

2nd Edition

# THE JOHN ZINK HAMWORTHY COMBUSTION HANDBOOK

FUNDAMENTALS | Vol.1

 **JOHN ZINK  
HAMWORTHY**  
COMBUSTION

**CHARLES E. BAUKAL, JR.**  
*Editor*

 **CRC Press**  
Taylor & Francis Group

THE JOHN ZINK HAMWORTHY

---

# **COMBUSTION HANDBOOK**

SECOND EDITION

Volume 1

**FUNDAMENTALS**



# INDUSTRIAL COMBUSTION SERIES

*Series Editors:*

Charles E. Baukal, Jr.

The John Zink Hamworthy Combustion Handbook, Second Edition

Volume I — Fundamentals

Volume II — Design and Operations

Volume III — Applications

*Charles E. Baukal, Jr.*

Industrial Burners Handbook

*Charles E. Baukal, Jr.*

The John Zink Combustion Handbook

*Charles E. Baukal, Jr.*

Computational Fluid Dynamics in Industrial Combustion

*Charles E. Baukal, Jr., Vladimir Gershtein, and Xianming Jimmy Li*

Heat Transfer in Industrial Combustion

*Charles E. Baukal, Jr.*

Oxygen-Enhanced Combustion

*Charles E. Baukal, Jr.*

THE JOHN ZINK HAMWORTHY

---

# COMBUSTION HANDBOOK

SECOND EDITION

Volume 1

**FUNDAMENTALS**

Edited by

**Charles E. Baukal, Jr.**



**CRC Press**

Taylor & Francis Group

Boca Raton London New York

---

CRC Press is an imprint of the  
Taylor & Francis Group, an **informa** business



CRC Press  
Taylor & Francis Group  
6000 Broken Sound Parkway NW, Suite 300  
Boca Raton, FL 33487-2742

© 2013 by Taylor & Francis Group, LLC  
CRC Press is an imprint of Taylor & Francis Group, an Informa business

No claim to original U.S. Government works  
Version Date: 2012920

International Standard Book Number-13: 978-1-4398-3963-8 (eBook - PDF)

This book contains information obtained from authentic and highly regarded sources. Reasonable efforts have been made to publish reliable data and information, but the author and publisher cannot assume responsibility for the validity of all materials or the consequences of their use. The authors and publishers have attempted to trace the copyright holders of all material reproduced in this publication and apologize to copyright holders if permission to publish in this form has not been obtained. If any copyright material has not been acknowledged please write and let us know so we may rectify in any future reprint.

Except as permitted under U.S. Copyright Law, no part of this book may be reprinted, reproduced, transmitted, or utilized in any form by any electronic, mechanical, or other means, now known or hereafter invented, including photocopying, microfilming, and recording, or in any information storage or retrieval system, without written permission from the publishers.

For permission to photocopy or use material electronically from this work, please access [www.copyright.com](http://www.copyright.com) (<http://www.copyright.com/>) or contact the Copyright Clearance Center, Inc. (CCC), 222 Rosewood Drive, Danvers, MA 01923, 978-750-8400. CCC is a not-for-profit organization that provides licenses and registration for a variety of users. For organizations that have been granted a photocopy license by the CCC, a separate system of payment has been arranged.

**Trademark Notice:** Product or corporate names may be trademarks or registered trademarks, and are used only for identification and explanation without intent to infringe.

**Visit the Taylor & Francis Web site at**  
**<http://www.taylorandfrancis.com>**

**and the CRC Press Web site at**  
**<http://www.crcpress.com>**

### *Dedication*

This book is dedicated to the memory of Richard T. Waibel, PhD. From 1961 to 1969, Dick attended Penn State University, where he received his BA and his PhD in fuel science. He started his career as an assistant director of industrial energy utilization at the Institute of Gas Technology in Chicago as it was known at that time. During his tenure there from 1975 to 1983, Dick developed industrial scale combustion research projects with industrial clients, the U.S. Department of Energy, and the U.S. Environmental Protection Agency. Projects included combustion of coal, low heating value gases, oil and slurries, as well as pollutant emission studies. He continued his career with John Zink Company, LLC, in Tulsa, Oklahoma, where he was instrumental in establishing John Zink as a world leader in low emissions technology. Dick authored numerous publications and is listed as inventor on 11 U.S. patents. During many years as chairman of the American Flame Research Committee (AFRC) and president of the International Flame Research Foundation (IFRF), he developed numerous valuable relationships between the industrial and academic combustion worlds, making friends all over the world. In addition to his academic and industrial achievements “Dr. Dick,” as he was known by many, was an avid and accomplished fly fisherman, photographer, and world traveler.



This page intentionally left blank

---

# Contents

---

List of Figures .....	ix
List of Tables .....	xxix
Foreword to the First Edition .....	xxxiii
Preface to the First Edition.....	xxxv
Preface to the Second Edition.....	xxxvii
Acknowledgments .....	xxxix
Editor.....	xli
Contributors.....	xliii
Prologue.....	xlvi
<b>1. Introduction .....</b>	<b>1</b>
<i>Charles E. Baukal, Jr.</i>	
<b>2. Refining and Petrochemical Industries .....</b>	<b>31</b>
<i>Erwin Platvoet, Rasik Patel, David Brown, Jason D. McAdams, and James G. Seebold</i>	
<b>3. Fuels.....</b>	<b>45</b>
<i>John Ackland, Jeff White, and Richard T. Waibel</i>	
<b>4. Combustion Fundamentals .....</b>	<b>79</b>
<i>Steve Londerville, Joseph Colannino, and Charles E. Baukal, Jr.</i>	
<b>5. Solid Fuel Combustion in Suspension.....</b>	<b>125</b>
<i>Steve Londerville and Timothy Webster</i>	
<b>6. Catalytic Combustion .....</b>	<b>137</b>
<i>Klaus-Dieter Zschorsch</i>	
<b>7. Heat Transfer .....</b>	<b>159</b>
<i>Jay Karan and Charles E. Baukal, Jr.</i>	
<b>8. Flare Radiation.....</b>	<b>207</b>
<i>Wes Bussman and Jeff White</i>	
<b>9. Fundamentals of Fluid Dynamics.....</b>	<b>227</b>
<i>Wes Bussman, Zachary L. Kodesh, and Robert E. Schwartz</i>	
<b>10. Oil Atomization .....</b>	<b>309</b>
<i>I.-Ping Chung and Steve Londerville</i>	
<b>11. Cold Flow Modeling .....</b>	<b>327</b>
<i>Christopher Q. Jian</i>	
<b>12. Thermal Efficiency .....</b>	<b>339</b>
<i>Charles E. Baukal, Jr. and Wes Bussman</i>	
<b>13. CFD-Based Combustion Modeling .....</b>	<b>353</b>
<i>Michael A. Lorra and Shirley X. Chen</i>	



<b>14. Pollutant Emissions</b> .....	381
<i>Charles E. Baukal, Jr., I.-Ping Chung, Steve Londerville, James G. Seebold, and Richard T. Waibel</i>	
<b>15. NO<sub>x</sub> Emissions</b> .....	417
<i>Charles E. Baukal, Jr. and Wes Bussman</i>	
<b>16. Noise</b> .....	479
<i>Wes Bussman, Jay Karan, Carl-Christian Hantschk, and Edwin Schorer</i>	
<b>17. Combustion Training</b> .....	513
<i>Charles E. Baukal, Jr. and Myra N. Crawford-Fanning</i>	
<b>Appendix A: Units and Conversions</b> .....	551
<b>Appendix B: Physical Properties of Materials</b> .....	555
<b>Appendix C: Properties of Gases and Liquids</b> .....	563
<b>Appendix D: Properties of Solids</b> .....	583
<b>Index</b> .....	587

## List of Figures

<b>Figure 1.1</b>	Operating refineries capacity and gross input (thousands of barrels per day) and number of operating refineries in the United States from 1949 to 2011.....	3
<b>Figure 1.2</b>	Product mix for U.S. refineries from 1949 to 2011.....	3
<b>Figure 1.3</b>	Annual final energy consumption for U.S. refineries from 1986 to 2010.....	4
<b>Figure 1.4</b>	Energy cost for U.S. refineries from 1988 to 2005 .....	4
<b>Figure 1.5</b>	Typical petroleum refinery. ....	5
<b>Figure 1.6</b>	Offshore oil rig flare. ....	6
<b>Figure 1.7</b>	Flare pilot. ....	6
<b>Figure 1.8</b>	Duct burner flame.....	6
<b>Figure 1.9</b>	Schematic of a duct burner used to enhance the power from a gas turbine.....	6
<b>Figure 1.10</b>	Front of a boiler burner. ....	7
<b>Figure 1.11</b>	Thermal oxidizer drawing.....	7
<b>Figure 1.12</b>	Vapor combustor system.....	7
<b>Figure 1.13</b>	Biogas flare system.....	8
<b>Figure 1.14</b>	Vapor recovery system. ....	8
<b>Figure 1.15</b>	Flare gas recovery system.....	8
<b>Figure 1.16</b>	Schematics of (a) side- and (b) top-fired reformers .....	11
<b>Figure 1.17</b>	Down-fired burner commonly used in top-fired reformers.....	11
<b>Figure 1.18</b>	Elevation view of a terrace-wall-fired furnace.....	11
<b>Figure 1.19</b>	Schematic of a process heater .....	12
<b>Figure 1.20</b>	Schematic of a typical process heater .....	12
<b>Figure 1.21</b>	Fired heater size distribution .....	13
<b>Figure 1.22</b>	Schematic of center or target wall firing configuration. ....	14
<b>Figure 1.23</b>	Horizontal floor-fired burners firing toward a center wall. ....	14
<b>Figure 1.24</b>	Wall-fired burner. ....	14
<b>Figure 1.25</b>	Schematic of a horizontally mounted, vertically fired burner configuration.....	14
<b>Figure 1.26</b>	Examples of process heaters.....	15
<b>Figure 1.27</b>	Typical heater types.....	16
<b>Figure 1.28</b>	Cabin heater.....	17
<b>Figure 1.29</b>	Crude unit burners.....	18
<b>Figure 1.30</b>	Typical burner arrangements.....	19
<b>Figure 1.31</b>	Drawing of a typical combination oil and gas burner. ....	20
<b>Figure 1.32</b>	Process heater heat balance .....	20



<b>Figure 1.33</b>	Schematic of a burner (B) arrangement in the floor of vertical cylindrical furnaces. ....	20
<b>Figure 1.34</b>	Schematic of a burner (B) arrangement in the floor of rectangular cabin heaters. ....	21
<b>Figure 1.35</b>	Adiabatic equilibrium NO and CO as a function of the equivalence ratio for an air/CH <sub>4</sub> flame.....	21
<b>Figure 1.36</b>	Schematic of an oxy/fuel burner.....	22
<b>Figure 1.37</b>	Schematic of an oxygen-enriched air/fuel burner. ....	22
<b>Figure 1.38</b>	Schematic of a burner using oxygen + recycled combustion products. ....	23
<b>Figure 1.39</b>	Schematic of flue gas recirculation.....	23
<b>Figure 1.40</b>	HALO <sup>®</sup> ™ burner designed to entrain furnace gases into the flame.....	23
<b>Figure 1.41</b>	Schematic of a premix burner. ....	24
<b>Figure 1.42</b>	Drawing of a typical premix (radiant wall) gas burner. ....	24
<b>Figure 1.43</b>	Painting of a diffusion flame.....	24
<b>Figure 1.44</b>	Schematic of a diffusion burner.....	25
<b>Figure 1.45</b>	Schematic of a partially premixed burner.....	25
<b>Figure 1.46</b>	Schematic of a staged-air burner. ....	25
<b>Figure 1.47</b>	Drawing of a typical staged-air combination oil and gas burner.....	25
<b>Figure 1.48</b>	Schematic of a staged-fuel burner. ....	25
<b>Figure 1.49</b>	Drawing of a typical staged-fuel gas burner. ....	25
<b>Figure 1.50</b>	Drawing of a typical natural draft gas burner. ....	26
<b>Figure 1.51</b>	Natural draft burner.....	26
<b>Figure 1.52</b>	Flames impinging on tubes in a cabin heater.....	27
<b>Figure 1.53</b>	Flames pulled toward the wall.....	27
<b>Figure 1.54</b>	Oil burner needing service.....	27
<b>Figure 1.55</b>	Highly lifted down-fired burner flame. ....	27
<b>Figure 1.56</b>	John Zink Co. LLC (Tulsa, Oklahoma) R&D Test Facility.....	28
<b>Figure 1.57</b>	Cold flow testing. ....	28
<b>Figure 1.58</b>	Example of CFD model result.....	28
<b>Figure 1.59</b>	Virtual reality engineering simulation.....	29
<b>Figure 2.1</b>	Typical refinery process flow diagram. ....	34
<b>Figure 2.2</b>	Simplified crude distillation flow diagram.....	35
<b>Figure 2.3</b>	Typical visbreaking flow diagram. ....	35
<b>Figure 2.4</b>	Typical hydrotreating flow diagram. ....	36
<b>Figure 2.5</b>	Catalytic reforming process flow diagram. ....	37
<b>Figure 2.6</b>	Simplified process diagram for delayed coking.....	37
<b>Figure 2.7</b>	Simplified process diagram of a steam reforming based hydrogen plant. ....	39
<b>Figure 2.8</b>	Typical PSA system flow diagram.....	40
<b>Figure 2.9</b>	Typical flow diagram of an ammonia plant.....	40
<b>Figure 2.10</b>	Typical methanol plant process flow diagram .....	41

<b>Figure 3.1</b>	Capping a burning oil well.....	46
<b>Figure 3.2</b>	Refinery flow diagram .....	49
<b>Figure 3.3</b>	Flow diagram of UOP fluid catalytic cracking complex .....	50
<b>Figure 3.4</b>	Simplified process flow diagram for hydrogen reforming/pressure swing adsorption .....	53
<b>Figure 3.5</b>	Simplified process flow diagram for Flexicoking .....	54
<b>Figure 3.6</b>	Viewing oil flame through a burner plenum.....	56
<b>Figure 3.7</b>	Burner firing heavy oil (1).....	56
<b>Figure 3.8</b>	Burner firing heavy oil (2).....	56
<b>Figure 3.9</b>	Naphtha distillation curve.....	57
<b>Figure 3.10</b>	Flame speed for various gases .....	64
<b>Figure 3.11</b>	Crude oil distillation curve.....	65
<b>Figure 3.12</b>	Viscosity of fuel oils.....	67
<b>Figure 3.13</b>	100% TNG flame.....	69
<b>Figure 3.14</b>	80% TNG/20% N <sub>2</sub> flame. ....	69
<b>Figure 3.15</b>	90% TNG/10% N <sub>2</sub> flame. ....	70
<b>Figure 3.16</b>	90% TNG/10% H <sub>2</sub> flame. ....	70
<b>Figure 3.17</b>	75% TNG/25% H <sub>2</sub> flame. ....	70
<b>Figure 3.18</b>	25% TNG/75% H <sub>2</sub> flame. ....	70
<b>Figure 3.19</b>	50% TNG/50% H <sub>2</sub> flame.....	71
<b>Figure 3.20</b>	100% H <sub>2</sub> flame.....	71
<b>Figure 3.21</b>	50% TNG/25% H <sub>2</sub> /25% C <sub>3</sub> H <sub>8</sub> flame.....	71
<b>Figure 3.22</b>	100% C <sub>3</sub> H <sub>8</sub> flame.....	71
<b>Figure 3.23</b>	50% TNG/50% C <sub>3</sub> H <sub>8</sub> flame.....	72
<b>Figure 3.24</b>	100% C <sub>4</sub> H <sub>10</sub> flame.....	72
<b>Figure 3.25</b>	Simulated cracked gas flame.....	72
<b>Figure 3.26</b>	Simulated FCC gas flame.....	72
<b>Figure 3.27</b>	Simulated coking gas flame.....	73
<b>Figure 3.28</b>	Simulated reforming gas flame. ....	73
<b>Figure 3.29</b>	100% Tulsa natural gas.....	73
<b>Figure 3.30</b>	100% hydrogen.....	73
<b>Figure 3.31</b>	100% propane.....	74
<b>Figure 3.32</b>	50% hydrogen/50% propane.....	74
<b>Figure 3.33</b>	50% hydrogen/50% Tulsa natural gas. ....	74
<b>Figure 3.34</b>	50% propane/50% Tulsa natural gas.....	74
<b>Figure 3.35</b>	25% hydrogen/75% propane.....	75
<b>Figure 3.36</b>	75% hydrogen/25% propane.....	75
<b>Figure 3.37</b>	25% hydrogen/75% Tulsa natural gas. ....	75

<b>Figure 3.38</b>	75% hydrogen/25% Tulsa natural gas. ....	75
<b>Figure 3.39</b>	25% propane/75% Tulsa natural gas. ....	76
<b>Figure 3.40</b>	75% propane/25% Tulsa natural gas. ....	76
<b>Figure 3.41</b>	25% hydrogen/25% propane/50% Tulsa natural gas. ....	76
<b>Figure 3.42</b>	50% hydrogen/25% propane/25% Tulsa natural gas. ....	76
<b>Figure 4.1</b>	Typical cabin-style process heater. ....	81
<b>Figure 4.2</b>	Carbon atom with six protons, neutrons, and electrons. ....	82
<b>Figure 4.3</b>	Periodic table. ....	83
<b>Figure 4.4</b>	Composition of air by volume. ....	86
<b>Figure 4.5</b>	Species concentration versus excess air for the following fuels ....	90
<b>Figure 4.6</b>	Adiabatic flame temperature versus equivalence ratio for air/H <sub>2</sub> , air/CH <sub>4</sub> , and air/C <sub>3</sub> H <sub>8</sub> flames where the air and fuel are at ambient temperature and pressure. ....	104
<b>Figure 4.7</b>	Adiabatic flame temperature versus air preheat temperature for stoichiometric air/H <sub>2</sub> , air/CH <sub>4</sub> , and air/C <sub>3</sub> H <sub>8</sub> flames where the fuel is at ambient temperature and pressure. ....	104
<b>Figure 4.8</b>	Adiabatic flame temperature versus fuel preheat temperature for stoichiometric air/H <sub>2</sub> , air/CH <sub>4</sub> , and air/C <sub>3</sub> H <sub>8</sub> flames where the air is at ambient temperature and pressure. ....	105
<b>Figure 4.9</b>	Adiabatic flame temperature versus fuel blend (CH <sub>4</sub> /H <sub>2</sub> and CH <sub>4</sub> /N <sub>2</sub> ) composition for stoichiometric air/fuel flames where the air and fuel are at ambient temperature and pressure. ....	106
<b>Figure 4.10</b>	Adiabatic flame temperature versus fuel blend (CH <sub>4</sub> /H <sub>2</sub> ) composition and air preheat temperature for stoichiometric air/fuel flames where the fuel is at ambient temperature and pressure. ....	107
<b>Figure 4.11</b>	Sample Sankey diagram showing distribution of energy in a combustion system. ....	107
<b>Figure 4.12</b>	Available heat versus gas temperature for stoichiometric air/H <sub>2</sub> , air/CH <sub>4</sub> , and air/C <sub>3</sub> H <sub>8</sub> flames where the air and fuel are at ambient temperature and pressure. ....	108
<b>Figure 4.13</b>	Available heat versus air preheat temperature for stoichiometric air/H <sub>2</sub> , air/CH <sub>4</sub> , and air/C <sub>3</sub> H <sub>8</sub> flames at an exhaust gas temperature of 2000°F (1100°C) where the fuel is at ambient temperature and pressure. ....	109
<b>Figure 4.14</b>	Available heat versus fuel preheat temperature for stoichiometric air/H <sub>2</sub> , air/CH <sub>4</sub> , and air/C <sub>3</sub> H <sub>8</sub> flames at an exhaust gas temperature of 2000°F (1100°C) where the air is at ambient temperature and pressure. ....	110
<b>Figure 4.15</b>	Graphical representation of ignition and heat release. ....	110
<b>Figure 4.16</b>	Species concentration versus stoichiometric ratio for the following fuels ....	113
<b>Figure 4.17</b>	Adiabatic equilibrium reaction process. ....	116
<b>Figure 4.18</b>	Adiabatic equilibrium calculations for the predicted gas composition as a function of the O <sub>2</sub> :CH <sub>4</sub> stoichiometry for air/CH <sub>4</sub> flames where the air and CH <sub>4</sub> are at ambient temperature and pressure. ....	116
<b>Figure 4.19</b>	Adiabatic equilibrium stoichiometric calculations for the predicted gas composition of the major species as a function of the air preheat temperature for air/CH <sub>4</sub> flames where the CH <sub>4</sub> is at ambient temperature and pressure. ....	117
<b>Figure 4.20</b>	Adiabatic equilibrium stoichiometric calculations for the predicted gas composition of the minor species as a function of the air preheat temperature for air/CH <sub>4</sub> flames where the CH <sub>4</sub> is at ambient temperature and pressure. ....	118

<b>Figure 4.21</b>	Adiabatic equilibrium stoichiometric calculations for the predicted gas composition of the major species as a function of the fuel preheat temperature for air/CH <sub>4</sub> flames where the air is at ambient temperature and pressure.....	119
<b>Figure 4.22</b>	Adiabatic equilibrium stoichiometric calculations for the predicted gas composition of the minor species as a function of the fuel preheat temperature for air/CH <sub>4</sub> flames where the air is at ambient temperature and pressure.....	120
<b>Figure 4.23</b>	Adiabatic equilibrium stoichiometric calculations for the predicted gas composition of the major species as a function of the fuel blend (H <sub>2</sub> + CH <sub>4</sub> ) composition for air/fuel flames where the air and fuel are at ambient temperature and pressure.....	120
<b>Figure 4.24</b>	Adiabatic equilibrium stoichiometric calculations for the predicted gas composition of the minor species as a function of the fuel blend (H <sub>2</sub> + CH <sub>4</sub> ) composition for air/fuel flames where the air and fuel are at ambient temperature and pressure.....	121
<b>Figure 4.25</b>	Adiabatic equilibrium stoichiometric calculations for the predicted gas composition of the major species as a function of the fuel blend (N <sub>2</sub> + CH <sub>4</sub> ) composition for air/fuel flames where the air and fuel are at ambient temperature and pressure.....	121
<b>Figure 4.26</b>	Adiabatic equilibrium stoichiometric calculations for the predicted gas composition of the minor species as a function of the fuel blend (N <sub>2</sub> + CH <sub>4</sub> ) composition for air/fuel flames where the air and fuel are at ambient temperature and pressure.....	122
<b>Figure 4.27</b>	Equilibrium calculations for the predicted gas composition of the major species as a function of the combustion product temperature for air/CH <sub>4</sub> flames where the air and fuel are at ambient temperature and pressure.....	122
<b>Figure 4.28</b>	Equilibrium calculations for the predicted gas composition of the minor species as a function of the combustion product temperature for air/CH <sub>4</sub> flames where the air and fuel are at ambient temperature and pressure.....	123
<b>Figure 5.1</b>	Subbituminous char burnout Coen code A = 60 and E = 17,150. ....	129
<b>Figure 5.2</b>	Pet coke char burnout Coen Code A = 15 and E = 19,000. ....	129
<b>Figure 5.3</b>	Coal dust flame velocity versus equivalence ratio.....	129
<b>Figure 5.4</b>	Fuel introduction for conveying options.....	131
<b>Figure 5.5</b>	Front of Coen biomass burner.....	132
<b>Figure 6.1</b>	Catalyst's function. ....	138
<b>Figure 6.2</b>	(a) Bulk materials: pellets catalyst–spheres and rings (balls, rings, and cylinders) and (b) types of monolith catalyst monolith (honeycomb) material. ....	140
<b>Figure 6.3</b>	Typical horizontal catalytic system with a preheat exchanger. ....	143
<b>Figure 6.4</b>	Typical compact catalytic waste gas cleaning system. ....	144
<b>Figure 6.5</b>	Typical required reactor inlet/reaction temperature, $T_c$ . ....	145
<b>Figure 6.6</b>	The arrangement is a catalyst facility consisting of ceramic monoliths. ....	147
<b>Figure 6.7</b>	Reactor designs and flows: (a) Single-bed reactor, (b) vertical two-bed reactor (operating temperature > 480°C, $\Delta T_c > 150$ K), (c) horizontal cylinder two-bed reactor (operating temperature > 480°C, $\Delta T_c > 150$ K), and (d) multiple-bed reactor.....	148
<b>Figure 6.8</b>	Simple catalytic waste gas cleaning system.....	152
<b>Figure 6.9</b>	Catalytic waste gas cleaning system with a burner and blower. ....	153
<b>Figure 6.10</b>	Catalytic waste gas cleaning system with a heat exchanger. ....	153
<b>Figure 6.11</b>	Catalytic waste gas cleaning system with hot water/air production.....	154

<b>Figure 6.12</b>	Catalytic waste gas cleaning system with steam production and waste liquid injection.....	154
<b>Figure 6.13</b>	Simple catalytic waste gas cleaning system with regenerative heat transfer system. ....	155
<b>Figure 6.14</b>	Regenerative heat transfer system, temperature profile.....	155
<b>Figure 6.15</b>	Catalytic waste gas cleaning system with regenerative heat transfer system including back purge flow system.....	156
<b>Figure 6.16</b>	Catalytic waste gas cleaning system with regenerative heat transfer system, one-way flow reactor. ....	157
<b>Figure 7.1</b>	Typical fired heater.....	161
<b>Figure 7.2</b>	Heat transfer through a plane wall: (a) temperature distribution and (b) equivalent thermal circuit .....	164
<b>Figure 7.3</b>	Equivalent thermal circuit for a series composite wall .....	164
<b>Figure 7.4</b>	Temperature drop due to thermal contact resistance. ....	165
<b>Figure 7.5</b>	Temperature distribution for a composite cylindrical wall .....	166
<b>Figure 7.6</b>	Thermal conductivity of (a) some commonly used steels and alloys and (b) some refractory materials. ....	169
<b>Figure 7.7</b>	Temperature–thickness relationships corresponding to different thermal conductivities.....	170
<b>Figure 7.8</b>	Thermal boundary layer development in a heated circular tube .....	171
<b>Figure 7.9</b>	Orthogonal oscillations of electric and magnetic waves in the propagation of electromagnetic waves.....	177
<b>Figure 7.10</b>	Spectrum of electromagnetic radiation.....	177
<b>Figure 7.11</b>	Spectral blackbody emissive power.....	179
<b>Figure 7.12</b>	Radiation transfer between two surfaces approximated as gray bodies.....	180
<b>Figure 7.13</b>	Network representation of radiative exchange between surface $i$ and the remaining surfaces of an enclosure.....	181
<b>Figure 7.14</b>	View factor of radiation exchange between faces of area $dA_i$ and $dA_j$ .....	181
<b>Figure 7.15</b>	View factor for aligned parallel rectangles.....	184
<b>Figure 7.16</b>	View factor for coaxial parallel disks .....	184
<b>Figure 7.17</b>	View factor for perpendicular rectangles with a common edge.....	185
<b>Figure 7.18</b>	Infrared thermal image of a flame in a furnace.....	185
<b>Figure 7.19</b>	Emission bands of (a) $\text{CO}_2$ and (b) $\text{H}_2\text{O}$ .....	186
<b>Figure 7.20</b>	Total emissivity of water vapor at the reference state of a total gas pressure $p = 1$ bar and a partial pressure of $\text{H}_2\text{O}$ $p_a \rightarrow 0$ .....	188
<b>Figure 7.21</b>	Total emissivity of carbon dioxide at the reference state of a total gas pressure $p = 1$ bar and a partial pressure of $\text{CO}_2$ $p_a \rightarrow 0$ .....	188
<b>Figure 7.22</b>	Radiation heat transfer correction factor for mixtures of water vapor and carbon dioxide .....	189
<b>Figure 7.23</b>	Photographic view of a luminous flame.....	192
<b>Figure 7.24</b>	Photographic view of a nonluminous flame.....	192
<b>Figure 7.25</b>	Photographic view of a radiant wall burner. ....	193
<b>Figure 7.26</b>	Vertical heat flux distribution for oil and gas firing in a vertical tube furnace.....	193



<b>Figure 7.27</b>	Distribution of dimensionless average radiant flux density at the tube surfaces for various flame lengths.....	194
<b>Figure 7.28</b>	Maximum flame radiation as a function of the C/H weight ratio in the fuel.....	195
<b>Figure 7.29</b>	Radiation heat transfer in a cylindrical furnace.....	197
<b>Figure 7.30</b>	Cross section of a furnace wall. ....	198
<b>Figure 7.31</b>	Cross section of a process tube. ....	199
<b>Figure 8.1</b>	Electromagnetic spectrum.....	208
<b>Figure 8.2</b>	Flare firing propane at 60,000 lb/h (27,000 kg/h) corresponding to an HR rate equal to 1.2 billion Btu/h (350 MW). ....	209
<b>Figure 8.3</b>	Illustration defining radiation level. ....	209
<b>Figure 8.4</b>	Solar radiation level at angles normal to the solar beam and horizontal to the surface of the Earth in Tulsa, Oklahoma. ....	210
<b>Figure 8.5</b>	View of Tulsa from the sun during the months of January and July. ....	210
<b>Figure 8.6</b>	Effects of doubling the distance of the flame epicenter from an observer. ....	211
<b>Figure 8.7</b>	Relative radiation level as a function of distance from the source.....	212
<b>Figure 8.8</b>	Spectral emission of radiation from luminous and nonluminous flames .....	212
<b>Figure 8.9</b>	Generalized diagram showing relative atmospheric radiation transmission of different wavelengths .....	213
<b>Figure 8.10</b>	Estimates of the fraction of flame radiation transmitted through the atmosphere at various distances and percent relative humidity .....	214
<b>Figure 8.11</b>	API 521 recommendations.....	216
<b>Figure 8.12</b>	Various models commonly used in industry to estimate flare radiation.....	217
<b>Figure 8.13</b>	Illustration for example calculation. ....	218
<b>Figure 8.14</b>	Steam-assisted flare (a) without steam and (b) with steam.....	219
<b>Figure 8.15</b>	Smoking flare.....	219
<b>Figure 8.16</b>	A couple brands of handheld radiometers.....	220
<b>Figure 8.17</b>	The major components that make up a flare radiometer. ....	220
<b>Figure 8.18</b>	A radiometer certificate of calibration. ....	221
<b>Figure 8.19</b>	Illustration showing a radiometer not viewing the entire flare flame.....	222
<b>Figure 8.20</b>	Radiometers with different types of windows.....	222
<b>Figure 8.21</b>	Transmissivity curve of zinc selenide.....	223
<b>Figure 8.22</b>	Transmissivity curve of sapphire.....	223
<b>Figure 8.23</b>	Reflected radiation at a wavelength of $1 \times 10^{-6}$ m for zinc selenide.....	223
<b>Figure 8.24</b>	The John Zink radiometer cube.....	224
<b>Figure 9.1</b>	(a and b) Ratio of specific heat ( $k$ ) for various pure-component gases at different temperatures.....	232
<b>Figure 9.2</b>	The pitch drop experiment is a <i>long-term experiment</i> , which measures the flow of a piece of <i>pitch</i> through a funnel .....	233
<b>Figure 9.3</b>	Dynamic viscosity as a function of temperature for various fluids.....	235
<b>Figure 9.4</b>	Temperature versus viscosity for various hydrocarbons.....	236

<b>Figure 9.5</b>	Viscosity of mid-continent oils .....	237
<b>Figure 9.6</b>	Osborn Reynold's experimental apparatus used to study the transition from laminar to turbulent flow.....	238
<b>Figure 9.7</b>	Smoke rising from a soldering iron.....	238
<b>Figure 9.8</b>	Photograph showing examples of a (a) laminar and (b) turbulent flame.....	239
<b>Figure 9.9</b>	Various sizes of Pitot-static tubes.....	239
<b>Figure 9.10</b>	The simple Pitot tube illustrating the difference between the static, velocity, and total pressure. ....	240
<b>Figure 9.11</b>	Illustration showing measurements of static, velocity, and total pressure inside a pipe .....	240
<b>Figure 9.12</b>	Illustration of the Pitot-static tube. ....	240
<b>Figure 9.13</b>	Photograph of the Pitot-static tube. ....	241
<b>Figure 9.14</b>	Illustration showing the fluid flow pattern through a long-radius elbow. ....	242
<b>Figure 9.15</b>	Loss coefficients through various fittings .....	243
<b>Figure 9.16</b>	Well-rounded bell inlet on a premixed burner.....	243
<b>Figure 9.17</b>	Moody diagram showing friction factor versus Re .....	245
<b>Figure 9.18</b>	Flow past a cylinder at a Reynolds number of 10,000.....	246
<b>Figure 9.19</b>	Stack downwash.....	246
<b>Figure 9.20</b>	Steam washing down the downwind side of a stack .....	246
<b>Figure 9.21</b>	Flame pulled down on the outside of a flare tip due to stack downwash effect.....	247
<b>Figure 9.22</b>	Flame pulled down on the outside of a flare tip due to stack downwash effect (closer view).....	247
<b>Figure 9.23</b>	An upward projecting flame.....	248
<b>Figure 9.24</b>	Damaged flare tip and appurtenances caused by external burning: (a) flare tip and (b) flare pilot. ....	248
<b>Figure 9.25</b>	Wind tunnel test showing flow past a small-scale building .....	248
<b>Figure 9.26</b>	Illustration showing a gas plume being pulled into the downwind side of a building.....	248
<b>Figure 9.27</b>	Photograph showing recirculation pattern created between two small-scale buildings .....	248
<b>Figure 9.28</b>	Photographs showing a recirculation pattern created on the downwind side of a small-scale hill located inside a wind tunnel.....	249
<b>Figure 9.29</b>	Downwash on the backside of a volcano (Mount Mayon, Philippines) bellowing steam and ash.....	249
<b>Figure 9.30</b>	Illustration showing the effect of stack height on the plume downwind of a mountain.....	249
<b>Figure 9.31</b>	Internal burning inside a steam-assisted flare tip. ....	249
<b>Figure 9.32</b>	Schlieren photographs showing airflow patterns near a cup filled with hot coffee and another filled with ice water .....	250
<b>Figure 9.33</b>	Illustration showing air falling into a flare tip creating internal burning. ....	250
<b>Figure 9.34</b>	Flow past a cavity .....	250
<b>Figure 9.35</b>	Illustration showing internal burning by action of wind.....	251
<b>Figure 9.36</b>	A view looking inside a wind tunnel showing a small-scale model .....	251
<b>Figure 9.37</b>	Scale model wind tunnel test analyzing the gas plume downstream of a vent stack.....	252

<b>Figure 9.38</b>	Satellite photograph showing the plume of smoke and ash from a volcano .....	252
<b>Figure 9.39</b>	Smoke venting from a stack and dispersing downwind .....	252
<b>Figure 9.40</b>	Illustration defining the plume rise of a buoyant gas vented from a stack.....	253
<b>Figure 9.41</b>	(a) Vent stack with a low plume rise and (b) vent stack with high plume rise .....	253
<b>Figure 9.42</b>	(a) Smoke dissipating in an unstable atmosphere (high turbulence) and (b) smoke dissipating in a stable atmosphere (low turbulence).....	254
<b>Figure 9.43</b>	Heavier-than-air plume vented from a stack in a stable atmosphere .....	254
<b>Figure 9.44</b>	Illustration showing how the heater draft typically varies inside a heater at various elevations.....	255
<b>Figure 9.45</b>	Four methods air is commonly supplied in process heaters.....	255
<b>Figure 9.46</b>	Illustration showing a U-tube manometer connected to the side of a natural draft heater.....	258
<b>Figure 9.47</b>	U.S. standard for variation of atmospheric pressure with elevation.....	258
<b>Figure 9.48</b>	Plot showing that the atmospheric pressure is approximately linear at altitudes less than about 500 ft (150 m). .....	259
<b>Figure 9.49</b>	Illustration showing how the pressure varies inside a stack filled with hot air.....	259
<b>Figure 9.50</b>	Illustration showing how the hydrostatic pressure and draft varies inside a stack filled with hot air.....	260
<b>Figure 9.51</b>	Illustration showing how the hydrostatic pressure and draft inside a stack filled with hot, warm, and cooler ambient air varies with elevation. ....	260
<b>Figure 9.52</b>	Illustration showing how the hydrostatic pressure and draft varies with stack height. ....	261
<b>Figure 9.53</b>	Example problem illustrating effects of temperature and height on draft. ....	261
<b>Figure 9.54</b>	Illustration showing the hydrostatic pressure and draft profile at various elevations inside a stack filled with hot air.....	262
<b>Figure 9.55</b>	Illustration showing how the heater pressure profile changes as the stack damper is closed and the burner damper opened.....	263
<b>Figure 9.56</b>	Illustration showing the pressure and draft profile for a typical natural draft heater.....	264
<b>Figure 9.57</b>	Positive draft inside a heater forcing flame out through the burner intake.....	264
<b>Figure 9.58</b>	(a) Refractory brick dislodged from the heater wall due to warping of the heater casing. (b) Large chunk of refractory that has fallen from the heater wall into the throat of a burner.....	265
<b>Figure 9.59</b>	(a) Coke buildup on a burner tip caused by low draft through the burner. (b) Long flame impinging on process tubes caused by low draft at the burner elevation. ....	265
<b>Figure 9.60</b>	A process tube penetrating the convection section of a heater. ....	265
<b>Figure 9.61</b>	Sight ports on a heater left open allowing tramp air to enter.....	266
<b>Figure 9.62</b>	Access door on a heater not properly sealed allowing tramp air to enter. ....	266
<b>Figure 9.63</b>	Illustration showing the effects of closing the burner and stack damper on draft and excess O <sub>2</sub> . ....	267
<b>Figure 9.64</b>	Results showing the draft profile for various burner and stack damper settings operating at a constant burner heat release and heater O <sub>2</sub> . ....	267
<b>Figure 9.65</b>	Schematic of a heater used in the SMR industry for hydrogen production.....	268
<b>Figure 9.66</b>	Example of a typical draft profile inside a down-fired heater.....	268

<b>Figure 9.67</b>	Illustration comparing the pressure inside of a down-fired heater and the pressure inside a vacuum cleaner hose. ....	269
<b>Figure 9.68</b>	Illustration showing inclined manometers essentially expand the scale of a U-tube manometer by orienting it at an angle. ....	270
<b>Figure 9.69</b>	Inclined manometer typically used to measure heater draft. ....	270
<b>Figure 9.70</b>	Inclined manometer reading 0.2 and 0 in. of WC. ....	271
<b>Figure 9.71</b>	(a) Dial pressure gauge reading 0.2 in. WC and (b) electronic pressure transmitter used to measure heater draft. ....	271
<b>Figure 9.72</b>	Illustration used in example problem to demonstrate how much the draft varies with elevation inside a heater. ....	272
<b>Figure 9.73</b>	Plot showing how the draft per foot of heater height varies with flue gas temperature for two different ambient conditions. ....	272
<b>Figure 9.74</b>	Illustration showing ways the wind can impact heater draft levels. ....	273
<b>Figure 9.75</b>	Data trends showing wind effects on heater draft and excess O <sub>2</sub> at high- and low-wind speeds over a 10-min period. ....	274
<b>Figure 9.76</b>	(a–c) Illustrations showing burner designs with various air intake configurations. ....	274
<b>Figure 9.77</b>	Experimental data showing effects of a crosswind past a burner intake on excess O <sub>2</sub> . ....	275
<b>Figure 9.78</b>	Illustration showing the path of combustion air as it passes through a burner. ....	275
<b>Figure 9.79</b>	A typical air-side capacity curve for a natural draft burner. ....	276
<b>Figure 9.80</b>	Example of a fuel capacity curve. ....	278
<b>Figure 9.81</b>	Graph showing how the fuel capacity curve varies in the subsonic and sonic flow regimes. ....	279
<b>Figure 9.82</b>	Photographs of gas exiting a nozzle at sonic and subsonic flow conditions. ....	280
<b>Figure 9.83</b>	Example of a fuel capacity curve for a particular burner firing several fuels. ....	281
<b>Figure 9.84</b>	Burner tips commonly used in the burner industry ....	281
<b>Figure 9.85</b>	Illustration showing four nozzles having the same port area but with different internal designs. ....	282
<b>Figure 9.86</b>	Photographs of a PSA gas burner showing rounded port inlets caused by corrosion from metal dusting. ....	283
<b>Figure 9.87</b>	Illustration showing a several important factors that influence the flow rate through nozzles. ....	283
<b>Figure 9.88</b>	Example showing how the orifice discharge coefficient affects the fuel pressure of a burner operating at a constant HR. ....	284
<b>Figure 9.89</b>	Fuel ports plugged with pipe scale and dirt. ....	284
<b>Figure 9.90</b>	Fuel ports plugged with mortar. ....	284
<b>Figure 9.91</b>	Flame patterns (a) before and (b) after cleaning coke from fuel ports. ....	285
<b>Figure 9.92</b>	Coke buildup in the main body of the fuel nozzle. ....	285
<b>Figure 9.93</b>	Illustration showing partial blockage near the outlet of a fuel port. ....	285
<b>Figure 9.94</b>	Comparing a burner (a) without and (b) with partially plugged primary fuel tips. ....	286
<b>Figure 9.95</b>	Example showing the effects of fuel port blockage on the fuel capacity curves. ....	287
<b>Figure 9.96</b>	Burner tip with coking on the inside. ....	287
<b>Figure 9.97</b>	Fuel tips partially plugged upstream of the ports. ....	288

<b>Figure 9.98</b>	Photograph of a gas exiting a nozzle.....	289
<b>Figure 9.99</b>	Mixing downstream of a free jet.....	289
<b>Figure 9.100</b>	General structure of a turbulent free jet.....	290
<b>Figure 9.101</b>	Illustration showing a simple version of an eductor.....	291
<b>Figure 9.102</b>	The basic components of an eductor system.....	292
<b>Figure 9.103</b>	Flow path of secondary gas entrained into an eductor designed with a well-rounded bell inlet.....	292
<b>Figure 9.104</b>	Eductor tubes on a steam-assisted flare.....	293
<b>Figure 9.105</b>	Eductor system on a flare pilot.....	293
<b>Figure 9.106</b>	Eductor systems on pre-mixed wall-fired burners. ....	293
<b>Figure 9.107</b>	Eductor systems on premixed burners and pilots. ....	294
<b>Figure 9.108</b>	A general representation of how the pressure of the primary jet influences the entrainment performance of an eductor system. ....	294
<b>Figure 9.109</b>	A Venturi inlet on a premixed burner pilot covered with heavy fuel oil.....	294
<b>Figure 9.110</b>	Illustration showing a premixed burner flashing back.....	295
<b>Figure 9.111</b>	Schlieren photograph showing a turbulent flame front downstream of a premixed burner.....	295
<b>Figure 9.112</b>	Illustration that demonstrates flame propagation.....	296
<b>Figure 9.113</b>	Premix radiant-wall burner (a) tip and (b) firing in a heater. ....	296
<b>Figure 9.114</b>	Flashback of a premixed radiant wall burner with the flame stabilized inside the burner tip. ....	297
<b>Figure 9.115</b>	Flashback of a premixed radiant wall burner with the flame stabilized inside the venturi (glowing red from heat).....	297
<b>Figure 9.116</b>	Premixed radiant wall burner tip damaged from flashback.....	297
<b>Figure 9.117</b>	Laminar flame speed of several fuel components.....	297
<b>Figure 9.118</b>	(a) Twenty-two birthday candles arranged in 8 in. (20 cm) diameter circle. (b) Twenty-two birthday candles arranged in 2 in. (5 cm) diameter circle. ....	298
<b>Figure 9.119</b>	Burners firing in a vertical-cylindrical (VC) heater showing no signs of flame-flame interactions.....	299
<b>Figure 9.120</b>	Burners arranged in a tight circle causing flames to collapse toward the center of the burner circle.....	299
<b>Figure 9.121</b>	Two steam jets starting out parallel and being attracted to each other due to the low-pressure zone .....	299
<b>Figure 9.122</b>	Red smoke pulled into the low-pressure zone created on the back side of an airplane wing .....	300
<b>Figure 9.123</b>	Illustration showing the flow pattern and static pressure along the centerline between two unventilated (bounded by a lower wall) parallel flowing jets. ....	300
<b>Figure 9.124</b>	Flames impinging on process tubes in radiant section.....	300
<b>Figure 9.125</b>	Flame impinging on process tubes in convection section. ....	301
<b>Figure 9.126</b>	Ruptured process tube caused by prolonged flame impingement.....	301
<b>Figure 9.127</b>	(a) Candle flame held next to a piece of glass. (b) Soot particle.....	301
<b>Figure 9.128</b>	Burners arranged in a tight circle causing flames to collapse toward the center.....	302

<b>Figure 9.129</b>	Diffusion burners arranged in a straight line.....	303
<b>Figure 9.130</b>	Loss coefficients used for estimating the mass flow rate of tramp air flowing through an open heater sight port. ....	304
<b>Figure 9.131</b>	Illustration of air leaking into a flare system filled with methane. ....	305
<b>Figure 10.1</b>	Liquid disintegration of a cylindrical jet caused by wave formations on liquid surface. ....	311
<b>Figure 10.2</b>	A hollow-cone swirl spray with high viscosity liquid ( $v = 6 \text{ mm}^2/\text{s}$ ) .....	313
<b>Figure 10.3</b>	John Zink Spray Laboratory equipped with a PDPA. ....	315
<b>Figure 10.4</b>	Spray angle relative to a stable oil flame .....	315
<b>Figure 10.5</b>	A gun with a $90^\circ$ machine angle, its spray angle actually is about $30^\circ$ .....	315
<b>Figure 10.6</b>	Patternator to collect water sprayed out of an oil gun.....	315
<b>Figure 10.7</b>	Patternation measurements for a gun shown in Figure 10.5. ....	316
<b>Figure 10.8</b>	Simplex swirl atomizer.....	316
<b>Figure 10.9</b>	Simplex swirl atomizer with return flow.....	317
<b>Figure 10.10</b>	John Zink EA oil gun.....	317
<b>Figure 10.11</b>	John Zink MEA gun. ....	317
<b>Figure 10.12</b>	John Zink High Efficiency Residual Oil (HERO) gun.. ....	318
<b>Figure 10.13</b>	Y-jet atomization principle.....	318
<b>Figure 10.14</b>	WDH waste aqueous gun design with one liquid exit port surrounded with eight atomizing ports. ....	318
<b>Figure 10.15</b>	Patternation comparison for HERO and WDH guns. ....	319
<b>Figure 10.16</b>	Coen elliptical cap slots for low- $\text{NO}_x$ .....	319
<b>Figure 10.17</b>	Droplet size measurements of the MEA oil gun at different air pressures.....	319
<b>Figure 10.18</b>	Droplet size measurements of the MEA oil gun at similar air–water differential pressures.....	320
<b>Figure 10.19</b>	Droplet size measurements of MEA oil gun at the same air–water differential pressure but different mass ratios. ....	320
<b>Figure 10.20</b>	Droplet size comparison measured by PDPA for different oil gun designs. ....	320
<b>Figure 10.21</b>	Steam consumption for different oil gun designs. ....	321
<b>Figure 10.22</b>	Steam consumption curve for a constant steam–oil differential pressure oil gun.....	321
<b>Figure 10.23</b>	A typical oil gun capacity curve showing oil gun turndown ratio. ....	321
<b>Figure 10.24</b>	Comparison of $\text{NO}_x$ emissions for the HERO and MEA oil guns. ....	322
<b>Figure 10.25</b>	Diagram of Y-jet. ....	323
<b>Figure 11.1</b>	Illustration of geometric similarity.....	328
<b>Figure 11.2</b>	Typical relationship of $\text{Eu} = f(\text{Re})$ .....	330
<b>Figure 11.3</b>	Velocity measurement using a Pitot tube and manometer.....	331
<b>Figure 11.4</b>	Airflow/helium bubble analog flow visualization. ....	332
<b>Figure 11.5</b>	Illustration of mixing.....	332
<b>Figure 11.6</b>	Cutaway view of the burner to be installed on the prototype. ....	333
<b>Figure 11.7</b>	Scale physical model of the combustion air system.....	333

<b>Figure 11.8</b>	Burner no. 1 exit air velocity—Baseline.....	335
<b>Figure 11.9</b>	Burner no. 1 exit air velocity—After modifications. ....	335
<b>Figure 11.10</b>	Burner no. 2 exit air velocity—Baseline.....	335
<b>Figure 11.11</b>	Burner no. 2 exit air velocity—After modifications. ....	335
<b>Figure 11.12</b>	Burner no. 1 peripheral velocity distribution. ....	336
<b>Figure 11.13</b>	Burner no. 2 peripheral velocity distribution. ....	337
<b>Figure 12.1</b>	Historical (1980–2010) world energy consumption.....	340
<b>Figure 12.2</b>	2010 World energy consumption.....	340
<b>Figure 12.3</b>	U.S. energy consumption by industry sector.....	341
<b>Figure 12.4</b>	2010 Energy flow by source and end use in the United States.....	341
<b>Figure 12.5</b>	Sankey diagram for the energy flows into and out of a furnace. ....	342
<b>Figure 12.6</b>	Available heat lost due to increased excess O <sub>2</sub> as a function of the flue gas exit temperature for methane as the fuel.....	342
<b>Figure 12.7</b>	Available heat lost due to increased excess O <sub>2</sub> as a function of the fuel for a fixed flue gas exit temperature (400°F). ....	342
<b>Figure 12.8</b>	Ratio of NO <sub>x</sub> formed at a given excess O <sub>2</sub> level compared to the amount of NO <sub>x</sub> formed at 1% excess O <sub>2</sub> .....	343
<b>Figure 12.9</b>	Example demonstrating how variations in ambient temperature and humidity can result in dramatic changes in CO emissions.....	343
<b>Figure 12.10</b>	Cabin-style process heater. ....	344
<b>Figure 12.11</b>	Process burners in a cabin heater. ....	344
<b>Figure 12.12</b>	Air leak around a tube penetration in the convection section.....	346
<b>Figure 12.13</b>	Open sight port in the floor of a process heater. ....	346
<b>Figure 12.14</b>	Poorly sealed sight port on the side of a process heater. ....	346
<b>Figure 12.15</b>	Example of a convection section removed so that tubes can be cleaned.....	346
<b>Figure 12.16</b>	Air infiltration as a function of heater draft. ....	347
<b>Figure 12.17</b>	Typical draft profile in a process heater ( $\Delta P$ = pressure drop). ....	348
<b>Figure 12.18</b>	End wall photo of an operating process heater. ....	348
<b>Figure 12.19</b>	Smoke bomb test to find leaks in a heater. ....	349
<b>Figure 12.20</b>	Thermal image showing a partially open explosion door.....	349
<b>Figure 12.21</b>	Plugged convection section tubes. ....	350
<b>Figure 12.22</b>	Sight port refractory plug seal.....	350
<b>Figure 12.23</b>	Sight port designed to reduce air leaks and protect operators against hot furnace flue gases, high radiant heat, and positive pressure surges in the heater. ....	351
<b>Figure 12.24</b>	Engineered tube seals.....	351
<b>Figure 13.1</b>	Investigation of an isothermal flow field.....	354
<b>Figure 13.2</b>	Original topographic data. ....	354
<b>Figure 13.3</b>	Representation of topographical data in a CFD model (blue showing lower elevation, red showing higher elevation). ....	354



<b>Figure 13.4</b>	Close-up view of a burner in a test furnace. ....	355
<b>Figure 13.5</b>	Representation of a process burner, colored by temperature (blue showing low temperatures, red high temperatures). ....	355
<b>Figure 13.6</b>	Point measurement of a scalar in a turbulent flow. ....	357
<b>Figure 13.7</b>	Plot of the $\beta$ -function for several values of $Z$ and $Z''$ . ....	367
<b>Figure 13.8</b>	Representation of a luminous flame utilizing a soot model. ....	371
<b>Figure 13.9</b>	Discretized geometry of a typical process burner. ....	372
<b>Figure 13.10</b>	Discretized geometry of a typical boiler burner. ....	372
<b>Figure 13.11</b>	Close-up view of primary and secondary tips. ....	373
<b>Figure 13.12</b>	Rendered view inside an ethylene cracker showing flow patterns near the premixed radiant wall burners. ....	374
<b>Figure 13.13</b>	Illustration of a flame envelope defined as an isocontour of 2500 ppm CO. ....	375
<b>Figure 13.14</b>	Illustration of combustion products indicating poor mixing between fuel and oxidizer. ....	375
<b>Figure 13.15</b>	Smaller combustion product envelopes indicate improved mixing between oxidizer and fuel. ....	375
<b>Figure 13.16</b>	CFD model of two burners. ....	376
<b>Figure 13.17</b>	CFD simulation optimizes burner performance leading to uniform heat flux on process tubes. ....	376
<b>Figure 13.18</b>	Improved flame pattern maximizes burner performance. ....	376
<b>Figure 13.19</b>	Combining John Zink's (a) physical and (b) CFD simulation capabilities allows them to provide comprehensive solutions for their customers. ....	377
<b>Figure 13.20</b>	(a) Before—testing reveals a wide flame with an unacceptable appearance. CFD calculations indicate flame spreading out above the burner tile. (b) After—Design modifications were developed using CFD simulation. ....	377
<b>Figure 14.1</b>	Number of people (in millions) living in counties with air quality concentrations above the level of the primary (health-based) National Ambient Air Quality Standards (NAAQS) in 2008. ....	382
<b>Figure 14.2</b>	Comparison of growth measures (gross domestic product, vehicle miles traveled, population, and energy consumption) and emissions ( $\text{CO}_2$ and aggregate emissions) from 1970 to 2010 in the United States. ....	383
<b>Figure 14.3</b>	Distribution of air pollution emissions by pollutant type and source category. ....	383
<b>Figure 14.4</b>	Adiabatic equilibrium CO as a function of equivalence ratio for air/fuel flames. ....	388
<b>Figure 14.5</b>	Adiabatic equilibrium CO as a function of gas temperature for stoichiometric air/fuel flames. ....	388
<b>Figure 14.6</b>	Adiabatic equilibrium CO as a function of air preheat temperature for stoichiometric air/fuel flames. ....	389
<b>Figure 14.7</b>	Adiabatic equilibrium CO as a function of fuel preheat temperature for a stoichiometric air/ $\text{CH}_4$ flame. ....	389
<b>Figure 14.8</b>	Adiabatic equilibrium CO as a function of fuel composition ( $\text{CH}_4/\text{H}_2$ ) for a stoichiometric air/fuel flame. ....	390
<b>Figure 14.9</b>	Adiabatic equilibrium CO as a function of fuel composition ( $\text{CH}_4/\text{N}_2$ ) for a stoichiometric air/fuel flame. ....	390
<b>Figure 14.10</b>	Bacharach smoke tester included a hand pump, filter papers, and spot scale sheet. ....	392
<b>Figure 14.11</b>	Particulate sampling train. ....	393

<b>Figure 14.12</b>	Sampling at different isokinetic variations. ....	394
<b>Figure 14.13</b>	Minimum number of traverse points for particulate traverses. ....	395
<b>Figure 14.14</b>	Type S pitot tube. ....	396
<b>Figure 14.15</b>	BERL experimental facility. ....	400
<b>Figure 14.16</b>	CSS. ....	400
<b>Figure 14.17</b>	CDFB. ....	401
<b>Figure 14.18</b>	Low NO <sub>x</sub> diffusion flame burner (LDFB). ....	401
<b>Figure 14.19</b>	CDFB total hydrocarbon emissions versus heating value of HC fuel mixture. ....	402
<b>Figure 14.20</b>	CDFB total hydrocarbon emissions versus combustion zone stoichiometry. ....	402
<b>Figure 14.21</b>	CDFB total hydrocarbon emissions versus propylene and ethylene spikes. ....	402
<b>Figure 14.22</b>	CDFB total hydrocarbon emissions versus hydrogen content of HC fuel mixture. ....	402
<b>Figure 14.23</b>	CDFB total PAH at stack outlet. ....	403
<b>Figure 14.24</b>	CDFB total PAH and benzo(a)pyrene at furnace outlet compared to stack outlet. ....	404
<b>Figure 14.25</b>	Lagrangian jet model predictions. ....	405
<b>Figure 14.26</b>	CDFB photoionization current (pA) versus theoretical air (%). ....	406
<b>Figure 14.27</b>	Range and average of emissions at the stack outlet for the CDFB. ....	407
<b>Figure 14.28</b>	Range of measurements of HAPs at the stack outlet for the CDFB. ....	408
<b>Figure 14.29</b>	Emissions for refinery fuel gas (16% H <sub>2</sub> , propane, natural gas) for the CDFB. ....	408
<b>Figure 14.30</b>	Range of emissions for natural gas and refinery fuel gas for the CDFB and the ultralow NO <sub>x</sub> diffusion burner. ....	409
<b>Figure 14.31</b>	Emission factor comparison for low NO <sub>x</sub> burner and conventional burner. ....	409
<b>Figure 14.32</b>	Total PAH emissions 4 rings and greater versus stoichiometric ratio. ....	410
<b>Figure 14.33</b>	Benzene and PAH emissions versus stoichiometric ratio for the CDFB. ....	410
<b>Figure 14.34</b>	CO and PAH emissions versus stoichiometric ratio for the CDFB. ....	411
<b>Figure 14.35</b>	HC and PAH emissions versus stoichiometric ratio for the CDFB. ....	411
<b>Figure 14.36</b>	HC, aldehyde, VOC, and PAH emissions versus stoichiometric ratio for the CDFB. ....	412
<b>Figure 14.37</b>	Total heavy VOC emissions vs. stoichiometric ratio for the CDFB. ....	412
<b>Figure 14.38</b>	Typical process heater, petroleum refinery emissions factors. ....	413
<b>Figure 15.1</b>	Schematic of NO exiting a stack and combining with O <sub>2</sub> to form NO <sub>2</sub> . ....	418
<b>Figure 15.2</b>	Schematic of acid rain. ....	419
<b>Figure 15.3</b>	Acid rain deterioration examples. ....	419
<b>Figure 15.4</b>	Schematic of smog formation. ....	420
<b>Figure 15.5</b>	NO <sub>x</sub> emissions in the United States between 1970 and 1999 based on the process. ....	420
<b>Figure 15.6</b>	Schematic of fuel NO <sub>x</sub> formation pathways. ....	422
<b>Figure 15.7</b>	Adiabatic equilibrium NO as a function of equivalence ratio for air/fuel flames. ....	423
<b>Figure 15.8</b>	Adiabatic equilibrium NO as a function of gas temperature for stoichiometric air/fuel flames. ....	424

<b>Figure 15.9</b>	Adiabatic equilibrium NO as a function of air preheat temperature for stoichiometric air/fuel flames. ....	424
<b>Figure 15.10</b>	Adiabatic equilibrium NO as a function of fuel preheat temperature for a stoichiometric air/CH <sub>4</sub> flame. ....	425
<b>Figure 15.11</b>	Adiabatic equilibrium NO as a function of fuel composition (CH <sub>4</sub> /H <sub>2</sub> ) for a stoichiometric air/fuel flame. ....	425
<b>Figure 15.12</b>	Adiabatic equilibrium NO as a function of fuel composition (CH <sub>4</sub> /N <sub>2</sub> ) for a stoichiometric air/fuel flame. ....	426
<b>Figure 15.13</b>	Conversion ratio of fuel-bound nitrogen to NO <sub>2</sub> of various nitrogen-containing fuels as a function of fuel-nitrogen content.....	426
<b>Figure 15.14</b>	Conversion rate of fuel-bound nitrogen to NO <sub>x</sub> for two different oil-fired burners. ....	427
<b>Figure 15.15</b>	Relative NO <sub>x</sub> versus air/fuel ratio for premix and diffusion flames. ....	427
<b>Figure 15.16</b>	National NO <sub>2</sub> ambient air quality trends .....	428
<b>Figure 15.17</b>	Sampling system schematic as recommended by the U.S. EPA. ....	430
<b>Figure 15.18</b>	Schematic of four general strategies for reducing NO <sub>x</sub> emissions.....	431
<b>Figure 15.19</b>	Example of a staged fuel burner .....	435
<b>Figure 15.20</b>	Example of a staged air burner (Hamworthy DFR burner).....	435
<b>Figure 15.21</b>	Schematic of FuGR.....	436
<b>Figure 15.22</b>	Example of a burner incorporating FuGR (John Zink Halo™ burner). ....	436
<b>Figure 15.23</b>	Remote stage fuel tip. ....	436
<b>Figure 15.24</b>	Illustration showing how the remote stage method provides lower NO <sub>x</sub> emissions. ....	437
<b>Figure 15.25</b>	Radiant wall burners firing (a) without remote staging, NO <sub>x</sub> = 24 ppmvd and (b) with remote staging, NO <sub>x</sub> = 16 ppmvd.....	437
<b>Figure 15.26</b>	Flameless combustion system.....	440
<b>Figure 15.27</b>	TANGENT™ technology low NO <sub>x</sub> thermal oxidizer burner.....	440
<b>Figure 15.28</b>	History of low NO burner development for (a) round flame burners and (b) radiant wall burners, firing on gaseous fuels. ....	441
<b>Figure 15.29</b>	COOLstar burner. ....	442
<b>Figure 15.30</b>	Computational fluid dynamic modeling of the COOLstar burner .....	442
<b>Figure 15.31</b>	Schematic of the selective catalytic reduction process .....	444
<b>Figure 15.32</b>	NO <sub>x</sub> removal efficiency versus temperature for SCR .....	444
<b>Figure 15.33</b>	Common catalyst configuration used in SCR systems .....	445
<b>Figure 15.34</b>	SCR process flow diagram .....	446
<b>Figure 15.35</b>	Typical catalyst deactivation for an SCR as a function of operating time.....	447
<b>Figure 15.36</b>	Selective non-catalytic reduction system .....	447
<b>Figure 15.37</b>	SNCR temperature window .....	447
<b>Figure 15.38</b>	Effect of residence time on SNCR NO <sub>x</sub> reduction efficiency .....	448
<b>Figure 15.39</b>	Effect of ammonia slip on SNCR NO <sub>x</sub> reduction efficiency.....	448
<b>Figure 15.40</b>	Catalytic cleaning NO <sub>x</sub> reduction system .....	449

<b>Figure 15.41</b>	Adiabatic equilibrium NO as a function of the fuel blend composition for $H_2/CH_4$ blends combusted with 15% excess air where both the fuel and the air are at ambient temperature and pressure. ....	451
<b>Figure 15.42</b>	Adiabatic equilibrium NO as a function of the fuel blend composition for $C_3H_8/CH_4$ blends combusted with 15% excess air where both the fuel and the air are at ambient temperature and pressure. ....	451
<b>Figure 15.43</b>	Adiabatic equilibrium NO as a function of the fuel blend composition for $H_2/C_3H_8$ blends combusted with 15% excess air where both the fuel and the air are at ambient temperature and pressure. ....	451
<b>Figure 15.44</b>	Ternary plot of adiabatic equilibrium (a) temperature and (b) relative NO (fraction of the maximum value) as a function of the fuel blend composition for $H_2/CH_4/C_3H_8$ blends combusted with 15% excess air where both the fuel and the air are at ambient temperature and pressure. ....	452
<b>Figure 15.45</b>	Raw gas (VYD) burner. ....	452
<b>Figure 15.46</b>	VYD burner closeup. ....	452
<b>Figure 15.47</b>	Test furnace. ....	453
<b>Figure 15.48</b>	Measured NOx (percent of the maximum ppmv value) as a function of the fuel blend composition for $H_2/TNG$ blends combusted with 15% excess air where both the fuel and the air were at ambient temperature and pressure. ....	453
<b>Figure 15.49</b>	Measured NOx (percent of the maximum ppmv value) as a function of the fuel blend composition for $C_3H_8/TNG$ blends combusted with 15% excess air where both the fuel and the air were at ambient temperature and pressure. ....	454
<b>Figure 15.50</b>	Measured NOx (percent of the maximum value in both ppmv and lb/MMBtu) as a function of the fuel blend composition for $H_2/C_3H_8$ blends combusted with 15% excess air where both the fuel and the air were at ambient temperature and pressure. ....	455
<b>Figure 15.51</b>	Measured NOx (fraction of the maximum value in both ppmv and lb/MMBtu) as a function of the fuel blend composition for $TNG/H_2/C_3H_8$ blends combusted with 15% excess air where both the fuel and the air were at ambient temperature and pressure for gas tip #2. ....	456
<b>Figure 15.52</b>	Measured NOx (fraction of the maximum value in both ppmv and lb/MMBtu) as a function of the fuel blend composition for $TNG/H_2/C_3H_8$ blends combusted with 15% excess air where both the fuel and the air were at ambient temperature and pressure for gas tip #4. ....	456
<b>Figure 15.53</b>	Measured NOx (fraction of the maximum value in both ppmv and lb/MMBtu) as a function of the fuel blend composition for $TNG/H_2/C_3H_8$ blends combusted with 15% excess air where both the fuel and the air were at ambient temperature and pressure for gas tip #6. ....	457
<b>Figure 15.54</b>	Measured NOx (fraction of the maximum value) in (a) ppmv and (b) lb/MMBtu as a function of the fuel blend composition for $TNG/H_2/C_3H_8$ blends combusted with 15% excess air where both the fuel and the air were at ambient temperature and pressure for a constant fuel gas pressure of 21 psig. ....	457
<b>Figure 15.55</b>	Measured NOx (fraction of the maximum value in ppmvd) as a function of the fuel pressure for all 15 different $TNG/H_2/C_3H_8$ blends (A through O) combusted with 15% excess air where both the fuel and the air were at ambient temperature and pressure. ....	458
<b>Figure 15.56</b>	Measured NOx (fraction of the maximum value) in (a) ppmv and (b) lb/MMBtu as a function of the fuel blend composition, fuel gas pressure and calculated adiabatic flame temperature for $TNG/H_2/C_3H_8$ blends combusted with 15% excess air where both the fuel and the air were at ambient temperature and pressure. ....	458
<b>Figure 15.57</b>	Effects of firebox temperature on NOx. ....	459
<b>Figure 15.58</b>	Velocity thermocouple (suction pyrometer). ....	460

<b>Figure 15.59</b>	Effect of firebox temperature on NO <sub>x</sub> for various types of diffusion burners firing NG at 3% excess O <sub>2</sub> .....	461
<b>Figure 15.60</b>	Effect of firebox temperature on NO <sub>x</sub> for various types of diffusion burners firing NG at various excess O <sub>2</sub> levels.....	462
<b>Figure 15.61</b>	Effect of firebox temperature on NO <sub>x</sub> for various types of diffusion burners firing NG at 3% excess O <sub>2</sub> and various air preheat temperatures.....	462
<b>Figure 15.62</b>	Effect of firebox temperature on NO <sub>x</sub> for various types of partially premixed burners firing NG at 3% excess O <sub>2</sub> .....	463
<b>Figure 15.63</b>	Effect of firebox temperature on NO <sub>x</sub> for diffusion and partially premixed low NO <sub>x</sub> burners firing on NG at 3% excess O <sub>2</sub> .....	463
<b>Figure 15.64</b>	Schematic showing the effect of chromium in Fe–Cr alloys on an oxide scale structure based on isothermal oxidation studies at 1000°C (1800°F).....	465
<b>Figure 15.65</b>	A plot showing predicted NO concentration as a function of time for various exhaust gas temperatures.....	465
<b>Figure 15.66</b>	Schematic showing test furnace and sample probe locations.....	467
<b>Figure 15.67</b>	(a) NO emissions at locations before and in the middle of the convection section at various depths and (b) top surface is in middle of convection section, bottom surface before convection section.....	468
<b>Figure 15.68</b>	Illustration showing theorized flow pattern within test furnace.....	468
<b>Figure 15.69</b>	(a) NO <sub>x</sub> (NO + NO <sub>2</sub> ) at locations before and in the middle of the convection section at various depths and (b) top surface is in middle of convection section, bottom surface before convection section.....	469
<b>Figure 15.70</b>	(a) NO <sub>x</sub> (NO + NO <sub>2</sub> ) at various locations in the upper 10' (3 m) of the radiant section of the field test furnace and (b) NO and NO <sub>2</sub> at various locations in the upper 10' (3.0 m) of the radiant section of the field test furnace.....	469
<b>Figure 15.71</b>	Schematic showing the layout of a typical reforming furnace.....	470
<b>Figure 15.72</b>	Test furnace and MK-II™ burner.....	471
<b>Figure 15.73</b>	Schematic of the MK-II™ burner.....	471
<b>Figure 15.74</b>	Effects of furnace temperature on NO <sub>x</sub> emissions.....	471
<b>Figure 15.75</b>	Effects of combustion air temperature on NO <sub>x</sub> emissions at various turndown conditions.....	472
<b>Figure 15.76</b>	Effects of furnace O <sub>2</sub> concentration (excess air) on NO <sub>x</sub> emissions at various combustion air temperatures.....	472
<b>Figure 15.77</b>	Photographs of (a) MK-II™, (b) low-NO <sub>x</sub> , and (c) conventional burner technologies.....	473
<b>Figure 15.78</b>	Comparison of NO <sub>x</sub> emissions for the conventional, low-NO <sub>x</sub> and MK-II™ burner technologies.....	473
<b>Figure 15.79</b>	Effects of percent PSA gas duty on flame appearance firing the MK-II™ burner.....	473
<b>Figure 15.80</b>	Effects of PSA gas composition on flame appearance firing the MK-II™ burner at a constant heat release.....	474
<b>Figure 16.1</b>	Community located close to an industrial plant.....	480
<b>Figure 16.2</b>	Tree falling in the forest.....	481
<b>Figure 16.3</b>	Pressure peaks and troughs.....	482
<b>Figure 16.4</b>	Cross-section of the human ear.....	482

<b>Figure 16.5</b>	Relationship of decibels to watts. ....	483
<b>Figure 16.6</b>	Calculating SPL at a distance $r$ . ....	484
<b>Figure 16.7</b>	Threshold of hearing in humans. ....	485
<b>Figure 16.8</b>	Threshold of hearing and threshold of pain in humans. ....	485
<b>Figure 16.9</b>	A-weighted scale for human hearing threshold. ....	485
<b>Figure 16.10</b>	A-weighted burner noise curve. ....	485
<b>Figure 16.11</b>	Weighting curves A, B, C, and D. ....	486
<b>Figure 16.12</b>	Block diagram of a sound level meter. ....	486
<b>Figure 16.13</b>	Same sound spectrum on three different intervals. ....	487
<b>Figure 16.14</b>	Typical burner noise curve. ....	488
<b>Figure 16.15</b>	Nomogram for noise level addition. ....	489
<b>Figure 16.16</b>	Atmospheric attenuation. ....	490
<b>Figure 16.17</b>	Typical earplugs and muffs. ....	492
<b>Figure 16.18</b>	Test flare at John Zink test site in Tulsa, OK. Combustion of identical fuel flow rates with different degrees of mixing. ....	494
<b>Figure 16.19</b>	Typical noise signature emitted from a flare. ....	494
<b>Figure 16.20</b>	Photograph of a high-pressure and low-pressure flare burning the same fuel. ....	495
<b>Figure 16.21</b>	Shadow photograph of a burning butane lighter. ....	495
<b>Figure 16.22</b>	Engineer measuring flare noise. ....	496
<b>Figure 16.23</b>	PWL $L_w$ calculated from measured noise data, plotted versus heat release rate, $\dot{Q}_{\text{combust}}$ for different types of industrial flares under various operating conditions. ....	496
<b>Figure 16.24</b>	Predicted sound pressure field contour plots for a multipoint LRGO flare system. ....	497
<b>Figure 16.25</b>	SPL emitted from a steam-assisted flare operating at normal conditions and at over-steamed conditions (combustion instability). ....	498
<b>Figure 16.26</b>	Burner SPL normal and with instability. ....	499
<b>Figure 16.27</b>	Development of orderly wave patterns within a high-speed gas jet. ....	500
<b>Figure 16.28</b>	Illustration showing the region of maximum jet mixing noise. ....	500
<b>Figure 16.29</b>	Photograph showing shock waves downstream of an air jet. ....	500
<b>Figure 16.30</b>	Screech tone emissions. ....	501
<b>Figure 16.31</b>	Noise radiating from a valve. ....	501
<b>Figure 16.32</b>	Photograph of two enclosed flares. ....	502
<b>Figure 16.33</b>	A steam-assisted flare with a muffler. ....	503
<b>Figure 16.34</b>	Steam jet noise emitted with and without muffler. ....	503
<b>Figure 16.35</b>	Example for noise abatement in steam-assisted flares by reducing the amount of steam required to ensure smokeless combustion. ....	504
<b>Figure 16.36</b>	Water injected into a high-pressure flare. ....	504
<b>Figure 16.37</b>	Noise spectrum from a high-pressure flare with and without water injection. ....	505
<b>Figure 16.38</b>	Sound pressure versus frequency for a burner operating with and without a muffler. ....	505

<b>Figure 16.39</b>	Illustration showing two different muffler designs. ....	506
<b>Figure 16.40</b>	Illustration showing a common plenum chamber for floor burners in a furnace. ....	506
<b>Figure 16.41</b>	Noise emissions from a steam control valve.....	506
<b>Figure 16.42</b>	Illustration used for burner noise example.....	507
<b>Figure 16.43</b>	SPL spectrum for high-pressure flaring. ....	508
<b>Figure 16.44</b>	Noise contributions separately based on the mathematical model.....	508
<b>Figure 16.45</b>	Effect of distance on flare noise. ....	509
<b>Figure 17.1</b>	Quiz cards example .....	518
<b>Figure 17.2</b>	Molecule modules example. ....	519
<b>Figure 17.3</b>	ASTD competency model. ....	531
<b>Figure 17.4</b>	Example of a PowerPoint template slide. ....	534
<b>Figure 17.5</b>	Example of an introduction slide. ....	537
<b>Figure 17.6</b>	BP, Texas City, Texas refinery. ....	538
<b>Figure 17.7</b>	Free-standing diffusion burner slide. ....	540
<b>Figure 17.8</b>	(a) Irregular flame patterns in an operating process heater and (b) closed air registers on the two improperly adjusted burners. ....	540
<b>Figure 17.9</b>	Burners firing across the floor in a process heater (a) before adjustment and (b) after adjustment. ....	541
<b>Figure 17.10</b>	Schematic of flame rollover in a cabin heater. ....	541
<b>Figure 17.11</b>	Main computer screen for Jeopardy game used to review for final test.....	541
<b>Figure 17.12</b>	Overall ratings by students on their interest in and the benefit of each course section. ....	542
<b>Figure 17.13</b>	Shintech plant in Plaquemine, Louisiana. ....	542
<b>Figure 17.14</b>	Photo of part of the thermal oxidation system during installation. ....	543
<b>Figure 17.15</b>	Series of furnaces showing the progression towards blow-off of a burner flame. ....	543
<b>Figure 17.16</b>	Slide showing the 3Ts of combustion: time, temperature, and turbulence.....	545
<b>Figure 17.17</b>	Animated P&ID with a picture of an actual control valve.....	545
<b>Figure 17.18</b>	Student ratings of interest and benefit of each course topic.....	546



---

## List of Tables

---

<b>Table 1.1</b>	Summary of Process Heating Operations.....	2
<b>Table 1.2</b>	Summary of Emissions from Refinery Processes .....	5
<b>Table 1.3</b>	Some American Petroleum Institute–Recommended Practices Related to Combustion Equipment .....	9
<b>Table 1.4</b>	Average Burner Configuration by Heater Type.....	13
<b>Table 1.5</b>	Major Fired Heater Applications in the Chemical Industry.....	13
<b>Table 2.1</b>	Major Petroleum Refining Processes .....	32
<b>Table 2.2</b>	Major Refinery Processes Requiring a Fired Heater .....	33
<b>Table 2.3</b>	Hydrogen Usage by Industry.....	38
<b>Table 2.4</b>	Typical Product Distributions for Common Pyrolysis Feeds.....	43
<b>Table 3.1</b>	Example Pipeline Quality Natural Gas .....	47
<b>Table 3.2</b>	Commercial Natural Gas Components and Typical Ranges of Composition .....	47
<b>Table 3.3</b>	Quantitative Listing of Products Made by the U.S. Petroleum Industry .....	48
<b>Table 3.4</b>	General Fraction Boiling Points .....	50
<b>Table 3.5</b>	Composition of a Typical Refinery Gas .....	51
<b>Table 3.6</b>	Typical Composition of Steam Reforming/PSA Tail Gas .....	52
<b>Table 3.7</b>	Typical Composition of Flexicoking Waste Gas .....	53
<b>Table 3.8</b>	Requirements for Fuel Oils (per ASTM D 396).....	55
<b>Table 3.9</b>	Typical Analysis of Different Fuel Oils.....	55
<b>Table 3.10</b>	Naphtha Elemental Analysis.....	57
<b>Table 3.11</b>	Distillation Fractions as a Function of Temperature Determined by ASTM Method D86 .....	57
<b>Table 3.12</b>	Typical Flared Gas Compositions.....	58
<b>Table 3.13</b>	Volumetric Analysis Summary.....	59
<b>Table 3.14</b>	Constants of FG Mixtures .....	60
<b>Table 3.15</b>	Constants of Components.....	62
<b>Table 3.16</b>	Viscosity Conversion Chart .....	68
<b>Table 4.1</b>	Density Comparison of Average Air and 79% N <sub>2</sub> 21% O <sub>2</sub> Assumption .....	87
<b>Table 4.2</b>	Common Gaseous Fuels .....	88
<b>Table 4.3</b>	Combustion Data for Hydrocarbons.....	93
<b>Table 4.4</b>	Specific Gravity and Properties of Common Liquid Fuels .....	100
<b>Table 4.5</b>	Liquid Fuel Properties by API Gravity as well as Common Coals .....	101
<b>Table 4.6</b>	Adiabatic Flame Temperatures.....	103
<b>Table 5.1</b>	Coal Analyses As-Received Basis .....	126
<b>Table 5.2</b>	Class of Coals .....	126

<b>Table 5.3</b>	Fuel Properties of Biomass and Solid Fuels .....	127
<b>Table 6.1</b>	Catalyst Types in Different Processes .....	140
<b>Table 6.2</b>	Typical Reactions in Catalytic Waste Gas Cleaning .....	145
<b>Table 6.3</b>	Examples of Minimum Inlet Temperature for Various Fresh Catalysts .....	146
<b>Table 6.4</b>	Notes on Material Selection.....	148
<b>Table 7.1</b>	Thermal Conductivity of Common Materials.....	162
<b>Table 7.2</b>	Properties of Various Substances at 32°F (0°C) .....	162
<b>Table 7.3</b>	Properties of Selected Gases at 14.696 psi.....	163
<b>Table 7.4</b>	One-Dimensional, Steady-State Solutions to the Heat Equation with No Generation .....	164
<b>Table 7.5</b>	Typical Convective Heat Transfer Coefficients .....	171
<b>Table 7.6</b>	Summary of Convection Correlations for Flow in a Circular Tube.....	174
<b>Table 7.7</b>	Constants of Equation 7.56 for Circular Cylinder in Cross Flow .....	175
<b>Table 7.8</b>	Constants of Equation 7.61 for the Tube Bank in Cross Flow .....	175
<b>Table 7.9</b>	Spectrum of Electromagnetic Radiation.....	178
<b>Table 7.10</b>	View Factors for Two-Dimensional Geometries .....	182
<b>Table 7.11</b>	View Factors for Three-Dimensional Geometries .....	183
<b>Table 7.12</b>	Correlation Constants for the Determination of the Total Emissivity for Water Vapor and Carbon Dioxide.....	187
<b>Table 7.13</b>	Mean Beam Lengths for Radiation from a Gas Volume to a Surface on Its Boundary.....	190
<b>Table 8.1</b>	Approximate Composition of Dry Air.....	213
<b>Table 8.2</b>	American Petroleum Institute 521 Recommendations for Radiation Exposure to Personnel.....	216
<b>Table 9.1</b>	Properties of Various Gases.....	231
<b>Table 9.2</b>	Equivalent Sand Grain Roughness ( $\epsilon$ ) for Various Pipe Material and Surfaces.....	244
<b>Table 9.3</b>	Advantages and Disadvantages of Each Draft Technique.....	257
<b>Table 10.1</b>	Liquid Fuel Properties.....	310
<b>Table 10.2</b>	Effect of Dimensionless Parameters on Liquid Breakup Length.....	313
<b>Table 10.3</b>	Combustion Performance of the HERO Gun.....	322
<b>Table 10.4</b>	Combustion Test Results for the MEA Oil Gun .....	322
<b>Table 10.5</b>	Effect of Operational Parameters on Pollutant Emissions .....	322
<b>Table 11.1</b>	Mass Flow Measurements .....	334
<b>Table 12.1</b>	Importance of Combustion to Industry.....	340
<b>Table 12.2</b>	Major Process Heating Operations .....	340
<b>Table 12.3</b>	Examples of Processes in the Process Industries Requiring Industrial Combustion .....	340
<b>Table 13.1</b>	Universal “Empirical” Constants Used in the Standard $k$ - $\epsilon$ Turbulence Model.....	358
<b>Table 13.2</b>	Cartesian Differential Equation Set .....	359
<b>Table 13.3</b>	Cylindrical Differential Equation Set .....	360
<b>Table 13.4</b>	Discrete Ordinates for the $S_N$ Approximation ( $N = 2, 4,$ and $6$ ) .....	369

<b>Table 14.1</b>	U.S. National Ambient Air Quality Standards (NAAQS) as of October 2011 .....	382
<b>Table 14.2</b>	Combustion Emission Factors (lb/10 <sup>6</sup> Btu) by Fuel Type .....	384
<b>Table 14.3</b>	Location of Traverse Points in Circular Stacks .....	395
<b>Table 15.1</b>	NO <sub>x</sub> Emission Factors by Fuel Type .....	422
<b>Table 15.2</b>	Uncontrolled NO <sub>x</sub> Emission Factors for Typical Process Heaters .....	422
<b>Table 15.3</b>	Summary of NO <sub>x</sub> Control Techniques .....	431
<b>Table 15.4</b>	Reduction Efficiencies for NO <sub>x</sub> Control Techniques .....	432
<b>Table 15.5</b>	NO <sub>x</sub> Control Technologies in Process Heaters .....	432
<b>Table 15.6</b>	NO <sub>x</sub> Reductions for Different Low-NO <sub>x</sub> Burner Types .....	440
<b>Table 15.7</b>	Data for NO <sub>2</sub> Decomposition over Metal Oxides at 773 K (842°F) .....	464
<b>Table 16.1</b>	Speed of Sound in Different Media and at Different Temperatures .....	482
<b>Table 16.2</b>	The 10 Octave Bands .....	483
<b>Table 16.3</b>	Octave and One-Third Octave Bands .....	487
<b>Table 16.4</b>	A-Weighting of the Burner Sound Curve from Figure 16.14 .....	488
<b>Table 16.5</b>	Addition Rules .....	489
<b>Table 16.6</b>	Sound Levels of Various Sources .....	492
<b>Table 16.7</b>	OSHA Permissible Noise Exposure .....	492
<b>Table 16.8</b>	Calculation of the Typical Combustion Noise Spectrum of a Stable Burning Flare from the Overall Sound Pressure Level (OASPL) .....	495
<b>Table 16.9</b>	OASPL Determined Experimentally and Using the Mathematical Model .....	509
<b>Table 17.1</b>	Course Outline .....	539

This page intentionally left blank

---

## *Foreword to the First Edition*

---

As we enter the twenty-first century, the importance of energy for industry, transportation, and electricity generation in our daily lives is profound. Combustion of fossil fuels is by far the predominant source of energy today and will likely remain that way for many years to come.

Combustion has played major roles in human civilization, including both practical and mystical ones. Since man discovered how to create fire, we have relied on combustion to perform a variety of tasks. Fire was first used for heating and cooking, and later to manufacture tools and weapons. For all practical purposes, it was not until the onset of the Industrial Revolution in the nineteenth century that man started to harness power from combustion. We have made rapid progress in the application of combustion systems since then, and many industries have come into existence as a direct result of this achievement.

Demands placed on combustion systems change continuously with time and are becoming more stringent. The safety of combustion systems has always been essential, but emphasis on effective heat transfer, temperature uniformity, equipment scale-up, efficiency, controls, and—more recently—environmental emissions and combustion-generated noise has evolved over time. Such demands create tremendous challenges for combustion engineers. These challenges have been successfully met in most applications by combining experience and sound engineering practices with creative and innovative problem-solving.

Understanding combustion requires knowledge of the fundamentals: turbulent mixing, heat transfer, and chemical kinetics. The complex nature of practical combustion systems, combined with the lack of reliable analytical models in the past, encouraged researchers to rely heavily on empirical methods to predict performance and to develop new products. Fortunately, the combustion field has gained considerable scientific knowledge in the last few decades, and such knowledge is now utilized in industry by engineers to evaluate and design combustion systems in a more rigorous manner. This progress is the result of efforts in academia, government laboratories, private labs, and companies like John Zink.

The advent of ever-faster and more powerful computers has had a profound impact on the manner in which engineers model combustion systems. Computational fluid dynamics (CFD) was born from these developments.

Combined with validation by experimental techniques, CFD is an essential tool in combustion research, development, analysis, and equipment design.

Today's diagnostic tools and instrumentation—with capabilities unimaginable just a few years ago—allow engineers and scientists to gather detailed information in hostile combustion environments at both microscopic and macroscopic levels. Lasers, spectroscopy, advanced infrared, and ultraviolet camera systems are used to nonintrusively gather quantitative and qualitative information, including combustion temperature, velocity, species concentration, flow visualization, particle size, and loading. Advanced diagnostic systems and instrumentation are being transferred beyond the laboratory to implementation in practical field applications. The information obtained with these systems has considerably advanced our knowledge of combustion equipment and has been an indispensable source of CFD model validation.

Oil refining, chemical processes, and power generation are energy-intensive industries with combustion applications in burners, process heaters, boilers, and cogeneration systems, as well as flares and thermal oxidizers. Combustion for these industries presents unique challenges related to the variety of fuel compositions encountered. Combustion equipment must be flexible to be able to operate in a safe, reliable, efficient, and environmentally responsible manner under a wide array of fuel compositions and conditions.

Combustion is an exciting and intellectually challenging field containing plenty of opportunities to enhance fundamental and practical knowledge that will ultimately lead to the development of new products with improved performance.

This book represents the tireless efforts of many John Zink engineers willing to share their unique knowledge and experience with other combustion engineers, researchers, operators of combustion equipment, and college students. We have tried to include insightful and helpful information on combustion fundamentals, combustion noise, CFD design, experimental techniques, equipment, controls, maintenance, and troubleshooting. We hope our readers will agree that we have done so.

**David H. Koch**  
*Executive Vice President*  
*Koch Industries*

This page intentionally left blank



---

## Preface to the First Edition

---

Combustion is described as “the rapid oxidation of a fuel resulting in the release of usable heat and production of a visible flame.”<sup>1</sup> Combustion is used to generate 90% of the world’s power.<sup>2</sup> Regarding the science of combustion, Liñán and Williams wrote the following:

Although combustion has a long history and great economic and technical importance, its scientific investigation is of relatively recent origin. Combustion science can be defined as the science of exothermic chemical reactions in flows with heat and mass transfer. As such, it involves thermodynamics, chemical kinetics, fluid mechanics, and transport processes. Since the foundations of the second and last of these subjects were not laid until the middle of the nineteenth century, combustion did not emerge as a science until the beginning of the twentieth century.<sup>3</sup>

Chomiak wrote the following: “In spite of their fundamental importance and practical applications, combustion processes are far from being fully understood.”<sup>4</sup> In Strahle’s opinion, “combustion is a difficult subject, being truly interdisciplinary and requiring the merging of knowledge in several fields.”<sup>5</sup> It involves the study of chemistry, kinetics, thermodynamics, electromagnetic radiation, aerodynamics, and fluid mechanics, including multiphase flow and turbulence, heat and mass transfer, and quantum mechanics to name a few. Regarding combustion research,

The pioneering experiments in combustion research, some 600,000 years ago, were concerned with flame propagation rather than ignition. The initial ignition source was provided by Mother Nature in the form of the electrical discharge plasma of a thunderstorm or as volcanic lava, depending on location. ... Thus, in the beginning, Nature provided an arc-augmented diffusion flame and the first of man’s combustion experiments established that the heat of combustion was very much greater than the activation energy—i.e., that quite a small flame on a stick would spontaneously propagate itself into a very large fire, given a sufficient supply of fuel.<sup>6</sup>

In one of the classic books on combustion, Lewis and von Elbe wrote the following:

Substantial progress has been made in establishing a common understanding of combustion

phenomena. However, this process of consolidation of the scientific approach to the subject is not yet complete. Much remains to be done to advance the phenomenological understanding of flame processes so that theoretical correlations and predictions can be made on the basis of secure and realistic models.<sup>7</sup>

Despite the length of time it has been around, despite its importance to man, and despite vast amounts of research, combustion is still far from being completely understood. One of the purposes of this book is to improve that understanding, particularly in industrial combustion applications in the process and power generation industries.

This book is generally organized in two parts. Part I deals with the basic theory of some of the disciplines (combustion, heat transfer, fluid flow, etc.) important for the understanding of any combustion process and consists of Chapters 1 through 13. While these topics have been satisfactorily covered in many combustion textbooks, this book treats them from the context of the process and power generation industries. Part II deals with specific equipment design issues and applications in the process and power generation industries.

---

## References

1. Industrial Heating Equipment Association, *Combustion Technology Manual*, 5th edn. Combustion Division of the Industrial Heating Equipment Association, Arlington, VA, 1994, p. 1.
2. N. Chigier, *Energy, Combustion, and Environment*. McGraw-Hill, New York, 1981, p. ix.
3. A. Liñán and F.A. Williams, *Fundamental Aspects of Combustion*. Oxford University Press, Oxford, U.K., 1993, p. 3.
4. Chomiak, *Combustion: A Study in Theory, Fact and Application*, p. 1.
5. W.C. Strahle, *An Introduction to Combustion*. Gordon & Breach, Langhorne, PA, 1993, p. ix.
6. F.J. Weinberg, The first half-million years of combustion research and today’s burning problems, in *Fifteenth Symposium (International) on Combustion*, The Combustion Institute, Pittsburgh, PA, 1974, p. 1.
7. B. Lewis and G. von Elbe, *Combustion, Flames and Explosions of Gases*, 3rd edn. Academic Press, New York, 1987, p. xv.



This page intentionally left blank

---

## *Preface to the Second Edition*

---

The first edition of the *John Zink Combustion Handbook* was published in 2001. It replaced the previous industry standard book (*Furnace Operations*, 3rd edition, Gulf Publishing, Houston, 1981) written by Dr. Robert Reed, who was the former technical director of the John Zink Company. The first edition of the *Zink Handbook* consisted of 800 oversized pages, was in full color, and was written by 30 authors as compared to *Furnace Operations*, which consisted of 230 pages in black and white and was written by a single author. The first edition of the *Zink Handbook* was a major expansion compared to *Furnace Operations*. The second edition of the *Zink Handbook* is another major expansion compared to the first edition.

The second edition consists of three volumes, collectively about twice as large as the single-volume first edition. Volume I concerns the fundamentals of industrial combustion such as chemistry, fluid flow, and heat transfer. While the basic theory is presented for each topic, the unique treatment compared to standard textbooks is how these topics apply to industrial combustion. Volume II concerns design and operations and includes topics related to equipment used in industrial combustion such as installation, maintenance, and troubleshooting. It also includes an extensive appendix with data relevant to industrial combustion equipment and processes.

Volume III concerns applications and covers topics such as process burners, boiler burners, process flares, thermal oxidizers, and vapor control. It shows how the information in volumes I and II is used to design and operate equipment in particular industry applications.

There were several reasons for writing a second edition. The first is the natural improvement in technology with time. For example, NO<sub>x</sub> emissions from process burners are lower than ever and continue to decrease with advancements in technology. A second reason for the new edition is to make improvements to the first edition as recommended by readers. One example is to have more property data useful for the design and operation of combustion equipment. Another reason for the new edition is to expand the coverage to include technologies not covered in the first edition such as metallurgy, refractories, blowers, and vapor control equipment.

While these three volumes represent a significant expansion of the first edition, some topics could have been covered in greater detail and some topics have received little if any attention. There is still much to learn on the subject of industrial combustion, which is far more complicated than the average person would ever imagine. This is what makes it such an exciting and dynamic area of technology that has a significant impact on society because it affects nearly every aspect of our lives.

This page intentionally left blank

---

## *Acknowledgments*

---

The authors would like to collectively thank the John Zink and Coen companies for their help and support during the preparation of these materials. Many colleagues helped with ideas, content, and the preparation of figures and tables. The authors would also like to thank Rick Ketchum, Andrew Walter, Vincent Wong, and Jeffrey Ma for their help in preparing the materials for this book.

Chuck Baukal would like to thank his wife, Beth, and his daughters, Christine, Caitlyn, and Courtney, for their continued support. He would also like to thank the good Lord above, without whom this would not have been possible. Wes Bussman would like to thank his family for their support. He would also like to thank all of his colleagues at John Zink Company for their encouragement and for the knowledge they have shared with him throughout his career. Myra

Fanning would like to thank God, her parents, Willia and Frank Crawford, for their guidance, and her sister, Marisa Crawford-Gray, for her never-ending support and encouragement. Special thanks to Chuck Baukal for his mentoring abilities and belief that she could be part of this book. Christopher Jian would like to thank his wife, Sylvia, for her love and support without which his career would not have been possible. He would also like to thank his mentors William Talley and Harry Adams for their career-long guidance and encouragement. Jason McAdams would like to thank his wife, Heather, and his sons, Ian and Nathan, for their support and for their understanding of the extra time and effort that being in the combustion business sometimes takes. He also thanks all of those who have given their time to help him learn throughout his career.

This page intentionally left blank

---

## Editor

---

**Charles E. Baukal, Jr.**, is the director of the John Zink Institute for the John Zink Co. LLC (Tulsa, Oklahoma), where he has been since 1998. He has also been the director of R&D and the director of the R&D Test Center at Zink. He previously worked for 13 years at Air Products and Chemicals, Inc. (Allentown, Pennsylvania) in the areas of oxygen-enhanced combustion and rapid gas quenching in the ferrous and nonferrous metals, minerals, and waste incineration industries. He has also worked for Marsden, Inc. (a burner supplier in Pennsauken, New Jersey) for five years in the paper, printing, and textile industries and for Selas Corp. (a burner supplier in Dresher, Pennsylvania) in the metals industry, both of whom make industrial combustion equipment. He has over 30 years of experience in the fields of industrial combustion, pollution control, and heat transfer and has authored more than 100 publications in those areas. Dr. Baukal is an adjunct instructor for Oral Roberts University, the University of Oklahoma, the University of Tulsa, and the University of Utah. He is the author/editor of eight books in the field of industrial combustion, including *Oxygen-Enhanced Combustion*

(1998), *Heat Transfer in Industrial Combustion* (2000), *Computational Fluid Dynamics in Industrial Combustion* (2001), *The John Zink Combustion Handbook* (2001), *Industrial Combustion Pollution and Control* (2004), *Handbook of Industrial Burners* (2004), *Heat Transfer from Flame Impingement Normal to a Plane Surface* (2009), and *Industrial Combustion Testing* (2011).

He has a PhD in mechanical engineering from the University of Pennsylvania (Philadelphia, Pennsylvania), an MBA from the University of Tulsa, and is a licensed professional engineer in the state of Pennsylvania, a board-certified environmental engineer (BCEE), and a qualified environmental professional (QEP). He has also served as an expert witness in the field of combustion, has 11 U.S. patents, and is a member of numerous honorary societies and *Who's Who* compilations. Dr. Baukal is a member of the American Society of Mechanical Engineers, the American Society for Engineering Education (ASEE), and the Combustion Institute. He serves on several advisory boards, holds offices in the Combustion Institute and ASEE, and is a reviewer for combustion, heat transfer, environmental, and energy journals.

This page intentionally left blank

---

## Contributors

---

**John Ackland** works in the process flare group and has been at John Zink Company LLC (Tulsa) and John Zink International Luxembourg Sarl since 1998 in various technical and business roles within the process burner and process flare departments. He received his BS in chemical engineering from the University of Tulsa.

**David Brown** is a cracking furnace expert working for Total Research and Technology Feluy (TRTF) in Belgium. Prior to joining TPRF in 2009, David worked for Shaw Energy & Chemicals (formerly Stone & Webster) for 28 years in a leading role in the development, sales, design, commissioning, and operation of cracking furnaces. David received his MA and MEng from the University of Cambridge and his DPhil from the University of Oxford. He is a chartered engineer and a fellow of the (British) Institution of Chemical Engineers. He served as session chair for Fundamentals & Technology (Ethylene Producers' Conference). He is also the joint holder of five patents and has presented papers on combustion in cracking furnaces on numerous occasions.

**Wes Bussman** is a senior research and development engineer for John Zink Co. LLC. He received his PhD in mechanical engineering from the University of Tulsa. He has 20 years of experience in basic scientific research work, industrial technology research and development, and combustion design engineering. He holds ten patents and has authored several published articles and conference papers. He has also been a contributing author to several combustion-related books. He has taught engineering courses at several universities and is a member of Kappa Mu Epsilon Mathematical Society and Sigma Xi Research Society.

**Shirley X. Chen** is a senior CFD engineer at John Zink Company's Simulation Technology Solutions Group. She has over ten years of experience in the power generation and eight years of experience in the petrochemical industries. Her areas of expertise include radiative heat transfer, flow and heat transfer in porous media, and combustion simulations. She has published over 15 papers in peer-reviewed journals and conference proceedings. Shirley received her PhD in aerospace and mechanical engineering from the University of Oklahoma.

**I-Ping Chung** is a senior development engineer in the Technology and Commercial Development Group at the

John Zink Company LLC (Tulsa, Oklahoma). She has worked in the field of industrial combustion and equipment, fluid dynamics, atomization and sprays, spray combustion, and laser diagnosis in combustion and has a PhD in mechanical and aerospace engineering. She has 24 publications and holds 9 patents. She is a registered professional engineer of mechanical engineering in the states of California and Iowa.

**Joseph Colannino** is chief technology officer of ClearSign Combustion Corporation—a company that applies low power electric fields to flames to improve their shape and emissions. Prior to joining ClearSign, Colannino was director of research and development at John Zink Company, LLC, where he led global R&D efforts. His responsibilities included management of intellectual property, oversight of John Zink's testing facility, and leading knowledge management efforts. He has more than 25 years of experience in the combustion industry and has authored or contributed to several books, including *Industrial Combustion Testing*, *The Air Pollution Control Guide*, *The John Zink Combustion Handbook*, and *Modeling of Combustion Systems—A Practical Approach*. He is a registered professional engineer and has written and reviewed problems appearing on the NCEES professional engineering exam, given in all 50 states for professional engineering licensure. His areas of experience include R&D management, combustion, pollutant formation and control, and statistical experimental design. Past and present memberships include the American Institute of Chemical Engineers, the American Chemical Society, the Air and Waste Management Association, the American Statistical Association, and the National Association of Professional Engineers. He received his BS from the California Polytechnic University in Pomona and his master's degree in knowledge management from the University of Oklahoma.

**Myra N. Crawford-Fanning** is the school administrator for the John Zink Institute/John Zink Company LLC (Tulsa, Oklahoma), coordinating and facilitating training for customers around the world. Previously, she was employed with the Wichita Public Schools for 20 years. She is a graduate of Wichita State University with a BA in speech communications. Since working for John Zink in 2000, she has received various certifications, including the American Society for Training & Development (ASTD) training certificate and a training generalist



certificate through Langevin Learning Services. She has served on the Northeast Oklahoma (NEOK) Chapter of ASTD Board for a number of years as secretary, president elect, president, and past president. As a repeat presenter at the annual North American Process Technology Alliance (NAPTA, formerly GCPTA) Instructor Skills Conference, her knowledge and skills are shared and received positively by other instructors in the combustion field. She has also presented for the ASTD Call Center Forum to remind instructors that learning can be fun.

**Carl-Christian Hantschk** has been working as a consulting engineer in industrial acoustics for Müller-BBM GmbH (Munich, Germany) since 2001. He was promoted to managing director in 2009. He works on industrial acoustics in general, including theoretical and applied acoustics, environmental acoustics, aero-acoustics, and numerical acoustics, with special focus on the interdisciplinary field between combustion and acoustics. He holds a diploma in mechanical engineering and received his doctorate in thermodynamics from the Technical University Munich, Germany. His research focuses on combustion-driven acoustic oscillations in burners and combustion-acoustic interactions. He has also given lectures on chemical thermodynamics, thermal radiation, and heat transfer and acoustics at his university, international conferences, and for industrial clients. His work has resulted in 30 publications and 4 invention disclosures. As one of his main research projects, he codeveloped an active acoustic feedback control for industrial combustion systems.

**Christopher Q. Jian** is currently senior R&D manager at The Dow Chemical Company (Midland, Michigan). He previously served as director of Simulation Technology Solutions Group at the John Zink Company LLC (Tulsa, Oklahoma). He has worked in fossil fuel combustion, CFD simulations, and physical modeling of fluid flow-related processes. He has a PhD in mechanical engineering and an MBA. He also has 4 patents and over 40 publications in various engineering fields.

**Jay Karan** (Jaiwant Jayakaran) is director of thermal oxidizer systems at the John Zink Company LLC (Tulsa, Oklahoma). He has over 25 years of experience in the fields of combustion, petrochemicals, and power, with responsibilities in R&D, plant operations, and engineering. Jay has an MS in mechanical engineering. He has authored several technical articles and papers over the years and has several patents.

**Zachary L. Kodesh** is the technology manager in the Flare Systems Division of the John Zink Company LLC (Tulsa, Oklahoma). He received his BS and MS in mechanical

engineering from Oklahoma State University and has worked for John Zink Co. since 1990. He is a registered professional engineer, a certified functional safety expert, a member of ASME, and is an active participant in the American Petroleum Institute.

**Steve Londerville** is currently chief engineer at Coen Company, San Mateo City, California. Previous positions since 1978 at Coen were chief technical officer, vice president R&D, director R&D, and chief engineer. During the past 35 years, he has been involved with all aspects of product development at Coen Co. He received his mechanical engineering degree from San Jose State University in 1977. He holds 7 patents and has authored 16 publications. He is a member of ASME, AIChE, the Combustion Institute, Tau Beta Pi, and the Institute for Liquid Atomization and Spray Systems (ILASS) including past officer in the board of directors of ILASS. He was recognized as the ASME 1990 Distinguished Mechanical Engineer of the year, Santa Clara Valley Section.

**Michael A. Lorra** currently works as a senior process engineer/CFD specialist at John Zink KEU GmbH in Krefeld, Germany. He started as a CFD engineer for the John Zink Company, LLC, Tulsa, Oklahoma in 1999. Prior to this, he worked at Gaswaerme Institut e.V., Essen, Germany, for eight years, where he also completed his PhD. He gained experience in NO<sub>x</sub> reduction techniques, especially in reburning technology. He developed his own software code for the computation of turbulent reacting flow problems using laminar flamelet libraries. During his time at John Zink, he specialized in CFD models for thermal oxidizers and flare systems.

**Jason D. McAdams** is the director of applications engineering for the Process Burner Group of the John Zink Company LLC (Tulsa, Oklahoma). He has been with John Zink since 1999, serving in several roles including product development, design engineering, project management, technical sales, and management. Prior to this, he worked for more than five years at Koch Refining Company, where he gained experience with the application of combustion equipment as a project engineer and reliability engineer. He received his BS in mechanical engineering from the University of Tulsa and has authored multiple publications in journals and conference proceedings. McAdams is a registered professional engineer in the state of Oklahoma.

**Rasik Patel** is the vice president of process technology with OnQuest Inc. located in San Dimas, California. He has 36 years of experience in designing fired process heaters, coker heaters, steam methane reformers, and pyrolysis furnaces for the refining and petrochemical

industries. He is an active member in the heat transfer subgroup of the API task force, working on fired heater standards. He received his MS in chemical engineering from the Imperial College of Science & Technology, University of London, England.

**Erwin Platvoet** is director of process burner engineering at John Zink Company in Tulsa, Oklahoma. He has over 20 years of experience in CFD and heat transfer engineering for various companies in Europe and the United States. He received his MS in chemical engineering from Twente University of Technology in the Netherlands and currently holds six patents.

**Edwin Schorer** has been working as a consulting engineer in industrial acoustics for Müller-BBM GmbH (Munich, Germany) since 1989. He received his degree in electrical engineering and his doctorate in psychoacoustics from the Technical University Munich, Germany. He was promoted to managing director in 2006. He works in industrial acoustics in general, including theoretical and applied acoustics, with special focus on noise predictions for flare noise and fan noise, fluid mechanics, ship acoustics, and acoustic optimization of postal automation systems. His research work resulted in 15 publications on psychoacoustics as well as industrial and technical acoustics. Dr. Schorer is a member of the German Institute for Standardization, the Noise Control and Vibration Engineering Standards Committee, and the German Acoustical Society. His research focuses on a functional schematic of just noticeable frequency and amplitude variations. He has worked as temporary academic counsel at his university, lecturing in electroacoustics and technical acoustics. He has also acted as supervising tutor for students' diploma theses and practical trainings.

**Robert E. Schwartz** retired as a senior technical specialist at John Zink Company, LLC (Tulsa, Oklahoma). He worked in the fields of combustion, flares, pressure relieving systems, fluid flow, and heat transfer for more than 40 years, including 42 years with Zink, where he has provided technical and business leadership in all product areas and has extensive international experience. He has 51 U.S. patents for inventions of apparatus and methods that are in use throughout Zink. He was also the associate editor of first edition of *The John Zink Hamworthy Combustion Handbook*. His areas of technical expertise include development, design, fabrication, and operation of combustion equipment, including flares, incinerators, process burners, boiler burners, and vapor control; reduction of NO<sub>x</sub> and other emissions from combustion processes; fluid flow and heat transfer in process and combustion equipment; noise elimination and control; vapor

emissions control using recovery processes; hazardous waste site remediation; and permitting and operation of hazardous waste storage and disposal sites. His professional organizations and awards include membership in the American Society of Mechanical Engineers, the American Institute of Chemical Engineers and Sigma Xi, the Scientific Research Society, Registered Professional Engineer in the state of Oklahoma, recipient of the University of Missouri Honor Award for Distinguished Service in Engineering, and election to The University of Tulsa Engineering Hall of Fame. He received his BS and MS in mechanical engineering from the University of Missouri.

**James G. Seebold**, Chevron (retired), has more than 40 years experience in the design, operation, and maintenance of burners, fired heaters, furnaces, incinerators, boilers, and flares, including low-NO<sub>x</sub> burners, selective catalytic and noncatalytic NO<sub>x</sub> reduction systems, and hazardous air pollutant emissions. He conceived and led the 4-year, \$7 million, 20-participant industry-government-university collaboration that provided the basis for this volume's chapter on pollutant emissions. Jim received his a PhD in mechanical engineering from Stanford University.

**Richard T. Waibel** was a senior principal engineer in the Burner Process Engineering Group at the John Zink Company, LLC (Tulsa, Oklahoma). He worked in the field of burner design and development and has a doctorate in fuel science from Pennsylvania State University. He published over 70 technical papers, publications, and presentations. Dr. Waibel was the chairman of the American Flame Research Committee for many years starting in 1995.

**Timothy Webster** is the president of Coen Company, Inc. He has worked in the field of industrial combustion for 18 years and received his MS in engineering from the University of Wisconsin. He has over 40 publications and is a licensed professional mechanical engineer in California.

**Jeff White** is a senior flare design engineer at the John Zink Company LLC (Tulsa, Oklahoma). He has worked in the field of flare system design at John Zink Company for 30 years. He received his MS in mechanical engineering from The University of Texas at Austin. He has published two articles, one on flare radiation methods and the other on flow measurement by ASME nozzles.

**Klaus-Dieter Zschorsch** is a senior process and application engineer in the Catalytic and Thermal Oxidizer Engineering Group of the John Zink KEU GmbH (Krefeld, Hamburg, Germany). He has a degree in

process engineering from the University of Applied Sciences (UAS), Hamburg, and has worked for John Zink KEU GmbH in the field of catalytic oxidizers, condensation units, and selective catalytic reduction since 1990 and in the field of thermal oxidizers since 2010. He has been appointed as a guideline committee member of Verein Deutscher Ingenieure e.V. (VDI).

As a committee member, he serves in an honorary capacity for the VDI Guideline "Method of Catalytic Waste Gas Cleaning." He supports the committee by formulating technical rules and coauthoring papers and presentations covering fundamentals of catalytic oxidizers, oxidative processes, and selective catalytic reduction.

---

## Prologue

---

### Fred Koch and John Zink—Pioneers in the Petroleum Industry

The early decades of the twentieth century saw the birth and growth of the petroleum industry in Oklahoma. Drilling derricks sprouted like wildflowers throughout the state, making it among the top oil producers in the nation and Tulsa the “Oil Capital of the World” by the 1920s.

Refining operations accompanied oil production. Many of the early refineries were so small that today they would be called pilot plants. They were often merely topping processes, skimming off natural gasoline and other light fuel products and sending the remainder to larger refineries with more complex processing facilities.

Along with oil, enough natural gas was found to make its gathering and sale a viable business as well. Refineries frequently purchased this natural gas to fuel their boilers and process heaters. At the same time, these refineries vented propane, butane, and other light gaseous hydrocarbons into the atmosphere because their burners could not burn them safely and efficiently. Early burner designs made even natural gas difficult to burn as traditional practice and safety concerns led to the use of large amounts of excess air and flames that nearly filled the fire box. Such poor burning qualities hurt plant profitability.

Among firms engaged in natural gas gathering and sales in the northeastern part of the state was Oklahoma Natural Gas Company (ONG). It was there that John Steele Zink (Figure P.1b), after completing his studies at the University of Oklahoma in 1917, went to work as a chemist. Zink’s chemistry and engineering education enabled him to advance to the position of manager of industrial sales. But while the wasteful use of natural gas due to inefficient burners increased those sales, it troubled Zink and awakened his talents first as an innovator and inventor and then as an entrepreneur.

Seeing the problems with existing burners, Zink responded by creating one that needed less excess air and produced a compact, well-defined flame shape. A superior burner for that era, it was technically a pre-mix burner with partial primary air and partial draft-induced secondary air. The use of two airflows led to its trade name, BI-MIX®. The BI-MIX® burner is shown in a drawing from one of Zink’s earliest patents (Figure P.2).

ONG showed no interest in selling its improved burners to its customers, so in 1929 Zink resigned and founded Mid-Continent Gas Appliance Co., which he later renamed the John Zink Company.



(a)



(b)

**FIGURE P.1**  
Fred Koch (a) and John Zink (b).



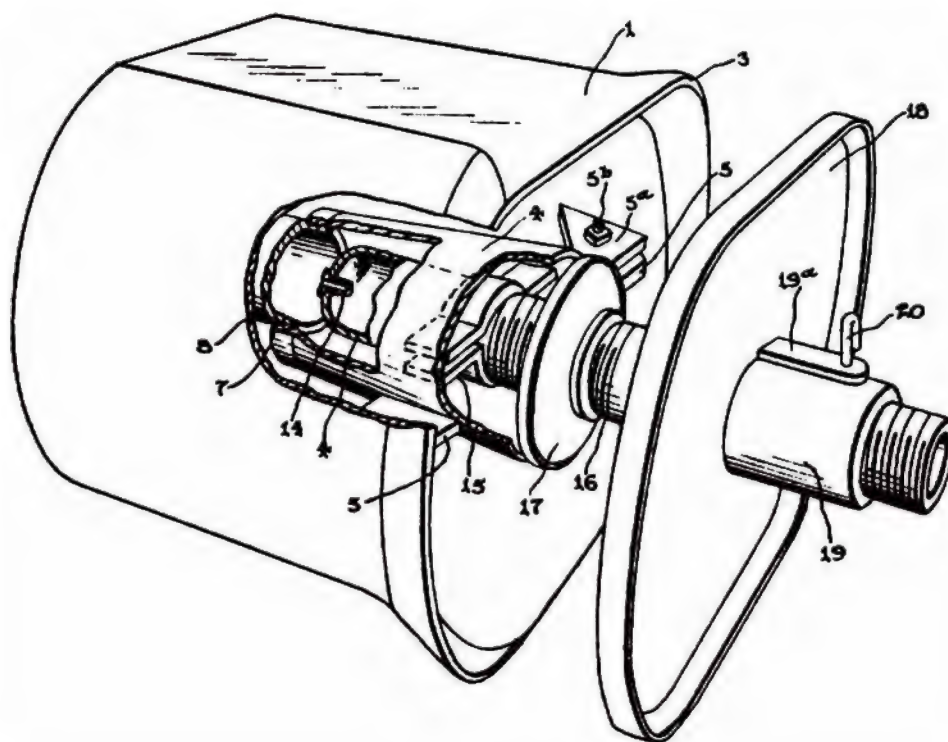


FIGURE P.2

Drawing of BI-MIX® From Zink's patent.

Zink's BI-MIX® burner was the first of many advances in technology made by his company, which to date has seen over 250 U.S. patents awarded to nearly 80 of its employees. He carried out early manufacturing of the burner in the garage of his Tulsa-area home and sold it from the back of his automobile as he traveled the Oklahoma oil fields, generating the money he needed to buy the components required to fabricate the new burners.

The novel burners attracted customers by reducing their fuel costs, producing a more compact flame for more efficient heater operation, burning a wide range of gases, and generally being safer to use. Word of mouth among operators helped spread their use throughout not only Oklahoma but, by the late 1930s, to foreign refineries as well.

Growth of the company required Zink to relocate his family and business to larger facilities on the outskirts of Tulsa. In 1935, he moved into a set of farm buildings on Peoria Avenue, a few miles to the south of the city downtown, a location Zink thought would allow for plenty of future expansion.

As time passed, Zink's company became engaged in making numerous other products, sparked by its founder's beliefs in customer service and solving customer problems. After World War II, Zink was the largest sole proprietorship west of the Mississippi River. Zink's reputation for innovation attracted customers who wanted new burners and, eventually, whole new families

of products. For example, customers began asking for reliable pilots and pilot igniters, when atmospheric venting of waste gases and emergency discharges was replaced by combustion in flares in the late 1940s. This in turn was followed by requests for flare burners and finally complete flare systems, marking the start of the flare equipment industry. Similar customer requests for help in dealing with gas and liquid waste streams and hydrocarbon vapor led the Zink Company to become a leading supplier of gas and liquid waste incinerators and also of hydrocarbon vapor recovery and other vapor control products.

Zink's great interest in product development and innovation led to the construction of the company's first furnace for testing burners. This furnace was specially designed to simulate the heat absorption that takes place in a process heater. Zink had the furnace built in the middle of the employee parking lot, a seemingly odd placement. He had good reason for this because he wanted his engineers to pass the test furnace every day as they came and went from work as a reminder of the importance of product development to the company's success.

Zink went beyond encouraging innovation and motivating his own employees. During the late 1940s, Zink and his technical team leader, Robert Reed (who together with Zink developed the first smokeless flare), sensed a need for an industry-wide meeting to discuss technologies and experiences associated with process heating. In 1950, they hosted the first of four annual process heating

seminars in Tulsa. Interest in the seminars was high, with the attendance level reaching 300. Attendees of the first process heating seminar asked Zink and Reed to conduct training sessions for their operators and engineers. These training sessions, which combined lectures and practical hands-on burner operation in Zink's small research and development center, were the start of the John Zink Burner School®. The year 2010 marked the 60th anniversary of the original seminar and the 50th year in which the Burner School has been offered. Over the years, other schools were added to provide customer training in the technology and operation of hydrocarbon vapor recovery systems, vapor combustors, and flares.

Included among the 150 industry leaders attending the first seminar was Harry Litwin, former president and part owner of Koch Engineering Co., now part of Koch Industries of Wichita, Kansas. Litwin was a panelist at the closing session. Koch Engineering was established in 1943 to provide engineering services to the oil refining industry. In the early 1950s, it developed an improved design for distillation trays and because of their commercial success the company chose to exit the engineering business. Litwin left Koch at that time and set up his own firm, the Litwin Engineering Co., which grew into a sizeable business.

During the same period that John Zink founded his business, another talented young engineer and industry innovator, Fred C. Koch, was establishing his reputation as an expert in oil processing. The predecessor to Koch Engineering Co. was the Winkler-Koch Engineering Co., jointly owned by Fred Koch with Lewis Winkler, which designed processing units for oil refineries. Fred Koch had developed a unique and very successful thermal cracking process that was sold to many independent refineries throughout the United States, Europe, and the former Soviet Union. One of the first of these processing units was installed in a refinery in Duncan, Oklahoma, in 1928, one year before Zink started his own company.

While the two men were not personally acquainted, Koch's and Zink's companies knew each other well in those early years. Winkler-Koch Engineering was an early customer for Zink burners. The burners were also used in the Wood River refinery in Hartford, Illinois. Winkler-Koch constructed this refinery in 1940 with Fred Koch as a significant part owner and the head of refining operations. Winkler-Koch Engineering, and later Koch Engineering, continued to buy Zink burners for many years.

Fred Koch and two of his sons, Charles and David, were even more successful in growing their family business than were Zink and his family. When the Zink family sold the John Zink Company to Sunbeam Corporation\* in 1972, the company's annual revenues

were \$15 million. By that time, Koch Industries, Inc., the parent of Koch Engineering, had revenues of almost \$1 billion. Since then, Koch has continued to grow; its revenues in the year 2011 were over \$100 billion.

When the John Zink Company was offered for sale in 1989, its long association with Koch made Koch Industries a very interested bidder. Acting through its Chemical Technology Group, Koch Industries quickly formed an acquisition team, headed by David Koch, which succeeded in purchasing the John Zink Company.

Koch's management philosophy and focus on innovation and customer service sparked a new era of revitalization and expansion for the John Zink Company. Koch recognized that the Peoria Avenue research, manufacturing, and office facilities were outdated. The growth of Tulsa after World War II had made Zink's facilities an industrial island in the middle of a residential area. The seven test furnaces on Peoria Avenue at the time of the acquisition, in particular, were cramped, with such inadequate infrastructure and obsolete instrumentation they could not handle the sophisticated research and development required for modern burners.

A fast-track design and construction effort by Koch resulted in a new office and manufacturing complex in the northeastern sector of Tulsa that was completed at the end of 1991. In addition, a spacious R&D facility adjacent to the new office and manufacturing building replaced the Peoria test facility.

The initial multimillion dollar investment in R&D facilities included an office building housing the R&D staff and support personnel, a burner prototype fabrication shop, and an indoor laboratory building. Additional features included steam boilers, fuel storage and handling, data gathering centers, and measurement instrumentation and data logging for performance parameters from fuel flow to flue gas analysis.

Koch has repeatedly expanded the R&D facility. When the new facility began testing activities in 1992, nine furnaces and a multipurpose flare testing area were in service. Today, there are 14 outdoor test furnaces and 2 indoor research furnaces. Control systems are frequently updated to keep them state of the art.

Zink is now able to monitor burner tests from an elevated customer center that has a broad view of the entire test facility. The customer center includes complete automation of burner testing with live data on control panels and flame shape viewing on color video monitors.

A new flare testing facility (Figure P.3) was constructed in the early 2000s to dramatically expand and improve Zink's capabilities. This project represents the company's largest single R&D investment since the original construction of the R&D facility in 1991. The new facilities accommodate the firing of a wide variety of fuel blends (propane, propylene, butane, ethylene, natural gas, hydrogen, and diluents such as

\* Sunbeam Corporation was primarily known as an appliance maker. Less well known was Sunbeam's group of industrial specialty companies such as John Zink Company.



**FIGURE P.3**  
Flare testing facility.

nitrogen and carbon dioxide) to reproduce or closely simulate a customer's fuel composition. Multiple cameras provide video images along with the electronic monitoring and recording of a wide range of flare test data, including noise emissions. The facility can test all varieties of flare systems with very large sustained gas flow rates at or near those levels that customers will encounter in the field. Indeed, flow capacity matches or exceeds the smokeless rate of gas flow for virtually all customers' industrial plants, giving the new flare facility a capability unmatched in the world.

These world-class test facilities are staffed with engineers and technicians who combine theoretical training with practical experience. They use the latest design and

analytical tools, such as computational fluid dynamics, physical modeling, and a phase Doppler particle analyzer. The team can act quickly to deliver innovative products that work successfully, based on designs that can be exactly verified before the equipment is installed in the field.

Koch's investment in facilities and highly trained technical staff carries on the tradition John Zink began more than 80 years ago: providing our customers today, as he did in his time, with solutions to their combustion needs through better products, applications, information, and service.

**Robert E. Schwartz**  
*Tulsa, Oklahoma*



# 1

## Introduction

Charles E. Baukal, Jr.

### CONTENTS

1.1	Process Industries .....	1
1.1.1	Hydrocarbon and Petrochemical.....	1
1.1.2	Power Generation.....	6
1.1.3	Pollution Control.....	7
1.2	Literature Review.....	8
1.2.1	Combustion.....	8
1.2.2	Process Industries .....	9
1.2.3	Combustion in the Process Industries .....	10
1.3	Fired Heaters .....	10
1.3.1	Reformers.....	10
1.3.2	Process Heaters .....	12
1.4	Burners .....	17
1.4.1	Competing Priorities .....	18
1.4.2	Design Factors .....	19
1.4.2.1	Fuel .....	21
1.4.2.2	Oxidizer .....	22
1.4.2.3	Gas Recirculation .....	22
1.4.3	General Burner Types.....	23
1.4.3.1	Mixing Type.....	23
1.4.3.2	Fuel Type .....	25
1.4.3.3	Combustion Air Temperature .....	26
1.4.3.4	Draft Type .....	26
1.4.3.5	Location .....	26
1.4.4	Potential Problems.....	26
1.5	Design Tools .....	27
1.6	Conclusions.....	29
	References.....	29

### 1.1 Process Industries

Process industries encompass the production of a wide range of products like fuels (e.g., oil and natural gas), glass, metals (e.g., steel and aluminum), minerals (e.g., refractories, bricks, and ceramics), and power, to name a few. The treatment and disposal of waste materials is another example of a process industry. In this book, only a few of these are considered and are briefly discussed in this chapter. Typical process heating operations are shown in Table 1.1. They include fluid heating (common in petroleum refining and chemical manufacturing) and thermal oxidation.<sup>1</sup> The main focus of this book is

on the hydrocarbon, petrochemical, power generation, and thermal oxidation industries.

#### 1.1.1 Hydrocarbon and Petrochemical

Figure 1.1 shows that the number of operating refineries in the United States has been declining since 1949. The graph also shows that capacity and throughput have been increasing over that same time period. A peak occurred in the late 1970s and early 1980s during the oil crisis. Since that time, smaller and older refineries have been closing because they are no longer profitable. In many cases, it is too expensive to modernize them to meet current emissions standards and



TABLE 1.1

Summary of Process Heating Operations

Process	Application	Equipment	Industry
Agglomeration sintering	Metals production	Various furnace types, kilns, microwave	Primary metals
Calcining	Lime calcining	Various furnace types	Cement, wallboard, pulp and paper manufacturing, primary metals
Curing and forming	Coating, polymer production, enameling	Various furnace types, ovens, kilns, lehrs, infrared, UV, electron beam, induction	Ceramics, stone, glass, primary metals, chemicals, plastics, and rubber
Drying	Water and organic compound removal	Fuel-based dryers, infrared, resistance, microwave, radio-frequency	Stone, clay, petroleum refining, agricultural and food, pulp and paper, textile
Forming	Extrusion, molding	Various ovens and furnaces	Rubber, plastics, glass
Fluid heating	Food preparation, chemical production, reforming, distillation, cracking, hydrotreating, visbreaking	Various furnace types, reactors, resistance heaters, microwave, infrared, fuel-based fluid heaters, immersion heaters	Agricultural and food, chemical manufacturing, petroleum refining
Heating and melting high-temperature	Casting, steelmaking, glass production	Fuel-based furnaces, kilns, reactors, direct arc, induction, plasma, resistance	Primary metals, glass
Heating and melting low-temperature	Softening, liquefying, warming	Ovens, infrared, microwave, resistance	Plastics, rubber, food, chemicals
Heat treating	Hardening, annealing, tempering	Various fuel-based furnace types, ovens, kilns, lehrs, laser, resistance, induction, electron beam	Primary metals, fabricated metal products, glass, ceramics
Incineration/thermal oxidation	Waste handling/disposal	Incinerators, thermal oxidizers, resistance, plasma	Fabricated metals, food, plastics and rubber, chemicals
Metals reheating	Forging, rolling, extruding, annealing, galvanizing, coating, joining	Various furnace types, ovens, kilns, heaters, reactors, induction, infrared	Primary metals, fabricated metal products, glass, ceramics
Separating	Air separation, refining, chemical cracking	Distillation, membranes, filter presses	Chemicals
Smelting	Steelmaking and other metals (e.g., silver)	Various furnace types	Primary metals
Other heating processes	Food production (including baking, roasting, and frying), sterilization, chemical production	Various furnace types, ovens, reactors, resistance heaters, microwave, steam, induction, infrared	Agricultural and food, glass, ceramics, plastics and rubber, chemicals

Source: Lawrence Berkeley National Laboratory and Resource Dynamics Corporation, *Improving Process Heating System Performance: A Sourcebook for Industry*, 2nd Edition, U.S. Department of Energy and Industrial Heating Equipment Association, Washington, DC, 2007, Table 1.

to process sour crude oils. However, existing refineries continue to be upgraded and expanded. Figure 1.2 shows the mix of products produced by U.S. refineries. Some trends are evident. Aviation gasoline, residual fuel oil, and kerosene have decreased, while jet fuel, motor gasoline, liquefied petroleum gases, and petroleum coke have increased. Figure 1.3 shows the average energy consumption in a U.S. refinery. The three largest sources of energy are still gas (by-product gases reused in the plant), petroleum coke, and natural gas. Still gas and natural gas are particularly relevant here as they are commonly combusted in the types of equipment discussed in this book. Figure 1.4 shows that the

cost of fuel in U.S. refineries rose significantly between 2000 and 2005. This emphasizes the importance of energy-efficient combustion processes (see Chapter 12). Table 1.2 shows the largest sources of air emissions from various processes in a refinery.<sup>2</sup> Nearly all of them are related to combustion processes involving heaters and boilers. These emissions are discussed in detail in Chapters 14 and 15.

The hydrocarbon and petrochemical industries (see Chapter 2) present unique challenges to the combustion engineer, compared to other industrial combustion processes. One of the more important challenges is the wide variety of fuels, which are usually off-gases from

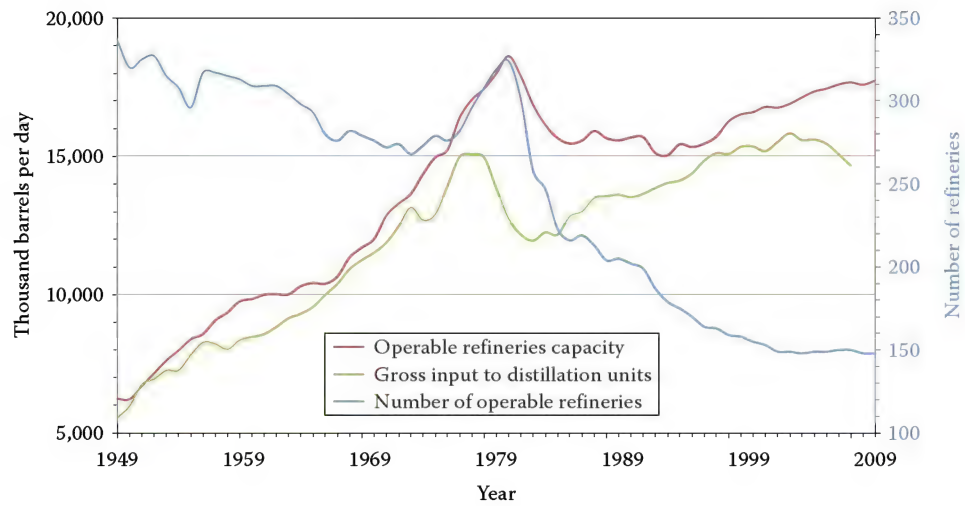


FIGURE 1.1

Operating refineries capacity and gross input (thousands of barrels per day) and number of operating refineries in the United States from 1949 to 2011. (Courtesy of Energy Information Administration, Washington, DC.)

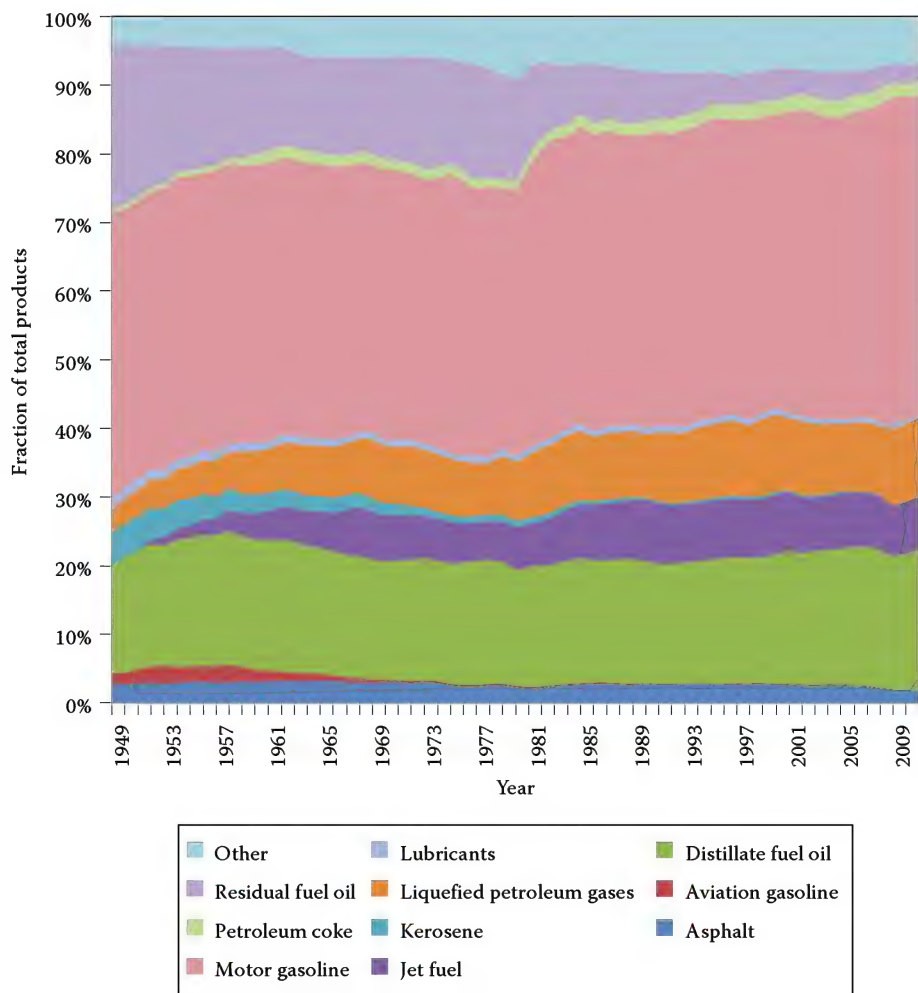


FIGURE 1.2

Product mix for U.S. refineries from 1949 to 2011. (Courtesy of Energy Information Administration, Washington, DC.)

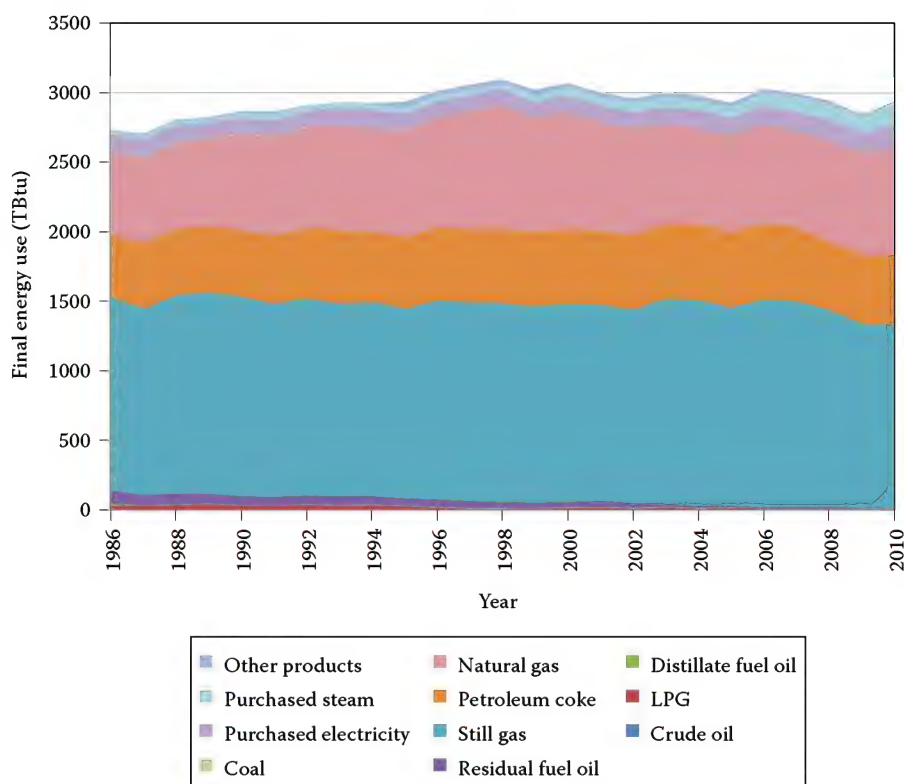


FIGURE 1.3

Annual final energy consumption for U.S. refineries from 1986 to 2010. (Courtesy of Energy Information Administration, Washington, DC.)

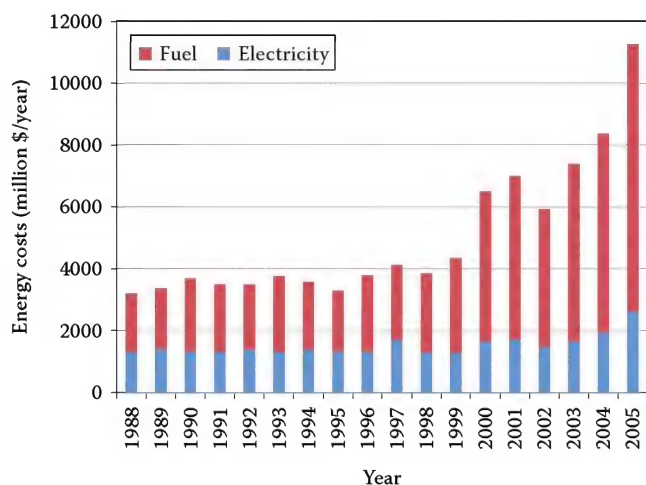


FIGURE 1.4

Energy cost for U.S. refineries from 1988 to 2005. (Courtesy of U.S. Census, Annual Survey of Manufacturers, Retrieved from [http://www.factfinder2.census.gov/faces/tableservices/jsf/pages/productview.xhtml?pid=ASM\\_2005\\_31GS104&prodType=table](http://www.factfinder2.census.gov/faces/tableservices/jsf/pages/productview.xhtml?pid=ASM_2005_31GS104&prodType=table).)

the petroleum refining processes that are used in a typical plant (see Figure 1.5). This differs significantly from most other industrial combustion systems that normally fire a single purchased fuel such as natural gas or fuel oil. Another important challenge is that many

of the burners commonly used in the hydrocarbon and petrochemical industries are natural draft, where the buoyant combustion exhaust products create a draft that induces the combustion air to enter the burners (see Chapter 9). This is different from nearly all other industrial combustion processes, which utilize a combustion air blower to supply the air used for combustion in the burner (see Volume 2, Chapter 3). Natural draft burners are not as easy to control as forced draft burners and are subject to environmental conditions such as the wind that can disturb the conditions in a process heater.

The U.S. Department of Energy Office of Industrial Technologies has prepared a Technology Roadmap for industrial combustion.<sup>3</sup> For process heating systems, some key performance targets for the year 2020 have been identified for burners and for the overall system. For the burners, the targets include reducing criteria pollutant emissions by 90%, reducing CO<sub>2</sub> emissions to levels agreed upon by the international community, reducing specific fuel consumption by 20%–50%, and maximizing the ability to use multiple fuels. For the heating system, the targets include reducing the total cost of combustion in manufacturing, enhancing system integration, reducing product loss rate by 50%, maximizing system robustness, and zero accidents.



TABLE 1.2

Summary of Emissions from Refinery Processes

Main Process	Subprocess	Largest Sources of Air Emissions
Topping/separation processes	Crude oil desalting	Heater stack gas (CO, SO <sub>x</sub> , NO <sub>x</sub> , hydrocarbons, and particulates)
	Crude distillation (atmospheric and vacuum)	Heater stack gas (CO, SO <sub>x</sub> , NO <sub>x</sub> , hydrocarbons, and particulates) and steam injector emissions (hydrocarbons)
Thermal and catalytic cracking processes	Visbreaking	Fugitive emissions from process vents
	Coking	Heater stack gas (CO, SO <sub>x</sub> , NO <sub>x</sub> , hydrocarbons, and particulates); particulate emissions from decoking can also be considerable
	Fluid catalytic cracking	Catalyst regeneration and CO boilers (hydrocarbons, CO, SO <sub>x</sub> , NO <sub>x</sub> , and particulates)
	Catalytic hydrocracking	Heater stack gas (CO, SO <sub>x</sub> , NO <sub>x</sub> , hydrocarbons, and particulates)
Combination/rearrangement processes	Alkylation	Process vents, fugitive emissions
	Catalytic reforming	Heater stack gas (CO, SO <sub>x</sub> , NO <sub>x</sub> , hydrocarbons, and particulates), fugitive emissions, and catalyst regeneration
	Isomerization	Boiler/heater stack gas (CO, SO <sub>x</sub> , NO <sub>x</sub> , hydrocarbons, and particulates), HCl (possible in fuel gas) vents, and fugitive emissions (hydrocarbons)
	Ethers manufacture	Boiler stack gas (CO, SO <sub>x</sub> , NO <sub>x</sub> , hydrocarbons, and particulates)
Treatment processes	Catalytic hydrotreating	Heater stack gas (CO, SO <sub>x</sub> , NO <sub>x</sub> , hydrocarbons, and particulates)
	Sweetening/Merox process	Vents and fugitive emissions
	Sulfur removal/Claus process	Process tail gas (NO <sub>x</sub> , SO <sub>x</sub> , hydrogen sulfide), fugitive emissions
Specialty products manufacture	Lubricating oil manufacture (deasphalting solvent extraction, dewaxing)	Heater stack gas (CO, SO <sub>x</sub> , NO <sub>x</sub> , hydrocarbons, and particulates), fugitive propane, and fugitive solvents

Source: Adapted from Pellegrino, J. et al., Energy and environmental profile of the U.S. petroleum refining industry, Report prepared for the U.S. Department of Energy, Washington, DC, November 2007, Tables 2.3 through 2.7.

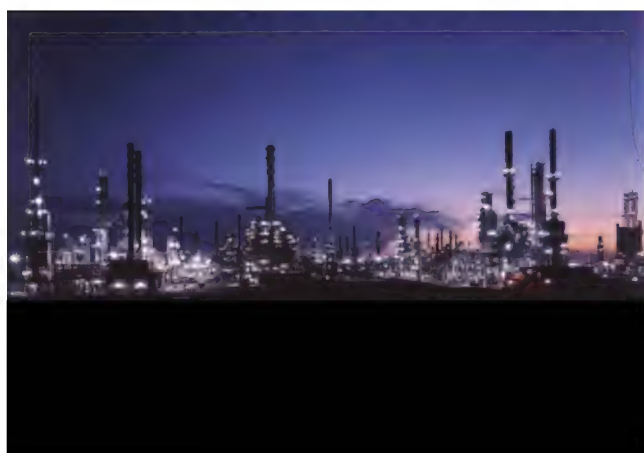


FIGURE 1.5  
Typical petroleum refinery.

The following were identified as top priority R&D needs in process heating: burner capable of adjusting operating parameters in real time, advanced burner stabilization methods, robust design tools, and economical methods to premix fuel and air. The following were

identified as top priority R&D needs in process heating: new furnace designs, advanced sensors, cost-effective heat recovery processes, and new methods to generate heat without environmental impact. Both the burners and the process heaters are considered in a number of chapters within this book.

Worrell and Galitsky<sup>4</sup> wrote, "Combustion is the key in many of the processes used in the refinery." They identified low NO<sub>x</sub> burners and high efficiency burners as major technology development areas for the petroleum refining industry. They further noted that 60% of all the fuel consumed in a refinery is used in heaters, furnaces, and boilers.<sup>5</sup>

Flares (see Figure 1.6 and Volume 3, Chapter 11) are used to combust unwanted hydrocarbon fuels, typically in the gaseous state. There are several conditions that may require flaring. The most common is in control of the process where gases or liquids are vented. Another is in an upset condition where materials in the midst of processing need to be safely combusted to avoid a dangerous build-up and unsafe conditions during the restart of the process. Another common reason is excess by-product fuels that cannot be economically



FIGURE 1.6  
Offshore oil rig flare.



FIGURE 1.7  
Flare pilot.

recovered during a transient condition such as a product change. Whatever the reason, flares must reliably combust fuels whenever they are called upon. One of the challenges for flares is maintaining a pilot flame (see Figure 1.7) to ignite the fuels (see Volume 3, Chapter 12), especially in very high wind conditions.<sup>6</sup> Another challenge is an extremely wide turndown ratio, because of the wide variety of venting conditions. Environmental challenges include minimizing the radiation heat load and noise to the surrounding environment and the NO<sub>x</sub>, CO, and particulate (smoke-producing) emissions to the atmosphere. Flares are covered in Volumes 2 and 3.

### 1.1.2 Power Generation

Duct burners and boiler burners are used in the power generation industries. Duct burners (see a typical flame in Figure 1.8) are burners that are inserted into large ducts (see Figure 1.9) to boost the temperature of the gases flowing through the ducts. These burners are frequently used in cogeneration projects, electrical utility peaking stations, repowering programs, and industrial mechanical driver systems employing gas turbines with site requirements for steam. They are also used in fluidized bed combustors and chemical process plants. The efficiency of a duct burner to supply additional heat approaches 95%, which is much higher than, for example, a backup boiler system in generating more steam. Duct burners are often easily retrofitted into existing ductwork. Several important factors in duct burner applications include: low pollutant emissions, safe operation,

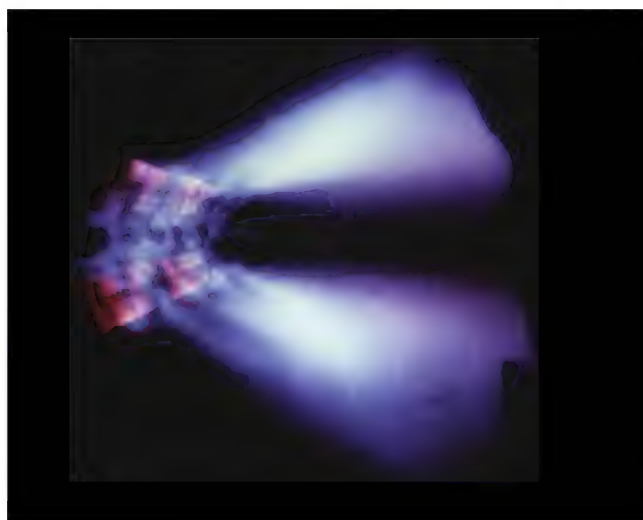


FIGURE 1.8  
Duct burner flame.

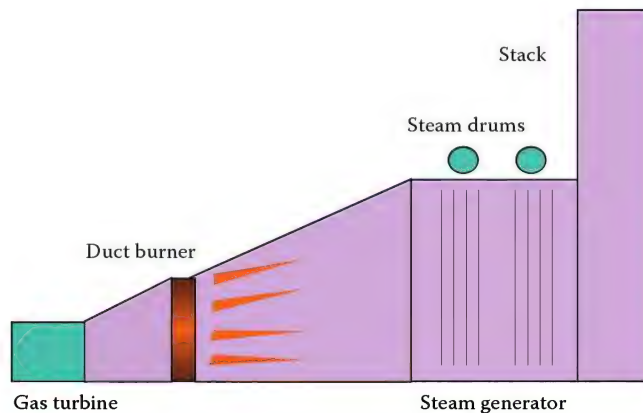


FIGURE 1.9  
Schematic of a duct burner used to enhance the power from a gas turbine.





**FIGURE 1.10**  
Front of a boiler burner.

uniform heat distribution from the duct burners to the gases flowing through the duct, getting uniform gas distribution through the duct burners, and having adequate turndown to meet fluctuating demands. Duct burners typically use gaseous fuels, but occasionally fire on oil.

Boiler burners (see Figure 1.10) are used to combust fuels, commonly natural gas or fuel oil, in the production of steam, which is often used to produce electrical energy for power generation. These burners produce radiation and convection used to heat water flowing through the boiler. The water is vaporized into steam. Sometimes the steam is used in the plant in the case of smaller industrial boilers. Larger utility boilers produce steam to drive turbines for electrical energy production. While boiler burners have been around for many years, there have been many design changes in recent years due to the current emphasis on minimizing pollutant emissions. Duct and boiler burners are discussed in Volume 3 of this Handbook.

### 1.1.3 Pollution Control

Thermal oxidizers (see Figure 1.11) are used to treat unwanted by-product materials that may be solids, liquids, or gases. The composition of the by-products varies widely and may range from minute quantities (e.g., parts per million [ppm]) of a contaminant up to 100%. These by-products come from a variety of industrial processes and often have some heating value, which aids in their thermal treatment.

There are often many options to choose from to eliminate the by-product materials. While the most



**FIGURE 1.11**  
Thermal oxidizer drawing.

preferable is recycling so that the by-products are reused in the process, this is not always an option in some processes. Land-filling may be an option for some of the solid waste materials. However, it is often preferable to completely destroy the waste in an environmentally safe way. Many other methods are possible, but thermal treatment is often the most economical and effective. The waste products must be treated in a way that any emissions from the treatment process must be below regulatory limits. Thermal oxidation is discussed in Volumes 2 and 3 of this Handbook.

Other processes used to control waste streams from the process industries are vapor control and biogas flaring (see Volume 3 for these topics). Figure 1.12 shows a photograph of a vapor combustion system used to



**FIGURE 1.12**  
Vapor combustor system.



**FIGURE 1.13**  
Biogas flare system.



**FIGURE 1.15**  
Flare gas recovery system.



**FIGURE 1.14**  
Vapor recovery system.

destroy waste streams such as volatile organics released during the off-loading of oil tankers. Figure 1.13 shows an example of a biogas flare system, where, for example, combustible gases such as methane released from a landfill are safely combusted rather than being released into the atmosphere. Figure 1.14 shows a vapor recovery where hydrocarbon gases are recovered instead of combusted. The recovered gases are normally recycled back into the process. Figure 1.15 shows a flare gas recovery system typically used in refineries and chemical plants to capture waste gases that would normally be sent to a flare for destruction. The recovered gases may be reused elsewhere in the plant or sold. This dramatically reduces the amount of gas flared.<sup>7</sup>

## 1.2 Literature Review

Numerous books are available on the subjects of both combustion and process industries. However, few books have been written on the combination of the two. This section briefly surveys some of the relevant literature on the subjects of combustion, the process industries, and the combination of combustion in those industries. Most of these combustion books are written at a highly technical level for use in upper level undergraduate or graduate level courses. The books typically have a broad coverage with less emphasis on practical applications due to the nature of their target audience.

### 1.2.1 Combustion

Many good textbooks are available on the fundamentals of combustion, which have little if anything on its use in the hydrocarbon and petrochemical industries.<sup>8–16</sup> Khavkin<sup>17</sup> has written a book that combines theory and practice on gas turbines and industrial combustion chambers. Of relevance here, the Khavkin book has a discussion of tube furnaces used in hydrogen production. Turns<sup>18</sup> book, which is designed for both undergraduate and graduate combustion courses, contains more discussions of practical combustion equipment than most similar books.

There have also been many books written on the more practical aspects of combustion. Griswold's<sup>19</sup> book



not only has a substantial treatment of the theory of combustion, but is also very practically oriented and includes chapters on gas burners, oil burners, stokers and pulverized coal burners, heat transfer (although brief), furnace refractories, tube heaters, process furnaces, and kilns. Stambuleanu's<sup>20</sup> book on industrial combustion has information on actual furnaces and on aerospace applications, particularly rockets. There are much data in the book on flame lengths, flame shapes, velocity profiles, species concentrations, and liquid and solid fuel combustion, with a limited amount of information on heat transfer. A book by Perthuis on industrial combustion has significant discussions on flame chemistry, and some discussion of heat transfer from flames.<sup>21</sup> Keating's<sup>22</sup> book on applied combustion is aimed at engines and has no treatment of industrial combustion processes. A recent book by Ragland and Bryden<sup>23</sup> attempts to bridge the gap between the theoretical and practical books on combustion. However, the book has little discussion about the types of industrial applications considered here. Even handbooks on combustion applications have little, if anything, on industrial combustion systems.<sup>24–28</sup> *Furnace Operations* by Robert Reed is the only book that has any significant coverage of combustion in the hydrocarbon and petrochemical industries. However, this book was last updated in 1981 and is more of an introduction to the subject with few equations, graphs, figures, pictures, charts, and references.

### 1.2.2 Process Industries

Anderson<sup>29</sup> has written a general introductory book on the petroleum industry, tracing its development from the beginning up to some projections for the future of oil. There is no specific discussion of combustion in petroleum refining. Leffler<sup>30</sup> has written an introductory book on the major processes in petroleum refining, including cat cracking, hydrocracking, and ethylene production among many others. The book is written from an overall process perspective and has no discussion of the heaters in a plant. Meyers<sup>31</sup> has edited a recently updated handbook on petroleum refining processes. The book is divided into 14 parts, each on a different type of overall process, including catalytic cracking and reforming, gasification and hydrogen production, hydrocracking, and visbreaking and coking, among others. Each part is further divided into the individual subtypes and variations of the given overall process. Companies such as Exxon, Dow-Kellogg, UOP, Stone & Webster, and Foster Wheeler have written about the processes they developed, which they license to other companies. Many aspects of the processes are discussed including flow diagrams, chemistry, thermodynamics, economics, and environmental considerations, but there is very little discussion of the

combustion systems. Gary et al.<sup>32</sup> have written a good overview of petroleum refining. The book discusses many of the processes involved in petroleum refining operations, including coking, catalytic cracking, and catalytic reforming, among others. However, it does not specifically discuss the combustion processes involved in heating the refinery fluids.

There are a number of excellent recommended practices published by the American Petroleum Institute related to combustion equipment in the hydrocarbon and petrochemical industries (see Table 1.3). These recommended practices contain specific guidelines for the design of equipment used in the petrochemical industry. For example, Section 14.1.1 of API 560 states the following:

Burner design, selection, spacing, location, installation, and operation shall ensure against flame impingement on tubes, tube supports and flame exiting the radiant section of the heater throughout the entire operating range of the burners. The location and operation of burners shall ensure complete combustion within the radiant section of the heater.

That standard further gives specific minimum clearance guidelines between burners (oil-fired and gas-fired), process tubes, and heater walls for both natural draft and forced draft operation. The standard also recommends materials of construction for the various components in a fired heater. Extensive and detailed data sheets are provided for all aspects of heater design. The guidelines in the API recommended practices have been formulated and periodically reviewed by industry experts in the particular subject area based on extensive experience with the equipment.

**TABLE 1.3**

Some American Petroleum Institute–Recommended Practices Related to Combustion Equipment

#	Title	Edition	Date
521	Pressure-relieving and depressuring systems	5th	January 2007
531M	Measurement of noise from fired process heaters	1st	March 1980
535	Burners for fired heaters in general refinery services	2nd	January 2006
536	Post-combustion NO <sub>x</sub> control for fired equipment in General Refinery Services	2nd	December 2006
537	Flare details for general refinery and petrochemical service	2nd	December 2008
556	Instrumentation, control, and protective systems for gas-fired heaters	2nd	April 2011
573	Inspection of fired boilers and heaters	2nd	February 2003



### 1.2.3 Combustion in the Process Industries

The standard book on the subject of combustion in the hydrocarbon and petrochemical industries that has been used for decades is *Furnace Operations* by Robert Reed, formerly the chief technical officer of John Zink.<sup>25</sup> This book gives a good introduction to many of the subjects important in burner and heater operation. However, it is somewhat outdated, especially with regard to pollution regulations and new trends in burner designs. The first edition of *The John Zink Hamworthy Combustion Handbook*<sup>33</sup> was designed to be a greatly expanded version of that book, with many more equations, figures, tables, references, and much wider coverage. The present edition updates the information from the first edition and adds new technologies and topics not covered in the first edition such as biogas flaring, vapor control, flare gas recovery, metallurgy, and refractories, among many others.

## 1.3 Fired Heaters

Fired or tubestill heaters are used in the petrochemical and hydrocarbon industries to heat fluids in tubes for further processing. In this type of process, fluids flow through an array of tubes located inside a furnace or heater. The tubes are heated by direct-fired burners that often use fuels that are by-products from processes in the plant and that vary widely in composition.

Using tubes to contain the load is somewhat unique compared to the other types of industrial combustion applications. It was found that heating the fluids in tubes has many advantages over heating them in the shell of a furnace.<sup>34</sup> Advantages include better suitability for continuous operation, better controllability, higher heating rates, more flexibility, less chance of fire, and more compact equipment.

One of the problems encountered in refinery-fired heaters is an imbalance in the heat flux in the individual heater passes.<sup>35</sup> This imbalance can cause high coke formation rates and high tube metal temperatures, which reduce a unit's capacity and can cause premature failures. Coke formation on the inside of the heater tubes reduces the heat transfer through the tubes that leads to the reduced capacity. One cause of coking is flame impingement directly on a tube, which causes localized heating and increases coke formation there. This flame impingement may be caused by operating without all of the burners in service, insufficient primary or secondary air to the burner, operating the heater at excessive firing rates, fouled burner tips, eroded burner tip orifices, or insufficient draft. The problem of flame impingement shows the importance

of proper design<sup>36</sup> to assure even heat flux distribution inside the fired heater.

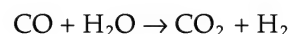
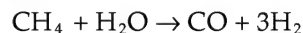
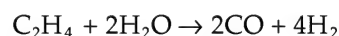
Recently, the major emphasis has been on increasing the capacity of existing heaters rather than installing new heaters. The limitations of over-firing a heater are

- High tube metal temperatures
- Flame impingement causing high coke formation rates
- Positive pressure at the arch of the heater
- Exceeding the capacity of induced-draft and forced-draft fans
- Exceeding the capacity of the process fluid feed pump

Garg<sup>37</sup> noted the importance of good heater specifications to ensure suitable performance for a given process. Some of the basic process conditions needed for the specifications include heater type (cabin, vertical cylindrical, etc.), number of fluid passes, the tube coil size and material, fluid data (types, compositions, properties, and flow rates), heat duty required, fuel data (composition, pressure, and temperature), heat flux loading (heat flux split between the radiant and convection sections), burner data (number, type, arrangement, etc.), draft requirement, required instrumentation, as well as a number of other details such as the number of peepholes, access doors, and platforms.

### 1.3.1 Reformers

As the name indicates, reformers are used to reformulate a material into another product. For example, a hydrogen reformer takes natural gas and reformulates it into hydrogen in a catalytic chemical process that involves a significant amount of heat. A sample set of reactions are given in the following for converting propane to hydrogen:<sup>38</sup>



The reformer is a direct-fired combustor containing numerous tubes, filled with catalyst, inside the combustor.<sup>39</sup> The reformer is heated with burners, firing either vertically downward, vertically upward, or horizontally, with the exhaust on the opposite end, depending on the specific design of the unit. The raw feed material flows through the catalyst in the tubes which, under the proper conditions, converts that material to the desired

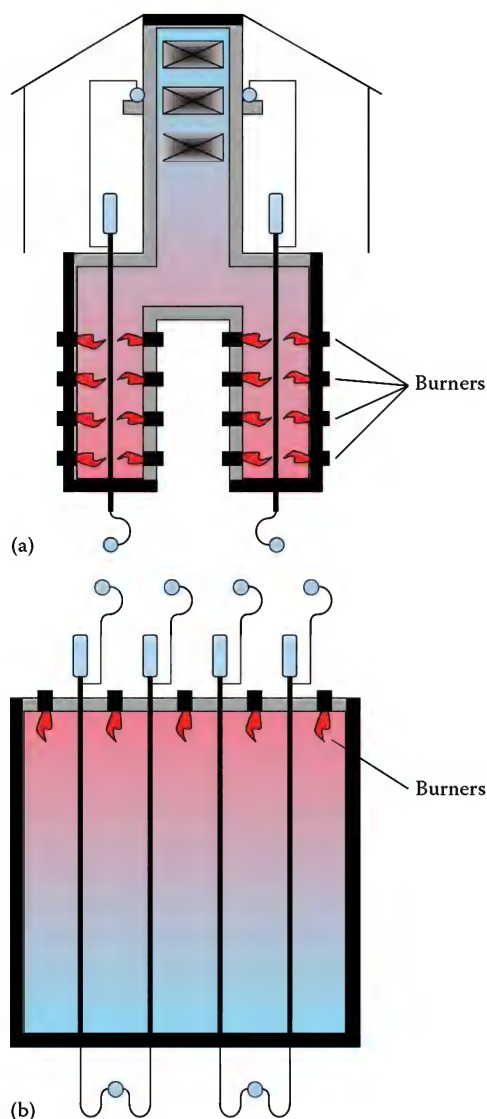


**FIGURE 1.16** Schematics of (a) side- and (b) top-fired reformers. (Adapted from Gunardson, H., *Industrial Gases in Petrochemical Processing*, Marcel Dekker, New York, 1998, p. 45, Figs 1 and 2.)

end product. The burners provide the heat needed for the highly endothermic chemical reactions. The fluid being reformulated typically flows through a reformer combustor containing many tubes (see Figure 1.16). The side-fired reformer has multiple burners on the side of the furnace with a single row of tubes centrally located. The heat is transferred primarily by radiation from the hot refractory walls to the tubes. Top-fired reformers have multiple rows of tubes in the firebox. In that design, the heat is transferred primarily from radiation from the flame to the tubes. Figure 1.17 shows a down-fired burner commonly used in top-fired reformers. In a design sometimes referred to as terrace firing, burners may be located in the side wall but be firing up the wall at a slight angle (see Figure 1.18). Foster Wheeler uses



**FIGURE 1.17** Down-fired burner commonly used in top-fired reformers.

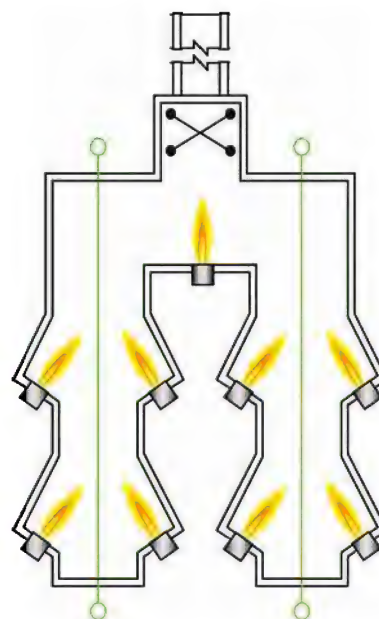


**FIGURE 1.18** Elevation view of a terrace-wall-fired furnace.

terrace wall reformers in the production of hydrogen by steam reformation of natural gas or light refinery gas.<sup>40</sup>

The reformer tubes are a critical element in the overall design of the reformer. Since they operate at pressures up to 350 psig (24 barg), they are typically made from a high temperature and pressure nickel alloy like incolon to ensure that they can withstand the operating conditions inside the reformer. Failure of the tubes can

be very expensive because of the downtime of the unit, lost product, damaged catalyst, and possibly, damaged reformer. New reactor technologies are being developed to improve the process for converting natural gas to precursor synthesis gas (syngas).<sup>41</sup>

### 1.3.2 Process Heaters

Process heaters are sometimes referred to as process furnaces or direct-fired heaters. They are heat transfer units designed to heat petroleum products, chemicals, and other liquids and gases flowing through tubes. Typical petroleum fluids include gasoline, naphtha, kerosene, distillate oil, lube oil, gas oil, and light ends.<sup>42</sup> The heating is done to raise the temperature of the fluid for further processing downstream or to promote chemical reactions in the tubes, often in the presence of a catalyst. Refinery heaters may carry liquids at temperatures as high as 1500°F (810°C) and pressures up to 1600 psig (110 barg). The primary modes of heat transfer in process heaters are radiation and convection. The initial part of the fluid heating is done in the convection section of the furnace, while the latter heating is done in the radiant section (see Figure 1.19). Each section has a bank of tubes in it where the fluids flow through, as shown in Figure 1.20.<sup>43</sup> Early heater designs had only a single bank of tubes that failed prematurely because designers did not understand the importance of radiation on the process.<sup>34</sup> The tubes closest to the burners would overheat. Overheating caused the hydrocarbons

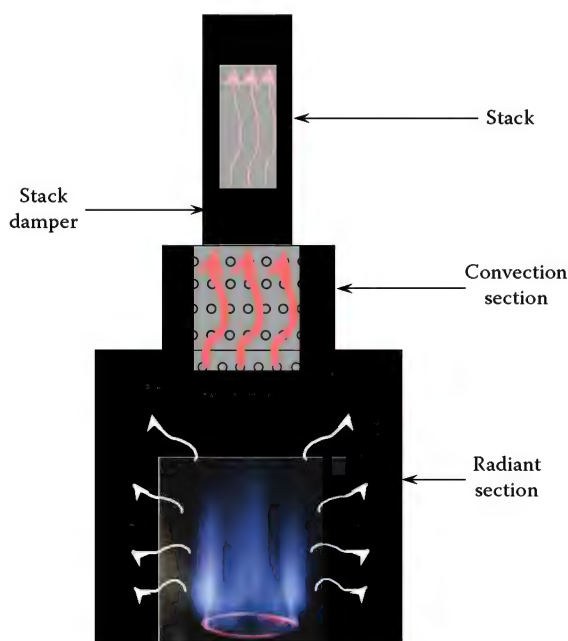


FIGURE 1.19

Schematic of a process heater. (Adapted from Lieberman, N.P., *Troubleshooting Process Operations*, PennWell Books, Tulsa, OK, 1991, p. 316, Fig. 15-1.)

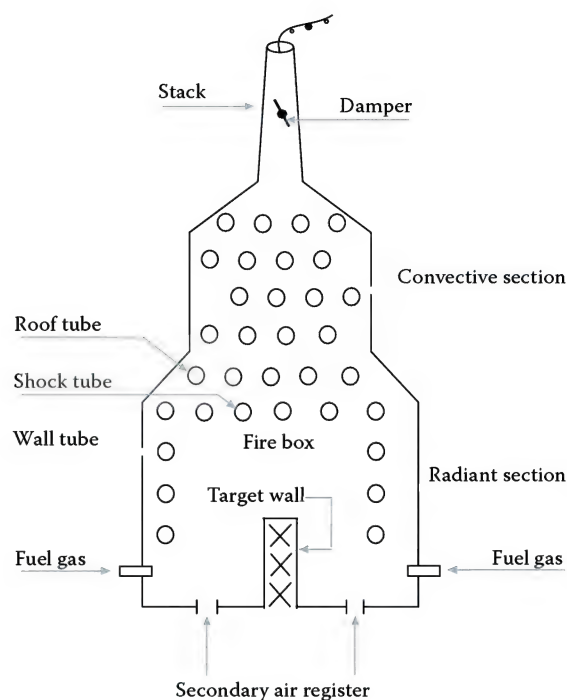


FIGURE 1.20

Schematic of a typical process heater. (Adapted from Sanderford, E.B., *Alternative control techniques document—NO<sub>x</sub> emissions from process heaters*, U.S. Environmental Protection Agency report EPA-453/R-93-015, February 1993, p. 3–11, Fig. 3-4.)

to form coke inside the tube. The coke further aggravated the problem by reducing the thermal conductivity through the coke layer inside the tube. The reduced thermal conductivity prevented the process fluids from absorbing adequate heat to cool the tubes, resulting in overheating and failure of the tubes. One of the key challenges for the heater designer is to get even heat distribution inside the combustor to prevent coking inside the tubes. Bell and Lowy<sup>44</sup> estimated that approximately 70% of the energy is transferred to the fluids in the radiant section of a typical heater and the balance in the convection section. The tubes in the convection section often have fins to improve convective heat transfer efficiency. These fins are designed to withstand temperatures up to about 1200°F (650°C). If delayed combustion occurs in the convection section, the fins can be exposed to temperatures up to 2000°F (1100°C), which can damage the fins.<sup>43</sup>

Process heaters are typically designed around the burners.<sup>42</sup> There may be anywhere from 1 to over 100 burners in a typical process heater, depending on the design and process requirements. In the refinery industry, the average number of burners in a heater varies by the heater type, as shown in Table 1.4.<sup>45</sup> On average, mechanical draft burners have higher firing rates than natural draft. For forced draft systems, burners with air preheat typically have higher heat releases than burners



TABLE 1.4

Average Burner Configuration by Heater Type

Heater Type	Average Number of Burners	Average Design Total Heat Release (10 <sup>6</sup> Btu/h)	Average Firing Rate per Burner (10 <sup>6</sup> Btu/h)
Natural draft	24	69.4	2.89
Mechanical draft, no air preheat	20	103.6	5.18
Mechanical draft, with air preheat	14	135.4	9.67

Source: From Sanderford, E.B., Alternative control techniques document—NO<sub>x</sub> emissions from process heaters, U.S. Environmental Protection Agency Report EPA-453/R-93-015, February, 1993.

without air preheat. According to one survey, 89.6% of the burners in oil refineries are natural draft, 8.0% are forced draft with no air preheat, and 2.4% are forced draft with air preheat.<sup>46</sup> The mean size of all process heaters is  $72 \times 10^6$  Btu/h (21 MW), which are mostly natural draft. The mean size of forced draft heaters is  $110 \times 10^6$  Btu/h (32 MW). Figure 1.21 shows the distribution for the overall firing rate for fired heaters.

Table 1.5 shows the major applications for fired heaters in the chemical industry. These can be broadly classified into two categories: (1) low- and medium-firebox temperature applications such as feed preheaters, reboilers, and steam superheaters and (2) high-firebox

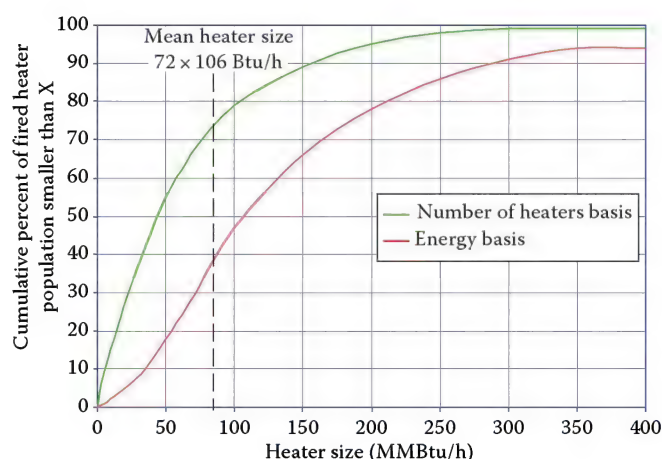


FIGURE 1.21

Fired heater size distribution. (From Sanderford, E.B., Alternative control techniques document—NO<sub>x</sub> emissions from process heaters, U.S. Environmental Protection Agency report EPA-453/R-93-015, February 1993.)

temperature applications such as olefins pyrolysis furnaces and steam-hydrocarbon reformers. The low- and medium-firebox temperature heaters represent about 20% of the chemical industry requirements and are similar to those in the petroleum refining industry.<sup>47</sup> The high-firebox temperature heaters represent the remaining 80% of the chemical industry heater requirements and are unique to the chemical industry.

TABLE 1.5

Major Fired Heater Applications in the Chemical Industry

Chemical	Process	Heater Type	Firebox Temperature (°F)	1985 Fired Heater Energy Requirement, (10 <sup>12</sup> Btu/year)	% of Known Chemical Industry Heater Requirements
<i>Low- and medium-temperature applications</i>					
Benzene	Reformate extraction	Reboiler	700	64.8	9.9
Styrene	Ethylbenzene dehydrogenation	Steam superheater	1500–1600	32.1	4.9
Vinyl chloride monomer	Ethylene dichloride cracking	Cracking furnace	N/A	12.6	1.9
P-xylene	Xylene isomerization	Reactor fired preheater	N/A	13.0	2.0
Dimethyl terephthalate	Reaction of p-xylene and methanol	Preheater, hot oil furnace	480–540	11.1	1.7
Butadiene	Butylene dehydrogenation	Preheater, reboiler	1100	2.6	0.4
Ethanol (synthetic)	Ethylene hydration	Preheater	750	1.3	0.2
Acetone	Various	Hot oil furnace	N/A	0.8	0.1
<i>High-temperature applications</i>					
Ethylene/propylene	Thermal cracking	Pyrolysis furnace	1900–2300	337.9	51.8
Ammonia	Natural gas reforming	Steam hydrocarbon reformer	1500–1600	150.5	23.1
Methanol	Hydrocarbon reforming	Steam hydrocarbon	1000–2000	25.7	4.0
<i>Total known fired heater energy requirement</i>				652.4	100.0

Source: Sanderford, E.B., Alternative control techniques document—NO<sub>x</sub> emissions from process heaters, U.S. Environmental Protection Agency Report EPA-453/R-93-015, February 1993.

Berman<sup>48</sup> discussed the different burner designs used in fired heaters. Burners may be located in the floor firing vertically upward. In vertical cylindrical (VC) furnaces, those burners are located in a circle in the floor of the furnace. The VC furnace itself serves as a part of the exhaust stack to help create draft to increase the chimney effect.<sup>49</sup> In cabin heaters, which are rectangular, there are one or more rows of burners located in the floor. Burners may be at a low-level firing parallel to the floor. In that configuration, they may be firing from two opposite sides toward a partial wall in the middle of the furnace that acts as a radiator to distribute the heat (see Figures 1.22 and 1.23). Burners may be located on the wall firing radially along the wall (see Figure 1.24), which are referred to as radiant wall burners. There are also combinations of these burners in certain heater designs. For example, in ethylene production heaters, both floor-mounted vertically fired

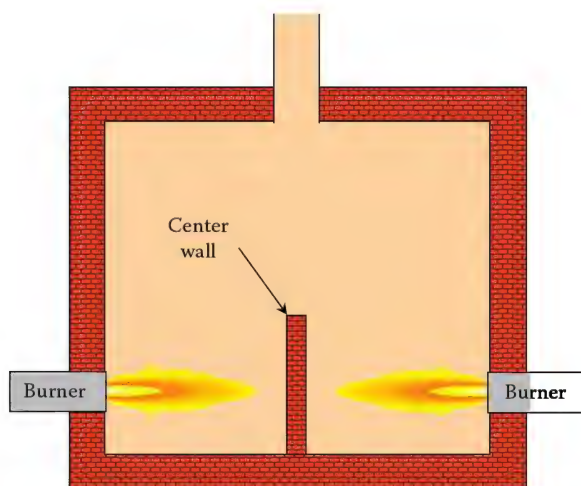


**FIGURE 1.22**  
Schematic of center or target wall firing configuration.



**FIGURE 1.23**  
Horizontal floor-fired burners firing toward a center wall.



**FIGURE 1.24**  
Wall-fired burner.

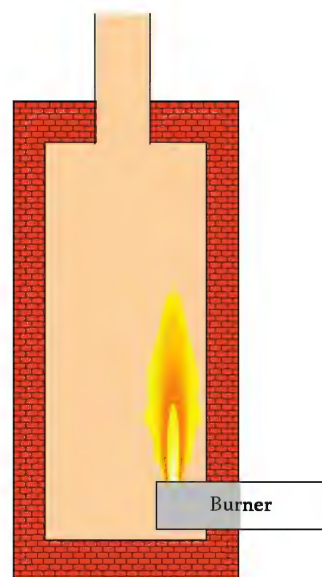


**FIGURE 1.25**  
Schematic of a horizontally mounted, vertically fired burner configuration.

burners (see Figure 1.25) and radiant wall burners are used in the same heater.

Typical examples of process heaters are shown in Figures 1.26 and 1.27. A cabin heater is shown in Figure 1.28. Burners firing in a crude unit are shown in Figure 1.29. Typical burner arrangements are shown in Figure 1.30. Berman<sup>50</sup> noted the following categories of process heaters: column reboilers, fractionating-column feed preheaters, reactor-feed preheaters including reformers, heat supplied to heat transfer media (e.g., a circulating fluid or molten salt), heat supplied to viscous fluids, and fired reactors including steam reformers and pyrolysis heaters. Six types of vertical-cylindrical fired heaters were given: all radiant, helical coil, cross flow with convection section, integral convection section, arbor or wicket type, and single-row/double-fired. Six basic designs were also given for horizontal tube-fired heaters: cabin, two-cell box,

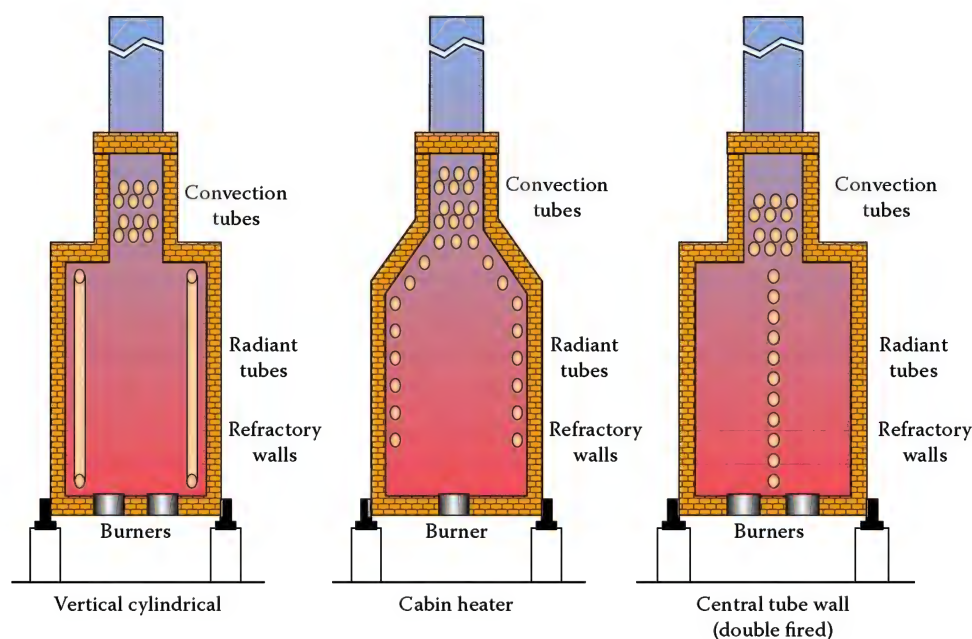


FIGURE 1.26

Examples of process heaters. (From Shires, G.L., Furnaces, in *The International Encyclopedia of Heat and Mass Transfer*, Hewitt, G.F., Shires G.L., and Polezhaev, Y.V. (eds.), pp. 493–497, CRC Press, Boca Raton, FL, 1997, p. 495, Figure 3.)

cabin with dividing bridgewall, end-fired box, end-fired box with side-mounted convection section and horizontal-tube/single-row/double-fired.

Many commonly used process heaters typically have a radiant section and a convection section. Burners are fired in the radiant section to heat up tubes. Fluids flow through the tubes and are heated to the desired temperature for further processing. The fluids are preheated in the convection section and heated to the desired process temperature in the radiant section. Radiant heat transfer from the flames to the tubes is the most critical aspect of this heater because overheating of the tubes leads to tube failure and shutdown of the heater.<sup>51</sup> The tubes may be horizontally or vertically oriented, depending on the particular heater design.

A unique aspect of process heaters is that they are often natural draft. This means that no combustion air blower is used. The air is inspired into the furnace by the suction created by the hot gases rising through the combustion chamber and exhausting to the atmosphere. Another unique aspect of these heaters is the wide range of fuels that are used which are often by-products of the petroleum refining process. These fuels may contain significant amounts of hydrogen, which has a large impact on the burner design. It is also fairly common for multiple fuel compositions to be used, depending on the operating conditions of the plant at any given time. In addition to hydrocarbons ranging up to  $C_5$ , the gaseous fuels may also contain hydrogen and inerts (like  $CO_2$  or  $N_2$ ).

The compositions can range from gases containing high levels of inerts to fuels containing high levels of  $H_2$ . The flame characteristics for fuels with high levels of inerts are very different than for fuels with high levels of  $H_2$  (see Chapter 3). Add to that the requirement for turndown conditions, and it becomes very challenging to design burners that will maintain stability, low emissions, and the desired heat flux distribution, over the range of conditions that are possible. Some plants use liquid fuels, like no. 2 to no. 6 fuel oil, sometimes by themselves and sometimes in combination with gaseous fuels. The so-called combination burners (see Figure 1.31) use both a liquid and a gaseous fuel, which are normally injected separately through each burner.

Shires gave a general heat balance for a process heater:<sup>52</sup>

$$\dot{Q}_f = \dot{Q}_g + \dot{Q}_l + \dot{Q}_p \quad (1.1)$$

where

$\dot{Q}_f$  is the heat generated by combusting the fuel

$\dot{Q}_g$  is the heat going to the load

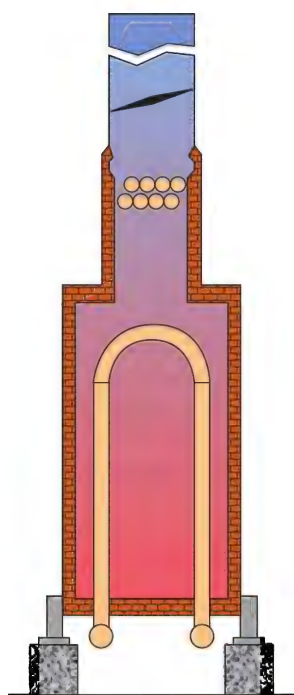
$\dot{Q}_l$  is the heat lost through the walls

$\dot{Q}_p$  is the heat carried out by the exhaust products

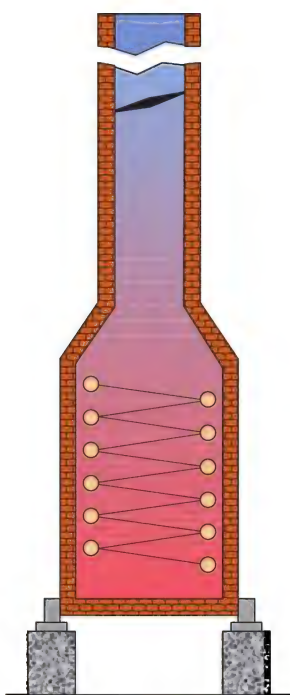
This is shown schematically in Figure 1.32.

Talmor<sup>53</sup> has written a book dealing with the prediction, control, and troubleshooting of hot spots in process heaters. The book gives a method for estimating

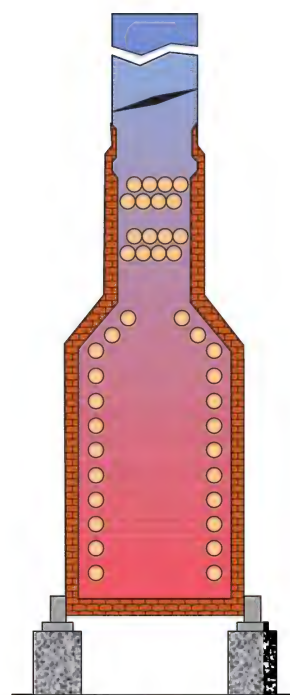




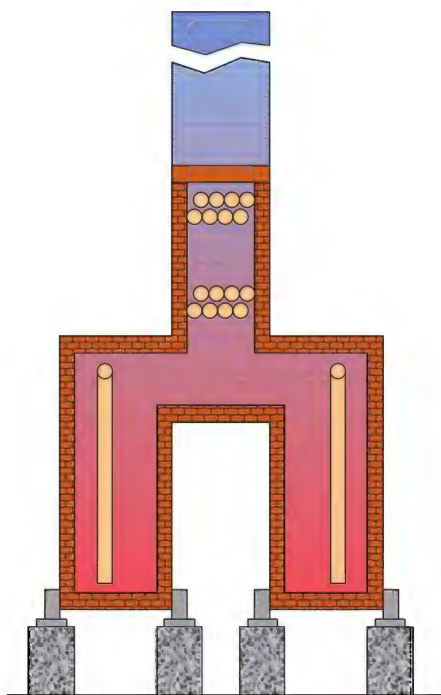
Type A -  
box heater with  
arbor coil



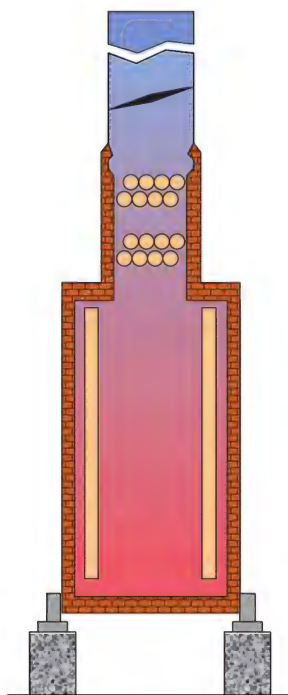
Type B -  
cylindrical heater  
with helical coil



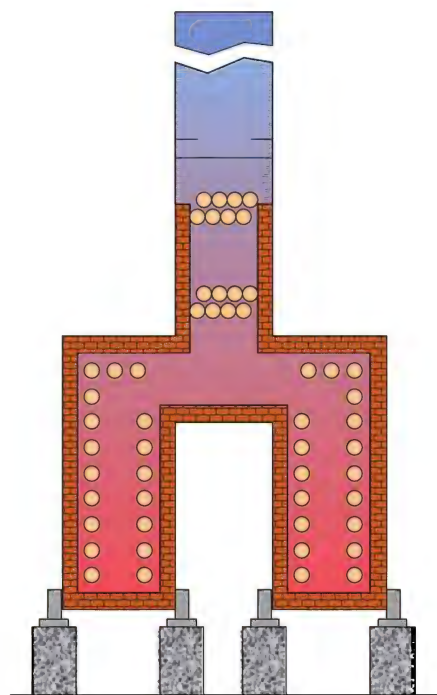
Type C -  
cabin heater with  
horizontal tube coil



Type D -  
box heater with  
vertical tube coil



Type E -  
cylindrical heater  
with vertical coil



Type F -  
box heater with  
horizontal tube coil

FIGURE 1.27

Typical heater types. (Adapted from API Publication 535, *Burner for Fired Heaters in General Refinery Services*, 1st Edition, American Petroleum Institute, Washington, DC, July 1995.)



FIGURE 1.28  
Cabin heater.

the magnitude and location of the maximum heat flux in the combustion zone. It takes into account the firing rate of each burner, the number of burners, the flame length, the flame emissivity, the spacing between the burner and the tubes, the spacing between the burners, and the geometry of the firebox. The book includes much empirical data specific to a variety of different process heaters and also gives many detailed examples that have been worked out.

---

## 1.4 Burners

The burner is the device that is used to combust the fuel with an oxidizer to convert the chemical energy in the fuel into thermal energy. A given combustion system may have a single burner or many burners,

depending on the size and type of the application. For example, in a vertical cylindrical furnace, one or more burners are located in the floor of a cylindrically shaped furnace (see Figure 1.33). The heat from the burner radiates in all directions and is efficiently absorbed by the tubes. Another type of heater geometry is rectangular (see Figure 1.34). This type of system is generally more difficult to analyze because of the multiplicity of heat sources and because of the interactions between the flames and their associated products of combustion.

There are many factors that go into the design of a burner.<sup>54</sup> This section will briefly consider some of the important factors that are taken into account for a particular type of burner, with how those factors impact things like heat transfer and pollutant emissions. Burner design is discussed in detail in Volume 2 of this Handbook.





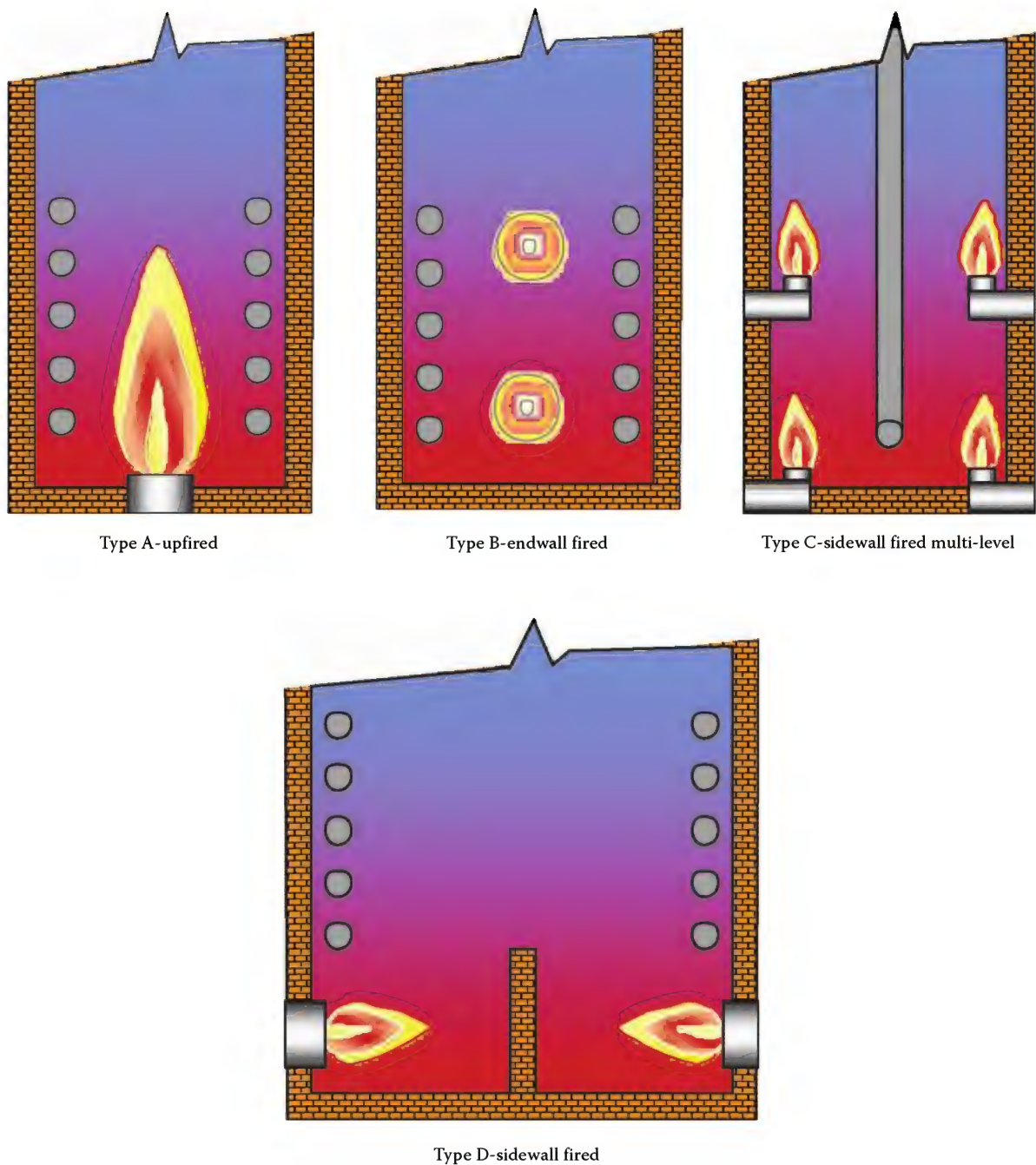
FIGURE 1.29  
Crude unit burners.

#### 1.4.1 Competing Priorities

There have been many changes in the traditional designs used in burners, primarily because of the interest in reducing pollutant emissions. In the past, the burner designer was primarily concerned with efficiently combusting the fuel and transferring the energy to a heat load. New and increasingly more stringent environmental regulations have added the need to consider the pollutant emissions produced by the burner. In many cases, reducing pollutant emissions and maximizing combustion efficiency are at odds with each other. For example, a well-accepted technique for reducing NO<sub>x</sub> emissions is known as staging, where the primary flame zone is deficient of either fuel or oxidizer (see Chapter 15).<sup>55,56</sup> The balance of the fuel or oxidizer may be injected into the burner in a secondary flame zone or, in a more extreme case, may be injected somewhere else in the combustion chamber. Staging reduces the peak temperatures in the primary flame zone and also alters the chemistry in a way that reduces NO<sub>x</sub> emissions because fuel-rich or fuel-lean zones are less conducive to NO<sub>x</sub> formation than near

stoichiometric zones. NO<sub>x</sub> emissions increase rapidly with the exhaust product temperature (see Figure 15.8). Since thermal NO<sub>x</sub> is exponentially dependent on the gas temperature (see Chapter 15), even small reductions in the peak flame temperature can dramatically reduce NO<sub>x</sub> emissions. However, lower flame temperatures often reduce the radiant heat transfer from the flame since radiation is dependent on the fourth power of the absolute temperature of the gases. Another potential problem with staging is that it may increase CO emissions (see Chapter 14), which is an indication of incomplete combustion and reduced combustion efficiency. However, it is also possible that staged combustion may produce soot in the flame, which can increase flame radiation. The actual impact of staging on the heat transfer from the flame is highly dependent on the actual burner design.

In the past, the challenge for the burner designer was to maximize the mixing between the fuel and the oxidizer to ensure complete combustion. If the fuel was difficult to burn, as in the case of low heating value fuels such as waste liquid fuels or process gases from

**FIGURE 1.30**

Typical burner arrangements. (Adapted from API Publication 535, *Burner for Fired Heaters in General Refinery Services*, 1st Edition, American Petroleum Institute, Washington, DC, July 1995.)

chemical production, the task could be very challenging. Now, the burner designer must balance the mixing of the fuel and the oxidizer to maximize combustion efficiency while simultaneously minimizing all types of pollutant emissions. This is no easy task as, for example, NO<sub>x</sub> and CO emissions often go in opposite directions (see Figure 1.35). When CO is low, NO<sub>x</sub> may be high and vice versa. Modern burners must be environmentally

friendly, while simultaneously efficiently transferring heat to the load.

#### 1.4.2 Design Factors

There are many types of burner designs that exist due to the wide variety of fuels, oxidizers, combustion chamber geometries, environmental regulations,

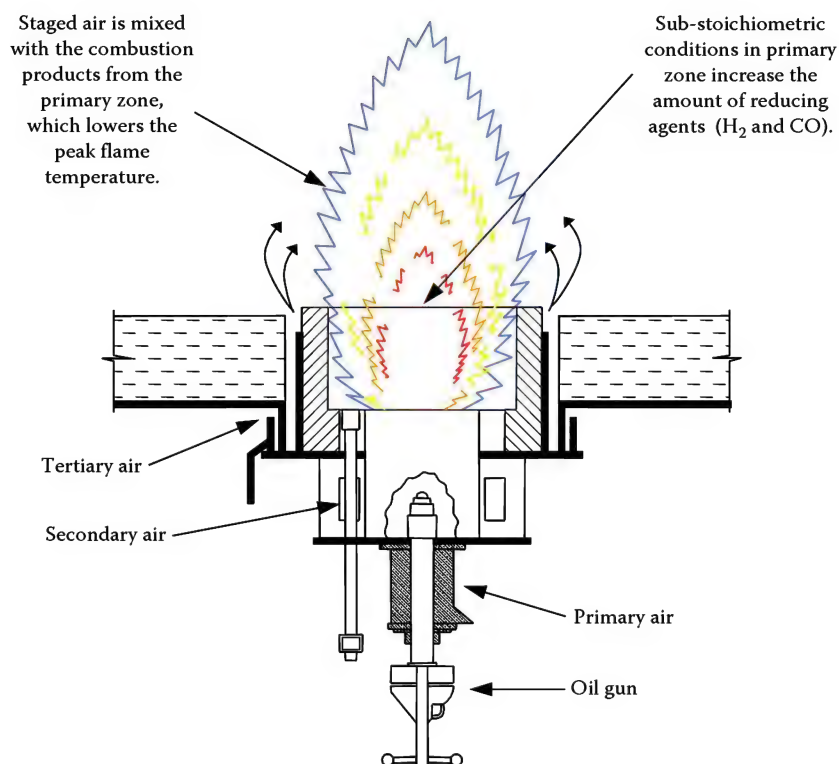


**FIGURE 1.31**  
Drawing of a typical combination oil and gas burner.

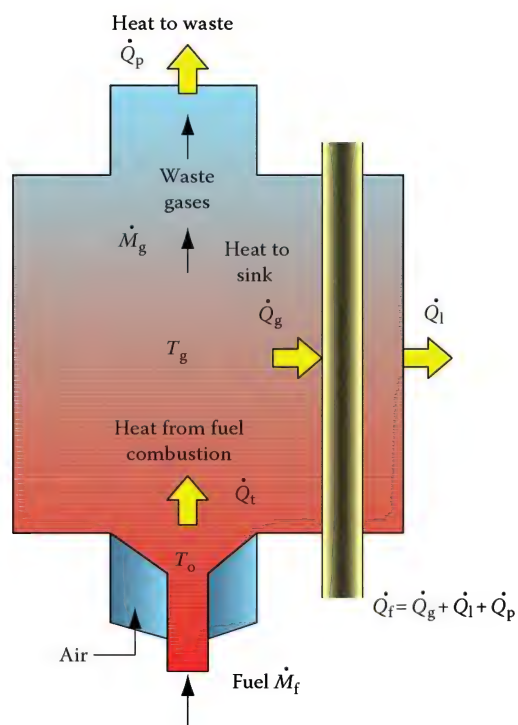


**FIGURE 1.32**  
Process heater heat balance. (Adapted from Shires, G.L., Furnaces, in *The International Encyclopedia of Heat and Mass Transfer*, Hewitt, G.F., Shires G.L., and Polezhaev, Y.V. (eds.), pp. 493–497, CRC Press, Boca Raton, FL, 1997.)

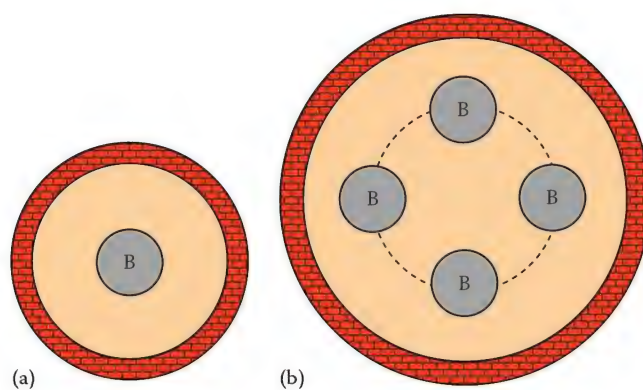


**FIGURE 1.33**  
Schematic of a burner (B) arrangement in the floor of vertical cylindrical furnaces: (a) small diameter furnace with a single centered burner and (b) larger diameter furnace with four burners symmetrically arranged at a radius from the centerline.

thermal input sizes, and heat transfer requirements. Additionally, heat transfer requirements include flame temperature, flame momentum, and heat distribution. Garg<sup>57</sup> lists the following burner specifications that are needed to properly choose a burner for a given application: burner type, heat release and turndown, air supply (natural draft, forced draft, or balanced draft), excess air level, fuel composition(s), firing position, flame dimensions, ignition type, atomization media for liquid fuel



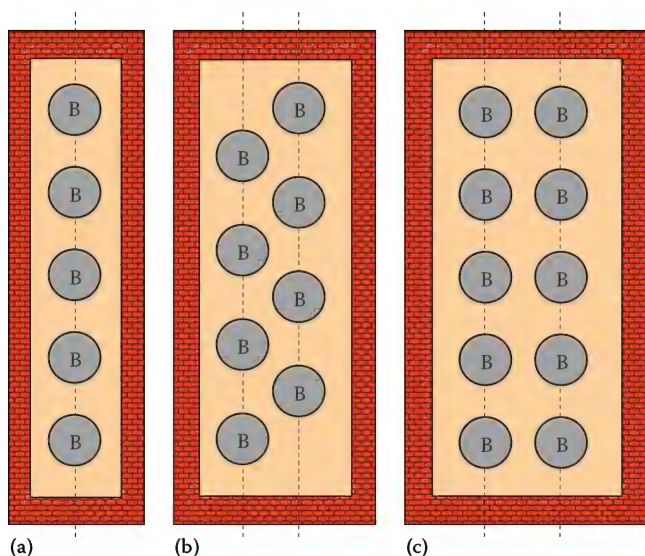


FIGURE 1.34

Schematic of a burner (B) arrangement in the floor of rectangular cabin heaters: (a) single row of burners in a narrower heater, (b) two rows of staggered burners in a slightly wider heater, and (c) two rows of parallel burners in an even wider heater.

firing, noise, NO<sub>x</sub> emission rate, and whether waste gas firing will be used. Some of these design factors are briefly considered in the following sections.

#### 1.4.2.1 Fuel

Depending upon many factors, certain types of fuels are preferred for certain geographic locations due to cost and availability considerations. Gaseous fuels, particularly

natural gas, are commonly used in most industrial heating applications in the United States. In Europe, natural gas is also commonly used along with light fuel oil. In Asia and South America, heavy fuel oils are generally preferred although the use of gaseous fuels is on the rise.

Fuels also vary depending on the application. For example, in incineration processes, waste fuels are commonly used either by themselves or with other fuels like natural gas. In the petrochemical industry, fuel gases often consist of a blend of several fuels, including gases like hydrogen, methane, propane, butane, propylene, nitrogen, and carbon dioxide (see Chapter 3).

The fuel has an important influence on the heat transfer from a flame (see Chapter 7). In general, solid fuels like coal and liquid fuels like oil produce very luminous flames, which contain soot particles that radiate like blackbodies to the heat load. Gaseous fuels like natural gas often produce nonluminous flames because they burn so cleanly and completely without producing many soot particles. A fuel such as hydrogen is completely nonluminous as there is no carbon available to produce soot.

In cases where highly radiant flames are required, a luminous flame is preferred. In cases where convection heat transfer is preferred, a nonluminous flame may be preferred in order to minimize the possibility of contaminating the heat load with soot particles from a luminous flame. Where natural gas is the preferred fuel and highly radiant flames are desired, new technologies are being developed to produce more luminous flames. These include things like pyrolyzing the fuel in a partial oxidation process,<sup>58</sup> using a plasma to produce soot in the fuel,<sup>59</sup> and generally controlling the mixing of the

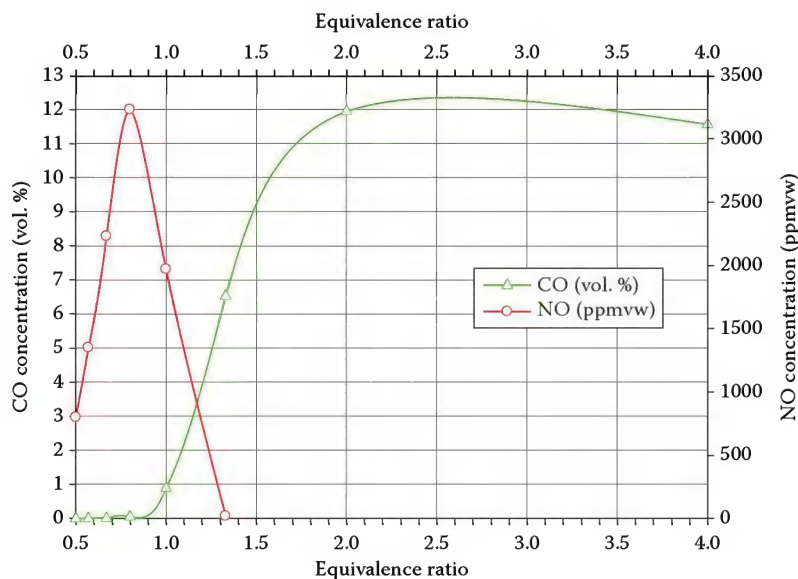


FIGURE 1.35

Adiabatic equilibrium NO and CO as a function of the equivalence ratio for an air/CH<sub>4</sub> flame.

fuel and oxidizer to produce fuel-rich flame zones that generate soot particles.<sup>60</sup>

Therefore, the fuel itself has a significant impact on the heat transfer mechanisms between the flame and the load. In most cases, the fuel choice is dictated by the customer as part of the specifications for the system and is not chosen by the burner designer. The designer must make the best of whatever fuel is being used. In most cases, the burner design is optimized based on the choice of the fuel.

In some cases, the burner may have more than one type of fuel. An example is shown in Figure 1.31.<sup>61</sup> Dual-fuel burners are designed to operate typically on either gaseous or liquid fuels. These burners are used, usually for economic reasons, where the customer may need to switch between a gaseous fuel such as natural gas and a liquid fuel such as oil. These burners normally operate on one fuel or the other, and sometimes on both fuels simultaneously. Another application where multiple fuels may be used is in waste incineration. One method of disposing of waste liquids contaminated with hydrocarbons is to combust them by direct injection through a burner. The waste liquids are fed through the burner, which is powered by a traditional fuel such as natural gas or oil. The waste liquids often have very low heating values and are difficult to combust without auxiliary fuel. This further complicates the burner design where the waste liquid must be vaporized and combusted concurrently with the normal fuel used in the burner.

#### 1.4.2.2 Oxidizer

The predominant oxidizer used in most industrial heating processes is atmospheric air. This can present challenges in some applications where highly accurate control is required due to the daily variations in the temperature, barometric pressure, and humidity of ambient air. The combustion air is sometimes preheated to increase the overall thermal efficiency of a process. Combustion air is also sometimes blended with some of the products of combustion—a process usually referred to as flue gas recirculation (FGR).

FGR is used to both increase thermal efficiency and reduce NO<sub>x</sub> emissions (see Chapter 15). Capturing some of the energy in the exhaust gases and using it to preheat the incoming combustion oxidizer increases thermal efficiency. FGR also reduces peak flame temperatures resulting in reduced NO<sub>x</sub> emissions, since NO<sub>x</sub> emissions are highly temperature dependent.

Another type of oxidizer sometimes used in process heaters is turbine exhaust gas which as the name implies is gas coming from the exhaust of a gas turbine. This exhaust gas generally has between 13% and 17% O<sub>2</sub> and is at temperatures between 850°F and 1050°F (450°C and 566°C).<sup>61</sup> Burners are specially designed for this type of oxidizer where flame stability becomes an issue at lower levels of O<sub>2</sub> content in the exhaust gas.

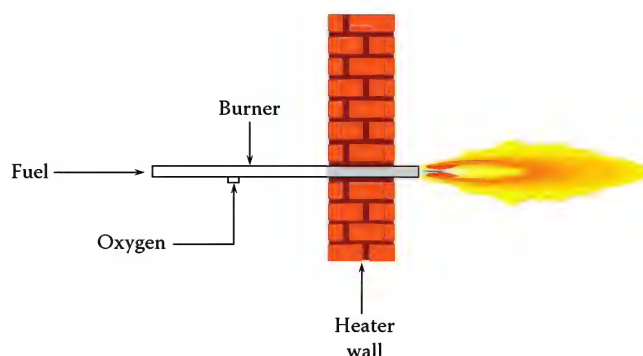


FIGURE 1.36  
Schematic of an oxy/fuel burner.

The use of pure oxygen as the oxidizer in industrial combustion processes has been used for many years.<sup>62</sup> This includes using high purity oxygen as the sole oxidizer (see Figure 1.36), as well as using both air and oxygen as the oxidizer. Mixing oxygen into an air stream for combustion is referred to as *oxygen enrichment* (see Figure 1.37). Oxygen-enhanced combustion technology has generally not been economically viable in lower temperature applications such as process heaters and boilers. However, because of the increased interest in capturing CO<sub>2</sub> emissions from combustion processes, the use of oxygen is now being considered in a wide range of applications that were previously uneconomical, including process heaters and boilers. For example, oxygen enrichment is being considered for use in steam methane reformers<sup>63</sup> and oxygen blended with recirculated combustion products in a process heater (see Figure 1.38).<sup>64</sup> At the time of this writing, the use of oxygen in process heaters is in its infancy but is expected to grow in popularity.

#### 1.4.2.3 Gas Recirculation

A common technique used in combustion systems is to design the burner to induce furnace gases to be drawn into the burner to dilute the flame, usually referred to

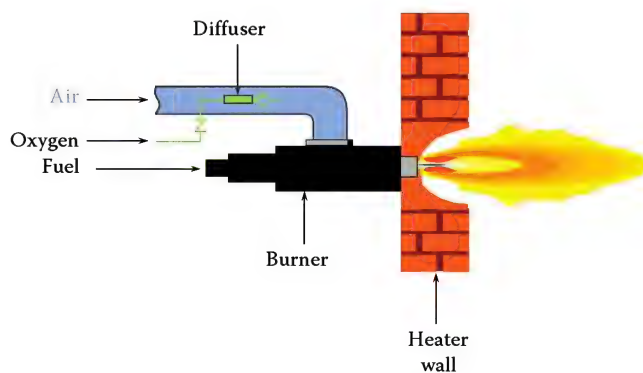
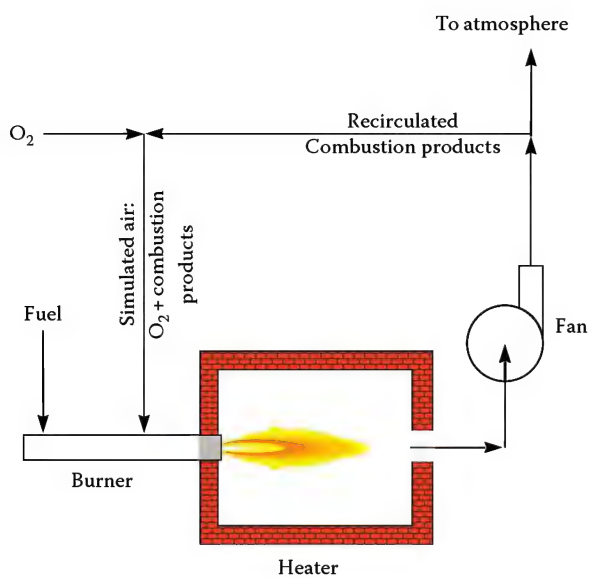


FIGURE 1.37  
Schematic of an oxygen-enriched air/fuel burner.





**FIGURE 1.38**  
Schematic a burner using oxygen + recycled combustion products.

as flue or furnace gas recirculation. Even though the furnace gases are hot, they are still much cooler than the flame itself. This dilution may accomplish several purposes. One is to minimize NO<sub>x</sub> emissions by reducing the peak temperatures in the flame, as in flue gas recirculation. However, furnace gas recirculation may be preferred to flue gas recirculation (see Figure 1.39) because no external high temperature ductwork or fans are needed to bring the product gases back into the flame zone. Another reason to use furnace gas recirculation may be to increase the convective heating from the flame because of the added gas volume and momentum. An example of a burner designed to entrain furnace gases into the flame is shown in Figure 1.40.

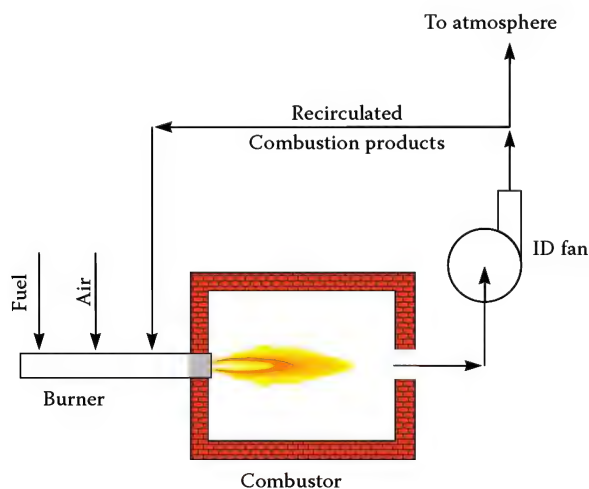
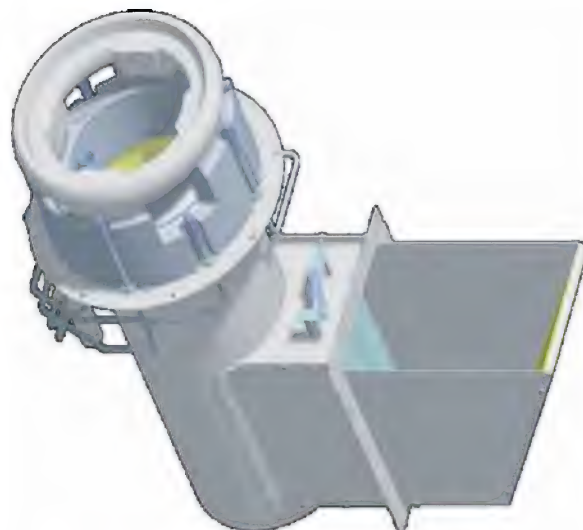


**FIGURE 1.39**  
Schematic of flue gas recirculation.



(a)



(b)

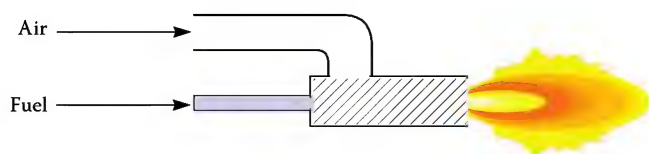
**FIGURE 1.40**  
HALO<sup>TM</sup> burner designed to entrain furnace gases into the flame  
(a) 3D model of burner (b) Photo of burner top and flame.

### 1.4.3 General Burner Types

There are numerous ways that burners can be classified. Some of the common ones are discussed in this section along with a brief description of implications for heat transfer.

#### 1.4.3.1 Mixing Type

One common method for classifying burners is according to how the fuel and the oxidizer are mixed. In pre-mixed burners, shown as a schematic in Figure 1.41 and

**FIGURE 1.41**

Schematic of a premix burner.

as a drawing in Figure 1.42, the fuel and the oxidizer are completely mixed before combustion begins. Radiant wall burners usually are of the premixed type. Premixed burners often produce shorter and more intense flames, compared to diffusion flames. This type of flame is often preferred in, for example, ethylene cracking furnaces because the radiant wall burners are close to the process tubes. This can produce high temperature regions in the flame leading to nonuniform heating of the load and higher NO<sub>x</sub> emissions.

In diffusion-mixed flames, the fuel and the oxidizer are separated and unmixed prior to combustion, which begins where the oxidizer/fuel mixture is within the flammability range. An example of a diffusion flame is a candle (see Figure 1.43). A diffusion-mixed gas burner is shown schematically in Figure 1.44. This is sometimes referred to as a “nozzle-mix” or “raw gas” burner because the fuel gas exits the burner essentially as raw gas having no air mixed with it. Diffusion burners typically have longer flames than premixed burners, a lower temperature hot spot, and a more uniform temperature and heat flux distribution.

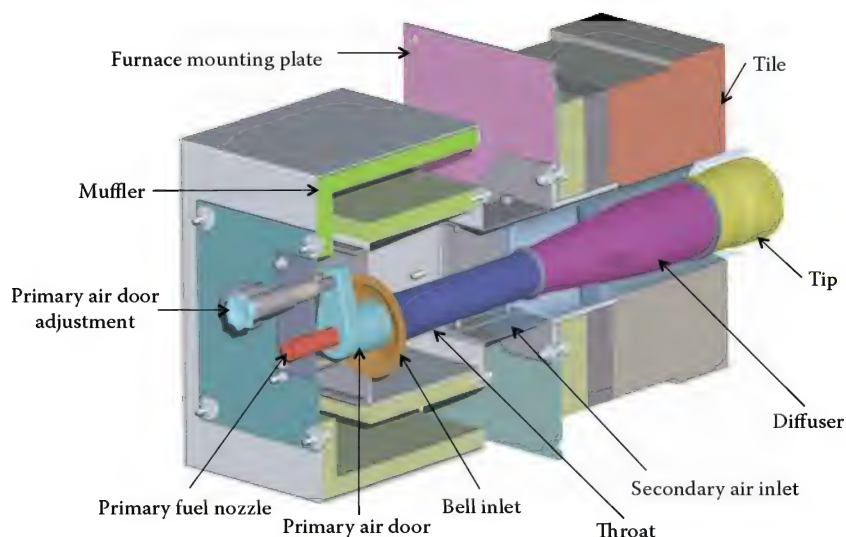
It is also possible to have partially premixed burners, shown schematically in Figure 1.45, where some fraction of the fuel is mixed with the oxidizer. Partial premixing is often done for stability and safety reasons since it not only helps anchor the flame, but also reduces the chance for flashback (see Chapter 1 in Volume 2), which is sometimes a problem in fully premixed burners. This

**FIGURE 1.43**

Painting of a diffusion flame. (Courtesy of the Los Angeles County Museum of Art, Los Angeles, CA.)

type of burner often has a flame length, temperature, and heat flux distribution that is somewhere between the fully premixed and diffusion flames.

Another burner classification based on mixing is known as staging—staged air and/or staged fuel. A staged air

**FIGURE 1.42**

Drawing of a typical premix (radiant wall) gas burner.





**FIGURE 1.44**  
Schematic of a diffusion burner.

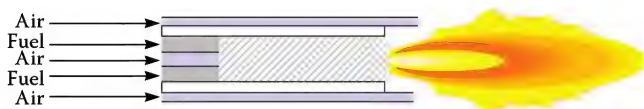


**FIGURE 1.45**  
Schematic of a partially premixed burner.

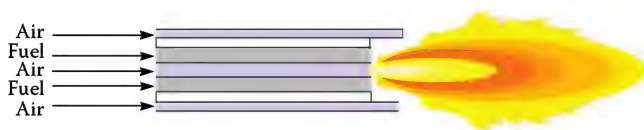


**FIGURE 1.46**  
Schematic of a staged-air burner.

burner is shown in a schematic in Figure 1.46 and in a drawing in Figure 1.47. A staged fuel burner is shown in a schematic in Figure 1.48 and in a drawing in Figure 1.49. Secondary and sometimes tertiary injectors in the burner are used to inject a portion of the fuel and/or the air into the flame, downstream of the base of the flame. Staging is often done to reduce NO<sub>x</sub> emissions and to produce longer flames (see Chapter 15). These longer flames typically

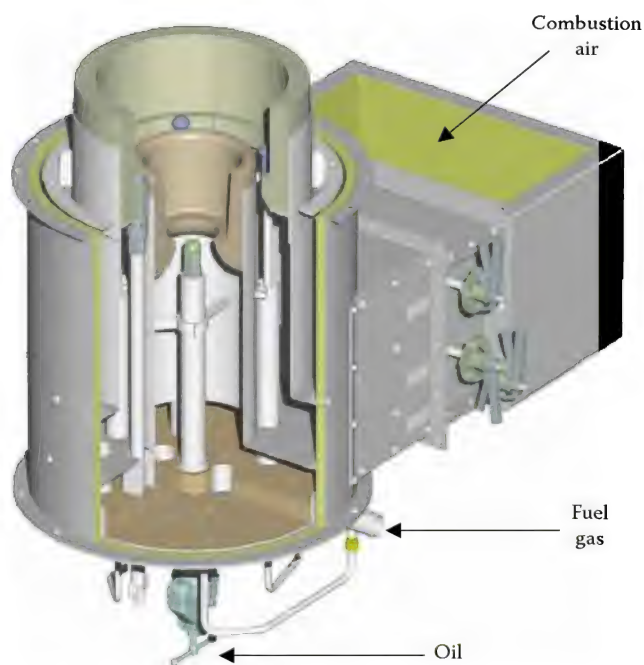


**FIGURE 1.47**  
Drawing of a typical staged-air combination oil and gas burner.

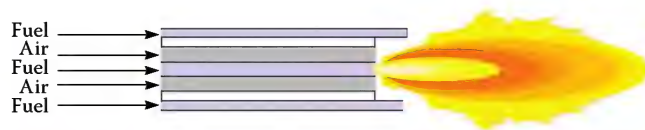


**FIGURE 1.48**  
Schematic of a staged-fuel burner.

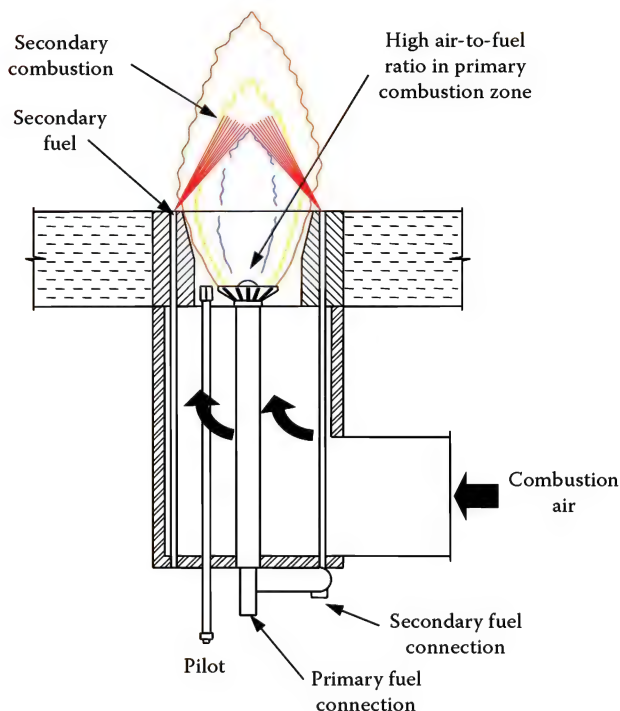


**FIGURE 1.49**  
Drawing of a typical staged-fuel gas burner.

have a lower peak flame temperature and more uniform heat flux distribution than nonstaged flames.

### 1.4.3.2 Fuel Type

There are three common fuel classifications for burners used in the process industries which are generally listed in order of increasing complexity as follows: gas, oil, or a combination of gas and oil. Gas burners are either diffusion (raw gas or no premixing), premixed, or partially premixed. The gas composition can vary widely as it is often a by-product from the plant. Burners often need to be able to fire multiple fuels that may be produced by the plant depending on the process conditions and depending on start-up versus normal operation. These gaseous fuels, typically referred to as refinery fuel gases, often have significant amounts of methane, hydrogen, and higher hydrocarbons like propane and propylene (see Chapter 3). They may also contain inerts like CO<sub>2</sub> and N<sub>2</sub>. The heating value may range from 500 to 1500 Btu/ft<sup>3</sup> (19–56 MJ/m<sup>3</sup>). Burners firing oil require some type of liquid atomization (see Chapter 10), commonly



mechanical (pressurizing the liquid high enough to force it through an atomizer), air, or steam. Steam is the most commonly used because it is economical, readily available, gives a wide turndown ratio, and gives good flame control. Combination burners can usually fire 100% oil, 100% gas, or any combination in between.

### 1.4.3.3 Combustion Air Temperature

Another way commonly used to classify the oxidizer is by its temperature. It is common in many industrial applications to recover heat from the exhaust gases by preheating the incoming combustion air, either with a recuperator or a regenerator. Such a burner is often referred to as a preheated air burner. This is typically done for forced draft burners in what is referred to as a balanced draft system.

### 1.4.3.4 Draft Type

Most industrial burners are known as forced-draft or mechanical-draft burners. This means that the oxidizer is supplied to the burner under pressure. For example, in a forced-draft air burner, the air used for combustion is supplied to the burner by a blower (see Volume 2, Chapter 3). In natural-draft burners, the air used for combustion is induced into the burner by the negative draft produced in the combustor. A drawing is shown in Figure 1.50 and a photo is shown in Figure 1.51. In this type of burner, the pressure drop and combustor stack height are critical in producing enough suction to induce enough combustion air into the burners. This type of burner is commonly

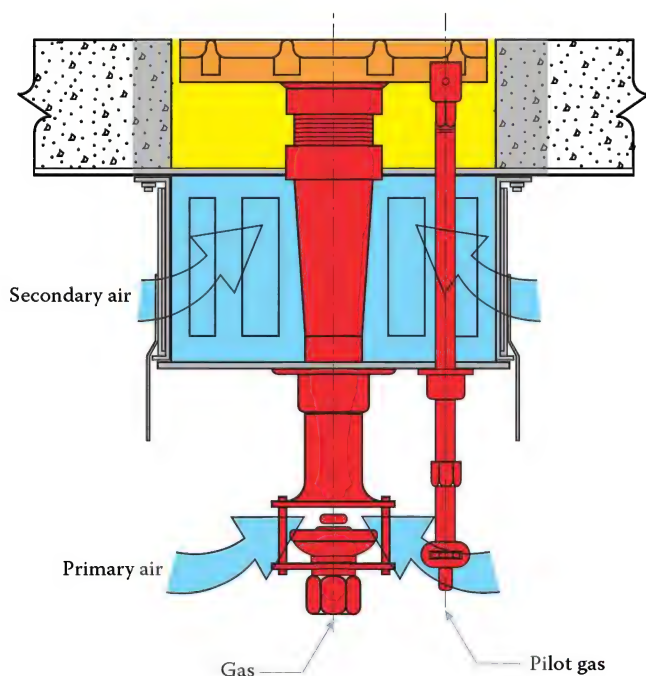


FIGURE 1.50  
Drawing of a typical natural draft gas burner.



FIGURE 1.51  
Natural draft burner.

used in the chemical and petrochemical industries in fluid heaters. The main consequence of the draft type on heat transfer is that the natural-draft flames are usually longer than the forced-draft flames so that the heat flux from the flame is distributed over a longer distance and the peak temperature in the flame is often lower. Note that burners in forced-draft applications are often designed to operate as natural-draft burners in the event of a problem with the combustion air fan (e.g., a power failure).<sup>61</sup> Generally, the heat capacity is reduced when forced-draft burners are operated in the natural-draft condition.

### 1.4.3.5 Location

Process burners are often classified by their location in the furnace or heater. Floor or hearth burners (see Figure 1.30, Type A) are located in the bottom of the combustor and fire vertically upward. Roof or down-fired burners (see Figure 1.17) are located in the ceiling and fire vertically downward. Wall burners (see Figure 1.24) may be located in the wall or in the floor firing along the wall. Their function is to heat a refractory wall to radiate heat to process tubes. Side wall burners are located on the side or end walls of a heater and fire horizontally (see Figure 1.30, Types B or D) or vertically (see Figure 1.30, Type C).

### 1.4.4 Potential Problems

There are many potential problems that could affect the performance of burners and therefore the performance of the heaters, boilers, and furnaces used to process the materials of interest to the end user. A few examples will

illustrate some of the potential problems that may be encountered. Figure 1.52 shows flames impinging on the process tubes in a cabin heater. Flame impingement on the tubes can cause premature coking and significantly reduce the operational run time. Figure 1.53 shows flames pulled toward the wall of a heater. This may be caused by burner design problems or by gas flow currents in the furnace. While flames leaning away from the tubes may reduce coking, they also reduce performance because the heater is designed for vertical flames. Less heat is transferred to the tubes when the flames lean away from the tubes. This reduces the throughput of the entire process. Figure 1.54



**FIGURE 1.52**  
Flames impinging on tubes in a cabin heater.



**FIGURE 1.53**  
Flames pulled toward the wall.



**FIGURE 1.54**  
Oil burner needing service.

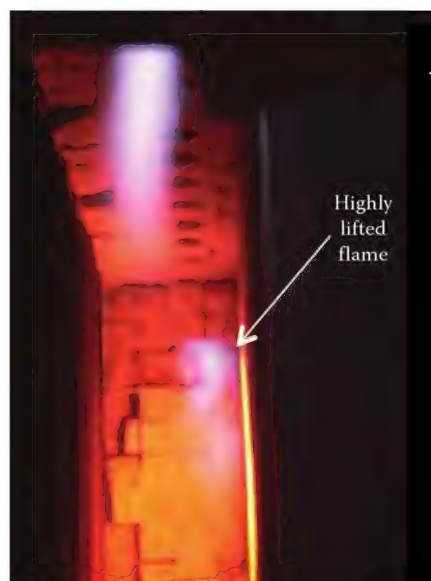


**FIGURE 1.55**  
Highly lifted down-fired burner flame.

shows a single oil burner that needs some type of service or adjustment. Figure 1.55 shows an example of a highly lifted down-fired burner flame in a hydrogen reformer. In all of these examples, the performance of the combustion system is reduced. Volume 2 discusses some of the common problems encountered and how to fix them.

## 1.5 Design Tools

Today's equipment designer has more tools available compared to the past. Some of these tools are physical in nature. Comprehensive and sophisticated test facilities are available to test both pilot-scale and full-scale





**FIGURE 1.56**  
John Zink Co. LLC (Tulsa, Oklahoma) R&D Test Facility.



**FIGURE 1.57**  
Cold flow testing.

equipment.<sup>65</sup> Figure 1.56 shows a photograph of the John Zink Co. LLC test facility located in Tulsa, Oklahoma which has equipment for testing process burners, boiler burners, flares, flare pilots, biogas flares, thermal oxidizers, and vapor combustors. Various types of testing are discussed in Volume 2. Cold flow modeling (see Figure 1.57) is sometimes used to study the airflow in scale model combustion air ducts (see Chapter 11).

Some of today's design tools are virtual in nature. Computational fluid dynamic (CFD) modeling (Figure 1.58; see Chapter 13) provides highly sophisticated analyses of combustion processes.<sup>66</sup> These are among the most complicated problems to model because

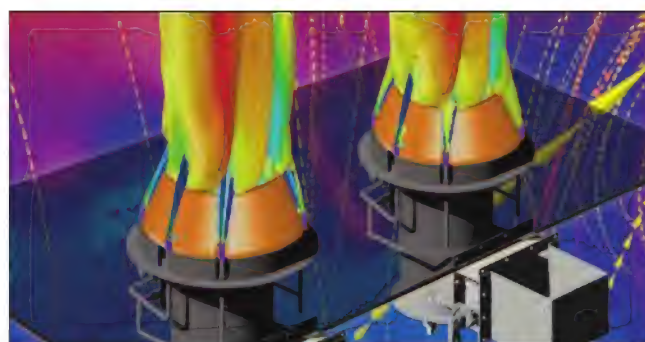


**FIGURE 1.58**  
Example of CFD model result.

of the physics. The fluid flow is often turbulent which is difficult to model. The heat transfer is nonlinear because of radiation which has a fourth power dependence. The radiation may also have a wavelength dependence because of the spectral properties of important combustion products such as  $\text{H}_2\text{O}$  and  $\text{CO}_2$ . The combustion chemistry is exceedingly complex and depending on the fuel could include thousands of reactions. In many cases, the exact chemistry and rate constants are not completely known. Another challenge for combustion modeling is the huge disparity in length scales where the holes in the fuel injectors are on the order of millimeters while the combustor itself is often on the scale of tens of meters. This means that many millions of control volumes may be required to properly simulate the geometry. A more recent virtual tool is sometimes referred to as virtual reality which is an advanced visualization technique for



**FIGURE 1.59**  
Virtual reality engineering simulation.

viewing CFD results. Figure 1.59 shows a photograph of an example of a virtual reality simulation result. In actuality, these results are viewed with 3D glasses to get a true 3D representation of the computational results.

## 1.6 Conclusions

This book considers all aspects of combustion, with particular emphasis on applications in the process industries including the petrochemical, hydrocarbon, power generation, and thermal oxidation industries. The fundamentals of combustion, heat transfer, and fluid flow are discussed from a more applied approach. Many other aspects of combustion, such as fuel composition, pollutant emissions, noise, safety, and control, are also discussed. Topics of specific interest to burners are also treated including design, testing, installation, maintenance, and troubleshooting. There are also very detailed considerations of process burners, flares, boiler burners, duct burners, and thermal oxidizers. Many of these topics have never been adequately covered in other combustion books. The extensive use of color illustrations further enhances the usefulness of this book as an essential tool for the combustion engineer.

## References

1. Lawrence Berkeley National Laboratory and Resource Dynamics Corporation, *Improving Process Heating System Performance: A Sourcebook for Industry*, 2nd Edition, U.S. Department of Energy and Industrial Heating Equipment Association, Washington, DC, 2007.
2. J. Pellegrino, S. Brueske, T. Carole, and H. Andres, Energy and environmental profile of the U.S. petroleum refining industry, Report prepared for the U.S. Department of Energy, Washington, DC, November 2007.
3. U.S. Department of Energy Office of Industrial Technology, *Industrial Combustion Technology Roadmap*, U.S. DOE, Washington, DC, April 1999.
4. E. Worrell and C. Galitsky, Profile of the petroleum refining industry in California, Ernest Orlando Lawrence Berkeley National Laboratory Report LBNL-55450, U.S. Department of Energy, Washington, DC, 2004.
5. E. Worrell and C. Galitsky, Energy efficiency improvement and cost saving opportunities for petroleum refineries, Lawrence Berkeley National Laboratory Report LBNL-56183, U.S. Department of Energy, Washington, DC, 2005.
6. J. Bellovich, J. Franklin, and C. Baukal, The last line of defence (sic), *Hydrocarbon Engineering*, 11(4), 47–54, 2006.
7. J. Peterson, N. Tuttle, H. Cooper, and C. Baukal, Minimize facility flaring, *Hydrocarbon Processing*, 86(6), 111–115, 2007.
8. R.A. Strehlow, *Fundamentals of Combustion*, International Textbook Company, Scranton, PA, 1968.
9. F.A. Williams, *Combustion Theory*, Benjamin/Cummings Publishing, Menlo Park, CA, 1985.
10. J.A. Barnard and J.N. Bradley, *Flame and Combustion*, 2nd Edition, Chapman and Hall, London, U.K., 1985.
11. B. Lewis and G. von Elbe, *Combustion, Flames and Explosions of Gases*, 3rd Edition, Academic Press, New York, 1987.
12. W. Bartok and A.F. Sarofim (eds.), *Fossil Fuel Combustion*, Wiley, New York, 1991.
13. I. Glassman and R.A. Yetter, *Combustion*, 4th Edition, Academic Press, New York, 2008.
14. M. Lackner, F. Winter, and A.K. Agarwal, *Handbook of Combustion*, Vol. 1: Fundamentals and Safety, Vol. 2: Combustion Diagnostics and Pollutants, Vol. 3: Gaseous and Liquid Fuels, Vol. 4: Solid Fuels, Vol. 5: New Technologies, Wiley-VCH, Weinheim, Germany, 2010.
15. A.W. Date, *Analytic Combustion*, Cambridge University Press, Cambridge, U.K., 2011.
16. S. McAllister, J-Y Chen, and A.C. Fernandez-Pello, *Fundamentals of Combustion Processes*, Springer, New York, 2011.
17. Y.I. Khavkin, *Combustion System Design: A New Approach*, PennWell Books, Tulsa, OK, 1996.
18. S.R. Turns, *An Introduction to Combustion: Concepts and Applications*, 3rd Edition, McGraw-Hill, New York, 2012.
19. J. Griswold, *Fuels, Combustion and Furnaces*, McGraw-Hill, New York, 1946.
20. A. Stambuleanu, *Flame Combustion Processes in Industry*, Abacus Press, Tunbridge Wells, U.K., 1976.
21. E. Perthuis, *La Combustion Industrielle*, Éditions Technip, Paris, 1983.
22. E.L. Keating, *Applied Combustion*, Marcel Dekker, New York, 1993.
23. K.W. Ragland and K.M. Borland, *Combustion Engineering*, 2nd Edition, McGraw-Hill, New York, 2011.



24. C.G. Segeler (ed.), *Gas Engineers Handbook*, Industrial Press, New York, 1965.
25. R.D. Reed, *Furnace Operations*, 3rd Edition, Gulf Publishing, Houston, TX, 1981.
26. R. Pritchard, J.J. Guy, and N.E. Connor, *Handbook of Industrial Gas Utilization*, Van Nostrand Reinhold, New York, 1977.
27. R.J. Reed, *North American Combustion Handbook*, Vol. I, 3rd Edition, North American Mfg. Co., Cleveland, OH, 1986.
28. IHEA, *Combustion Technology Manual*, 5th Edition, Industrial Heating Equipment Association, Arlington, VA, 1994.
29. R.O. Anderson, *Fundamentals of the Petroleum Industry*, University of Oklahoma Press, Norman, OK, 1984.
30. W.L. Leffler, *Petroleum Refining for the Nontechnical Person*, Pennwell Books, Tulsa, OK, 1985.
31. R.A. Meyers, *Handbook of Petroleum Refining Processes*, 2nd Edition, McGraw-Hill, New York, 1997.
32. J.H. Gary, G.E. Handwerk, and M.J. Kaiser, *Petroleum Refining: Technology and Economics*, 5th Edition, CRC Press, Boca Raton, FL, 2007.
33. C.E. Baukal (ed.), *The John Zink Combustion Handbook*, CRC Press, Boca Raton, FL, 2001.
34. W.L. Nelson, *Petroleum Refinery Engineering*, 2nd Edition, McGraw-Hill, New York, 1941.
35. G.R. Martin, Heat-flux imbalances in fired heaters cause operating problems, *Hydrocarbon Processing*, 77(5), 103–109, 1998.
36. R. Nogay and A. Prasad, Better design method for fired heaters, *Hydrocarbon Processing*, 64(11), 91–95, 1985.
37. A. Garg and H. Ghosh, Good heater specifications pay off, *Chemical Engineering*, 95(10), 77–80, 1988.
38. H. Futami, R. Hashimoto, and H. Uchida, Development of new catalyst and heat-transfer design method for steam reformer, *Journal of the Fuel Society of Japan*, 68(743), 236–243, 1989.
39. H. Gunardson, *Industrial Gases in Petrochemical Processing*, Marcel Dekker, New York, 1998.
40. J.D. Fleshman, FW Hydrogen Production, in *Handbook of Petroleum Refining Processes*, 2nd Edition, R.A. Myers (ed.), McGraw-Hill, New York, Chapter 6.2, 1996.
41. J.S. Plotkin and A.B. Swanson, New technologies key to revamping petrochemicals, *Oil and Gas Journal*, 97(50), 108–114, 1999.
42. D.Q. Kern, *Process Heat Transfer*, McGraw-Hill, New York, 1950.
43. N.P. Lieberman, *Troubleshooting Process Operations*, PennWell Books, Tulsa, OK, 1991.
44. H.S. Bell and L. Lowy, Equipment, in *Petroleum Processing Handbook*, W.F. Bland and R.L. Davidson (eds.), Chapter 4, McGraw-Hill, New York, 1967.
45. E.B. Sanderford, Alternative control techniques document—NO<sub>x</sub> emissions from process heaters, U.S. Environmental Protection Agency report EPA-453/R-93-015, February 1993.
46. L.A. Thrash, Annual refining survey, *Oil and Gas Journal*, 89(11), 86–105, 1991.
47. S.A. Shareef, C.L. Anderson, and L.E. Keller, *Fired Heaters: Nitrogen Oxides Emissions and Controls*, U.S. Environmental Protection Agency, Research Triangle Park, NC, EPA Contract No. 68-02-4286, June 1988.
48. H.L. Berman, Fired heaters—II: Construction materials, mechanical features, performance monitoring, in *Process Heat Exchange*, V. Cavaseno (ed.), Chemical Engineering, McGraw-Hill, New York, pp. 293–302, 1979.
49. A.J. Johnson and G.H. Auth, *Fuels and Combustion Handbook*, 1st Edition, McGraw-Hill, New York, 1951.
50. H.L. Berman, Fired heaters—I: Finding the basic design for your application, in *Process Heat Exchange*, V. Cavaseno (ed.), Chemical Engineering, McGraw-Hill, New York, pp. 287–292, 1979.
51. V. Ganapathy, *Applied Heat Transfer*, PennWell Books, Tulsa, OK, 1982.
52. G.L. Shires, Furnaces, in *The International Encyclopedia of Heat and Mass Transfer*, G.F. Hewitt, G.L. Shires and Y.V. Polezhaev (eds.), CRC Press, Boca Raton, FL, pp. 493–497, 1997.
53. E. Talmor, *Combustion Hot Spot Analysis for Fired Process Heaters*, Gulf Publishing, Houston, TX, 1982.
54. C.E. Baukal (ed.), *Industrial Burners Handbook*, CRC Press, Boca Raton, FL, 2004.
55. J.L. Reese, G.L. Moilanen, R. Borkowicz, C. Baukal, D. Czerniak and R. Batten, State-of-the-art of NO<sub>x</sub> emission control technology, ASME paper 94-JPGC-EC-15, *Proceedings of Int'l Joint Power Generation Conference*, Phoenix, AZ, October 3–5, 1994.
56. C.E. Baukal, *Industrial Combustion Pollution and Control*, Marcel Dekker, New York, 2004.
57. A. Garg, Better burner specifications, *Hydrocarbon Processing*, 68(8), 71–72, 1989.
58. M.L. Joshi, M.E. Tester, G.C. Neff, and S.K. Panahi, Flame particle seeding with oxygen enrichment for NO<sub>x</sub> reduction and increased efficiency, *Glass*, 68(6), 212–213, 1990.
59. R. Ruiz and J.C. Hilliard, Luminosity enhancement of natural gas flames, *Proceedings of 1989 International Gas Research Conference*, T.L. Cramer (ed.), Govt. Institutes, Rockville, MD, pp. 1345–1353, 1990.
60. A.G. Slavejkov, T.M. Gosling, and R.E. Knorr, Low-NO<sub>x</sub> staged combustion device for controlled radiative heating in high temperature furnaces, U.S. Patent 5,611,682, March 18, 1997.
61. API Publication 535, *Burner for Fired Heaters in General Refinery Services*, 1st Edition, American Petroleum Institute, Washington, DC, July 1995.
62. C.E. Baukal (ed.), *Oxygen-Enhanced Combustion*, CRC Press, Boca Raton, FL, 1998.
63. J. Lambert, M. Sorin, and J. Paris, Analysis of oxygen-enriched combustion for steam methane reforming (SMR), *Energy*, 22(8), 817–825, 1997.
64. M.B. Wilkinson, J.C. Boden, T. Gilmartin, C. Ward, D.A. Cross, R.J. Allam, and N.W. Ivens, CO<sub>2</sub> capture from oil refinery process heaters through oxyfuel combustion, in *Greenhouse Gas Control Technologies*, J. Gale and Y. Kaya (eds.), *Proceedings of the 6th International Conference on Greenhouse Gas Control Technologies*, Kyoto, Japan, Vol. 1, pp. 69–74, October 1–4, 2002.
65. C.E. Baukal, *Industrial Combustion Testing*, CRC Press, Boca Raton, FL, 2011.
66. C.E. Baukal, V.Y. Gershtein, and X. Li (eds.), *Computational Fluid Dynamics in Industrial Combustion*, CRC Press, Boca Raton, FL, 2001.

# 2

## *Refining and Petrochemical Industries*

Erwin Platvoet, Rasik Patel, David Brown, Jason D. McAdams, and James G. Seebold

### CONTENTS

2.1	Introduction.....	31
2.2	Refining.....	32
2.2.1	Introduction.....	32
2.2.2	Examples of Refining Processes .....	32
2.2.2.1	Crude Distillation .....	32
2.2.2.2	Visbreaking.....	33
2.2.2.3	Hydrotreating.....	33
2.2.2.4	Catalytic Reforming.....	36
2.2.2.5	Delayed Coking.....	36
2.3	Reforming .....	38
2.3.1	Introduction.....	38
2.3.2	Reforming Reactions .....	38
2.3.3	Reforming Catalyst.....	39
2.3.4	Reforming for Hydrogen .....	39
2.3.5	Reforming for Ammonia .....	39
2.3.6	Reforming for Methanol .....	41
2.4	Ethylene.....	42
2.4.1	Introduction.....	42
2.4.2	Kinetics of Thermal Cracking.....	42
2.4.3	Severity of Cracking .....	42
2.4.4	Typical Product Distribution.....	42
2.4.5	Coking .....	42
2.4.6	Decoking .....	43
	References.....	43

### 2.1 Introduction

The hydrocarbon processing industry (HPI) and chemical processing industry (CPI) collectively comprise the manufacturing arm of the oil and gas industries. These industries cover all aspects of producing petroleum-based products and chemicals, including refining of petroleum, manufacturing of chemical and petrochemicals from petroleum feedstocks, processing of gases, and production of synthetic fuels.

These industries take raw materials such as crude oil, natural gas, and bitumen from tar sands and convert them into useable products without which the world today would not be able to operate. These products

include the gasoline, diesel, and jet fuel used for vehicles, liquid and gaseous fuels to generate steam for power generation and to drive operations in a myriad of industrial applications, precursor materials for the generation of plastics that go into everything from clothing, to carpet, to automobile interiors, to plastic bottles, pharmaceuticals, and several other specialty products.

Heat is absolutely critical to all of these processes. It is used for separation of the various hydrocarbon molecules, to bring process flows into a reactor to the proper temperature for a chemical conversion to take place (or to take place under optimum conditions), to generate the steam necessary for these processes, and to safely destroy by-products or waste gases that result from these processes. The only way to supply the intense

energy demands of these industries is through the combustion of hydrocarbon fuels. In fact, combustion is the very lifeblood of the petroleum, petrochemical, and chemical sector.

Because the combustion processes in a refinery or chemical plant take place in large, stationary sources, such as fired heaters or boilers, the emissions from these pieces of equipment are significantly easier to regulate than the equivalent combustion reaction emissions from thousands of smaller, mobile sources, such as automobiles. Consequently, this means that refinery and chemical combustion processes are almost always chosen as candidates for environmental regulation. As these regulations have tightened over the years, “combustion” problems the industry has experienced become “emissions” problems since the performance of the combustion equipment is inexorably linked to its emissions performance. When faced with operation under some of the most stringent environmental regulations, industry companies and combustion equipment manufacturers have worked together to jointly develop cutting-edge low-emission combustion technology.<sup>1</sup>

It is sometimes easy for industry functionaries to take combustion functions like process heating for granted. They should not. Without a comprehensive understanding of combustion and its industrial application, these plants would not run, and modern life as we know it would not exist.

## 2.2 Refining

### 2.2.1 Introduction

A majority of operations within the HPI are within petroleum refining. The refining industry, or petroleum refining industry, converts crude oil into fuels, specialty chemicals and feeds for use in making more highly purified chemical components. According to the U.S. Energy Information Administration, petroleum refining is the most energy-intensive manufacturing industry in the United States, accounting for about 31% of total U.S. industrial energy consumption in 2006.<sup>2</sup>

Table 2.1<sup>3</sup> and Table 2.2<sup>4</sup> show the major processes in petroleum refining, most of which require combustion in one form or another. Figure 2.1 shows the process flow through a typical refinery.

### 2.2.2 Examples of Refining Processes

A large number of processes exist in which petroleum fractions are upgraded or converted to more valuable products. The examples selected in the following text are characterized by the presence of a heater.

**TABLE 2.1**

Major Petroleum Refining Processes

Category	Major Process
Topping (separation of crude oil)	Atmospheric distillation Vacuum distillation Solvent deasphalting
Thermal and catalytic cracking	Delayed coking Fluid coking/flexicoking Visbreaking Catalytic cracking Catalytic hydrocracking
Combination/rearrangement of hydrocarbon	Alkylation Catalytic reforming Polymerization Isomerization Ethers manufacture
Treating	Catalytic hydrotreating/hydroprocessing Sweetening/sulfur removal Gas treatment
Specialty product manufacture	Lube oil Grease Asphalt

Source: U.S. Department of Energy Office of Industrial Technology, *Petroleum—Industry of the Future: Energy and Environmental Profile of the U.S. Petroleum Refining Industry*, U.S. DOE, Washington, DC, December 1998.

#### 2.2.2.1 Crude Distillation

A simplified flow diagram of a crude distillation process (see Figure 2.2) shows a typical use of process heaters in a refinery process.

The crude heater preheats the crude oil to a temperature of around 700°F (370°C) before it enters the crude distillation tower. The tower separates the crude oil into various components such as light gases (C<sub>1</sub>–C<sub>4</sub>), light and heavy naphtha, kerosene, and diesel. The heavy residue from the bottom of the crude distillation tower (called “atmospheric resid” or “atmospheric reduced crude (ARC)”) is sent to another fired heater where it is further heated to approximately 750°F (400°C) and then delivered to a vacuum tower for additional separation by fractionation. The vacuum tower operates at negative pressures to aid with separation of these heavier components in the crude oil into gas oils and vacuum residue (asphalt).

There are numerous hydroconversion processes such as hydrotreating and hydrocracking where the vacuum residue and other heavier oil fractions are reacted in the presence of hydrogen and a catalyst in order to upgrade to lighter products and reduce the sulfur, nitrogen, or asphaltene content. The majority of these processes use charge and/or reboiler heaters similar to the aforementioned example.



TABLE 2.2

Major Refinery Processes Requiring a Fired Heater

Process	Process Description	Heaters Used	Process Heat Requirements		Feedstock Temperature Outlet of Heater, °F
			KJ/L	10 <sup>3</sup> Btu/bbl	
<i>Distillation</i>					
Atmospheric	Separates light hydrocarbons from crude in a distillation column under atmospheric conditions	Preheater, reboiler	590	89	700
Vacuum	Separates heavy gas oils from atmospheric distillation bottoms under vacuum	Preheater, reboiler	418	63	750–830
<i>Thermal processes</i>					
Thermal cracking	Thermal decomposition of large molecules into lighter, more valuable products	Fired reactor	4650	700	850–1000
Coking	Cracking reactions allowed to go to completion; lighter products and coke produced.	Preheater	1520	230	900–975
Visbreaking	Mild cracking of residuals to improve their viscosity and produce lighter gas oils	Fired reactor	961	145	850–950
<i>Catalytic cracking</i>					
Fluidized catalytic cracking	Cracking of heavy petroleum products; a catalyst is used to aid the reaction	Preheater	663	100	600–885
Catalytic hydrocracking	Cracking heavy feedstocks to produce lighter products in the presence of hydrogen and a catalyst	Preheater	1290	195	400–850
<i>Hydroprocessing</i>					
Hydrodesulfurization	Remove contaminating metals, sulfur, and nitrogen from the feedstock; hydrogen is added and reacted over a catalyst	Preheater	431	65 <sup>a</sup>	390–850
Hydrotreating	Less severe than hydrodesulfurization; removes metals, nitrogen, and sulfur from lighter feedstocks; hydrogen is added and reacted over a catalyst	Preheater	497	75 <sup>b</sup>	600–800
<i>Hydroconversion</i>					
Alkylation	Combination of two hydrocarbons to produce a higher molecular weight hydrocarbon; heater used on the fractionator	Reboiler	2500	377 <sup>c</sup>	400
Catalytic reforming	Low-octane naphthas are converted to high-octane, aromatic naphthas; feedstock is contacted with hydrogen over a catalyst	Preheater	1790	270	850–1000

Source: Sanderford, E.B., *Alternative Control Techniques Document—NO<sub>x</sub> Emissions from Process Heaters*, U.S. Environment Protection Agency Report EPA-453/R-93-015, February, 1993.

<sup>a</sup> Heavy gas oils and middle distillates.

<sup>b</sup> Light distillate.

<sup>c</sup> Btu bbl<sup>-1</sup> of total alkylate.

### 2.2.2.2 Visbreaking

One example of such a hydrocracking process is visbreaking. Its main goal is to manufacture incremental gas and distillate products, while reducing the viscosity and pour point of vacuum and atmospheric residues. Figure 2.3 shows a typical process flow diagram. Vacuum residue is fed to the visbreaker charge heater where it is heated to high temperature (850°F–900°F) (450°C–480°C), causing partial vaporization and mild cracking. In some

processes, it is then fed to a soaker drum where additional conversion takes place. The cracked feed is then charged to a fractionator to produce the desired products. The tar product can be further processed in a vacuum flasher to produce additional gas oil and waxy distillates.

### 2.2.2.3 Hydrotreating

Hydrotreating is a common name for a wide variety of processes in which naphtha, middle distillates, or

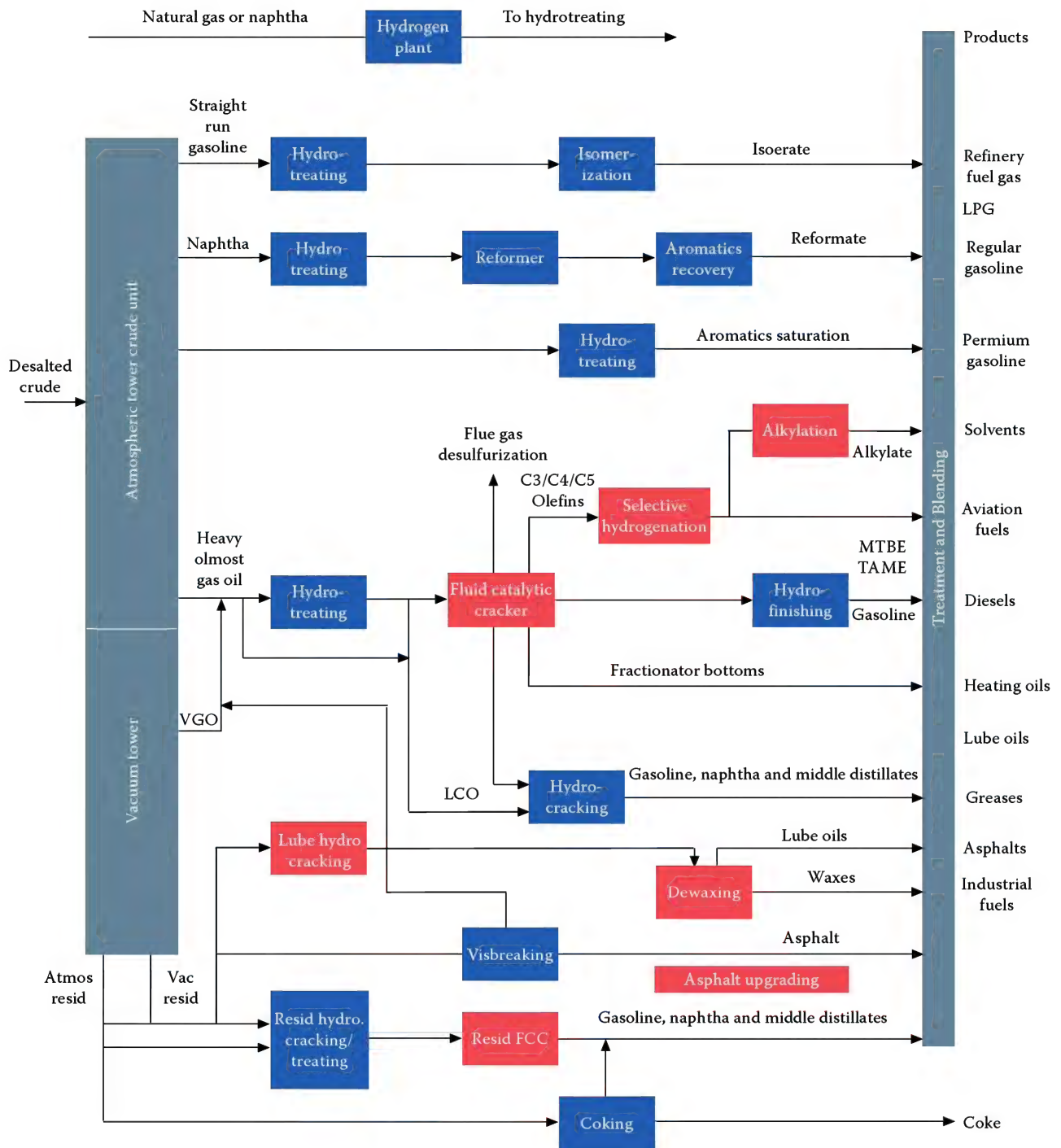


FIGURE 2.1  
Typical refinery process flow diagram.

vacuum residues are treated in order to improve their properties, such as

- Reduction of sulfur content (hydrosulfurization) and color improvement of diesel
- Reduction of nitrogen and metal content

- Reduction of aromatic content (hydrodearomatization)
- Conversion to lighter products and reduction of viscosity

Due to the variety of different applications and processes, there are many different process flow diagrams.

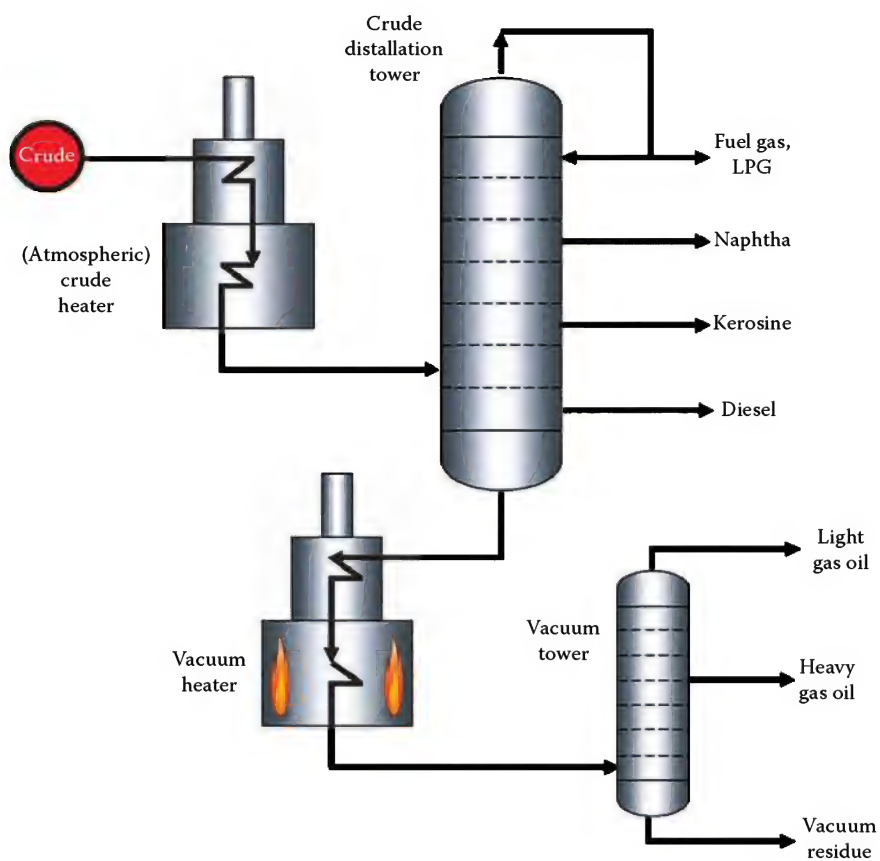


FIGURE 2.2  
Simplified crude distillation flow diagram.

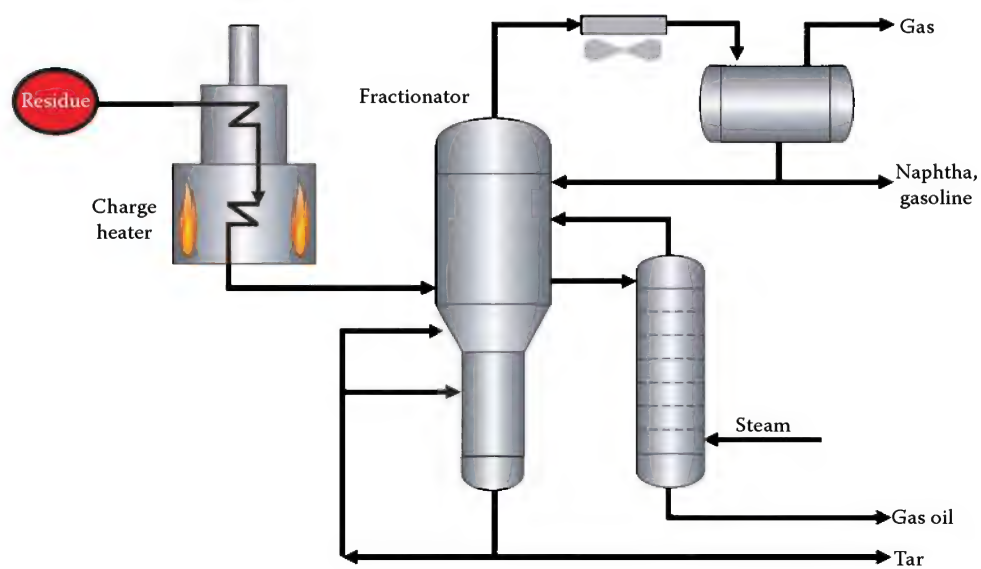
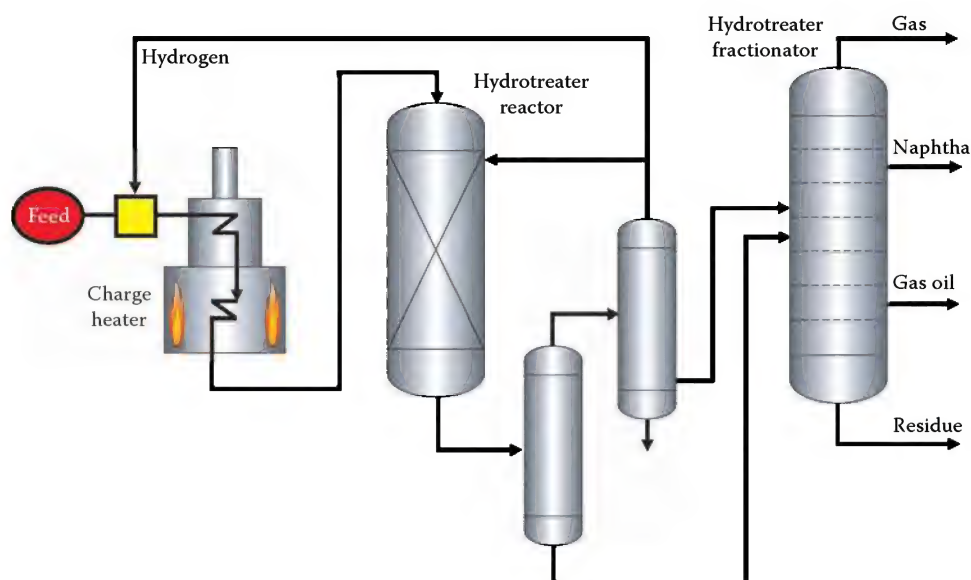


FIGURE 2.3  
Typical visbreaking flow diagram.



**FIGURE 2.4**  
Typical hydrotreating flow diagram.

In a typical version (see Figure 2.4), the feed is mixed with makeup hydrogen before it is heated and partially vaporized in the heater. The feed then enters the hydrotreater reactor, which is usually a one or two stage catalytic reactor. The reactor effluent is then separated through flashing in a gas and a liquid phase and sent to a fractionator.

#### 2.2.2.4 Catalytic Reforming

Another major hydroconversion process is catalytic reforming. It is a catalytic process to convert low-octane naphthas into high-octane aromatic products called reformates for use in high-octane gasoline. The process produces very significant amounts of by-product hydrogen gas for use in a number of the other processes involved in a modern petroleum refinery. Other by-products are small amounts of methane, ethane, propane, and butanes. A simplified process scheme is shown in Figure 2.5. The naphtha feed is blended with the hydrogen-rich recycle stream and preheated to the reaction temperature (910°F–970°F, 490°C–520°C) before the mixture enters the first reactor stage. Since the catalytic reactions in reactor beds A, B, and C are highly endothermic, the fired heater modules are used to reheat the process gas between the reactor stages. Downstream of the last reactor stage, the effluent is separated into the hydrogen-rich gas fraction, a fraction containing the  $C_1$ – $C_4$  gases, and the reformate.

#### 2.2.2.5 Delayed Coking

The delayed coking process is used to convert vacuum residues to lighter hydrocarbon fractions such as LPG,

naphtha, light gas oil, and heavy gas oil. Other feeds that can be used are tar sand bitumen, deasphalter bottoms, and tars. Portions of the feed that do not upgrade to these lighter components are reacted to form petroleum coke and tars. Ideally, as much of the feed as possible is upgraded to the lighter, higher value product streams. The petroleum coke, or pet coke, is relatively pure carbon and is typically used as fuel. It can also be used for the production of electrodes and other chemicals.

A simplified flow diagram of the semicontinuous delayed coking process is shown in Figure 2.6. Feedstock is introduced to the bottom of the coker fractionator where it mixes with the condensed recycle. The mixture is then pumped through the coker heater where it is heated to coking temperature, while it is partially vaporized. Some cracking may occur inside the heater tubes, but large-scale decomposition has to be prevented since that would significantly increase coking inside the tubes and reduce the heater run length. For that reason, the typical residence time in a coker heater is small while the heat flux is relatively high and needs to be well controlled.

After the coker heater, the vapor–liquid mixture enters a coke drum that provides the long required residence time to complete thermal cracking while forming coke. Since the reactions in the coking drum are endothermic, the heater outlet temperature is about 100°F (55°C) above the drum temperature. There are at least two parallel coke drums, so one can be in operation with incoming heater effluent, while the coke that previously formed in the other drum is drilled out using high-pressure water. The drum operation cycle is

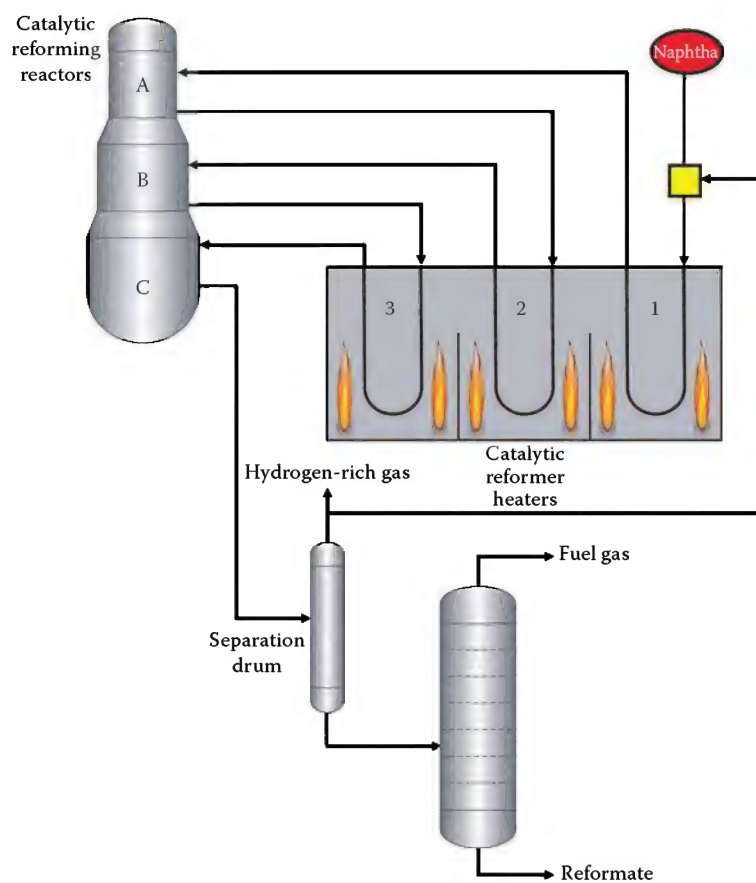


FIGURE 2.5  
Catalytic reforming process flow diagram.

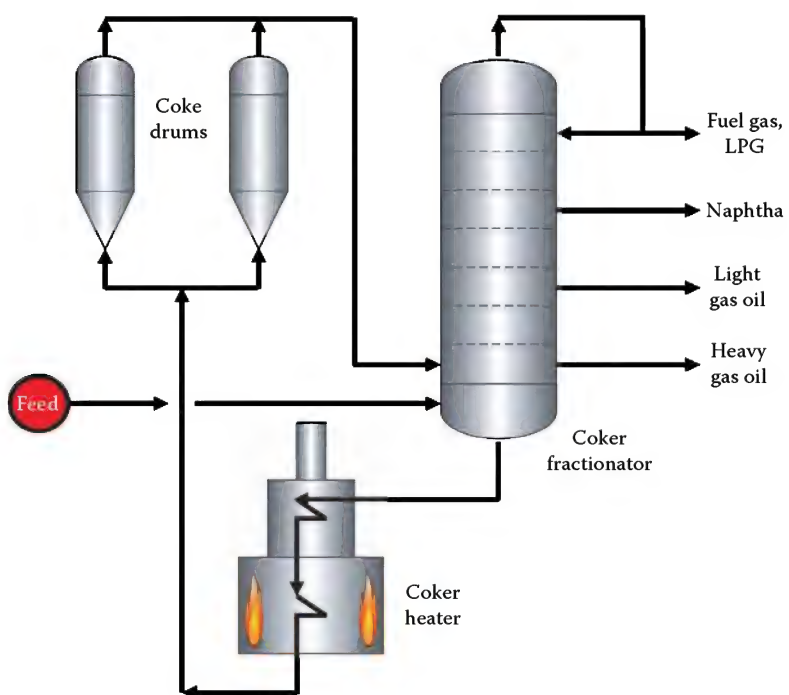


FIGURE 2.6  
Simplified process diagram for delayed coking.



typically 48 hours, with the drum being on-stream for 24 hours and cleaned for another 24 hours.

The coke drum overhead is fed back to the fractionator where it is separated into the product streams (gas, naphtha, light and heavy oils).

Typical operating conditions are as follows:

Heater outlet temperature: 900°F–950°F (480°C–510°C)

Coke drum pressure: 15–100 psig (1–7 barg)

The typical product slate of a vacuum residue feed is<sup>5</sup>

Gas:	8–10 wt%
Naphtha:	10–20 wt%
Gas oil:	30–50 wt%
Coke:	25–40 wt%

## 2.3 Reforming

### 2.3.1 Introduction

Hydrogen, carbon monoxide, and syngas ( $H_2 + CO$ ) continue to play an important role in the refining (e.g., production of ultralow sulfur clean fuels) and petrochemical industries (such as the production of ammonia and methanol). Table 2.3<sup>6</sup> provides a listing of typical uses of hydrogen in industry and the relative percentage of overall hydrogen production.

While there are many commercial technologies available to manufacture these products from hydrocarbons,

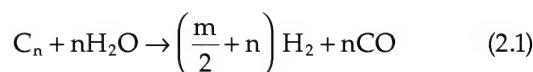
the primary ones are steam reforming, autothermal reforming, and partial oxidation. Of these, the steam reforming process continues to be the most cost-effective means for large-scale hydrogen production.

The main process steps in the steam reforming process are feed compression and purification (to remove sulfur), steam reforming and steam production, shift conversion (for increased hydrogen production) followed by purification. A layout of a typical steam reforming unit is included in Figure 2.7.

At the heart of the steam reforming unit is the reforming furnace, a heat transfer device that is part furnace, part reactor. It is within this furnace that all of the initial reactions of the reforming process take place.

### 2.3.2 Reforming Reactions

In a steam reformer, hydrocarbon feed mixed with steam is passed through tubes in a reforming furnace that are filled with nickel-based catalyst. This catalytic process can be represented by the following reactions:



Equation 2.1 is the steam reforming reaction and is strongly endothermic while Equation 2.2 is referred to as the water-gas shift reaction and is exothermic. While both reactions produce hydrogen, they are limited by thermodynamic equilibrium. The reforming reaction is favored by low pressure and high temperature while the shift reaction is independent of pressure. From plant economic considerations, however, operation at higher pressure is favored to minimize the cost of product compression. A steam reformer for hydrogen production typically runs at an outlet pressure between 150 psig (10.4 barg) and 450 psig (31.0 barg) with outlet temperatures up to 1600°F (870°C). The third parameter that influences the makeup of the reformed gas is the steam to carbon ratio, commonly expressed as moles of steam per atom of carbon in the hydrocarbon feed entering the reformer. Typical values of steam to carbon ratio for new reformers are between 2.8 and 3.1. These ratios help avoid carbon (coke) formation on the catalyst.

Reforming furnaces can have several configurations including down fired, side fired, terrace wall fired, and bottom fired. Volume 3, Chapter 5 of this handbook provides additional details about each of these various reforming furnace configurations. Burners for each of these configurations are specifically designed to supply heat per the demands of that furnace configuration.

TABLE 2.3

Hydrogen Usage by Industry

Hydrogen Final Usage Category	Usage by Industry (%)	Comments
Ammonia	37	An ammonia plant is typically a hydrogen plant with a second converter that reacts hydrogen with nitrogen
Merchant	3	This includes all bottled users, liquid hydrogen supplied in tank trucks, and gaseous hydrogen in short pipe lines (not including the over-the-fence hydrogen suppliers)
Methanol	10	
Refinery hydrogenation	19	Hydrocracking and hydrotreating
Cryogenics	17	
Refinery fuel gas	14	Last resort

Source: Elshout, R., *Chem. Eng.*, 117(5), 34, 2010.



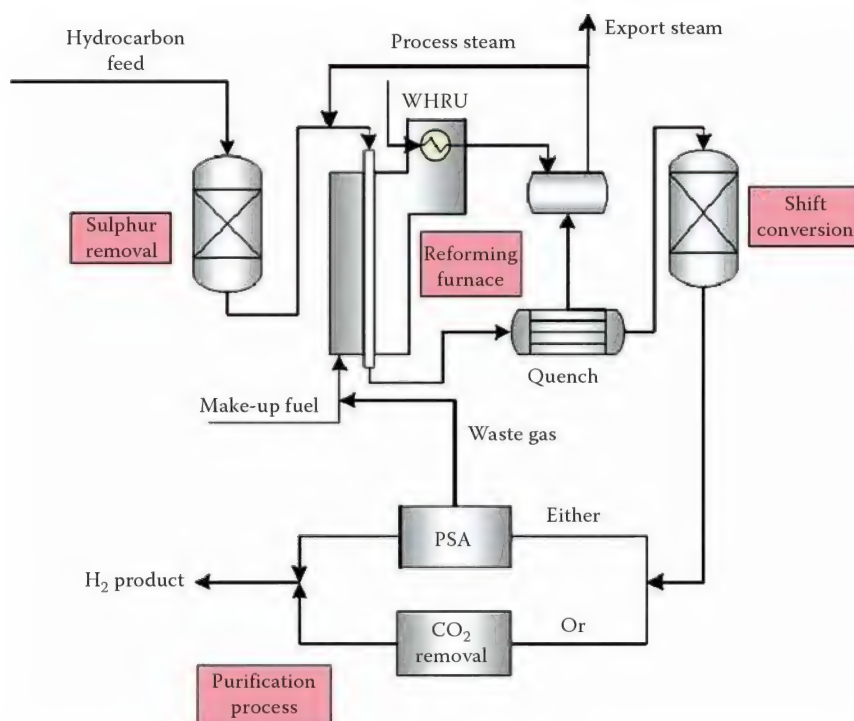


**FIGURE 2.7**  
Simplified process diagram of a steam reforming based hydrogen plant.

### 2.3.3 Reforming Catalyst

The endothermic steam reforming reaction is promoted by the presence of a catalyst. As the mixture of hydrocarbons and steam pass through the steam reformer tubes, the catalyst acts as a heat sink over which the reaction can occur more rapidly. The steam reforming catalyst is nickel based and is supplied in a pellet form in varying shapes. The common underlying features are

- Selective to promote the reforming reaction for a given feedstock
- High strength to withstand the loading and operating cycles
- Shaped to provide a large geometric surface area to promote rapid reaction
- Sized to meet the process side pressure drop demand

### 2.3.4 Reforming for Hydrogen

When the intended end product of the steam reforming reaction is high purity hydrogen for use in refinery or other processes, the produced syngas will pass through a purification system to extract and concentrate the hydrogen out of the stream. Modern hydrogen plants use the pressure swing adsorption (PSA) process to

achieve hydrogen product purity above 99.9%. This is in contrast to the purity of 90%–98% achieved in older plants using an amine-based CO<sub>2</sub> removal system followed by methanation of the remaining carbon oxides.

Figure 2.8<sup>6</sup> shows a typical flow diagram of a PSA system.

The portions of the syngas that are not recovered into the hydrogen stream by the PSA system are recycled back to the burners for use as a fuel. This stream, called “PSA off gas” or just “PSA gas,” is typically supplied to the burners at a pressure of only 2–3 psig 0.15–0.2 barg. Burners for these applications must be able to burn both this low pressure PSA off gas and a makeup fuel that is typically supplied at higher pressure. This may require two gas connections, or blending of these two fuels into a combined low-pressure fuel.

### 2.3.5 Reforming for Ammonia

Steam reforming of hydrocarbons is also the first step in chemical plants that produce ammonia (NH<sub>3</sub>).<sup>7</sup> Demand for ammonia continues to rise as it is a key ingredient in the fertilizer used to produce crops to feed an ever-increasing world population. The worldwide ammonia production using hydrogen derived from steam reforming was estimated at 131 million metric tons in 2010.<sup>8</sup> Figure 2.9 shows a simplified flow sheet of a typical

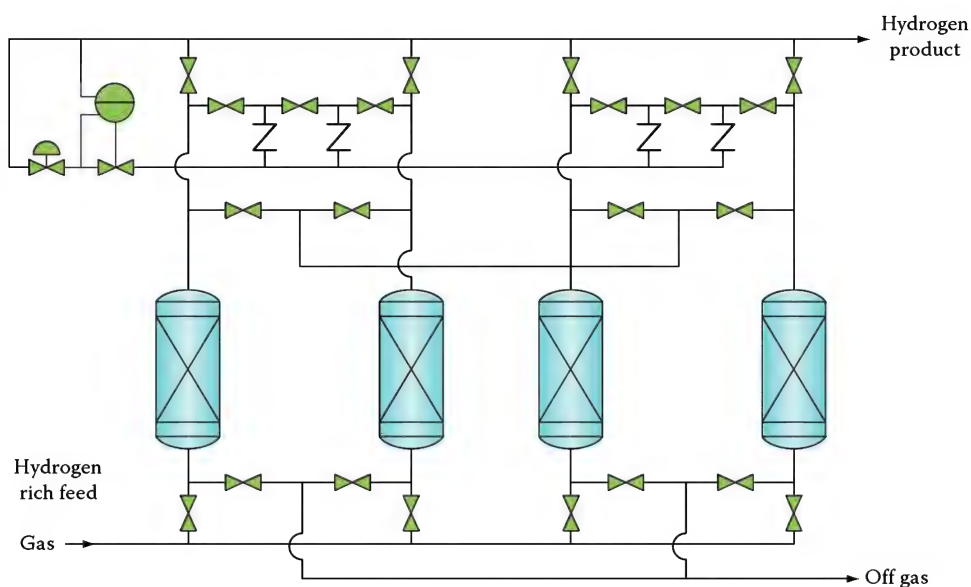


FIGURE 2.8  
Typical PSA system flow diagram. (From Elshout, R., *Chem. Eng.*, 117(5), 34, 2010.)

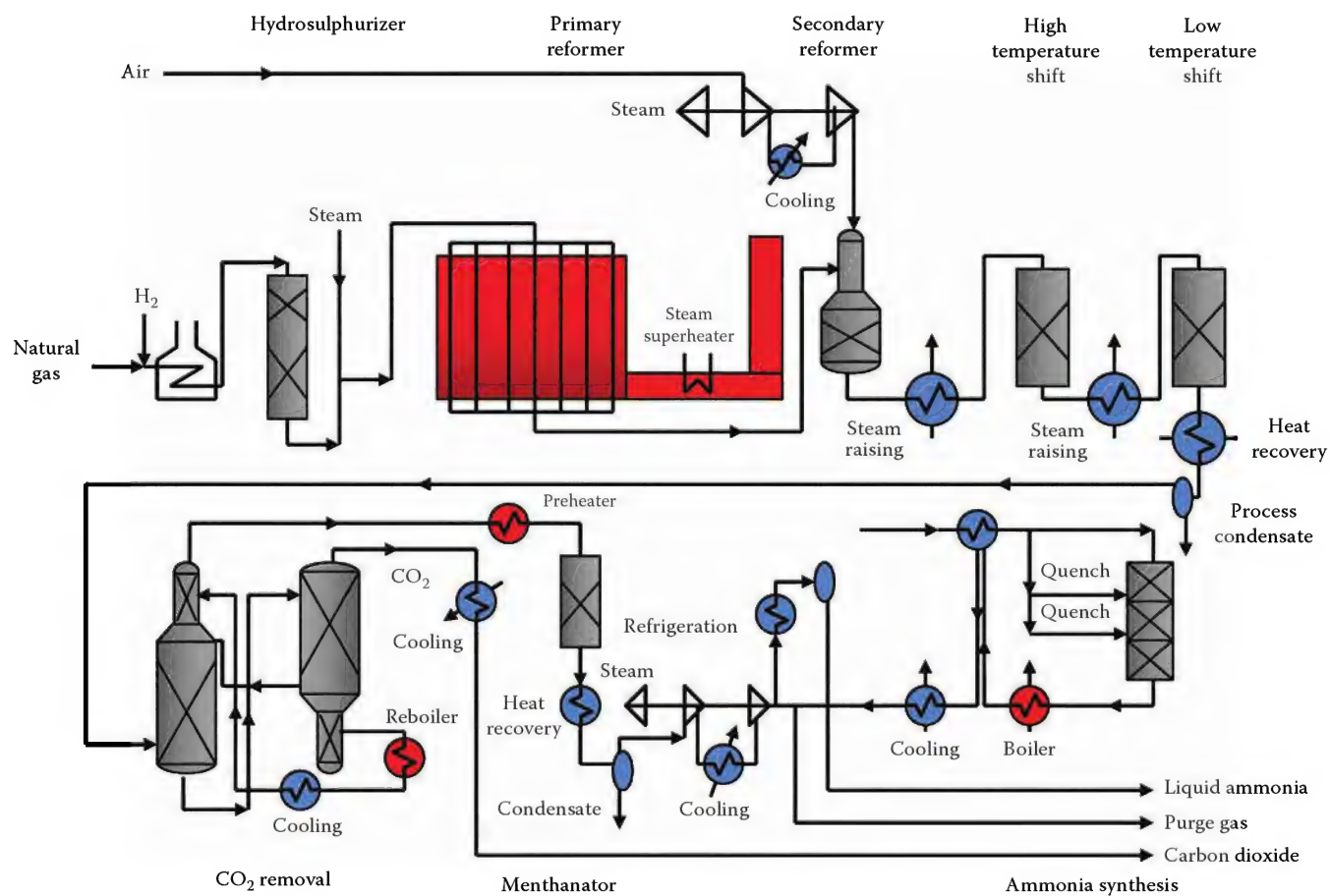
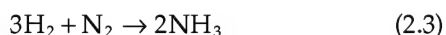


FIGURE 2.9  
Typical flow diagram of an ammonia plant. (Adapted from Synetix, Introduction to ammonia manufacture.)

ammonia plant with a primary reforming furnace and secondary reformer.

In an ammonia plant, the CO in the syngas is converted to CO<sub>2</sub> in the water-gas shift reactor, and then is extracted from the stream using amine solvents, or a PSA system. The remaining hydrogen (H<sub>2</sub>) and nitrogen (N<sub>2</sub>) from earlier air injection are routed through a secondary reformer that reacts them together using an iron catalyst promoted with K<sub>2</sub>O, CaO, and Al<sub>2</sub>O<sub>3</sub> to produce the ammonia molecule (NH<sub>3</sub>) per the following reaction:



The liquid ammonia formed by this reaction is then recovered out of the resulting stream through condensation.

Burners used in ammonia plants typically burn a purge stream from the process that is high in hydrogen (H<sub>2</sub>). This purge stream is typically mixed with the main burner fuel gas since it is supplied at higher pressures. This purge stream can contain traces of the ammonia (NH<sub>3</sub>) product. Since ammonia in fuel gas directly converts to NO<sub>x</sub> emissions through combustion, these trace amounts of ammonia in the fuel gas must be watched when emissions from the furnace are critical.

### 2.3.6 Reforming for Methanol

Although not as widely produced as ammonia or hydrogen, demand for methanol (CH<sub>3</sub>OH) is also

increasing because of its use in gasoline blendstocks, as a gasoline or biodiesel production feedstock, and as precursor materials for plastics. As with hydrogen and ammonia, the first major step in a methanol plant after feed purification is the steam hydrocarbon reformer furnace where syngas is produced. The reformer effluent gas is then cooled before being sent to synthesis reactor. Here the carbon monoxide (CO) and carbon dioxide (CO<sub>2</sub>) in the syngas are reacted with the hydrogen (H<sub>2</sub>) in the syngas across a catalyst bed at high pressure (5–10 MPa [725–1450 psi]) and high temperature (250°C [480°F]) to form methanol (CH<sub>3</sub>OH) by the following primary reactions:



As the conversion to methanol is relatively low, continual recycling of the unreacted gases is done. This process results in a build-up of inert gases rich in hydrogen which are then sent to the reformer to be burned as fuel. The final step in the process involves purification using distillation of the crude product from the synthesis loop. Figure 2.10 shows the layout of a typical, large-scale methanol plant.

Reforming furnaces in methanol plants can have some of the largest number of burners of any kind of chemical process industry furnace, with large-scale plants having hundreds of down fired burners in each reforming furnace.<sup>9</sup>

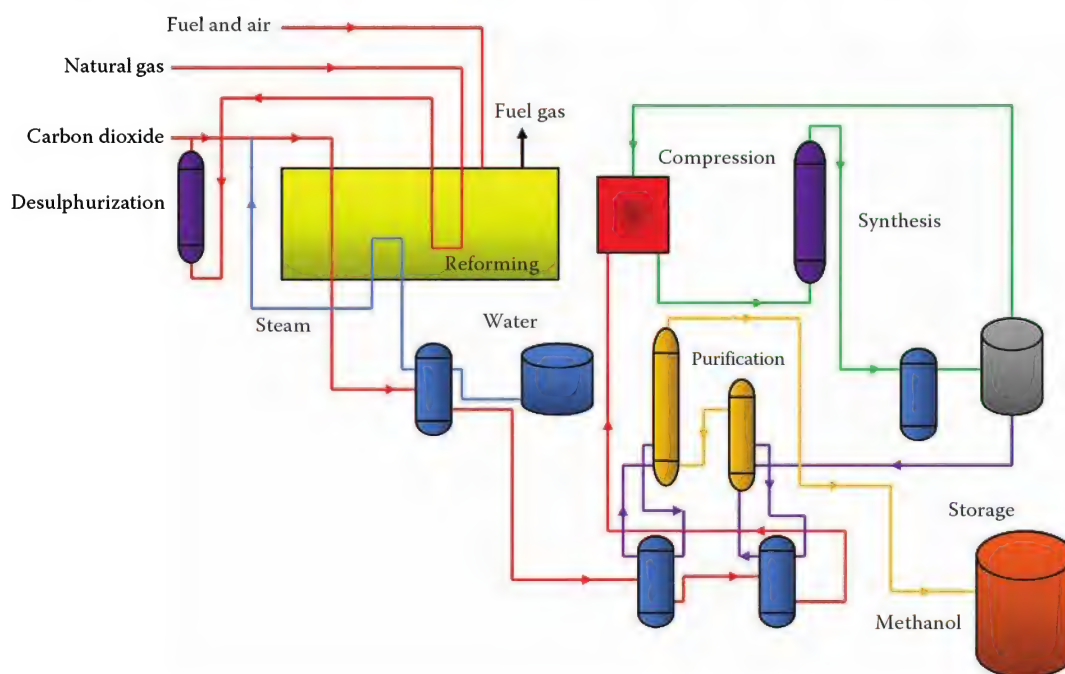


FIGURE 2.10

Typical methanol plant process flow diagram. (Adapted from ICI Low Pressure Process, [www.ttmmethanol.com](http://www.ttmmethanol.com))



## 2.4 Ethylene

### 2.4.1 Introduction

Ethylene is the largest volume building block for many petrochemicals. It can be produced via a myriad of different processes, such as a number of different catalytic pyrolysis and hydrolysis processes<sup>10</sup> fluidized bed cracking, paraffin dehydrogenation, and oxydehydrogenation<sup>11</sup> among others. More recently, there have been significant advances in the methanol to olefins (MTO) routes with several commercial plants in the world. It can be combined with other technologies that convert higher olefins to ethylene and propylene, in order to achieve high overall product yields. Examples are Total's olefin cracking process (OCP) and Lummus' olefins conversion technology (OCT).

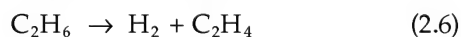
OCP converts low-value olefins in mixed by-product streams to propylene and ethylene at propylene-to-ethylene (P/E) ratios in the range of 3.5–4. It is capable of processing a wide range of C<sub>4</sub>–C<sub>8</sub> olefins without any ethylene loss.

OCT combines metathesis and isomerization chemistry, reacting C<sub>4</sub> products with ethylene to produce propylene. It is used together with MTO type processes, but can also be combined with a conventional naphtha cracker in order to increase the maximum propylene-to-ethylene ratio from 0.6 to 1.1.

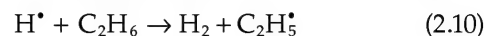
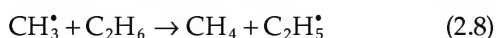
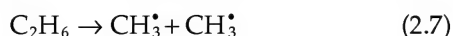
However, steam cracking remains still by far the most important route to produce ethylene.

### 2.4.2 Kinetics of Thermal Cracking

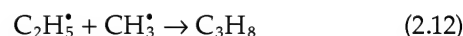
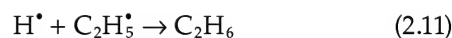
Steam cracking furnaces produce ethylene by heating hydrocarbons such as ethane, propane, butane, naphtha, or gas oils to very high temperatures in the presence of steam. Depending on the type of feed and the severity of cracking, typical reactor coil outlet temperatures are in the range of 1450°F–1625°F (788°C–885°C). As the hydrocarbons reach cracking temperature they decompose through a complex series of free radical reactions into a mixture consisting mostly of olefins such as ethylene and propylene, as well as hydrogen, methane, and other species. For example, ethane typically decomposes into hydrogen and ethylene, for which the molecular reaction is as follows:



This is a very simplified representation. In reality, this reaction proceeds via a number of radical reactions that include the following initiation and propagation steps:



Besides forming the desired products hydrogen and ethylene, the radical reactions also terminate by recombination to form undesired products, e.g.,



Thermodynamic equilibrium favors the formation of olefins only at high temperatures and low pressures. Typical reactor coil outlet pressures are 25–35 psia (1.7–2.4 bara). The hydrocarbon partial pressures are lowered further by the presence of the dilution steam. A high selectivity is achieved by operating with very low residence times, typically 0.1–0.5 s.

### 2.4.3 Severity of Cracking

Conversion and severity are measures for the extent of cracking. Conversion is used when the feed consists of one or two components, and describes how much of the component is converted into products. When the feed consists of many different components, as is the case for example for naphtha, conversion is not a practical manner to describe the extent of the reactions. Instead, the composition of the product is used instead. A typical measure for severity is the ratio of propylene to ethylene, or the ratio of methane to propylene. A simpler way to judge the severity of cracking is by monitoring the coil outlet temperature. Since the actual product yields also depend on coil pressure, steam ratio, and feed properties, this is not a very accurate method.

### 2.4.4 Typical Product Distribution

Typical product distributions for various types of feeds are shown in Table 2.4.

### 2.4.5 Coking

The high endothermic heats of cracking combined with very short residence times require high heat fluxes and result in very high tube skin temperatures ranging typically between 1825°F–2050°F (1000°C–1125°C). An undesired side reaction is the formation of coke (carbon) on the inside of process tube walls. Coke production is a strong function of skin temperature. It can exist in various morphologies, depending on feed composition and tube



TABLE 2.4

Typical Product Distributions for Common Pyrolysis Feeds

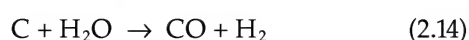
Feed	Ethane	Propane	Butane	Naphtha	Naphtha
Conversion/ Severity	65%	95%	96%	High	Low
Steam/ Hydrocarbon Ratio	0.3	0.3	0.4	0.5	0.5
H <sub>2</sub>	3.9	1.6	1.2	1.0	0.8
CH <sub>4</sub>	3.8	25.3	21.7	18.0	12.6
C <sub>2</sub> H <sub>2</sub>	0.5	0.6	0.8	1.0	0.4
C <sub>2</sub> H <sub>4</sub>	52.0	39.0	39.2	34.3	25.5
C <sub>2</sub> H <sub>6</sub>	35.0	3.9	3.0	3.8	4.3
C <sub>3</sub> H <sub>6</sub>	1.0	11.3	15.3	14.1	17.0
C <sub>3</sub> H <sub>8</sub>	0.2	5.0	0.2	0.4	0.5
C <sub>4</sub> H <sub>6</sub>	1.4	4.5	4.1	4.5	4.5
C <sub>4</sub> H <sub>8</sub>	0.2	0.8	1.7	3.7	6.5
C <sub>4</sub> H <sub>10</sub>	0.2	0.1	4.0	0.2	0.8
C <sub>5</sub> -C <sub>8</sub>					
Non-aromatic	0.7	1.9	2.8	2.9	11.4
Aromatics	0.5	3.5	3.4	9.7	10.7
C <sub>9+</sub>	0.0	0.9	0.9	1.4	2.2
Fuel oil	0.0	0.4	0.6	4.2	2.5

metallurgy.<sup>12</sup> Typically, it can be categorized as two types: catalytic and pyrolytic. Catalytic coke is formed by the reaction between hydrocarbon and metal surface components (mostly nickel and iron) of the reactor tube. The resulting catalytic coke is somewhat rigid and branch-like in structure, creating “trapping” sites that promote pyrolytic coke formation and accumulation. On the other hand, pyrolytic coke is softer and less structured than catalytic coke, and can be easily flushed through the system. It is formed by several related mechanisms, including dehydrogenation, polymerization, and condensation of both light olefinic and heavy aromatic compounds.

As the coke layer gets thicker, both the process pressure drop and the tube skin temperature increase. When either a pressure drop limit (typical for the hard, high thermal conductivity coke produced from a low molecular weight feed like ethane) or a tube skin temperature limit (typical for the soft, low thermal conductivity coke produced from a high molecular weight feed like gas oil) is reached, the furnace tubes must be decoked using a steam/air mixture.

#### 2.4.6 Decoking

Decoking is the process where a mixture of steam and air is introduced into the coils to gasify and burn the coke. There are two parallel reaction mechanisms in effect, gasification and oxidation of the carbon. The endothermic steam gasification reaction produces carbon monoxide and hydrogen as follows:



A small minority of producers use steam-only decoking. For this operation, much higher temperatures are required—typically 1850°F (~1000°C). Some ethylene producers carry out all of their decoking using only steam, which means that their radiant coil inlet temperatures must be high in order to achieve an efficient decoke.

An efficient way for coke removal is burning the coke directly with oxygen:



Like any other combustion reaction, it is exothermic. The speed of the reaction must be limited; otherwise, the local metal temperatures become too high. This is why most producers use a steam/air mixture for decoking. In addition to acting as a heat sink for the combustion heat and preventing thermal shocks, the steam is also used to maintain the optimum velocity inside the tubes.

The coke burn-off starts as soon as the oxygen and the coke meet inside the heated tubes: therefore the decoking progresses from the beginning to the end of the coil. Because of its exothermic nature, the procedure itself must be carried out carefully, since there are risks of

- Overheating the tubes, when the reaction proceeds too rapidly
- Breaking the coils, when thermal shocks cause the tubes to contract faster than the coke
- Erosion, due to excessive velocities of spalled coke particles
- Plugging the tubes or the downstream transfer line exchanger (or “TLE”) tube sheets due to excessive spalling
- Tube carburization, oxidation, bowing

#### References

1. Seebold, J. G., Waibel, R. T., and Webster, T. L., Control refinery NOx emissions cost-effectively, *Hydrocarbon Processing*, 80(11), 55–59, 2001.
2. U.S. Energy Information Administration, 2006 energy consumption by manufacturers—Data tables, Table 1.2. <http://www.gov/emeu/mecs/mecs2006/2006tables.html>
3. U.S. Department of Energy, Office of Industrial Technology, *Petroleum—Industry of the Future: Energy and Environmental Profile of the U.S. Petroleum Refining Industry*, U.S. Department of Energy, Washington, DC, December 1998.

4. Sanderford, E. B., *Alternative Control Techniques Document—NO<sub>x</sub> Emissions from Process Heaters*, U.S. Environment Protection Agency Report EPA-453/R-93-015, February, 1993.
5. Speight, J. G. and Özüm, B., *Petroleum Refining Processes*, Marcel Dekker Inc., New York, 2002.
6. Elshout, R., Hydrogen production by steam reforming, *Chemical Engineering*, 117(5), 34–38, 2010.
7. West-Toolsee, E. and Patel, R., Maximize ammonia production cost-effectively, *Hydrocarbon Processing*, 82(4), 67–72, 2006.
8. McNutt, M. K., U.S. Geological Survey, *Mineral Commodity Summaries*, January 2011. <http://minerals.usgs.gov/minerals/pubs/mcs/2011/mcs2011.pdf>
9. McAdams, J. D. and Waibel, R., Methanol furnace combustion troubleshooting, *Proceedings of International Methanol Technology and Operators Forum (IMTOF)*, Johnson Matthey Catalysts, Billingham, Cleveland, England, June 2007.
10. Baukal, C. E., Ed. *Industrial Combustion Testing*, CRC Press LLC, Boca Raton, FL, 2010.
11. Picciotti, M., Novel ethylene technologies developing, but steam cracking remains king, *Oil & Gas Journal*, 95(25), 53–58, 1997.
12. Sundaram, K. M., Olszewski, E. F., and Shreehan, M. M., Ethylene, *Kirk-Othmer Encyclopedia of Chemical Technology*, 4th edn., Vol. 9, John Wiley & Sons, New York, 1994.

# 3

## Fuels

John Ackland, Jeff White, and Richard T. Waibel

### CONTENTS

3.1	Introduction .....	46
3.2	Oil Recovery .....	46
3.3	Natural Gas.....	47
3.4	Processing, Refining, and Fuel Use.....	48
3.4.1	Liquefied Petroleum Gas .....	50
3.4.2	Refinery Gases.....	51
3.4.3	Combustible Off-Gas Streams .....	52
3.4.3.1	Pressure Swing Adsorption (PSA) Tail Gas .....	52
3.4.3.2	Flexicoking Waste Gas.....	53
3.4.4	Liquid Fuels .....	54
3.4.4.1	Light Oils.....	54
3.4.4.2	Heavy Oils.....	54
3.4.4.3	Residual Oils.....	54
3.4.5	Liquid Naphtha .....	55
3.4.6	Typical Flared Gas Compositions.....	55
3.4.6.1	Oil Field/Production Plant Gases.....	55
3.4.6.2	Refinery Gases.....	57
3.4.6.3	Ethylene/Polyethylene Gases .....	57
3.4.6.4	Other Special Cases .....	57
3.5	Fuel Properties .....	58
3.5.1	Molecular Weight.....	58
3.5.2	Lower and Higher Heating Values.....	63
3.5.3	Specific Heat Capacity.....	63
3.5.4	Flammability Limits.....	63
3.5.5	Flame Speed.....	63
3.5.6	Viscosity .....	64
3.5.7	Derived Quantities .....	64
3.5.7.1	Partial Pressure .....	64
3.5.7.2	Adiabatic Flame Temperature .....	64
3.5.7.3	Heat Release .....	65
3.5.7.4	Volume Equivalent of Flow .....	65
3.5.8	Liquid Fuel Properties.....	65
3.5.8.1	Flash Point.....	65
3.5.8.2	Pour Point.....	65
3.5.8.3	Distillation.....	65
3.5.8.4	Viscosity .....	65
3.5.8.5	Density, Gravity, Specific Volume, and Specific Weight.....	66
3.5.8.6	Heat Capacity (Specific Heat) .....	66
3.5.9	Photographs of Gaseous Fuel Flames .....	69
	References.....	77



### 3.1 Introduction

Gaseous and liquid fuels are a key component in today's energy processes. During the Industrial Revolution, starting in the mid-eighteenth century, the major energy source used in the world changed from charcoal (wood) to various forms of coal. As technology developed, the world began moving from the use of coal to crude oil (the most abundant liquid fuel used in industry today), and its derivatives, to provide the energy and heating requirements needed. The modern era of viable crude oil production and use began with commercial wells in the mid-1800s. An increasing need for oil products in technology (such as gasoline for the internal combustion engine and automobiles) spurred massive efforts in oil exploration and recovery in the early 1900s.

Major oil deposits found in the United States prompted it to become a major world oil producer. The successes of American oil discovery and production inspired oil companies in other countries to start a worldwide exploration for oil reserves. In the mid-1950s, major U.S. oil companies provided approximately two-thirds of the world's oil supply at prices near \$1 per barrel (a dramatic difference from today's, per barrel, rate).<sup>1</sup> In 1960, the Organization of Petroleum Exporting Countries (OPEC) was founded by the governments of major oil-exporting countries for the purpose of stabilizing oil production and prices. As the demand for oil increased, the production inevitably increased, leading to new technological developments in drilling and exploration techniques that have identified and exploited oil reserves throughout the world. The vast majority of the known oil reserves in the world are located in the Middle East (approximately two-thirds), while the United States ranks eighth on the known reserve list.

Oil exploration, which initially was confined to land, has led to recovery efforts on the bottom of the ocean floor. The most abundant forms of oil deposits found in the world today are oil shale, heavy oil deposits, and tar sands. However, difficulty with, and the high cost of, extracting oil from these complicated mediums keeps conventional crude oil recovery as the leading source of usable raw material for refining processes. Figure 3.1 shows the capping of a burning oil well.

Similar to oil exploration, gas exploration is booming in a world that is looking for every possible energy source. Enormous gas deposits have been found in sites all over the world, and these are currently being exploited at an incredible rate. New methods of recovering gas are also allowing previously unreachable reserves to be tapped and utilized.



**FIGURE 3.1**  
Capping a burning oil well.

### 3.2 Oil Recovery

Crude oil is found in deep, high-pressure reservoirs, encased in rock, beneath the earth's surface. Oil companies use complicated drilling techniques to tap into these pockets and bring the crude oil to the surface so that it can be collected. Oil drilling is an expensive process that can be complicated by the location of the oil in the earth. Therefore, oil companies spend millions of dollars annually in exploration and cost analysis of potential, new oil reserves. Incredibly hard rock and deep reserves (sometimes greater than 3000 ft [~900 m] below the surface) necessitate the use of specially designed drill bits that will stand up to the high pressures and constant mechanical trauma encountered in drilling. Once an oil reservoir is "hit," the oil, now having an avenue to expand, will rush out of the drilling channel that was cleared by the drilling rig. The oil will be continuously extracted until the reservoir becomes depleted to the extent that it is no longer economically viable for a company to spend time and money to retrieve it. When the oil pressure in the reservoir becomes too low for natural extraction, pumps can be used to help with the extraction. Other means of keeping reservoirs "active" include injecting water, steam, or chemicals into the reservoir to help make low-pressure or viscous oil easier to extract.

Once the crude oil has been collected, and temporary storage facilities are nearing their capacity, it must be off-loaded so that further collection is possible. The most common methods of off-loading and transporting crude oil are pipelines (such as the Great Alaskan Pipeline), seafaring oil tankers, and barges. These transportation methods deliver the crude oil to locations around the world for refining into usable petroleum products.





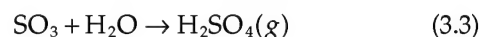
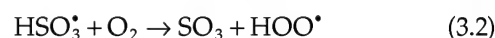
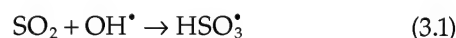
After the necessary purification processes have been completed, the “commercial-grade” natural gas is compressed to approximately 1000 psig (6.9 MPa) and is introduced to a natural gas pipeline distribution network where it is recompressed, if necessary, on its way to the consumer.

### 3.4 Processing, Refining, and Fuel Use

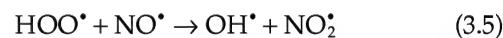
The primary concern for a typical refinery is to convert a barrel of crude oil, 42 U.S. gal (159 L) into usable products. A barrel of crude oil can typically be refined to provide 11 gal (42 L) of gasoline, 5.3 gal (20 L) of kerosene, 20.4 gal (77 L) of gas oil and distillates, and 5.3 gal (20 L) of heavier distillates.<sup>7</sup> The end products derived from crude oil number in the thousands, many of which can be found in Table 3.3. The processes that produce these different products are vast and complicated. Figure 3.2<sup>7</sup> provides a general refinery flow diagram.

The primary chemical components of crude oil are carbon, hydrogen, sulfur, oxygen, and nitrogen. The percentages of these elements found in a crude oil are most frequently used to characterize the oil. Two terms frequently used when referring to crude oil are “sweet” crude and “sour” crude. Sweet crude is the oil that contains less than 0.5 wt.% sulfur, while sour crude

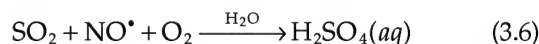
contains greater than 0.5 wt.% sulfur. Sulfur content is of importance and concern, due to the sulfur oxides (SO<sub>x</sub>) that are produced during combustion. SO<sub>2</sub>, for example, is a gas that has been shown to contribute significantly to several different environmental problems—namely, in acid rain formation and in its ready conversion to sulfuric acid, H<sub>2</sub>SO<sub>4</sub>. The nitrogen content of crude oil is of special interest to the combustion industry due to the high levels of nitrogen oxides or NO<sub>x</sub> (see Chapter 15) produced during combustion of these fuels (e.g., approximately 0.2 lb per MMBtu NO<sub>x</sub> or 142 ppm (291 mg/N-m<sup>3</sup>) can be attributed to “Fuel NO<sub>x</sub>” for an oil that contains 0.47 wt.% nitrogen when fired in a “conventional” oil burner). Like SO<sub>x</sub>, NO<sub>x</sub> is an environmentally damaging group of gases. Any time a fuel is burned in air with a hot flame, NO<sub>x</sub> are produced. The greater the flame temperature of the combustion, the greater the amount of NO that will be produced. NO is then oxidized to form NO<sub>2</sub> (over a period of minutes or hours), which is a major contributor to photochemical smog. In general, the fate of SO<sub>2</sub> and NO are intertwined, as can be seen by the following reaction sequence:<sup>8</sup>



The following is a parallel reaction that takes place between nitrogen oxide and the hydroperoxy radical, thus producing more of the hydroxyl radical to feed the aforementioned initial reaction:



The overall reaction is then



Crude oil compositions are relatively constant. However, slight deviations in composition can result in vastly different refining methods. Crude oils also contain inorganic elements such as vanadium, nickel, and sodium, and usually contain some amount of water and ash (noncombustible material). The main hydrocarbon constituents of crude oils are alkanes (paraffins), cycloalkanes (naphthenes), and aromatics.

Alkanes (also called paraffins after the Latin *parum affinis*, “little affinity”) are those chemical structures that are based on carbon atoms having only single bonds

TABLE 3.3

Quantitative Listing of Products Made by the U.S. Petroleum Industry

Product Classification	Number of Individual Products
Lubricating oils	1156
Chemicals, solvents, misc.	300
Greases	271
Asphalts	209
Waxes	113
White oils	100
Rust preventatives	65
Diesel and light fuel oils	27
Motor gasolines	19
Residual fuel oil	16
Liquified gases	13
Other gasolines	12
Transformer and cable oils	12
Kerosenes	10
Aviation gasolines	9
Jet fuels	5
Carbon blacks	5
Cokes	4
Fuel gas	1
Total	2347

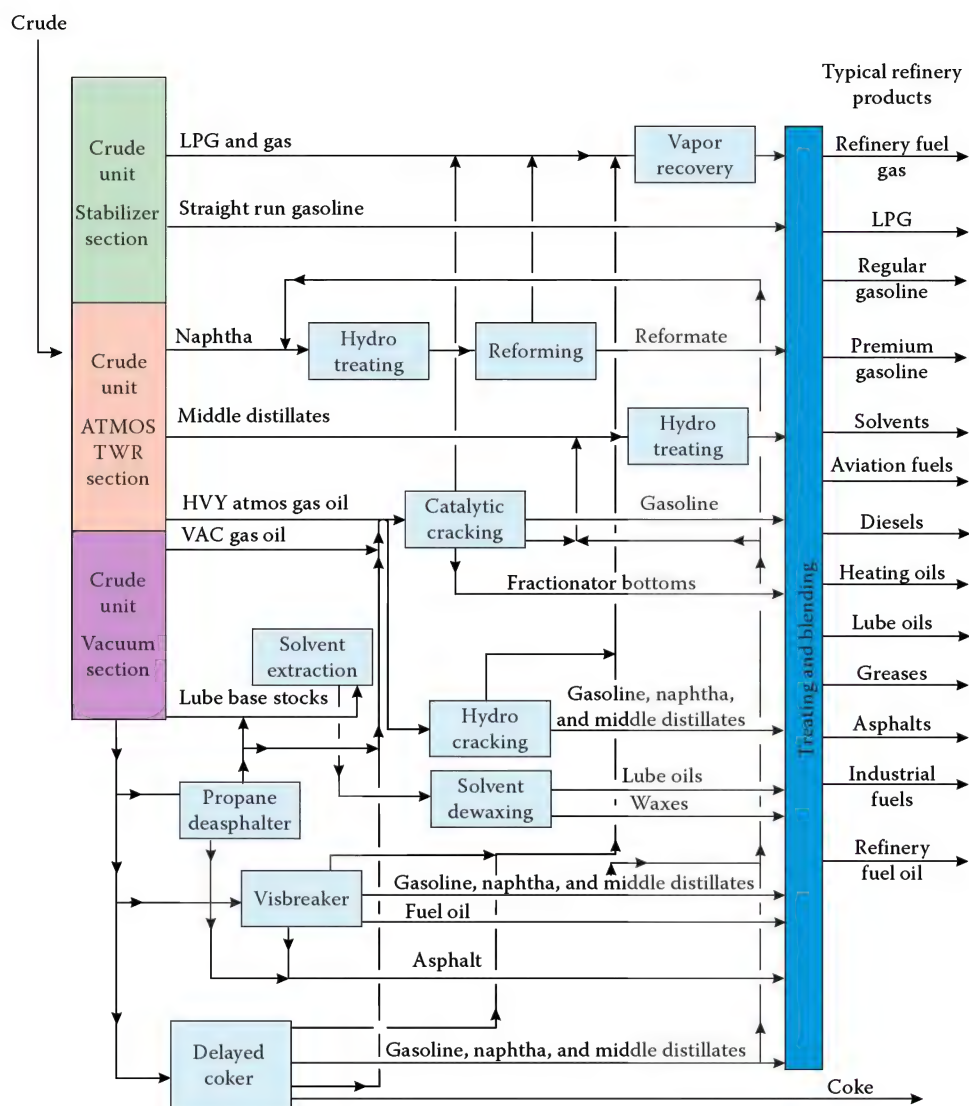


FIGURE 3.2

Refinery flow diagram. (From Gary, J.H. and Handwerk, G.E., *Petroleum Refining*, 3rd edn., Marcel Dekker, New York, 1994.)

and that are completely saturated with hydrogen atoms. Some of the alkane hydrocarbons are listed in Table 3.14. The basic chemical formula for an alkane is  $C_xH_{2x+2}$ , where "x" is the number of carbon atoms present. Crude oils can contain structures with up to 70 carbon atoms.<sup>7</sup> However, the vast majority of the compounds contain 40 carbon atoms or less. When the number of different constitutional isomers (different chemical connectivity and different physical properties, yet identical chemical formulae) is considered (tetracontane [ $C_{40}H_{82}$ ] has over 62 trillion possible isomers<sup>9</sup>), it is evident that the compositional diversity between differing crude oils is almost limitless.

Cycloalkanes (cycloparaffins or naphthenes) are alkanes in which all or some of the carbon atoms are arranged in a ring. When a cycloalkane contains only one ring, the general formula is  $C_xH_{2x}$ . The most

stable cycloalkane is cyclohexane, while cyclobutane and cyclopropane are the least stable. The properties of cycloalkanes are very similar to those of alkanes, as shown in Table 3.14.

Aromatic compounds are those compounds that contain at least one benzene-like ring. Benzene, discovered in 1825, has a chemical formula of  $C_6H_6$ , and is stable and nonreactive relative to alkanes and cycloalkanes. Aromatics, such as the heterocyclic compounds pyridine and furan, are composed of rings that contain elements other than carbon. For example, the benzene ring contains six carbon atoms, whereas the pyridine ring contains five carbon atoms and one nitrogen atom. Properties of some of the aromatic compounds are contained in Table 3.14.

It is worth mentioning the group of compounds called alkenes (olefins). Alkene compounds do not



TABLE 3.4

General Fraction Boiling Points

Distillation Fraction	Temperature Range (°F)
Butanes and lighter	<90
Gasoline	90–220
Naphtha	220–315
Kerosene	315–450
Fuel oils	450–800
Residue	>800

occur naturally in crude oil, but are produced by reaction during the refining process. Therefore, it should be expected that a refined end product will have some percentage of ethylene, propylene, or butylene, for example. Alkenes have the general formula  $C_xH_{2x}$  and contain a carbon-carbon double bond. Properties of some of the alkenes are contained in Table 3.14.

When a crude oil is refined, the first step is, invariably, distillation. The purpose of distillation is to separate lighter components from heavier ones, based on their respective volatility. The target of distillation is to separate the crude oil into different fractions. Each fraction consists of a boiling point range that will yield a mixture of hydrocarbons (see Table 3.4). Some of these mixtures can then be used as product (fuels, solvents, etc.) or further refined into gasoline or other desirable mixtures. Catalytic cracking is a typical process used to break down and rearrange alkane mixtures produced via distillation into smaller, highly branched alkanes by heating the mixtures to high temperatures in the presence of a variety of catalysts. Figure 3.3<sup>10</sup> shows a fluid catalytic cracking process. Due to the reactions that take place during catalytic cracking, the product streams are generally heavier than the feed streams.

Alkanes that are more highly branched are desirable because they have a higher octane rating than their unbranched cousins.

There are numerous “gases” that make up the base of the refinery or chemical plant. Among others, natural gas and LPG are used as standard “back-up” and emergency fuels, and other specialty refinery gas and off-gas mixes (such as PSA or Flexicoking gas) are often “recycled” since natural gas and LPG may be purchased utilities that bear a financial burden along with their use.

### 3.4.1 Liquefied Petroleum Gas

Liquefied petroleum gas (LPG) is the general term used to describe a hydrocarbon that is stored as a liquid under moderate pressure but is a gas under normal atmospheric conditions. LPG is vaporized for use as a fuel. The primary chemical components of LPG are propane, propylene, normal butane, isobutane, and butylene.<sup>11</sup> The GPSA Engineering Data Book contains industry standard product specifications for commercial propane (predominantly propane and/or propylene), commercial butane (predominantly butane and/or butylene), and commercial butane-propane mixtures.<sup>3</sup> LPG produced via the separation of heavier hydrocarbons from natural gas is mainly paraffinic, containing primarily propane, normal butane, and isobutane. LPG derived from oil-refinery gas may contain varying small amounts of olefins such as propylene and butylene.<sup>11</sup>

Most of the LPG used in the United States consists primarily of propane.<sup>12</sup> Elsewhere, however, LPG compositions may contain high fractions of butane and iso-butane. Due to their relatively high boiling point, LPG mixtures containing high concentrations of normal butane (boiling point = 31°F or -1°C at atmospheric

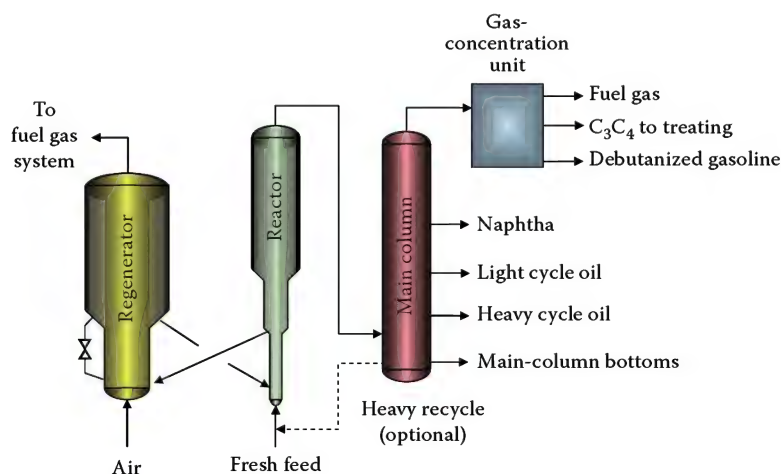


FIGURE 3.3

Flow diagram of UOP fluid catalytic cracking complex. (From Meyers, R.A., *Handbook of Petroleum Refining Processes*, 2nd edn., McGraw-Hill, New York, 1997, Chapter 3.3.)



pressure) or isobutane (boiling point = 11°F or -12°C at atmospheric pressure) are preferred for use in warm climates. Conversely, LPG mixtures containing high concentrations of propane (boiling point = -44°F or -49°C) are typically preferred for use in cold climates.<sup>4</sup>

### 3.4.2 Refinery Gases

Internally generated refinery fuel gases serve as the primary fuel component for most refineries, petrochemical plants, and hydrocarbon facilities. It is not usual for a process unit to produce its own fuel supply and usually fuel gas streams from various processing units are delivered to a common mixing point within the plant, before the new gas mixture is returned to the processing units as refinery gas. Refinery fuel gases contain an extremely wide variety of chemical constituents, including paraffins, olefins, diolefins, aromatics, mercaptans, organic sulfides, ammonia, hydrogen sulfide, carbon monoxide, carbon dioxide, etc. Because plants must operate in a manner best suited to maximize profit, the individual fuel gas streams originating at each process unit will vary in composition and quantity, depending on numerous economic and technical factors.<sup>13</sup> Table 3.5 contains typical chemical compositions of fuel gas streams originating from various process units within a petroleum refinery.<sup>14</sup>

It is very important that the refinery fuel gas leaving the common mixing point is a homogeneous mixture of the fuel gas streams supplied. If the individual fuel gas supply streams vary significantly in calorific value, and if the supply streams are not combined in a homogeneous

manner, the calorific value of the nonhomogeneous refinery fuel gas mixture will also vary widely and often instantaneously, which can wreak havoc on furnace and burner control systems unless the equipment is specifically adapted for such use. All of the combustion performance parameters—including burner stability, emissions control, heat transfer efficiency, and heat flux—will suffer as a result of the nonhomogeneous fuel mixture.<sup>13</sup> Static mixers are often used in various segments of industry to ensure a well-mixed, homogeneous fuel gas mixture, but they require high pressure drop that may push the pressure drop limits of the typically overloaded refinery fuel gas system.

Another problem often associated with the combustion of refinery fuel gases is the presence of liquid hydrocarbons in the refinery fuel gas stream, which can accelerate the coking and plugging rates of downstream gas burner components. Sources of unwanted liquid hydrocarbons in refinery fuel gas streams include condensation of heavier fuel gas components (C<sub>5</sub> and higher) due to natural cooling of the fuel gas stream, liquid entrainment into absorber or fractionator overhead gas streams, and lubrication oil contamination of the fuel gas stream. Potential solutions for the problems associated with these liquid hydrocarbons include liquid extraction of the heavier chemical components (C<sub>5</sub> and heavier) and filtration/coalescence of liquid components from the gas stream. In addition, increasing the velocity of the flowing gas through burner components (tips, risers, etc.) has been proven to cool the hardware and inhibit the cracking reactions that eventually lead to plugging and coking. However, when “dirty” fuel

**TABLE 3.5**

Composition of a Typical Refinery Gas

Fuel Gas Component	Refinery Fuel Gas Source (Dry Gas)					
	Cracked Gas (%)	Coking Gas (%)	Reforming Gas (%)	FCC Gas (%)	Combined Refinery Gas—Sample 1 (%)	Combined Refinery Gas—Sample 2 (%)
CH <sub>4</sub>	65	40	28	32	36	53
C <sub>2</sub> H <sub>4</sub>	3	3	7	7	5	2
C <sub>2</sub> H <sub>6</sub>	16	21	28	9	18	19
C <sub>3</sub> H <sub>6</sub>	2	1	3	15	8	6
C <sub>3</sub> H <sub>8</sub>	7	24	22	25	20	14
C <sub>4</sub> H <sub>8</sub>	1	—	—	—	—	—
C <sub>4</sub> H <sub>10</sub>	3	7	7	0	2	1
C <sub>5</sub> and higher	1	—	—	—	—	—
H <sub>2</sub>	3	4	5	6	3	3
CO	—	—	—	—	—	—
CO <sub>2</sub>	—	—	—	—	—	—
N <sub>2</sub>	—	—	—	7	8	3
H <sub>2</sub> O	—	—	—	—	—	—
O <sub>2</sub>	—	—	—	—	—	—
H <sub>2</sub> S	—	—	—	—	—	—
Total	100	100	100	100	100	100

gases are involved, an appropriate and regimented maintenance plan is crucial for long-term viability and performance of the equipment.

Wet fuel gas can introduce problems in cooler climates associated with the condensation and subsequent freezing of water vapor inside the fuel gas system. If the water vapor reaches the dew point in a cold atmospheric environment, there is danger of frost stoppage, freezing, or bursting of lines—a considerable fire safety hazard that merits serious thought. Options to combat water present in the fuel gas system include dehydration systems (as discussed in Section 3.3) and steam/electric tracing of refinery fuel gas lines.<sup>13</sup>

### 3.4.3 Combustible Off-Gas Streams

The quantity and variety of combustible off-gas streams in the hydrocarbon and petrochemical industries are virtually unlimited. Many of these waste gas streams are relatively high in inert concentration, with large amounts of nitrogen and carbon dioxide often present. As a result, these waste fuels are often low in heat content, with lower heating values in the range of 200–800 Btu/scf (7.9–31.5 MJ/Nm<sup>3</sup>). Additionally, as a result of the processes responsible for their creation, they are frequently only available at low pressure (<7 psig or 0.48 barg). For these reasons, off-gases are not usually compressed into the main refinery fuel gas system. Two of the most widely used combustible off-gases—Pressure Swing Adsorption (PSA) tail gas and Flexicoking gas—are discussed in detail in the following sections.

#### 3.4.3.1 Pressure Swing Adsorption (PSA) Tail Gas

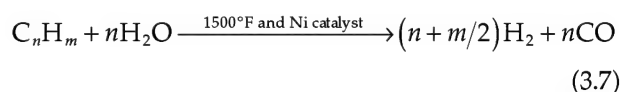
PSA tail gas is a low-pressure, low-heating value fuel gas produced as a by-product of a PSA process—a key purification component in the steam reforming hydrogen production process. Table 3.6 contains the approximate composition of a typical PSA tail gas fuel stream.

PSA is a cyclic process that uses beds of solid adsorbent to remove impurities such as carbon dioxide, carbon

monoxide, methane, and nitrogen from the hydrogen production stream. A simplified process flow diagram of a typical steam reforming hydrogen production unit using PSA is shown in Figure 3.4.<sup>15</sup>

The steam reforming process is conducted in four stages:<sup>7,12,15</sup>

1. Feedstock preparation: feedstock (light hydrocarbons such as methane, propane, butane, and light liquid naphtha) at approximately 450 psig (30.6 barg) is preheated and purified to remove reformer catalyst poisons such as halogens and sulfur-containing compounds.
2. Reforming: the purified feedstock is reacted with steam to form carbon monoxide and hydrogen:



The reaction is endothermic and occurs within the process tubes of a reformer furnace in the presence of nickel catalyst at approximately 1500°F (815°C).

3. Shift conversion: the water-gas shift reaction is employed to convert the carbon monoxide produced in the reforming step into additional hydrogen and carbon dioxide:



The shift conversion step is exothermic and is conducted at approximately 650°F (340°C) in the presence of a chromium/iron oxide catalyst.

4. Hydrogen purification/PSA: following the shift conversion step, the hydrogen production stream enters the PSA portion of the process. Adsorbent beds remove the impurities (carbon dioxide, carbon monoxide, methane, and nitrogen) and a small portion of the product. Typical hydrogen recovery is 80% or greater, with product purity of approximately 99.9 vol%.

The PSA unit must be frequently regenerated via depressurization of the adsorbent beds. When depressurization occurs, PSA off-gas is produced at a pressure of about 5 psig (0.34 barg) or less. The PSA off-gas consists of the impurities removed by the adsorbent beds, as well as the hydrogen that is not recovered in the product stream. The off-gas serves as the primary fuel for the reformer furnace burners. Due to difficulties associated with firing the low-pressure, high-inert concentration (carbon dioxide and nitrogen) PSA off-gas alone, the PSA off-gas is typically supplemented by refinery fuel gas or natural gas, in a “typical” ratio of 85% volume PSA gas to 15% supplementary gas. The PSA and

TABLE 3.6

Typical Composition of Steam Reforming/PSA Tail Gas

Fuel Gas Component	PSA Tail Gas Composition (Vol%)
CH <sub>4</sub>	17%
H <sub>2</sub> O	<1%
H <sub>2</sub>	28%
CO <sub>2</sub>	44%
CO	10%
N <sub>2</sub>	<1%
Total	100%

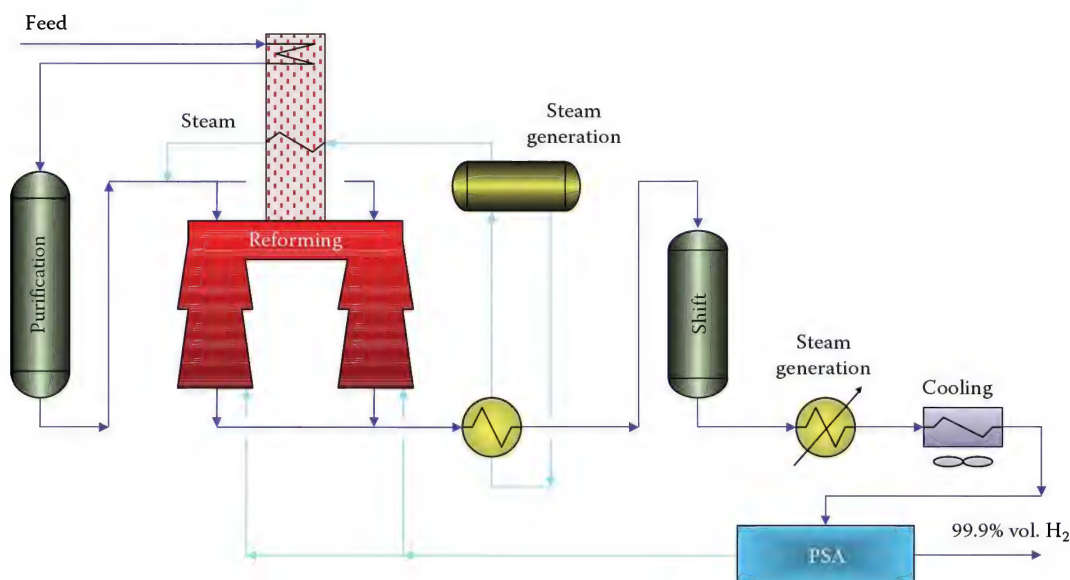


FIGURE 3.4

Simplified process flow diagram for hydrogen reforming/pressure swing adsorption. (Adapted from Meyers, R.A., *Handbook of Petroleum Refining Processes*, 2nd edn., McGraw-Hill, New York, 1997, Chapter 6.2.)

refinery fuel gases are fired in dual-fuel burners specifically designed for the steam reforming/PSA process.

### 3.4.3.2 Flexicoking Waste Gas

Flexicoking waste gas is a low-pressure, low-heating value fuel gas produced by petroleum refiners as a by-product of the Exxon Flexicoking process. Flexicoking is a continuous fluidized-bed thermal cracking process used in the conversion of heavy hydrocarbon feedstocks (typically heavy gas oils from atmospheric and vacuum distillation) to various gaseous and liquid hydrocarbon products. Table 3.7 contains the approximate

composition of two sample Flexicoking waste gas fuel streams.<sup>16</sup>

A simplified process flow diagram of the Flexicoking process is shown in Figure 3.5.<sup>16</sup> In the Flexicoking process, hot (500°F–700°F or 260°C–370°C) gas oil is injected into the reactor vessel containing hot, fluidized coke particles. Thermal cracking reactions inside the reactor vessel produce fresh petroleum coke that is deposited as a thin film on the surface of existing coke particles inside the reactor bed. Cracked vapor products exit the Flexicoking process through the reactor vessel overhead stream for additional downstream processing. Coke from the reactor vessel is continuously injected into the top of a second fluidized vessel, the coke heater, where it is heated and recycled to maintain a reactor bed temperature of 950°F–1000°F (510°C–540°C). A portion of the coke fed into the top section of the coke heater is injected into the bottom of a third fluidized vessel, the gasifier. Inside the gasifier, the coke is reacted with air and steam at approximately 1500°F–1800°F (820°C–980°C), producing a low-Btu fuel gas, or Flexicoking gas, consisting primarily of nitrogen, hydrogen, carbon monoxide, and carbon dioxide. The Flexicoking gas flows from the top of the gasifier to the bottom of the heater, where it provides the heat necessary to maintain the reactor bed temperature and helps fluidize the coke heater bed. The high-temperature Flexicoking gas leaving the coke heater is used for high-pressure steam generation before entrained coke fines are removed in a cyclone/venturi scrubber system. Because the low-Btu gas stream leaving the Flexicoking process contains substantial concentrations of H<sub>2</sub>S (~150 ppm by volume), the gas must first be sent through a hydrogen sulfide removal system before it can be burned as fuel.<sup>7,16</sup>

TABLE 3.7

Typical Composition of Flexicoking Waste Gas

Fuel Gas Component	Flexicoking Waste Gas Composition (by Volume)	
	Sample 1	Sample 2
CH <sub>4</sub>	1.0%	0.8%
H <sub>2</sub>	20.0%	21.0%
CO <sub>2</sub>	10.0%	10.5%
CO	20.0%	18.6%
N <sub>2</sub>	45.0%	45.6%
H <sub>2</sub> O	4.0%	3.5%
H <sub>2</sub> S	150 ppm	0
COS	120 ppm	120 ppm
Total	100.0%	100.0%

Source: Meyers, R.A., *Handbook of Petroleum Refining Processes*, 2nd edn., Chapter 12.1, McGraw-Hill, New York, 1997.







TABLE 3.8

Requirements for Fuel Oils (per ASTM D 396)

	No. 1	No. 2	No. 4	No. 6
Classification	Distillate	Distillate	Distillate (Heavy)	Residual
Density (kg/m <sup>3</sup> ) at 60°F (15°C), max	850	876	—	—
Viscosity at 104°F (40°C) mm/s <sup>2</sup>				
Min	1.3	1.9	>5.5	—
Max	2.1	3.4	24	—
Viscosity at 212°F (100°C) mm/s <sup>2</sup>				
Min	—	—	—	15
Max	—	—	—	50
Flash point °F (°C), min	100 (38)	100 (38)	131 (55)	140 (60)
Pour point °F (°C), max	−0.4 (−18)	21 (−6)	21 (−6)	—
Ash, % mass, max	—	—	0.1	—
Sulfur, % mass, max	0.5	0.5	—	—
Water and sediment, % vol., max	0.05	0.05	0.5	2.0
Distillation temperature °F (°C)				
10% volume recovered, max	419 (215)	—	—	—
90% volume recovered, min	—	540 (282)	—	—
90% volume recovered, max	550 (288)	640 (338)	—	—

TABLE 3.9

Typical Analysis of Different Fuel Oils

	No. 1 Fuel Oil	No. 2 Fuel Oil	No. 4 Fuel Oil	No. 6 Fuel Oil (Sour)
Ash (%)	<0.01	<0.01	0.02	0.05
Hydrogen (%)	13.6	13.6	11.7	11.2
Nitrogen (%)	0.003	0.007	0.24	0.37
Sulfur (%)	0.09	0.1	1.35	2.1
Carbon (%)	86.4	86.6	86.5	85.7
Heat of combustion (HHV), Btu/lb	20187	19639	19382	18343
Specific gravity 60/60°F	0.825	0.84	0.898	0.97
Density (lb/US gal)	6.877	6.96	7.488	8.08

for proper combustion. Due to its high viscosity, No. 6 oil requires heating during handling and further heating prior to combustion chamber injection. No. 6 oil is usually preheated to 150°F–200°F (66°C–93°C), to decrease its viscosity, before being atomized and injected into the burner. Depending on the quality of the heavy oil, John Zink recommends a maximum viscosity of 20–42 cSt for use in its standard oil guns. Figures 3.6 through 3.8 show burners firing heavy fuel oil.

### 3.4.5 Liquid Naphtha

Liquid naphtha is similar in its characteristics to kerosene (Tables 3.10 and 3.11). Figure 3.9 shows a typical naphtha distillation curve. In general, naphtha will boil out of a mixture between 220°F and 315°F (100°C–157°C). Naphtha is categorized, based on its volatility, into light,

intermediate, and heavy naphtha. Naphtha is a major constituent of gasoline; however, it generally requires further refining to make suitable quality gasoline. Prior to firing naphtha in a burner, care must be taken to vaporize it so that the combustion will be more complete and uniform.

### 3.4.6 Typical Flared Gas Compositions

During emergency situations, or when there is no practical use for the gases, they must be sent to a flare for safe and efficient disposal (see Volume 3, Chapter 11 for a discussion of flares). Gas compositions sent to flares include a large variety of individual compounds. The proportions of these compounds vary widely from one facility to another and even within a single facility from minute to minute. The following sections describe in general terms the kinds of gas streams commonly encountered in flare systems. Table 3.12 includes a brief overview of typical flare gas compositions.

#### 3.4.6.1 Oil Field/Production Plant Gases

Gases produced in oil fields generally consist of saturated hydrocarbon gases (paraffins), together with a certain amount of inerts (e.g., nitrogen or CO<sub>2</sub>). Oil field gases range in molecular weight (MW) from 19 to 25. Such gases may contain significant amounts of H<sub>2</sub>S (sour gas wells) or CO<sub>2</sub>. In some cases, especially offshore, these associated gases are burned continuously in the immediate vicinity of the oil wells. In other cases, the gas is sent to a production plant where it is treated in preparation for pipeline use. The gas can also be reinjected into the underground formation to help maintain operating pressure and flow from the field.



**FIGURE 3.6**  
Viewing oil flame through a burner plenum.



**FIGURE 3.7**  
Burner firing heavy oil (1).

Production plants convert the raw associated gas into several, more valuable products. Undesirable components such as  $H_2S$ ,  $CO_2$ , and water vapor are removed in treatment units. Depending on the composition of the feedstock, production plants may include a debutanizer, a depropanizer, and a deethanizer to separate the large majority of these valuable components. The remainder, mostly methane, becomes pipeline quality natural gas after the addition of odorants such as mercaptans. Within the production plant, it may become necessary to flare the raw associated gas, the pipeline product, or the overhead streams from any of the separation units.



**FIGURE 3.8**  
Burner firing heavy oil (2).

TABLE 3.10

## Naphtha Elemental Analysis

Component	Vol.%
<i>n</i> -Heptane	1.610
Methylcyclohexane	2.433
2-Methylheptane	5.618
4-Methylheptane	1.824
3-Methylheptane	4.841
1 <i>c</i> ,3-Dimethylcyclohexane	3.252
1 <i>t</i> ,4-Dimethylcyclohexane	1.040
1 <i>t</i> ,2-Dimethylcyclohexane	1.169
<i>n</i> -Octane	16.334
1 <i>c</i> ,2-Dimethylcyclohexane	1.674
1,1,4-Trimethylcyclohexane	3.500
2,6-Dimethylheptane	2.094
1 <i>c</i> ,3 <i>c</i> ,5-Trimethylcyclohexane	2.638
<i>m</i> -Xylene	2.426
<i>p</i> -Xylene	0.797
2,3-Dimethylheptane	1.475
4-Methyloctane	3.417
2-Methyloctane	4.491
3-Methyloctane	4.576
<i>o</i> -Xylene	1.137
<i>n</i> -Nonane	10.120
Other	23.534
Total	100.000

TABLE 3.11

## Distillation Fractions as a Function of Temperature Determined by ASTM Method D86

D86 Distillation	°F
0%	250
5%	258
10%	259
20%	262
30%	264
40%	267
50%	270
60%	273
70%	277
80%	282
90%	291
95%	300
97%	309

## 3.4.6.2 Refinery Gases

Refineries treat the liquids produced in the oil fields to generate many essential materials for public consumption as well as further chemical processing. As a result of various treatment processes, hydrogen and unsaturated hydrocarbon gases (olefins, diolefins, aromatics,

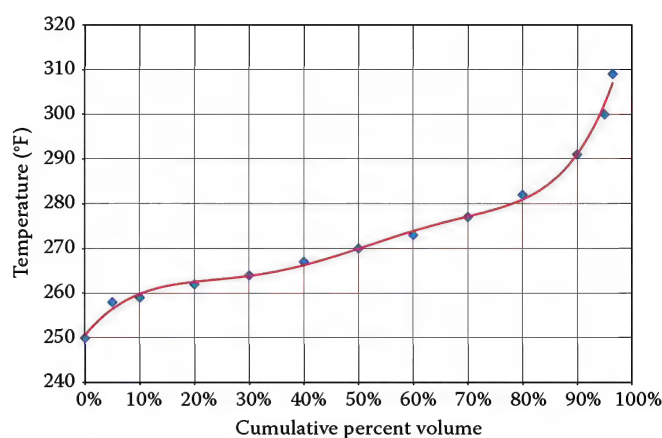


FIGURE 3.9

Naphtha distillation curve.

etc.) are produced in abundance in a refinery. Due to the wide variety of treatment processes, the composition of flared gases in a refinery is almost entirely unpredictable. Refinery flaring generally involves hydrogen, paraffins up to decane, olefins up to hexene, diolefins up to butadiene, and aromatics up to ethylbenzene, as well as contaminants such as  $H_2S$ ,  $CO_2$ , and water vapor.

## 3.4.6.3 Ethylene/Polyethylene Gases

Ethylene plants use cracking furnaces to convert feedstock into high-quality ethylene. Some plants use ethane as feedstock. The gas produced by such plants is often referred to as light cracked gas, and consists of approximately equal portions of hydrogen, ethane, and ethylene with relatively little else. Other plants use oil as feedstock and produce heavy cracked gas. Heavy cracked gas is also approximately equal portions of hydrogen, ethane, and ethylene, but a substantial fraction of the composition consists of heavy hydrocarbon gases such as aromatics and butadiene.

Polyethylene plants take the ethylene from the ethylene plant and polymerize it in a variety of ways. In some cases, the ethylene is mixed with heavier hydrocarbons (pentane, hexane, hexene, etc.) to alter the properties of the polymer. Random mixtures of ethylene and other hydrocarbons may be sent to the flare from the main process area. In addition, reliefs from various special chemical storage areas may send relatively pure materials such as hexane or hexene to the flare.

## 3.4.6.4 Other Special Cases

Landfills and digester facilities produce an off-gas that must be disposed of to prevent odor problems in the community. The gas is generally a mixture of  $CO_2$  and methane. Landfills are rarely above 30%–40% methane, while digesters may be as high as 60%–70% methane. In some landfills, perimeter wells are used to draw air into the



TABLE 3.12

Typical Flared Gas Compositions

	Production Gases	LNG Plants	Refinery Fuel Gas	Landfill	Digester	Marine/Truck Loading	Fertilizer Plants	Incineration Plants
Typical molecular weight	19–25	18–44	2.5–100+ <sup>a</sup>				17–18	20–30
Vol% methane	70–90	80–90	Up to 70–80	30–40	60–70	Up to 20		<5
Vol% ethane	10–15	<10	Up to 40–50			Up to 20		
Vol% propane	5–10	Up to 100	Up to 100			Up to 20		
Vol% butane +	<10					Up to 45–50		
Vol% unsaturates			Up to 100					
Vol% carbon monoxide			Up to 10					Up to 20
Vol% carbon dioxide	<1	<1	Up to 10	Up to 60	20–40			Up to 50
Vol% nitrogen	<5	<5	Up to 15			Up to 40		
Vol% H <sub>2</sub> S	Up to 5–10	<2	Up to 5					
Vol% hydrogen			Up to 90					20–30
Vol% air						3–90		
Vol% ammonia							Up to 100	
Vol% water vapor	1–2		Up to 2				<2–3	Up to 10

<sup>a</sup> Refinery gas composition can be almost anything from high hydrogen to decanes.

edges of the landfill, which prevents the spread of anaerobic bacteria and methane. In these cases, the methane content is even lower and some air is also sent to the flare.

Marine and truck loading facilities burn the vapor displaced from the tankers or trucks during the loading operation. In many cases, the displaced vapor is mostly air with some amount of evaporated gasoline or diesel fuel. Depending on the ambient temperature, the resulting mixture could be very rich in hydrocarbon vapor, or very lean.

Medical equipment, such as bandages or hypodermic needles, is often sterilized by contact with ethylene oxide (ETO) vapors. ETO sterilizer flares are designed to receive the ETO vapor after the sterilization process is complete. The composition coming to these flares generally consists of a mixture of ETO and either air or nitrogen. It should be noted that ETO has a flammability range from 3% to 100% and a very low ignition temperature.

Flares are often used as backup equipment for incinerators during maintenance or malfunctions. In this type of service, the waste gas is usually enriched with a substantial amount of clean fuel gas to ensure reliable burning. Steel mills produce off-gases that consist mainly of H<sub>2</sub>, H<sub>2</sub>O, CO, CO<sub>2</sub>, and air. These are generally low lower heating value (LHV) mixtures that also require enrichment and supplemental fuel firing to maintain ignition. Fertilizer plants and other chemical plants produce ammonia, which may be sent to a flare in an emergency. Waste gases that are sent to flares in these facilities may be pure ammonia or diluted with nitrogen or water vapor.

The variety of gases and the hazards associated with each requires careful review of all aspects of system

design to ensure that these fuels are safely handled, whether in a flare, a furnace, or an incinerator.

### 3.5 Fuel Properties

Tables 3.13 through 3.15 provide physical and combustion property data for a large variety of common fuel gas mixtures and their chemical components.

#### 3.5.1 Molecular Weight

Molecular weight is the mass in grams of 1 g-mol of a chemical compound. Avogadro's number defines the number of molecules in a g-mol to be  $6.02252 \times 10^{23}$ , a fundamental constant. To determine the MW of a mixture of gases, it is necessary to know the MW of each compound and the composition of the gases in terms of mole or mass fractions. Having assembled this information, the following formulae are used to calculate MW:

$$MW = \sum MW_i \times y_i = \frac{1}{\sum \frac{x_i}{MW_i}} \quad (3.9)$$

where

MW is the molecular weight of mixture

MW<sub>*i*</sub> is the molecular weight of component *i*

*y<sub>i</sub>* is the mole fraction of component *i*

*x<sub>i</sub>* is the mass fraction of component *i*



[illegible]

## of FG Mixtures

Component	Natural Gas				LPG		Refinery Gases (Dry)						Waste Gases	
	Tulsa, OK, USA	Alaska, USA	Netherlands	Algeria	Propane	Butane	Cracked Gas	Coking Gas	Reforming Gas	FCC Gas	Refinery Gas Sample 1	Refinery Gas Sample 2	PSA Gas	Flexicoking Gas
Weight	17.16	16.1	18.51	18.49	44.1	58.12	22.76	28.62	30.21	29.18	28.02	24.61	25.68	23.73
Heating value (LHV), Btu/lb	913	905	799	1,025	2,316	3,010	1,247	1,542	1,622	1,459	1,389	1,297	263	131
Heating value (HHV), Btu/lb	1,012	1,005	886	1,133	2,517	3,262	1,369	1,686	1,769	1,587	1,515	1,421	294	142
Specific gravity (air = 1.0)	0.59	0.56	0.64	0.64	1.53	1.1	0.79	0.99	1.05	1.01	0.97	0.85	0.89	0.82
Specific heat, Btu/lb-°F	1,318	1,343	1,108	1,416	2,035	3,110	1,540	1,694	1,726	1,579	1,538	1,541	312	157
Thermal efficiency (C <sub>p</sub> /C <sub>v</sub> )	1.30	1.31	1.31	1.28	1.13	1.10	1.24	1.19	1.19	1.20	1.21	1.23	1.33	1.38
Specific air required, lb/lb	10,554	10,567	10,554	10,525	10,369	10,371	10,402	10,379	10,322	10,234	10,311	10,375	9,667	8,265
Specific air required, lb/lb	805	806	805	803	791	791	794	792	787	781	787	792	738	630
Energy for 15% excess air, MBtu	12,138	12,152	12,138	12,104	11,925	11,926	11,962	11,936	11,870	11,769	11,858	11,931	11,117	9,505
Energy for 15% excess air, MBtu	923	924	923	920	907	907	910	908	903	895	902	907	845	723
Energy combustion, CF/MMBtu	10,983	10,956	11,141	10,953	10,962	10,996	10,890	10,909	10,871	10,847	10,911	10,904	11,722	13,511
Energy combustion, lb/MMBtu	865	862	876	863	870	874	861	864	862	860	864	862	985	1,103
Net combustion, CF/MMBtu	13,257	13,258	13,415	13,163	12,788	12,757	12,935	12,862	12,771	12,689	12,821	12,902	14,198	15,581
Net combustion, lb/MMBtu	973	971	984	968	957	958	958	957	952	948	864	957	1102	1,201
Temperature, °F	3,306	3,308	3,284	3,317	3,351	3,351	3,342	3,348	3,359	3,371	3,353	3,345	3,001	2,856

Values calculated using 60°F fuel gas and 60°F, 50% relative humidity combustion air.

TABLE 3.15

## Constants of Components

								Gas Density Ideal Gas, 14.696						
								psia, 60°F			Heating Value			
								Specific	Gas	Specific	Btu/scf		Btu/lbm	
								Gravity	Density	Volume	LHV	HHV	LHV	HHV
No.	Fuel Gas Component	Chemical Formula	Molecular Weight	14.696 psia (°F)	Vapor Pressure 100°F (psia)	Specific Heat Capacity, C <sub>p</sub> 14.696 psia (Btu/lbm/°F)	Latent Heat of Vaporization 14.696 psia and Boiling Point (Btu/lbm)	(Air = 1)	(lbm/ft³)	(ft³/lbm)	(Net)	(Gross)	(Net)	(Gross)
Paraffin (alkane) series (C <sub>n</sub> H <sub>2n+2</sub> )														
1	Methane	CH <sub>4</sub>	16.04	−258.69	—	0.5266	219.22	0.554	0.042	23.651	912	1,013	21,495	23,875
2	Ethane	C <sub>2</sub> H <sub>6</sub>	30.07	−127.48	—	0.4097	210.41	1.038	0.079	12.618	1,639	1,792	20,418	22,323
3	Propane	C <sub>3</sub> H <sub>8</sub>	44.10	−43.67	190	0.3881	183.05	1.522	0.116	8.604	2,385	2,592	19,937	21,669
4	<i>n</i> -Butane	C <sub>4</sub> H <sub>10</sub>	58.12	31.10	51.6	0.3867	165.65	2.007	0.153	6.528	3,113	3,373	19,679	21,321
5	Isobutane	C <sub>4</sub> H <sub>10</sub>	58.12	10.90	72.2	0.3872	157.53	2.007	0.153	6.528	3,105	3,365	19,629	21,271
6	<i>n</i> -Pentane	C <sub>5</sub> H <sub>12</sub>	72.15	96.92	15.57	0.3883	153.59	2.491	0.190	5.259	3,714	4,017	19,507	21,095
7	Isopentane	C <sub>5</sub> H <sub>12</sub>	72.15	82.12	20.44	0.3827	147.13	2.491	0.190	5.259	3,705	4,007	19,459	21,047
8	Neopentane	C <sub>5</sub> H <sub>12</sub>	72.15	49.10	35.9	0.3866	135.58	2.491	0.190	5.259	3,692	3,994	19,390	20,978
9	<i>n</i> -Hexane	C <sub>6</sub> H <sub>14</sub>	86.18	155.72	4.956	0.3864	143.95	2.975	0.227	4.403	4,415	4,767	19,415	20,966
Naphthene (cycloalkane) series (C <sub>n</sub> H <sub>2n</sub> )														
10	Cyclopentane	C <sub>5</sub> H <sub>10</sub>	70.13	120.60	9.917	0.2712	167.35	2.420	0.180	5.556	3,512	3,764	19,005	20,368
11	Cyclohexane	C <sub>6</sub> H <sub>12</sub>	84.16	177.40	3.267	0.2901	153.25	2.910	0.220	4.545	4,180	4,482	18,849	20,211
Olefin series (C <sub>n</sub> H <sub>2n</sub> )														
12	Ethene (Ethylene)	C <sub>2</sub> H <sub>4</sub>	28.05	−154.62	—	0.3622	207.57	0.969	0.074	13.525	1,512	1,613	20,275	21,636
13	Propene (Propylene)	C <sub>3</sub> H <sub>6</sub>	42.08	−53.90	226.4	0.3541	188.18	1.453	0.111	9.017	2,185	2,336	19,687	21,048
14	1-Butene (Butylene)	C <sub>4</sub> H <sub>8</sub>	56.11	20.75	63.05	0.3548	167.94	1.937	0.148	6.762	2,885	3,086	19,493	20,854
15	Isobutene	C <sub>4</sub> H <sub>8</sub>	56.11	19.59	63.4	0.3701	169.48	1.937	0.148	6.762	2,868	3,069	19,376	20,737
16	1-Pentene	C <sub>5</sub> H <sub>10</sub>	70.13	85.93	19.115	0.3635	154.46	2.421	0.185	5.410	3,585	3,837	19,359	20,720
Aromatic series (C <sub>n</sub> H <sub>2n-6</sub> )														
17	Benzene	C <sub>6</sub> H <sub>6</sub>	78.11	176.17	3.224	0.2429	169.31	2.697	0.206	4.857	3,595	3,746	17,451	18,184
18	Toluene	C <sub>7</sub> H <sub>8</sub>	92.14	231.13	1.032	0.2598	154.84	3.181	0.243	4.118	4,296	4,497	17,672	18,501
19	<i>o</i> -Xylene	C <sub>8</sub> H <sub>10</sub>	106.17	291.97	0.264	0.2914	149.1	3.665	0.280	3.574	4,970	5,222	17,734	18,633
20	<i>m</i> -Xylene	C <sub>8</sub> H <sub>10</sub>	106.17	282.41	0.326	0.2782	147.2	3.665	0.280	3.574	4,970	5,222	17,734	18,633
21	<i>p</i> -Xylene	C <sub>8</sub> H <sub>10</sub>	106.17	281.05	0.342	0.2769	144.52	3.665	0.280	3.574	4,970	5,222	17,734	18,633
Additional fuel gas components														
22	Acetylene	C <sub>2</sub> H <sub>2</sub>	26.04	−119	—	0.3966	—	0.899	0.069	14.572	1,448	1,499	20,769	21,502
23	Methyl alcohol	CH <sub>3</sub> OH	32.04	148.1	4.63	0.3231	473	1.106	0.084	11.841	767	868	9,066	10,258
24	Ethyl alcohol	C <sub>2</sub> H <sub>5</sub> OH	46.07	172.92	2.3	0.3323	367	1.590	0.121	8.236	1,449	1,600	11,918	13,161
25	Ammonia	NH <sub>3</sub>	17.03	−28.2	212	0.5002	587.2	0.588	0.045	22.279	364	441	7,986	9,667
26	Hydrogen	H <sub>2</sub>	2.02	−423.0	—	3.4080	193.9	0.070	0.005	188.217	274.6	325.0	51,625	61,095
27	Oxygen	O <sub>2</sub>	32.00	−297.4	—	0.2188	91.6	1.105	0.084	11.858	—	—	—	—
28	Nitrogen	N <sub>2</sub>	28.16	−320.4	—	0.2482	87.8	0.972	0.074	13.473	—	—	—	—
29	Carbon monoxide	CO	28.01	−313.6	—	0.2484	92.7	0.967	0.074	13.546	321.9	321.9	4,347	4,347
30	Carbon dioxide	CO <sub>2</sub>	44.01	−109.3	—	0.1991	238.2	1.519	0.116	8.621	—	—	—	—
31	Hydrogen sulfide	H <sub>2</sub> S	34.08	−76.6	394.0	0.2380	235.6	1.177	0.090	11.133	595	646	6,537	7,097
32	Sulfur dioxide	SO <sub>2</sub>	64.06	14.0	88	0.1450	166.7	2.212	0.169	5.923	—	—	—	—
33	Water vapor	H <sub>2</sub> O	18.02	212.0	0.9492	0.4446	970.3	0.622	0.047	21.061	—	—	—	—
34	Air	—	28.97	−317.6	—	0.2400	92	1.000	0.076	13.099	—	—	—	—

(continued)

**TABLE 3.15 (continued)**  
**Constants of Components**

Fuel Gas		Unit Volume per Unit Volume of Combustible								Unit Mass per Unit Mass of Combustible								Theoretical Air Required (lbm/10,000 Btu)	Flammability Limits (vol% in Air Mixture)		No.
		Required for Combustion			Flue Gas Products					Required for Combustion			Flue Gas Products						Lower	Upper	
		O <sub>2</sub>	N <sub>2</sub>	Air	CO <sub>2</sub>	H <sub>2</sub> O	N <sub>2</sub>	SO <sub>2</sub>	O <sub>2</sub>	N <sub>2</sub>	Air	CO <sub>2</sub>	H <sub>2</sub> O	N <sub>2</sub>	SO <sub>2</sub>						
No.	Component	O <sub>2</sub>	N <sub>2</sub>	Air	CO <sub>2</sub>	H <sub>2</sub> O	N <sub>2</sub>	SO <sub>2</sub>	O <sub>2</sub>	N <sub>2</sub>	Air	CO <sub>2</sub>	H <sub>2</sub> O	N <sub>2</sub>	SO <sub>2</sub>	(lbm/10,000 Btu)	Lower	Upper	No.		
Paraffin (alkane) series (C <sub>n</sub> H <sub>2n+2</sub> )																					
1	Methane	2.0	7.547	9.547	1.0	2.0	7.547	—	3.989	13.246	17.235	2.743	2.246	13.246	—	7.219	5.0	15.0	1		
2	Ethane	3.5	13.206	16.706	2.0	3.0	13.206	—	3.724	12.367	16.092	2.927	1.797	12.367	—	7.209	2.9	13.0	2		
3	Propane	5.0	18.866	23.866	3.0	4.0	18.866	—	3.628	12.047	15.676	2.994	1.634	12.047	—	7.234	2.1	9.5	3		
4	<i>n</i> -Butane	6.5	24.526	31.026	4.0	5.0	24.526	—	3.578	11.882	15.460	3.029	1.550	11.882	—	7.251	1.8	8.4	4		
5	Isobutane	6.5	24.526	31.026	4.0	5.0	24.526	—	3.578	11.882	15.460	3.029	1.550	11.882	—	7.268	1.8	8.4	5		
6	<i>n</i> -Pentane	8.0	30.186	38.186	5.0	6.0	30.186	—	3.548	11.781	15.329	3.050	1.498	11.781	—	7.267	1.4	8.3	6		
7	Isopentane	8.0	30.186	38.186	5.0	6.0	30.186	—	3.548	11.781	15.329	3.050	1.498	11.781	—	7.283	1.4	8.3	7		
8	Neopentane	8.0	30.186	38.186	5.0	6.0	30.186	—	3.548	11.781	15.329	3.050	1.498	11.781	—	7.307	1.4	8.3	8		
9	<i>n</i> -Hexane	9.5	35.846	45.346	6.0	7.0	35.846	—	3.527	11.713	15.240	3.064	1.463	11.713	—	7.269	1.2	7.7	9		
Naphthene (cycloalkane) series (C <sub>n</sub> H <sub>2n</sub> )																					
10	Cyclopentane	7.5	27.939	35.810	5.0	5.0	27.939	—	3.850	11.155	14.793	3.146	1.283	11.155	—	7.262			10		
11	Cyclohexane	9.0	33.528	42.970	6.0	6.0	33.528	—	4.620	13.386	17.750	3.146	1.283	11.155	—	7.848	1.3	8.4	11		
Olefin series (C <sub>n</sub> H <sub>2n</sub> )																					
12	Ethene (Ethylene)	3.0	11.320	14.320	2.0	2.0	11.320	—	3.422	11.362	14.784	3.138	1.284	11.362	—	6.833	2.7	34.0	12		
13	Propene (Propylene)	4.5	16.980	21.480	3.0	3.0	16.980	—	3.422	11.362	14.784	3.138	1.284	11.362	—	7.024	2.0	10.0	13		
14	1-Butene (Butylene)	6.0	22.640	28.640	4.0	4.0	22.640	—	3.422	11.362	14.784	3.138	1.284	11.362	—	7.089	1.6	9.3	14		
15	Isobutene	6.0	22.640	28.640	4.0	4.0	22.640	—	3.422	11.362	14.784	3.138	1.284	11.362	—	7.129	1.6	—	15		
16	1-Pentene	7.5	28.300	35.800	5.0	5.0	28.300	—	3.422	11.362	14.784	3.138	1.284	11.362	—	7.135	1.4	8.7	16		
Aromatic series (C <sub>n</sub> H <sub>2n-6</sub> )																					
17	Benzene	7.5	28.300	35.800	6.0	3.0	28.300	—	3.072	10.201	13.274	3.380	0.692	10.201	—	7.300	1.38	7.98	17		
18	Toluene	9.0	33.959	42.959	7.0	4.0	33.959	—	3.125	10.378	13.504	3.343	0.782	10.378	—	7.299	1.28	7.18	18		
19	<i>o</i> -Xylene	10.5	39.619	50.119	8.0	5.0	39.619	—	3.164	10.508	13.673	3.316	0.848	10.508	—	7.338	1.18	6.48	19		
20	<i>m</i> -Xylene	10.5	39.619	50.119	8.0	5.0	39.619	—	3.164	10.508	13.673	3.316	0.848	10.508	—	7.338	1.18	6.48	20		
21	<i>p</i> -Xylene	10.5	39.619	50.119	8.0	5.0	39.619	—	3.164	10.508	13.673	3.316	0.848	10.508	—	7.338	1.18	6.48	21		
Additional fuel gas components																					
22	Acetylene	2.5	9.433	11.933	2.0	1.0	9.433	—	3.072	10.201	13.274	3.380	0.692	10.201	—	7.300	2.5	80	22		
23	Methyl alcohol	1.5	5.660	7.160	1.0	2.0	5.660	—	1.498	4.974	6.472	1.373	1.124	4.974	—	6.309	6.72	36.5	23		
24	Ethyl alcohol	3.0	11.320	14.320	2.0	3.0	11.320	—	2.084	6.919	9.003	1.911	1.173	6.919	—	6.841	3.28	18.95	24		
25	Ammonia	0.75	2.830	3.580	—	1.5	3.330	—	1.409	4.679	6.088	—	1.587	5.502	—	6.298	15.50	27.00	25		
26	Hydrogen	0.5	1.887	2.387	—	1.0	1.887	—	7.936	26.353	34.290	—	8.937	26.353	—	5.613	4.00	74.20	26		
27	Oxygen	—	—	—	—	—	—	—	—	—	—	—	—	—	—	—	—	—	27		
28	Nitrogen	—	—	—	—	—	—	—	—	—	—	—	—	—	—	—	—	—	28		
29	Carbon monoxide	0.5	1.877	2.387	1.0	—	1.887	—	—	1.897	2.468	1.571	—	1.870	—	5.677	12.50	74.20	29		
30	Carbon dioxide	—	—	—	—	—	—	—	—	—	—	—	—	—	—	—	—	—	30		
31	Hydrogen sulfide	1.5	5.660	7.160	—	1.0	5.660	1.0	1.410	4.682	6.093	—	0.529	4.682	1.880	8.585	4.30	45.50	31		
32	Sulfur dioxide	—	—	—	—	—	—	—	—	—	—	—	—	—	—	—	—	—	32		
33	Water vapor	—	—	—	—	—	—	—	—	—	—	—	—	—	—	—	—	—	33		
34	Air	—	—	—	—	—	—	—	—	—	—	—	—	—	—	—	—	—	34		



### 3.5.2 Lower and Higher Heating Values

The LHV of a gas is the heat released by combustion of a specific quantity of that gas with the products of combustion remaining as vapor. The higher heating value (HHV) adds the latent heat, of any steam produced as a combustion product, to the LHV. It represents the total heat obtained by first burning a fuel and then cooling the products to standard temperature. Heating values may be provided on a volume basis, typically Btu/scf (MJ/Nm<sup>3</sup>) or a mass basis such as Btu/lbm (kJ/kg).

To determine the heating value of a mixture of gases, it is necessary to know the heating value of each compound and the composition of the gases in terms of mole or mass fractions. Having assembled this information, the following formulae are used to calculate heating values:

$$HV_v = \sum HV_{v,i} \times y_i \quad (3.10)$$

$$HV_m = \sum HV_{m,i} \times x_i \quad (3.11)$$

where

$HV_v$  is the heating value of mixture, volume basis

$HV_{v,i}$  is the heating value of component  $i$ , volume basis

$HV_m$  is the heating value of mixture, mass basis

$HV_{m,i}$  is the heating value of component  $i$ , mass basis

### 3.5.3 Specific Heat Capacity

The specific heat capacity of a gas is the energy that must be added to a specific amount of the gas to raise its temperature by 1°. If the gas is maintained at constant pressure during this heating process, the value is referred to as " $c_p$ ." If the gas is maintained at constant volume, the value is referred to as " $c_v$ ." Specific heat is not a constant for a given gas; it is a function of temperature. Specific heat can be defined on a volume basis, typically Btu/lb mole-°F; or on a mass basis such as Btu/lb-°F.

To determine the specific heat of a mixture of gases, it is necessary to know the specific heat of each compound at the mixture temperature and the composition of the gases in terms of mole or mass fractions. Having assembled this information, the following formulae are used to calculate specific heat ( $c_p$  and  $c_v$  formulae are analogous, only  $c_p$  formulae are shown):

$$c_p(\text{vol.}) = \sum c_{p,i}(\text{vol.}) \times y_i \quad (3.12)$$

$$c_p(\text{mass}) = \sum c_{p,i}(\text{mass}) \times x_i \quad (3.13)$$

where

$c_p(\text{vol.})$  is the specific heat of mixture, volume basis

$c_{p,i}(\text{vol.})$  is the specific heat of component  $i$ , volume basis

$c_p(\text{mass})$  is the specific heat of mixture, mass basis

$c_{p,i}(\text{mass})$  is the specific heat of component  $i$ , mass basis

### 3.5.4 Flammability Limits

Flammability limits define the range of fuel concentrations in air that will sustain a flame without additional air or fuel. The upper flammability limit (UFL) is the maximum fuel concentration that can sustain a flame and the lower flammability limit (LFL) is the minimum. These limits are often tabulated for fuels at some standard temperature, typically 60°F (16°C). Flammability limits are not constant for a given gas; they are functions of the air/fuel mixture temperature. An extensive discussion of this subject can be found in Coward and Jones.<sup>18</sup>

Wierzba and Karim<sup>19</sup> present a method for estimating the flammability limits as a function of mixture temperature by calculating adiabatic flame temperature (AFT). First, the AFT for the standard temperature mixture is determined. Next, the mixture temperature is set to the desired level and the fuel concentration is varied until the calculated AFT for the nonstandard temperature matches the AFT for the standard temperature. They provide an approximating method for calculating AFT for sub-stoichiometric mixtures.

Both the Coward and Jones manuscript and the Wierzba and Karim article indicate that a form of Le Chatelier's rule can be used to calculate LFL and UFL for many combinations of fuels and inerts. Both references also mention that this rule fails to accurately predict for a few important situations. One notable example is a mixture of ethylene and carbon dioxide that differs substantially from normal calculated LFL and UFL. Another example is any mixture of chemicals that is prone to react with another at temperatures below the ignition point, such as ethylene and hydrogen. Mixtures involving significant amounts of inert compounds (e.g., H<sub>2</sub>O, N<sub>2</sub>, and CO<sub>2</sub>) require special treatment either by the AFT method described earlier or by grouping the inerts with fuel components in known proportions matching conditions for which LFL and UFL have been measured. This latter method is described in detail by Coward and Jones.<sup>18</sup>

With these exceptions in mind, the following mixing rules can be used to calculate LFL and UFL for most common gas mixtures:

$$\text{LFL} = \frac{100}{\sum \frac{y_i}{\text{LFL}_i}} \quad (3.14)$$

$$\text{UFL} = \frac{100}{\sum \frac{y_i}{\text{UFL}_i}} \quad (3.15)$$

### 3.5.5 Flame Speed

Flame speed and burning velocity are terms that are often used for the rate of propagation of a flame through a flammable mixture. The flame speed is not only

dependent on the fuel gas composition, gas/air mixture ratio, and temperature of the mixture, but also the physical dimensions of the combustion device and the interaction of the flame with heat absorbing surfaces. Flame speed is, thus, not an absolute value, but a device-dependent measurement. Quoted values for flame speed should include information regarding the method of measurement. Since the measured flame speed is not an absolute value, comparisons of flame speeds for various fuels must be made on the basis of data collected on identical test instruments.

Figure 3.10<sup>20</sup> shows flame speed data for a variety of fuel gases. Note that the maximum velocity generally occurs in a fuel-rich mixture with less than 100% theoretical combustion air in the fuel/air mixture.

### 3.5.6 Viscosity

Viscosity is discussed in detail in Chapter 9, "Fundamentals of Fluid Dynamics."

### 3.5.7 Derived Quantities

In addition to the specific properties described earlier, there are a number of useful derived parameters that may be of interest when studying combustion systems.

#### 3.5.7.1 Partial Pressure

Partial pressure is the pressure exerted by a single component of a mixture when that component alone occupies the entire volume at the mixture temperature. Dalton's law states that the total pressure of a mixture is the sum of the partial pressures of the components. While this law has been demonstrated to be somewhat in error, especially at high pressures, it is often useful for estimating purposes to determine whether a more detailed analysis is justified. The basic relationship is

$$p_i = y_i \leftrightarrow TP \quad (3.16)$$

Partial pressures are of interest when estimating the probability of forming condensate in a gas mixture. When the partial pressure of a component exceeds the vapor pressure of that component at the mixture temperature, condensation is likely.

#### 3.5.7.2 Adiabatic Flame Temperature

The AFT is the temperature that the combustion products would reach with no heat loss. Heat loss due to radiation, convection, or conduction is not included; hence the reference to adiabatic. Accounting for dissociation of combustion products is important. Customarily, the

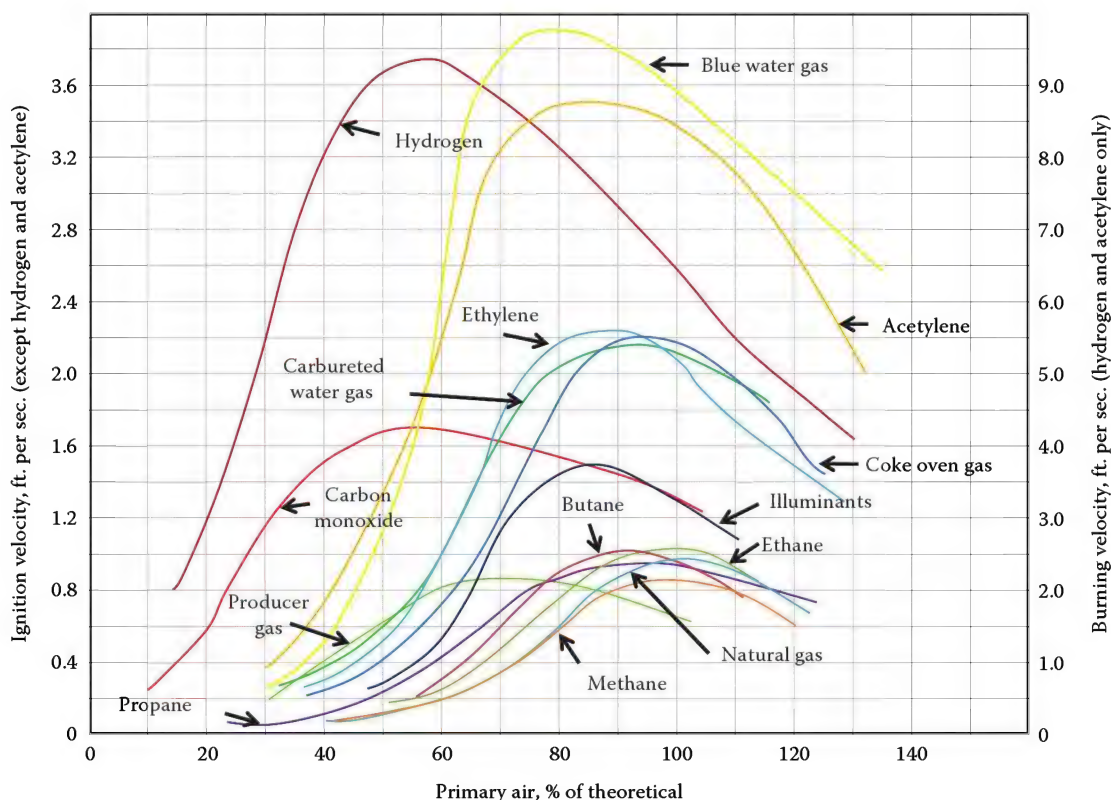


FIGURE 3.10

Flame speed for various gases. (Adapted from *Gas Engineers Handbook*, Industrial Press, 1965 (original reference is Weil, S. A. et al., *Fundamentals of Combustion of Gaseous Fuels*, IGT Research Bulletin 15, Chicago, IL, 1957).)

AFT is determined for a stoichiometric fuel/air mixture, although other mixtures such as LFL and UFL are sometimes studied for special purposes, as discussed in Section 3.5.4.

### 3.5.7.3 Heat Release

Heat release is the product of the flow rate and the heating value of the fuel using compatible units. This quantity is used throughout many areas of interest in combustion, including equipment sizing, radiation, and emissions. Unless the process involves the recovery of the heat of vaporization of the water vapor, the LHV is usually used when calculating heat release:

$$HR = \dot{w} \leftrightarrow LHV_m = Q \leftrightarrow LHV_v \quad (3.17)$$

where

HR is the heat release (energy/hour)

$\dot{w}$  is the mass flow (mass/hour)

$LHV_m$  is the lower heating value (energy/mass)

$Q$  is the volumetric flow (volume/hour)

$LHV_v$  is the lower heating value (energy/volume)

Typical units of heat release are MMBtu/hour, or MMkcal/hour, where MM =  $1 \times 10^6$ .

### 3.5.7.4 Volume Equivalent of Flow

Volume equivalent of flow ( $V_{eq}$ ) is the volumetric flow of air at standard temperature and pressure that produces the same velocity pressure in the same size line. This quantity is often used to provide generalized capacity curves for equipment that may need to handle several different gas streams. When designing equipment for this situation, the stream with the highest  $V_{eq}$  will often dominate the hydraulic design, unless the different streams have different allowable pressure drops. Caution should be used in cases where friction is expected to be a major factor in the system pressure drop because  $V_{eq}$  does not account for variations in viscosity.

$$V_{eq} = Q \sqrt{\frac{MW}{29} \frac{T_{gas}}{520}} = 13.1 \dot{w} \sqrt{\frac{29}{MW} \frac{T_{gas}}{520}} \quad (3.18)$$

where

$V_{eq}$  is the volume equivalent (SCFH)

$T_{gas}$  is the gas temperature (°R)

## 3.5.8 Liquid Fuel Properties

When liquid fuels are encountered, there are certain properties that determine into which category they are divided, and for what processes they are suitable.

### 3.5.8.1 Flash Point

The flash point of a liquid is the lowest temperature at which enough vapors are given off to form a mixture that will ignite when exposed to an ignition source. The standard method for determining flash point is ASTM D-93. Under certain conditions, ASTM D-56 can be used for light distillate oils. Some flash point values are provided in Table 3.8. The flash point is an important property for indication of volatility and for storage requirements.

### 3.5.8.2 Pour Point

The pour point of a liquid is determined by ASTM D-99 and indicates the lowest temperature at which an oil will flow at a controlled rate. If the fluid temperature goes below this point, flow will be inhibited.

### 3.5.8.3 Distillation

The distillation of a liquid gives an indication of its volatility, as well as the ease with which it can be vaporized. The test evaluates the vaporization range of a fuel between its end point (the point at which 100% of the volume has vaporized) and the initial boiling point (the point at which the liquid begins to vaporize). Figure 3.11 shows a typical crude oil distillation curve.

### 3.5.8.4 Viscosity

In layman's terms, the viscosity is a fluid's resistance to flow. Technically, the viscosity is the ratio of shear stress to shear rate of a fluid in motion. Most fluids considered in this chapter (gases, fuel oils) are Newtonian fluids because the aforementioned ratio is constant with respect to time, at a given temperature and pressure. A very important factor in the determination of fluid

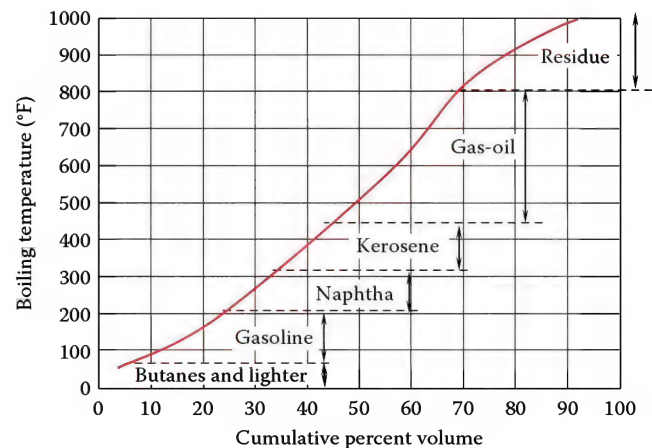


FIGURE 3.11  
Crude oil distillation curve.

flow is the dimensionless quantity called the Reynolds number. The Reynolds number is calculated as

$$\text{Re} = \frac{DV\rho}{\mu} \quad \text{or} \quad \text{Re} = \frac{DV}{\nu} \quad (3.19)$$

where

$D$  is the pipe diameter

$V$  is the fluid velocity

$\rho$  is the fluid density

$\mu$  is the fluid absolute viscosity

$\nu$  is the fluid kinematic viscosity

When the Reynolds number is less than 2100, the flow is typically streamlined and smooth and is called laminar. However, when the Reynolds number increases above 2100, internal agitation takes place and the flow is considered turbulent. As seen in Equation 3.19, as the viscosity increases, the flow becomes more laminar, assuming the other properties stay constant. Viscosity is divided into two different categories: kinematic viscosity and absolute viscosity.

Kinematic viscosity ( $\nu$ ) is dependent on fluid density, and has units of length<sup>2</sup> time<sup>-1</sup>. Typical units for kinematic viscosity are stokes (0.001 m<sup>2</sup> s<sup>-1</sup>), centistokes (stoke/100), Seconds Saybolt Universal (SSU), and Seconds Saybolt Furol (SSF). Because the density of a fluid is dependent on temperature, the viscosity of a fluid is likewise dependent on temperature. As the temperature increases, the viscosity of a fluid will decrease (become more fluid, or less viscous), and vice versa.

Absolute viscosity ( $\mu$ ) can be calculated by multiplying the kinematic viscosity by the density of the fluid. The most common units for absolute viscosity are poise (1 Pa-sec) and centipoise (cp), which is poise/100.

The viscosity of oil is a very important consideration in proper burner design. As previously mentioned, the more viscous the fluid, the more preheating required prior to burning. Several useful conversions are listed in the following:

$$1 \text{ lbm/ft hour} = 0.00413 \text{ g/cm s}$$

$$0.000413 \text{ kg/m s}$$

$$1 \text{ centipoise} = 0.01 \text{ poise}$$

$$0.01 \text{ g/cm s}$$

$$0.001 \text{ kg/m s}$$

$$6.72 \times 10^{-4} \text{ lbm/ft s}$$

$$1 \text{ stoke} = 0.0001 \text{ m}^2/\text{s} = 100 \text{ centistokes}$$

$$\text{centistokes} = (0.266 \times \text{SSU}) - (195/\text{SSU}) \text{ for SSU } 32 \text{ to } 100$$

$$(0.220 \times \text{SSU}) - (135/\text{SSU}) \text{ for SSU} > 100$$

See also Figure 3.12 and Table 3.16.

### 3.5.8.5 Density, Gravity, Specific Volume, and Specific Weight

Density is a fluid's mass per unit volume and is important due to its effect on other properties, such as viscosity. Additionally, the density is used to calculate the heat capacity. The densities of liquids are frequently given as the °API or the specific gravity (SG). The specific gravity of a liquid can be calculated by the formula

$$\text{SG} = \rho/\rho_{\text{ref}} \quad (3.20)$$

where

$\rho$  is the density of the substance in question at specific conditions

$\rho_{\text{ref}}$  is the density of a reference substance at a specific condition

Water is frequently used as a reference substance and, at 60°F (16°C), has a specific gravity of 1.0 and a density of 1.94 slugs/ft<sup>3</sup> (999 kg/m<sup>3</sup>), where 1 slug = 1 lb<sub>f</sub>/s<sup>2</sup>. Specific gravity for gases requires an additional assumption relating to pressure and temperature. Gas-specific gravity is defined relative to air as the reference substance and is generally determined at a standard temperature and pressure. Under those conditions, gas-specific gravity can be calculated as the ratio of MWs.

°API runs opposite that of specific gravity; therefore, as °API increases, the density decreases. When a fluid and water are compared at 60°F (16°C), the °API can be calculated as

$$^\circ\text{API} = \frac{141.5}{\text{SG}} - 131.5 \quad (3.21)$$

The specific volume (volume per unit mass) is the reciprocal of the density, and is commonly used in thermodynamic calculations.

The specific weight of a fluid ( $\gamma$ ) is defined as its weight per unit volume. The relationship that relates specific weight to the density is  $\gamma = \rho \times g$ , where  $\rho$  is the density and  $g$  is the local acceleration (32.174 ft/s<sup>2</sup> or 9.8067 m/s<sup>2</sup>). The specific weight of water at 60°F (16°C) is 62.4 lbm/ft<sup>3</sup> (9.80 kN/m<sup>3</sup>).

### 3.5.8.6 Heat Capacity (Specific Heat)

The heat capacity, or specific heat, of a fluid is defined as the amount of heat that is required, per unit mass, to



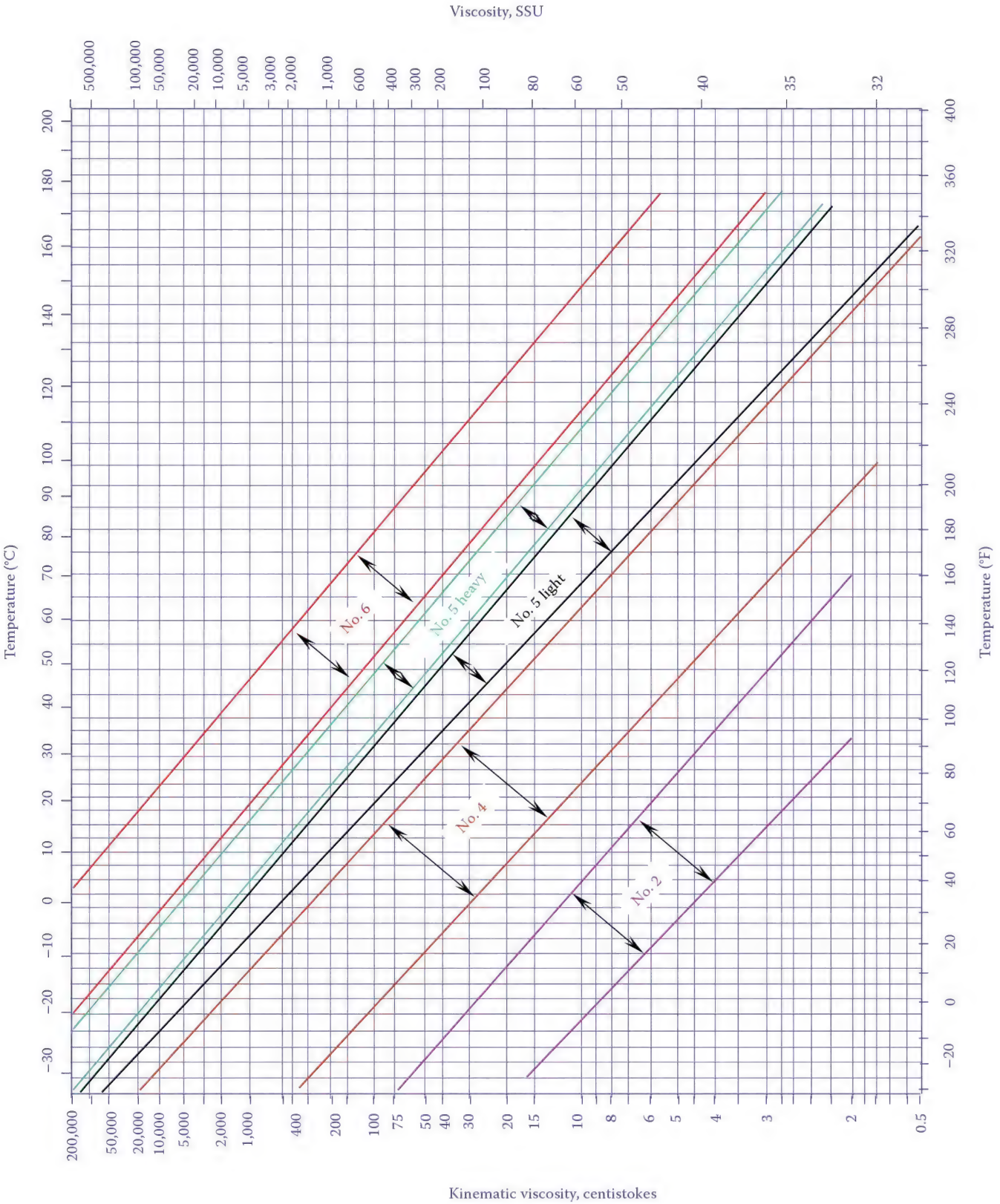


FIGURE 3.12  
Viscosity of fuel oils.

TABLE 3.16

## Viscosity Conversion Chart

Kinematic Viscosity Centipoises K	Seconds Saybolt Universal (SSU)	Seconds Saybolt Furoi (SSF)	Seconds Redwood	Seconds Redwood Admiralty	Degrees Engler	Degrees Barbey
1	31		29		1	6200
2.56	35		32.1		1.16	2420
4.3	40		36.2	5.1	1.31	1440
5.9	45		40.3	5.52	1.46	1050
7.4	50		44.3	5.83	1.58	838
8.83	55		48.5	6.35	1.73	702
10.2	60		52.3	6.77	1.88	618
11.53	65		56.7	7.17	2.03	538
12.83	70	12.95	60.9	7.6	2.17	483
14.1	75	13.33	65	8	2.31	440
15.35	80	13.7	69.2	8.44	2.45	404
16.58	85	14.1	73.3	8.86	2.59	374
17.8	90	14.44	77.6	9.3	2.73	348
19	95	14.85	81.5	9.7	2.88	326
20.2	100	15.24	85.6	10.12	3.02	307
31.8	150	19.3	128	14.48	4.48	195
43.1	200	23.5	170	18.9	5.92	144
54.3	250	28	212	23.45	7.35	114
65.4	300	32.5	254	28	8.79	95
76.5	350	35.1	296	32.5	10.25	81
87.6	400	41.9	338	37.1	11.7	70.8
98.6	450	46.8	381	41.7	13.15	62.9
110	500	51.6	423	46.2	14.6	56.4
121	550	56.6	465	50.8	16.05	51.3
132	600	61.4	508	55.4	17.5	47
143	650	66.2	550	60.1	19	43.4
154	700	71.1	592	64.6	20.45	40.3
165	750	76	635	69.2	21.9	37.6
176	800	81	677	73.8	23.35	35.2
187	850	86	719	78.4	24.8	33.2
198	900	91	762	83	26.3	31.3
209	950	95.8	804	87.6	27.7	29.7
220	1,000	100.7	846	92.2	29.2	28.2
330	1,500	150	1270	138.2	43.8	18.7
440	2,000	200	1690	184.2	58.4	14.1
550	2,500	250	2120	230	73	11.3
660	3,000	300	2540	276	87.6	9.4
770	3,500	350	2960	322	100.2	8.05
880	4,000	400	3380	368	117	7.05
990	4,500	450	3810	414	131.5	6.26
1100	5,000	500	4230	461	146	5.64
1210	5,500	550	4650	507	160.5	5.13
1320	6,000	600	5080	553	175	4.7
1430	6,500	650	5500	559	190	4.34
1540	7,000	700	5920	645	204.5	4.03
1650	7,500	750	6350	691	219	3.76
1760	8,000	800	6770	737	233.5	3.52
1870	8,500	850	7190	783	248	3.32
1980	9,000	900	7620	829	263	3.13
2090	9,500	950	8040	875	277	2.97
2200	10,000	1000	8460	921	292	2.82

raise the temperature by 1°. Typical units of heat capacity are Btu/(lbm·°R) (kJ/(kg·K)). Heat capacity is temperature dependent, and is defined in terms of constant volume or constant pressure, as can be seen by the following equations:

$$C_p \left( \frac{\delta h}{\delta T} \right)_p \quad (3.22)$$

$$C_v \left( \frac{\delta h}{\delta T} \right)_v \quad (3.23)$$

where

$C_p$  is the heat capacity at constant pressure

$C_v$  is the heat capacity at constant volume

$\delta h$  is the change in enthalpy

$\delta T$  is the change in temperature

To calculate the heat capacity of a petroleum liquid, to within 2%–4% accuracy, the following equations can be employed:

$$C = \frac{0.388 + (0.00045 \cdot ^\circ\text{F})}{\sqrt{\text{SG}}} \quad \text{for units of Btu/(lbm} \cdot ^\circ\text{R)} \quad (3.24)$$

$$C = \frac{1.685 + (0.039 \cdot ^\circ\text{C})}{\sqrt{\text{SG}}} \quad \text{for units of kJ/(kg} \cdot \text{K)} \quad (3.25)$$

where

$C$  is the heat capacity

$\text{SG}$  is the specific gravity (relative density), so long as the liquid temperature is between 32°F and 400°F (0°C and 205°C) and the specific gravity is between 0.75 and 0.96 at 60°F (16°C)<sup>11</sup>

Further information about gaseous and liquid fuels and their properties can be obtained from the references listed at the end of this chapter.<sup>21–24</sup>

### 3.5.9 Photographs of Gaseous Fuel Flames

Figures 3.13 through 3.28 are photographs of a John Zink, staged fuel, gas burner, firing a wide variety of fuel gas mixtures into open air (i.e., not in a furnace). In each photograph, the burner is being operated at the same heat release rate (energy released per unit time) and under the same general ambient conditions. Fuel composition is the only parameter that is varied throughout the series. The images are provided to illustrate the differences in flame appearance (shape and color) produced by various fuel compositions.

Figures 3.29 through 3.42 show a similar series of photos of a John Zink “raw gas” burner firing a wide variety of fuels inside a furnace all at the same firing rate.

There is a widely held misconception that yellow-flame burning is solely the direct result of combustion air deficiency. Inadequate or unsatisfactory fuel/air mixing will certainly result in the production of yellow

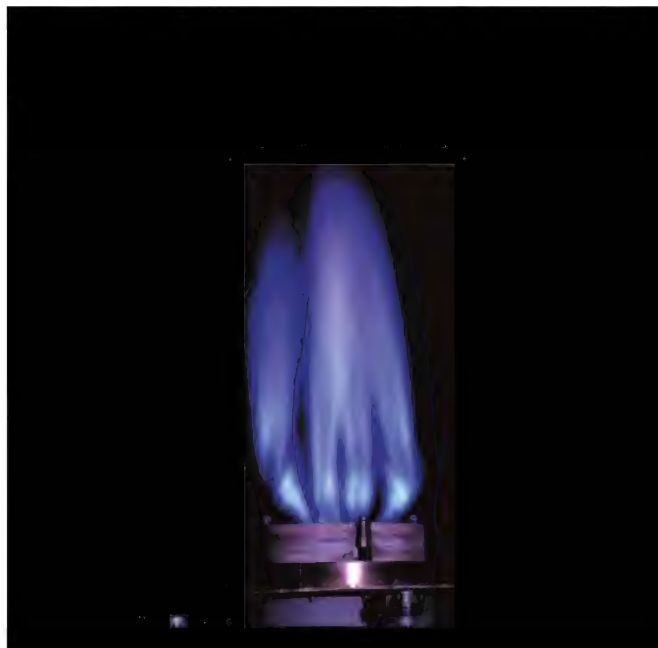


FIGURE 3.13  
100% TNG flame.



FIGURE 3.14  
80% TNG/20% N<sub>2</sub> flame.

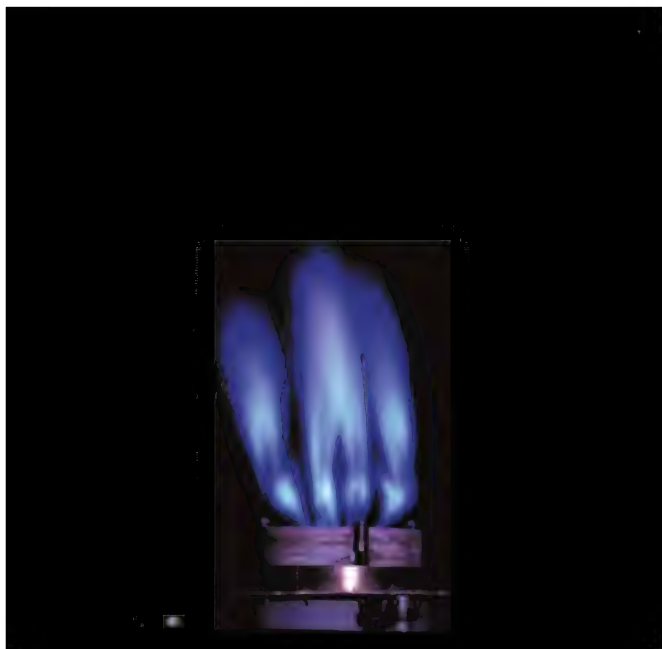


FIGURE 3.15  
90% TNG/10%  $N_2$  flame.



FIGURE 3.17  
75% TNG/25%  $H_2$  flame.

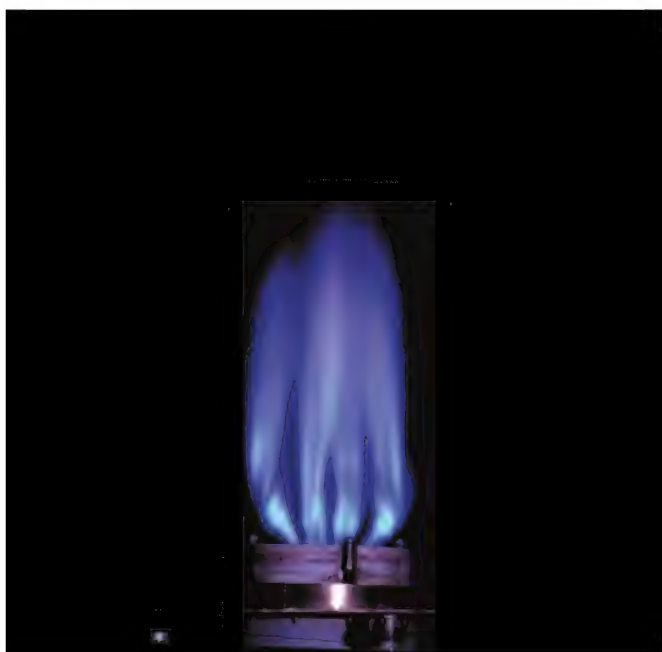


FIGURE 3.16  
90% TNG/10%  $H_2$  flame.



FIGURE 3.18  
25% TNG/75%  $H_2$  flame.



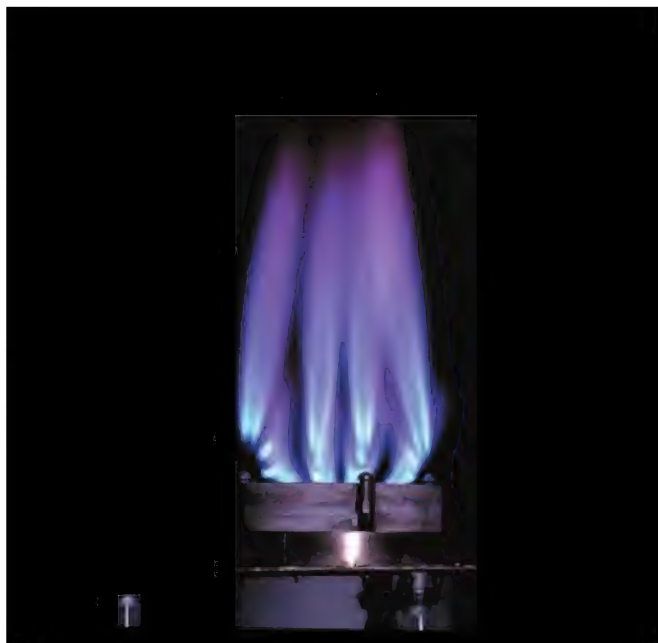


FIGURE 3.19  
50% TNG/50%  $\text{H}_2$  flame.



FIGURE 3.21  
50% TNG/25%  $\text{H}_2$ /25%  $\text{C}_3\text{H}_8$  flame.

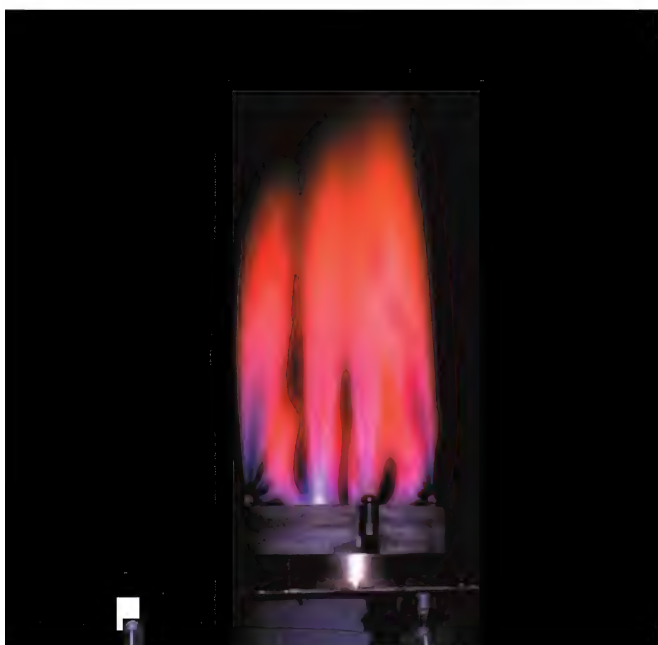


FIGURE 3.20  
100%  $\text{H}_2$  flame.

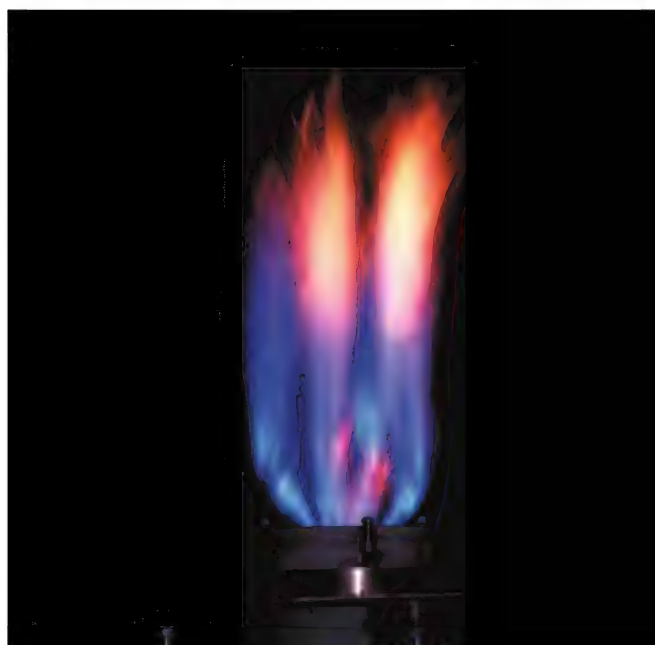


FIGURE 3.22  
100%  $\text{C}_3\text{H}_8$  flame.



FIGURE 3.23  
50% TNG/50% C<sub>3</sub>H<sub>8</sub> flame.

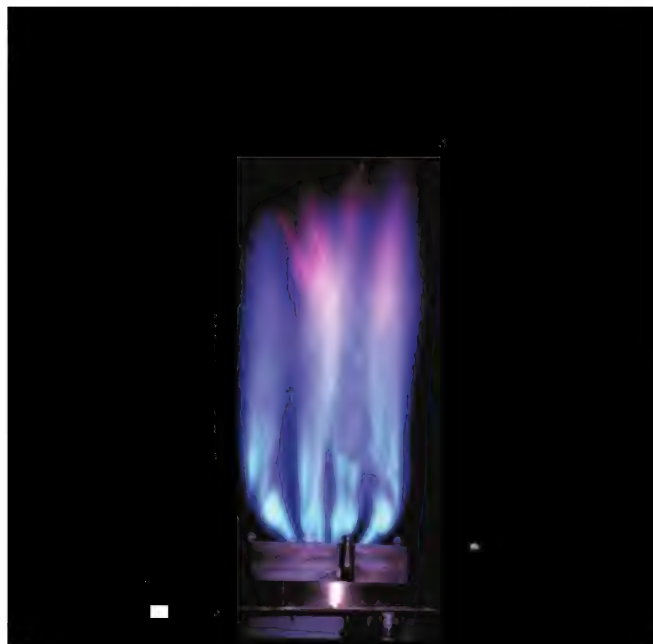


FIGURE 3.25  
Simulated cracked gas flame.



FIGURE 3.24  
100% C<sub>4</sub>H<sub>10</sub> flame.

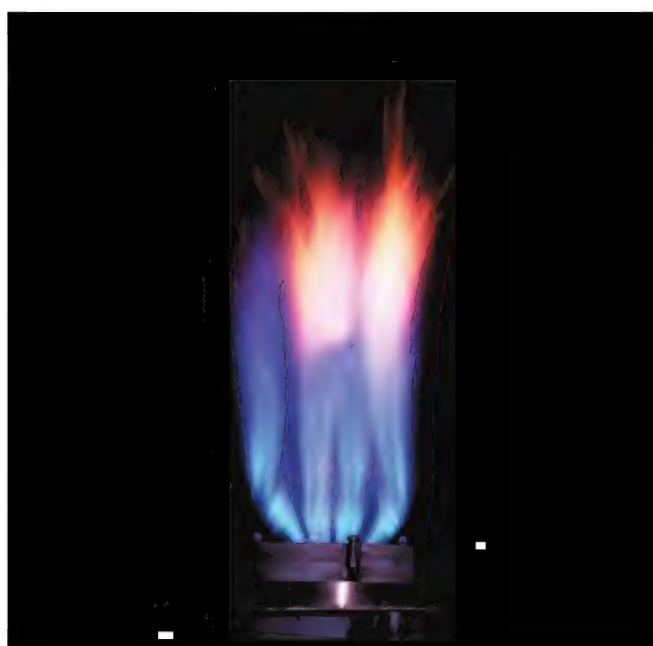


FIGURE 3.26  
Simulated FCC gas flame.

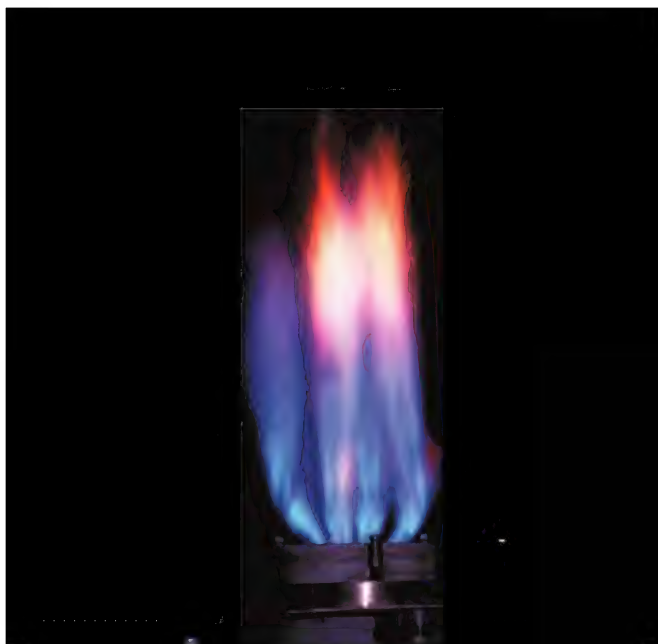


FIGURE 3.27  
Simulated coking gas flame.



FIGURE 3.29  
100% Tulsa natural gas.

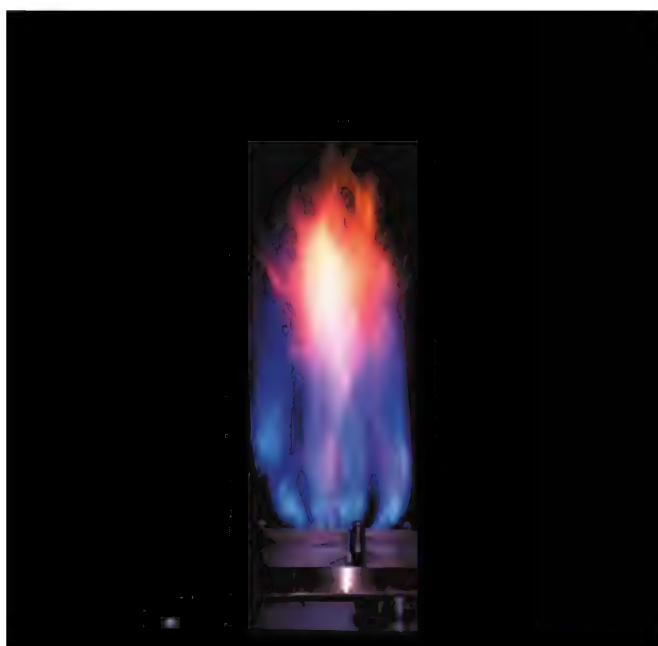


FIGURE 3.28  
Simulated reforming gas flame.



FIGURE 3.30  
100% hydrogen.



FIGURE 3.31  
100% propane.



FIGURE 3.33  
50% hydrogen/50% Tulsa natural gas.



FIGURE 3.32  
50% hydrogen/50% propane.



FIGURE 3.34  
50% propane/50% Tulsa natural gas.





FIGURE 3.35  
25% hydrogen/75% propane.



FIGURE 3.37  
25% hydrogen/75% Tulsa natural gas.



FIGURE 3.36  
75% hydrogen/25% propane.



FIGURE 3.38  
75% hydrogen/25% Tulsa natural gas.



FIGURE 3.39  
25% propane/75% Tulsa natural gas.



FIGURE 3.41  
25% hydrogen/25% propane/50% Tulsa natural gas.



FIGURE 3.40  
75% propane/25% Tulsa natural gas.



FIGURE 3.42  
50% hydrogen/25% propane/25% Tulsa natural gas.



flame. However, both yellow and blue flame burning can occur at virtually any condition of deficient or excess combustion air. Contrary to popular belief, it is possible to have a yellowish, smoky natural gas flame.

Yellow flame burning is the direct result of the cracking of a hydrocarbon fuel into its hydrogen and carbon components, followed by separate burning of the two constituents. The hydrogen constituents are burned in a rapid process that produces a pale lavender-pink flame that is very difficult to see except against a dark background. The carbon "solid" burns slowly in a bright, yellow, luminescent flame that is radiant across the full visible spectrum. This is why looking at a combination of oil and gas burner, firing in mixed oil/gas duty, will generally render the gas flame invisible, since the oil flame and the slow burning, luminescent, oil particles will dominate the human eye.

Blue flame burning is the direct result of progressive oxygenation of the fuel in a manner that does not allow uncombined carbon to be present in the reaction (flame) envelope. Inadequate fuel/air mixing can severely limit this reaction process, producing a greater tendency toward yellow flame. Both yellow and blue flame burnings are possible with any hydrocarbon fuel, and both kinds of flame produce equivalent quantities of heat.

The hydrogen-to-carbon weight ratio (H:C) is a good indicator of a fuel mixture's relative tendency to produce yellow flame burning, with low H:C ratios corresponding to an increased movement toward yellow flame burning. Again, pure hydrogen ( $H:C = \infty$ ) typically burns as a pale lavender-pink flame that is very difficult to see except against a dark background. Pure methane ( $H:C = 0.33$ ) typically burns as a light blue flame. Fuel mixtures containing propane ( $H:C = 0.22$ ), butane ( $H:C = 0.21$ ), and the olefins ( $H:C = 0.166$ ) all have a greater tendency to exhibit yellow flame burning than pure methane fuels.<sup>13</sup>

## References

1. Web site for Energy Information Administration, Office of Gas and Oil, [www.eia.doe.gov](http://www.eia.doe.gov), Crude Oil Watch, May 24, 2000.
2. Reed, R.J., *North American Combustion Handbook*, Vol. I, North American Mfg. Co., Cleveland, OH, 1986.
3. Gas Processors and Suppliers Association, *GPSA Engineering Data Book*, Vol. I, 10th edn., Gas Processors Suppliers Association, Tulsa, OK, 1987.
4. Austin, G.T., *Shreve's Chemical Process Industries*, 5th edn., McGraw-Hill, New York, 1984.
5. Gas Processors and Suppliers Association, *GPSA Engineering Data Book*, Vol. II, 10th edn., Gas Processors Suppliers Association, Tulsa, OK, 1987.
6. McCabe, W.L., Smith, J.C., and Harriot, P., *Unit Operations of Chemical Engineering*, 5th edn., McGraw-Hill, New York, 1993.
7. Gary, J.H. and Handwerk, G.E., *Petroleum Refining*, 3rd edn., Marcel Dekker, New York, 1994.
8. Baird, C., *Environmental Chemistry*, W.H. Freeman, New York, 1995.
9. Solomons, T.W., *Organic Chemistry*, 5th edn., John Wiley & Sons, New York, 1992.
10. Meyers, R.A., *Handbook of Petroleum Refining Processes*, 2nd edn., McGraw-Hill, New York, 1997, Chapter 3.3.
11. Perry, R.H., Green, D.W., and Maloney, J.O., Eds., *Perry's Chemical Engineers' Handbook*, 7th edn., McGraw-Hill, New York, 1997, Chapter 27.
12. Leffler, W.L., *Petroleum Refining for the Non-Technical Person*, PennWell Publishing, Tulsa, OK, 1985.
13. Reed, R.D., *Furnace Operations*, 3rd edn., Gulf Publishing, Houston, TX, 1981.
14. Nelson, W.L., *Petroleum Refining Engineering*, 3rd edn., McGraw-Hill, New York, 1949.
15. Meyers, R.A., *Handbook of Petroleum Refining Processes*, 2nd edn., McGraw-Hill, New York, 1997, Chapter 6.2.
16. Meyers, R.A., *Handbook of Petroleum Refining Processes*, 2nd edn., McGraw-Hill, New York, 1997, Chapter 12.1.
17. American Standard Testing Methods, ASTM D-396: Standard Specification for Fuel Oils, 1998.
18. Coward, H.F. and Jones, G.W., *Limits of Flammability of Gases and Vapors*, U.S. Bureau of Mines, Dept. of Interior, Bulletin 503, Pittsburgh, PA, 1952.
19. Wierzbza, I. and Karim, G.A., Prediction of the flammability limits of fuel mixtures, *AFRC/JFRC International Symposium*, October, Maui, Hawaii, 1998.
20. Gas Engineers Handbook, Industrial Press 1965 (Original reference is Weil, S. A. et al., *Fundamentals of Combustion of Gaseous Fuels*, (IGT Research Bulletin 15) Chicago, IL, 1957)
21. Dean, J., *Lange's Handbook of Chemistry*, 14th edn., McGraw-Hill, New York, 1992.
22. Munson, B.R., Young, D.F., and Okiishi, T.H., *Fundamentals of Fluid Mechanics*, 2nd edn., John Wiley & Sons, New York, 1994.
23. Heald, C.C., *Cameron Hydraulic Data*, 18th edn., Ingersoll-Dresser Pumps, Fairfield, NJ, 1994.
24. Van Wylen, G.J., Sonntag, R.E., and Borgnakke, C., *Fundamentals of Classical Thermodynamics*, 4th edn., John Wiley & Sons, New York, 1994.

This page intentionally left blank



# 4

## Combustion Fundamentals

Steve Londerville, Joseph Colannino, and Charles E. Baukal, Jr.

### CONTENTS

4.1	Introduction .....	80
4.2	Uses for Combustion .....	80
4.3	Brief Overview of Combustion Equipment and Heat Transfer .....	80
4.4	Chemical Combustion Fundamentals .....	81
4.4.1	States of Matter .....	81
4.4.2	Physical Properties of Matter .....	81
4.4.3	Chemical Structure .....	81
4.4.4	Periodic Table .....	82
4.4.5	Equations and Avogadro's Number .....	82
4.5	Gaseous State .....	84
4.5.1	Kinetic Molecular Theory .....	84
4.5.2	Gas Laws .....	84
4.5.3	Standard and Normal Air .....	86
4.5.4	Properties of Air .....	86
4.5.5	Humidity .....	86
4.5.6	Psychrometric Chart .....	87
4.5.7	Dalton's Law of Partial Pressures, Saturation, and Superheated Vapor .....	87
4.6	Oxidation-Reduction Equations .....	87
4.6.1	Redox Reactions of Gaseous Fuels and Excess Air .....	88
4.6.2	Flue Gas .....	89
4.7	Air-to-Fuel Ratio .....	89
4.7.1	Air-to-Fuel Mixture Ratio .....	94
4.7.2	Air-to-Fuel Mass Ratio .....	94
4.7.3	Turbine Exhaust Gas .....	95
4.8	Chemical Thermodynamics .....	97
4.8.1	Enthalpy, Entropy, and Heat Capacity .....	97
4.8.2	Heat of Combustion .....	97
4.8.3	Adiabatic Flame Temperature .....	98
4.8.4	Dissociation .....	99
4.9	Practical Liquid Fuels .....	100
4.10	Combustion Kinetics .....	101
4.10.1	Thermal NO <sub>x</sub> Formation .....	102
4.10.2	Prompt NO <sub>x</sub> Formation .....	102
4.10.3	Fuel-Bound NO <sub>x</sub> .....	103
4.11	Flame Properties .....	103
4.11.1	Flame Temperature .....	103
4.11.2	Available Heat .....	105
4.11.3	Minimum Ignition Energy .....	106
4.11.4	Flammability Limits .....	106
4.11.5	Flame Speeds .....	109

4.12 Substoichiometric Combustion.....	111
4.12.1 Equilibrium and Thermodynamics .....	111
4.12.2 Substoichiometric Combustion Revisited .....	111
4.13 General Discussion.....	112
4.13.1 Air Preheat Effects.....	112
4.13.2 Fuel Blend Effects.....	116
4.14 Emissions .....	117
4.15 Quick Sizing .....	118
4.15.1 Finding Saturated Humidity.....	118
4.15.2 Stoichiometric Combustion of Air Simplified .....	119
4.15.3 Density of Low Pressure Gases .....	119
References.....	123

---

## 4.1 Introduction

Combustion is the controlled release of heat and energy from the chemical reaction between a fuel and an oxidizer. The fuels in the refining, petrochemical, and power generation industries are almost exclusively hydrocarbons ( $C_xH_y$ ). Hydrocarbons comprise only hydrogen (H) and carbon (C) in their molecular structure. Natural gas and fuel oil are examples of hydrocarbon fuels. Practical fuels containing small contaminants such as nitrogen ( $N_2$ ) and oxygen ( $O_2$ ) are described later in this chapter and in other chapters of this book such as Chapter 3.

---

## 4.2 Uses for Combustion

Combustion is used either directly or indirectly to produce virtually every product in common use. Combustion processes produce and refine fuel, generate electricity, prepare foods and pharmaceuticals, and transport goods. Fire has transformed mankind and separated it from the beasts, illuminated nations, and safeguarded generations. It has been used in war and peace, to tear down and build up; it is both feared and respected. It is a most powerful tool and worthy of study and understanding.

---

## 4.3 Brief Overview of Combustion Equipment and Heat Transfer

In the process industries, combustion powers gas turbines, process heaters, reactors, and boilers. The burner combusts fuel and generates products of combustion and heat. A firebox contains the flame envelope. In boilers, the fire heats water in the tubes to boiling. The steam rises to a steam drum that separates the liquid

and vapor phases, returning water to the tubes and passing steam. The steam may be further heated in a superheater. Superheaters raise the temperature of the steam above the boiling point, using either radiant and/or convective heat transfer mechanisms.

Radiant heat transfer requires a line-of-sight to the flame. Only this heat transfer mechanism can operate in a vacuum. For example, the Earth receives essentially all its heat from the sun through this mechanism. Convection requires the bulk movement of a hot fluid. In a boiler, hot combustion gases transfer heat to the outer tube wall *via* convection. Convection occurs naturally by means of buoyancy differences between hot and cool fluids, termed natural convection, or by motive devices such as fans or blowers creating high velocities, termed forced convection. Heat transfers from the outer to inner tube wall by conduction—the predominant heat transfer mode through metals. Inside the tube, convection is the predominant mode of heat transfer to the inside fluid. A more complete discussion of heat transfer is given in Chapter 7.

Most large boilers have water in the tubes and fire outside—called water-tube boilers. Fire-tube boilers put the fire and hot gases in tubes surrounded by water. This system is applicable to smaller, unattended boilers.

Process heaters are akin to water-tube boilers, but with some very important differences. First, process heaters contain a process fluid in the tubes, rather than water. The process fluid is usually a hydrocarbon, for example, crude oil. Process heaters come in two main varieties: vertical cylindrical (VC) and cabin style (see Volume 3, Chapter 5). VCs comprise a cylindrical flame zone surrounded by process tubes. Cabin-style heaters are rectangular with wall and roof tubes (see Figure 4.1). The radiant section comprises the space surrounded by tubes having a direct view of the flame. Most process heaters also have a convective section comprised of overhead tubes that cannot directly view the flame. Convective tubes receive their heat from the direct contact of the combustion gases. The transition from the radiant to convective sections is known as the bridgewall.



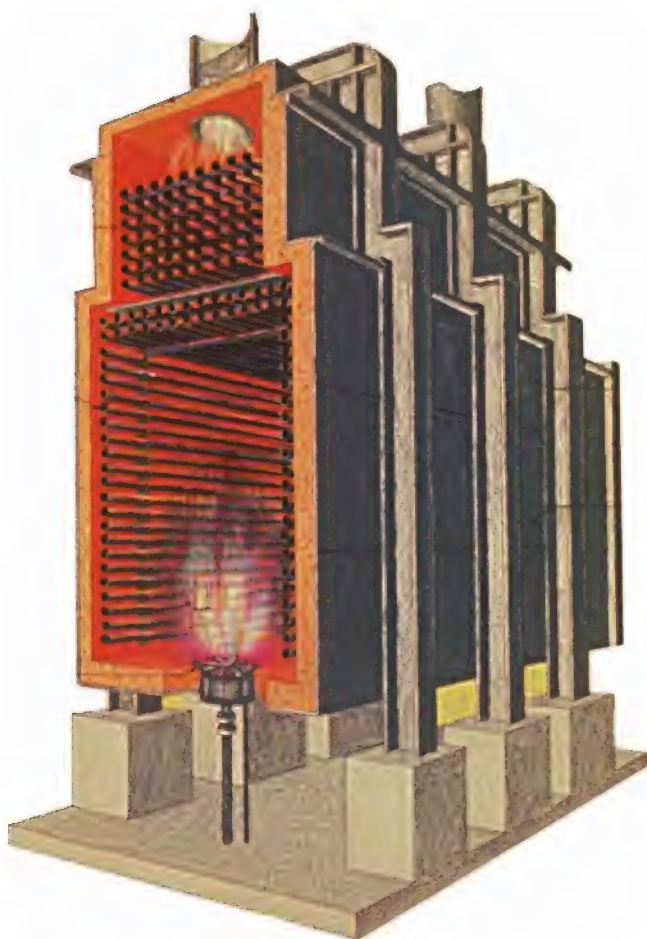


**FIGURE 4.1**  
Typical cabin-style process heater.

Reactors such as cracking furnaces and reforming furnaces are more extreme versions of process heaters. Here, the process fluid undergoes chemical transformations to a different substance. For example, in an ethylene cracking furnace, liquid or gas feedstock transforms to ethylene ( $C_2H_4$ )—an intermediate in the production of polyethylene and other plastics. There are many specialized types of reactors using combustion as the heat source.

## 4.4 Chemical Combustion Fundamentals

Chemistry is the fundamental backbone of combustion. Advanced concepts in combustion are founded upon the application of chemistry. It is, therefore, important to review and highlight the fundamental concepts that will play a key role in later topics.

### 4.4.1 States of Matter

Matter is the term for the substance of which all physical objects consist. Matter includes atoms and other

particles that have mass and occupy volume. Classically, matter exists in three distinct states: solid, liquid, and gaseous vapor.

In solid state matter, molecules are packed closely together. The forces between these molecules are strong enough to create an object that is rigid and occupies a definite shape and volume. As a result, particles in solid state matter are not free to move and can only vibrate. Solid matter is the most difficult to compress and generally has a very high bulk modulus.

In liquid state matter, molecules flow easily despite strong intermolecular force between molecules. Liquids take shape of the container and will remain in an open container. Liquid matter is difficult to compress but still has a considerably lower bulk modulus than solids.

In gaseous state matter, molecules move freely with little interactions except during collisions. Gases expand to fill a closed container. Gaseous matter is the most compressible state with a substantially lower bulk modulus than liquids.<sup>1</sup>

### 4.4.2 Physical Properties of Matter

Mass is the measure of the amount of matter within a substance. Mass differs from weight as mass is an invariable quantity and does not depend on the acceleration of gravity. The International System of Units (SI) unit for mass is the kilogram (kg) while imperial units are measured in pound-mass (lbm).

Volume is the space of which a body of matter occupies. The SI unit for volume is cubic meter ( $m^3$ ) and cubic feet ( $ft^3$ ) in imperial units.

Density is defined as the mass per unit volume of a substance. Density is commonly represented by the Greek letter  $\rho$  (rho). Density is normally expressed in ( $kg/m^3$ ) for SI units and ( $lbm/ft^3$ ) for imperial units.

$$\text{Density} = \frac{\text{mass}}{\text{volume}} \quad (4.1)$$

Specific gravity is an important parameter that is used to compare many parameters and is defined as the ratio of the density of a fluid to the density of water. In the case of gases, specific gravity is the ratio of the density of the gas to the density of air.<sup>1</sup> The density of air and water used for specific gravity is referenced at standard air conditions which are discussed in a later section of this chapter.

### 4.4.3 Chemical Structure

Atoms are the almost infinitesimally small building blocks of matter. The early experiments of Ernest Rutherford and Niels Bohr depict the atom with a densely packed center, called a nucleus, surrounded by a large cloud of negatively charged electrons. The nucleus is composed of electrically neutral neutrons

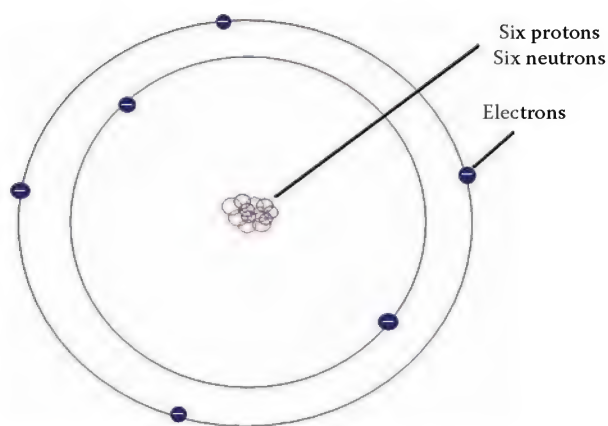


**FIGURE 4.2**  
Carbon atom with six protons, neutrons, and electrons.

and positively charged protons. Atoms with different quantities of neutrons, protons, and electrons are what make up different elements.<sup>2</sup>

The first category of substances is an element. An element is a pure substance that cannot be decomposed chemically. Currently 116 elements are known, with familiar examples being carbon (see Figure 4.2), nitrogen, and oxygen. Each element is assigned a unique atomic number which is equal to the number of protons found in the nucleus of the atom.

The second category of substances is a molecule. Molecules are the smallest collection of chemically bound atoms that define a substance, for example, nitrogen, which exists as the gaseous molecule  $N_2$  at room conditions.

Physical and chemical properties of an atom are primarily determined by the energy associated with the movement and number of electrons, especially pertaining to the outermost electrons of an atom called valence electrons. The exchange of electrons between atoms is the result of chemical bonding.

Ionic bonding holds two or more atoms together through electrostatic forces that exist between ions of opposite charge. Ionic bonding most commonly occurs between a metallic element (cation) and a non-metallic element (anion). Table salt is a familiar example of an ionic bond, where the positively charged sodium bonds with the negatively charged chlorine.

In covalent bonding, two or more atoms are bonded together from sharing electrons. Such bonding most commonly occurs between the interactions of non-metallic elements with one another. Carbon dioxide is an example of covalent bonding as oxygen atoms share their excess electrons with carbon.<sup>2</sup>

Bond energy is the energy change that accompanies the formation of a chemical bond. In bond formation, energy is either released (exothermic) or absorbed (endothermic). The amount of energy released or absorbed determines the bond strength; the larger the energy

difference, the more stable the bond. Compounds with weak bond energies tend to readily dissolve within a solution, whereas compounds with stronger bond energies may not be readily soluble.<sup>3</sup>

#### 4.4.4 Periodic Table

Every element is represented by one or two unique letters that often abbreviate the full element name in English, Latin, or German. For example, the symbol C represents carbon, H for hydrogen, and Ca for calcium.

A chemical formula is a symbol or a group of symbols that represent the elements and their respective quantities which make up the composition of a substance. The formula for water is  $H_2O$ , which specifies two atoms of hydrogen and one atom of oxygen.

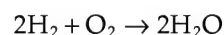
In the early 1869, Dmitri Mendeleev developed the periodic table through chemical observations to predict trends in and group regular patterns of chemical behavior. Consequently, the periodic table organizes elements by increasing atomic number in the horizontal rows and by similar properties in the vertical columns.<sup>3</sup>

The periodic table (see Figure 4.3) can be separated into two main categories—metals and non-metals. With the exception of hydrogen, all metals are located to the left and in the middle of the table. These elements are prone to having fewer valence electrons than protons, giving the element a positive charge also known as a cation. Conversely, non-metals are located to the right of the table. Non-metals are prone to having more valence electrons than protons, giving the element a negative charge known as an anion.

Elements on the 8A column—often called noble gases, includes He, Ne, Ar, Kr, Xe, and Rn—have completely filled their respective valence electron orbital making their chemical reactivity very low. Elements in the 1A column have relatively empty valence electrons and are thus very chemically reactive in comparison to noble gases.

#### 4.4.5 Equations and Avogadro's Number

Chemical reactions can be represented concisely through chemical equations.



In a chemical equation, the starting substances, or reactants, are placed on the left side of the arrow and to the right of the arrow are the substances produced by the reaction called the products.

From the law of conservation of mass, atoms are neither created nor destroyed in a chemical reaction, thus a chemical equation must have an equal amount of items on both the reactant and product side. Once the formulas of the reactants and products in a reaction are



Group

1 IA A	2 IIA A	<div>Key to chart</div> <div>Atomic number Symbol Atomic weight</div>										13 IIIA 3A	14 IVA 4A	15 VA 5A	16 VIA 6A	17 VIIA 7A	18 VIIIA 8A
1 H 1.008	2 He 4.003	3 Li 6.94	4 Be 9.012	5 B 10.81	6 C 12.01	7 N 14.01	8 O 16.00	9 F 19.00	10 Ne 20.18	11 Na 22.99	12 Mg 24.31	13 Al 26.98	14 Si 28.09	15 P 30.97	16 S 32.06	17 Cl 35.45	18 Ar 39.95
19 K 39.10	20 Ca 40.08	21 Sc 44.96	22 Ti 47.88	23 V 50.94	24 Cr 52.00	25 Mn 54.94	26 Fe 55.85	27 Co 58.93	28 Ni 58.69	29 Cu 63.55	30 Zn 65.39	31 Ga 69.72	32 Ge 72.64	33 As 74.92	34 Se 78.96	35 Br 79.90	36 Kr 83.79
37 Rb 85.47	38 Sr 87.62	39 Y 88.91	40 Zr 91.22	41 Nb 92.91	42 Mo 95.94	43 Tc (98)	44 Ru 101.1	45 Rh 102.9	46 Pd 106.4	47 Ag 107.9	48 Cd 112.4	49 In 114.8	50 Sn 118.7	51 Sb 121.8	52 Te 127.6	53 I 126.9	54 Xe 131.3
55 Cs 132.9	56 Ba 137.3	*	72 Hf 178.5	73 Ta 180.9	74 W 183.9	75 Re 186.2	76 Os 190.2	77 Ir 192.2	78 Pt 195.1	79 Au 197.0	80 Hg 200.5	81 Tl 204.4	82 Pb 207.2	83 Bi 209.0	84 Po (209)	85 At (210)	86 Rn (222)
87 Fr (223)	88 Ra (226)	**	104 Rf (265)	105 Db (268)	106 Sg (271)	107 Bh (270)	108 Hs (277)	109 Mt (276)	110 Ds (281)	111 Rg (280)	112 Cn (285)	113 Uut (284)	114 Fl (289)	115 Uup (288)	116 Lv (293)	117 Uus (294)	118 Uuo (294)

Lanthanide series\*

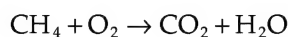
actinide series\*\*

57 La 138.9	58 Ce 140.1	59 Pr 140.9	60 Nd 144.2	61 Pm 144.9	62 Sm 150.4	63 Eu 152.0	64 Gd 157.3	65 Tb 158.9	66 Dy 162.5	67 Ho 164.9	68 Er 167.3	69 Tm 168.9	70 Yb 173.0	71 Lu 175.0
89 Ac (227)	90 Th 232	91 Pa 231	92 U 238	93 Np (237)	94 Pu (242)	95 Am (243)	96 Cm (247)	97 Bk (247)	98 Cf (251)	99 Es (252)	100 Fm (257)	101 Md (258)	102 No (259)	103 Lr (262)

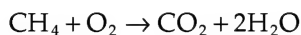
e.

known, the equation can be balanced by determining the coefficients that provide equal numbers of each type of atom on the reactant and product sides.<sup>2</sup>

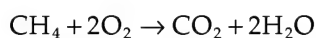
Step 1: Unbalanced Equation



Step 2: Match H on product side



Step 3: Match O<sub>2</sub> on reactant side



The weight of an atom is almost infinitesimally small; for example, a hydrogen atom weighs  $1.67 \times 10^{-24}$  g ( $3.68 \times 10^{-27}$  lb). Expressing weight in this way poses an inconvenience to scientists and engineers. Thus, atomic weight is introduced as the relative weight of atoms in different elements which is proportional to their actual weight.

Molecular weight uses atomic weight as the mass of an element of a molecule. For example, the element oxygen has an atomic weight of 16 atomic mass units (amu) and thus a molecular weight of 16 grams per mole (g/mol). Likewise, imperial units may be used as well, H<sub>2</sub>O has an atomic weight of 18 amu [(2 × 1) + 16] and thus a molecular weight of 18 pounds per mole (lb/mol).

The number  $6.023 \times 10^{23}$  was proposed by Jean Perrin in honor of Avogadro, who found that the volume of gas is proportional to the number of atoms. Avogadro's number is the exact number of carbon atoms in 12 g of the isotope carbon-12. Further,  $6.023 \times 10^{23}$  is now used to represent the exact number of atoms in one gram per mole of any molecule.<sup>2</sup> With Avogadro's number, one can calculate the weight of a single atom of any element.

## 4.5 Gaseous State

Combustion is a chemical reaction that occurs between gaseous air and fuel. Further, many fuels both exist and are ignited in the gaseous state. The study of gases will help to predict vital parameters of air and fuels.

### 4.5.1 Kinetic Molecular Theory

The kinetic molecular theory was developed in the nineteenth century to describe the motion of gaseous

molecules and provides the foundation for gas laws. This theory can be summarized in three postulates.

- Gases are composed of molecules which occupy a volume that is far smaller than the total volume occupied by gas. Molecules are relatively far apart.
- Gas molecules are in continuous motion moving in straight lines, often colliding with one another. Pressure is formed when gas molecules collide with the walls of the container.
- The kinetic energy of gas molecules increases as temperature rises. Molecules travel at higher velocities with increasing pressure.<sup>3</sup>

### 4.5.2 Gas Laws

From the kinetic molecular theory, early experiments with gases reveal four variables that are needed to define the physical state of a gas: temperature, pressure, volume, and the amount of gas expressed in moles. Boyle's law states that for a fixed amount of gas at a fixed temperature, pressure and volume are inversely proportional.

$$PV = \text{constant} \quad (4.2)$$

where

$P$  is the pressure of the gas, psia or kPa

$V$  is the volume of the gas, ft<sup>3</sup> or m<sup>3</sup>

Charles's law states that for a fixed amount of gas at a fixed pressure, the volume and temperature are proportional.

$$\frac{V}{T} = \text{constant} \quad (4.3)$$

where

$T$  is the absolute temperature, °R or °K

$V$  is the volume of the gas, ft<sup>3</sup> or m<sup>3</sup>

The ideal law gas is the culmination of all gas laws as it is derived from combining Boyle's law, Charles's law, and Avogadro's law. The law applies for typical combustion reactions and relates the pressure, volume, and number of moles:

$$PV = nRT \quad (4.4)$$

where

$P$  is the pressure of the gas, psia or kPa

$V$  is the volume of the gas, ft<sup>3</sup> or m<sup>3</sup>

$n$  is the number of moles

$R$  is the gas constant = 10.73 psia-ft<sup>3</sup>/lb mol °R or 8.314 kJ/kmol °K

$T$  is the absolute temperature, °R or °K

Degrees Rankine (°R) are defined as the number of Fahrenheit degrees above absolute zero—the coldest possible theoretical temperature. Equation 4.4 shows that gas volume and moles are directly proportional.

Another useful form of the ideal gas law is

$$PM = \rho RT \quad (4.5)$$

where

$\rho$  is the density of the gas, lb/ft<sup>3</sup> or kg/m<sup>3</sup>

$M$  is the molecular weight of the gas, lb/lb mol or g/mol

Also the ideal gas law can provide solutions in terms of mass by replacing number of moles ( $n$ ) with mass in Equation 4.4 and replacing the gas constant ( $R$ ) with the corresponding constant for mass. An example best reinforces these points.

#### Example 4.1

Given a 1000 ft<sup>3</sup> vessel containing methane at 30 psig at 70°F, how many lb mol of methane does the vessel contain? what is the gas density? and how much does the gas weigh? The solutions follow.

At standard temperature and pressure (STP, see Section 4.5.3 for more explanation), the pressure will be 14.7 psia or 2117 lb/ft<sup>3</sup> and absolute temperature of 529.7°R (or rounding to yield 530°R):

From Equation 4.4,

$$n = \frac{PV}{RT} = \frac{(30 + 14.7) [\text{psia}] \times 1000 [\text{ft}^3]}{10.73 \left[ \frac{\text{psia ft}^3}{\text{lb mol } ^\circ\text{R}} \right] \times (459.7 + 70) [^\circ\text{R}]}$$

$$= 7.86 \text{ lb mol}$$

From Equation 4.5,

$$\rho = \frac{PM}{RT} = \frac{(30 + 14.7) [\text{psia}] \times 16.05 [\text{lb/lb mol}]}{10.73 \left[ \frac{\text{psia ft}^3}{\text{lb mol } ^\circ\text{R}} \right] \times (459.7 + 70) [^\circ\text{R}]}$$

$$= 0.126 \text{ lb/ft}^3$$

Finally, multiply the density by the volume to obtain the weight of gas,  $m = \rho V = 0.126 \text{ lb/ft}^3 \times 1000 \text{ ft}^3 = 126 \text{ lb}$ . Furthermore, using the ideal gas law one can determine the molar density for any gas.

$$PV = nRT$$

where

$n$  is the molar density, lb mol/ft<sup>3</sup>

$R$  is the gas constant = 1545 ft – lb<sub>f</sub>/lb mol °R

$$n = \frac{2117 \text{ psfa}}{1545 \left[ \frac{\text{ft – lb}_f}{\text{lb mol – } ^\circ\text{R}} \right] \times 530 ^\circ\text{R}} = 0.00258 \frac{\text{lb mol}}{\text{ft}^3}$$

Inverting the value yields

$$= 387 \frac{\text{ft}^3}{\text{lb mol}}$$

For any gas at STP, independent of molecular weight (MW).

Another helpful equation derived from the ideal gas law (used to relate with MW) can be used to calculate density of any gas relating to temperature and pressure.

$$PV = mRT$$

$$\rho = \frac{m}{V} = \frac{P}{RT}$$

with

$$R = 1545 \frac{\text{ft – lb}_f/\text{lb mol}}{\text{lb mol } ^\circ\text{R}(\text{MW}) \text{ lb}_m}$$

At STP, the density of air is 0.075 lb<sub>m</sub>/ft<sup>3</sup> and MW is 28.85:

$$0.075 = \frac{2117 \text{ psfa}}{\left( \frac{1545}{28.85} \right) \left[ \frac{\text{ft – lb}_f}{\text{lb}_m \text{ – } ^\circ\text{R}} \right] \times 530 ^\circ\text{R}}$$

Since

$$PV = m \frac{R}{\text{MW}} T \quad \text{and} \quad \rho = \frac{P \times \text{MW}}{RT}$$

$$\text{and} \quad R = \frac{P \times \text{MW}}{\rho T} = \text{Constant}$$

Then, the density of any gas can be related to another *via*:

$$\rho_2 = \rho_1 \frac{\text{MW}_2}{\text{MW}_1} \frac{P_2}{P_1} \frac{T_1}{T_2} \quad (4.6)$$

**Example 4.2**

For methane ( $\text{CH}_4$ ) at 100°F and 10 psig, what is the gas density?

From Equation 4.6, using air at STP, the gas density will be

$$\begin{aligned} \rho_{\text{methane}} &= 0.075 \times \frac{\text{MW}_{\text{methane}}}{28.85} \times \frac{P_2}{14.7} \times \frac{530}{T_2} \\ &= 0.075 \frac{16 \times (10 + 14.7 \text{ psia}) \times 530^\circ\text{R}}{28.85 \times 14.7 \text{ psia} \times (460 + 100)^\circ\text{R}} \\ &= 0.066 \frac{\text{lb}}{\text{ft}^3} \end{aligned}$$

Alternate units of R:

8.314  $\text{J K}^{-1} \text{mol}^{-1}$   
 $8.314 \times 10^{-5} \text{ m}^3 \text{ atm K}^{-1} \text{mol}^{-1}$   
 $1545 \text{ ft} - \text{lb}_f - \text{lb mol}^{-1} \text{ }^\circ\text{R}^{-1}$   
 $10.731 \text{ ft}^3 \text{ psi } ^\circ\text{R}^{-1} \text{ lb mol}^{-1}$   
 $1.986 \text{ Btu} - \text{lb mol}^{-1} \text{ }^\circ\text{R}^{-1}$   
 $82.057 \text{ cm}^3 \text{ atm K}^{-1} \text{mol}^{-1}$   
 $62.363 \text{ LTorr K}^{-1} \text{mol}^{-1}$

**4.5.3 Standard and Normal Air**

Air pressure and density are standardized at the weight of the earth's atmosphere exerted on a surface at sea level. There are two commonly used standards for air pressure and density: normal temperature and pressure (NTP) and standard temperature and pressure (STP).<sup>4</sup>

STP is defined by International Union of Pure and Applied Chemistry (IUPAC) as referring to 0°C (273.15 K, 32°F) and 10<sup>5</sup> Pa. Alternately, STP is defined in Imperial and U.S. system of units as air at 60°F (520°R) and 14.696 psia (15.6°C, 1 atm). In the United States, NTP is sometimes referenced to 1 atm and 32°F (0°C). To further complicate the situation, there are other standards, such as SATP, ISA, and ICAO. It is best to be clear on actual temperature and pressure used as a reference and to state what conditions are being used for "STP" or "NTP." Further, it is important to note that the two standards also apply for other gases, such as gaseous fuels.<sup>5</sup>

Many times the properties for air are based on the composition of 78% nitrogen, 21% oxygen, and 1% argon. For combustion calculations, dry air is often defined as 21%  $\text{O}_2$  and 79%  $\text{N}_2$ . This composition for dry air is used throughout this chapter for computations. For actual sizing of equipment, air with moisture should be considered.

60°F (15.6°C)	Air @ 14.7 psia (1 atm) at 60°F
	Density: 0.075 lb/ft <sup>3</sup> (1.201 kg/m <sup>3</sup> )
32°F (0°C)	Air @ 14.7 psia (1 atm) at 32°F (0°C)
	Density: 0.080 lb/ft <sup>3</sup> (1.281 kg/m <sup>3</sup> )

Atmospheric pressure decreases with elevation and can be corrected using the following formula<sup>1</sup>:

$$P = p_o \left[ \frac{T_o - \alpha(z - z_o)}{T_o} \right]^{g/\alpha R} \quad (4.7)$$

where

$P$  is the atmospheric pressure

$P_o$  is the known reference atmospheric pressure

$T_o$  is the known reference temperature

$z$  is the elevation

$z_o$  is the known reference elevation

$\alpha$  is the lapse rate =  $5.87 \times 10^{-3} \text{ K/m}$

$g$  is the acceleration of gravity

$R$  is the specific gas constant = 1716 ft – lb/slug × °R

**4.5.4 Properties of Air**

As air is a key component of combustion, the composition of air will be very important in future calculations to predict chemical reactions. The average composition of air is as shown in Figure 4.4. Table 4.1 lists the density of dry air using 79% nitrogen and 21% oxygen as well as average composition which is sometimes used. The molecular weight of average air is 28.966 while the 79% nitrogen and 21% oxygen assumption has the molecular weight of 28.842. For most engineering calculations these are small differences.

**4.5.5 Humidity**

In this chapter, the calculations for dry air have been idealized. However, the amount of water vapor in the air is important in many applications, such as fan sizing, flame temperature, and air heaters/dryers. Three types of humidity exist: absolute, relative, and specific humidity.

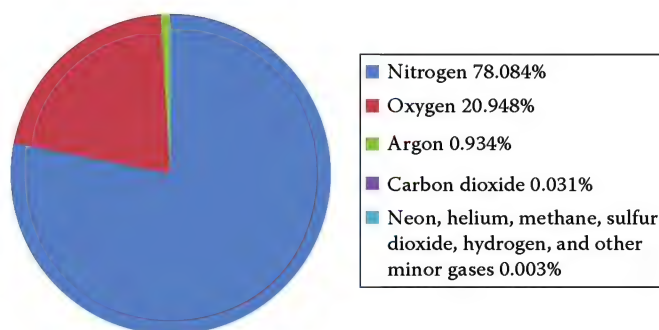


**FIGURE 4.4**

Composition of air by volume. (Modified from McQuiston, C. and Parker, J.D., *Heating, Ventilating, and Air Conditioning*, John Wiley & Sons, New York, 1982.)



TABLE 4.1

Density Comparison of Average Air and 79% N<sub>2</sub> 21% O<sub>2</sub> Assumption

Temp (°F)	Density of Air			
	lb/ft <sup>3</sup>		kg/m <sup>3</sup>	
	Average	79/21	Average	79/21
32	0.0862	0.0859	1.381	1.376
60	0.0763	0.0761	1.222	1.217
70	0.0748	0.0745	1.1982	1.194

Absolute humidity is the mass of water per unit volume of air:

$$\text{Absolute Humidity} = \frac{\text{Mass}_{\text{vapor}}}{\text{Volume}_{\text{net}}} \quad (4.8)$$

Relative humidity is the ratio of moisture in the air at a given temperature and vapor pressure, to the maximum amount of moisture air can hold at that temperature and saturation pressure. Relative humidity ranges from 0 for completely dry air to 100 for saturated air.

$$\phi = \frac{P_v}{P_{\text{sat}}} \quad (4.9)$$

Specific humidity is the ratio of the mass of vapor to mass of dry air:

$$\text{Specific Humidity} = \frac{\text{Mass}_{\text{vapor}}}{\text{Mass}_{\text{dry-air}}} \quad (4.10)$$

#### 4.5.6 Psychrometric Chart

When working with gas–vapor mixtures, calculating the physical properties can become tedious. Thus, engineers have tabulated air–vapor properties graphically in a complex chart generally referred to as the psychrometric chart (see Volume 2). The chart relates six parameters: dry bulb temperature, wet bulb temperature, relative humidity, humidity ratio, enthalpy, and specific volume. If any two of the mentioned independent parameters are known, the four other properties can be looked up through the chart. See the Quick Sizing section at the end of this chapter for a practical method of finding saturated humidity through steam tables.

#### 4.5.7 Dalton's Law of Partial Pressures, Saturation, and Superheated Vapor

Gases are usually comprised of a mixture of molecules. Partial pressure is the pressure that each molecule would exert if it occupied the same volume alone at the

same temperature; it is also representative of the volume fraction of an enclosed component. The total pressure of the gas mixture is the sum of the partial pressure for each individual gas molecule.

$$P_{\text{Total}} = \sum_{i=1}^n P_i \quad (4.11)$$

Example:  $P_{\text{Total}} = P_{\text{N}_2} + P_{\text{O}_2} + P_{\text{CO}_2}$

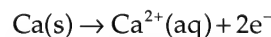
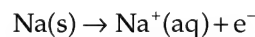
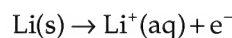
(Example of Dalton's law of partial pressures for nitrogen, oxygen, and carbon dioxide.)

Saturation is the process in which liquid boils into a vapor phase. Saturation temperature and pressure are the conditions required for saturation to occur. Saturation temperatures and saturated pressures vary for each liquid, but are always directly related: as saturation pressure increases for a liquid so does saturation temperature. Thus, for a given saturation temperature there is a corresponding saturation pressure.

In superheated vapors, the temperature exceeds the saturation temperature at corresponding saturation pressure. All molecules of a superheated vapor are completely in the vapor phase.

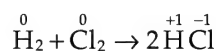
### 4.6 Oxidation–Reduction Equations

Combustion is a chemical reaction in which fuel undergoes oxidation. Oxidation and reduction, often called "Redox," are chemical reactions that transfer electrons between reactants. In an oxidation, an atom becomes more positively charged by losing an electron.



(Examples of oxidation reactants)

Conversely, reduction occurs when an atom gains an electron and is more negatively charged.



(Example of a redox equation where H<sub>2</sub> is oxidized by Cl<sub>2</sub> to form HCl.)

Oxidation numbers are assigned for good book-keeping of electrons gained by reduction and lost by oxidation. In the example given earlier, hydrogen's oxidation number increased from 0 to +1 as it is oxidized. Similarly, chlorine's oxidation number decreases from 0 to –1 because it is reduced.

The method of balancing redox reactions is defined in the following:

1.  $\text{CH}_4 + \text{O}_2 \rightarrow \text{CO}_2 + \text{H}_2\text{O}$
2.  $\text{CH}_4 + \text{O}_2 \rightarrow \text{CO}_2 + 2 \text{H}_2\text{O}$
3.  $\text{CH}_4 + 2\text{O}_2 \rightarrow \text{CO}_2 + 2 \text{H}_2\text{O}$ 
  - a. Balance C
  - b. Balance H
  - c. Balance required  $\text{O}_2$

#### 4.6.1 Redox Reactions of Gaseous Fuels and Excess Air

As discussed earlier, fuels in their purest form are composed of hydrogen and carbon, called hydrocarbons. Very few fuels originally contain oxygen and nitrogen, but some compounds do have the tendency to pick up oxygen, nitrogen, and sometimes sulfur. Fuels can be categorized into gaseous fuels or liquid fuels and are discussed extensively in the fuels chapter, however in this section, the chemical reactions for gaseous hydrocarbons will be developed.<sup>7-9</sup> Table 4.2 shows some common gaseous fuels.

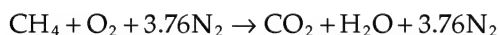
The following is an introduction of a redox example of methane ( $\text{CH}_4$ ) combustion.

Assume dry air is composed of 21% oxygen and 79% nitrogen. Thus, it yields 21 moles  $\text{O}_2$  and 79 moles  $\text{N}_2$ . To simplify this fraction, divide the number of moles of nitrogen with oxygen.

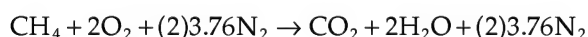
$$\frac{79 \text{ mol N}_2}{21 \text{ mol O}_2} = 3.76$$

Showing 3.76 mol of  $\text{N}_2$  for every 1 mol of  $\text{O}_2$ .

The unbalanced equation of methane combustion:



Balancing the equation of methane combustion:

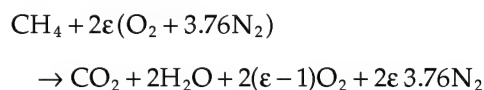


The products of chemical combustion reactions are called flue gas, as they are the gaseous exhaust that

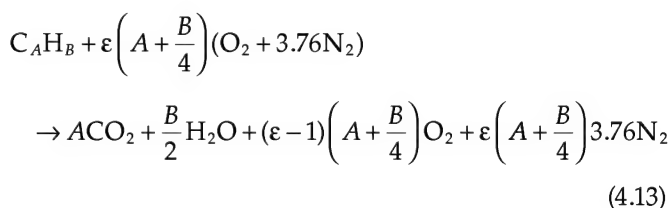
exits through the chimney or flue. The previous equation is theoretical in that it presumes that all the oxygen and fuel react and that nitrogen does not. Actually, trace amounts of nitrogen will react with oxygen to form nitrogen oxides ( $\text{NO}_x$ ). Further, in industrial practice, perfect mixing cannot be achieved. It is actually more cost-effective to ensure complete combustion with the addition of air above the theoretical requirements.

This introduces the concept of excess air. Excess air is an added amount of air to the burner system which is in excess of the amount required for perfect stoichiometric combustion. Excess air is intentionally added to provide a more thorough mixture for more complete combustion and control of combustion chamber temperatures or to produce hot air. Excess air, represented by  $\epsilon$ , is introduced into the chemical reaction as a multiplier of air (predominantly  $\text{O}_2$  and  $\text{N}_2$ ).

$$\epsilon = \frac{\% \text{Excess Air}}{100} + 1 \quad (4.12)$$



The previous equation shows two important chemical features of complete combustion: no carbon monoxide ( $\text{CO}$ ) and some unreacted oxygen appears in the combustion products. To account for any hydrocarbon fuel, variables  $A$  and  $B$  are introduced as moles of Carbon and moles of hydrogen, respectively. Equation 4.13 gives a generic equation for gaseous hydrocarbon fuels with air.



where  $A$  and  $B$  are defined as  $\text{C}_A\text{H}_B$ .

Further, for gases, if nitrogen and oxygen are introduced, Equation 4.14 may be generalized:

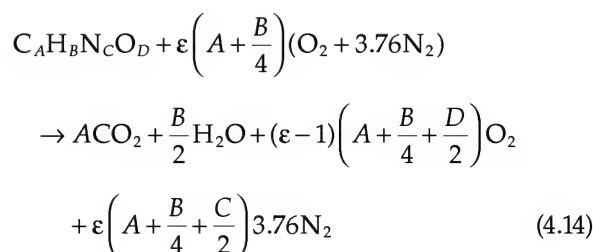


TABLE 4.2

Common Gaseous Fuels

$\text{CH}_4$	Methane
$\text{C}_2\text{H}_6$	Ethane
$\text{C}_3\text{H}_8$	Propane
$\text{C}_4\text{H}_{10}$	Butane

### 4.6.2 Flue Gas

In situ, analyzers measure the flue gas species in the actual hot-wet environment. In contrast, extractive analyzers remove the flue gas, condense the water, and measure the concentration of the flue gas species in the dry gas. Therefore, two sets of equations are needed for wet and dry measurements extracted from Equation 4.13.

Total wet products:

$$\text{TWP} = A + (\epsilon - 1) \left( A + \frac{B}{4} \right) + \epsilon \left( A + \frac{B}{4} \right) 3.76 + \frac{B}{2} \quad (4.15)$$

Total dry products:

$$\text{TDP} = A + (\epsilon - 1) \left( A + \frac{B}{4} \right) + \epsilon \left( A + \frac{B}{4} \right) 3.76 \quad (4.16)$$

$$f_{\text{O}_2, \text{wet}} = \frac{(\epsilon - 1) \left( A + \frac{B}{4} \right)}{\text{TWP}} \quad f_{\text{O}_2, \text{dry}} = \frac{(\epsilon - 1) \left( A + \frac{B}{4} \right)}{\text{TDP}} \quad (4.17)$$

$$f_{\text{CO}_2, \text{wet}} = \frac{A}{\text{TWP}} \quad f_{\text{CO}_2, \text{dry}} = \frac{A}{\text{TDP}} \quad (4.18)$$

$$f_{\text{N}_2, \text{wet}} = \frac{\epsilon \left( A + \frac{B}{4} \right)}{\text{TWP}} \quad f_{\text{N}_2, \text{dry}} = \frac{\epsilon \left( A + \frac{B}{4} \right)}{\text{TDP}} \quad (4.19)$$

$$f_{\text{H}_2\text{O}, \text{wet}} = \frac{B}{2} \frac{1}{\text{TWP}} \quad (4.20)$$

where

$f$  is the mole or volume fraction of the subscripted species,  $0 < f < 1$

Subscripts <sub>wet</sub> or <sub>dry</sub> refer to in situ or extractive measurements, respectively

Because of the strong relationship between oxygen and excess air, the excess oxygen can be used as a measure of excess air. (See Figure 4.5a through f.)

## 4.7 Air-to-Fuel Ratio

The air-to-fuel ratio is an important parameter that will dictate many later combustion calculations (see Table 4.3). The air-to-fuel ratio will be found by both volume and weight. The general form of air-to-fuel ratios will be presented, and then an example calculation will be provided.

Air-fuel ratio by volume can be found in the general form of hydrocarbon gaseous fuels, Equation 4.13, through

$$\left( \frac{A}{F} \right)_v = 4.76\epsilon \left( A + \frac{B}{4} \right) \quad (4.21)$$

where  $C_A H_B$  is the fuel.

To find air-fuel weight, use the molecular weight:

$$\left( \frac{A}{F} \right)_w = \left( \frac{A}{F} \right)_v \times \frac{\text{MW}_{\text{air}}}{\text{MW}_{\text{fuel}}} = \left( \frac{A}{F} \right)_v \times \frac{1}{\text{S.G. fuel}} \quad (4.22)$$

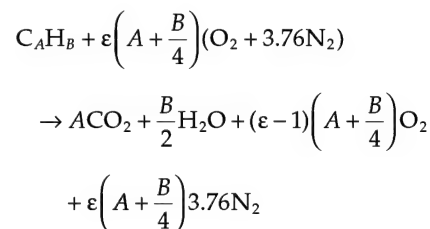
Flue gas-fuel weight can also be calculated in general form using

$$\left( \frac{FG}{F} \right)_w = \left( \frac{A}{F} \right)_w + \left( \frac{\text{Fuel}}{\text{Fuel}} \right)_w = \left( \frac{A}{F} \right)_w + 1 \quad (4.23)$$

### Example 4.3

For the combustion of methane ( $\text{CH}_4$ ), find the air-to-fuel ratio by volume and weight as well as flue gas to fuel by weight when there is 20% excess air.

Using the general equation (4.13) for gaseous fuels results as follows:



The hydrocarbon  $\text{CH}_4$  and 20% excess air yields as follows:

$$\epsilon = 1 + 20\% = 1.20$$

Now solve using the equations presented earlier.

Air-fuel volume:

$$\left( \frac{A}{F} \right)_v = 4.76\epsilon \left( A + \frac{B}{4} \right) = 11.424$$

The specific gravity ( $\text{SG}_{\text{fuel}}$ ) of methane is 0.554.

Solving for air-fuel weight yields,

$$\left( \frac{A}{F} \right)_w = \left( \frac{A}{F} \right)_v \times \frac{1}{\text{SG}_{\text{fuel}}} = 20.62 \frac{\text{lb}_m \text{air}}{\text{lb}_m \text{fuel}}$$

Lastly, the flue gas-to-fuel ratio can be found:

$$\left( \frac{FG}{F} \right)_w = \left( \frac{A}{F} \right)_w + 1 = 21.62 \frac{\text{lb}_m \text{FG}}{\text{lb}_m \text{fuel}}$$

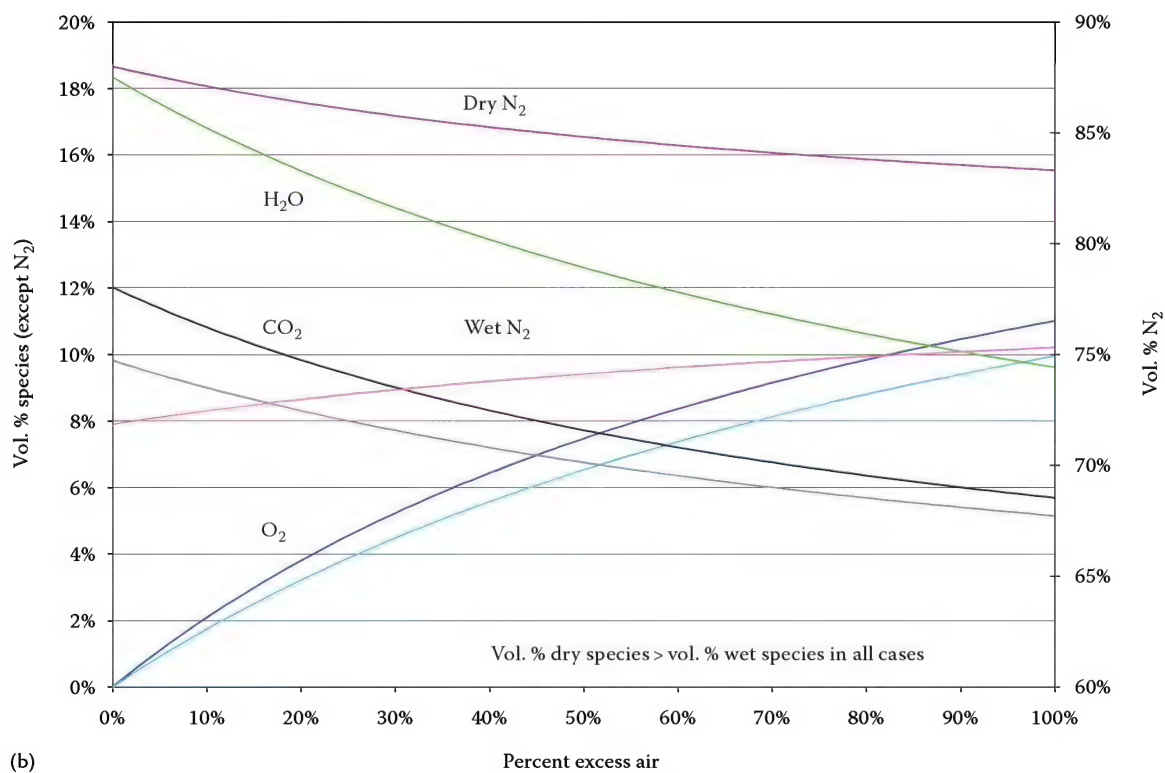
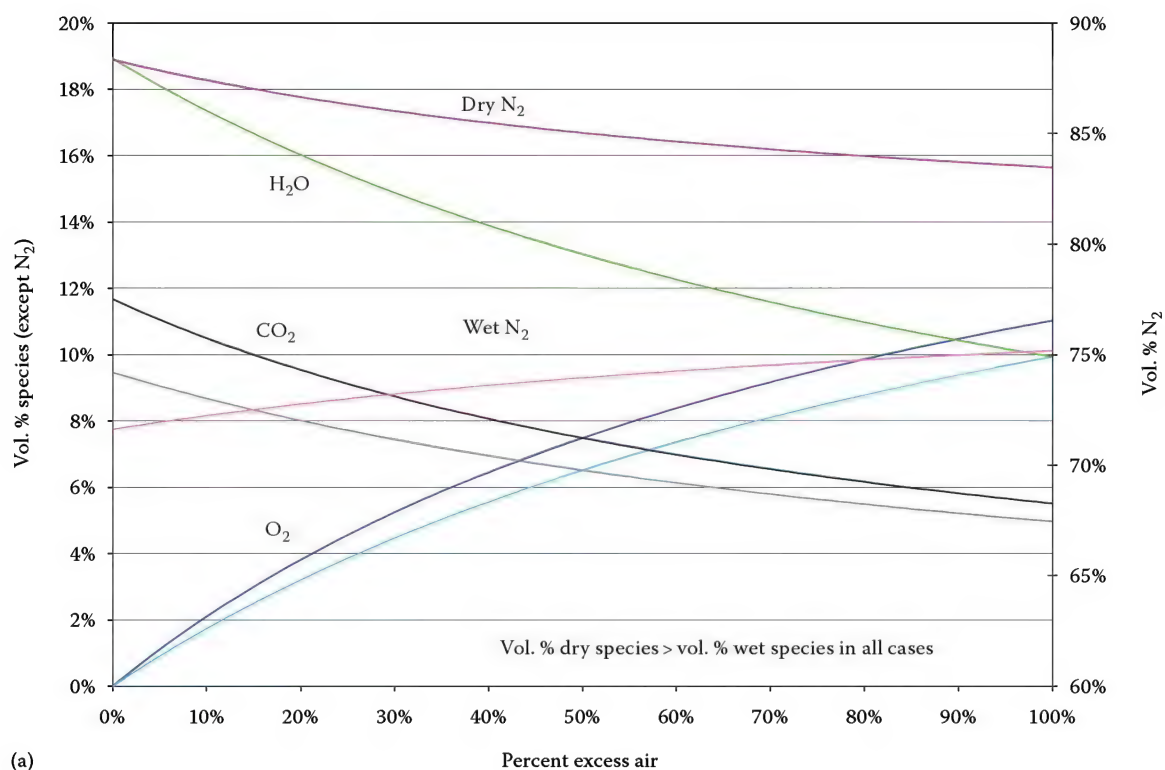
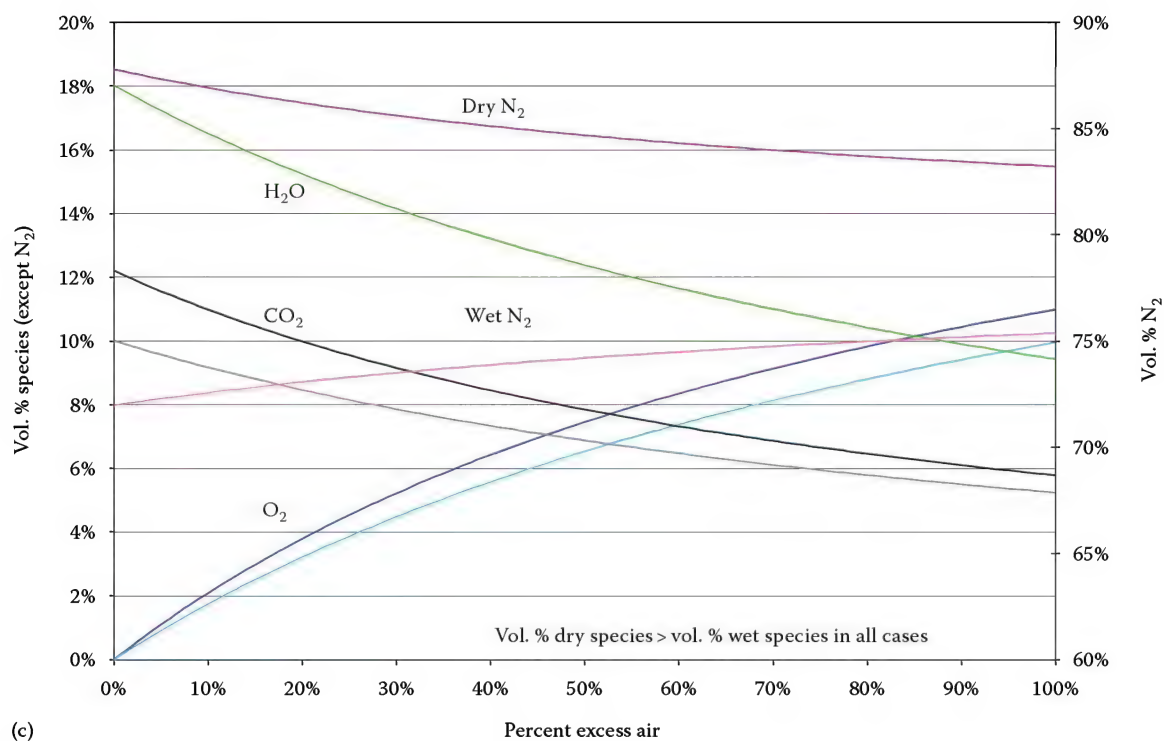


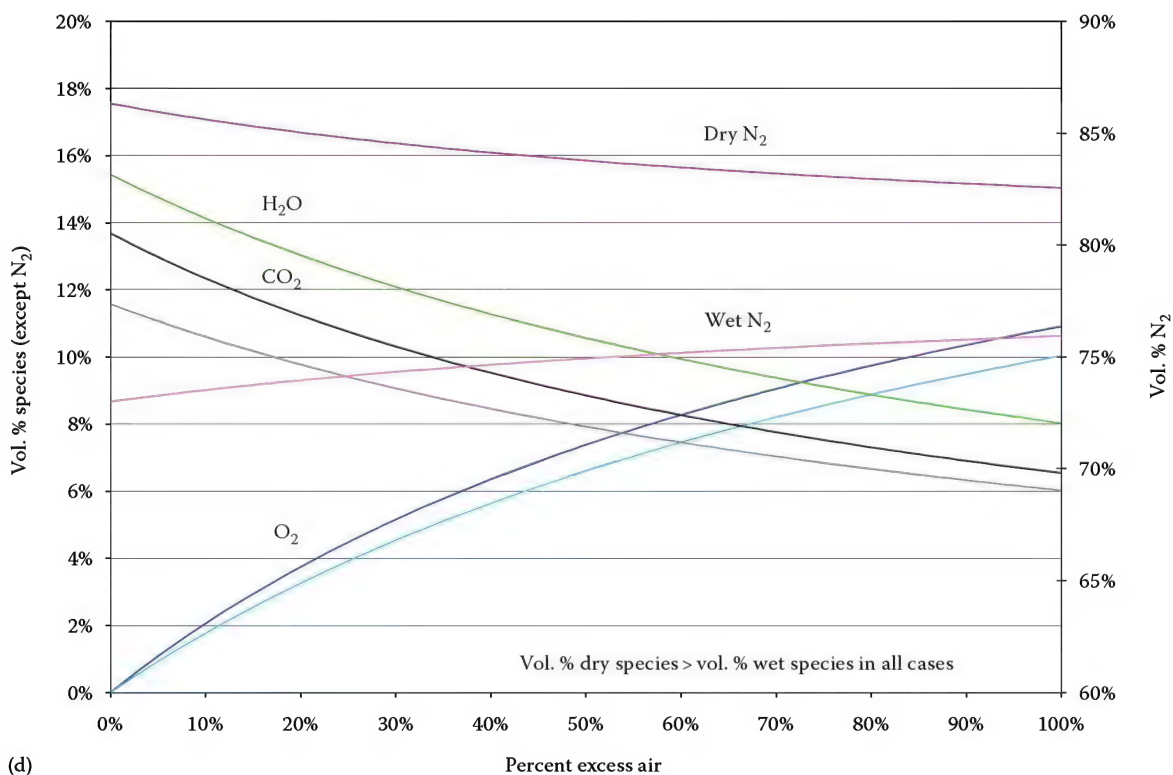
FIGURE 4.5

Species concentration versus excess air for the following fuels: (a)  $\text{CH}_4$ , (b) natural gas.





(c)

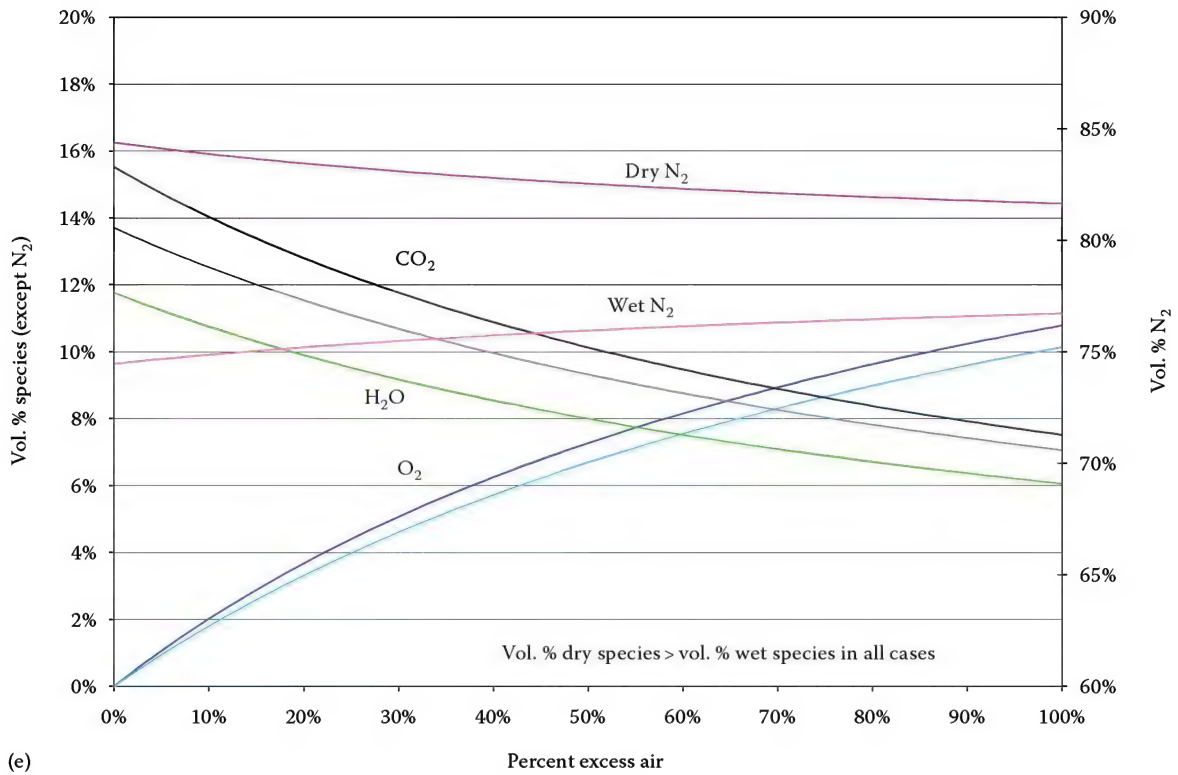


(d)

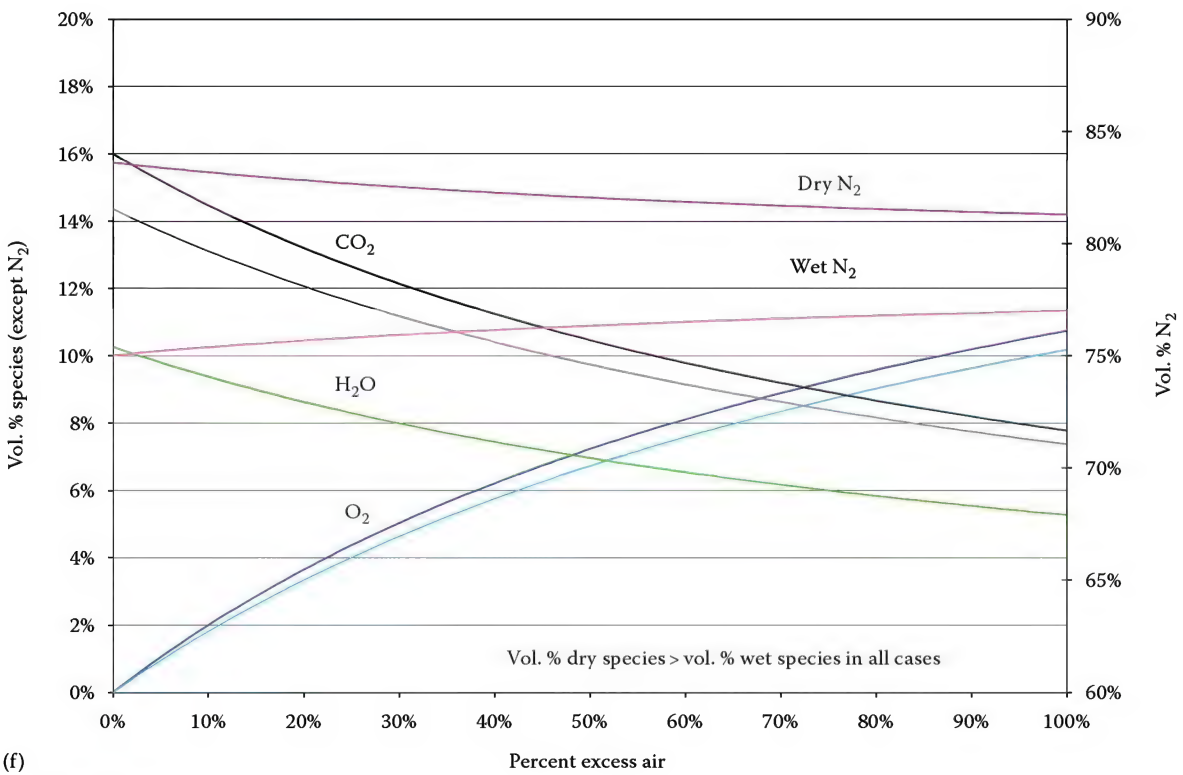
FIGURE 4.5 (continued)

Species concentration versus excess air for the following fuels: (c) simulated refinery gas (25%  $H_2$ , 50%  $CH_4$ , 25%  $C_3H_8$ ) (d)  $C_3H_8$ .

(continued)



(e)



(f)

FIGURE 4.5 (continued)

Species concentration versus excess air for the following fuels: (e) No. 2 oil, and (f) No. 6 oil.

TABLE 4.3

Combustion Data for Hydrocarbons

Hydrocarbon	Formula	Higher Heating Value (Vapor), Btu lb <sub>m</sub> <sup>-1</sup>	Theor. Air/Fuel Ratio, by Mass	Max Flame Speed, (ft s <sup>-1</sup> )	Adiabatic Flame Temp (in Air) (°F)	Ignition Temp (in Air) (°F)	Flash Point (°F)	Flammability Limits (in Air) (% by Volume)	
Paraffins or alkanes									
Methane	CH <sub>4</sub>	23,875	17.195	1.1	3484	1301	Gas	5.0	15.0
Ethane	C <sub>2</sub> H <sub>6</sub>	22,323	15.899	1.3	3540	968–1166	Gas	3.0	12.5
Propane	C <sub>3</sub> H <sub>8</sub>	21,669	15.246	1.3	3573	871	Gas	2.1	10.1
<i>n</i> -Butane	C <sub>4</sub> H <sub>10</sub>	21,321	14.984	1.2	3583	761	−76	1.86	8.41
<i>iso</i> -Butane	C <sub>4</sub> H <sub>10</sub>	21,271	14.984	1.2	3583	864	−117	1.80	8.44
<i>n</i> -Pentane	C <sub>5</sub> H <sub>12</sub>	21,095	15.323	1.3	4050	588	<−40	1.40	7.80
<i>iso</i> -Pentane	C <sub>5</sub> H <sub>12</sub>	21,047	15.323	1.2	4055	788	<−60	1.32	9.16
Neopentane	C <sub>5</sub> H <sub>12</sub>	20,978	15.323	1.1	4060	842	Gas	1.38	7.22
<i>n</i> -Hexane	C <sub>6</sub> H <sub>14</sub>	20,966	15.238	1.3	4030	478	−7	1.25	7.0
Neohexane	C <sub>6</sub> H <sub>14</sub>	20,931	15.238	1.2	4055	797	−54	1.19	7.58
<i>n</i> -Heptane	C <sub>7</sub> H <sub>16</sub>	20,854	15.141	1.3	3985	433	25	1.00	6.00
Triptane	C <sub>7</sub> H <sub>16</sub>	20,824	15.151	1.2	4035	849	—	1.08	6.69
<i>n</i> -Octane	C <sub>8</sub> H <sub>18</sub>	20,796	15.093	—	—	428	56	0.95	3.20
<i>iso</i> -Octane	C <sub>8</sub> H <sub>18</sub>	20,770	15.093	1.1	—	837	10	0.79	5.94
Olefins or alkenes									
Ethylene	C <sub>2</sub> H <sub>4</sub>	21,636	14.807	2.2	4250	914	Gas	2.75	28.6
Propylene	C <sub>3</sub> H <sub>6</sub>	21,048	14.807	1.4	4090	856	Gas	2.00	11.1
Butylene	C <sub>4</sub> H <sub>8</sub>	20,854	14.807	1.4	4030	829	Gas	1.98	9.65
<i>iso</i> -Butene	C <sub>4</sub> H <sub>8</sub>	20,737	14.807	1.2	—	869	Gas	1.8	9.0
<i>n</i> -Pentene	C <sub>5</sub> H <sub>10</sub>	20,720	14.807	1.4	4165	569	—	1.65	7.70
Aromatics									
Benzene	C <sub>6</sub> H <sub>6</sub>	18,184	13.297	1.3	4110	1044	12	1.35	6.65
Toluene	C <sub>7</sub> H <sub>8</sub>	18,501	13.503	1.2	4050	997	40	1.27	6.75
<i>p</i> -Xylene	C <sub>8</sub> H <sub>10</sub>	18,663	13.663	—	4010	867	63	1.00	6.00
Other hydrocarbons									
Acetylene	C <sub>2</sub> H <sub>2</sub>	21,502	13.297	4.6	4770	763–824	Gas	2.50	81
Naphthalene	C <sub>10</sub> H <sub>8</sub>	17,303	12.932	—	4100	959	174	0.90	5.9

Sources: Gray, D.E., Ed., *American Institute of Physics Handbook*, 2nd edn., McGraw-Hill Book Company, New York, 1963; Perry, R.H. et al., S.D., Eds., *Chemical Engineers' Handbook*, 4th edn., McGraw-Hill Book Company, New York, 1963; Weast, R.C., Ed., *Handbook of Chemistry and Physics*, 53rd edn., The Chemical Rubber Company, Cleveland, OH, 1972; gives the heat of combustion of 500 organic compounds; Steere, N.V., Ed., *Handbook of Laboratory Safety*, 2nd edn., The Chemical Rubber Company, Cleveland, OH, 1971; Landenburg, R.W. and Taylor, H.S., *Physical Measurements in Gas Dynamics and Combustion*, Princeton University Press, Princeton, NJ, 1954.

Note: Based largely on "Gas Engineers' Handbook", American Gas Association, Inc., Industrial Press, 1967. For heating value in J kg<sup>-1</sup>, multiply the value in Btu lb<sub>m</sub><sup>-1</sup> by 2324. For flame speed in m s<sup>-1</sup>, multiply the value in ft s<sup>-1</sup> by 0.3048.

Further the molecular weight of the flue gas in general form, Equation 5.12, can be determined by

MW<sub>FG</sub>

$$= \frac{A44 + \frac{B}{2}(18) + (\epsilon - 1)\left(A + \frac{B}{4}\right)32 + \epsilon\left(A + \frac{B}{4}\right)3.76(28)}{A + \frac{B}{2} + (\epsilon - 1)\left(A + \frac{B}{4}\right) + \epsilon\left(A + \frac{B}{4}\right)3.76} \quad (4.24)$$

The molecular weight is introduced as a ratio of the actual weight of the fuel.

$$MW_{\text{fuel}} = 12A + B$$

It is important to note that these equations assume air is composed of 21% O<sub>2</sub> and 79% N<sub>2</sub>.

### 4.7.1 Air-to-Fuel Mixture Ratio

Gases are not always isotropic; fuels often contain a mixture of gaseous compounds. Example 4.4 provides a sample solution for a given gas mixture.

#### Example 4.4

Find the air-to-fuel ratio by weight of a gas mixture composed of:

50% CH<sub>4</sub>  
30% C<sub>2</sub>H<sub>6</sub>      20% excess air  
20% H<sub>2</sub>

Estimate the hydrocarbon formula by calculating the moles of carbon and hydrogen:

$$\text{mole C} = 50\%(1) + 30\%(2) = 1.1 = A$$

$$\text{mole H} = 50\%(4) + 30\%(6) + 20\%(2) = 4.2 = B$$

$$C_A H_B = C_{1.1} H_{4.2}$$

The air-fuel by volume equation (4.21) yields

$$\left(\frac{A}{F}\right)_v = 4.76(1.2) \left(1.1 + \frac{4.2}{4}\right) = 12.28$$

Further, the molecular weight of the fuel can be found as follows:

$$MW_{\text{fuel}} = 12A + B = 12(1.1) + 4.2 = 17.4$$

$$\text{Specific gravity (SG}_{\text{fuel}}) = \frac{17.4}{28.842} = 0.6$$

$$\left(\frac{A}{F}\right)_{\text{WT}} = \frac{12.28}{0.6} = 20.4$$

### 4.7.2 Air-to-Fuel Mass Ratio

Solid and liquid fuel compositions are often given on a mass basis. The following is an example calculating the air-to-fuel ratio when given the mass of C and H<sub>2</sub>.

#### Example 4.5

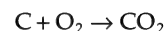
Mass	g-mol/g-Fuel	Mole O <sub>2</sub> φ = 1
85% C	.0708	.0708
15% H <sub>2</sub>	.075	.0375
		.1083

Convert to mole/gram fuel.

$$\frac{.85 \text{ g C}}{\text{g Fuel}} \times \frac{\text{g} \cdot \text{mole}}{12 \text{ g C}} = .0708 \frac{\text{g} \cdot \text{mol C}}{\text{g Fuel}}$$

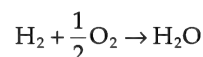
$$\frac{.15 \text{ g H}_2}{\text{g Fuel}} \times \frac{\text{g} \cdot \text{mole}}{2 \text{ g H}_2} = .075 \frac{\text{g} \cdot \text{mole H}_2}{\text{g Fuel}}$$

Developing a relation between weight of C and moles of O<sub>2</sub>:



$$\frac{.0708 \text{ mol C}}{\text{g Fuel}} \times \frac{1 \text{ mol O}_2}{1 \text{ mol C}} = \frac{.0708 \text{ mol O}_2}{\text{g Fuel}}$$

Developing a relation between weight of H<sub>2</sub> and moles of O<sub>2</sub>:



$$\frac{.075 \text{ mol H}_2}{\text{g Fuel}} \times \frac{\frac{1}{2} \text{ mol O}_2}{1 \text{ mol H}_2} = \frac{.0375 \text{ mol O}_2}{\text{g Fuel}}$$

Combining the two relationships, the required amount of O<sub>2</sub> per mass of fuel is found.

$$\frac{.1083 \text{ mol O}_2}{\text{g Fuel}} \times \frac{1 \text{ mol Air}}{.21 \text{ mol O}_2} \times \frac{28.85 \text{ g Air}}{1 \text{ mol Air}} = \frac{14.87 \text{ g Air}}{1 \text{ g Fuel}}$$

$$\left(\frac{A}{F}\right)_{\text{WT}} = 14.87$$

Many solid and liquid fuels cannot be defined with C<sub>A</sub>H<sub>B</sub>. In such cases, use the general equation for hydrocarbon combustion along with the fuel's mole ratio as defined in the following example.

#### Example 4.6

Given the same fuel as Example 4.5 with a mass comprised of 85% carbon and 15% hydrogen, find the air-fuel ratio by weight and the chemical equation with no excess air using the new mole ratio:

$$\left(\frac{\text{H}}{\text{C}}\right)_{\text{mole}} = x$$

$$\text{CH}_x + \epsilon \left(1 + \frac{x}{4}\right) (\text{O}_2 + 3.76 \text{N}_2)$$

$$\rightarrow \text{CO}_2 + \frac{x}{2} \text{H}_2\text{O} + (\epsilon - 1) \left(1 + \frac{x}{4}\right) \text{O}_2$$

$$+ \epsilon \left(1 + \frac{x}{4}\right) 3.76 \text{N}_2$$



Because there is no excess air,

$$\epsilon = 1$$

Convert mass percentage to mole fraction:

$$\frac{.15 \text{ g H}}{.85 \text{ g C}} \times \frac{12 \text{ g C}}{1 \text{ mol C}} \times \frac{1 \text{ mol H}}{1 \text{ g H}} = 2.11 \frac{\text{mole H}}{\text{mole C}} = x$$

Finding the molecular weight of the fuel:

$$\text{MW}_{\text{fuel}} = 12 + x = 14.11$$

$$\left(\frac{A}{F}\right)_{\text{WT}} = \epsilon \left(1 + \frac{x}{4}\right) \times \frac{4.76 \text{ mol Air}}{\text{mole Fuel}} \times \frac{\text{mole Fuel}}{(12 + x) \text{ g Fuel}} \\ \times \frac{28.85 \text{ g Air}}{\text{mole Air}} = 14.87$$

This yields the same answer as Example 4.5

Note that one cannot find  $\left(\frac{A}{F}\right)_v$  with this form of the oxidation equation. However, one can find volume of flue gas products, molecular weight,  $\text{O}_2$ , etc.

### 4.7.3 Turbine Exhaust Gas

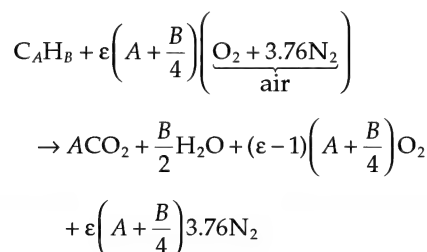
In turbine exhaust gases (TEGs), the products are delivered to the burner at elevated temperatures, (1200°F or 650°C) which, in turn, reduces the oxygen content in air to roughly 12%. Thus, in cases like this as well as other oxidizer streams,  $\text{O}_2$  with  $\text{N}_2$ ,  $\text{CO}_2$ , and  $\text{H}_2\text{O}$  must be normalized. This method is best illustrated through an example.

#### Example 4.7

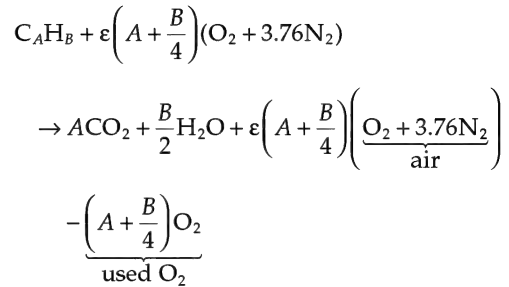
Given a mole percentage composition of a turbine exhaust gas, find the turbine exhaust gas to fuel by weight and the percentage of wet oxygen of  $\text{CO}_2$  with an excess air of 300%.

12%  $\text{O}_2$   
4%  $\text{H}_2\text{O}$   
5%  $\text{CO}_2$   
79%  $\text{N}_2$

The general equation is as follows:



The products can be rewritten as



As developed in Equation 4.13 from air with 21%  $\text{O}_2$  and 79%  $\text{N}_2$ , a similar process is done using TEG by normalizing the TEG stream to a mole of  $\text{O}_2$  and the balance of  $\text{N}_2$ ,  $\text{H}_2\text{O}$ , and  $\text{CO}_2$  follows. For example,

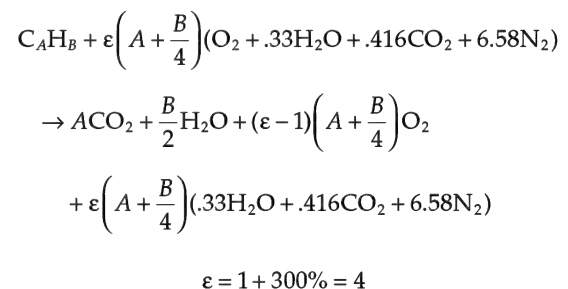
$$12\% \text{O}_2 \rightarrow .12 \text{ mol O}_2 \times \left(\frac{1}{.12}\right) = 1 \text{ mol O}_2$$

Thus, in this case, the multiplier is  $\left(\frac{1}{.12}\right) = 8.33$

TEG

	Normalize	
12% $\text{O}_2$	$.12 \text{ mol O}_2 \rightarrow 1 \text{ mol O}_2$	
4% $\text{H}_2\text{O}$	$.04 \text{ H}_2\text{O} \rightarrow .33 \text{ mol H}_2\text{O}$	the "air"
5% $\text{CO}_2$	$.05 \text{ CO}_2 \rightarrow .416 \text{ mol CO}_2$	
79% $\text{N}_2$	$.79 \text{ N}_2 \rightarrow 6.58 \text{ mol N}_2$	

Applying the multiplier with each molecule normalizes the quantities and provides the stoichiometric coefficients as shown in the following.



Solving for TEG by weight,

$$\left(\frac{\text{TEG}}{F}\right)_v = \epsilon \left(A + \frac{B}{4}\right) (1 + .33 + .416 + 6.58) \\ = 4 \left(1 + \frac{1}{4}\right) (8.326) = 66.6$$

$$\text{MW}_{\text{TEG}} = .12(32) + .04(18) + .05(44) + .79(28) = 28.88$$

$$\left(\frac{\text{TEG}}{F}\right)_w = \left(\frac{\text{TEG}}{F}\right)_v \left(\frac{\text{MW}_{\text{TEG}}}{\text{MW}_F}\right) \\ = 66.6 \times \frac{28.88}{16}$$

Note that specific gravity should be used in this case because TEG  $\neq$  air.

Manipulating the general equation for chemical combustion for  $O_2$  yields

% $O_{2wet}$

$$= \frac{(\epsilon - 1) \left( A + \frac{B}{4} \right)}{A + \frac{B}{2} + (\epsilon - 1) \left( A + \frac{B}{4} \right) + \epsilon \left( A + \frac{B}{4} \right) (.33 + .416 + 6.58)} \times 100$$

$$= \frac{3(2)}{1 + 2 + 3(2) + 4(2)(8.326)} = \frac{600}{75.61} = 7.93\%wet$$

TEG examples are typically given in  $lb_m/h$  or  $kg/h$  basis and are sometimes best solved with a table.

#### Example 4.8

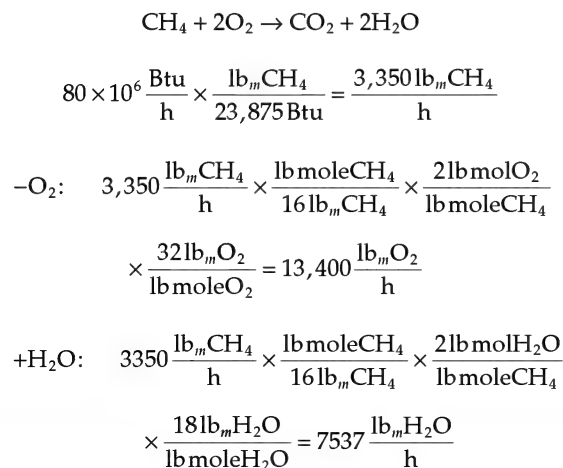
Given the combustion of methane yielding  $10^6$   $lb_m/h$  TEG at  $1000^\circ F$  with a fuel input of  $80 \times 10^6$  Btu/h HHV. Find the molecular weight of TEG, the emission of  $O_2$ ,  $H_2O$ , and  $CO_2$  in lbm per hour, TEG to fuel by weight, % $O_2$  and  $\epsilon$ .

The given TEG flow breakdown:

$lb_m/h$ TEG		$lb_m/h$	$lb_m/h$ Products	k lb mol/h TEG
120 k $O_2$	-	13,400	106.6 k $O_2$	3.75
40 k $H_2O$	+	7,537.5	47.54 k $H_2O$	2.22
50 k $CO_2$	+	9,212	59.21 k $CO_2$	1.136
790 k $N_2$	—	—	790 k $N_2$	28.2
$10^6$ $lb_m/h$			1003.35 k	35.306

$$MW_{TEG} = \frac{10^6}{35,306} = 28.32.$$

The combustion reaction consumes  $O_2$  and forms  $H_2O$  and  $CO_2$



$$CO_2: \quad 3350 \frac{lb_m CH_4}{h} \times \frac{lb \text{ mole } CH_4}{16 lb_m CH_4} \times \frac{1 lb \text{ mole } CO_2}{1 lb \text{ mole } CH_4}$$

$$\times \frac{44 lb_m CO_2}{lb \text{ mole } CO_2} = 9212 \frac{lb_m CO_2}{h}$$

mF G k pph	k lb mole/h
$O_2$ 106.6	3.33
$H_2O$ 47.54	2.64
$CO_2$ 59.21	1.345
$N_2$ 790	28.21
1003.35	35.53

$$MW_{FG} = 1003.35 \frac{k lb_m}{h} \times \frac{h}{35.53 k lb \text{ mole}}$$

$$= 28.24 \frac{lb_m}{\text{mole } FG}$$

$$\left( \frac{TEG}{F} \right)_{WT} = \frac{10^6}{3350} = 298.5$$

$$\%O_{2wet} = \frac{3.33}{35.53} \times 100 = 9.37\%$$

Finding  $\epsilon$ :

$$\text{For } \epsilon = 1 \rightarrow 13,400 lb_m O_2 \times \frac{10^6 lb \text{ TEG}}{120 k lb O_2}$$

$$= 111.6 k lb \text{ TEG}$$

$$\epsilon = \frac{10^6}{111.6K} = 8.96$$

#### Example 4.9

The same example given earlier can be solved using the general formula of hydrocarbon combustion.

TEG pph	k lb mol/h	Normalized $O_2 = 1$
120 k $O_2$	3.75	1
40 k $H_2O$	2.22	.592
50 k $CO_2$	1.136	.303
790 k $N_2$	28.2	7.52

$$C_A H_B + \epsilon \left( A + \frac{B}{4} \right) (O_2 + .592 H_2O + .303 CO_2 + 7.52 N_2)$$

$$\rightarrow A CO_2 + \frac{B}{2} H_2O + (\epsilon - 1) \left( A + \frac{B}{4} \right) O_2$$

$$+ \epsilon \left( A + \frac{B}{4} \right) (.592 H_2O + .303 CO_2 + 7.52 N_2)$$

$$\text{MWTEG} = 28.32$$

$$\left(\frac{\text{TEG}}{F}\right)_{\text{WT}} = \frac{\epsilon \left(1 + \frac{4}{4}\right) (1 + .592 + .303 + 7.52) 28.32}{16}$$

$$\text{TEG} = 10^6 \text{ lb/h}$$

$$\text{Fuel} = 3350 \text{ lb/h}$$

$$\frac{10^6}{3350} = \frac{\epsilon \left(1 + \frac{4}{4}\right) (9.415) 28.32}{16} \rightarrow \epsilon = 8.96$$

The method used in Example 4.8 yields the same results as Example 4.9.

## 4.8 Chemical Thermodynamics

The amount of heating energy released in a chemical reaction can be calculated through thermodynamics.

### 4.8.1 Enthalpy, Entropy, and Heat Capacity

How hot can a flame be? First, there is a difference between heat ( $Q$ ) and temperature ( $T$ ). Heat is energy in transit. When a body absorbs heat, it stores it as another form of energy, increasing the body's temperature and expanding it. That is, the material uses some of the thermal energy to raise the temperature and some of the energy to expand the body against the atmosphere. The same amount of heat absorbed in different materials will yield different temperature increases and expansions.

For example, 100 Btu of heat will raise the temperature of 1 lb of water by 100°F and expand the volume of that water by approximately 2.2%. The same 100 Btu of heat absorbed by 1 lb of air will increase the temperature by 400°F and expand the volume by approximately 62%. The total energy used to raise the temperature and increase the volume is called enthalpy ( $H$ ), classically defined as the measure of total energy content of a substance in a thermodynamic system.<sup>15</sup> Enthalpy relates to temperature by a quantity known as the isobaric heat capacity,  $C_p$ . Heat capacity is the amount of heat required to raise the temperature of 1 unit mass of a substance by one degree of temperature. The change in internal energy or enthalpy for an ideal gas during a process can be determined by integrating Equation 4.25:

$$h_2 - h_1 = \int_1^2 C_p(T) dT \quad (4.25)$$

From Equation 4.25, it is important to note that  $C_p$  varies as a function of temperature.

### 4.8.2 Heat of Combustion

In addition to the conservation of mass, energy is also conserved in a combustion reaction. One measure of the chemical energy of a fuel is the *heat of combustion*. Table 4.3 gives heats of combustion for some typical fuels on a HHV mass basis.<sup>16</sup> Heat of combustion is reported as either net heating value (lower heating value, LHV) or gross heating value (higher heating value, HHV). To understand the difference, reconsider the chemical equation for methane combustion. When methane burns, it produces two products:  $\text{CO}_2$  and  $\text{H}_2\text{O}$ . The  $\text{CO}_2$  will remain a gas under all conceivable industrial combustion conditions. However,  $\text{H}_2\text{O}$  can exist as either a liquid or a vapor, depending on how much heat is extracted from the process. If so much heat is extracted that the  $\text{H}_2\text{O}$  condenses, then the combustion yields its HHV. If water is released from the stack as a vapor, then combustion yields the LHV. The process industry usually uses the LHV. Boiler and turbine calculations usually use the HHV. However, either measure can be used in combustion calculations as long as one is consistent.

For the purpose of combustion, the concern is with the changes in the energy of a system as opposed to energy of a particular state; because of this, any state may be chosen as the initial state and assigned a zero value of enthalpy for that substance. However, when the process involves chemical change, the composition of the system is no longer the same as it was in the beginning of the process. It is thus necessary to choose a reference state for all substances which has been defined by engineers to be at 77°F (25°C) and 1 atm (101.3 kPa), known as the standard reference state. Heat of formation is the enthalpy of a substance at the standard reference state.<sup>15</sup>

By definition, these heating values can be related by

$$\text{HHV} - \text{LHV} = (h_{\text{vap}}) \frac{m_{\text{H}_2\text{O}}}{m_{\text{fuel}}} \quad (4.26)$$

where

$m_{\text{H}_2\text{O}}$  is the mass of  $\text{H}_2\text{O}$

$m_{\text{fuel}}$  is the mass of fuel

$h_{\text{vap}}$  is the enthalpy of vaporization of  $\text{H}_2\text{O}$  at the specified temperature

#### Example 4.10

Here, an example of calculations for enthalpy of combustion, HHV and LHV, of methane gas is presented.



Heat of formation at standard reference state:

$$\text{CH}_{4\text{g}} = -17.88 \text{ kcal/g mol}$$

$$\text{CO}_{2g} = -94.051 \text{ kcal/g mol}$$

$$\text{H}_2\text{O}_{\text{liq}} = -68.315 \text{ kcal/g mol}$$

$$\text{H}_2\text{O}_g = -57.796 \text{ kcal/g mol}$$

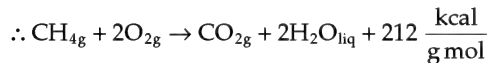
For  $\text{H}_2\text{O}_{\text{liq}}$ ,

$$\Delta h = \sum (\text{products}) - \sum (\text{reactants})$$

$$\Delta h = [(1 \times -94.051) + (2 \times -68.315)] - [-17.88]$$

$$= -212.8 \frac{\text{kcal}}{\text{g mol}}$$

Negative enthalpy denotes exothermic reactions



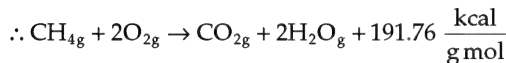
$$212 \frac{\text{kcal}}{\text{g mol}} = \text{HHV since H}_2\text{O is condensed.}$$

Conversely, for  $\text{H}_2\text{O}_g$ ,

$$\Delta h = \sum (\text{products}) - \sum (\text{reactants})$$

$$\Delta h = [(1 \times -94.051) + (2 \times -57.796)] - [-17.88]$$

$$= -191.76 \frac{\text{kcal}}{\text{g mol}}$$



$$191.76 \frac{\text{kcal}}{\text{g mol}} = \text{LHV since H}_2\text{O is not condensed.}$$

Conversion to  $\frac{\text{Btu}}{\text{lb}_m}$ :

$$212 \frac{\text{kcal}}{\text{g mol}} \times 1,000 \frac{\text{C}}{\text{kcal}} 4.186 \frac{\text{J}}{\text{C}} \times 9.47 \times 10^{-4} \frac{\text{Btu}}{\text{J}}$$

$$\times \frac{1 \text{ g mol}}{16 \text{ g}} \times 454 \frac{\text{g}}{\text{lb}_m} = 23,868 \frac{\text{Btu}}{\text{lb}_m}$$

Finding density of methane,

$$\rho_{\text{CH}_4} = .076 \frac{\text{lb}_m}{\text{Sft}^3} \times \frac{16}{28.85} = .042 \frac{\text{lb}_m}{\text{Sft}^3}$$

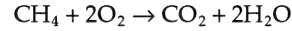
Now one can find Btu per unit volume:

$$23,868 \frac{\text{Btu}}{\text{lb}_m} \times .042 \frac{\text{lb}_m}{\text{Sft}^3} = 1006 \frac{\text{Btu}}{\text{Sft}^3}$$

To find enthalpy at vaporization,

$$\text{HHV} - \text{LHV} = (h_{\text{vap}}) \frac{m_{\text{H}_2\text{O}}}{m_{\text{fuel}}}$$

$$h_{\text{vap}} = 970 \frac{\text{Btu}}{\text{lb}_m}$$



$$2 \frac{\text{mole H}_2\text{O}}{\text{mole CH}_4} \times 18 \frac{\text{lb}_m}{\text{mole H}_2\text{O}} \times \frac{1 \text{ mole CH}_4}{16 \text{ lb}_m} = 2.25$$

$$\text{mass ratio} = \frac{m_{\text{H}_2\text{O}}}{m_{\text{fuel}}}$$

Converting:

$$\text{LHV} = 191.76 \frac{\text{kcal}}{\text{g mol}} \Rightarrow 21,589 \frac{\text{Btu}}{\text{lb}_m}$$

#### 4.8.3 Adiabatic Flame Temperature

An adiabatic flame is an idealized situation where there is no heat loss to the surroundings during combustion; that is to say that all generated heat is applied to the products. Once the reactants and their states are specified, the enthalpy of the reactants can easily be determined through tables. However, the calculations of the enthalpy of the products are not as simple because the specific heat varies as a function of temperature. To be able to predict the enthalpy of products, engineers have created tables that provide the enthalpy of combustion products given varying temperatures of adiabatic flame. Through these tables, engineers can very closely predict the adiabatic flame temperature by interpolating enthalpy solutions.<sup>15</sup>

##### Example 4.11

The following example will find adiabatic flame temperature through the enthalpy solutions using standard gas tables.

##### Given

$\text{CH}_4$  at 20% EA  
find adiabatic flame temperature.

From the general form,

$$\begin{aligned} C_A H_B + \epsilon \left( A + \frac{B}{4} \right) (\text{O}_2 + 3.76 \text{N}_2) \\ \rightarrow A \text{CO}_2 + \frac{B}{2} \text{H}_2\text{O} + (\epsilon - 1) \left( A + \frac{B}{4} \right) \text{O}_2 \\ + \epsilon \left( A + \frac{B}{4} \right) 3.76 \text{N}_2 \end{aligned}$$



The products are as follows:

From the Gas Tables				
$ACO_2$	=	1 lb mol $CO_2$	$h$ (70°F)	= 3968.3 Btu/ lb mol
$B/2 H_2O$	=	2 lb mol $H_2O$	$h$ (70°F)	= 4202.2
$(\epsilon - 1)\left(A + \frac{B}{4}\right)O_2$	=	.4 lb mol $O_2$	$h$ (70°F)	= 3676.1
$\epsilon\left(A + \frac{B}{4}\right)3.76N_2$	=	9.04 lb mol $N_2$	$h$ (70°F)	= 3680.8

By definition,

$$\text{Heating value} = \sum \text{moles of product} \times \left( \sum h_{\text{products}} - \sum h_{\text{reactants}} \right)$$

In practical application, LHV is used when the  $H_2O$  product of the reaction exists in vapor phase, while HHV is used when the  $H_2O$  product is in a liquid phase.

In most cases, the  $H_2O$  product is in gaseous phase and from the previous example LHV in the combustion of methane was calculated and now the units of lb mole need to be converted:

$$\text{LHV} = 21,589 \frac{\text{Btu}}{\text{lb}_m} \times 16 \frac{\text{lb}_m}{\text{lbmol}} = 344 \frac{\text{kBtu}}{\text{lbmol}}$$

Now, set up the heating value equation:

$$344,000 = 1(h_{CO_2} - 3,968.3) + 2(h_{H_2O} - 4,202.2) + .4(h_{O_2} - 3,676.1) + 9.04(h_{N_2} - 3,680.8)$$

Looking up enthalpy from temperature in gas tables, one can then calculate the LHV solutions as tabulated in the following:

Temp <sub>AD</sub>	CO <sub>2</sub>	H <sub>2</sub> O	h <sub>O<sub>2</sub></sub>	h <sub>N<sub>2</sub></sub>	Calculated LHV	Result
3500°F	48,646.80	39,988	32,440	30,982	338,242	Too low
3200°F	44,280	36,274	29,715	28,390	374,557	Too high

Interpolating temperature from enthalpy yields

$$\text{temp}_{AD} = 3247 \Rightarrow \text{next guess}$$

Next interpolate again for enthalpy from interpolated temp<sub>AD</sub>:

CO <sub>2</sub>		H <sub>2</sub> O	
3240°F	44,860	3240°F	36,765
3247°F	44,961	3247°F	36,851
3260°F	45,151	3260°F	37,011
O <sub>2</sub>		N <sub>2</sub>	
3240°F	30,077.5	3240°F	28,735.1
3247°F	30,140	3247°F	29,145
3260°F	30,258	3260°F	29,907.5

Interpolating once more for temp<sub>AD</sub> from the calculated LHV.

Guess:

Temp <sub>AD</sub>	LHV
3200°F	338,242
X	344,000
3247°F	347,312

$$\left( \frac{344,000 - 338,242}{347,312 - 338,242} \right) 47 + 3,200 = 3,231^\circ\text{F}$$

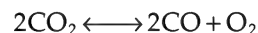
This provides a fairly good approximation.

Note that the actual flame temperature will be much cooler than this, because heat will transfer from the flame to the surroundings *via* convection and radiation. This example was used to show the hand calculation of adiabatic flame temperatures. In practice, solutions would be generated using a curve fit of enthalpy versus temperature. This can be done using a simple computer solution.

#### 4.8.4 Dissociation

At elevated temperatures, bonds that hold gas molecules together weaken. These gas molecules are said to dissociate and form new molecules from their respective constituents. Dissociation is a reversible process and when undergoing dissociation, gases are heterogeneous in composition, normally only 1%–2% of a given gas dissociates under typical combustion temperatures.

Dissociation of carbon dioxide gas:



Dissociation of water:



The measure of a gas's stability against dissociation is represented by the equilibrium constant,  $K_p$ , the smaller the value of the constant, the more stable the gas.

Given the chemical equation  $aA + bB \leftrightarrow cC + dD$ ,

$$K_p = \frac{(p_C)^c (p_D)^d}{(p_A)^a (p_B)^b} \quad (4.27)$$

where

$p_A$  is the partial pressure of element A  
 $p_B$  is the partial pressure of element B  
 $p_C$  is the partial pressure of element C  
 $p_D$  is the partial pressure of element D  
 $p$  is the mixture pressure

The process of finding the equilibrium constant through Equation 4.27 can become very time consuming when calculating for multiple partial pressures. Fortunately, the equilibrium constant is a property that can be looked up in tables, such as the *Janaf Thermochemical Tables*.<sup>17</sup> In these charts, the  $K_p$  for many gases are tabulated as a function of temperature. It is also important to note that the values for equilibrium constants are commonly given in base 10, that is,  $\log_{10} K_p$ .

Dissociation is an important factor to consider, as high percentages of dissociation will decrease the theoretically attainable temperature of a gas.

## 4.9 Practical Liquid Fuels

As mentioned earlier, the topic of fuels will be extensively covered in other chapters; the scope of this section is only to introduce the chemical properties of liquid fuels. A parameter that can predict many properties of a liquid fuel is API gravity. API gravity was devised by the American Petroleum Institute as a standard measure of a fuel's density and is defined as

$$\text{Degree API gravity} = \frac{141.5}{\text{Specific gravity @ } 60^\circ\text{F}} - 131.5 \quad (4.28)$$

The API gravity of liquid fuels holds many relationships with several of the fuel's properties. The following are some relationships between properties and API gravity for liquid fuels (see Tables 4.4<sup>6</sup> and 4.5<sup>18</sup>):

- The lower a fuel's API gravity, the heavier a fuel is in viscosity, the higher the carbon residue, and the heavier the weight.
- Conversely, the higher a fuel's API gravity, the lighter a fuel is in viscosity, the lower the carbon residue, and the lower the weight.

**TABLE 4.4**

Specific Gravity and Properties of Common Liquid Fuels

Grade Fuel	No. 1	No. 2	No. 4 (Light)	No. 4	No. 5 (Light)	No. 5 (Heavy)	No. 6
Specific gravity, 60/60°F	0.8499	0.8762	0.8762	—	—	—	—
(deg API), max	35 min	30 min	30 max	—	—	—	—
Flash point °F min	100	100	100	130	130	130	140
Pour point °F max	0	20	20	20	—	—	—
Kinematic viscosity mm <sup>2</sup> /s [cSt]							
At 100°F min	1.4	2	2	5.8	>26.4	>65	—
Max	2.2	3.6	5.8	26.4	65	194	—
At 104°F min	1.3	1.9	—	5.5	>24	>58	—
Max	2.1	3.4	—	24	58	168	—
Saybolt viscosity							
Universal at 100°F							
Min	—	32.6	32.6	45	>125	>300	>900
Max	—	37.9	45	125	300	900	9000
Furol at 122°F							
Min	—	—	—	—	—	23	>45
Max	—	—	—	—	—	40	300
Distillation temperature, °F							
10% Point max	420	—	—	—	—	—	—
90% Point min	—	540	—	—	—	—	—
Max	550	640	—	—	—	—	—
Sulfur content, mass, max	0.5	0.5	—	—	—	—	—
Corrosion copper strip, max	3	3	—	—	—	—	—
Carbon residue, 10% b;% m, max	0.15	0.35	—	—	—	—	—
Water and sediment, % vol, max	0.05	0.05	0.5	0.5	1	1	2

Source: Schmidt, P., *Fuel Oil Manual*, 4th edn., Industrial Press, New York, 1985.

TABLE 4.5

Liquid Fuel Properties by API Gravity as well as Common Coals

Liquid Fuel Heating Properties							
API Gravity	Specific Gravity	Percent Hydrogen	Heating Values (Btu/gal)		Heating Values (Btu/lbm)		BTU Fired/Cubic Foot of Air <sup>a</sup>
			Higher	Lower	Higher	Lower	
0.000	1.076	8.940	158,610	149,470	17,684	16,665	98.32
2.000	1.060	9.152	157,380	148,330	17,815	16,791	98.67
4.000	1.044	9.364	156,110	147,250	17,935	16,918	99.00
6.000	1.029	9.577	154,860	146,340	18,055	17,062	99.29
8.000	1.014	9.789	153,570	145,260	18,165	17,182	99.55
10.000	1.000	10.002	152,280	144,000	18,270	17,277	99.78
12.000	0.986	10.214	151,000	142,720	18,372	17,365	99.99
14.000	0.973	10.426	149,720	141,440	18,470	17,449	100.17
16.000	0.959	10.639	148,440	140,160	18,564	17,529	100.33
18.000	0.946	10.851	147,160	138,790	18,654	17,593	100.47
20.000	0.934	11.064	145,880	137,510	18,739	17,663	100.59
22.000	0.922	11.276	144,600	136,230	18,821	17,731	100.69
24.000	0.910	11.488	143,420	135,040	18,908	17,804	100.77
26.000	0.898	11.701	142,140	133,760	18,982	17,863	100.83
28.000	0.887	11.913	140,950	132,580	19,063	17,931	100.88
30.000	0.876	12.126	139,660	131,300	19,124	17,979	100.91
32.000	0.865	12.338	138,490	130,120	19,200	18,040	100.94
34.000	0.855	12.550	137,310	128,940	19,269	18,094	100.95
36.000	0.845	12.763	136,130	127,560	19,334	18,117	100.95
38.000	0.835	12.975	134,960	126,570	19,396	18,191	100.95
40.000	0.825	13.188	133,760	125,390	19,450	18,233	100.94
Coal							
Pittsburg #8 bituminous	—	—	95,166	—	—	—	97.400
Anthracite	—	—	90,233	—	—	—	96.530

Source: Adapted from Stultz, S.C. and Kitto, J.B., *Steam: Its Generation and Use*, 40th edn., Babcock & Wilcox Company, Barberton, OH, 1992; Schmidt, P., *Fuel Oil Manual*, 4th edn., Industrial Press, New York, 1985.

<sup>a</sup> Air referenced at 70°F.

- The higher the API gravity, the greater the HHV on a mass basis created when burning the fuel.
- The higher the API gravity, the lower the unit weight of the fuel.
- The higher the API gravity, the higher the hydrogen and the lower the carbon content.
- API gravity can indicate the grade of a fuel.
- As API gravity decreases, the rate of combustion also decreases while the flame length increases. (Schmidt<sup>9</sup>)

#### 4.10 Combustion Kinetics

Combustion systems operate with moderate to high temperatures and, as such—exact chemical kinetics are very important for emissions prediction—they must be correct. Generally first-order reaction rates perform very well. For first-order oxidation the general expression is as follows:

$$\frac{d(\text{chemical})}{dt} = -K[\text{O}_2][\text{chemical}] \quad (4.29)$$

where

$$K = Ae^{\left[\frac{-E}{RT}\right]}$$

and

$A$  is the pre-exponential factor/frequency factor in appropriate units

$R$  is the universal gas constant in appropriate units

$T$  is the absolute temperature

$E$  is the activation energy, usually listed in kcal/mol

$t$  = time in seconds

For perfectly stirred reactors well downstream of the initial mixing, integration of the first-order equation results in a simple equation for constant temperature and  $O_2$  mole fraction in a time step may be expressed as

$$1 - \left( \frac{\text{Chemical final}}{\text{Chemical initial}} \right) = \left[ 1 - e^{-k(O_2)(\Delta t)} \right] \quad (4.30)$$

For utilization, and performance prediction, kinetic data can be utilized from literature such as Battelle Columbus Laboratories' "Chemical Aspects of Afterburner Systems."<sup>19</sup> For instance for CO destruction, several kinetic data are available such as found in Ref. [20].

$$\frac{d[CO]}{dt} = -1.8 \times 10^7 e^{\left[\frac{-25,000}{RT}\right]} (CO)(O_2)^{0.5} (H_2O)^{0.5} \left( \frac{P}{RT} \right)^2 \quad (4.31)$$

Most published CO rates involve  $H_2O$  because CO destruction requires the  $(OH)^{-1}$  radical to produce the reaction.

For HC and VOC incineration, several sources are available, such as Ref. [21], where, in general,

$$\frac{d(C_a H_b)}{dt} = -5.52 \times 10^8 P^{-0.815} T e^{\left(\frac{12,200}{T}\right)} (C_a H_b)^{0.5} (O_2) \frac{\text{mol}}{\text{cm}^2 \text{ s}} \quad (4.32)$$

#### 4.10.1 Thermal NO<sub>x</sub> Formation

Thermal NO<sub>x</sub> (see Chapter 15) is formed at high temperatures when molecular  $N_2$  and  $O_2$  dissociate and react to form NO. For formation, rather than destruction such as NO<sub>x</sub>, the equations are similar to the formation of thermal NO<sub>x</sub>.

$$\frac{d(NO)}{dt} = 2Ae^{\left(\frac{-E}{RT}\right)} (O)_{eq} (N_2) \quad (4.33)$$

and

$$(O)_{eq} = \frac{K_0}{(RT)^{0.5}} (O_2)_{eq}^{0.5} \quad (4.34)$$

One generally accepted practice to compute NO using Equations 4.33 and 4.34 is to assume  $O_2$  in equilibrium with O and  $O_2$  concentration using the Westenburg results for  $K_0$  (see Ref. [22]) for  $O_2$  equilibrium and Zeldovich constants,  $A$  and  $E$ , as measured by Bowman.<sup>23</sup>

The utilization of gas kinetic data for emission formation can be computed from detailed temperature and species concentration in the flow field in many ways, such as the Rayleigh flux theorem. Simply stated in all cases, one can post process thermal map data in some discrete volume form or insert into a CFD code (see Chapter 13) using the Rayleigh flux theorem as follows:

$$\frac{\partial}{\partial t} \int n \rho dv = \int n \rho (V \cdot da) \quad (4.35)$$

where

$n$  is the chemical in mass units

$t$  is the time

$\rho$  is the density

$v$  is the volume

$a$  is the area

$V$  is the velocity vector

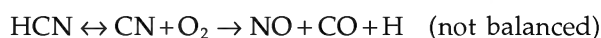
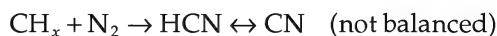
When described in words, the formation of  $(n)$  through the volume surface is equal to the integrated rate of formation over the control volume. It is then a simple extrapolation to extend this concept for even coarse volumes as follows:

$$\sum \frac{dn}{dt} \rho \Delta v = n \rho (V \cdot a) \quad (4.36)$$

This method can be very useful for fully mixed downstream products even with coarse volumes. But one must be careful with coarse volumes to be sure that the temperature and concentrations are uniform.

#### 4.10.2 Prompt NO<sub>x</sub> Formation

Another NO<sub>x</sub> formation mechanism is prompt NO<sub>x</sub>. This occurs at the flame front and is responsible for no more than 20 parts per million (ppm) NO<sub>x</sub> in refinery or natural-gas fueled equipment. The mechanism can be summarized as





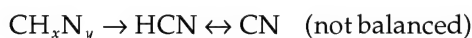
Both of these reactions are very fast and do not require high temperature. It would appear that one way to reduce NO<sub>x</sub> from the prompt mechanism would be to dilute the HCN and CN species on the fuel side of the combustion zone or reduce the available oxygen. The use of premix combustion is very effective for prompt NO<sub>x</sub> reduction.

### 4.10.3 Fuel-Bound NO<sub>x</sub>

The fuel-bound NO<sub>x</sub> mechanism is similar to prompt NO<sub>x</sub> and proceeds through the same HCN–CN chemistry. However, the fuel-bound mechanism differs in the following ways:

- The fuel-bound mechanism requires nitrogen as part of the fuel molecule.
- At low fuel–nitrogen concentrations, all of the bound nitrogen converts to NO<sub>x</sub>.
- The fuel-bound mechanism can be responsible for hundreds of ppm NO<sub>x</sub>, depending on the amount of nitrogen bound in the fuel.

The first steps in the chemistry differ in that the intermediates are formed directly from pyrolysis of the parent molecule. Ambient nitrogen is unimportant.



The subsequent chemistry (oxidation pathways for HCN and CN) is identical to prompt NO<sub>x</sub>.

Reducing the available oxygen, reducing the nitrogen content in the fuel, or diluting the fuel species with an inert gas reduces NO<sub>x</sub>.

## 4.11 Flame Properties

The flame temperature is a critical variable in determining the heat transfer, as is shown in Chapter 7. This section shows how the adiabatic flame temperature is affected by the fuel composition, the equivalence ratio, and the air and fuel preheat temperatures. As previously mentioned, real flame temperatures are not as high as the adiabatic flame temperature, but the trends are comparable and representative of actual conditions.

### 4.11.1 Flame Temperature

Table 4.6 shows the adiabatic flame temperature for common hydrocarbon fuels combusted with air. Figure 4.6

TABLE 4.6

Adiabatic Flame Temperatures

Fuel	Air	
	°F	°C
H <sub>2</sub>	3807	2097
CH <sub>4</sub>	3542	1950
C <sub>2</sub> H <sub>2</sub>	4104	2262
C <sub>2</sub> H <sub>4</sub>	3790	2088
C <sub>2</sub> H <sub>6</sub>	3607	1986
C <sub>3</sub> H <sub>6</sub>	4725	2061
C <sub>3</sub> H <sub>8</sub>	3610	1988
C <sub>4</sub> H <sub>10</sub>	3583	1973
CO	3826	2108

shows the adiabatic flame temperature as a function of the equivalence ratio for three fuels: H<sub>2</sub>, CH<sub>4</sub>, and C<sub>3</sub>H<sub>8</sub>. The peak temperature occurs at about stoichiometric conditions ( $\phi = 1.0$ ). In that case, there is just enough oxidizer to fully combust all the fuel. Any additional oxidizer absorbs sensible energy from the flame and reduces the flame temperature. In most real flames, the peak flame temperature often occurs at slightly fuel lean conditions ( $\phi < 1.0$ ). This is due to imperfect mixing where slightly more O<sub>2</sub> is needed to fully combust all the fuel. Nearly all industrial combustion applications are run at fuel-lean conditions to ensure that CO emissions are low. Therefore, depending on the actual burner design, the flame temperature may be close to its peak—a condition that is often desirable for maximizing heat transfer. One problem often encountered by maximizing the flame temperature is that high flame temperature maximizes NO<sub>x</sub> emissions. NO<sub>x</sub> increases approximately exponentially with gas temperature. This has led to many design concepts for reducing the peak flame temperature to minimize NO<sub>x</sub> emissions.<sup>24</sup>

Figure 4.7 shows how preheating the air in the combustion of the three fuels shown dramatically increases the adiabatic flame temperature. The increase is nearly linear for the air preheat temperature range shown. Air preheating is commonly done to both increase the overall system efficiency (which will be graphically shown later) and to increase the flame temperature, especially for higher temperature heating and melting processes like melting metal or glass. Figure 4.8 shows the effect of preheating the fuel on the adiabatic flame temperature. Again, there is a nearly linear rise in the flame temperature, but the magnitude of the increase is much less than for air preheating. This is due to the much larger mass of air compared to the mass of fuel in the combustion process. Preheating the air to a given temperature requires much more energy than

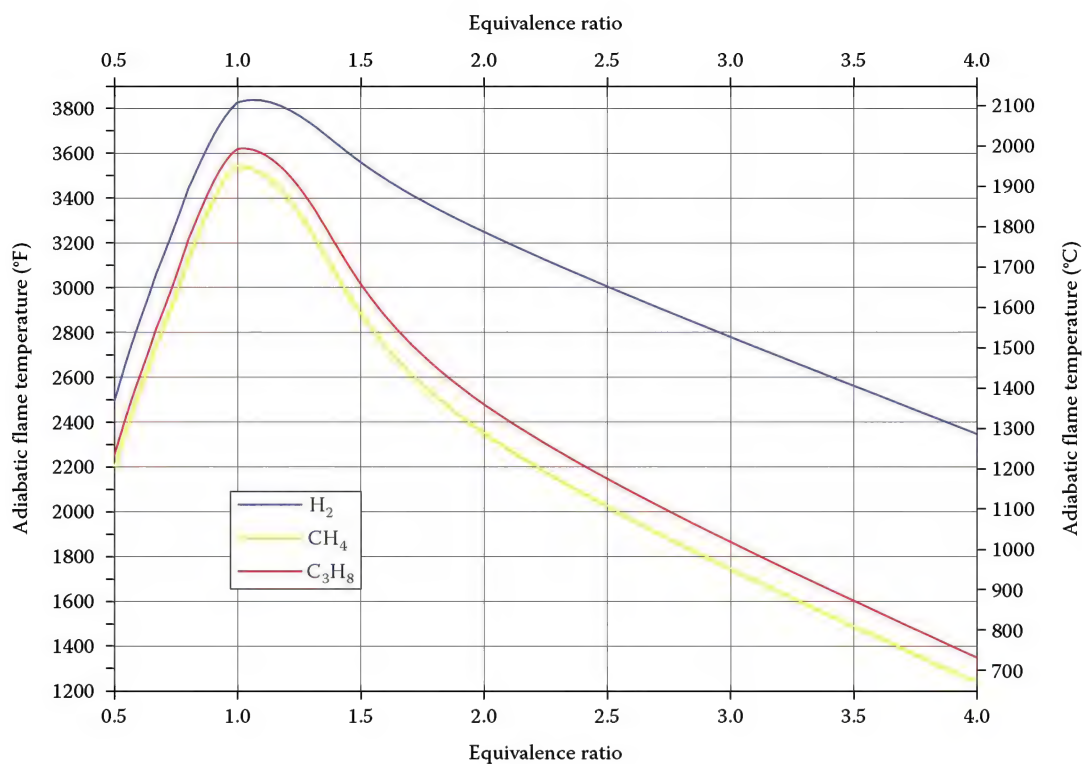


FIGURE 4.6

Adiabatic flame temperature versus equivalence ratio for air/H<sub>2</sub>, air/CH<sub>4</sub>, and air/C<sub>3</sub>H<sub>8</sub> flames where the air and fuel are at ambient temperature and pressure.

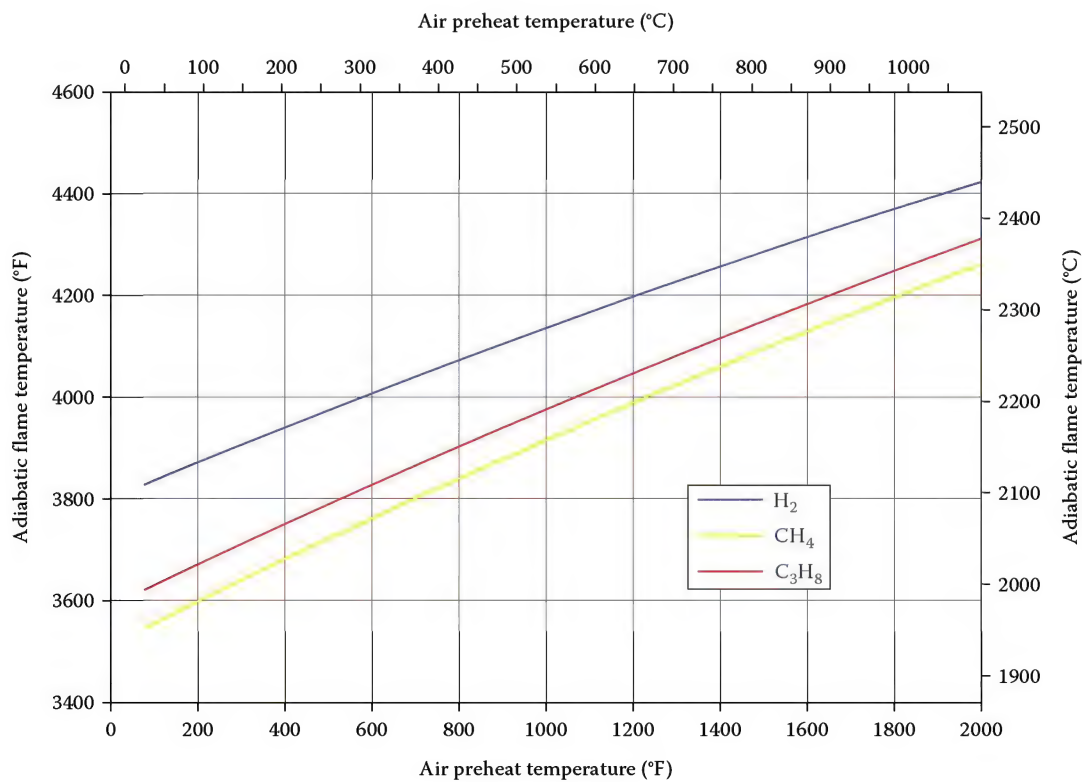


FIGURE 4.7

Adiabatic flame temperature versus air preheat temperature for stoichiometric air/H<sub>2</sub>, air/CH<sub>4</sub>, and air/C<sub>3</sub>H<sub>8</sub> flames where the fuel is at ambient temperature and pressure.

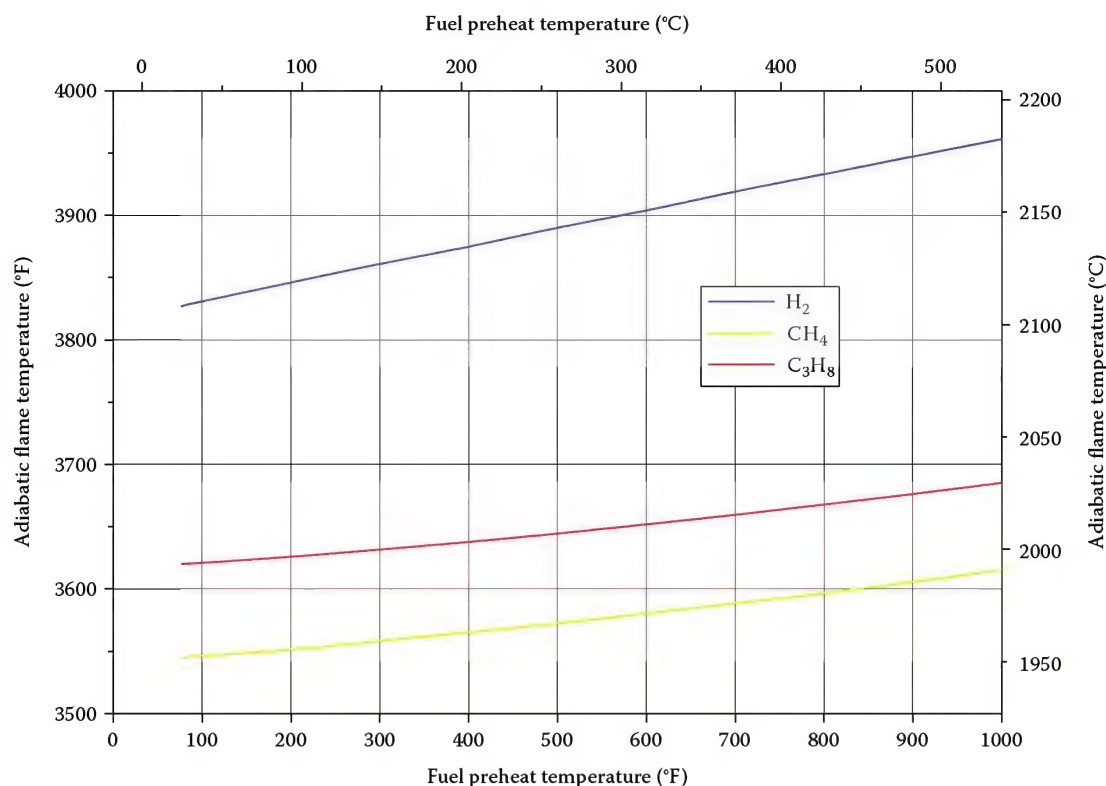


FIGURE 4.8

Adiabatic flame temperature versus fuel preheat temperature for stoichiometric air/H<sub>2</sub>, air/CH<sub>4</sub>, and air/C<sub>3</sub>H<sub>8</sub> flames where the air is at ambient temperature and pressure.

preheating the fuel to that same temperature, because of the difference in mass.

Figure 4.9 shows how the flame temperature varies for fuel blends of H<sub>2</sub>/CH<sub>4</sub> and N<sub>2</sub>/CH<sub>4</sub>. The flame temperature increases as the H<sub>2</sub> content in the blend increases. It is important to note that the increase is not linear; the increase is more rapid at higher levels of H<sub>2</sub>. Because of the relatively high cost of H<sub>2</sub> compared to CH<sub>4</sub> and C<sub>3</sub>H<sub>8</sub>, it is not used in many industrial applications. However, high H<sub>2</sub> fuels are often used in many of the hydrocarbon and petrochemical applications for fluid heating. Because such fuels are by-products of the chemical manufacturing process, their use is much less expensive than purchasing H<sub>2</sub> from an industrial gas supplier as well as being more cost-effective than purchasing other fuels. The graph also shows that the adiabatic flame temperature decreases for N<sub>2</sub>/CH<sub>4</sub> fuel blends as the N<sub>2</sub> content increases. Again, the decrease is not linear and rapidly decelerates at higher N<sub>2</sub> contents until no flame is present for a “fuel” having 100% N<sub>2</sub>. Figure 4.10 shows how preheating the combustion air for fuel blends of H<sub>2</sub> and CH<sub>4</sub> increases the adiabatic flame temperature. However, the increase is not a dramatic rise from pure CH<sub>4</sub> to pure H<sub>2</sub>. Again, the change in flame temperature with blend composition is nonlinear.

#### 4.11.2 Available Heat

The available heat in a process is defined as the gross heating value of the fuel, minus the energy carried out of the exhaust stack by the flue gases. This difference is the energy that is available to do work. However, some of that energy will be lost by conduction through the heater walls, by radiation through openings, by air infiltration that will absorb sensible energy, as well as by other types of energy losses that are dependent on the burner and heater designs, and by the process operations. The accounting of the distribution for where energy goes in a process is sometimes graphically depicted using a Sankey diagram. Figure 4.11 presents a very simplified Sankey diagram showing that only 40% of the energy goes to the load in that example. The available heat for that example is 50%, which includes the 40% to the load and the 10% lost to various sources. Figure 4.12 shows the calculated available heat for three different fuels as a function of the exhaust or flue gas temperature. As expected, there is a rapid decrease in available heat as the exhaust gas temperature increases. This indicates that more and more energy is being carried out of the exhaust instead of being transferred to the load as the exhaust temperature increases. At the adiabatic flame temperature for each fuel, there is no available heat as

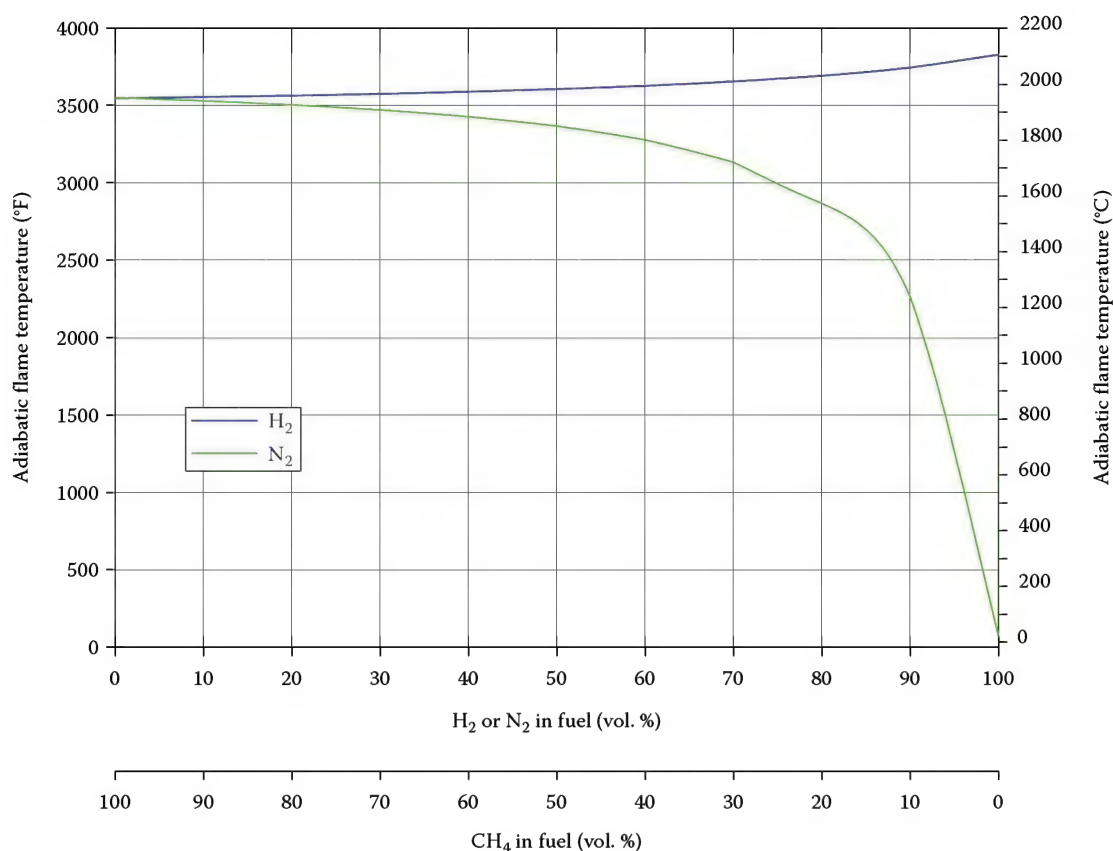


FIGURE 4.9

Adiabatic flame temperature versus fuel blend ( $\text{CH}_4/\text{H}_2$  and  $\text{CH}_4/\text{N}_2$ ) composition for stoichiometric air/fuel flames where the air and fuel are at ambient temperature and pressure.

all the energy was carried out in the exhaust. Figure 4.13 shows that the available heat increases with the air pre-heat temperature, which simply indicates that energy was recovered in the process and was used to preheat the combustion air. Figure 4.14 shows that preheating the fuel increases the efficiency, but to a much lesser extent than air preheating. The mass of air is much greater than the mass of fuel, so preheating the fuel is less effective than preheating the air, if the preheat temperature is the same.

#### 4.11.3 Minimum Ignition Energy

Ignition energy graphs usually have the vertical axis as the relative energy of the fuel mixture (see Figure 4.15). The reactants start from an initial state. If the minimum ignition energy is supplied, the reactant bonds will rupture, producing intermediate species such as  $\text{CH}_3$ ,  $\text{H}$ , and  $\text{O}$ . Such species are extremely reactive and recombine to form the final products,  $\text{CO}_2$  and  $\text{H}_2\text{O}$ . Since the net heat release is greater than the minimum ignition energy, the reaction, once started, will continue until virtually all of the reactants are consumed. The horizontal axis shows the progress of the reaction. At the upper left, the diagram

shows that the fuel–air mixture has a high potential energy. At the lower right, it is noted that the products of combustion have relatively little remaining chemical energy. Because energy must be conserved, the difference between the upper and lower energy levels must be the amount of heat that the combustion reaction liberates. Note, however, that the energy diagram does not slope monotonically along the reaction coordinate, but contains a hump. This hump is the minimum ignition energy.

What the diagram says is that fuel and air comprising a very high chemical energy may exist in a metastable state, until one introduces a spark or flame of sufficient energy. Once the system reaches the minimum ignition energy, the reaction will be self-sustaining until the reaction consumes enough of the reactants. At that point, the reaction cannot liberate enough heat to supply the minimum ignition energy and the flame goes out.

#### 4.11.4 Flammability Limits

Suppose that fuel and air are not provided in stoichiometric proportions, but have excess of fuel or air. Will the flame continue to propagate if the ignition source is removed? That depends on whether the fuel–air mixture



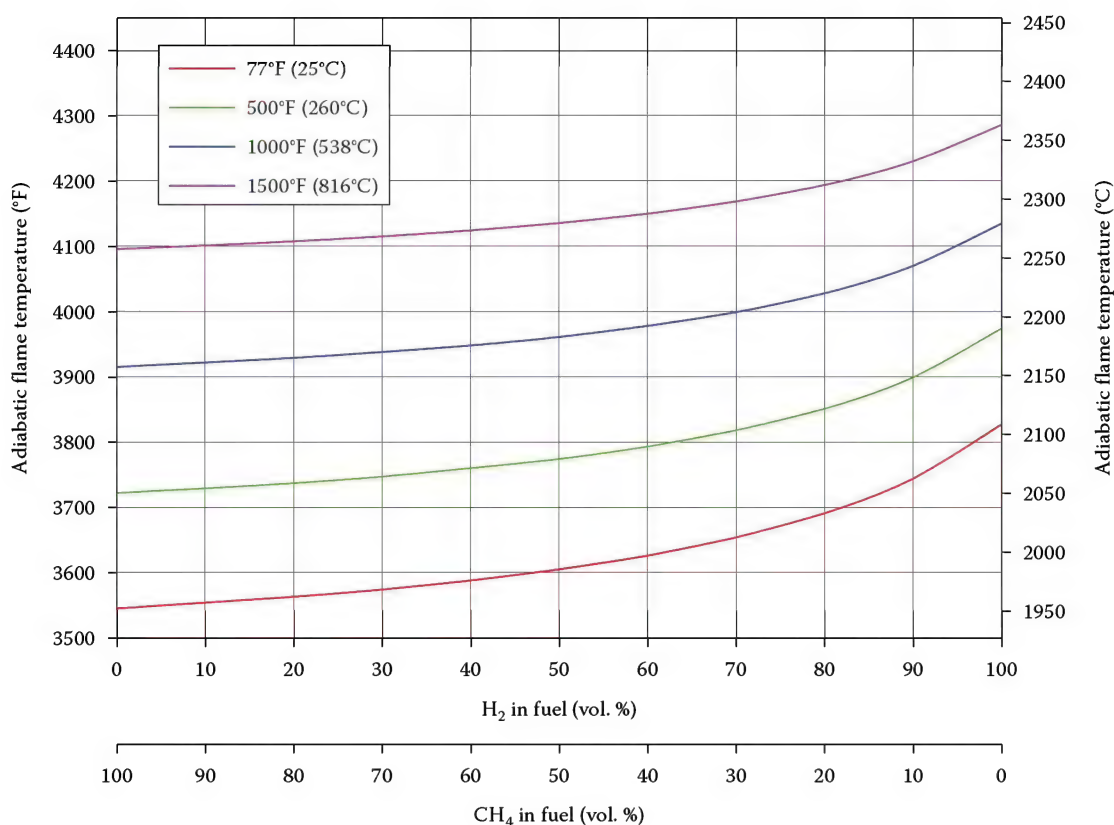


FIGURE 4.10

Adiabatic flame temperature versus fuel blend ( $\text{CH}_4/\text{H}_2$ ) composition and air preheat temperature for stoichiometric air/fuel flames where the fuel is at ambient temperature and pressure.

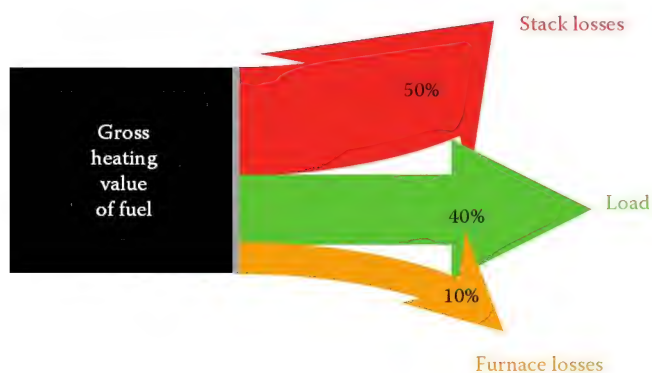


FIGURE 4.11

Sample Sankey diagram showing distribution of energy in a combustion system.

has enough chemical energy to exceed the minimum ignition energy. If not, the flame will extinguish. This leads to a lower and upper flammability limit. The limits of flammability define the limiting chemical composition in which the gas mixture will no longer ignite and continue to produce flames. The lower limit (fuel lean) of flammability represents the smallest ratio of fuel that, when mixed with air, can maintain a flame without the

input of an external heat source. Past the upper limit (fuel rich), the large ratio of gas begins to act as a diluent so that flames cannot be self-sustaining.<sup>4,25</sup> A list of the upper and lower limits of flammability for common gases is available in Table 4.3. For gas mixtures, one can use Le Chatelier's rule to estimate flammability limits for gas mixtures. Because this is only an estimate, one must confirm the flammability limit of the actual mixture. Such experiments are relatively inexpensive and many third parties exist that can perform this kind of analysis.

Le Chatelier's rule states that the flammability limit of a mixture is equal to the reciprocal of the sum of reciprocal flammability limits weighted by their mole fractions.

$$\text{Limit of flammability} = \frac{100}{\frac{a}{A} + \frac{b}{B} + \frac{c}{C} + \dots} \quad (4.37)$$

where

$a, b, c, \dots$  is the percentage represented by the respective gas combination in the mixture

$A, B, C, \dots$  is the respective flammability limits of gas combination from flammability tables

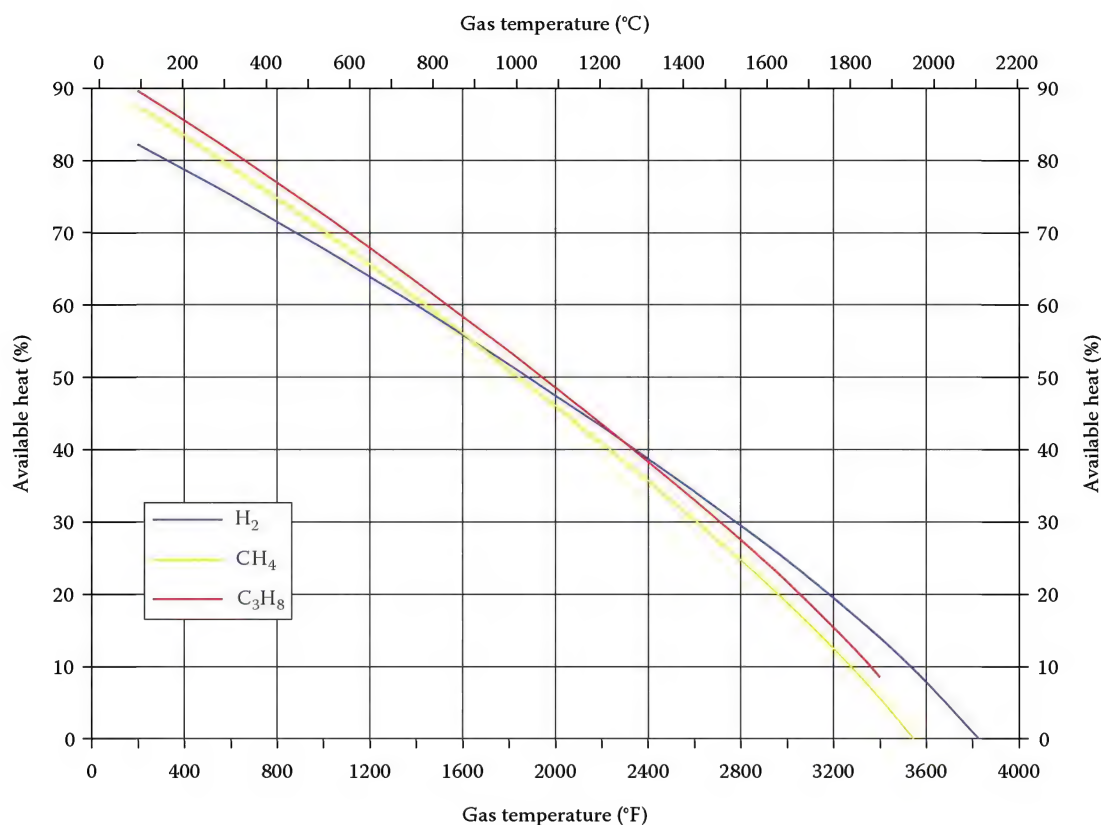


FIGURE 4.12

Available heat versus gas temperature for stoichiometric air/ $H_2$ , air/ $CH_4$ , and air/ $C_3H_8$  flames where the air and fuel are at ambient temperature and pressure.

**Example 4.12**

The following will present a practical example of calculating upper and lower flammability limits:

**Given**

A natural gas is composed of the flammable gases 79%  $CH_4$ , 17%  $C_2H_6$ , and the inert gases 3%  $N_2$ , 1%  $CO_2$ .

**Problem**

Find upper and lower limits of flammability of the gas mixture.

- The gas must first be dissected into combinations of flammable gas alone and flammable gas with inert gas. In this case the four combinations:  $CH_4$ ,  $CH_4 + N_2$ ,  $C_2H_6$ , and  $C_2H_6 + CO_2$ , are available.
- Then choose a ratio of inert gas to combustible gas by allocating a percentage of "pure" combustible gas to the combinations of combustible and inert gas.
- Totaling up the percentage of dissectioned gas gives the percentage of mixture of each respective gas combination.

- With the ratio of inert to combustible gas of each combination now known, use the flammability tables to find the upper and lower limits of flammability.

Combustible Gas	Ratio of Inert to Combustible Gas	Dissection%				Total %	Limits of Flammability	
		$CH_4$	$CH_4 + N_2$	$C_2H_6$	$C_2H_6 + CO_2$		Lower	Upper
$CH_4$	1	3	...	3	...	6	10.5	23
$CH_4$	0	76	...	...	...	76	5	15
$C_2H_6$	1	...	1	...	1	2	6.5	18.5
$C_2H_6$	0	...	16	...	...	16	3	12.5
Total		79	17	3	1	100		

With the percentage of each respective gas combinations and their limits of flammability, calculate the fuel's limits of flammability using Le Chatelier's equation.

Lower limit of flammability

$$= \frac{100}{\frac{a}{A} + \frac{b}{B} + \frac{c}{C} + \frac{d}{D}} = \frac{100}{\frac{6}{10.5} + \frac{76}{5} + \frac{2}{6.5} + \frac{16}{3}}$$

$$= 4.7 \left( \frac{F}{A} \right)_v$$

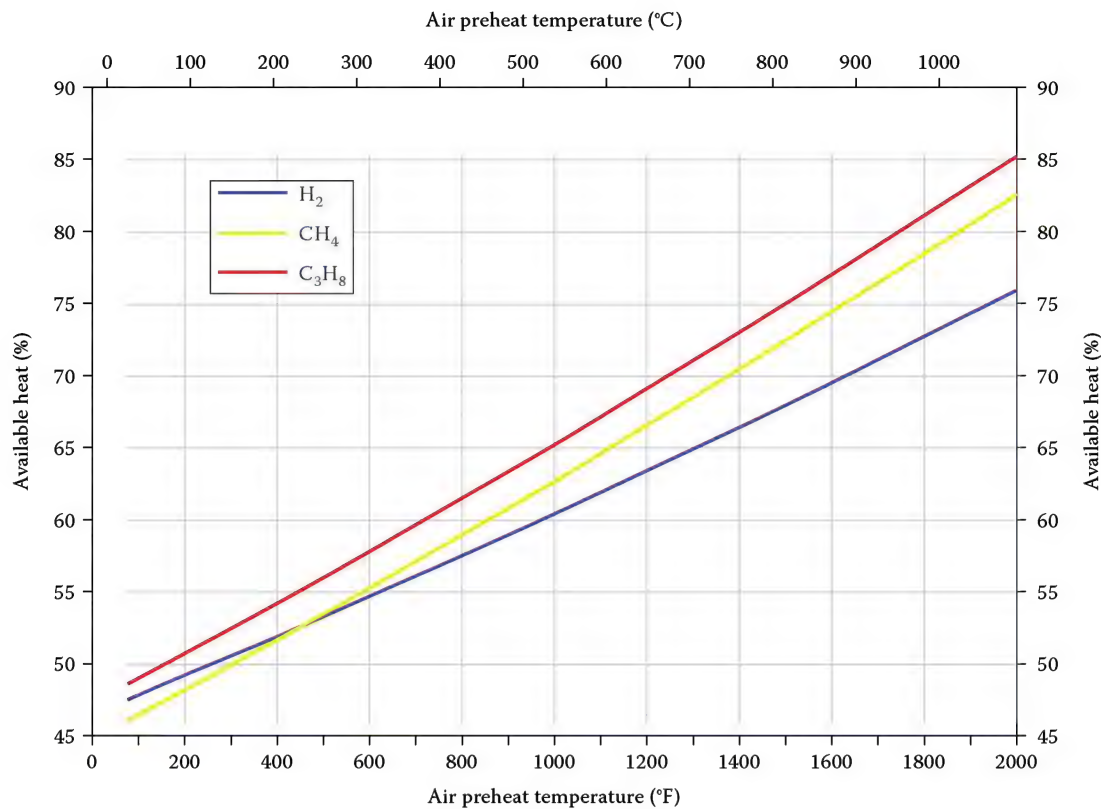


FIGURE 4.13

Available heat versus air preheat temperature for stoichiometric air/H<sub>2</sub>, air/CH<sub>4</sub>, and air/C<sub>3</sub>H<sub>8</sub> flames at an exhaust gas temperature of 2000°F (1100°C) where the fuel is at ambient temperature and pressure.

Upper limit of flammability

$$= \frac{100}{\frac{a}{A} + \frac{b}{B} + \frac{c}{C} + \frac{d}{D}} = \frac{100}{\frac{6}{23} + \frac{76}{15} + \frac{2}{18.5} + \frac{16}{12.5}}$$

$$= 14.9 \left( \frac{F}{A} \right)_v$$

The range of flammability narrows when pressures fall below atmospheric. The increase of temperature tends to widen the range of flammability. The lower limit of flammability can be predicted at different temperatures using the Burgess–Wheeler law:

$$L_T = L_{298} \left[ 1 - \frac{3.14(T - 298)}{L_{298}(\text{LHV})} \right] \quad (4.38)$$

where

$L_T$  is the adjusted lower limit of flammability

$L_{298}$  is the lower limit of flammability

LHV is the lower heating value

$T$  is the temperature to be adjusted in Kelvins

#### 4.11.5 Flame Speeds

The reaction between fuel and air can only occur at a finite speed. That finite speed depends on the speed of

the reaction (chemical) and the amount of turbulence in the flame (physical). If the flame has a lot of turbulence, hot pockets of gas recirculate and the mixture burns faster. To first focus on the chemical part, suppose a long tube is filled with a flammable mixture. If one end of the tube is ignited, the flame front will move along the tube at a precise velocity. A flame that has no turbulence is a laminar flame. Accordingly, the flame speed of a laminar flame is known as the *laminar flame speed* and is a function of the kinetics of the combustion reaction. Under standard conditions, this is a function of the fuel chemistry alone. Now suppose that instead of a stationary fuel mixture with a moving flame front, the fuel is moved. If the fuel is metered exactly at its flame speed, the flame front will remain stationary. If the fuel is metered faster than the flame speed, the flame front will move forward (called *lift-off* or *blow-off*). If the fuel is metered slower than its flame speed, the flame front will travel backward (called *burnback* or *flashback*).

Typical burners operate with fuel flows in excess of the laminar flame speed. To avoid lift-off, several devices are used. Consider premix burners first. Fuel flows across an orifice into the throat of a venturi. The venturi is designed to entrain air near the stoichiometric ratio. Gradual flow passages are used to avoid turbulence, and hot gases are recirculated back to the burner.

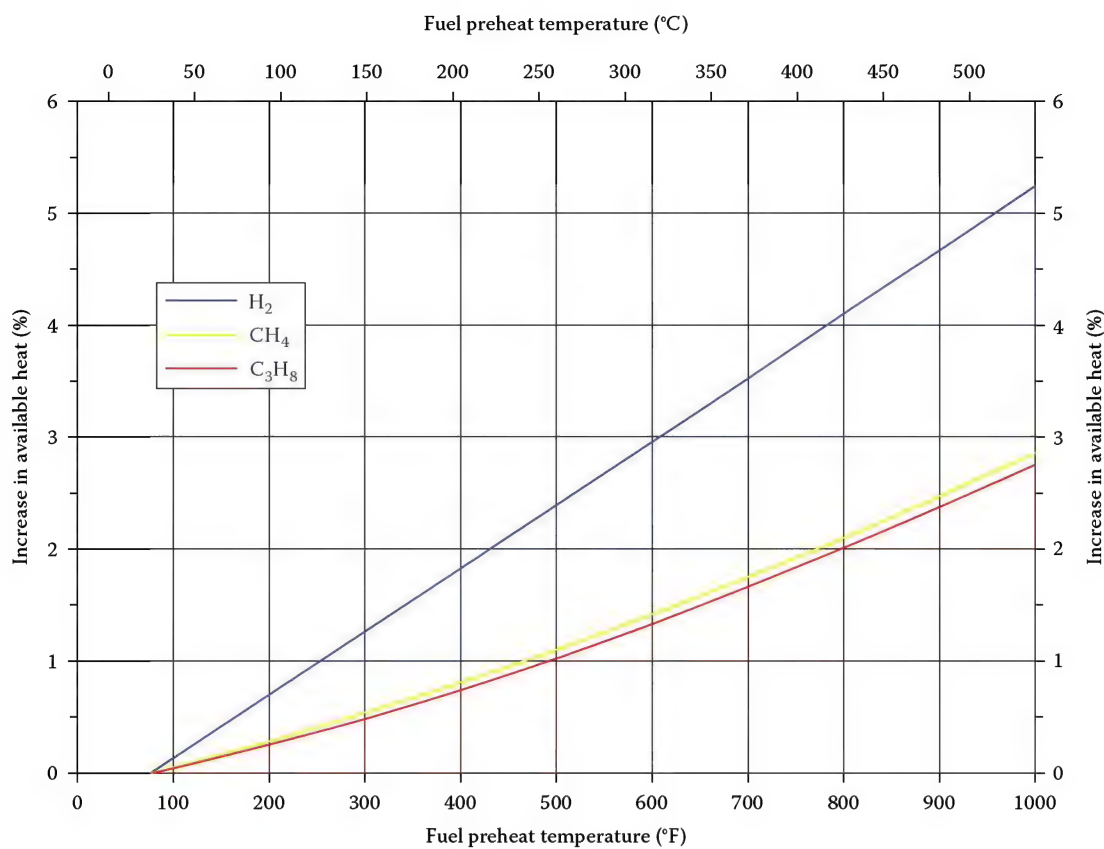


FIGURE 4.14

Available heat versus fuel preheat temperature for stoichiometric air/H<sub>2</sub>, air/CH<sub>4</sub>, and air/C<sub>3</sub>H<sub>8</sub> flames at an exhaust gas temperature of 2000°F (1100°C) where the air is at ambient temperature and pressure.

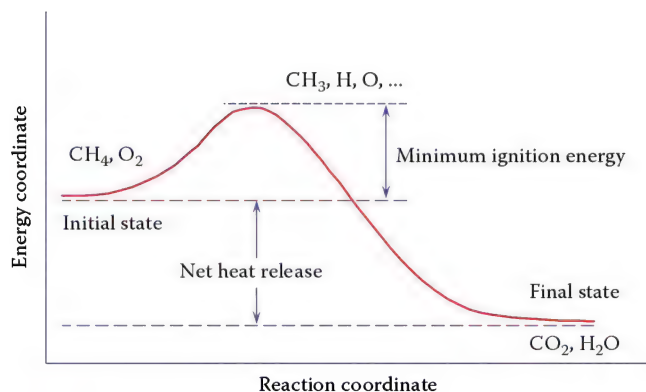


FIGURE 4.15

Graphical representation of ignition and heat release.

The fuel–air mixture is supplied at velocities above the laminar flame speed. As the fuel jet issues from the burner, the velocity slows considerably. The flame front establishes where the flame and gas velocities are equal. The sudden expansion from the burner avoids liftoff as the velocity rapidly slows. The high fuel–air velocity avoids burnback. Sudden expansions of this type are used as flame holders because they stabilize the flame front and keep it from moving forward or backward.

Another concept used in premix burners is quench distance—the distance needed to remove sufficient heat from the flame to extinguish it. Here, burner slots or orifices have a finite thickness that exceeds the quench distance. Because the burner is cooler than the flame, if the flame does begin to burnback, the heavy metal will remove sufficient heat and cool the flame below its minimum ignition energy. Without this feature, a flame that finds its way into a premix burner could flashback. With flashback, the combustion occurs in the burner, rather than at the flame holder. Sustained burnback will destroy the burner in a short time.

Diffusion burners supply fuel with no premix chamber. The fuel meets the air outside the fuel nozzle. With diffusion burners, flashback is not an issue because the fuel alone cannot support combustion (i.e., the upper flammability limit is exceeded). However, liftoff is still a concern. If the flame lifts off the burner, it may travel to a place beyond the flammability limits and extinguish. Under certain conditions, the flame can repeatedly lift-off and reestablish. This behavior is dangerous because the fuel may burn incompletely during one part of the cycle and reignite later, causing an explosion. The cycle of liftoff and burnback can occur many times a second,



causing rumble or vibration. Such rumble can be a sign of dangerous instabilities.

Modern burners are designed to give high heat release in short distances. This necessitates fuel velocities that greatly exceed the laminar flame speed. To stabilize such flames, various flame holders are used. For example, an ignition ledge on a burner is a type of flame holder known as a *bluff body*. Even if the air flows by the ledge at very high speed, the air speed very close to the ledge will be very slow. The flame will then establish very near the ignition ledge and be quite stable even over a wide range of firing rates. The burner tile itself is designed with a sudden expansion into the furnace, which also acts as a flame holder because the gas velocity decreases rapidly just after the expansion.

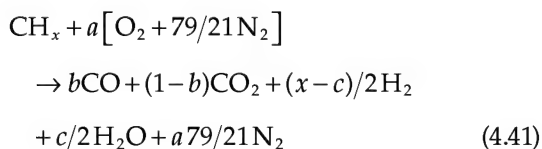
## 4.12 Substoichiometric Combustion

The concept of excess air presumes air in addition to that required for combustion. However, if one does not provide enough air, combustion may still continue, generating large quantities of CO and combustibles. This is referred to as substoichiometric combustion. Process heaters and boilers should NEVER be operated in this mode. Suddenly adding air to such a hot mixture could result in explosion. Because substoichiometric combustion may have DEADLY consequences, it is useful to consider the process, observe its features, and normally avoid it. Further, substoichiometric combustion is an important mechanism in the development and use of low NO<sub>x</sub> burners when the substoichiometric products may be important in the design. The stoichiometric ratio,  $\Phi$ , is a fuel-to-air ratio. It has the following relationship with  $\epsilon$ .

$$\Phi = \frac{1}{(1 + \epsilon)} \quad (4.39)$$

$$\epsilon = \frac{(1 - \Phi)}{\Phi} \quad (4.40)$$

Equation 4.41 shows a modified form of the general equation for hydrocarbon combustion.



where

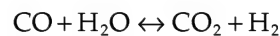
$a, x$  are specified

$b, c$  are unknown having the relation  $2a = 2 - b + c/2$

The reader should note that the formulation neglects soot. Turns<sup>26</sup> has pointed out that using an equilibrium calculation with the water–gas shift reaction arrives at a good approximation for substoichiometric species. This is adequate for investigating the general features of substoichiometric combustion.

### 4.12.1 Equilibrium and Thermodynamics

The chemical equation gives the water–gas shift reaction:



The double-headed arrow indicates that the reaction proceeds in both directions simultaneously. When the rate of the forward reaction equals that of the reverse, the process is in dynamic equilibrium. Equilibrium is characterized by the following relation:

$$K = \frac{[\text{CO}_2][\text{H}_2]}{[\text{CO}][\text{H}_2\text{O}]} \quad (4.42)$$

where the brackets denote wet volume concentrations of the enclosed species. For substoichiometric combustion, it will be useful to define the following quantities:  $\alpha = [\text{H}_2]/[\text{H}_2\text{O}]$ ,  $\beta = [\text{CO}]/[\text{CO}_2]$ , then  $K = \alpha/\beta$ .

### 4.12.2 Substoichiometric Combustion Revisited

Now that equilibrium and the water–gas shift reaction have been defined, one can define substoichiometric combustion. Solving the mass balance for C, H, and O<sub>2</sub>, in turn for  $\alpha$  and  $\beta$ , and using the relation  $K = \alpha/\beta$ , one obtains the following equations:

$$\begin{aligned} & \text{CH}_x + \frac{1}{2} \left[ \frac{2 + \beta}{1 + \beta} + \frac{x}{2(1 + \beta K)} \right] \left( \text{O}_2 + \frac{79}{21} \text{N}_2 \right) \\ & \rightarrow \left( \frac{1}{1 + \beta} \right) \text{CO}_2 + \left( \frac{\beta}{1 + \beta} \right) \text{CO} + \frac{1}{2} \left( \frac{x}{1 + \beta K} \right) \text{H}_2\text{O} \\ & + \frac{1}{2} \left( \frac{\beta K x}{1 + \beta K} \right) \text{H}_2 + \left( \frac{79}{21} \right) \left( \frac{1}{2} \right) \left[ \frac{2 + \beta}{1 + \beta} + \frac{x}{2(1 + \beta K)} \right] \text{N}_2 \end{aligned} \quad (4.43)$$

Now, by combining equations for the left side of the relation, one knows that  $a$  must have the following expression.

$$a = \frac{1}{\Phi} \left( 1 + \frac{x}{4} \right) = \frac{1}{2} \left[ \frac{2 + \beta}{1 + \beta} + \frac{x}{2(1 + \beta K)} \right] \quad (4.44)$$

One could solve for  $\Phi$  and substitute into Equation 4.43. However, the equation is quadratic and complicated. An easier solution is to solve for both  $\Phi$  and the desired species using a parametric relation in  $\beta$ . Equation 4.45 gives the relation for  $\Phi$ :

$$\Phi = \frac{(x+4)(1+\beta)(1+\beta K)}{2(2+\beta)(1+\beta K) + x(1+\beta)} \quad (4.45)$$

Solving for the species as a function of  $\beta$  gives the following:

$$\text{TWP} = 1 + \frac{x}{2} + \frac{79}{21} \left[ \frac{1}{1+\beta} + \frac{\beta}{2(1+\beta)} + \frac{x}{4(1+\beta K)} \right]$$

$$\text{TDP} = 1 + \frac{1}{2} \left( \frac{\beta K x}{1+\beta K} \right) + \frac{79}{21} \left[ \frac{1}{1+\beta} + \frac{\beta}{2(1+\beta)} + \frac{x}{4(1+\beta K)} \right]$$

$$f_{\text{O}_2, \text{wet}} = 0 \quad f_{\text{O}_2, \text{dry}} = 0 \quad (4.46)$$

$$f_{\text{CO}_2, \text{wet}} = \frac{1}{\text{TWP}} \left( \frac{1}{1+\beta} \right) \quad f_{\text{CO}_2, \text{dry}} = \frac{1}{\text{TDP}} \left( \frac{1}{1+\beta} \right) \quad (4.47)$$

$$f_{\text{CO}, \text{wet}} = \frac{1}{\text{TWP}} \left( \frac{\beta}{1+\beta} \right) \quad f_{\text{CO}, \text{dry}} = \frac{1}{\text{TDP}} \left( \frac{\beta}{1+\beta} \right) \quad (4.48)$$

$$f_{\text{H}_2\text{O}, \text{wet}} = \frac{1}{2 \text{TWP}} \left( \frac{x}{1+\beta K} \right) \quad (4.49)$$

$$f_{\text{H}_2, \text{wet}} = \frac{1}{2 \text{TWP}} \left( \frac{\beta K x}{1+\beta K} \right) \quad f_{\text{H}_2, \text{dry}} = \frac{1}{2 \text{TDP}} \left( \frac{\beta K x}{1+\beta K} \right) \quad (4.50)$$

$$f_{\text{N}_2, \text{wet}} = \frac{79}{21} \frac{1}{2 \text{TWP}} \left[ \frac{2+\beta}{1+\beta} + \frac{x}{2(1+\beta K)} \right]$$

$$f_{\text{N}_2, \text{dry}} = \frac{79}{21} \frac{1}{2 \text{TDP}} \left[ \frac{2+\beta}{1+\beta} + \frac{x}{2(1+\beta K)} \right] \quad (4.51)$$

Combining the excess air and substoichiometric equations, one can construct a graph of species concentrations versus  $\Phi$ , as shown in Figure 4.16a through f for various fuels on a wet and dry basis. In particular, the substoichiometric portion of the graphs use  $K = 0.19$ , which corresponds to a temperature of  $\sim 2200^\circ\text{F}$  ( $1100^\circ\text{C}$ ). As Turns<sup>26</sup> has pointed out for propane, this gives excellent agreement with rigorous equilibrium calculations. Note that one can generate considerable CO and  $\text{H}_2$  from substoichiometric combustion. If air is suddenly admitted to such a hot mixture, explosion is likely.

### 4.13 General Discussion

In this section, the concepts discussed so far are applied to combustion in general. Figure 4.17 shows a schematic of an adiabatic equilibrium process. The boxes represent perfectly insulated enclosures, which do not exist in reality, but are useful for illustrating the concept. The boxes are filled with a combustible mixture of a fuel and an oxidizer, in this case methane and air, respectively. The left box represents the process at the time just before a spark is applied to ignite the mixture. The only species in the box are  $\text{CH}_4$  and air ( $\text{O}_2 + 3.76\text{N}_2$ ) in proportions to make the mixture flammable. A spark is then initiated to ignite the mixture. The right box represents the process an infinite time later to ensure all the reactions have gone to completion (i.e., reached equilibrium). In reality, most combustion reactions are completed in only a fraction of a second. Many species are then present after the reaction is completed. The exact composition depends on the ratio of the fuel to air. For example, if not enough air is present, then CO will be generated. If sufficient air is present, then little or no CO will be present. This is illustrated in Figure 4.18 which shows the predicted species for the adiabatic equilibrium combustion of methane and air as a function of the stoichiometry. For methane, the stoichiometric  $\text{O}_2\text{:CH}_4$  ratio for theoretically perfect combustion is 2.0. Stoichiometries less than 2.0 are fuel rich, as insufficient oxygen is present to fully combust the fuel. Stoichiometries greater than 2.0 are fuel lean, as excess oxygen is present. Figure 4.18 shows that the exhaust product composition is highly dependent on the ratio of the fuel to the oxidizer.

#### 4.13.1 Air Preheat Effects

Figure 4.19 shows the major species for the predicted exhaust gas composition for the stoichiometric combustion of methane with preheated air. There is almost no change up to temperatures of about  $1000^\circ\text{F}$  ( $540^\circ\text{C}$ ), and only a relatively small change at higher temperatures. Figure 4.20 shows the predicted minor species in the exhaust gas for the same reaction of ambient temperature methane with preheated air. This graph shows that there is a dramatic increase in all the minor species as the air preheat temperature increases. This is due to chemical dissociation. Figure 4.21 shows the predicted major species in the exhaust products for the combustion of preheated methane with ambient air. There is very little change in the species concentration with fuel preheat. Note that higher fuel preheat temperatures present safety problems because of the auto-ignition temperature of methane, which is approximately  $1200^\circ\text{F}$  ( $650^\circ\text{C}$ ) in air. Figure 4.22 also shows that the predicted minor species concentrations increase with fuel preheat temperature.

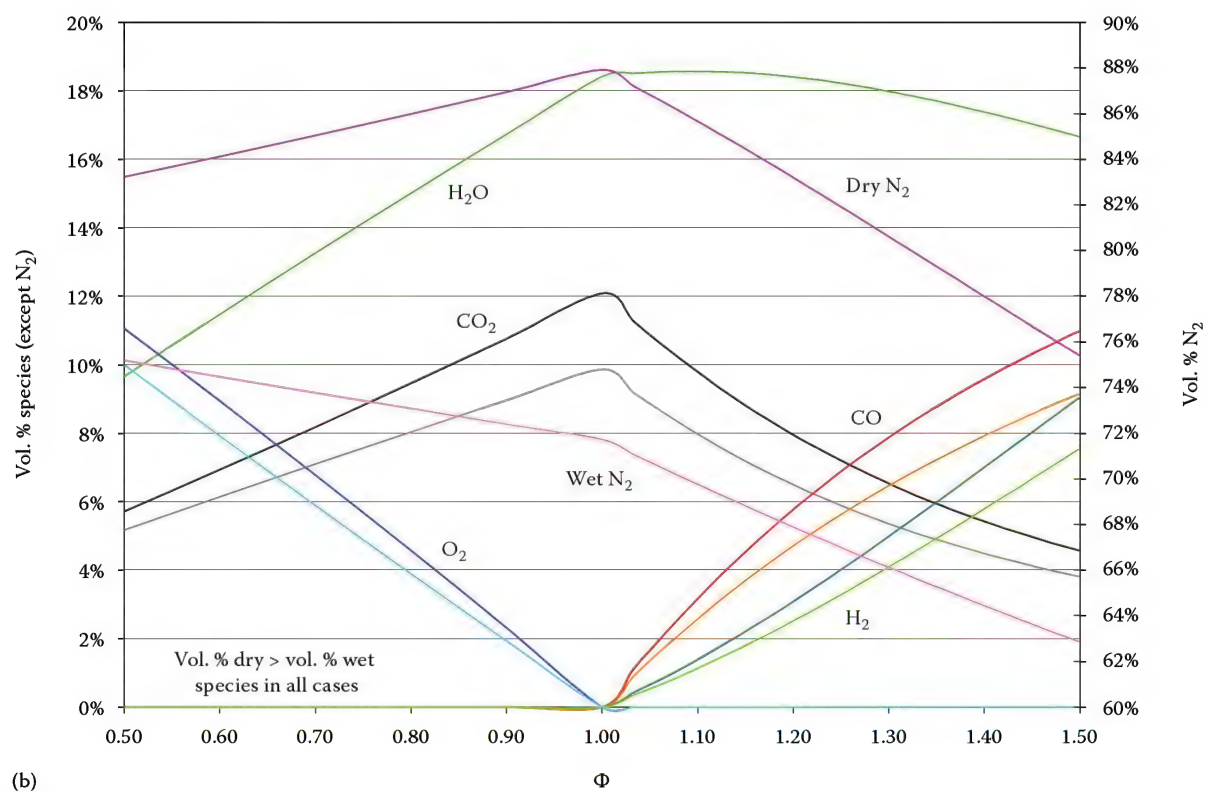
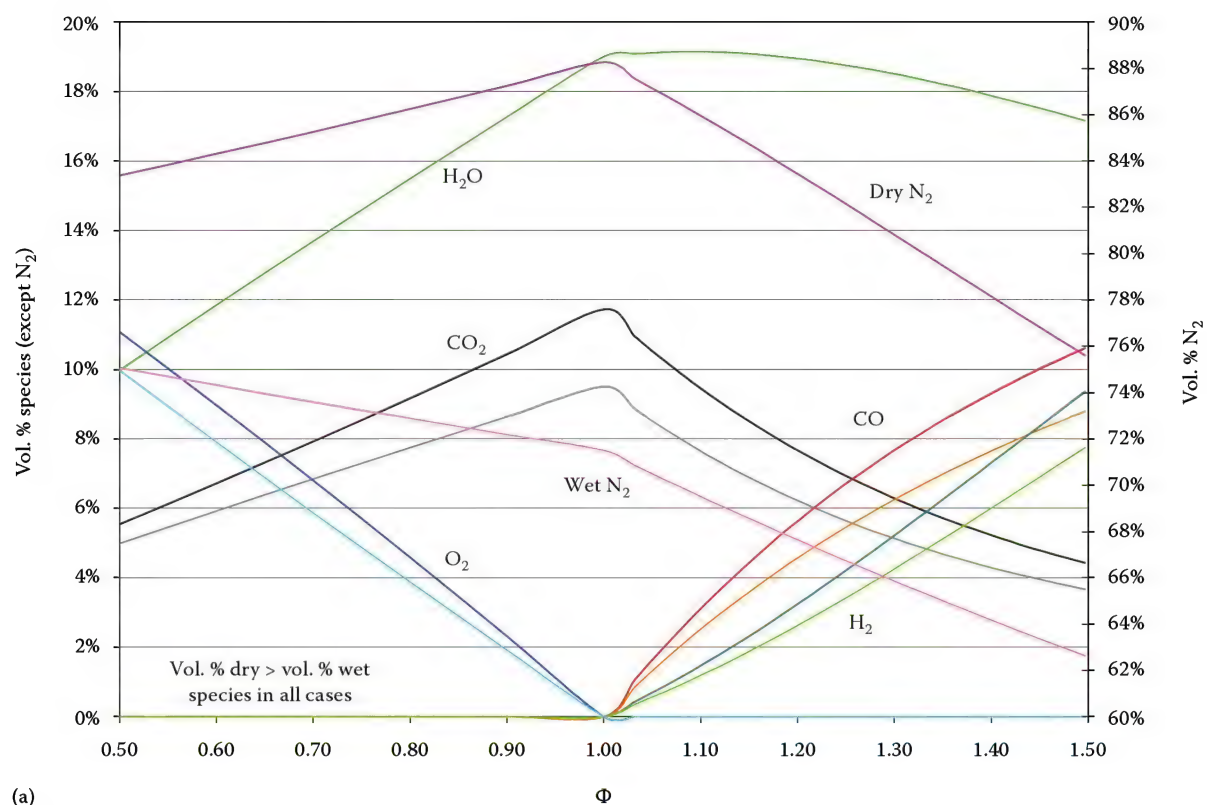
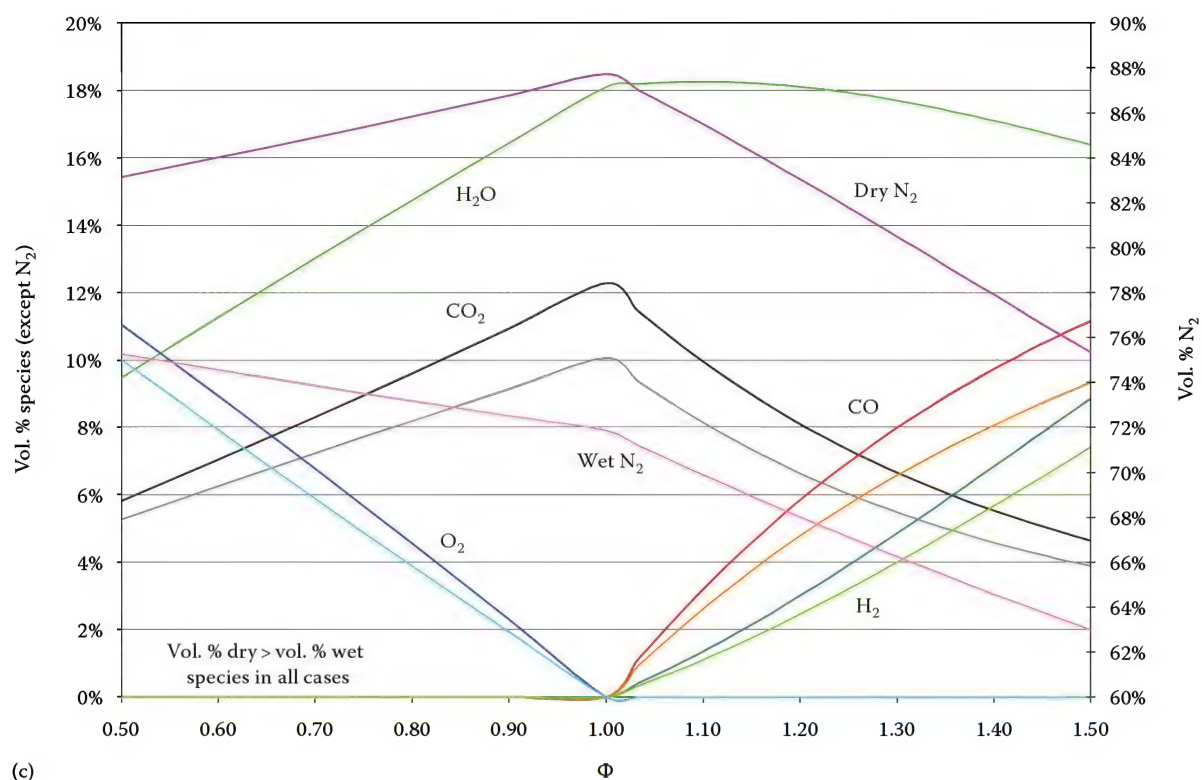


FIGURE 4.16

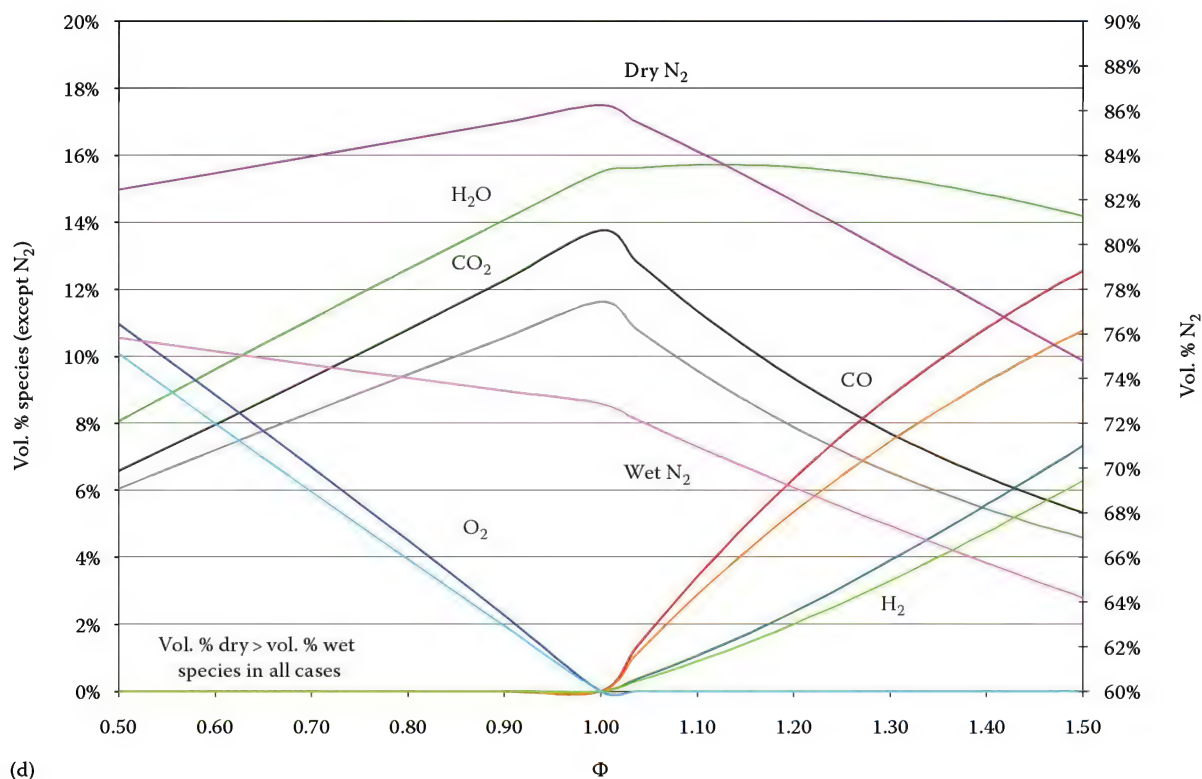
Species concentration versus stoichiometric ratio for the following fuels: (a)  $\text{CH}_4$ , (b) natural gas.

(continued)





(c)

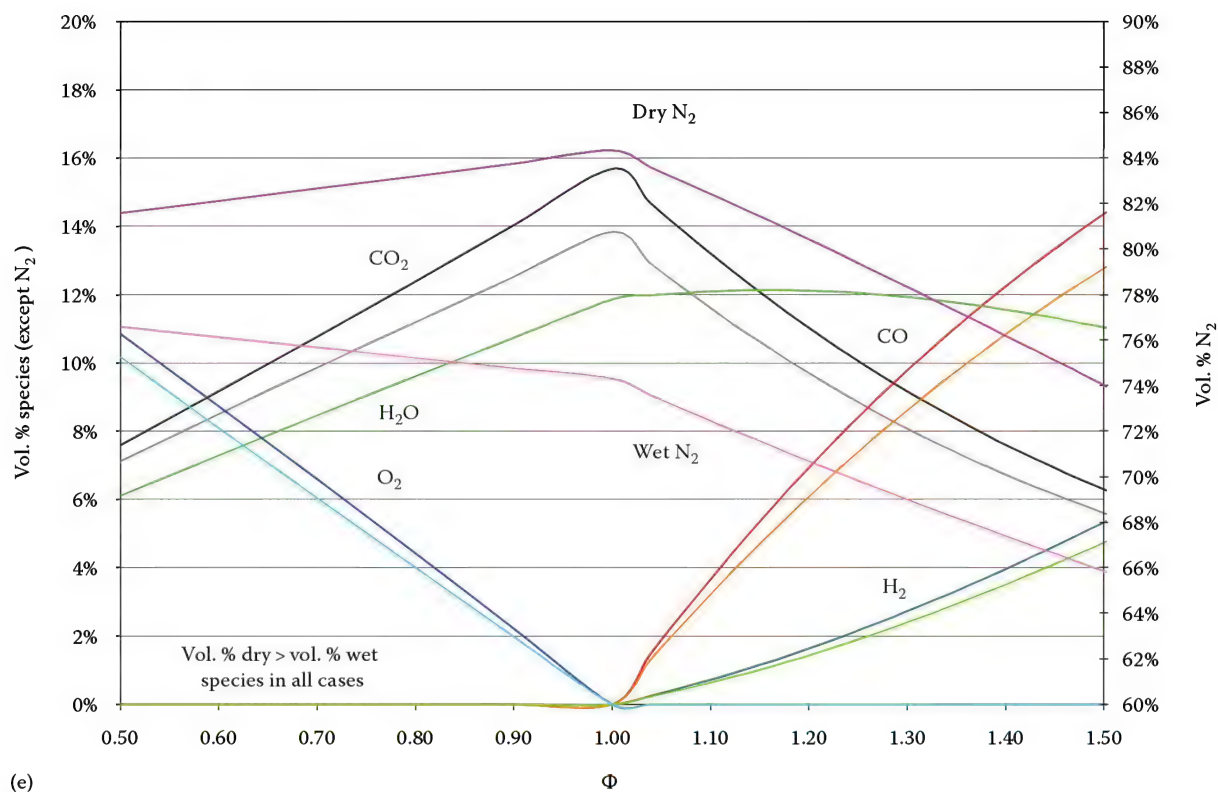


(d)

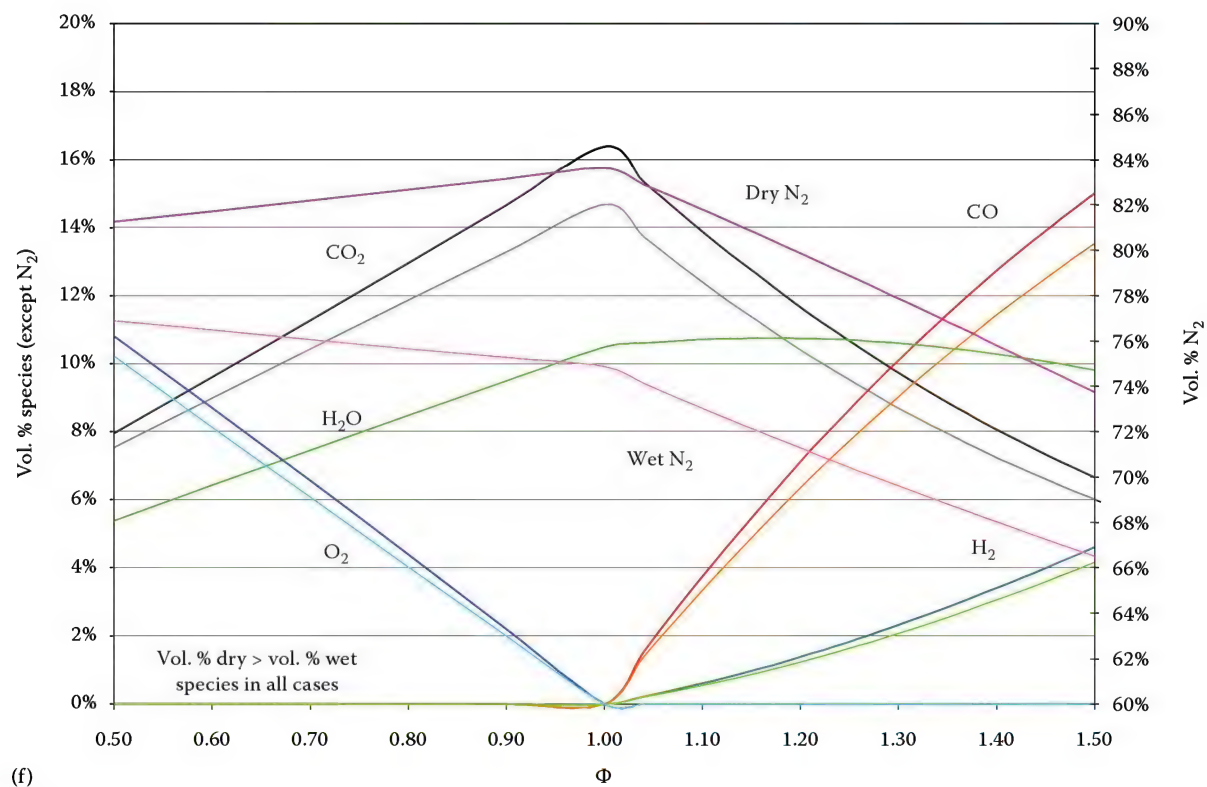
FIGURE 4.16 (continued)

Species concentration versus stoichiometric ratio for the following fuels: (c) simulated refinery gas (25%  $H_2$ , 50%  $CH_4$ , 25%  $C_3H_8$ ), (d)  $C_3H_8$ .





(e)



(f)

FIGURE 4.16 (continued)

Species concentration versus stoichiometric ratio for the following fuels: (e) No. 2 oil, and (f) No. 6 oil.

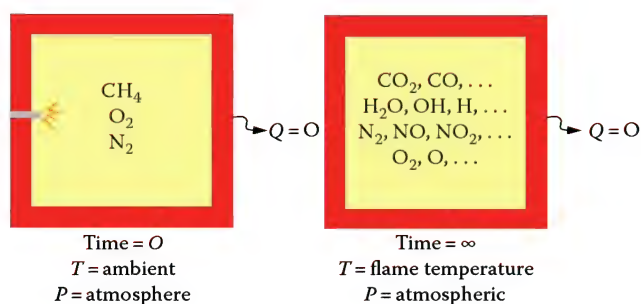


**FIGURE 4.17**  
Adiabatic equilibrium reaction process.

#### 4.13.2 Fuel Blend Effects

Fuel blends are particularly important in many of the hydrocarbon and petrochemical industries. Figure 4.23 shows the predicted major species for the combustion of air with fuel blends consisting of  $H_2$  and  $CH_4$ .  $CO_2$  and  $N_2$  decline and  $H_2O$  increases as the  $H_2$  content in the fuel increases. It is important to note that the species concentrations are not linear functions of the blend composition, where the change occurs more rapidly at higher  $H_2$  compositions. Figure 4.24 is a similar plot of the predicted minor species as functions of the  $H_2/CH_4$  fuel blend. This

graph also shows strong nonlinearities as the  $H_2$  content increases. Figure 4.25 shows the predicted major species for the combustion of air with fuel blends consisting of an inert ( $N_2$ ) and  $CH_4$ . At the extreme of 100%  $N_2$ , there is no fuel left in the “fuel blend” and no combustion takes place. There is a rapid change in the species concentrations as the  $N_2$  content increases. Figure 4.26 shows the predicted minor species for the combustion of  $N_2/CH_4$  fuel blends. This graph also shows a rapid decline in the species concentration, in this case for the minor species.

Real combustion processes are not adiabatic, as the whole intent is to transfer heat from the flame to some type of load. The amount of heat lost from the process determines the temperature of the exhaust gases. The higher the heat losses from the flame, the lower the exhaust gas temperature. Figure 4.27 shows the predicted major species for the combustion of air and methane as a function of the exhaust gas temperature. The peak temperature is the adiabatic flame temperature. There is relatively little change in the major species concentration as a function of temperature. Figure 4.28 shows the predicted minor species for the combustion of air and methane as a function of the exhaust gas temperature. The concentrations are

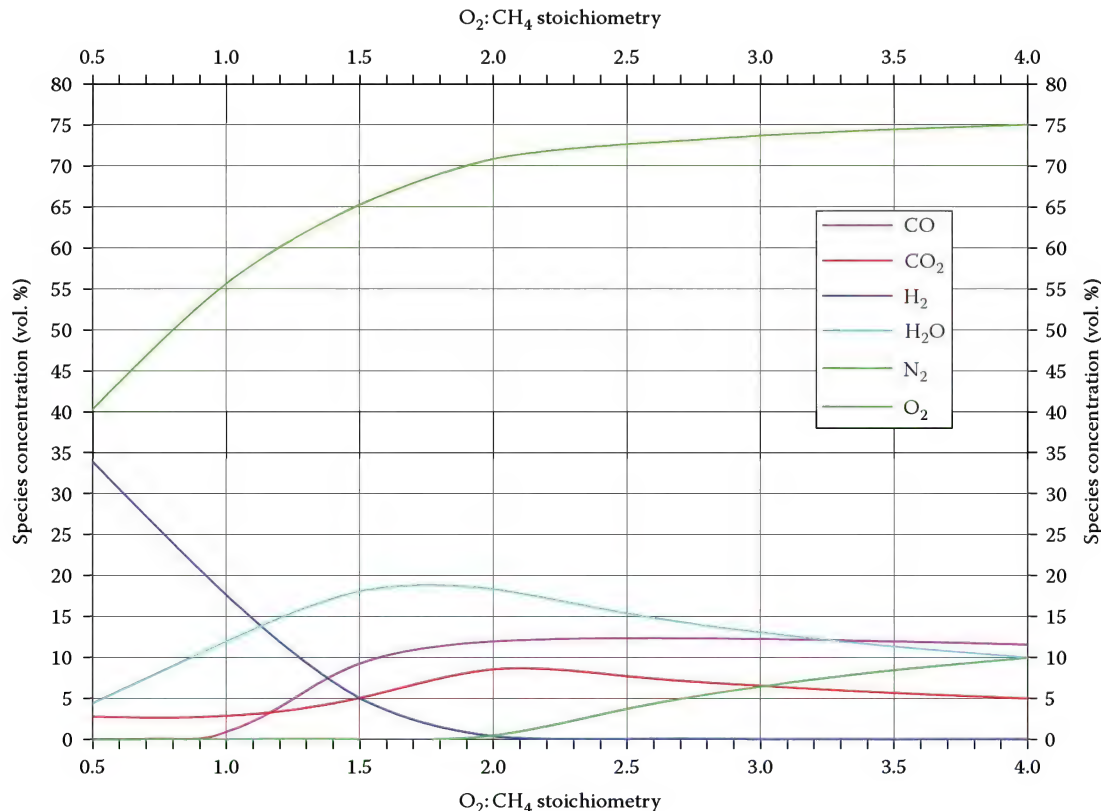


**FIGURE 4.18**  
Adiabatic equilibrium calculations for the predicted gas composition as a function of the  $O_2:CH_4$  stoichiometry for air/ $CH_4$  flames where the air and  $CH_4$  are at ambient temperature and pressure.

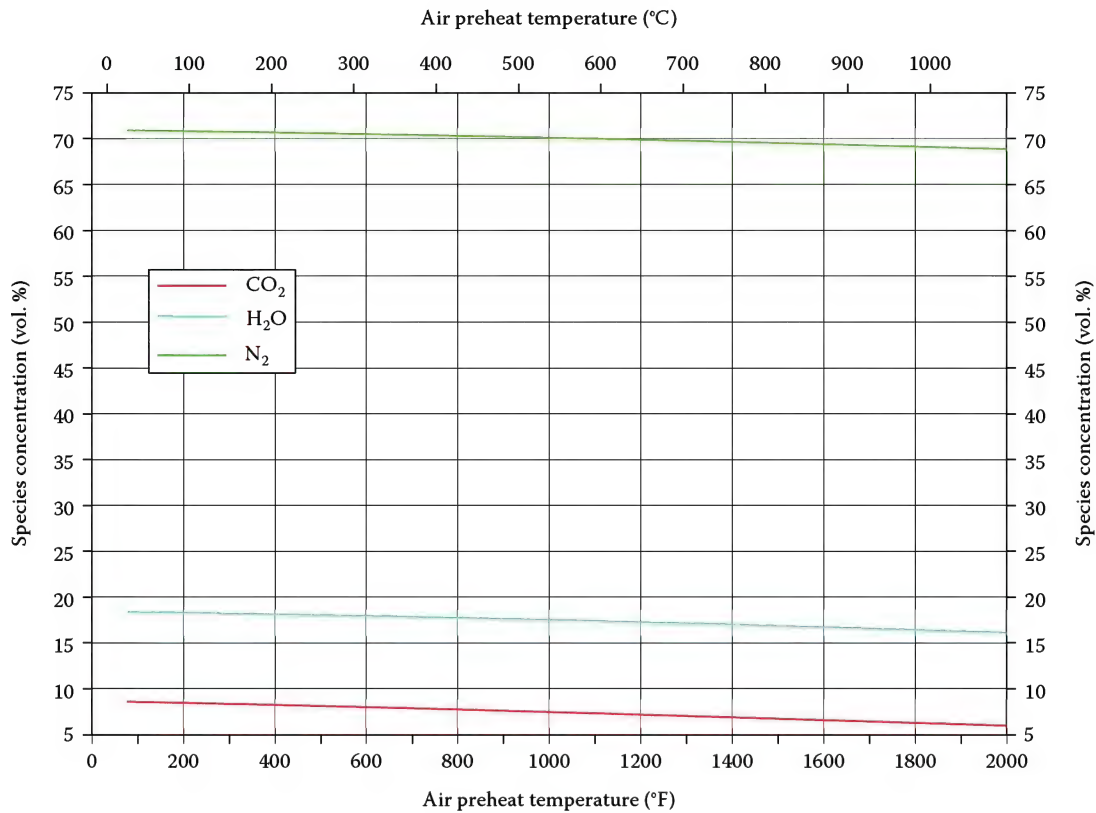


FIGURE 4.19

Adiabatic equilibrium stoichiometric calculations for the predicted gas composition of the major species as a function of the air preheat temperature for air/CH<sub>4</sub> flames where the CH<sub>4</sub> is at ambient temperature and pressure.

essentially zero up to temperatures of about 2000°F (1100°C) and rapidly increase up to the adiabatic flame temperature.

From the products of the general form of hydrocarbon reactions given earlier, one can obtain

$$\text{O}_2 \%_{\text{dry}} = \frac{(\epsilon - 1) \left(1 + \frac{x}{4}\right) 100}{1 + (\epsilon - 1) \left(1 + \frac{x}{4}\right) + \epsilon \left(1 + \frac{x}{4}\right) 3.76} \quad (4.52)$$

#### 4.14 Emissions

Common examples of gaseous emissions are NO<sub>x</sub>, CO, and SO<sub>x</sub>. (For a more detailed discussion see Chapters 14 and 15). The concentration of each pollutant is measured at the stack in dry parts per million volume (ppmvd). As ppmvd varies with the amount of O<sub>2</sub> in the stack, it is necessary to establish a reference percentage of O<sub>2</sub>. For example, 100 ppm NO<sub>x</sub> at 3% O<sub>2</sub>.

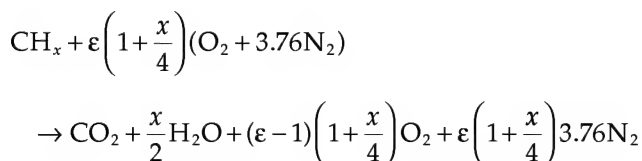
In order to establish the percentage of dry O<sub>2</sub>, use the excess air measured in the stack.

where

$$\left(\frac{H}{C}\right)_{\text{mol}} = "x"$$

$$\text{Substituting } \phi = \frac{\% \text{Excess Air}}{100} + 1$$

The general relation for EA and O<sub>2</sub> dry for any HC fuel is as follows:



$$\text{O}_2 \%_{\text{dry}} = \frac{1}{\left[ \frac{1}{\left(1 + \frac{x}{4}\right)} + 3.76 \right] \frac{1}{\text{EA}} + .0476} \quad (4.53)$$

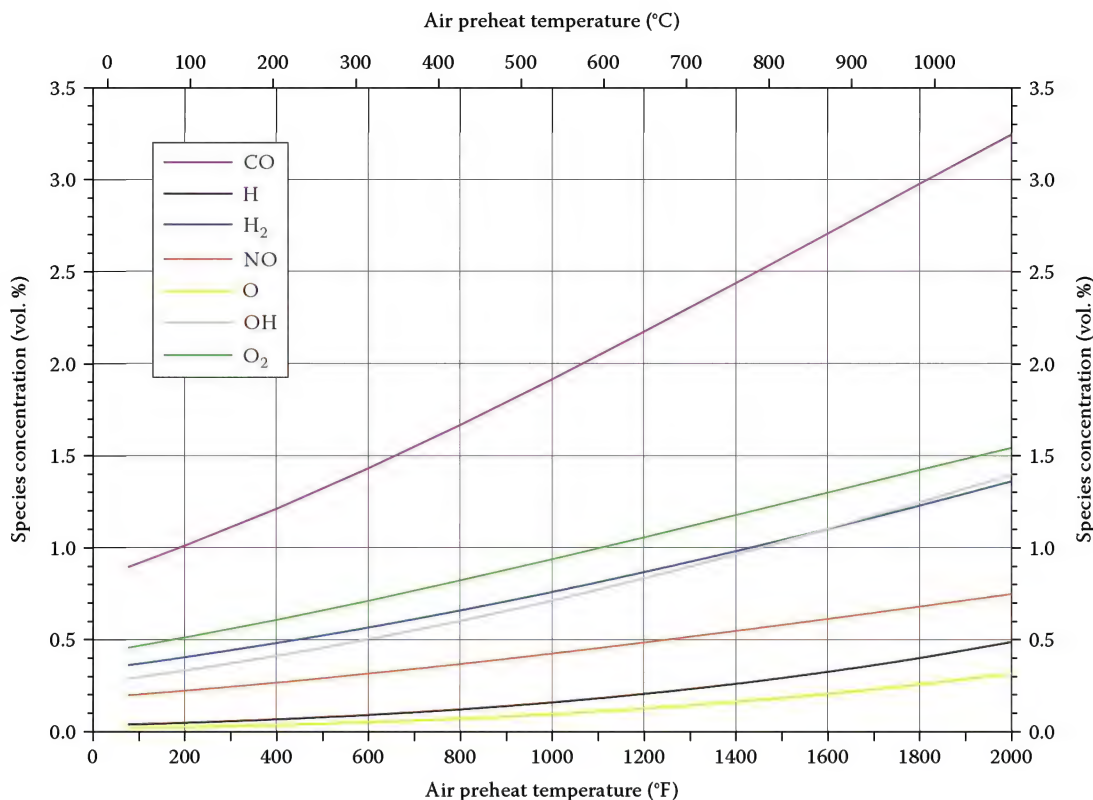


FIGURE 4.20

Adiabatic equilibrium stoichiometric calculations for the predicted gas composition of the minor species as a function of the air preheat temperature for air/CH<sub>4</sub> flames where the CH<sub>4</sub> is at ambient temperature and pressure.

It is often necessary to calculate mass emission rate per Btu produced  $\left(\frac{\text{lbs}}{10^6 \text{ Btu}}\right)$  from ppmvd. Using the general chemical equation for fuel oxidation given in Example 4.6 and repeated above, compute

$$\begin{aligned} & \frac{N_{\text{ppmvd}}}{10^6} \times \frac{\text{lb Mol Chem}}{\text{lb Mol FG}} \times \frac{\text{lb Mol} \left( \frac{FG}{F} \right)}{\text{lb Mol} \left( \frac{FG}{F} \right)} \\ & \times \frac{1 - \text{lb Mol Fuel}}{(\text{MW}_F) \text{ lb Fuel}} \times \frac{\text{MW}_{\text{chem}} \text{ lbm}}{\text{lb Mol Chem}} \times \frac{\text{lbm Fuel}}{\text{HHV}} \\ & \times \frac{10^6 \text{ Btu}}{\text{million}} = \frac{\text{lbm}}{10^6 \text{ Btu}} \end{aligned}$$

where  $N_{\text{ppmvd}}$  = ppmv of chemical X

$$\left( \frac{FG}{F} \right)_{\text{dry, vol}} = 1 + (\epsilon - 1) \left( 1 + \frac{x}{4} \right) + \epsilon \left( 1 + \frac{x}{4} \right) \quad (4.54)$$

Substituting  $\phi = \frac{\% \text{Excess Air}}{100} + 1$  and simplifying gives

$$\frac{N_{\text{ppmvd}} \text{ MW}_{\text{chem}}}{\text{HHV}(12 + x)} \left[ 1 + \left( 1 + \frac{x}{4} \right) \left( \frac{4.76 \text{ EA}}{100} + 3.76 \right) \right] = \frac{\text{lbm N}}{10^6 \text{ Btu}} \quad (4.55)$$

The previous equation is a general relationship between a product species in dry ppm by volume and  $\frac{\text{lb}_m}{10^6 \text{ Btu}}$  for any chemical compound.

$$\text{HHV} = \frac{\text{Btu}}{\text{lb}_m}$$

and

$\text{MW}_c$  = molecular weight of "N" chemical EA = % excess air

## 4.15 Quick Sizing

### 4.15.1 Finding Saturated Humidity

A shortcut is to use steam property tables of saturated pressure versus temperature to find the saturated humidity in the air. Water vaporizes at 100°C (212°F) which, according to the steam tables, yields a saturation pressure of 101.42 kPa (14.7 psia). To get saturated humidity then, simply take the ratio of  $P_{\text{sat}}$  at any temperature to 101.32 kPa in order to get saturation humidity.

$$\text{Saturated Humidity} = \frac{P_{\text{sat}} @ \text{Temp}}{P_{\text{sat}} @ \text{Boiling Temp}} \quad (4.56)$$



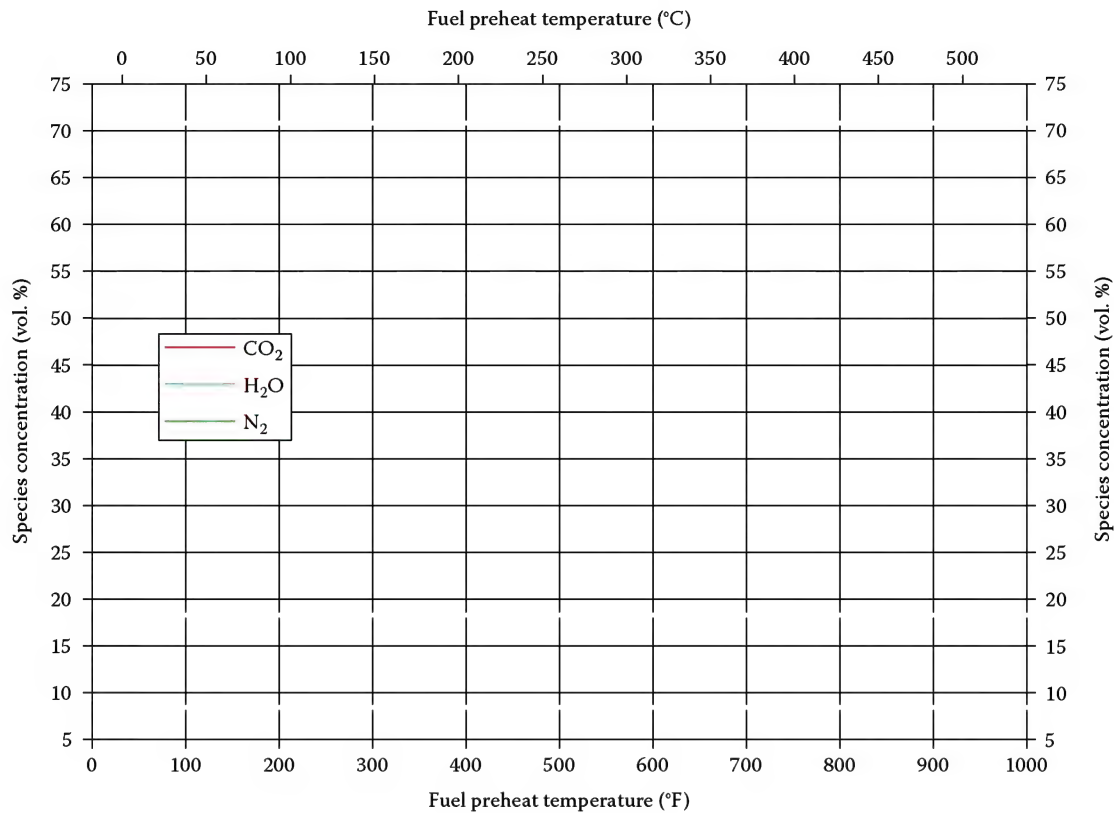


FIGURE 4.21

Adiabatic equilibrium stoichiometric calculations for the predicted gas composition of the major species as a function of the fuel preheat temperature for air/CH<sub>4</sub> flames where the air is at ambient temperature and pressure.

#### Example 4.13

For example, suppose a room of 35°C; then looking up the properties of steam at 35°C in the steam tables yields

At 35°C →  $P_{\text{sat}}$  of 5.63 kPa.

And  $P_{\text{sat}}$  at boiling = 101.42 kPa at boiling °C

$$\text{Saturated Humidity} = \frac{5.63 \text{ kPa}}{101.42 \text{ kPa}} = 5.55\%$$

Thus a room at 35°C yields a saturated humidity of 5.55%.

#### 4.15.2 Stoichiometric Combustion of Air Simplified

In finding air-to-fuel ratio by volume it is generally accepted to assume that all gaseous paraffinic hydrocarbons consume a cubic foot of air for every 106 Btu

fired  $\left(106 \frac{\text{Btu}}{\text{ft}^3_{\text{air}}}\right)$ . In the case of liquid fuels, it is also accepted that the reaction consumes a cubic foot of air for every 100 Btu fired  $\left(100 \frac{\text{Btu}}{\text{ft}^3_{\text{air}}}\right)$ . Similarly, coal reactions, on average, consume a cubic foot of air for every 98 Btu fired  $\left(98 \frac{\text{Btu}}{\text{ft}^3_{\text{air}}}\right)$ . The actual  $\frac{\text{Btu}}{\text{ft}^3_{\text{air}}}$  for coal and oil can be found in Table 4.5. For gaseous fuels the reader can compute using the methods outlined in Section 4.7 or computed from Table 4.3.

#### 4.15.3 Density of Low Pressure Gases

A practical shortcut to find the density of a gas at low pressures is to use the following equation:

$$\text{Pressure} = (0.075) \left( \frac{\text{MW}_{\text{gas}}}{\text{MW}_{\text{air}}} \right) \left( \frac{P_{\text{gas}}}{P_{\text{airSTP}}} \right) \left( \frac{T_{\text{gas}}}{T_{\text{airSTP}}} \right) \quad (4.57)$$

Specific gravity

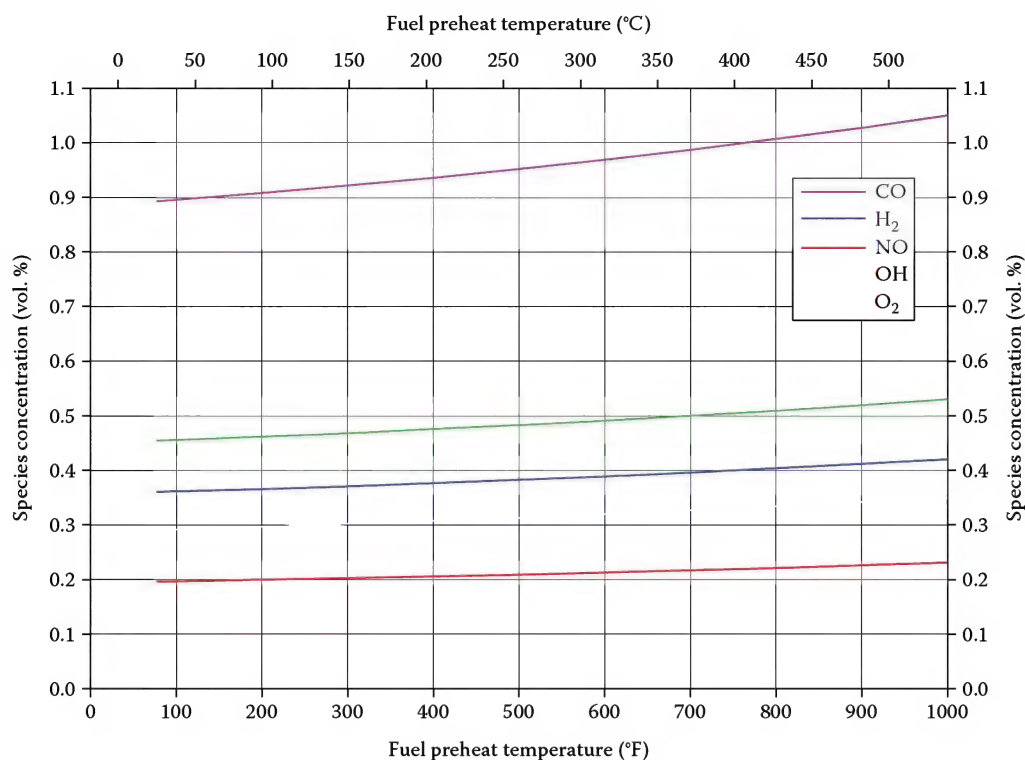


FIGURE 4.22

Adiabatic equilibrium stoichiometric calculations for the predicted gas composition of the minor species as a function of the fuel preheat temperature for air/CH<sub>4</sub> flames where the air is at ambient temperature and pressure.

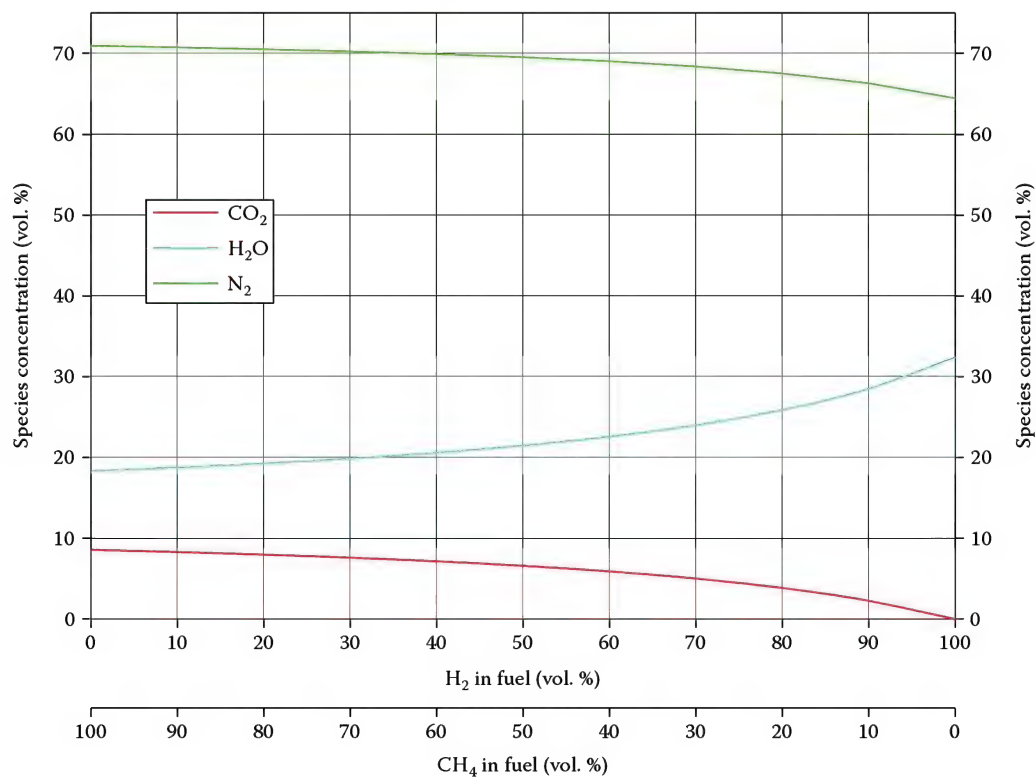


FIGURE 4.23

Adiabatic equilibrium stoichiometric calculations for the predicted gas composition of the major species as a function of the fuel blend (H<sub>2</sub> + CH<sub>4</sub>) composition for air/fuel flames where the air and fuel are at ambient temperature and pressure.

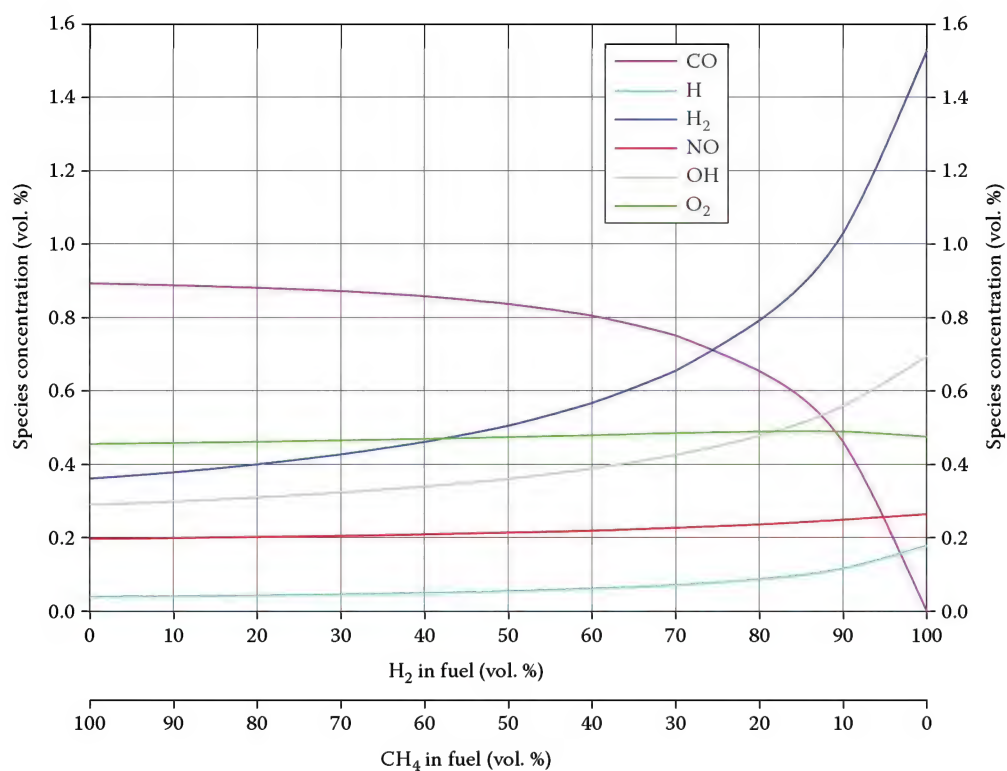


FIGURE 4.24

Adiabatic equilibrium stoichiometric calculations for the predicted gas composition of the minor species as a function of the fuel blend ( $H_2 + CH_4$ ) composition for air/fuel flames where the air and fuel are at ambient temperature and pressure.

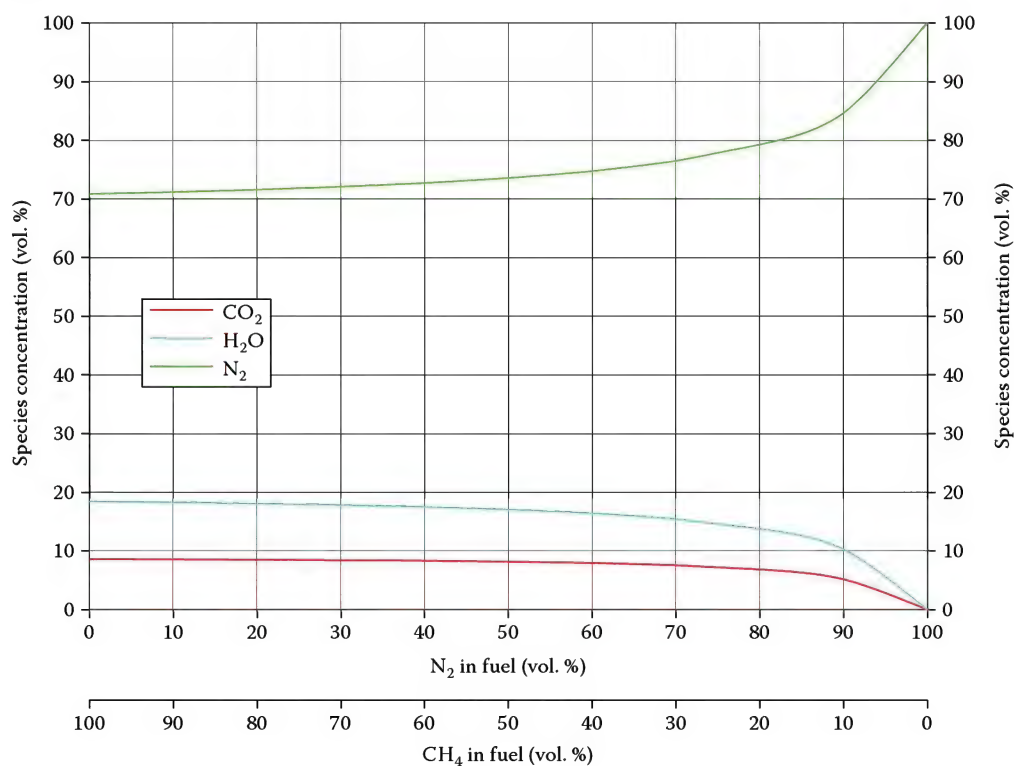


FIGURE 4.25

Adiabatic equilibrium stoichiometric calculations for the predicted gas composition of the major species as a function of the fuel blend ( $N_2 + CH_4$ ) composition for air/fuel flames where the air and fuel are at ambient temperature and pressure.

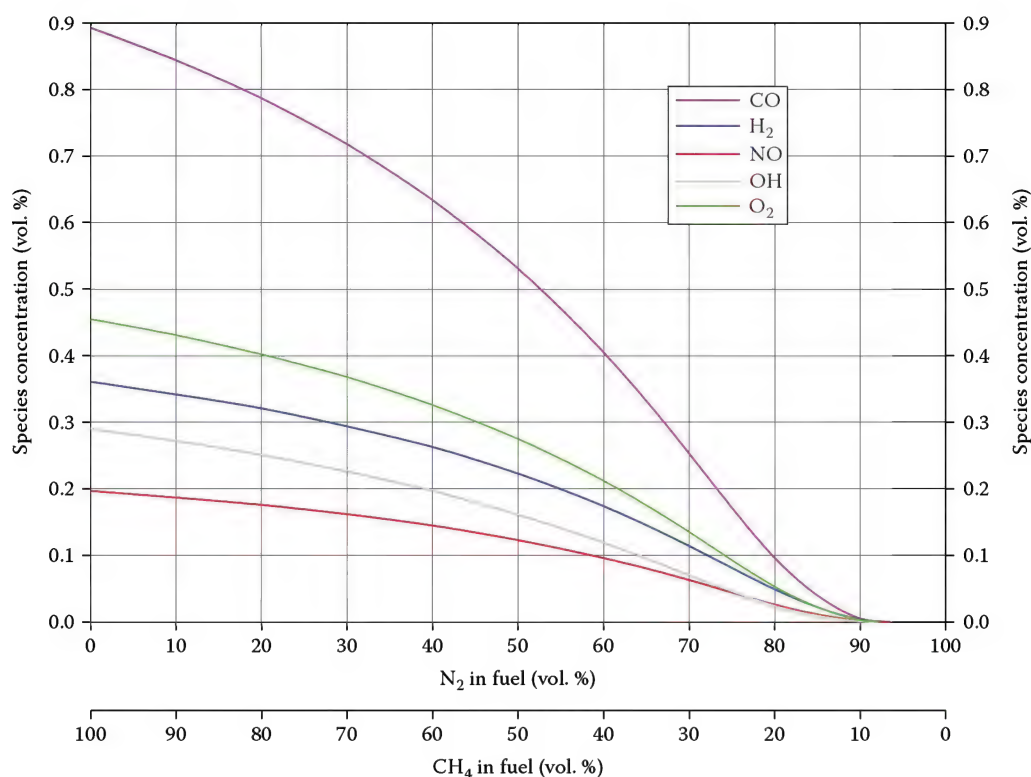


FIGURE 4.26

Adiabatic equilibrium stoichiometric calculations for the predicted gas composition of the minor species as a function of the fuel blend ( $N_2 + CH_4$ ) composition for air/fuel flames where the air and fuel are at ambient temperature and pressure.

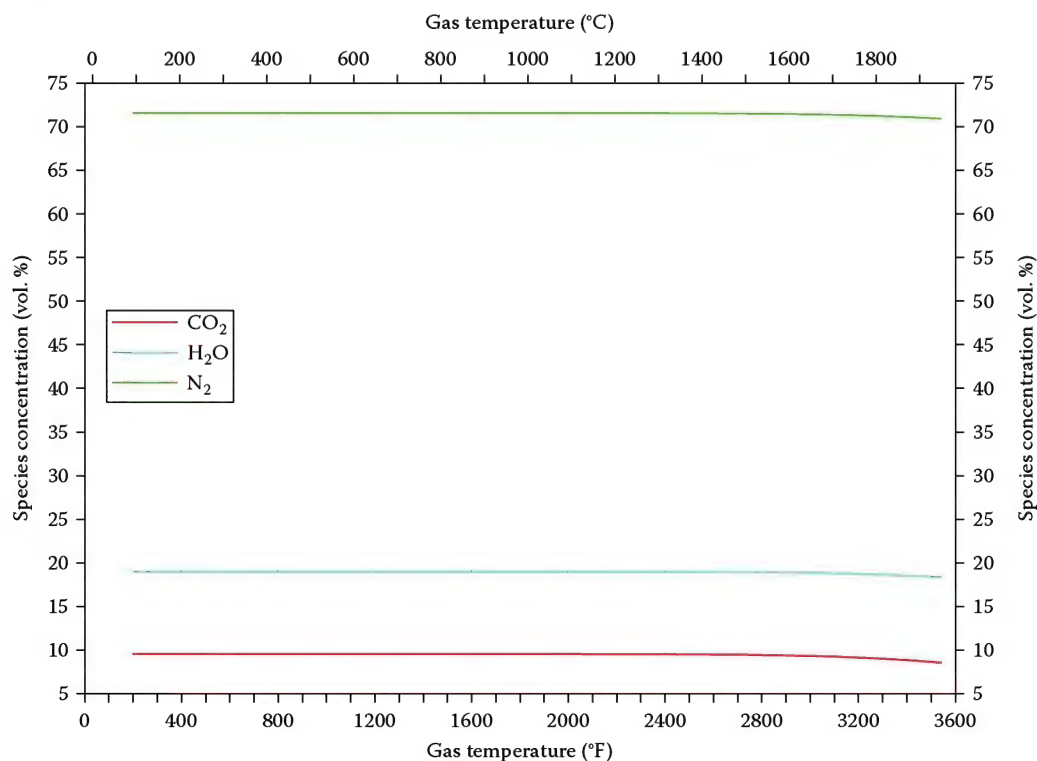


FIGURE 4.27

Equilibrium calculations for the predicted gas composition of the major species as a function of the combustion product temperature for air/ $CH_4$  flames where the air and fuel are at ambient temperature and pressure.



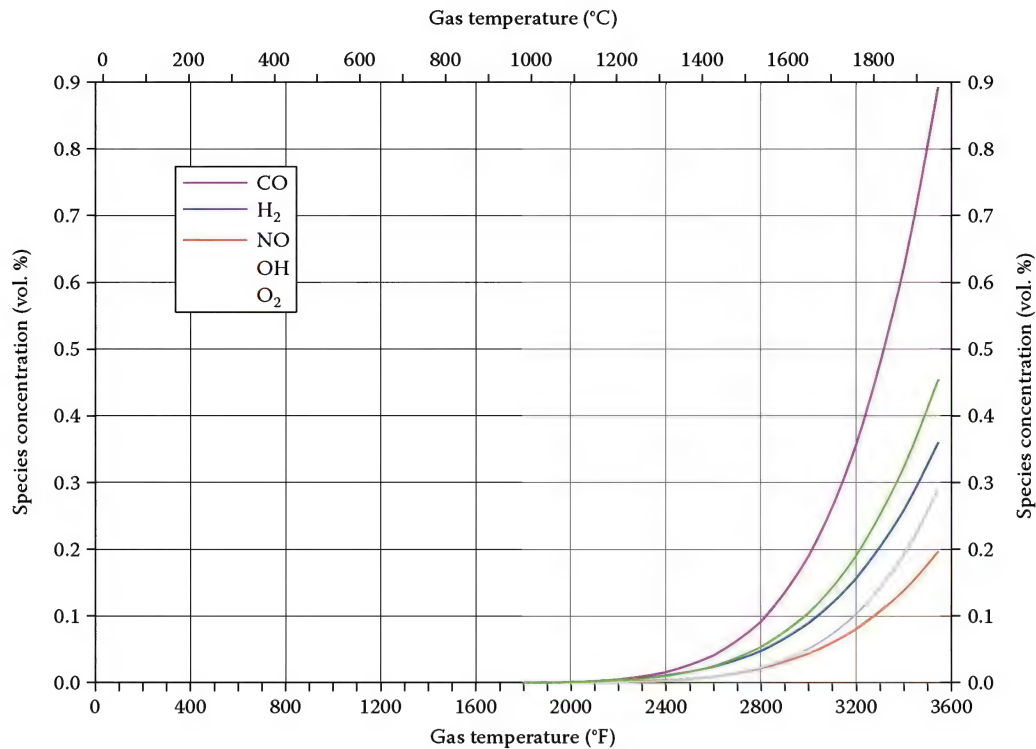


FIGURE 4.28

Equilibrium calculations for the predicted gas composition of the minor species as a function of the combustion product temperature for air/CH<sub>4</sub> flames where the air and fuel are at ambient temperature and pressure.

**Example 4.14**

Find the density of steam at 300°F and 35.3 psig.

Convert temperature to rankine and gauge pressure to atmospheric.

$$T_{\text{gas}} = 300 + 460 = 760^{\circ}\text{R}$$

$$P_{\text{gas}} = 25.3 + 14.7 = 40 \text{ psia}$$

At STP conditions,

$$T_{\text{STP}} = 530^{\circ}\text{R}$$

$$P_{\text{STP}} = 14.7 \text{ psia}$$

$$\rho_{\text{air STP}} = .075 \frac{\text{lb}_m}{\text{ft}^3}$$

$$SG_{\text{H}_2\text{O}} = \frac{18}{28.97} = .621$$

Applying Equation 4.57,

$$\rho_{\text{steam}} = (.075)(.621) \left( \frac{40 \text{ psia}}{14.7 \text{ psia}} \right) \left( \frac{760^{\circ}\text{R}}{530^{\circ}\text{R}} \right) = .0884 \frac{\text{lb}_m}{\text{ft}^3}$$

From standard steam tables, the exact density =  $.0906 \frac{\text{lb}_m}{\text{ft}^3}$ , yielding a small 2.4% difference.

**References**

1. C. Crowe et al., Eds., *Engineering Fluid Mechanics*, 9th edn., John Wiley & Sons, Inc., Hoboken, NJ, 2009.
2. W. Nebergall, *General Chemistry*, 4th edn., D.C. Heath and Company, Lexington, MA, 1972.
3. T. Brown et al., *Chemistry: The Central Science*, 10th edn., Pearson Education, Upper Saddle River, NJ, 2006.
4. F. Vandaveer, *Gas Engineers Handbook*, 1st edn., Industrial Press, New York, 1965.
5. Y. Cengel, *Heat and Mass Transfer: A Practical Approach*, 3rd edn., McGraw Hill, Willard, OH, 2007.
6. C. McQuiston and J.D. Parker, *Heating, Ventilating, and Air Conditioning*, John Wiley & Sons, New York, 1982.
7. R. Bolz et al., *Handbook of Tables for Applied Engineering Science*, 2nd edn., CRC Press, Cleveland, OH, 1973.
8. F. Huang, *Engineering Thermodynamics: Fundamentals and Applications*, Macmillan Publishing Co., New York, 1976.
9. P. Schmidt, *Fuel Oil Manual*, 4th edn., Industrial Press, New York, 1985.
10. D.E. Gray, Ed., *American Institute of Physics Handbook*, 2nd edn., McGraw-Hill Book Company, New York, 1963.
11. R.H. Perry, C.H. Chilton, and S.D. Kirkpatrick, Eds., *Chemical Engineers' Handbook*, 4th edn., McGraw-Hill Book Company, New York, 1963.
12. R.C. Weast, Ed., *Handbook of Chemistry and Physics*, 53rd edn., The Chemical Rubber Company, Cleveland, OH, 1972.

13. N.V. Steere, Ed., *Handbook of Laboratory Safety*, 2nd edn., The Chemical Rubber Company, Cleveland, OH, 1971.
14. R.W. Landenburg and H.S. Taylor, *Physical Measurements in Gas Dynamics and Combustion*, Princeton University Press, Princeton, NJ, 1954.
15. Y. Cengel et al., *Thermodynamics: An Engineering Approach*, 6th edn., McGraw Hill, Willard, OH, 2008.
16. F. Kreith, Ed., *The CRC Handbook of Mechanical Engineering*, CRC Press, Boca Raton, FL, 1998.
17. D.R. Stull and H. Prophet, *JANAF Thermochemical Tables*, 2nd edn., National Standards Reference Data System, National Bureau of Standards, Washington, DC, 1971.
18. S.C. Stultz and J.B. Kitto, *Steam: Its Generation and Use*, 40th edn., Babcock & Wilcox Company, Barberton, OH, 1992.
19. R.H. Barnes, M.J. Saxton, R.E. Barrett, and A. Levy, Chemical Aspects of Afterburner Systems, Battelle Columbus Laboratories, IPA-600/7-79-096, NTIS publication PB298465, April 1979.
20. G.C. Williams, H.C. Hottel, and A.C. Morgan, The combustion of methane in a jet-mixed reactor, *12th Symposium (International) on Combustion*, The Combustion Institute, Pittsburgh, PA, 1969.
21. V.S. Engleman, W. Bartok, J.P. Longwell, and R.B. Edelman, Experimental and theoretical studies of NO<sub>x</sub> formation in a jet stirred combustor, *14th Symposium (International) on Combustion*, The Combustion Institute, Pittsburgh, PA, 1973.
22. A.E. Westenberg, Turbulence modeling for CFD, *Combustion Science and Technology* 4: 59–67, 1971.
23. C.T. Bowman, Kinetics of pollution formation and destruction in combustion, *Progress in Energy and Combustion Science* 1: 33–45, 1975.
24. J.L. Reese et al., State-of-the-art of nox emission control technology, *Proceedings of the International Joint Power Generation Conference*, Phoenix, AZ, October 3–5, 1994.
25. M. Zabethakis, *Flammability Characteristics of Combustible Gases and Vapors*, U.S. Department of Commerce, Springfield, CA, 1965.
26. S.R. Turns, *An Introduction to Combustion*, McGraw-Hill, New York, 1996.

# 5

## *Solid Fuel Combustion in Suspension*

Steve Londerville and Timothy Webster

### CONTENTS

5.1	Introduction .....	125
5.2	Fuel Properties and Characterization .....	125
5.2.1	Coal .....	126
5.2.2	Wood, Biomass, and Pet Coke .....	126
5.3	Oxidation of Solid Fuels .....	126
5.3.1	Heat-up, Devolatilization, and Volatile Oxidation .....	126
5.3.2	Char Oxidation .....	128
5.3.3	Flammability Characteristics .....	129
5.4	Fuel Conveying .....	129
5.4.1	Pressure Drop Calculations in Solid/Gas Conveying .....	129
5.4.2	Horizontal Transport .....	130
5.4.3	Vertical Transport and Minor Losses .....	130
5.4.4	Conveying Options .....	130
5.5	Burner Designs .....	130
5.5.1	Utility and Multiburner Applications .....	132
5.5.2	Industrial Burners .....	132
5.5.3	Support Fuel .....	132
5.6	Furnace and Control Considerations .....	132
5.7	Combustion Controls .....	133
5.8	Emission Formation and Prediction .....	133
5.9	Conclusions .....	134
	References .....	135

### 5.1 Introduction

The utilization of solid fuels dates back to early civilization, and fire used for cooking and warmth was discovered long before liquid or gaseous fuels were in use. Early utilization of solid fuels in the last few centuries started with cut wood or chunk coal burned in stoves and fireplaces. Early industrial use of solid fuels utilized various forms of grates with chunk wood or coal. Today, solid fuels are used in boilers (both industrial and utility), kilns, and air heaters.

This chapter presents the use of solid fuels pneumatically conveyed in suspension. This means that solid fuels need to be ground or “pulverized” into much smaller sizes and pneumatically conveyed, usually with air, to a burner system. The preparation of the fuel and delivery to the burner system can be very complex. Only the

basics of this preparation will be presented with more concentration dedicated to conveying, burners, and the actual oxidation of solids in suspension.

### 5.2 Fuel Properties and Characterization

For all solid fuels, the primary properties are defined by proximate and ultimate analyses. An example of each type of analysis is shown in Table 5.1 for Pittsburgh Seam Coal, West Virginia. Generally, both proximate and ultimate analyses are required to design a system. This allows computation of heat input, combustion air calculations, and most emissions. Each solid fuel type will have grind size requirements for conveying and unit performance with respect to heat

TABLE 5.1

Coal Analyses As-Received Basis

ASTM D3172		ASTM D3176	
Proximate Analysis		Ultimate Analysis	
Component	%weight	Component	%weight
Moisture	2.5	Moisture	2.5
Volatile matter	37.6	Carbon	75.0
Fixed carbon	52.9	Hydrogen	5.0
Ash	7.0	Sulfur	2.3
Total	100	Nitrogen	1.5
Heating value	13,000 BTU/lb <sub>m</sub>	Oxygen	6.7
		Total	100
		Heating value	30,238 KJ/kg

Source: Adapted from Stultz, S.C. and Kitto, J.B., *Steam: Its Generation and Use*, 40th edn., Babcock and Wilcox Company, New York, 1992, p. 8.5.

transfer and emissions. The following sections detail some specifics for some common, but not all, solid fuels.

### 5.2.1 Coal

Coal is, by far, the most commonly used solid fuel, supplying 32% of the world's energy. Coal starts initially forming from vegetation and wood under pressure and temperature over a long period of time. During this time period, the initial formation goes from humates to anaerobic and then peat. Final formation to coal then proceeds in order to yield lignite, subbituminous, bituminous and finally anthracitic coal over time. Coal is defined by class as shown in Table 5.2.

In recent years, coal has been dubbed the "dirty fuel," primarily because of the increased use of natural gas, which has lower emissions as opposed to actual coal emissions that are generally reduced with post-combustion cleanup.

TABLE 5.2

Class of Coals

Class 1	Anthracitic	High rank with high carbon, low moisture, but high heating value, greater than 14,000 Btu/lb <sub>m</sub> . It is low in sulfur and volatiles. Premium fuel most commonly used in domestic markets
Class 2	Bituminous	Commonly burned in utilities with medium heating values, volatiles, and fixed carbon
Class 3	Subbituminous	High in moisture and volatiles. Low ash and sulfur. Heating values at 10,000 BTU/lb <sub>m</sub>
Class 4	Lignitic	Lowest heating values, below 8000 BTU/lb <sub>m</sub> , and high moisture and volatiles. Lowest in fixed carbon and ash

Source: Adapted from Stultz, S.C. and Kitto, J.B., *Steam: Its Generation and Use*, 40th edn., Babcock and Wilcox Company, New York, 1992, p. 8.5.

Sulfur contributes to acid rain, opacity, and particulates. The ash content contributes to opacity and particulates. Even with zero carbon loss, the stack gas of almost all coal installations will require sulfur and particulate cleanup that is quite expensive for all but large capacity users. A great deal of information is known about coal fuels, as it has been a utility fuel for 100 years or so.

### 5.2.2 Wood, Biomass, and Pet Coke

Less common solid fuels include wood, various biomasses, and petroleum coke. Many of these fuels are "renewable." All have specific and sometimes unique requirements for grinding, conveying, ignition, burn-out, erosion, and emissions. All of these fuels can be pneumatically conveyed and burned in suspension. The low volatility fuels may require support fuel. The high sulfur and ash fuels usually require some kind of post-combustion cleanup. Rice hulls, coke, char fines, and coal are the most erosive fuels and will require special wear plates. The high nitrogen fuels will need to address conversion to NO<sub>x</sub> emissions. Staging air and fuel has shown to be effective in the reduction of NO<sub>x</sub> emissions (see Chapter 15).

Other fuels such as planer shavings, sander dust, sunflower seed hulls, peanut shells, and olive pits have also been used. Wood waste from manufacturing may need to include the glues used in the product not specified by the parent wood for emission calculations. Table 5.3 outlines some of these fuels' properties.

## 5.3 Oxidation of Solid Fuels

All solid fuels oxidize in a similar manner. The process includes the following steps: heat up, devolatilization, volatile oxidation, and, finally, char burnout. During the process, the solid particle can swell or shrink and can break up or not, and this is very specific to the fuel.

### 5.3.1 Heat-up, Devolatilization, and Volatile Oxidation

All solid fuels require initial heat up as the first step in oxidation to dry the material. Depending on the fuel type, swelling, shrinking, and breakup may occur partially at this stage. In normal burners, heat-up rates are very high, on the order of  $10^5 \frac{K}{s}$  Ref. [2]. For normal burners where fuel is delivered pneumatically in suspension, these heat-up times are very low (<5–15 ms) and can generally be neglected. Coal devolatilization can



TABLE 5.3

Fuel Properties of Biomass and Solid Fuels (CoenBCS 1983 Bulletin)

	Fuel Properties of Biomass and Solid Fuels Chemical Composition (% by wt., Dry Basis)												
Fuel Characteristics	Bark		Wood			Rice Hulls	Coffee Grounds	Apple Pomace	Peat	Delayed Coke	Char Fines	Coal	
	Pine	Oak	Pine	Fir	Bagasse							Sub A	Bit A
Proximate analysis													
Volatile matter	72.9	76.0	79.4	75.1	83.8	64.3	86.0	71.3	67.3	12.1	2.0		34.3
Fixed carbon	24.2	18.7	20.1	24.5	12.7	20.7	13.1	23.0	22.7	87.6	58.4	56.4	59.2
Ash	2.9	5.3	0.5	0.4	3.5	15.0	0.9	5.7	10.0	0.3	39.6	4.7	6.5
Ultimate analysis													
Hydrogen	5.6	5.4	6.3	6.3	5.8	5.7	7.7	5.9	5.3	3.9	0.4	5.0	5.2
Carbon	53.4	49.7	51.8	50.7	48.8	44.9	57.3	42.2	52.2	89.6	58.6	75.1	79.5
Sulfur	0.1	0.1	0.0	0.0	0.0	0.1	0.2	0.1	0.4	4.2	1.0	1.0	1.3
Nitrogen	0.1	0.2	0.1	2.4	0.2	0.5	1.4	0.7	1.8	1.2	0.4	1.4	1.4
Oxygen	37.9	39.3	41.3	40.2	41.7	33.8	32.5	45.4	30.3	0.8	0.0	12.8	6.1
Ash	2.6	5.3	0.5	0.4	3.5	15.0	0.9	5.7	10.0	0.3	39.6	4.7	6.5
Heating value													
Dry basis (Btu/lb)	9030	8370	9130	8795	8100	7226	10,950	8090	9057	15,400	8758	13,595	14,366

be modeled by the method of Kobayashi.<sup>3</sup> This method uses a parallel pair of first-order irreversible reactions and seems to fit measured data very well. Combined, the rate of devolatilization can be expressed in first order as

$$\frac{dv}{dt} = (y_1 k_1 + y_2 k_2) c \quad (5.1)$$

where

$\frac{dv}{dt}$  = Rate of devolatilization on a mass basis

$y_1$  = Fraction of volatiles close to the proximate analysis

$y_2$  = Fraction of volatiles at high temperatures, often near unity

$k_1 = B_1 \exp \frac{E_1}{RT}$  = Arrhenius rate at low temperatures

$k_2 = B_2 \exp \frac{E_2}{RT}$  = Arrhenius rate at high temperatures

$c$  = Coal particle mass

$T$  = Absolute temperature in Kelvin

$R$  = Universal gas constant in consistent units

At high temperatures, as experienced in real flames, coal devolatilization ranges from 40 to 10 ms from lignite to bituminous coals.

For wood and biomass, a first-order reaction is also commonly used as described by Roberts<sup>4</sup>, using a constant diameter, shrinking density model:

$$\frac{dp}{dt} = -\rho K \quad (5.2)$$

and on integration

$$f = \epsilon^{-K\Delta T} \quad (5.3)$$

where

$\rho$  = Density in consistent units

$f$  = Fraction devolatilized

$\Delta T$  = Time of devolatilization in seconds

$K = A \exp \left( \frac{E}{RT} \right)$ , an Arrhenius rate with units of inverse seconds

Considerable variations in the rate data have been recorded and summarized by Malte.<sup>5</sup> Suggested values for  $A$  and  $E$  are  $7 \times 10^7 \text{ s}^{-1}$  and  $-30 \text{ Kcal/gmol}$ , respectively.

However, for the devolatilization of biomass, the author shows that not only does the density decrease, but the biomass particles also undergo breakup according to the aspect ratio of the particle and material type.<sup>6</sup> Thus, the primary function of devolatilization in biomass oxidation is the reduction in size and density for the next oxidation step; the reduction of the resultant char is called char burnout.

A final note on devolatilization for a variety of petroleum coke-derived fuels—these fuels are usually void of significant volatiles and tend to oxidize as constant density shrinking diameter char discussed later under the section on char oxidation. They are treated as near solid carbon spheres for practical burnout times.

At high temperatures, a long list of kinetic data is available for computing volatile oxidation. Generally, a two-step

mechanism is used where the hydrocarbons (HCs) oxidize to CO and then CO oxidizes to CO<sub>2</sub>. References for HC oxidation include several sources such as Edelman.<sup>7</sup>

In general,

$$\frac{d(C_a H_b)}{dt} = -5.52 \times 10^8 (P^{-0.815})(T)e^{(12,200/T)}(C_a H_b)^{0.5}(O_2) \frac{\text{mol}}{\text{cm}^2 \text{ s}} \quad (5.4)$$

For CO destruction, several kinetic data are available such as Williams and Hottel<sup>8</sup>

$$\frac{d[\text{CO}]}{dt} = -1.8 \times 10^7 e^{(-25,000/RT)}(\text{CO})(O_2)^{.5}(\text{H}_2\text{O})^5 \left( \frac{P}{RT} \right)^2 \quad (5.5)$$

Almost all published CO rates involve H<sub>2</sub>O because CO destruction requires the (OH)<sup>-1</sup> radical to produce the reaction.

After, and partially during, gaseous oxidation, the original solid particle becomes void of HCs and becomes a char "particle" that can be treated as mostly carbon. The resultant char is rarely spherical except in the case of pet coke.

### 5.3.2 Char Oxidation

Despite the fact that the final char is not always spherical, it is convenient to treat it as such. With this assumption for a solid char, the relationship is

$$(1 - V) = \frac{D_c^3 \rho_c}{D_o^3 \rho_o} \quad (5.6)$$

where

$D_c$  is the char diameter, consistent units

$D_o$  is the initial particle diameter corrected for breakup, swelling or shrinking

$\rho_o$  is the density of initial particle, consistent units

$\rho_c$  is the density of char particle assuming it is carbon

$V$  is the proximate volatile fraction

After determining the char size and structure, a char burnout model can be applied to determine the burnout time. The char will oxidize by diffusion of oxygen to the surface and surface reactivity. Two different models can be used depending on the initial char size and fuel type. First, the more common model is shrinking diameter constant density. The second model is generally used for large cenosphere constant diameter, shrinking density. In either case, the oxidation is defined as follows:<sup>2</sup>

$$\frac{dm}{dt} = \frac{-12 C_{og} A_p}{\frac{1}{K_m} + \frac{1}{K_r}} \quad (5.7)$$

where

$\frac{dm}{dt}$  in grams carbon/second consumed

$C_{og}$  is the molar density of O<sub>2</sub> gmol/cm<sup>3</sup>

$A_p$  is the area of initial char, cm<sup>2</sup>

$K_r$  is the surface reaction coefficient in cm/s

$K_m$  is the diffusion coefficient in cm/s

and

$$K_r = \frac{K_p \bar{R} T_k}{32} \text{ cm/s} \quad (5.8)$$

where

$$K_p = A e^{(-E/T_k R')}, \text{ reaction rate char data in } \frac{\text{g}}{\text{cm}^2 \times \text{s} \times \text{atmO}_2} \quad (5.9)$$

where

$E$  is the activation energy in cal/g-mol

$R' = 1.98 \text{ cal/g-mole K}$

$A$  is the pre-exponential factor  $\frac{\text{g}}{\text{cm}^2 \cdot \text{s} \cdot \text{atmO}_2}$

$$\bar{R} = 82.057 \frac{\text{cm}^3 \text{ atm}}{(\text{gmol K})}$$

$T_k$  is the temperature in K

and

$$K_m = \frac{2 D_{O_2 N_2}}{D_c} \text{ cm/s} \quad (5.10)$$

where Bird, Stewart, and Lightfoot<sup>9</sup> demonstrated that

$$D_{O_2 N_2} \cong 0.00026 T_k^3 \sqrt{\left( \frac{1}{M W O_2} + \frac{1}{M W N_2} \right)} \quad (5.11)$$

and

$D_{O_2 N_2}$  = Diffusivity in cm<sup>2</sup>/s

MW = Molecular weight O<sub>2</sub> or N<sub>2</sub>

Combining 5.7 and 5.11 yields the final char loss formula:

$$\frac{dm}{dt} = \frac{-12 C_{og} A_p}{\left( \frac{D_c}{(0.000116) T_k^{1.5}} + \frac{32}{K_p \bar{R} T_k} \right) s} \frac{\text{gC}}{\text{s}} \quad (5.12)$$

Combining these equations,  $\frac{dm}{dt}$  can be integrated numerically or directly integrated for the case of

constant diameter/shrinking density with constant  $O_2$  and temperature. Since this is rarely the case, the normal solution will involve char size distribution, reducing  $O_2$ , changing the temperature, and a simple “marching” solution that is simple enough to do in a spreadsheet. Either the constant diameter or constant density model can be used after defining the char size distribution. Further, this procedure will yield not only the final particulate, but the size distribution as well. From this distribution and mass loading, opacity can be predicted using simple light scattering equations.

See Figures 5.1 and 5.2 for examples of computed char burnout for subbituminous coal char and pet coke char. Note the pet coke char requires longer to burnout due to the low surface reactivity.

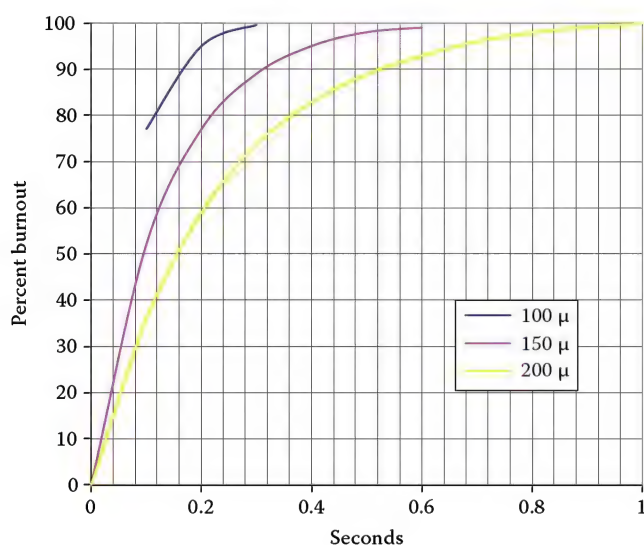


FIGURE 5.1  
Subbituminous char burnout Coen code A = 60 and E = 17,150.

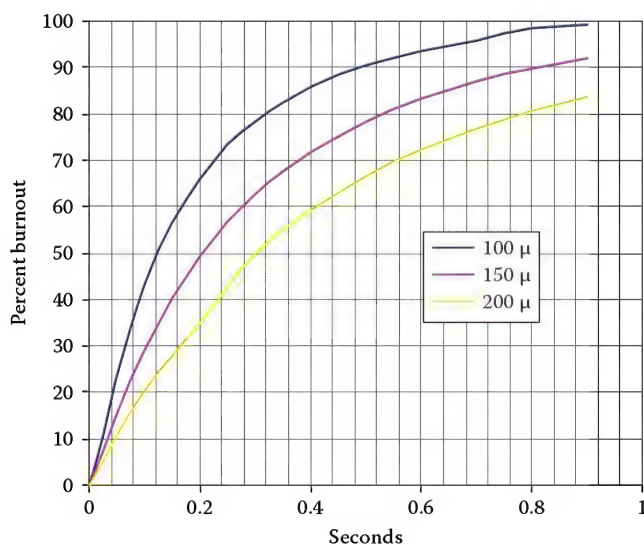


FIGURE 5.2  
Pet coke char burnout Coen Code A = 15 and E = 19,000.

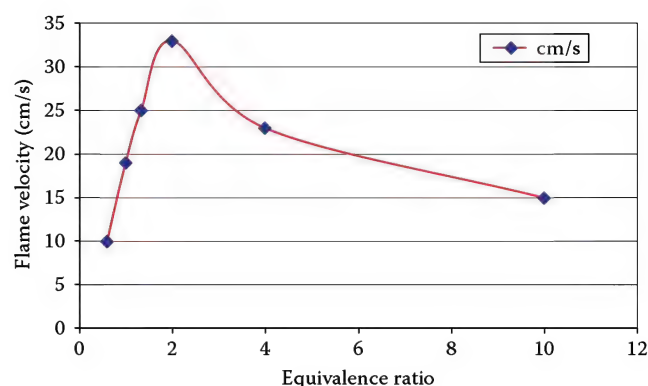


FIGURE 5.3  
Coal dust flame velocity vs equivalence ratio. (Adapted from Smoot, L.D. et al., *Propagation of laminar pulverized coal-air flames*, 16th Symposium International on Combustion, The Combustion Institute, Pittsburgh, PA, p. 375, 1976.)

### 5.3.3 Flammability Characteristics

The oxidation mechanism for solid fuels has been discussed from heat-up to devolatilization and char burnout. These mechanisms define the flame volume and the emissions. The local flammability of the HC volatiles is described in Chapters 3 and 4 of this book and will not be repeated here. However, solid fuels exhibit unusual flammability characteristics not found in liquid or gaseous fuels. The rich limit of flammability is almost infinite for solid fuel/air mixtures. This is due to the fact that all of the air is present, but much of the fuel still exists as unreacted char or volatiles. The gaseous air does not initially blend with fuel vapor as the fuel vapor is still in solid form and thus the ignitable gaseous mixture remains lean over a wide range, even though the actual mixture of air and solids can be very rich. In addition, the range of local stoichiometric mixtures near and around the solid particle ranges widely from high excess air to near zero when reacting. The situation can be quantified as shown by measurements of Smoot et al.<sup>10</sup> plotted in Figure 5.3.

## 5.4 Fuel Conveying

The pneumatic conveying of solid fuels can cause erosion depending on the fuel properties, pipe materials, and conveying velocity. Further, it is critical to be able to keep the solid material in suspension and be able to predict piping pressure drop for proper fan selection and distribution at the burner.

### 5.4.1 Pressure Drop Calculations in Solid/Gas Conveying

Pneumatic conveying of solids can be classified as dense phase or dilute phase transport. In the literature and

industry, there are varying definitions for these flows.<sup>11,12</sup> Dilute transport generally means that particles are pneumatically transported at many times their settling velocity. For example, 10%–20% of the stoichiometric air is a typical flow with a velocity at 60–100 ft/s (18–30 m/s). Actual flow and velocity will depend on particle sizes. Dense phase is used more for transport than in combustion systems.

When dense phase flow is used to transport solid fuels to a burner, the limit is usually about 5% stoichiometric airflow at a minimum of 80 ft/s (24 m/s). Dense phase flow is not recommended for solid fuel delivery due to slugging and plugging issues. An excellent treatment of dilute phase transport has been presented by Hinkle<sup>13</sup> and is summarized here for convenience.

#### 5.4.2 Horizontal Transport

For horizontal transport, Hinkle proposed the following relationships:

$$\Delta P_h = \frac{V_g^2 \gamma_g}{2g} + \frac{WV_p}{g} + \frac{fL\gamma_g V_g^2}{2gD} \left( 1 + \left( \frac{4f_p V_p}{fV_g} \right) \frac{W}{V_g \gamma_g} \right) \quad (5.13)$$

The first term is the initial acceleration of the gas, the second is the initial acceleration of the particles, and the last term is composed of fluid losses and losses based on friction of solids to fluid.

where

$\Delta P_h$  is the horizontal pressure drop in lbf/sq foot

$V_g$  is the gas velocity in ft/s

$\gamma_g$  is the specific weight of the gas in lbf/cubic ft

$g = 32.2$  ft/s<sup>2</sup>

$W$  is the solids loading in lb<sub>m</sub>/s/ft<sup>2</sup>

$V_p$  is the particle velocity in ft/s

$f$  is Darcy pipe friction factor

$L$  is pipe length in ft

$D$  is pipe diameter in ft

$f_p$  is the fluid to solid friction loss, defined as follows:

$$f_p = \frac{3\gamma_g C_d}{2\gamma_p} \frac{D}{D_p} \left( \frac{V_g - V_p}{V_p} \right)^2 \quad (5.14)$$

In addition,

$$\frac{V_p}{V_g} = \left( 1 - 0.179 D_p^{0.3} \gamma_p^{0.5} \right) \quad (5.15)$$

where

$C_d$  is the particle drag coefficient

$D_p$  is the diameter of the particle in inches

$\gamma_p$  is the specific weight of the particle in lbf/cubic ft

It should further be noted that the following term must always be less than unity or set to unity:

$$\frac{4f_p V_p}{fV_g} \leq 1$$

#### 5.4.3 Vertical Transport and Minor Losses

For vertical transport, Hinkel proposed the following:

$$\Delta P_v = \frac{fL\gamma_g V_g^2}{2gD} \left( 1 + \left( \frac{4f_p V_p}{fV_g} \right) \frac{W}{V_g \gamma_g} \right) + \frac{WL}{V_p} \quad (5.16)$$

where  $\Delta P_v$  is the vertical pressure drop in lbf/ft<sup>2</sup>.

After reviewing minor losses from a variety of references for many years, substitution of equivalent length of pipe for minor losses and the use of Hinkel's horizontal transport equation is recommended. For pneumatic conveying, always use large radius elbows. Pressure drop for short radius elbows can be modeled using *solids handling*,<sup>14</sup> but it is not recommended due to the large pressure drop.

The authors' experience with using Hinkel's method compares very closely with Ogawa.<sup>15</sup>

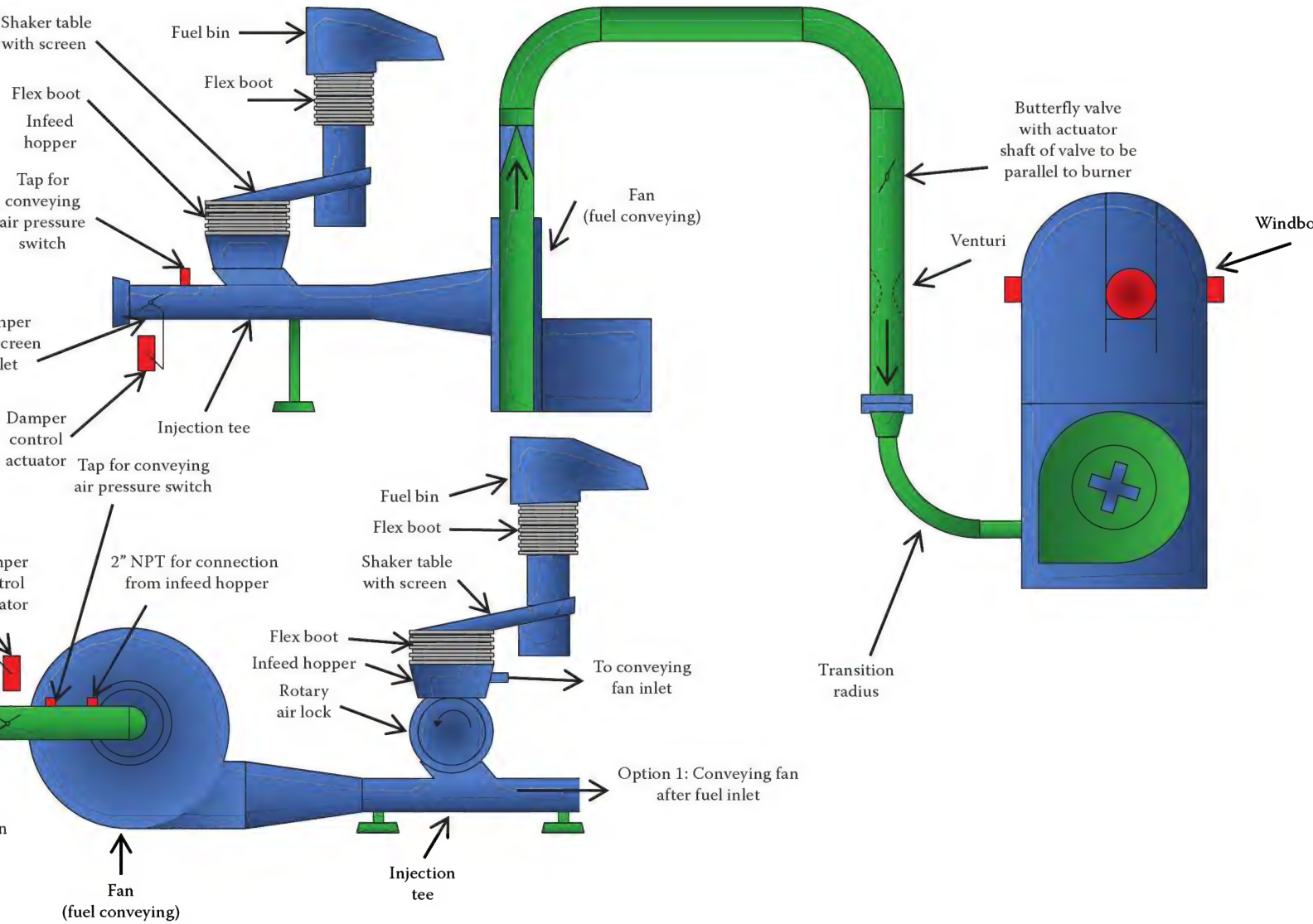
#### 5.4.4 Conveying Options

Figure 5.4 illustrates a standard arrangement for conveying solid fuels from the fuel bin to the burner in what is known as indirect firing. In this conveying option, the solid fuel is preground and delivered/metered to a fuel bin. The fuel can be introduced upstream of the fan under negative pressure and conveyed through the fan. Alternatively, the fuel can be introduced downstream from the fan via a rotary air lock feed and supply fuel under positive pressure. Both systems can be used and both have obvious and subtle pros and cons. For example, rotary air locks can leak and running solid fuel through a blower can cause fan problems. Note the recommended minimum horizontal run and the fivefold larger pipe radius elbows. In direct fired systems, as are commonly used in utilities, the fuel is metered and delivered directly to the mill and conveyed to the burners.

### 5.5 Burner Designs

Burners for solid fuel share many of the same features as gas and oil burners (see Volumes 2 and 3). Many of them may also be equipped to fire at a maximum on gas





ection for conveying options.

and/or liquid fuel. The key differences are the installation of a solid fuel injection pipe or annular scroll. Depending on whether the solid fuel is conveyed in the dense or dilute phase to the burner affects the burner internal area required to accommodate this.

Since the control of fuel and air mixing is also very important in controlling the fuel NO<sub>x</sub> generated by these burners, solid fuel burners often employ multiple air zones to delay fuel air mixing. The burners will likely have to accommodate a variety of changes in fuel conditions, such as moisture content, grind size, volatility, and heating value over their operational life. To help optimize performance as these conditions change, the burner will often have the ability to adjust ratios between the different air zones. The burner will also have features like adjustable register louvers to control the amount, and sometimes even the direction of combustion air spin.

Because solid fuel is abrasive, it will abrade away the burner components that it contacts over time. To accommodate this, solid fuels burners are typically equipped with replaceable components such as nozzles and wear plates.

#### 5.5.1 Utility and Multiburner Applications

In utility and multiburner applications, it is common to use multiple mills for grinding the solid materials to the right size and multiple conveying lines for distribution. The solids are pneumatically conveyed and supplied to the burners in the form of a round pipe in the center of the burner. Various styles of “register” burners are utilized to deliver the secondary air around the center in one or more zones with or without swirl. The furnaces are generally large for solid fuel burnout. At times, some units collect and reinject any unoxidized char.

For NO<sub>x</sub> control, it is common to use over-fired air (OFA), staged levels, or burners out of service (BOOS). Multiple variants to the simple round pipe have been implemented to control NO<sub>x</sub> by limiting mixing with the secondary register air.

#### 5.5.2 Industrial Burners

Industrial burners designed for solid fuels generally use an annular zone to inject pneumatically conveyed fuel into the furnace. These applications are usually a single burner and the furnace is small requiring more rapid mixing of the fuel and air. The burner is designed for higher turn down and may have features to reduce emissions (see Figure 5.5).

#### 5.5.3 Support Fuel

The use of support fuel varies according to specific job applications. Fuels with high ash and or moisture as



**FIGURE 5.5**  
Front of Coen biomass burner.

well as low volatility fuels may require support fuel at all times. Size distribution may be important depending on the fuel type. In many cases, the fuel delivery rate can vary requiring support fuel. In general, the amount of support fuel can vary from 2% to 10%. For utility applications, support fuel is generally not required due to preheated air and multiple burners. Many utility applications employ warm up and stabilizing fuel injectors using either natural gas or oil. They are used for startup and stabilization as the fuel properties vary.

### 5.6 Furnace and Control Considerations

The primary furnace considerations when firing solid fuels revolve around the high levels of ash that are generated. Furnace designs must contain provisions to minimize this ash from contacting cool boiler surfaces until the ash has cooled enough that it is no longer liquid or “sticky” and will generate slag formation. This typically involves increasing the size of the combustion chamber relative to what is used in a gas- or oil-fired application. For example, package boilers firing gas or oil may have a volumetric heat release in the furnace between 60,000 and 80,000 Btu/(h ft<sup>3</sup>) (620 and 830 kW/m<sup>3</sup>), while those same designs, when employed in solid fuel applications, may be derated to a range 30,000–50,000 Btu/(h ft<sup>3</sup>) (310–520 kW/m<sup>3</sup>).

Once the ash has cooled, some portion of it will drop out in the furnace, called “bottom ash,” and some portion will be carried out of the boiler with the flue gas, called “fly ash.” The boiler furnace must have some provision, such as drop-out sections, to allow the bottom ash to be collected and then removed from the



furnace. The fly ash is typically captured in the exhaust gas cleaning systems with baghouses, cyclones, or precipitators.

One alternative to the aforementioned system, where the ash is allowed to cool and be removed “dry” from the system, is to design the boiler furnace to operate in a “slagging” mode. In this case, the temperatures in the system are designed to keep any “bottom ash” at a high enough temperature that it remains liquid. This liquid ash, or “slag,” is then allowed to drain to a low point in the furnace and exit through a “slag tap” into a cooling pool.

---

## 5.7 Combustion Controls

Control of solid fuel firing is complicated by the fact that it is more subject to changes in fuel heating value than gas or liquid fuels. One of the major factors influencing the change in heating value is solid fuel’s ability to absorb moisture during its transport and storage. Through annual changes in humidity and rainfall, the moisture content of solid fuels can vary throughout the year. Since the fuel metering systems are based on providing either a metered mass or volume of fuel to the burner, changes in heating value due to either composition changes, moisture content, or grind size need to be addressed. In most cases, the use of oxygen trim systems that monitor the oxygen in the flue gas and make adjustments to the combustion air flow are used to compensate for these changes. For boiler systems that utilize induced draft fans, the furnace is controlled at a negative pressure, less than atmospheric. Therefore, care must be taken to minimize the amount of infiltrated air from leakages (tramp air) into the system as this will interfere with the ability of oxygen trim systems to effectively control the combustion airflow.

---

## 5.8 Emission Formation and Prediction

Coal is a domestically abundant hydrocarbon fuel with a lower cost per unit of energy than other common industrial or utility fuels, such as natural gas or fuel oil. Biomass combustion can make use of many waste products found in the timber, manufactured wood products, and agricultural industries. It not only provides a source of essentially free fuel, but can also eliminate many of the disposal problems associated with these byproducts. The environmental regulations faced by industry are one of the primary governing

factors that must be addressed when designing a new system. The associated costs to comply with mandated NO<sub>x</sub> emissions limits can be significant, especially if it requires the addition of costly flue gas treatment equipment. In these cases, the ability to reduce NO<sub>x</sub> emissions significantly through changes to the combustion equipment can make the difference as to whether a system can meet required NO<sub>x</sub> levels in a cost-effective manner.

In order to make significant reductions in the NO<sub>x</sub> emissions from solid fuel combustion without the use of flue gas treatment, a method must be found to reduce the conversion of fuel bound nitrogen (FBN) to NO<sub>x</sub>. Through the use of air staging, it has been possible to reduce the total NO<sub>x</sub> emissions by more than 50% over that of an unstaged system.

Coal, depending on type and origin, will contain between 1% and 3% FBN by weight. Raw wood typically contains 0%–0.25% nitrogen by weight. However, the glues used in manufacturing the panels can increase the nitrogen content of this waste to as high as 7%, with the largest FBN being observed with plants that are using new faster drying resins. The agricultural industry also produces a significant amount of biomass waste, such as rice husks or wheat straw, and increasing air quality regulations are greatly restricting the amount of field burning allowed. Plowing this material back into the soil can result in increased levels of crop disease and lower crop yields. These raw biomass materials can also contain comparatively high nitrogen levels, with typical values ranging from 0.5% to 2.5% by weight.

One major concern to utilizing these materials as an industrial fuel is the effect that they may have on the amount of regulated emissions being generated. In order to significantly reduce the amount of NO<sub>x</sub> from the biomass fuels, it is necessary to target the “Fuel NO<sub>x</sub>” conversion, since this results in the largest single contribution to the NO<sub>x</sub>. One proven method of reducing the amount of bound nitrogen that converts to NO<sub>x</sub> is to introduce the fuel into a primary combustion zone that is oxygen deficient, or substoichiometric. In this way, the nitrogen that is liberated from the fuel has little or no free oxygen with which to bond and therefore, mostly recombines to the inert N<sub>2</sub>. The balance of the air required to complete the combustion is introduced further downstream in a secondary combustion zone. This guarantees complete burnout of the fuel and reduces the temperature of the combustion products.

Solid fuel applications require similar emission predictions as in gas fuel burners. Carbon monoxide, UBHC, VOCs, and NO<sub>x</sub> are all important emissions. Kinetic rate equations such as 5.4 and 5.5 can be utilized when the flow and temperature fields are known to predict reduction in emissions. For the formation of emissions, rather

than destruction or oxidation of hydrocarbons, the equations are similar as shown in the following:

$$\frac{d(NO)}{dt} = 2Ae^{(-E/RT)}(O_2)_{eq}(N_2) \quad (5.17)$$

and

$$(O_2)_{eq} = \frac{k_o}{(RT)^{0.5}} (O_2)_{eq}^{0.5}$$

One generally accepted practice is to assume  $(O_2)$  in equilibrium with  $(O)$  and  $(O_2)$  concentration using the Westenburg (1971) results for  $k_o$ <sup>16</sup> for  $(O_2)$  equilibrium and Zeldovich constants,  $A$ ,  $E$  as measured by Bowman.<sup>17</sup>

The utilization of gas kinetic data for emission formation or hydrocarbon oxidation can be computed from detailed temperatures and species concentrations in the flow field in many ways such as the Rayleigh flux theorem.

Simply stated, in all cases, one can post-process thermal map data in some discrete volume form and/or insert into a CFD code using the Rayleigh flux theorem as follows:

$$\frac{\partial}{\partial t} \int_{Cv} n \rho dv = \int_{Cs} n \rho (V \cdot da) \quad (5.18)$$

where

- $n$  is chemical in mass units
- $t$  is time
- $\rho$  is density
- $v$  is volume
- $a$  is area
- $V$  is velocity vector

Where, described in words, the formation of  $(n)$  through the volume surface is equal to the integrated rate of formation over the control volume.

It is a simple extrapolation to extend this concept for even coarse volumes as follows:

$$\sum \frac{dn}{dt} \rho \Delta v = n \rho (V \cdot a) \quad (5.19)$$

Solid fuels generally contain a significant amount of elemental nitrogen in the fuel. A portion of the elemental fuel nitrogen is converted to  $NO_x$  during the entire process of oxidation. The range of this conversion is very dependent on the burner and furnace type as well as any  $NO_x$  reduction techniques utilized. The range can vary from 4% to 60% and is highly dependent on the amount of FBN in the fuel. The FBN contribution can be more or less than the thermal  $NO_x$  contribution.

From a practical perspective, carbon particulate can be calculated on every application as outlined with great accuracy using Equation 5.12. For most solid fuel applications, ash and sulfur compounds need to be added to the total particulate. Then, opacity can be computed based on total particulate loading and size distribution.

Very expensive or large applications will utilize computational fluid dynamics (CFD) to compute the total flow field, and post-process emissions utilizing the equations in this chapter with the appropriate destruction and formation kinetics (see Chapter 13). The fuel contribution to  $NO_x$  is a function of many factors and each burner manufactured will have a set of algorithms used for prediction.

## 5.9 Conclusions

The solid fuel fired burner system is a complex process involving heat-up, devolatilization, kinetics oxidation, char oxidation, diffusion, surface reactivity, and two-phase particle/gas flow. Solid fuel firing offers the advantage of being able to utilize lower cost hydrocarbon fuels such as coal or petroleum coke. Unique breakup/swelling or shrinking particle models will need to be applied based on experience with different fuel characteristics. Erosion needs to be considered for many solid fuels. Equally important is the up-front handling, supply, grinding, and conveying of the solid material.

Biomass fuels have potential additional advantages, such as being carbon neutral or eliminating waste disposal costs. Overall, there are many unique challenges that must be considered in the design of the system, including the following:

1. Fuel storage, preparation, and transport complexity
2. Higher  $NO_x$  emissions due to FBN
3. Higher particulate emissions due to ash content
4. Higher  $SO_x$  emissions due to sulfur content
5. Ash collection and disposal
6. Potential for slag formation, corrosion, and erosion in the boiler
7. Larger furnace requirements than gas- or oil-fired boilers
8. Increased fuel delivery system and burner wear due to abrasion
9. Increased monitoring of changes to fuel composition, such as moisture content



Although this chapter only briefly touched on upfront fuel handling, such handling can be a major problem to get everything sized correctly and this should be only left to truly experienced professionals for design.

## References

1. S.C. Stultz and J.B. Kitto, *Steam: Its Generation and Use*, 40th edn., Babcock and Wilcox, New York, p. 8.5, 1992.
2. L.D. Smoot and P.J. Smith, *Coal Combustion and Gasification*, Plenum Press, New York, pp. 81–90, 1985.
3. H. Kobayashi, J.B. Howard, and A.F. Sarofim, Coal devolatilization at high temperatures, *16th Symposium International*, p. 411, 1976.
4. A.F. Roberts, A review of kinetic data for the pyrolysis of wood and related substances, *Combustion and Flame* 14, 261–272, 1970.
5. P.C. Malte and B. Dorri, *The Behavior of Fuel Particles in Wood Waste Furnaces*, Western States Section of the Combustion Institute, Pullman, WA, April 13–14, 1981.
6. S. Londerville, Coen company internal files and codes on wood oxidation. 1982–2010.
7. R.B. Edelman, V.S. Engleman, W. Bartok, and J.P. Longwell, Experimental and theoretical studies of NO<sub>x</sub> formation in a jet stirred combustor, *14th Symposium (International) on Combustion*, The Combustion Institute, Pittsburgh, PA, 1973.
8. G.C. Williams, H.C. Hottel, and A.C. Morgan, The combustion of methane in a jet-mixed reactor, *12th Symposium (International) on Combustion*, p. 913, The Combustion Institute, Pittsburgh, PA, 1969.
9. R.B. Bird, W.E. Stewart, and E.N. Lightfoot. *Transport Phenomena*, John Wiley, New York, 1960.
10. L.D. Smoot, M.D. Horton, and G.A. Williams, Propagation of laminar pulverized coal-air flames, *16th Symposium International on Combustion*, The Combustion Institute, Pittsburgh, PA, p. 375, 1976.
11. D. Mills, M. Jones, and V. Agarwal, *Handbook of Pneumatic Conveying Engineering*, Marcel Dekker, Inc., New York, 2004.
12. F. Zenz and D.F. Othmer, *Fluidization and Fluid-Particle Systems*, Reinhold Pub. Co., New York, 1960.
13. B.L. Hinkle, PhD thesis, Georgia Institute of Technology, Atlanta, GA, June 1953.
14. K. McNaughton (ed.), *Solids Handling, Chemical Engineering*, McGraw Hill, New York, p. 130, 1981.
15. A. Ogawa, *Separation of Particles from Air and Gases*, Vol. 1, CRC Press, Boca Raton, FL, pp. 124–129, 1985.
16. A.E. Westenberg, Kinetics of NO and CO lean, premixed hydrocarbon-air flames, *Combust. Sci. and Technol.*, 4(1), 59–64.
17. C.T. Bowman, Kinetics of pollution formation and destruction in combustion, *Prog. Energy Combust. Sci.* 1, 33–45, 1975.

This page intentionally left blank

# 6

## Catalytic Combustion

Klaus-Dieter Zschorsch

### CONTENTS

6.1	Catalytic Combustion.....	137
6.2	Fundamentals.....	138
6.2.1	Process.....	138
6.2.2	Measurement and Control Engineering.....	139
6.2.2.1	Selection of Catalyst.....	139
6.2.2.2	Deactivation and Reactivation of Catalysts.....	141
6.2.2.3	Criteria for Selecting a Suitable Catalyst.....	141
6.2.2.4	Protective Measures against Catalyst Deactivation.....	142
6.2.2.5	Reactivation of Catalysts.....	142
6.3	Process Details.....	143
6.3.1	Reactor Types.....	146
6.3.2	Safety Systems.....	149
6.3.3	Prevention of Pollutant Enrichment and Overheating.....	149
6.3.4	Emergency Bypass.....	149
6.4	Detail Process Measuring and Control Engineering.....	150
6.5	Other Facility Components.....	150
6.5.1	Buffer Systems.....	150
6.6	Energy Demand and Heat Recovery.....	151
6.7	Different Design of Catalytic Waste Gas Cleaning Systems.....	152
	References.....	157

### 6.1 Catalytic Combustion

A wide variety of plants in the industrial sector emit polluted air containing volatile organic compounds (VOCs) and/or various inorganic compounds (e.g., carbon monoxide, hydrogen sulfide, hydrogen cyanide, and ammonia). Emission of these compounds can have harmful effects on human health, the environment, and the nearby surroundings of the factory, or they can be irritating due to bad odor. Throughout the world, there is a growing interest in reducing the emissions to prevent these harmful effects. Legislation, imposing of different directives, and implementation of environmental programs are being used to minimize air pollution. One of the ways to avoid the emission of undesirable compounds is to clean the polluted air stream before discharging it into the atmosphere. This can be achieved by combustion—thermal or catalytic—of the off-gas. The industrial sectors using combustion for air cleaning are

primarily chemical, pharmaceutical, paper and printing, painting and coating, petroleum refining, metal finishing, or rubber production.

The purpose of combustion is to convert the contaminants in the waste gas into harmless gaseous compounds such as CO<sub>2</sub> and H<sub>2</sub>O. Traditionally, thermal combustion has been used, requiring a combustion temperature of approximately 800°C–900°C (1500°F–1700°F). That means in a typical thermal incinerator, waste destruction occurs in the flame or by thermal oxidation because of high-temperature, gas-phase oxidation reactions. However, by using a catalyst, the rate of reaction is enhanced and the combustion can take place at much lower temperatures of 200°C–400°C (400°F–750°F) and with a shorter residence time in the “combustion chamber.” This results in lower energy consumption and a more energy-efficient process combined with a lower CO<sub>2</sub> emission. The lower combustion temperature also means lower NO<sub>x</sub> and CO emissions, and finally, it gives the possibility of using normal carbon steel as construction material.

Catalyst replacement costs must be considered regarding the use of catalytic combustion. The average lifetime of a catalyst is around 30,000–40,000 h of operation, making the catalyst costs comparatively low compared to the extra energy costs incurred if a catalyst was not used.

The design and construction of combustion units must comply with valid quality management standards, according to the latest technical rules and in full accordance with all relevant statutory directives. The fundamentals and method of catalytic combustion must be considered when designing and constructing a waste gas cleaning system. This includes the detailed catalytic selections, process layout and apparatus sizing, catalyst volume, and energy consumption in a catalytic system. While the description of the fundamentals and methods is a guideline, experience is necessary for efficient designs.

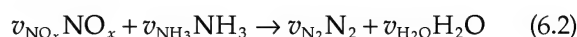
## 6.2 Fundamentals

### 6.2.1 Process

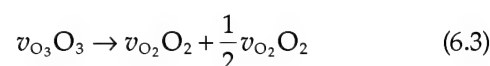
During catalytic waste gas cleaning, pollutants generally react with another compound on the catalyst's surface. This compound must either be available in the waste gas or must be added. One catalytic cleaning method or reaction is the oxidation of hydrocarbon combustion shown in the following:



The reduction of nitrogen oxides (e.g., in waste gas) from nitric acid plants with ammonia is a possible catalytic reaction as follows:



Another possibility is a simple decomposition of a pollutant such as ozone ( $O_3$ ):



Technical catalysts in catalytic oxidation systems are often bulk materials or molds. Bulk material can be balls, cylinders, or rings. The molds are in the shape of honeycombs or monoliths. The catalyst material is crossed by small and tiny capillary tubes and contains small cavities. This kind of porous catalyst has, in addition to their outer geometric surface, an inner surface. The inner surface is many times greater than the size of the outer surface and therefore is determinate of the catalyst activity. Nonporous catalysts (e.g., wires coated with precious metal) are not often used. Chemical reactions can occur on both the outer and the inner surfaces. A schematic illustration of the combustion process, taking place in a catalytic reactor, is shown in Figure 6.1.

The chemical conversion rate or destruction and removal efficiency (DRE) in catalytic combustion systems depends on the catalyst activity, the concentrations of the reacting partners and the reaction temperature. The activity of catalyst defines the quantity of the substance, which is converted per contact volume of catalyst and time measured under standard conditions. For a continued gas reaction in a reactor, the reaction partners in the gas-filled space must pass through the diffusion boundary layer

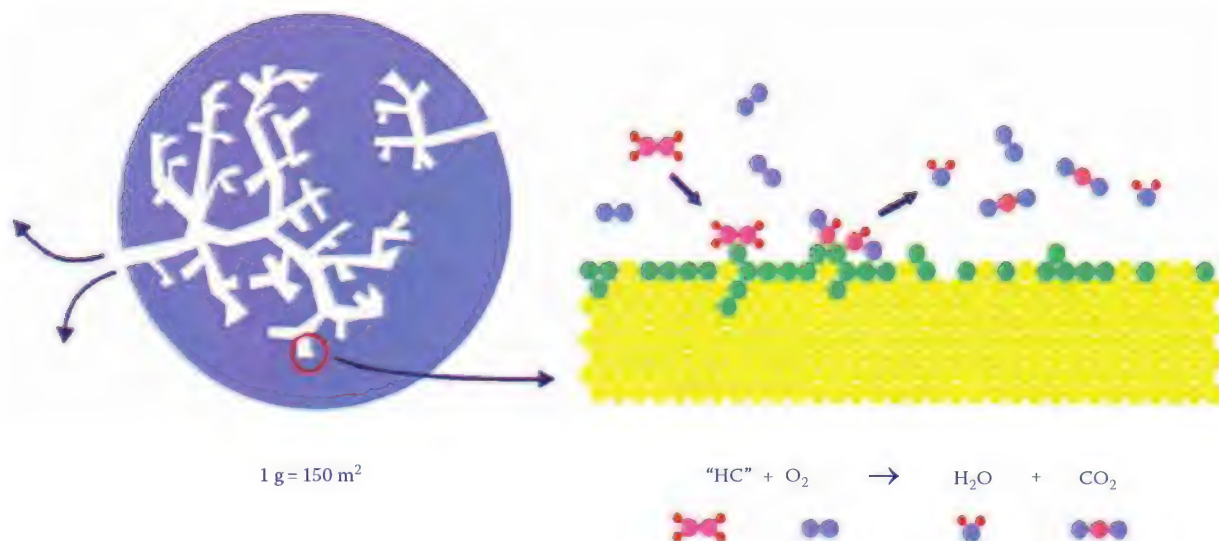


FIGURE 6.1  
Catalyst's function.



surrounding the catalyst to reach the outer surface. Gases are then diffused through the pores to the inner surface.

The reaction rate, which is exponentially dependent on the temperature, interacts with transport processes, which are generally much less dependent on the temperature. Isothermal methods can be differentiated into three areas (1) kinetic area, (2) pore diffusion area, and (3) substance crossover area (boundary layer diffusion area). The term “space velocity” is used for the catalytic system design of a reactor in reference to the isothermal method. Space velocity ( $R_G$ ) is defined as the ratio of gas volumetric flow  $\dot{V}$  to catalyst volume  $V_K$  in a standard state:

$$V_K = \frac{V}{R_G} \quad V \left[ \frac{m_{N^3}}{h} \right], \quad V_K [m^3], \quad R_G \left[ \frac{m_{N^3}}{(h \times m^3)} \right] \text{ or } [h^{-1}] \quad (6.4)$$

In practice, the  $h^{-1}$  unit is commonly used. The gas volumetric flow  $V$  is commonly related to the standard state (damp).

## 6.2.2 Measurement and Control Engineering

The measurement, recording, and control engineering of the catalytic system has to be performed so that all subsequent operating states can be controlled safely and reliably, and dangerous situations can be avoided. Specific operating conditions and various process parameters must be monitored specific to the application. Generally, minimum gas flow rate, mass flow rate, and the intake temperature of the catalyst should be monitored. The supply of waste gas into the catalytic system must be interrupted if the minimum temperature falls below acceptable operational levels. The delay between the measurement and the shut-off device must be taken into consideration. The oxygen content (minimum  $O_2$  content) may need to be monitored depending on waste gas conditions. The intake concentration of pollutants in the waste gas or polluted gas, which can be oxidized, must maintain a certain level before entry into the reaction zone.

For proper operation, monitoring of the catalyst bed temperature is necessary. Depending on the bulk height, it is important to take two or three quick temperature measurements (or a single measurement of the reactor emissions in the case of a honeycomb shape). At the start, the system will be heated with fresh air or circulated air. After a plant failure, the entire waste gas cleaning system must be cleaned using a flushing procedure. During a plant shut-down, the supply piping must be purged and the emission concentration of the organic components monitored.

Depending on the application, important safety control elements may have to be performed with integrated fault detection. In the case of a failure, the plant must not be restarted automatically. To safely operate the unit, safety control circuits are provided. Necessary control functions

are safeguarded with hardwire interlocks or programmable fail-safe control systems. (Volume 2, Chapter 2 provides a general overview of combustion controls.)

### 6.2.2.1 Selection of Catalyst

The popular definition of a catalyst is that it is a substance that accelerates a chemical process without being consumed during this process. A catalyst is composed of a carrier coated with an active material. The reason for the carrier is that often the active material has a very low mechanical strength and is very expensive. By placing the active material on a carrier, the required strength is provided, and at the same time, the expensive active material is spread out over a large accessible area.

Catalyst structures may be either full contact or supported catalysts. Full contact catalysts consist of an active phase. Various pollutants and catalyst poisons call for different types of active material, and the diverse sizes of plants and different dust loadings call for different physical shapes of the carrier. The active material is a metal oxide, a noble metal, or a combination the two.

Generally, noble metals such as palladium (Pd) and platinum (Pt) or transition metal oxide like oxides of titanium (Ti), vanadium (V), chromium (Cr), manganese (Mn), iron (Fe), cobalt (Co), nickel (Ni), and copper (Cu) are used for active materials. The oxides can be used in pure form, as compounds and with various additives. Additives in low quantities often cause a significant increase in activity. Full contacts are often inferior to the supported catalysts with regard to activity, but can in some cases provide certain advantages regarding the considerable activity reserve of the solid material. The activity reserve is useful with regard to poisoning or mechanical stress (abrasion). Supported catalysts are all catalysts with an active phase applied on a structural material—the carrier. The active phase determines the catalytic properties in interaction with the carrier. The mass fraction of the active phase in the catalyst is low (typical values for precious metal catalysts lie between 0.1% and 0.5%).

The active phase is applied preferably on the surface or in the surface layer (surface impregnation) and operate in the boundary layer diffusion area.

The carriers of the catalysts available today are pellets—formed as spheres (alumina) or rings (alumina or silica)—and monoliths made of alumina placed on a skeleton (see Figure 6.2). Carrier materials are metals and may be in the form of monoliths (honeycombs), formed sheets (expanded grids), turnings, wires, webbing, or nets. In many cases, metal oxides such as  $Al_2O_3$ ,  $SiO_2$ ,  $TiO_2$ ,  $ZrO_2$ , and  $MgO$  are either molded or natural, and synthetic minerals such as bims, mullite, cordierite, stellite, and zeolite are molded and used as carrier material.

Chemical or physical properties of the carrier can either exacerbate or even prevent the direct raising of

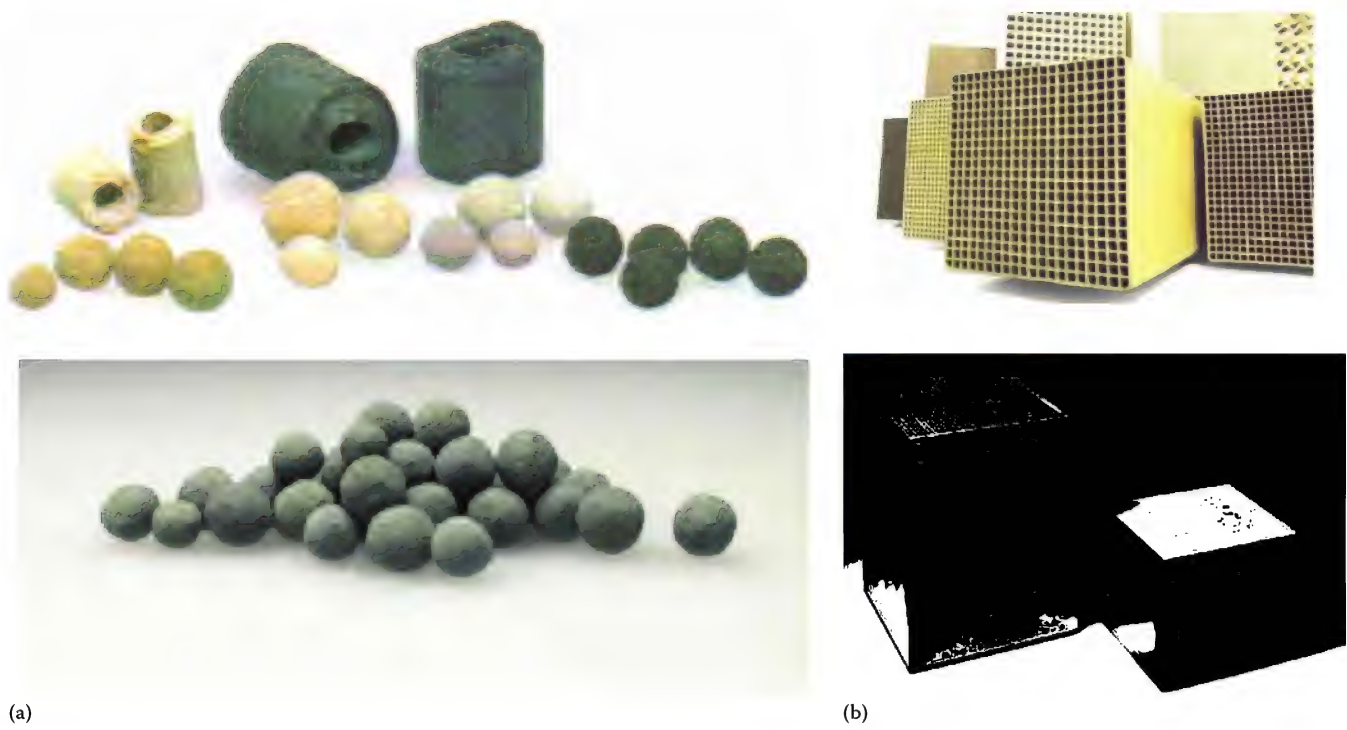


**FIGURE 6.2**  
(a) Bulk materials: pellets catalyst–spheres and rings (balls, rings, and cylinders) and (b) types of monolith catalyst monolith (honeycomb) material.

the active phase. In these cases, a thin intermediate layer (wash coat) of ceramic or synthetic fibers is applied on the substrate and then impregnated with the catalytic active component. By applying an intermediate layer, a large surface can be covered, which is important for both kinetics and the diffusion area.

The advantages of pellets are that they are less sensitive to poisoning due to more active material per air volume treated, and the cost is lower than monoliths. The greatest advantages of monoliths are a lower volume due to a higher activity per volume, a lower pressure drop, and the ability to let dust pass through the catalyst (see Table 6.1).

**TABLE 6.1**  
Catalyst Types in Different Processes

Process	Application in	Pollutants to Be Converted	Catalyst Form	Components
Oxidative methods	Refineries	CO, HCs, VOC	Monoliths, bulk materials	Metal oxides
	Chemical industry foundries			Precious metal catalyst
	Waste incinerators	VOC, PCDDF		Metal oxides
	Stationary motors	CO, HCs		Precious metal catalyst (three-way catalyst, precious catalyst)
	Food industries (roasting facilities, smokehouses)	VOC		Precious metal catalyst, metal oxides
	Paint manufacturers, printing plants	VOC		Precious metal catalyst, metal oxides
Reductive methods	Glass/mineral oil/chemical/steel/non-ferrous metal industrial	NO <sub>x</sub>	Monoliths, bulk materials (extrudates, balls, and pellets)	V <sub>2</sub> O <sub>5</sub> /TiO <sub>2</sub> /SiO <sub>2</sub> /WO <sub>3</sub> and other metal oxides
	Power plants, waste incinerators, stationary motors			
	Nitric acid manufacture	NO, NO <sub>2</sub> , N <sub>2</sub> O		Precious metal/Al <sub>2</sub> O <sub>3</sub> Metal oxides (e.g., Fe) zeolithes

General requirements of catalysts include high catalytic activity at a low working temperature; selectivity (only desired reactions accelerated); thermal, chemical, and mechanical reliability (temperature, knocks, friction, vibrations); high service life; low pressure loss; regenerability; environmentally friendly disposal; and ease of handling.

Catalysts may undergo physical or chemical changes during operation. Reasons for these changes include diffusion and migratory processes on the surface or in the catalyst interior, phase changes, recrystallization, and formation or decomposition of surface compounds or of functional groups on the carrier surface. In practice, a waste gas catalyst must be able to cope with different operating conditions.

Depending on the area of application and the catalyst type, the space velocities must be between approximately 2,000 L/h (reductive method) and approximately 300,000 L/h (CO oxidation for stationary motors) and the operating temperatures of waste gas cleaning catalysts range between room temperature (ozone disintegration) and a maximum of approximately 800°C (1500°F).

#### 6.2.2.2 Deactivation and Reactivation of Catalysts

Catalysts are deactivated and reactivated in catalytic waste gas treatment systems.<sup>1-4</sup> Catalysts naturally age and have a limited expected service life. Under certain marginal conditions, deactivation mechanisms can also cause a premature loss of function. The term, "catalyst deactivation," describes the reduction of operational activity compared to the initial activity.

Several parameters determine the activity of the waste gas catalyst material including kind, type, and composition of the catalytic material, distribution of active components on the catalyst, specific contact surface, size, and number of pores, and mass transport of the substance to and from the reaction sites.

Causes of catalyst deactivation mechanisms may be chemical, thermal, or mechanical. Chemical deactivation is a result of unwanted reaction between the waste gas and the catalyst. This can result in the catalytic properties being directly impaired due to substance changes in the catalyst and the reaction sites, fouling by reaction products specifically over the active sites, blocking the catalyst surface with strong sorptive bonds and/or chemical reactions, or covering the catalyst non-specifically. Additionally, a contact reaction with the waste gas can lead to loss of mechanical stability in the catalyst, which in turn can cause deactivation due to material degradation or the loss of structure. Chemical changes in the catalytic material are often irreversible; however, deactivation caused by deposits can be partially rectified. The substances responsible for chemical

deactivation include halogen compounds (HCl, HBr, and HF), compounds that contain sulfur (reversible poisons), elements such as phosphorus, arsenic, silicon, and lead, and alkaline earth metals (irreversible poisons).

Thermal deactivation is either caused by extreme temperature peaks or by a constant excessive operating temperature. The conversion of high concentration of pollutants will occur generally at the extreme temperature peaks of the catalyst. Also, if the pollutants are sorptively bonded to the catalyst, sudden oxidation, when the catalytic waste gas cleaning process is started, may result. The valid temperature ranges to prevent thermal deactivation are specified by the catalyst manufacturer and are based on the catalyst type. Thermal deactivation is not reversible.

If subjected to temperatures between 1200°F (650°C) and 1350°F (730°C) for extended periods of time, many catalysts will begin to suffer significant damage as a result of sintering. Sintering is the melting and coalescence of the active catalyst material, which results in a loss of available catalyst surface area and, consequently, a loss of catalytic activity. The rate of sintering increases rapidly with increasing temperature. A catalyst that shows the first signs of damage at 1200°F (650°C) will likely be severely damaged in a matter of hours at 1500°F (820°C). Therefore, for long-term operation and the best DRE, the catalyst bed needs to be maintained above the temperature at which high-rate reactions occur, but below the temperature at which significant sintering occurs. Typical catalyst outlet temperatures are in the range of 600°F (320°C)–1000°F (540°C). The reduction of activity may trigger sintering on the catalyst surface, changes in shape and structure (e.g., crystal grating, modification), and material migration on the catalyst's surface (active sites).

Deactivation due to mechanical influences is caused by wearing of catalyst material, either due to abrasive particles in the waste gas being treated or due to frictional movements in the catalyst when in operation (plant vibrations), or deposits of particles on the catalyst's surface together with impaired substance conveyance.

#### 6.2.2.3 Criteria for Selecting a Suitable Catalyst

When selecting a suitable catalyst, resistance to chemical attacks or thermal deactivation must be taken into consideration. Also, the presence of deactivating substances in the waste gas should be considered from the outset. An analysis of the waste gas is generally required to determine valid concentrations. Substances and processes that influence the composition of the waste gas must be taken into account. If the operating conditions and failures are variable or unknown, pilot studies should be conducted to determine the deactivating effect of the waste gas.

The activity of used catalysts is determined by standardized activity tests. These tests use conversion temperature patterns and start temperatures to determine the activity with synthetic waste gas mixtures. The causes for the reduction in activity can be determined by studying the substance composition and morphology of the catalyst. These studies can also reveal the deactivation process conditions, the remaining lifetime of the catalyst, and the possibilities for reactivation.

#### **6.2.2.4 Protective Measures against Catalyst Deactivation**

The treatment process and the method of protecting a catalyst require a careful design with a good understanding of the operating conditions and a thorough knowledge of the waste gas composition. Adequate or sufficient experience should be available combined with pilot test results. Only waste gases with a known composition should be cleaned in the catalyst. Catalytic waste gas cleaning must comply with legal regulations based upon technical guidelines or specified air quality standards. Problems may arise during the removal of certain compounds, such as sulfur, halogen, nitrogen compounds, or carcinogenic substances. Here, it is best to use a combination of methods or use a more suitable catalyst material.

The protection against chemical deactivation requires measures for preventing catalyst poisoning due to chemical reactions and must be implemented in specific manners. Possible prevention measures are selecting stable carriers and active components, operation at high temperatures, thereby preventing the condensation of organic substances, coking and strong adsorption of reaction partners or products, regular regeneration due to combustion or curing (e.g., in the event of coking, adsorption), desorption (e.g., by blowing out with air in the event of adsorption), and additional heating if necessary. The measures also include use of combined pretreatment processing stages, such as pre-separation of aerosols, catalyst poisons, and particles by prefiltration and prewashing, condensing substances contained in the waste gas (e.g., low-boiling organic compounds), and preceding adsorption. Often suitable prevention can be achieved by adding guard beds or sacrificial layers to protect the main catalyst, using a multi-bed catalyst arrangement for selective progressive reactions, and providing a suitable temperature profile to prevent fouling and insufficient temperatures.

An increase in structural changes (e.g., crystal formation, sintering, and phase change) in the catalytic material, together with the attrition of the inner surface and impaired distribution of active components can be caused by increasing temperatures. The use of

temperature-stable catalysts allows waste gases to be treated at high temperatures. Temperature increases that result from higher concentrations (e.g., in the event of solvent oxidation) must be prevented through the implementation of control measures.

The stability and instability of the reactor must be considered when estimating the expected temperature increase in the catalyst bed. Fixed-bed catalytic reactors have a two-phase system (solid/gas). Within the system, unsteady relationships are sporadically established, influenced by current substance transport and heat transfer rates, heat retention and reaction kinetics, and where the waste gas temperature does not correspond to the temperature in the reaction zone. The differences may be higher or lower than the adiabatically calculated temperatures. They are also noticeable by a migration of the reaction zone within the reactor—this is the layer of the catalyst in which the main substance conversion takes place. The site of the reaction zone can be measured using a steep temperature increase in the catalyst bed. These effects and their negative influence on the thermal demands on the catalyst can be counteracted by controlling the preheat temperature of the waste gas, by external heating or cooling, integrated heat exchangers, or a controlled operation of an additional heater (gas fired or electrical). Catalyst manufacturers allow for unsteady procedures with a short-term maximum temperature capacity.

At low temperatures, catalysts work as an adsorption material. To prevent spontaneous oxidation and related spontaneous heating of adsorbed pollutants at these temperatures, the catalyst must only be supplied with waste gas containing pollutants during normal operating temperatures. This requires the catalyst to be preheated to the required operation temperature.

The catalyst can be protected from mechanical deactivation by implementing technical measures for reducing the mechanical demands on the catalyst. The protection can be provided by suitable flow routing, reactor construction, monitored plant operation, operationally oriented maintenance intervals, and pre-separation of particles. Further, selecting a suitable catalyst shape protects it against damage due to mechanical loads.

#### **6.2.2.5 Reactivation of Catalysts**

After the performance of the catalyst has been reduced by deactivation, the original activity level may be partially or fully restored, depending on the condition of the catalyst. This is achieved by reactivation measures selected according to the condition of the catalyst. Determining the best reactivation measure depends on the condition of the catalyst using methods such as visual observations to check for fouling,



discoloration, and cracks. Also, x-ray fluorescence analysis (XRF) may be done to determine changes in the basic composition compared to a reference model and a wet chemical analysis may be done to determine the concentration of the elements, which have been identified as deactivating. The most widely used technique for estimating surface area is the so-called BET method.<sup>5</sup> The BET surface analysis to determine the amount of reduction in the catalytic surface or an activity test, to measure the activity of the used pattern before and after the reactivation compared to a reference model may also be used.

### 6.3 Process Details

A variety of catalysts are used in catalytic incineration for initiating and supporting the reaction. The operating temperatures normally lie in the range between 250°C (480°F) and 600°C (1100°F). However, some applications have operating temperatures as high as 800°C (1500°F). The operating temperature is dependent on the type and concentration of pollutants and on the properties of catalyst. Given sufficient reaction enthalpy of the substances to be oxidized, it is possible to omit the use of additional energy.<sup>6-10</sup>

The process of catalytic waste gas cleaning can be divided into three fundamental steps: (1) treatment or pretreatment of the waste gas, (2) mixture of the reaction partners, reaction (oxidation) at the catalyst, and, if necessary, (3) after-treatment of the cleaned waste gas. However, in special cases, to ensure operation within the permissible working range, the waste or raw gas should undergo conditioning or precleaning. To protect the catalyst, ensure safe facility operation and prepare the reaction, it is often necessary to condition the waste gas being treated.<sup>6</sup> This conditioning can take place in one, or several process steps and depends on the chemical and physical properties of the treated waste gas, the required clean gas parameters, and the required operational parameters of the catalyst.

The construction of catalytic waste gas cleaning facilities depends on the application and the catalytic method chosen. Generally, heating to the necessary reaction temperature or minimum inlet temperature is required. Usually heating takes place by means of a heat transfer unit, with extensive utilization of the heat energy of the cleaned waste gas, and by means of an additional heating system. Only when reactions are already at the raw gas temperature will no preheating be necessary. Figure 6.3 shows the construction principles of a catalytic waste gas cleaning facility. In a heat transfer unit, the raw gas is already largely preheated and, if required, subsequently heated again to the necessary catalyst operating temperature.

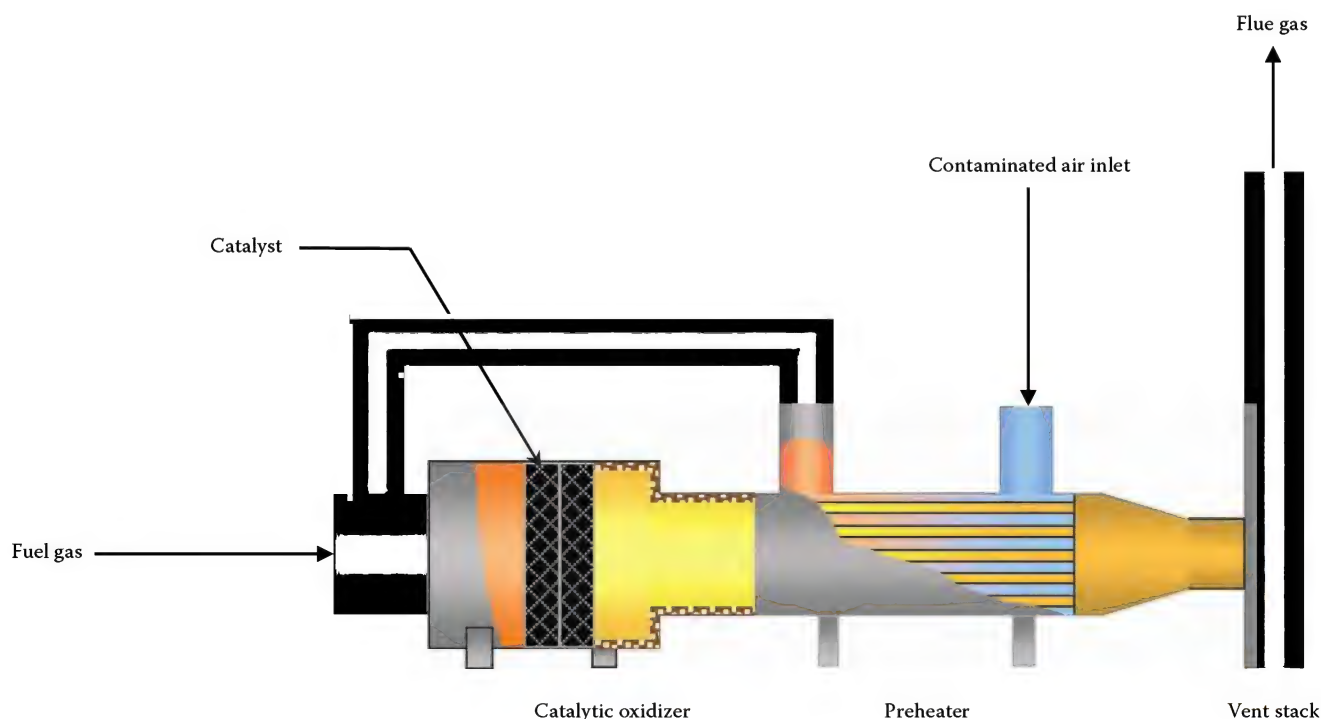


**FIGURE 6.3**  
Typical horizontal catalytic system with a preheat exchanger.



**FIGURE 6.4**  
Typical compact catalytic waste gas cleaning system.

Possible heaters include gas and oil burners (in the event of direct heating, the catalyst's suitability should be checked) or indirect heating by means of a heat transfer unit or electrical heaters. Indirect heating can be provided with heat-exchanger oil, steam, or hot water. The catalytic reaction is exothermic (i.e., the conversion releases heat energy) such that the waste gas temperature increases in accordance with the heating value of the pollutants. The needed heating power is then reduced and, if possible, turned off entirely. In this case, the system operates autothermically meaning without external additional heat. The clean gas is discharged into the atmosphere via the heat transfer unit (recuperative or regenerative).

The catalytic waste gas cleaning system can be provided in a compact design (see Figure 6.4), which includes all the required equipment parts in one vessel. The vessel consists of the heat exchanger, electrical heater, the reactor filled with catalyst, and also internal ducting for connection to other equipment.

Important parameters of the catalytic process for waste gas cleaning are waste gas properties, reaction temperature (or minimum temperature), pressure, and space velocity. The catalyst itself and the reactor that accommodates the catalyst are the most important components of the catalytic method. The form, manufacturing, types, and disposal of catalysts are described in Sections 6.1 and 6.2. The catalysts used predominantly for industrial applications are bulk catalysts. Honeycomb catalysts (monolithic catalysts) are preferred for larger volume flows and in internal combustion engines. Filter systems with catalytic action are also used for special applications such as the oxidation of special components.

Depending on the waste gas properties, there are typical applications for an oxidative catalytic waste gas cleaning system.

Table 6.2 lists the pollutants that can be decomposed with the help of such a system. The presence of substances that can act as catalyst poisons must be considered.

The reaction temperature (see Figure 6.5) required to achieve a desired conversion rate  $>99.5\%$  is determined essentially by the pollutant that needs to be removed and the specified space velocity. The catalyst's "conversion temperature behavior" during catalytic waste gas cleaning describes the percentage of pollutant removal as a function of reaction temperature. Conversion rates greater than  $99.5\%$  require a significant amount of catalyst, which increases the capital cost.

The polar properties of compound and number of multiple bonds in the molecule have an impact on how easily components can be oxidized. If the composition of the organic components of the waste gas is known, the required input temperature range should be established. Aromatic compounds and most aliphatic ones can be oxidized between  $210^{\circ}\text{C}$  ( $410^{\circ}\text{F}$ ) and  $350^{\circ}\text{C}$  ( $660^{\circ}\text{F}$ ), inorganic nitrogen and sulfur compounds and CO at very low temperatures between  $150^{\circ}\text{C}$  ( $300^{\circ}\text{F}$ ) and  $250^{\circ}\text{C}$  ( $480^{\circ}\text{F}$ ). Heterocompounds that contain oxygen, nitrogen, or sulfur can be oxidized very easily with a temperature range between  $180^{\circ}\text{C}$  ( $360^{\circ}\text{F}$ ) and  $250^{\circ}\text{C}$  ( $480^{\circ}\text{F}$ ). The temperatures for the conversion of halogen-containing pollutant components (e.g., during the removal by suction of soil atmosphere) are higher than those for hydrocarbons.

For safety reasons, the catalyst's inlet temperature must be chosen to be sufficiently high to avoid adsorptive effects by the pollutants on the catalyst. Odors and low pollutant loads (e.g., in the food industry) can be oxidized or minimized with the help of conventional catalysts in the temperature range between  $210^{\circ}\text{C}$  ( $410^{\circ}\text{F}$ ) and  $350^{\circ}\text{C}$  ( $660^{\circ}\text{F}$ ). Odor minimization can be carried out at room temperature with special catalysts, provided that adequate preliminary precipitation of aerosols and grease particles takes place.

The temperatures listed earlier, at which a conversion rate  $>99.5\%$  takes place, are important for the design of catalytic waste gas cleaning facilities. Conversion rates as a function of temperature determine the input temperature range and thus the facility's cost-effectiveness.

The minimum temperature necessary for a catalytic reaction is specific to each catalyst and is not a fixed property. This depends on the substance or mixture to be converted, the space velocity, and other parameters (e.g., on temperature elevation ( $\Delta T$ ) during the reaction). In the case of aging, poisoning, or deposits, the minimum temperature can be adjusted (i.e., increased). The waste gas temperature rises due to the exothermic nature of the oxidation process. The temperature elevation,  $\Delta T$ , depends on the concentration and the conversion rate of the components contained in the waste gas stream.

TABLE 6.2

Typical Reactions in Catalytic Waste Gas Cleaning

Pollutant Group	Overall Reaction	Catalyst Type	Products	By-Products	Applications	Impacts/ Risks
VOC, formaldehyde	$C_mH_n + (m + n/4) O_2 \rightarrow mCO_2 + n/2 H_2O$ $HCHO + O_2 \rightarrow H_2O + CO_2$	Noble metal, mixed oxide	$CO_2, H_2O$	$NO_x$	Cleaning, chem./pharm. production, industrial degreasing, film manufacturing, groundwater/soil decontamination, combustion engines	
Halogenated hydrocarbons (e.g., chlorinated CHC, $C_2H_4Cl_2$ , etc.)	$C_2H_4Cl_2 + 2.5O_2 \rightarrow 2 CO_2 + H_2O + 2 HCl$	Noble metal, mixed oxide	$CO_2, H_2O, HCl, Cl_2^{b)}$	$Cl_2$	Waste incineration facilities, pharmaceutical and chemical industry	Poisoning, corrosion
Carbon monoxide	$CO + \frac{1}{2}O_2 \rightarrow CO_2$	Noble metal, mixed oxide	$CO_2$	—	Combustion engines, wet oxidation, therm. Waste gas incineration	Poisoning, halogens, powders
Soot	$C + O_2 \rightarrow CO_2$ $C + 2NO_2 \rightarrow CO_2 + 2NO$	Noble metal,	$CO_2$		Engines, soot particle filters	
$NH_3, HCN$	$NH_3 + \frac{3}{4}O_2 \rightarrow \frac{1}{2} H_2O + \frac{1}{2}N_2$ $HCN + \frac{1}{4}O_2 \rightarrow CO_2 + \frac{1}{2}H_2O + \frac{1}{2}N_2$	Noble metal, mixed oxide	$N_2, H_2O, CO_2$	$NO_x$	Combustion engines, furnaces, stripping facilities (waste water cleaning)	
Ozone	$O_3 \rightarrow O_2 + \frac{1}{2} O_2$	Noble metal, mixed oxide	$O_2$		Ozone decomposition, ozone generators, ultraviolet drying	Efficiency depends on air humidity
Sulfur dioxide $SO_2$	$2SO_2 + O_2 \rightarrow 2 SO_3 (Abs.)$	Noble metal, mixed oxide	$SO_3, H_2SO_4$		Waste gas from paper manufacturing, waste gas from starch production, Claus unit power stations, $DeSO_{NO_x}, SNO_x$	
$H_2S, CS_2, COS$	$H_2S + 2O_2 \rightarrow SO_3 + H_2O$ $CS_2 + 4O_2 \rightarrow CO_2 + 2SO_3$ $2COS + 3O_2 \rightarrow 2CO_2 + 2SO_2$	Noble metal, mixed oxide	$CO_2, SO_2$	$SO_3$	Iron ore calcinations, catalytic waste gas desulphurization	
Special components (e.g., CDD/F, PAH)		$TiO_2, V_2O_5, WO_3$	$CO_2, H_2O, HCl,$		Waste incineration facilities, special waste incineration facilities, sintering facilities, crematoriums	

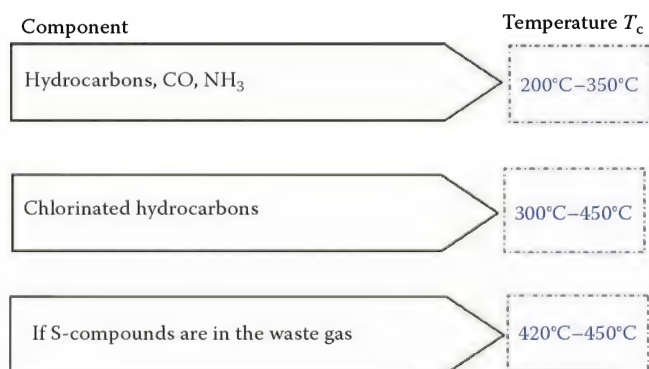


FIGURE 6.5

Typical required reactor inlet/reaction temperature,  $T_c$ .

Table 6.3 lists examples of the minimum catalyst inlet reaction temperatures for a number of compounds that are required in order to achieve a conversion rate >99.5%.

Normally, the process works under atmospheric pressure. However, it can also be used at other pressures that are adapted to the operating pressure of the process causing the emissions. As a rule, catalytic oxidation efficiency increases with increasing working pressure. Typical high-pressure applications are inert gas treatment systems. It is possible to treat an inert gas stream, such as nitrogen or  $CO_2$ , which may be contained by a small amount of hydrocarbon. This requires adding of small amount of oxygen. A minimum outlet concentration of approximately 1000 ppm is required.



TABLE 6.3

Examples of Minimum Inlet Temperature for Various Fresh Catalysts

Raw Gas Components		Raw Gas Components	
Ethylene	300°C	Dibutyl phthalate	275°C
Butane	290°C	Pyridine	250°C
Butylene	230°C	Dibutyl phthalate	275°C
Heptane	275°C	Pyridine	250°C
Benzene	300°C	Tributylamine	200°C
Toluene	270°C	Dimethylformamide	230°C
Xylene	280°C	Toluol diisocyanate	285°C
Naphthalene	270°C	Chlorobenzene	350°C
Methane	450°C	Chloroform	350°C
Methanol	190°C	Thiophene	320°C
Formaldehyde	190°C	Offset printing solvent	260°C
Ethanol	210°C		
Propanol-1	210°C	CO	180°C
Pentanol-1	200°C	HCN	250°C
Cresol	240°C	<i>Odor removal in the processing of onion/garlic</i>	200°C
Di-isobutyl ketone	210°C	H <sub>2</sub> S and CS <sub>2</sub>	200°C
Methyl ethyl ketone	240°C	Coffee	180°C
Butyric acid	200°C	Carcasses in rendering plants	200°C
Phthalic acid anhydride	270°C	NH <sub>3</sub>	270°C
Malenic acid anhydride	200°C	Large kitchens, restaurants	From 20°C

The central component of the catalytic process is the reactor that accommodates the catalyst. The reactor's design and dimensions are determined by the volume flow, the required space velocity, and the selection of catalyst type and form. The reactor's dimensions are a function of the specified reaction conditions, according to the permissible flow velocity resulting from the cross section.

### 6.3.1 Reactor Types

The reactor's design and form depend on the type of catalyst, the operating temperature, the working pressure, and the conduction of the flow. For bulk catalysts, a cylindrical reactor cross section (Figure 6.6) is preferred for high operating temperatures. Experience has shown that the cylindrical design works best if the operation temperature is greater than 480°C (900°F) and temperature difference will be greater than ( $\Delta T_c$ ) 150 K (270°F). The catalyst is arranged here as a packed bed layer and is normally placed on a grid with a wire screen. Under low thermal specifications (low internal stresses), reactors with square or rectangular cross sections can also be used. They can be designed as single-bed reactors

or, if larger cross sections are required, as multiple-bed reactors (see Figure 6.6). Horizontal arrangements can be chosen in cylindrical or, in compact facilities, rectangular form. (This design is, however, limited by a maximum operating temperature of 480°C (900°F) and temperature difference ( $\Delta T_c$ ) lower than 150 K = 270°F.) Catalyst beds in the form of a cylindrical ring are less common. This arrangement is susceptible to bed settling, which can cause undesirable marginal flows.

In facility designs that incorporate regenerative heat recovery, often the reactor is equipped with two separate chambers, each of which holds a catalyst bulk bed and a filling body packed bed as a regenerative heat transfer system.

Channeling in the perfusion flow and undesirable cavities at the reactor's wall or within the packed bed decreases the system efficiency and can lead to problems. Structural approaches to the prevention of channeling include a suitable sealing of the grids or of the wire cloth relative to the container's wall. The wire cloth should be attached in packed beds such that the catalyst cannot be deformed or run off as a result of mechanical or temperature-dependent movements in the bed or in the reactor material.

Reactors constructed for monolithic (honeycomb and plate) catalysts are different from those constructed for bulk material catalysts. Monolithic catalysts are used either in cylindrical or in cuboids form. Unlike packed beds, no transverse mixing takes place inside a monolith. These designs require a uniform incoming flow and a successful flow distribution.

Cylindrical catalysts consist normally of a catalytically coated metal matrix framed by a sheet-metal jacket. With small waste gas volume flows in particular, such cylindrical catalysts are assembled into reactors by way of simple welded construction, by welding the sheet-metal jacket to the required pipeline part (cone, flange, etc.). This form offers the advantage of an especially low pressure drop, in any assembled position.

More expensive reactors permit the replacement of cylindrical catalyst modules without disassembling the reactor itself. The systems feature removable side-sections. One or several catalyst modules are inserted with a resilient sealing ("soft sealing") and can be removed again at any time. The resilient sealing serves to space the elements apart and prevent bypass flows.

Cuboid catalysts are based either on metallic or ceramic monoliths (see Figure 6.7). Metal monolithic catalysts with rectangular flow cross sections are also available as modules with a sheet-metal jacket. In the event of larger waste gas volume flows, several of these modules are assembled into a rectangular flow cross section of any required size. If necessary, multiples of such a system can be arranged in sequence in the flow direction in "layers."



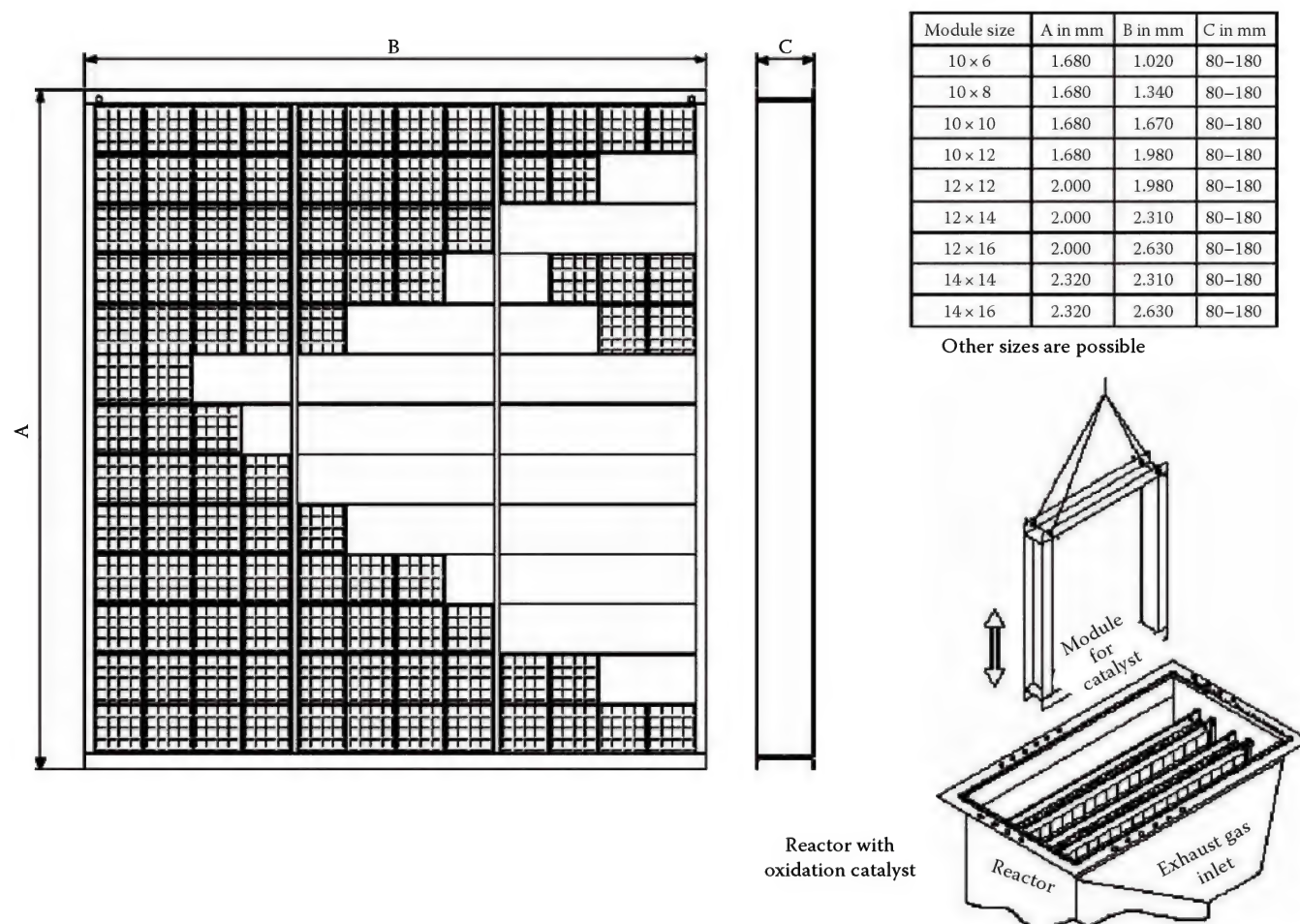


FIGURE 6.6

The arrangement is a catalyst facility consisting of ceramic monoliths.

Ceramic catalyst monoliths (Figure 6.7) are available as standard with a flow cross section of 150 mm × 150 mm (5.9 in. × 5.9 in.). Normally, several such monoliths are packed with “soft sealing” in a frame or a sheet-metal jacket. The resulting module is used either as a complete catalyst layer in a reactor or as a component of one. Depending on the reactor’s construction, one or several catalyst layers may be used. Both vertical and horizontal flow reactors are common; in principle, tilted arrangements are also possible. When assembling monolithic modules, leaks between the modules or cassettes and at the seating surfaces should be prevented structurally and by means of sealing.

Depending on the design of particular catalytic waste gas cleaning facilities, the excess heat released during the catalytic reaction should be removed by means of suitable systems. The design is determined by the type of primary heat recovery (regenerative or recuperative) or the installed waste heat usage, since unregulated operation may cause the catalyst to overheat.

To ensure a homogenous temperature profile across the entire catalyst bed, the reactor’s container should be thermally insulated in accordance with the specific requirements.

The choice of the reactor’s fabrication material is based on the gas composition (paying careful attention to the reaction products) and the design temperature, taking into account a possible temperature rise. When selecting the material, consider acid formation in the process gas, especially through halogen-containing pollutants, which requires the use of special corrosion-resistant materials (e.g., austenitic steels). Table 6.4 contains some general suggestions for material selection.

The calculation of catalytic reactors proceeds on the basis of the specific conditions and problems associated with any given case, the known waste gas data and the technical reaction quantities (kinetic and thermodynamic quantities). These can be determined experimentally for the particular components undergoing treatment, or found in manuals or tabulated reference books. Where, for example, a multicomponent mixture

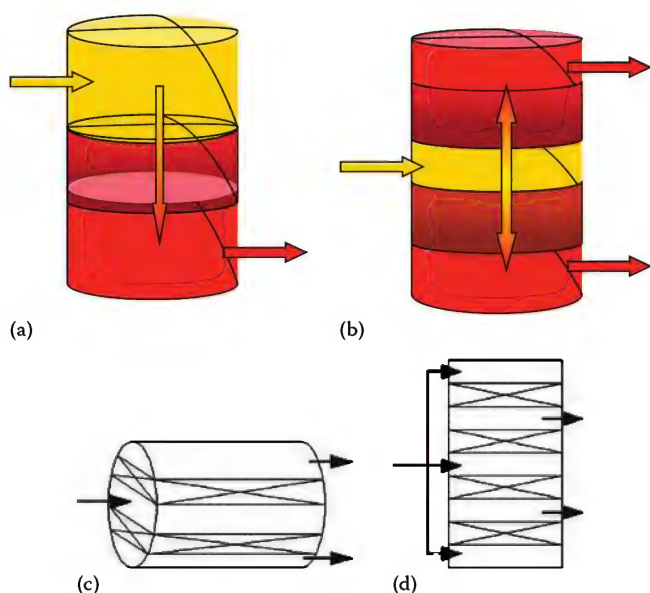


FIGURE 6.7

Reactor designs and flows: (a) Single-bed reactor, (b) vertical two-bed reactor (operating temperature  $> 480^{\circ}\text{C}$ ,  $\Delta T_c > 150\text{ K}$ ), (c) horizontal cylinder two-bed reactor (operating temperature  $> 480^{\circ}\text{C}$ ,  $\Delta T_c > 150\text{ K}$ ), and (d) multiple-bed reactor.

TABLE 6.4

Notes on Material Selection

Design Temperature in $^{\circ}\text{C}$	Construction Material
Up to 450	Ferritic steels
500	High-temperature ferritic steels
$>550$	Austenitic steels
$>600$ (700)	High-temperatures austenitic steels

of unknown composition is involved, such reactor calculations are only possible to a limited degree. Therefore, sufficiently extensive measurements should be performed on the raw gas being cleaned. In practice, semi-empirical reactor designs are referenced. Often, the calculations are based on conversion-temperature curves obtained experimentally in testing facilities.

The conversion rate for particular substances is affected by factors such as temperature, space velocity and geometry, empty space velocity, catalyst type and active components, active catalyst surface, activity loss/aging or catalyst poisoning, partial oxygen pressure, and partial water vapor pressure.

At the heart of the catalytic method lies the reactor that serves to hold the catalyst. The reactor's design and dimensions should be established by the size and shape of the catalyst bed. The size and shape of the catalyst bed is determined by the specified process conditions, required reaction temperature curve, the permissible space velocity, the permissible pressure drop over the catalyst bed, the selected catalyst type and reaction behavior.

Begin by selecting a suitable space velocity as a function of the associated temperature. The space velocity and, thus, the catalyst's content should be selected on the basis of factors such as catalyst type and geometry, required service life (operating hours), gas composition, possible catalyst poisons, required conversion rate, and accruing operating costs (fuel, catalyst, blower operation).

The space velocity  $RG$  is defined as the ratio of the total volume flow  $\dot{V}$  to catalyst volume  $V_K$ :

$$RG = \frac{\dot{V}}{V_K} \quad (6.5)$$

The space velocity  $RG$  is, therefore, the volume flow that can be fed in 1 h over  $1\text{ m}^3$  of catalyst, and is the parameter that determines the facility's size. The catalyst's content is calculated as follows:

$$V_K = \frac{\dot{V}}{RG} \quad (6.6)$$

$\dot{V}$  in  $\text{m}^3/\text{h}$ ,  $V_K$  in  $\text{m}^3$ , and  $RG$  in  $\text{m}^3/(\text{h} \cdot \text{m}^3)$  or in  $\text{h}^{-1}$

In the event of additional heating, the waste gas from the burner's operation should be considered when determining the space velocity. The space velocity for pollutants that decompose with difficulty can be under  $5000\text{ h}^{-1}$ . Gases with normal and easily decomposable pollutants can be cleaned with space velocities of  $10,000$ – $40,000\text{ h}^{-1}$  (even up to over  $100,000\text{ h}^{-1}$  for an engine waste gas catalyst).

The catalyst bed's design can be varied as a function of the available space and the reactor type. The catalyst's leading surface  $A$  is obtained from the ratio of the total volume flow to the empty space velocity  $v$ :

$$A = \frac{\dot{V}}{v} \quad (6.7)$$

$A$  in  $\text{m}^2$ ,  $\dot{V}$  in  $\text{m}^3/\text{h}$ , and  $v$  in  $\text{m/s}$

The common values for empty space velocities are  $0.7$ – $1.5\text{ m/s}$  ( $2.3$ – $4.9\text{ ft/s}$ ). The bed height  $H$  is obtained from the catalyst volume  $V_K$ :

$$H = \frac{V_K}{A} \quad (6.8)$$

$H$  in  $\text{m}$ ,  $A$  in  $\text{m}^2$ , and  $V_K$  in  $\text{m}^3$

The bed height  $H$  can be obtained also from the ratio of the empty space velocity  $v$  to the space velocity  $RG$ :

$$H = \frac{v}{RG} \quad (6.9)$$

$RG$  in  $\text{h}^{-1}$  and  $v$  in  $\text{m}/\text{h}$ .

Gas velocity, catalyst form and dimensions, and bed height determine the pressure loss that, for example, a blower needs to overcome. A minimum pressure loss is necessary for adequate gas distribution. The pressure loss of the catalyst layers is usually determined experimentally, or stated by the catalyst's manufacturer as a function of empty space velocity for the relevant catalyst type.

### 6.3.2 Safety Systems

The design of the waste gas cleaning system must ensure that the raw gas is not present in explosive form or as an ignitable mixture. For safe operation, the concentration of pollutants must be kept below the 25% lower explosion level (LEL) and overloading or overheating the catalyst must be avoided. The lower explosion limit of components is dependent on temperature. The calculation of real lower explosion limits has to be based on the actual waste gas temperature. Here, observe that various waste gas temperatures will exist as a result of warming the waste gas in a heat exchanger. One cause for the formation of ignitable mixtures is short-term departures from what is regarded as normal operation (e.g., in the event of operational disruption of the connected processes, pressure relief, cleaning procedures, etc.). The prevention of explosive mixtures can be ensured through various methods including raw gas concentration monitoring at the inlet to the catalytic cleaning facility, concentration-dependent limiting of waste gas preheating temperature or, in the event of waste gas mixtures loaded with inert gases, through oxygen monitoring.

If the possibility of an explosive waste gas stream cannot be ruled out due to the nature and the operation of the emitting processes and the physical conditions, then, pursuant to the explosion safety guidelines, this waste gas stream must be allocated to an explosion zone according to the occurrence probability of an explosive gas mixture. The allocation indicates the number of the independent explosion-safety systems required for separating the production process from the waste gas cleaning facility.

If required, the measuring equipment for concentration monitoring should be installed at the necessary distance from the inlet of the catalytic cleaning facility taking into account the relevant response times. The monitoring device should be arranged such that the path length of the loaded raw gases from the device to the cleaning facility is adequate for a safe switchover to the emergency discharge systems or safe shut-off of the discharge. After exceeding the ignition concentration, the pipeline system and the facility should be flushed. In addition, any electrostatic charges during transport of the organic components through synthetic pipes or

lined systems should be prevented (e.g., by grounding the pipelines and by using electrically conducting materials).<sup>11–19</sup>

In smaller facilities, the parts at risk can also be designed to be resistant to pressure surges and/or with pressure relief systems. All safety-relevant facility parts, especially safety-relevant process control engineering systems, should be designed either in accordance with valid rules and guidelines as a protective device or with redundancy. This includes concentration meters and fans. The catalyst layer, and, where relevant, the waste gas blower, constitute a constant ignition source. In general, safety planning should differentiate between electric and non-electric ignition sources. See Volume 2, Chapter 1 for a general discussion of safety.

### 6.3.3 Prevention of Pollutant Enrichment and Overheating

In order to prevent excessive heating of the chosen catalyst and of the materials used beyond the deployment limits, continuous temperature monitoring systems should be installed in the reactor or at the reactor's outlet (see also Section 6.2.2). Under excessively low temperatures, pollutants can become enriched at the catalyst resulting in a risk of uncontrolled incineration. The lower temperature limit (activation temperature of the catalyst) should be monitored continuously at the reactor's inlet in order to prevent the temperature from falling below it. The measurement sites should be arranged so that the entire catalyst bed is recorded systematically. If the temperature is outside the permissible range, the waste gas cleaning facility should be shut down and the waste gas diverted to the bypass via an emergency system.

### 6.3.4 Emergency Bypass

When the permissible limit of safety-relevant substances (gases or dusts) in the raw gas is exceeded as per Section 6.2, if the upper or lower temperature limit as per Section 6.2.2 is reached, or if some other safety-relevant facility fault occurs, the feeding of waste gas into the cleaning facility should be stopped immediately and the waste gas discharged via an emergency bypass directly into the atmosphere for safety reasons. The appropriate changeover dampers should be latched to each other in such a way that an open ventilation discharge path is always ensured. This allows the upstream process to be shut down in a safe and orderly manner and/or the fault in the waste gas cleaning facility to be rectified. Use of the emergency bypass can be temporarily restricted by the competent authority or automatically subject to the conditions.



---

## 6.4 Detail Process Measuring and Control Engineering

To achieve the most reliable and safe mode of operation, often it is advantageous to measure the temperatures at the raw gas inlet, after the raw gas preheating stage, at a representative point at the reactor's inlet and in the reactor bed and/or at the reactor's outlet. In addition, other parameters can be recorded such as raw gas concentration at the inlet to the facility, raw gas volume flow at the inlet to the facility, clean gas volume flow at the facility's outlet, clean gas concentration, and oxygen content in the raw or clean gas (for oxygen-free or low-oxygen waste gases).

Once the facility's functionality has been tested, the dependence of the required clean gas values on the raw gas concentration calculated, the waste gas throughput and the reaction temperature (characteristic temperature at a defined place) has been calculated, the reaction temperature can be used as a control quantity for additional heating or for diluting the raw gas in the event of very high concentrations. In the event of rapid fluctuations in waste gas properties (concentration, temperature, volume flow) (e.g., due to the upstream lot or batch processes), the load change velocities of the processes should be adjusted to the physically limited reaction times of the instrumentation and control systems, or steps taken to achieve uniform raw gas values.

---

## 6.5 Other Facility Components

In applications where increased dust quantities in the raw gas may be expected, a filter system should be installed upstream for reducing the dust load to the relevant catalyst's permissible value. Special aerosol precipitators should be used for aerosols. If inorganic pollutants, dust, and aerosols are present in only trace amounts, the waste gas can also be precleaned in a suitable scrubber.

If the waste gas contains components that tend to condense, condensation can be adequately prevented by heating the feed or overheating the waste gas. A condensation stage may be useful where there are large quantities of condensable substances.

### 6.5.1 Buffer Systems

If the emitting facilities deliver short-term elevated pollutant loads, these emission spikes can be smoothed or rendered more uniform by means of systems referred to as "smoothers" that contain appropriate adsorbers (e.g., active carbon or zeolite) placed upstream. As a general

rule, it is more cost-effective to carry out the smoothing of spikes at the emission source. The buffer systems can also be equipped with "sacrificial layers." Their task consists of removing poisonous components from the raw gas stream. The spent material needs to be reconditioned or disposed.

A blower (see Volume 2, Chapter 3 for a discussion of blowers) installed on the raw gas side of the catalytic waste gas cleaning facility serves to boost the movement of the raw gas to be cleaned and to overcome the pressure loss in the facility. The choice of materials for the blower's construction should take into account the substances contained in the raw gas, the explosion safety zone, the temperatures to be encountered, and the possibility of the temperature dropping below the dew point as a result of the need to draw fresh air in the event of high incoming concentrations.

In special applications, the blower can be installed on the clean gas side of the facility. The reaction products released during the catalytic process and the elevated operating temperature should be considered in the blower's design. The entire facility works under negative pressure, such that pollutants in the raw gas cannot escape.

Where the emitting units supply the raw gas under adequate primary pressure, a conveying system is not necessary. A supplementary fan may be necessary for the start-up process to introduce fresh air for starting up the facility. A supplementary fan or a fresh-air damper can be installed for safety reasons or in order to prevent thermal overloading in the case of raw gas rarefaction.

A suitable pipeline system should be provided for the raw and clean gas streams. The important factors in designing the pipelines, and the type and execution of their arrangements, include the possible temperature rise in the catalytic process, the composition of the reaction products on the clean gas side, and the substances contained in the raw gas. The choice of pipeline material is based on the gas composition and on the temperature of the medium being transported. For unpressurized operations, the specifications for ventilation facilities are normally adequate for the pipelines and flange connectors. In the event of waste gas temperatures exceeding 400°C (750°F), welded connections are preferable to flange connectors. In simple applications, gas ducts as well as the classic pipeline design may be selected.

Normally, the heating system is installed before the reactor. However, if incineration products are released that may impair the catalyst's activity, heat transfer may take place indirectly by placing the burner after the reactor.

Heating the catalyst's facility to the required reaction temperature or for auxiliary firing relies normally on electric heaters, natural gas or propane gas-fired burners, or heat transfer medium operated heaters.



Determining the incineration products is vital when considering the fuel suitability for the burner operation in a catalytic waste gas facility.

The energy content of the clean gases can be recovered in two different ways—primary heat recovery for heating the raw gas within a heat transfer system (minimizing fuel input) and secondary heat recovery for heating a heat transfer medium for further use as may be possible within the emitting process. The facility's parts should be provided with suitable thermal insulation, depending on the thermal requirements and the permissible surface temperatures.

---

## 6.6 Energy Demand and Heat Recovery

The energy demand of a catalytic waste gas cleaning facility consists of additional energy in the form of indirect or direct heating, provided that there is no autothermic process management, electric energy for waste gas and/or raw gas transportation (ventilators) and for the operation of other consumers (e.g., dampers, valves, instrumentation, and control systems), compressed air for controlling dampers and valves. The energy demand is dependent on the size of the raw gas stream, pollutant concentration, the heating value of the raw gas, the difference between the temperature of the raw gas, the minimum temperature needed at the reactor's inlet, the reactor's construction, and the construction and the efficiencies of the heat transfer systems.

The energy efficiency of the catalytic cleaning facility is improved by using one or several heat transfer units for heat recovery. There are two options: (1) to preheat the waste gas in order to reduce the fuel demand (primary heat recovery) where the lowest additional energy demand exists during the autothermic operating mode; or (2) to use the heat and feed it by means of heat transfer systems to the production process, or to utilize it in some other way (e.g., to heat a water circuit or rooms (secondary heat recovery).

The bulk of the energy demand of a catalytic waste gas cleaning facility derives from the waste gas transport and the heating system. The latter's task is to heat up the facility during start-up and to heat the raw gas for the catalytic operation, in order to achieve a sufficiently high catalyst inlet temperature.

The raw gas stream to be cleaned is normally drawn in by the facility's blower, and fed to the reactor under increased pressure. The temperature, the required compression, and the raw gas volume stream determine the blower's size, and, in combination with its efficiency, its energy demand. The required compression is the sum

of the pressure losses in the facility's parts (heat transfer unit, heater, reactor, pipelines, and auxiliary components). In the reactor, the gas velocity, the catalyst's form and dimensions, and the bed height determine the pressure loss that the blower needs to overcome. A minimum pressure loss is required for sufficiently uniform gas distribution. The pressure loss in the catalyst layers is usually obtained experimentally or is stated by the catalyst's manufacturer as a function of gas velocity.

Before the facility's start-up, the catalyst bed and the reactor need to be heated up to the required reaction temperature. This is done with fresh air, to avoid increased emissions of untreated raw gas and a situation where flammable substances are adsorbed on the catalyst at low temperatures causing damage to the catalyst.

The energy demand for heating up the catalyst's facility depends on the physical construction, the masses, and heat capacities of the catalyst, reactor chamber, heat transfer unit and insulation, and on the start-up strategy (e.g., heating up the facility with a small gas stream). This should be determined empirically on a case-by-case basis. In practice, the raw gas can be introduced once the outlet temperature exceeds the minimum reaction temperature.

For primary heat recovery, a heat transfer system is fitted between the hot clean gas and the cold raw gas. Depending on the application, there may be two different heat transfer units and constructions in use. One is a recuperative heat transfer unit, consisting of plate heat transfer units and tube bundle heat transfer units ( $\eta = 50\%–80\%$ ). The other is the regenerative heat transfer unit, consisting of rotating systems ( $\eta = 50\%–80\%$ ) and stationary ceramic multi-bed systems ( $\eta = 80\%–97\%$ ).

The choice of a suitable heat transfer system depends essentially on the encountered concentrations and, thus, on the expected facility temperatures. Other criteria include the possible need for corrosion-resistant materials, condensate discharge, and good accessibility for inspection, servicing, and cleaning (especially, if there is a risk of condensation or dust deposits in the raw gas). Plate and tube bundle heat transfer units are usually operated in crosscurrent flow, and are recuperative heat transfer units. The heat is transferred directly via a separating surface (plate, tube) from the hot to the cold side. The transfer is continuous and without contact between the media.

In regenerative heat transfer systems, heat transfer takes place via a heat storage medium (e.g., a ceramic body with a high specific heat capacity). The cold raw gas is fed via an appropriate damper or valve control system or a rotary slide valve to a heat storage bed. The raw gas is preheated in the first packed bed. This is followed by oxidation in the catalyst layer, which,

depending on the facility's construction, may be either distributed on the heat accumulator or be arranged separately. The hot clean gas then flows over the second heat storage bed and gives off the majority of the heat energy contained in it to the ceramic body. Regenerative heat transfer methods work discontinuously. As a result of the high heat transfer area of the heat accumulator, very good efficiency can be achieved with comparatively small unit sizes. Nonetheless, in this approach the heat accumulators are exposed alternately to raw gas and clean gas. Complete, clean flushing of the entire container and reliable, leak-proof air-control systems are important to prevent carry-over of raw gas when switching over (important for odor-intensive or high-load waste gases).

Given sufficiently high pollutant concentration in the raw gas, and consequently an overautothermic mode of operation, there is excess energy present, which can be fed back via secondary heat recovery into the production process. It may be possible to concentrate the process exhaust air (i.e., reduce the quantity of waste gas) and correspondingly increase pollutant concentration up to the permissible safety limit. Examples of secondary heat recovery include heat transfer oil waste heat systems, hot water waste heat systems, steam generation, preheating of process gas, direct heat recovery for the process, heat pump, or an organic Rankine cycle (ORC) process.

Depending on the heat transfer medium's required temperature, the waste heat system can be integrated (arranged between the reactor and the facility's heat transfer unit) or be located downstream and for odor-intensive or high-load waste gases.

## 6.7 Different Design of Catalytic Waste Gas Cleaning Systems

If the waste gas has the necessary temperature for the combustion, the unit can be designed very simply. In this case, the only equipment needed is a catalytic reactor and catalyst (Figure 6.8.)

Normally, it is necessary to include a burner to provide the required  $T_c$  and a blower to obtain a pressure high enough to push the waste gas through the system. It is also possible to replace the gas burner with a suitable electric heater if this would be more convenient. Units treating small flows have a small and acceptable energy consumption so often they are only equipped with a burner. The typical layout for small units (<1000 N-m<sup>3</sup>/h) is illustrated in Figure 6.9.

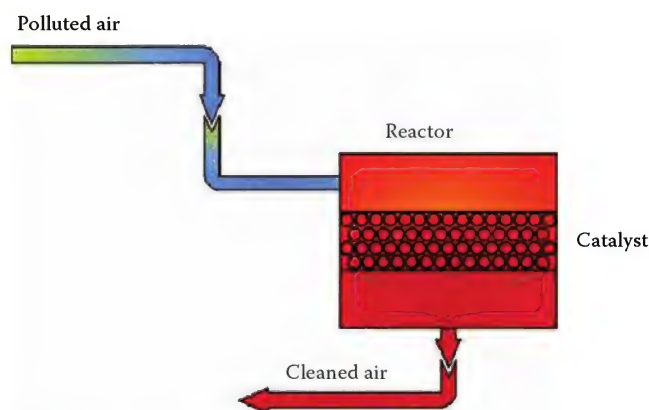


FIGURE 6.8  
Simple catalytic waste gas cleaning system.

To heat the waste gas solely by means of a gas burner or an electric heater can be very expensive due to the high cost of both fuel and electricity. For units larger than 1000 N-m<sup>3</sup>/h, it is, in general, economically feasible to install a heat exchanger. See the layout in Figure 6.10.

$$\eta = \frac{(T_c - T_H) - T_{\text{inlet}}}{T_{\text{R,out}} - T_{\text{inlet}}} \quad (6.10)$$

where

$T_c$  is the combustion temperature already introduced

$T_H$  is the temperature provided by the burner

$T_{\text{inlet}}$  is the inlet temperature to the heat exchanger (which normally is the temperature of the waste gas)

$T_{\text{R,out}}$  is the outlet temperature from the catalytic reactor. In the case of an autothermal operation,  $T_{\text{R,out}} - T_c = \Delta T_c$ .

The optimum size of a heat exchanger is a compromise between the fuel price and the price of the heat exchanger. In locations where the fuel price is low, the best option is a small heat exchanger ( $\eta \sim 50\%$ ), whereas in locations with very high fuel prices, the best solution is a larger heat exchanger ( $\eta = 70\% - 74\%$  or higher). These figures, of course, also depend on the length of payback time that one is willing to accept for an additional investment in a larger heat exchanger.

The design always incorporates a bypass of the heat exchanger in order to control the inlet temperature to the catalyst. The bypass can be either on the cold or on the hot side of the heat exchanger, and both solutions have their advantages and disadvantages.



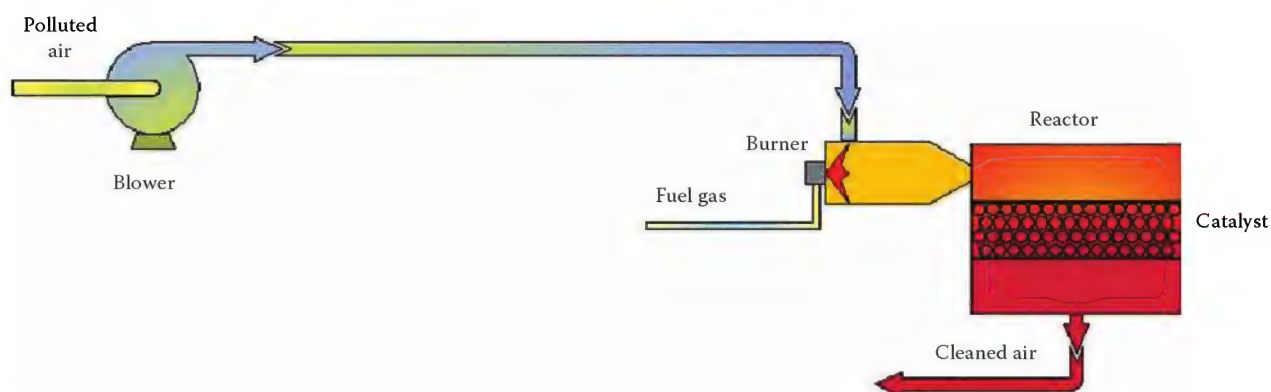


FIGURE 6.9  
Catalytic waste gas cleaning system with a burner and blower.

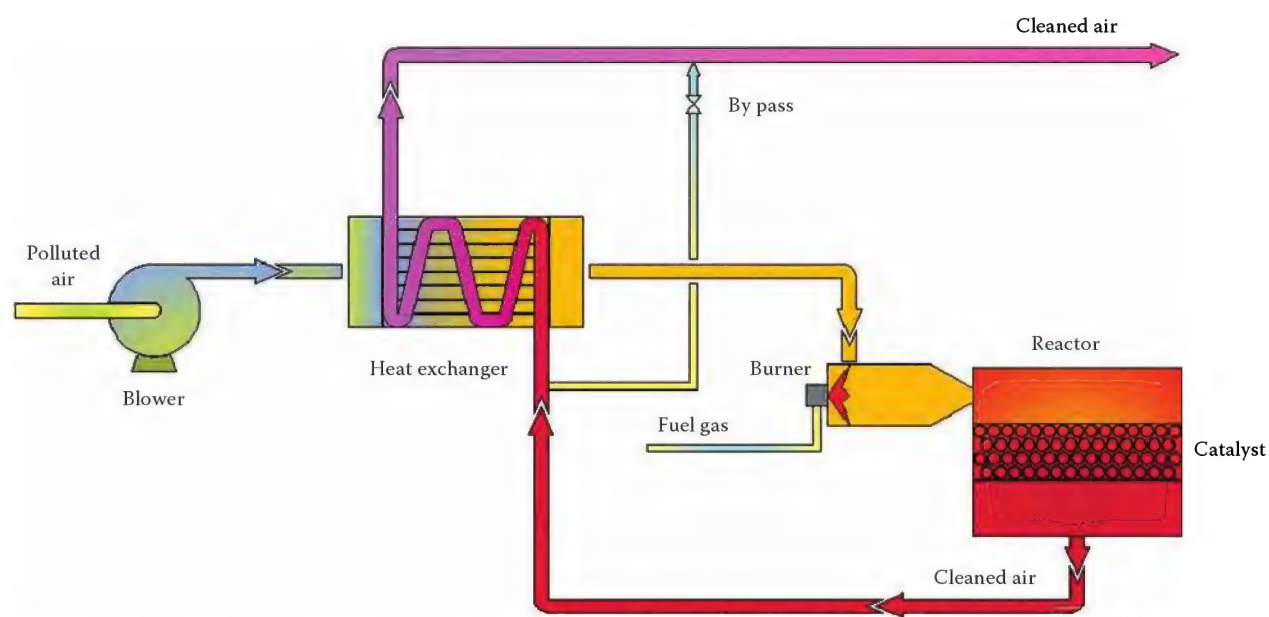


FIGURE 6.10  
Catalytic waste gas cleaning system with a heat exchanger.

Excess heat in a catalytic waste gas cleaning system (due to high inlet temperature of the waste gas or high concentration of combustibles, etc.) can be used for production of hot water/air. This is performed by recovering the excess heat, in the clean outlet stream from the heat exchanger, before emitting it to the atmosphere. The principle is shown in Figure 6.11.

If there is a lot of excess heat after combustion, it is possible to equip the unit with a steam boiler. The steam boiler can be placed at the clean air outlet from the heat exchanger, where it normally can produce low-pressure steam. Alternatively, it can be placed right after the reactor where the temperature is the highest,

producing high-pressure steam. However, in the latter case it will be necessary with a larger heat exchanger as some of the energy for heat recovery is extracted as steam. This system (illustrated in Figure 6.12) is often seen in the maleic anhydride industry where  $\Delta T_c$  is normally very high.

In Figure 6.12, the possibility of waste liquid injection is illustrated. This is an option if there are waste liquids with a certain amount of VOCs that need to be removed. Co-combustion of the waste liquid adds to the temperature increase in the catalytic reactor and thereby enhances the fuel economy of the system. The liquid is injected just before the burner where the

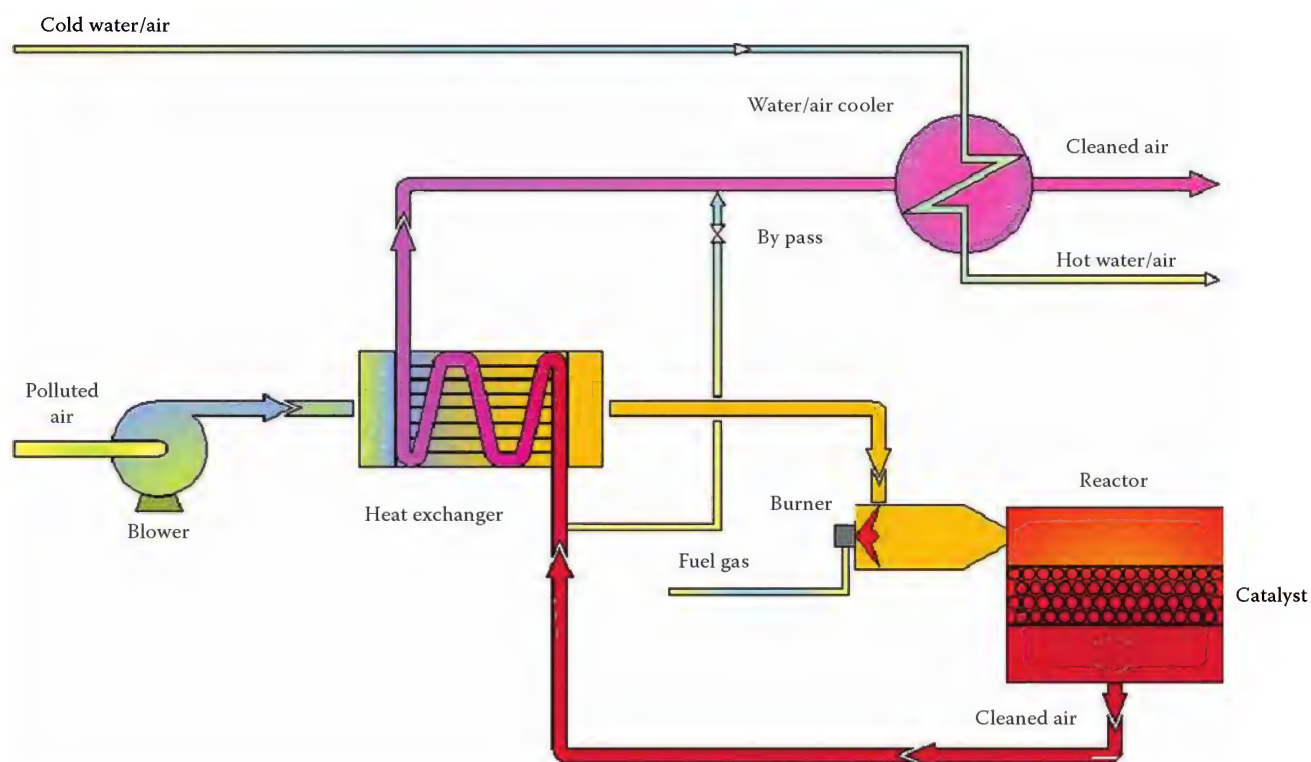


FIGURE 6.11  
Catalytic waste gas cleaning system with hot water/air production.

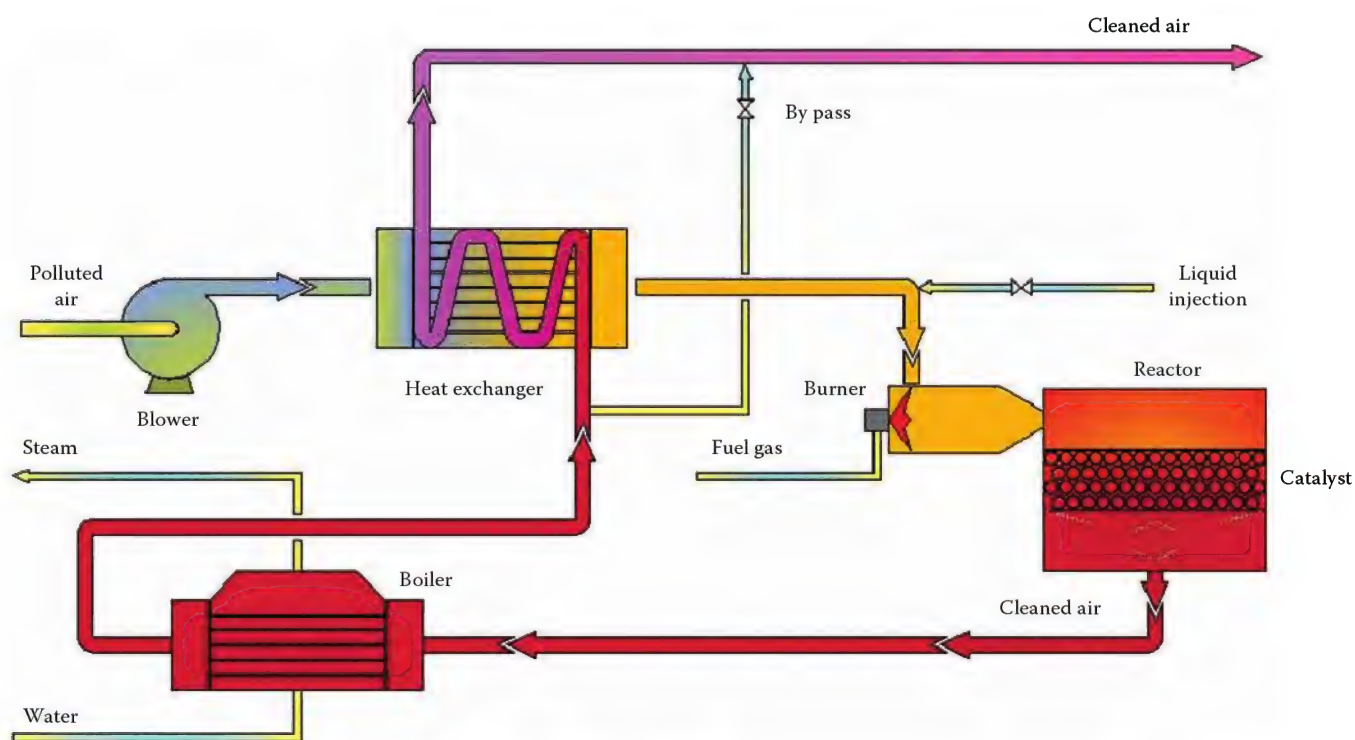


FIGURE 6.12  
Catalytic waste gas cleaning system with steam production and waste liquid injection.



waste gas is hot enough to ensure evaporation. When flowing through the catalytic reactor, the evaporated liquid will contribute to an even higher  $\Delta T_c$  and, thus, higher steam production. It is also possible to inject organic dust through this valve with the same advantages.

In cases with low concentration ( $0\text{--}4\text{ g/m}_N^3$ ) of combustibles, the catalytic waste gas cleaning system unit will consume a considerable amount of energy. In these situations, the best solution is, in general, to supply a system with a regenerative heat transfer system, instead. The process is based on regenerative heat exchange meaning that the heat from the cleaned gas is absorbed in a bed of ceramics and later released from this bed to the cold uncleaned waste gas. In that case, the ceramic beds are doing the preheating that in the standard catalytic waste gas cleaning system was performed by the heat exchanger. This provides a very high heat efficiency (larger than 95%) exchange, which makes this process applicable to low concentrations.

A very important consideration when designing this kind of system is to ensure absolutely tight valves. Small leaks will result in a flow of uncleaned gas into the clean gas and the consequence will be a lower cleaning efficiency. A special type of butterfly valve with two blades may be used. The valve in itself is not 100% tight, but air is discharged between the blades so that any leaks of process air will be discharged and returned to the inlet of the unit for cleaning. These valves can also be made as three- or four-way valves.

The simplest catalytic waste gas cleaning with regenerative heat transfer system is shown in Figure 6.13. The waste gas enters the catalytic reactor

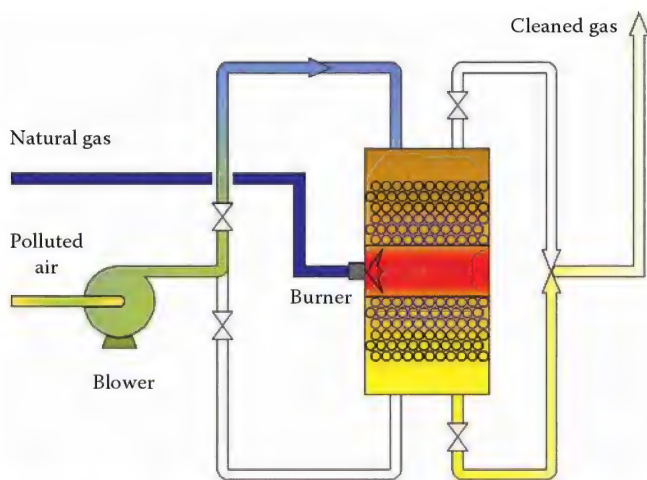


FIGURE 6.13

Simple catalytic waste gas cleaning system with regenerative heat transfer system.

at the top, flows through the first ceramic bed, and onto the central portion where the burner is mounted. The waste gas now flows through the second catalyst bed, where the remaining part of the combustibles is burned, and on to the second ceramic bed, where most of the heat is absorbed. After some time of operation (typically, 10–15 min), the flow is reversed. Now, the waste gas enters at the bottom where it is warmed up by the heat absorbed in the ceramic bed. If the content of combustibles is not high enough to obtain the required combustion temperature, the burner provides the additional heat. Autothermal operation is normally obtained at a concentration of about  $0.5\text{ g/Nm}^3$  (depending on the type of organics), and, in that case, the burner will only be necessary during start-up.

The average cleaning efficiency for this simple unit is only about 95%. The reason is that each time the flow is reversed a small amount of uncleaned gas will be left either at the top or at the bottom (depending on the flow direction). This will be emitted to the stack together with the cleaned gas, causing peaks with a higher concentration of organics as a consequence of the flow reversal.

As a result of the constant change of flow direction, the heat is kept in the central part of the unit containing the catalytic and the ceramic beds, and the temperature of the cleaned gas will only be slightly higher than the inlet temperature of the waste gas (see Figure 6.14).

To avoid the high concentration peaks and obtain a better cleaning efficiency, the system unit can be equipped with a “back purge system” (see Figure 6.15). The purpose of this system is to pull the “trapped”

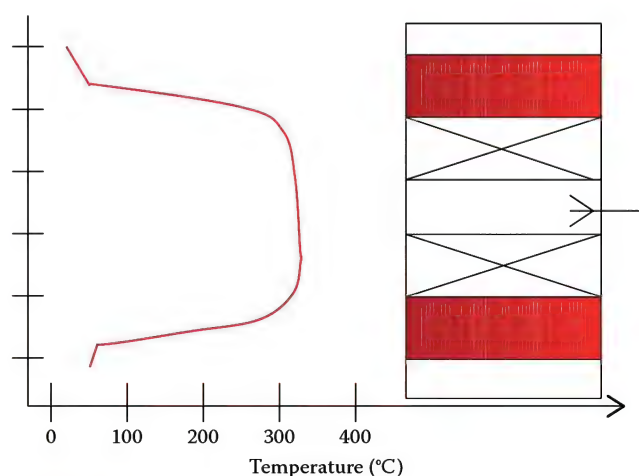


FIGURE 6.14

Regenerative heat transfer system, temperature profile.

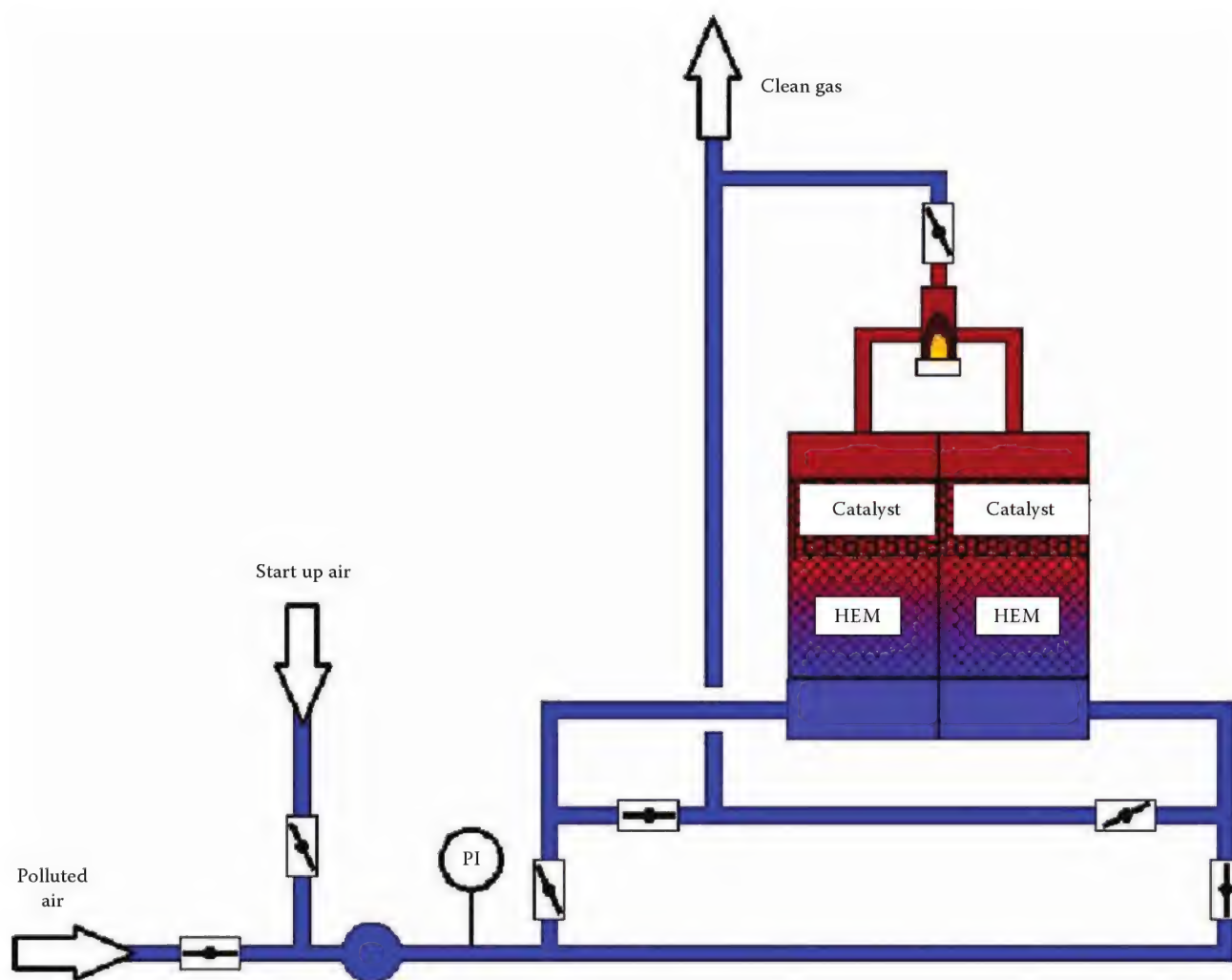


FIGURE 6.15

Catalytic waste gas cleaning system with regenerative heat transfer system including back purge flow system.

uncleaned gas in the end of the reactor back to the inlet of the unit, when the flow is reversed. In this way, peaks will be avoided and a cleaning efficiency of about 99% will be obtained. The system unit with back purge system will be operated autothermally at a concentration of combustibles of about  $0.8 \text{ g/Nm}^3$ , depending on the type of organics, of course.

The valve placed in the center, opposite the burner allows release of excess heat by sending hot cleaned air directly to the stack without passage through the second ceramic bed. This can be a necessity in those cases where the inlet concentration of combustibles is higher than what is actually needed for autothermal operation.

In the case of large fluctuations in the concentration of combustibles or large units with multiple bed reactors, it can be very difficult to control the temperature

level in the reactor. A solution is to use the one-way flow catalytic waste gas cleaning system with regenerative heat transfer system where the flow always goes in the same direction through the catalyst. This design enables the system to keep a constant inlet temperature to the catalyst, which is necessary in cases with a high demand for the cleaning efficiency. This unit can also be equipped with the back purge system. However, for the sake of simplicity the back purge system is omitted on the schematic drawing of the unit given in Figures 6.15 and 6.16.

One-way flow also gives the possibility of recovering some heat. The types of heat recovery are the same as for the catalytic waste gas cleaning system and the heat recovery system is placed after the catalytic reactor, to take advantage of the clean gas at the high and constant temperature. In addition, injection of waste liquid or

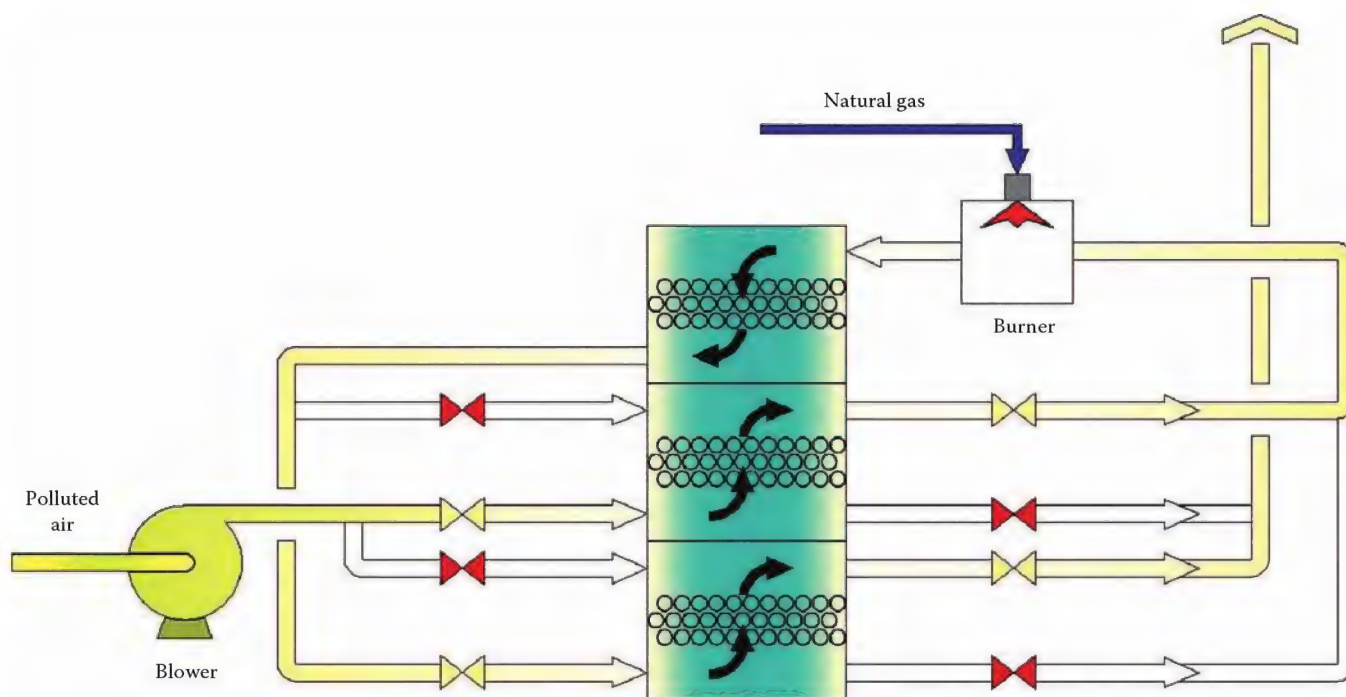


FIGURE 6.16

Catalytic waste gas cleaning system with regenerative heat transfer system, one-way flow reactor.

organic dust is possible, which is performed upstream from the catalyst before the inlet to the burner. A schematic illustration is given in Figure 6.16.

## References

- Andersen, J.R. and M. Roudart: *Catalysis*. Vol. 1,2. Heidelberg, Berlin: Springer Verlag 1981.
- Kirchner, K. and M. Elsholz: Deactivation of catalysts by phosphorous, arsenic and silicon compounds. Preprints 9th World Clean Air Congress Air Congress CDN/ Montreal, August 29–30, 1992.
- Stanischewski, D. und K. Kirchner: Die Vergiftung von oxidischen Katalysatoren zur Abluftreinigung mit Siliziumverbindungen, *Staub—Reinhaltung der Luft* 53(2), 53–58, 1993.
- Thomas, J.M. and W.J. Thomas: *Introduction to the Principles of Heterogeneous Catalysis*. New York: Academic Press 1967.
- Brunauer, S., Emmett, P.H., and E. Teller, Adsorption of gases in multimolecular layers, *Journal of the American Chemical Society*, 60(2), 309–319, 1938.
- VDI-Berichte 525: Katalytische und thermische Verfahren der Abgasreinigung, Kolloquium Mannheim, 7/8.3.1985. Düsseldorf: VDI Verlag 1985.
- Menig, H.: *Luftreinhaltung durch Adsorption, Absorption und Oxidation*, Wiesbaden: Deutscher Fachschriften Verlag, 1977.
- Kirchner, K. and B. Angele: Beitrag zur katalytischen Abgasreinigung. *Verfahrenstechnik*.
- Eigenberger, G. and U. Nicken: Katalytische Abluftreinigung: Verfahrenstechnische Aufgaben und neue Lösungen. *Chem.Eng.-Tech.* 63(8), 781–791.
- Bournbach, C: *Luftreinhaltung*, 2. Auflage, Springer Verlag, 1992.
- Bartknecht, W.: *Explosionsschutz—Grundlagen und Anwendung*. Springer Verlag Berlin, Heidelberg, New York, 1993.
- Nabert, K. and G. Schön: *Sicherheitstechnische Kennzahlen brennbarer Gase und Dämpfe*. Deutscher Eichverlag, Braunschweig, 2. Auflage, Nachdruck 1978 mit 6. Nachtrag (T. Redecker und G. Schön), 1990.
- Schampel, K.: *Flammendurchschlagsicherungen*, Kontakt & Studium Band 170. Expert Verlag, 1988.
- Leinemann, H. and V. Halstrick: *Explosionsschutz durch den Einsatz flammendurchschlagsicherer Armaturen—neuester Stand der Technik*. Braunschweiger Flammenfilter, 1989.
- Stall, D.R.: *Fundamentals of Fire and Explosion*. New York: American Institute of Chemical Engineers, Vol. 73, 1977.
- Bartknecht, K.: Prüfung einer Tauchsicherung auf Flammendurchschlag bei Propan-Explosionen und -Detonationen. D3/81, Ciba-Geigy, 1981.
- Peter, H.K.: Prüfen von Flammendurchschlagsicherungen gegen dynamischen und statischen Durchschlag. *Chemische Rundschau* (1981) 11.
- ESCIS-Hefte Schriftenreihe der Expertenkommission für Sicherheit in der chemischen Industrie der Schweiz.
- Sicherheitstechnische Informationen über Protego-Armaturen, Sachregister über Prüfungen und Zulassungen. Sicherheitstechnische Kenndaten, 1991.

This page intentionally left blank



# 7

## *Heat Transfer*

Jay Karan and Charles E. Baukal, Jr.

### CONTENTS

7.1	Introduction .....	160
7.2	Conduction.....	161
7.2.1	Thermal Conductivity and Specific Heat.....	162
7.2.2	One-Dimensional Steady-State Conduction .....	163
7.2.2.1	Plane Wall .....	163
7.2.2.2	Composite Wall .....	164
7.2.2.3	Contact Resistance .....	165
7.2.2.4	Cylinder.....	165
7.2.3	Transient Conduction.....	166
7.3	Convection .....	168
7.3.1	Dimensionless Numbers.....	170
7.3.2	Newton's Law of Cooling .....	170
7.3.3	Laminar Flow Convection.....	171
7.3.3.1	Fully Developed Velocity and Temperature Profiles.....	172
7.3.4	Turbulent Internal Flow .....	172
7.3.4.1	Circular Tubes .....	172
7.3.4.2	Non-circular Tubes/Sections.....	173
7.3.5	Turbulent External Flow .....	173
7.3.5.1	Convection Heat Transfer for the Cylinders in Cross Flow .....	174
7.3.5.2	Convection Heat Transfer in Banks of Tubes.....	175
7.3.6	Forced Convection from Flames.....	175
7.3.7	Natural Convection .....	176
7.4	Radiation .....	177
7.4.1	Blackbody Radiation/Planck Distribution.....	178
7.4.1.1	Planck Distribution.....	178
7.4.1.2	Wien's Displacement Law .....	179
7.4.1.3	Stefan-Boltzmann Law .....	179
7.4.2	Radiant Exchange between Black Surfaces.....	180
7.4.3	Radiant Exchange between Gray/Diffuse Surfaces.....	180
7.4.4	View Factors for Diffuse Surfaces .....	180
7.4.5	Infrared Temperature Measurement .....	181
7.4.6	Radiation in Absorbing/Emitting/Scattering Media.....	185
7.4.7	Mean-Beam-Length Method .....	186
7.4.8	Equation of Radiative Transfer .....	191
7.4.9	Radiation Emitted by a Flame.....	192
7.5	Heat Transfer in Process Furnaces .....	193
7.5.1	Flame Radiation .....	195
7.5.2	Furnace Gas Radiation.....	196
7.5.3	Refractory Surface Radiation .....	196

7.5.4	Analysis of Radiation Heat Transfer .....	197
7.5.5	Heat Transfer through the Wall of a Furnace .....	198
7.5.6	Heat Transfer in the Process Tube .....	199
7.5.7	Furnace Gas Flow Patterns .....	199
7.5.8	Role of the Burner in Heat Transfer .....	200
7.6	Conclusions .....	202
	References .....	202

## 7.1 Introduction

Heat transfer is one of the fundamental purposes of combustion in the hydrocarbon and petrochemical industries. The objective of many industrial combustion applications is to transfer energy, in the form of heat, to some type of load for thermal processing of that load.<sup>1</sup> An understanding of heat transfer is essential to the successful design and operation of fired equipment. The objective of this chapter is to review helpful concepts of heat transfer, focusing on those topics as applied to combustion, particularly in the hydrocarbon and petrochemical industries.

Numerous excellent books have been written on the subject of heat transfer. However, almost none of them have any significant discussion of combustion. This is not surprising as the field of heat transfer is very broad, making it difficult to be exhaustively comprehensive. Many of the heat transfer text books have no specific discussion of heat transfer in industrial combustion but do treat gaseous radiation heat transfer.<sup>1-24</sup>

The heat transfer books written specifically about radiation often have sections covering heat transfer from luminous and nonluminous flames. Hottel and Sarofim's<sup>25</sup> book has a good blend of theory and practice regarding radiation. It also has a chapter specifically on applications in furnaces. Love's<sup>26</sup> book on radiation has short theoretical discussions of radiative heat transfer in flames and measuring flame parameters, but no other significant discussions of flames and combustion. Özisik's<sup>27</sup> book focuses more on interactions between radiation, conduction, and convection, with no specific treatment of combustion or flames. A short book by Gray and Müller<sup>28</sup> aims toward more practical applications of radiation. Sparrow and Cess<sup>29</sup> have a brief chapter on nonluminous gaseous radiation where they discuss the various band models.

Some of the older books on heat transfer are more practically oriented with less emphasis on theory. Kern's<sup>30</sup> classic book *Process Heat Transfer* has a chapter specifically on heat transfer in furnaces, primarily

boilers and petroleum refinery furnaces. Hutchinson<sup>31</sup> gives many graphical solutions for conduction, radiation, and convection heat transfer problems, but nothing specifically for flames or combustion. Hsu<sup>32</sup> has helpful discussions on nonluminous gaseous radiation and luminous radiation from flames. Welty<sup>33</sup> discusses heat exchangers, but not combustors or flames. Karlekar and Desmond<sup>34</sup> give a brief presentation on nonluminous gaseous radiation, but no discussion of flames or combustion. Ganapathy's<sup>35</sup> book on applied heat transfer is one of the better ones concerning heat transfer in industrial combustion and includes a chapter on fired-heater design. Blokh's<sup>36</sup> book is also a good reference for heat transfer in industrial combustion, although it is aimed at power boilers and does not specifically address industrial combustion processes. It has much information on flame radiation from a wide range of fuels including pulverized coal, oils, and gases. Deshmukh's<sup>37</sup> book on industrial heating has many useful chapters on topics such as fuel burning devices and refractories. Xu<sup>38</sup> has written a chapter specifically on heat transfer in combustion systems, which is a useful reference. Some handbooks on heat transfer have been written, but these also tend to have little if anything on industrial combustion systems.<sup>39-42</sup> Hewitt et al.<sup>43</sup> have written a useful encyclopedia on the subjects of heat and mass transfer.

Heat is a form of energy upon which the majority of all refinery processes are based. Heat transfer is that science that seeks to understand and predict the energy transfer between masses, resulting from differences in temperature.<sup>2,10</sup> Heat transfer is commonly divided into three mechanisms or modes for classification: conduction, convection, and radiation. Phase change modes of heat transfer such as boiling and condensation are not covered in this chapter.

The three major heat transfer mechanisms all have importance as applied to combustion in refinery processes. Consider a typical fired heater as shown in Figure 7.1, which consists of tubes with flowing fluid to be heated, a burner, or group of burners, designed to provide the required energy for the desired process, and a radiant section and a convection section

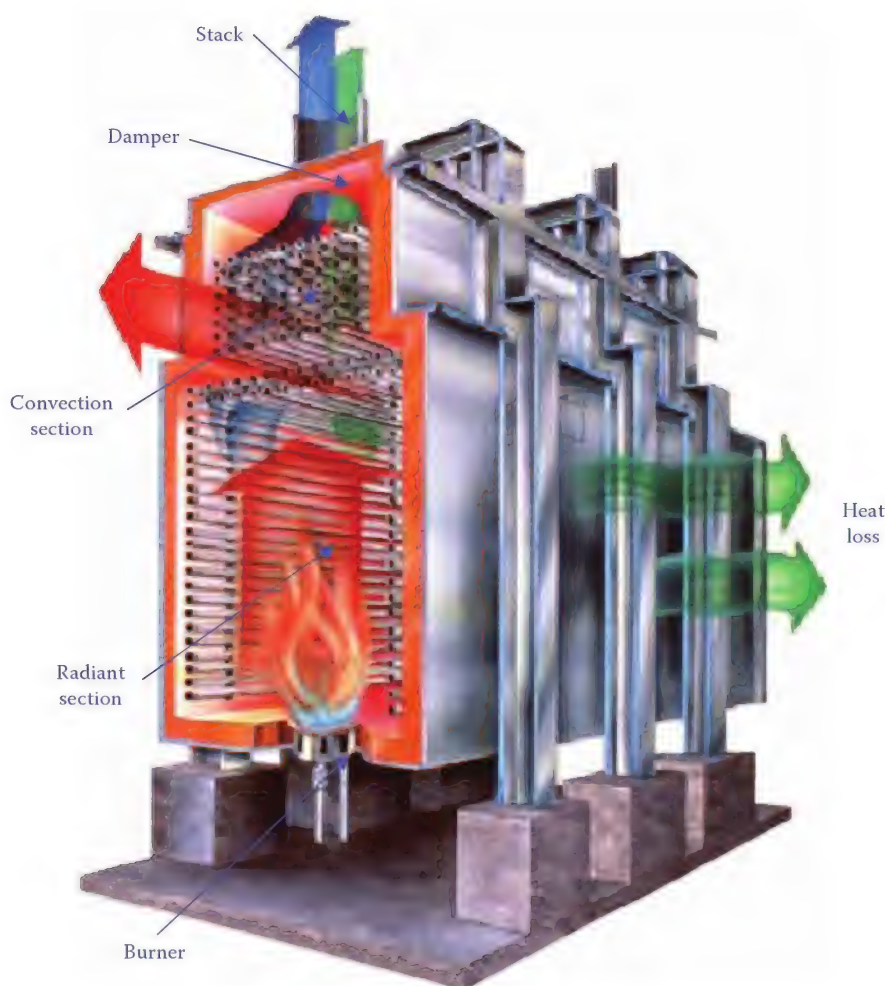


**FIGURE 7.1**  
Typical fired heater.

for heating. Major heat transfer processes in petrochemical or refinery heaters include

1. Conduction through the furnace refractory and convection from the wall of the furnace to the surrounding air
2. Radiation exchange between the flame, the surrounding walls, and process tubes
3. Convection from the hot furnace gases to the process tubes and from process tube walls to the fluid flowing through the tubes

See the end of the chapter for a more comprehensive discussion on the various heat transfer processes taking place in a furnace and how one may calculate various effects.

The consequences of the performance of these heat transfer mechanisms may significantly impact product throughput and quality, furnace efficiency, equipment

lifetime, and safety. Other critical phenomena for consideration may include the effect of heat transfer mechanisms on the fired equipment itself (e.g., heat transfer effects on burner fuel tips) or the effect of heat transfer on the performance of the fired equipment with respect to  $\text{NO}_x$  emissions, flame stability, and flame shape.

## 7.2 Conduction

Conduction heat transfer refers to the transfer of energy from the more energetic to the less energetic particles of a substance, resulting from interaction between the particles. Conduction is the net transfer of energy by random molecular motion—also called diffusion of energy. Conduction in gases and liquids is by such molecular motion, except that, in liquids, the molecules are more closely spaced and



the molecular interactions are stronger and more frequent. In the case of solids, conduction refers to the energy transfer by lattice waves induced by atomic motion. When the solid is a conductor, the translational motion of free electrons transfers energy. In nonconductors, the transfer of energy takes place only via lattice waves.

Heat conduction occurs in both stationary and moving solids, liquids, and gases. The primary postulate of classical heat conduction theory is that the rate of heat conduction in a material is proportional to the temperature gradient. This is consistent with the second law of thermodynamics, indicating that heat flows in the direction of decreasing temperature or from hot bodies to cold bodies:

$$\vec{q} = -k\nabla T \quad (7.1)$$

This equation states that heat flux is proportional to the temperature gradient, and the proportionality constant is called the thermal conductivity of the material transferring heat. More detailed information on thermal conduction heat transfer is available in books specifically written on that subject.<sup>44–49</sup>

### 7.2.1 Thermal Conductivity and Specific Heat

Thermal conductivity is a material property that is expressed in Btu/(h-ft-°F) or W/(m-K) and is dependent on the chemical composition of the substance. Typical values for some materials are shown in Tables 7.1 and 7.2.

The thermal conductivity of solids is generally higher than that of liquids, and that of liquids is higher than that of gases. Among solids, the insulating materials have the lowest conductivities. Thermal conductivity of pure metals typically decreases with an increase in temperature, while the conductivity of alloys may either increase or decrease (see Table 7.1). Thermal conductivities of various refractory materials are shown in Figure 7.6b. For many heat transfer calculations, it is sufficiently accurate to assume a constant thermal conductivity corresponding to the average temperature of the material.

The thermal conductivities of most nonmetallic liquids range from 0.05 to 0.15 Btu/h-ft-°F (0.09–0.26 W/m-K), and the thermal conductivities of many liquids tend to decrease as temperature increases.

**TABLE 7.1**

Thermal Conductivity of Common Materials

Material	Btu/h ft F	W/m K
Gases at atmospheric pressure	0.004–0.70	0.007–1.2
Insulating materials	0.01–0.12	0.02–0.21
Nonmetallic liquids	0.05–0.40	0.09–0.70
Nonmetallic solids (brick, stone, concrete)	0.02–1.5	0.04–2.6
Liquid metals	5.0–45	8.6–78
Alloys	8.0–70	14–121
Pure metals	30–240	52–415

**TABLE 7.2**

Properties of Various Substances at 32°F (0°C)  
(Except for Steam as Noted Here)

	$\rho$ Lb/ft <sup>3</sup>	$c_p$ Btu/lb°F	$k$ Btu/h ft°F
<i>Metals</i>			
Copper	559	0.09	223
Aluminum	169	0.21	132
Nickel	556	0.12	52
Iron	493	0.11	42
Carbon Steel	487	0.11	25
Alloy Steel 18Cr 8Ni	488	0.11	9.4
<i>Nonmetal solids</i>			
Limestone	105	~0.2	0.87
Glass Pyrex	170	~0.2	0.58
Brick K-28	27	~0.2	0.14
Plaster	140	~0.2	0.075
Kaowool	8	~0.2	0.016
<i>Gases</i>			
Hydrogen	0.006	3.3	0.099
Oxygen	0.09	0.22	0.014
Air	0.08	0.24	0.014
Nitrogen	0.08	0.25	0.014
Steam <sup>a</sup>	0.04	0.45	0.015
<i>Liquids</i>			
Water	62.4	1.0	0.32
Sulfur dioxide (liquid)	89.8	0.33	0.12

<sup>a</sup> Reference temperature for steam is 212°F (100°C). All other temperatures are 32°F (0°C).

The thermal conductivities of gases increase with temperature and are independent of pressure at the conditions at which most furnaces operate. Generally, gas thermal conductivities decrease with increasing molecular weight. Thus, a light gas such as hydrogen has a relatively high conductivity.

When calculating the thermal conductivity of non-homogeneous materials, one must use the apparent thermal conductivity to account for the porous or layered construction of the material. In furnace refractory walls, the thermal conductivity may vary from site to site for the same material. This is because the thermal conductivity of these materials is strongly dependent on their apparent bulk density (mass per unit volume). For higher temperature insulations, the apparent thermal conductivity of fibrous insulations and insulating firebrick increases as bulk density increases. However, there is a limit at which an increase in density will no longer contribute to a significant increase in the thermal conductivity. See Volume 2 of the Handbook for more information about refractories.

It is known that the specific heats of solids and liquids are generally independent of pressure. Table 7.2



also shows the specific heats of various metals, alloys, and nonhomogeneous materials at 32°F (0°C). These values may be used at other temperatures without significant error.

Gases on the other hand demonstrate more temperature dependence with regard to their specific heat. For all practical purposes, in furnace analyses any pressure dependence can be neglected. Table 7.3 gives the specific heat data for air and other gases at different temperatures. In the case of steam and water, the variation of both thermal conductivity and specific heat can be significant over the ranges of temperatures and pressures encountered in industrial steam systems. Refer to the ASME steam tables for data on water and steam.<sup>50</sup>

TABLE 7.3

Properties of Selected Gases at 14.696 psi

Temperature °F	$\rho$ lb/ft <sup>3</sup>	$c_p$	$k$	$\rho$ lb/ft <sup>3</sup>	$c_p$	$k$
		Btu/ lb°F	Btu/h ft°F		Btu/ lb°F	Btu/h ft°F
		Air				CO <sub>2</sub>
0	0.0855	0.240	0.0131	0.1320	0.184	0.0076
500	0.0408	0.248	0.0247	0.0630	0.247	0.0198
1000	0.0268	0.263	0.0334	0.0414	0.280	0.0318
1500	0.0200	0.276	0.0410	0.0308	0.298	0.042
2000	0.0159	0.287	0.0508	0.0247	0.309	0.050
2500	0.0132	0.300	0.0630	0.0122	0.311	0.055
3000	0.0113	0.314	0.0751	0.0175	0.322	0.061
		O <sub>2</sub>				N <sub>2</sub>
0	0.0945	0.219	0.0133	0.0826	0.249	0.0131
500	0.0451	0.235	0.0249	0.0395	0.254	0.0236
1000	0.0297	0.252	0.0344	0.0260	0.269	0.0320
1500	0.0221	0.263	0.0435	0.0193	0.283	0.0401
2000	0.0178		0.0672	0.0156		0.0468
2500	0.0148		0.0792	0.0130		0.0528
3000	0.0127		0.0912	0.0111		
		H <sub>2</sub>				
0	0.0059	3.421	0.1071			
500	0.0028	3.470	0.1610			
1000	0.0019	3.515	0.2206			
1500	0.0014	3.619	0.2794			
2000	0.0011	3.759	0.3444			
2500	0.0009	3.920	0.4143			
3000	0.0008	4.218	0.4880			
Flue gases						
	Natural Gas k	Fuel Oil k	Coal k			
0	—	—	—			
500	0.022	0.022	0.022			
1000	0.030	0.029	0.029			
1500	0.037	0.036	0.036			
2000	0.044	0.043	0.043			
2500	0.051	0.049	0.050			

In the use of thermal insulators as a heat barrier, it must be kept in mind that the effectiveness of an insulator depends greatly on the temperature of its cold face. So it is not possible to protect a metal object in a furnace by insulating all around it, unless there is an adequate path for the heat to escape from the object to a cooler location, such as the atmosphere outside the furnace. Regardless of the thickness of insulation on an object that is in a furnace, if it is not attached to a cold sink, the object will attain the furnace temperature in a short time. This heat-up time period is governed by the specific heat of the material and is merely the time (and heat input) required to heat the mass of insulation (and mass of the object) up to the furnace temperature. The quantity of heat required to reach furnace temperature is given by

$$Q = m C_p \Delta T \quad (7.2)$$

where

$m$  is the mass of the material

$C_p$  is the specific heat of the material

$\Delta T$  is the temperature difference between ambient and furnace temperatures

## 7.2.2 One-Dimensional Steady-State Conduction

In a one-dimensional steady-state conduction situation, the temperature change occurs only in one direction. The system is described as steady state when the temperature at every point remains the same over time. This assumption is usually valid for analysis of a furnace wall under steady-state furnace operation, when the firing rate and temperature gradient through the furnace wall may be considered constant for all practical purposes. However, during startup and shutdown, the heat input and temperature gradients are changing over time and must be treated differently. Common solutions to Equation 7.1 are given in Table 7.4; some of these are discussed next.

### 7.2.2.1 Plane Wall

It can be shown that the general heat equation in an isotropic medium is

$$\frac{\partial}{\partial x} \left( k \frac{\partial T}{\partial x} \right) + \frac{\partial}{\partial y} \left( k \frac{\partial T}{\partial y} \right) + \frac{\partial}{\partial z} \left( k \frac{\partial T}{\partial z} \right) + \dot{q} = \rho c_p \frac{\partial T}{\partial t} \quad (7.3)$$

where

$k$  is the thermal conductivity of the medium

$\dot{q}$  is the rate of energy generation within the system

$\rho c_p \partial T / \partial t$  is the time rate of change of sensible energy of the system

TABLE 7.4

One-Dimensional, Steady-State Solutions to the Heat Equation with No Generation

	Plane Wall	Cylindrical Wall <sup>a</sup>	Spherical Wall <sup>a</sup>
Heat equation	$\frac{d^2T}{dx^2} = 0$	$\frac{1}{r} \frac{d}{dr} \left( r \frac{dT}{dr} \right) = 0$	$\frac{1}{r^2} \frac{d}{dr} \left( r^2 \frac{dT}{dr} \right) = 0$
Temperature distribution	$T_{s,1} - \Delta T \frac{x}{L}$	$T_{s,2} + \Delta T \frac{\ln(r/r_2)}{\ln(r_1/r_2)}$	$T_{s,1} - \Delta T \left[ \frac{1 - (r_1/r)}{1 - (r_1/r_2)} \right]$
Heat flux ( $q''$ )	$k \frac{\Delta T}{L}$	$\frac{k \Delta T}{r \ln(r_2/r_1)}$	$\frac{k \Delta T}{r^2 [(1/r_1) - (1/r_2)]}$
Heat rate ( $q$ )	$kA \frac{\Delta T}{L}$	$\frac{2\pi L k \Delta T}{\ln(r_2/r_1)}$	$\frac{4\pi k \Delta T}{(1/r_1) - (1/r_2)}$
Thermal resistance ( $R_{t, \text{cond}}$ )	$\frac{L}{kA}$	$\frac{\ln(r_2/r_1)}{2\pi Lk}$	$\frac{(1/r_1) - (1/r_2)}{4\pi k}$

Source: Incropera, F.P. and DeWitt, D.P., *Fundamentals of Heat and Mass Transfer*, John Wiley & Sons, New York, 1996.

<sup>a</sup> The critical radius of insulation is  $r_{cr} = k/h$  for the cylinder and  $r_{cr} = 2k/h$  for the sphere where  $k$  is the thermal conductivity of the insulation and  $h$  is the convective heat transfer coefficient on the outside of the insulation.

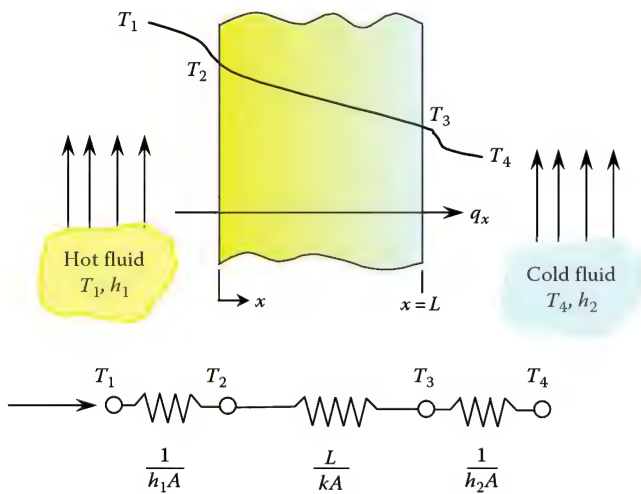


FIGURE 7.2

Heat transfer through a plane wall: (a) temperature distribution and (b) equivalent thermal circuit. (From Incropera, F.P. and DeWitt, D.P., *Fundamentals of Heat and Mass Transfer*, John Wiley & Sons, New York, 1996.)

For the plane wall shown in Figure 7.2, Equation 7.3 can be solved to obtain the following energy flux equation:

$$q_x = \frac{kA}{L} (T_{s,1} - T_{s,2}) \quad (7.4)$$

This equation can also be written as

$$q_x = \frac{(T_{s,1} - T_{s,2})}{\frac{L}{kA}} \quad (7.5)$$

where the quantity  $L/kA$  has the unit of h-ft/Btu (K/W) and is called thermal resistance. Figure 7.2 also includes an equivalent thermal circuit. One side of the plane wall ( $x = 0$ ) is being heated by the surrounding fluid at  $T_{\infty,1}$  and the other side ( $x = L$ ) is being cooled by the surrounding cold fluid at  $T_{\infty,2}$ . The thermal circuit in Figure 7.2 includes both convective heating and cooling as well as conduction through the material of the wall.

### 7.2.2.2 Composite Wall

In industry, different furnace designs are used for different heat transfer operations. Design economics require that these furnaces often have several layers in series to reduce costs, or to increase strength, or to provide better insulation. The one-dimensional steady-state heat transfer analysis can be applied to these cases also. A composite wall can be considered to be multiple walls in series as shown in Figure 7.3. The heat flux in the  $x$  direction is expressed as

$$q_x = \frac{T_1 - T_6}{\sum R_t} \quad (7.6)$$

where

$T_1$  and  $T_2$  are the surrounding temperatures

$\sum R_t$  is the total thermal resistance of the system

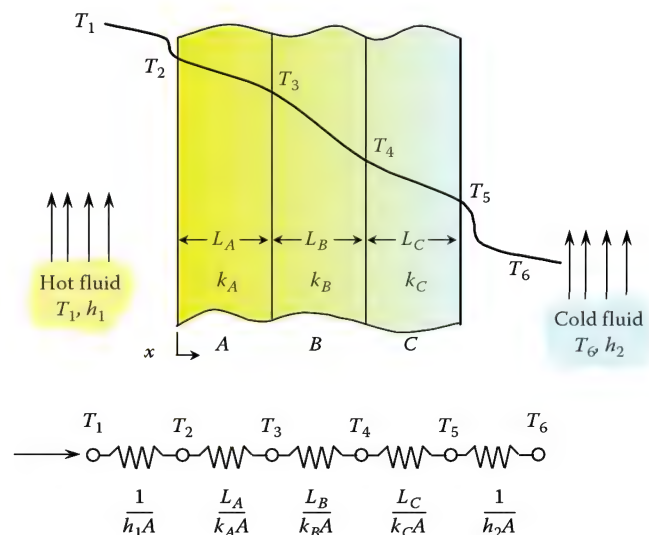


FIGURE 7.3

Equivalent thermal circuit for a series composite wall. (From Incropera, F.P. and DeWitt, D.P., *Fundamentals of Heat and Mass Transfer*, John Wiley & Sons, New York, 1996.)

The total thermal resistance for a wall with three layers is evaluated as

$$\sum R_t = \frac{1}{h_1 A} + \frac{L_A}{k_A A} + \frac{L_B}{k_B A} + \frac{L_C}{k_C A} + \frac{1}{h_2 A} \quad (7.7)$$

where

$h_1$  and  $h_2$  are convection heat transfer coefficients on the two sides of the composite wall, respectively  
 $k_A$ ,  $k_B$ , and  $k_C$  are the thermal conductivities of walls A, B, and C, respectively

The heat transfer rate can also be expressed as

$$q_x = \frac{T_{\infty,1} - T_{s,1}}{\frac{1}{h_1 A}} = \frac{T_{s,1} - T_2}{\frac{L_A}{k_A A}} = \frac{T_2 - T_3}{\frac{L_B}{k_B A}} = \dots \quad (7.8)$$

An overall heat transfer coefficient  $U$  can then be defined:

$$U = \frac{1}{R_{tot} A} = \frac{1}{\left(\frac{1}{h_1}\right) + \left(\frac{L_A}{k_A}\right) + \left(\frac{L_B}{k_B}\right) + \left(\frac{L_C}{k_C}\right) + \left(\frac{1}{h_2}\right)} \quad (7.9)$$

A circuit diagram of the thermal resistance of the composite walls is also shown in Figure 7.3.

### 7.2.2.3 Contact Resistance

In composite systems, the temperature drop across the interface between the walls might be appreciable. This temperature drop as caused by the contact resistance,  $R_{t,c}$ , between two solid materials A and B, is illustrated in Figure 7.4. If the heat flux for a unit area of interface is  $q_x$  ( $q_x = q_{contact} + q_{gap}$ ), then the contact resistance can be defined as

$$R_{t,c} = \frac{T_A - T_B}{q_x} \quad (7.10)$$

The thermal contact resistance for different combinations of solids is available in standard texts.<sup>51</sup>

### 7.2.2.4 Cylinder

For steady-state heat conduction with no generation of energy during conduction, the transfer in a hollow cylinder of radius  $r$  is

$$\frac{1}{r} \frac{d}{dr} \left( kr \frac{dT}{dr} \right) = 0 \quad (7.11)$$

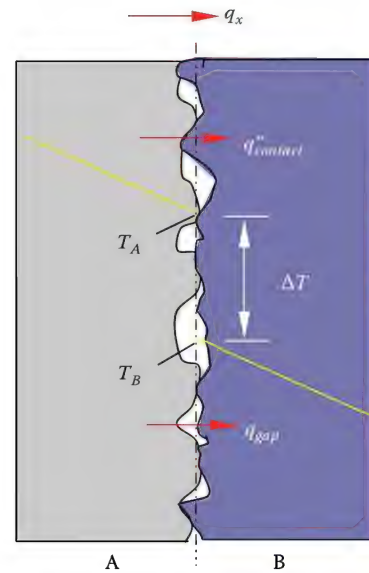


FIGURE 7.4

Temperature drop due to thermal contact resistance.

Energy generation refers to the exothermic or endothermic energy release within the medium that is conducting. This would not be the case in the wall of a pipe. However, if one were considering heat transfer through a gas that is reacting, as in combustion, then energy generation would have to be included.

From Equation 7.11 the heat flux in a cylinder can be defined as

$$q_r = \frac{2\pi Lk (T_{s,1} - T_{s,2})}{\ln(r_2/r_1)} \quad (7.12)$$

From this equation, the conduction thermal resistance can be given by

$$R = \frac{\ln(r_2/r_1)}{2\pi Lk} \quad (7.13)$$

The aforementioned concept can be extended to derive the equation for heat transfer in a system of multiple concentric cylinders, see Figure 7.5, with radii  $r_1$ ,  $r_2$ ,  $r_3$ , and  $r_4$ ; corresponding temperatures  $T_2$ ,  $T_3$ ,  $T_4$ , and  $T_5$ ; and thermal conductivities of  $k_A$ ,  $k_B$ , and  $k_C$ , all having length,  $L$ :

$$q_r = \frac{T_1 - T_6}{\frac{1}{2\pi r_1 L h_2} + \frac{\ln(r_2/r_1)}{2\pi k_A L} + \frac{\ln(r_3/r_2)}{2\pi k_B L} + \frac{\ln(r_4/r_3)}{2\pi k_C L} + \frac{1}{2\pi r_6 L h_6}} \quad (7.14)$$

where

$T_1$  and  $T_6$  represent surrounding temperatures

$h_2$  and  $h_6$  represent convection heat transfer coefficients on the surfaces 2 and 6, respectively



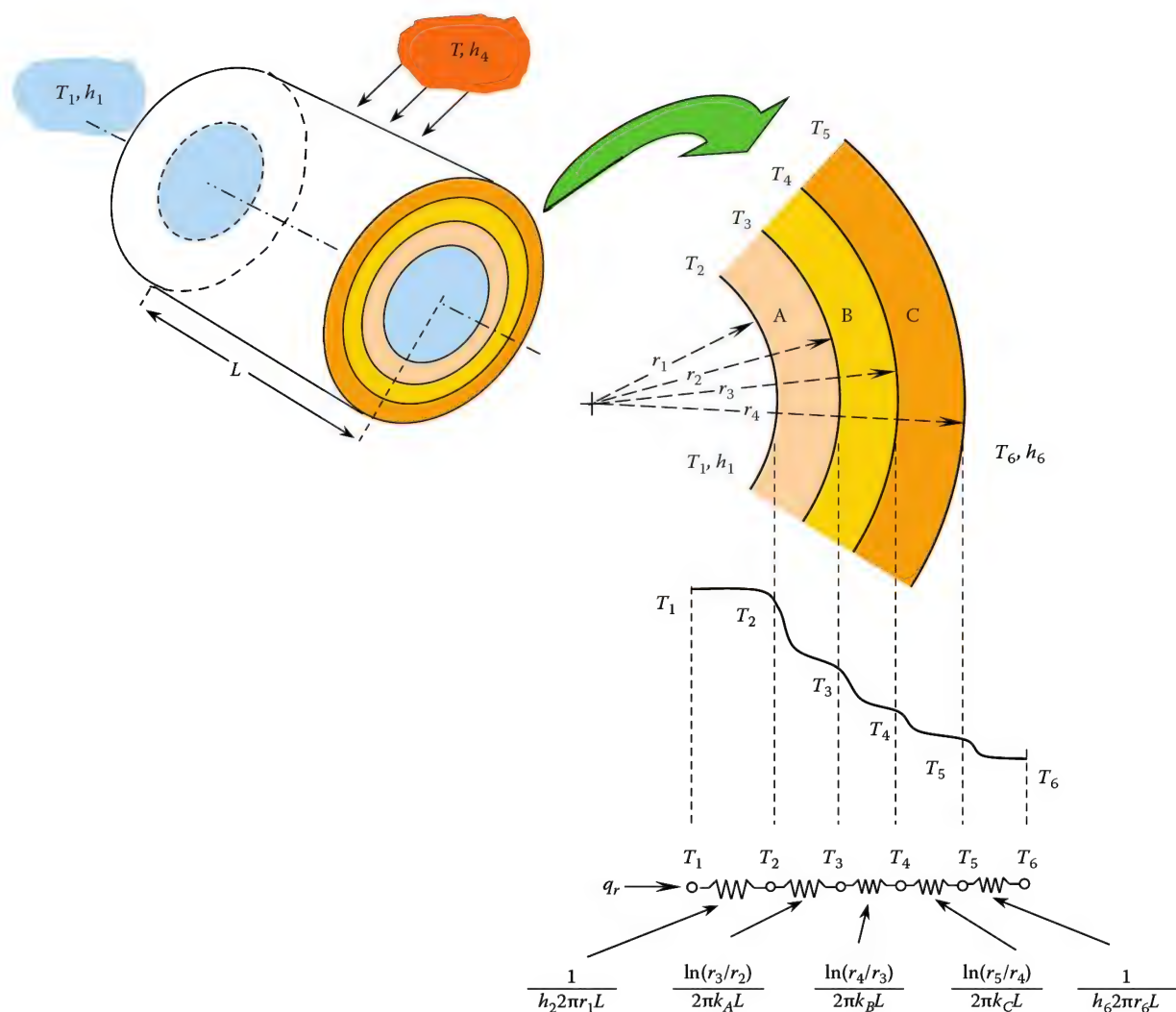


FIGURE 7.5

Temperature distribution for a composite cylindrical wall. (From Incropera, F.P. and DeWitt, D.P., *Fundamentals of Heat and Mass Transfer*, John Wiley & Sons, New York, 1996.)

Figure 7.5 also shows the thermal circuit of the system.

In terms of overall heat transfer coefficient,  $U$ , and total thermal resistance,  $R_{tot}$ ,

$$q_r = \frac{T_2 - T_6}{R_{tot}} = UA(T_2 - T_6) \quad (7.15)$$

### 7.2.3 Transient Conduction

Transient or unsteady-state conduction involves storage of heat. For instance, in heating up a furnace during startup, heat must be supplied to bring the walls to the operating temperature and to overcome the steady-state losses of normal operation. In typical continuous furnace operation, the heat stored in the walls and the metal of the tubes is insignificant compared to the total heat input. In heaters that are heated and cooled

periodically, such as in batch process work, the heat stored in the walls may be a significant cost.

Unsteady-state conduction occurs in heating or cooling processes where the temperatures change with time. Examples include operating regenerative heaters, raising boiler pressure, and turndown conditions on process furnaces. By introducing time as an additional variable, conduction analyses become more complicated.

One case is that unsteady-state conduction problems can be easily solved if the temperature gradient within a solid material can be ignored. The conditions under which temperature gradients can be ignored are considered later. A common example would be dropping a hot metal sphere into a cold water bath. The high thermal conductivity of the metal (compared with the convection coefficient as discussed later) usually allows analyzing the time-temperature



history of the metal's temperature without regard to temperature variations within the sphere. The simplified approach, based on neglecting the temperature gradient in the metal, is called the lumped capacitance method.

In a furnace setting, it is usually possible to neglect the temperature gradient in metal pipe walls, since the thermal conductivity is high compared to the rest of the heat transfer path. However, insulating refractory cannot be treated as lumped capacitance. Obviously, a lumped capacitance approximation is the first resort in the analysis of a transient problem due to its simplicity. However, it should be noted that the simplicity also makes it the least accurate approach.

If a hot solid initially ( $t = 0$ ) at a temperature  $T_i$  is cooled and attains any temperature  $T(t)$  at any time ( $t > 0$ ), a general heat balance equation can be written as

$$-hA_s(T - T_\infty) = \rho Vc \left( \frac{dT}{dt} \right) \quad (7.16)$$

where

$h$  is the convection heat transfer coefficient

$A_s$  is the surface area of the solid

$\rho$  is the density of the solid

$c$  is the specific heat of the solid

$T_\infty$  is the temperature of the surrounding medium

Solving the aforementioned differential equation gives

$$\frac{\theta}{\theta_i} = \frac{T - T_\infty}{T_i - T_\infty} = \exp \left[ - \left( \frac{hA_s}{\rho Vc} \right) t \right] \quad (7.17)$$

Here, the quantity  $(\rho Vc/hA_s)$  is called the thermal time constant, expressed as  $\tau_t$ . It can also be written as

$$\tau_t = \left( \frac{1}{hA_s} \right) (\rho Vc) = R_t C_t \quad (7.18)$$

Here  $R_t$  is the resistance to convection heat transfer and  $C_t$  is the lumped thermal capacitance of the solid. The physical significance of the aforementioned equation is the fact that any increase in the value of  $C_t$  or  $R_t$  will cause the system to respond more slowly for any change in the temperature.

Considering a plane wall with temperatures  $T_1$  and  $T_2$  ( $T_1 > T_2$ ) at the sides 1 and 2, surrounding temperature of  $T_\infty$ , the surface energy balance will give

$$\frac{kA}{L} (T_1 - T_2) = hA(T_2 - T_\infty) \quad (7.19)$$

where

$A$  is the surface area

$k$  is the thermal conductivity of the solid

This equation can be rearranged to give

$$\frac{(T_1 - T_2)}{(T_2 - T_\infty)} = \frac{\frac{L}{kA}}{\frac{1}{hA}} = \frac{hL}{k} \equiv Bi \quad (7.20)$$

The dimensionless quantity  $(hL/k)$  is called the Biot number ( $Bi$ ). It is a measure of the temperature drop in a solid as compared to the temperature drop between the surface and the fluid. It can also be interpreted as the ratio of resistance due to conduction and resistance due to convection. Obviously, when the conduction resistance is negligible as compared to the convection resistance (i.e.,  $Bi \ll 1$ ), the lumped capacitance assumption is valid. In the case of uneven surfaces or complicated shapes, the estimation of length,  $L$ , is difficult and therefore a characteristic length,  $L_c$ , is usually taken, which is the ratio of volume to the surface area.

The exponent in Equation 7.17 can now be rewritten as

$$\frac{hA_s t}{\rho Vc} = \frac{hL_c}{k} \frac{k}{pc} \frac{t}{L_c^2} = \frac{hL_c}{k} \frac{\alpha t}{L_c^2} = Bi \cdot Fo \quad (7.21)$$

where

$\alpha$  is the thermal diffusivity

$Fo$  is the Fourier number  $\equiv \alpha t/L_c^2$

Thus, the temperature distribution can be expressed as

$$\frac{\theta}{\theta_i} = \frac{T - T_\infty}{T_i - T_\infty} = \exp(-Bi \cdot Fo) \quad (7.22)$$

If the condition of the solid is affected simultaneously by convection, radiation, applied surface heat flux, and internal energy generation, the situation could be complicated and difficult to solve. Thus, the more general form of Equation 7.16 is

$$-hA_s(T - T_\infty) + \epsilon A_s \sigma (T^4 - T_{sur}^4) + E_g + q_s = \rho Vc \frac{dT}{dt} \quad (7.23)$$

where

$E_g$  is the heat generated within the system

$q_s$  is the heat supplied to the system

$\epsilon$  is the emissivity of the solid

$\sigma$  is the Stefan-Boltzmann's constant

Equation 7.23 is a nonlinear, first-order, nonhomogeneous differential equation, which cannot be integrated

to obtain an exact solution. However, when there is no imposed heat flux and negligible convection compared to radiation, this equation can be simplified to be solved and finally give

$$t = \frac{\rho V c}{3\epsilon A_s \sigma} \left( \frac{1}{T^3} - \frac{1}{T_i^3} \right) \quad (7.24)$$

Here it is assumed that the surrounding temperature ( $T_{sur}$ ) is zero.

On the other hand, if radiation is negligible compared to convection and the convection coefficient,  $h$ , is constant with respect to time, the differential equation can be solved to give

$$\frac{T - T_\infty}{T_i - T_\infty} = \exp(-at) + \frac{b/a}{T_i - T_\infty} [1 - \exp(-at)] \quad (7.25)$$

where  $a = \frac{hA_s}{\rho V c}$  and  $b = \frac{q_s + E_g}{\rho V c}$ . The second term on the right-hand side of Equation 7.25 is the outcome of the applied flux and the heat generated within the system.

Further discussion about transient conduction is beyond the scope of this book and the reader is referred to other texts on the subject.

Figure 7.6a shows thermal conductivities of some commonly used steels and alloys as a function of temperature. Figure 7.7 shows temperature variation in a slab, as a function of thickness, under three different conditions: (1) constant thermal conductivity, (2) thermal conductivity increasing with temperature, and (3) thermal conductivity decreasing with temperature. In the first case, the temperature profile is straight, in the second case it curves upward, and in the third case it curves downward.

### 7.3 Convection

Convection heat transfer occurs due to fluid movement. A combination of molecular conduction and macroscopic fluid motion contributes to convective heat transfer. Convection takes place adjacent to surfaces as a result of fluid motion past the surface. All convection processes fall into three categories: natural convection, forced convection, and mixed convection.

Natural convection occurs when fluid motion is created as a result of local density differences alone, without any mechanical driving force such as a fan or pump. Theoretical analyses of natural convection require the

simultaneous solution of the coupled equations of motion and energy.

Forced convection can occur when mechanical forces from devices such as fans and pumps give motion to the fluid. Forced convection is the most commonly employed mechanism in the process industries where hot and cold fluids, separated by a solid boundary, are pumped through heat-transfer equipment such as heat exchangers. The rate of heat transfer is a function of the physical properties of the fluids and surfaces, the flow rates, and the geometry of the system. Flow is generally turbulent and the flow duct varies in complexity from circular tubes to baffled and finned tubes. Theoretical analyses of forced convection heat transfer have been limited to relatively simple geometries and laminar flow. Usually, for complicated geometries, only empirical relationships are available. However, computational fluid dynamics (CFD) (see Chapter 13), the science of computer modeling flows and heat transfer, has advanced enough, to provide good information based on the available semi-empirical CFD models.<sup>52</sup> In forced convection, heat transfer coefficients are strongly influenced by the mechanics of the flow. The turbulence intensity, entrance conditions, and wall conditions are some of the factors that must be considered when calculating forced convection heat transfer.

Mixed convection refers to those situations where both natural and forced convection are at work. A good example would be the convective heat transfer process taking place on the outside surface of a furnace wall when there is some low velocity wind blowing. In the absence of wind, the wall would be cooled purely by natural convection, but with wind, both mechanisms are present simultaneously. If one mode is much more dominant than another, then the convection heat transfer can often be simplified by ignoring the much weaker mode. For example, if very high speed winds are blowing over the outside walls of a furnace, it is reasonable to ignore the natural convection heat transfer that would be insignificant.

One example of the importance of forced convection in the process industries is the convection section in process heaters. This is the downstream section of the heater that is heated by the combustion exhaust gases exiting the radiant or primary heating section (see Volume 3 for a more detailed discussion of process heaters). Not all heaters have a convection section, but Garg<sup>53</sup> estimates that the heater efficiency can be increased from 55%–65%, to 80% or more with the addition of a convection section. A number of books are dedicated specifically to convection heat transfer.<sup>54–65</sup> These should be consulted for a complete development of the theory and equations discussed in this section.

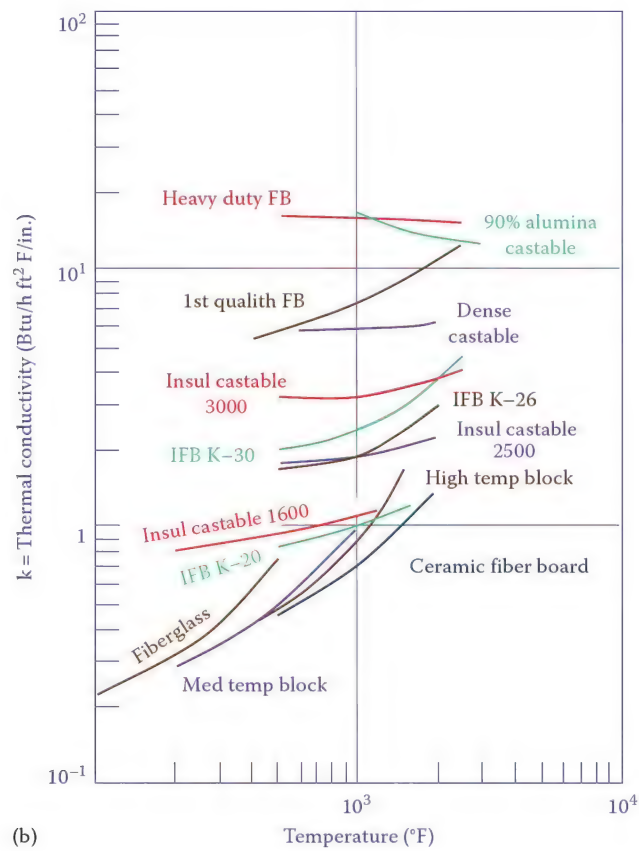
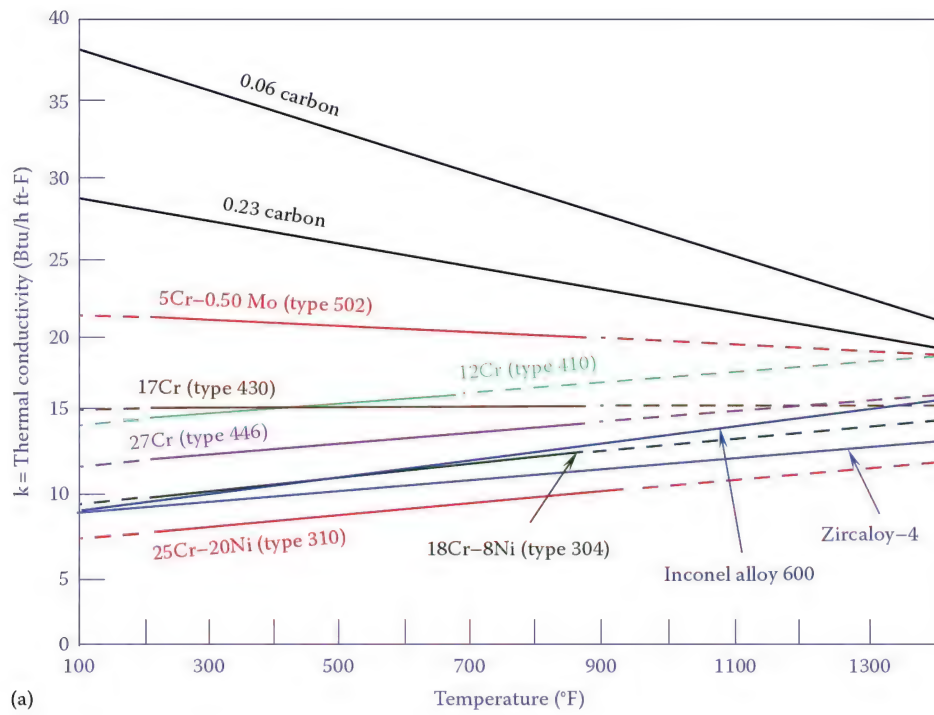
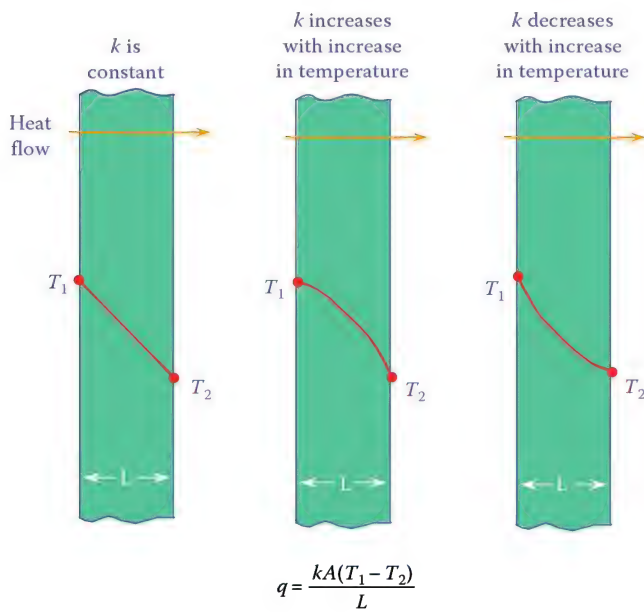


FIGURE 7.6

Thermal conductivity of (a) some commonly used steels and alloys and (b) some refractory materials.



**FIGURE 7.7**  
Temperature–thickness relationships corresponding to different thermal conductivities.

### 7.3.1 Dimensionless Numbers

There are some important nondimensional numbers that are commonly used in convection heat transfer analysis. The Reynolds number is the ratio of the inertial forces to the viscous forces in a flow:

$$Re = \frac{\rho v l}{\mu} = \frac{v l}{\nu} \quad (7.26)$$

where

$\rho$  is the fluid density

$v$  is the fluid velocity

$l$  is the characteristic length scale (e.g., diameter for a pipe for flow through a pipe)

$\mu$  is the absolute viscosity

$\nu$  is the kinematic viscosity

The Reynolds number is low for laminar flows and high for turbulent flows, with transition flows at values in between. The actual range for each type of flow depends on the flow geometry (e.g., internal flow through a pipe vs. external flow over a surface). The Prandtl number is the ratio of momentum diffusivity to thermal diffusivity and is defined as

$$Pr = \frac{c_p \mu}{k} \quad (7.27)$$

where

$c_p$  is the fluid constant pressure specific heat

$k$  is the fluid thermal conductivity

For many gases,  $Pr \approx 0.7$ . The Nusselt number is the ratio of the convective and conductive heat transfer rates:

$$Nu = \frac{h l}{k} \quad (7.28)$$

where  $h$  is the convective heat transfer coefficient.

In forced convection flows  $Nu$  is commonly a function of the  $Pr$  and  $Re$  and is used to determine the convection coefficient  $h$ .

Convection heat transfer is caused by fluid motion past a material, where the fluid is either at a higher or lower temperature than the material. In industrial combustion applications, the fluid is usually at a higher temperature than the medium it is heating. At least one person has argued that convection is not actually a separate mode of heat transfer, but that it is a subset of conduction because the energy must still conduct from the fluid to the material.<sup>66</sup> While that may be true on a microscopic scale in the boundary layer next to the material, convection is a fundamentally different process than conduction and is treated here as such, which is the convention in standard heat transfer texts. Forced convection is often a very important mode of heat transfer in industrial combustion systems. In some limited applications, natural convection may also be important because of high temperature gradients that may exist.

### 7.3.2 Newton's Law of Cooling

When a fan or a blower causes a fluid such as air to flow over a surface at a different temperature than the fluid, the heat transfer to the surface is by forced convection. When the fluid is simply moving due to buoyancy forces caused by a density difference, the transfer of heat is taking place by free, or natural, convection. Advection is energy transfer by bulk motion alone. In convection, heat transfer takes place due to random molecular motion and bulk motion combined. Any convective transfer of heat can be represented by a general heat balance equation:

$$q'' = h(T_s - T_\infty) \quad (7.29)$$

where

$q''$  is the heat flux from the surface

$h$  is the convective heat transfer coefficient

$T_s$  is the temperature of a surface  $s$

$T_\infty$  is the temperature of the fluid

If  $T_s > T_\infty$  where the surface is hotter than the fluid, then heat is convected away from the surface by the fluid and the surface is cooled. If  $T_s < T_\infty$ , where the surface



**TABLE 7.5**

Typical Convective Heat Transfer Coefficients

Condition	Btu/h ft <sup>2</sup> F	W/m <sup>2</sup> C
Air, free convection	1–5	6–30
Air, forced convection	5–50	30–300
Steam, forced convection	300–800	1,800–4,800
Oil, forced convection	5–300	30–1,800
Water, forced convection	50–2,000	300–1,200
Water, boiling	500–20,000	3,000–120,000

is cooler than the fluid, then heat is convected to the surface by the fluid. The aforementioned expression is called Newton's law of cooling. Typical convective heat transfer coefficients are shown in Table 7.5.

### 7.3.3 Laminar Flow Convection

An important factor that influences convective heat transfer is the laminar sublayer. In a turbulent flow of a fluid past a solid, in the immediate neighborhood of the surface, there exists a relatively quiet zone of fluid called the laminar sublayer. As one approaches the wall from the body of the fluid, the flow slows down. The region next to the wall where the flow velocity is much less than in the free stream is known as the boundary layer. The boundary layer itself has fluid that is turbulent closer to the core of the flow followed by a transition zone and finally becomes laminar very close to the wall. The portion of the flow that is essentially laminar is called the laminar sublayer. In the laminar sublayer, the heat is transferred by molecular conduction. The resistance of the laminar layer to heat flow will vary according to its thickness and can range

from 95% of the total resistance for some fluids to only 1% for others like liquid metals.

In highly turbulent flows, the sublayer is thinner, and so, greater turbulence makes for better heat transfer in general. Similarly, surface roughness and other mechanisms, such as oscillating flow or phase change, will aid in heat transfer by disturbing the boundary layer. From a heat transfer perspective, it is beneficial in process tubes used in reformers and crackers to have a rough surface finish that results from the spin-cast process used to make the tubes. Similarly, many boiler manufacturers and other heat exchanger manufacturers use heat transfer tubes with internal "rifling" to enhance the convective heat transfer.

In most cases, the boundary layer effect is dominant in gases. In a system transferring heat from a gas to a liquid, usually the resistance on the liquid side can be neglected because it is so much smaller than the resistance on the gas side.

Consider a fluid at a uniform temperature  $T(r, 0)$  entering a tube where the heat transfer takes place from the wall of the tube (maintained either at a constant temperature or with a constant wall heat flux), a thermal entrance region is formed as shown in Figure 7.8. For laminar flow conditions, the thermal entry length is given by Kays and Crawford<sup>58</sup> as

$$(x_{fd,t}/D)_{lam} = 0.05 \text{ Re}_D \text{ Pr} \quad (7.30)$$

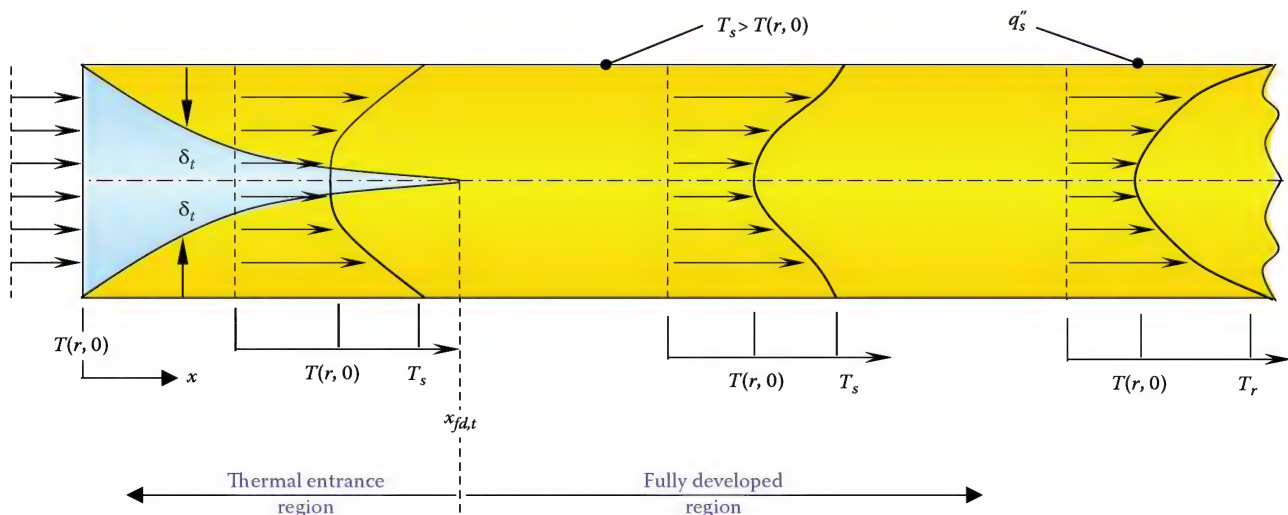
where

$x_{fd,t}$  is the thermal entrance length

$D$  is the diameter of the tube

$\text{Re}_D$  is the Reynolds number based on tube diameter

$\text{Pr}$  is the Prandtl number

**FIGURE 7.8**

Thermal boundary layer development in a heated circular tube. (From Incropera, F.P. and DeWitt, D.P., *Fundamentals of Heat and Mass Transfer*, John Wiley & Sons, New York, 1996.)

The thermal entry length then increases with the Reynolds number, which is directly dependent on fluid velocity. The equation for thermal entry length is very similar to the equation for hydrodynamic entry length, which is

$$(x_{fd,h}/D)_{lam} = 0.05 \text{ Re}_D \quad (7.31)$$

where  $x_{fd,h}$  is the hydrodynamic entry length.

### 7.3.3.1 Fully Developed Velocity and Temperature Profiles

For a particular set of conditions, the velocity in a tube may be approximated as uniform and the temperature as given by a parabolic profile, that is,

$$u(r) = C_1 \text{ and } T(r) - T_s = C_2 [1 - (r/r_0)^2] \quad (7.32)$$

where  $u(r)$  is the velocity as a function of radial distance from the centerline,  $C_1$  and  $C_2$  are constants,  $r$  is the radial distance from the centerline and  $r_0$  is the inside radius of the pipe. From Equation 7.29, the convection coefficient,  $h$ , is given by

$$h = \frac{q_s''}{T_s - T_m} \quad (7.33)$$

where  $T_s$  and  $T_m$  are the tube surface temperature and the mean temperature of the fluid in the tube, respectively. The mean temperature is given by

$$T_m = \frac{2}{u_m r_0^2} \int_0^{r_0} u T r dr \quad (7.34)$$

where  $u_m$  is the mean velocity in the pipe. Noting that the temperature is parabolic and the velocity is uniform throughout from Equation 7.32, it can be shown that

$$q_s'' = k \left( \frac{\partial T}{\partial r} \right)_{r=r_0} = \frac{-2kC_2}{r_0} \quad (7.35)$$

Therefore,

$$h = \frac{q_s''}{T_s - T_m} = \frac{4k}{r_0} \quad (7.36)$$

or

$$\text{Nu}_D = \frac{hD}{k} = 8 \quad (7.37)$$

where  $\text{Nu}_D$  is the Nusselt number based on tube diameter.

Similarly, in a circular tube characterized by uniform surface heat flux and fully developed conditions, the Nusselt number is given as

$$\text{Nu}_D = 4.36 \quad (7.38)$$

and for laminar, fully developed conditions, with a constant surface temperature, the Nusselt number is

$$\text{Nu}_D = 3.66 \quad (7.39)$$

### 7.3.4 Turbulent Internal Flow

#### 7.3.4.1 Circular Tubes

Internal or conduit flow is a flow field where the fluid completely fills a closed stationary duct or pipe. On the other hand, external or immersed flow is where the fluid flows past a stationary immersed solid. With internal flow, the heat-transfer coefficient is theoretically infinite at the location where heat transfer begins. The local heat-transfer coefficient rapidly decreases and becomes constant, so that after a certain length, the average coefficient in the conduit is independent of the length. The local coefficient may follow an irregular pattern, however, if obstructions or turbulence promoters are present in the duct.

Since the analysis of turbulent flow heat transfer is quite complex, empirical correlations are typically used in calculations. The Chilton–Colburn analogy provides an important correlation for the Nusselt number in turbulent flow heat transfer:

$$\text{St Pr}^{2/3} = \frac{\text{Nu}_D}{\text{Re}_D \text{ Pr}} \text{ Pr}^{2/3} = \frac{f}{8} \quad (7.40)$$

where

St is the Stanton number

$f$  is the friction factor

given by

$$f = 0.184(\text{Re}_D)^{-1/5} \quad (7.41)$$

Combining Equations 7.40 and 7.41,

$$\text{Nu}_D = 0.023 (\text{Re}_D)^{4/5} (\text{Pr})^{1/3} \quad (7.42)$$

Dittus and Boelter<sup>67</sup> suggested a modification in Equation 7.42 by replacing the exponent of Prandtl number by  $n$ , where  $n$  is 0.4 for heating and 0.3 for cooling. Equation 7.42, or its modification, is valid for the cases where the temperature difference ( $T_s - T_m$ ) is moderate. When the temperature difference is large,

the equation suggested by Sieder and Tate<sup>68</sup> is recommended as follows:

$$\text{Nu}_D = 0.027 (\text{Re}_D)^{4/5} (\text{Pr})^{1/3} (\mu/\mu_s)^{0.14} \quad (743)$$

where  $\mu_s$  is the viscosity of the fluid determined at the surface temperature and all the other properties are calculated at the mean temperature. The Dittus–Boelter and Sieder–Tate equations are applicable for both the cases of uniform surface temperature and heat flux conditions. Petukhov<sup>69</sup> gave a correlation that is more accurate than the Dittus–Boelter or Sieder–Tate equations, but is more complex to use

$$\text{Nu}_D = \frac{(f/8)\text{Re}_D \text{Pr}}{1.07 + 12.7(f/8)^{1/2}(\text{Pr}^{2/3} - 1)} \quad (744)$$

where the friction factor,  $f$ , is obtained from the Moody diagram in Figure 9.17.<sup>70</sup>

For the special cases of liquid metals, where the Prandtl number is very small ( $0.003 \leq \text{Pr} \leq 0.05$ ), Skupinski et al.<sup>71</sup> gave a correlation for heat transfer in fully developed turbulent flow. For constant surface heat flux, that correlation is

$$\text{Nu}_D = 4.82 + 0.0185 \text{Pe}_D^{0.827} \quad (745)$$

for  $3.6 \times 10^3 < \text{Re}_D < 9.05 \times 10^5$  and  $10^2 < \text{Pe}_D < 10^4$  where the Peclet number is defined as  $\text{Pe}_D = \text{Re}_D \text{Pr}$ . For constant surface temperature,<sup>72</sup>

$$\text{Nu}_D = 5.0 + 0.025 \text{Pe}_D^{0.8} \quad (746)$$

Reed et al.<sup>73</sup> have presented extensive literature on different correlations for heat transfer in laminar and turbulent flow conditions.

### 7.3.4.2 Non-circular Tubes/Sections

Although the correlations discussed so far have been presented for circular tubes, these relationships can be extended to noncircular tubes and sections simply by replacing the tube diameter by a hydraulic diameter defined as

$$D_h = 4 \frac{A_c}{P} \quad (747)$$

where

$A_c$  is the flow cross-sectional area

$P$  is the wetted perimeter

Reynolds number and Nusselt number calculations are based on the hydraulic diameter. In the case of flow

through an annulus produced by two concentric tubes, the hydraulic diameter is given by

$$D_h = \frac{4 \left( \frac{\pi}{4} \right) (D_o^2 - D_i^2)}{\pi D_o + \pi D_i} = D_o - D_i \quad (748)$$

Table 7.6 summarizes the convection correlations in circular tubes.<sup>51</sup>

### 7.3.5 Turbulent External Flow

External flow or immersed flow occurs when a fluid flows past a stationary immersed solid. Similar to internal flow, for immersed flow the local coefficient is again infinite at the point where heating begins. Subsequently, it decreases and may show irregularities depending upon the configuration of the body. Usually, the local coefficient does not become constant as flow proceeds downstream over the body.

When heat transfer occurs during immersed flow, the rate depends on the configuration of the body, the position of the body, the proximity of other bodies, and the flow rate and turbulence of the fluid stream. The heat transfer coefficient varies over the immersed body, since both the thermal and momentum boundary layers vary even for simple configurations immersed in an infinite flowing fluid. For complicated configurations and assemblages of bodies such as those found on the shell side of a heat exchanger, little is known about the local heat transfer coefficient; empirical relationships giving average coefficients are all that are usually available. Research that has been conducted on local coefficients in complicated geometries has not been extensive enough to extrapolate into useful design relationships.

For turbulent flow with the Reynolds number up to about  $10^8$ , the local friction coefficient is given by<sup>74</sup>

$$C_{f,x} = 0.0592 \text{Re}_x^{-1/5} \quad (749)$$

where  $x$  is the distance from the leading edge. The velocity boundary layer thickness is given by

$$\delta = 0.37 \times \text{Re}_x^{-1/5} \quad (750)$$

where  $x$  is the distance in the direction of flow. Thus the local Nusselt number for external turbulent flow is

$$\text{Nu}_x = \text{St} \text{Re}_x \text{Pr} = 0.0296 \text{Re}_x^{4/5} \text{Pr}^{1/3} \quad (751)$$

where  $\text{St}$  is the Stanton number.

Complications arise when the boundary layer formation caused by the external flow consists of both laminar and turbulent portions. Under these circumstances, neither laminar nor turbulent correlations are satisfactory.

TABLE 7.6

Summary of Convection Correlations for Flow in a Circular Tube

Correlation	Conditions
$f = 64/\text{Re}_D$	Laminar, fully developed
$\text{Nu}_D = 4.36$	Laminar, fully developed, uniform $q_s''$ , $\text{Pr} \geq 0.6$
$\text{Nu}_D = 3.66$	Laminar, fully developed, uniform $T_s$ , $\text{Pr} \geq 0.6$
$\overline{\text{Nu}}_D = 3.66 + \frac{0.0668(D/L)\text{Re}_D \text{Pr}}{1 + 0.04[(D/L)\text{Re}_D \text{Pr}]^{2/3}}$	Laminar, thermal entry length ( $\text{Pr} \gg 1$ or an unheated starting length), uniform $T_s$
or, $\overline{\text{Nu}}_D = 1.86 + \left(\frac{\text{Re}_D \text{Pr}}{L/D}\right)^{2/3} \left(\frac{\mu}{\mu_s}\right)^{0.14}$	Laminar, combined entry length $\{[\text{Re}_D \text{Pr}/(L/D)]^{1/3} (\mu/\mu_s)^{0.14}\} \geq 2$ ; uniform $T_s$ , $0.48 < \text{Pr} < 16,700$ , $0.0044 < (\mu/\mu_s) < 9.75$
$f = 0.316 \text{Re}_D^{-1/4}$	Turbulent, fully developed, $\text{Re}_D \leq 2 \times 10^4$
$f = 0.184 \text{Re}_D^{-1/5}$	Turbulent, fully developed, $\text{Re}_D \leq 2 \times 10^4$
or, $f = (0.790 \ln \text{Re}_D - 1.64)^{-2}$	Turbulent, fully developed, $3000 \leq \text{Re}_D \leq 5 \times 10^6$
$\text{Nu}_D = 0.023 \text{Re}_D^{4/5} \text{Pr}^n$	Turbulent, fully developed, $0.6 \leq \text{Pr} \leq 160$ , $\text{Re}_D \geq 10,000$ , $(L/D) \geq 10$ , $n = 0.4$ for $T_s > T_m$ and $n = 0.3$ for $T_s > T_m$
or	
$\text{Nu}_D = 0.027 \text{Re}_D^{4/5} \text{Pr}^{1/3} \left(\frac{\mu}{\mu_s}\right)^{0.14}$	Turbulent, fully developed, $0.7 \leq \text{Pr} \leq 16,700$ , $\text{Re}_D \geq 10,000$ , $(L/D) \geq 10$
or	
$\text{Nu}_D = \left(\frac{(f/8)(\text{Re}_D - 1000)\text{Pr}}{1 + 12.7(f/8)^{1/2}(\text{Pr}^{2/3} + 1)}\right)$	Turbulent, fully developed, $0.5 \leq \text{Pr} \leq 2000$ , $3000 \leq \text{Re}_D \leq 5 \times 10^6$ , $(L/D) \geq 10$
$\text{Nu}_D = 4.82 + 0.0185(\text{Re}_D \text{Pr})^{0.827}$	Liquid metals, turbulent, fully developed, uniform $q_s''$ , $3.6 \times 10^3 < \text{Re}_D < 9.05 \times 10^5$ , $10^2 < \text{Pe}_D < 10^4$
$\text{Nu}_D = 5.0 + 0.025(\text{Re}_D \text{Pr})^{0.8}$	Liquid metals, turbulent, fully developed, uniform $T_s$ , $\text{Pe}_D > 100$

Source: Incropera, F.P. and DeWitt, D.P., *Fundamentals of Heat and Mass Transfer*, John Wiley & Sons, New York, 1996.

A reasonably good correlation for mixed boundary layer conditions is

$$\text{Nu}_L = [0.037 \text{Re}_L^{4/5} - 871] \text{Pr}^{1/3} \quad (7.52)$$

where  $L$  is the length of the surface in the flow direction, with the conditions that  $0.6 < \text{Pr} < 60$ ;  $5 \times 10^5 < \text{Re}_L < 10^8$ ;  $\text{Re}_{x,c} = 5 \times 10^5$  and where  $\text{Re}_L$  is based on the total length of the surface and  $\text{Re}_{x,c}$  is the critical Reynolds number for transition from laminar to turbulent.

Similarly, the suitable correlation for the friction coefficient in mixed boundary cases is given by

$$C_{f,L} = [0.074/\text{Re}_L^{1/5}] - [1742/\text{Re}_L] \quad (7.53)$$

with the conditions  $5 \times 10^5 < \text{Re}_L < 10^8$  and  $\text{Re}_{x,c} = 5 \times 10^5$ .

When  $L$  is very high as compared to  $x_c$  (i.e., the entire surface is covered by a turbulent layer), the correlation for heat transfer simplifies to

$$\text{Nu}_L = 0.037 \text{Re}_L^{4/5} \text{Pr}^{1/3} \quad (7.54)$$

and similarly, the friction coefficient becomes

$$C_{f,L} = 0.074 \text{Re}_L^{-1/5} \quad (7.55)$$

### 7.3.5.1 Convection Heat Transfer for the Cylinders in Cross Flow

Hilpert<sup>75</sup> presented a correlation for the average Nusselt number for convection heat transfer for cylinders in cross flow:

$$\text{Nu}_D = \frac{hD}{k} = C \text{Re}_D^m \text{Pr}^{1/3} \quad (7.56)$$

where Nusselt and Reynolds numbers are based on the diameter of the cylinder, and constants  $C$  and  $m$  are as presented by Hilpert<sup>75</sup> and Knudsen and Katz<sup>76</sup> in Table 7.7.

In Equation 7.56, Churchill and Bernstein<sup>77</sup> suggest a more comprehensive correlation covering a wider range of Reynolds and Prandtl numbers and suitable for the entire range of experimental data available:

$$\text{Nu}_D = 0.3 + \frac{0.62 \text{Re}_D^{1/2} \text{Pr}^{1/3}}{[(1 + (0.4/\text{Pr})^{2/3})]^{1/4}} \left[ 1 + \left( \frac{\text{Re}_D}{282,000} \right)^{5/8} \right]^{4/5} \quad (7.57)$$

where all the physical properties are determined at the film temperature.



TABLE 7.7

Constants of Equation 7.56 for Circular Cylinder in Cross Flow

$Re_D$	$C$	$m$
0.4–4	0.989	0.330
4–40	0.911	0.385
40–4 × 103	0.683	0.466
4 × 103–4 × 104	0.193	0.618
4 × 104–4 × 105	0.027	0.805

Source: Hilpert, R., *Forschungsarbeiten auf dem Gebiet des Ingenieurwesens*, 4, 215, 1933; Knudsen, J.D. and Katz, D.L., *Fluid Dynamics and Heat Transfer*, McGraw-Hill, New York, 1958.

### 7.3.5.2 Convection Heat Transfer in Banks of Tubes

Grimison<sup>78</sup> suggested a correlation for convection heat transfer in aligned or staggered banks of tubes for 10 or more rows of tubes:

$$Nu_D = 1.13 C_1 Re_{D,max}^m Pr^{1/3} \quad (7.58)$$

for the conditions  $2000 < Re_{D,max} < 40,000$  and  $Pr \geq 0.7$ .

For the number of rows less than 10 a correction factor must be used.<sup>51</sup> In the aforementioned equation, the Reynolds number is based on the maximum fluid velocity occurring within the tube bank. The maximum velocity for the aligned arrangement is given by

$$V_{max} = \frac{S_T}{S_T - D} V \quad (7.59)$$

and the maximum velocity for the staggered arrangement is

$$V_{max} = \frac{S_T}{2(S_T - D)} V \quad (7.60)$$

Zhukauskas<sup>79</sup> has presented a correlation that is more recent and widely used:

$$Nu_D = C \cdot Re_{D,max}^m Pr^{0.36} \left( \frac{Pr}{Pr_s} \right)^{1/4} \quad (7.61)$$

The equation is valid for the following conditions: number of rows,  $N_L \geq 20$ ;  $0.7 < Pr < 500$ ;  $1000 < Re_{D,max} < 2 \times 10^6$ , where all the properties, except  $Pr_s$ , have been determined at the arithmetic mean of the inlet and outlet fluid temperatures, and constants  $C$  and  $m$  are listed in Table 7.8.

TABLE 7.8

Constants of Equation 7.61 for the Tube Bank in Cross Flow

Configuration	$Re_{D,max}$	$C$	$m$
Aligned	$10-10^2$	0.80	0.40
Staggered	$10-10^2$	0.90	0.40
Aligned	$10^2-10^3$	Approximate as a single (isolated) cylinder	
Staggered	$10^2-10^3$		
Aligned ( $S_T/S_L > 0.7$ ) <sup>a</sup>	$10^3-2 \times 10^5$	0.27	0.63
Staggered ( $S_T/S_L > 2$ )	$10^3-2 \times 10^5$	$0.35 (S_T/S_L)^{1/5}$	0.60
Staggered ( $S_T/S_L > 2$ )	$10^3-2 \times 10^5$	0.40	0.60
Aligned	$2 \times 10^5-2 \times 10^6$	0.021	0.84
Staggered	$2 \times 10^5-2 \times 10^6$	0.022	0.84

Source: Zhukauskas, A., Heat transfer from tubes in cross flow, in J. P. Hartnett and T. F. Irvine, Jr., (eds.), *Advances in Heat Transfer*, Vol. 8, Academic Press, New York, 1972.

<sup>a</sup> For  $(S_T/S_L < 0.7)$ , heat transfer is inefficient and aligned tubes should not be used.

### 7.3.6 Forced Convection from Flames

In many conventional furnace heating processes, forced convection is only a small fraction of the total heat transfer to the product. Most of the heating comes from the radiation from the hot refractory walls. However, in flame impingement, with no furnace enclosure, forced convection may be 70%–90% of the total heat flux.<sup>80,81</sup> For flame temperatures up to about 2600°F (1700 K), forced convection is the dominant mechanism in flame impingement heat transfer.<sup>82</sup>

For low temperature flames, as is common in air/fuel combustion systems, forced convection has generally been the only mechanism considered. In highly dissociated oxygen/fuel flames, a large fraction of the heat release is from exothermic reactions. However, even for those flames, forced convection is still an important contributor to the overall heat transfer to the target.

The turbulence level directly affects the importance of forced convection. The flow regime is determined by the Reynolds number, defined in Equation 7.26. For example, for flame jet impingement<sup>83</sup> there are many possible choices for the length  $l$ . One is the burner outlet nozzle diameter,  $d_n$ . Another is the axial distance from the nozzle exit to the surface being heated,  $l_j$ . A third possibility is the width of the jet at the edge of the stagnation zone,  $d_j$ . Still another is some dimension of the material being heated. For a disk or cylinder, it may be the diameter,  $d_b$ . For a plane surface, it may be the radial distance from the stagnation point,  $r$ . In one case, the width of the water cooling channel in a target used in a flame impingement study was used.<sup>82</sup>

Laminar flames have been used in many flame impingement studies.<sup>82,84–93</sup> Sibulkin<sup>94</sup> developed a semi-analytic solution for the heat transfer for laminar

flow, normal to the stagnation point of an axisymmetric, blunt-nosed target:

$$q''_s = 0.763(\beta_s \rho_e \mu_e)^{0.5} \text{Pr}_e^{-0.6} c_{p_e}(T_e - T_w) \quad (7.62)$$

where  $\beta_s$  is the velocity gradient at the edge of the stagnation zone in front of the stagnation point and is defined as

$$\beta_s = \left( \frac{\partial v_x}{\partial x} \right)_{x=0, y=\delta}$$

This result has been the basis for all other semi-analytical flame impingement heat transfer solutions.<sup>95</sup>

Turbulent flames have also been commonly used.<sup>81,96–108</sup> A typical example of an empirical equation, incorporating the turbulence intensity  $Tu$ , was given by Hustad and Sønju as

$$q''_s = \frac{k_e}{d_b} \left\{ 0.41 \text{Re}_{b,e}^{0.6} \text{Pr}_e^{0.35} Tu^{0.15} \left( \frac{\text{Pr}_e}{\text{Pr}_w} \right)^{0.25} \right\} (T_e - T_w) \quad (7.63)$$

where subscript  $b$  refers to the body of revolution. This was developed for flames produced by jets of  $\text{CH}_4$  and  $\text{C}_3\text{H}_8$  into ambient air. These are known as pure diffusion ( $\phi = \infty$ ) flames. The flames impinged normal to uncooled steel pipes. These experiments were done to simulate fires, caused by ruptured fuel pipes in the petrochemical industry.

Babiy<sup>109</sup> presents a correlation for the convective heat transfer from combustion gases to carbon particles in pulverized coal combustion processes. A commonly used equation for the convective heat transfer between a gas and a sphere is given by

$$\text{Nu}_d = 2 + 0.17 \text{Re}_d^{0.66} \quad (7.64)$$

where  $d$  is the diameter of the sphere.

For pulverized coal combustion, this equation is modified as follows:

$$\text{Nu}_d^* = \text{Nu}_d \left[ 145 \exp \left( \frac{-5000}{T_g} \right) \right] \quad (7.65)$$

where  $T_g$  is the absolute temperature of the gas (K).

The equation applies for  $T_g = 1200\text{--}1600$  K ( $1700^\circ\text{F}\text{--}2400^\circ\text{F}$ ),  $\text{O}_2 = 5\%\text{--}21\%$ ,  $d = 150\text{--}1000$   $\mu\text{m}$ , and  $\text{Re}_d < 1$ .

### 7.3.7 Natural Convection

Natural convection is sometimes referred to as buoyancy-induced flow.<sup>110</sup> These flows can occur where the

gas velocities are very low. Natural convection heat transfer from flames may be important in industrial combustion systems.

One measure of the intensity of natural convection is the Rayleigh number:

$$\text{Ra} = \frac{g \tilde{\beta}_e q_f l_j^2}{\rho_e c_{p_e} \nu_e^3} \quad (7.66)$$

which is analogous to the Reynolds number for forced convection. Higher Rayleigh numbers indicate more natural convection. Another measure of intensity is the Grashof number:

$$\text{Gr} = \frac{g \tilde{\beta}_e (T_w - T_\infty) l^3}{\nu^2} \quad (7.67)$$

where

$g$  is the gravity constant

$\tilde{\beta}$  is the volume coefficient of expansion ( $= 1/T$  for an ideal gas)

$\nu$  is the kinematic viscosity

The Richardson number,  $Ri$ , is one measure of the importance of buoyancy compared to forced convection. It is defined as

$$\text{Ri} = \frac{\text{Gr}}{\text{Re}_n^2} \quad (7.68)$$

which is the ratio of the buoyant force to the inertial force. Conolly and Davies<sup>89</sup> studied stoichiometric, laminar flames impinging on a hemi-nosed cylinder. The flame was parallel to the cylinder and impinging on the nose. A variety of fuels and oxidizers were used. Buoyancy effects were negligible. The criterion was that buoyancy may be neglected, compared to forced convection, for  $Ri < 0.05$ . Wang et al.<sup>111</sup> numerically modeled a non-reacting jet of ambient air, impinging on an infinite flat plate. It was concluded that natural convection is important only when  $\text{Re}_j$  is low, and the temperature difference between the jet and the stagnation surface is large. The critical  $Ri$  was estimated to be approximately 0.02. You<sup>93</sup> determined the heat transfer from a buoyant flame to a flat plate, in terms of the Rayleigh number, as

$$q''_b = 31.2 \left( q_f / l_j^2 \right) \text{Ra}_e^{-1/6} \text{Pr}_e^{-3/5} \quad (7.69)$$

where  $q_f$  is the heat release and  $l_j$  is the jet length. The flames were produced by upward jets of pure natural gas into ambient air. The jets impinged on a horizontal surface, to simulate a fire spreading over the ceiling of a room. Natural convection is more important in low velocity flames. Both Beér<sup>80</sup> and Vizioz<sup>97</sup> stated that the

effects of buoyancy were negligible in their studies, due to the high burner exit velocities.

## 7.4 Radiation

Thermal radiation heat transfer is the movement of energy by electromagnetic waves. Quantum theory describes electromagnetic energy as photons or quanta. Unlike conduction or convection, radiation does not require any intervening medium for transfer. Electromagnetic radiation, in the wavelength range of 0.1–100  $\mu\text{m}$ , is produced solely by the temperature of a body. Energy at the body's surface is converted into electromagnetic waves that emanate from the surface and strike another body. Some of the thermal radiation is absorbed by the receiving body and reconverted into internal energy, while the remaining energy is reflected from or transmitted through the body. The fractions of radiation reflected, transmitted, and absorbed by a surface are known, respectively, as reflectivity  $\rho$ , transmissivity  $\tau$ , and absorptivity  $\alpha$ . The sum of these fractions equals one:

$$\rho + \tau + \alpha = 1 \quad (7.70)$$

Thermal radiation is emitted by all surfaces whose temperatures are above absolute zero.

Thermal radiation can pass through some gases like air without absorption taking place. So these gases do not affect radiative transfer. On the other hand, gases like carbon dioxide, water vapor, and carbon monoxide affect radiation to some extent and are known as participating gases. These participating gases are, of course, common constituents of furnace flue gases (see Chapter 4) and, as such, play a significant part in the transfer and distribution of heat to the heater tubes.

All surfaces emit radiation in amounts that are determined by the temperature and the nature of the surface.

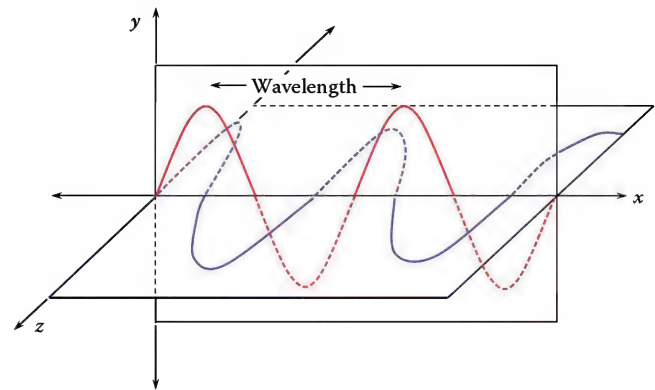


FIGURE 7.9

Orthogonal oscillations of electric and magnetic waves in the propagation of electromagnetic waves.

The perfect radiator, commonly known as a “blackbody” absorbs all the radiant energy reaching its surface and emits radiant energy at the maximum theoretical limit according to the Stefan–Boltzmann law:

$$Q_r = A\sigma T_s^4 \quad (7.71)$$

where

$\sigma$  is the Stefan–Boltzmann constant  $0.1713 \times 10^{-8}$  Btu/h-ft<sup>2</sup>-R<sup>4</sup> or  $(5.669 \times 10^{-8} \text{ W/m}^2\text{-K}^4)$

$T_s$  is the absolute temperature in Rankine (Kelvin)

The product  $\sigma T_s^4$  is also known as the blackbody emissive power  $E_b$ .

Radiation plays an important role in many industrial processes that require heating, cooling, drying, combustion, and solar energy. Figure 7.9 shows a schematic of the propagation of electromagnetic waves. The electrical and magnetic oscillations can be seen to be orthogonal to each other. Figure 7.10 shows the spectrum of electromagnetic radiation and Table 7.9 gives

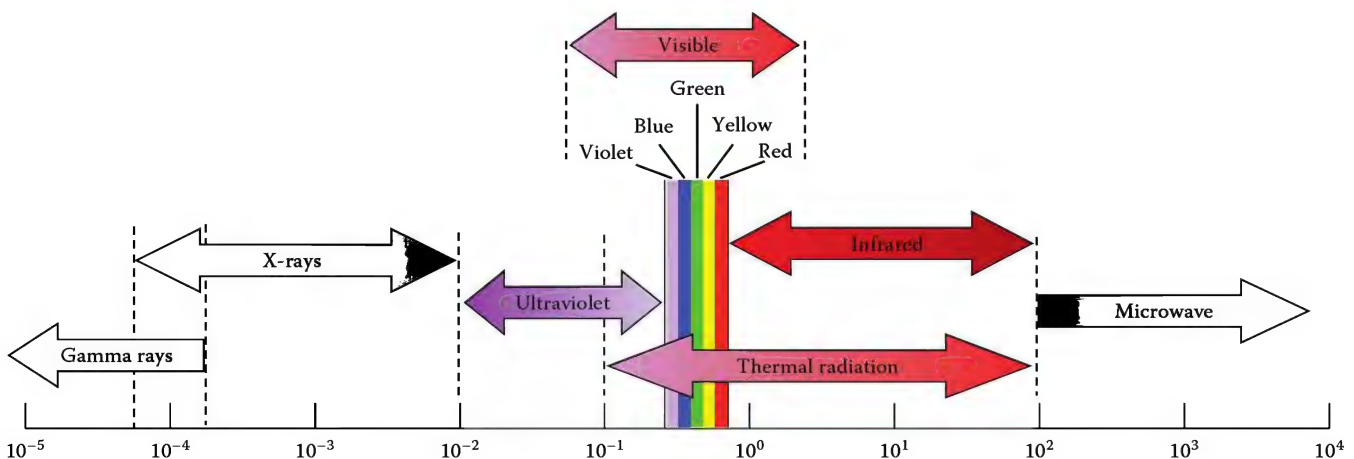


FIGURE 7.10

Spectrum of electromagnetic radiation.



TABLE 7.9

Spectrum of Electromagnetic Radiation

Region	Wavelength (Å)	Wavelength (cm)	Frequency (Hz)	Energy (eV)
Microwave	10 <sup>9</sup> –10 <sup>6</sup>	10–0.01	3 × 10 <sup>9</sup> –3 × 10 <sup>12</sup>	10 <sup>–5</sup> –0.01
Infrared	10 <sup>6</sup> –7000	0.01–7 × 10 <sup>–5</sup>	3 × 10 <sup>12</sup> –4.3 × 10 <sup>14</sup>	0.01–2
Visible	7000–4000	7 × 10 <sup>–5</sup> –4 × 10 <sup>–5</sup>	4.3 × 10 <sup>14</sup> –7.5 × 10 <sup>14</sup>	2–3
Ultraviolet	4000–10	4 × 10 <sup>–5</sup> –10 <sup>–7</sup>	7.5 × 10 <sup>14</sup> –3 × 10 <sup>17</sup>	3–10 <sup>3</sup>
X-rays	10–0.1	10 <sup>–7</sup> –10 <sup>–9</sup>	3 × 10 <sup>17</sup> –3 × 10 <sup>19</sup>	10 <sup>3</sup> –10 <sup>5</sup>
Gamma rays	<0.1	<10 <sup>–9</sup>	>3 × 10 <sup>19</sup>	>10 <sup>5</sup>

approximate wavelengths, frequencies, and energies for selected regions of the spectrum. Books dedicated to dealing with general radiation heat transfer are available.<sup>25, 28, 29, 112–115</sup>

This section will first treat thermal radiation heat transfer between surfaces in enclosures. Each surface is assumed to be isothermal, gray, and diffuse. The assumption that the surfaces are gray means that they emit and absorb thermal radiation without regard to the *wavelength* or *frequency* of the radiation. Since thermal radiation is a wave, it has all of the properties of a wave. It has a wavelength, a frequency, and a wave number. It can be reflected, refracted, and diffracted. The assumption of diffuse surfaces implies that the surfaces emit, absorb, and reflect radiation energy without regard to the direction (relative to the surface). Real surfaces are neither gray nor diffuse, but usually their behavior can reasonably be approximated as such. Many real surfaces have surface imperfections or oxide layers that may be on the order of 1 × 10<sup>–6</sup> m (1 μm) in thickness. This surface layer will interact with radiation of wavelengths near this value. Additionally, electromagnetic theory can be used to predict both the directional and wavelength dependence of pure metal surfaces. Analysis of radiation heat transfer in an industrial setting is complicated by these factors. Furthermore, the radiative properties of real surfaces can be strongly dependent on the surface preparation. For instance, a polished metal will have an emissivity that may be an order of magnitude below the emissivity of the same surface with an oxide layer. Uncertainties in radiative properties are always a consideration when conducting radiation heat transfer analyses. However, when used appropriately and with care, values of properties obtained from literature surfaces can be used to make reasonably accurate heat transfer calculations.

#### 7.4.1 Blackbody Radiation/Planck Distribution

A blackbody is an ideal body, useful as a reference in discussion of radiant heat transfer theory, that is both an ideal and diffuse emitter and absorber of radiant energy. It absorbs all incident radiation, regardless of wavelength and direction. No real surface can emit more energy than a blackbody at a given temperature and wavelength. Since the emission from a blackbody is diffuse, the intensity of a blackbody is given as

$$I_b = \frac{E_b}{\pi} \quad (7.72)$$

where  $E_b$  is the emissive power of the blackbody.

A relatively small opening to a cavity with a uniform interior surface temperature closely approximates the radiation characteristics of a blackbody. Radiation that enters the surface will be partially absorbed and partially reflected by the first internal surface of incidence. If the opening is small compared to the cavity dimension, then virtually all of the energy that enters the cavity will undergo multiple internal reflections and eventually be absorbed. Further, even though the surfaces within the cavity are not black and they do not emit blackbody radiation, their *radiosity* (radiosity is the total radiation leaving a surface, in this case, it will be the emitted radiation plus the reflected radiation) will be that of a blackbody. The proof of this is given in Siegel and Howell.<sup>114</sup>

##### 7.4.1.1 Planck Distribution

Spectral distribution of a blackbody emission was first determined by Planck<sup>116</sup> and is given by

$$I_{\lambda,b}(\lambda, T) = \frac{2hc_0^2}{\lambda^5 [\exp(hc_0/\lambda kT) - 1]} \quad (7.73)$$

where

$h = 6.6256 \times 10^{-34}$  J · s (Planck constant)

$k = 1.3805 \times 10^{-23}$  J/K (Boltzmann constant)

$c_0 = 2.998 \times 10^8$  m/s (speed of light in vacuum)

$T$  is the absolute temperature of the blackbody in K

On the assumption that the blackbody is a diffuse emitter, its spectral emissive power is given by

$$E_{\lambda,b}(\lambda, T) = \pi I_{\lambda,b}(\lambda, T) = \frac{2h\pi c_0^2}{\lambda^5 [\exp(hc_0/\lambda kT) - 1]} \quad (7.74)$$

Equation 7.74 is known as the Planck distribution. Figure 7.11 shows the variation of spectral emissive



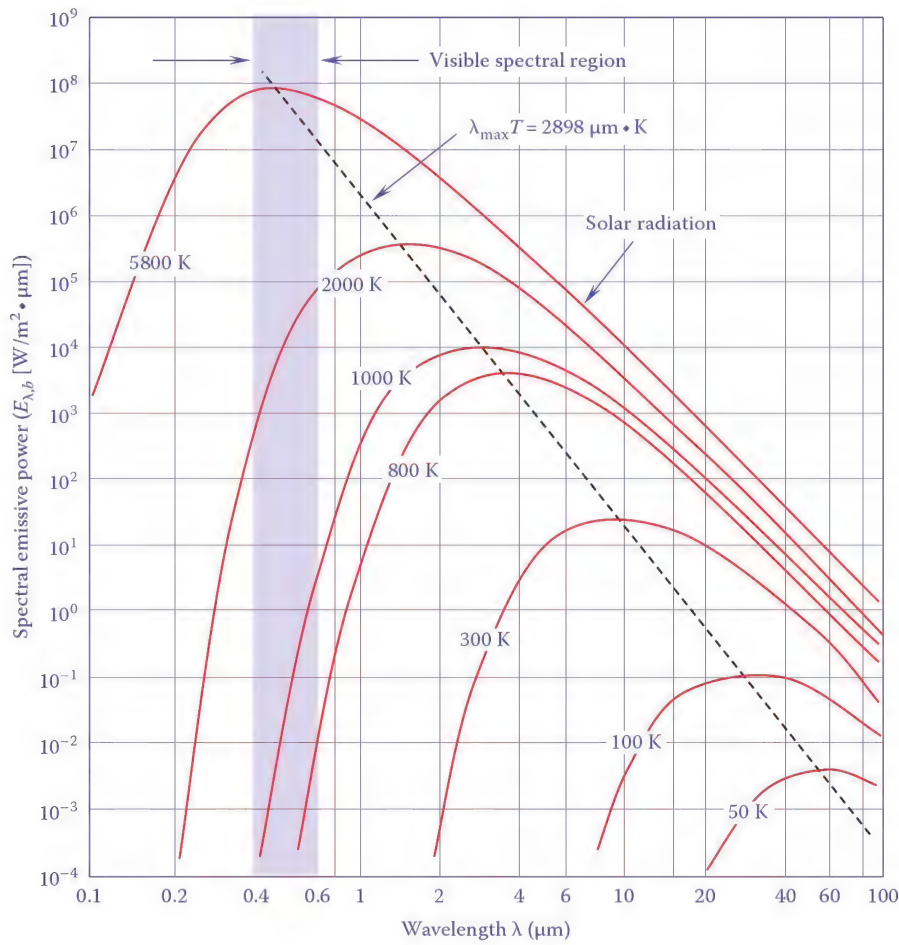


**FIGURE 7.11**  
Spectral blackbody emissive power.

power as a function of wavelength for selected temperatures. The figure indicates that as temperature increases, the blackbody emissive power at every wavelength increases and the wavelength of peak emission decreases. Radiation from the sun is approximated by radiation from a 5800 K (9980°F) blackbody source. The temperature at which radiant energy emissions from a surface become visible to the human eye is called the Draper point, occurring at approximately 800 K (980°F).

#### 7.4.1.2 Wien's Displacement Law

From Figure 7.11 it is clear that the blackbody spectral distribution has a maximum and the corresponding  $\lambda_{max}$  depends on temperature. Differentiating Equation 7.73 with respect to  $\lambda$  and setting the result equal to zero gives

$$\lambda_{max} T = 2897.8 \mu\text{m} \cdot \text{K} \quad (7.75)$$

Equation 7.75 is known as Wien's displacement law. The dotted line in Figure 7.11 shows the locus of points of the maximum in the spectral distribution curves.

#### 7.4.1.3 Stefan–Boltzmann Law

Integration of the Planck distribution equation shows that the emissive power of a blackbody is given as

$$E_b = \sigma T^4 \quad (7.76)$$

where  $\sigma$  is the Stefan–Boltzmann constant and has the numerical value of  $5.670 \times 10^{-8} \text{ W/m}^2 \cdot \text{K}^4$ . Equation 7.76 is known as the Stefan–Boltzmann law. The importance of this law is that the emissive power of a blackbody can be directly obtained for any temperature. Also, if the emissivity of any real surface is known, its emissive power can be calculated by using the blackbody emissive power.

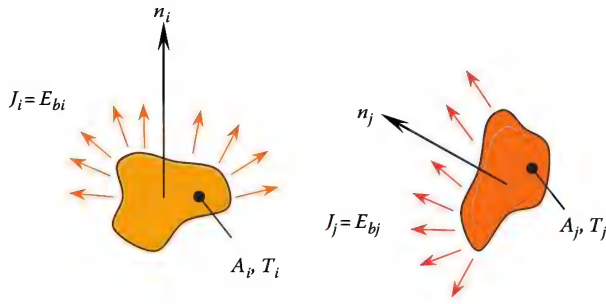


FIGURE 7.12

Radiation transfer between two surfaces approximated as gray bodies.

### 7.4.2 Radiant Exchange between Black Surfaces

Since in a blackbody there is no reflection, energy leaves exclusively as emission and is absorbed completely by another blackbody. Figure 7.12 shows exchange between two black surfaces of arbitrary shape and size. If  $q_{ipj}$  is the rate at which radiation leaves surface  $i$  and is intercepted by surface  $j$ ,

$$q_{ipj} = (A_i J_i) F_{ij} \quad (7.77)$$

where  $F_{ij}$  is the shape factor.

Since the radiosity of a black surface equals the emissive power,

$$q_{ipj} = A_i F_{ij} E_{bi} \quad (7.78)$$

Similarly,

$$q_{jpi} = A_j F_{ji} E_{bj} \quad (7.79)$$

Thus, the net exchange between the two black surfaces is

$$q_{ij} = A_i F_{ij} (T_i^4 - T_j^4) \quad (7.80)$$

### 7.4.3 Radiant Exchange between Gray/Diffuse Surfaces

The main problem in the radiation exchange between non-blackbodies is the surface reflection. Consider an exchange between surfaces in an enclosure. Assume that they are isothermal, opaque, and gray, with uniform radiosity and irradiation. The net rate of heat transfer from a surface is given by

$$q_i = A_i (J_i - G_i) \quad (7.81)$$

where

$J$  is the radiosity

$G$  is the irradiation

Also,

$$J_i = E_i + \rho_i G_i \quad (7.82)$$

where

$E$  is emissive power

$\rho$  is the reflectivity of the surface

Thus,

$$q_i = A_i (E_i - \alpha_i G_i) \quad (7.83)$$

where  $\rho_i = (1 - \alpha_i) = (1 - \epsilon_i)$  for an opaque, diffuse, gray surface. Therefore, the radiosity is given as

$$J_i = \epsilon_i E_{bi} + (1 - \epsilon_i) G_i \quad (7.84)$$

and,

$$q_i = \frac{E_{bi} - J_i}{(1 - \epsilon_i)/(A_i \epsilon_i)} \quad (7.85)$$

Thus, the total rate at which radiation reaches surface  $i$  from all surfaces is

$$A_i G_i = \sum_j F_{ji} A_j J_j \quad (7.86)$$

Using reciprocity and summation rule, the net rate of radiation transfer to surface  $i$  becomes

$$q_i = \sum F_{ij} A_i (J_i - J_j) = \sum q_{ij} \quad (7.87)$$

Equation 7.87 is a relationship between the net rate of radiation transfer from surface  $i$  and the sum of radiant exchange with the other surfaces. The aforementioned exchange may also be represented as

$$\frac{E_{bi} - J_i}{(1 - \epsilon_i)/(A_i \epsilon_i)} = \sum_{j=1}^N \frac{J_i - J_j}{(A_i F_{ij})^{-1}} \quad (7.88)$$

A network representation of this equation is shown in Figure 7.13.

In situations where the net radiation transfer rate is known and not the temperature, Equation 7.88 is used in the alternate form:

$$q_i = \sum \frac{J_i - J_j}{(A_i F_{ij})^{-1}} \quad (7.89)$$

The solutions of Equation 7.87 or 7.89 are easily accomplished by matrix inversion or iteration methods.<sup>51</sup>

### 7.4.4 View Factors for Diffuse Surfaces

View factor or shape factor or configuration factor is defined as the fraction of the radiation leaving surface

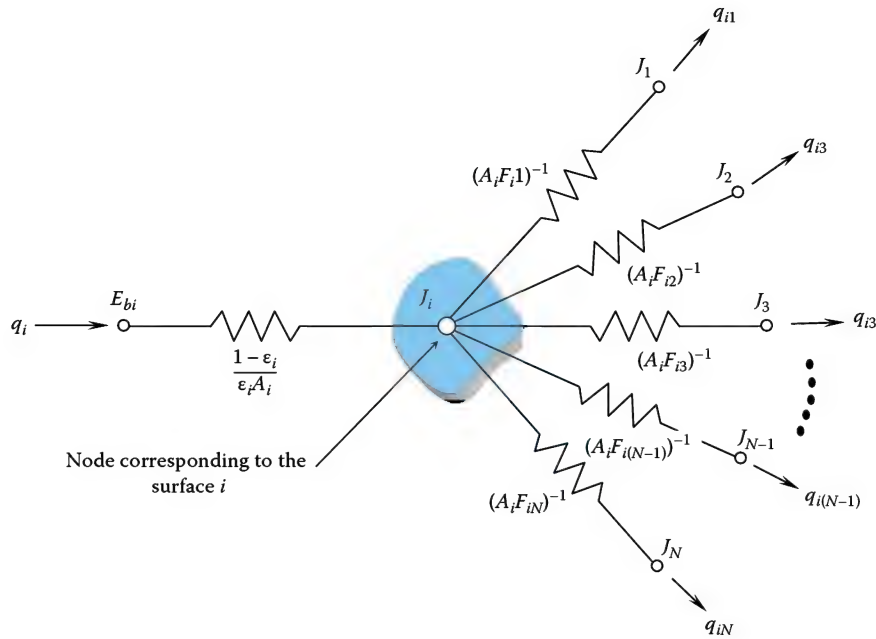


FIGURE 7.13

Network representation of radiative exchange between surface  $i$  and the remaining surfaces of an enclosure. (From Incropera, F.P. and DeWitt, D.P., *Fundamentals of Heat and Mass Transfer*, John Wiley & Sons, New York, 1996.)

$i$  that is intercepted by surface  $j$ . In Figure 7.14, two arbitrary surfaces are exchanging radiation. They have areas  $A_i$  and  $A_j$ , temperatures  $T_i$  and  $T_j$ , and are separated by a distance  $R$ . They are at angles  $\theta_i$  and  $\theta_j$  from normals  $n_i$  and  $n_j$ . It can be shown that the total rate at which radiation leaves surface  $i$  and is intercepted by  $j$  is

$$q_{i \rightarrow j} = J_i \iint \frac{\cos \theta_i \cos \theta_j}{\pi R^2} dA_i dA_j \quad (7.90)$$

Thus, the view factor, which is the fraction of radiation that leaves  $A_i$  and is intercepted by  $A_j$ , is given as

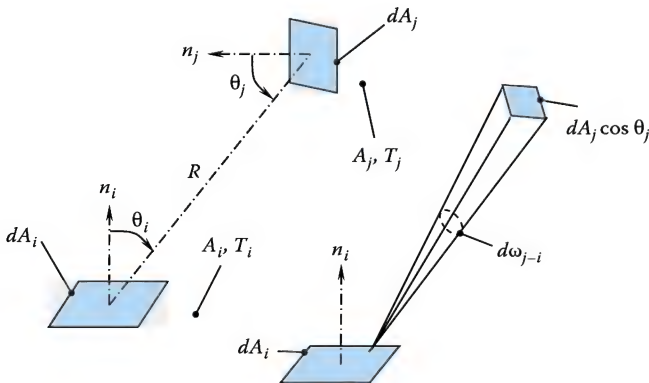


FIGURE 7.14

View factor of radiation exchange between faces of area  $dA_i$  and  $dA_j$ . (From Incropera, F.P. and DeWitt, D.P., *Fundamentals of Heat and Mass Transfer*, John Wiley & Sons, New York, 1996.)

$$F_{ij} = \frac{q_{i \rightarrow j}}{A_i J_i} \quad (7.91)$$

or, assuming that the two surfaces are diffuse emitters and reflectors and have uniform radiosity, the shape factor is given as

$$F_{ij} = \frac{1}{A_i} \iint \frac{\cos \theta_i \cos \theta_j}{\pi R^2} dA_i dA_j \quad (7.92)$$

Similarly, view factor  $F_{ji}$  can be calculated for the radiation leaving surface  $j$  and intercepted by surface  $i$ .

View factors follow reciprocity and summation rules given as follows:

$$A_i F_{ij} = A_j F_{ji} \text{ (reciprocity rule)} \quad (7.93a)$$

$$\sum F_{ij} = 1 \text{ (summation rule)} \quad (7.93b)$$

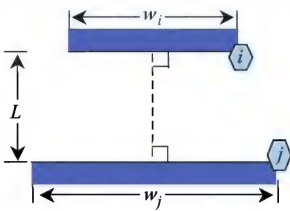
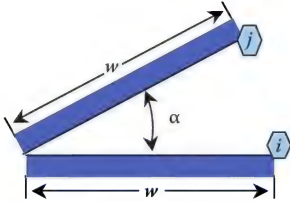
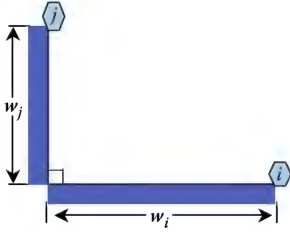
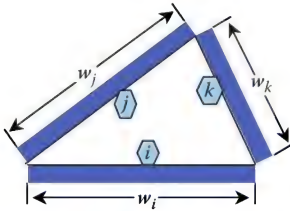
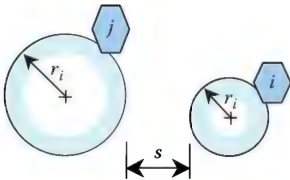
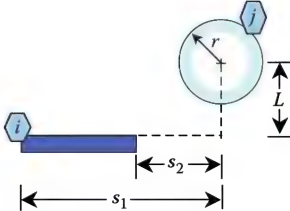
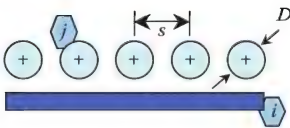
Tables 7.10 and 7.11 show view factors for two and three-dimensional geometries, respectively, and Figures 7.15 through 7.17 show the view factors for three very common configurations.

#### 7.4.5 Infrared Temperature Measurement

Planck's distribution relates the radiation emitted by a blackbody to its temperature. This relation is used in heat transfer analysis to determine how much energy is emitted by a surface. A further application of this relation is to

TABLE 7.10

View Factors for Two-Dimensional Geometries

Geometry	Relation
<p>Parallel plates with sidelines connected by a perpendicular</p> 	$F_{ij} = \frac{[(W_i + W_j)^2 + 4]^{1/2} - [(W_j - W_i)^2 + 4]^{1/2}}{2W_i}$ $W_i = w_i/L, W_j = w_j/L$
<p>Inclined parallel plates of equal width and a common edge</p> 	$F_{ij} = 1 - \sin\left(\frac{\alpha}{2}\right)$
<p>Perpendicular plates with a common edge</p> 	$F_{ij} = \frac{1 + (w_i/w_j) - [1 + (w_j/w_i)^2]^{1/2}}{2}$
<p>Three-sided enclosure</p> 	$F_{ij} = \frac{w_i + w_j - w_k}{2w_i}$
<p>Parallel cylinders of different radii</p> 	$F_{ij} = \frac{1}{2\pi} \left\{ \pi + [C^2 - (R+1)^2]^{1/2} - [C^2 - (R-1)^2]^{1/2} \dots \right. \\ \left. + (R-1) \cos^{-1} \left[ \frac{R}{C} - \frac{1}{C} \right] - (R+1) \cos^{-1} \left[ \frac{R}{C} + \frac{1}{C} \right] \right\}$ $R = r_j/r_i, S = s/r_i$ $R = r_i/r_j, S = s/r_j$
<p>Cylinder and parallel rectangle</p> 	$F_{ij} = \frac{r}{s_1 - s_2} \left[ \tan^{-1} \frac{s_1}{L} - \tan^{-1} \frac{s_2}{L} \right]$
<p>Infinite plane and row of cylinders</p> 	$F_{ij} = 1 - \left[ 1 - \left( \frac{D}{s} \right)^2 \right]^{1/2} + \left( \frac{D}{s} \right) \tan^{-1} \left( \frac{s^2 - D^2}{D^2} \right)^{1/2}$

Source: Incropera, F.P. and DeWitt, D.P., *Fundamentals of Heat and Mass Transfer*, John Wiley & Sons, New York, 1996.



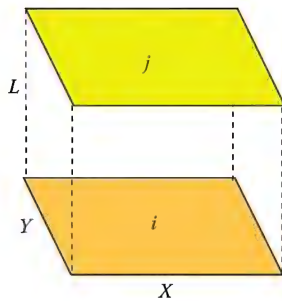
TABLE 7.11

View Factors for Three-Dimensional Geometries

## Geometry

## Relation

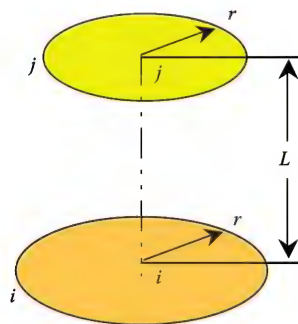
Aligned parallel rectangles



$$\bar{X} = X/L, \bar{Y} = Y/L$$

$$F_{ij} = \frac{2}{\pi \bar{X} \bar{Y}} \left\{ \ln \left[ \frac{(1 + \bar{X}^2)(1 + \bar{Y}^2)}{1 + \bar{X}^2 + \bar{Y}^2} \right]^{1/2} + \bar{X}(1 + \bar{Y}^2)^{1/2} \tan^{-1} \frac{\bar{X}}{(1 + \bar{Y}^2)^{1/2}} \dots \right. \\ \left. + \bar{Y}(1 + \bar{X}^2)^{1/2} \tan^{-1} \frac{\bar{Y}}{(1 + \bar{X}^2)^{1/2}} - \bar{X} \tan^{-1} \bar{X} - \bar{Y} \tan^{-1} \bar{Y} \right\}$$

Coaxial parallel disks

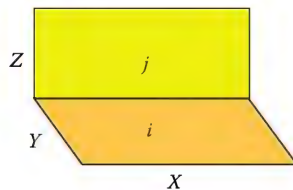


$$R_i = r_i/L, R_j = r_j/L$$

$$S = 1 + \frac{1 + R_j^2}{R_i^2}$$

$$F_{ij} = \frac{1}{2} \left\{ S - [S^2 - 4(r_j/r_i)^2]^{1/2} \right\}$$

Perpendicular rectangles with a common edge



$$H = Z/X, W = Y/X$$

$$F_{ij} = \frac{1}{\pi W} \left\{ W \tan^{-1} \frac{1}{W} + H \tan^{-1} \frac{1}{H} - (H^2 + W^2)^{1/2} \dots \right. \\ \times \tan^{-1} \frac{1}{(H^2 + W^2)^{1/2}} + \frac{1}{4} \ln \left[ \frac{(1 + W^2)(1 + H^2)}{(1 + W^2 + H^2)} \right] \dots \\ \left. \times \left[ \frac{W^2(1 + W^2 + H^2)}{(1 + W^2)(W^2 + H^2)} \right]^{W^2} \times \left[ \frac{H^2(1 + H^2 + W^2)}{(1 + H^2)(H^2 + W^2)} \right]^{H^2} \right\}$$

Source: Incropera, F.P. and DeWitt, D.P., *Fundamentals of Heat and Mass Transfer*, John Wiley & Sons, New York, 1996.

measure the *intensity* of the emitted radiation and use this measurement to determine the surface temperature. In practice, a number of complicating factors make it impossible to use Planck's distribution to convert the measured intensity to the surface temperature. In reality, there are no perfectly black surfaces. Real surfaces are at best gray and not always diffuse. In addition, compensation must be made for radiation reflected from the surface during the measurement. While it is possible to make these corrections analytically, vendors of infrared temperature measuring devices invariably make extensive use of calibration. Calibration allows the measurement device to be corrected for spectral selectivity of the detector and for nonlinearities in the detector's response.

Figure 7.18 shows infrared temperature measurements made on a burner. By selecting an appropriate wavelength for the intensity measurement (in this case, the wavelength is 3.9  $\mu\text{m}$ ), the effects of  $\text{CO}_2$  and  $\text{H}_2\text{O}$  between the emitting surface and the infrared camera are negated. Surface temperatures can then be readily measured "through" a flame. It is very difficult to make reliable gas temperature measurements by measuring the infrared emission because the emission from gases depends on the temperature of the gas volume, the composition of the gas volume, as well as the dimension of the gas volume. Since most real applications involve non-isothermal gas volumes (such as a flame in a furnace), IR measurements are not feasible.

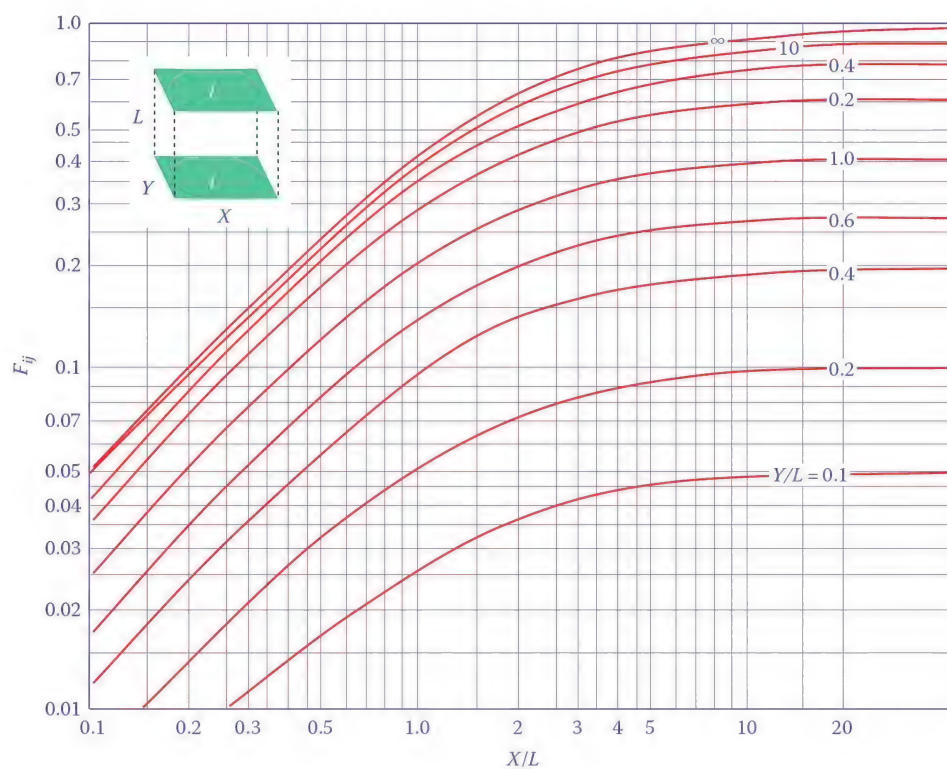


FIGURE 7.15

View factor for aligned parallel rectangles. (From Incropera, F.P. and DeWitt, D.P., *Fundamentals of Heat and Mass Transfer*, John Wiley & Sons, New York, 1996.)

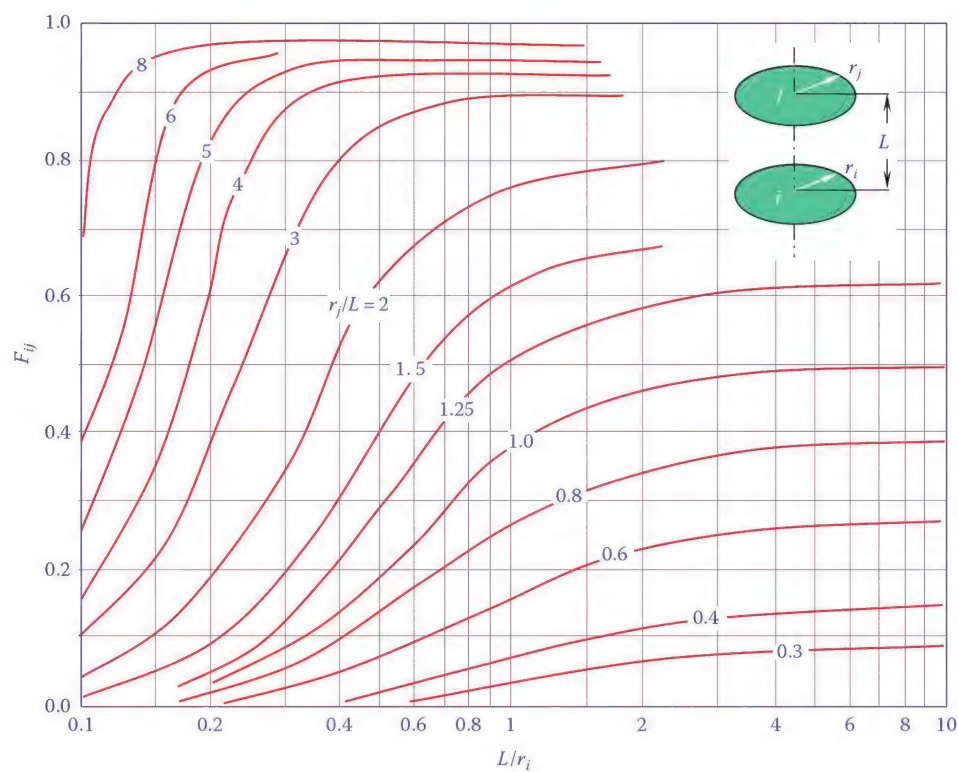


FIGURE 7.16

View factor for coaxial parallel disks. (From Incropera, F.P. and DeWitt, D.P., *Fundamentals of Heat and Mass Transfer*, John Wiley & Sons, New York, 1996.)

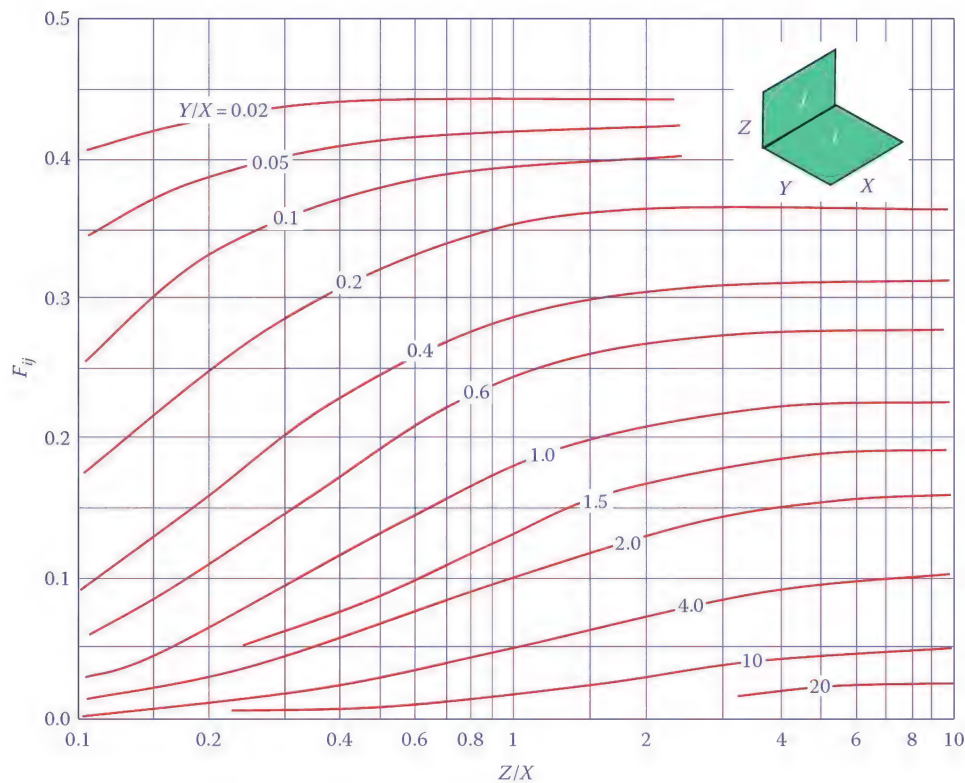


FIGURE 7.17

View factor for perpendicular rectangles with a common edge. (From Incropera, F.P. and DeWitt, D.P., *Fundamentals of Heat and Mass Transfer*, John Wiley & Sons, New York, 1996.)

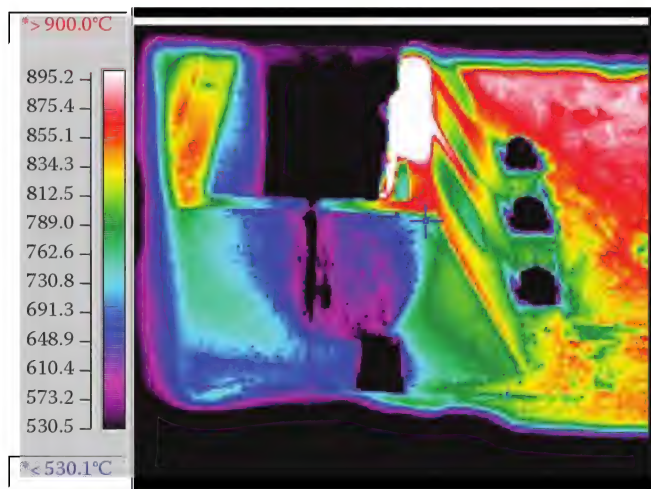


FIGURE 7.18

Infrared thermal image of a flame in a furnace.

#### 7.4.6 Radiation in Absorbing/Emitting/Scattering Media

The foregoing discussion on radiation heat transfer is limited to *surface exchange*. Surface exchange is radiation heat transfer from one surface to another, assuming that the medium between the two surfaces is a vacuum or a

transparent substance. The notion of surface exchange is actually an idealization. When radiant energy is incident on a surface, it actually penetrates that surface some distance when considered at the molecular level. For most metals, this distance is only several Å ( $= 10^{-10}$  m), while for most nonmetals, it is several  $\mu\text{m}$  ( $\mu = 10^{-6}$  m).

Radiation absorption and emission in gases is due to the quantum energy levels of the gas molecules. An in-depth analysis and discussion of the topic is beyond the scope of this section, but some understanding of gas spectra is necessary to understand gas radiation. Since air is primarily composed of symmetric diatomic molecules (which typically do not emit or absorb in the infrared) and inert gases ( $\text{N}_2$ ,  $\text{O}_2$ , and Ar), air is usually considered as a transparent medium. Humid air, however, does absorb some radiation. Normally this absorption is neglected as it is usually not significant. Other molecules that are commonly found in combustion applications, such as  $\text{CH}_4$  and other hydrocarbons,  $\text{CO}_2$ ,  $\text{H}_2\text{O}$ , CO, etc., do emit and absorb in the infrared. Unlike many solid surfaces, however, their emission and absorption do not smoothly vary with wavelength. Rather, their emission and absorption spectra oscillate violently with wavelength, but only in narrow “bands” centered around wavelengths particular to the species under consideration.



If the medium between surfaces is not transparent to thermal radiation, it is called a participating medium. The notion of emissive power, so useful in analyzing surface exchange, is meaningless in a participating medium. Instead, we must consider the *intensity* of radiation. From the study of surface exchange, we know that the intensity of radiation emitted by a diffuse surface is independent of angle, while emissive power varies as the cosine of the normal angle. In Section 7.4.8, how radiant intensity is absorbed, emitted, and scattered by participating media will be shown. Radiant intensity within a participating medium is a function of location (typically three independent variables in a three-dimensional problem), direction (two independent angles are required to describe direction in a three-dimensional problem), and wavelength or wavenumber (one independent variable) if the problem is steady state. The fact that radiant intensity is a function of six independent variables indicates immediately that the analysis will be significantly more complicated than, for instance, conduction heat transfer, where there are only three independent variables in a three-dimensional, steady-state problem. Further, if scattering is to be considered, the equation of radiative transfer will have an integro-differential form.

#### 7.4.7 Mean-Beam-Length Method

Gases emit and absorb radiation in discrete energy bands dictated by the allowed energy states within the molecule. While the energy emitted by a solid shows a continuous spectrum, the radiation emitted and absorbed by a gas is restricted to bands. Figure 7.19 shows the  $\text{CO}_2$  and  $\text{H}_2\text{O}$  spectra relative to blackbody radiation at 600 K (620°F), 1200 K (1700°F), and 2400 K (3860°F).<sup>117</sup> The emission of radiation for these gases occurs in the infrared region of spectrum. The inert gases and diatomic gases of symmetrical composition such as  $\text{O}_2$ ,  $\text{N}_2$ , and  $\text{H}_2$  are transparent to thermal radiation. Important gases that absorb and emit radiation are polyatomic gases such as  $\text{CO}_2$  and  $\text{H}_2\text{O}$  and asymmetric molecules such as  $\text{CO}$ . Determination of radiant flux from gases is highly complex. But it can be simplified by using Hottel's assumption<sup>121</sup> that involves determination of emission from a hemispherical mass of gas at temperature  $T_g$  to a surface element located at the center of the hemisphere's base as

$$E_g = \epsilon_g \sigma T_g^4 \quad (7.94)$$

where

$E_g$  is emissive power

$\epsilon_g$  is the gas emissivity

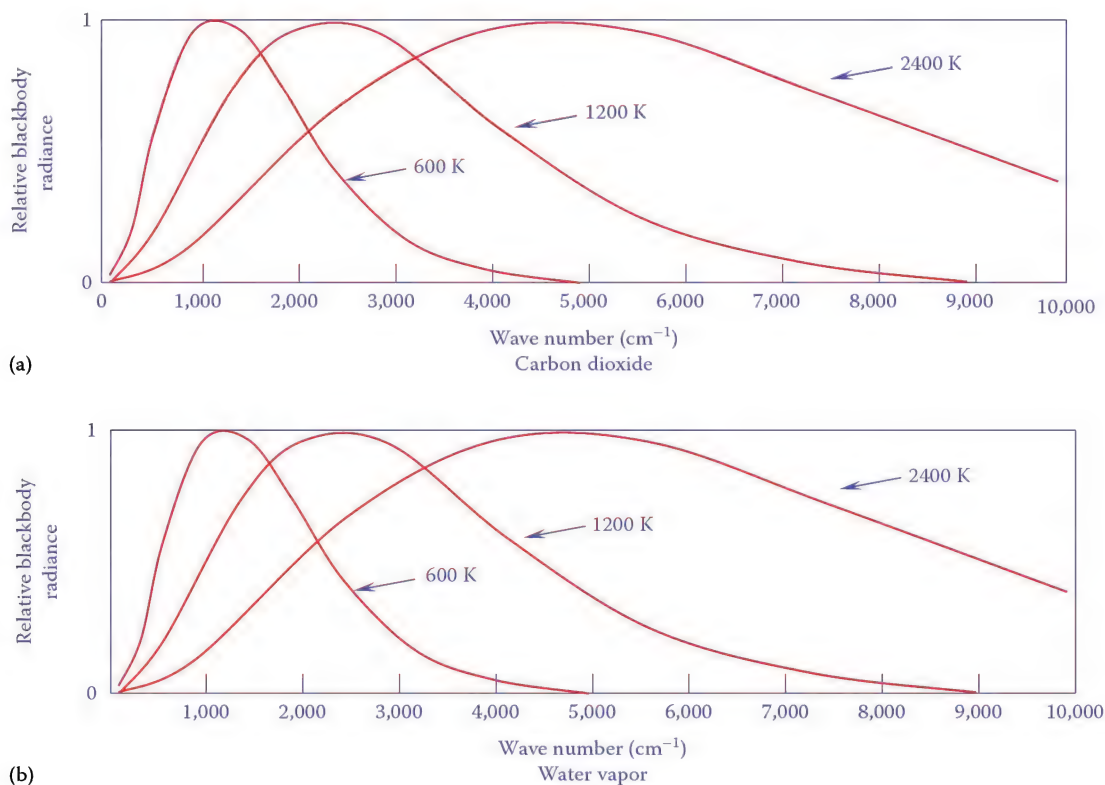


FIGURE 7.19

Emission bands of (a)  $\text{CO}_2$  and (b)  $\text{H}_2\text{O}$ . (From Ludwig, C.B. et al., *Handbook of Infrared Radiation from Combustion Gases*, NASA SP-3080, NASA, Washington, DC, 1973.)



The total emissivity may be calculated from Leckner.<sup>118</sup> The individual emissivity of either CO<sub>2</sub> or H<sub>2</sub>O is given by

$$\epsilon_i(p_a L, p, T_g) = \epsilon_0(p_a L, T_g) \left( \frac{\epsilon}{\epsilon_0} \right) (p_a L, p, T_g) \quad (7.95)$$

where

$\epsilon_i$  = emissivity of the individual gas

$p_a$  = partial pressure of the gas

$L$  = path length through the gas

$T_g$  = absolute temperature of the gas

$\epsilon_0$  = emissivity of the individual gas at a reference state (atmospheric pressure and  $p_a \rightarrow 0$  but  $p_a L > 0$ ).

The first term in Equation 7.95 is calculated using

$$\epsilon_0(p_a L, T_g) = \exp \left[ \sum_{i=0}^M \sum_{j=0}^N c_{ij} \left( \frac{T_g}{T_0} \right)^j \left( \log_{10} \frac{p_a L}{(p_a L)_0} \right)^i \right] \quad (7.96)$$

where

$T_0$  = absolute reference temperature of the gas (1000 K  $\approx 1800^\circ\text{F}$ )

$c_{ij}$  are constants

The second term of the equation is calculated from

$$\left( \frac{\epsilon}{\epsilon_0} \right) (p_a L, p, T_g) = \left\{ 1 - \frac{(a-1)(1-P_E)}{a+b-1+P_E} \exp \left[ -c \left( \log_{10} \frac{(p_a L)_m}{p_a L} \right)^2 \right] \right\} \quad (7.97)$$

where  $a, b, c, P_E$  and  $(p_a L)_m/p_a L$  are given in Table 7.12

Graphical results for H<sub>2</sub>O and CO<sub>2</sub> are shown in Figures 7.20 and 7.21, respectively.<sup>119–120</sup> The total emissivity is then calculated using

$$\epsilon_{\text{CO}_2 + \text{H}_2\text{O}} = \epsilon_{\text{CO}_2} + \epsilon_{\text{H}_2\text{O}} - \Delta\epsilon \quad (7.98)$$

where the  $\Delta\epsilon$  accounts for the overlap between the H<sub>2</sub>O and CO<sub>2</sub> bands which can be estimated from Figure 7.22 or can be calculated from

$$\Delta\epsilon = \left( \frac{\xi}{10.7 + 101\xi} - 0.0089\xi^{10.4} \right) \left( \log_{10} \frac{(p_{\text{H}_2\text{O}} + p_{\text{CO}_2})L}{(p_a L)_0} \right)^{2.76} \quad (7.99)$$

and

$$\xi = \frac{p_{\text{H}_2\text{O}}}{p_{\text{H}_2\text{O}} + p_{\text{CO}_2}} \quad (7.100)$$

### Example 7.1

Given: Combustion products containing 9% CO<sub>2</sub>, 18% H<sub>2</sub>O, and the balance N<sub>2</sub>, at a temperature of 1500°F, with a mean beam length of 10 ft, at atmospheric pressure.

**Find:** Gas emissivity.

**Solution:** Calculate  $p_a L$  for CO<sub>2</sub> and H<sub>2</sub>O to use graphs:

$$\text{CO}_2: p_a L = (0.09 \text{ bar})(305 \text{ cm}) = 27 \text{ bar-cm}$$

$$\text{H}_2\text{O}: p_a L = (0.18 \text{ bar})(305 \text{ cm}) = 55 \text{ bar-cm}$$

Look up Figures 7.20 and 7.21 to find the  $\epsilon_0$  for CO<sub>2</sub> and H<sub>2</sub>O at a temperature of 820°C:

$$\text{CO}_2: \epsilon_0 \approx 0.12$$

$$\text{H}_2\text{O}: \epsilon_0 \approx 0.29$$

**TABLE 7.12**

Correlation Constants for the Determination of the Total Emissivity for Water Vapor and Carbon Dioxide

Gas	Water Vapor				Carbon Dioxide		
$M, N$		2, 2			2, 3		
$c_{00} \dots c_{N0}$	-2.2118	-1.1987	0.035596	-3.9893	2.7669	-2.1081	0.39163
	0.85667	0.93048	-0.14391	1.2710	-1.1090	1.0195	-0.21897
$\vdots \quad \ddots \quad \vdots$	-0.10838	-0.17156	0.045915	-0.23678	0.19731	-0.19544	0.044644
$c_{0M} \dots c_{NM}$							
$P_E$		$(P + 2.5bp_a/\sqrt{t})/p_0$			$(p + 0.28p_a)/p_0$		
$(p_0 L)_m/(p_a L)_0$		13.2 $t^2$			0.054/ $t^2$ , $t < 0.7$		
$a$	2.144,	$t < 0.7$			0.225 $t^2$ , $t > 0.7$		
	1.88 – 2.053 $\log_{10} t$ ,	$t > 0.7$			1 + 0.1/ $t^{1.45}$		
$b$		1.10/ $t^{1.4}$			0.23		
$c$		0.5			1.47		

Source: Kreith, F. Ed., *CRC Handbook of Mechanical Engineering*, CRC Press, Boca Raton, FL, 1998, p. 4–73.

Note:  $T_0$ , 1000 K;  $p_0$ , 1 bar;  $t = T/T_0$ ;  $(p_a L)_0$ , 1 bar-cm.

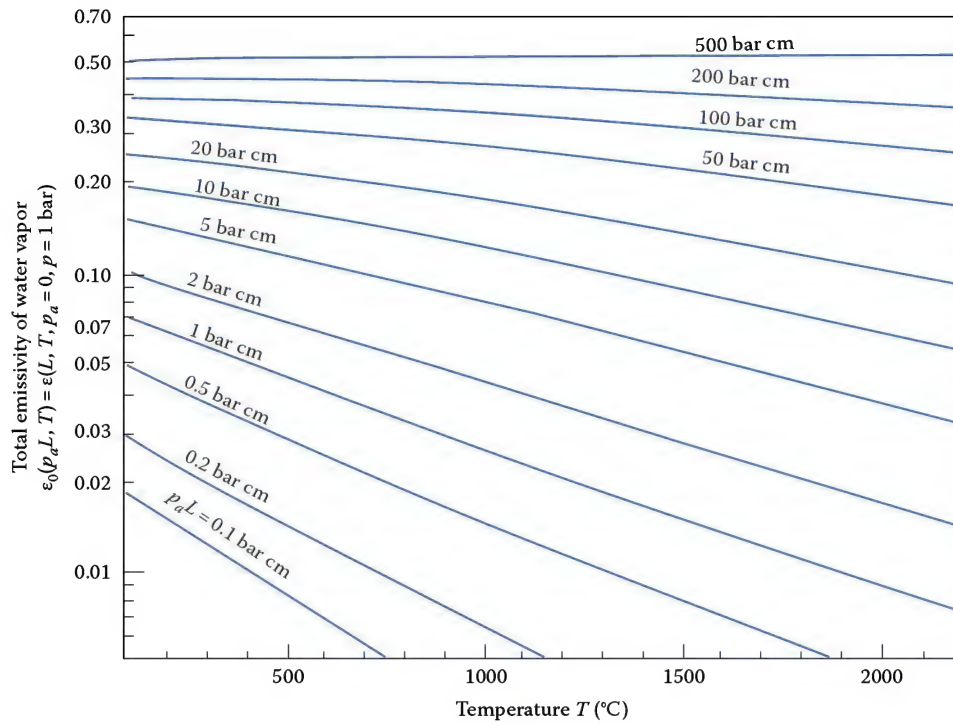


FIGURE 7.20

Total emissivity of water vapor at the reference state of a total gas pressure  $p = 1$  bar and a partial pressure of  $\text{H}_2\text{O}$   $p_a \rightarrow 0$ . (Adapted from Modest, M.F., Radiation, Section 4.3, in *The CRC Handbook of Mechanical Engineering*, ed. F. Kreith, CRC Press, Boca Raton, FL, 1998.)

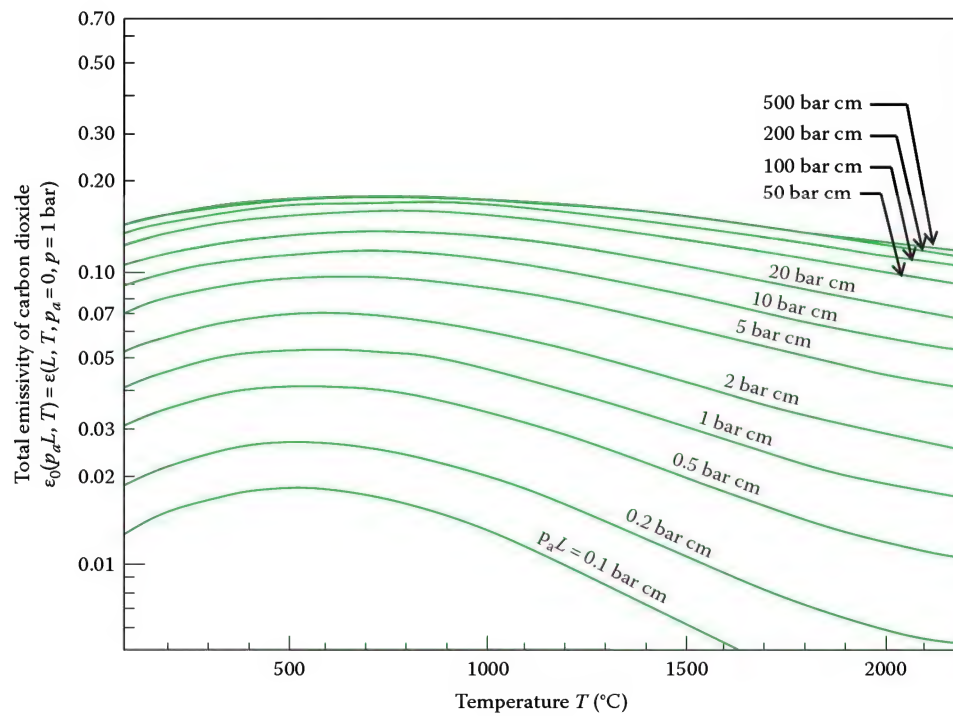


FIGURE 7.21

Total emissivity of carbon dioxide at the reference state of a total gas pressure  $p = 1$  bar and a partial pressure of  $\text{CO}_2$   $p_a \rightarrow 0$ . (Adapted from Modest, M.F., Radiation, Section 4.3, in *The CRC Handbook of Mechanical Engineering*, ed. F. Kreith, CRC Press, Boca Raton, FL, 1998.)

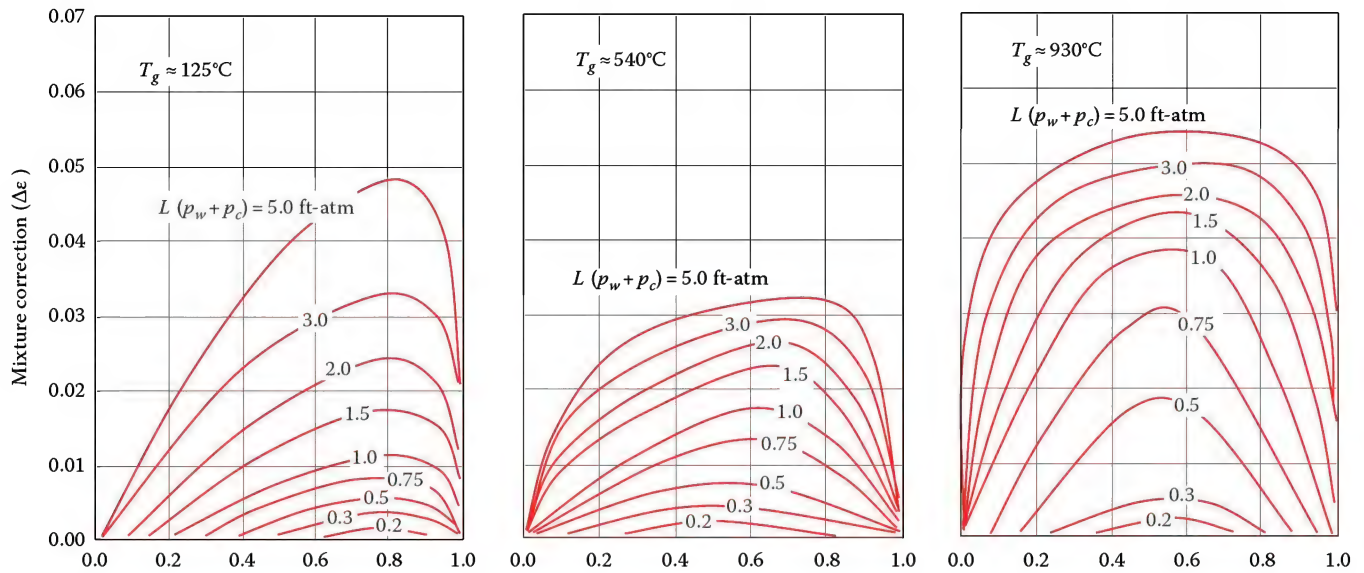


FIGURE 7.22

Radiation heat transfer correction factor for mixtures of water vapor and carbon dioxide.

Calculate correction factors  $\epsilon/\epsilon_0$  using Equation 7.97 and Table 7.12

$$t = T/T_0 = (1090 \text{ K}/1000 \text{ K}) = 1.09$$

$$\text{CO}_2: P_E = (1.0 + 0.28(0.09))/1.0 = 1.03$$

$$\text{H}_2\text{O}: P_E = (1.0 + 2.56/\sqrt{1.09})/1.0 = 3.45$$

$$\text{CO}_2: \frac{(p_a L)_m}{p_a L} = 0.225t^2 = 0.225(1.09)^2 = 0.267$$

$$\text{H}_2\text{O}: \frac{(p_a L)_m}{p_a L} = 13.2t^2 = 13.2(1.09)^2 = 15.7$$

$$\text{CO}_2: a = 1 + 0.1/(1.09)^{1.45} = 1.09; b = 0.23; c = 1.47$$

$$\text{H}_2\text{O}: a = 1.88 - 2.053 \log_{10}(1.09) = 1.80;$$

$$b = 1.10/(1.09)^{1.4} = 0.97; c = 0.5$$

$$\begin{aligned} \text{CO}_2: \left( \frac{\epsilon}{\epsilon_0} \right) &= \left\{ 1 - \frac{(1.09 - 1)(1 - 1.03)}{1.09 + 0.23 - 1 + 1.03} \exp[-1.47(\log_{10} 0.267)^2] \right\} \\ &= 1.001 \end{aligned}$$

$$\begin{aligned} \text{H}_2\text{O}: \left( \frac{\epsilon}{\epsilon_0} \right) &= \left\{ 1 - \frac{(1.80 - 1)(1 - 3.45)}{1.80 + 0.97 - 1 + 3.45} \exp[-0.5(\log_{10} 15.7)^2] \right\} \\ &= 1.184 \end{aligned}$$

$$\text{CO}_2: \epsilon = (\epsilon/\epsilon_0) \epsilon_0 = (1.001)(0.12) = 0.120$$

$$\text{H}_2\text{O}: \epsilon = (\epsilon/\epsilon_0) \epsilon_0 = (1.184)(0.29) = 0.343$$

$$\text{Calculate } \xi: \xi = \frac{0.18}{0.18 + 0.09} = 0.67$$

Calculate  $\Delta\epsilon$ :

$$\begin{aligned} \Delta\epsilon &= \left( \frac{0.67}{10.7 + 101(0.67)} - 0.0089(0.67)^{10.4} \right) \\ &\quad \times \left( \log_{10} \frac{(0.18 + 0.09)(305 \text{ cm})}{1 \text{ bar-cm}} \right)^{2.76} \\ \Delta\epsilon &= 0.051 \end{aligned}$$

$$\epsilon = 0.120 + 0.343 - 0.051 = 0.412$$

The mean beam length,  $L_e$ , can be defined as the radius of a hemispherical gas mass whose emissivity is equivalent to that of the geometry of interest.

Table 7.13 gives the mean beam length of numerous gas geometries and shapes from Hottel.<sup>121</sup> For geometries not covered in Table 7.13, the mean beam length may be approximated as

$$L_e = 3.4 (\text{volume})/(\text{surface area}) \quad (7.101)$$

Using mean beam length  $L_e$ , instead of  $L$  (the radius of hemisphere), gas emissivity is obtained, which, in turn, gives radiant heat transfer to a surface due to emission from an adjoining gas:

$$q = \epsilon_g A_s \sigma T_g^4 \quad (7.102)$$

where  $A_s$  is the surface area.

TABLE 7.13

Mean Beam Lengths for Radiation from a Gas Volume to a Surface on Its Boundary

Geometry of Gas Volume	Characterizing Dimension, $L$	Geometric Mean Beam Length, $L_g/L$	Average Mean Beam Length, $L_m/L$	$L_m/L_0$
Sphere radiating to its surface	Diameter, $L = D$	0.67	0.65	0.97
Infinite circular cylinder to bounding surface	Diameter, $L = D$	1.00	0.94	0.94
Semi-infinite circular cylinder to:	Diameter, $L = D$			
Element at center of base		1.00	0.90	0.90
Entire base		0.81	0.65	0.80
Circular cylinder (height/diameter = 1) to:	Diameter, $L = D$			
Element at center of base		0.76	0.71	0.92
Entire surface		0.67	0.60	0.90
Circular cylinder (height/diameter = 2) to:	Diameter, $L = D$			
Plane base		0.73	0.60	0.82
Concave surface		0.82	0.76	0.93
Entire surface		0.80	0.73	0.91
Circular cylinder (height/diameter = 0.5) to:	Diameter, $L = D$			
Plane base		0.48	0.43	0.90
Concave surface		0.53	0.46	0.88
Entire surface		0.50	0.45	0.90
Infinite semicircular cylinder to center of plane rectangular face	Radius, $L = R$	—	1.26	—
Infinite slab to its surface	Slab thickness, $L$	2.00	1.76	0.88
Cube to a face	Edge $L$	0.67	0.6	0.90
Rectangular $1 \times 1 \times 4$ parallelepipeds to:	Shortest edge, $L$			
$1 \times 4$ face		0.90	0.82	0.91
$1 \times 1$ face		0.86	0.71	0.83
All faces		0.89	0.81	0.91

The net radiation exchange rate between the surface at temperature  $T_s$  and the gas at  $T_g$  is then given by

$$q_{net} = A_s \sigma (\epsilon_g T_g^4 - \alpha_g T_s^4) \quad (7.103)$$

The absorptivity of  $H_2O$  and  $CO_2$  can be estimated using

$$\alpha(p_a L, p, T_g, T_s) = \left( \frac{T_g}{T_s} \right)^{1/2} \epsilon \left( p_a L \frac{T_s}{T_g}, p, T_s \right) \quad (7.104)$$

where  $T_s$  is the surface temperature such as a furnace wall.

The correction for the band overlap between  $H_2O$  and  $CO_2$  is calculated using

$$\alpha_{CO_2+H_2O} = \alpha_{CO_2} + \alpha_{H_2O} - \Delta\epsilon \quad (7.105)$$

where  $\Delta\epsilon$  is estimated with a pressure-path length of  $p_a L T_s / T_g$

### Example 7.2

Given: Using the data from the previous example and a wall temperature of  $1000^\circ F$ .

Find: Gas absorptivity.

Solution: Calculate  $p_a L T_s / T_g$  for  $CO_2$  and  $H_2O$  to use graphs:

$$\begin{aligned} CO_2: p_a L T_s / T_g &= (0.09 \text{ bar})(305 \text{ cm})(1000 + 460)/(1500 + 460) \\ &= 20 \text{ bar-cm} \end{aligned}$$

$$\begin{aligned} H_2O: p_a L T_s / T_g &= (0.18 \text{ bar})(305 \text{ cm})(1000 + 460)/(1500 + 460) \\ &= 41 \text{ bar-cm} \end{aligned}$$



Look up Figures 7.20 and 7.21 to find the  $\epsilon_0$  for CO<sub>2</sub> and H<sub>2</sub>O at a temperature of 540°C (1000°F):

$$\text{CO}_2: \epsilon_0 \approx 0.12, \text{H}_2\text{O}: \epsilon_0 \approx 0.28$$

Calculate correction factors  $\epsilon/\epsilon_0$  using Equation 7.97 and Table 7.12:

$$t = (811 \text{ K}/1000 \text{ K}) = 0.811$$

$$\text{CO}_2: P_E = (1.0 + 0.28(0.09))/1.0 = 1.03$$

$$\text{H}_2\text{O}: P_E = (1.0 + 2.56/\sqrt{0.811})/1.0 = 3.84$$

$$\text{CO}_2: \frac{(p_a L)_m}{p_a L} = 0.225t^2 = 0.225(0.811)^2 = 0.148$$

$$\text{H}_2\text{O}: \frac{(p_a L)_m}{p_a L} = 13.2t^2 = 13.2(0.811)^2 = 8.68$$

$$\text{CO}_2: a = 1 + 0.1/(0.811)^{1.45} = 1.14; \quad b = 0.23; \quad c = 1.47$$

$$\text{H}_2\text{O}: a = 1.88 - 2.053 \log_{10}(0.811) = 2.07;$$

$$b = 1.10/(0.811)^{1.4} = 1.47; \quad c = 0.5$$

$$\begin{aligned} \text{CO}_2: \left( \frac{\epsilon}{\epsilon_0} \right) &= \left\{ 1 - \frac{(1.14 - 1)(1 - 1.03)}{1.14 + 0.23 - 1 + 1.03} \exp[-1.47(\log_{10} 0.148)^2] \right\} \\ &= 1.001 \end{aligned}$$

$$\begin{aligned} \text{H}_2\text{O}: \left( \frac{\epsilon}{\epsilon_0} \right) &= \left\{ 1 - \frac{(2.07 - 1)(1 - 3.84)}{2.07 + 1.47 - 1 + 3.84} \exp[-0.5(\log_{10} 8.68)^2] \right\} \\ &= 1.307 \end{aligned}$$

$$\text{CO}_2: \epsilon = (\epsilon/\epsilon_0) \epsilon_0 = (1.001)(0.12) = 0.120$$

$$\text{H}_2\text{O}: \epsilon = (\epsilon/\epsilon_0) \epsilon_0 = (1.307)(0.28) = 0.366$$

$$\text{CO}_2: \alpha = \sqrt{\frac{1500 + 460}{1000 + 460}} (0.120) = 0.139$$

$$\text{H}_2\text{O}: \alpha = \sqrt{\frac{1500 + 460}{1000 + 460}} 0.366 = 0.424$$

$$\alpha = 0.139 + 0.424 - 0.051 = 0.512$$

#### 7.4.8 Equation of Radiative Transfer

Consider the propagation of a “pencil” beam of radiant energy through a participating medium. The radiant energy is absorbed by the medium, decreasing the intensity of the radiant energy according to

$$\left( \frac{\partial I_\lambda}{\partial s} \right)_{\text{absorption}} = -a_\lambda I_\lambda, \quad (7.106)$$

where

$a_\lambda$  is the spectral absorption coefficient

$s$  is a coordinate along the path

Additionally, the intensity of the radiation is increased by emission from the medium. The increase in the radiant intensity is given by

$$\left( \frac{\partial I_\lambda}{\partial s} \right)_{\text{emission}} = a_\lambda I_{b\lambda}. \quad (7.107)$$

A further effect to be considered when particulate medium is present is scattering. When radiant energy strikes a solid particle within the medium, the radiation may be reflected or diffracted so that its direction changes. When radiant energy strikes a solid particle within the medium, the radiation may be reflected or diffracted so that its direction changes. As radiation propagates, its intensity is decreased by *out-scattering* and increased by *in-scattering*. Attenuation by (out) scattering is described by

$$\left( \frac{\partial I_\lambda}{\partial s} \right)_{\text{outscatter}} = -a_\lambda I_\lambda. \quad (7.108)$$

The increase in intensity due to in-scatter is given by

$$\left( \frac{\partial I_\lambda}{\partial s} \right)_{\text{inscatter}} = \frac{\sigma_{s\lambda}}{4\pi} \int_{4\pi} I_\lambda(s_i) \Phi(s_i, s) d\Omega_i, \quad (7.109)$$

where the subscript  $i$  in the integrand denotes the incident direction. Physically, this integral can be described as a summation over all possible directions of the radiation entering a particular location multiplied by the scattering phase function, which represents the fraction of radiation traveling in a particular direction  $s$  that is scattered into a new direction  $s$ .

Summing all of these effects results in the equation of transfer for radiation in a participating medium:

$$\frac{\partial I_\lambda}{\partial s} = -(a_\lambda + \sigma_{s\lambda}) I_\lambda + a_\lambda I_{b\lambda} + \frac{\sigma_{s\lambda}}{4\pi} \int_{4\pi} I_\lambda(s_i) \Phi(s_i, s) d\Omega_i \quad (7.110)$$

This equation describes the propagation of radiation through absorbing/emitting/scattering media. It is an integro-differential equation when scattering is considered. Analytical solutions of the equation of transfer are possible only for very simple geometries and boundary conditions. In more complex geometries and boundary conditions, approximate solution techniques such as the spherical harmonics method and the discrete ordinates method can be used. These methods are discussed further in Chapter 13. These approximate solution techniques are more fully discussed in texts such as Siegel and Howell<sup>114</sup> and Modest.<sup>122</sup>

#### 7.4.9 Radiation Emitted by a Flame

Accurate estimation of the heat emitted from a flame is very difficult for a number of reasons:

1. The flame temperature is not known. While one can readily calculate an adiabatic flame temperature for a given fuel, the actual flame temperature will be below this value because the flame emits radiant heat.
2. The often used term *flame radiation* suggests that some special mechanism is at work within the reaction zone emitting radiant energy. This is not true. Radiant energy is emitted only by the gases and solids (particularly carbon) present in the flame. The gaseous combustion products  $\text{H}_2\text{O}$  and  $\text{CO}_2$  are the gases that emit radiation in significant quantities, while any species (such as CO and radicals) in the flame are present at such small fractions and such thin path lengths that their emission is typically negligible. However, determining the concentration and temperature of  $\text{H}_2\text{O}$  and  $\text{CO}_2$  within the flame is nontrivial, and in fact, the gases are clearly nonisothermal.
3. The presence of solid carbon particles within the flame (which give flames a yellowish color) can dominate the radiant emission from the flame. Again, predicting the concentration (measured as a volume fraction) and temperature of these carbon particles is very difficult.

Figure 7.23 shows a yellow luminous flame. The yellowish color of the flame is due to broad band radiation by carbon particles. The flame shown was produced by combusting a fuel oil atomized by steam. Flames with significant soot fractions radiate significantly directly from the flame. In contrast, nonluminous or slightly luminous flames (as shown in Figure 7.24) emit only a small fraction of the energy liberated by the combustion process.

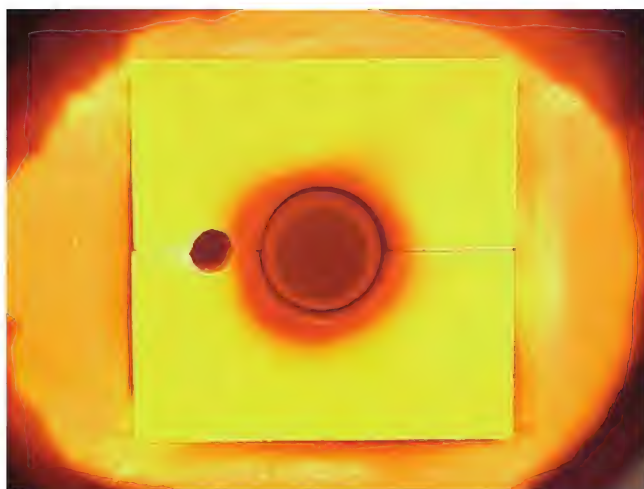


FIGURE 7.23  
Photographic view of a luminous flame.



FIGURE 7.24  
Photographic view of a nonluminous flame.

Figure 7.25 shows a radiant wall burner. In this burner, a mixture of fuel and air jets out radially from the burner. Very near the burner, the wall is dark because the flame “stands off” the burner exit. Further away from the burner, the refractory surface is a bright yellow color. In this particular application, the temperature of this refractory is above 2000°F (1100°C). As illustrated in the photograph, the visible radiation from the hot refractory surface dominates any flame radiation in the visible region, rendering the flame invisible to the human eye. This burner is very common in ethylene pyrolysis furnaces, where the burner is used to heat a refractory wall. The primary heat transfer mode to the refractory wall is



**FIGURE 7.25**  
Photographic view of a radiant wall burner.

probably convective, although gas radiation plays a role. The hot wall then radiates energy to process tubes that run parallel to the wall at a distance of approximately 3 ft (1 m).

## 7.5 Heat Transfer in Process Furnaces

A complete treatment of heat transfer in process furnaces is beyond the scope of this chapter, but the chapter would not be complete either, without describing, albeit briefly, the phenomena at play in process furnace heat transfer. Some examples of heat transfer in process furnaces are briefly considered next. Hoogendoorn et al.<sup>123</sup> made heat flux measurements in a rectangular, vertical tube furnace with two round burners firing vertically upward. Both oil and gas flames were tested. The objective of the study was to determine the validity of the assumption of a constant furnace temperature often used to calculate the heat flux to process tubes. A 1 in. (25 mm) diameter, water-cooled heat flux probe, with and without air screens, was used to measure radiation and total heat flux, respectively. Forced convection was calculated from the difference between the total and radiant heat flux measurements. The heat flux was found to be significantly nonuniform in the furnace. Gas flames were found to have a more uniform heat flux distribution than oil flames, as shown in Figure 7.26.

Selçuk et al.<sup>124</sup> studied the effect of flame length on the radiative heat flux distribution in a process fluid heater. This information is important in the design of the heater to prevent premature damage to the process tubes due to improper flame heights. It will also help to optimize the heat transfer rate to the tubes to maximize thermal efficiency. A two-flux radiation model was used to predict

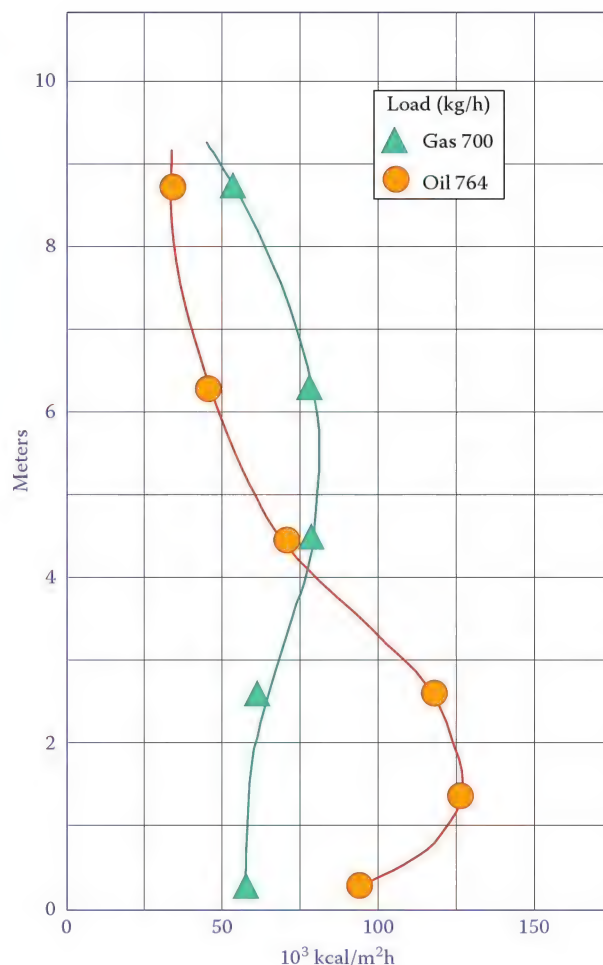


**FIGURE 7.26**  
Vertical heat flux distribution for oil and gas firing in a vertical tube furnace. (From Hoogendoorn, C.J. et al., *J. Inst. Fuel*, 43, 511, 1970.)

the radiant heat transfer in the heater. The predictions were in good agreement with a set of experimental data. The results showed that the radiant flux at the tube surface was a strong function of the flame height, as shown in Figure 7.27.

Process furnaces are a good example of systems that incorporate all the heat transfer mechanisms concurrently at work in gases, liquids, and solids. The challenge is to achieve good heat transfer in the radiation and convection mechanisms. Conduction plays only a minor role in getting the heat from the flame to the process fluid, but it is the primary mechanism at work in preventing heat loss to the surroundings.

Refer to Figure 7.1 at the beginning of this chapter for the following discussion. The main part of the furnace that contains the burner flames is the radiant section. The process heating tubes are located in the radiant section in various arrangements. In low temperature furnaces where the gases exit the radiant section at less than 800°C (1500°F), the process tubes are often located



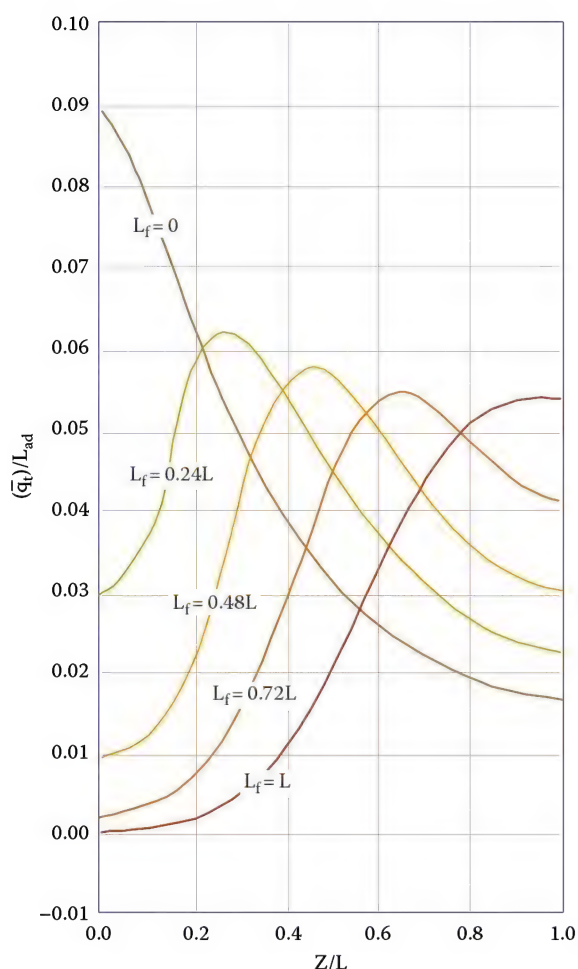


**FIGURE 7.27**

Distribution of dimensionless average radiant flux density at the tube surfaces for various flame lengths ( $L_f$  = flame length,  $L$  = heater height,  $Z$  = height). (From Hoogendoorn, C.J. et al., *J. Inst. Fuel*, 43, 511, 1970.)

close to the walls of the furnaces. In high temperature furnaces where gases exit the radiant section at more than 980°C (1800°F), the tubes are usually suspended in the main furnace space, away from the walls.

In many furnace designs, a convection section is located downstream of the radiant section. The combustion gases that leave the radiant section flow through the convection section and then through the stack to be vented to atmosphere. Depending on the design, an air preheater may be installed in the path to the stack to further extract heat from the flue gas. The convection section may be used to preheat the process fluid or may be used to generate steam or heat another process fluid. Since the radiant section is the high temperature section of the furnace, the final passes of the heating process are located there.

Radiation is the dominant heat transfer mechanism in the radiant section. Both participating medium (gaseous) radiation and surface exchange are significant.

It should be noted that even though gas flames emit only a little in the visible spectrum, their emission into the infrared spectrum will be quite large. In typical cracking furnaces and some boilers where temperatures are very high (above about 1800°F = 1000°C), the furnace walls will glow bright orange or even yellow. In these furnaces, it is frequently difficult to see a gas flame visually. This is because the walls are radiating in the visual spectrum. However, even though the naked eye cannot see any gas radiation from the flame, radiation from the flame is still a significant contributor to heat transfer. Recall from Figure 7.11 (the blackbody emissive power graph) that the blackbody curves do not cross. This means that at any given wavelength, the hotter the radiator is, the higher the blackbody emissive power is. The governing factor in heat transfer in the radiation section is temperature because the radiant heat transfer coefficient is directly proportional to the fourth power of the temperature.

Convection also contributes to heat transfer in the radiant section. The furnace gases circulate vigorously inside the radiant section driven by the in-flow of combustion air, gas expansion due to combustion, and the temperature gradients through the furnace. These flow patterns are very difficult to predict a priori, but they are very important in assessing heat transfer to the process tubes. In the convection section of the furnace, most of the heat is transferred by convection. The first row or two of tubes in the convection section that have a “line of sight” view of the radiant section experience a lot of radiant transfer. Consequently, the first two or three rows of tubes are usually not equipped with fins, to avoid excessive localized heat flux; these tubes are called shock tubes. The subsequent rows of tubes in the convection section are often finned to maximize the convective heat transfer per unit tube length. The governing factor in heat transfer in the convection section is mass velocity, since the convective heat transfer coefficient is strongly dependent on the velocity.

In the average heater, about 60%–80% of the total heat is transferred in the radiant section and approximately 20%–40% comes from the convection section. With this ratio of heat transfer in the heater sections, it is obvious that the greatest benefit will result from improvements in the radiant section.

Detailed analysis of furnace heat transfer is complex. There exist well-defined methods to calculate the heat transferred in the many varieties of heat exchangers, (e.g., parallel, counterflow, shell-and-tube, compact), but furnace heat transfer calculation methods are less well documented. Many furnace vendors do have proprietary methods for computing the heat transferred to the process load, but these are largely based on empirical data and are not documented in the open literature. Furthermore, furnace heat transfer



seems to be the source of controversy and disagreement among engineering professionals in the field. There exists much disagreement as to the relative importance of gas radiation and surface radiation, for instance. Sometimes rules-of-thumb are used to determine certain types of heat transfer in a furnace. For example, the American Petroleum Institute Standard 560 recommends using a radiation loss of 1.5% of the lower heating value of the fuel when calculating the fuel efficiency of a process heater.<sup>125</sup>

The function of the burner is to deliver heat to the process load as uniformly as possible. Reaching this ideal condition is difficult. The burner equipment used must possess superior ability to disperse heat to the gaseous furnace atmosphere if the heater operation is to be satisfactory. It is the relative ability to disperse heat by a particular burner that makes it suitable to firing in a particular heater. If the burner is applied to a different furnace design, it may not be as effective.<sup>126</sup>

### 7.5.1 Flame Radiation

The radiant sources in the furnace are the flame, the radiant furnace surfaces, and the radiant furnace gases ( $H_2O$  and  $CO_2$ ). Gas flames produce some radiation directly from the flame, more or less, depending on how luminous the flame is. An oil flame can radiate three to four times as much as a gas flame due to the high

quantities of soot formed in the flame that makes it luminescent. Figure 7.28 shows that the higher the carbon-to-hydrogen weight ratio in the fuel, the higher the flame emissivity.<sup>127</sup> Solid fuels have higher emissivities than liquid fuels, which have higher emissivities than gaseous fuels. A gas flame also may produce soot under certain conditions of mixing and can radiate relatively more, but not as much as an oil flame. The distance from the flame to the heat transfer surface at various locations in the furnace varies widely. Since radiant transfer varies inversely as the square of the distance between the radiant and the absorptive bodies, flame radiation will not be uniformly delivered to all portions of the furnace. The heightened requirement of uniformity of heat flux in ethylene cracking furnaces has driven the design of furnaces with multiple small burners distributed uniformly over the furnace walls.

Flame radiation does not dominate the radiation process in the furnace. As an illustration, consider a combination burner (see Figure 1.47) that can provide both a gas flame and oil flame in the same location in a furnace. Even though the oil flame is three to four times as radiant as the gas flame the furnace performance and tube surface temperatures are not significantly changed. It is issues such as these that introduce controversy in the various schools of thought regarding furnace heat transfer. Experimentally determining the true radiant behavior in the furnace is very difficult.

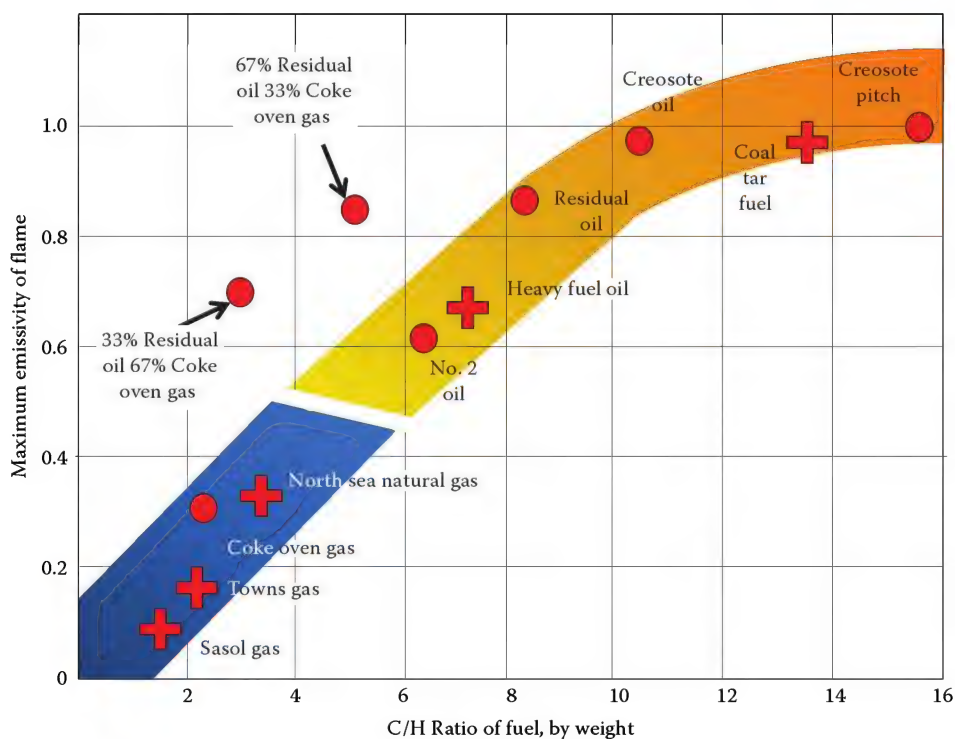


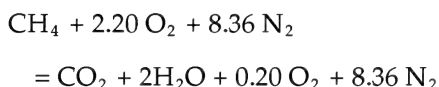
FIGURE 7.28

Maximum flame radiation as a function of the C/H weight ratio in the fuel. (Adapted from Reed, R.D. *Furnace Operations*, Gulf Publishing, Houston, TX, 1981.)

### 7.5.2 Furnace Gas Radiation

An analysis of the heat capacities of the furnace gases indicates that the gases that radiate in the infrared, carbon dioxide and water, only carry about 33% of the total heat released. Conversely, 63% of the heat is contained in the other gases, namely, oxygen and nitrogen.

Consider the chemistry of burning methane at 10% excess air:



Gaseous products are 1 mol of  $\text{CO}_2$ , 2 mol  $\text{H}_2\text{O}$ , 8.36 mol  $\text{N}_2$ , and 0.20 mol of  $\text{O}_2$ . Consider a lb-mol of methane as 380 SCF (10.8 SCM). At 910 Btu/scf (33,900 kJ/m<sup>3</sup>), the lower heating value of a lb-mol of methane is 345,800 Btu (364,800 kJ). If it is presumed that 10% of the heat is radiated directly by the flame burst, the heat content of the gases is 311,220 Btu (328,340 kJ). The respective heat contents of the component gases based on their specific heats are as follows:

$\text{CO}_2 = 37,700 \text{ Btu (39,800 kJ)}$ ,  $\text{H}_2\text{O} = 67,200 \text{ Btu (70,900 kJ)}$

$\text{CO}_2 + \text{H}_2\text{O} = 104,900 \text{ Btu (110,700 kJ)} = 33.7\%$

$\text{O}_2 = 4,800 \text{ Btu (5,060 kJ)}$ ,  $\text{N}_2 = 201,520 \text{ Btu (212,600 kJ)}$

$\text{O}_2 + \text{N}_2 = 206,320 \text{ Btu (217,700 kJ)} = 63.3\%$

The total heat content of the radiating gases carbon dioxide and water is 104,900 Btu (110,700 kJ). The heat content of the nitrogen and oxygen is 206,320 Btu (217,700 kJ) immediately following the radiant part of the flame. These gases are in a homogeneous mixture in which a portion of the gases is radiant capable and a portion is not. The heat energy of a portion of the gases is being dissipated by radiation to produce a steady decrease in heat content within these gases. The other portion that does not radiate then transfers its heat to the radiating gases as their temperature decreases.

However, the emissivity of radiating gases is quite low. The quantity of heat radiated is a relatively small portion of the total heat content of the gases. So a significant amount of the heat transfer occurs when the gases come into close proximity of the heat transfer tubes. First, the contact of the gases with the surface of the tubes and refractory walls transfers heat by convection. Second, the close proximity of the gases to these surfaces makes the radiation transfer higher since distance is minimized. Thus, the heat transfer in this combination mode depends on the vigorous furnace hot gas currents.

### 7.5.3 Refractory Surface Radiation

The furnace interior refractory walls have a much greater surface area than the surface area of the heat transfer tubes. Therefore proportionally greater energy is delivered to the furnace refractory surfaces. Refractory has a very high heat capacity. The refractory's ability to store heat exceeds that of the gases and tube materials. Thus, initially, a significant portion of the furnace heat up time is due to the heat capacity of the refractory.

Refer back to Table 7.2 for the specific heats of some common materials. One can see that an average refractory brick has a specific heat of approximately 0.2 Btu/lb-°F (0.84 kJ/kg-K). This is almost double that of carbon steel. The largest heat storage occurs in the refractory. To illustrate the magnitude, let us consider a furnace that is 30 ft × 30 ft × 40 ft (9 m × 9 m × 12 m). With six inches (15 cm) of refractory thickness the furnace now has approximately 200,000 lb (90,800 kg) of refractory. The quantity of heat stored in the refractory can be estimated using the formula

$$Q = m \times C_p \times (T_1 - T_2) \quad (7.111)$$

Assume the refractory heats up from an ambient temperature of  $T_2 = 70^\circ\text{F (21}^\circ\text{C)}$  to a steady-state average temperature of  $500^\circ\text{F (260}^\circ\text{C)}$ . The average is the temperature midway in the thickness of the refractory. The hot surface will be considerably hotter and the cold surface typically around  $200^\circ\text{F (93}^\circ\text{C)}$ . The amount of heat stored in the refractory is

$$\begin{aligned}Q &= 200,000 \text{ lb} \times 0.2 \text{ Btu/lb-}^\circ\text{F} \times (500 - 70)^\circ\text{F} \\ &= 17.2 \times 10^6 \text{ Btu}\end{aligned}$$

At steady state, the refractory reaches and maintains a thermal equilibrium. The amount of energy reaching the refractory is either re-radiated back or lost to the surroundings through conduction to the outside of the furnace. Analysis of the possible radiant heat transfer components that could transfer energy to the refractory do not account for all the heat that is, in fact, reaching the refractory. The difference, a significant portion, is therefore coming from convection. As the hot gases sweep down the walls of the furnace, they heat the walls by a combination of radiation and convection. To achieve these rates of convection, the gas velocity in the proximity of the walls has to be quite high. Reed stated that gas velocities could reach 50 ft/s (16 m/s) in the vicinity of the walls.<sup>126</sup>

It is common to think of only the refractory areas that glow as being radiant. In reality all the hot surfaces, whether they are visibly elevated in temperature or not, are radiating. The visibly glowing surfaces, of course, are radiating more than the darker surfaces. Generally

speaking, refractory surfaces possess high emissivity and thus readily deliver their heat by radiation.

#### 7.5.4 Analysis of Radiation Heat Transfer

In this discussion and the following, the flame radiation will be approximated by treating the flame as an isothermal cylinder of gases. These gases can be reasonably assumed to be 17% H<sub>2</sub>O (by volume) and 8% CO<sub>2</sub> (by volume) at 1540°C (2800°F). For purposes of illustration, the mean beam length of the flame will be assumed to be 1 m (3.3 ft), however, this is only an approximation. Better accuracy requires more information to calculate the mean beam length. The pressure-pathlength for H<sub>2</sub>O is then 0.56 atm-ft, and for CO<sub>2</sub>, the pressure-pathlength is 0.264 atm-ft. From Figures 7.20 and 7.21, the emissivity of the water vapor is about 0.1, while the emissivity of the CO<sub>2</sub> is about 0.065. The total emissivity (uncorrected) is then 0.165.

Figure 7.22 indicates a 5% correction to the combined emissivity, so the corrected flame emissivity is 0.157. At 1540°C (2800°F), the blackbody emissive power is  $E_{b-flame} = \sigma T^4 = 5.67 \times 10^{-8}(1540 + 273)^4 = 610 \text{ kW/m}^2 = 194,000 \text{ Btu/ft}^2$ .

Figure 7.29 is an illustration of a vertical cylindrical furnace. In this style of furnace, the burners (shown here as a single flame) are surrounded by process tubes. The furnace shell is just outside the process tubes. The radiative circuit diagram in the figure shows how radiative heat flows from the flame to the tubes and refractory walls. To use this diagram, the emissivity values for the flame, refractory wall, and tube surfaces are required. For purposes of illustration, the flame emissivity determined earlier (0.157 for a flame temperature of 2800°F = 1540°C), a typical refractory emissivity of 0.65, and a typical tube surface emissivity (oxidized metal) of 0.85 will be used. To compute view factors, some dimensions need to be assumed as follows: a furnace diameter

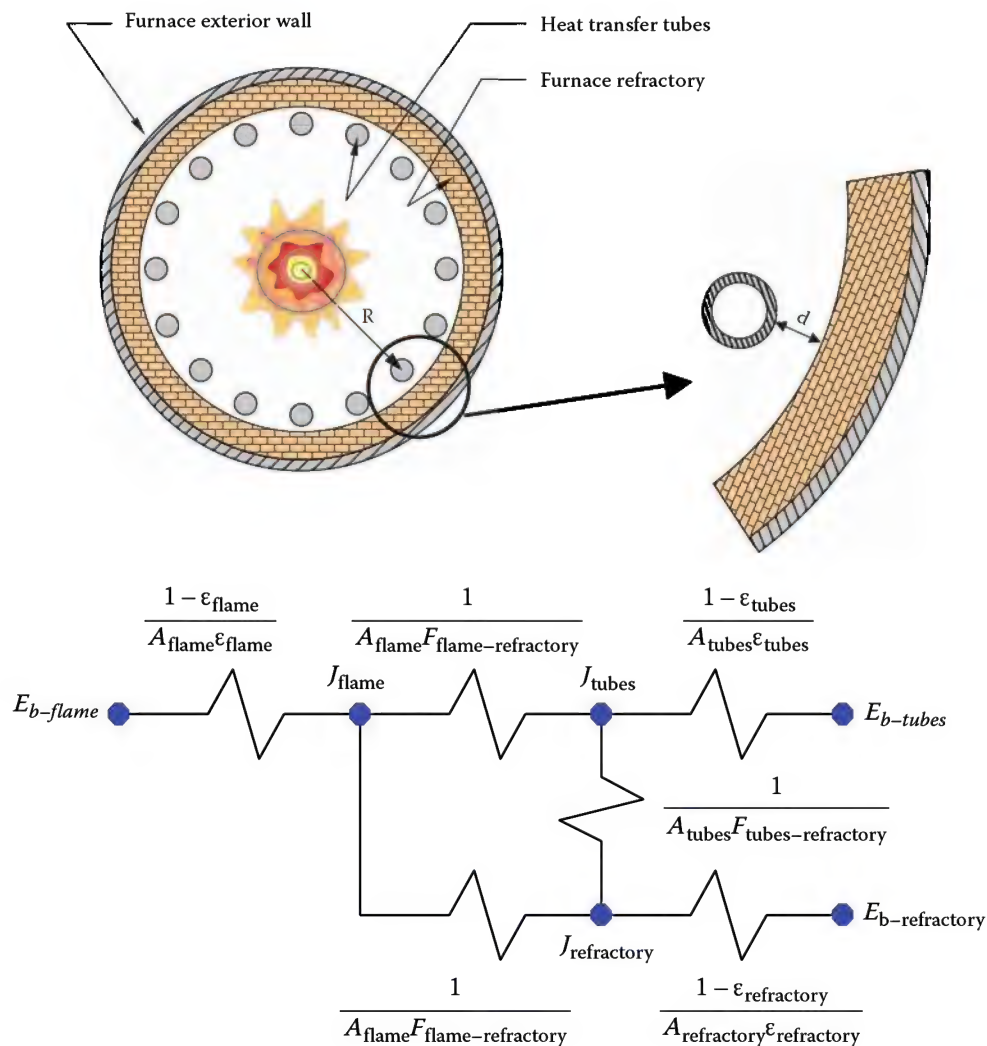


FIGURE 7.29  
Radiation heat transfer in a cylindrical furnace.

of 10 m (33 ft), a flame diameter of 1 m (3.3 ft), and a tube diameter of 20 cm (8 in.). Then a calculation using the formula in Table 7.10 gives the view factor from the flame to a single tube as 0.022. If it is assumed that there are 16 tubes in the furnace, then the view factor from the flame to the tubes is  $F_{\text{flame-tubes}} = 16 \times 0.022 = 0.352$ . Assume that the flame radiation that is not incident on the tubes is incident on the refractory, so that  $F_{\text{flame-refractory}} = 1 - F_{\text{flame-tubes}} = 0.648$ . Since there is no view factor catalog entry to help in computing the view factor from the tubes to the refractory, this value will be assumed to be one. This neglects the view factor from the tubes to the flame (which really is small) and the fact that the tubes "see each other" (which probably is not that small). For calculation purposes, an inside surface refractory temperature of 650°C (1200°F) and a tube surface temperature of 430°C (800°F) will be assumed.

The circuit diagram shown in Figure 7.29 leads to a system of three linear equations. Since the height of the furnace has not been specified, all the results will be per unit height. The solution of these equations gives the radiative heat flux from the flame as 284 kW/m (294,000 Btu/h-ft), the heat flux to the tubes is 251 kW/m (260,000 Btu/h-ft), and the heat flux to the furnace refractory is 33 kW/m (34,000 Btu/h-ft). These results mean, for instance, that the heat flux to the tubes is 260,000 Btu/ft (900,000 kJ/m) of tube length. If the tubes were 50 ft (15 m) long, then the total heat flux into the tubes would be  $13 \times 10^6$  Btu/h (3.8 MW).

### 7.5.5 Heat Transfer through the Wall of a Furnace

Figure 7.30 illustrates a typical furnace wall. The outer layer of the furnace wall is the steel furnace shell.

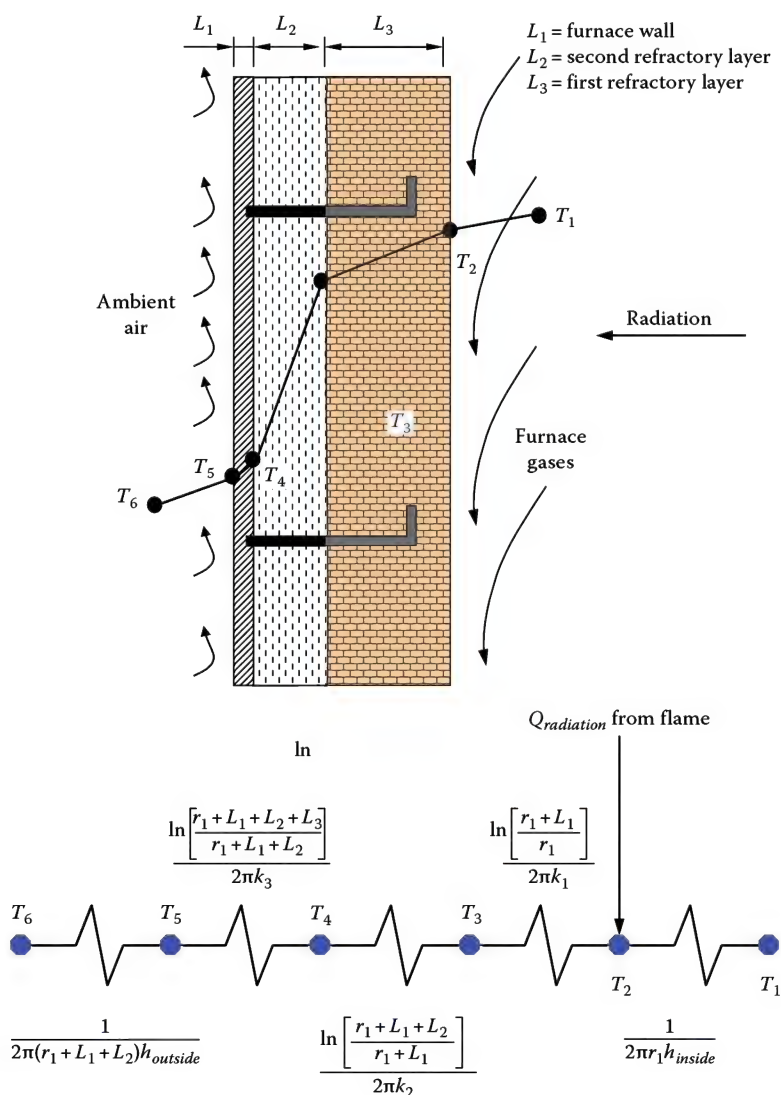


FIGURE 7.30

Cross section of a furnace wall.



The inner layers typically consist of refractory bricks and perhaps soft refractory blankets. The circuit diagram in the figure indicates how the heat transfer through the wall can be analyzed. All three heat transfer mechanisms are indicated. The inside surface is subjected to both convective and radiative heat transfer from the flue gases and flame, respectively. This heat is conducted through the refractory and eventually is convected away by natural and forced (wind) convection on the outside of the shell. A typical inside heat transfer coefficient is  $30 \text{ W/m}^2\text{-K}$  ( $5.3 \text{ Btu/h-ft}^2\text{-}^\circ\text{R}$ ). A typical outside heat transfer coefficient is  $17 \text{ W/m}^2\text{-K}$  ( $3.0 \text{ Btu/h-ft}^2\text{-}^\circ\text{R}$ ). If the refractory (both blanket and brick together) conductivity is assumed to be  $0.5 \text{ W/m-K}$  ( $0.3 \text{ Btu/h-ft}^2\text{-}^\circ\text{R}$ ) and the steel conductivity is  $100 \text{ W/m-K}$  ( $58 \text{ Btu/h-ft}^2\text{-}^\circ\text{R}$ ), then the heat flux through the wall can be computed. Using the radiative heat flux from the previous analysis as  $33 \text{ kW/m}$  ( $34,000 \text{ Btu/h-ft}$ ), assume a refractory surface temperature of  $650^\circ\text{C}$  ( $1200^\circ\text{F}$ ) and a flue gas temperature of  $675^\circ\text{C}$  ( $1250^\circ\text{F}$ ). Assume that the blanket thickness ( $L_1$ ) is  $5 \text{ cm}$  ( $2 \text{ in.}$ ), the brick thickness ( $L_2$ ) is  $5 \text{ cm}$  ( $2 \text{ in.}$ ), and the steel thickness is  $1.25 \text{ cm}$  ( $0.5 \text{ in.}$ ), then the circuit analysis gives the total heat flux through the furnace wall as  $56 \text{ kW/m}$  ( $58,000 \text{ Btu/h-ft}$ ) and the outer skin temperature is  $92^\circ\text{C}$  ( $200^\circ\text{F}$ ). Refer to the chapter on Process Heaters in Volume 3 of the Handbook for more details on heat transfer in furnaces.

### 7.5.6 Heat Transfer in the Process Tube

Figure 7.31 shows a cross-sectional view of a process fluid flowing through a tube. Radiant heat is incident on the outer surface of the tube, along with convection

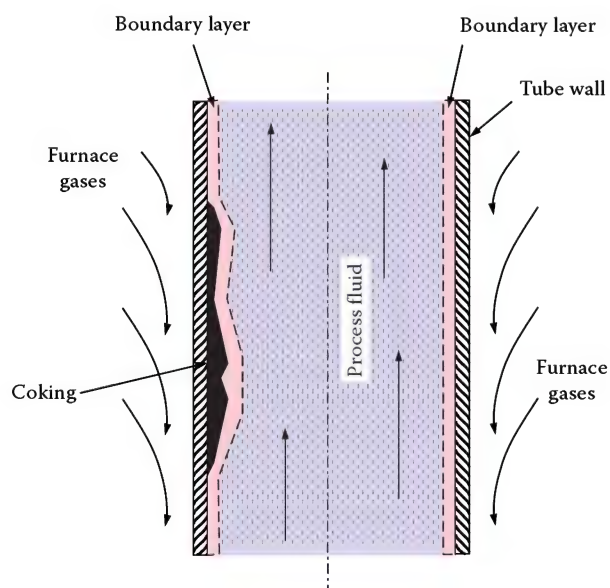


**FIGURE 7.31**  
Cross section of a process tube.

heat transfer from the furnace gases. This heat is conducted through the wall of the tube. Any coking or scaling on the inside or outside surface of the tube will add to the heat transfer resistance, which will subsequently increase the outside surface temperature. Heat transfer into the process fluid can be analyzed using the formulas given earlier in this chapter. The circuit analysis shown in the previous two examples can also be applied to this example. Additionally, the effects of extra heat transfer resistance due to coke or scale buildup on the tube surfaces could be readily added to get a more physically realistic calculation.

### 7.5.7 Furnace Gas Flow Patterns

As previously noted, in the low temperature furnaces the tubes are usually located very close to the walls. Again since the radiation is inversely proportional to the square of the distance, the radiation from the walls to the tube is significant when the tubes are close to the walls.

In the case of radiant wall furnaces, used in ethylene cracking operations, the wall is directly heated by the flame in order to capitalize on the high heat capacity of the refractory. The quantity of ethylene produced is maximized when the heat is applied evenly to the entire length of the tube. The ideal way to accomplish this is to heat the wall and allow it to radiate to the tubes. The high heat capacity of the refractory acts as a huge capacitance that helps to smooth out peaks in the temperature profile.

The heating of the refractory walls is caused by the hot gases sweeping down the walls. In fact the flow of gases between the tubes and the walls is important as the following example will illustrate. The flames heat the gases and buoyancy causes them to rise. As the gases close to the tubes deliver heat to the tubes and walls, they cool down, become denser, and flow down toward the bottom of the furnace. This establishes a circulation pattern within the furnace such that the gases rise up from the flames and reverse direction higher up in the furnace and flow down the wall and tubes to the furnace floor. On reaching the floor, the gases are reheated by the burner and rise up again to either make another circuit or to exit from the furnace through the stack. The benefits of recirculation are optimum when the tubes are on typical two-diameter centers and decrease as the center-to-center distance is reduced to less than two diameters.

Gases in such recirculation flow pass over the entire tube areas as well as the wall behind the tubes, scrubbing the tube surfaces for heat transfer by convection. Far more importantly, they also scrub the refractory wall behind the tubes to continually deliver heat to the wall surface. Whether the tubes are horizontal or vertical does not seem to make much difference.

There are several methods to visualize furnace gas flow patterns. Today CFD is the preferred engineering tool to study furnace flue gas patterns. Chapter 13 shows several examples of such studies. On the other hand, in the furnace one may use various powdery substances such as baking soda, particulate carbon, etc., to observe furnace flow patterns. The powder is usually introduced in the air stream to the burners and is seen to glow briefly in the furnace. The glowing particles trace the flow patterns. This is a useful but approximate technique because the persistence of the glowing is short and if it is too short, it may adversely bias the conclusions being drawn.

Reed in his book on *Furnace Operations*<sup>126</sup> mentions an incident to illustrate the importance of furnace gas flow between the tubes and walls. A heater had operated satisfactorily for years. As operation progressed, it was noted that the heater was rapidly losing heat transfer ability despite the fact that there had been no change in operation, which might account for the decrease. There was no change in pressure drop, so the possibility of coke lay-down was rejected. The deterioration in performance came about in less than six months and was noticeable on a day-to-day basis as the heater operated.

The heater had been in service for many years and was due for repairs, which included replacement of refractory side walls that were sagging inward. The walls, supported independently of the steel, which supported the tubes, had gradually moved toward the tubes. The space between the walls and the back sides of the tubes was reduced to such a degree that most of the side walls were actually resting against the tubes.

The heater was shut down and the side walls were repaired to make the space between the tubes and the wall one full tube diameter, which in this case was four inches. When the heater was put back into service, it had regained its original heat transfer capability. No change other than the refractory repair had been implemented. From this, it was surprisingly evident that the increased space between the tubes and the wall accounted for increased heat absorbing ability.

Reed conducted experiments at reduced scale to evaluate the influence of tube-to-wall spacing. A test heater was constructed using tubes with an outer diameter of 1/4 in. (6 mm). The test furnace dimensions were 18 × 18 × 27 in. (46 × 46 × 69 cm). There was a provision to accurately adjust the tube-to-wall spacing and to adjust the relationship of the burner to the tubes. Accurately metered, saturated air was passed through the 3/16-in. (4.8 mm) ID tubes as the source of heat absorption. A thermocouple was used in the air stream at the exit from the tubes to measure temperature of the exiting air and so measure the heat absorbed. The firing rate and excess

air, as well as furnace temperature, were closely controlled to identical conditions for all tests.

Reed reports that for a tube spaced one-half diameter off the wall, the heat transfer to the tube is increased 13% over the condition where the tube is tangent to the wall. If the tube is spaced one diameter off the wall, the heat transfer to the tube is increased approximately 29% over the condition where the tube is tangent to the wall. Further increasing the tube-to-wall spacing to as much as three to four diameters provided no increase in heat transfer. Still greater spacing actually created a decrease in heat transfer.

To verify that the gas flow behind the tubes was the contributor to the enhanced heat transfer at a tube-to-wall distance of one tube diameter, an additional experiment was conducted. In this experiment, the tubes were spaced one diameter off the wall to produce the 29% increase in transfer. Strips of mica 0.003 in. (0.08 mm) thick were placed in the space between the tubes and the wall at the centerlines of the tubes so as to block the space between the tubes and the wall with material that is substantially transparent to infrared. The purpose was to avoid blocking radiant transfer but to completely block the flow path for gases in the space between the tubes and the wall behind them. With the mica strips, the heat transfer to the tubes was exactly the same as was observed with the tubes tangent to the wall. In other words the 29% performance gain was lost due to the blockage.

### 7.5.8 Role of the Burner in Heat Transfer

Simple release of an adequate amount of heat to the furnace atmosphere is not the only objective for the burner. Proper choice of burners is critical to the performance of the heater. There are no hard and fast rules to govern the choice of burners. The design of the furnace and the burner must be matched carefully to achieve good overall performance. There is no single burner design that can be universally applied.

The function of the burner equipment is usually to deliver heat to the furnace as uniformly as possible. Reaching this ideal condition would require an infinitely large number of small burners. Ethylene cracking and hydrogen reforming furnaces most closely approximate this ideal arrangement by using many small burners. Over the last 100 years the quest for better heat transfer has resulted in a myriad of furnace designs. It follows that many burner designs were developed to fit the various furnace designs. Back when emissions were not regulated, the primary requirement for the burner was effective heat transfer. Typically the old burner designs rapidly mixed the fuel and air resulting in short flames. Emissions regulations have now driven the design of burners for the last two or three decades. The primary requirement is now to meet the emissions regulations,

but not compromise furnace performance. This conflicting challenge has been met with considerable engineering ingenuity over the years. Low-NO<sub>x</sub> burners designed in the last two decades tend to have longer flames because the strategy for NO<sub>x</sub> reduction was to delay mixing and thereby reduce the peak flame temperatures.

Over the years, furnace manufacturers as well as burner manufacturers have researched heat flux profiles in various burner–furnace combinations. Again CFD (see Chapter 13) is a great help in studying heat flux profiles but even with today's sophisticated modeling capabilities and advanced instrumentation, exact measurements are not possible. Exact measurements are difficult to obtain because apart from the obvious problem of working in a high temperature zone, the geometry of the furnace and the re-radiation from various furnace surfaces make the analysis complicated. With wall-fired burners, whether floor mounted or wall mounted, it is somewhat easier to predict heat flux patterns. However, in furnaces that have free standing flames the heat flux patterns tend to be specific to that burner–furnace combination.

If a desired heat flux pattern is identified, it is possible to engineer the flame shape to attempt to meet the requirement. Previous experience can help define the burner design required. On the other hand the outcome can only be estimated if there is no previous experience with that particular furnace–burner combination. In such cases, some final testing and adjustment is usually required. Consequently burners have been developed over the years with flames of every conceivable shape.

Burner flames must be shaped and directed to allow the required heat diffusion to the furnace gases without delivering excessive heat to any local heat transfer area. Local overheating and flame impingement must be avoided at all costs. Flame impingement does not occur solely due to burner performance. The burner has only limited control over the characteristic flow patterns of a furnace. It is possible to modify a burner to eliminate flame impingement by changing the fuel jet configurations, but there is only a narrow window of opportunity here because radical modifications will require compromises in other areas of burner performance, such as capacity or emissions.

Flame length is of utmost importance in burner design, although flame length and heat dispersion are not necessarily in a fixed relationship. Providing short flames exclusively for all applications is not the answer either, because some applications require long flames to reach further into large furnaces, or to deliver heat to locations further away from the burner. For example, in the typical floor-fired steam reformer it is necessary to drive the hot gases from the furnace floor to the top of the furnace to distribute heat to the tube areas where maximum heat density is demanded. Today most steam reforming furnaces (see Figure 1.16b) are down-fired for

this reason. The contrary is true in side-wall-fired steam reformers (see Figure 1.16a).

In side-wall firing, the burners are located in areas where maximum heat transfer is demanded. The flame is expected to remain close to the wall and not penetrate forward into the furnace at all. This is because the furnaces are narrow and the burners are located quite close to the tubes, which may be either vertically or horizontally suspended at the center of the furnace. The “terrace wall” furnace design (see Figure 1.18) for the same application is a prime example of the differentiation between heat dispersion and flame length. The burners are mounted in terraces on the side wall in much the same way a floor-mounted burner would be, and the flame is fired vertically up the wall. In this design, the flame is considerably longer than the small wall burners, yet the service performed is identical.

In a typical process heater, the demand for very precise control of heat density per linear length of tube is not as great as in a steam-reformer furnace. It is possible to use a smaller number of larger burners to obtain satisfactory firing conditions and heat dispersion, but the burners must be suited to the service. Sometimes, burners capable of reasonably short flames have not had satisfactory heat dispersion characteristics and must be replaced to reduce tube damage.

Some designs have burners that are mounted on the side walls of the furnace with the flame fired horizontally into the furnace space. This is not the same as the ethylene cracking or reforming radiant wall arrangements. These are lower temperature furnaces where the design decision has been made to mount a burner on the side wall instead of the floor to reduce the initial cost of the furnace. Side-wall mounting costs less since the furnace does not have to be elevated to install burners below it, and, often, fewer burners are required. However, floor firing has some advantages over side-wall firing. With floor-mounted burners the heater can typically be fired 25% harder. This is because floor mounting makes better use of the combustion volume and provides more uniform heat distribution.

Either way, there will be greater service from the heater when a relatively large number of small burners are used rather than a small number of large burners. If there is a relatively small number of large burners, there is a greater mass of gas issuing from each burner and a greater concentration of heat before the burner. This larger mass of gases and quantity of heat must then be dispersed evenly to the furnace atmosphere for good performance. It is far easier to disperse smaller amounts of gas and heat as issued by several smaller burners.

To conclude, in general, the heat transfer role of the burner in a furnace is to provide the required amount of



heat with appropriate flame dimensions without localized hot spots or flame impingement. The sizing and selection of the burner must help to make the temperature of the bulk of the furnace gases as uniform as possible in as short a distance as possible from the burner.

## 7.6 Conclusions

This chapter has presented some of the fundamentals of heat transfer. Basic relations for conduction, convection, and radiation heat transfer have been provided and discussed. This chapter, by necessity, has been a very brief and dense presentation of the subject of heat transfer, specifically targeted toward process heaters and burners. The interested reader is encouraged to consult with heat transfer texts (see references) for more detailed information or explanation. The subject of heat transfer is vast and interesting. The focus of this chapter has been on heat transfer in combustion systems, but there are a multitude of other heat transfer applications to which these basic principles may be applied. It is hoped that this brief introduction has given the reader an interest in pursuing the subject further.

The difficulties that may arise when trying to apply heat transfer relationships to furnace heat transfer problems were considered here. Some of the approximations that can be made to complete such an analysis were considered. Again, the reader interested in more information should consult the references given at the end of this chapter. In particular, the book by Baukal<sup>128</sup> provides a thorough overview of industrial combustion heat transfer and cites many additional references.

## References

1. B. Gebhart, *Heat Transfer*, 2nd edn., McGraw-Hill, New York, 1971.
2. A. Bejan, *Heat Transfer*, Wiley, New York, 1993.
3. A.F. Mills, *Heat Transfer*, 2nd edn., Prentice Hall, Englewood Cliffs, NJ, 1998.
4. L.M. Latif, *Heat Transfer Essentials: A Textbook*, Begell House, New York, 2002.
5. R.J. Ribando, *Heat Transfer Tools*, McGraw-Hill, Boston, MA, 2002.
6. K. Jorge, T. Muneer, and G. Thomas, *Heat Transfer: A Problem Solving Approach*, Taylor & Francis, New York, 2003.
7. P.S. Ghoshdastidar, *Heat Transfer*, Oxford University Press, Oxford, U.K., 2004.
8. P.D. Hills, *Practical Heat Transfer*, Begell House, New York, 2005.
9. M. Kutz (ed.), *Heat Transfer Calculations*, McGraw-Hill, New York, 2006.
10. M. Kaviany, *Heat Transfer Physics*, Cambridge University Press, Cambridge, U.K., 2008.
11. J.R. Welty, *Fundamentals of Momentum, Heat, and Mass Transfer*, 5th edn., Wiley, Denver, MA, 2008.
12. J.P. Holman, *Heat Transfer*, 10th edn., McGraw-Hill, New York, 2009.
13. W.X. Janna, *Engineering Heat Transfer*, 3rd edn., CRC Press, Boca Raton, FL, 2009.
14. G. Nellis and S. Klein, *Heat Transfer*, Cambridge University Press, Cambridge, U.K., 2009.
15. F. Kreith, R.M. Manglik, and M.S. Bohn, *Principles of Heat Transfer*, 7th edn., CL Engineering, Mason, OH, 2010.
16. M.M. Rathore and R.R. Kapuno, Jr., *Engineering Heat Transfer*, Jones & Bartlett Learning, Sudbury, MA, 2010.
17. H.D. Baehr, *Heat and Mass-Transfer*, Springer, New York, 2011.
18. T.L. Bergman, A.S. Levine, D.P. Dewitt, and F.P. Incropera, *Introduction to Heat Transfer*, 6th edn., Wiley, New York, 2011.
19. Y.A. Çengel and A.J. Ghajar, *Heat and Mass Transfer: Fundamentals & Applications*, McGraw-Hill, New York, 2011.
20. J.-C. Han, *Analytical Heat Transfer*, CRC Press, Boca Raton, FL, 2011.
21. M. Kaviany, *Essentials of Heat Transfer*, Cambridge University Press, Cambridge, U.K., 2011.
22. J.H. Lienhard IV and J.H. Lienhard V, *A Heat Transfer Textbook*, 4th edn., Dover Publications, Mineola, NY, 2011.
23. L. Theodore, *Heat Transfer Applications for the Practicing Engineer*, Wiley, Hoboken, NJ, 2011.
24. P. von Böckh and T. Wetzel, *Heat Transfer: Basics and Practice*, Springer, New York, 2011.
25. H.C. Hottel and A.F. Sarofim, *Radiative Transfer*, McGraw-Hill, New York, 1967.
26. T.J. Love, *Radiative Heat Transfer*, Merrill Publishing, Columbus, OH, 1968.
27. M. Özisik, *Radiative Transfer and Interactions with Conduction and Convection*, Wiley, New York, 1973.
28. W.A. Gray and R. Müller, *Engineering Calculations in Radiative Heat Transfer*, Pergamon, Oxford, U.K., 1974.
29. E.M. Sparrow and R.D. Cess, *Radiation Heat Transfer*, Augmented Edition, Hemisphere, Washington, DC, 1978.
30. J.B. Dwyer, Furnace calculations, in *Process Heat Transfer*, (ed.) D.Q. Kern, McGraw-Hill, New York, 1950.
31. F.W. Hutchinson, *Industrial Heat Transfer*, Industrial Press, New York, 1952.
32. S.T. Hsu, *Engineering Heat Transfer*, D. Van Nostrand Co., Princeton, NJ, 1963.
33. J.R. Welty, *Engineering Heat Transfer*, Wiley, New York, 1974.
34. B.V. Karlekar and R.M. Desmond, *Engineering Heat Transfer*, West Pub. Co., St. Paul, MN, 1977.
35. V. Ganapathy, *Applied Heat Transfer*, PennWell Books, Tulsa, OK, 1982.
36. A.G. Blokh, *Heat Transfer in Steam Boiler Furnaces*, Hemisphere, Washington, DC, 1988.



37. Y.V. Deshmukh, *Industrial Heating: Principles, Techniques, Materials, Applications, and Design*, CRC Press, Boca Raton, FL, 2005.
38. J. Xu, Heat transfer in combustion systems, Chapter 5 in *Handbook of Combustion: Vol. 1: Fundamentals and Safety*, (ed.) M. Lackner, F. Winter, and A.K. Agarwal, John Wiley, New York, 2010.
39. W.M. Rohsenow, J.P. Hartnett, and Y. Cho, *Handbook of Heat Transfer*, 3rd edn., McGraw-Hill Book Company, New York, 1998.
40. N.P. Cheremisinoff (ed.), *Handbook of Heat and Mass Transfer*, 4 volumes, Vol. 1: Heat Transfer Operations, Vol. 2: Mass Transfer and Reactor Design, Vol. 3: Catalysis, Kinetics, and Reactor Engineering, and Vol. 4: Advances in Reactor Design and Combustion Science, Gulf Pub. Co., Houston, TX, 1986.
41. F. Kreith (ed.) *The CRC Handbook of Thermal Engineering*, CRC Press, Boca Raton, FL, 2000.
42. A. Bejan and A.D. Kraus, *Heat Transfer Handbook*, Wiley, New York, 2003.
43. G.F. Hewitt, G.L. Shires, and Y.V. Polezhaev, *International Encyclopedia of Heat and Mass Transfer*, CRC Press, Boca Raton, FL, 1997.
44. V.S. Arpaci, *Conduction Heat Transfer*, Addison-Wesley, Reading, MA, 1966.
45. M.N. Özisik, *Boundary Value Problems of Heat Conduction*, Dover, New York, 1968.
46. U. Grigull and H. Sandner, *Heat Conduction*, Hemisphere, Washington, DC, 1984.
47. G.E. Myers, *Analytical Methods in Conduction Heat Transfer*, Genium Publishing, Schenectady, NY, 1987.
48. B. Gebhart, *Heat Transfer and Mass Diffusion*, McGraw-Hill, New York, 1993.
49. D. Poulikakos, *Conduction Heat Transfer*, Prentice-Hall, Englewood Cliffs, NJ, 1994.
50. ASME, *ASME Steam Tables for Industrial Use*, 2nd edn., American Society of Mechanical Engineers, Washington, DC, 2009.
51. F.P. Incropera and D.P. DeWitt, *Fundamentals of Heat and Mass Transfer*, 4th edn., John Wiley & Sons, New York, 1996.
52. C.E. Baukal, V.Y. Gershtein, and X. Li, *Computational Fluid Dynamics in Industrial Combustion*, CRC Press, Boca Raton, FL, 2001.
53. A. Garg, How to boost the performance of fired heaters, *Chem. Eng.*, 96(11), 239–244, 1989.
54. V.S. Arpaci, *Convection Heat Transfer*, Prentice-Hall, Englewood Cliffs, NJ, 1984.
55. C.S. Fang, *Convective Heat Transfer*, Gulf Publishing, Houston, TX, 1985.
56. S. Kakac, R.K. Shah, and W. Aung (eds.), *Handbook of Single-Phase Convective Heat Transfer*, Wiley, New York, 1987.
57. L.C. Burmeister, *Convective Heat Transfer*, 2nd edn., Wiley, New York, 1993.
58. S. Kakac and Y. Yener, *Convective Heat Transfer*, 2nd edn., CRC Press, Boca Raton, FL, 1995.
59. P.H. Oosthuizen and D. Naylor, *Introduction to Convective Heat Transfer Analysis*, McGraw-Hill, New York, 1999.
60. T. Cebeci, *Convective Heat Transfer*, 2nd Rev. ed., Horizons, Long Beach, CA, 2002.
61. A. Bejan, *Convection Heat Transfer*, 3rd edn., Wiley, New York, 2004.
62. W.M. Kays, M.E. Crawford, and B. Weigand, *Convective Heat and Mass Transfer*, 4th edn., McGraw-Hill, New York, 2004.
63. M. Favre-Marinet and S. Tardu, *Convective Heat Transfer: Solved Problems*, Wiley, Hoboken, NJ, 2009.
64. M. Ghiaasiaan, *Convective Heat and Mass Transfer*, Cambridge University Press, Cambridge, U.K., 2011.
65. M. Kaviany, *Principles of Convective Heat Transfer*, 2nd edn., Springer-Verlag, New York, 2011.
66. T.M. Smith, President of Marsden, Inc., Pennsauken, NJ, private communication, 1982.
67. F.W. Dittus and L.M.K. Boelter, Heat transfer in automobile radiators of the tubular type, *Uni. Calif. Berkeley Publ. Eng.*, 2, 443, 1930.
68. E.N. Sieder and G.E. Tate, Heat transfer and pressure drop of liquids in tubes, *Ind. Eng. Chem.*, 28(12), 1429–1435, 1936.
69. B.S. Petukhov, T.F. Irvine and J.P. Hartnett (eds.), *Advances in Heat Transfer*, Vol. 6, Academic Press, New York, 1970.
70. L.F. Moody, Friction factors for pipe flow, *Trans. ASME*, 66, 671–684, 1944.
71. E.S. Skupinski, J. Tortel, and L. Vautrey, Determination des coefficients de convection d'un alliage sodium-potassium dans un tube circulaire, *Int. J. Heat Mass Transfer*, 8, 937–951, 1965.
72. R.A. Seban and T.T. Shimazaki, Heat transfer to a fluid flowing turbulently in a smooth pipe with walls at constant temperature, *Trans. ASME J. Heat Transfer*, 73, 803–809, 1951.
73. C.B. Reed, S. Kakac, R.K. Shah, and W. Aung (eds.), *Handbook of Single-Phase Convective Heat Transfer*, Chap. 8, Wiley Interscience, New York, 1987.
74. H. Schlichting, *Boundary Layer Theory*, 6th edn., McGraw-Hill, New York, 1968.
75. R. Hilpert, Wärmeabgabe von geheizten drähten und rohren im luftstrom. *Forschungsarbeiten auf dem Gebiet des Ingenieurwesens*, 4, 215–224, 1933.
76. J.D. Knudsen and D.L. Katz, *Fluid Dynamics and Heat Transfer*, McGraw-Hill, New York, 1958.
77. S.W. Churchill and M. Bernstein, A correlating equation for forced convection from gases to liquids to a circular cylinder in crossflow, *J. Heat Transfer*, 99(2), 300–306, 1977.
78. E.D. Grimison, Correlation and utilization of new data on flow resistance and heat transfer for cross flow of gases over tube banks, *Trans. ASME*, 59, 583–594, 1937.
79. A. Zhukauskas, Heat transfer from tubes in cross flow, in J.P. Hartnett and T.F. Irvine, Jr. (eds.), *Advances in Heat Transfer*, Vol. 8, Academic Press, New York, 1972.
80. J.M. Beér and N.A. Chigier, Impinging jet flames, *Comb. Flame*, 12, 575–586, 1968.
81. A. Milson and N.A. Chigier, Studies of methane-air flames impinging on a cold plate, *Comb. Flame*, 21, 295–305, 1973.

82. E.G. Jackson and J.K. Kilham, Heat transfer from combustion products by forced convection, *Ind. Eng. Chem.*, 48(11), 2077–2079, 1956.
83. C.E. Baukal and B. Gebhart, A review of empirical correlations for flame impingement heat transfer, *Int. J. Heat Fluid Flow.*, 17(4), 386–396, 1996.
84. J.K. Kilham, Energy transfer from flame gases to solids, *Third Symposium on Combustion and Flame and Explosion Phenomena*, The Williams and Wilkins Co., Baltimore, MD, pp. 733–740, 1949.
85. R.A. Cookson and J.K. Kilham, Energy transfer from hydrogen-air flames, *Ninth Symposium (International) on Combustion*, Academic Press, New York, pp. 257–263, 1963.
86. Woodruff, L.W. and W.H. Giedt, Heat transfer measurements from a partially dissociated gas with high lewis number, *J. Heat Trans.*, 88, 415–420, 1966.
87. J.K. Kilham and P.G. Dunham, Energy transfer from carbon monoxide flames, *Eleventh Symposium (International) on Combustion*, The Comb. Inst., Pittsburgh, PA, pp. 899–905, 1967.
88. J.K. Kilham and M.R.I. Purvis, Heat transfer from hydrocarbon-oxygen flames, *Comb. Flame*, 16, 47–54, 1971.
89. R. Conolly and R.M. Davies, A study of convective heat transfer from flames, *Int. J. Heat Mass Trans.*, 15, 2155–2172, 1972.
90. S. Nawaz, Heat transfer from oxygen enriched methane flames, PhD thesis, The University of Leeds, Leeds, U.K., 1973.
91. C.J. Hoogendoorn, C.O. Popiel, and T.H. van der Meer, Turbulent heat transfer on a plane surface in impingement round premixed flame jets, *Proc. of 6th Int. Heat Trans. Conf.*, Toronto, 4, 107–112, 1978.
92. J.K. Kilham and M.R.I. Purvis, Heat transfer from normally impinging flames, *Comb. Sci. Tech.*, 18, 81–90, 1978.
93. You, H-Z., An investigation of fire-plume impingement on a horizontal ceiling: 2—Impingement and ceiling-jet regions, *Fire & Materials*, 9(1), 46–56, 1985.
94. M. Sibulkin, Heat transfer near the forward stagnation point of a body of revolution, *J. Aero. Sci.*, 19, 570–571, 1952.
95. C.E. Baukal and B. Gebhart, A review of semi-analytical solutions for flame impingement heat transfer, *Int. J. Heat Mass Trans.*, 39(14), 2989–3002, 1996.
96. S.N. Shorin and V.A. Pechurkin, Effectivnost' teploperenosa na poverkhnost' plity ot vysokotemperaturnoi strui produktov sgoraniya razlichnykh gazov, *Teoriya i Praktika Szhiganiya Gaza*, 4, 134–143, 1968.
97. J.-P. Vizioz and T.M. Lowes, Convective heat transfer from impinging flame jets, *Int'l Flame Res. Found. report F 35/a/6*, IJmuiden, the Netherlands, 1971.
98. E. Buhr, G. Haupt and H. Kremer, Heat transfer from impinging turbulent jet flames to plane surfaces, *Combustion Institute European Symposium 1973*, (ed.) F.J. Weinberg, Academic Press, New York, pp. 607–612, 1973.
99. R.B. Smith and T.M. Lowes, Convective heat transfer from impinging tunnel burner flames—A short report on the NG-4 trials, *Int'l Flame Res. Found. Report F 35/a/9*, IJmuiden, the Netherlands, 1974.
100. M. Matsuo, M. Hattori, T. Ohta, and S. Kishimoto, The experimental results of the heat transfer by flame impingement, *Int'l Flame Res. Found. Report F 29/1a/1*, IJmuiden, the Netherlands, 1978.
101. J.B. Rajani, R. Payne, and S. Michelfelder, Convective heat transfer from impinging oxygen-natural gas flames—Experimental results from the NG5 Trials, *Int'l Flame Res. Found. Report F 35/a/12*, IJmuiden, the Netherlands, 1978.
102. A. Ivernel and P. Vernotte, Etude expérimentale de l'amélioration des transferts convectifs dans les fours par suroxygénation du comburant, *Rev. Gén. Therm., Fr.*, Nos. 210–211, 1979.
103. G.K. Hargrave and J.K. Kilham, The effect of turbulence intensity on convective heat transfer from premixed methane-air flames, *Inst. Chem. Eng. Symp. Ser.*, 2(86), pp. 1025–1034, 1984.
104. M.E. Horsley, M.R.I. Purvis, and A.S. Tariq, Convective heat transfer from laminar and turbulent premixed flames, *Heat Transfer 1982*, (eds.) U. Grigull, E. Hahne, K. Stephan, and J. Straub, Hemisphere, Washington, DC, Vol. 3, pp. 409–415, 1982.
105. Rauenzahn, R.M., Analysis of Rock Mechanics and Gas Dynamics of Flame-Jet Thermal Spallation Drilling, PhD thesis, MIT, Cambridge, MA, 1986.
106. G.K. Hargrave, M. Fairweather, and J.K. Kilham, Forced convective heat transfer from premixed flames—Part 2: Impingement heat transfer, *Int. J. Heat Fluid Flow*, 8(2), 132–138, 1987.
107. J.E. Hustad and O.K. Sønju, Heat transfer to pipes submerged in turbulent jet diffusion flames, in *Heat Transfer in Radiating and Combusting Systems*, Springer-Verlag, Berlin, pp. 474–490, 1991.
108. T.H. van der Meer, Stagnation point heat transfer from turbulent low reynolds number jets and flame jets, *Exper. Therm. Fluid Sci.*, 4, 115–126, 1991.
109. V.I. Babi, Solid/gas phase heat exchange in combustion of powdered fuel, in *Heat Transfer in Flames*, (eds.) N.H. Afgan and J.M. Beer, Chapter 7, Scripta Book Company, Washington, DC, pp. 131–139, 1974.
110. B. Gebhart, Y. Jaluria, R. Mahajan, and B. Sammakia, *Buoyancy-Induced Flows and Transport*, Hemisphere, New York, 1988.
111. Y.B. Wang, C. Chaussavoine, and F. Teyssandier, Two-dimensional modelling of a non-confined circular impinging jet reactor—Fluid dynamics and heat transfer, *Int. J. Heat Mass Trans.*, 36(4), 857–873, 1993.
112. J.A. Wiebelt, *Engineering Radiation Heat Transfer*, Holt, Rinehart and Winston, New York, 1966.
113. D.K. Edwards, *Radiation Heat Transfer Notes*, Hemisphere, Washington, DC, 1981.
114. R. Siegel and J.R. Howell, *Thermal Radiation Heat Transfer*, 2nd edn., Hemisphere, Washington, 1981.
115. M.Q. Brewster, *Thermal Radiative Transfer and Properties*, Wiley, New York, 1992.
116. M. Planck, *The Theory of Heat Radiation*, Dover Publications, New York, 1959.
117. C.B. Ludwig, W. Malkmus, J.E. Reardon, and J.A.L. Thomson, *Handbook of Infrared Radiation from Combustion Gases*, NASA SP-3080, NASA, Washington, DC, 1973.

118. B. Leckner, Spectral and total emissivity of water vapor and carbon dioxide, *Comb. Flame*, 19, 1972.
119. C.B. Ludwig, W. Malkmus, J.E. Reardon, and J.A.L. Thomson, Handbook of infrared radiation, NASA Report SP-3080, Scientific and Technical Information Office, Washington, DC, 1973.
120. M.F. Modest, Radiation, Section 4.3, in *The CRC Handbook of Mechanical Engineering*, ed. F. Kreith, CRC Press, Boca Raton, FL, 1998.
121. H.C. Hottel, *Radiant Heat Transmission*, in W.H. McAdams, ed. *Heat Transmission*, 3rd edn., McGraw-Hill, New York, 1954.
122. M.F. Modest, *Radiative Heat Transfer*, McGraw-Hill, New York, 1993.
123. C.J. Hoogendoorn, C.M. Ballintijn, and W.R. Dorresteyn, Heat-flux studies in vertical tube furnaces, *J. Inst. Fuel*, 43, 511–516, 1970.
124. N. Selçuk, R.G. Siddall, and J.M. Beér, Prediction of the effect of flame length on temperature and radiative heat flux distributions in a process fluid heater, *J. Inst. Fuel*, 43, 89–96, 1975.
125. ANSI/API standard 560, *Fired Heaters for General Refinery Service*, 4th edn., American Petroleum Institute, Washington, DC, August 2007.
126. R.D. Reed, *Furnace Operations*, 3rd edn., Gulf Publishing, Houston, TX, 1981.
127. W. Trinks, M.H. Mawhinney, R.A. Shannon, R.J. Reed, and J.R. Garvey, *Industrial Furnaces*, 6th edn., John Wiley, New York, 2004.
128. C.E. Baukal, *Heat Transfer in Industrial Combustion*, CRC Press, Boca Raton, FL, 2000.

This page intentionally left blank



## Flare Radiation

Wes Bussman and Jeff White

### CONTENTS

8.1	Introduction .....	207
8.2	Properties and Characteristics of Radiation .....	208
8.2.1	Electromagnetic Spectrum .....	208
8.2.2	Flare Radiation Units.....	208
8.2.3	Solar Radiation Level .....	209
8.2.4	Radiation Level as a Function of Distance from Source .....	211
8.2.5	Flare Radiation Spectrum.....	212
8.2.6	Radiation Transmission Losses through the Atmosphere.....	213
8.3	Environmental Concerns .....	214
8.3.1	Radiation Effects on Equipment .....	214
8.3.2	Ignition of Flammable Material from Radiant Heating .....	214
8.3.3	Radiation Effects on Humans .....	215
8.3.4	API 521 Recommendations.....	215
8.4	Estimating Flare Radiation.....	217
8.5	Measuring Flare Radiation.....	219
8.5.1	Description of the Radiometer .....	219
8.5.2	Useful Tips When Measuring Flare Radiation.....	220
8.5.2.1	Radiometer Selection.....	220
8.5.2.2	Sun Interference .....	221
8.5.2.3	View Angle.....	221
8.5.2.4	Convective Cooling Effects.....	222
8.5.2.5	Measuring Technique.....	223
8.5.3	Radiometer Cube .....	224
	References.....	224

### 8.1 Introduction

The hydrocarbon and petrochemical industries use flare systems to dispose of waste gases in a safe, effective manner.<sup>1</sup> During an emergency flaring situation, today's plants might burn more than  $1 \times 10^6$  lb/h ( $5 \times 10^5$  kg/h) of gas producing an open flame over several hundred feet (100 m) long.<sup>2</sup> A portion of the heat produced by the flame will radiate to its immediate surroundings. In many cases, heat radiated from the flare flame during emergency flaring forms the basis for determining how tall to design the flare stack, where to locate it, and what area surrounding the flare is to have limited access to personnel and equipment.

One of the greatest challenges in designing a flare system is predicting the amount of heat radiated from

the flame. It is extremely important to accurately predict thermal radiation. Underestimating thermal radiation levels may result in a flare stack that is too short, which could expose personnel and equipment to potentially dangerous levels of heat.

Estimating flare radiation from a purely theoretical approach is currently not feasible due to the complexity of the problem. To overcome this problem, engineers have historically estimated radiation using semi-empirical models based on experimental data. Although each flare vendor uses their own proprietary models to estimate flare radiation, each model must rely heavily on experimental data. Therefore, it is extremely important that radiation data gathered from flare testing are accurate.

This chapter will present the properties and characteristics of thermal radiation followed by a discussion

on the effects of thermal radiation on equipment, structures and personnel. Methods used in the flare industry to estimate radiation from a flare flame will then be shown. Finally, typical industrial measurement of flare radiation will be explored.

## 8.2 Properties and Characteristics of Radiation

### 8.2.1 Electromagnetic Spectrum

Everyone has experienced the effect of heat transfer by thermal radiation; for example, the warmth of sunshine or the heat one feels when standing next to a campfire. Unlike conduction or convection, heat transfer by thermal radiation does not require a medium to transfer heat. Thermal radiation is transferred through space by electromagnetic wave phenomena that travel at the speed of light (see Chapter 7).

Radiation consists of a wide range of wavelengths as illustrated in Figure 8.1. Each wavelength corresponds to a frequency and an energy level: the shorter the wavelength of radiation, the higher the frequency and greater the energy. Very short wave lengths fall into a category of gamma rays or x-ray. Radiation with longer wavelengths, such as TV and radio waves, falls on the other end of the spectrum and has much less energy. *Thermal radiation* falls between these two ends and is defined as the

portion of the spectrum between  $1 \times 10^{-7}$  and  $1 \times 10^{-4}$  m wavelengths<sup>3</sup> that is emitted from solid, liquids, and gases by way of the temperature above absolute zero.<sup>4</sup>

The human eye is not able to see all of the energy in the thermal radiation spectrum; the range that the human eye can detect is referred to as the *visible spectrum* and ranges in wavelength from about  $0.4 \times 10^{-6}$  to  $0.7 \times 10^{-6}$  m.

The sun emits thermal radiation with wavelengths primarily in the range from  $0.3 \times 10^{-6}$  to  $3 \times 10^{-6}$  m. In general, about 47% of the radiation from the sun (at the surface of the Earth) falls in the visible spectrum, 46% falls in the infrared spectrum and about 8% in the ultra violet spectrum.<sup>5</sup>

The radiation emitted from a flare flame ranges from about  $0.3 \times 10^{-6}$  to  $30 \times 10^{-6}$  m. Although flare radiation covers a wide spectrum, the human eye cannot see about 99.9% of the radiation emitted because almost all of the energy falls in the infrared region but, one can definitely feel the radiation as heat. Only about 0.1% of the radiation emitted from a flare flame is in the visible spectrum; this small percent allows us to see the flame.

### 8.2.2 Flare Radiation Units

Figure 8.2 shows a flare burning propane at a rate of 60,000 lb/h corresponding to a total heat release (HR) of about  $1.2 \times 10^9$  Btu/h. Experimental data collected from this test reveal that approximately 25% of the total heat produced by this flame is radiated to its immediate surroundings; this is referred to as *flare radiation*.

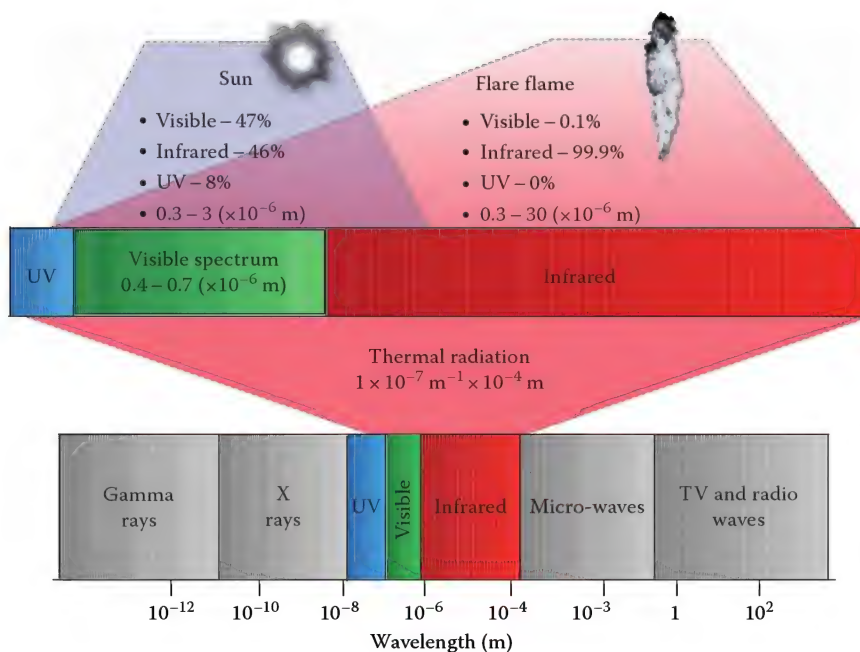


FIGURE 8.1  
Electromagnetic spectrum.



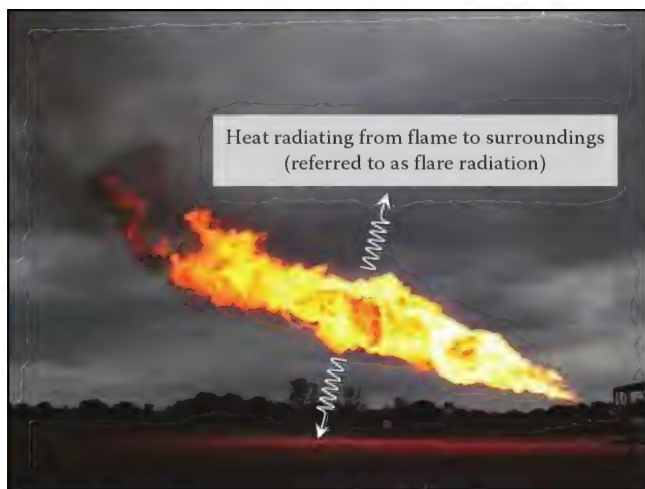


FIGURE 8.2

Flare firing propane at 60,000 lb/h (27,000 kg/h) corresponding to an HR rate equal to 1.2 billion Btu/h (350 MW).

The amount of flare radiation received at a given location (or point of interest) is referred to as the *flare radiation level*. The radiation level is defined as the amount of heat passing through a given area in a given amount of time. For example, suppose an observer stands at a distance from a flame and holds a  $1 \times 1$  ft ( $30 \times 30$  cm) square frame facing in the direction normal to the radiation incidence as illustrated in Figure 8.3. Assume the observer measures the amount of heat passing through the frame and finds that in a time period of 1 h 1000 Btu (1055 kJ) of energy passes through the frame. The observer has measured a radiation level of 1000 Btu/h-ft<sup>2</sup>. In the flare industry, radiation levels are commonly written in units of Btu/h-ft<sup>2</sup> or W/m<sup>2</sup>. The conversion from one Btu/h-ft<sup>2</sup> to W/m<sup>2</sup> is 3.154. For example, a radiation level of 1000 Btu/h-ft<sup>2</sup> corresponds to 3154 W/m<sup>2</sup>.

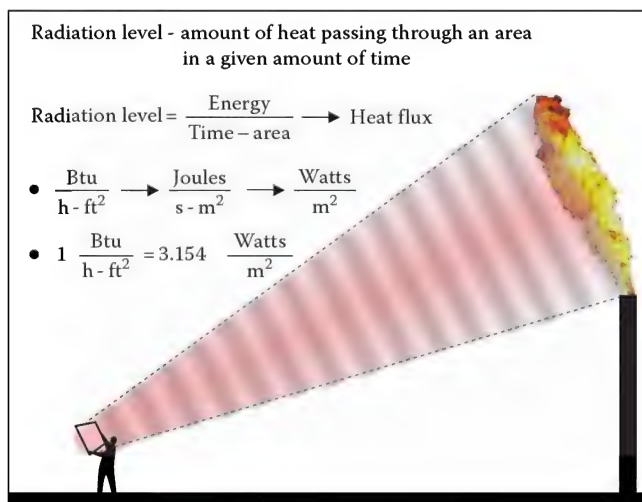


FIGURE 8.3

Illustration defining radiation level.

### 8.2.3 Solar Radiation Level

When personnel and equipment are exposed to flare radiation, it is likely that they are also being exposed to the radiation from the sun: referred to as solar radiation. Flare radiation and solar radiation levels can be cumulative. For example, suppose the flare radiation level at a point of interest is 500 Btu/h-ft<sup>2</sup> (1600 W/m<sup>2</sup>) on a cloudy day. On a clear day, however, when the sun is in full view, the radiation level could increase to over 800 Btu/h-ft<sup>2</sup> (2500 W/m<sup>2</sup>). Therefore, when estimating flare radiation, it is important that design engineers take into account the contribution from solar radiation because it can impact flare boom lengths and stack heights.

Solar radiation should also be taken into account when measuring flare radiation levels. If instrumentation is pointed directly into the sun during data collection, then solar radiation might have a significant contribution to the overall flare radiation level. The purpose of this section is to discuss the solar radiation levels.

The amount of thermal radiation received from the sun varies with the time of year and depends largely on the path length in the Earth's atmosphere that the sun's energy must traverse.<sup>6</sup> For example, Figure 8.4 shows radiation levels throughout the year, at high noon, on a clear day in Tulsa, Oklahoma. These levels are based on the solar radiation received at the Earth's surface at angles normal to the solar beam and horizontal to the surface of the Earth using a model developed by Bird.<sup>7</sup>

In Tulsa, the radiation level received on an object, positioned normal to the solar beam, varies from about 290–305 Btu/h-ft<sup>2</sup> (915–946 W/m<sup>2</sup>). Notice, in winter and fall (September through February), the normal radiation is lower than in spring and summer (March through August). This trend occurs because during the fall and winter months, the solar radiation passes through a greater thickness of the Earth's atmospheric air than in the spring and summer months; this can be better explained by referring to Figure 8.5.

Figure 8.5 shows the view of Tulsa, relative to the sun, during the months of January and July. Notice in July, Tulsa faces almost directly toward the sun, however, in January, Tulsa is at a much greater angle relative to the sun; this angle is referred to as the *angle of incidence*. During the summer months, Tulsa is positioned with an angle of incidence of approximately 15° while in the winter months the angle is approximately 75°. A larger angle of incidence requires the solar radiation to pass through a greater thickness of air resulting in more radiation transmission losses. It should be mentioned that the Earth's distance from the sun during its yearly elliptical orbit also affects the amount of radiation the Earth receives; this variation in distance

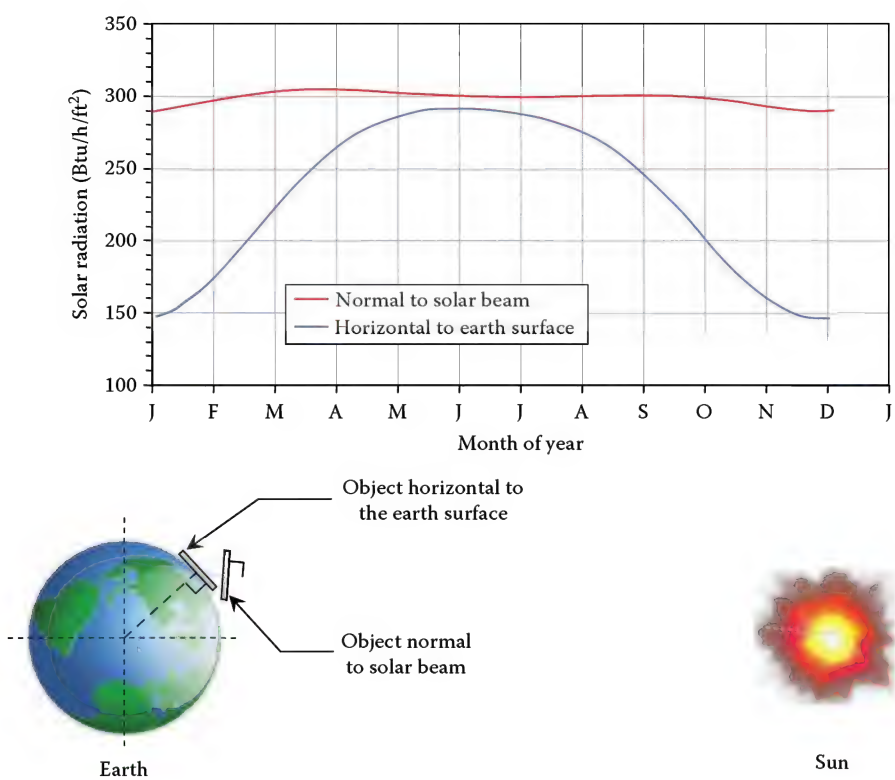


FIGURE 8.4 Solar radiation level at angles normal to the solar beam and horizontal to the surface of the Earth in Tulsa, Oklahoma.

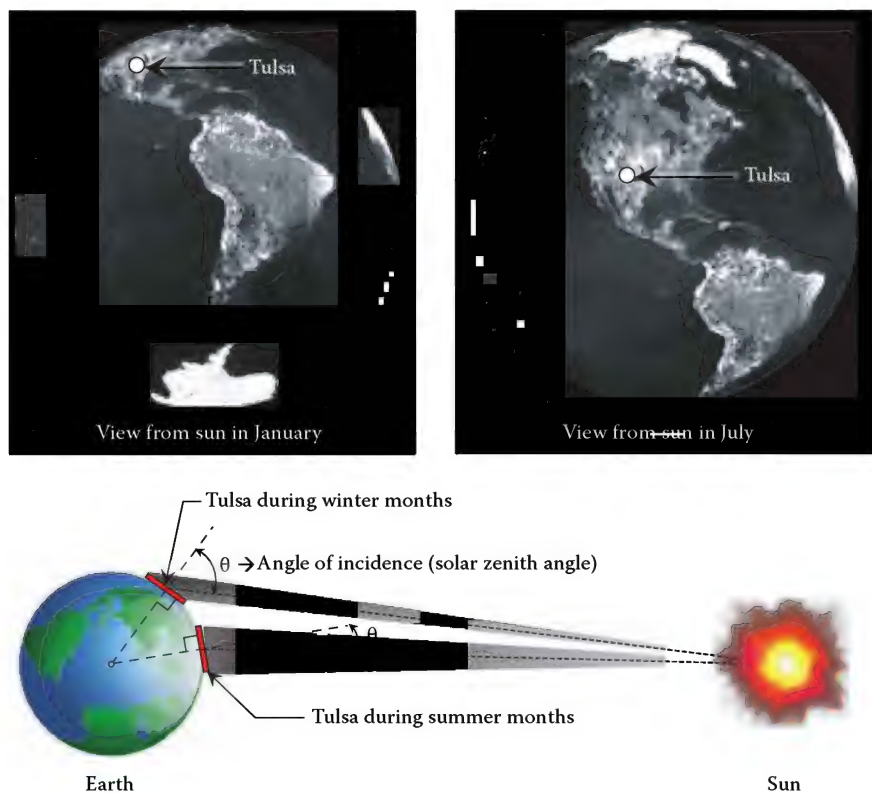


FIGURE 8.5 View of Tulsa from the sun during the months of January and July.



changes by about 3.4% resulting in a 6.9% change in the amount of solar energy reaching the Earth.<sup>8</sup>

Figure 8.4 also shows the radiation level in Tulsa for an object positioned horizontal to the Earth's surface. For this case, the radiation varies much more dramatically: from about 150 to 290 Btu/h-ft<sup>2</sup> (473–915 W/m<sup>2</sup>) throughout the year. Peak radiation levels occur during the summer months mainly because the view allows more solar radiation to strike an area positioned horizontal to the Earth. The amount of radiation that strikes an area positioned horizontal to the Earth can be described by the Lambert cosine law:

$$I(\theta) = I_{\theta=0} \cos \theta \quad (8.1)$$

where

$\theta$  is the angle of incidence

$I_{\theta=0}$  is the radiant flux with an angle of incidence of zero

$I(\theta)$  is the radiant flux at a given angle of incidence

#### 8.2.4 Radiation Level as a Function of Distance from Source

As previously discussed, the distance from the Earth to the sun can affect the amount of solar energy reaching the Earth. Similarly, the length of a flare boom or stack height can have a significant impact on the flare radiation level at a point of interest. To gain better insight into how much the thermal radiation level varies with the distance from a flame, consider an observer located near the base of a flare stack as illustrated in Figure 8.6. To simplify this analysis, assume that all of the heat

radiated from the flame is emitted from a single point located near the center of the flame; this point is referred to as the *flame epicenter*. Let us further assume that the heat emitted from the epicenter radiates outwardly in all directions and that the heat is evenly distributed over the surface of a sphere. For Case 1, the observer is located at a distance,  $r$ , from the epicenter while in Case 2 the observer is located at twice the distance,  $2r$ . The surface area ( $A$ ) of each sphere can be written as  $A_1 = 4\pi r^2$  and  $A_2 = 4\pi(2r)^2$  where subscript 1 and 2 represent Case 1 and Case 2, respectively. Taking the ratio of  $A_2$  to  $A_1$  results in  $A_2/A_1 = 4$ ; this result shows that doubling the distance from the flame epicenter yields a four-fold increase in surface area. Since the heat is evenly distributed over each sphere, one can conclude that the observer will experience a radiation level four times greater for Case 1 as compared to Case 2. Or in other words, doubling the distance from the radiation source reduces the radiation level by a factor of four.

Since the surface area of the sphere increases by a factor of  $r^2$ , then theoretically the radiation level should fall off by a factor of  $1/r^2$ , where  $r$  is the distance from the radiation source or epicenter. Figure 8.7 is a plot showing how the radiation level falls off relative to an observer located at a distance  $r$  from the flame epicenter. Again, notice that as the observer moves out to a distance  $2r$  from the epicenter, the radiation falls off by a factor of four. If the observer further increases her distance from the epicenter by  $4r$  notice that the radiation level falls off by a factor of 16. This example demonstrates that sizing the flare boom lengths and stack heights is critical because relatively small changes in distance can have a significant impact on the radiation levels at a point of interest.

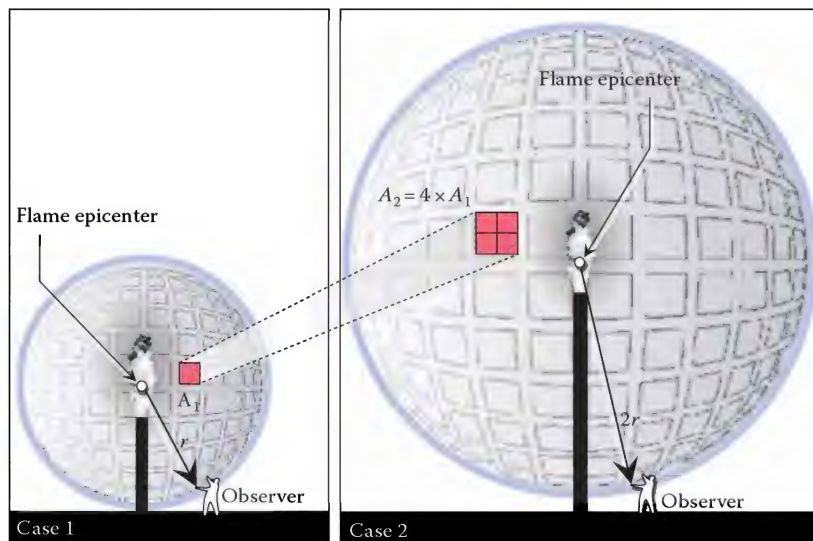


**FIGURE 8.6**  
Effects of doubling the distance of the flame epicenter from an observer.

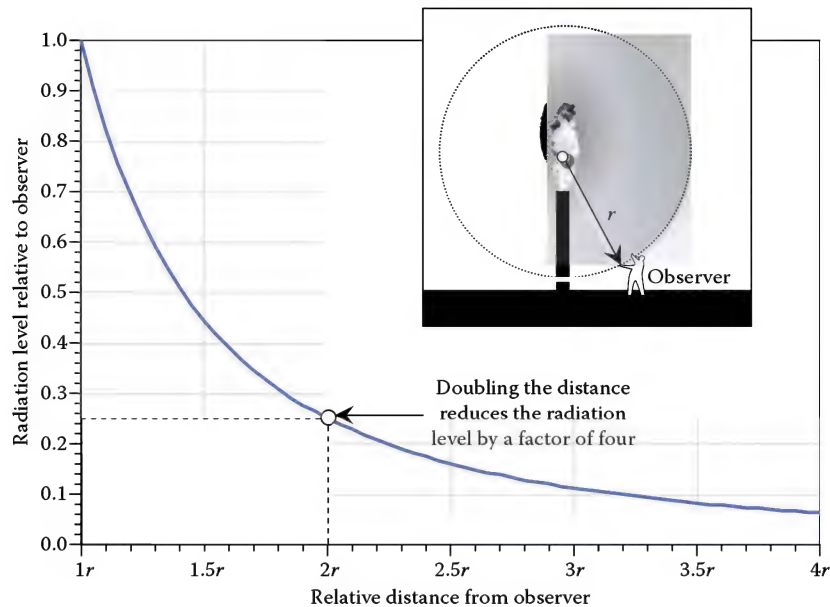


FIGURE 8.7

Relative radiation level as a function of distance from the source.

### 8.2.5 Flare Radiation Spectrum

When a flare burns a waste gas, the stable products of combustion typically consist of soot particles and a variety of gases such as carbon dioxide ( $\text{CO}_2$ ), water vapor ( $\text{H}_2\text{O}$ ), carbon monoxide ( $\text{CO}$ ), hydrogen ( $\text{H}_2$ ), oxygen ( $\text{O}_2$ ), nitrogen ( $\text{N}_2$ ), and nitric oxide ( $\text{NO}$ ). The principal contributors of thermal radiation come from two sources: (1) hot  $\text{CO}_2$  and  $\text{H}_2\text{O}$  vapor and (2) solid particles of soot.

Both  $\text{H}_2\text{O}$  and  $\text{CO}_2$  emit radiation in the infrared region and do not contribute to the visible

light emitted from the flame; this is referred to as *nonluminous radiation*.  $\text{H}_2\text{O}$  and  $\text{CO}_2$  emit radiation at distinct band wavelengths:  $\text{H}_2\text{O}$  at 2.7, 6.3, and  $20 \times 10^{-6}$  m and  $\text{CO}_2$  at 2.7, 4.3, and  $15 \times 10^{-6}$  m. Radiation levels emitted from nonluminous gases depend on the thickness of the gas (optical path) and temperature of the gas; the hotter the gas and thicker the optical path, the higher the radiation. Figure 8.8<sup>9</sup> shows the spectral emission of radiation from a nonluminous flame of a jet engine combustor. Notice that radiation falls

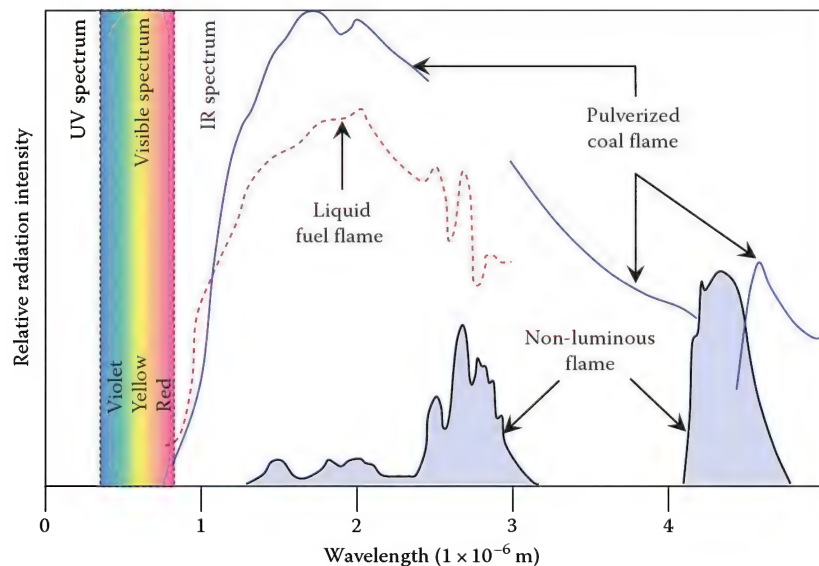


FIGURE 8.8

Spectral emission of radiation from luminous and nonluminous flames. (Adapted from Palmer, H.B. and Beer, J.M., *Combustion Technology, Some Modern Developments*, Academy Press, New York, 1974, p. 216.)

within the infrared spectrum at distinct band wavelengths. Figure 8.8 also shows the radiation spectrum emitted from flames containing soot particles (coal and liquid flame); these types of flames are referred to as *luminous flames*.

The presence of soot particles in a flame can dominate the thermal radiation. A flame containing a significant amount of soot can radiate three to four times as much radiation as a nonluminous flame.<sup>1,10</sup> The radiation emitted from soot particles is unlike gaseous radiation with distinct bands; instead, the radiation is continuous over a wide range of wavelengths. Notice in Figure 8.8 that the radiation from the luminous flame falls within the visible spectrum; this is what gives flames a yellow-orange color.

### 8.2.6 Radiation Transmission Losses through the Atmosphere

As radiation passes through the Earth's atmosphere, some of the radiation is attenuated. The amount of atmospheric attenuation depends largely on the composition of the air and the spectral characteristics of the radiation.

Atmospheric air consists of a mixture of several gases, water vapor, numerous pollutants, and small particles. Table 8.1 gives the approximate composition of dry air by volume fraction.<sup>11</sup> Some of the gases have concentrations that are constant while others are variable. Nitrogen, oxygen, and argon account for about 99.99% (by volume) of the permanent gases in the atmosphere. The concentration of carbon dioxide can be somewhat variable but,

TABLE 8.1

Approximate Composition of Dry Air

Constituent	Volume Fraction
Nitrogen	0.78084
Oxygen	0.20948
Argon	0.00934
Carbon dioxide	0.00031
Neon, helium, methane, sulfur dioxide, Hydrogen, and other minor gases	0.00003

Adapted from McQuiston, C. and Parker, J.D., *Heating, Ventilating, and Air Conditioning*, John Wiley & Sons, New York, 1982.

is typically around 0.03%. Water vapor in the atmosphere is also variable but typically varies between 0% and 4%.

Some wavelengths in the infrared, TV, and radio spectrum will pass through the air unabsorbed; the wavelengths that pass through the air unabsorbed are referred to as *atmospheric windows*. Figure 8.9 shows a generalized diagram of atmospheric radiation transmission through the air in the region of interest for flare radiation. Notice that the atmospheric windows occur at distinct wavelengths. Water vapor and carbon dioxide are largely responsible for the radiation absorption in these bands with water vapor dominant. Water vapor in the atmosphere absorbs thermal radiation at wavelengths similar to where water vapor in the products of combustion emits radiation.<sup>12</sup> For nonluminous flames, where radiation from hot H<sub>2</sub>O contributes a significant

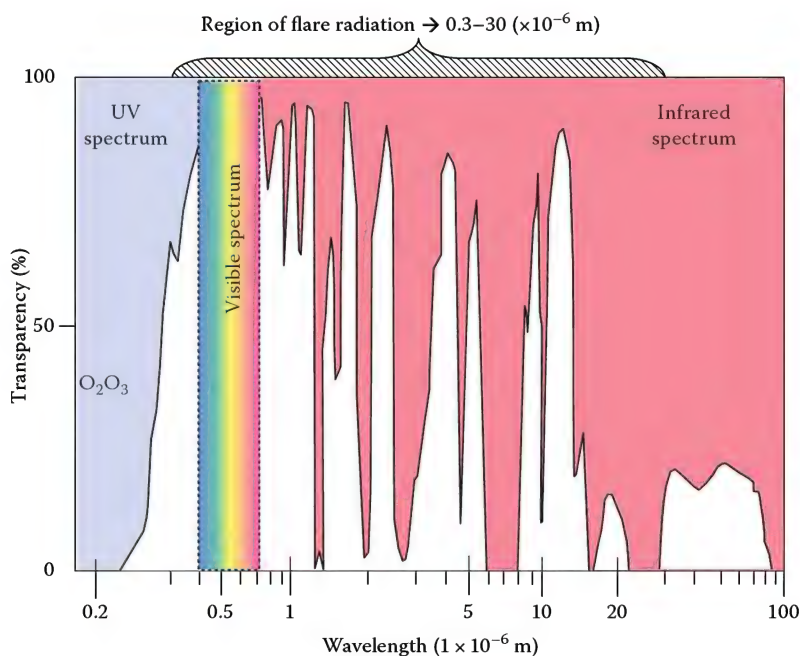


FIGURE 8.9

Generalized diagram showing relative atmospheric radiation transmission of different wavelengths. (Adapted from Brzustowski, T.A. and Sommer, E.C., Predicting radiant heating from flares, *Proceedings—Division of Refining*, API Washington, DC, pp. 865–893, 1973.)



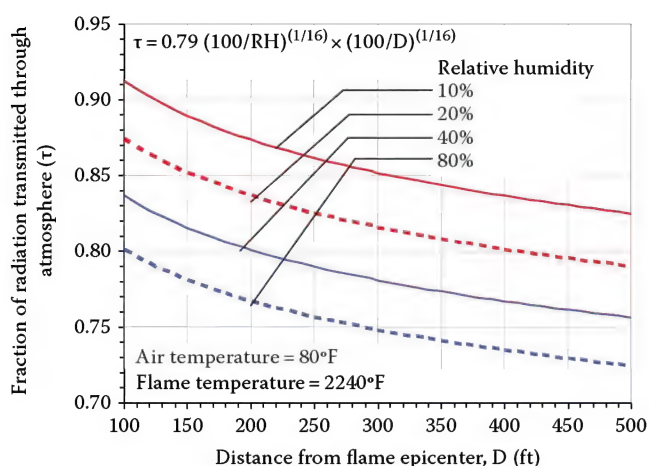


FIGURE 8.10

Estimates of the fraction of flame radiation transmitted through the atmosphere at various distances and percent relative humidity. (From Brzustowski, T.A. and Sommer, E.C., Predicting radiant heating from flares, *Proceedings—Division of Refining*, API Washington, DC, pp. 865–893, 1973.)

portion of the total emitted energy, absorption by water vapor in the atmosphere has a significantly greater attenuating effect than for a luminous flame.

The amount of atmospheric absorption depends largely on the relative humidity and distance from the point of interest to the flame as demonstrated in Figure 8.10.<sup>12</sup> Brzustowski et al. state that these curves are strictly applicable only under the following conditions: luminous hydrocarbon flame radiating at 2240°F (1227°C), 80°F (27°C) dry bulb ambient temperature, relative humidity greater than 10%, and distance from the flame between 100 and 500 ft (30 and 150 m); however, it can be used to estimate the order of magnitude of  $\tau$  under a wider range of conditions. Notice for these conditions, it is estimated that approximately 15%–25% of the radiation can be attenuated over a distance of 500 ft (150 m).

### 8.3 Environmental Concerns

Excessive thermal radiation from flares can cause equipment and structural damage, ignite flammable material, and pose a safety risk to personnel. The purpose of this section is to discuss the importance of exposure to high levels of flare radiation.

#### 8.3.1 Radiation Effects on Equipment

When equipment is exposed to radiant heating, the outer surface of the equipment heats; the heat can then be transferred to the internal components by convection, conduction, and radiation. If enough heat is transferred, it could melt plastic parts such as valve seals, wiring insulation

and gages. Many plastics will melt at a radiation level of about 12 kW/m<sup>2</sup> (3800 Btu/h-ft<sup>2</sup>) while electrical cable insulation will start to degrade at 18–20 kW/m<sup>2</sup> (5700–6300 Btu/h-ft<sup>2</sup>).<sup>13</sup> High heat can also dry out lubricated parts such as motors or valves. The amount of damage incurred can vary dramatically from equipment to equipment and depends largely on the design of the equipment, time period of exposure, and local ambient conditions.

Due to the multiple parameters involved in the heat transfer of equipment under radiant heating, it is difficult to recommend threshold levels. It is common practice to position equipment where it cannot be in direct view of the flare flame or provide adequate protection to shield it from the radiation.

#### 8.3.2 Ignition of Flammable Material from Radiant Heating

Flammable objects near a flare, such as wood objects and vegetation, can ignite if exposed to high levels of thermal radiation. For ignition to occur, the material must be heated to a temperature high enough to vaporize the solid fuel within the material. The vaporized gas must then mix with the surrounding air to form a flammable air-fuel mixture. If an ignition source, such as a small flame or a spark is present, the air-fuel mixture can ignite; this is referred to as *piloted ignition*. If the air-fuel mixture is ignited without the presence of a piloted source it is referred to as *auto-ignition* or *spontaneous ignition*. Piloted ignition requires a much lower temperature than auto-ignition.

The surface temperature of the material at which ignition occurs is referred to as the *ignition temperature*. Babrauskas<sup>14</sup> gives a good summary of the data reported in the literature regarding ignition temperatures of wood for piloted and auto-ignition under radiant heating. Results from numerous experimental studies show that wood will ignite over a wide range of temperatures under radiant heating. Babrauskas states that the large variation in ignition temperature is due to several reasons: definition of ignition, design of test apparatus, and operating conditions, specimen conditions (size, moisture, and orientation), and species of wood. Based on a summary of the data reported in the literature, Babrauskas concludes that 250°C (480°F) is the best estimate of the ignition temperature of wood regardless if it is piloted or auto-ignition; this value is a suitable limit for design or hazard analysis purposes.<sup>15</sup>

In 1965, McGuire<sup>17</sup> suggested that the minimum radiation level for piloted ignition of most wood material is 12.5 kW/m<sup>2</sup> (3960 Btu/h-ft<sup>2</sup>). At these radiation levels, the time required for ignition is about 10–20 min. These test results are based on radiant heat oriented along the grain of the wood (along-grain exposure). Spearpoint,<sup>18</sup> however, found that if the wood is exposed to radiation on the end-grain, piloted ignition occurs at lower



radiation levels. For end-grain exposure, Spearpoint found piloted ignition for maple occurs at  $8 \text{ kW/m}^2$  ( $2500 \text{ Btu/h-ft}^2$ ) in about 45 min; for along-grain exposure, maple will ignite at  $12 \text{ kW/m}^2$  ( $3800 \text{ Btu/h-ft}^2$ ) in about 70 min. The time required for piloted ignition of wood depends on several factors such as size and shape of the piece of wood, rate of heat loss from the surface, type of wood, orientation, and radiation level.

The auto-ignition of wood has not been studied as extensively as piloted ignition. Test results indicate that wood will auto-ignite at about  $4.3 \text{ kW/m}^2$  ( $1400 \text{ Btu/h-ft}^2$ ) if exposed for hours, rather than minutes. For short-term exposures, a radiation level of  $20 \text{ kW/m}^2$  ( $6300 \text{ Btu/h-ft}^2$ ) is typical for the auto-ignition of wood.<sup>14</sup>

Vegetation in the area of a flare should also be considered such as grass and trees. A radiation level of  $25 \text{ kW}$  ( $7900 \text{ Btu/h-ft}^2$ ) is capable of auto-ignition of trees if the exposure duration is long enough.<sup>18</sup> Dry grass, being much lighter in weight, reaches ignition temperature more quickly and can ignite within a few minutes.

### 8.3.3 Radiation Effects on Humans

In this section, we will discuss the effects of various levels of radiation on humans. As a bench-mark reference, keep in mind that the amount of radiation that reaches sea level at high noon on a clear day is about  $317 \text{ Btu/h-ft}^2$  ( $1000 \text{ W/m}^2$ ).

Living human skin absorbs heat radiated from a fire nearly as a blackbody.<sup>19</sup> When exposed to high levels of thermal radiation on the bare skin, one will first experience pain: a hot, tingling sensation felt when the skin temperature rises to just above  $111^\circ\text{F}$  ( $44^\circ\text{C}$ ) at a depth of over  $0.1 \text{ mm}$  ( $0.004 \text{ in.}$ ). If the temperature of the skin remains above  $111^\circ\text{F}$  ( $44^\circ\text{C}$ ) pain and injury will occur. The burn injury for human skin is categorized as first-, second-, and third-degree burns.

If one is exposed to a radiation level of  $1600 \text{ Btu/h-ft}^2$  ( $5 \text{ kW/m}^2$ ) on the bare skin (about five times the level from the sun), a first-degree burn will occur in approximately 20 s. The injury will result in damage to the outer layer of skin; this type of burn is extremely painful, leaving the skin reddened that will heal in 2–5 days.

Second-degree injuries burn through the first layer of the skin and damage the second layer of skin. This degree of injury results in intense pain with reddening and blistering of the skin. If treated properly, second-degree burns will heal themselves with very little scarring. This degree of injury is considered minor if it involves less than 15% of the body surface area in adults. If the skin is exposed to  $1600 \text{ Btu/h-ft}^2$  ( $5 \text{ kW/m}^2$ ) for more than 50 s a third-degree burn will occur. These types of burns may require skin grafting and leave deep scars.

In 1959, Stoll and Green<sup>17</sup> conducted an experiment using human subjects to determine the effects of thermal

radiation on the skin. A  $1000 \text{ W}$  ( $3400 \text{ Btu/h}$ ) projection lamp was used to expose a known amount of radiation on an area of the forearm. From the data, they were able to establish the time to reach the *threshold of pain* and the *threshold of blistering* (second-degree burn) for various levels of radiation. The threshold of pain is defined as when a person first starts to feel pain when exposed to a particular level of radiation. The threshold of blistering is defined as blistering of the skin occurring within a 24 h period after being exposed to a particular level of radiation.

The data from Stoll and Green show that one can tolerate  $1000 \text{ Btu/h-ft}^2$  ( $3.2 \text{ kW/m}^2$ ) (about three times the radiation from the sun) directly on the bare skin for about 40 s before experiencing pain. At a radiation level of  $1500 \text{ Btu/h-ft}^2$  ( $4.7 \text{ kW/m}^2$ ) one would feel pain in about 20 s. At  $3000 \text{ Btu/h-ft}^2$  ( $9.4 \text{ kW/m}^2$ ), pain would occur within about 6 s and above  $6000 \text{ Btu/h-ft}^2$  ( $18.8 \text{ kW/m}^2$ ) one would feel pain almost immediately. The data show that once pain is felt, blistering will occur fairly quickly if the skin remains exposed to the radiation.

### 8.3.4 API 521 Recommendations

The American Petroleum Institute 521 (API 521) provides design radiation levels for personnel working in the vicinity of a flare; these recommendations are listed in Table 8.2 and separated into four radiation levels: 500, 1500, 2000, and  $3000 \text{ Btu/h-ft}^2$  ( $1.6, 4.7, 6.3,$  and  $9.4 \text{ kW/m}^2$ ).<sup>20</sup>

The API 521 recommends a maximum radiation level of  $500 \text{ Btu/h-ft}^2$  ( $1.6 \text{ kW/m}^2$ ) at any location where personnel, with *appropriate clothing*, can be continuously exposed. Appropriate clothing consists of a hard hat, long-sleeved shirt with cuffs buttoned, work gloves, long-legged pants, and work shoes. The API 521 states, however, that three major factors can impact this permissible level: (1) ambient conditions, (2) flare design, and (3) personnel training. Ambient conditions such as wind speed, temperature, and relative humidity can have a significant impact on personnel working in a  $500 \text{ Btu/h-ft}^2$  ( $1.6 \text{ kW/m}^2$ ) environment. Increasing the ambient temperature and relative humidity increases the heat index and stress on workers. For example, a  $500 \text{ Btu/h-ft}^2$  ( $1.6 \text{ kW/m}^2$ ) environment might feel comfortable to someone working in Canada on a cold winter day. However, a  $500 \text{ Btu/h-ft}^2$  ( $1.6 \text{ kW/m}^2$ ) environment might be stressful to someone working in Houston on a hot, humid day during the summer. If a worker is exposed to an additional heat load from a flare flame, his heat stress tolerance will be reduced. In such a case, appropriate adjustments should be made to the design radiant heat intensity.

The design of the flare system also impacts personnel working in a  $500 \text{ Btu/h-ft}^2$  environment. If personnel are able to temporarily shield themselves from the flare radiation by positioning themselves under catwalks, scaffolding, or behind the flare stack, they should be able

TABLE 8.2

American Petroleum Institute 521 Recommendations for Radiation Exposure to Personnel

Permissible Design Level (Btu/h-ft <sup>2</sup> )	Conditions
3000	Maximum radiant heat intensity at any location where urgent emergency action by personnel is required. When personnel enter or work in an area with the potential for radiant heat intensity greater than 2000 Btu/h-ft <sup>2</sup> , radiation shielding and/or special protective apparel (e.g., a fire approach suit) should be considered <i>Safety precaution</i> —It is important to recognize that personnel with appropriate clothing <sup>a</sup> cannot tolerate thermal radiation at 2000 Btu/h-ft <sup>2</sup> more than a few seconds
2000	Maximum radiant heat intensity in areas where emergency actions lasting up to 30 s can be required by personnel without shielding but with appropriate clothing <sup>a</sup>
1500	Maximum radiant heat intensity in areas where emergency actions lasting 2–3 minutes can be required by personnel without shielding but with appropriate clothing <sup>a</sup>
500	Maximum radiant heat intensity at any location where personnel with appropriate clothing <sup>a</sup> can be continuously exposed

<sup>a</sup> Appropriate clothing consists of hard hat, long-sleeved shirt with cuffs buttoned, work gloves, long-legged pants, and work shoes. Appropriate clothing minimizes direct skin exposure to thermal radiation.

to more effectively tolerate the environment. Finally, training can impact the amount of time personnel can work in a 500 Btu/h-ft<sup>2</sup> (1.6 kW/m<sup>2</sup>) environment. If personnel are trained to wear appropriate clothing to minimize direct radiation and can work upwind of the flare to minimize flare radiation levels, they should be more tolerant to the environment.

If appropriately clothed, the API 521 recommends that personnel not be exposed to a radiation level greater than 1500 Btu/h-ft<sup>2</sup> (4.7 kW/m<sup>2</sup>) for more than two to three minutes. As discussed previously, one would feel pain after about 20 s if the skin is exposed to 1500 Btu/h-ft<sup>2</sup> (4.7 kW/m<sup>2</sup>); in about 40–50 s a second-degree burn would result. It is common for flare manufacturers to design flare stack heights so that the maximum radiation level at grade does not exceed 1500 Btu/h-ft<sup>2</sup> (4.7 kW/m<sup>2</sup>) during emergency flaring; this allows personnel time to evacuate the area.

The API 521 recommends that personnel not be exposed to a radiation level greater than 2000 Btu/h-ft<sup>2</sup> (6.3 kW/m<sup>2</sup>) for more than 30 s if appropriately clothed. If radiation levels exceed 2000 Btu/h-ft<sup>2</sup> (6.3 kW/m<sup>2</sup>) a fire protection suit must be worn. A fire protection suit consists of a silver, non flammable material containing an air supply bottle. The silver suit helps reflect some of the radiation while the air supply prevents personnel from breathing in the hot ambient air. The suit also consists of a hood designed with a mirrored window that helps reflect some of the incoming radiation but, allows personnel to see through.

Several other important recommendations API 521 makes include restricted access area to personnel, use of

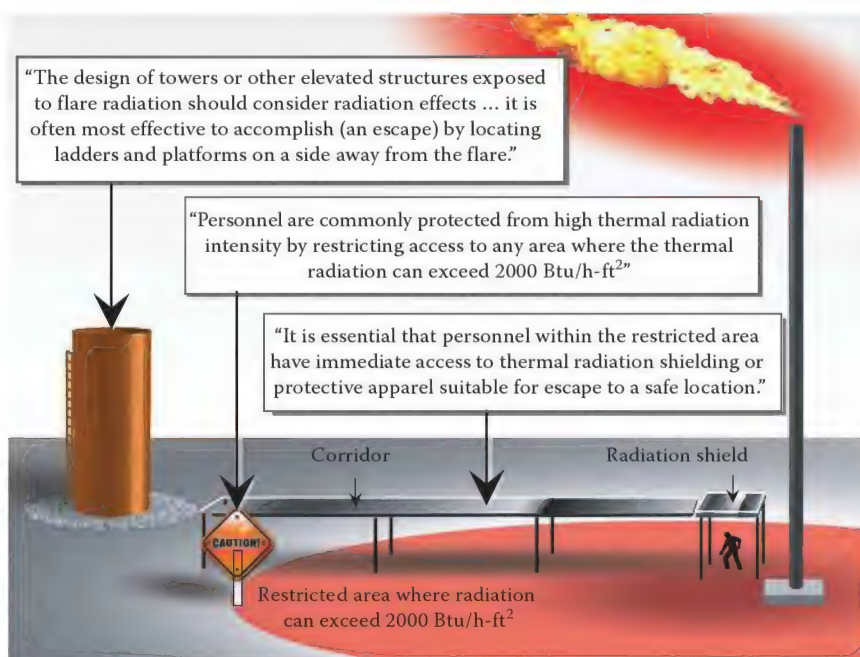


FIGURE 8.11

API 521 recommendations.

radiation shielding, and location of ladders and platforms; these recommendations are summarized with an illustration in Figure 8.11. The API 521 states that personnel are commonly protected from high thermal radiation intensity by restricting access to any area where the thermal radiation can exceed 2000 Btu/h-ft<sup>2</sup> (6.3 kW/m<sup>2</sup>). Some plants locate fences and warning signs around areas where flare radiation levels can exceed 2000 Btu/h-ft<sup>2</sup> (6.3 kW/m<sup>2</sup>).

The API 521 also states that it is essential that personnel within the restricted area have immediate access to thermal radiation shielding or protective apparel suitable for escape to a safe location. Radiation shields are structures sometimes located near the base of the flare stack designed with a galvanized or reflective steel roof. Some plants design a roofed corridor that leads from the base of the stack to a safe location away from high radiation levels.

The API 521 also recommends locating ladders and platforms on towers and elevated structures on a side away from the flare. Designing in this manner provides personnel a shield from the radiant heat allowing them more time to evacuate the area.

## 8.4 Estimating Flare Radiation

Manufacturers of flares usually provide estimates of flare radiation based on proprietary models. These models are commonly semi-empirical in nature in that they use a combination of theory and experimental data. The purpose of this section is to discuss, in general, why and how semi-empirical modeling is used to estimate flare radiation and why accurate experimental data are crucial for these models.

Every point within a flame radiates heat, however not every point radiates the same amount of heat. As previously discussed, radiant energy is emitted by the gases and solids present in the flame. The amount of heat radiated from a point within the flame depends largely on the concentration and temperature of H<sub>2</sub>O, CO<sub>2</sub>, and soot at that point. Predicting the concentration of gases and solids within the flame, using a theoretical approach, is nontrivial and challenging even with today's computer power; therefore, it is not a practical method for determining flare radiation for day-to-day engineering design work. As a result, those involved in flare design applications commonly rely on a more practical approach: semi-empirical modeling.

In general, there are three fundamental approaches for semi-empirically modeling flare radiation. The simplest approach is to assume that all of the heat emitted from the flame is concentrated at a single point within the flame (epicenter). All of the heat emitted from the epicenter radiates outward and evenly distributes its energy over the entire surface of a sphere; this type

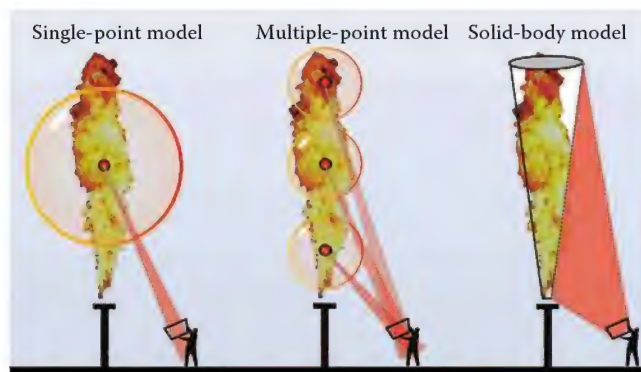


FIGURE 8.12

Various models commonly used in industry to estimate flare radiation.

of model is referred to as the *single-point model* and is illustrated in Figure 8.12. Another method commonly used is the *multi-point model*. This model separates the flame into several segments of equal or varying length and assumes that the heat radiates from the epicenter of each segment and is evenly distributed over the surface of each sphere as illustrated in Figure 8.12; this illustration represents a three-point model. The *solid-body model* assumes that the flame is a solid-body, typically shaped like a cone, cylinder, or frustum, and that every point on the surface of the solid-body radiates heat.

The advantage of the single-point model is that it is the simplest, mathematically, of the three models. The disadvantage, however, is that when the point of interest is located near the flame, the flame cannot be treated as a single-point source. That is, the distance from the point of interest to various locations within the flame differs significantly. On the other hand, when the point of interest is at a significant distance from the flame, the flame can be treated as a single-point source because the distance from the point of interest to every point on the flame is approximately the same. As a rule of thumb, the single-point model is typically valid for distance of at least three flame lengths away from the epicenter. Flare manufacturers commonly use the multi-point or solid-body model to improve the accuracy at points of interest in close proximity to the flame. To gain better insight into how these models are used, a hypothetical example demonstrating the single-point model is presented in the following.

### Example 8.1

Suppose a flare is firing propane at a rate of 50,000 lb/h (23,000 kg/h) and that an observer is located at a distance of 150 ft away (46 m) from the flame epicenter as illustrated in Figure 8.13. What is the maximum theoretical radiation level at the point of interest?

First, calculate the total amount of heat released (or firing rate) from the flame. The total HR is



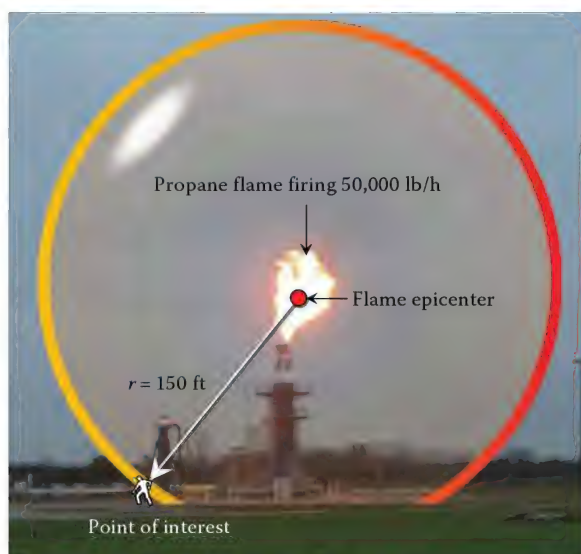


FIGURE 8.13  
Illustration for example calculation.

calculated by multiplying the fuel flow rate,  $\dot{m}$ , by the lower heating value (LHV) of fuel. Knowing the LHV of propane is 21,500 Btu/lb<sub>m</sub>, the HR can be determined:

$$\begin{aligned} HR &= \dot{m} \times LHV = 50,000 \frac{\text{lb}_m}{\text{h}} \times 21,500 \frac{\text{Btu}}{\text{lb}_m} \\ &= 1,075 \times 10^6 \frac{\text{Btu}}{\text{h}} \end{aligned}$$

Next, calculate the surface area ( $A_s$ ) of the sphere with a radius ( $r$ ) equal to 150 ft:

$$A_s = 4 \times \pi \times r^2 = 282,743 \text{ ft}^2$$

Assuming all of the heat is evenly distributed over the surface area of the sphere, the maximum theoretical radiation level ( $I$ ), at a distance of 150 ft from the flame epicenter, can be determined by dividing the total HR by the surface area of the sphere:

$$I = \frac{HR}{A_s} = \frac{1,075 \frac{\text{Btu}}{\text{h}}}{282,743 \text{ ft}^2} = 3,802 \frac{\text{Btu}}{\text{h-ft}^2}$$

The actual or measured radiation level would be significantly lower than the maximum theoretical value just calculated because not all of the heat from the flame is transferred to its immediate surroundings by thermal radiation. The fraction of total heat radiated from the flame is referred to as the *radiant fraction*,  $F$ , and is written mathematically as follows:

$$F = \frac{\text{Actual measured radiation level}}{\text{Maximum theoretical radiation level}}$$

Suppose the actual measured radiation level for this example is 1000 Btu/h-ft<sup>2</sup> (3.2 kW/m<sup>2</sup>) at a distance of 150 ft (46 m) from the epicenter; this would correspond to a radiant fraction of 0.26 (1000/3802). That is, 26% of the total heat released from this flame is transferred to the surroundings by thermal radiation. It should be mentioned that in this example the transmission loss of the radiation through the air was ignored. Recall that as a rule of thumb, 15%–25% of the radiation is absorbed by the atmosphere over a distance of 500 ft (150 m).

The general equation commonly found in the literature for calculating flare radiation levels,  $I$ , is written as follows:

$$I = \frac{HR \times F \times \tau}{4 \times \pi \times r^2} \quad (8.2)$$

The term,  $\tau$ , is referred to as the transmissivity, and is the fraction of radiation loss through the atmosphere. (Usually, the transmissivity is ignored and set equal to a value of one.) The flare radiant fraction,  $F$ , typically varies from a value of about 0.1–0.4 and is determined from experimental data. The radiant fraction is an overall characteristic of a flame that can be influenced by several variables; three key variables include (1) flare gas composition, (2) mixing, and (3) smoke formation.

The composition of the gas being flared can have a tremendous impact on the fraction of total heat radiated from a flame. As mentioned earlier, the presence of soot in a flame usually dominates the radiation emitted over CO<sub>2</sub> and H<sub>2</sub>O. Therefore, hydrocarbon fuels that have a higher carbon-to-hydrogen mass ratio will typically have a higher radiant fraction under similar firing conditions. For example, the carbon-to-hydrogen mass ratio of propane (C<sub>3</sub>H<sub>8</sub>) and methane (CH<sub>4</sub>) is 4.5 and 3, respectively. Since propane has more carbon available to form soot, one would expect it to have a higher radiant fraction than methane under similar firing conditions.

The amount of air mixed with the flare gas prior to combustion can also impact flame radiant fractions. If a hydrocarbon is not mixed with an appropriate amount of air prior to combustion, it will have a tendency to create soot within the flame envelope resulting in higher radiant fractions. Propane, for example, chemically “cracks” at about 500°F (260°C) forming acetylene. At about 750°F (400°C) acetylene combines with radicals to form benzene. Finally, at about 1650°F (900°C) benzene agglomerates to form soot particles that are roughly 0.1–10 μm in diameter. This type of reaction is referred to as pyrolysis, a chemical reaction that does not involve oxygen. To reduce the tendency of soot formation, or pyrolysis, an appropriate amount of ambient air must be mixed with the flare gas. Flare manufacturers use various flare designs to assist mixing. One type is a steam-assisted flare.





**FIGURE 8.14**  
Steam-assisted flare (a) without steam and (b) with steam.

Steam assist-flares use high pressure steam to entrain surrounding air and inject it into the core of the flare gas stream. The rapid mixing of the steam and air with the flare gas helps reduce soot formation which tends to lower the flame radiant fraction. Figure 8.14 shows a steam-assisted flare operating under identical flare gas flow conditions with and without steam-assist. Notice without steam-assist, the flame is more luminous and contains more soot; this results in higher radiant fractions. The fraction of heat radiated from a flame can also

be greatly increased by the presence of liquid droplets in the gas. Droplets within a hot flame can easily be converted to soot.<sup>21</sup>

The amount of smoke formation can significantly impact flare radiant fractions. If soot does not burn completely within the flame envelope, it will cool, creating black smoke leaving the flame as demonstrated in Figure 8.15. The carbon particles, or smoke, are an excellent absorber of radiation and can act as a shield to block thermal radiation. Notice in the photograph that a majority of the upper part of the flame is shrouded or blocked by the smoke. This can have a dramatic impact on the amount of heat radiated from the flame to its immediate surroundings.



**FIGURE 8.15**  
Smoking flare.

## 8.5 Measuring Flare Radiation

As previously discussed, the models used in the flare industry for estimating flare radiation rely heavily on flare radiation data from full-scale test equipment. In this section, the instrumentation commonly used in the flare industry to measure radiation levels will be discussed.

### 8.5.1 Description of the Radiometer

Flare radiation is commonly measured using an instrument called a *radiometer*. There are several brands of radiometers available on the market; Figure 8.16 shows a couple of handheld thermopile-type radiometers. Radiometers are meters used to detect and measure radiant electromagnetic energy. There are many types



**FIGURE 8.16**  
A couple brands of handheld radiometers.

of radiometers based on their physics of detection and the intended applications. Due to the spectral range of thermal radiation from flares, it is common to use thermopile-type radiometers to measure flare radiation. A thermopile is a kind of thermometer for measuring heat radiation, consisting of multiple thermocouple junctions in series. A thermocouple is a junction between two different metals that produces a voltage related to a temperature difference relative to a reference temperature.

Flare radiometers typically consist of three main components: (1) sensor surface, (2) thermopile, and (3) heat sink as illustrated in Figure 8.17.<sup>22</sup> The incoming radiation is absorbed on the sensor surface which typically consists of a dark material designed to absorb most of the flare radiation that it receives. The absorbing material is typically very thin, without a lot of thermal mass, so that it will reach temperatures quickly resulting in a fast response time. The heat absorbed on the sensor surface is then transferred through thermopiles located just beneath the absorbing material.

Thermopiles consist of very small thermocouples joined together in series. The heat flows through the thermopiles and into a heat sink located just below.

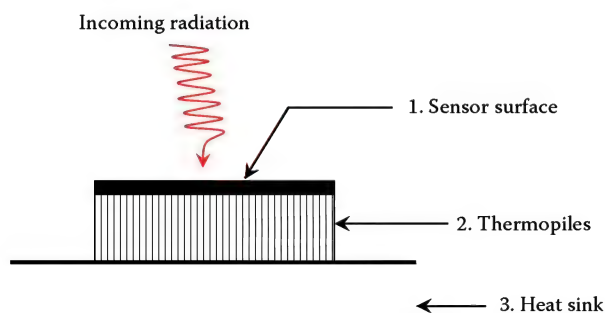


**FIGURE 8.17**  
The major components that make up a flare radiometer.

The difference in temperature between the sensor surface and heat sink is a function of the heat being transferred and a function of the net absorbed heat flux.<sup>22</sup> The thermopile converts this flow of heat to an electrical signal which is then converted into a radiation level. Radiometers of this type do not require a power supply since the electrical output signal is generated by heat transfer.

Some radiometers are designed to give a direct display of the radiation level in units of Btu/h/ft<sup>2</sup> or W/m<sup>2</sup>. Some require one to measure the electrical output signal and convert the reading to a radiation level. The output signal is usually in units of millivolts (mV) and can be measured using a handheld voltmeter. Manufacturers of radiometers usually supply the customer with a certificate of calibration which usually consists of a plot showing the response of the output signal at various levels of incident radiation.

A Certificate of Calibration for one particular radiometer is shown in Figure 8.18. For this radiometer, the output signal response is linear with the incident radiation level. This particular radiometer has a constant of 293.6 Btu/h-ft<sup>2</sup> (925.6 W/m<sup>2</sup>) per mV. So, for example, suppose one aims this radiometer at a flame and the voltmeter reads 743 mV. Taking that number and multiplying it by the constant yields the radiation level  $293.6 \times 743 = 2181$  Btu/h-ft<sup>2</sup> (6.877 kW/m<sup>2</sup>).

Radiometers are sometimes equipped with optical covers to limit convection by wind effects which can interfere with radiation measurements. When flare radiometers are designed with optical covers, the manufacturer will usually provide two calibration constants; one with the cover material on, and one with the cover material off. The calibration constant with the cover material on should be used. However, for more advanced users that wish to change the cover material, the calibration with the cover material off is often useful.

### 8.5.2 Useful Tips When Measuring Flare Radiation

Radiation data gathered from full-scale testing are critical information used to design a flare; therefore, accurate measurements are important. Several tips to help eliminate potential error and improve the accuracy of radiation measurements include the following: (1) select the right radiometer, (2) avoid convective cooling effects, (3) measure without sun interference, (4) position the radiometer so that it views the entire flame, and (5) vary the angle of the radiometer to find the maximum radiation level.

#### 8.5.2.1 Radiometer Selection

The reader should be aware that there are several types of radiometers available in the marketplace.



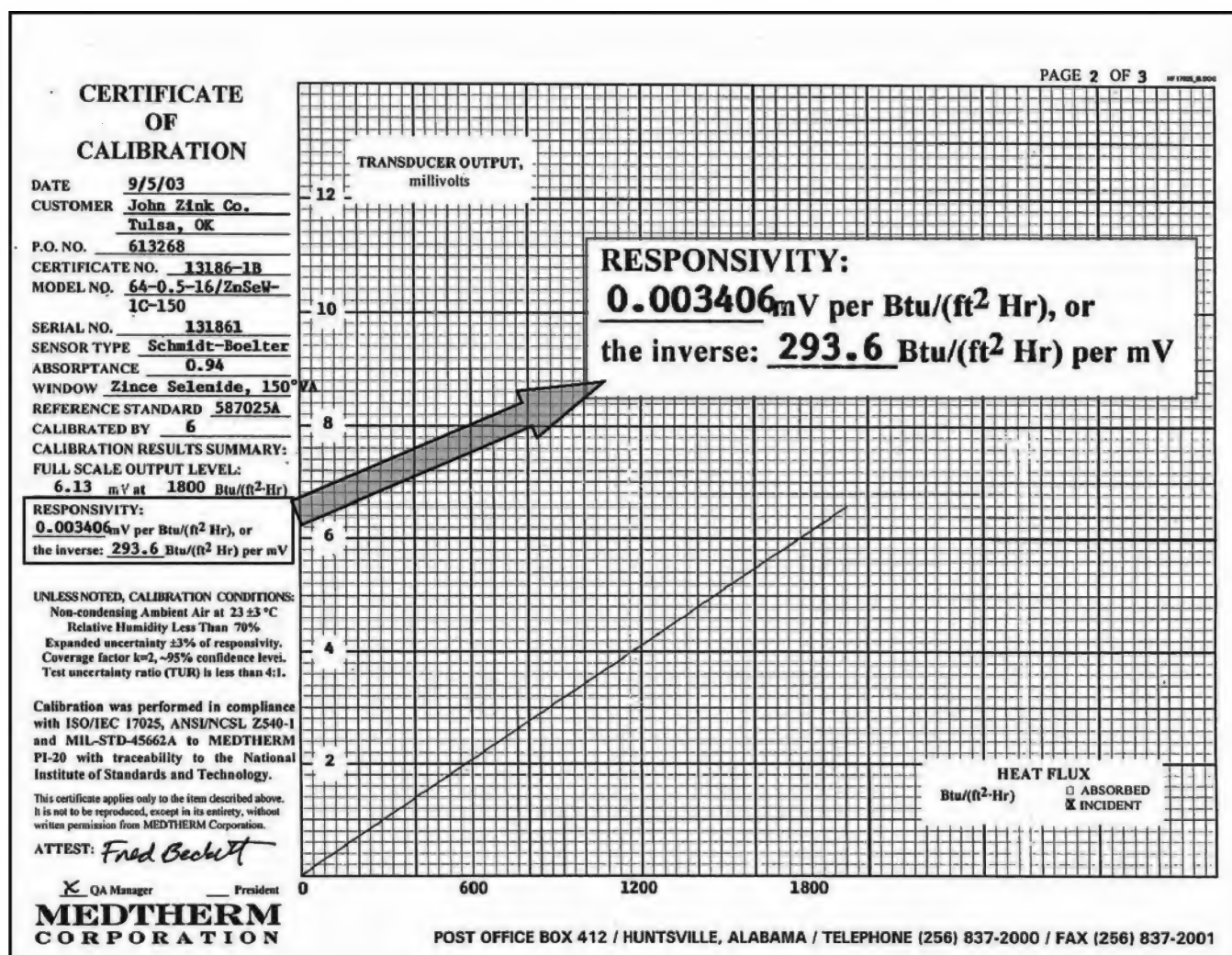


FIGURE 8.18

A radiometer certificate of calibration.

Many of these radiometers are designed to measure solar radiation and, therefore, are not capable of measuring the radiation in the far infrared region where most flare radiation is found; recall that approximately 99.9% of the radiation emitted resides in the infrared spectrum. If radiometers specifically designed for solar radiation are used to measure flare radiation, a majority of the radiation in the infrared spectrum will not be captured; this will result in a measured value that will be significantly lower than the actual radiation level. It is, therefore, important to use a radiometer that will capture radiation over a broad infrared spectrum when measuring flare radiation; a radiometer that will measure in the wavelength range from about  $0.3 \times 10^{-6}$  to  $30 \times 10^{-6}$  m is usually adequate. It is important to select the correct type of radiometer to ensure the sensor can respond to the range of radiation wavelengths of interest, and to select the correct type of optical cover.

#### 8.5.2.2 Sun Interference

It is preferred to measure flare radiation with the sun at your back where it will not contribute to the measurement. This is especially important on partly cloudy days because clouds could alter the sun's contribution during a test. It should also be noted that sky conditions that create a bright glare can interfere with radiometers.

#### 8.5.2.3 View Angle

The radiometer should be positioned so that the sensor surface views the entire flame. Some radiometers have a narrower view angle depending on how far back the absorbing material is set back into the cavity. If it is set deeply into a cavity, the view angle might be fairly narrow. Caution should be exercised to ensure the entire flare flame can be covered in the view angle of the

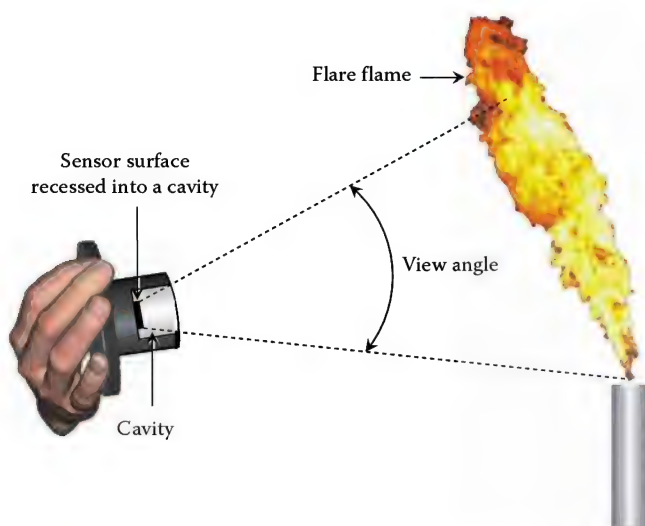


**FIGURE 8.19**  
Illustration showing a radiometer not viewing the entire flare flame.

radiometer. Figure 8.19 illustrates an example of a radiometer not viewing the entire flare flame.

#### 8.5.2.4 Convective Cooling Effects

Wind blowing over a radiometer sensor surface during a measurement could result in an erroneous reading. As wind blows past the radiometer sensor surface, it can cool the sensor surface, resulting in a radiation level reading lower than the actual level. To eliminate the convective cooling effects, radiometer manufacturers commonly use one of the two methods: (1) position the sensor surface into a recessed cavity or (2) cover it with a special window as shown in Figure 8.20.

The effectiveness of the cavity method is not well understood at different wind speeds and directions. It is possible that even at quiescent ambient conditions; natural convective cooling can occur and result in lower-than-actual radiation readings. The second method is to use a special optical material placed over the surface of the absorbing material. The cover material is typically in close proximity, but not in direct contact with the sensor surface. The cavity formed between the cover and the sensor surface is sometimes filled with an inert gas to prevent oxidation of the sensor surface. This cover material blocks the wind from cooling the absorbing material on the sensor surface. It is important to use the proper cover material. For example, typical glass that one would find in a window would not work. Although it is transparent to the human eye, a large portion of the infrared radiation emitted from the flare flame will not pass through it resulting in a low radiation reading. One might argue that some sort of lab calibration may correct the problem. However, the percentage of flare radiation that can penetrate the cover material may vary

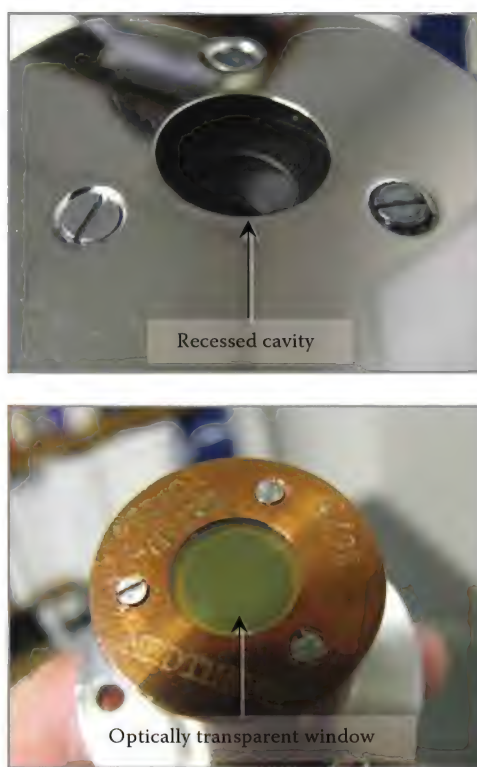


**FIGURE 8.20**  
Radiometers with different types of windows.

significantly depending on the spectral distribution of the flare flame; this is affected by various factors such as how sooty the flame is, the temperature and concentration fields of the flame, etc.

Several materials can be used to shield a radiometer from the wind; a common material used for flare radiometers is zinc selenide. Zinc selenide is a light-yellow, man-made material rarely found in nature and is highly transparent to the radiation emitted from a flare flame. Figure 8.21 shows the transmissivity curve as a function of wavelength for zinc selenide. The transmissivity of zinc selenide is relatively constant over the wavelength range between  $0.7 \times 10^{-6}$  to  $16 \times 10^{-6}$  m, making it an excellent choice for flare radiation measurement.

Figure 8.22 shows the transmissivity curve as a function of wavelength for sapphire. The transmissivity varies with the wavelength between  $0.7 \times 10^{-6}$  and  $4.0 \times 10^{-6}$  m, and more importantly, drops off rapidly at wavelength above  $4.0 \times 10^{-6}$  m. A significant fraction of flare radiation will be clipped and not measured by the sensor if a sapphire cover is used to measure flare radiation.

Flare radiometers are often designed with flat optical covers. One shortcoming of a flat optical cover is that the amount of reflected radiation increases dramatically when the angle of incidence is high (Snell's law).<sup>23</sup> For example, Figure 8.23 shows the fraction of reflected radiation of zinc selenide at a wavelength of  $1 \times 10^{-6}$  m (refractive index of 2.49). It can be seen that the reflectivity



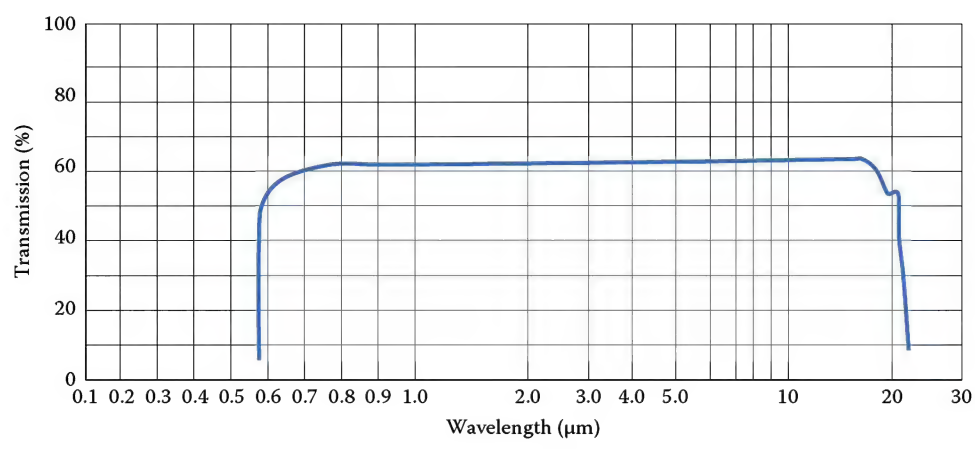


**FIGURE 8.21**  
Transmissivity curve of zinc selenide.

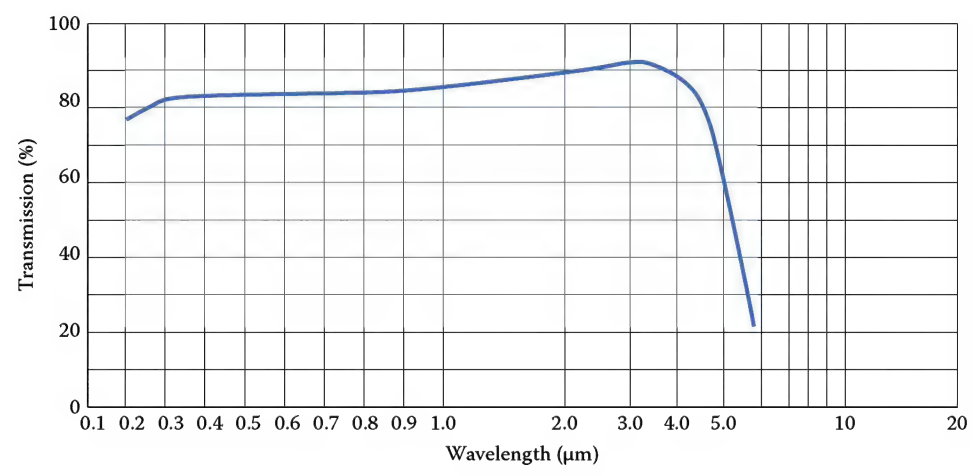


**FIGURE 8.22**  
Transmissivity curve of sapphire.

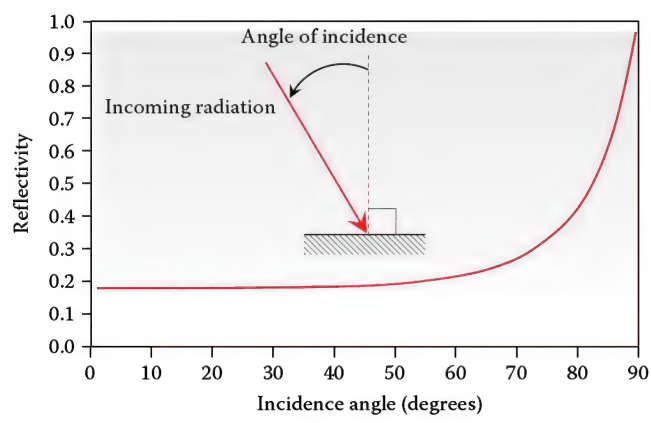


**FIGURE 8.23**  
Reflected radiation at a wavelength of  $1 \times 10^{-6}$  m for zinc selenide.

remains virtually constant when the incidence angle is between  $0^\circ$  and  $60^\circ$ , but starts to deviate at greater angles. Besides the view angle limit set by physical blockage of the radiometer, reflectivity is another important factor affecting the view angle of a radiometer. Dome-shaped

optical covers can help reduce reflection; however, constructing a dome-shape cover out of high performance optical material is not cost effective and is therefore typically not used for flare radiometers.

**8.5.2.5 Measuring Technique**

Flare gas flow rate and composition, wind speed and direction, the location of the flare flame's epicenter can vary during a flare test. Due to the Lambert cosine law, the maximum radiation reading will be measured when the radiometer is aimed directly at the flare epicenter. It is often difficult to predict the location of the epicenter and to position the radiometer to aim at the epicenter prior to a flare test.

Traditionally, flare radiation is measured manually by trained personnel properly clothed. During measurement, the operator varies the angle of the radiometer between left and right and between up and down, continuously searching for the maximum reading. This approach is often called manual scanning.

Manual scanning suffers two significant shortcomings. First, if the flare epicenter fluctuates in space, this searching method is not effective in tracking the epicenter. Second, if the flare gas flow rate or composition varies in time, this method cannot distinguish the effects from these variations in flow conditions from those caused by the angle perturbation, and therefore fails to track the flame epicenter. As a result, flare radiation measurements using manual scanning are often associated with relatively large errors. The magnitude of these errors depends largely on the specific individuals conducting these tests and flow conditions.

### 8.5.3 Radiometer Cube

A radiometer cube is a state-of-the-art device developed by the John Zink Company to accurately measure flare radiation and is shown in Figure 8.24. This instrument is designed with three radiometers, attached to the three adjacent surfaces of a cube near a corner. The radiometer cube<sup>24</sup> is placed on a tripod and located in the field at a certain distance from the base of the flare stack. A bubble level, attached to the top surface of the cube, is used to ensure that the top surface is positioned in a horizontal plane. A sighting tube is attached to the top surface of the cube to allow the orientation of the cube to be accurately controlled and determined. The corner of the cube is pointed in the general direction of the flare flame, with the sighting tube pointing at an object with known coordinates.

A set of at least two cubes are used to achieve the full capability of the instrument. The relative locations of the

radiometer cubes and the flare, as well as the orientations of the cubes are determined prior to the flare test and entered into the computer to allow real-time tracking of key flare radiation parameters. Each radiometer on the cubes is connected to a data acquisition system. The data acquisition system collects the data from each sensor and performs trigonometric calculations using a complex set of equations. The results are real-time parameters of the flare radiation: total radiation levels from both cubes, incidence angles, and the flare epicenter coordinates. This instrument has four main advantages over the hand held instrument:

1. Reduces measurement errors
2. Avoids placing personnel in hazardous situations
3. Locates the flame epicenter
4. Provides continuous measurement throughout a test

The John Zink proprietary radiometer cubes can be used in conjunction with the API 521 single-point epicenter flare radiation model to obtain objective, experimental values for the radiant fraction and the epicenter locations, which have previously been regarded as somewhat subjective and difficult to quantify.



**FIGURE 8.24**  
The John Zink radiometer cube.

## References

1. Baukal, C.E., *The John Zink Combustion Handbook*, CRC Press, Boca Raton, FL, 2001, p. 105.
2. Baukal, C.E., *Industrial Combustion Pollution and Control*, Marcel Dekker, Inc., New York, 2004, p. 508.
3. efunda (Engineering Fundamentals), Heat transfer: Radiation, [http://www.efunda.com/formulae/heat\\_transfer/radiation/overview\\_rad.cfm](http://www.efunda.com/formulae/heat_transfer/radiation/overview_rad.cfm), 2012.
4. Cornforth, J.R., *Combustion Engineering and Gas Utilizations*, E&FN Spon, London, U.K., 1992.
5. Wikipedia, the free encyclopedia, "Infrared," <http://wikipedia.org/wiki/Infrared>
6. Solar Energy Technologies Program: Light and the PV Cell, U.S. Department of Energy, <http://www.eere.energy.gov>, 2012.
7. Bird and Hulstrom's model from the publication, A simplified clear sky model for direct and diffuse insolation on horizontal surfaces, by R.E. Bird and R.L. Hulstrom, SERI Technical Report SERI/TR-642-761, Solar Energy Research Institute, Golden, CO, Feb 1991.
8. <http://en.wikipedia.org/wiki/Earth>, "Earth.", 2012.
9. Palmer, H.B. and Beer, J.M., *Combustion Technology, Some Modern Developments*, Academy Press, New York, 1974, p. 216.
10. Bussman, W.R. and Knott, D., Unique concept for noise and radiation reduction in high-pressure flaring, OTC 12160, Offshore Technology Conference, Houston, TX, May 2000.

11. McQuiston, C. and Parker, J.D., *Heating, Ventilating, and Air Conditioning*, John Wiley & Sons, New York, 1982.
12. Brzustowski, T.A. and Sommer, E.C., Jr., Predicting radiant heating from flares, *Proceedings—Division of Refining*, Vol. 53, API Washington, DC, 1973, p. 865–893.
13. DiNenno, P.J., Simplified radiation heat transfer calculations from large open hydrocarbon fires, Society of Fire Protection Engineers, SFPE Technology Report 82–9, 1982.
14. Babrauskas, V., Ignition of Wood: A Review of the State of the Art, pp. 71–88 *Interflam 2001*, Interscience Communications Ltd., London, U.K., 2001.
15. Society of Wood Science and Technology, <http://www.sswst.org>, Teaching unit number 2, 2012.
16. McGuire, J.H., Fire and Spatial Separation of Building, *Fire Technology* 1(4), 278–287, 1965.
17. Spearpoint, M.J., *Predicting the Ignition and Burning Rate of Wood in the Cone Calorimeter Using an Integral Model (NIST GCR 99-775)*, National Institute of Standards and Technology, Gaithersburg, MD, 1999.
18. Bilo, M. and Kinsman, P.R., Thermal radiation criteria used in pipeline risk assessment, *Pipes and Pipelines International* 42(6), 17–25, November–December, 1997.
19. Hymes, I., Boydell, W., and Prescott, B., *Thermal Radiation: Physiological and Pathological Effects*, Institute of Chemical Engineers, Rugby, U.K., 1996.
20. American Petroleum Institute 521 *Pressure-relieving and Depressuring Systems*, 5th edn., Washington, DC, January 2007.
21. Schwartz, R.E. and White, J.W., Flare Radiation Prediction: A Critical Review, presented at the 30th Annual Loss Prevention Symposium of the American Institute of Chemical Engineers, February 1996, Session 12.
22. Hukseflux Thermal Sensors, <http://www.hukseflux.com/thermsens.htm>, 2012.
23. Siegel, R. and Howell, J.R., *Thermal Radiation Heat Transfer*, 3rd edn., Taylor & Francis, New York, 1992.
24. Hong, J., White, J., and Baukal, C., Accurately Predict Radiation From Flare Stacks, *Hydrocarbon Processing* 85(6), 79–81, June 2006.

This page intentionally left blank



# 9

## *Fundamentals of Fluid Dynamics*

Wes Bussman, Zachary L. Kodesh, and Robert E. Schwartz

### CONTENTS

9.1	Introduction .....	228
9.2	Properties of Fluids .....	229
9.2.1	Density of Gases .....	229
9.2.2	Ratio of Specific Heat for Gases .....	230
9.2.2.1	Definition .....	230
9.2.2.2	Ratio of Specific Heat of Mixtures .....	231
9.2.2.3	Ratio of Specific Heat as a Function of Temperature .....	231
9.2.3	Viscosity of Gases and Liquids .....	231
9.2.3.1	General Description of Viscosity .....	233
9.2.3.2	Dynamic Viscosity .....	233
9.2.3.3	Kinematic Viscosity .....	233
9.2.3.4	Other Units of Viscosity .....	234
9.2.3.5	Viscosity as a Function of Temperature and Pressure .....	234
9.2.3.6	Viscosity of Fluid Mixtures .....	234
9.3	Laminar and Turbulent Flow .....	235
9.4	Pressure .....	236
9.4.1	Units of Pressure .....	236
9.4.2	Atmospheric Pressure .....	236
9.4.3	Gauge and Absolute Pressure .....	238
9.4.4	Static, Velocity, and Total Pressure .....	239
9.4.5	Pressure Loss through Fittings .....	241
9.4.6	Flow Resistance through Straight Pipe .....	242
9.5	Downwash .....	245
9.5.1	Over and around Flare Stacks .....	245
9.5.2	Over Buildings .....	246
9.5.3	Over Terrain .....	246
9.6	Flare Tip Internal Burning .....	249
9.6.1	Buoyancy Effects .....	249
9.6.2	Wind Action .....	250
9.7	Gas Dispersion from an Elevated Flare .....	250
9.7.1	Atmospheric Dispersion Modeling .....	251
9.7.2	Major Factors Affecting GLC .....	252
9.8	Heater Draft .....	254
9.8.1	Background .....	254
9.8.2	Draft Systems .....	255
9.8.2.1	Natural-Draft Heaters .....	256
9.8.2.2	Mechanical-Draft Heaters .....	256
9.8.3	Fundamental Concepts of Draft .....	257
9.8.4	Natural Draft Heaters .....	262
9.8.4.1	Draft Profile .....	262

9.8.4.2	Draft Measurement Location .....	263
9.8.4.3	Adjusting Draft .....	266
9.8.5	Mechanical Draft Heaters.....	266
9.8.6	Instrumentation Used to Measure Heater Draft.....	269
9.8.7	Heater Draft Calculations.....	270
9.8.8	Effects of Ambient Wind Conditions on Natural Draft Heaters .....	273
9.9	Air-Side Pressure Drop through Burners .....	274
9.9.1	Definition of Burner Pressure Drop .....	275
9.9.2	API 560 Burner Pressure Drop Design Recommendations .....	276
9.9.3	Air-Side Capacity Curves .....	276
9.10	Burner Fuel Capacity Curves .....	277
9.10.1	Background.....	277
9.10.2	Discussion of Burner Heat Release .....	278
9.10.3	Description of Fuel Capacity Curves .....	278
9.10.4	Effects of Internal Nozzle Design on Fuel Capacity Curves .....	281
9.10.5	Effects of Orifice Plugging on Fuel Capacity Curves .....	284
9.10.6	Generating Fuel Capacity Curves.....	286
9.11	Free Jet Flow .....	289
9.12	Eduction Processes .....	291
9.12.1	Description of Eductor Systems.....	291
9.12.2	Application of Eductor Systems.....	292
9.12.3	Factors Influencing Eductor Performance.....	294
9.13	Flashback.....	295
9.13.1	Definition of Flashback in a Burner .....	295
9.13.2	Description of Flashback .....	295
9.13.3	Major Factors Affecting Flashback.....	296
9.14	Flame–Flame Interference Inside Heaters.....	298
9.14.1	Description of Flame–Flame Interference .....	298
9.14.2	Flow Dynamics Associated with Flame–Flame Interference .....	299
9.14.3	Detrimental Effects of Flame–Flame Interference .....	300
9.15	Air Leakage into Heaters and Flare Stacks .....	303
9.15.1	Estimating Air Infiltration.....	303
9.15.2	Heaters.....	303
9.15.3	Flare Stacks .....	304
	Nomenclature .....	306
	Greek Letters.....	306
	References.....	306

## 9.1 Introduction

Ancient civilizations were able to solve fluid mechanic problems that enabled them to build boats, ships, canals, irrigation systems, bridges, and water lifting machines.<sup>1</sup> These advances were brought about without the aid of any mathematical analysis of fluid mechanics, but through trial and error and everyday life experiences. The first analytical analysis of fluid mechanics was not recorded until the third century BC when Archimedes (285–212 BC) began formulating equations to analyze the buoyancy of objects in a fluid. About 1900 years later, the science of fluid mechanics began to be routinely analyzed mathematically by men such as Newton, Bernoulli,

Euler, Navier, and Stokes who are attributed to some of the fundamental equations of fluid dynamics.<sup>2</sup>

Today, fluid dynamics is one of the most important areas of engineering endeavor. Over the last 100 years, research into the science of fluid dynamics has grown at an exponential rate. Today, there are hundreds of papers published and dozens of conferences and symposia every year devoted to fluid dynamic research. Fluid dynamics is a broad subject because it is an important tool used in many engineering fields, for example, turbulence, acoustics, and aerodynamics. There are many good textbooks written on the subject; Panton,<sup>3</sup> White,<sup>4</sup> Fox and McDonald,<sup>5</sup> Vennard and Street,<sup>6</sup> Hinze,<sup>7</sup> Schlichting,<sup>8</sup> and Hughes and Brighton<sup>9</sup> are a few examples.

Fluid dynamics plays an important role in the design and operation of combustion equipment. For example, industrial burners and flares require analysis and control of the flow of air, steam, fuel, and hot combustion products through complex networks of pipes, ducts, valves, dampers, regulators, pumps, etc. Engineers rely extensively on empirical fluid dynamic models, computational fluid dynamic models, cold flow physical models, and experience gained from day-to-day observation of flow dynamics to help facilitate and guide in the design of combustion equipment. Fluid dynamics also plays a key role in the operation of flare and burner equipment. In general, the more familiar the operators are with the flow dynamics associated with their combustion equipment, the better they are equipped to operate and troubleshoot their system in a safe and efficient manner.

The purpose of this chapter is to (1) provide the reader with some of the practical fluid dynamic concepts and terminology commonly used in the burner and flare industry, (2) demonstrate several ways combustion engineers apply fluid dynamics to assist in the design of combustion equipment, and (3) describe some of the instrumentation often used in the combustion industry.

## 9.2 Properties of Fluids

The properties of a fluid (gas or liquid) describe its physical characteristics. This section presents a brief description of these properties and discusses how the properties of a mixture are calculated. For a list of additional gas properties, the reader is referred to the following sources: Geerssen,<sup>10</sup> Turns,<sup>11</sup> and Bartok and Sarofim.<sup>12</sup>

### 9.2.1 Density of Gases

Atmospheric air is a mixture of many gases plus water vapor and other pollutants. Aside from pollutants, which may vary considerably from place to place, the composition of dry air is relatively constant; the composition varies slightly with time, location, and altitude.<sup>13</sup> The *ASHRAE Handbook of Fundamentals*<sup>14</sup> gives the following approximate composition of dry air on a volume fraction basis:

Nitrogen	0.78084
Oxygen	0.20948
Argon	0.00934
Carbon dioxide	0.00031
Neon, helium, methane, sulfur dioxide, hydrogen, etc.	0.00003

In 1949, a standard composition of dry air was fixed by the International Joint Committee on Psychrometric Data<sup>15</sup> as shown in the following.

Constituent	Molecular Weight	Volume Fraction
Oxygen	32.000	0.2095
Nitrogen	28.016	0.7809
Argon	39.944	0.0093
Carbon dioxide	44.010	0.0003
	28.965	1.0000

Density is defined as the mass per unit volume of a fluid and is usually given the Greek symbol  $\rho$  (rho). The units of density can be written as  $\text{lb}_m/\text{ft}^3$  ( $\text{kg}/\text{m}^3$ ). Based on the composition of dry air given earlier, the density is  $0.0765 \text{ lb}_m/\text{ft}^3$  ( $1.225 \text{ kg}/\text{m}^3$ ) at standard temperature and pressure. An informal notation for standard temperature and pressure is STP which is based on  $59.0^\circ\text{F}$  ( $15^\circ\text{C}$ ) and  $14.696 \text{ lb}_f/\text{in}^2$  ( $101.325 \text{ kPa}$ ). The temperature and pressure, which constitutes standard conditions, can vary from industry to industry as well as country to country. Care should be taken when utilizing properties based on STP to ensure the correct basis is known. Table 9.1 contains a list of several pure-component gases with corresponding density and molecular weight (mole weight).

The density of a gas varies with temperature and pressure. For example, the density of dry air at  $59.0^\circ\text{F}$  and at  $14.696 \text{ psia}$  is  $0.0765 \text{ lb}_m/\text{ft}^3$ ; however, if the air is compressed or the temperature is reduced, the density of the air will increase. The density of a gas at a given temperature and pressure can be calculated using the following equation:

U.S. customary units

$$\rho_{\text{actual}} = \rho_{\text{STP}} \underbrace{\left( \frac{460 + T_{\text{standard}}(^{\circ}\text{F})}{460 + T_{\text{gas}}(^{\circ}\text{F})} \right)}_{\text{correcting for temperature}} \underbrace{\left( \frac{P_{\text{atm}}(\text{psia}) + P_{\text{gas}}(\text{psig})}{P_{\text{standard}}(\text{psia})} \right)}_{\text{correcting for pressure}} \quad (9.1a)$$

SI units

$$\rho_{\text{actual}} = \rho_{\text{STP}} \underbrace{\left( \frac{273.15 + T_{\text{standard}}(^{\circ}\text{C})}{273.15 + T_{\text{gas}}(^{\circ}\text{C})} \right)}_{\text{correcting for temperature}} \times \underbrace{\left( \frac{P_{\text{atm}}(\text{kPa(abs)}) + P_{\text{gas}}(\text{kPa g})}{P_{\text{standard}}(\text{kPa(abs)})} \right)}_{\text{correcting for pressure}} \quad (9.1b)$$

where  $T_{\text{standard}}$  and  $P_{\text{standard}}$  are the standard temperature and pressure on which  $\rho_{\text{STP}}$  is based. To demonstrate how this equation is used, consider the following example:

**Example 9.1**

A vessel contains air at 10 psig and 30°F. If the atmospheric pressure is 13.9 psia, determine the density of the air inside the tank. Substituting the appropriate values into Equation 9.1a gives

$$\rho_{\text{actual}} = 0.0765 \left( \frac{460 + 59}{460 + 30} \right) \left( \frac{13.9 + 10}{14.696} \right) = 0.1318 \frac{\text{lb}_m}{\text{ft}^3}$$

In this example, the density of the air inside the tank is 0.1318 lb<sub>m</sub>/ft<sup>3</sup>; this is the density at actual conditions inside the tank. Notice as the temperature of the gas increases, the density decreases, but as the pressure increases, the density increases.

If the molecular weight of a gas is known, the density of the gas at actual conditions can be determined. First, the density of the gas at STP is calculated using the following equation:

U.S. customary units and SI units

$$\rho_{\text{gas,STP}} = \rho_{\text{air,STP}} \left( \frac{MW_{\text{gas}}}{MW_{\text{air}}} \right) \quad (9.2)$$

where

$MW_{\text{gas}}$  is the molecular weight of gas

$MW_{\text{air}}$  is the molecular weight of air

$\rho_{\text{gas,STP}}$  is the density of the gas at STP

After the density of the gas is calculated at standard conditions, the density at actual conditions can be determined using Equation 9.1.

**Example 9.2**

Calculate the density of methane at 100°F and 30 psig at an atmospheric pressure of 14.0 psia.

Using Equation 9.2, calculate the density of methane at standard conditions.

$$\begin{aligned} \rho_{\text{gas,STP}} &= \rho_{\text{air,STP}} \left( \frac{MW_{\text{gas}}}{MW_{\text{air}}} \right) = 0.0765 \frac{\text{lb}_m}{\text{ft}^3} \left( \frac{16.043}{28.965} \right) \\ &= 0.0424 \frac{\text{lb}_m}{\text{ft}^3} \text{STP} \end{aligned}$$

Using Equation 9.1, calculate the density of methane at actual conditions. *Note:* since the density of air at 59°F and 14.696 psia was utilized, these values for temperature and pressure will be used as the standard conditions.

$$\begin{aligned} \rho_{\text{methane,100°F,30psig}} &= 0.0424 \left( \frac{460 + 59}{460 + 100} \right) \left( \frac{14.0 + 30}{14.696} \right) \\ &= 0.1176 \frac{\text{lb}_m}{\text{ft}^3} \end{aligned}$$

The molecular weight of a mixture can be calculated using the following equation:

$$MW_{\text{mixture}} = [MW_1x_1 + MW_2x_2 + \dots + MW_nx_n] \quad (9.3)$$

where  $MW_n$  and  $x_n$  are the molecular weight and volume fraction of the  $n$ th component, respectively.

**Example 9.3**

Calculate the density of a gas mixture containing 25% hydrogen and 75% methane (volume basis) at STP.

The values for each variable used in Equation 9.3 are listed as follows:

$$MW_1 = MW_{\text{hydrogen}} = 2.0159$$

$$MW_2 = MW_{\text{methane}} = 16.043$$

$$x_1 = x_{\text{hydrogen}} = \frac{25\%}{100} = 0.25$$

$$x_2 = x_{\text{methane}} = \frac{75\%}{100} = 0.75$$

Substituting these values into Equation 9.3 gives

$$MW_{\text{mixture}} = [2.0159 \times 0.25 + 16.043 \times 0.75] = 12.536$$

The following variables will be utilized in Equation 9.2

$$\rho_{\text{air,STP}} = 0.0765 \text{ lb}_m/\text{ft}^3$$

$$MW_{\text{air}} = 28.965$$

$$\begin{aligned} \rho_{\text{mixture,STP}} &= 0.0765 \left( \frac{12.536}{28.965} \right) \\ &= 0.0331 \frac{\text{lb}_m}{\text{ft}^3} \text{STP}(59^\circ\text{F}, 14.696 \text{ psia}) \end{aligned}$$

**9.2.2 Ratio of Specific Heat for Gases****9.2.2.1 Definition**

The ratio of specific heat is a fluid property commonly used in combustion industry and is usually denoted by the letter  $k$  (in some books it is denoted by  $\gamma$ ). Mathematically, the ratio of specific heat is defined as follows:

$$k = \frac{c_p}{c_v} \quad (9.4)$$



TABLE 9.1

Properties of Various Gases

Gas Composition	Molecular Weight	Density <sup>a</sup> (lb/scf)	Ratio of Specific Heat <sup>a</sup>
Methane (CH <sub>4</sub> )	16.043	0.04238	1.31
Ethane (C <sub>2</sub> H <sub>6</sub> )	30.070	0.07943	1.19
Propane (C <sub>3</sub> H <sub>8</sub> )	44.097	0.11648	1.13
<i>n</i> -Butane (C <sub>4</sub> H <sub>10</sub> )	58.123	0.15352	1.10
Pentane (C <sub>5</sub> H <sub>12</sub> )	72.150	0.19057	1.08
<i>n</i> -Hexane (C <sub>6</sub> H <sub>14</sub> )	86.177	0.22762	1.06
Cyclopentane (C <sub>5</sub> H <sub>10</sub> )	70.134	0.18525	1.12
Cyclohexane (C <sub>6</sub> H <sub>12</sub> )	84.161	0.22230	1.09
Ethylene (C <sub>2</sub> H <sub>4</sub> )	28.054	0.07410	1.25
Propene (C <sub>3</sub> H <sub>6</sub> )	42.081	0.11115	1.15
Butene (C <sub>4</sub> H <sub>8</sub> )	56.108	0.14820	1.11
Pentene (C <sub>5</sub> H <sub>10</sub> )	70.134	0.18525	1.08
Butadiene (C <sub>4</sub> H <sub>6</sub> )	54.092	0.14288	1.12
Carbon dioxide (CO <sub>2</sub> )	44.010	0.11625	1.29
Water (H <sub>2</sub> O)	18.015	0.04758	1.33
Oxygen (O <sub>2</sub> )	31.999	0.08452	1.40
Nitrogen (N <sub>2</sub> )	28.013	0.07399	1.40
Sulfur dioxide (SO <sub>2</sub> )	64.060	0.16920	1.27
Hydrogen sulfide (H <sub>2</sub> S)	34.080	0.09002	1.32
Carbon monoxide (CO)	28.010	0.07398	1.40
Ammonia (NH <sub>3</sub> )	17.031	0.04498	1.31
Hydrogen (H <sub>2</sub> )	2.016	0.00532	1.41
Argon (Ar)	39.944	0.10551	1.67
Acetylene (C <sub>2</sub> H <sub>2</sub> )	26.038	0.06878	1.24
Benzene (C <sub>6</sub> H <sub>6</sub> )	78.114	0.20633	1.12

<sup>a</sup> At 59°F (standard temperature) and 14.696 psi.

where  $c_p$  and  $c_v$  are the specific heat at constant pressure and volume, respectively. For most hydrocarbons, the ratio of specific heat varies between a value of nearly 1.0 and 1.7 and exhibits a strong dependence on the gas temperature and composition. For example, methane at standard temperature (59°F) has a  $k$  value of approximately 1.31, while propane has a value of 1.13. However, at 200°F, the ratio of specific heat of methane and propane decrease to a value of approximately 1.27 and 1.10, respectively. Values of  $k$  for several pure-component gases at standard temperature are listed in Table 9.1.

The ratio of specific heat can be thought of as being a value that relates to the compressibility of a gas. How much a gas compresses when a pressure is applied to it is an important property that influences the flow rate of a gas through a fuel orifice. Later in this chapter, it will be shown how the ratio of specific heat is utilized in orifice calculations.

### 9.2.2.2 Ratio of Specific Heat of Mixtures

For a mixture of gases, the ratio of specific heat ( $k_{\text{mixture}}$ ) can be determined with the following equation:

$$k_{\text{mixture}} = \frac{\frac{k_1 x_1}{k_1 - 1} + \frac{k_2 x_2}{k_2 - 1} + \dots + \frac{k_n x_n}{k_n - 1}}{\frac{x_1}{k_1 - 1} + \frac{x_2}{k_2 - 1} + \dots + \frac{x_n}{k_n - 1}} \quad (9.5)$$

where

$k_n$  is the ratio of specific heat

$x_n$  is the volume fraction of  $n$ th component

### Example 9.4

Determine the ratio of specific heat of the following fuel mixture (percentage by volume): 50% hydrogen, 20% methane, and 30% propane.

The volume fraction of each gas component is

$x_1 = 0.5$  (hydrogen)

$x_2 = 0.2$  (methane)

$x_3 = 0.3$  (propane)

The ratio of specific heat of each gas component can be obtained from Table 9.1.

$k_1 = 1.41$  (hydrogen)

$k_2 = 1.31$  (methane)

$k_3 = 1.13$  (propane)

Substituting the values given earlier into Equation 9.5 and solving gives the ratio of specific heat of the fuel mixture at a temperature of 59°F.

$$k_{\text{mixture}} = \frac{\frac{1.41 \times 0.5}{1.41 - 1} + \frac{1.31 \times 0.2}{1.31 - 1} + \frac{1.13 \times 0.3}{1.13 - 1}}{\frac{0.5}{1.41 - 1} + \frac{0.2}{1.31 - 1} + \frac{0.3}{1.13 - 1}} = 1.24$$

### 9.2.2.3 Ratio of Specific Heat as a Function of Temperature

As mentioned, the ratio of specific heat also varies with the temperature of the gas. Typically, as the temperature increases, the ratio of specific heat decreases as shown in Figure 9.1 for several pure-gas components. To determine the ratio of specific heat of a fuel mixture at various temperatures, the ratio of specific heat must be determined for each gas component at that given temperature. Using these values, Equation 9.5 can be used to determine the ratio of specific heat of the mixture at the given temperature.

### 9.2.3 Viscosity of Gases and Liquids

The viscosity of fluids (gases and liquids) is an important property that must be considered in the design of burner and flare equipment. For example, fuel oil must be heated to the right temperature in order to reduce the viscosity and achieve good atomization for combustion.

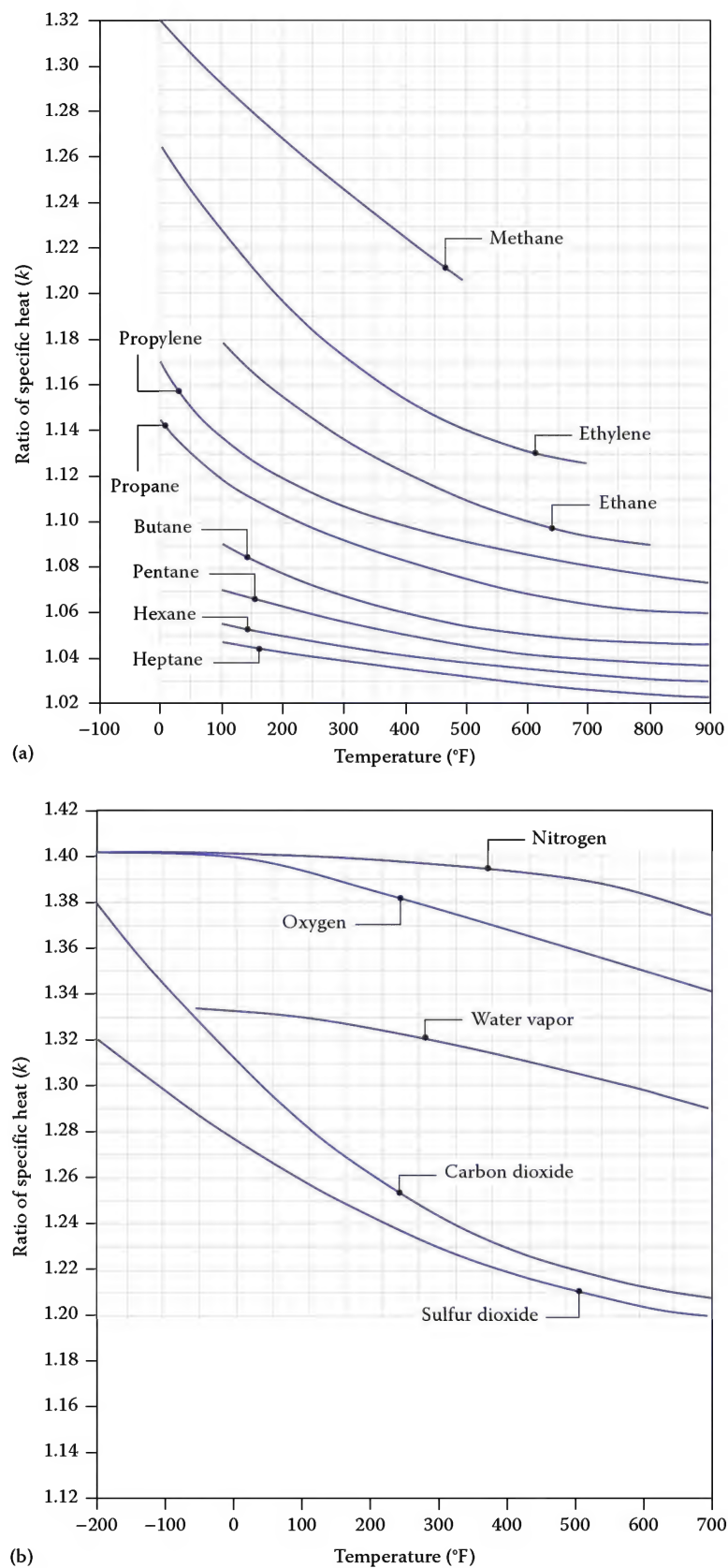


FIGURE 9.1

(a and b) Ratio of specific heat ( $k$ ) for various pure-component gases at different temperatures.

In addition, viscosity of gases and liquids must be considered when designing burner and flare piping networks so that equipment can be properly sized.

### 9.2.3.1 General Description of Viscosity

All fluids exhibit a resistance to flow; this property is called *viscosity*. In general, viscosity determines the rate at which the motion of fluid flow is slowed or damped. Some fluids exhibit a higher viscosity than other fluids. For example, a highly viscous liquid called pitch flows much slower than water under the influence of gravity; pitch is approximately 230 billion ( $2.3 \times 10^{11}$ ) times more viscous than water.<sup>16</sup> Figure 9.2 is a photograph showing pitch flowing out from a funnel; the flow started in 1927 and is still flowing today.



FIGURE 9.2

The pitch drop experiment is a *long-term experiment*, which measures the flow of a piece of *pitch* through a funnel. The experiment shown in this photograph started in 1927 at the University of Queensland in Brisbane, Australia. The experiment is still in progress today, currently under the direction of John Mainstone. (Courtesy of the University of Queensland.)

### 9.2.3.2 Dynamic Viscosity

The dynamic viscosity is typically represented by the Greek letter  $\mu$  (pronounced mu) and is sometimes referred to as the *absolute* viscosity or *pure* viscosity. The dynamic viscosity is dimensionally equal to mass per length per time (mass/length-time). For example, in SI units one can write kg/m-s, which is equivalent to N-s/m<sup>2</sup> or Pa-s or dyne-s/cm<sup>2</sup>. The most common unit of viscosity is the dyne-second per square centimeter (dyne-s/cm<sup>2</sup>) which is usually referred to as poise (P); named after the French physician Jean Louis Marie Poiseuille. Water at 68.4°F (20.2°C) has a dynamic viscosity of 1 cP. Several useful conversions are listed as follows:

$$1 \text{ poise (P)} = 1 \text{ dyne-s/cm}^2 = 1 \text{ g/cm-s}$$

$$1 \text{ poise (P)} = 100 \text{ centiPoise (cP)}$$

$$1 \text{ poise (P)} = 0.1 \text{ Pa-s} = 0.1 \text{ N-s/m}^2 = 0.1 \text{ kg/m-s}$$

$$1 \text{ poise (P)} = 0.0020885 \text{ lb}_f\text{-s/ft}^2$$

### 9.2.3.3 Kinematic Viscosity

Often times the viscosity is reported in literature as the dynamic viscosity divided by the density of the fluid ( $\mu/\rho$ ). This quantity is called the kinematic viscosity and is usually represented by the Greek letter  $\nu$  (pronounced nu):

$$\nu = \frac{\mu}{\rho} \quad (9.6)$$

One reason the kinematic viscosity is often tabulated is because it frequently appears in flow calculations. The kinematic viscosity is dimensionally equal to length squared per unit time (length<sup>2</sup>/time); for example, m<sup>2</sup>/s or ft<sup>2</sup>/s. A commonly used unit for kinematic viscosity is the Stoke (St). Several useful conversions are listed as follows:

$$1 \text{ Stoke (St)} = 1 \text{ cm}^2/\text{s} = 100 \text{ centiStokes (cSt)}$$

$$1 \text{ m}^2/\text{s} = 10,000 \text{ cm}^2/\text{s} = 10,000 \text{ St} = 1,000,000 \text{ (cSt)} \\ = 10.76 \text{ ft}^2/\text{s}$$

The following example demonstrates how the kinematic viscosity is determined knowing the dynamic viscosity.

**Example 9.5**

Determine the kinematic viscosity of water at 68.4°F in units of cSt.

The density of water at 68.4°F is approximately 1000 kg/m<sup>3</sup>. Using Equation 9.6, the kinematic viscosity is calculated as follows:

$$\begin{aligned} \nu &= \frac{\mu}{\rho} = \frac{1 \text{ cP}}{1000 \text{ kg/m}^3} \times \frac{1 \text{ P}}{100 \text{ cP}} \times \frac{0.1 \text{ kg/m-s}}{1 \text{ P}} \\ &= 1 \times 10^{-6} \text{ m}^2/\text{s} \\ 1 \times 10^{-6} \text{ m}^2/\text{s} \times \frac{1 \times 10^6 \text{ cSt}}{1 \text{ m}^2/\text{s}} &= 1 \text{ cSt} \end{aligned}$$

**9.2.3.4 Other Units of Viscosity**

Another unit commonly used in the petrochemical industry for defining the kinematic viscosity is the Saybolt universal second (SUS or SSU). The SSU is a measure of the time, in seconds, required for a volume of 60 mL of petroleum product to flow through a calibrated tube under a carefully controlled temperature. The kinematic viscosity can be converted from SSU to centiStokes using the following equations:

$$\begin{aligned} \text{centiStokes (cSt)} &= (0.266 \times \text{SSU}) \\ &\quad - (195/\text{SSU}) \quad \text{for SSU} = 32 - 100 \end{aligned} \quad (9.7)$$

$$\begin{aligned} \text{centiStokes (cSt)} &= (0.220 \times \text{SSU}) \\ &\quad - (135/\text{SSU}) \quad \text{for SSU} > 100 \end{aligned} \quad (9.8)$$

In addition, there are a number of other historic units used in the hydrocarbon and petrochemical industries such as the Redwood seconds and degree Engler. These units are a consequence of various historic viscosity measurement techniques, especially for crude oil and various cuts.<sup>17</sup>

Redwood second is a measure of the time, in seconds, for 50 mL of the liquid to flow through a Redwood viscometer. A rough conversion of Redwood seconds to centistokes is given by the formula:

$$\text{Centistokes (cSt)} = 0.260 \times t - (0.0188/t) \quad (9.9)$$

where  $t$  is the time in Redwood seconds

Degree Engler is still occasionally used in the United Kingdom. The kinematic viscosity in unit of Engler degrees is the ratio of the time to flow 200 mL of the test fluid to the time to flow 200 mL of water at the same temperature in an Engler viscosity meter.

**9.2.3.5 Viscosity as a Function of Temperature and Pressure**

Viscosity of a fluid is dependent on pressure and temperature. The viscosity always increases with pressure.<sup>5</sup> However, at conditions normally encountered in the burner and flare industry, pressure has little effect on the viscosity and is usually ignored. Temperature, on the other hand, can have a significant impact on the viscosity of liquids and gases.

In general, liquids become more viscous as they get colder. For example, an automobile is more difficult to start on cold days because the oil exhibits a higher resistance to flow due to higher viscosity. Water also becomes more viscous as it gets colder, but the effect is not as significant as motor oil. While liquids become more viscous as they get colder, gases become less viscous; that is, they behave in just the opposite way. The graph in Figure 9.3 clearly shows these trends for several common liquids and gases.

The reason the viscosity–temperature relationship between liquids and gases behave differently is due to the difference in molecular structure. Liquid molecules are spaced much closer together than gas molecules. As the spacing between molecules decreases, the attractive force between them becomes stronger. This strong, intermolecular attraction makes it more difficult for molecules to slip or move around each other corresponding to an increase in viscosity. As the temperature of the liquid increases, the attractive forces become weaker corresponding to a reduction in resistance to flow. The attractive forces in gases, however, are negligible since they are spaced further apart. Therefore, the resistance to motion is governed by the collision of the randomly moving molecules. As the temperature of a gas increases, the randomly moving molecules become more active inducing more collisions and corresponding to an increase in viscosity.

**9.2.3.6 Viscosity of Fluid Mixtures**

Fuel gases in the petrochemical industry typically consist of mixtures of several pure components. Unfortunately, the viscosity of gases is rarely a linear function of the composition. Some procedures for estimating the viscosity of gas mixtures are published in Bird,<sup>18</sup> Reid,<sup>19</sup> and Lyman.<sup>20</sup> Empirical rules have been developed to provide reasonable viscosity estimates of hydrocarbon mixtures. For example, Figure 9.4 shows the dynamic viscosity of hydrocarbon gas mixtures based on molecular weight.<sup>21</sup>

Liquid mixtures tend to be less predictable. Crude oils and heavy fuel oils in particular are mostly dependent upon cut temperatures and origination of the crude. A typical chart of viscosity versus temperature for various



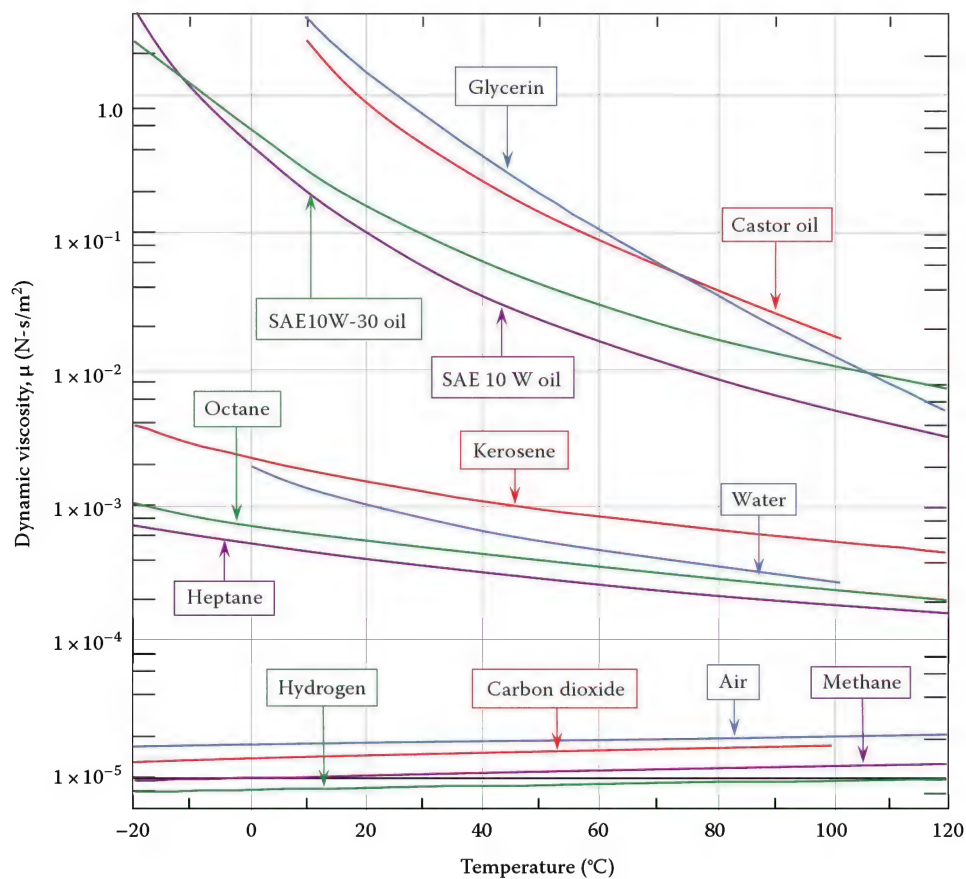


**FIGURE 9.3**  
Dynamic viscosity as a function of temperature for various fluids.

oils is provided in Figure 9.5 to illustrate the point.<sup>21</sup> Normally, it is recommended that information, provided by the fuel supplier, be used to determine the viscosity for mixtures of liquids.

### 9.3 Laminar and Turbulent Flow

Visual observations of fluids in motion have resulted in two broad classifications of flow regimes: *laminar* and *turbulent*. Laminar flows have no fluctuations and tend to flow for long distances with very little mixing occurring in the flow; however, turbulent flows have fluctuations and eddies associated with them that increase mixing rates substantially.

In 1883, Osborn Reynolds published results from a famous experiment he performed that quantified laminar and turbulent flows. A schematic of his experimental apparatus is shown in Figure 9.6.<sup>22</sup> Reynolds used this apparatus to feed water from a large tank through a glass pipe designed with a bell-mouthed inlet. Colored liquid (dye) from a reservoir was injected into the entrance to

the glass pipe. Reynolds discovered that when the water velocity was low, the stream of dye issuing from the tube traveled downstream in a fine line, which did not mix with the water. However, he observed that when the velocity of the water in the tube reached a certain value, the dye would rapidly mix with the water, causing the entire flow in the glass tube to be colored.

Reynolds concluded from these experiments that two flow regimes existed: one is orderly and the other is chaotic. The orderly flow is referred to as *laminar flow* while the chaotic regime is referred to as *turbulent flow*. A familiar example demonstrating laminar and turbulent flow regimes is shown in Figure 9.7. In Figure 9.7, smoke rises from soldering iron in a room of still air. Notice the smoke initially rises up in a fine line and flows smoothly (laminar) for a distance of about 6 in. When the smoke line rises up some distance, it suddenly transitions into a chaotic motion (turbulent). Turbulent flows are easier to find than laminar flows; for example, flow from volcanoes, wind, rivers, and exhaust from a jet engines are all turbulent.

From his experiments, Reynolds made a famous discovery. He found that below a certain velocity, the flow always became laminar. As the velocity was increased, turbulent flow could always be achieved. In addition,

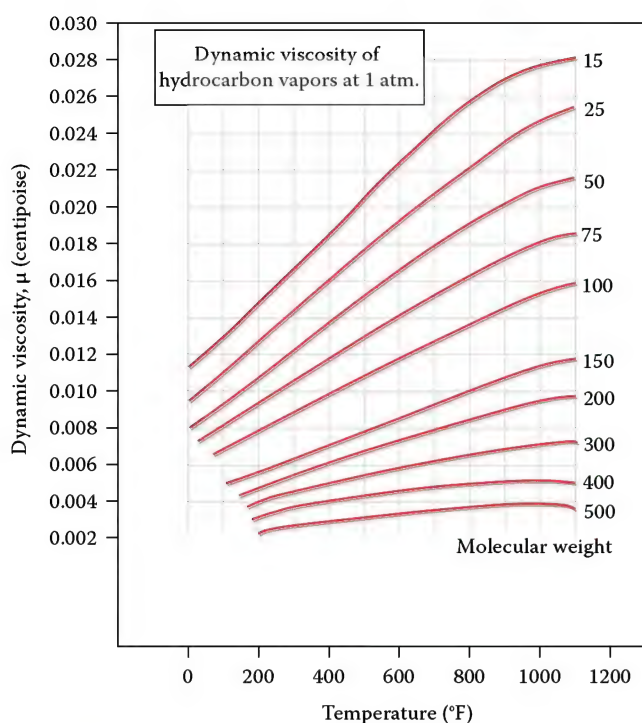


**FIGURE 9.4** Temperature versus viscosity for various hydrocarbons. (From Maxwell, J.B., *Data Book on Hydrocarbons*, D. Van Nostrand Company, Princeton, NJ, 1950.)

Reynolds was able to generalize his results into a non-dimensional parameter, which today is known as the Reynolds number,  $Re$ . It is defined as follows:

$$Re = \frac{VD}{\nu} \quad (9.10)$$

where

$V$  is the velocity in the pipe

$D$  is the pipe diameter

$\nu$  is the kinematic viscosity

As a practical matter, pipe flows having a Reynolds number less than 2300 are laminar, and flows having a Reynolds number greater than 4000 are turbulent. In addition to determining the type of flow, Reynolds numbers have been proven to also scale the intensity of turbulence in a flow. That is, higher Reynolds numbers result in greater vortex generation and faster mixing rates. As a result, Reynolds number calculations are very common in the petrochemical industry. They are used to scale flow coefficients, friction factors, heat transfer rates, and mass transfer rates.

Flames are also classified as either laminar or turbulent. For example, Figure 9.8 shows a burning match and an industrial flare. One can easily recognize the flare flame as being a turbulent flame and the burning match as a laminar flame. Notice that the flame front

on the burning match is smooth while the flare fire is chaotic. These are examples of *diffusion flames*; that is, the oxidizer (air in this case) and fuel are separate and unmixed and only react when they diffuse together to form a flammable mixture. In general, diffusion flames tend to burn slower and produce more soot than flames where the air and fuel are premixed. *Premixed flames* are defined as flames in which the fuel and oxidizer are completely mixed before combustion begins. Premixed flames often produce shorter and more intense flames as compared to diffusion flames.

## 9.4 Pressure

### 9.4.1 Units of Pressure

Pressure is created by the collision of molecules on a surface and is defined as the force exerted per unit area on that surface. In the burner and flare industry, it is common for engineers to use a variety of units for pressure. The choice usually depends on the applications and end user. For example, engineers in the United States will typically use English units such as pounds per square inch (psi) when measuring fuel pressure or inches of water column (inches WC) when measuring heater draft. In Europe and Asia, however, it is common to use SI units such as kilopascal (kPa) and millimeters of water column (mm WC). Several useful units of conversion include the following:

$$\begin{aligned} 1 \text{ N/m}^2 &= 1 \text{ Pa} = 10 \text{ dyne-s/cm}^2 \\ &= 9.869233 \times 10^{-6} \text{ atmospheres (atm)} \\ &= 2.089 \times 10^{-2} \text{ lb}_f/\text{ft}^2 \end{aligned}$$

$$\begin{aligned} 1 \text{ lb}_f/\text{in.}^2 &= 6895 \text{ N/m}^2 = 5.171 \text{ cm mercury} \\ &= 0.0703 \text{ kg/cm}^2 = 27.68 \text{ in. WC} \end{aligned}$$

$$1 \text{ atm} = 101,325 \text{ N/m}^2 = 1.03323 \text{ kg/cm}^2 = 14.696 \text{ psi}$$

$$1 \text{ atm} = 1.01325 \text{ bar} = 76 \text{ cm mercury} = 406.8 \text{ in. WC}$$

$$\begin{aligned} 1 \text{ bar} &= 0.9869 \text{ atm} = 100 \text{ kPa} = 14.5038 \text{ psi} \\ &= 1.01972 \text{ kg/cm}^2 = 29.53 \text{ in. mercury} \end{aligned}$$

### 9.4.2 Atmospheric Pressure

*Atmospheric pressure* refers to the pressure created by a column of air that extends from the surface of the earth

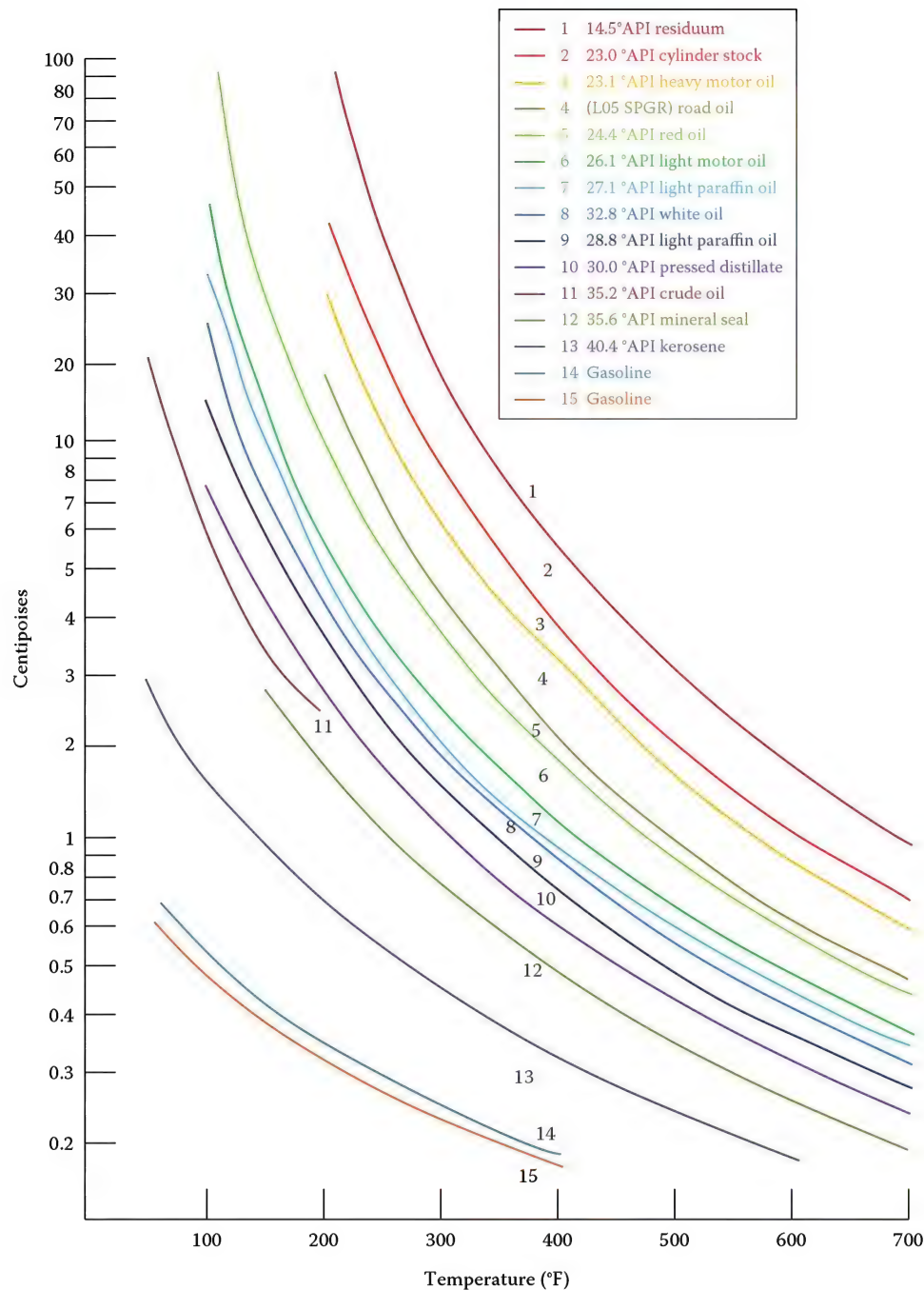


FIGURE 9.5

Viscosity of mid-continent oils. (Adapted from Maxwell, J.B., *Data Book on Hydrocarbons*, D. Van Nostrand Company, Princeton, NJ, 1950.)

to several miles above. Initially, engineers developed a *Standard Atmospheric Pressure* so that the performance of aircraft and missiles could be evaluated at a standard condition. The idea of a standard atmospheric pressure was first introduced in the 1920s.<sup>23</sup> In 1976, a revised report was published which defined the U.S. standard atmosphere that is the currently accepted standard. This standard is an idealized representation of the mean conditions of the earth's atmosphere in 1 year. The standard

atmospheric pressure at sea level is equal to 14.696 psi (407 in. of WC or 101,325 N/m<sup>2</sup>).

The atmospheric pressure varies with elevation. As one moves away from the surface of the earth the atmospheric pressure decreases because there is less atmosphere overhead to create pressure. For example, in Denver Colorado the elevation is about 1 mile above sea level. The atmospheric pressure at this elevation is approximately 12.0 psi. The atmospheric pressure, in the



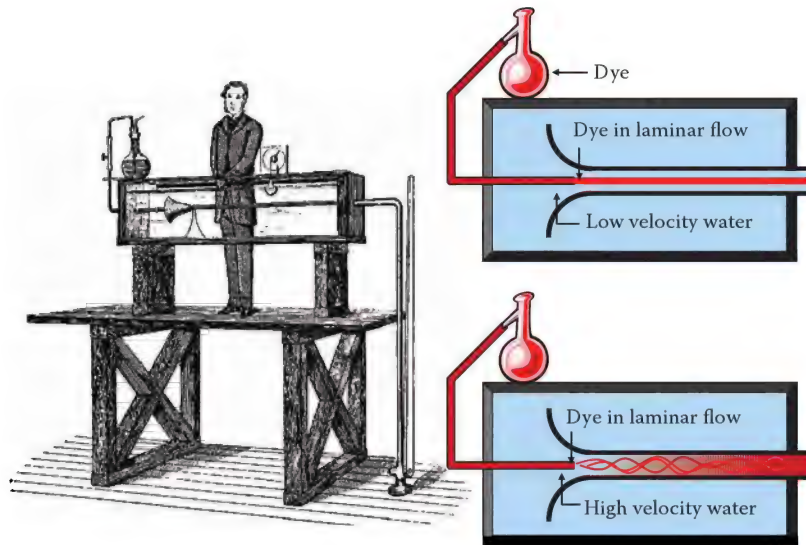


FIGURE 9.6

Osborn Reynold's experimental apparatus used to study the transition from laminar to turbulent flow.

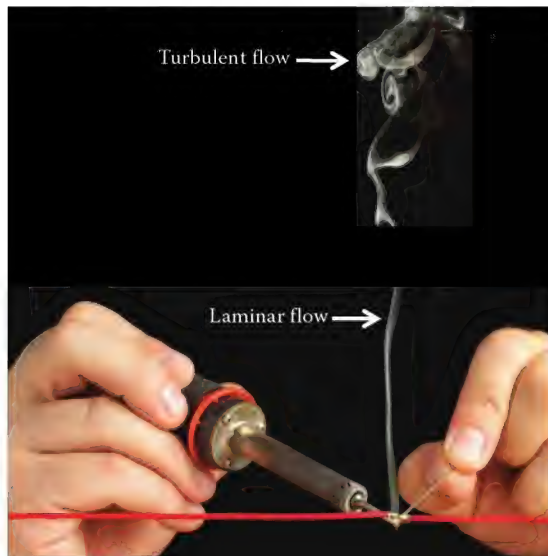


FIGURE 9.7

Smoke rising from a soldering iron. (From Dreamstime).

troposphere, defined as the layer between sea level and 10,769 m (6.7 miles), can be estimated using the following equation.<sup>24</sup>

$$P = 101,325 \left[ \frac{T_o - 6.5 \times 10^{-3}(H)}{T_o} \right]^{5.259} \quad (9.11)$$

where

$P$  is the atmospheric pressure in  $\text{N/m}^2$

$T_o$  is the atmospheric temperature at sea level in Kelvin

$H$  is the height above sea level in meters

#### Example 9.6

If the temperature at sea level is 60°F, what is the atmospheric pressure at an elevation 1 mile above sea level?

First, determine the temperature at sea level in units of Kelvin (K).

$$\begin{aligned} T_o(\text{K}) &= \frac{T_o(^{\circ}\text{F}) - 32}{1.8} + 273.15 = \frac{60 - 32}{1.8} + 273.15 \\ &= 277.17 \text{ K} \end{aligned}$$

Next, convert the height above sea level ( $H$ ) to units of meters.

$$H(\text{m}) = 1 \text{ mile} = 5280 \text{ ft} \frac{1 \text{ m}}{3.281 \text{ ft}} = 1609 \text{ m}$$

Substituting these values into Equation 9.11 gives

$$\begin{aligned} P &= 101,325 \left[ \frac{277.17 - 6.5 \times 10^{-3}(1609)}{277.17} \right]^{5.259} \\ &= 82,766.14 \text{ N/m}^2 \times \frac{1 \text{ psi}}{6895 \text{ N/m}^2} = 12.00 \text{ psi} \end{aligned}$$

#### 9.4.3 Gauge and Absolute Pressure

If the earth were in a perfect vacuum, there would be no column of air above the surface; hence, the atmospheric pressure would be zero. The *absolute pressure* is measured relative to a perfect vacuum. Therefore, when a pressure measurement is taken at the surface of the





(a)



(b)

**FIGURE 9.8**  
Photograph showing examples of a (a) laminar and (b) turbulent flame.

earth, the absolute pressure is equal to the atmospheric pressure. When writing the units for pressure it is customary to designate absolute pressure with the letter “a” or “abs” after the units; for example, psia, psi (abs), or kPa (abs). The absolute pressure can never be less than zero, however, the gauge pressure can. The relationship between absolute, gage, and atmospheric pressures is  $P(\text{abs}) = P(\text{gage}) + P(\text{atmosphere})$ . The *gage pressure* is always measured relative to the atmospheric pressure. A gauge pressure of less than zero can exist. For example, suppose there is a sealed container that holds a gas at 10 psia at sea level. The gauge pressure, which is measured relative to the absolute pressure, would be  $10 \text{ psia} - 14.696 \text{ psia} = -4.696 \text{ psig}$ . The letter “g” after the pressure units represents gauge pressure. Now, suppose the container is pressurized to 20 psia. The gauge

pressure will then be  $20 \text{ psia} - 14.696 \text{ psia} = 5.304 \text{ psig}$ . Therefore, the gauge pressure can either be a positive or negative number and is just the difference in pressure between the atmospheric pressure and the pressure of interest.

#### 9.4.4 Static, Velocity, and Total Pressure

The terms static, velocity, and total pressure are important concepts commonly used in the flare and burner industries. To explain these concepts, the design of the Pitot tube will be discussed and examples will be provided to demonstrate how they are mathematically defined.

Pitot tubes are commonly used in industry to measure the velocity of a flowing fluid. They are manufactured in a variety of sizes as shown in Figure 9.9 and are commonly referred to as Pitot-static tubes. Before discussing the Pitot-static tube design, consider the more basic design referred to as the simple Pitot tube.

The simple Pitot tube consists of a tube bent at a right angle as illustrated in Figure 9.10. One end of the tube is placed directly into a flowing fluid stream, parallel to the flow direction or streamlines. As the fluid impacts the open end of the Pitot tube it is brought to rest or stagnates, with zero velocity, directly in front of the opening of the tube. The pressure at this point is the *total* pressure (or stagnation pressure). That is, the total pressure is a measure of the pressure created by the fluid as it impacts the tip of the Pitot tube plus the pressure inside the pipe itself. By attaching a pressure gauge on the opposite end of the Pitot tube, as shown in the

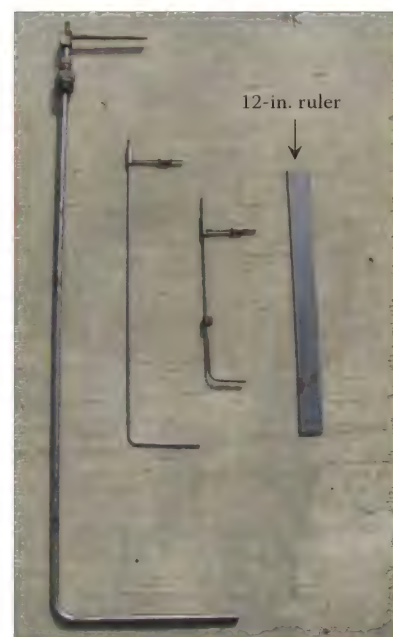


**FIGURE 9.9**  
Various sizes of Pitot-static tubes.

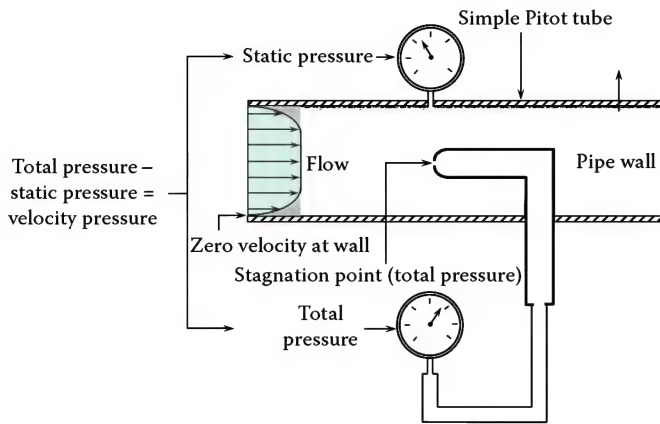


FIGURE 9.10

The simple Pitot tube illustrating the difference between the static, velocity, and total pressure.

illustration, one can measure directly the total pressure in the flowing stream.

The pressure inside the pipe can be measured by placing a pressure gauge on the pipe wall as shown in the illustration; this pressure is referred to as the *static* pressure. At a specific location, the static pressure is constant across the entire traverse of the pipe diameter, however, the static pressure decreases in the downstream direction due to pressure losses created by friction between the fluid and wall. The difference between the total pressure and the static pressure is referred to as the *velocity* pressure; sometimes it is also referred to as the dynamic pressure. Again, the total pressure is the sum of the static and velocity pressures. Mathematically, this is written as follows:

$$P_T = P_V + P_S \quad (9.12)$$

where

$P_T$  is the total pressure

$P_V$  is the velocity pressure

$P_S$  is the static pressure

Figure 9.11 is an illustration showing measurements of static, velocity, and total pressure inside a pipe.

Pitot-static tubes are usually designed as illustrated in Figures 9.12 and 9.13. Pitot-static tubes consist of a coaxial tube placed around the outside of the simple Pitot tube. Several pressure ports located around the perimeter of the outside coaxial tube are used to measure the static pressure within the flow stream; these holes are called the static ports and sense the static pressure due to zero velocity of the fluid perpendicular to the static port openings. Attaching a pressure-sensing device, such as a U-tube manometer (see Volume 2, Chapter 7), and measuring the differential pressure between the total and static pressure allows one to determine the

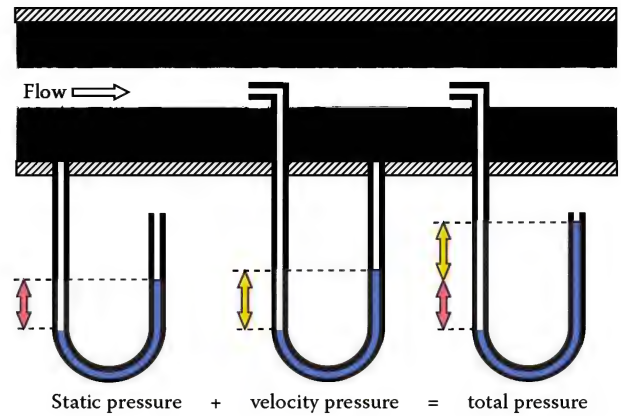


FIGURE 9.11

Illustration showing measurements of static, velocity, and total pressure inside a pipe. (Illustration adapted from Engineeringtoolbox.com)

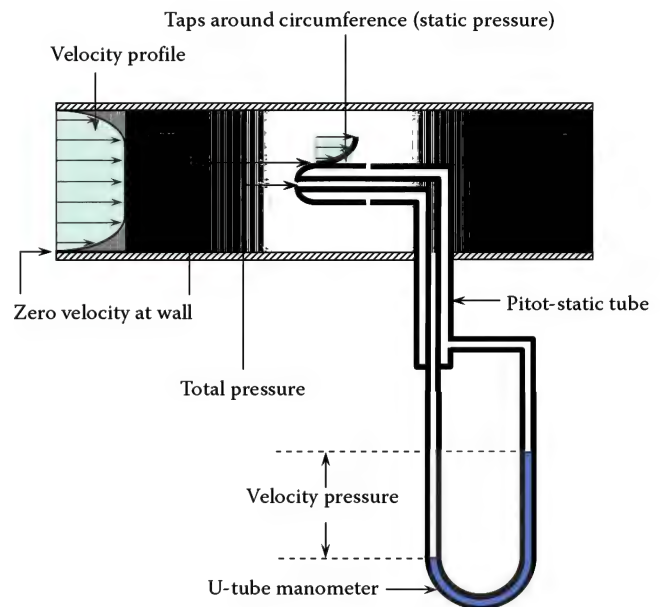


FIGURE 9.12

Illustration of the Pitot-static tube.

velocity pressure. Mathematically, the velocity pressure can be written as follows:

$$P_V = \frac{\rho V^2}{2}, \quad (9.13)$$

where  $V$  is the velocity of the fluid impacting the Pitot tube inlet. With the velocity pressure known, the velocity of the fluid at the point of measurement can be determined by solving Equation 9.10 for  $V$ .

$$V = \sqrt{\frac{2P_V}{\rho}} = \sqrt{\frac{2(P_T - P_S)}{\rho}} \quad (9.14)$$

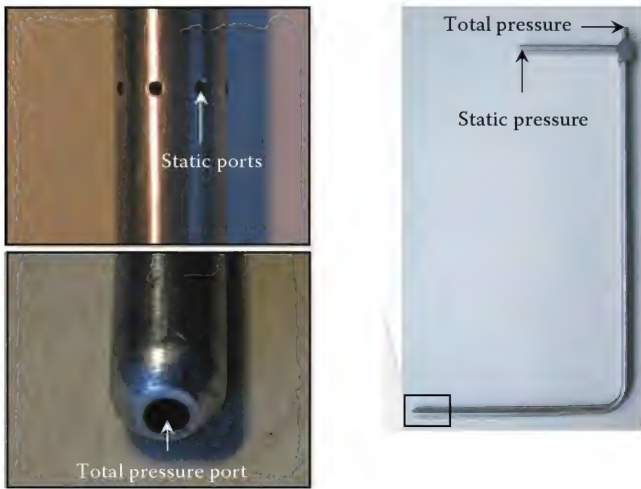


FIGURE 9.13  
Photograph of the Pitot-static tube.

The following example demonstrates how Equation 9.14 is used:

#### Example 9.7

A Pitot-static tube is placed within a duct flowing air with a temperature of 200°F. The static pressure within the duct is 1 psig and the atmospheric pressure is 14.3 psia. A U-tube manometer measures a velocity pressure of 4 in. WC between the total pressure tap and static tap on the Pitot tube. Determine the velocity of the air at the measurement point.

First, determine the density of the air flowing within the duct.

$$\begin{aligned} \rho_{\text{air, duct}} &= \underbrace{0.0765 \frac{\text{lb}_m}{\text{ft}^3}}_{\text{density of air at standard temperature and pressure (59°F and 14.696 psia)}} \times \underbrace{\frac{14.3 \text{ psia} + 1 \text{ psig}}{14.696 \text{ psia}}}_{\text{correcting for the actual air pressure inside the duct}} \\ &\times \underbrace{\frac{59^\circ\text{F} + 460}{200^\circ\text{F} + 460}}_{\text{correcting for the actual air temperature inside the duct}} \times \underbrace{\frac{1 \text{ slug}}{32.2 \text{ lb}_m}}_{\text{converting pounds mass to slugs}} \\ &= 0.001945 \frac{\text{slugs}}{\text{ft}^3} \end{aligned}$$

The slug is a unit of mass and is defined as

$$\text{slug} = \text{lb}_f \cdot \text{s}^2 / \text{ft}$$

Next, convert the velocity pressure,  $P_v$ , to units of  $\text{lb}_f/\text{ft}^2$ .

$$P_v = 4 \text{ in. WC} \times \frac{1 \frac{\text{lb}_f}{\text{in}^2} \times \frac{144 \text{ in}^2}{\text{ft}^2}}{27.68 \text{ in. WC}} = 20.81 \frac{\text{lb}_f}{\text{ft}^2}$$

Finally, the velocity can be calculated as follows:

$$\begin{aligned} V &= \left( \frac{2 \times P_v}{\rho} \right)^{\frac{1}{2}} = \left( \frac{2 \times 20.81 \frac{\text{lb}_f}{\text{ft}^2} \times \frac{1 \frac{\text{slug} \cdot \text{ft}}{\text{s}^2}}{1 \text{ lb}_f}}{0.001944 \frac{\text{slugs}}{\text{ft}^3}} \right)^{\frac{1}{2}} \\ &= 146 \frac{\text{ft}}{\text{s}} \end{aligned}$$

#### 9.4.5 Pressure Loss through Fittings

Obstructions within the flow stream of a pipe or duct can alter the flow direction and pattern of a fluid resulting in a pressure drop. For example, consider the long radius elbow as illustrated in Figure 9.14. When fluid flows through the elbow, the flow separates and creates a recirculation zone and counter rotating vortices just downstream of the bend. Pressure losses are the result of additional turbulence and/or flow separation created by sudden changes in the fluid momentum. Examples of other obstructions include fittings such as tees, contractions, or expansions. The purpose of this section is to discuss the general procedure for estimating the pressure drop through various fittings.

A complete theoretical analysis for calculating the flow through fittings has not yet been developed; therefore, the pressure drop is based on equations that rely heavily on experimental data. The most common method used to determine the pressure loss is to specify the *loss coefficient*,  $K_L$ , defined as follows:

$$K_L = \frac{dP}{\frac{1}{2} \rho V^2} \quad (9.15)$$

where

$dP$  is the pressure drop through the fitting

$\rho$  is the approaching fluid density

$V$  is the fluid velocity specified either upstream or downstream of the obstruction

Notice that the loss coefficient is a dimensionless number and is defined as the ratio of the pressure drop through a fitting to the velocity pressure of the fluid stream. Solving Equation 9.15 for  $dP$  relates the pressure drop through a fitting:

$$dP = K_L \frac{\rho V^2}{2} \quad (9.16)$$

Equation 9.16 shows that if the loss coefficient,  $K_L$ , is equal to 1.0, then the pressure loss through that fitting will equal the velocity pressure of the fluid stream,



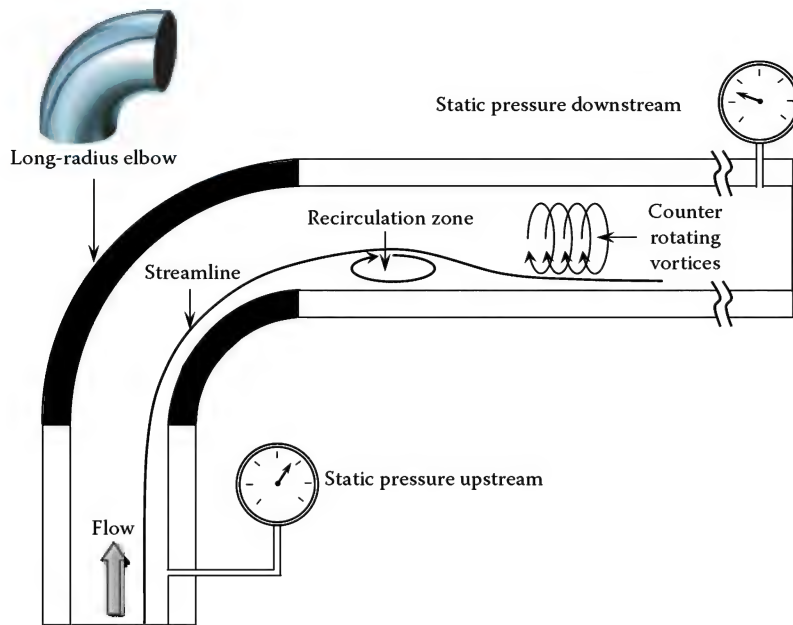


**FIGURE 9.14**  
Illustration showing the fluid flow pattern through a long-radius elbow.

$\frac{1}{2}\rho V^2$ . The loss coefficient is strongly dependent on the geometry of the obstruction and the Reynolds number. The loss coefficient for turbulent flow through a few fittings is given in Figure 9.15. For more detailed information on loss coefficients through various fittings, refer to Idelchik<sup>25</sup> and Crane technical paper No. 410.<sup>26</sup>

#### Example 9.8

Combustion air flows through the entrance of an eductor system. Compare the pressure drop through the entrance of a well-rounded inlet with a radius of 0.4 in. to a straight pipe inlet ( $R = 0$ ). The diameter of the downstream pipe is 2 in. and the air velocity and density is 100 ft/s and 0.0765 lb<sub>m</sub>/ft<sup>3</sup>, respectively.

First, determine the density of the air in units of slugs/ft<sup>3</sup>.

$$\rho_{\text{air, duct}} = 0.0765 \frac{\text{lb}_m}{\text{ft}^3} \times \frac{1 \text{ slug}}{32.2 \text{ lb}_m} = 0.002376 \frac{\text{slugs}}{\text{ft}^3}$$

From Figure 9.15, the loss coefficient for the well-rounded inlet ( $R/D = 0.4/2 = 0.2$ ) is 0.03 and for the straight pipe inlet ( $R/D = 0$ ) the loss coefficient is 0.5. Substituting the appropriate values into Equation 9.16, the pressure loss can be determined.

$$\begin{aligned} dP_{\text{bell}} &= K_L \frac{\rho V^2}{2} = 0.03 \frac{0.002376 \frac{\text{slugs}}{\text{ft}^3} \times (100)^2 \frac{\text{ft}^2}{\text{s}^2}}{2 \times \frac{1 \frac{\text{slug-ft}}{\text{s}^2}}{1 \text{ lb}_f}} \\ &= 0.356 \frac{\text{lb}_f}{\text{ft}^2} = 0.069 \text{ in. WC} \end{aligned}$$

$$\begin{aligned} dP_{\text{straight pipe}} &= K_L \frac{\rho V^2}{2} \\ &= 0.5 \frac{0.002376 \frac{\text{slugs}}{\text{ft}^3} \times (100)^2 \frac{\text{ft}^2}{\text{s}^2}}{2 \times \frac{1 \frac{\text{slug-ft}}{\text{s}^2}}{1 \text{ lb}_f}} \\ &= 5.94 \frac{\text{lb}_f}{\text{ft}^2} = 1.14 \text{ in. WC} \end{aligned}$$

Notice that the straight pipe inlet has a pressure drop that is approximately 16.5 times more than the well-rounded-bell inlet. In industry, it is not uncommon to see burner and flare appurtenances designed with well-rounded inlets in order to reduce pressure drop through the system. For example, well-rounded-bell inlets are commonly used on flare and burner pilots, premixed burners (Figure 9.16) and steam eduction tubes on flares.

#### 9.4.6 Flow Resistance through Straight Pipe

When a fluid flows through a straight section of pipe, the static pressure inside the pipe becomes smaller as the fluid flows downstream, often referred to as a pressure drop or head loss. The pressure loss is created by the friction between the pipe wall and the flowing fluid and results in a loss of energy available for work.



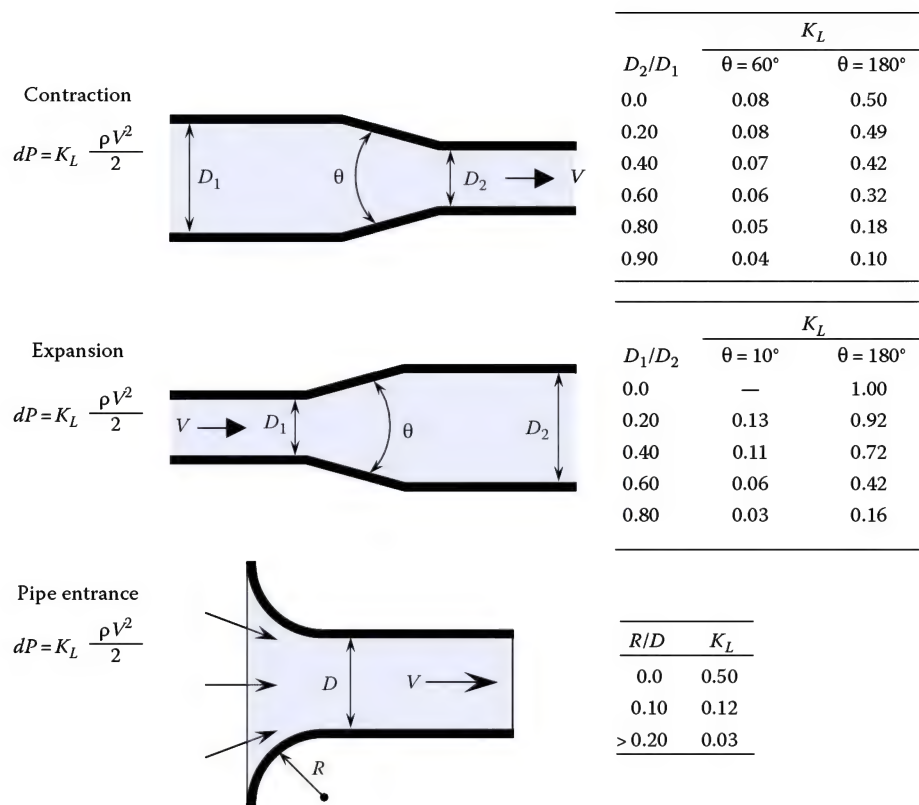


**FIGURE 9.15** Loss coefficients through various fittings. (From Roberson, J.A. and Crowe, T., *Engineering Fluid Mechanics*, Houghton Mifflin Company, Boston, MA, 1965.)

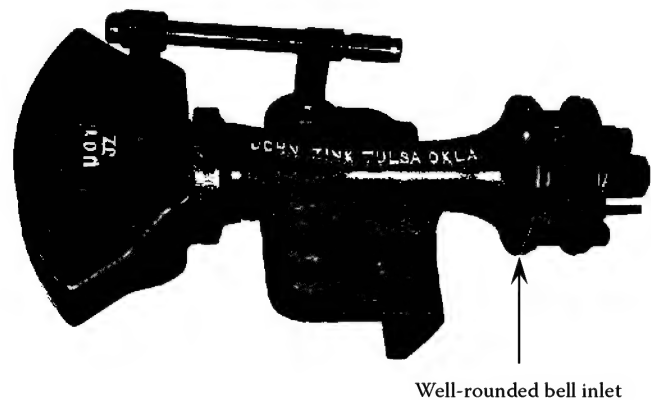


**FIGURE 9.16** Well-rounded bell inlet on a premixed burner.

Accurate estimates of pressure drop through straight pipe are important in the flare and burner industry because it has a significant impact on the design of the equipment. Several applications include the following:

1. Gas flow in flare stacks and headers
2. Steam flow in a pipe feeding steam-assisted flare tips
3. Air from a blower feeding air-assisted flare tips

4. Gas flow through burner manifold and riser pipes
5. Oil flow through pipes feeding atomizing guns

The pressure drop for a fully developed flow (implies the velocity profile does not change in the fluid flow direction) inside a pipe can be estimated using the Darcy–Weisbach equation (often referred to as the Darcy equation).

$$dP = f \times \underbrace{\frac{L}{D}}_{\text{Geometry of the pipe}} \times \underbrace{\frac{\rho V^2}{2}}_{\text{Velocity pressure of flowing fluid}} \quad (9.17)$$

where  
 $dP$  is the pressure drop  
 $f$  is a dimensionless number known as the Darcy *friction factor*  
 $L$  is the pipe length  
 $D$  is the inside pipe diameter  
 $\rho$  is the density of the fluid  
 $V$  is the average velocity of the fluid flowing inside the pipe

Nikuradse<sup>27</sup> carried out experiments to determine how the friction factor varies with flow rate and the roughness of the pipe wall. In his experiments, Nikuradse used artificially roughened pipes made by attaching

grains of sand of known size to the inside of a pipe wall.<sup>27</sup> Nikuradse's experiments revealed two important characteristics of flow through pipes. First, if the flow is laminar, the roughness of the pipe wall has no effect on the friction factor. Second, for turbulent flows, the friction factor depends only on two dimensionless parameters: the Reynolds number ( $Re$ ) and the *relative roughness* of the pipe. The relative roughness is defined as the ratio of the average height of the sand grains ( $\epsilon$ ) to the diameter of the pipe ( $D$ ). Although Nikuradse's artificially roughened pipe does not simulate the true roughness of commercially available pipe, it can be used to get a measure of the effective roughness. For example, Table 9.2 shows a list of various pipe material and surfaces corresponding to an equivalent sand grain roughness (size). It should be mentioned that the buildup of corrosion or scale on the inside of a pipe can significantly increase the roughness. Also, very old pipes can be so badly eroded on the inside that the effective inside diameter of the pipe is increased. Figure 9.17 is a plot showing how the friction factor ( $f$ ) varies as a function of Reynolds number ( $Re$ ) and relative roughness ( $\epsilon/D$ ). This plot is called the Moody chart or Moody diagram, in honor of L.F. Moody, who correlated Nikuradse's original data in terms of the relative roughness with commercial pipe material.

Notice for fully developed laminar flow in a pipe ( $Re < 2100$ ), the friction factor is independent of the relative roughness and can be simply written as

$$f = \frac{64}{Re} \quad (9.18)$$

**TABLE 9.2**

Equivalent Sand Grain Roughness ( $\epsilon$ ) for Various Pipe Material and Surfaces

Surface	Equivalent Sand Grain Roughness, $\epsilon$	
	(mm)	(ft)
Copper, lead, brass, aluminum (new)	0.001–0.002	$3.33 \times 10^{-6}$ – $6.7 \times 10^{-6}$
PVC and plastic pipes	0.0015–0.002	$0.5 \times 10^{-5}$ – $2.33 \times 10^{-5}$
Epoxy, vinyl ester, and isophthalic pipe	0.005	$1.7 \times 10^{-5}$
Stainless steel	0.015	$5 \times 10^{-5}$
Commercial steel pipe	0.045–0.09	$1.5 \times 10^{-4}$ – $3 \times 10^{-4}$
Rusted steel (corrosion)	0.15–4	$5 \times 10^{-4}$ – $133 \times 10^{-4}$
Galvanized steel	0.15	$5 \times 10^{-4}$
New cast iron	0.25–0.8	$8 \times 10^{-4}$ – $27 \times 10^{-4}$
Worn cast iron	0.8–1.5	$2.7 \times 10^{-3}$ – $5 \times 10^{-3}$
Rusty cast iron	1.5–2.5	$5 \times 10^{-3}$ – $8.3 \times 10^{-3}$
Smoothed cement	0.3	$1 \times 10^{-3}$
Ordinary concrete	0.3–1	$1 \times 10^{-3}$ – $3.33 \times 10^{-3}$
Coarse concrete	0.3–5	$1 \times 10^{-3}$ – $16.7 \times 10^{-3}$

Source: Adapted from Engineeringtoolbox.com, *Roughness & Surface Coefficients for Ventilation Ducts*, accessed 14 September 2012.

At moderate Reynolds numbers, however, the friction factor is a function of both the Reynolds number and the relative roughness of the pipe. For an extremely high Reynolds number, the curves become horizontal and are no longer a function of the Reynolds number as discovered by Nikuradse. For smooth pipe ( $\epsilon = 0$ ), the friction factor is not zero implying that no matter how smooth the inside surface of a pipe wall is, even if it is perfectly smooth, there will always be a head loss because the friction factor is greater than zero. On a microscopic level, a wall will always have a surface roughness and therefore, the relative roughness will always be greater than zero.

Several researchers have attempted to develop an analytical expression for the friction factor as a function of the Reynolds number and relative roughness. One well-known equation is the Colebrook–White formula:

$$\frac{1}{\sqrt{f}} = -2 \log_{10} \left( \frac{\epsilon/D}{3.7} + \frac{2.51}{Re \sqrt{f}} \right) \quad (9.19)$$

This formula is typically used to generate curves in the Moody diagram. The difficulty in using the Colebrook–White formula is that the solution is implicit; that is, in order to solve for the friction factor  $f$ , an iterative scheme must be used; this is not too difficult, however, if a computer is used. Swamee and Jain<sup>28</sup> developed a friction factor equation that can be solved explicitly:

$$f = \frac{0.25}{\log_{10} \left[ \left( \frac{\epsilon/D}{3.7} + \frac{5.74}{Re^{0.9}} \right) \right]^2} \quad (9.20)$$

This equation predicts friction factor values within 3% error from those on the Moody diagram for  $4000 < Re < 10^8$  and  $10^{-5} < \epsilon/D < 0.02$ .

In addition to circular pipe flows, these equations can also be utilized to analyze flows in non-circular pipe such as square, rectangular or triangular, for example. For pipe with no geometric variations with no obvious “diameter,” a concept termed the *hydraulic diameter* is useful. Essentially, it is the ratio of the flow area to the wetted perimeter, multiplied by four. In analytical form, this ratio is expressed as follows:

$$\text{Hydraulic diameter} = \frac{4 \times \text{Area}}{\text{Wetted perimeter}} \quad (9.21)$$

For circular pipes, the use of Equation 9.21 produces a hydraulic diameter equal to the diameter of the pipe. The previous equation provides reasonable accuracy for

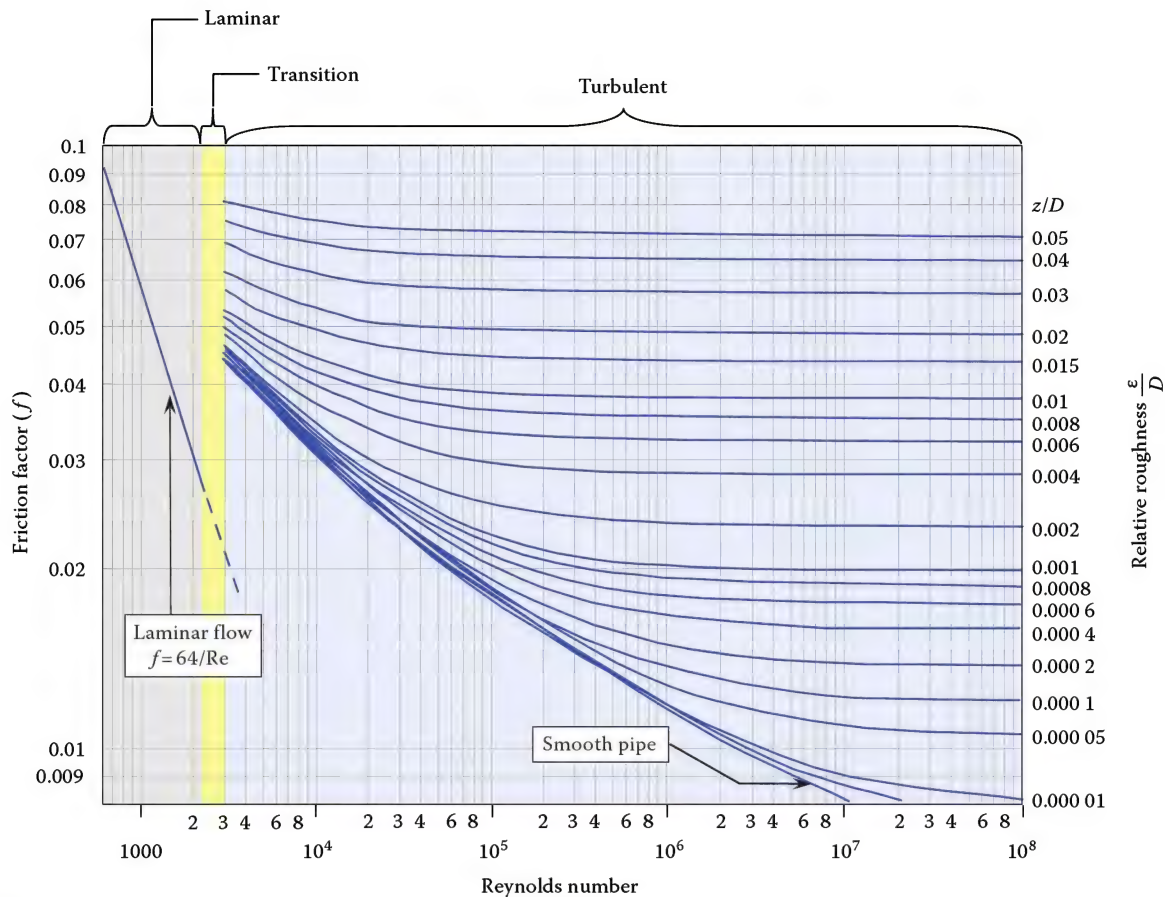


FIGURE 9.17

Moody diagram showing friction factor versus Re. (Adapted from Roberson, J.A. and Crowe, T., *Engineering Fluid Mechanics*, Houghton Mifflin Company, Boston, MA, 1965.)

calculations involving turbulent flow, but large errors will occur for laminar flow calculations. See Vennard and Street<sup>7</sup> for additional details.

## 9.5 Downwash

### 9.5.1 Over and around Flare Stacks

When a fluid flows past a cylinder, a low-pressure region is created on the backside (downwind side) as shown in the photograph in Figure 9.18. The strength of this low-pressure region depends largely on the velocity and density of the flowing stream; the higher the velocity and density, the stronger the low-pressure region.

When wind blows past a stack oriented in the vertical direction, the vented gas can be pulled toward the downwind side of the stack into the low-pressure region as shown in Figure 9.19. This photograph shows fluid flowing past a vertical, cylindrical stack

being tested in a laboratory. Notice that the yellow smoke venting from the stack is pulled into the low-pressure region and flows down the backside of the stack; this phenomenon is commonly referred to as *stack downwash*.

Stack downwash is common in industry. For example, Figure 9.20 shows steam issuing from a large stack. Notice the downwash on the downwind side of the stack. As winds strike a flare tip and stack, the low-pressure region on the backside can cause flames to downwash as shown in Figures 9.21 and 9.22; in the flare industry, this is commonly referred to as *flame pull down*. Pull down can cause flames to burn on the external surface of a flare tip and/or its appurtenances and is referred to as *external burning*.

External burning most commonly occurs at low to modest waste gas flow rates and under windy conditions. If the waste gas flow rate is high enough, the momentum of the exiting gas will overcome the low-pressure zone and produce an upward projecting flame as shown in Figure 9.23. However, at some lower gas flow rate, the waste gas is pulled into the low-pressure zone on the downwind side and burns adjacent



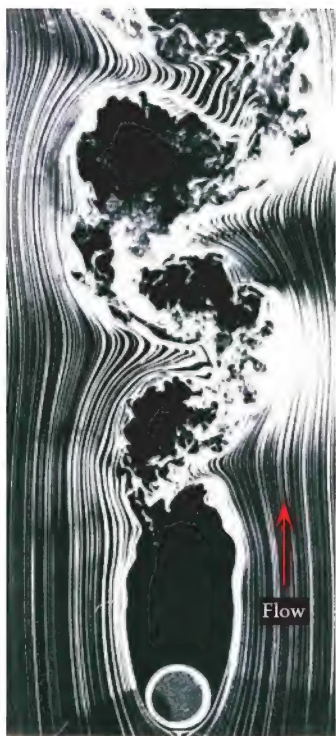


FIGURE 9.18

Flow past a cylinder at a Reynolds number of 10,000. (From Corke, T. and Nagib, H., *An Album of Fluid Motion*, The Parabolic Press, Stanford, CA, 1982, p. 97).

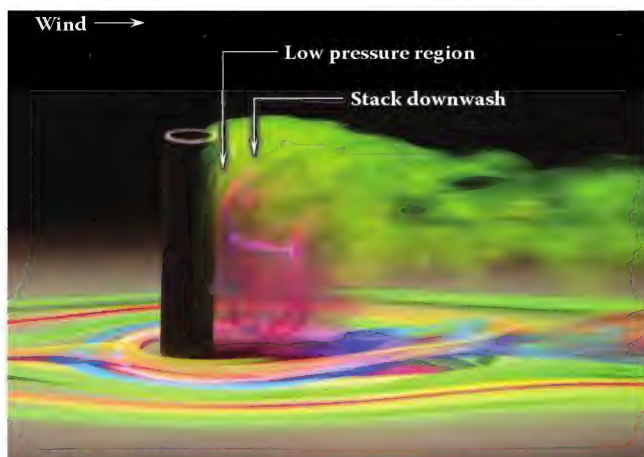


FIGURE 9.19

Stack downwash. (Photograph by Henry Werlé. Copyright ONERA—The French Aerospace Laboratory, Toulouse, France.)

to the flare tip. The depth of flame pull down varies largely with tip diameter, waste gas velocity, and wind velocity.

The American Petroleum Institute (API) 537 states that "...many flare burner material failures occur at low relief gas flow rates. At these low rates, the flare burner is most subjected to the detrimental effects of internally or externally attached flames."<sup>29</sup> When external burning

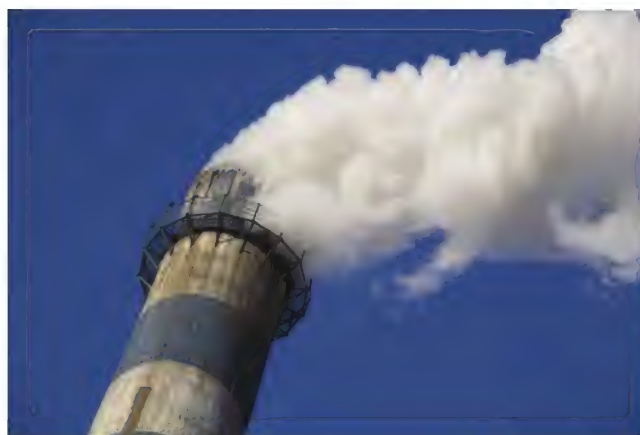


FIGURE 9.20

Steam washing down the downwind side of a stack. (From Dreamstime.)

occurs, the flare tip is exposed to high temperatures in a predominantly reducing atmosphere. These conditions are typically cyclic due to continuous changes in wind speed, direction, and gas flow rate and can severely damage a flare tip and/or its appurtenances as shown in Figure 9.24. Flare tip life can be improved by minimizing external flame impingement.<sup>30</sup>

### 9.5.2 Over Buildings

Figure 9.25 shows wind blowing past a small-scale building tested in a wind tunnel. The white streak-lines in the photograph are created by small particles released upstream and reveal the flow path of the fluid. Notice the large recirculation zone behind the structure; a similar flow pattern occurs over full-scale buildings.

If a vent stack or flare is located upwind of a building, as illustrated in Figure 9.26, the recirculation zone can cause the gas plume to be pulled in behind the building creating a downwash effect; this can drive the gas plume down the backside of the building substantially increasing ground level concentrations (GLCs). Although the flow pattern becomes more complicated for groups of building located close together, the downwash effect can still occur as demonstrated in Figure 9.27. This photograph shows wind blowing past two small-scale buildings tested in a wind tunnel. Notice the strong recirculation zone between the two structures.

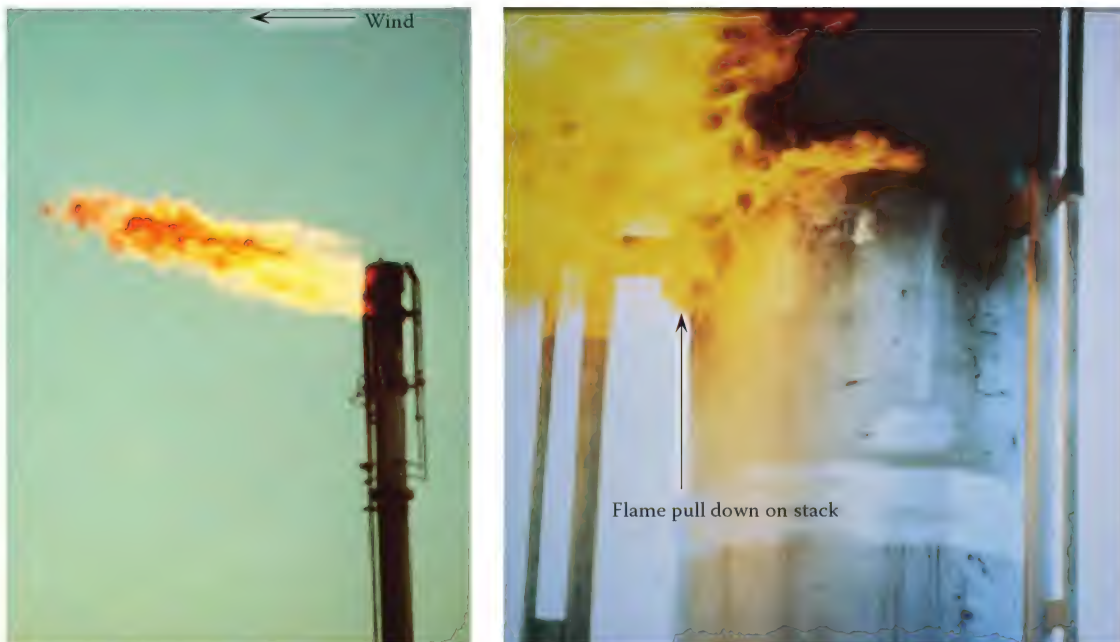
### 9.5.3 Over Terrain

Figure 9.28 shows a small-scale hill tested in a wind tunnel; notice the large recirculation zone on the downwind side. The recirculation zone can create a





**FIGURE 9.21**  
Flame pulled down on the outside of a flare tip due to stack downwash effect.



**FIGURE 9.22**  
Flame pulled down on the outside of a flare tip due to stack downwash effect (closer view).

downwash effect. For example, Figure 9.29 shows a volcano spewing smoke. Notice that the recirculation zone is washing the smoke down the backside of the volcano.

The downwash effect over terrain can play an important role when designing the height of a flare

stack. For example, imagine a community located on the downwind side of a mountain with a flare stack located at the top as illustrated in Figure 9.30. It is possible that if the height of the stack is short, the plume could be pulled down into the low-pressure region on the backside of the mountain resulting in



FIGURE 9.23  
An upward projecting flame.

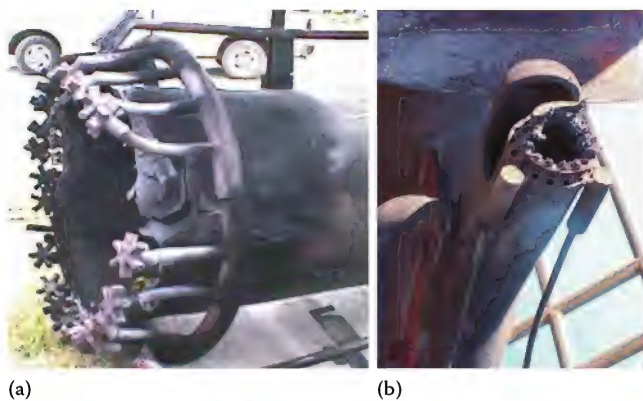


FIGURE 9.24  
Damaged flare tip and appurtenances caused by external burning: (a) flare tip, (b) flare pilot, and (c) steam manifold on flare.

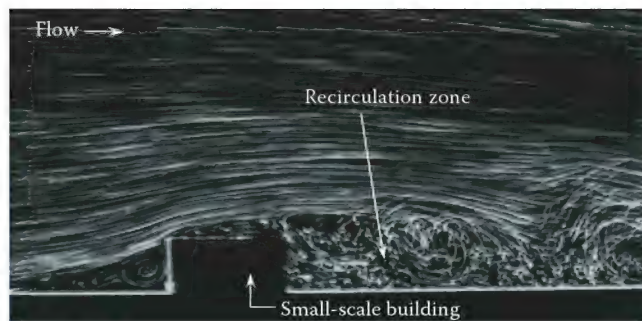


FIGURE 9.25  
Wind tunnel test showing flow past a small-scale building. (From ONERA photograph, Werlé, *An Album of Fluid Motion*, The Parabolic Press, Stanford, CA, 1982, p. 31.)

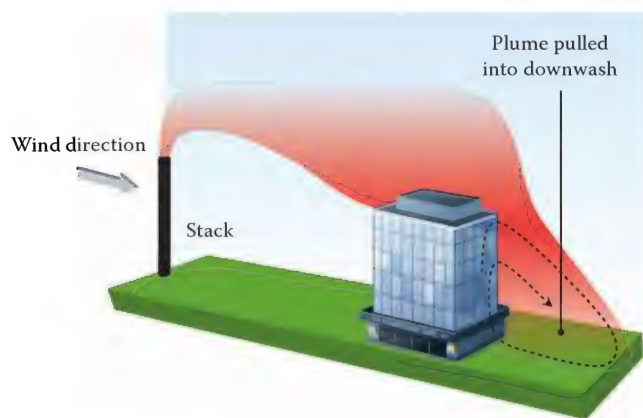


FIGURE 9.26  
Illustration showing a gas plume being pulled into the downwind side of a building.

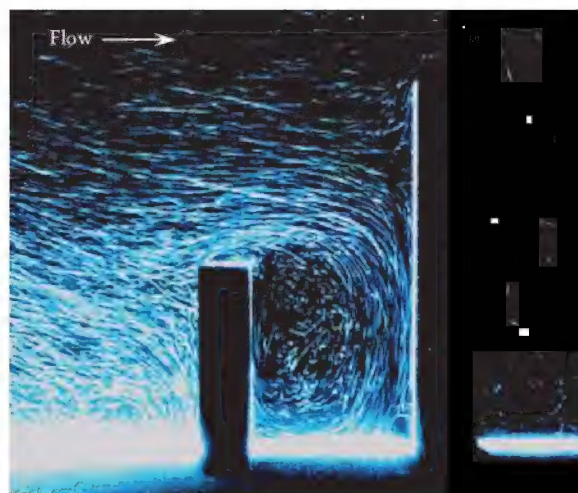
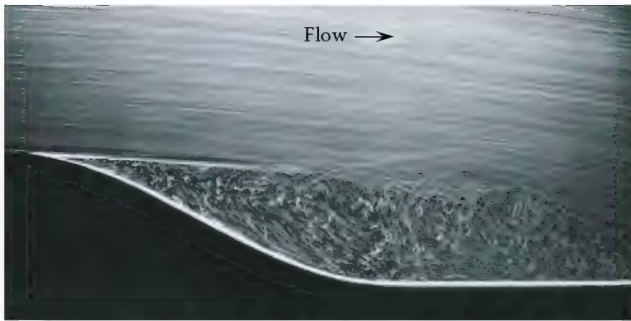
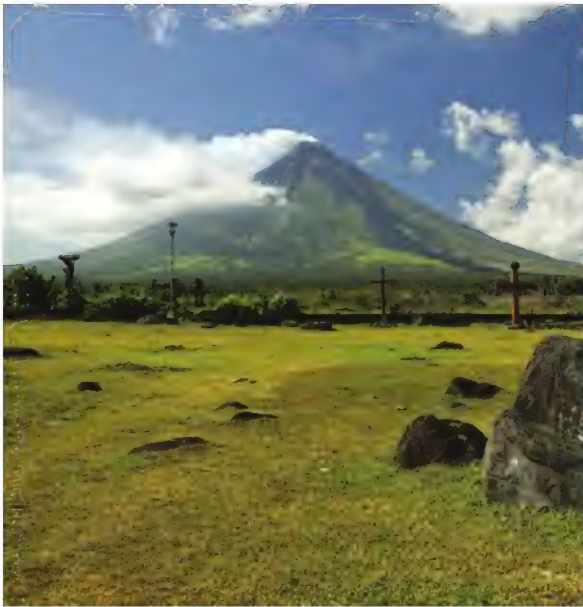


FIGURE 9.27  
Photograph showing recirculation pattern created between two small-scale buildings. (Photograph courtesy of Kato Lab. and Ooka Lab. IIS, the University of Tokyo, Tokyo, Japan.)



**FIGURE 9.28**

Photographs showing a recirculation pattern created on the downwind side of a small-scale hill located inside a wind tunnel. (From ONERA photograph, Werlé, *An Album of Fluid Motion*, The Parabolic Press, Stanford, CA, 1982, p. 27.)

**FIGURE 9.29**

Downwash on the backside of a volcano (Mount Mayon, Philippines) bellowing steam and ash. (Courtesy of Dreamstime.)

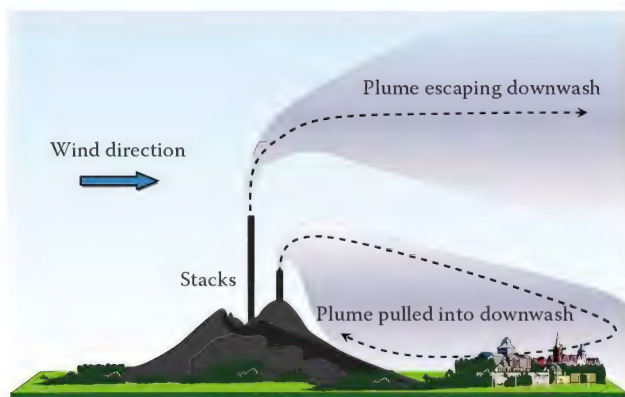
**FIGURE 9.30**

Illustration showing the effect of stack height on the plume downwind of a mountain.

high concentrations of combustion products within the community. However, if the stack height is tall enough, the plume flows over the top of the low-pressure region and the community may not be affected by flare operations.

## 9.6 Flare Tip Internal Burning

Internal burning occurs when air infiltrates into a flare system, mixes with the waste gas, and burns on the interior surface of the tip as shown in Figure 9.31. Internal burning is the most prominent mechanism responsible for the failure of a flare tip. Buoyancy effects and wind action are two common ways air infiltrates into flare tips.

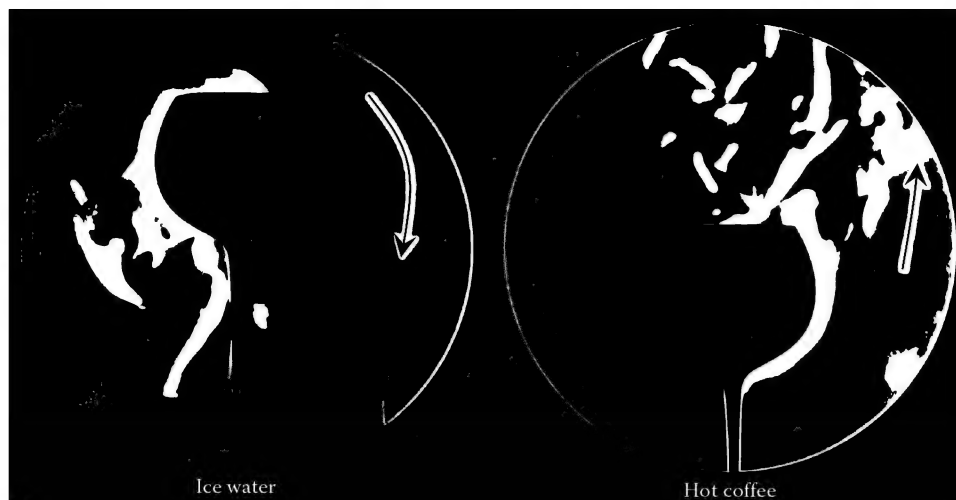
### 9.6.1 Buoyancy Effects

Figure 9.32 shows Schlieren photographs revealing the flow pattern of air around a cup filled with hot coffee and another filled with ice water. Notice that as the air comes in contact with the hot cup, it heats and becomes lighter than the surrounding air causing it to become buoyant and rise. As the air comes in contact with the cold cup, however, the air cools, becomes heavier than the surrounding air and falls. Buoyancy of gases plays a key role in air migration into a flare tip.

When flaring lighter-than-air waste gas at low flow rates, ambient air will tend to migrate into the flare tip since it is heavier than the gas inside the flare. As the air falls into the tip, it mixes with the waste gas and forms a flammable mixture inside as illustrated in Figure 9.33. When this flammable mixture is ignited by the flare pilots, internal burning occurs.

**FIGURE 9.31**

Internal burning inside a steam-assisted flare tip.

**FIGURE 9.32**

Schlieren photographs showing airflow patterns near a cup filled with hot coffee and another filled with ice water. (Photograph courtesy of Professor Andrew Davidhazy.)

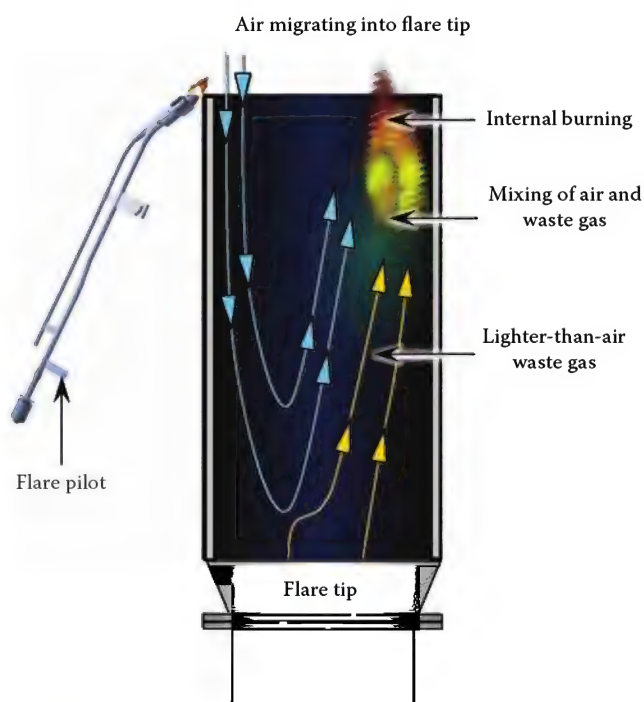
**FIGURE 9.33**

Illustration showing air falling into a flare tip creating internal burning.

### 9.6.2 Wind Action

The extent of internal burning can be compounded by the action of wind. As wind blows past the tip, it can generate an internal re-circulation pattern near the outlet of the flare tip similar to the photograph shown in Figure 9.34. This re-circulation zone promotes air migration and mixing inside the tip. When a flammable air-fuel mixture forms, the flare pilots ignite the mixture causing internal burning (Figure 9.35). The

**FIGURE 9.34**

Flow past a cavity. (From Taneda, *An Album of Fluid Motion*, The Parabolic Press, Stanford, CA, 1982, p. 15.)

penetration depth and intensity of the internal flame typically becomes more severe with larger tip diameters and higher wind speeds.

## 9.7 Gas Dispersion from an Elevated Flare

If a flare does not properly dispose of a pollutant such as a toxic, corrosive, or flammable vapor, it could pose a serious health hazard to personnel in the area and surrounding



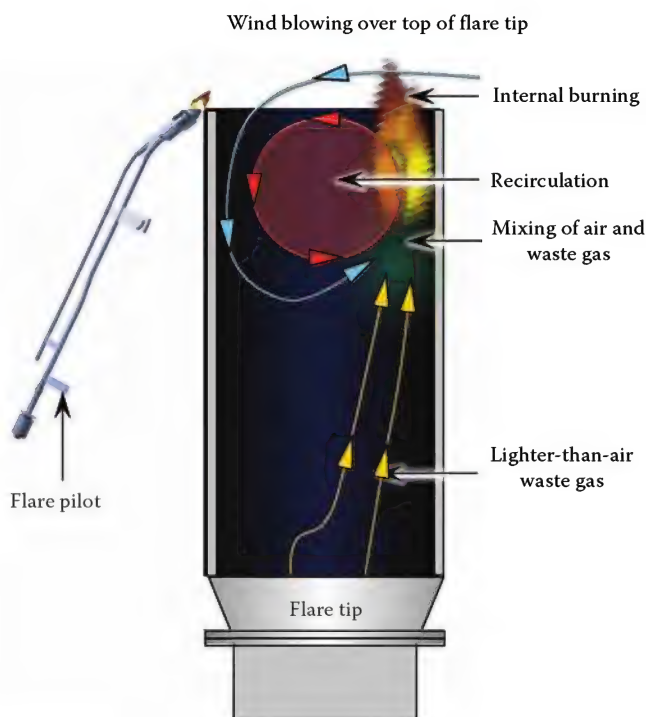


**FIGURE 9.35**  
Illustration showing internal burning by action of wind.

communities. The purpose of this section is to discuss methods used to estimate GLCs and describe several important factors that influence how a pollutant, emitted from an elevated flare, disperses into the atmosphere.

### 9.7.1 Atmospheric Dispersion Modeling

Consider the following scenario: An industrial plant has an upset condition. In order to prevent overpressurizing process equipment, gas is diverted to an elevated flare at a rate of several-million pounds per hour. During the flaring event, the flow rate of the gas dramatically exceeds the design flow rate of the flare causing the flare to not properly combust all of the waste gas. Assume that the vented flare gas contains some hydrogen sulfide ( $H_2S$ ) and that a community is located directly downwind of the flare stack. As the unburned gas from the flare is carried by the wind toward the community, it mixes with the ambient air and becomes less concentrated. Hydrogen sulfide is a colorless, flammable gas with a characteristic rotten egg odor. It takes only a concentration of about 4.7 ppb (parts per billion) of  $H_2S$  in air for humans to smell. At a concentration of only 150 ppm (parts per million), we can no longer smell the odor because we become desensitized after a few breathes. When our nose becomes desensitized to the odor, the situation can become seriously dangerous because a concentration level of only 320 ppm can lead

to death. At a concentration of 800 ppm, death can occur in about 5 min. The outcome of this scenario depends on many factors such as the ambient wind conditions, type of terrain, flow rate of pollutants, velocity of pollutants out of the flare tip, and height of the flare stack, just to name a few. Dispersion modeling can provide valuable information to help determine (1) protective actions in the event of a release, (2) location of impacted areas, and (3) GLCs of pollutants.<sup>31</sup> Dispersion of air pollutants can be modeled experimentally or mathematically.

Experiments using wind tunnels can be a very useful tool to model pollutant dispersion. Testing requires a scaled-down model to be built inside a wind tunnel as shown in Figure 9.36. The main objective of using wind tunnel testing is to reproduce the important characteristics of the atmospheric boundary layer and the resulting dispersion patterns of pollutants at a small scale.<sup>32</sup>

Figure 9.37 shows a wind tunnel test analyzing the gas plume downstream of the vent stack. In order to get meaningful results, the experimentalist must have the right flow measurement equipment and design the experiment to take into account the atmospheric turbulence and appropriate scaling parameters. This analysis requires someone skilled in the art to properly design the model and interpret the results.

Mathematical modeling of stack gas dispersion began in the 1930s. Earlier models were somewhat simplified; however, with the advent of computers, these models have become more sophisticated and able to capture much more detail of the dispersion problem. There are many models available in the marketplace. Some of the more complex models require several days or even weeks of computational time using today's most sophisticated high-speed computers. They also require



**FIGURE 9.36**  
A view looking inside a wind tunnel showing a small-scale model. (Photograph courtesy of CPP, Inc., Wind Engineering consultants, Fort Collins, CO.)



**FIGURE 9.37**  
Scale model wind tunnel test analyzing the gas plume downstream of a vent stack. (Photograph courtesy of CPP, Inc., Wind Engineering consultants, Fort Collins, CO.)

someone skilled in the art to perform the analysis and interpret the results (see Chapter 13).

### 9.7.2 Major Factors Affecting GLC

In 2008, a volcano erupted in Chile sending a cloud of smoke and ash into the air. The wind carried the pollutant across Argentina and into the Atlantic Ocean as shown in the satellite photograph in Figure 9.38. Notice as the smoke moves downwind, it slowly disperses and becomes less concentrated. In general, the concentration of the pollutant at ground level depends on two factors: (1) the height of the plume above the ground and (2) how fast the plume spreads in the direction perpendicular to the wind.

Figure 9.39 shows a buoyant plume dispersing downwind. The dispersion of the pollutant is largely attributed to the turbulence in the atmosphere; molecular diffusion also contributes, but to a much lesser extent. If the maximum concentration of a buoyant plume were mapped downwind, the curve would ideally look similar to the one illustrated in Figure 9.40. That is,

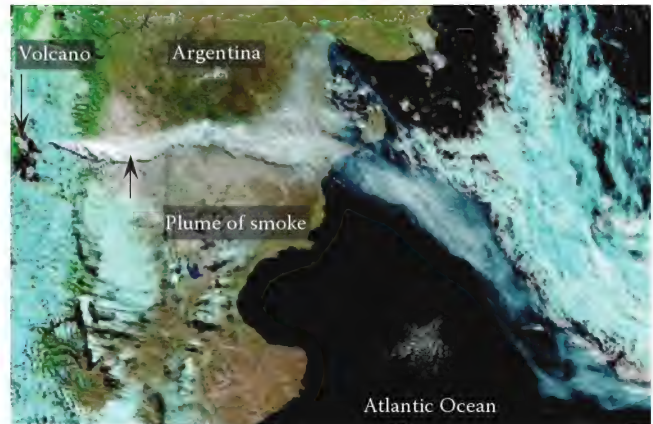


**FIGURE 9.38**  
Satellite photograph showing the plume of smoke and ash from a volcano. (From NASA, Washington, DC.)



**FIGURE 9.39**  
Smoke venting from a stack and dispersing downwind. (From Dreamstime.)

the line of maximum pollutant concentration would initially curve in the downwind direction and then eventually level off, horizontally, at a location further downwind. The distance from the horizontal line of maximum concentration to the exit of the stack exit is referred to as the *plume rise*. Plume rise can have a significant impact on the GLC. For instance, under identical ambient conditions and flat terrain, a short plume rise results in higher GLC as compared to one with a higher plume rises.

The velocity of the gas out of the stack can have a significant impact on the plume rise. Higher stack exit velocities result in more vertical momentum increasing



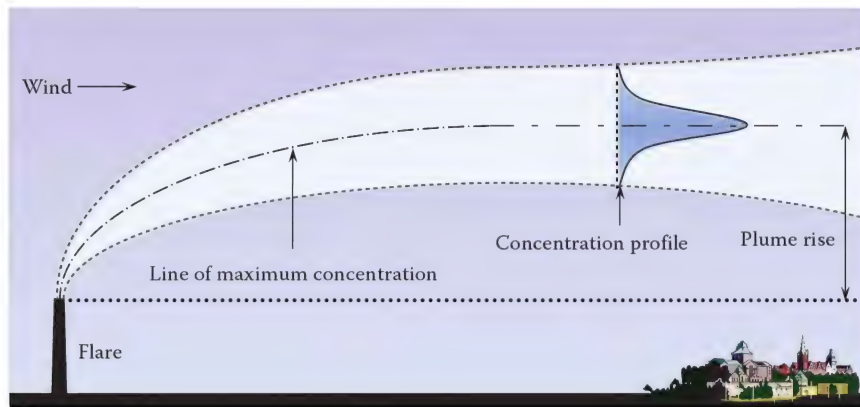


FIGURE 9.40

Illustration defining the plume rise of a buoyant gas vented from a stack.

the plume rise. Ambient wind speed also plays a significant role in the plume rise; high wind speeds tend to bend the plume at a faster rate in the horizontal direction, reducing the plume rise. The density of the waste gas is also important. A lighter gas will tend to have a higher plume rise as compared to a heavier gas. Figure 9.41 shows photographs with examples of vented stacks demonstrating various plume rises.

Probably the most obvious factor affecting GLC is the height of the flare stack. In general, a taller stack will allow the vented gas plume more time and distance to mix with the atmospheric air before reaching the ground, resulting in lower GLCs of pollutants. In the flare industry, the height of a flare stack is typically determined based on thermal radiation levels emitted from the flare flame. In some instances, however, the stack height is determined based on estimates of GLC using dispersion models.

Atmospheric turbulence also has a big impact on how fast a gas plume will disperse. There are many variables that can influence atmospheric turbulence, but two key factors are (1) time of day and (2) type of terrain. During the day, radiation from the sun heats the surface of the earth. The heat absorbed by the ground is transferred to the air causing it to rise. The rising warm air then causes the cooler air above to fall toward the ground; this is referred to as an *inversion*. An inversion creates a lot of turbulence in the atmosphere and is referred to as a *highly unstable atmosphere*. During the nighttime, however, the opposite phenomena can occur. At night, the surface of the earth cools allowing the cold air to remain near the ground and the warmer air to remain overhead. These atmospheric conditions produce little turbulence and are referred to as a *stable atmosphere*. Under stable atmospheric conditions, a plume of gas will disperse more slowly. For example, Figure 9.42 show photographs of a vented stack under different atmospheric conditions. The upper photograph shows



(a)

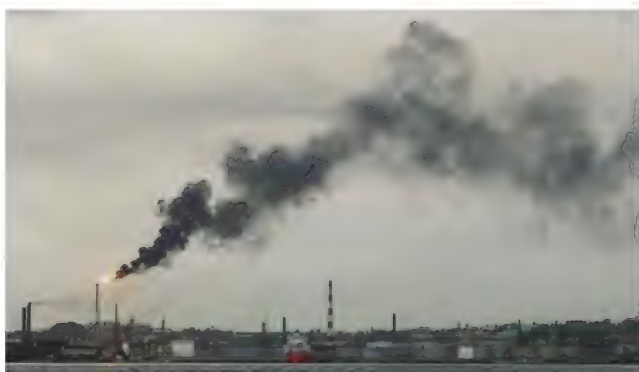


(b)

FIGURE 9.41

(a) Vent stack with a low plume rise and (b) vent stack with high plume rise. (From Dreamstime.)

smoke emitted from a flare quickly dissipating downwind indicating high levels of atmospheric turbulence. However, the lower photograph shows a plume of gas slowly dispersing into the atmosphere indicating a much more stable atmosphere.



(a)



(b)

**FIGURE 9.42**

(a) Smoke dissipating in an unstable atmosphere (high turbulence) and (b) smoke dissipating in a stable atmosphere (low turbulence). (From Dreamstime.)

During stable wind conditions, heavier-than-air gas exiting a stack can descend to the ground fairly rapidly with little dispersion as shown in Figure 9.43. When this situation occurs, the gas can travel a great distance near the ground and remain highly concentrated. If the gas is flammable, it could come in contact with an ignition source creating an explosion.

Atmospheric turbulence can also be impacted by the type of terrain. For example, wind blowing past

**FIGURE 9.43**

Heavier-than-air plume vented from a stack in a stable atmosphere. (Photograph courtesy of Jean-Marc Duyckaerts.)

buildings, trees, hills, or rough terrain generates additional atmospheric turbulence that can increase the dispersion rate of a gas plume. However, wind blowing over a grass plain or the surface of calm water generates significantly less atmospheric turbulence reducing dispersion rates of pollutants.

The variables just discussed are a few that can influence GLC. There are many other variables that can also affect GLC such as (1) time varying flow rate of the flare gas, (2) time varying wind speeds, (3) gas condensation, and (4) velocity profile of the wind. For more information refer to Turner,<sup>33</sup> Moses,<sup>34</sup> Seigneur,<sup>35</sup> and Barratt.<sup>36</sup>

## 9.8 Heater Draft

### 9.8.1 Background

The difference between the pressure inside the heater and atmospheric pressure, at a given elevation, is called heater *draft*. Draft is not constant throughout a heater, but changes with elevation as illustrated in Figure 9.44. Notice in this example that the pressure inside the heater is less than the atmospheric pressure at every elevation. If the pressure inside the heater is less than the atmospheric pressure, the heater is said to be operating at a *negative* pressure (vacuum); if the pressure inside the heater is greater than the atmospheric pressure, the heater is said to be operating at a *positive* pressure.<sup>37</sup>

Heaters used in the refining/petrochemical industries are designed to operate at a negative pressure; that is, the pressure throughout the entire heater is always lower than the atmospheric pressure. If a heater operates at a positive pressure, it can cause hot flue gases or flame to exit the heater through leaks and open sight ports, which can cause serious structural damage to the heater and is a safety concern to personnel working in the area. On the other hand, if the heater is operating at too negative of a pressure, it could create other problems. For example, additional air entering through leaks in the heater can reduce heater efficiency. Therefore, it is important that the draft inside a heater be properly controlled (see Volume 2).

The dynamics associated with heater draft can be a challenging subject matter to fully appreciate and understand. The purpose of this section is to present the reader with an explanation of how draft is created and why it varies with elevation inside a heater using basic fluid dynamic principles coupled with several illustrations. This section will also cover (1) the various techniques used in industry to supply process heaters with combustion air, (2) the proper locations to measure draft, (3) the instrumentation commonly used to



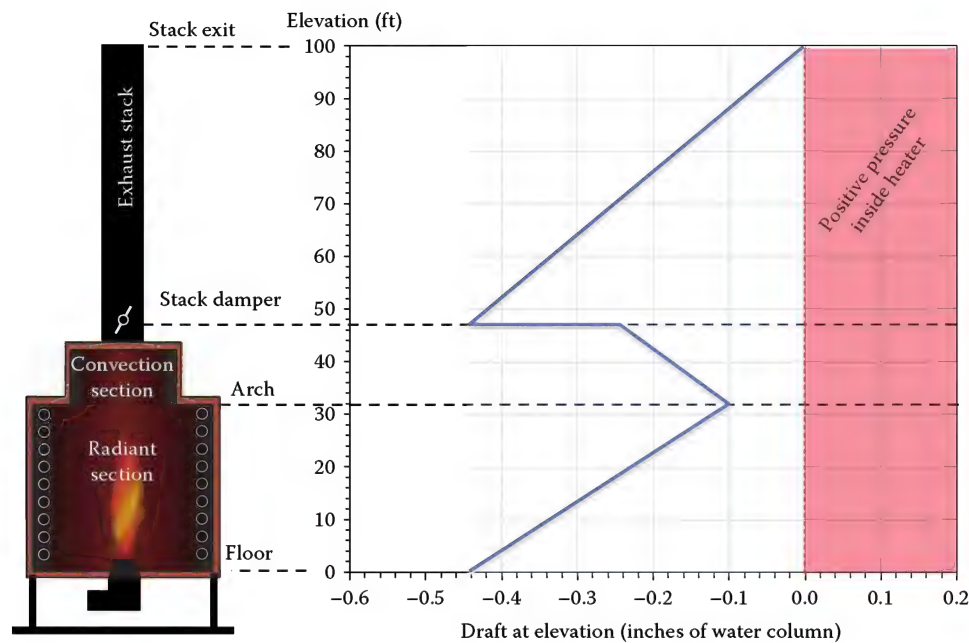


FIGURE 9.44

Illustration showing how the heater draft typically varies inside a heater at various elevations.

measure draft, (4) the problems associated with not maintaining a proper draft, and (5) the effects of ambient wind on heater draft.

### 9.8.2 Draft Systems

Heaters require a continuous supply of air for combustion. Combustion air can be supplied by means of a

*mechanical-draft* system or *natural-draft* system as illustrated in Figure 9.45. Mechanical-draft systems use man-made devices such as fans or blowers to supply air into the heater. In natural-draft systems, the airflow is produced by a driving force (draft) created by the difference in density of the hot flue gas inside the heater and the ambient air.<sup>38</sup> Heaters that use this technique are called *natural-draft heaters*.

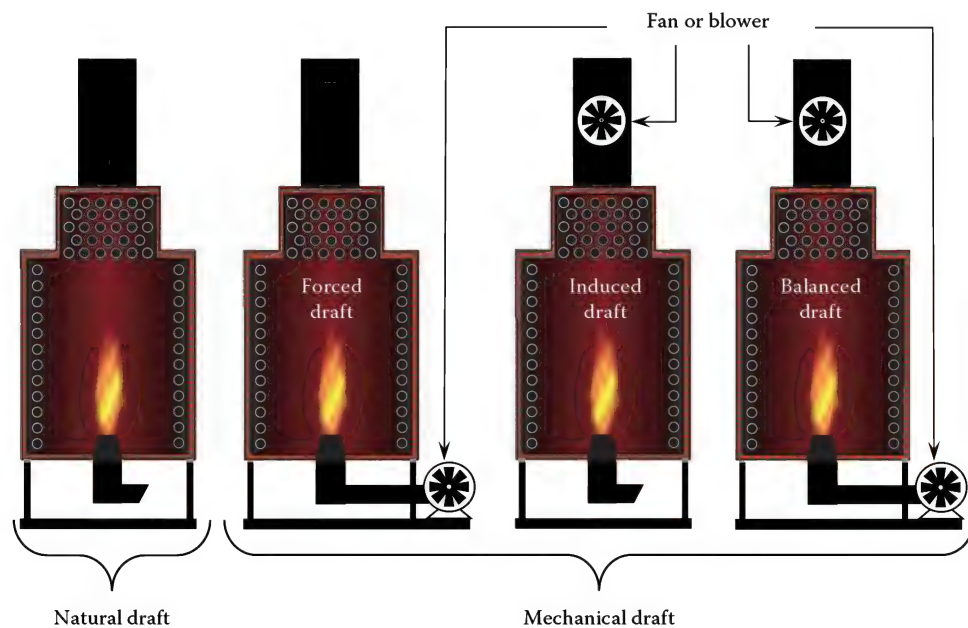


FIGURE 9.45

Four methods air is commonly supplied in process heaters.

### 9.8.2.1 Natural-Draft Heaters

Natural-draft heaters are the most common type of heater used in the process industry. An advantage of natural-draft heaters, compared to mechanical-draft heaters is that no fans are needed as a driving force to deliver the air for combustion; therefore, no capital cost is required to install the fan and ductwork, no electrical cost to operate fans, less noise, and obviously, they are not subject to fan failure (i.e., circuit breakers, bearings, blades, etc.). Natural-draft systems, however, can have several disadvantages compared to mechanical-draft systems: (1) size of burners are larger, (2) heater excess  $O_2$  (a measure of heater efficiency) is more affected by ambient wind, (3) air control requires manual adjustment of individual burner dampers, (4) heat recuperation cannot be used, (5) exhaust stack is relatively long, and (6) heater excess  $O_2$  can be significantly affected by large swings in ambient air temperature and humidity.

Natural-draft burners are usually larger in physical size than mechanically forced draft burners because they typically do not have as much air-side pressure drop available across the burner. Larger size burners can create problems in some instances where available space is limited. Also, larger burners are usually heavier and in some cases, the added weight can create structural issues.

Natural-draft burners typically operate with an air-side pressure drop of less than 1 in. WC across the burner; however, mechanically forced draft burners typically operate with an air-side pressure drop in the range of 2–10 in. of WC. Since natural-draft heaters do not have as much air-side pressure drop available across the burner as mechanically forced draft burners, the flames tend to be longer and have less momentum (lazier flame). Although longer, lazier flames tend to be more prone to impinge on process tubes, they can provide a more even heat distribution within the radiant section, which can improve process throughput. Longer flames also have a tendency to produce lower  $NO_x$  emissions than shorter flames.

Ambient winds can change the pressure at the burner intake and at the exit of the exhaust stack, which can impact heater draft levels resulting in swings in excess  $O_2$ . Since natural-draft heaters are open to the atmosphere at both the exit of the exhaust stack and burner inlet, they are more susceptible to wind effects than mechanical-draft heaters. In locations where high winds are common, devices have been added to the top of exhaust stacks to help mitigate wind effects. Also, wind fences have been erected around the perimeter of some natural-draft heaters to help reduce the high velocity wind sweeping beneath the heater.<sup>39</sup>

Changes in ambient air temperature can have a significant impact on the excess  $O_2$  in a heater. As the

temperature of the ambient air changes, its density also changes. If a burner, operating at a given draft, experiences an increase in air density due to a decrease in temperature, it will pull more combustion air into the heater on a mass basis, resulting in higher excess  $O_2$ ; conversely, as the air temperature increases, excess  $O_2$  decreases. In some locations, like in the Middle East, air temperatures can vary by more than 80°F (26.7°C) in a single day. This can cause dramatic swings in excess  $O_2$ . Heater excess  $O_2$  can also be affected by the relative humidity of the ambient air. When the moisture in the air increases, the excess  $O_2$  drops because part of the combustion air is displaced by the water vapor. When excess  $O_2$  varies in a natural-draft heater, operators must manually adjust the dampers on individual burners to correct the  $O_2$ . Mechanical-draft heaters, however, can allow operators to make  $O_2$  adjustments from a control room.

### 9.8.2.2 Mechanical-Draft Heaters

There are three types of mechanical-draft heater designs: *forced-draft*, *induced-draft*, and *balanced-draft*. Forced-draft heaters use a fan (see Volume 2, Chapter 3), located upstream of the burner inlet, to pump air through the burner and into the heater. A primary advantage of this technique is that a heat recuperation system can be utilized to improve heater efficiency. Compared to natural-draft heaters, forced-draft heaters also allow operators to better control and maintain the combustion airflow, which further helps improve heater efficiency. Another advantage is that a higher air-side pressure drop across the burners can be utilized; this can be beneficial in some applications because it allows for relatively smaller, lighter weight burner designs. Several disadvantages of forced-draft systems include (1) higher capital cost to install the fan and ductwork, (2) higher electrical cost to operate the fan, (3) higher noise levels, and (4) fan maintenance issues. After-treatment for  $NO_x$  abatement (such as selective catalytic reduction) could be used on these systems, but it would create a positive pressure within the firebox, which has several disadvantages (discussed later in this section).

In the induced-draft heater, air is drawn through the burners and into the heater using a fan located in the exhaust stack. Similar to forced-draft heaters, induced-draft heaters can be designed with heat recuperation to improve heater efficiency. However, the cost (initial, operating and maintenance) of a “hot” (flue gas) fan is more than the cost of a “cold” (ambient) fan. Induced-draft heaters also allow for the design of shorter exhaust stack heights; this can be beneficial on heaters that have large convection sections that require a large pressure drop such as in some ethylene cracking furnaces. Induced-draft heaters also allow better control of excess air (using a variable speed drive) as compared to the natural-draft heaters. These heaters can also be designed

with after-treatment systems for  $\text{NO}_x$  abatement. Several disadvantages of this technique are (1) higher capital cost to install the hot fan, (2) higher electrical cost to operate the fan, (3) higher noise levels, (4) larger burner required as compared to forced-draft system, (5) heater draft can be affected by high winds blowing past burner intake, (6) burner air control requires individual adjustment, and (7) fan maintenance issues.

In the balanced-draft heater, air is forced into the heater with a fan located upstream of the burner and assisted by an induced draft fan (ID fan) located in the exhaust stack. The FD fan overcomes the pressure drop through the combustion air ductwork and burner while the ID fan overcomes the pressure drop through the exhaust gas section of the heater. Balanced-draft heaters are the most complex of the four types of heater designs because they need sophisticated systems to control airflow rates and heater draft. The advantages of using balanced-draft systems are that (1) smaller burners can be used, (2) heater draft is not significantly affected by high winds because the burner intake and

exhaust stack are isolated, (3) burner air control does not require individual adjustment, (4) heat recuperation can be used, (5) exhaust stacks can be designed shorter, and (6) after-treatment systems for  $\text{NO}_x$  abatement can be used. Several disadvantages with this technique are (1) higher capital cost to install the fans, (2) higher electrical cost to operate fans, (3) higher noise levels, and (4) fan maintenance issues. A summary of the advantages and disadvantages of each draft method discussed are summarized in Table 9.3.

### 9.8.3 Fundamental Concepts of Draft

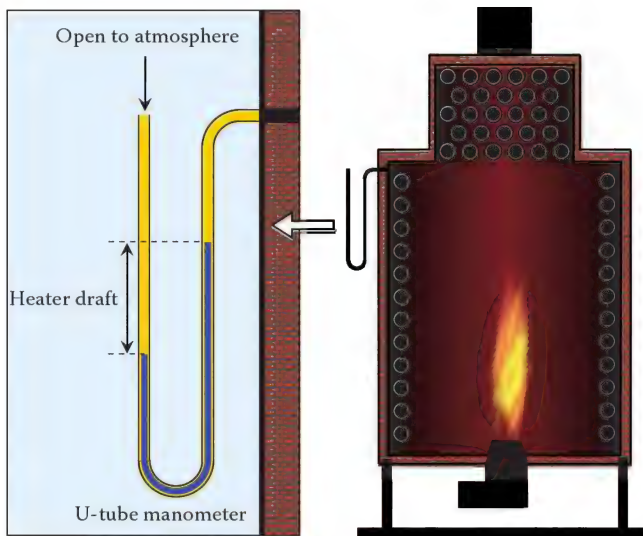
As mentioned, furnace draft is defined as the pressure inside of the heater minus the pressure outside of the heater measured at the same elevation. For example, consider a tube shaped in the form of a "U" that is partially filled with water (referred to as a U-tube manometer). If both ends of the U-tube are open to the atmosphere, the water will equalize to the same level in each arm of the tube. Now, suppose one arm of the U-tube is connected to

TABLE 9.3

Advantages and Disadvantages of Each Draft Technique

Parameter	Natural Draft	Forced Draft	Induced Draft	Balanced Draft
Capital cost	None	Fan and ductwork	Fan	Fans and ductwork
Electricity cost	No	Yes	Yes	Yes
Noise	Less	More	More	More
Flame height	Longer	Shorter	Longer	Shorter
Burner size	Bigger	Smaller	Bigger	Smaller
Wind affected	Burner and stack	Stack	Burner	No
Burner air control	Individual	Multiple	Individual	Multiple
Heat recuperation	No	Yes	Yes	Yes
Stack height	Longer	Shorter	Shorter	Shorter
Subject to fan failure	No	Yes	Yes	Yes
Ambient temp. swings	Yes	No	No	No
Process swing concerns	Yes	No	No	No
After-treatment	No	Yes	Yes	Yes





**FIGURE 9.46**  
Illustration showing a U-tube manometer connected to the side of a natural draft heater.

a port on the side of a heater while the other is left open to the atmosphere as illustrated in Figure 9.46. How would the water inside the tube react? If the pressure inside of the heater is less than the atmospheric pressure outside the heater, then one would expect the water to travel up the tube in the arm that is connected to the heater. The difference in height of the two water columns is a measure of the heater draft at that particular elevation. For example, if the difference in the two columns of water is 1/2 in., the heater draft is  $-0.5$  in. of water column; typically written

as inches WC or inches  $H_2O$ . If the draft is written with a negative sign ( $-$ ), it implies that the pressure inside the furnace is lower than the atmospheric pressure while a positive sign ( $+$ ) indicates the opposite. A useful conversion to keep in mind is that  $1 \text{ psi} = 27.68 \text{ in. WC}$ . This implies that if a pressure of  $1 \text{ psig}$  is applied to one arm of a U-tube manometer while the other arm is open to the atmosphere, one would measure a difference of  $27.68 \text{ in.}$  between the two columns of water.

Understanding how the pressure varies inside a natural draft heater requires one to be somewhat familiar with a few basic fluid dynamic concepts. These concepts are discussed in detail next.

First, consider how the atmospheric pressure on earth varies with elevation. The atmospheric pressure on earth comes from the weight of all of the air above us. The earth is surrounded by a layer of air (atmosphere) which is about 300 miles thick and weighs about  $11 \times 10^{18} \text{ lb}_m$ .<sup>40</sup> Since we live at the bottom of this layer of air, we are subjected to the pressure that it exerts upon us. At sea level, the average pressure exerted by the atmosphere is  $14.696 \text{ psi}$  ( $101.325 \text{ kPa}$  or  $406.8 \text{ in. WC}$ ). As one moves to elevations above sea level, the atmospheric pressure decreases because there is less mass of air overhead and therefore less pressure. This pressure variation is similar to what one experiences when swimming underwater; the deeper one dives, the greater the hydrostatic pressure experienced due to the increase in the weight of water overhead.

Figure 9.47 is a plot showing the U.S. standard for atmospheric pressure at different elevations.<sup>42</sup> Notice at sea level the atmospheric pressure is  $14.696 \text{ psi}$  while in

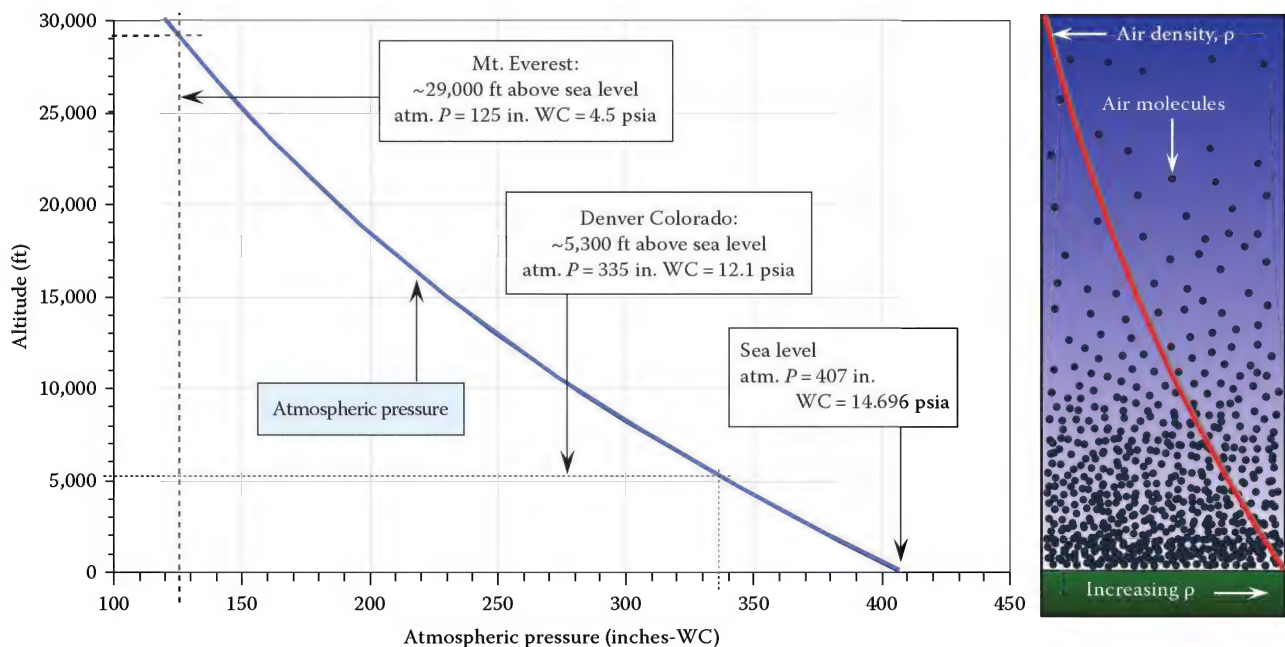


**FIGURE 9.47**  
U.S. standard for variation of atmospheric pressure with elevation.



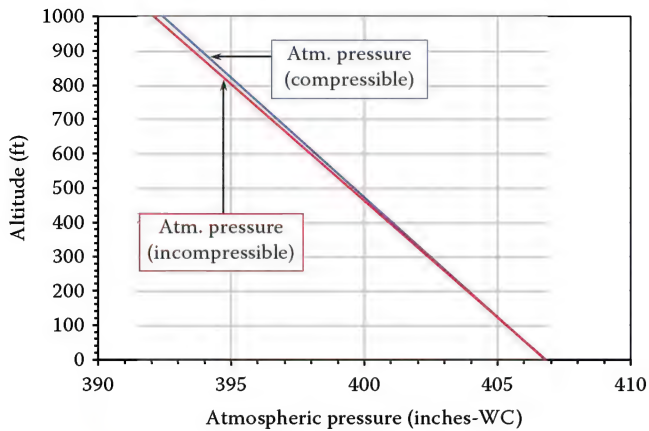


FIGURE 9.48

Plot showing that the atmospheric pressure is approximately linear at altitudes less than about 500 ft (150 m).

Denver Colorado, which is located about 1 mile above sea level (~5300 ft), the atmospheric pressure is only 12.1 psia (335 in. WC). In comparison, the highest point on earth is the top of Mt. Everest at 29,028 ft above sea level; here, the atmospheric pressure is about 4.5 psia. Also notice that the atmospheric pressure versus altitude is not a straight line, but rather a curve. The reason the line is not straight is due to compressibility effects. At lower altitudes, the additional weight of air overhead causes it to compress and become denser than the air above; the denser the air, the more sensitive the atmospheric pressure becomes with variations in altitude. At elevations ranging from sea level to about 500 ft (150 m) above sea level the atmospheric pressure varies almost linearly (Figure 9.48) and can be approximated by an equation that assumes the air is incompressible:

$$P (\text{in.WC}) = \left[ 14.696 - \frac{0.0765 \times H(\text{ft})}{144} \right] 27.68 \quad (9.22)$$

where

$P$  is the atmospheric pressure in units of inches of water column

$H$  is the altitude in units of feet

For simplicity, the draft inside of a stack will be used as a basis for initial discussion. Consider two identical stacks with the base of each stack located at sea level as illustrated in Figure 9.49. Assume that one of the stacks contains air at the same temperature as the surrounding ambient air (cool stack) while the other stack contains hot air (hot stack). Also, assume that the air inside both stacks is at rest (static). Since the density of the air inside the cool stack is the same as the surrounding ambient air, the pressure at different elevations within this stack must be identical to the

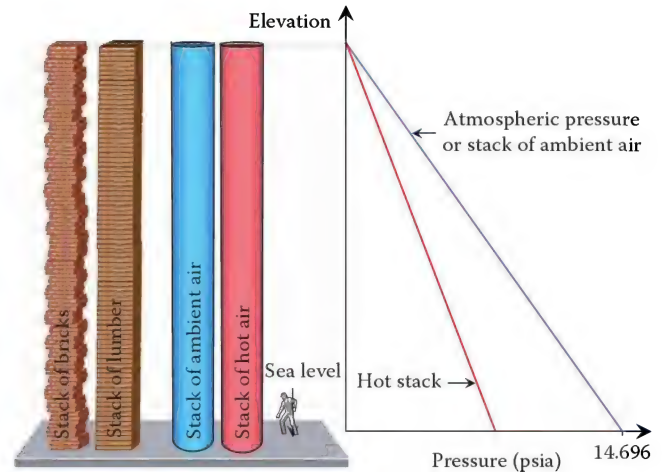


FIGURE 9.49

Illustration showing how the pressure varies inside a stack filled with hot air.

atmospheric pressure; this is represented by the blue line in Figure 9.49 and is referred to as the hydrostatic pressure since the gas is at rest. Notice that at the base of the cool stack, the hydrostatic pressure is equal to 14.696 psia since it is located at sea level. If one measured the mass of air above any given elevation within the hot stack and cold stack, they would find that the mass is always greater inside the cool stack due to the higher density of cool air. Since the hot stack has less air mass than the cold stack, it is not able to exert as much pressure; this is represented by the red line in Figure 9.49. Therefore, the hydrostatic pressure inside the hot stack is less than the pressure inside the cool stack at every elevation. For a further explanation, consider the following analogy.

Bricks and lumber are stacked to the same height and cross-sectional area as illustrated in Figure 9.49. If one were to measure the weight of the bricks and lumber above any given elevation in each stack, they would find that the weight of bricks is greater than the weight of the lumber, assuming that the density of the brick is greater than the density of the lumber. Since the cross-sectional area of each stack is the same, the pressure exerted at any elevation would also be greater within the stack of bricks. In this analogy, the bricks represent the air inside cool stack while the lumber represents the air inside the hot stack. In summary, a low-density column of gas will exert less pressure relative to a denser column of gas at any given elevation. A discussion of how the draft varies with elevation within the hot stack is presented next.

Figure 9.50 is an illustration showing a stack containing hot air with U-tube manometers connected at three different elevations. To the left of the stack is a plot showing how the hydrostatic pressure inside and outside the stack varies with elevation. At the stack exit, the pressure is equal to the atmospheric

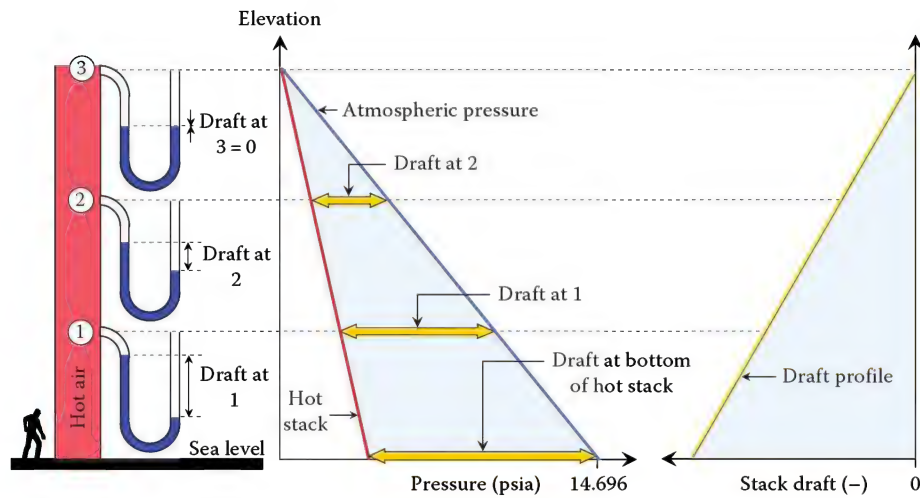


FIGURE 9.50

Illustration showing how the hydrostatic pressure and draft varies inside a stack filled with hot air.

pressure since the total mass of air above this point is the same. At this location, the water level in each arm of the U-tube manometer is the same indicating zero draft. However, below the exit, the pressure inside the stack is less than the pressure outside the stack (atmospheric pressure). Again, the draft is the difference between these two pressures. Notice that the draft is greatest at the bottom of the stack and decreases linearly to zero at the stack exit as shown in the plot on the far right-hand side. A plot showing the draft at various elevations is referred to as the draft profile.

The draft profile changes as the temperature of the gas inside the stack varies. Figure 9.51 is an illustration showing three identical stacks filled with air at different temperatures: hot air, warm air, and ambient air. The plots to the right of the stacks show how

the hydrostatic pressure and draft vary within each stack. Notice that as the temperature of the air inside the stack increases, the stack draft also increases. Also notice that when the air temperature in the stack is equal to the ambient air temperature, the pressure inside the stack is the same as the atmospheric pressure at any given elevation; therefore, the draft is zero throughout this stack. Another important variable influencing the draft profile is the height of the stack.

As the height of a stack changes, the draft profile also varies. For example, Figure 9.52 is an illustration showing two stacks of different heights filled with hot air at the same temperature. Even though the stacks are filled with air at the same temperature, the taller stack has the potential to create more draft than a shorter stack.

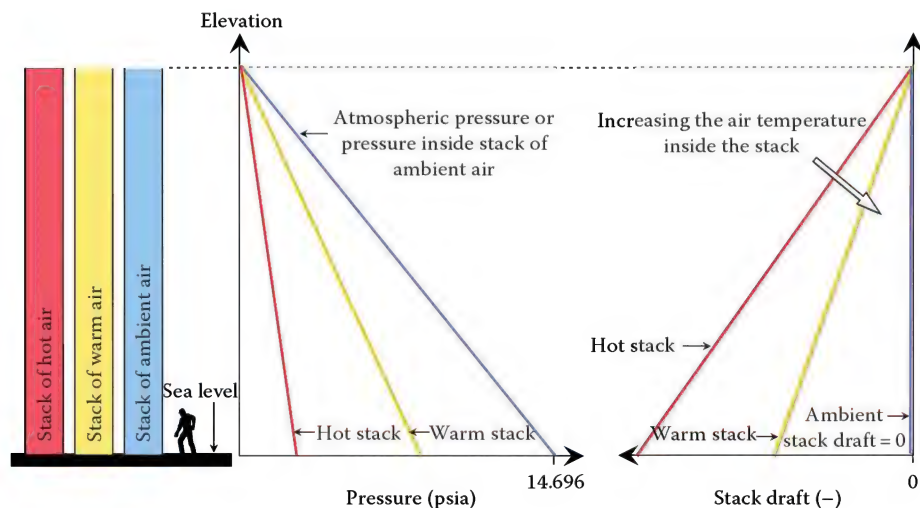


FIGURE 9.51

Illustration showing how the hydrostatic pressure and draft inside a stack filled with hot, warm, and ambient air varies with elevation.

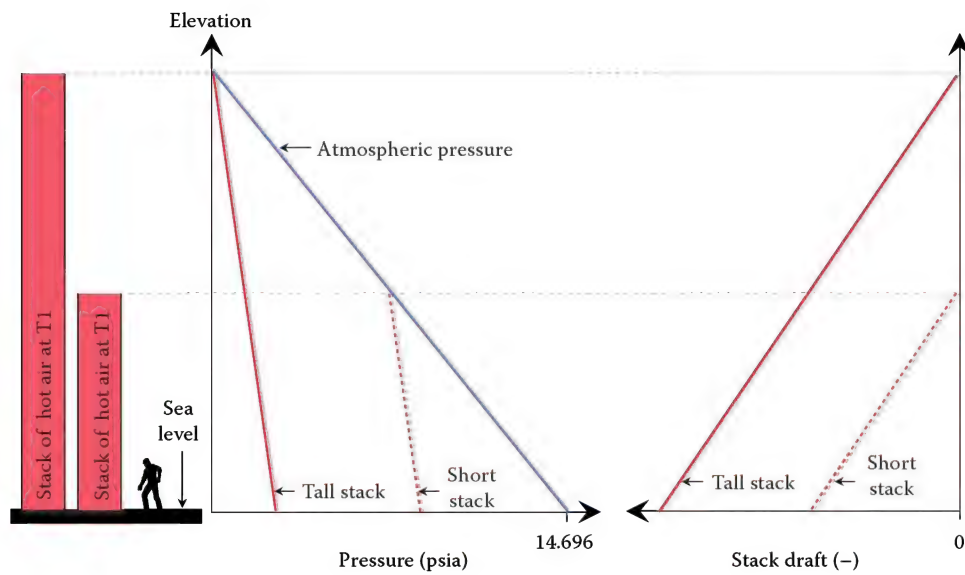


FIGURE 9.52

Illustration showing how the hydrostatic pressure and draft varies with stack height.

Assuming the temperature of the flue gas in the convection section and stack are the same for each heater, which heater has the potential to achieve the highest draft level?

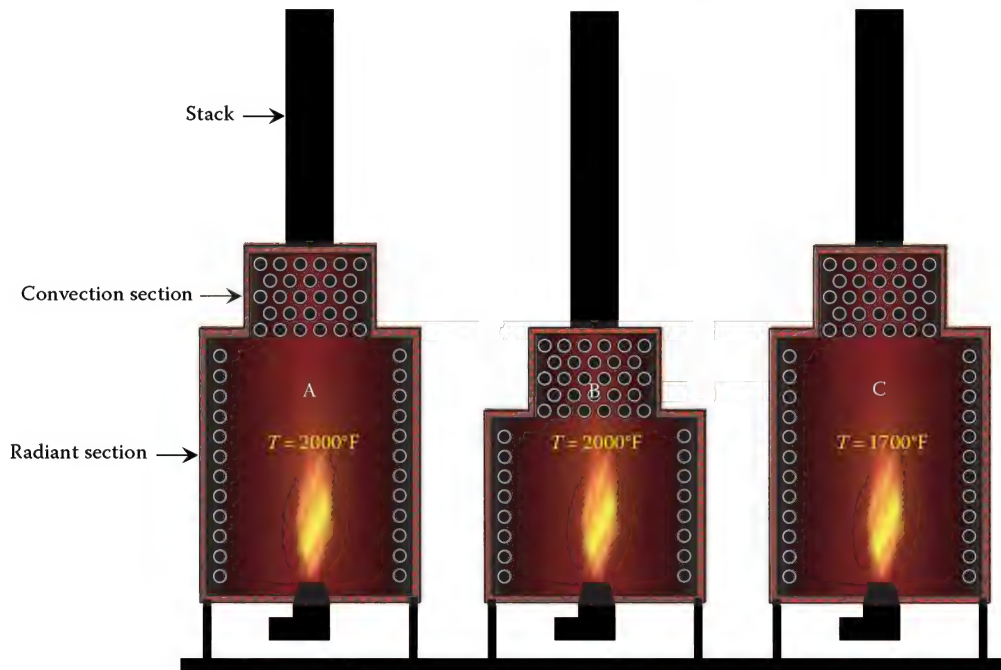


FIGURE 9.53

Example problem illustrating effects of temperature and height on draft.

### Example 9.9

Which of the three heaters illustrated in Figure 9.53 has the potential of creating the highest draft assuming the temperature of the flue gas in the convection section and the stack are the same for each heater?

First, comparing heaters A and B: Notice the flue gas temperature in each radiant section is the same, however, the radiant section in heater A is taller. Since heater A has more of its height filled with high temperature gas (lower density gas), heater A has the potential to create



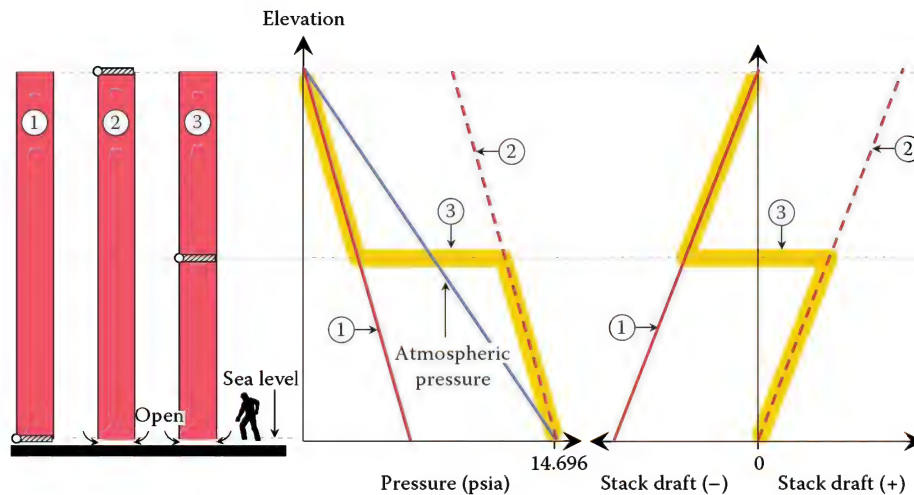
**FIGURE 9.54**

Illustration showing the hydrostatic pressure and draft profile at various elevations inside a stack filled with hot air. The damper in each stack is located at different elevations; top bottom and middle of the stack.

a higher draft than heater *B*. Next, comparing heaters *A* and *C*: Notice the height of the radiant sections are the same, however, the flue gas temperature is higher in heater *A*. Therefore, heater *A* has the potential for producing the highest draft.

Finally, before getting into the discussion of the draft profile inside a heater, consider the three stacks illustrated in Figure 9.54. Assume each stack is the same height, at the same elevation, and contains hot air at the same temperature. Also assume that each stack is designed with a damper, that when closed provides a perfect seal. The damper is located at different elevations on each stack: the damper is located at the bottom of stack 1, midway between top and bottom of stack 3, and at the top of stack 2. Notice the hydrostatic pressure at the top of stack 1 is equal to the atmospheric pressure and decreases linearly below the stack exit as discussed earlier. The hydrostatic pressure inside stack 2, however, is equal to the atmospheric pressure at the bottom since it is open to the atmosphere at this location. Moving up from the bottom of stack 2, the pressure decreases linearly, but does not decrease as much with elevation as the atmospheric pressure due to the lower density of gas in the stack; this results in a positive pressure inside stack 2. The hydrostatic pressure inside stack 3 is equal to the pressure inside stack 1 at locations above the damper and equal to the pressure inside stack 2 at locations below the damper. Next, consider the draft profile in each stack. Notice that for stack 3, the draft is always negative within the stack at locations above the damper and positive within the stack at location below the damper.

## 9.8.4 Natural Draft Heaters

### 9.8.4.1 Draft Profile

Consider a natural draft heater as illustrated in Figure 9.55. Assume the heater floor is located at sea level with an ambient temperature of 59°F; this corresponds to an atmospheric pressure of 406.8 in. WC (14.696 psia). At the stack exit, an elevation of 160 ft (49 m) above the floor, the atmospheric pressure decreases to 404.4 in. WC; this pressure profile is represented by the blue line in the plot. The difference in the atmospheric pressure at grade and at an elevation of 160 ft (49 m) is the maximum draft that can be achieved for this particular heater. That is, 2.3 in. WC (407–404.7) is the maximum achievable draft assuming the density of the gas inside of the heater was equal to zero and there were no pressure losses as the flue gases flow through the heater and stack.

Next, consider a stack containing a column of hot flue gas with dampers located at the same elevation as the dampers on the burner and heater stack as illustrated in Figure 9.55. Suppose that the gas inside the stack is sectioned into three zones with temperatures identical to those inside the heater; the temperature in the radiant section, convection section, and stack of the heater, is 2000°F, 1000°F, and 500°F, respectively. If the lower damper on the column of gas is closed and the upper is open, the hydrostatic pressure inside will fall below the atmospheric pressure; the pressure profile is shown as the red line in the plot. Notice that since there are three different temperature zones, the pressure profile is not a straight line like the atmospheric pressure profile. That is, as the flue gas temperature increases in each zone,



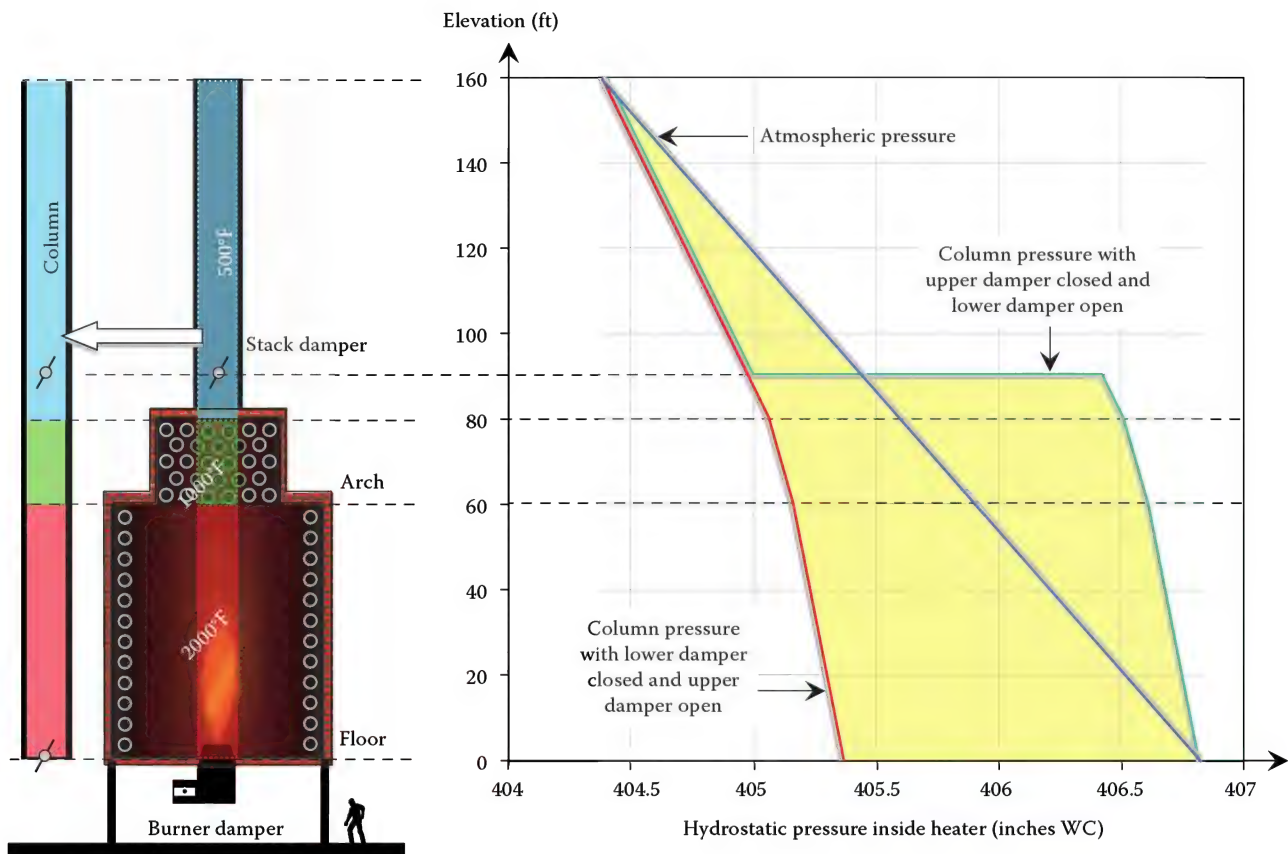


FIGURE 9.55

Illustration showing how the heater pressure profile changes as the stack damper is closed and the burner damper is opened.

the line representing the hydrostatic pressure becomes vertical. Next, suppose the upper damper is closed and the lower is open. As discussed previously, the hydrostatic pressure below the upper damper will be greater than the atmospheric pressure and less than atmospheric pressure above the damper; this profile is shown as the green line in the plot. The yellow-shaded area in the plot represents the maximum and minimum values of hydrostatic pressure from the three profiles plotted. The actual draft profile of this particular heater will fall somewhere within this envelope.

The plot in Figure 9.56 is an illustration showing how the pressure inside the heater varies with elevation. Starting at the stack exit, the hydrostatic and static pressures are equal. However, at elevations below the stack exit, the static pressure inside the heater begins to deviate from the hydrostatic pressure. This deviation is caused by the pressure drop ( $\Delta P$ ) associated with frictional losses as the flue gas flows along the stack wall and is influenced by the roughness. Notice that this pressure drop increases the static pressure inside the heater shifting the profile to the right. Similarly, the pressure drop across the stack damper, convection section, and radiant section increases the static pressure inside the heater and further

shifts the profile to the right; the larger the pressure drop, the more the shift. Notice that the lowest draft inside the heater occurs at the arch. In a properly designed heater, this is typically the location of minimum draft and is one of the most important locations to measure and control draft. By maintaining a slight negative pressure throughout the heater; this will be discussed in more detail later. Also notice that the draft in the radiant section decreases with height. Therefore, burners located lower in the heater will experience more draft than the burners located higher in the heater. In this particular example, the burners located at the floor have about  $-0.5$  in. WC draft available while the burners located 20 ft (6 m) above the floor only have about  $-0.4$  in. WC available. Therefore, burners located at different elevations within a heater should have the burner dampers adjusted to take into account the variations in draft to help maintain similar combustion air-flow rates to all burners.

#### 9.8.4.2 Draft Measurement Location

Potentially, draft can be measured at many different places along the height of a heater. However, the two

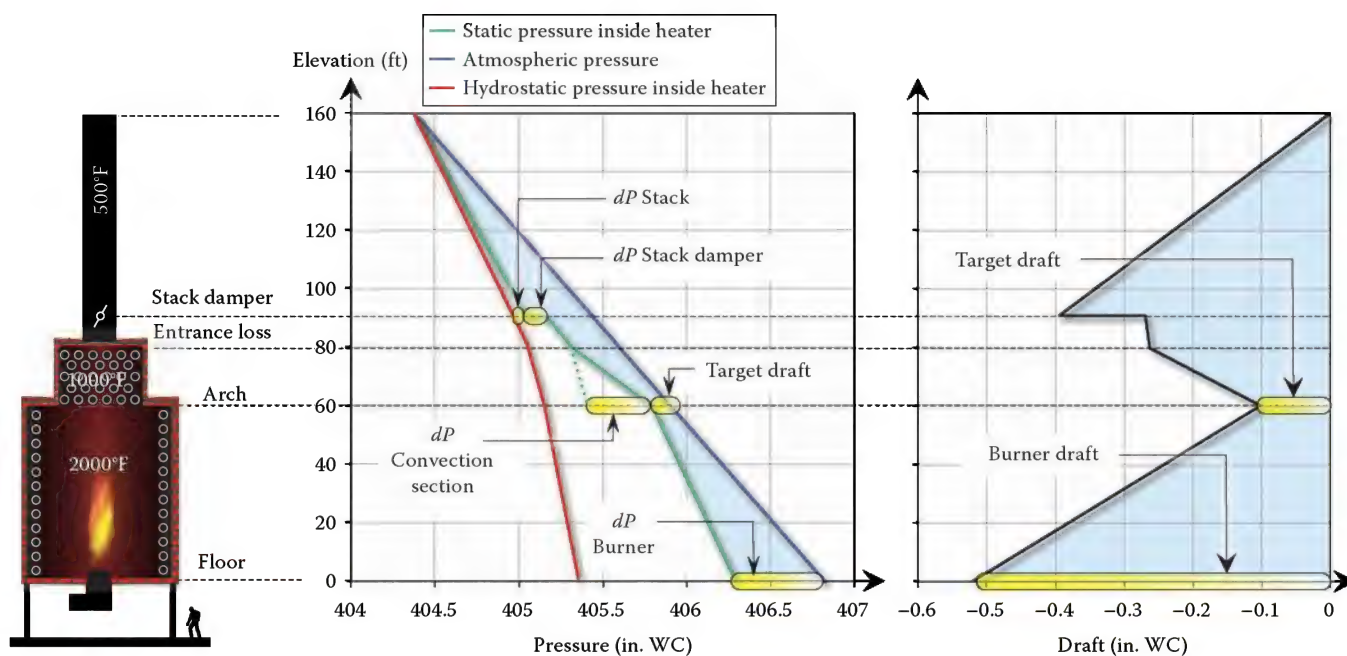


FIGURE 9.56

Illustration showing the pressure and draft profile for a typical natural draft heater.

most important places to measure draft are at the top of the radiant section (arch or roof) and at the elevation of the burners.

It is important to measure the draft at the arch to ensure that the entire heater is operating at a negative pressure. Typically, when heaters initially start to go positive, it happens at a location where the draft is the lowest; as previously discussed, this normally occurs at the arch in a properly designed heater. It is important that heaters always operate at a negative pressure because when heaters run positive, flame or hot flue gas can flow out through openings in the heater, which can pose a safety risk to personnel and damage the structure of the heater.

Hot flue gas escaping a heater is a safety concern because it can potentially burn personnel working within the area. Figure 9.57 is a photograph showing a heater operating with a positive pressure, which is forcing the flame to be pushed out through the burner inlet. Although this photograph clearly shows hot flue gas escaping the heater, it cannot always be detected by the eye. When opening a sight port on the heater, it is important not to stand directly in front of a port in case the furnace is operating positive.

Hot flue gases flowing out through openings can damage the structure of the heater. When hot flue gases come in contact with the furnace casing (shell), it heats the metal causing it to expand and warp. When the metal warps, it can cause welds that hold the refractory anchors in place to crack and fail and dislodge the brick lining. Brick or pieces of castable refractory that break loose from the wall of the heater can fall into the throat of the burner



FIGURE 9.57

Positive draft inside a heater forcing flame out through the burner intake.

as shown in Figure 9.58. Refractory inside the throat can reduce the airflow rate through the burner and starve the fuel for air. This can lead to (1) coke buildup on the outside of burner tips, (2) unstable flame, (3) high levels of unburned hydrocarbon (UHC) and carbon monoxide (CO) emissions out the stack, and (4) the formation of long, lazy flames that are more prone to impinge on process tubes (Figure 9.59). Hot flue gas leaks can also corrode the heater casing when water vapor in the flue gas condenses and collects on the outside surface of the heater.

Typically, draft levels at the arch are maintained at a pressure of  $-0.05$  to  $-0.1$  in. of WC. Maintaining a slight



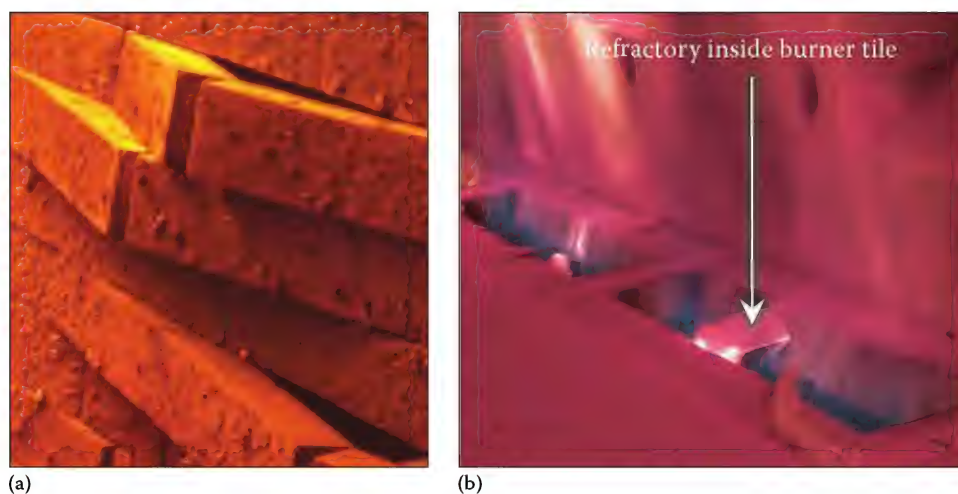


FIGURE 9.58

(a) Refractory brick dislodged from the heater wall due to warping of the heater casing. (b) Large chunk of refractory that has fallen from the heater wall into the throat of a burner.

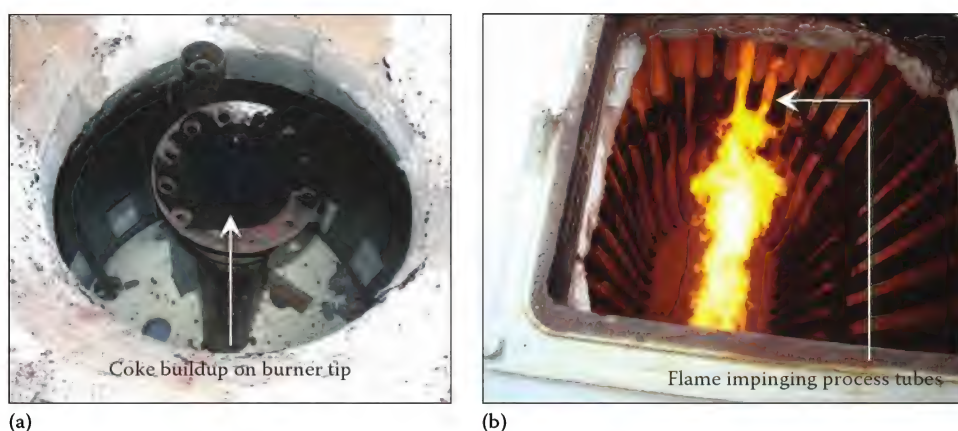


FIGURE 9.59

(a) Coke buildup on a burner tip caused by low draft through the burner. (b) Long flame impinging on process tubes caused by low draft at the burner elevation.

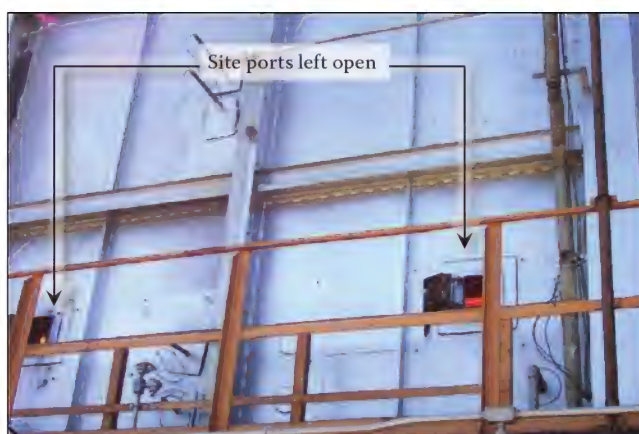
negative pressure at this location normally insures a negative pressure or vacuum throughout the entire heater. If the target draft is too negative, however, excess air can leak through openings and cracks into the heater. A common place for unwanted air (tramp air) to enter the furnace is through the convection section because it is difficult to get a tight seal around the process tubes penetrating the shell of the heater as shown in Figure 9.60. Tramp air infiltration into a heater can lead to a reduction in heater efficiency (see Chapter 12), increased  $\text{NO}_x$  emissions, poor burner performance, and afterburning in the convection section.

Heater draft should also be measured at the elevation of the burners. Knowing the draft at the burners, operators can determine if the proper amount of air is available to the burners for complete combustion. For example, if the heater  $\text{O}_2$  is on target but the draft at the floor of the heater is too low, this could indicate that



FIGURE 9.60

A process tube penetrating the convection section of a heater.

**FIGURE 9.61**

Sight ports on a heater left open allowing tramp air to enter.

tramp air is entering the heater. Air can leak into heaters through (1) cracks in walls, (2) sight ports that are not properly sealed or that might be left open (Figure 9.61), (3) out-of-service burners with air registers left open, and (4) penetrations through heater walls that are not properly sealed (Figure 9.62).

#### 9.8.4.3 Adjusting Draft

Airflow into natural draft heaters can be regulated using the stack damper and burner dampers. In general, using the stack damper is the preferred way to control the heater draft while the burner dampers are used to control the heater  $O_2$  level. However, they are not completely independent of each other. That is, if an operator

**FIGURE 9.62**

Access door on a heater not properly sealed allowing tramp air to enter.

adjusts the burner damper to control the  $O_2$ , the furnace draft will also be affected and vice versa. Therefore, it may be necessary to adjust both the stack damper and the burner dampers to achieve the desired target draft and  $O_2$  level. As an example to illustrate this point, consider the operation of a vacuum cleaner.

Suppose an inclined manometer is connected to the hose of a vacuum cleaner downstream of the inlet as shown in Figure 9.63. What would happen if one covered the inlet to the vacuum cleaner with their hand? The pressure inside of the hose would become more negative and the flow rate of air would decrease. This is similar to what takes place when the burner damper is closed on a heater; the draft increases and the heater  $O_2$  decreases. Next, consider what would happen if the vacuum hose is pinched downstream of the manometer tap? The pressure inside of the hose would become more positive and the flow rate of air would decrease. This similar effect happens when the stack damper is closed; both the draft and heater  $O_2$  decrease. Adjusting dampers to achieve the desired result is not intuitive and at times can be confusing even for those with experience.

Figure 9.64 is an illustration showing how the draft profile changes as the stack damper is closed and the burner damper opened while maintaining a constant  $O_2$  level inside the heater. These results are from a computer program designed to simulate the dynamics of a heater.<sup>42</sup> The plot shows that as the stack damper is closed and the burner damper opened, the draft profiles shift more toward positive pressure. Notice that if the stack damper is closed too much, the draft becomes positive at the arch (target draft). However, as the stack damper is opened and the burner damper is closed, the target draft eventually becomes negative. The middle yellow profile shows the design conditions for a typical heater. The left blue line shows a condition where the draft is too negative, while the right red profile shows a condition where the draft is not negative enough and where the heater actually is positive at the arch.

#### 9.8.5 Mechanical Draft Heaters

Process heaters equipped with mechanical draft systems also operate with negative pressure throughout the entire heater. Similar to a natural draft heater, a negative pressure insures that hot combustion products do not exit the heater through cracks and sight ports, damaging the structure and posing a safety risk to personnel. The draft profile in mechanical draft heaters is also similar to natural draft heaters. For example, consider a heater used in steam-methane reforming (SMR).

SMR is a technology commonly used for hydrogen production (see Chapter 2). The process involves flowing a mixture of steam and lighter hydrocarbons such as natural gas (methane) or refinery feedstock



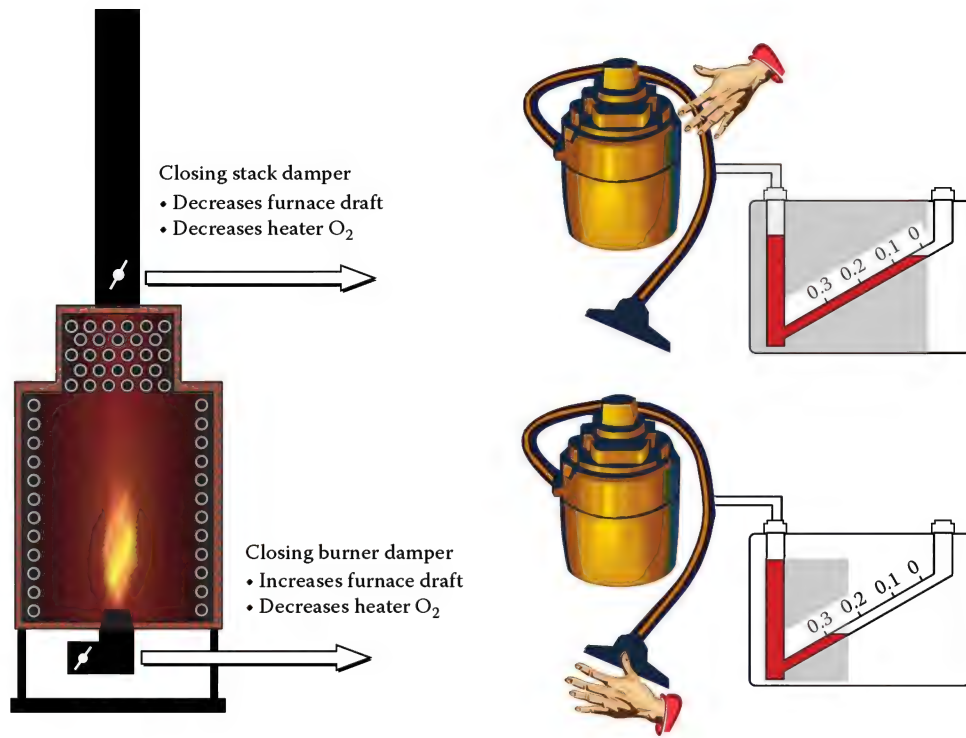


FIGURE 9.63

Illustration showing the effects of closing the burner and stack damper on draft and excess  $O_2$ .

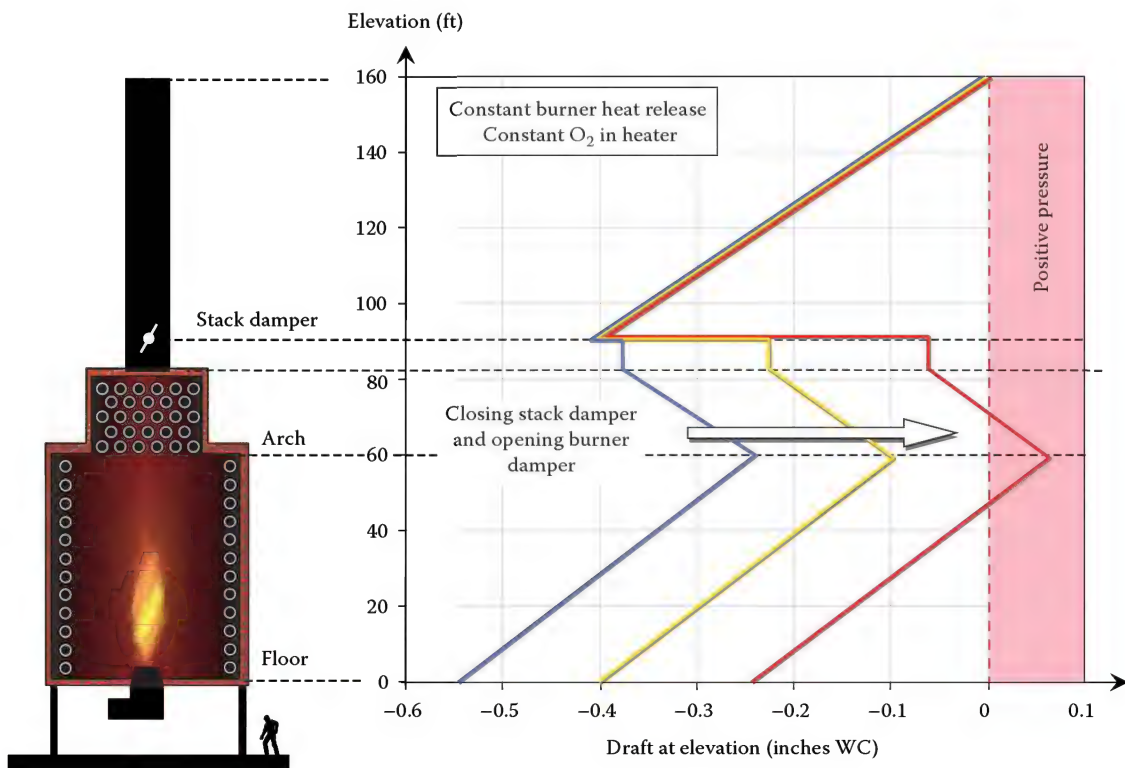
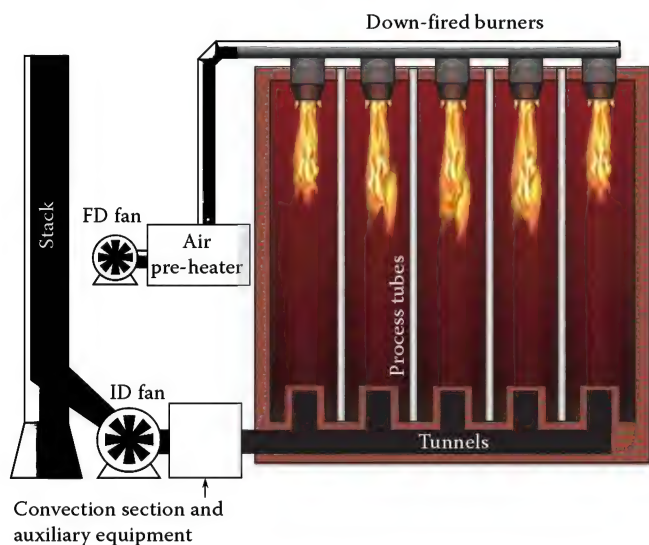


FIGURE 9.64

Results showing the draft profile for various burner and stack damper settings operating at a constant burner heat release and heater  $O_2$ .

over hot catalyst.<sup>43,44</sup> The hot catalyst creates a reaction converting the steam-hydrocarbon mixture into hydrogen and carbon monoxide (syngas). The catalyst is contained within process tubes and heated inside of a furnace. The furnace is typically rectangular and designed with several rows of burners that fire vertically down from the ceiling between multiple rows of catalyst-filled tubes<sup>45</sup> as illustrated in Figure 9.65; this



**FIGURE 9.65**  
Schematic of a heater used in the SMR industry for hydrogen production.

type of heater is commonly referred to as a “down-fired” heater. Hot combustion products exit the heater by way of several tunnels located at the floor and flow through the convection section and auxiliary equipment. Many of these heaters are designed as balanced draft systems; that is, air is pushed into the heater using a forced draft fan (FD fan) located upstream of the burners and assisted by an ID fan located near the exhaust stack. The balance between the ID fan and FD fan is critical in order to ensure that a proper amount of air is delivered through the burners and that heater draft remains negative.

Figure 9.66 shows a typical draft profile inside a down-fired heater. The draft is highest at the floor and decreases linearly with elevation, similar to a natural draft heater. In this example, the draft at the burner level is  $-0.2$  in. WC and at the floor is  $-0.5$ ; this draft level is somewhat typical of SMR heaters. Notice as the flue gas flows through the tunnels, the pressure becomes more negative.

In a balanced draft system, the pressure is lowest at the inlet to the ID fan. In some cases, the pressure can be as low as  $-20$  to  $-30$  in. of WC, depending on the pressure drop through the tunnels, convection section, and auxiliary equipment. For example, consider a U-tube manometer connected to the hose of the vacuum cleaner as illustrated in Figure 9.67. If the inlet of the vacuum hose were restricted to flow by partially covering it, the static pressure inside the hose would become more

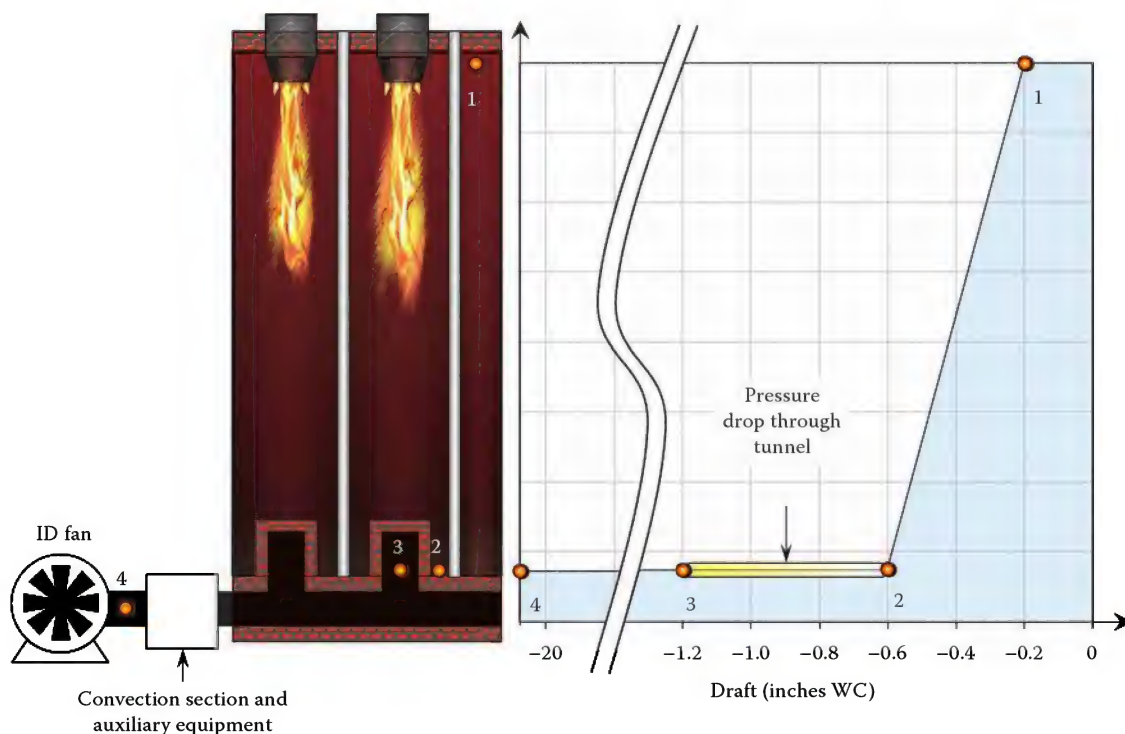


**FIGURE 9.66**  
Example of a typical draft profile inside a down-fired heater.

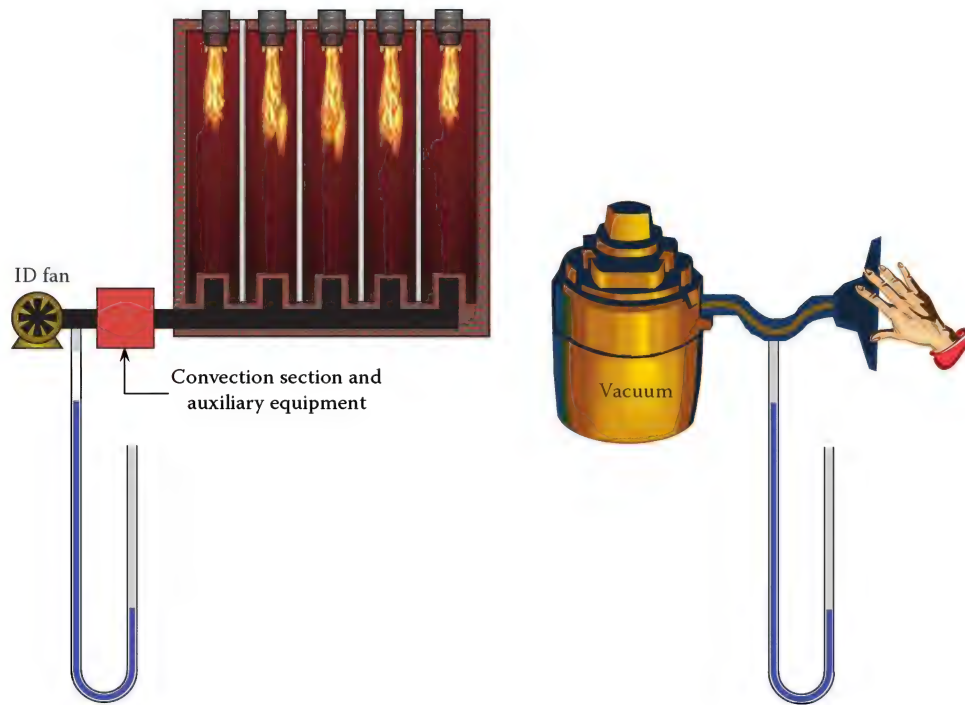
**FIGURE 9.67**

Illustration comparing the pressure inside of a down-fired heater and the pressure inside a vacuum cleaner hose.

negative and the water in the manometer would rise up the column; the static pressure in the hose becomes more negative as the inlet is more restricted. Similarly to the pressure drop through the tunnels, as the convection section and auxiliary equipment take larger pressure drops, the static pressure to the inlet of the ID fan becomes more negative.

### 9.8.6 Instrumentation Used to Measure Heater Draft

Heater draft is typically measured within an accuracy of 1/100th in. WC. With U-tube manometers, it is not possible to read pressures this accurately; instead, inclined manometers are commonly used. Inclined manometers essentially expand the scale of a U-tube manometer by orienting it at an angle, relative to the horizontal, as illustrated in Figure 9.68. Although the actual vertical rise of the liquid in the U-tube and inclined manometer are identical, the scale on the inclined manometer is spread out over a much larger horizontal distance; this expanded scale increases the instruments' accuracy.

Figure 9.69 shows a photograph of a typical inclined manometer used to measure heater draft. Usually, inclined manometers are filled with red gauge oil having a specific gravity of approximately 0.8. The low specific gravity oil allows the scale to be expanded (relative to water) for better accuracy. Also, the oil prevents freezing problems in cold climates. Located at the top of the manometer are two

pressure taps: a high-pressure side and low-pressure side. The low-pressure side tap contains the oil reservoir.

Before using the manometer, it is important that it is level with the horizontal; typically manometers are designed with a bubble level to assist in accurate leveling. It is also important that the manometer be zeroed. Manometers are typically designed with an adjustable piston located inside of a cylinder. By rotating a knob on the manometer, the user can manually adjust the position of the piston, which controls the level of oil in the reservoir; this allows the manometer to be zeroed. When zeroing the manometer, it is important that the high- and low-pressure taps are open to the atmosphere to ensure they are at the same pressure; be aware that wind blowing into one of the ports can have a significant effect. When taking a pressure measurement, it is common to read the oil interface near the center of the tube as shown in Figure 9.70; in this example, the manometer is reading 0.2 and 0.0 in. WC.<sup>46</sup>

A few common ways manometers are misused in the field, resulting in inaccurate draft readings, include the following: using the wrong fluid in the manometer, manometer is not level, water has collected in the line leading from the manometer to the measurement point, pressure taps are screwed down too tightly sealing the manometer, wind is blowing into an open pressure tap, manometer was not zeroed, and the pressure taps were not located at the same elevation. Draft can also be measured using a dial gauge or a pressure transmitter as shown in Figure 9.71.



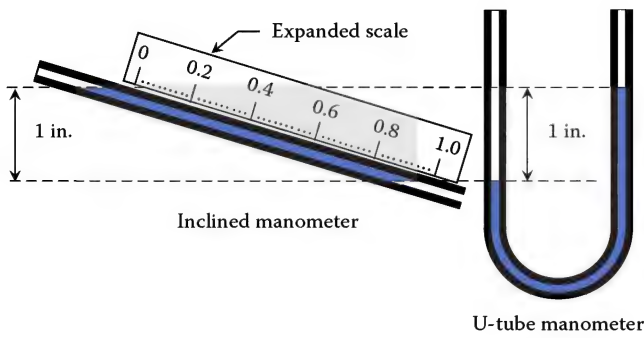


FIGURE 9.68

Illustration showing inclined manometers essentially expand the scale of a U-tube manometer by orienting it at an angle.

### 9.8.7 Heater Draft Calculations

The following equation can be used to estimate the draft at various elevations within a heater.

U.S. Customary Units:

$$\begin{aligned} \text{Draft}_{\text{per ft height}} (\text{inches WC}) \\ = -0.5193 P_{\text{atm}} (\text{psia}) \left[ \frac{1}{T_{\text{atm}} (^{\circ}\text{F}) + 460} - \frac{1}{T_{\text{heater}} (^{\circ}\text{F}) + 460} \right] \end{aligned} \quad (9.23a)$$

where

$\text{Draft}_{\text{per ft height}} \equiv$  Draft generated per foot of height (inches WC)

$P_{\text{atm}} \equiv$  Atmospheric pressure (psia)

$T_{\text{atm}} \equiv$  Atmospheric temperature ( $^{\circ}\text{F}$ )

$T_{\text{heater}} \equiv$  Temperature inside heater ( $^{\circ}\text{F}$ )

The coefficient 0.5193 is derived as follows:

$$\begin{aligned} 0.0765 \frac{\text{lb}_m}{\text{ft}^3} \times \frac{1}{14.696 \frac{\text{lb}_f}{\text{in}^2}} \times 519^{\circ}\text{R} \times \frac{32.2 \frac{\text{ft}}{\text{s}^2}}{32.2 \frac{\text{lb}_m - \text{ft}}{\text{lb}_f - \text{s}^2}} \times 1 \text{ ft} \\ \times \frac{\text{ft}^2}{144 \text{ in}^2} \times \frac{27.68'' \text{ WC}}{\frac{\text{lb}_f}{\text{in}^2}} = 0.5193 \frac{\text{inches WC} - ^{\circ}\text{R}}{\text{psia}} \end{aligned}$$

S.I. Units:

$$\begin{aligned} \text{Draft}_{\text{perm height}} (\text{inches WC}) = -0.1372 P_{\text{atm}} (\text{kPa(abs)}) \\ \times \left[ \frac{1}{T_{\text{atm}} (^{\circ}\text{C}) + 273.15} - \frac{1}{T_{\text{heater}} (^{\circ}\text{C}) + 273.15} \right] \end{aligned} \quad (9.23b)$$

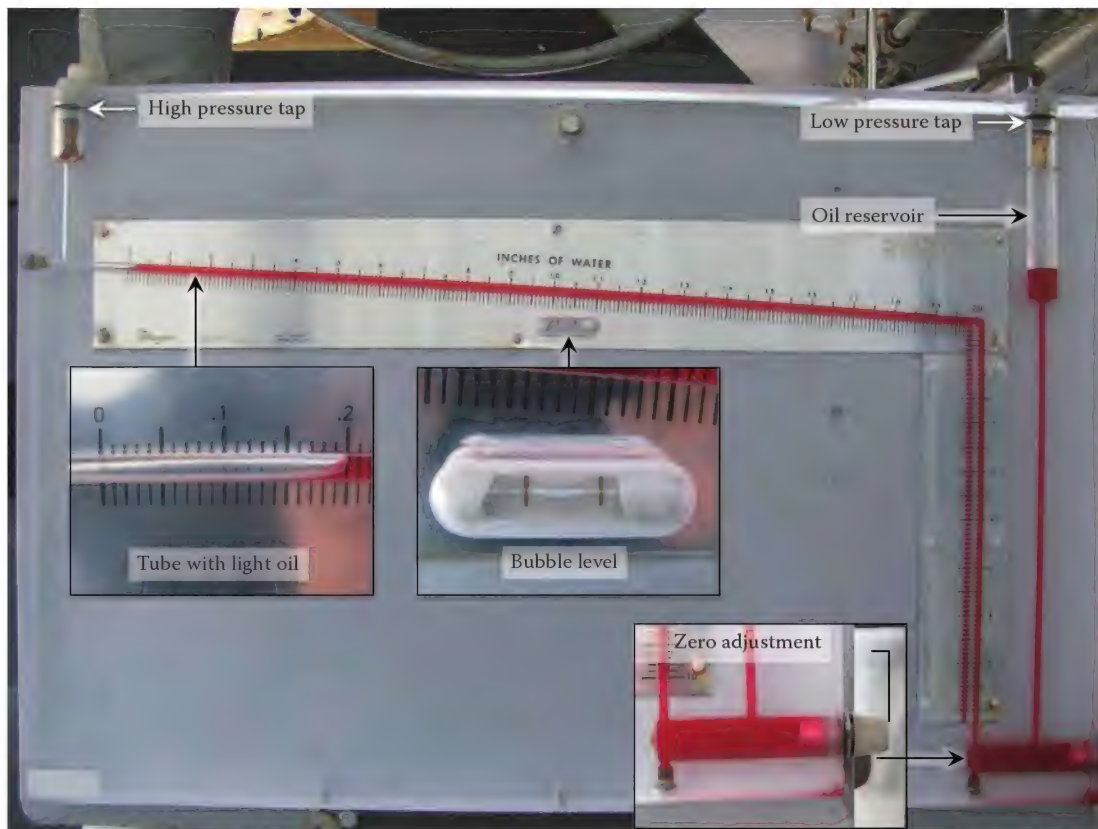
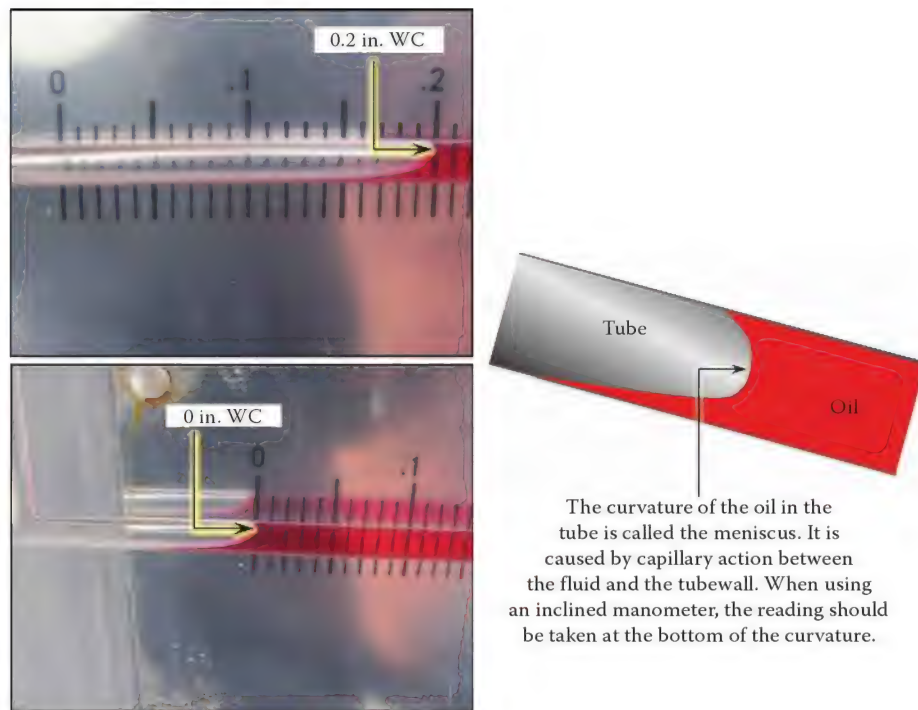


FIGURE 9.69

Inclined manometer typically used to measure heater draft.





**FIGURE 9.70**  
Inclined manometer reading 0.2 and 0 in. of WC.

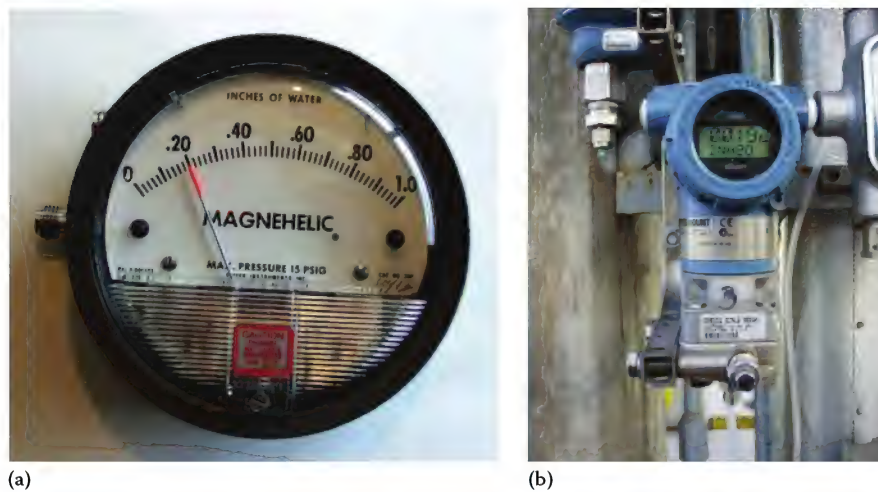


**FIGURE 9.71**  
(a) Dial pressure gauge reading 0.2 in. WC and (b) electronic pressure transmitter used to measure heater draft.

where

$\text{Draft}_{\text{perm height}} \equiv \text{Draft generated per meter of height (inches WC)}$

$P_{\text{atm}} \equiv \text{Atmospheric pressure (kPa(abs))}$

$T_{\text{atm}} \equiv \text{Atmospheric temperature (}^{\circ}\text{C)}$

$T_{\text{heater}} \equiv \text{Temperature inside heater (}^{\circ}\text{C)}$

$$1.225 \frac{\text{kg}}{\text{m}^3} \times \frac{1}{101.325 \text{ kPa (abs)}} \times 288.15^{\circ}\text{K} \times 1\text{m} \\ \times \frac{1\text{m}^2}{10,000\text{cm}^2} \times \frac{27.68''\text{WC}}{0.0703 \frac{\text{kg}}{\text{cm}^2}} = 0.1372 \frac{\text{inches WC} - ^{\circ}\text{K}}{\text{kPa (abs)}}$$

The coefficient 0.1372 is derived as follows:

To demonstrate how Equation 9.23 is used, consider the following example:

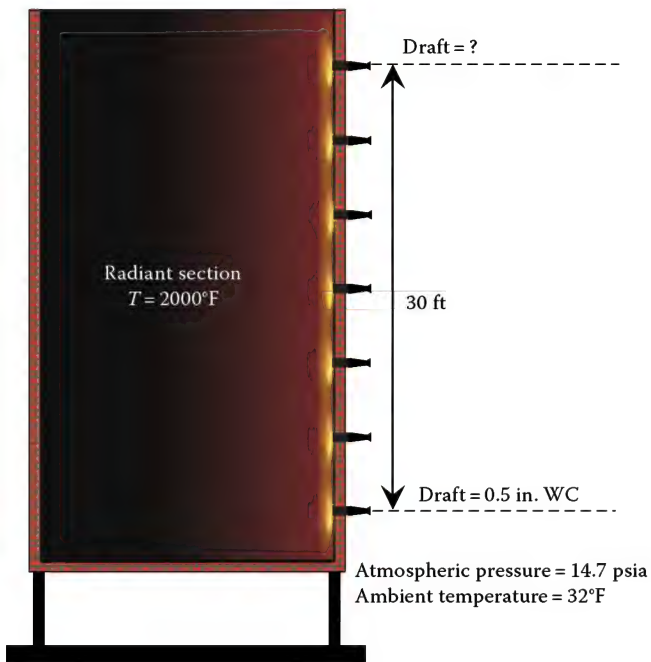


**FIGURE 9.72**  
Illustration used in example problem to demonstrate how much the draft varies with elevation inside a heater.

#### Example 9.10

An ethylene-cracking furnace is designed with seven rows of wall burners with a radiant section operating at a temperature of  $2000^{\circ}\text{F}$  as illustrated in Figure 9.72. At the bottom row of burners, the heater draft is  $-0.5$  in. WC and the atmospheric pressure is 14.7 psia. Assume that the ambient temperature is  $32^{\circ}\text{F}$  and does not vary with elevation. Determine the draft at the top row of burners located 30 ft above the bottom row.

Knowing  $P_{\text{atm}} = 14.7$ ,  $T_{\text{atm}} = 32^{\circ}\text{F}$ , and  $T_{\text{heater}} = 2000^{\circ}\text{F}$ , Equation 9.23 is used to determine the draft per foot of height inside the heater.

$$\begin{aligned}\text{Draft}_{\text{per ft height}} &= -(0.5193)(14.7) \left[ \frac{1}{32 + 460} - \frac{1}{2000 + 460} \right] \\ &= -0.0124 \text{ in. WC per foot}\end{aligned}$$

The draft at the top row of burners can now be determined at follows:

$$\text{Draft}_{\text{at 30 ft}} = \text{Draft}_{\text{at bottom}} - \text{Draft}_{\text{per ft height}} \times \text{height (ft)}$$

$$\text{Draft}_{\text{at 30 ft}} = -0.5 - (-0.0124 \times 30) = -0.128 \text{ in. WC}$$

In this particular example, the heater draft at the bottom row of burners is  $-0.5$  in. WC while the upper row is  $-0.128$  in. WC. If the air door on the burners at each level were adjusted to the same position, the lower burners would pull in more combustion air than the upper burners. This could result in the upper burners operating at fuel rich conditions that could lead to burner flashback, high  $\text{NO}_x$  emissions, and poor flame quality. Therefore, the burner air doors at each row should be adjusted to compensate for the variation in draft within the heater.

A rule-of-thumb commonly used in industry is that the draft generated in the radiant section of a heater is 0.01 in. WC for every foot of height (for radiant section temperatures greater than  $1100^{\circ}\text{F}$ ). This rule-of-thumb should only be used as a rough estimate because the potential for draft can vary significantly with the density of the ambient air and flue gas. For example, using Equation 9.23, the draft per foot of height for two extreme

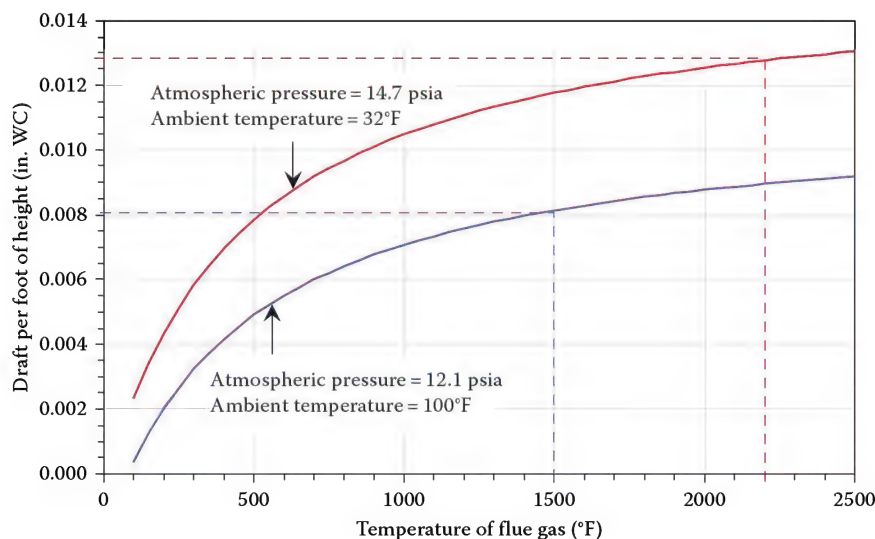
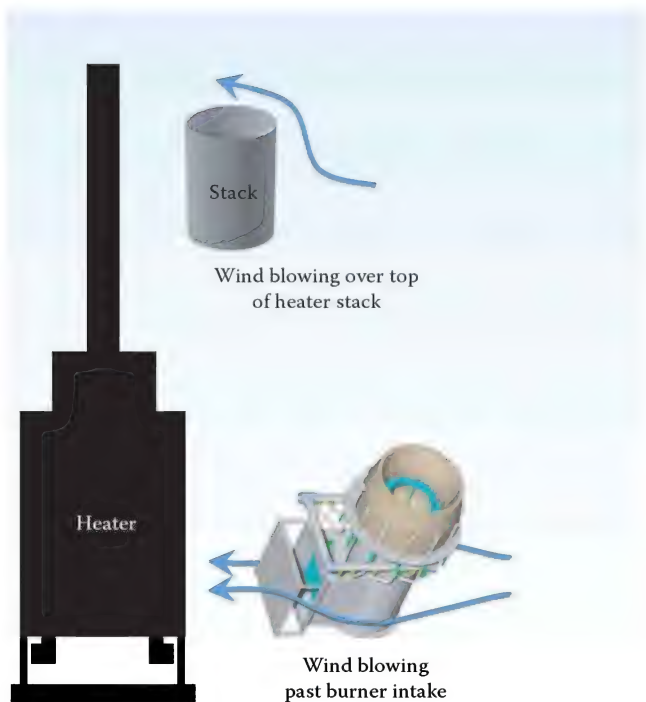


**FIGURE 9.73**  
Plot showing how the draft per foot of heater height varies with flue gas temperature for two different ambient conditions.

conditions is shown in Figure 9.73. A heater operating with a radiant section temperature of 1500°F in an ambient environment of 12.1 psia and 100°F can create a draft of about 0.008 in. of WC per foot of height. However, a heater operating with a radiant section temperature of 2200°F in an ambient environment of 14.7 psia and 32°F can create a draft of 0.13 in. of WC per foot of height.

### 9.8.8 Effects of Ambient Wind Conditions on Natural Draft Heaters

Ambient wind conditions, especially storm force winds, can cause significant swings in heater draft, which in turn, affects the excess  $O_2$ . Wind can influence heater draft by altering the pressure at the stack exit and burner intake. When wind blows over the top of a stack, as illustrated in Figure 9.74, it can contribute to either a backpressure or a suction pressure inside of the stack. If the momentum of the flue gas is low relative to the wind, then a negative pressure inside of the stack can be formed. Since the heater box is in direct dynamic communication with the stack, this will contribute to an increase in heater draft. However, if the momentum of the flue gas is dominant, the wind can create a backpressure resulting in a reduction in heater draft. Wind can also decrease draft if the heater is located just downwind of structures or near the base of a hill that is taller than the stack. Under these conditions, the recirculation zone downwind of the obstruction (Figures 9.25 and 9.28) can cause the air to flow downward creating a backpressure at the stack exit and reducing draft.



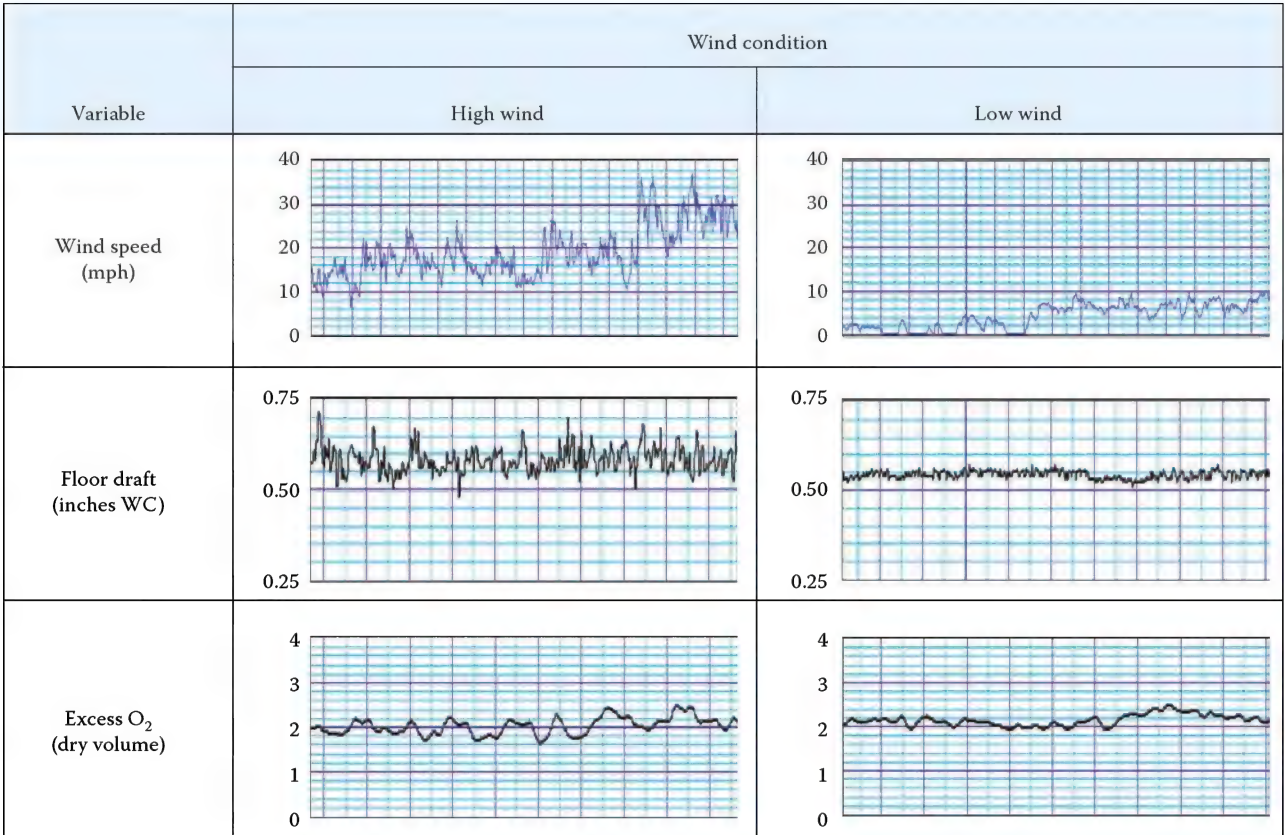
**FIGURE 9.74**  
Illustration showing ways the wind can impact heater draft levels.

Figure 9.75 shows draft and excess  $O_2$  data from a heater firing under high- and low-wind conditions with all other operating conditions being the same. For each wind condition, the burner damper was full open (100% open) and the stack-damper was set at 58% open. The stack damper was exposed to the full force of the wind while the burner inlet was somewhat isolated from the wind due to equipment and structures located in the area. Notice, for the high-wind case, the speed ranged from about 10 to 40 mph (64 km/h); these wind speeds caused variations in draft of about 0.25 in. WC and swings in excess  $O_2$  of about 1%. However, for the low-wind case, the speed varied from about 0 to 10 mph (0 to 16 km/h); this caused variations in draft of about 0.05 in. WC and swings in excess  $O_2$  of only about 0.2%. This data demonstrates that wind velocity can have a significant impact on heater draft and  $O_2$ .

A 40 mph (64 km/h) gust of wind (at 60°F = 16°C) will create a dynamic head of about 0.8 in. WC. A pressure of this magnitude, acting at the intake of a burner, can have a significant impact on heater draft, which in turn affects the excess  $O_2$ ; the impact depends on the burner intake design as well as wind speed and direction. For example, burners (b) and (c), as depicted in Figure 9.76, will be less susceptible to a headwind as compared to burner (a) because the mufflers act as a barrier to protect it from the direct force of the wind. A headwind blowing directly into the intake of burner (a) can increase the differential pressure across the burner driving more air across the burner and significantly raise the excess  $O_2$ . However, a crosswind can reduce the differential air pressure and significantly lower the excess  $O_2$ . Typically, the higher the draft available at the burner, the less susceptible it is to the effects of ambient wind.

A diffusion-style burner, firing natural gas at its designed maximum heat release (HR) of 10 MMBtu/h (2.9 MW) was tested in a crosswind with the damper set at 100% open as illustrated in Figure 9.77. Wind speeds up to 35 mph (56 km/h) were simulated using a variable speed blower positioned perpendicular to a burner intake. During all tests, the ambient wind speed remained less than 2 mph (3 km/h) and therefore, had an insignificant effect on the test results. Experimental data show that for this particular burner design and firing condition, a crosswind of 20 mph (32 km/h) did not have a significant impact on the airflow through the burner and did not influence the excess  $O_2$ . However, at a wind speed of 35 mph (56 km/h) the airflow through the burner was reduced causing the excess  $O_2$  to vary from 2.3% to 0.5% over a period of 5 min. During this time period, the CO emissions varied from zero to about 200 ppmvd (uncorrected for  $O_2$ ). One would expect that as the wind speed further increased the heater would eventually operate in a fuel-rich condition. Under these conditions, operators might be forced to increase heater





**FIGURE 9.75**  
Data trends showing wind effects on heater draft and excess O<sub>2</sub> at high- and low-wind speeds over a 10-min period.

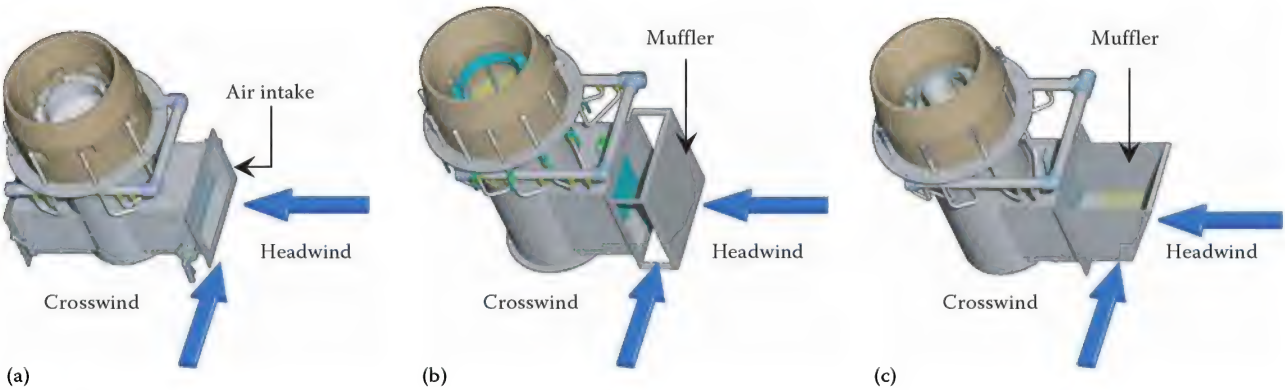


**FIGURE 9.76**  
(a–c) Illustrations showing burner designs with various air intake configurations.

excess O<sub>2</sub> margins to allow for the swings; increasing the excess O<sub>2</sub> lowers the thermal efficiency of the heater. To help eliminate crosswind effects, burner (c), as shown in Figure 9.76, might be a more efficient design. Although mufflers do not completely eliminate the effects of wind, they do help considerably.

### 9.9 Air-Side Pressure Drop through Burners

The purpose of this section is to discuss several important design issues associated with the flow of combustion air through natural draft burners.



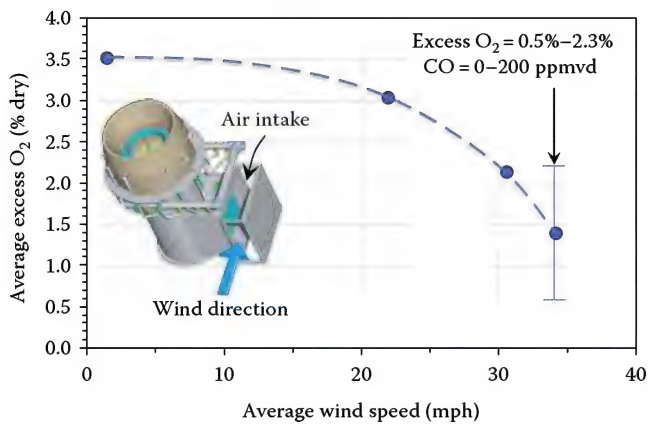


FIGURE 9.77

Experimental data showing effects of a crosswind past a burner intake on excess O<sub>2</sub>.

### 9.9.1 Definition of Burner Pressure Drop

When combustion air flows through a burner, it passes through various components such as the muffler, damper, plenum, and throat as illustrated in Figure 9.78. These components create a torturous path causing the

air to quickly change direction, accelerate, and decelerate. Each time the air changes velocity or direction through the burner, additional energy is consumed as the air molecules collide with one another resulting in a pressure drop through the burner.

The pressure drop through a burner is defined as the atmospheric pressure minus the total pressure inside the heater, both measured at the burner elevation; referring to Figure 9.78, this is the pressure at point 1 minus the pressure at point 8. Assuming that the velocity of the gas inside the heater is nearly zero, the velocity pressure is insignificant; therefore, the pressure inside the heater is the total pressure and equal to the static pressure.

The pressure drop through a burner can be measured using an inclined manometer (Figure 9.69). If the low-pressure side of the manometer is connected to the heater floor while the high-pressure side is left open to the atmosphere, the manometer will measure the pressure drop through the burner. This pressure difference is also referred to as the draft at the heater floor. In this illustration, the manometer shows a pressure drop through the burner equal to +0.4 in. WC or a draft at the heater floor equal to -0.4 in. of WC.

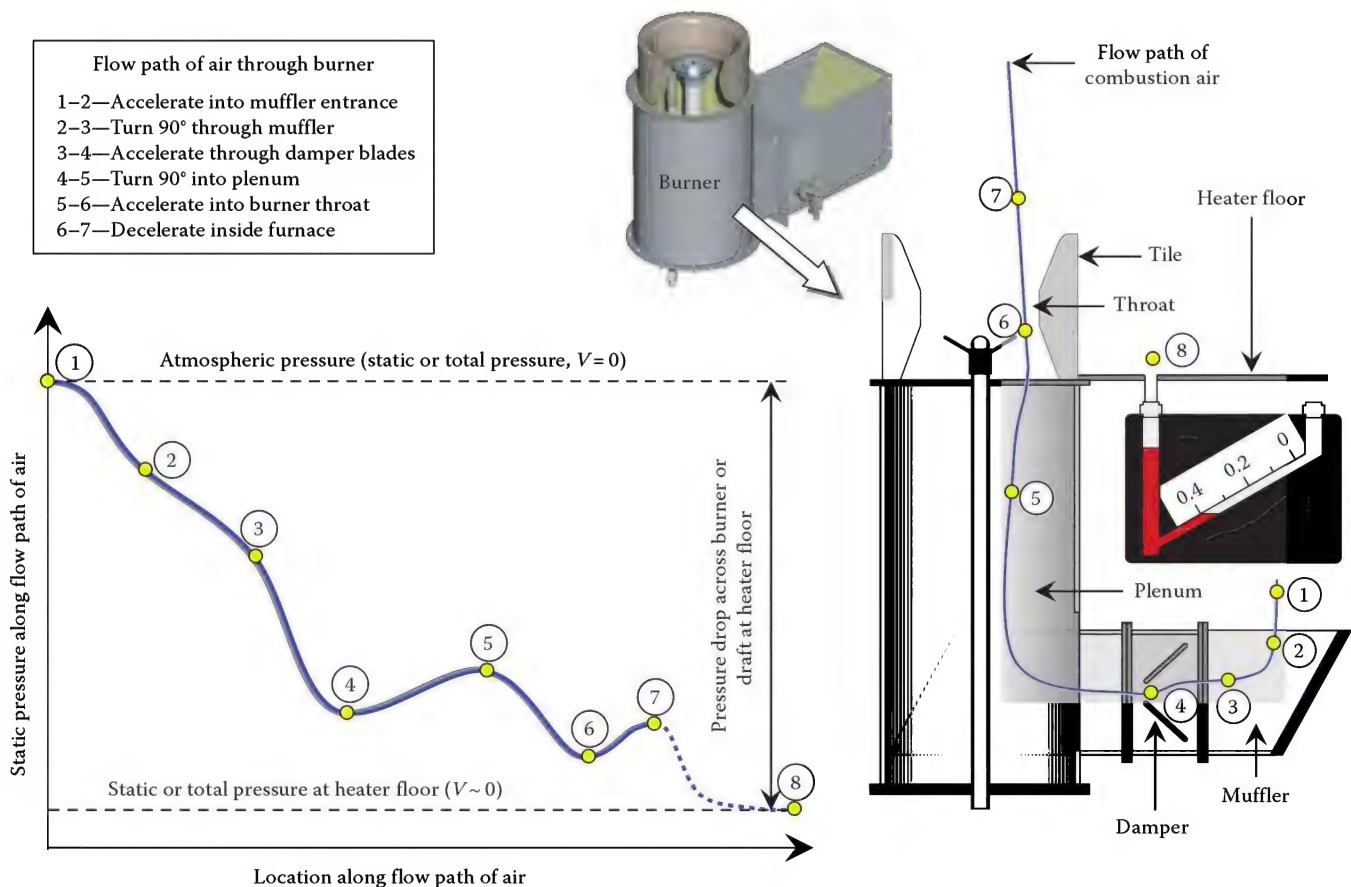


FIGURE 9.78

Illustration showing the path of combustion air as it passes through a burner.

### 9.9.2 API 560 Burner Pressure Drop Design Recommendations

According to the American Petroleum Institute 560 (API 560), it is a recommended practice to design burners to use at least 90% of the available heater draft when the burners are firing at the maximum duty with their dampers fully open. For example, suppose a heater, firing at maximum duty, is capable of producing a draft of  $-0.5$  in. of WC at the burners. According to the API recommendations, the burners should be designed to operate at a draft of  $-0.45$  in. WC ( $0.9 \times 0.5$  in. WC) or more when the burners are firing at their maximum rate (dampers fully open). The API 560 guidelines further recommends that 75% of the total pressure drop through the burner should be used at the throat of the burner. Burners designed according to these recommendations ensure that they are designed to utilize a majority of the available heater draft and that a significant portion of the draft is consumed in the throat of the burner. This is important because it helps promote a

burner design with high velocity air at the throat, which enhances mixing and provides a stiff flame that is less likely to impinge on furnace process tubes.

### 9.9.3 Air-Side Capacity Curves

Burner manufacturers usually have several different burner sizes available, of a given type, to accommodate the wide range of firing rates required in the industry. For example, since a 20 MMBtu/h (6 MW) burner requires twice as much combustion air as the 10 MMBtu/h (3 MW) burner at identical firing conditions, the muffler, damper plenum, and throat of the burner are typically larger in order to achieve the air flow required for combustion and to meet API 560 air-side pressure drop design recommendations.

Burner manufacturers often use air-side capacity curves to help them estimate the size of a burner required for a specific application. Figure 9.79 gives an example of a typical air-side capacity curve for a

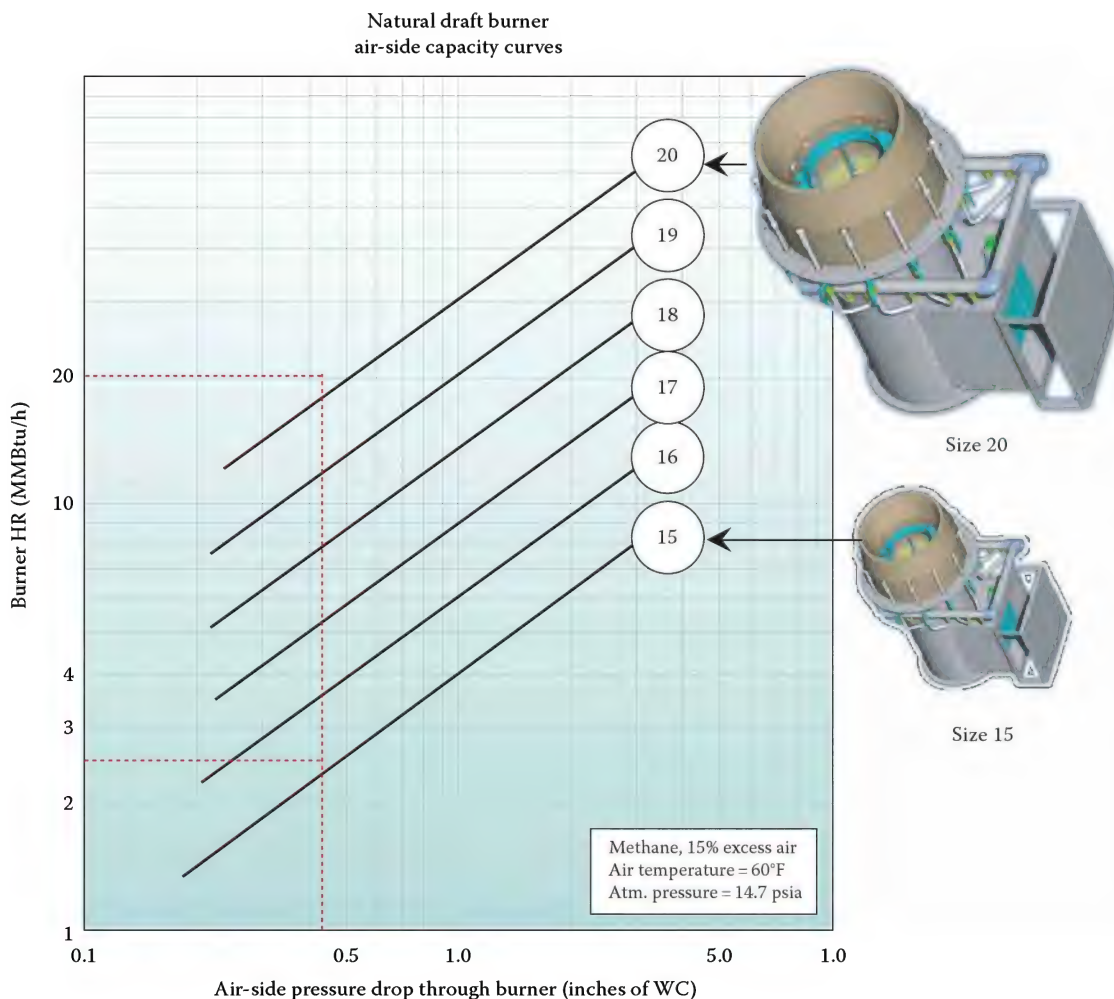


FIGURE 9.79

A typical air-side capacity curve for a natural draft burner.

particular type of burner. Air-side capacity curves basically show the firing capacity of a burner as a function of the air-side pressure drop (or burner draft) operating at a specific condition. These curves are usually generated from experimental data and are often plotted on a log-log scale to linearize the relationship. The curves shown in this particular example are based on burners operating with 15% excess air at an ambient temperature and pressure of 60°F (16°C) and 14.7 psia (1.013 bar, respectively). The numbers corresponding to each curve usually represent a nominal dimension of the burner such as the diameter of the tile throat. In this particular example, notice that a size 15 burner operating at -0.5 in. WC draft (or a burner pressure drop of 0.5 in. of WC) can achieve a maximum HR of about 2.5 MMBtu/h (0.73 MW); this is based on firing methane at 15% excess air with an ambient temperature and pressure of 60°F (16°C) and 14.7 psia (1.013 bar), respectively. Under identical firing conditions, notice a size 20 burner can achieve a maximum HR of about 20 MMBtu/h (6 MW).

When burners operate at conditions different from what is specified on the burner capacity curve, the air-side pressure drop must be corrected for those conditions. That is, one must correct the capacity curve for air temperature, altitude, or excess air conditions. The following equation can be used to correct the air-side pressure drop at actual firing conditions:

$$dP_{\text{Actual}} = dP_{\text{CC}} \times \left( \frac{100 + EA_{\text{Actual}}}{100 + EA_{\text{CC}}} \right)^2 \times \left( \frac{T_{\text{Actual}}}{T_{\text{CC}}} \right) \times \left( \frac{P_{\text{CC}}}{P_{\text{Actual}}} \right) \quad (9.24)$$

The subscript “Actual” represents the actual firing conditions and “CC” represents the value obtained from the capacity curves. The variable  $EA$  represents the percent excess air,  $T$  is the absolute temperature of the ambient air, and  $P$  is the absolute pressure of the atmosphere. For the air-side capacity curve shown in Figure 9.79,  $T_{\text{CC}} (\text{R}) = 460 + 60^\circ\text{F} = 520^\circ\text{R}$ ,  $P_{\text{CC}} = 14.7$  psia, and  $EA_{\text{CC}} = 15\%$ . Equation 9.24 shows that as the temperature of the combustion air increases, the air-side pressure drop through the burner also increases. This occurs because a higher temperature reduces the air density. Less dense air requires a larger volumetric flow rate to supply the same amount of oxygen through the burner, resulting in an increase in pressure drop. Similarly, if the atmospheric pressure is lowered, the air density is reduced resulting in an increase in air-side pressure drop. Finally, reducing the excess air requirement will lower the air-side pressure drop. To demonstrate how Equation 9.24 is used, consider the following example.

### Example 9.11

Using Figure 9.79, estimate the pressure drop through a size 15 burner firing 2.5 MMBtu/h with the heater operating at 13% excess air. The combustion air temperature is 100°F and atmospheric pressure is 14.0 psia.

A firing rate of 2.5 MMBtu/h corresponds to a pressure drop of approximately 0.5 in. WC through the size 15 burner. This represents the pressure drop for an air temperature of 60°F and atmospheric pressure of 14.7 psia. To correct the pressure drop for the actual firing conditions, Equation 9.24 is used.

$$\begin{aligned} dP &= 0.5 \times \left( \frac{100 + 13}{100 + 15} \right)^2 \times \left( \frac{460 + 100}{460 + 60} \right) \times \left( \frac{14.7}{14.0} \right) \\ &= 0.546 \text{ in. WC} \end{aligned}$$

Although the percent excess air is reduced from 15% to 13%, the pressure drop through the burner has increased because the density of the combustion air is lower at actual conditions than at standard conditions; this results in a higher volumetric flow rate of combustion air through the burner and hence a larger pressure loss.

## 9.10 Burner Fuel Capacity Curves

### 9.10.1 Background

It is important for operators to control and monitor the amount of heat fired into their furnace in order to maintain optimum throughput of their process and help prevent unsafe operating conditions. In order to control the amount of heat fired into a furnace, operators need to know the firing rate of each burner. Usually, it is too expensive to place fuel flow meters on each individual burner since most plants have multiple heaters with each heater having many burners. The most common method used in industry for determining the HR of each burner is with *fuel capacity curves*. Fuel capacity curves are graphs showing the operator how much heat is released per burner for a given fuel composition and pressure. These curves are normally supplied by the burner manufacturer and are specific to a given burner design.

The purpose of this section is to describe the fuel capacity curve, show how it is typically used by operators, and give an example calculation showing how burner manufacturers generate these curves. Before discussing the fuel capacity curve, however, it is important that the reader have a general understanding of burner HR.



### 9.10.2 Discussion of Burner Heat Release

When shopping for a light bulb, one will make a selection depending on the lighting condition that is needed. For example, one might buy a 25-Watt (W) bulb for a small reading lamp, but to light an entire room one might use a light bulb with more power, such as a 100 W bulb. The term power is a measure of how much energy is released in a given amount of time. For example, a 100 W light bulb will release 100 J of energy per second (1 Watt = 1 J/s). In industry, it is common to write the power released by a burner using kilowatts (1 kW = 1,000 W) or megawatts (1 MW = 1,000,000 W); in U.S. customary units, it is common to use MMBtu/h (millions of Btu/h). One MW is equal to 3.413 MMBtu/h. For example, a burner with an HR of 1,000,000 Btu/h can be written as 1 MMBtu/h = 0.293 MW.

The amount of power emitted from a burner is commonly referred to as the HR sometimes it is also referred to as the firing rate, firing duty, firing capacity, or heat output. The HR of a burner depends on how much fuel the burner consumes and how much energy the fuel releases when it is burned (fuel heating value). Mathematically, the HR of a burner can be written as follows:

$$HR = \dot{m} \times HV \quad (9.25)$$

where

$\dot{m}$  is the mass flow rate of the fuel  
 $HV$  is the heating value of the fuel

In the process burner industry, the lower heating value ( $LHV$ ) of the fuel is typically used to determine the HR. However, in the glass, steel, and boiler industry it is more common to use the higher heating value ( $HHV$ ) of the fuel. To demonstrate how Equation 9.25 is used, consider the following example.

#### Example 9.12

A process burner is firing methane at a rate of 100 lb/h. Determine the HR of the burner based on an  $LHV$  of 910.0 Btu/scf (the  $LHV$  is based on 59°F and 14.696 psia). First, calculate the density of the fuel,  $\rho_{\text{fuel,STP}}$ , at standard temperature and pressure (STP, 14.696 psia and 59°F) utilizing Equation 9.2.

$$\begin{aligned} \rho_{\text{fuel,STP}} &= \rho_{\text{air,STP}} \times \frac{MW_{\text{fuel}}}{MW_{\text{air}}} = 0.0765 \frac{\text{lb}}{\text{ft}^3} \times \frac{16}{29} \\ &= 0.0422 \frac{\text{lb}}{\text{ft}^3} \end{aligned}$$

where

$\rho_{\text{air,STP}}$  is the density of air at STP  
 $MW_{\text{fuel}}$  and  $MW_{\text{air}}$  are the molecular weights of the fuel and air, respectively

Next, determine the  $LHV$  of the fuel on a mass basis.

$$LHV_{\text{mass basis}} = \frac{LHV_{\text{volume basis}}}{\rho_{\text{fuel,STP}}} = \frac{910 \frac{\text{Btu}}{\text{ft}^3}}{0.0422 \frac{\text{lb}}{\text{ft}^3}} = 21,564 \frac{\text{Btu}}{\text{lb}}$$

Finally, calculate the HR of the burner.

$$\begin{aligned} HR &= \dot{m} \times LHV_{\text{mass basis}} \\ HR &= 100 \frac{\text{lb}}{\text{h}} \times 21,564 \frac{\text{Btu}}{\text{lb}} \times \frac{1 \text{ MMBtu}}{1,000,000 \text{ Btu}} \\ &= \underline{2.16 \text{ MMBtu/h}} \end{aligned}$$

In this example, the burner will release 2,160,000 Btu (2.16 MMBtu) of energy into the furnace every hour; this can be converted to megawatts by dividing by 3.413 (2.16 MMBtu/h ÷ 3.413 MW/MMBtu/h = 0.633 MW).

### 9.10.3 Description of Fuel Capacity Curves

Figure 9.80 shows an example of what a typical capacity curve might look like for a burner firing methane. Notice that the vertical axis corresponds to the HR of the burner in units of MMBtu/h and the horizontal axis corresponds to the fuel pressure in units of psig. Sometimes, capacity curves are represented using

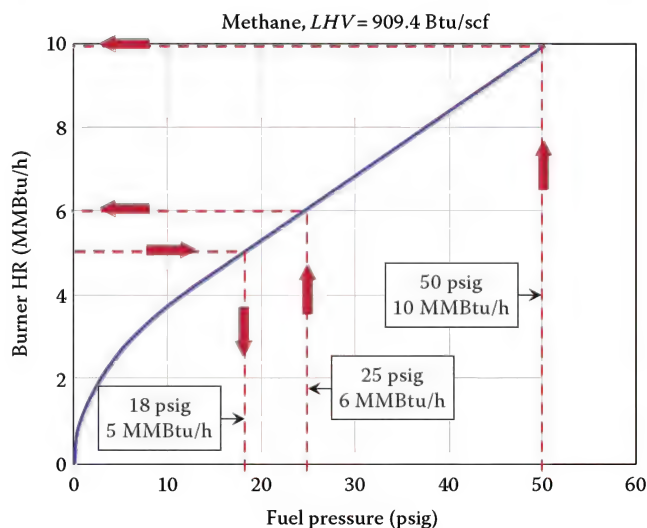


FIGURE 9.80  
Example of a fuel capacity curve.



different units. For example, a capacity curve might use units of megawatts (MW) for the burner HR and Pascal (Pa) for units of pressure. Next, an explanation will be provided showing how the capacity curve is used.

Referring to Figure 9.80, consider a burner is firing methane at 50 psig. The HR of the burner can be determined by locating 50 psig on the horizontal axis and moving up to the curve. Moving horizontally from this point to the vertical axis gives an HR of near 10 MMBtu/h. Now, suppose the burner HR is reduced by one-half (2:1 turndown). Should the fuel pressure be reduced by one-half? Notice that if the pressure is reduced by one-half (25 psig), the HR only drops to 6 MMBtu/h. This clearly demonstrates that reducing the fuel gauge pressure by one-half did not reduce the HR by one-half. That is, the fuel pressure and HR are not linearly proportional. In order to reduce the HR of the burner from 10 to 5 MMBtu/h, the fuel pressure would have to be lowered to about 18 psig. Next, an explanation will be provided showing how the HR varies with fuel pressure.

Referring to Figure 9.81, notice that as the fuel pressure increases from zero, the HR of the burner initially follows a curved path (shown in blue). As the fuel pressure further increases, however, the curve eventually transforms into a straight line (shown in red). The pressure corresponding to the point where the curve and straight line intersect each other is referred to as the *critical fuel pressure*. The critical pressure is a function of the atmospheric pressure

( $P_{\text{atm}}$ ) and ratio of specific heat ( $k$ ) and can be calculated as follows:

$$P_{c, \text{gage}} = \frac{P_{\text{atm}}}{\left(\frac{2}{k+1}\right)^{k/(k-1)}} - P_{\text{atm}} \quad (9.26)$$

### Example 9.13

Determine the critical pressure ( $P_c$ ) of a fuel with  $k = 1.31$  and  $P_{\text{atm}} = 14.7$  psia.

$$\begin{aligned} P_{c, \text{gage}} &= \frac{P_{\text{atm}}}{\left(\frac{2}{k+1}\right)^{k/(k-1)}} - P_{\text{atm}} \\ &= \frac{14.7 \text{ psia}}{\left(\frac{2}{1.31+1}\right)^{1.31/(1.31-1)}} - 14.7 \text{ psia} = 12.3 \text{ psig} \end{aligned}$$

The critical pressure, for example, of methane, propane, and hydrogen is 12.4, 10.7, and 13.2 psig, respectively, at an atmospheric pressure of 14.7 psia.

When a burner operates at a fuel pressure less than the critical pressure, the fuel at the exit of the nozzle flows at a velocity less than the speed of sound (based on the static temperature and pressure at the nozzle exit); this is referred to as *subsonic flow*. However, when the fuel pressure reaches the critical pressure or higher, the fuel exits the orifice at a velocity equal to the speed of sound; this is referred to as *sonic flow*. Figure 9.82 show photographs downstream of a nozzle for a gas flowing

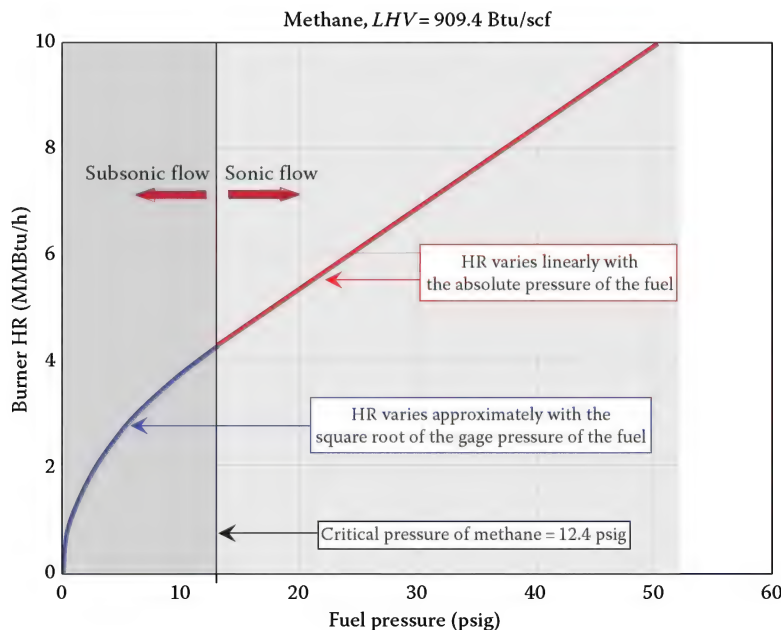
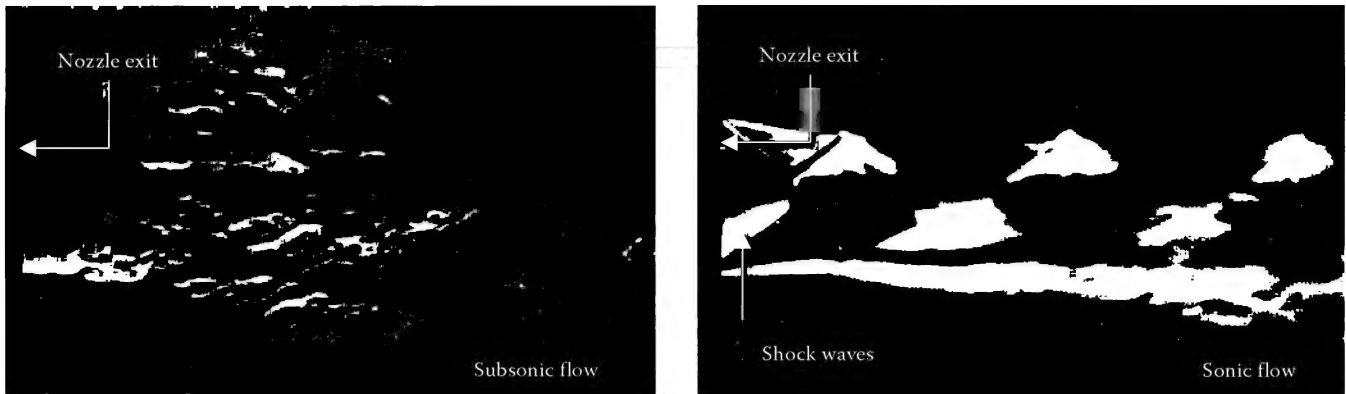


FIGURE 9.81

Graph showing how the fuel capacity curve varies in the subsonic and sonic flow regimes.

**FIGURE 9.82**

Photographs of gas exiting a nozzle at sonic and subsonic flow conditions. At sonic flow conditions, the gas exits the nozzle at the speed of sound creating shock waves downstream. At subsonic flow conditions, the gas exits the nozzle less than the speed of sound with no shock waves. (Sonic flow from Oertel 1975, subsonic flow from Bradshaw Ferriss and Johnson 1964, *An Album of Fluid Motion*, The Parabolic Press, Stanford, CA, 1982, p. 98.)

at sonic and subsonic conditions. Notice for sonic flow, shock waves form downstream of the nozzle, but do not form for the subsonic condition. When shock waves form downstream of the nozzle, it compresses the gas upstream resulting in the transformation from a curved profile to a linear profile on the fuel capacity curve.

Regardless of the fuel composition, all fuel capacity curves will exhibit a similar trend; that is, a curved profile in the subsonic regime (below critical pressure) and a linear profile in the sonic regime (at or above critical pressure). For fuel pressures lower than the critical pressure (subsonic flow regime), the burner HR varies approximately with the square root of the *gauge* pressure (psig). For values greater than the critical pressure (sonic flow regime), the burner HR varies linearly with the *absolute* pressure (psia). To demonstrate these concepts, consider the following examples.

**Example 9.14**

A burner is firing methane at 25 psig corresponding to an HR of 6 MMBtu/h. Determine the HR of the burner if the pressure of the fuel were to increase to 50 psig. Assume the atmospheric pressure is 14.7 psia.

Since the fuel pressures in this example are in the sonic regime (pressures greater than critical pressure), the burner HR varies linearly with the absolute pressure. Therefore, the following equation is used to determine the burner HR at 50 psig:

$$HR_2 = HR_1 \frac{P_{2,\text{psig}} + P_{\text{atmospheric,psia}}}{P_{1,\text{psig}} + P_{\text{atmospheric,psia}}} \quad (9.27)$$

$$HR_{\text{at } 50 \text{ psig}} = 6 \text{ MMBtu/h} \frac{50 + 14.7}{25 + 14.7} = 9.78 \text{ MMBtu/h}$$

**Example 9.15**

A burner is firing methane at 5 psig corresponding to an HR of 2.7 MMBtu/h. Estimate the HR of the burner if the pressure of the fuel were to increase to 10 psig.

Since the fuel pressures in this example are in the subsonic regime (pressures less than critical pressure), the HR varies approximately as the square root of the gauge pressure. Therefore, the following equation is used to determine the burner HR at 10 psig:

$$HR_2 = HR_1 \sqrt{\frac{P_{2,\text{psig}}}{P_{1,\text{psig}}}} \quad (9.28)$$

$$HR_{\text{at } 10 \text{ psig}} = 2.7 \text{ MMBtu/h} \sqrt{\frac{10}{5}} = 3.8 \text{ MMBtu/h}$$

It should be emphasized that the square root relationship of pressure versus HR is an approximation and is usually within a small percent of the exact solution. It should also be mentioned that the calculation procedure used in the earlier examples are different if the fuel pressures of interest fall on both sides of the critical fuel pressure. To demonstrate this concept, consider the following example:

**Example 9.16**

A burner is firing propane at 5 psig corresponding to an HR of 4 MMBtu/h. Estimate the HR of the burner if the pressure of the fuel were to increase to 30 psig. Assume the atmospheric pressure is 14.7 psia.

Since the fuel pressures in this example are in both the subsonic (5 psig) and sonic (30 psig) regime, the problem needs to be separated

into two parts. First, estimate the HR of the burner operating at the critical pressure of propane (10.7 psig). Knowing the HR at 5 psig, the square root relationship of the gauge pressure is used to estimate the HR at the critical pressure as follows:

$$HR_{at\ 10.7\ psig} = 4\ \text{MMBtu/h} \sqrt{\frac{10.7}{5}} = 5.9\ \text{MMBtu/h}$$

Next, using the HR at the critical pressure, the linear relationship with the absolute pressure is used to estimate the HR at 30 psig.

$$\begin{aligned} HR_{at\ 30\ psig} &= 5.9\ \text{MMBtu/h} \frac{30 + 14.7}{10.7 + 14.7} \\ &= 10.4\ \text{MMBtu/h} \end{aligned}$$

Burners are usually designed to fire more than one fuel composition. In this instance, burner manufacturers will usually provide a capacity plot that contains several curves representing each fuel. For example, Figure 9.83 shows a fuel capacity plot for a particular burner firing three different fuels: propane, methane, and hydrogen. Consider the following scenario using this capacity plot: Suppose an operator is firing a burner on propane at an HR of 8 MMBtu/h; this corresponds to a fuel pressure of 21 psig. If the fuel composition changes to methane, the plot shows that the operator would have to adjust the fuel to about 37 psig in order to maintain a constant HR. If no adjustments were made to the fuel pressure during the swing in fuel composition, notice the burner HR would fall to about 5.5 MMBtu/h.

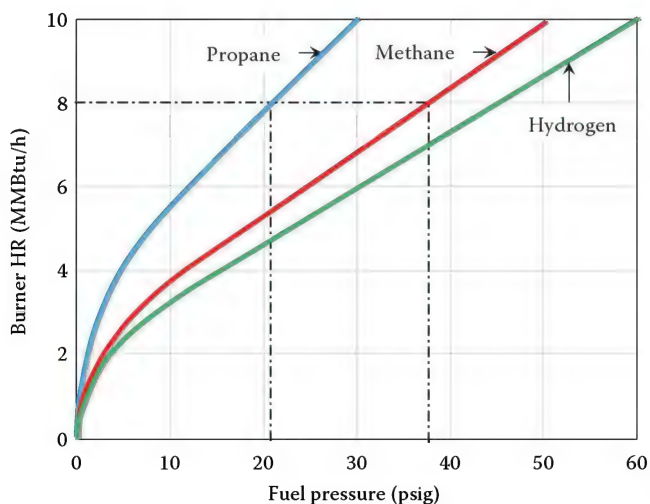


FIGURE 9.83

Example of a fuel capacity curve for a particular burner firing several fuels.

#### 9.10.4 Effects of Internal Nozzle Design on Fuel Capacity Curves

Burner tips, sometimes called nozzles or fuel injectors, are designed and used to control the amount of fuel delivered into a process burner. Tips are considered to be one of the most important components on a burner because they directly impacts safety, thermal efficiency, pollution emissions, and operability.<sup>47</sup> Burners usually have several fuel tips and each fuel tip typically has multiple holes (called fuel ports). The angle, size, number, and position of the fuel ports are designed to achieve a specific flame shape and burner performance. There are many different tip designs used in the burner industry as shown in Figure 9.84. Some applications use nozzles designed with multiple arms, commonly called spider tips, while others use nozzles with less complicated designs. Burner tips not only appear different on the outside, but their geometry is also different internally.

Variations in the internal design of a tip can have a significant impact on the flow rate of gas through the tip. When burner manufacturers design combustion equipment, the internal geometry of the tips is an integral part of the overall design of the equipment. For example, if a user were to replace a tip on a burner with a different internal design, it could significantly alter the flow rate of fuel to the equipment, even though the gas-side area and port arrangement of the replacement tip is identical to the original; this modification could significantly jeopardize the safety and performance of the equipment. When replacing tips on burner equipment, it is important that the user consult the manufacturer and use the appropriate replacement parts. The purpose of this section is to discuss how replacing nozzles that are not designed by the manufacturer can alter fuel



FIGURE 9.84

Burner tips commonly used in the burner industry. Burner tips not only appear different on the outside, but their geometry is also different internally. (Photograph by Wes Bussman.)



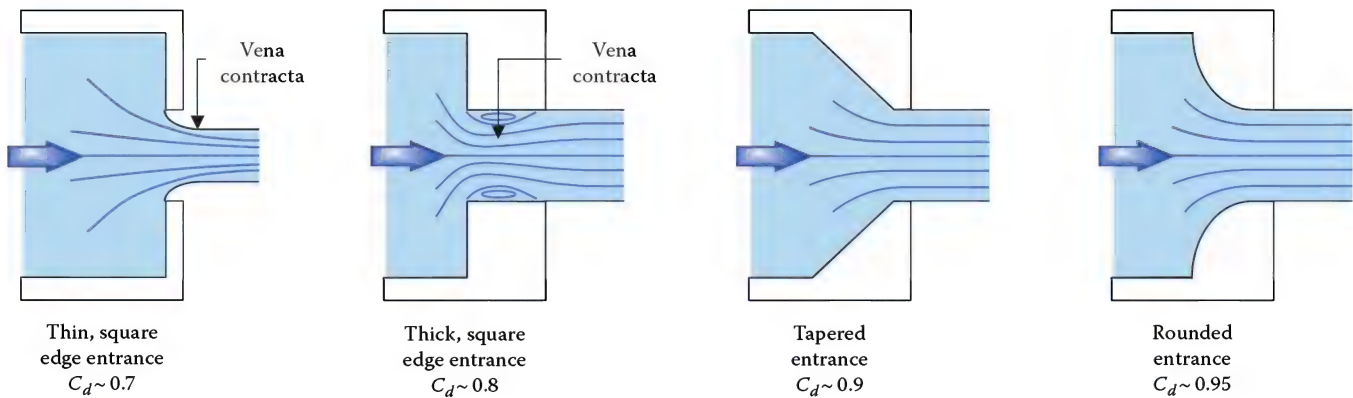


FIGURE 9.85

Illustration showing four nozzles having the same port area but with different internal designs. The more streamlined the orifice entrance is the more fuel it will flow at a given pressure.

capacity curves that could trigger several problems in the operation of a heater.

First, an explanation is provided showing how the internal design of a nozzle can affect the fuel flow rate. Figure 9.85 is an illustration showing four nozzles having the same port area but with different internal designs. Suppose these nozzles were firing methane at the same pressure, which nozzle would flow more fuel? The rounded entrance nozzle would flow more fuel because it has a more streamlined entrance design than the other nozzles. Notice the nozzles with square-edged entrances have streamlines that converge near the exit and that the area of the jet actually decreases; this point of minimum area is called the *vena contracta*. The vena contracta creates a restriction in the flow reducing the effective orifice area and hence flow rate.

To gain a better understanding of how much the internal design of a nozzle affects the fuel flow rate, a term called the *orifice discharge coefficient* is discussed next. When engineers generate fuel capacity curves, they use mathematical equations formulated to give the flow rate of a fuel through an orifice. These theoretical equations, however, are based on the assumption that the flow through the nozzle is perfect or ideal. That is, the equations assume that the fuel flows through the nozzle without any (1) pressure losses, (2) heat transfer, or (3) reduction in the cross-sectional area of the fuel jet (vena contracta). Since these assumptions do not reflect what really happens, the calculated flow rate is always greater than the actual flow rate through the nozzle. To compensate for the discrepancy, engineers multiply the ideal solution by a correction factor called the orifice discharge coefficient; mathematically, this can be written as follows:

$$\dot{m}_{\text{actual}} = C_d \dot{m}_{\text{ideal}} \quad (9.29)$$

where

$\dot{m}_{\text{actual}}$  is the actual mass flow rate through the nozzle

$C_d$  is the orifice discharge coefficient

$\dot{m}_{\text{ideal}}$  is the mass flow rate through the nozzle based on ideal mathematical equations

The orifice discharge coefficient of burner nozzles is determined experimentally.

Figure 9.85 shows that a nozzle designed with a thin, square-edged entrance will typically have a discharge coefficient of about 0.7. However, as the length of the port increases, the discharge coefficient increases to a value of about 0.8. If the entrance to the port is tapered, the flow becomes more streamlined and the discharge coefficient further increases to a value of about 0.9. A nozzle with a rounded entrance will typically have a discharge coefficient of about 0.95. Usually, nozzles in the burner industry are designed with square-edge or tapered entrance while rounded entrance designs are less common.

Typically, the discharge coefficient of burner nozzles varies from about 0.80 for square-edge inlets to about 0.92 for tapered inlets. It is possible that the discharge coefficients can vary over time. For example, Figure 9.86 shows photographs of a pressure swing absorption (PSA) gas tip that was in service for about four years. Upon inspection, it was found that the tip suffered severe corrosion from metal dusting. Initially, this nozzle was designed with square edge port inlets. Notice in the cut-away view, however, that the inlets to the ports are now rounded; this can have a significant impact on the fuel capacity curve. For this particular example, it would not be surprising that the HR increased by about 20%–25%.

The main factors that can affect the discharge coefficient of a nozzle include the following: (1) ratio of port length to port diameter, (2) ratio of port diameter to upstream diameter, (3) angle of tapered entrance, and (4) manufacturing tolerances. See Figure 9.87 for a





FIGURE 9.86

Photographs of a PSA gas burner showing rounded port inlets caused by corrosion from metal dusting.

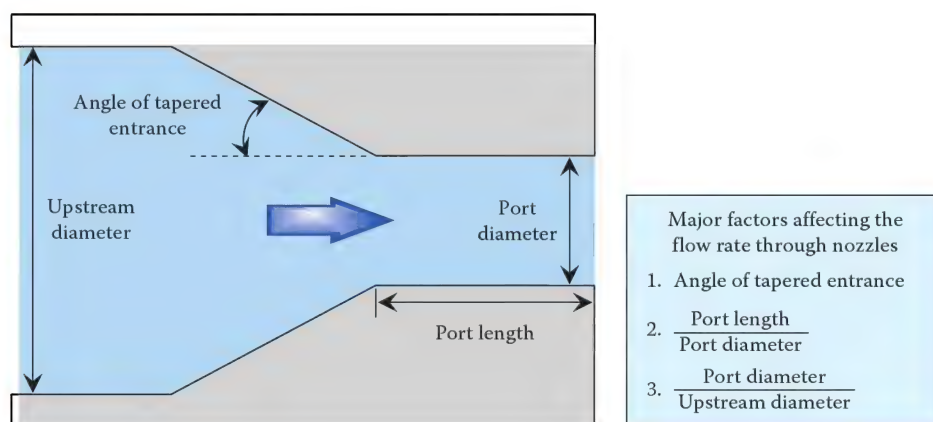


FIGURE 9.87

Illustration showing a several important factors that influence the flow rate through nozzles.

description of these variables. The burner designer must be aware of these variables and consider their effects on equipment performance.

To demonstrate how the internal design of burner tips can alter the heater operations, consider the following example:

#### Example 9.17

Burners installed in a furnace are designed to operate at a pressure of 32 psig in order to achieve the desired heat input. After several years of successful operation, the operators begin to notice that they cannot achieve the HR required for their operation. Upon inspection, they discover that the tips on many burners are starting to coke and plug. The operators decide to replace all the tips using their own fabricated tip with the same drilling area and pattern. What they did not realize is that the length-to-diameter ratio of the ports on their nozzles is different than the manufacturers' and they also failed to debur the ports; this results in an orifice discharge coefficient that is different than the manufacturers' tips. Suppose the orifice discharge

coefficient for their fabricated tip is 0.70 and the manufacturer's is 0.85. How could this affect the operability of the heater?

Figure 9.88 is a plot showing the fuel pressure required to maintain a constant HR for burner tips with identical fuel-side area, but with different orifice discharge coefficients. The manufacturer's tip is represented by the blue dashed line; that is, an orifice discharge coefficient of 0.85 requires a fuel pressure of 32 psig to achieve the desired HR. The operator's fabricated tip is represented by the orange dashed line; an orifice discharge coefficient of 0.70. Notice that in order to achieve the desired HR the fabricated tip would require a fuel pressure of about 42 psig. If the operators do not have this pressure available, they would not be able to achieve the desired heat input for their process. Now consider that they do have the fuel pressure available. How could this affect the operability of the heater? With the fabricated tips on the burners, the burners are now operating at a fuel pressure 10 psig higher than what they were designed for due to the smaller effective diameter of the ports

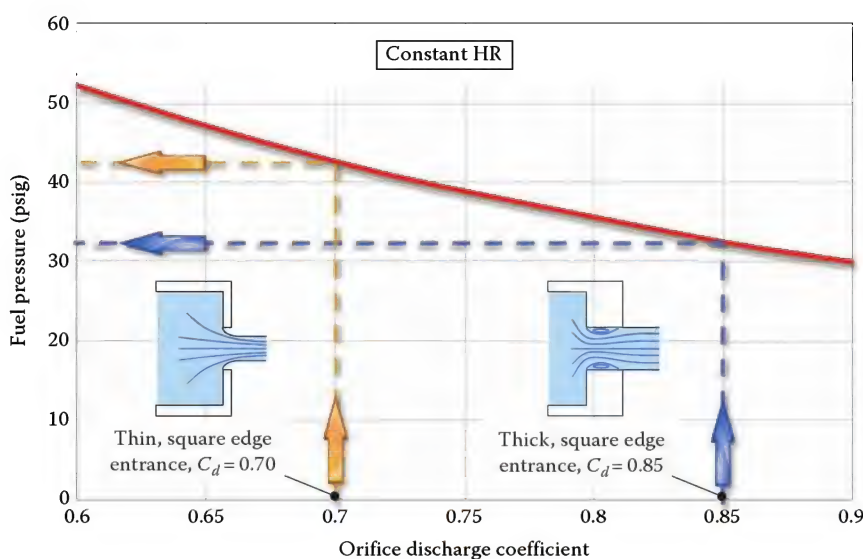


FIGURE 9.88

Example showing how the orifice discharge coefficient affects the fuel pressure of a burner operating at a constant HR. As the orifice discharge coefficient is lowered, the fuel pressure must increase significantly.

created by the vena contracta. The combination of higher fuel pressure and smaller effective port diameter would allow more flue gas to be entrain into the fuel jets; this could cause burner stability issues, longer flames, reduced burner turndown, and/or increased CO, and UHC emissions.

#### 9.10.5 Effects of Orifice Plugging on Fuel Capacity Curves

One of the most important maintenance issues with the fuel side of the burner is plugging of the burner tips. A few sources of material that can plug fuel tips include pipe-scale (Figure 9.89), dirt, salts, gums, polymers, and



FIGURE 9.89

Fuel ports plugged with pipe scale and dirt.

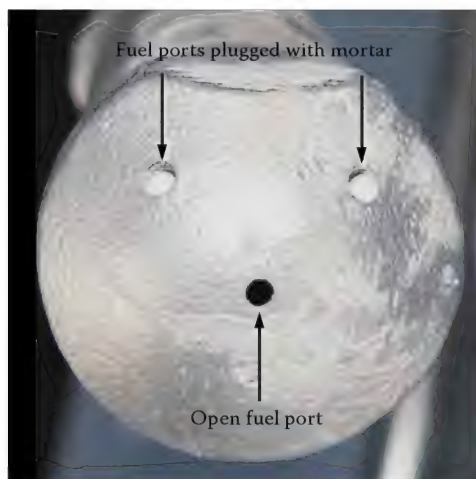


FIGURE 9.90

Fuel ports plugged with mortar.

amine compounds found in the fuel, coke, and refractory mortar (Figure 9.90). When fuel tips become fully or partially plugged, they can dramatically alter the flame pattern inside the heater as demonstrated in Figure 9.91. When fuel tips become plugged, they should be cleaned quickly to avoid more serious maintenance problems. The purpose of this section is to (1) discuss how flame patterns can be affected by partial plugging inside the fuel tip and fuel supply line, (2) demonstrate the effects of orifice plugging on fuel capacity curves, and (3) provide an example showing the analysis involved in generating a single point on a fuel capacity curve.

A common way tips become plugged is from *coking*. Coking is the buildup of a black carbonaceous material



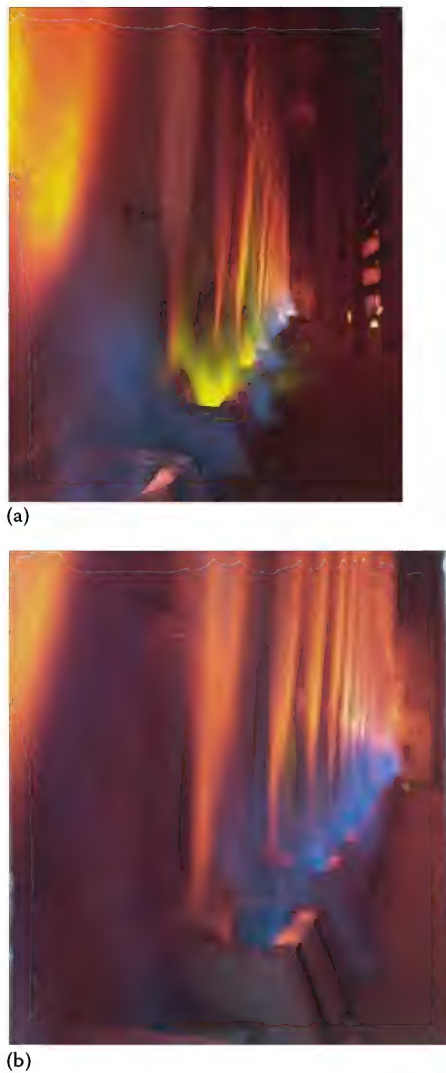


**FIGURE 9.91**  
Flame patterns (a) before and (b) after cleaning coke from fuel ports.

inside a burner tip. Under normal firing conditions, the high-velocity fuel flowing through burner tips extracts enough heat from the metal to prevent the tips from reaching extremely high temperatures. However, low firing conditions or when burners are taken out of service while the heater is hot can cause tips to overheat. When fuel tips are exposed to extremely high temperatures, they can cause the fuel to thermally crack and deposit carbon (coke) on the inside walls of the tips as shown in Figure 9.92. When the coke builds up on the walls, it can completely or partially plug the fuel ports and the main body of the tip. Also, as the inner wall of burner tips become covered with coke, the ability to transfer heat from the tip to the fuel is diminished and the tip temperature increases. The higher tip temperature causes the coke thickness to increase; thus, a cycle of coke buildup followed by temperature increase begins. If not promptly addressed, the tips will be destroyed.

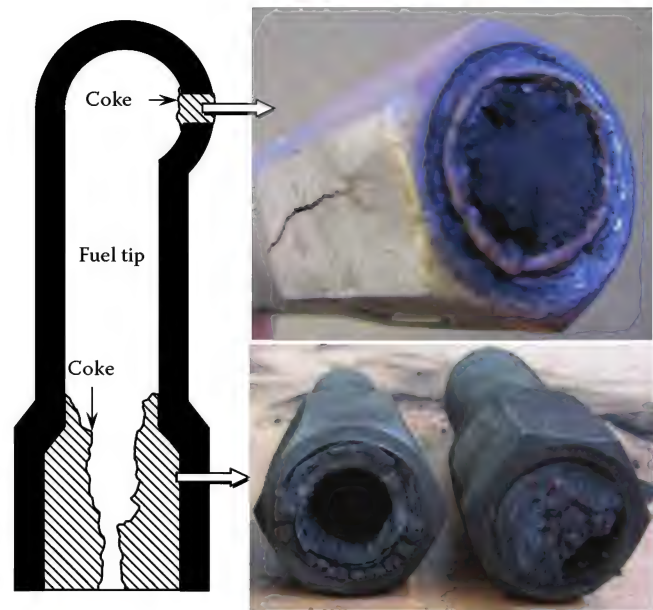


**FIGURE 9.92**  
Coke buildup in the main body of the fuel nozzle.

When coke deposits or other sources of material such as pipe scale partially block the fuel ports near the outlet as illustrated in Figure 9.93, the effective area of the fuel jet decreases. As the area of the port becomes smaller, the fuel jet exiting the nozzle is able to entrain the surrounding gas at a faster rate than what it was designed for. That is, for a given distance downstream of the nozzle exit, a smaller diameter fuel jet entrains more of the surrounding gas as compared to a larger jet at the same fuel flow rate. This effect can have a significant impact on the flame stability because if too much air or flue gas is mixed with the fuel, prior to combustion, it can reduce the stability of the flame causing it to lift from the burner or go out completely as demonstrated

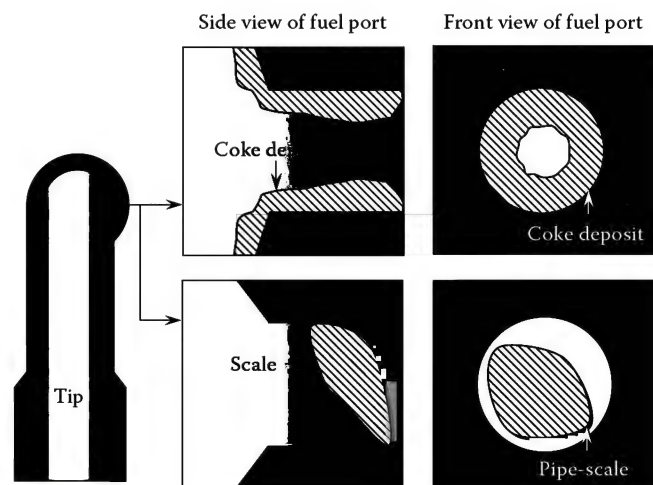
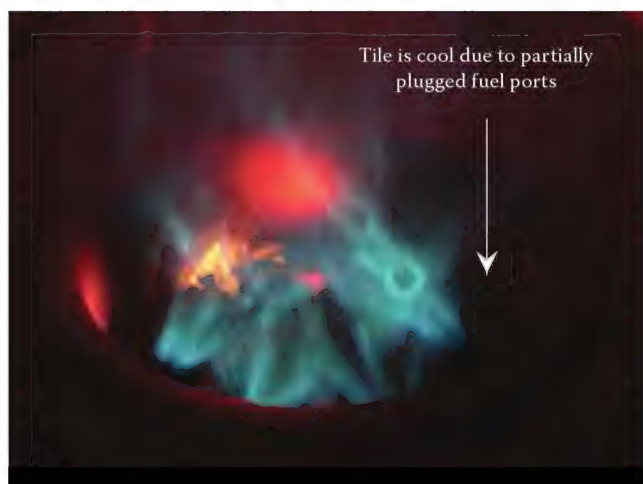


**FIGURE 9.93**  
Illustration showing partial blockage near the outlet of a fuel port.



(a)



(b)

**FIGURE 9.94**

Comparing a burner (a) without and (b) with partially plugged primary fuel tips.

in Figure 9.94. This photograph shows that the inside of the tile is not glowing hot due to primary fuel ports partially plugged with coke.

When fuel ports plug, it can significantly alter the capacity curves. For example, consider the following: Burners in a heater are designed to fire methane at an HR of 1.5 MMBtu/h (0.44 MW), corresponding to a fuel pressure of 30 psig (2 barg). During operation, the burner fuel ports start to partially plug with coke. How much does this affect the fuel capacity curves? Figure 9.95 is a plot showing the fuel capacity curve with the area of the nozzle ports blocked 0%, 25%, and 50%. Notice that with 0% blockage, a fuel pressure of 30 psig corresponds to the design HR of 1.5 MMBtu/h (0.44 MW). However, with 25% blockage the fuel pressure must be increased to about 45 psig (3 barg) to maintain a constant HR with 50% blockage the pressure must be increased to 75 psig (5 barg). Clearly, partial plugging of

fuel ports has a significant effect on fuel capacity curves. If the measured fuel pressure is higher than the pressure obtained from fuel capacity curves, the tips may be plugged.

If materials build up inside the main body of the fuel tip (see Figures 9.92 and 9.96) or in the fuel supply line that leads to the burners, the pressure drop through the piping will increase and the flow will be restricted; in this case, the flame can behave differently as compared to plugging that occurs near the outlet of a fuel port. The debris in the main body of a partially plugged tip or fuel supply line can act as a double drop orifice. That is, as the fuel flows past the debris, it loses pressure causing the fuel to exit the ports at a lower velocity. This not only reduces the HR of the burner, but it also reduces the mixing rate of the fuel with the combustion air and furnace flue gas. When this occurs, the flame usually appears short and bright yellow as shown in Figure 9.97.

### 9.10.6 Generating Fuel Capacity Curves

Before computers were common in the workplace, engineers used lookup tables and performed hand calculations using slide rules to generate fuel capacity curves. This was usually a time-consuming task. Today, fuel capacity curves are typically generated using computer programs. In this section, an example is provided that demonstrates the analysis involved in generating a single point on a fuel capacity curve.

#### Example 9.18

Determine the HR of a burner operating at a fuel pressure ( $P_{\text{fuel,gage}}$ ) of 30 psig with the following conditions:

LHV of fuel ( $LHV_{\text{volume basis}}$ ) = 1380.7 Btu/scf

Orifice area ( $A$ ) = 0.1254 in.<sup>2</sup>

Molecular weight of fuel ( $MW_{\text{fuel}}$ ) = 28.4

Ratio of specific heat of fuel ( $k$ ) = 1.19

Fuel temperature ( $T_{\text{fuel}}$ ) = 100° F

Atmospheric pressure ( $P_{\text{atm}}$ ) = 14.7 psia

Orifice discharge coefficient ( $C_d$ ) = 0.85

**Step #1.** Determine the LHV of the fuel on a mass basis,  $LHV_{\text{mass basis}}$

First, determine the density of the fuel,  $\rho_{\text{fuel}}$ .

$$\begin{aligned}\rho_{\text{fuel,STP}} &= \rho_{\text{air,STP}} \times \frac{MW_{\text{fuel}}}{MW_{\text{air}}} = 0.0765 \frac{\text{lb}}{\text{ft}^3} \times \frac{28.4}{29} \\ &= 0.0749 \frac{\text{lb}}{\text{ft}^3}\end{aligned}$$



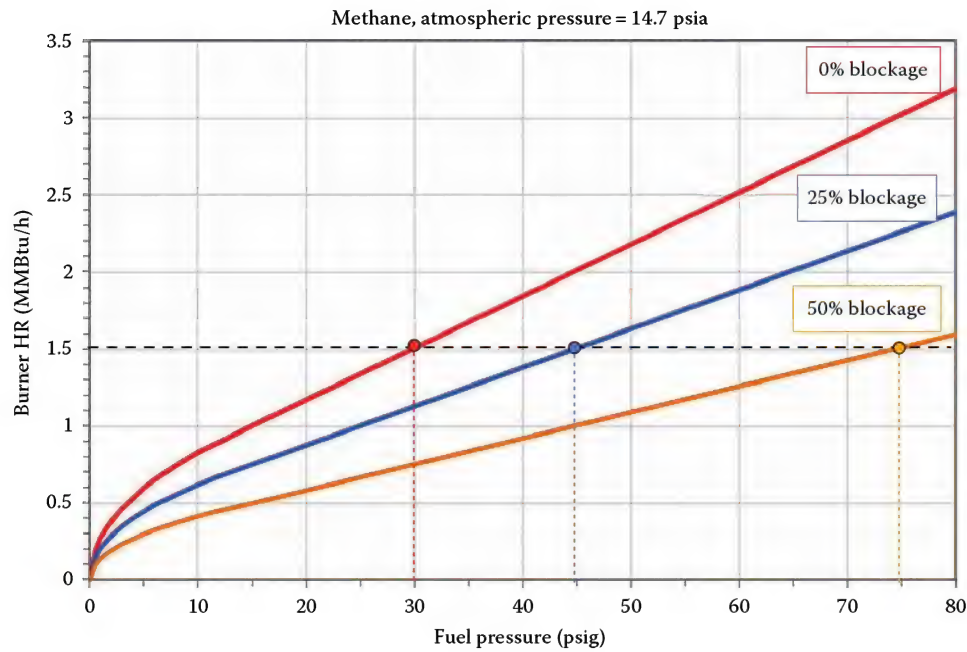


FIGURE 9.95

Example showing the effects of fuel port blockage on the fuel capacity curves.

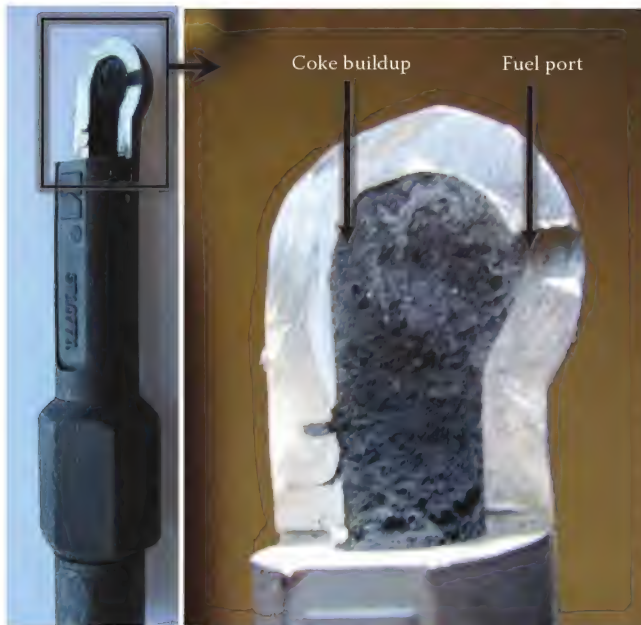


FIGURE 9.96

Burner tip with coking on the inside.

Next, calculate the *LHV* of the fuel on a mass basis.

$$LHV_{\text{mass basis}} = \frac{LHV_{\text{volume basis}}}{\rho_{\text{fuel}}} = \frac{1380.7 \frac{\text{Btu}}{\text{ft}^3}}{0.0749 \frac{\text{lb}}{\text{ft}^3}} = 18,433.9 \frac{\text{Btu}}{\text{lb}}$$

**Step #2.** Determine the Mach number of the fuel at the exit of the port,  $Ma_e$ .

The Mach number is defined as the velocity of the fuel at the port exit divided by the speed of sound of the fuel at the port exit based on the static pressure and temperature at that location. The Mach number at the exit can be determined as follows:

$$Ma_e = \left\{ \frac{2}{k-1} \left[ \left( \frac{P_{\text{fuel,gage}} + P_{\text{atm,absolute}}}{P_{\text{atm,absolute}}} \right)^{\frac{k-1}{k}} - 1 \right] \right\}^{1/2}$$

$$Ma_e = \left\{ \frac{2}{1.19-1} \left[ \left( \frac{30 \text{ psig} + 14.7 \text{ psia}}{14.7 \text{ psia}} \right)^{\frac{1.19-1}{1.19}} - 1 \right] \right\}^{1/2}$$

$$= 1.43$$

If the Mach number at the exit of a sonic nozzle can never be greater than a value of one, then why is the value just calculated greater than one? The calculated value indicates the maximum possible Mach number that could be achieved if the fuel were to flow through an ideal supersonic nozzle (converging-diverging nozzle). Since the fuel port is not a supersonic nozzle, the Mach number at the exit must be equal to one ( $Ma_e = 1$ ). If the calculated Mach number were less than a value of one, this would indicate that the flow at the nozzle exit is subsonic; that is, less than the speed of sound.



FIGURE 9.97

Fuel tips partially plugged upstream of the ports.

A question commonly asked is if the velocity of the gas cannot exceed sonic velocity at the nozzle exit, then how can the mass flow rate increase? Although the gas velocity does not exceed sonic velocity above the critical pressure, the density of the gas does increase with an increase in the upstream pressure; this increase in gas density at the nozzle exit is what leads to higher mass flow rate with an increase in upstream pressure.

**Step #3.** Determine the static pressure ( $P_e$ ) at the exit of the fuel port.

$$P_e = \frac{P_{\text{fuel,gage}} + P_{\text{atm,absolute}}}{\left[1 + \left(\frac{k-1}{2}\right)Ma_e^2\right]^{\frac{k}{k-1}}} = \frac{30 \text{ psig} + 14.7 \text{ psia}}{\left[1 + \left(\frac{1.19-1}{2}\right)1^2\right]^{\frac{1.19}{1.19-1}}} = 25.3 \text{ psia}$$

**Step #4.** Determine the static temperature ( $T_e$ ) at the exit of the fuel port.

$$T_e = \frac{T_{\text{fuel},^\circ\text{F}} + 460}{1 + \left(\frac{k-1}{2}\right)Ma_e^2} = \frac{100^\circ\text{F} + 460}{1 + \left(\frac{1.19-1}{2}\right)1^2} = 511.4 \text{ R}$$

**Step #5.** Determine the fuel density ( $\rho_e$ ) at the exit of the fuel port.

Knowing the static pressure and temperature at the exit of the fuel port, the ideal gas law is used to determine the density as follows:

$$\rho_e = \frac{P_e}{RT_e}$$

The gas constant ( $R$ ) is calculated as follows:

$$R = \frac{\bar{R}}{MW_{\text{fuel}}} = \frac{1545.32 \frac{\text{ft}\cdot\text{lb}_f}{\text{lb}_m\cdot\text{mole}\cdot\text{R}}}{28.4 \frac{\text{lb}_m}{\text{lb}_m\cdot\text{mole}} \times \frac{1 \text{ slug}}{32.2 \text{ lb}_m}} = 1757.15 \frac{\text{ft}\cdot\text{lb}_f}{\text{slug}\cdot\text{R}}$$

The density of the fuel at the burner exit becomes

$$\rho_e = \frac{P_e}{RT_e} = \frac{25.3 \frac{\text{lb}_f}{\text{in}^2} \times 144 \frac{\text{in}^2}{\text{ft}^2}}{1757.15 \frac{\text{ft}\cdot\text{lb}_f}{\text{slug}\cdot\text{R}} \times 511.4 \text{ R}} = 0.00405 \frac{\text{slug}}{\text{ft}^3}$$

**Step #6.** Determine the speed of sound ( $c_e$ ) at the exit of the fuel port.

$$c_e = (kRT_e)^{1/2}$$

$$= \left[ 1.19 \times \left( 1757.15 \frac{\text{ft} \cdot \text{lb}_f}{\text{slug} \cdot \text{R}} \times \frac{1 \frac{\text{slug} \cdot \text{ft}}{\text{s}^2}}{1 \text{lb}_f} \right) \times 511.4 \text{R} \right]^{1/2}$$

$$= 1034.2 \frac{\text{ft}}{\text{s}}$$

**Step #7.** Determine the mass flow rate of fuel.

$$\dot{m} = C_d \times \rho_e \times Ma_e \times c_e \times A$$

$$\dot{m} = (0.85) \left( 0.00405 \frac{\text{slug}}{\text{ft}^3} \times \frac{32.2 \text{lb}_m}{1 \text{slug}} \right) (1)$$

$$\times \left( 1034.2 \frac{\text{ft}}{\text{s}} \right) \left( 0.1254 \text{in.}^2 \times \frac{1 \text{ft}^2}{144 \text{in.}^2} \right)$$

$$\dot{m} = 0.10 \frac{\text{lb}_m}{\text{s}} = 360 \frac{\text{lb}_m}{\text{h}}$$

**Step #8.** Determine the HR of the burner.

$$HR = \dot{m} \times LHV = \left( 360 \frac{\text{lb}_m}{\text{h}} \right) \left( 18,429.7 \frac{\text{Btu}}{\text{lb}_m} \right)$$

$$= 6.63 \frac{\text{MMBtu}}{\text{h}}$$

It should be noted that if the Mach number calculated in step #2 is less than a value of one (subsonic flow) then that calculated number should be used throughout the calculation procedure.

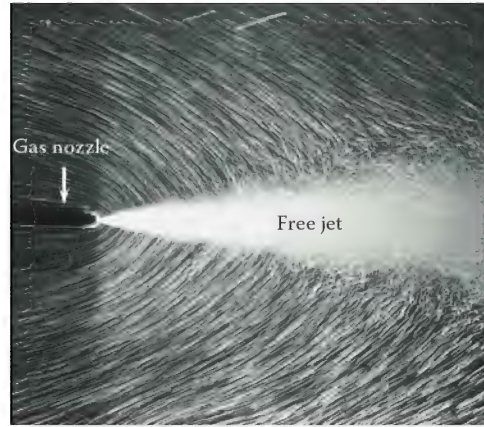


**FIGURE 9.98**

Photograph of a gas exiting a nozzle. The white streaks are small particles that have been released in the vicinity of the jet. (From ONERA photograph, Werlé, *An Album of Fluid Motion*, The Parabolic Press, Stanford, CA, 1982, p. 99.)

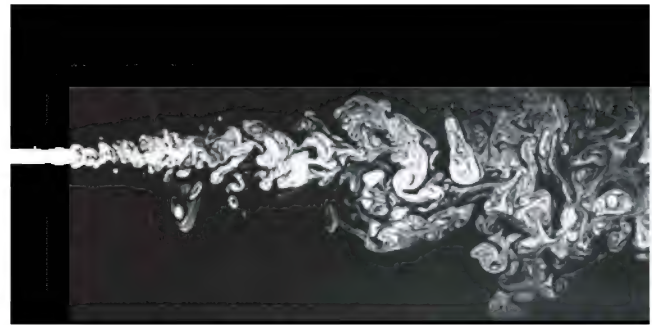


**FIGURE 9.99**

Mixing downstream of a free jet. (From Van Dyke, M., *An Album of Fluid Motion*, The Parabolic Press, Stanford, CA, 1982, p. 97.)

gas to entrain large quantities of furnace flue gas prior to combustion in order to reduce the flame temperature and lower  $\text{NO}_x$  emissions. However, when designing a burner firing low heating value gas that is difficult to burn, the engineer may want to reduce the mixing rate of the fuel gas with the furnace flue gas and/or combustion air in order to provide a stable flame. Likewise, some flares are designed to achieve rapid mixing of ambient air with the waste gas stream in order to increase the smokeless burning capacity. However, for flare gases that are more difficult to burn, the tip may be designed so that it prolongs the mixing of the air and waste gas in order to achieve a stabilized flame.

The purpose of this section is to discuss the structure and entrainment rates of free jets. The structure of a free jet can be separated into three regions: potential core, transition, and fully developed as illustrated in Figure 9.100.<sup>48</sup> The potential core is located just downstream of the nozzle exit and represents the region where the centerline of the fluid jet has not mixed with the

## 9.11 Free Jet Flow

Figure 9.98 shows a fluid jet emerging into a quiescent, surrounding fluid; this is referred to as a *free jet*. The white streaks in the photograph are small particles that have been released into the surrounding fluid, just upstream of the jet. A low-pressure region created within the free jet causes the particles to flow into the path of the jet and mix (Figure 9.99); this is referred to as *free jet entrainment*.

The rate at which a free jet entrains and mixes the surrounding fluid is a critical parameter when designing burner and flare equipment. For example, some process burners are designed to allow the fuel



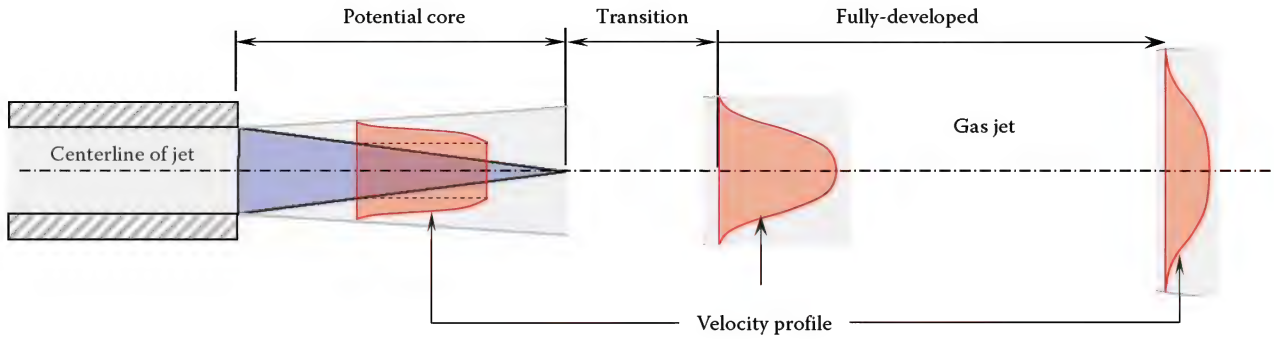


FIGURE 9.100

General structure of a turbulent free jet. (Adapted from Saddington, A.J. et al., *The Aeronautical Journal*, 108, 145, March 2004.)

ambient fluid. Mixing at the jet centerline does not occur until about three to five nozzle diameters downstream of the nozzle exit; at this location the mixing spreads to the centerline and the core region no longer exists. Beyond this core region, the flow enters the transition region. Within the transition region the jet continues to spread as the velocity decreases (decays) at a rate necessary to conserve axial momentum. Within the fully developed region (starts approximately 18 diameters downstream of the orifice), the velocity profile of the jet begins to take on a self-similar shape. That is, the centerline velocity, within the fully developed region of a circular, free jet can be described by the following equation:

$$\frac{U_o}{U_m} = 0.16 \frac{x_j}{d_o} - 1.5 \quad (9.30)$$

where

$U_o$  is the initial velocity at the nozzle exit (assuming uniform flow)

$U_m$  is the maximum (or centerline) velocity of the jet downstream

$x_j$  is the distance downstream from nozzle exit

$d_o$  is the diameter of nozzle

Notice the preceding equation is dimensionless; the only requirement for accuracy is that consistent units for velocity and length be used. The velocity profile in the radial direction can be described by the following equation:<sup>49</sup>

$$\frac{U}{U_m} = \exp \left[ -K_u \left( \frac{r_j}{x_j} \right)^2 \right] \quad (9.31)$$

where

$U$  is the actual velocity within the free jet

$U_m$  is the maximum (or centerline velocity) at the particular  $x$ -location

$r_j$  is the radial distance from jet centerline

$K_u$  is the Gauss constant, which has a value of about 92<sup>49</sup>

Equations for concentration decay are similar to the velocity equations, and are given by

$$\frac{C_o}{C_m} = 0.22 \frac{x_j}{d_o} - 1.5 \quad (9.32)$$

$$\frac{C}{C_m} = \exp \left[ -K_c \left( \frac{r_j}{x_j} \right)^2 \right], \quad (9.33)$$

where

$C$  is the actual concentration

$C_o$  is the initial concentration at the nozzle exit (assuming flat concentration profile)

$C_m$  is the maximum (or centerline) concentration of the jet downstream

$x$  is the distance from nozzle exit

$d_o$  is the diameter of the nozzle

$r_j$  is the radial distance from jet centerline

$K_c$  is the Gauss constant, which has a value of about 55.5<sup>50</sup>

It is important to note that the concentration of a free jet is independent of velocity. Intuition would lead one to believe that the faster a jet exits an orifice, the faster it mixes with the surrounding fluid. While it is true that it entrains more mass, it is not mixing at a faster rate; that is, downstream concentrations are not affected by the free jet exit velocity.

The mass entrainment rate of a circular, free jet can be estimated by the following equation:<sup>50</sup>

$$\frac{\dot{m}_\infty}{\dot{m}_j} = 0.28 \left( \frac{\rho_\infty}{\rho_j} \right)^{1/2} \left( \frac{x_j}{d_o} \right) \quad (9.34)$$

where

$\dot{m}_\infty$  is the mass of the surrounding gas entrained

$\dot{m}_j$  is the mass of the jet

$\rho_\infty$  is the density of the surrounding gas

$\rho_j$  is the density of the free jet calculated at the same pressure as the surrounding gas

$x_j$  is the distance downstream of the nozzle exit

$d_o$  is the diameter of the nozzle port



This equation is valid for  $x/d_o$  greater than about 18. The mixing rate of fuel with air and/or furnace flue gas can be controlled by varying the nozzle port diameter. For example, consider two fuel nozzles, each designed with a single port; nozzle *A* is designed with a 0.0625 in. (1.6 mm) diameter port while nozzle *B* with a 0.25 in. (6.4 mm) diameter. In order for each of these nozzles to fire the same HR (same mass flow rate) nozzle *A* must operate at a higher pressure than nozzle *B* since the fuel-side area is less. If the amount of surrounding gas entrained by each fuel nozzle were measured at a given downstream location, one would find that nozzle *A* would entrain more surrounding gas than nozzle *B*. Since more work went into compressing fuel *A* than fuel *B*, one should expect more work from fuel *A* as it exits the nozzle; this additional work or energy results in better free jet entrainment rates. The following example demonstrates the concept.

### Example 9.19

Consider two nozzles discharging methane into the ambient air. The temperature of the methane and air are both at 60°F. One nozzle has a port diameter equal to 0.0625 in. and the other nozzle has a port diameter equal to 0.25 in.. Determine the mass ratio of air-to-fuel for each nozzle at a location 8 in. downstream of the exit.

First, notice that the value of  $x/d$  is greater than 18 for both nozzles; therefore, Equation 9.34 is valid. The values of each variable in this example are the following:  $\rho_\infty = 0.0765 \text{ lb}_m/\text{ft}^3$ ,  $\rho_f = 0.0422 \text{ lb}_m/\text{ft}^3$ ,  $x = 8 \text{ in.}$ , and  $d = 0.0625 \text{ in.}$  and  $0.25 \text{ in.}$  Substituting these values into Equation 9.34, the mass ratio of air-to-fuel for the 0.0625 and 0.25 in. diameter nozzle are 48.3 and 12.1, respectively. Notice that the smaller port will entrain about four times more ambient air per unit of fuel than the larger port at a distance of 8 in. downstream of the nozzle exit. Again, this illustrates that burner engineers can control the rate of mixing of fuel with the surrounding gas by engineering the fuel nozzles' port diameter.

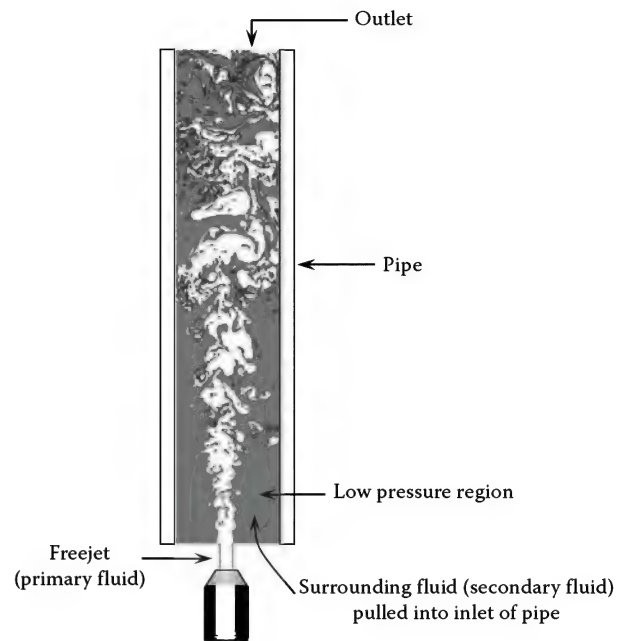


FIGURE 9.101

Illustration showing a simple version of an eductor.

the flare and burner industry, this system is typically referred to as an eductor.

Eductors are simple in design with no moving parts and have been used throughout industry for over a half a century. Some of the applications include exhausting fumes from buildings and vessels, refrigeration and air conditioning, drying, and filtration.<sup>51</sup> The simple eductor system described consists of two main components: a primary nozzle and a pipe. In the burner and flare industry, eductor system designs, in general, consist of six basic components: (1) primary nozzle, (2) inlet, (3) throat, (4) diffuser, (5) downstream section, and (6) tip as illustrated in Figure 9.102. The design of each component plays a major role in the entrainment performance of the eductor system.

The inlet typically consists of a well-rounded bell design as shown in Figure 9.103. This photograph shows steam at low pressure, issuing from small ports along the length of a tube. Notice the steam flowing into the well-rounded bell inlet. The purpose of a bell inlet is to reduce the pressure losses as the secondary gas enters into the eductor system. By reducing pressure losses, the engineer can improve the entrainment performance; sometimes this is critical, especially when designing premixed burners and pilots and steam-assisted flares. Located just downstream of the inlet is the throat.

The design of the throat is critical to the entrainment performance of an eductor system. Both the diameter of the throat and the ratio of length-to-diameter are the critical design parameters. Eductor systems can be designed with a specific throat diameter that will

## 9.12 Eduction Processes

### 9.12.1 Description of Eductor Systems

Consider a free jet positioned at one end of a section of pipe as illustrated in Figure 9.101. As the free jet (primary fluid) expands and impacts the wall of the pipe, it will act as a moving piston of fluid within the pipe. This so-called moving piston of fluid will draw the surrounding fluid (secondary fluid) into the low-pressure region created near the pipe inlet. The surrounding fluid will then be carried by the momentum of the jet through the pipe and exit at the outlet. This system is sometimes referred to as an *eductor*, *ejector*, *exhauster*, *injector*, or *jet pump*; in

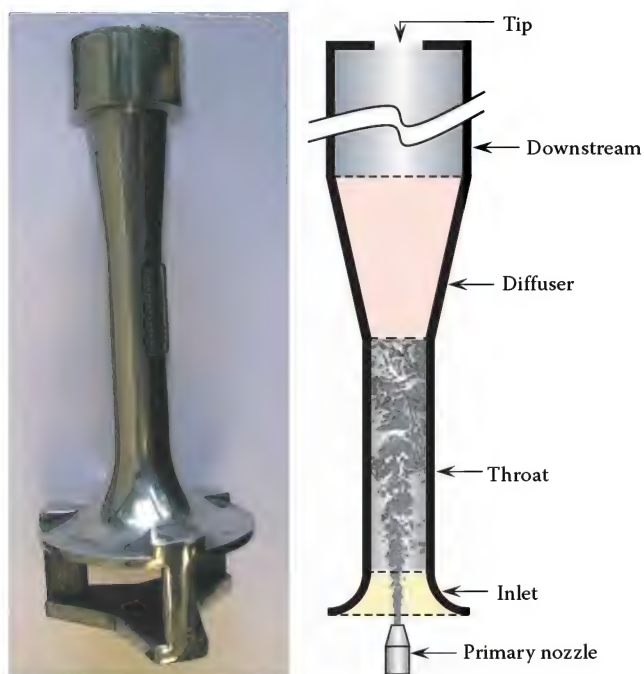


FIGURE 9.102

The basic components of an eductor system.

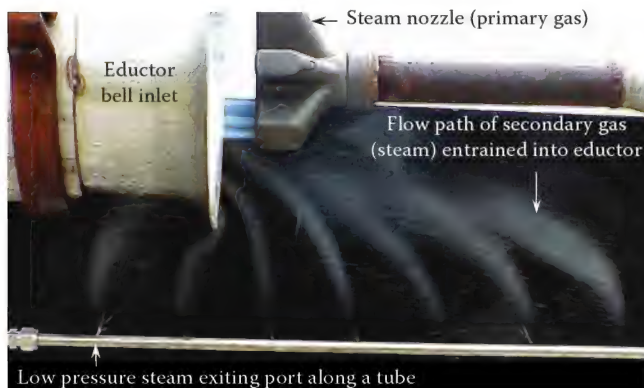


FIGURE 9.103

Flow path of secondary gas entrained into an eductor designed with a well-rounded bell inlet. (Photograph by Bob Schwartz.)

provide maximum entrainment performance. The throat diameter that provides the maximum entrainment performance depends on several factors such as the momentum of the jet and the overall pressure losses through the eductor system. The length-to-diameter ratio ( $L$  over  $D$  ratio) is also a critical design parameter and has an optimum value that provides maximum entrainment performance. If the  $L$  over  $D$  ratio is too large, additional momentum will be consumed by friction losses as the gas flows along the throat wall. If the  $L$  over  $D$  ratio is too small, the motive gas jet will not impinge the wall of the throat resulting in a reduction in entrainment performance. Values of  $L$  over  $D$  ratios that provide optimized entrainment performance typically vary from 5 to

7. Located just downstream of the throat is the diffuser section.

The diffuser consists of a conical shape that provides a transition from the throat to the downstream section. Typically, the diffuser is designed with a small transition angle to provide smooth flow in order to reduce the pressure losses as gas flows from the throat to the downstream section. The inlet, throat, and diffuser section is called the *venturi*. As the fluid exits the venturi, it enters into the downstream section of the eductor.

The design of the downstream section can be as simple as a straight pipe or complex, consisting of a variety of fittings. Sometimes, eductor systems are designed with a tip at the end of the downstream section. A variety of tip designs are used in industry depending on the application. The pressure loss associated with the gas flowing through the downstream section and tip can have a major influence on the design and entrainment performance of an eductor system.

### 9.12.2 Application of Eductor Systems

Eductor systems are quite common in the burner and flare industry. For example, multiple eductors are often used on steam-assisted flares to entrain ambient air and deliver it into the core of the waste gas stream as shown in Figure 9.104; this design increases the amount of waste gas that can be burned smokeless. Steam issuing from the nozzles, often designed for a maximum pressure of about 100 psig (6.8 barg), entrains about 5–15 lb of ambient air per pound of steam; the amount of air entrained depends on several factors such as the steam pressure and flow rate, design of the eductor tube (length, diameter, elbows, etc.), and ambient wind speed and temperature.

Eductors are also an important part of flare pilot design. Flare pilots (see Volume 3) are generally designed for a single flow rate with limited turndown and consist of premixed burners designed to mix fuel and air at a location remote from the flare tip exit as shown in Figure 9.105. The air–fuel mixture is delivered through a pipe to the pilot tip where it burns near the outlet of the flare. Locating the venturi remote from the flare tip helps ensure that inert purge gas or flue gas from the flare flame is not entrained into the inlet of the venturi; if this occurs, the air–fuel–inert gas mixture may not be flammable and could extinguish the pilot flame. It is also important that the pilot be designed so that the air–fuel mixture is not too fuel rich. If the air–fuel mixture is out of the flammable range because it is too fuel rich, the mixture must entrain and mix additional ambient air after it exits the pilot tip in order to burn. Under these conditions, the pilot flame would be extinguished if the tip were engulfed with inert purge gas or flue gas from the flare flame.

Historically, premixed burners have been used in many heater applications; particularly in the hydrogen-reforming





**FIGURE 9.104**  
Eductor tubes on a steam-assisted flare.

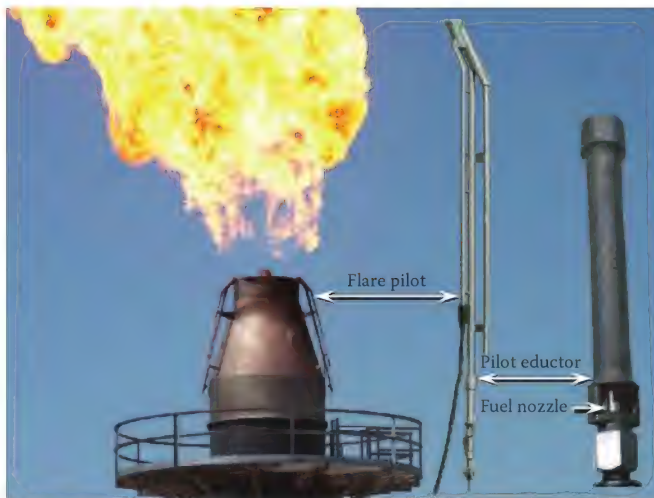


**FIGURE 9.105**  
Eductor system on a flare pilot.

and ethylene-cracking industry. These eductor-style burners inject fuel at high velocity from a port into the venturi throat where it mixes thoroughly with the educted air (Figures 9.16 and 9.106). The air–fuel mixture then flows through the diffuser and the downstream section before entering the premix burner tip. The flow then exits through openings in the burner tip and burns inside the

**FIGURE 9.106**  
Eductor systems on pre-mixed wall-fired burners.

heater. Figure 9.107 shows premixed burners and pilots mounted at the bottom of an industrial heater. Notice that each burner is designed with a bell-mouthed inlet. The diffuser section of the venturi cannot be seen because it is located inside the heater.



**FIGURE 9.107**  
Eductor systems on premixed burners and pilots.

### 9.12.3 Factors Influencing Eductor Performance

Some of the first theoretical and experimental studies on entrainment performance of eductor systems began in the early 1940s.<sup>51</sup> Since that time, a lot of work has been devoted to understanding the mechanisms governing the performance of these systems.<sup>53–55</sup> Due to the large number of variables involved, it can be challenging for burner and flare engineers to design and optimize eductor performance. To aid in the design, engineers usually rely on a combination of experiments and computer models.

The trends shown in Figure 9.108 provide a general representation of how the pressure of the primary jet influences the entrainment performance of an eductor system. It is convenient to plot the entrainment as the ratio of secondary-to-primary gas. These plots can provide valuable insight into the performance behavior of eductor systems. For a given venturi design, these trends can be summarized as follows:

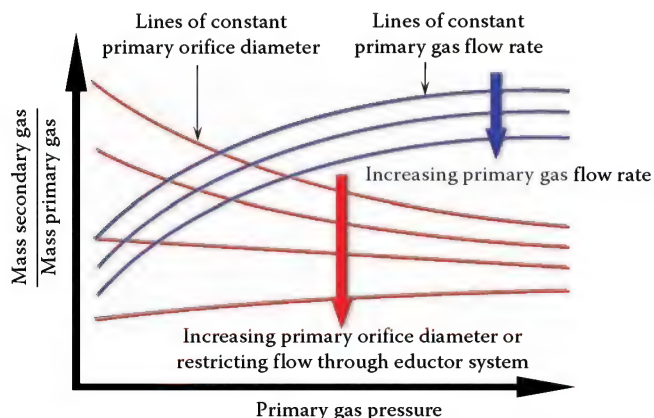


**FIGURE 9.108**  
A general representation of how the pressure of the primary jet influences the entrainment performance of an eductor system.

- At a constant primary gas pressure, increasing the orifice diameter decreases the entrainment performance; that is the ratio of secondary-to-primary gas decreases.
- At a constant primary gas pressure, restricting the flow through an eductor system decreases the entrainment performance. For example, Figure 9.109 shows a venturi inlet on a premixed burner pilot covered with heavy fuel oil; this restriction decreased the air entrainment performance to the point where the pilot was no longer stable.
- At a constant primary gas flow rate (represented by the blue lines in Figure 9.108), increasing the primary gas pressure and reducing the orifice diameter results in an increase in the entrainment performance. Typically, when designing premixed burners for heater applications, it is common to design the burner to utilize all of the fuel pressure available in order to optimize air entrainment performance.



**FIGURE 9.109**  
A Venturi inlet on a premixed burner pilot covered with heavy fuel oil.



- For a constant orifice diameter, increasing the primary gas pressure can result in either a reduction or increase in the entrainment performance; depending on the pressure losses associated with the system. For example, a venturi design that restricts the flow of the gas substantially may increase entrainment performance as the primary fuel pressure increases. However, a venturi design that does not restrict the flow of gas very much may decrease entrainment performance as the primary gas pressure increases.

## 9.13 Flashback

### 9.13.1 Definition of Flashback in a Burner

*Flashback* is a phenomenon that occurs in premix burners and pilots when the flame front propagates through the tip, as illustrated in Figure 9.110. Sometimes, flashback is also referred to as backflash, backburn, burn-back, blowback, flame inversion, or pop-back. When a flashback occurs, the flame can stabilize inside the venturi, downstream section, and/or tip. If flashback occurs and is left uncorrected, the eductor system can be quickly damaged due to overheating. The purpose of this section is to describe flashback in more detail and discuss the major factors affecting flashback.

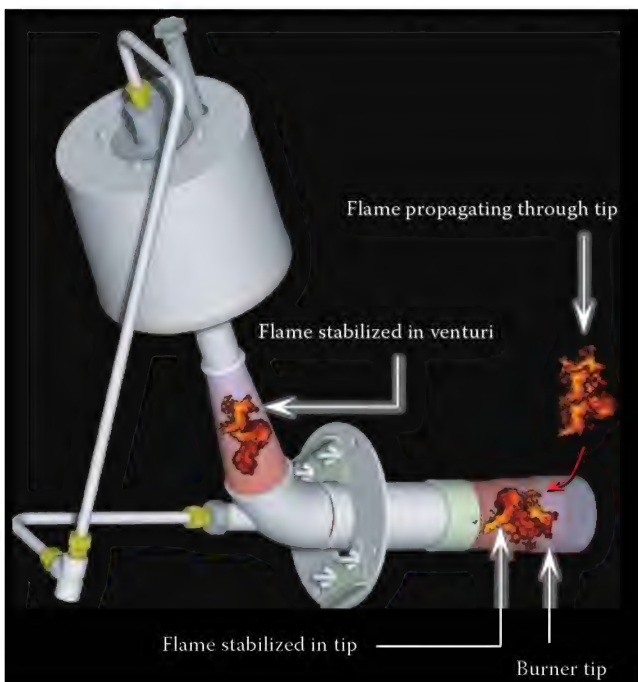


**FIGURE 9.110**  
Illustration showing a premixed burner flashing back.

### 9.13.2 Description of Flashback

Figure 9.111 shows a burner firing a premix of air and propane. Notice the wrinkled cone-shaped outline located just downstream of the burner exit. This wrinkled outline represents the location of where the air–fuel mixture just starts to react (burn) and is referred to as the *flame front*. Downstream of the flame front, the fuel continues burning in the flame zone. Within the flame zone, the gas heats from the reaction and expands which is clearly seen in the photograph. Upstream of the flame front, the air–fuel mixture has not yet started to react and is referred to as the unburned region.

The flame front in Figure 9.111 is in a stationary location; that is, it is not physically moving toward the burner or away from it and is referred to as a stable flame. Although the flame front is not physically moving, it is burning in the direction toward the inlet of the burner. The only reason it does not propagate back toward the burner is because the velocity of the unburned gas mixture at the flame front is equal and opposite to the burning velocity of the flame front. That is to say, the flame front establishes where the flame and unburned gas velocities are the same. This concept can be explained using a simple analogy. Consider a person walking on a moving sidewalk like those typically used in airports as

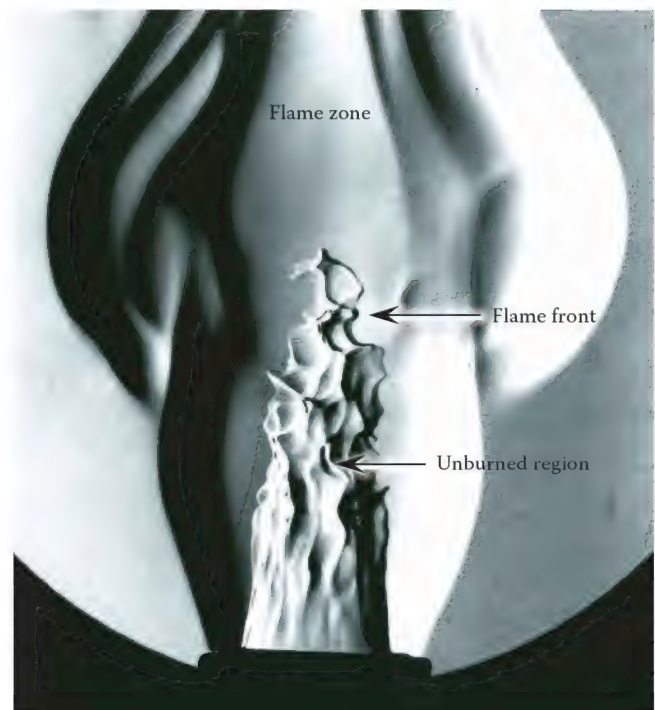


**FIGURE 9.111**  
Schlieren photograph showing a turbulent flame front downstream of a premixed burner. (Photograph by Akira Yoshida, Tokyo Denki University, Tokyo, Japan.)

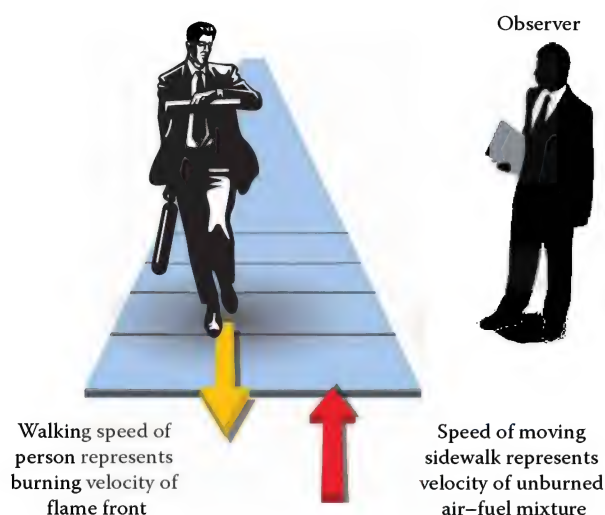
**FIGURE 9.112**

Illustration that demonstrates flame propagation.

illustrated in Figure 9.112. In this illustration, the walking speed of the person represents the burning velocity of the flame front. The moving sidewalk, which is moving in the opposite direction of the person, represents the velocity of the unburned air-fuel mixture at the flame front. If the velocity of the person walking is equal and opposite to the velocity of the sidewalk, then relative to an observer, the person is stationary.

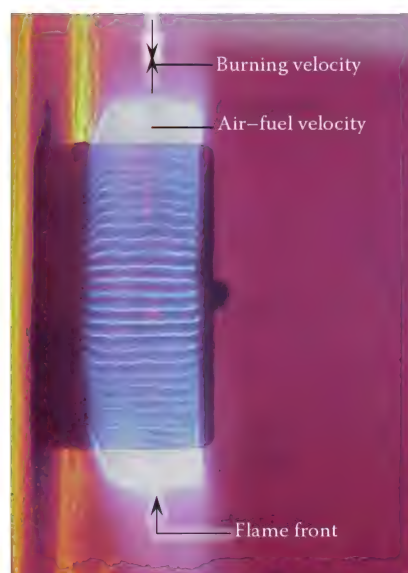
Figure 9.113 shows a premix radiant-wall burner firing in a heater. These burners are typically used in the hydrogen-reforming and ethylene-cracking industry and are designed to fire against a refractory wall. The upper photograph in this figure shows the burner tip. The tip is designed with thin, multiple slots. Air and fuel is premixed upstream of the tip and exit the burner through the slots. The lower photograph shows a flame front stabilized just outside the tip along each of these slots. As described, the velocity of the unburned air-fuel mixture at the flame front is equal to the propagation speed of the flame.

Suppose the velocity of the air-fuel mixture is moving faster than the propagation speed of the flame. In this case, the flame front will move forward, away from the burner tip (called lift off); in the analogy described earlier, this is similar to the sidewalk moving faster than the person walking. As the velocity of the air-fuel mixture continues to increase, the flame front will lift further from the burner tip. At some point, the velocity of the air-fuel mixture will exceed the burning velocity of the flame front causing the flame to blow out. Now suppose the velocity of the air-fuel mixture is moving slower than the propagation speed of the flame. In this case, the flame will travel backward into the burner (flashback).

Usually, flashback is easily recognized and can be detected audibly and/or visually. Sometimes, when flashback occurs, a loud, distinct bang will occur similar



(a)



(b)

**FIGURE 9.113**

Premix radiant-wall burner (a) tip and (b) firing in a heater.

to the sound of a gun firing. Other times, the sound may resemble a howling or a continuous popping noise as the flame burns inside the tip or venturi. Visually, flashback can sometimes be detected by an intermittent appearance of flame inside the burner tip with the tip metal glowing red from overheating as shown in Figure 9.114. Sometimes, flashback can be detected by the appearance of a flame at the fuel orifice. When this occurs, the venturi can glow red from the heat as shown in Figure 9.115.

If flashback occurs and is left uncorrected, the venturi and/or burner tip can be quickly damaged due to overheating. For example, Figure 9.116 shows a premixed radiant-wall burner tip damaged from flashback. When a flashback is detected, the operator should immediately shut off the burner and determine what actions must be taken to eliminate the unsafe operating condition.

### 9.13.3 Major Factors Affecting Flashback

Several factors governing the flashback potential of premix burners and pilots include the following: (1) fuel composition, (2) air-to-fuel ratio, and (3) tip



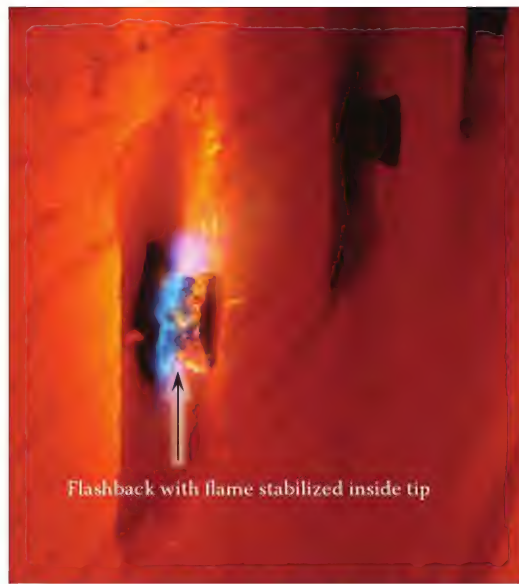


**FIGURE 9.114**  
Flashback of a premixed radiant wall burner with the flame stabilized inside the burner tip.



**FIGURE 9.115**  
Flashback of a premixed radiant wall burner with the flame stabilized inside the venturi (glowing red from heat).

design. The fuel gases most susceptible to causing flashback are the ones with higher flame speeds (see Section 3.5.6), such as hydrogen, acetylene, or ethylene. These fuels have characteristic flame speeds that are about 5–10 times greater than the characteristic flame speed of methane. In addition, the flame



**FIGURE 9.116**  
Premixed radiant wall burner tip damaged from flashback.

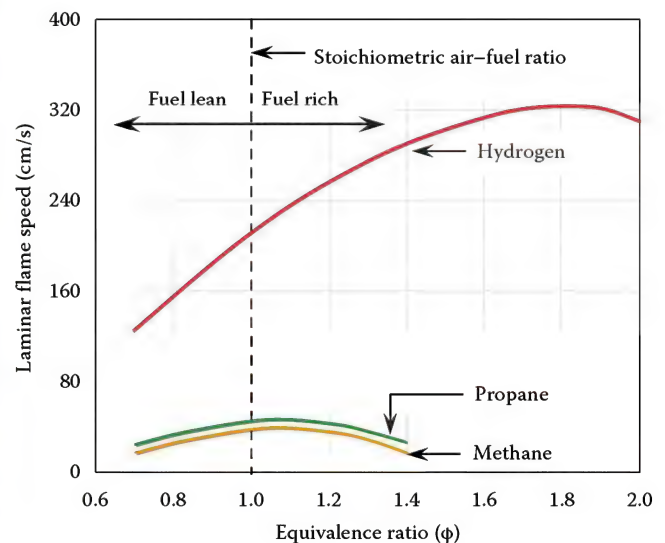


**FIGURE 9.117**  
Laminar flame speed of several fuel components.

speed of a fuel largely depends on the air–fuel ratio. For example, the laminar flame speeds of hydrogen, methane, and propane for various equivalence ratios is shown in Figure 9.117. The equivalence ratio,  $\phi$ , is defined as the air required for stoichiometric



combustion divided by the actual amount of air mixed with the fuel on a volume basis. For example, suppose 11 standard cubic feet of air are mixed with 1 standard cubic foot of methane. The equivalence ratio is determined as follows:

$$\begin{aligned}\phi &= \frac{\text{Volume of air required for stoichiometric combustion}}{\text{Volume of air actually mixed with fuel}} \\ &= \frac{9.52}{11} = 0.87\end{aligned}$$

If the equivalence ratio is less than one, the mixture is fuel lean (more air than stoichiometric amount); however, if the equivalence ratio is greater than one, the mixture is fuel rich (less air than stoichiometric amount). An equivalence ratio equal to one corresponds to a stoichiometric air–fuel mixture. The *laminar flame* speed is defined as the speed at which the flame front will propagate in a non-turbulent (laminar) environment. *Turbulent flame* speed is defined as the speed at which the flame front will propagate in a turbulent environment; the turbulent flame speed is significantly higher than the laminar flame speed and varies considerably with the amount of turbulence. Notice that the flame speed for the fuels plotted in Figure 9.117 varies with the equivalence ratio. For many hydrocarbons, the maximum flame speed generally occurs near stoichiometric or slightly substoichiometric (fuel-rich) conditions. For hydrogen, however, the maximum flame speed occurs considerably in the substoichiometric region. It should also be mentioned that the local temperature of the flame region also affects flame speed. For example, higher furnace operating temperatures or higher inlet air temperatures can result in increased flame velocities.

The design of the premix burner is critical in preventing flashback. The burner must be designed so that speed of the air–fuel mixture exiting the premix tip will always exceed the flame speed for the known operating conditions. The tip exit area, the shape and size of the tip exit (slot or hole), the air–fuel mixture exit velocity, and flow profile must be carefully engineered to help ensure that the burner will not flashback at any point in the normal operating range with the design fuels.

will merge. When flames from individual burners come in contact with each other, it is commonly referred to as *flame–flame interference*. Flame–flame interference can dramatically increase the overall flame length inside a heater and increase emission out the stack. The purpose of this section is to describe the flow behavior and detrimental effects associated with flame–flame interference inside process heaters.

#### 9.14.1 Description of Flame–Flame Interference

Consider a group of birthday candles arranged in a circle as shown in Figure 9.118. The upper photograph shows 22 candles arranged in an 8 in. (20 cm) diameter circle while the lower photograph shows the same number of candles arranged in a 2 in. (5 cm) diameter



(a)



(b)

FIGURE 9.118

(a) Twenty-two birthday candles arranged in 8 in. (20 cm) diameter circle. (b) Twenty-two birthday candles arranged in 2 in. (5 cm) diameter circle.

### 9.14 Flame–Flame Interference Inside Heaters

If the burners inside of a process heater are spaced at a proper distance from each other, the flames will remain separate and not interact with each other. However, if the burners are spaced too closely together, the flames

circle. Notice when the candles are spaced far apart, the flames do not interfere with each other and the flame length is relatively short with no signs of soot formation. However, when the candles are spaced closer together, an astonishingly visual change occurs: the flames (1) collapse toward the center, (2) increase in length, and (3) form a significant amount of soot.

#### 9.14.2 Flow Dynamics Associated with Flame–Flame Interference

Process burners can be arranged in various patterns inside a process heater; one common arrangement is a circular pattern as shown in Figure 9.119. Notice that the flames do not interfere with each other; that is, they are separate, individual flames that do not collapse toward the center of the burner circle. Figure 9.120, however, shows burners arranged in a tight circular pattern. Notice that the flames collapse toward the center and merge with each other. What flow behavior causes the flame to collapse toward the center?

Consider two steam nozzles oriented parallel to each other as shown in Figure 9.121. Although the nozzles are parallel, notice that the steam jets are drawn toward each other. The reason they flow toward one another is because a low-pressure zone is created between them. Figure 9.122 is a good example further demonstrating the nature of this flow behavior. This photograph shows an airplane flying past a smoke generator located on the ground. Notice that the smoke is drawn into the region on the backside of the airplane wing. The smoke flows toward the backside of the wing because the static pressure behind the wing is lower than the surrounding static pressure. Similarly, when two closely spaced jets flow parallel to each other, the low-pressure zone between them draws them together.



**FIGURE 9.119**  
Burners firing in a vertical-cylindrical (VC) heater showing no signs of flame–flame interactions.



**FIGURE 9.120**  
Burners arranged in a tight circle causing flames to collapse toward the center of the burner circle.



**FIGURE 9.121**  
Two steam jets starting out parallel and being attracted to each other due to the low-pressure zone. Notice the cyclic pattern in the steam jets; typically referred to as von Karman vortex streets. (Photograph from Dreamstime.)

Next, consider the flow of parallel flowing jets, bounded by a lower wall as illustrated in Figure 9.123. The flow field downstream of the jets can be separated into three regions:<sup>56</sup> converging region, merging region, and combined regions. The converging region represents the area below the point where the jets come together which is referred to as the merging





**FIGURE 9.122**  
Red smoke pulled into the low-pressure zone created on the back side of an airplane wing. (From NASA photograph, Washington, DC.)

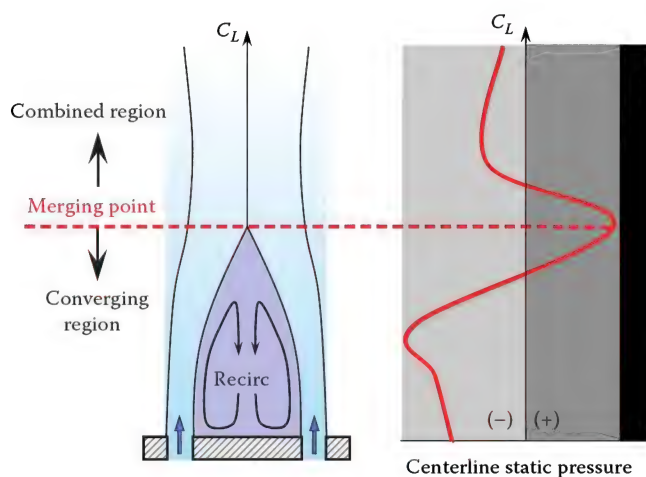


**FIGURE 9.123**  
Illustration showing the flow pattern and static pressure along the centerline between two unventilated (bounded by a lower wall) parallel flowing jets.

point. When the jets emerge from the wall, they can create two counter-rotating vortices within the converging region. Downstream of the merging point the jets continue to mix together, referred to as the combined region. Further downstream of the combined region, the two jets fully merge and resemble a single jet. Within the converging region, the static pressure can fall below the ambient pressure as illustrated in Figure 9.123. This low-pressure zone causes the jets to flow toward the center almost immediately after emerging from the nozzle exit. The strength of this low-pressure region is an important factor affecting how quickly the

jets merge together and depends on several factors such as the spacing between the jets and the momentum of the jets at the exit plane.

### 9.14.3 Detrimental Effects of Flame–Flame Interference

Flame–flame interference can create several detrimental effects inside a process heater. A few of these detrimental effects include the following: (1) flame impingement on process tubes, (2) soot deposit on process tubes, (3) higher emissions out of the stack, (4) afterburning in the convection section, and (5) erosion of heater refractory.

When flame–flame interference occurs, the mixing rate of the air and fuel, along the interface where the flames merge together, is reduced. This reduced mixing rate starves the fuel for combustion air causing the flames to stretch. As the flames stretch, they lose momentum and become more susceptible to following the currents inside the heater; this increases the risk of flames pulling over into process tubes in the radiant section as shown in Figure 9.124.

If the flames stretch too far, they could impinge or engulf the process tubes in the convection section of the heater as shown in Figure 9.125. Tubes are designed to last a long time; in some instances, 10 years. However, if flames impinge on process tubes, high temperatures can shorten the life of a tube to days. When flames impinge on process tubes, the tubes can overheat resulting in the formation of coke buildup on the inside surface.<sup>57</sup> The layer of coke on the inside surface will act as a thermal barrier reducing the heat transfer to the process fluid resulting in a reduction in heater efficiency. Sometimes, in order to maintain target production rates, plant operators will increase the firing rate, which further



**FIGURE 9.124**  
Flames impinging on process tubes in radiant section.





**FIGURE 9.125**  
Flame impinging on process tubes in convection section.



**FIGURE 9.126**  
Ruptured process tube caused by prolonged flame impingement.

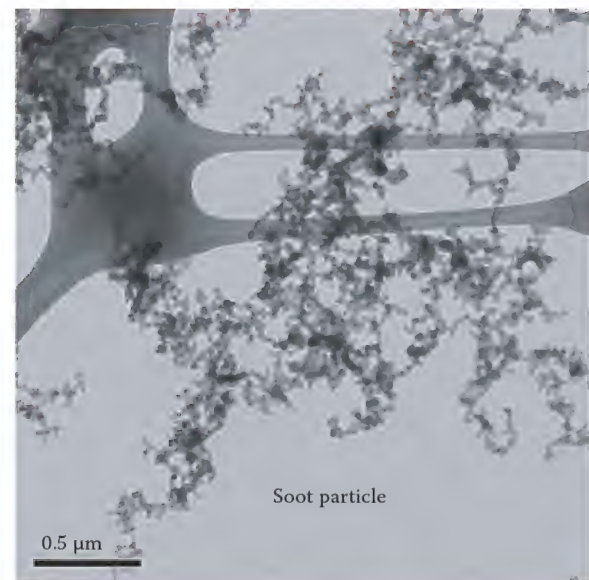
exacerbates the problem. Firing a heater above its design limit can cause long-term problems such as refractory damage, tube sagging or bowing, and tube leakage or rupture<sup>58</sup> as shown in Figure 9.126.

When flame–flame interference occurs, the fuel typically becomes starved for combustion air causing

the flame to produce soot. For example, when a piece of glass is held up against a candle flame as shown in Figure 9.127, the flame forms soot that collects on the surface of the glass. The glass acts as a flow barrier reducing the amount of ambient air entrained and mixed with the fuel; this causes the hydrocarbons in the fuel to heat and chemically crack. The cracked hydrocarbon eventually forms benzene, which agglomerates to create soot (carbon) particles that deposit on the surface of the glass. When soot is formed inside a process heater, the particles can easily adhere to the outside surface of process tubes and can build a thick layer. This soot layer acts as an excellent thermal barrier because it



(a)



(b)

**FIGURE 9.127**  
(a) Candle flame held next to a piece of glass. (b) Soot particle. (Photograph courtesy of JoAnn Lighty and Carlos Andres, University of Utah, Salt Lake City, UT.)

has a thermal conductivity about 1/100th that of stainless steel; as a result, the heat transfer efficiency to the process is reduced. Another detrimental effect is that the carbon deposited on the tube can slowly diffuse into the wall making the tube very brittle (see Volume 2, Chapter 4). When the tube experiences a thermal shock, it could prematurely fail.<sup>59</sup>

Flame–flame interference can increase CO and UHC emissions. If these flammable gases do not burn completely within the radiant section of the heater, they can be quenched when they come in contact with the cooler process tubes in the convection section. If quenched, unburned fuel can exit the stack resulting in wasted energy and/or emissions that exceed permitted levels. If the CO and UHC are not quenched by the process tubes, they may burn in the convection section; this is typically referred to as *afterburning*. Afterburning can damage the convection section and cause premature shutdown of the heater.

Flame–flame interference can also increase NO<sub>x</sub> emissions. When flames interfere with each other, it reduces the amount of inert furnace gas mixed with the fuel prior to combustion; as a result, this raises the temperature of the flame, which increases in the rate of thermal NO<sub>x</sub> production.

When burners are arranged in a tight circle, they can create a recirculation pattern in the center. Although not common, this strong recirculation pattern can erode the refractory lining on the floor of the heater as shown in Figure 9.128. Also notice the yellow flame; this indicates that the fuel is starved for combustion air.

This discussion has focused primarily on burners arranged in a circular pattern. It should be mentioned that flame–flame interference can also occur with burners arranged in a straight line. For example, Figure 9.129 shows 10 diffusion burners firing in the open. Notice when the burners are spaced further apart, the flame length is shorter and appears to produce less soot (less yellow color in the flame).

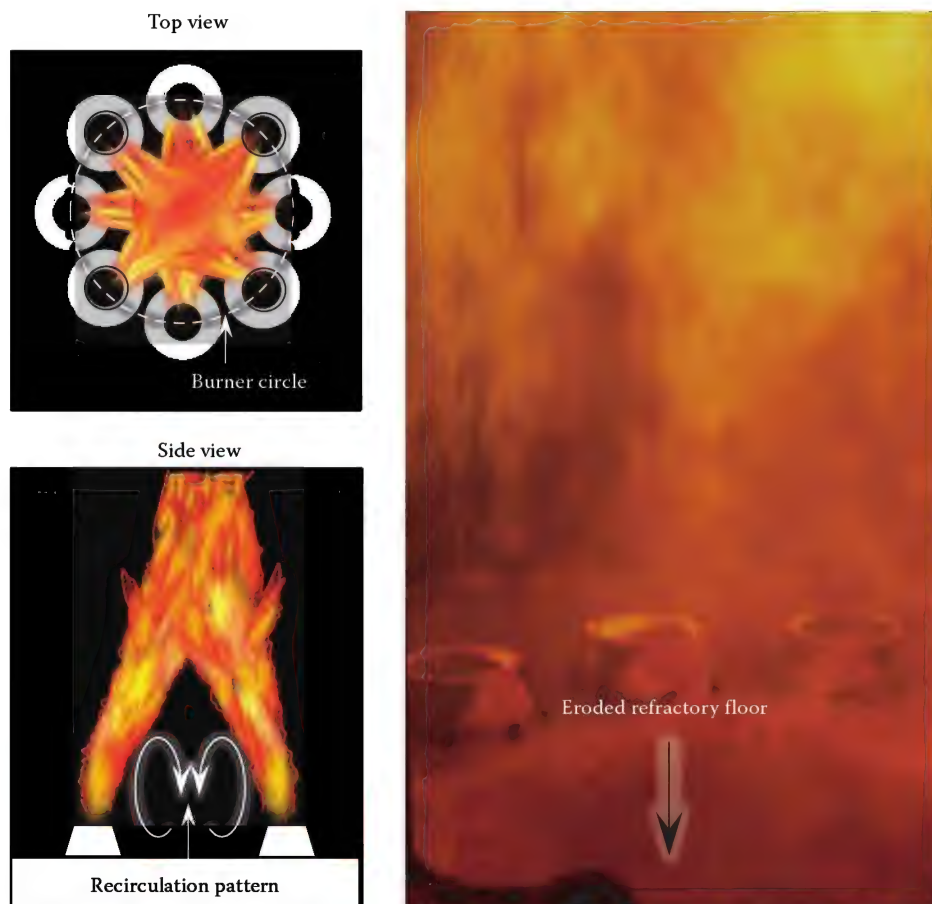


FIGURE 9.128

Burners arranged in a tight circle causing flames to collapse toward the center. Notice the erosion of the refractory floor at the center of the burner circle; this is caused by the large recirculation pattern in that area.



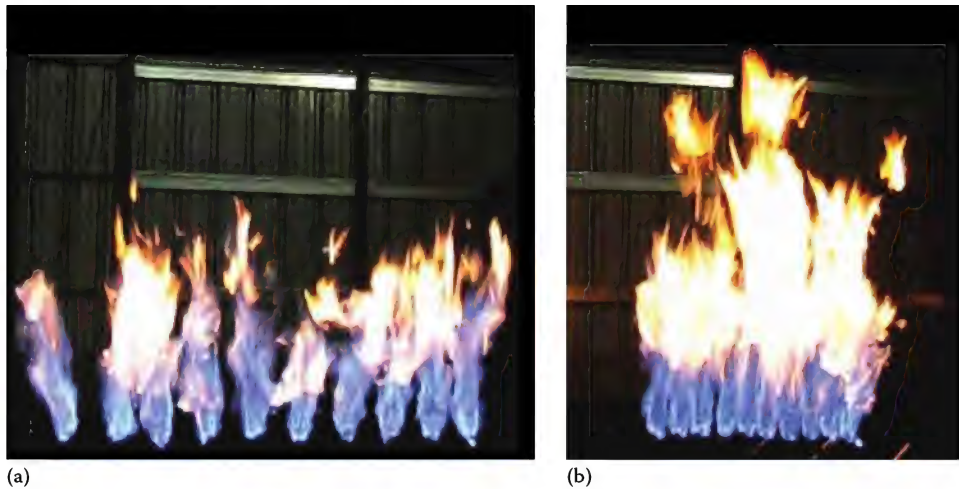


FIGURE 9.129

Diffusion burners arranged in a straight line: (a) burners at a spacing that produces no flame interaction and (b) burners spaced half the distance of that shown in (a).

## 9.15 Air Leakage into Heaters and Flare Stacks

When air leaks into heaters and flare stacks, it can pose serious safety risks, operational problems, equipment failure, and/or loss in efficiency. The purpose of this section is to describe a method for estimating air infiltration into flare and heater equipment.

### 9.15.1 Estimating Air Infiltration

The following equation can be used to estimate the mass flow rate of air leakage into heaters and flare stacks:

$$\dot{m} \left( \frac{\text{lb}_m}{\text{s}} \right) = 0.1271 \left( \frac{dP(\text{inches WC}) \times \rho_{\text{air}} \left( \frac{\text{lb}_m}{\text{ft}^3} \right) \times A^2(\text{in.}^2)}{K} \right)^{1/2} \quad (9.35)$$

where

$\dot{m}$  is the mass flow rate of air ( $\text{lb}_m/\text{s}$ )

$dP$  is the difference in ambient pressure and heater or flare stack pressure at leakage elevation (inches WC)

$\rho_{\text{air}}$  is the density of air at elevation of leakage (actual  $\text{lb}_m/\text{ft}^3$ )

$A$  is the open area of leak ( $\text{in.}^2$ )

$K$  is the loss coefficient through leak

### 9.15.2 Heaters

Air leakage (tramp air) can come from many areas of the heater including tube penetrations (Figure 9.60), sight ports (Figure 9.61), explosion doors, access doors (Figure 9.62), seams around burners, seams between heater wall plates, open sample connections, and burners that are out of service.<sup>60</sup> Small openings can allow a quantity of air to leak into the heater; this increases the excess  $\text{O}_2\%$  measured in the heater stack, independent of the air actually flowing through the burners making it appear that the burner dampers need to be adjusted to correct for the high excess  $\text{O}_2\%$  out the stack. Air leakage into a heater also increases the operating cost as demonstrated in the following example.

#### Example 9.20

An operator leaves a sight port door open on a heater; the sight port opening is  $4 \times 6$  in. ( $24 \text{ in.}^2$ ). The ambient temperature and pressure at the elevation of the leak is  $100^\circ\text{F}$  and  $14.3 \text{ psia}$ . Determine the air leakage rate into the heater if the draft at the sight port is  $-0.5 \text{ in. WC}$ .

The difference in ambient pressure and pressure inside the heater at the leakage elevation ( $dP$ ) is equal to  $0.5 \text{ in. WC}$ . The density of the ambient air is determined as follows:

$$\begin{aligned} \rho_{\text{air}} &= \underbrace{0.0765 \frac{\text{lb}_m}{\text{ft}^3}}_{\text{density of air at STSP}} \times \underbrace{\frac{59^\circ\text{F} + 460}{100^\circ\text{F} + 460}}_{\text{correcting density for temperature}} \times \underbrace{\frac{14.3}{14.696}}_{\text{correcting density for pressure}} \\ &= 0.0690 \frac{\text{lb}_m}{\text{ft}^3} \end{aligned}$$



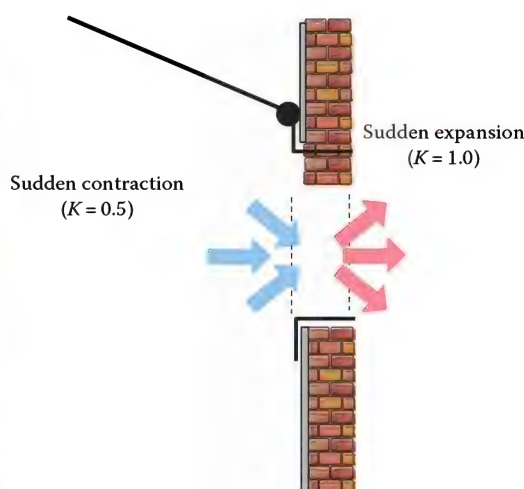


FIGURE 9.130

Loss coefficients used for estimating the mass flow rate of tramp air flowing through an open heater sight port.

The loss coefficient through the sight port is estimated assuming the air flows through a sudden contraction (entering the sight port) and a sudden expansion (exiting the sight port) as illustrated in Figure 9.130. Referring to Figure 9.15, the loss coefficient through the sight port is estimated as follows:

$$K_{\text{site port}} = K_{\text{sudden contraction}} + K_{\text{sudden expansion}} = 0.5 + 1.0 = 1.5$$

Substituting these values into Equation 9.35 gives

$$\begin{aligned} \dot{m} &= 0.1271 \left[ \frac{0.5 \text{ in. WC} \times 0.0690 \frac{\text{lb}_m}{\text{ft}^3} \times (24 \text{ in.}^2)^2}{1.5} \right]^{1/2} \\ &= 0.463 \frac{\text{lb}_m}{\text{s}} \end{aligned}$$

How much would this air leak cost a company annually, assuming the fuel cost to fire the heater is \$6/MMBtu and the stack exit temperature is 700°F? First, determine the mass flow rate of tramp air entering the heater on an annual basis:

$$\begin{aligned} \dot{m}_{\text{air}} &= 0.463 \frac{\text{lb}_m \text{ air}}{\text{s}} \times \frac{3600 \text{ s}}{1 \text{ h}} \times \frac{24 \text{ h}}{1 \text{ day}} \times \frac{365 \text{ days}}{1 \text{ year}} \\ &= 14.60 \times 10^6 \frac{\text{lb}_m \text{ air}}{\text{year}} \end{aligned}$$

Next, calculate the energy required to heat the tramp air from a temperature of 100°F–700°F. Knowing the specific heat of air ( $c_p$ ) at 100°F is equal to 0.24 Btu/lb<sub>m</sub>-°F the energy required to heat the air is calculated as follows:

$$\begin{aligned} q &= \dot{m}_{\text{air}} c_p \Delta T \\ &= \left( 14.60 \times 10^6 \frac{\text{lb}_m}{\text{year}} \right) \times \left( 0.24 \frac{\text{Btu}}{\text{lb}_m - ^\circ\text{F}} \right) \times (700^\circ\text{F} - 100^\circ\text{F}) \\ &= 2102.4 \times 10^6 \frac{\text{Btu}}{\text{year}} \end{aligned}$$

Finally, calculate the annual cost to heat the tramp air.

$$\begin{aligned} \text{Annual cost} &= q \times \text{fuel cost} \\ &= 2102.4 \times 10^6 \frac{\text{Btu}}{\text{year}} \times \frac{\$6}{1 \times 10^6 \text{ Btu}} \\ &= \$12,614 \text{ per year} \end{aligned}$$

This example demonstrates the importance of closing sight ports and sealing leaks in heaters.

### 9.15.3 Flare Stacks

An elevated flare stack filled with lighter-than-air gas will create a negative pressure at the base of the flare stack. This negative pressure is created by the difference in density between the stack gas and the ambient air (discussed in Section 9.8). If a negative static pressure exists within an elevated stack, then at low flare gas flow rates the entire header system will be under negative pressure. Operating a flare system under negative pressure increases the potential of air infiltration into the header system through leaks, open valves, or flanges, or through the tip exit. Infiltration of air can lead to internal burning in the flare stack or tip or could initiate a destructive detonation as demonstrated in the following example:

**Example 9.21**

A 48-in. diameter, 300-ft tall elevated flare stack is filled with methane as illustrated in Figure 9.131. The flow rate of methane produces an average velocity of 0.04 ft/s inside the stack. During routine maintenance, an operator forgets to close a drain line on the flare header; the open area of the drain line is 1 in.<sup>2</sup> The atmospheric temperature is 32°F and the atmospheric pressure at grade is 14.8 psia. The temperature of methane is 150°F throughout the entire flare stack. Estimate how much air is infiltrating into the flare system.

First, estimate the density of the ambient air at the atmospheric temperature and pressure.

$$\begin{aligned}\rho_{\text{amb air}} \frac{\text{lb}_m}{\text{ft}^3} &= \underbrace{\rho_{\text{air at STP}} \left( \frac{\text{lb}_m}{\text{ft}^3} \right)}_{\text{density of ambient air at standard T and P}} \times \underbrace{\frac{60 + 460}{T_{\text{amb air}}(^{\circ}\text{F}) + 460}}_{\text{correcting for temperature}} \\ &\times \underbrace{\frac{P_{\text{amb air}} \text{ psia}}{14.696}}_{\text{correcting for atmospheric pressure}} \\ \rho_{\text{amb air}} &= 0.0765 \frac{\text{lb}_m}{\text{ft}^3} \times \frac{60^{\circ}\text{F} + 460}{32^{\circ}\text{F} + 460} \times \frac{14.8}{14.696} \\ &= 0.0814 \frac{\text{lb}_m}{\text{ft}^3}\end{aligned}$$

Next, estimate the density of the gas inside the flare assuming methane (mole weight = 16) at a temperature of 150°F and at an atmospheric pressure of 14.8 psia.

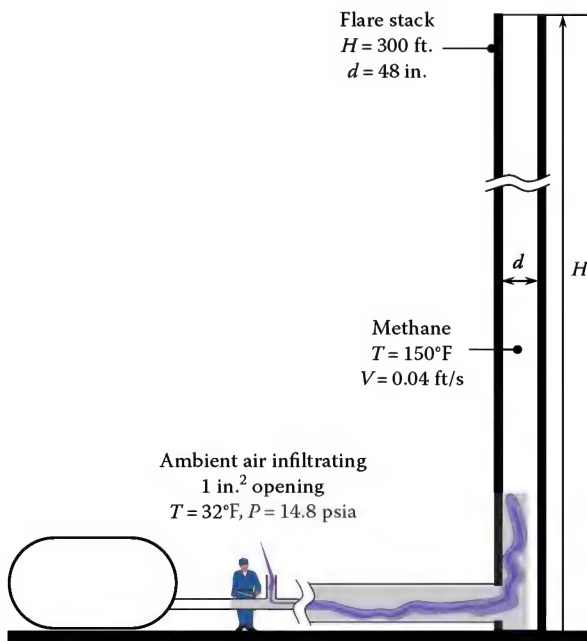
**FIGURE 9.131**

Illustration of air leaking into a flare system filled with methane.

$$\begin{aligned}\rho_{\text{flare gas}} &= \underbrace{0.0765 \frac{\text{lb}_m}{\text{ft}^3}}_{\text{density of air at STSP}} \times \underbrace{\frac{60^{\circ}\text{F} + 460}{150^{\circ}\text{F} + 460}}_{\text{correcting density for temperature}} \times \underbrace{\frac{14.8}{14.696}}_{\text{correcting density for pressure}} \\ &\times \underbrace{\frac{16}{29}}_{\text{correct for mole weight}} = 0.0362 \frac{\text{lb}_m}{\text{ft}^3}\end{aligned}$$

The pressure at the base of the flare stack, neglecting the pressure loss of the flare gas as it flows through the stack, can be calculated using the following equation:

$$P_{\text{base}} = 0.1922 \times H \times (\rho_{\text{flare gas}} - \rho_{\text{amb air}}), \quad (9.36)$$

where

$P_{\text{base}}$  is the static pressure at the base of the stack (inches WC)

$H$  is the height of stack (ft)

$\rho_{\text{flare gas}}$  is the density of flare gas ( $\text{lb}_m/\text{ft}^3$ )

$\rho_{\text{amb air}}$  is the density of ambient air ( $\text{lb}_m/\text{ft}^3$ )

Substituting the appropriate values into the pressure equation gives

$$P_{\text{base}} = 0.1922 \times 300 \times (0.0362 - 0.0814) = -2.61 \text{ in. WC}$$

Within the flare header, the pressure is approximately 2.61 in. WC lower than the atmospheric pressure. Assuming a loss coefficient ( $K$ ) of 1.5 through the open vent, Equation 9.35 is used to estimate the mass flow rate of air into the flare system.

$$\begin{aligned}\dot{m}_{\text{air}} &= 0.1271 \left[ \frac{2.61 \text{ in. WC} \times 0.0814 \frac{\text{lb}_m}{\text{ft}^3} \times (1 \text{ in.}^2)^2}{1.5} \right]^{1/2} \\ &= 0.376 \frac{\text{lb}_m}{\text{s}}\end{aligned}$$

Is the flow rate of air and fuel through the flare system flammable if fully mixed together? Converting the mass flow rate of air leakage into a standard volumetric flow rate gives

$$Q_{\text{air STSP}} = \frac{\dot{m}_{\text{air}}}{\rho_{\text{air STSP}}} = \frac{0.376 \frac{\text{lb}_m}{\text{s}}}{0.0765 \frac{\text{lb}_m}{\text{ft}^3}} = 4.92 \text{ scfs}$$

Assuming that the pressure throughout the stack is 14.8 psia, the volumetric flow rate of methane at standard conditions is calculated as follows:

$$Q_{\text{methane, STSP}} = \underbrace{0.04 \frac{\text{ft}}{\text{s}}}_{\text{average velocity of flare gas in stack}} \times \underbrace{\frac{\pi \left(\frac{48}{12}\right)^2}{4} \text{ft}^2}_{\text{cross-sectional area of flare stack}} \times \underbrace{\left(\frac{60^\circ\text{F} + 460}{150^\circ\text{F} + 460}\right)}_{\text{correcting for temperature of flare gas}} \times \underbrace{\left(\frac{14.8}{14.696}\right)}_{\text{correcting for atmospheric pressure}} = 0.432 \text{ scfs}$$

The volumetric air-to-fuel ratio entering the flare system is 4.92 scfs/0.432 scfs = 11.40. The flammability limits of methane as a volume percent of an air/fuel mixture is 5% and 15%. Converting these values to a volumetric air-to-fuel ratio produces 5.7–19. Since the air-to-fuel ratio in the stack falls between 5.7 and 19, if the air and methane fully mixed together within the flare system, it would create an explosive mixture.

## Nomenclature

$A$	Area
$c$	Speed of sound
$c_p$	Specific heat at constant pressure
$c_v$	Specific heat at constant volume
$C$	Concentration downstream of a free jet
$C_d$	Orifice discharge coefficient
$C_o$	Initial concentration at nozzle exit
$C_m$	Maximum (or centerline) concentration of a free jet
$D$	Diameter
$d_o$	Free jet nozzle diameter
$dP$	Pressure drop
$EA$	Excess air
$f$	Darcy friction factor
$g$	Acceleration of gravity
$h$	Height of liquid column
$H$	Altitude
$HR$	Heat release
$k$	Ratio of specific heat
$K_L$	Loss coefficient through a fitting
$K_u$	Gauss constant for free jet (~92)
$K_c$	Gauss constant for free jet (~55.5)
$LHV$	Lower heating value
$\dot{m}$	Mass flow rate
$\dot{m}_\infty$	Mass flow rate of ambient fluid into a free jet
$\dot{m}_j$	Mass flow rate of a free jet
$Ma$	Mach number
$MW$	Molecular weight
$P$	Pressure

$P_V$	Velocity pressure
$P_s$	Static pressure
$P_T$	Total pressure
$q$	Energy
$Q$	Volume flow rate
$r_j$	Distance from centerline of a free jet
$R$	Gas constant
$\bar{R}$	Universal gas constant
$Re$	Reynolds number
$T$	Temperature
$U$	Velocity of a free jet
$U_o$	Initial velocity at nozzle exit
$U_m$	Maximum (or centerline) velocity of a free jet
$V$	Velocity
$x_j$	Distance downstream of a free jet
$x$	Volume fraction
$Y_1$	Gas expansion factor for orifice metering run
$z$	Height of liquid column

## Greek Letters

$\beta$	Pipe inner diameter to orifice bore diameter
$\Delta T$	Difference in temperature
$\epsilon$	Equivalent sand grain roughness
$\epsilon/D$	Relative roughness
$\gamma$	Specific weight of fluid
$\mu$	Dynamic viscosity
$\nu$	Kinematic viscosity
$\phi$	Equivalence ratio
$\rho$	Density
$\rho_j$	Density of a free jet calculated at the same pressure as surrounding fluid
$\rho_\infty$	Density of surrounding fluid

## References

1. G. A. Tokaty, *A History and Philosophy of Fluid Mechanics*, Dover Publications, New York, 1994.
2. [www.wrightflyer.org/WindTunnel/testing1.html](http://www.wrightflyer.org/WindTunnel/testing1.html)
3. R. L. Panton, *Incompressible Flow*, John Wiley & Sons, New York, 1984.
4. F. M. White, *Viscous Fluid Flow*, McGraw-Hill, New York, 1991.
5. R. W. Fox and A. T. McDonald, *Introduction to Fluid Mechanics*, 2nd edn., John Wiley & Sons, New York, 1978.
6. J. K. Vennard and R. L. Street, *Elementary Fluid Mechanics*, 5th edn., John Wiley & Sons, Inc., 1975.
7. J. O. Hinze, *Turbulence*, McGraw-Hill, New York, 1975.
8. H. Schlichting, *Boundary-Layer Theory*, McGraw-Hill, New York, 1979.
9. W. F. Hughes and J. A. Brighton, *Schaum's Outline of Theory and Problems of Fluid Dynamics*, McGraw-Hill, New York, 1967.



10. T. M. Geerssen, *Physical Properties of Natural Gases*, N.V. Nederlandse Gasunie, Groningen, the Netherlands, 1980.
11. S. R. Turns, *An Introduction to Combustion*, McGraw-Hill, Boston, MA, 2000.
12. W. Bartok and A. F. Sarofim, *Fossil Fuel Combustion*, John Wiley & Sons, New York, 1991.
13. ASHRAE, *ASHRAE Handbook of Fundamental*, American Society of Heating, Refrigerating and Air-Conditioning Engineers, New York, 1977.
14. J. A. Goff, Standardization of thermodynamic properties of moist air, *Transactions of ASHVE*, 55, 1949.
15. K. K. Kuo, *Principles of Combustion*, John Wiley & Sons, New York, 1986.
16. Edgeworth, R., Dalton, B. J., and Parnell, T., The pitch drop experiment, University of Queensland, Brisbane, Queensland, Australia. [www.physics.uq.edu.au/physics\\_museum/pitchdrop.shtml](http://www.physics.uq.edu.au/physics_museum/pitchdrop.shtml). Retrieved March 03, 2009. A copy of: *European Journal of Physics*, 5, 198–200, 1984.
17. R. D. Reed, *Furnace Operation*, 3rd edn., Gulf Publishing, Houston, TX, 1981.
18. R. B. Bird, W. E. Stewart, and E. N. Lightfoot, *Transport Phenomena*, John Wiley & Sons, New York, 1976.
19. R. C. Reid et al., *The Properties of Gases and Liquids*, 3rd edn., McGraw-Hill, New York, 1977.
20. W. J. Lyman et al., *Handbook of Chemical Property Estimation Methods*, McGraw-Hill, New York, 1982.
21. J. B. Maxwell, *Data Book on Hydrocarbons*, D. Van Nostrand Company, Princeton, NJ, 1950.
22. Y. Nakayma (ed.), *Fantasy of Flow*, IOS Press, Tokyo, Japan, 1993.
23. R. R. Munson, D. F. Young, and T. H. Okiishi, *Fundamentals of Fluid Mechanics*, John Wiley & Sons, New York, 1990, p. 52.
24. J. A. Roberson and T. Crowe, *Engineering Fluid Mechanics*, Houghton Mifflin Company, Boston, MA, 1965.
25. I. E. Idelchik, *Handbook of Hydraulic Resistance*, Hemisphere, New York, 1986.
26. Engineering Division Crane, *Flow of Fluids through Valves, Fittings, and Pipe*, Crane Co., New York, 1969.
27. J. Nikuradse, Laws of flow in rough pipes, *VDI Forschungsheft*, 361, 1933; *NACA TM 1292*, 1950.
28. P. K. Swamee and A. K. Jain, Explicit equations for pipe-flow problems, *Journal Hydraulic Division of the ASCE*, 102(HY5), 657–664, May 1976.
29. American Petroleum Institute 537 Pressure-relieving and Depressuring Systems, ANSI/API standard, January 2007.
30. W. Bussman, R. Schwartz, and J. Franklin, Corrosions of flare tips, *Presented at NACE97*, Chicago, IL, 1997.
31. Atmospheric dispersion modeling, [www.en.wikipedia.org/wiki/Atmospheric\\_dispersion\\_modeling](http://www.en.wikipedia.org/wiki/Atmospheric_dispersion_modeling), accessed 2012.
32. R. L. Petersen, Applications of wind tunnel modeling for assessing odor impacts, *Proceeding of the 2008 WEF&AWMA Odor Specialty Conference*, Phoenix, AZ, 2008.
33. B. Turner, *Workbook of Atmospheric Dispersion Estimates*, U.S. Environmental Protection Agency, Washington, DC, 1970.
34. H. Moses, G. H. Strom, and J. E. Carson, Effects of meteorological and engineering factors on stack plume rise, *Nuclear Safety*, 6(1), 1–19, 1964.
35. C. Seigneur, Understanding the basics of air quality modeling, *Chemical Engineering Progress*, 88, 68, 1992.
36. R. Barratt, *Atmospheric Dispersion Modelling: An Introduction to Practical Applications*, Earthscan, London, U.K., 2001.
37. R. Reed, *North American Combustion Handbook*, 3rd edn., Vol. 1, North American Mfg. Co., Cleveland, OH, 2001.
38. A. W. Culp, *Principles of Energy Conversion*, McGraw-Hill Book Co., New York, 1979.
39. R. D. Reed, *Furnace Operations*, 3rd edn., Gulf Publishing Co., Houston, TX, 1981, p. 99.
40. Wikipedia, Atmosphere of Earth, [www.en.wikipedia.org/wiki/Atmosphere\\_of\\_Earth](http://www.en.wikipedia.org/wiki/Atmosphere_of_Earth), accessed 2012.
41. U.S. Standard Atmosphere, U.S. Government Printing Office, Washington, DC, 1962.
42. W. R. Bussman and C. Baukal, Process heater simulator, AFRC, Maui, HI, 2010.
43. V. K. Khanna, Hydrogen generation—A brief review, *Hydrocarbon Processing*, 80(7), 86A–86D, 2001.
44. K. Ruthardt, K. R. Radtke, and J. Larsen, Hydrogen trends, *Hydrocarbon Engineering*, 10(11), 41–46, 2005.
45. H. Gunardson, *Industrial Gases in Petrochemical Processing*, Marcel Dekker, New York, 1998.
46. J. Leecraft, *Field Handling of Natural Gas*, 4th edn., Petroleum Extension Service, Austin, TX, 1987.
47. C. Baukal, B. Johnson, K. Vaughn, and M. Pappe, Burner fuel tips, *Process Heating*, February 2010.
48. A. J. Saddington, N. J. Lawson, and K. Knowles, An experimental and numerical investigation of under-expanded turbulent jets, *The Aeronautical Journal*, 108, March 2004, Paper No. 2825.
49. M. A. Saad, *Compressible Fluid Flow*, Prentice-Hall, Englewood Cliffs, NJ, 1985.
50. P. M. Sforza and R. F. Mons, Mass, momentum and energy transport in turbulent free jets, *Journal of Heat and Mass Transfer*, 21, 371–384, 1978.
51. E. Kroll, The design of jet pumps, *Chemical Engineering Progress*, 1(2), 21, 1947.
52. J. H. Keenan and E. P. Newmann, A simple air ejector, *Journal of Applied Mechanics*, 64, A-75, 1942.
53. W. Bussman, A preliminary study of the mixing and inspiration performance of a Venturi Eductor system, John Zink Company Research Study, Tulsa, OK, Paper No. 92-03, 1992.
54. E. Kroll, The design of jet pumps, *Chemical Engineering Progress*, 1(2), 1947.
55. A. Namkhat, and S. Jugjai, Primary air entrainment characteristics for a self-aspirating burner: Model and experiments, *Energy*, 35, 1701–1708, 2010.
56. J. Lai and A. Nasr, Some mean flow characteristics of two parallel plane jets, *13th Australasian Fluid Mechanics Conference*, Melbourne, Victoria, Australia, December 1998.
57. K. Vinayagam, Minimizing flame impingements in fired heaters, *Chemical Engineering*, 114(5), 70–73, 2007.
58. G. Faagau, Resolve to trim that excess air, *Chemical Processing*, 71(1), 16, 2008.
59. G. Verdier and F. Carpentier, Consider new material for ethylene furnace applications, *Hydrocarbon Processing*, May 2011.
60. J. McAdams, J. Karan, R. Witte, and M. Claxton, Low NOx burner maintenance in high temperature furnaces, *Proceedings of the 14th Ethylene Producers' Conference*, New York, American Institute of Chemical Engineers, Vol. 1, pp. 351–370, 2002.

This page intentionally left blank

# 10

## *Oil Atomization*

I.-Ping Chung and Steve Londerville

### CONTENTS

10.1 Introduction .....	309
10.2 Liquid Fuel .....	309
10.3 Theoretical Basis of Atomization Process .....	311
10.4 Parameters Affecting Atomization .....	313
10.5 Spray Characteristics .....	314
10.5.1 Droplet Size.....	314
10.5.2 Spray Angle .....	315
10.5.3 Patternation.....	315
10.6 Atomizer Type.....	316
10.6.1 Single Fluid Atomizer .....	316
10.6.2 Twin Fluid Atomizer .....	316
10.6.2.1 Process Oil Gun.....	317
10.6.2.2 Boiler Burner Oil Gun .....	318
10.7 Oil Gun Performance .....	319
10.7.1 Process Oil Gun.....	319
10.7.1.1 Atomization Quality.....	319
10.7.1.2 Energy Consumption .....	321
10.7.1.3 Turndown Ratio .....	321
10.7.1.4 Pollutant Emissions .....	321
10.7.2 Boiler Oil Gun .....	322
10.8 Prediction Model.....	323
Nomenclature and Subscripts .....	324
References.....	325

### 10.1 Introduction

Atomization is a process of breaking up bulk liquid into many small droplets. In order to have good combustion, fuel and air must mix well. A bulk liquid has a limited surface area to contact with the air. This is the reason that liquid fuel, or more specifically, fuel oil, requires atomization before burning. Atomization increases the liquid surface area, which results in an increase of fuel evaporation rate and fuel-air mixing rate. This improves the combustion process.

The atomization mechanism can be kinetic energy from the liquid itself, or external mechanical energy through a special design, such as swirl, vibration, and

rotation, or even through assistance from other high-velocity mediums, such as air, gas, or steam. For a viscous liquid fuel (i.e., No. 6 heavy oil), it is especially effective to use other high-velocity mediums to assist in atomization. The air-assist or steam-assist atomization is called twin-fluid atomization.

### 10.2 Liquid Fuel

By definition, a liquid or fluid is a substance that deforms continuously when a shear stress is applied. The fluid is called “Newtonian” when the shear stress is



proportional to the rate of deformation. The proportionality constant is called viscosity.

$$\tau = \mu \frac{\partial u}{\partial y} \quad (10.1)$$

where

$\tau$  is the liquid shear stress

$\mu$  is the dynamic viscosity

$\frac{\partial u}{\partial y}$  is the rate of deformation or velocity gradient

The units and nomenclature used to define dynamic viscosity are almost endless, but essentially may be defined as (Force)(time)/(length)<sup>2</sup>. Often another measure, kinematic viscosity, is used and is defined as dynamic viscosity divided by density. The resultant unit is (length)<sup>2</sup>/(time). Kinematic viscosity is the most commonly reported and used type of viscosity in the industry. Kinematic viscosity in SI units is a Stoke, defined as cm<sup>2</sup>/s. The common SI unit is the centiStoke (cSt) = Stoke/100. Other common units are Saybolt Universal Seconds (SSU) and Saybolt Furol Seconds (SSF).

Most liquids are Newtonian. Exceptions are some long chain hydrocarbons and various kinds of mixtures

of solids with liquids, generally called slurries. Non-Newtonian fluids can be shear thickening or shear thinning. For atomizer considerations, these fluids have a special designation called "apparent viscosity" where the viscosity is rated at the atomizer high shear rates. The liquid viscosity is the single most important parameter defining atomizer performance in droplet generation.

Most common liquid fuels are hydrocarbon based with small amounts of non-hydrocarbon components such as sulfur, nitrogen, oxygen, ash, and other minor impurities. The American Society of Testing and Materials (ASTM) has divided fuel oils into five categories, designated as 1, 2, 4, 5, and 6. Numbers 1 and 2 are called distillate oils and have a viscosity close to water. Numbers 4 and 5 are typically blends and are uncommon today. Number 6 is a high viscosity oil that requires heating to reduce viscosity for transport via pipe or atomization. At room temperatures, the viscosity of number 6 oil is so high that it can appear to be a solid. Pitch is a fuel oil that has an even higher viscosity than number 6 oil.

Other important parameters for fuel oils are specific gravity, American Petroleum Institute (API) number, distillation temperature, impurities, and Conradson carbon or Ramsbottom carbon (Table 10.1).

**TABLE 10.1**

Liquid Fuel Properties

Grade Fuel	No. 1	No. 2	No. 4 (Light)	No. 4	No. 5 (Light)	No. 5 (Heavy)	No. 6
Specific gravity, 60/60°F	0.8499	0.8762	0.8762	—	—	—	—
(deg API), max	35 min	30 min	30 max	—	—	—	—
Flash point °F min	100	100	100	130	130	130	140
Pour point °F max	0	20	20	20	—	—	—
Kinematic viscosity mm <sup>2</sup> /s [cSt]							
At 100°F min	1.4	2	2	5.8	>26.4	>65	—
Max	2.2	3.6	5.8	26.4	65	194	—
At 104°F min	1.3	1.9	—	5.5	>24	>58	—
Max	2.1	3.4	—	24	58	168	—
Saybolt viscosity							
Universal at 100°F							
Min	—	32.6	32.6	45	>125	>300	>900
Max	—	37.9	45	125	300	900	9000
Furol at 122°F							
Min	—	—	—	—	—	23	>45
Max	—	—	—	—	—	40	300
Distillation temperature, °F							
10% point max	420	—	—	—	—	—	—
90% point min	—	540	—	—	—	—	—
Max	550	640	—	—	—	—	—
Sulfur content, mass, max	0.5	0.5	—	—	—	—	—
Corrosion copper strip, max	3	3	—	—	—	—	—
Carbon residue, 10% b; % m, max	0.15	0.35	—	—	—	—	—
Water and sediment, % vol, max	0.05	0.05	0.5	0.5	1	1	2

Source: Schmidt, P.F., (ed.), *Fuel Oil Manual*, Industrial Press, New York, 1985.

Specific gravity (SG) is the ratio of fuel density to that of water at 60°F (16°C). The National Bureau of Standards and the API devised another measure of gravity called the API number. They are related by the following formula:<sup>1</sup>

$$\text{API Gravity} = \frac{141.5}{\text{SG}} - 131.5 \quad (10.2)$$

Fuel oil impurities such as ash, sulfur, and nitrogen are important in emission predictions. Actual components in the ash such as vanadium, sulfur, and sodium are important parameters in the evaluation of atomizer corrosion and deposits. These deposits may be on or about the atomizer and in the furnace as well. Some heavy oil products may contain ash that is very erosive such as catalyst fines.

Many other fuels are used in industries that are not based on petroleum extraction. These are waste liquids that could be very corrosive or blends of fluids and solids (slurries) that could be both corrosive and erosive. At times, it is impossible to use internal mix or mechanical atomizers for corrosive or erosive fuels. Special external mix atomizers are used for such applications.

### 10.3 Theoretical Basis of Atomization Process

The process of atomization is to disintegrate the liquid into droplets by external forces. The literature on the theory of liquid disintegration is fairly extensive,<sup>2-9</sup> but generally addresses low-velocity liquid output from simple geometric openings. The analysis theory differs greatly from practical applications. Nevertheless, the theoretical analysis provides useful information, such as control parameters. This section presents the theoretical results for a simple single fluid jet for the purpose of understanding the effect of parameters on atomization.

The common process of atomization is described as a phenomenon where waves are developed on the liquid surface with gradually increased amplitudes as instability is approached until, finally, droplets are disintegrated from a continuous liquid body. Rayleigh<sup>10</sup> was the first to solve this problem in 1878. He considered the simplified case of vibration and breakup of a cylindrical jet for a nonviscous liquid in a vacuum environment. The waves developed on the liquid surface can be asymmetric waves, that is, sinuous waves,

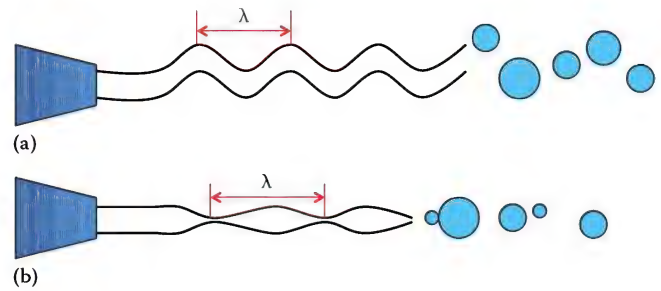


FIGURE 10.1

Liquid disintegration of a cylindrical jet caused by wave formations on liquid surface: either by sinuous wave (a) or dilatational wave (b).

or symmetric waves, that is, dilatational waves, as shown in Figure 10.1.

Later, Weber<sup>11</sup> extended Rayleigh's derivation to viscous liquid as follows:

$$\frac{D}{d_0} = 1.436 \left( 1 + 3 \frac{\text{We}_l^{0.5}}{\text{Re}} \right)^{1/6} \quad (10.3)$$

where

$D$  is the droplet diameter

$d_0$  is the jet diameter

$\text{We}_l$  (Weber number) and  $\text{Re}$  (Reynolds number) are defined as

$$\text{We}_l = \frac{\rho_l V_l^2 d_0}{\sigma} \quad (10.4)$$

$$\text{Re} = \frac{\rho_l V_l d_0}{\mu_l} \quad (10.5)$$

In these equations,  $\rho_l$  is the liquid density,  $V_l$  is the liquid exit velocity,  $\sigma$  is the liquid surface tension, and  $\mu_l$  is the liquid viscosity.

Obtaining a general solution for liquid jet disintegration requires solving Navier–Stokes equations by using the perturbation method. The perturbation method is a widely used technique in fluid mechanics using the superposition of an arbitrary small vibration onto the main fluid motion and then solving the equations. A simple example is illustrated in the following derivation:

For two-dimensional liquid jet disintegration, the Navier–Stokes equations can be expressed in the following forms:

$$\frac{\partial u}{\partial t} + u \frac{\partial u}{\partial x} + v \frac{\partial u}{\partial y} = -\frac{1}{\rho} \frac{\partial P}{\partial x} + \nu \left( \frac{\partial^2 u}{\partial x^2} + \frac{\partial^2 u}{\partial y^2} \right)$$

$$\frac{\partial v}{\partial t} + u \frac{\partial v}{\partial x} + v \frac{\partial v}{\partial y} = -\frac{1}{\rho} \frac{\partial P}{\partial x} + \nu \left( \frac{\partial^2 v}{\partial x^2} + \frac{\partial^2 v}{\partial y^2} \right)$$

$$\frac{\partial u}{\partial x} + \frac{\partial v}{\partial y} = 0. \quad (10.6)$$

The small perturbation, as indicated in Equation 10.7, is then substituted into the Navier–Stokes Equation 10.6,

$$\begin{aligned} u &= V + u_i \\ v &= v_i \\ P &= P_o + P_i, \end{aligned} \quad (10.7)$$

where

$V$  is liquid bulk velocity

$P_o$  is liquid pressure before superposition of perturbation

$u_i$ ,  $v_i$ , and  $P_i$  are small perturbations

After a series of substitutions, derivations, transformations, simplifications, and by adding some assumptions, Equation 10.6 can be written in a dimensionless form as

$$H(i\omega)^2 = 2(K + iL)i\omega + R + iS = 0$$

where

$$H = 1 + M \operatorname{ctg} h \epsilon$$

$$K = \sqrt{\frac{2}{Lp}} \epsilon^2 (1 + N \operatorname{ctg} h \epsilon)$$

$$L = \frac{1}{\sqrt{2}} \epsilon \sqrt{\operatorname{We}}$$

$$R = \epsilon^2 \left( \epsilon \operatorname{ctg} h \epsilon - \frac{1}{2} \operatorname{We} \right)$$

$$S = 2\epsilon^3 \sqrt{\frac{\operatorname{We}}{Lp}}, \quad \epsilon = kd_0, \quad i\omega_l = i\omega \sqrt{\frac{\rho_l d_0^3}{\sigma}}$$

and

$$\operatorname{We} = \frac{\rho_l V^2 2d_0}{\sigma}, \quad \frac{1}{Lp} = \frac{\mu_l^2}{\rho_l \sigma 2d_0}, \quad (10.8)$$

$$M = \frac{\rho_2}{\rho_1}, \quad N = \frac{\mu_2}{\mu_1}, \quad \operatorname{ctg} h \epsilon = \frac{\cosh \epsilon}{\sinh \epsilon}.$$

For a detailed derivation of these equations, see references [12,13]. In the preceding equations,  $\omega$  represents vibration frequency,  $d_0$  is the liquid jet diameter, and  $k$  is the wave number ( $k = 2\pi/\lambda$ ,  $\lambda$  is the wavelength). The solution of Equation 10.8 is a complex form. Its imaginary portion determines the character of motion's stability. The real portion denotes the vibration amplitude with positive sign for decay and negative sign for instability. It is obvious that the solution will include  $\operatorname{We}$  (Weber number),  $Lp$  (Laplace number or Ohnesorge number,  $Lp = 1/Oh$ ),  $M$  (gas–liquid density ratio), and  $N$  (gas–liquid viscosity ratio). Therefore, these four dimensionless numbers are the control parameters for the droplet diameter, which represents the liquid disintegration capability.

A simpler alternative method may be used to investigate the control parameters by using the dimensional analysis method, or called Buckingham PI theory.<sup>14</sup> Proper selection of the physical parameters is critical when using this method. Assume the atomization process can be characterized by the droplet diameter  $D$  and the following physical properties affect the droplet diameter:

$l$  = characteristic length of atomizer, (i.e., jet diameter or liquid sheet thickness, etc.).

$V$  = liquid exit velocity or liquid relative velocity to ambient environment

$\sigma$  = liquid surface tension

$\rho_l, \rho_g$  = liquid and ambient gas density, respectively

$\mu_l, \mu_g$  = liquid and ambient gas viscosity, respectively

Here, eight parameters ( $D, l, V, \sigma, \rho_l, \rho_g, \mu_l, \mu_g$ ) are listed, but only three primary dimensions— $M$  (mass),  $L$  (length), and  $T$  (time). Therefore,  $n = 8 - 3 = 5$  PI additional variables are needed to describe the relationship. Choosing  $l, V$ , and  $\rho_g$  as primary variables and reducing the other parameters to dimensionless (PI) variables yields

$$\Pi_1 = D l^{a1} V^{b1} \rho_g^{c1} = M^{-3c1} L^{1+a1+b1+c1} T^{-b1} = M^0 L^0 T^0$$

$$\Pi_2 = \sigma l^{a2} V^{b2} \rho_g^{c2} = M^{1+c2} L^{a2+b2-3c2} T^{-2-b2} = M^0 L^0 T^0$$

$$\Pi_3 = \mu_l l^{a3} V^{b3} \rho_g^{c3} = M^{1+c3} L^{a3+b3-c3-1} T^{-b3-c3} = M^0 L^0 T^0$$

$$\Pi_4 = \mu_g l^{a4} V^{b4} \rho_g^{c4} = M^{1+c4} L^{a4+b4-c4-1} T^{-b4-c4} = M^0 L^0 T^0$$

$$\Pi_5 = \rho_l l^{a5} V^{b5} \rho_g^{c5} = M^{1+c5} L^{a5+b5-3c5-3} T^{-b5} = M^0 L^0 T^0$$

(10.9)

Applying the power product method to zero the exponents in Equation 10.9, the following results:



$$\begin{aligned}
\Pi_1 &= \frac{D}{l} \\
\Pi_2 &= \frac{\sigma}{\rho_g V^2 l} = \frac{1}{We} \\
\Pi_3 &= \frac{\mu_l}{\rho_g V l} \\
\Pi_4 &= \frac{\mu_g}{\rho_g V l} \\
\Pi_5 &= \frac{\rho_l}{\rho_g} = M.
\end{aligned} \tag{10.10}$$

After rearranging  $\Pi_3$  and  $\Pi_4$  as

$$\begin{aligned}
\Pi_3' &= \frac{\Pi_3^2}{\Pi_2 \Pi_5} = \frac{\mu_l^2}{\rho_l \sigma l} = \frac{1}{L_p} \\
\Pi_4' &= \frac{\Pi_3}{\Pi_4} = \frac{\mu_l}{\mu_g} = N,
\end{aligned} \tag{10.11}$$

The equations become

$$\frac{D}{l} = f\left(\frac{\rho_g V^2 l}{\sigma}, \frac{\rho_l \sigma l}{\mu_l^2}, \frac{\rho_g}{\rho_l}, \frac{\mu_g}{\mu_l}\right) = f(We, L_p, M, N). \tag{10.12}$$

The results are the same as Equation 10.8.

In reality, the problem is much more complicated. For example, the disintegration of a liquid sheet can be also caused by liquid perforation, especially for high viscosity fluid as shown in Figure 10.2.<sup>15</sup> The photo is a swirl



**FIGURE 10.2**  
A hollow-cone swirl spray with high viscosity liquid ( $v = 6 \text{ mm}^2/\text{s}$ )  
The liquid surface shows perforation and waves developed before disintegration.

hollow-cone spray for a high viscosity liquid. The liquid viscosity is about six times that of typical water. From the photo, perforation on the liquid surface can be seen in addition to waves developed on the surface. Adding the perforation effect to the atomization process makes the analysis even more complex. It is difficult to have an analytical solution to describe this hydrodynamic and aerodynamic process. For this reason, empirical correlations are generally developed for real atomizations.<sup>14</sup>

## 10.4 Parameters Affecting Atomization

The analysis in Section 10.3 shows that a single fluid atomization is affected by the liquid exit velocity ( $V$ ), liquid characteristic length ( $l$ ), liquid density ( $\rho_l$ ), viscosity ( $\mu_l$ ), surface tension ( $\sigma_l$ ), ambient gas density ( $\rho_g$ ), and viscosity ( $\mu_g$ ). The exit velocity and characteristic length (i.e., jet diameter or liquid sheet thickness) are determined by the nozzle design. The liquid density, viscosity, and surface tension are the liquid properties. The gas density and viscosity are the ambient gas properties. Therefore, the atomization quality, which is represented by the droplet sizes, is determined by the nozzle design, liquid properties, and the ambient gas properties.

Before advanced laser instruments were available, measuring the droplet size was difficult. The atomization quality was investigated by the liquid breakup length—the shorter the breakup length, the better the atomization. Literature describing empirical relationships for breakup lengths with those parameters is fairly extensive.<sup>8,11,15–21</sup> A general trend of the breakup lengths varied with those parameters is summarized in Table 10.2. If the breakup length increases with an increase of the parameter, it is considered a positive effect.

**TABLE 10.2**

Effect of Dimensionless Parameters on Liquid Breakup Length

Parameter	Definition	Physical Meaning	Effect
Reynolds number	$Re = \frac{\rho_l V l}{\mu_l}$	$\frac{\text{Inertia}}{\text{Viscosity}}$	Negative
Weber number	$We = \frac{\rho_g V^2 l}{\sigma}$	$\frac{\text{Inertia}}{\text{Surface Tension}}$	Negative
Ohnesorge number	$Oh = \frac{\rho_l \sigma l}{\mu_l^2}$	$\frac{\text{Surface Tension}}{\text{Viscosity}}$	Positive
Density ratio	$M = \frac{\rho_g}{\rho_l}$	$\frac{\text{Gas Density}}{\text{Liquid Density}}$	Negative
Viscosity ratio	$N = \frac{\mu_g}{\mu_l}$	$\frac{\text{Gas Viscosity}}{\text{Liquid Viscosity}}$	Negative

If the breakup length decreases with an increase of the parameter, it is considered a negative effect.

Although the earlier discussions are mainly for a single jet fluid atomization, the results can be applied to the twin-fluid atomization process. In most process and utility burners, the liquid property (or oil) has wide variations in viscosity with small variations in surface tension and density. Process burners are generally used for the hydrocarbon, chemical, and petrochemical industries. Utility burners are mostly used for power generation or steam generation in commercial or industrial applications. The liquid fuel viscosity can vary 10- or even 100-fold, while surface tension and density usually only vary a few percentages making oil viscosity the dominant parameter. As mentioned in Section 10.2, oil viscosity, typically, varies inversely proportionally to temperature—the higher the temperature, the lower the oil viscosity. In industry, oil viscosity can be maintained in a reasonable range by heating the oil to a certain temperature. John Zink usually recommends maintaining oil viscosity at 200 SSU or 42 cSt. The Saybolt Universal Second is a kinematic viscosity used in classical mechanics and defined as the time that 60 cm<sup>3</sup> of oil takes to flow through a calibrated tube at a controlled temperature. (As discussed in Section 10.2, the cSt is a unit used for kinematic viscosity.)

The conversion of SSU to cSt may be approximated as follows:

$$\begin{aligned} 32 < \text{SSU} < 100 \text{ s}, \quad \text{cSt} &= 0.226 (\text{SSU}) - 195/(\text{SSU}) \\ \text{SSU} > 100 \text{ s}, \quad \text{cSt} &= 0.220 (\text{SSU}) - 135/(\text{SSU}) \end{aligned} \quad (10.13)$$

For viscous oils, sometimes the SSF is used. Conversion of SSF to cSt can be approximated as follows:

$$\begin{aligned} 25 < \text{SSF} < 40 \text{ s}, \quad \text{cSt} &= 2.24 (\text{SSF}) - 184/(\text{SSF}) \\ \text{SSF} > 40 \text{ s}, \quad \text{cSt} &= 2.16 (\text{SSF}) - 60/(\text{SSF}) \end{aligned} \quad (10.14)$$

Since the oil viscosity in industry can be maintained in an appropriate range, the atomization quality then is controlled mainly by the liquid characteristic length ( $l$ ), exit velocity ( $V$ ), and density ratio ( $M$ ). In other words, atomization quality in industrial applications is mainly a function of atomizer design and operational conditions.

contact surface area. Smaller droplets produce larger contact areas. The atomization quality, therefore, is usually indicated by the average droplet size. However, in addition to droplet size, other spray characteristics, such as spray angle and patternation, also affect liquid combustion. Droplet size, spray angle, and patternation are discussed in the following.

### 10.5.1 Droplet Size

The drops generated from atomization are heterogeneous, and the sizes vary greatly. It is, therefore, necessary to express the droplet diameter in a representative mean value. The most common mean values are defined as follows:

$$\begin{aligned} \text{Length Mean} = D_{10} &= \frac{\sum_i N_i D_i}{\sum_i N_i} \\ \text{Surface Mean} = D_{20} &= \left( \frac{\sum_i N_i D_i^2}{\sum_i N_i} \right)^{1/2} \\ \text{Volume Mean} = D_{30} &= \left( \frac{\sum_i N_i D_i^3}{\sum_i N_i} \right)^{1/3} \\ \text{Sauter Mean Diameter} = \text{SMD} = D_{32} &= \frac{\sum_i N_i D_i^3}{\sum_i N_i D_i^2} \end{aligned} \quad (10.15)$$

Droplet combustion involves liquid evaporation and combustion reaction, which consist of heat and mass transfer. Therefore, the mean value of droplet size should contain quantities of area and volume. The Sauter mean diameter (SMD), defined as a ratio of volume to area, is the most representative diameter for atomization applications.

In order to obtain the SMD droplet size, individual droplet sizes must be measured. The John Zink Spray Laboratory<sup>22</sup> is equipped with an advanced laser instrument called a phase Doppler particle anemometer (PDPA).<sup>23</sup> This device can measure individual droplet sizes within a spray and calculate the SMD value. The PDPA as shown in Figure 10.3 collects the droplet diameter and velocity simultaneously for each droplet passing through the laser sample volume. The detailed instrument description is discussed in Volume 2, Chapter 5 Combustion Diagnostics. (Section 10.7 contains a discussion of PDPA measurements on John Zink oil guns.)

## 10.5 Spray Characteristics

As stated earlier, good combustion requires good air-fuel mixing. The purpose of atomization is to create many small droplets to increase the liquid-to-air

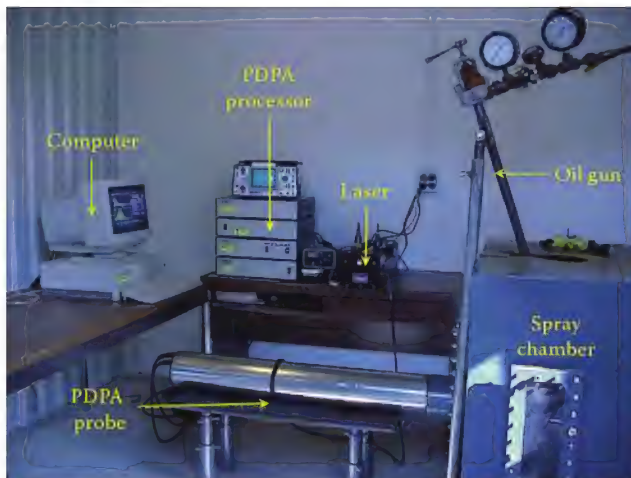


**FIGURE 10.3**  
John Zink Spray Laboratory equipped with a PDPA

### 10.5.2 Spray Angle

An appropriate spray angle is the key element to maintaining a stable oil flame. If the spray angle is too narrow, the recirculation vortex is too small to bring the high temperature flue gas back to the oil gun tip resulting in a lift-off flame as illustrated in Figure 10.4a. The lift-off oil flame could be extinguished. If the spray angle is too wide, the liquid fuel will spray on the tile edge resulting in coke built up as illustrated in Figure 10.4c. An appropriate spray angle recirculates high temperature flue gases back to the spray tip and keeps new droplets ignited resulting in a stable oil flame as shown in Figure 10.4b.

In reality, however, most oil guns have curved spray boundaries. The actual spray angle is not the same as the mechanical angle projected from the drilled hole. For example, the spray angle of a gun with a  $90^\circ$  machined angle could actually be about  $30^\circ$  as shown

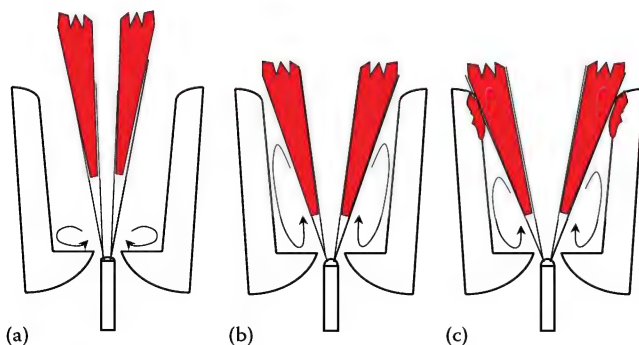


**FIGURE 10.4**  
Spray angle relative to a stable oil flame: (a) Narrow spray angle causes a lift-off oil flame, (b) Good spray angle brings hot flue gases back to the spray root and maintains a stable oil flame, and (c) Wide spray angle causes coking on the burner tile.

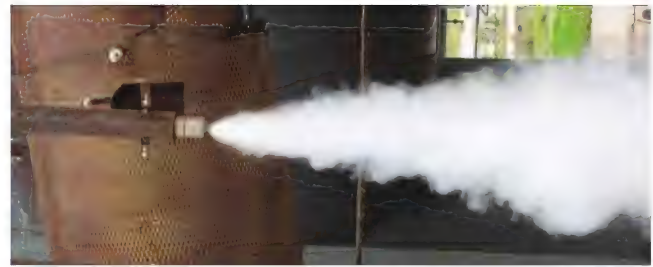


**FIGURE 10.5**  
A gun with a  $90^\circ$  machine angle, its spray angle actually is about  $30^\circ$ .

in Figure 10.5. Experimentation is required to measure the actual spray angle. One method of experimentation is to use a patternator.

### 10.5.3 Patterntation

Patterntation is the liquid distribution within the spray. Combustion requires uniform liquid fuel distribution to maintain a good combustion efficiency and low pollutant emissions. The apparatus used to measure the liquid distribution of an oil gun is called a patternator. A patternator that is designed by John Zink is shown in Figure 10.6. The oil gun is set at the center of a curved plate. Several small cups are mounted at the curvature to collect the water that is sprayed from the gun. The water collected in each cup is then measured by the graduated cylinder.

The typical patterntation sprayed out of a gun is shown in Figure 10.7. (The oil gun tested is pictured in Figure 10.5.) This graph indicates that water is distributed between  $-15^\circ$  and  $15^\circ$  resulting in a spray angle of about  $30^\circ$ . This method demonstrates that patterntation indicates both the uniformity of the liquid spray and the actual spray angle of an oil gun.

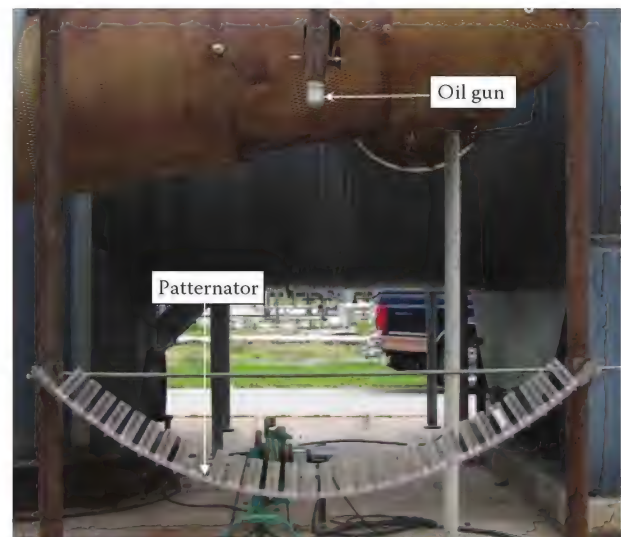


**FIGURE 10.6**  
Patternator to collect water sprayed out of an oil gun.



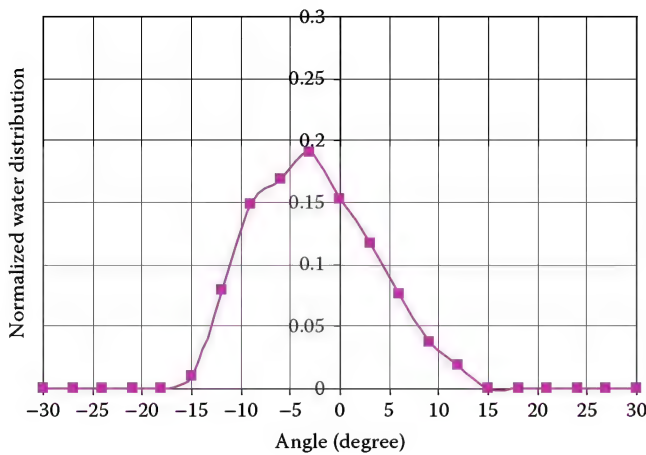


FIGURE 10.7  
Patternation measurements for a gun shown in Figure 10.5.

## 10.6 Atomizer Type

### 10.6.1 Single Fluid Atomizer

The single fluid atomizers are generally called “mechanical” because they use only the liquid fuel pressure for atomization. Many years ago, it was discovered that reasonably good atomization for combustion systems could be obtained by using mechanical atomizers. For a simple plain single orifice jet, fluids must be accelerated to about 400 ft/s (122 m/s).<sup>24</sup> The breakup mechanism is proportional to velocity as discussed in Section 10.3. This velocity corresponds to a liquid pressure of around 1000 psig (69 barg). Because of the high pressure requirement, single orifice atomizers are not generally used in atmospheric combustion applications.

A common mechanical atomizer used in combustion applications is the “pressure swirl” atomizer, sometimes called “simplex” (Figure 10.8). Fluid is introduced tangentially (swirled) creating an air core and then exits a small hole forming a hollow cone of liquid spray ranging from 50° to 80°. The operating parameters of this style of atomizer are well known and documented.<sup>25,26</sup>

The discharge coefficient for simplex swirl atomizer is approximated by:

$$C_d = .035 \left[ \frac{A_p}{D_s D_o} \right]^5 \left[ \frac{D_s}{D_o} \right]^{25} \quad (10.16)$$

where

- $C_d$  is the discharge coefficient
- $A_p$  is the area of swirled ports
- $D_s$  is the diameter of swirl chamber
- $D_o$  is the exit diameter

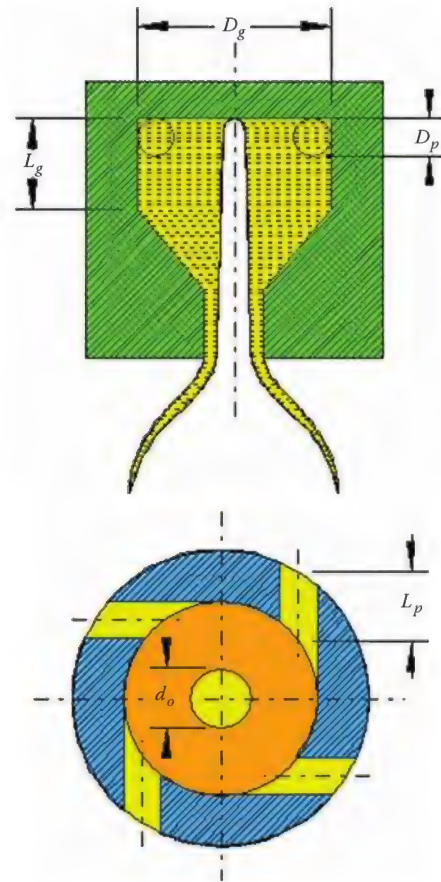


FIGURE 10.8  
Simplex swirl atomizer.

The cone angle is a direct function of atomizer geometry defined as  $\frac{A_p}{D_s D_o}$ .

Typical required oil pressures are 500–1000 psig (35–70 barg) with a lower operational pressure of about 300 psig (21 barg). The range of turn down can be extended enormously to 10:1 or more with the use of a wide range return flow (WRRF) atomizer. This design is essentially a simplex style with a return flow to keep the swirl high in the chamber, but limiting the discharge amount (Figure 10.9). A common problem with simplex atomizers is pulsation in the air core. Care must be taken in the design of the swirl chamber to prevent pulsation.

### 10.6.2 Twin Fluid Atomizer

Twin fluid atomizers are widely used in process burners and utility boiler burners. Typically, the heat released using a process burner is much smaller than that released in industrial and utility burners.

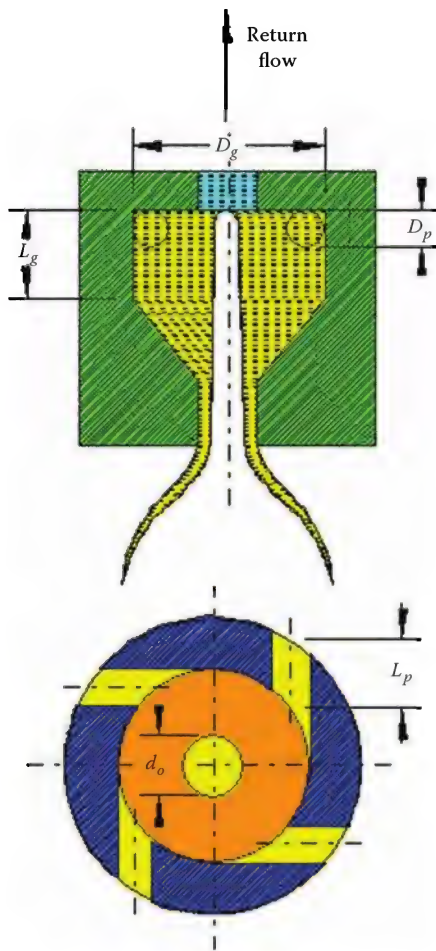


FIGURE 10.9  
Simplex swirl atomizer with return flow.

### 10.6.2.1 Process Oil Gun

As discussed in Section 10.3, the control parameters for atomization quality include the liquid characteristics of length, exit velocity, density, and viscosity. To achieve good atomization, those parameters should be manipulated in the correct direction within practical limits. For example, while it is well known that a smaller jet diameter produces better atomization, a small exit port may easily get clogged using heavy oil, especially No. 6 residual oil, which always contains solid particles. For process burner applications, the problem is more challenging. The heat released for each process burner is usually much smaller than that of boiler burners. In order to keep the process burner oil port diameter large enough to be free from clogs, the number of ports has to be reduced. This causes a poor oil gun spray pattern resulting in poor flame pattern. Because of this, most oil guns in process burners mix steam with oil. In this way, the fuel port diameters can be enlarged with a reasonable number of exit ports to

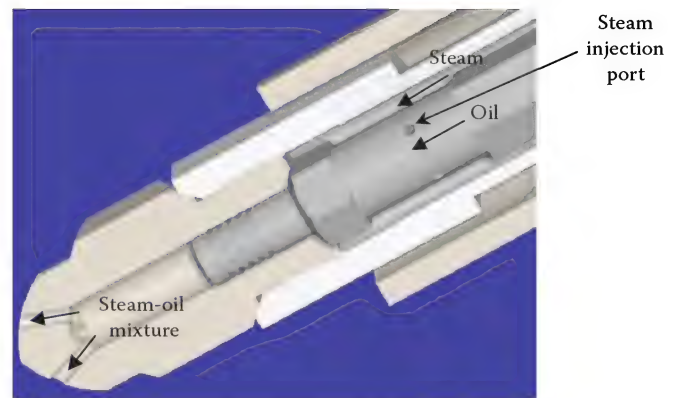


FIGURE 10.10  
John Zink EA oil gun.

maintain uniform spray patternation. The John Zink EA and MEA oil guns are the typical examples of this design. For the EA oil gun as shown in Figure 10.10, the fuel oil is mixed with the steam by injecting steam through small ports before exiting to the tip. The MEA design is similar to the EA oil gun except for a small modification on the tip design as shown in Figure 10.11. Mixing the oil with steam not only eliminates the clogging problem, but also reduces the fuel density and viscosity resulting in a good quality of atomization.

John Zink also developed a High Efficiency Residual Oil (HERO®) gun. Compared to the EA and MEA oil guns, the HERO gun has a much better atomization quality and consumes less atomizing medium (i.e., steam).<sup>22</sup> The HERO gun is a registered trademark of John Zink in the United States and is patented worldwide.<sup>27,28</sup>

The HERO gun, in addition to reducing the liquid density and viscosity as discussed for the EA and

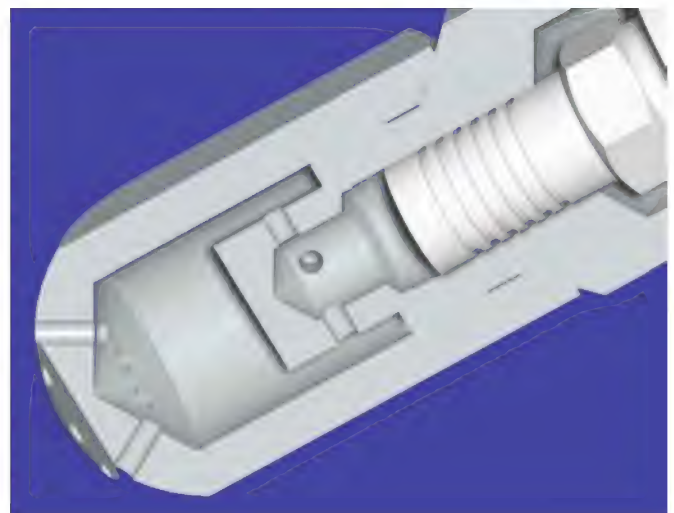


FIGURE 10.11  
John Zink MEA gun.



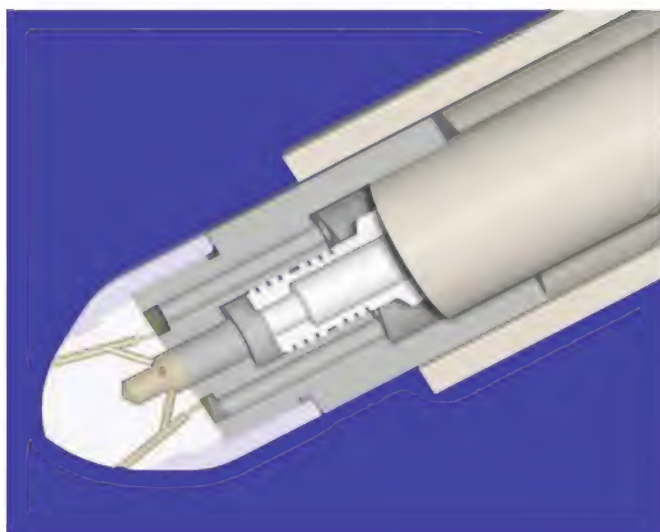


FIGURE 10.12

John Zink High Efficiency Residual Oil (HERO) gun. The tip is a modified Y-jet.

MEA oil guns, also employs a special design (a modification of the Y-jet) to decrease the characteristic length of liquid fluid. The HERO gun design is shown in Figure 10.12.

The Y-jet<sup>29</sup> is well known and widely used in large oil-fired boiler burners. In the Y-jet, fuel is injected into an atomizing medium stream with a certain angle as illustrated in Figure 10.13. As shown in Figure 10.13,

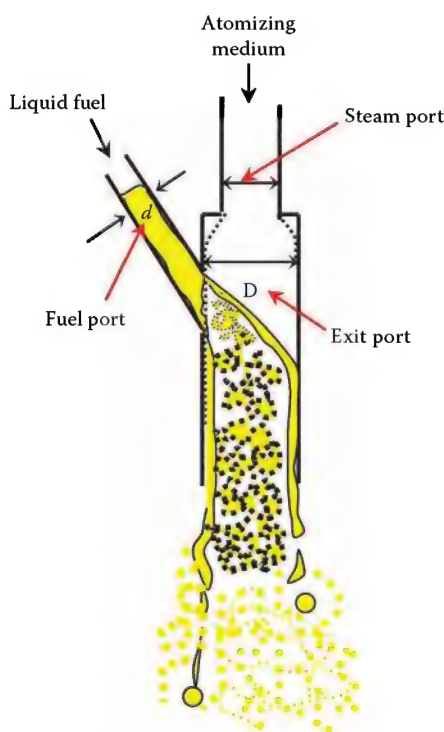


FIGURE 10.13

Y-jet atomization principle.

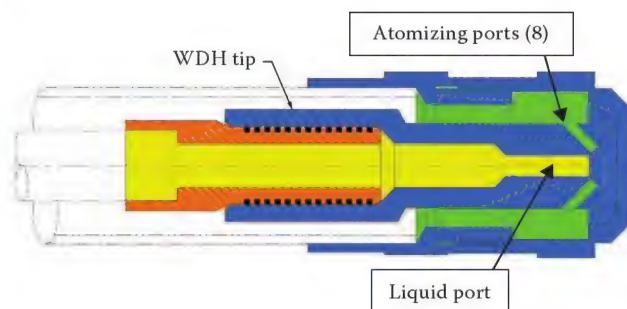


FIGURE 10.14

WDH waste aqueous gun design with one liquid exit port surrounded with eight atomizing ports.

the stream of atomizing medium pushes the liquid fuel against the wall, which makes the cylindrical liquid jet form an annular cone. Forming an annular liquid cone reduces the liquid characteristic length. For example, a liquid jet with a diameter  $d$  is injected into a mixing chamber of diameter  $D$ . If  $D = 1.1 d$ , the thickness of the liquid cone may become  $0.32 d$ , decreasing the liquid characteristic length by almost 70%. Forming a liquid cone also increases the contact surface area between liquid and gas. A large liquid–gas contact surface area improves the disintegration process.

The only limitation of the Y-jet is that every Y-jet has to be an individual port. Clogging becomes a problem for process oil guns with small heat releases. For this reason, the Y-jet design is not applied to process oil guns. The John Zink HERO gun eliminates this drawback by mixing fuel oil with steam before entering into individual Y-jet. The liquid fuel port,  $d$ , therefore, may be enlarged. Mixing the oil with steam also decreases the fuel oil density and viscosity resulting in even better atomization.

A good oil gun design results in a uniform patternation. In an attempt to prevent clogging, some oil gun designs sacrificed the patternation. For example, the WDH gun as shown in Figure 10.14 has liquid flowing straight through one exit port surrounded by several atomizing ports. While this design has no problem with clogging, the patternation has been sacrificed. The patternations for the WDH and the HERO gun are shown in Figure 10.15. The figure shows that liquid distribution for the HERO gun is much more uniform than that for the WDH gun. A uniform patternation has the advantage of less soot generation. The HERO gun is also found to have low particulate emissions compared to other oil guns.

#### 10.6.2.2 Boiler Burner Oil Gun

Boiler burner oil guns have capacities that range from 3 MW (10 MMBtu/h) to 130 MW (450 MMBtu/h). Smaller boilers, in the range of 50–1000 K lb/h (PPH)



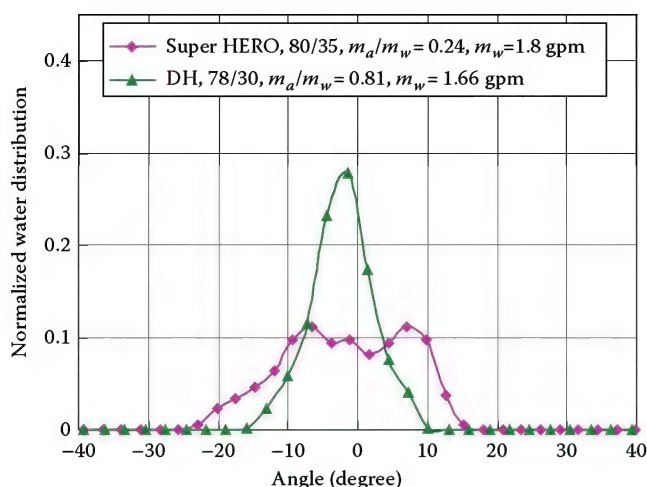


FIGURE 10.15

Patternation comparison for HERO and WDH guns. The HERO gun shows much more uniform liquid distribution than the WDH gun.

steam, generally use a variety of twin fluid internal mix atomizers or tip mix such as the Y-jet already discussed in detail earlier. Many years ago utility-size boilers almost always used mechanical atomizers such as the simplex WRRF design due to the excessive cost of atomizing steam and because the furnace residence time is high. Today, utilities' units have been changing to use twin fluid atomizers utilizing low steam consumption, typically 0.05–0.1 mass ratios. The driving decision to change is usually based on emission reductions.

It is common to design special cap drilling patterns for boiler applications. For package boilers, the tip patterns may be elliptical to produce elliptical flames to fit the aspect ratio of the furnace. Similar tip features can be utilized on tangentially fired utility units to prevent flame impingement (Figure 10.16). The drilling patterns can vary to produce staged combustion and reduce

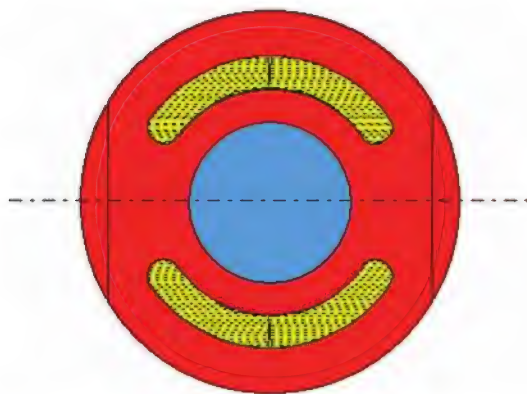


FIGURE 10.16

Coen elliptical cap slots for low- $\text{NO}_x$ .

$\text{NO}_x$  emissions, carbon loss, and opacity.<sup>30</sup> Internal mix atomizers are used rather than Y-jets due to the complex drilling patterns.

## 10.7 Oil Gun Performance

The oil gun performance can be evaluated by atomization quality (or droplet size), energy consumption (or atomizing medium consumption), turndown ratio, and pollutant emissions including particulate, CO, and  $\text{NO}_x$  emissions. In the following the process oil gun and boiler oil gun are discussed separately.

### 10.7.1 Process Oil Gun

#### 10.7.1.1 Atomization Quality

The atomization quality is determined by the mean droplet size. As mentioned in Section 10.5, the SMD is the most representative mean diameter for the atomization community. Differing operating conditions can change the oil gun's atomization quality. Some PDPA measurements for different oil guns at different operation conditions are presented here to demonstrate the control parameters. (In the PDPA experiments, the liquid is water and air is the atomizing medium.)

The PDPA measurements of the MEA oil gun for a given water pressure (=60 psig or 4 barg) at various air pressures are presented in Figure 10.17. In the Figure 10.17,  $P_w$  represents the water pressure and  $P_a$  is the

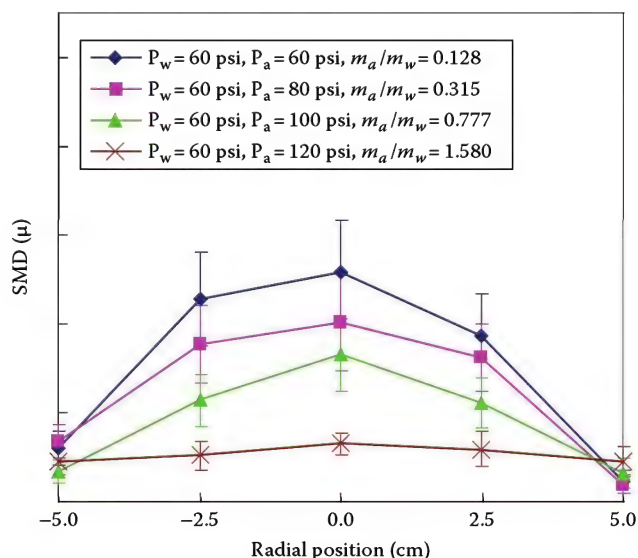
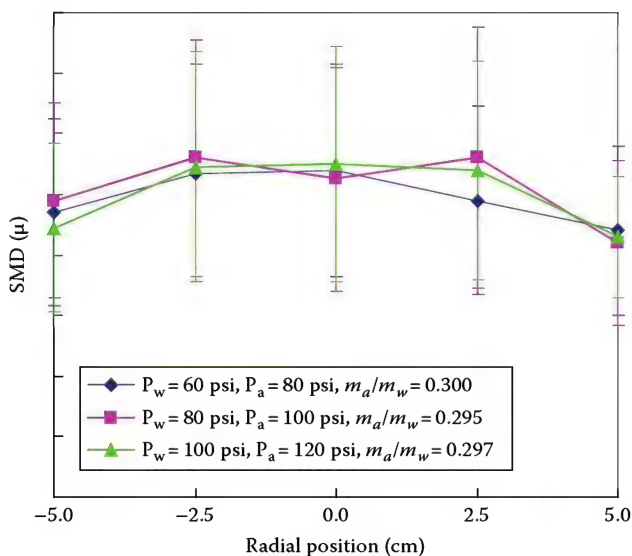


FIGURE 10.17

Droplet size measurements of the MEA oil gun at different air pressures.

air pressure. The abscissa represents the position across the spray cone of one exit port in an oil gun. The droplet size is represented by SMD with standard deviation. The results indicate that the higher air pressure generates smaller droplets. This is expected because high air pressure contains high momentum to break up the water jet.

Now, the question is which relative pressures play the more important role: water pressures or air–water differential pressure. The testing results for the oil gun at the same differential pressure, but different water pressures, are shown in Figures 10.18 and 10.19. With similar air–water differential pressures, the oil gun generates similar droplet sizes in Figure 10.18, but different results are shown in Figure 10.19. This indicates that the same air–water differential pressures do not necessarily generate the same droplet sizes. Also, note that the test case for water pressure of 60 psig (4 barg) in Figure 10.19 does *not* have a smaller droplet size than that for 40 psig (2.8 barg). This infers that neither water pressure nor differential pressure is a control parameter. By reviewing the calculation of the air–water mass ratio ( $m_a/m_w$ ), the parameter that dominates the droplet size becomes prominent. In Figure 10.18, the air–water mass ratios are similar; the oil gun generates similar droplet sizes. In Figure 10.19, even though the air–water differential pressures are the same, the mass ratios are different and consequently the atomization droplet sizes are different—the higher the mass ratio, the better the atomization. The same trend can be seen in Figure 10.20. The conclusion is that the mass ratio is the main control parameter for oil gun atomization quality.



**FIGURE 10.18**  
Droplet size measurements of the MEA oil gun at similar air–water differential pressures.

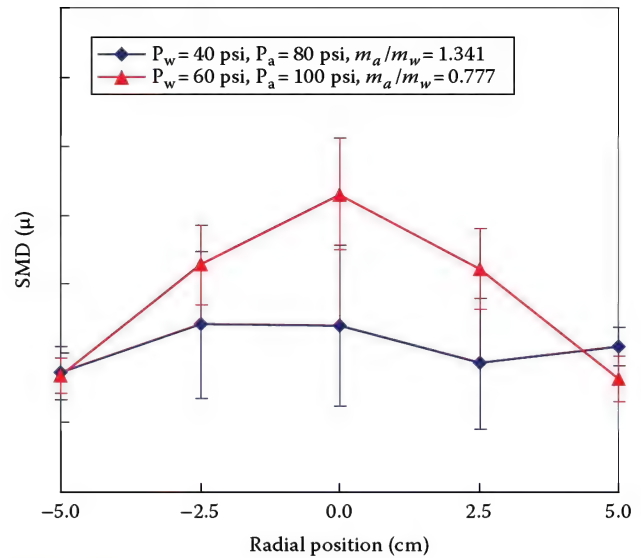


**FIGURE 10.19**  
Droplet size measurements of MEA oil gun at the same air–water differential pressure but different mass ratios.

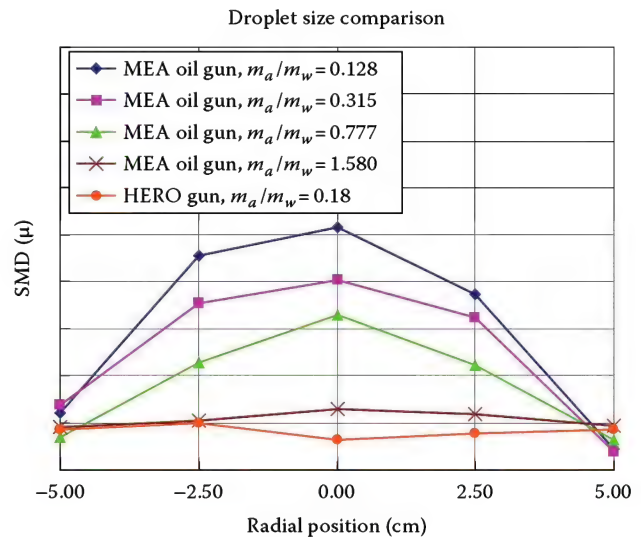


**FIGURE 10.20**  
Droplet size comparison measured by PDPA for different oil gun designs.

For different oil guns with similar mass ratios (e.g., 0.128 for the MEA and 0.18 for the HERO) the droplet size for the MEA oil gun is almost three times that of the HERO gun. From another perspective, to achieve the same droplet sizes, the MEA oil gun requires a mass ratio about eight times that of the HERO gun. This implies that the HERO gun is much more energy efficient. This validates the previous discussion in Section 10.3 that the liquid characteristic length is a dominant parameter for atomization quality. The HERO gun has a much smaller characteristic length than the EA or MEA oil guns. In other words, oil gun design is also, one of the control parameters.

### 10.7.1.2 Energy Consumption

In industry, steam is the most popular atomizing medium for the oil guns. The steam consumption for a typical oil gun in process burners is about 0.3–0.4 lb steam/lb oil. The John Zink MEA or EA guns fall in this category. The HERO gun is a much more energy-efficient oil gun consuming much less steam as shown in Figure 10.21.

In process oil burners, the oil gun is usually operated at a constant steam–oil differential pressure. The steam pressure is 20 psig (1.4 barg) or 30 psig (2.0 barg) higher than the oil pressure. Under this condition, the steam consumption for one specific oil gun is a function of heat release (or oil pressure) as indicated in Figure 10.22.

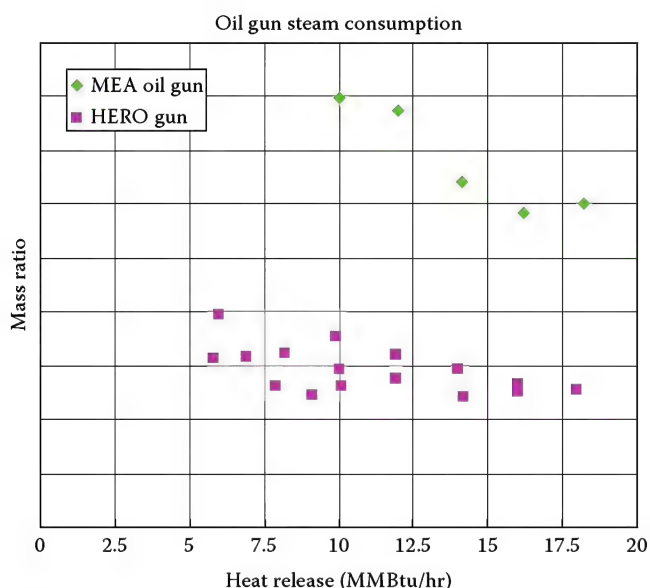


FIGURE 10.21 Steam consumption for different oil gun designs.

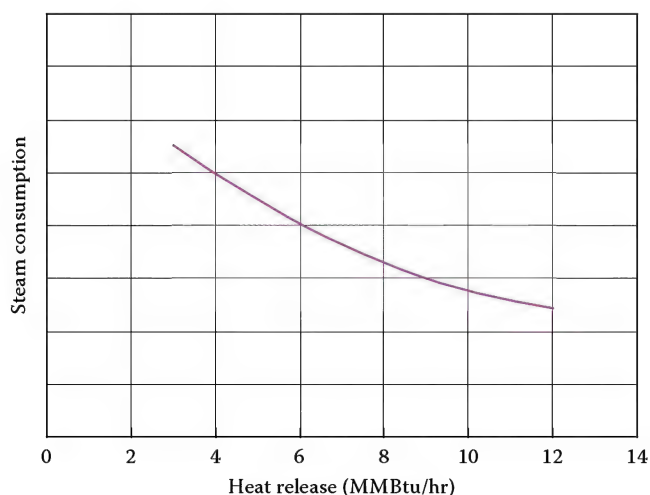


FIGURE 10.22 Steam consumption curve for a constant steam–oil differential pressure oil gun.

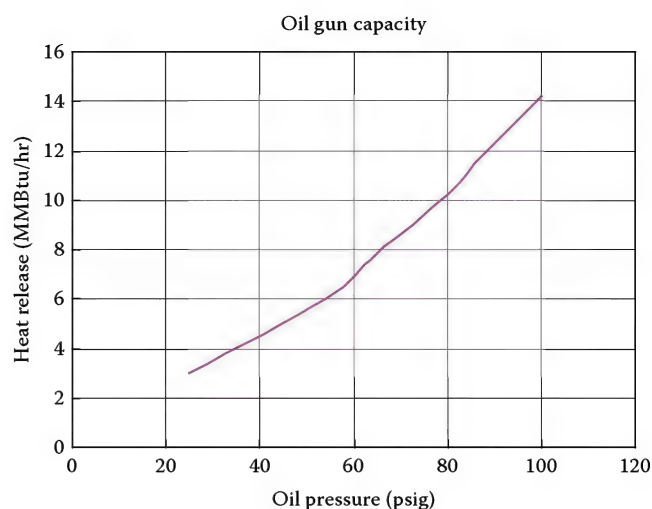


FIGURE 10.23 A typical oil gun capacity curve showing oil gun turndown ratio.

The steam consumption is high at low heat release and low at high heat release.

### 10.7.1.3 Turndown Ratio

An oil gun with a high turndown ratio is easy to operate. The turndown ratio of an oil gun is defined as the ratio of the maximum heat release to the minimum heat release with stable oil flames. A good atomization oil gun has a higher turndown ratio compared to a poor atomization oil gun. A good atomization oil gun generates small droplets. The small droplets vaporize quickly and are ignited easily. Consequently, it has the capability to maintain a stable flame at low oil pressures. The HERO gun typically achieves a turndown ratio of 4:1 at an oil pressure of 100 psig (6.9 barg), and the MEA or EA oil guns usually achieve a turndown ratio of 3:1 under the same condition.

The oil gun turndown ratio increases with higher available oil pressure. An example oil gun capacity curve is shown in Figure 10.23. From Figure 10.23, if the available oil pressure is 100 psig (6.9 barg), the oil gun can easily achieve a turndown ratio more than 4:1. If the oil pressure is only 80 psig (5.5 barg), the turndown ratio is reduced to around 3:1.

### 10.7.1.4 Pollutant Emissions

It is well understood that good atomization generates less particulate emissions. As indicated in Figure 10.17, an increase of mass ratio by increasing air–water differential pressure improves the atomization (i.e., the smaller droplet size). This infers that an increase of differential pressure reduces the particulate emissions. A combustion test of the HERO gun was conducted by varying the steam–oil differential pressures.



TABLE 10.3

Combustion Performance of the HERO Gun

Heat Release (MW)	Air Temperature (°C)	Furnace Temperature (°C)	Dry O <sub>2</sub> (%)	Differential Pressure (Bar)	Steam–Oil Mass Ratio (%)	Particulate Emission (%)	NO <sub>x</sub> (%)
4.5	232	867	3.9	2	100	100	100
4.5	232	846	4.0	2.7	110	65	108

The particulate emissions were measured using the EPA Method 5<sup>31</sup> and are listed in Table 10.3. The combustion results confirm the trend of the PDPA measurements (i.e., the higher the differential pressure, the lower the particulate emissions).

Table 10.3 also shows that increasing the mass ratio by increasing the differential pressure creates an increase in NO<sub>x</sub> emissions. The same trend is also observed by testing the MEA oil gun as listed in Table 10.4. In this test, the particulate emissions were not measured by a quantitative method, such as EPA Method 5, but by a qualitative method, the Bacharach test method. The Bacharach number is lower for the high differential pressure case. The EPA Method 5 and the Bacharach test method are described in detail in Chapter 14.

In the comparison, the first case in Table 10.3 is used as a baseline, or 100%, and the other cases (Table 10.4) are divided by its values. The comparison of NO<sub>x</sub> emissions for both oil guns is illustrated in Figure 10.24.

In conclusion, for one specific oil gun, the differential pressure may be increased to reduce the particulate emissions, but NO<sub>x</sub> emissions will be sacrificed. In order to reduce both particulate and NO<sub>x</sub> emissions, a different oil gun design should be employed. A comparison of the HERO case as shown in Table 10.3 to the MEA case in Table 10.4 demonstrates that the HERO gun has better performance on both pollutant emissions.<sup>32</sup>

CO emissions are usually correlated with the particulate emissions. The parameters that affect the particulate emissions have the same effect on the CO emissions. Other operational conditions, such as O<sub>2</sub> level, furnace temperature, and air temperature, also affect the pollutant emissions.<sup>33</sup> A general trend of pollutant emissions varied with operating condition parameters is summarized in Table 10.5. A positive effect is defined when emission increases with an increase of the parameter value. Conversely, a negative effect is defined when emission decreases with an increase of the parameter value.

TABLE 10.4

Combustion Test Results for the MEA Oil Gun

Heat Release (MW)	Differential Pressure (Bar)	O <sub>2</sub> (%)	Furnace Temperature (°C)	Steam–Oil Mass Ratio (%)	NO <sub>x</sub> (%)
4.6	1.1	3.08	1043	175	116
4.6	2.1	3.17	1001	275	136

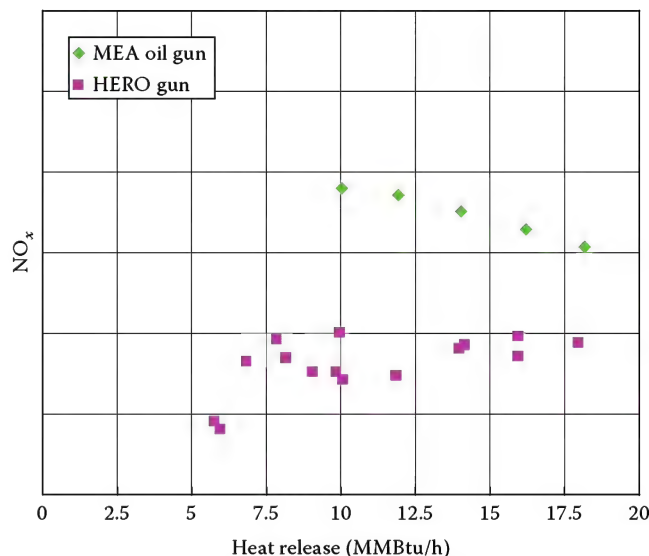
Oil gun NO<sub>x</sub> comparison

FIGURE 10.24

Comparison of NO<sub>x</sub> emissions for the HERO and MEA oil guns.

TABLE 10.5

Effect of Operational Parameters on Pollutant Emissions

Operational Parameters	NO <sub>x</sub> Emissions	CO Emissions	Particulate Emissions
O <sub>2</sub> level	Positive	Negative	Negative
Furnace temperature	Positive	Negative	Negative
Combustion air temperature	Positive	Negative	Negative
Differential pressure	Positive	Negative	Negative

In summary, a good oil gun design not only reduces the particulate and CO emissions, but also reduces NO<sub>x</sub> emissions. A strong understanding of the atomization principle is essential in the development of a good oil gun.

### 10.7.2 Boiler Oil Gun

Residence times for boilers are generally much lower than those of process applications. Thus, the importance of droplet distribution becomes paramount in the prediction of opacity and carbon loss. For mechanical simplex atomizers, a significant amount of work has been published to predict mean droplet size. An excellent summary can be

found in *Atomization and Sprays*.<sup>14</sup> An easy to use approximation for simplex atomizers SMD is<sup>34</sup>

$$SMD = 2.25\mu_L^{0.25} m_L^{0.25} (\Delta P)_L^{-0.5} \rho_A^{-0.25} \quad (10.17)$$

where

$\sigma$  is the surface tension liquid, kg/s<sup>2</sup>

$\mu$  is the kinematic viscosity liquid, kg/ms

$m$  is the mass flow rate liquid, kg/s

$\Delta P$  is the pressure drop liquid, Pa

$\rho$  is the density of ambient, kg/m<sup>3</sup>

Little work has been published on drop size relations for twin fluid atomizers since the early work of Wigg.<sup>35</sup> The industry usually relies on full scale testing for drop size relations as discussed previously. Subsequent correlations are empirically developed based upon atomizer geometry, liquid properties, and gas/liquid ratio. Similarly, the pressure and flow relations are developed based upon measured fluid losses, gas dynamics, and momentum exchange correlated to actual test data.

Atomizers are selected for boilers primarily based on emissions and turndown requirements. Utility boilers rarely require high turndown due to multiple burners and the need to generally fire at high load. For these reasons, a WRRF simplex atomizer is the overwhelming choice in these applications where it can be used.

When a large multi-burner boiler requires steam atomizers, the Y-jet atomizer is a good solution due to its ability to generate small enough droplets at low gas/liquid mass ratios of 0.05–0.1. The usual turndown requirement is 4 or 5:1. Large single burners are more difficult applications and may require 8–20:1 turndown.

Furnaces have small residence times and require small droplets to limit particulate and opacity emissions. Mechanical atomizers are almost never used in small furnaces with the exception of cold light off. Y-jet atomizers are preferred but may not be used if non-uniform flame patterns are needed. Generally for boiler applications, inside mix atomizers are used and require 0.1–0.15 gas/liquid ratios for normal applications.

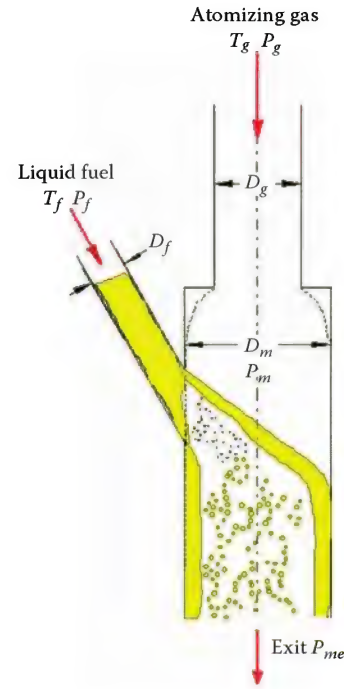


FIGURE 10.25  
Diagram of Y-jet.

predictions (see Figure 10.25) is given in the following. The solution involves compressible flow calculations, partial momentum exchange, orifice losses, and a multiple iterative solution.

Compute the Mach number through the gas orifice with known mixer pressure, mass flows and iterating on supply gas supply pressure as follows until convergence:

$$m_g = \frac{p_{tg}}{\sqrt{RT_t}} A_g M \sqrt{k} \left( 1 + \frac{k-1}{2} M^2 \right)^{(k+1)/(2-2k)} \quad (10.18)$$

Compute the gas temperature at orifice:

$$T_{go} = \frac{T_t}{1 + \left( \frac{k-1}{2} \right) M^2} \quad (10.19)$$

Compute the gas pressure at orifice:

$$P_{go} = \frac{P_{tg}}{\left( 1 + \frac{k-1}{2} M^2 \right)^{k/(k-1)}} \quad (10.20)$$

Compute the density at gas orifice:

$$\rho_{goi} = \frac{P_{goi}}{RT_{goi}} \quad (10.21)$$

## 10.8 Prediction Model

As discussed, predictive models have been developed for pressure swirl (simplex) atomizers for more than 50 years. Recently, Coen Co. has developed new predictive codes for Y-jet atomizers and internal mix atomizers. In prior years, testing full-scale atomizers was common. An outline of the Y-jet code used for flow and pressure

Compute the velocity through the gas orifice completing the first part of the converged solution with the assumed mixer pressure.

$$V_g = \frac{m_g}{(\rho_{go})A_g C d_g} \quad (10.22)$$

Next, using the same fixed flows, compute the mixer pressure by iterating on mixer inlet pressure assumed in the first iteration part one, above for the atomizing gas flow using partial conservation of momentum and compressible flow at the exit.

With the known fuel flow, compute the fuel velocity in the fuel orifice:

$$V_f = \frac{m_f}{(\rho_f A_f) C d_f} \quad (10.23)$$

With the known mixer pressure, compute the fuel supply pressure. Include the known formulas for viscosity corrections to find the actual fuel pressure.

$$(P_f - P_m) = (\rho_f V_f^2) \left( \frac{1}{2g_c C d_f^2} \right) \quad (10.24)$$

Next, balance the partial momentum exchange in the mixer before the exit orifice. Correct the gas density for actual mixer temperature and pressure. (For gas, the Mach numbers at 1, and under expanded flow in the first section, correct for normal shock.) From the conservation of mass, compute the gas velocity in the mixer.

Define  $V_r = \frac{V_{fm}}{V_{gm}}$  as the ratio of oil to gas velocity at the mixer outlet, a function of gas-to-liquid mass ratio. From the conservation of mass,

$$V_{gm} = \left\{ \frac{m_f}{(V_r)\rho_f} + \frac{m_g}{\rho_{gmi}} \right\} \left( \frac{1}{A_m} \right) \quad (10.25)$$

From the partial conservation of momentum, define

- $k_1$  = Fraction of oil inlet momentum conserved
- $k_2$  = Fraction of gas inlet momentum conserved

Compute the pressure rise or loss due to inlet momentum less exit momentum:

$$(\Delta p_m) A_m g_c = k_1 V_f m_f + k_2 V_g m_g - V_{gm} (m_g + V_r m_f) \quad (10.26)$$

Compute the mixer exit pressure by including the partial conservation of mixer gas stagnation velocity where the mixer gas density and temperature will depend on the partial heat transfer between fluids:

$k_3$  = Fraction of conserved gas stagnation velocity

$$P_{me} = P_m + \Delta P_m + \frac{k_3 \rho_{gm} V_{gm}^2}{2g_c} \quad (10.27)$$

Compute the exit  $C_{de}$  using conservation of mass:

$$C_{de} = \frac{m_g}{V_{gm} A_m r_g} \quad (10.28)$$

Compute the exit Mach number from pressure ratio:

$$\frac{P_{me}}{P_a} = \left( 1 + \frac{k-1}{2} M^2 \right)^{\frac{k}{k-1}} \quad (10.29)$$

Find the error in the part two iteration by the assumed mixer inlet pressure as follows:

$$m_g = \frac{P_{me}}{\sqrt{RT_m}} A_e (C_{de})(M) \sqrt{kg} \left( 1 + \frac{k-1}{2} M^2 \right)^{(k+1)/(2-2k)} \quad (10.30)$$

Iterate part two until the mixer pressure is found.

Iterate part one with new mixer pressure until the new gas supply pressure is found.

Continue back and forth until a solution for part one and part two is found.

This iterative technique requires experimental coefficients and heat transfer considerations to yield correct estimates. For simplicity, normal and oblique shock waves were omitted. When the gas inlet is choked, set the Mach number to 1, and correct the pressure and temperature. When the exit flow is choked, the resultant external shock wave can generally be ignored, however, excessive underexpansion at the exit can cause droplet deposition on the atomizer surface.

## Nomenclature and Subscripts

Nomenclature for Section 10.7 is as follows

- $A$  is the area
- $P$  is the pressure
- $T$  is the temperature
- $m$  is the mass flow rate
- $C_d$  is the discharge coefficient
- $R$  is the universal gas constant



- $K$  is the ratio of specific heats; constant pressure/  
volume
- $M$  is the mach number
- $g_c$  is the gravitational constant relation between  
lb mass and weight
- $\rho$  is the density
- $g_c$  is the proportionality constant between force,  
mass, and acceleration

## Subscripts:

- $g$  is the gas
- $t$  is the total pressure
- $o$  is the orifice
- $i$  is the inlet
- $m$  is the mixer
- $e$  is the exit
- $d$  is the discharge
- $a$  is the ambient
- $f$  is the fuel

The code is complicated and requires multiple simultaneous solutions. Experimental coefficients are obtained from full scale testing. Other codes based on similar principles are used for internal mix atomization with good success. The correlation of SMD test patterns to gas/liquid ratios has been shown to be strong.

## References

- Schmidt, P.F., (ed.), *Fuel Oil Manual*, 4th edn., Industrial Press, New York, pp. 34–35, 1985.
- Schweitzer, P.H., Mechanism of disintegration of liquid jets, *J. Appl. Phys.*, 8, 513–521, 1937.
- Giffen, E. and Muraszew, A., *The Atomization of Liquid Fuels*, Chapman & Hall, London, U.K., 1953.
- Krzywoblocki, M.A., Jets—Review of literature, *Jet Propul.*, 26, 760–779, 1957.
- Rutland, D.F. and Jameson, G.J., Theoretical prediction of the sizes of drops forms in the breakup of capillary jets, *Chem. Eng. Sci.*, 25, 11, 1970.
- Phinney, R.E., The breakup of a turbulent liquid jet in a gaseous atmosphere, *J. Fluid Mech.*, 60, 689–701, 1973.
- Kitamura, Y. and Takahashi, T., Influence of nozzle on breakup of a liquid jet, *Proceedings of ICLASS-78*, Tokyo, Japan, 1978.
- Mahoney, T.J. and Sterling, A.M., The breakup length of laminar liquid jets in air, *Proceedings of ICLASS-78*, Tokyo, Japan, 1978.
- Simmons, H.C., *The Atomization of Liquids: Principles and Methods*, Parker Hannifin, Cleveland, OH, Report No. 7901/2-0, 1979.
- Rayleigh, L., On the instability of jets, *Proc. London Math. Soc.*, 10, 4–13, 1878.
- Weber, C., Disintegration of liquid jets, *Z. Angew. Math. Mech.*, 11(2), 136–159, 1931.
- Lyshevskii, A.S., *Processes of Fuel Atomization in Diesel Nozzles (in Russian)*, Mashgiz, Moscow, 1963.
- Bayvel, L. and Orzechowski, Z., In *Liquid Atomization, Combustion: An International Series*, ed. N. Chigier, Taylor & Francis, London, U.K., 1993.
- Lefebvre, A.H., *Atomization and Sprays*, Hemisphere Publishing, New York, 1989.
- Chung, I.P. and Presser, C., Fluid property effects on sheet disintegration of a simplex pressure-swirl atomizer, *J. Prop. Power*, 17(1), 212–216, 2001.
- Buckingham, E., On physically similar systems: Illustrations of the use of dimensional equations, *Phys. Rev.*, 4(4), 345–376, 1914.
- Grant, R.P. and Middleman, S., Newtonian jet stability, *AIChE J.*, 12(4), 669–678, 1966.
- Hiroyasu, H., Shimizu, M., and Arai, M., The breakup of high speed jet in a high pressure gaseous atmosphere, *Proceedings of the 2nd ICLASS-82*, Madison, WI, pp. 69–74, 1982.
- Arai, M., Shimizu, M., and Hiroyasu, H., Breakup length and spray angle of high speed jet, *Proceedings of the 3rd ICLASS-82*, London, pp. 1B/4/1–10, 1985.
- Dombrowski, N. and Johns, W.R., The aerodynamic instability and disintegration of viscous liquid sheets, *Chem. Eng. Sci.*, 18, 203–214, 1963.
- York, J.L., Stubbs, H.F., and Tek, M.R., The mechanism of disintegration of liquid sheets, *Trans. ASME*, 75, 1279–1286.
- Chung, I.P., Karan, J., and Strupp, C., *High Efficiency Residual Oil (Hero®) Atomizer for Process Heater Burners*, AFRC Spring Meeting, Ottawa, Ontario, Canada, 2002.
- Bachalo, W.D., Method for measuring the size and velocity of spheres by dual-beam light scatter interferometry, *Appl. Opt.*, 19(3), 363–370, 1980.
- Castleman, R.A., Mechanism of the atomization of liquids, *Bur. Stand. J. Res.*, 6(3), 369–376, Research paper # 281 March 1931.
- Tanasawa, Y. and Kobayasi, K., Study on Swirl Atomizer, *Tech. Rep. Tohoku Univ.*, 20, Research paper # 1, pp. 27–58, 1955.
- Lefebvre, H., *Atomization and Sprays*, Hemisphere Publishing Corporation, Washington, DC, p. 171, 1989.
- High Efficiency Fuel Oil Atomizer, US Patent No. 6478239, John Zink Company, LLC, Tulsa, OK, January 2002.
- High Efficiency Oil Atomizer Method, US Patent No. 6691928, John Zink Company, LLC, Tulsa, OK, January 2003.
- Mullinger, P.J. and Chigier, N.A., The design and performance of internal mixing multijet twin fluid atomizers, *J. Inst. Fuel*, 47, 251–261, 1947.
- Drennan, S., Mandayam, V., and Rice, G., Low NOx experiences firing residual oil in industrial boilers, *AFRC International Symposium*, Ottawa, Ontario, Canada, 1997.

31. Environmental Protection Agency Method 5, Determination of particulate emissions from stationary sources, *40 CFR (Code of Federal Regulation) Chapter 1 Part 60 Appendixes A—Standards of Performance for New Stationary Sources Test Methods*, 2000.
32. Chung, I.P., Strupp, C., and Karan, J., New fuel oil atomizer for improved combustion performance and reduced emissions, presented at *6th European Conference on Industrial Furnaces and Boilers*, Lisbon, Portugal, 2002.
33. Chung, I.P., Baukal, C., and Ruiz, R., The effect of operational parameters on the burner NO<sub>x</sub> emissions, presented at *2004 International Flame Research Foundation Member's Conference*, Noordwijkerhout, the Netherlands, 2004.
34. Lefebvre, A., *Gas Turbine Combustion*, Hemisphere Publishing Corporation, Washington, DC, p. 400, 1983.
35. Wigg, L.D., *The Effect of Scale on Fine Sprays Produced by Large Airblast Atomizers*, Report 236, National Gas Turbines Establishment, Pyestock, England, 1959.

# 11

## Cold Flow Modeling

Christopher Q. Jian

### CONTENTS

11.1	Introduction .....	327
11.1.1	Basics of Similitude Theory .....	328
11.1.2	Geometric Similarity .....	328
11.1.3	Kinematic Similarity .....	328
11.1.4	Dynamic Similarity .....	328
11.1.5	Principle of Relaxation and Self-Similar Flow Regime .....	329
11.2	Physical Model Flow Measurement and Visualization Techniques .....	330
11.2.1	Flow Measurement .....	330
11.2.2	Velocity Measurement.....	331
11.2.3	Pressure Measurement.....	331
11.2.4	Temperature Measurement .....	331
11.3	Flow Visualization.....	331
11.4	Mixing Measurement Using Thermal Energy Balance Method.....	332
11.5	John Zink COOL <i>flow</i> Physical Modeling Case Study .....	333
11.5.1	Introduction.....	333
11.5.2	Boiler Technical Data—(Basis for the Model).....	334
11.5.3	Modeling Criteria.....	334
11.5.4	Scale Model Description .....	334
11.5.5	Instrumentation .....	334
11.5.6	Modeling Procedure.....	334
11.5.7	Physical Modeling Results.....	334
11.5.7.1	Mass Flow Distribution.....	334
11.5.7.2	Primary Air Velocity Distribution.....	335
11.5.7.3	Burner Exit Peripheral Air Velocity Distribution.....	336
11.5.8	Summary of Case Study .....	336
	References.....	337

### 11.1 Introduction

Physical modeling has been widely used in industry from geological studies to aerospace engineering to study complex fluid dynamics where engineering calculations or computational fluid dynamics (CFD) are deemed either unreliable (the former) or uneconomical (the latter).<sup>1</sup> In the field of combustion, physical modeling is employed in studying flow distribution involving combustion air, over-fire air (OFA), and flue gas recirculation (FGR) as well as isothermal flows in combustion chambers of furnaces, boilers, heat recovery and steam

generators (HRSG), etc. Physical modeling is often used to study flow patterns prior to the commissioning of new furnaces and boilers to gain a better understanding of the flow characteristics and the interactions between various flow streams inside the combustion chamber and then to fine tune operating strategies and parameter settings. For burners with a common windbox or furnaces with a large number of burners (e.g., 520 burners) connected with extensive ductwork, physical modeling is routinely used to identify flow maldistributions and to engineer flow solutions through the use of internals such as turning vanes, baffles, splitters, kickers, etc., to ensure desired flow distribution and flow patterns.



Examples of applications of physical modeling in combustion systems include

1. Air distribution in a single burner windbox
2. Air distribution in multiple burners sharing a common windbox
3. Distribution of OFA
4. Distribution and mixing of FGR
5. Determine and optimize primary, secondary, and tertiary air distribution
6. Air mass flow distribution among multiple burners with individual ductwork
7. Gas turbine exhaust flow distribution and duct burner auxiliary firing patterns
8. Combustion aerodynamics and partial load performance in furnaces and boilers
9. Combustion air and FGR pressure loss minimization
10. Air flow management in natural draft combustion systems

Construction of a scale model must be accompanied with an analysis to determine test conditions that ensure the test results from the scale model are representative of the processes in the prototype. In combustion applications, although most of the processes are inherently at elevated temperatures, physical modeling is usually carried out under isothermal conditions. The isothermal physical modeling technique is based on the principle of relaxation. Under this principle, the variables that are important for the phenomena under study are stressed. The variables that are stressed are replicated in the physical model as closely as possible to obtain a representative result. No scale physical model can be an exact model of the reality unless an exact full-scale prototype is made. However, by using accurate correlations, the modeling work can provide a good qualitative understanding of the fluid dynamics in the prototype. This chapter attempts to answer the question: How does one ensure that the scale model test results are representative of the actual processes in the prototype?

### 11.1.1 Basics of Similitude Theory

The theoretical basis of physical modeling is the similitude theory or similarity theory.<sup>2</sup> The basic requirements to achieve similitude are (1) geometric similarity, (2) kinematic similarity, and (3) dynamic similarity.

#### 11.1.2 Geometric Similarity

Geometric similarity requires that the scale physical model is dimensionally similar to the prototype.

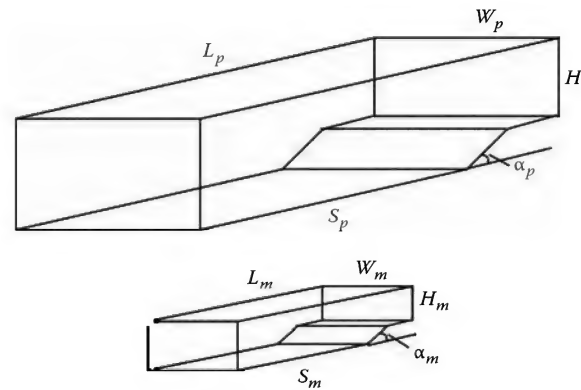


**FIGURE 11.1**  
Illustration of geometric similarity.

Such similarity exists between the scale model and the prototype if the ratio of all corresponding dimensions and all angles in the model and prototype are equal. Figure 11.1 illustrates the geometric similarity between a prototype (p) and a scale model (m).

Mathematically, geometric similarity can be expressed as

$$\frac{L_p}{W_p} = \frac{L_m}{W_m}, \quad \frac{L_p}{H_p} = \frac{L_m}{H_m}, \quad \frac{L_p}{S_p} = \frac{L_m}{S_m}, \quad \text{and} \quad \alpha_p = \alpha_m \quad (11.1)$$

#### 11.1.3 Kinematic Similarity

Kinematic similarity is the similarity of fluid flow behavior in terms of time within the similar geometries. Kinematic similarity requires that the motion of fluids of both the scale model and prototype undergo similar rate of change (velocity, acceleration, etc.). This similarity criterion ensures that streamlines in both the scale model and prototype are geometrically similar and spatial distributions of velocity are also similar.

Mathematically, kinematic similarity can be expressed as

$$\frac{V_p}{V_m} = \frac{L_p/T_p}{L_m/T_m} \quad \text{Velocity ratio} \quad (11.2)$$

$$\frac{a_p}{a_m} = \frac{L_p/T_p^2}{L_m/T_m^2} \quad \text{Acceleration ratio} \quad (11.3)$$

#### 11.1.4 Dynamic Similarity

Dynamic similarity ensures that the ratios of all forces, on the fluid flow and boundaries, in the prototype and scale model are the same and can be expressed as constants. Ratios of forces in fluid flows are often expressed in terms of dimensionless numbers. These dimensionless

numbers are derived using what is called dimensional analysis using the Buckingham\* theorem.

The Buckingham theorem is a key theorem in dimensional analysis. The theorem states that if there exists a physically meaningful equation involving a certain number of physical variables (e.g.,  $n$ ), and these variables are expressible in terms of  $k$  independent fundamental physical variables (such as length, mass, time, etc.), then the original equation is equivalent to an equation involving a set of  $p = n - k$  dimensionless variables constructed from the original variables.

In mathematical terms, if there is a physically meaningful equation such as

$$f(q_1, q_2, \dots, q_n) = 0 \quad (11.4)$$

where the  $q_i$  are the  $n$  physical variables, and they are expressed in terms of  $k$  independent physical units, then the preceding equation can be restated as

$$g(\pi_1, \pi_2, \dots, \pi_p) = 0 \quad (11.5)$$

where the  $\pi_i$  are dimensionless parameters constructed from the  $q_i$  by  $p = n - k$  equations of the form

$$\pi_i = q_1^{m_1} q_2^{m_2} \dots q_n^{m_n} \quad (11.6)$$

where the exponents  $m_i$  are rational numbers (they can always be taken to be integers: just raise it to a power to clear the denominators). The use of the  $\pi_i$  as the dimensionless parameters was introduced by Edgar Buckingham in his original 1914 paper on the subject from which the theorem draws its name.

The theorem provides a method for computing sets of dimensionless parameters from the given variables, even if the form of the equation is still unknown. However, the choice of dimensionless parameters, using this nondimensionalization scheme, is not unique: Buckingham's theorem only provides a way of generating sets of dimensionless parameters, and will not choose the most physically meaningful dimensionless parameters.

### 11.1.5 Principle of Relaxation and Self-Similar Flow Regime

In industrial combustion systems, fluid flows typically involve combustion air, fuel, FGR, and products

of combustion (POC) in the combustion chamber and various heat exchangers. These flows are usually subsonic with a Mach number of less than 0.3 and can be considered incompressible flows.<sup>3</sup> The dimensionless parameter that characterizes such flows is known as the Reynolds number (Re). The physical interpretation of the Re is that it is the ratio of two forces in the fluid flow, namely, the inertia force and the viscous force (or friction force).

In mathematical terms, Re is defined as

$$\text{Re} = \frac{\text{inertia force}}{\text{viscous force}} = \frac{F_i}{F_v} \quad (11.7)$$

where the inertia force and viscous force can be derived from dimensional analysis and the Buckingham  $\pi$  theorem:

$$\text{Inertial force: } F_i = \frac{mV^2}{D} = \rho D^2 V^2 \quad (11.8)$$

$$\text{Viscous force: } F_v = \tau D^2 = \frac{\mu V D^2}{D} = \mu V D \quad (11.9)$$

Substituting (11.8) and (11.9) into (11.7), Re becomes

$$\text{Re} = \frac{F_i}{F_v} = \frac{\rho V D}{\mu} = \frac{V D}{\nu} \quad (11.10)$$

where

$m$  is the mass

$D$  is the length dimension (or hydraulic diameter)

$V$  is the flow velocity

$\rho$  is the fluid density

$\mu$  is the dynamic viscosity

$\nu$  is the kinematic viscosity

$\tau$  is the shear stress

The dynamic similarity requires that in two geometrically and kinematically similar systems, the Re must be the same. With the constraints on length scale (satisfying geometric similarity) and velocity ratio (satisfying kinematic similarity), an identical Re can be obtained only by a dramatic change in the properties of the fluid. Since the scale model study typically uses air as the working medium and the properties of air do not change from the scale model to the prototype, the prototype Re cannot be achieved in the scale model. The solution to this complete similarity requirement is to apply a modeling technique based on the principle of relaxation. Under this principle, the variables that are important for the phenomena under study are stressed. The variables that are stressed are duplicated as necessary to obtain

\* Edgar Buckingham (1867–1940) was educated at Harvard and Leipzig, and worked at the (US) National Bureau of Standards (now the National Institute of Standards and Technology, or NIST) 1905–1937. His fields of expertise included soil physics, gas properties, acoustics, fluid mechanics, and blackbody radiation.

a representative result. To ensure that the scale model results are representative of the prototype, the concept of self-similar or self-preserving flow regime is applied.<sup>4</sup>

The objectives of performing scale model studies can be summarized as follows:

1. Assure desired flow patterns such as flow uniformity and minimization of flow recirculation.
2. Improve mixing performance of two or more flow streams.
3. Achieve equal flow mass distribution among multiple outlets.
4. Reduce total system pressure drop to reduce energy consumption or increase capacity.

Flows that develop a state that depends only on the local flow quantities, such as the local value of the mean velocity and the flow resistance, are said to be self-similar or self-preserving. This state of flow is present in the turbulent flow regime when sufficiently high  $Re$  are achieved. A majority of industrial combustion systems operate in this flow regime. When the scale model and prototype are both operating in the self-similar flow regime, they will manifest the same flow patterns and pressure drop coefficient despite different absolute local flow quantities.

The flow pressure drop coefficient ( $C_p$ ) is defined as the ratio between the static pressure and the dynamic pressure:

$$C_p = \frac{\text{Static pressure}}{\text{Dynamic pressure}} = \frac{p_1 - p_2}{\frac{1}{2} \rho V^2} \quad (11.11)$$

$$\begin{aligned} \text{Static pressure} &= p_1 - p_2 \\ \text{Dynamic pressure} &= \frac{1}{2} \rho V^2 \end{aligned}$$

The pressure drop coefficient can also be expressed as

$$C_p = \frac{p_1 - p_2}{\frac{1}{2} \rho V^2} = 2Eu \quad (11.12)$$

where

$$Eu = \frac{p_1 - p_2}{\rho V^2} = f(Re) \quad (11.13)$$

is the Euler number which is the ratio between pressure drop (flow friction) and twice the dynamic pressure. The Euler number is a function of the  $Re$ .

When the flow is in the self-similar regime, the Euler number becomes more or less a constant, independent

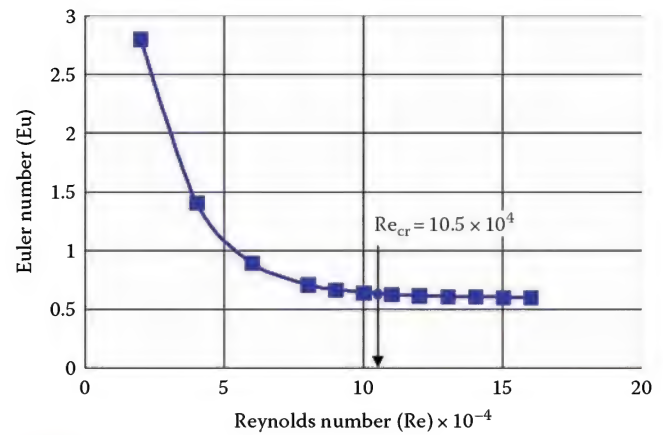


FIGURE 11.2  
Typical relationship of  $Eu = f(Re)$ .

of the Reynolds number. Figure 11.2 shows the relationship between the Reynolds and Euler number for a particular flow category.

In this particular system, if the  $Re$  is greater than the critical Reynolds number  $Re_{cr} = 10.5 \times 10^4$ , the Euler number becomes a constant of approximately 0.65. Since the flow pressure drop coefficient is twice the Euler number (11.12), a constant Euler number indicates that the pressure drop coefficient remains a constant at and beyond the critical  $Re$ . However, the critical  $Re$  that ensures self-similar flow state is system specific. As a general guide, for combustion air ductwork and FGR ducts,  $Re_{cr}$  should be maintained at  $>5 \times 10^4$ . For burners and combustion chambers, the recommended  $Re_{cr}$  is  $>2 \times 10^5$ .

In summary, in two geometrically and kinematically similar systems, when the flows are in the self-similar state, the flow characteristics such as flow patterns and streamlines are similar and the pressure drop coefficients in both the scale model and prototype are the same.

## 11.2 Physical Model Flow Measurement and Visualization Techniques

### 11.2.1 Flow Measurement

One of the advantages of physical modeling is that the direct measurements and observation of the fluid flow behavior inside the scale model represents a prototype's field operation. Typical flow measurements include velocity, pressure, and temperature. In some cases, species monitoring is also used to assess mixing performance of the scale model.



### 11.2.2 Velocity Measurement

A variety of instruments are available for measuring velocity. For isothermal physical modeling, velocity is usually measured using

- Pitot tube and a wide range of its variants
- Precision vane anemometer
- Hot wire anemometer
- Laser-Doppler velocimetry

Laser-Doppler velocimetry (LDV) is also applicable for velocity measurements at elevated temperature such as the region inside a flame zone. LDV requires that the flow field be seeded with tiny particles. For high temperature measurements, high melting point solid particles such as high alumina oxide particles on the order of  $1 \sim 2$  microns are used.

Figure 11.3 shows the velocity measurements using a Pitot tube and a digital manometer during a scale physical model study campaign. Detailed description of the various measurement apparatuses is out of the scope of this chapter.

### 11.2.3 Pressure Measurement

Many scale model measurements include quantitative measurement of pressure drops throughout the system. Maximum allowable system pressure drop is frequently a major constraint from the equipment manufacturer or end user when flow correction solutions are sought. System pressure drop directly relates to the operating cost due to blower/fan power consumption and the hydraulic head available for downstream power or steam generation. For scale model testing, pressure

measurements are usually performed using the following instruments:

- Pressure gauge
- Manometer
- Pressure transducer

### 11.2.4 Temperature Measurement

Temperature measurements are required when testing scale model mixing performance using the thermal mixing technique (see Section 11.4 for more information). Temperature measurements typically involve the following instruments:

- Thermometer
- Thermocouple
- Thermistor
- Infrared thermometer
- Infrared or charge coupled device (CCD) camera

The application of a CCD camera for temperature measurement is a recent development. A CCD camera is an apparatus which is designed to convert optical brightness into electrical amplitude signals using a variety of CCDs, and then reproduce the image of a subject using the electric signals without time restriction. Coupled with robust image analysis software, the advantage of a CCD camera based temperature measurement system is that it can take unlimited point measurements in the line of sight. Where most temperature measuring devices can only capture point data, the CCD camera system is capable of mapping an entire surface at the same instance.



**FIGURE 11.3**  
Velocity measurement using a Pitot tube and manometer.

## 11.3 Flow Visualization

Physical models in combustion related applications are typically built with transparent synthetic thermoplastic resin materials such as Plexiglas or Lexan. They offer the advantage of flow visualization for direct observation of complex flow patterns that are difficult, if not impossible, to visualize in the prototype. Efforts in prototype flow visualization have been made with limited success to gain a better understanding of flow patterns in critical areas. These flow visualization techniques typically involve setting up arrays of Tufts yarns as flow indicators and the use of sparks generated with burning saw dust. In many areas such as pipes and ducts, heat

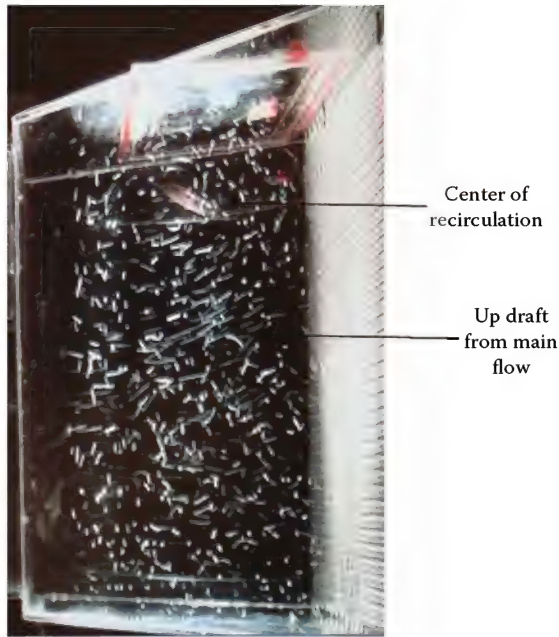


**FIGURE 11.4**  
Airflow/helium bubble analog flow visualization.

exchangers, fan inlets and outlets, etc., there are simply no observation stations that can provide the view of the entire flow field or it is not permissible to perform flow visualization.

The technique most commonly used for visualizing flow patterns in physical models is to inject smoke into the model. While the smoke serves as a good tracer to establish the flow field, after a short period, the entire flow passage is filled with smoke, making it difficult to track the streamlines in the flow domain. Furthermore, the smoke also tends to build up in the viewing area that further hampers continued visual observation.

At John Zink Company's COOLflow™ Physical Modeling Facility, a different flow visualization technique has been successfully applied to scale model studies. In this technique, small quantities of minute helium bubbles are suspended in the airflow and used as tracer spheres. The helium bubbles are neutrally buoyant with a nominal density close to that of the air at ambient temperatures. Figure 11.4 shows the helium bubble flow visualization technique applied to a scale model.

In order to visualize the movement of a large number of helium bubbles, collimated light sources are used to illuminate the bubbles at various planes. These collimated light sources are positioned perpendicular to the plane being viewed and the helium bubbles provide maximum light deflection at about 90° to the incident rays. Thus, the gross flow characteristics can be determined qualitatively and possible flow corrective measures evaluated.

## 11.4 Mixing Measurement Using Thermal Energy Balance Method

Study of the mixing performance of multiple streams is often an integral part of the combustion process to improve combustion efficiency, reduce emission, redistribute energy absorption, etc. Common gaseous streams include primary, secondary, and tertiary air, OFA, and FGR. The thermal energy balance method is the simplest way to determine the effectiveness of mixing. Under the steady state condition, the temperature of the mixture is a function of the temperature and mass fraction of each individual stream.

Consider a two-stream mixing point *A* as an example, one has

$$C_1 = \frac{\Delta m_{A1}}{\Delta m_A}, \quad C_2 = \frac{\Delta m_{A2}}{\Delta m_A}, \quad \text{and} \quad \Delta m_A = \Delta m_{A1} + \Delta m_{A2}$$

where (see Figure 11.5)

$\Delta m_{A1}$ ,  $\Delta m_{A2}$  represent the mass of stream  $m_1$  and  $m_2$  at point *A* and  $\Delta m_A$  is the total mass at point *A*.

Under the steady state condition, the energy balance at point *A* can be expressed as

$$c_{p1}T_1C_1 + c_{p2}T_2C_2 = c_pT_A \quad (11.14)$$

Equation 11.14 has two unknowns, namely,  $C_1$  and  $C_2$ ; hence, one additional equation is needed to solve for the two unknowns. This can easily be achieved by varying the temperature of one or more individual streams. In the current example,  $T_2$  is changed to  $T'_2$ . Under this condition, the energy balance equation (11.14) becomes

$$c'_{p1}T'_1C_1 + c'_{p2}T'_2C_2 = c'_pT'_A \quad (11.15)$$

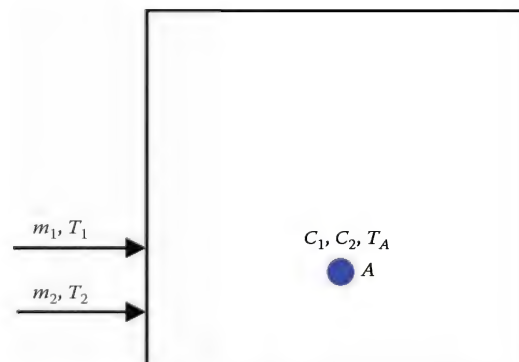


**FIGURE 11.5**  
Illustration of mixing.



Solving Equations (11.14) and (11.15), the mass fraction of the two streams can be determined as follows:

$$C_1 = \frac{c_p T_A c'_{p2} T'_2 - c_{p2} T_2 c'_p T'_A}{c_{p1} T_1 c'_{p2} T'_2 - c_{p2} T_2 c'_p T'_1} \quad (11.16)$$

$$C_2 = \frac{c_{p1} T_1 c'_p T'_A - c_p T_A c'_{p1} T'_1}{c_{p1} T_1 c'_{p2} T'_2 - c_{p2} T_2 c'_p T'_1}$$

The temperatures of the individual streams and at point A are measured by thermocouples. For combustion applications, air is the predominant medium used in scale model testing. The specific heats for air at various temperatures are readily available in most databases or handbooks (see Volume 2 of this handbook).

The thermal energy balance method is simple and fairly accurate in scale model testing. With an array of thermocouples, the thermal energy balance method can be further expanded to study the mixing intensity ( $dC/dx$ ,  $dC/dy$ ,  $dC/dz$ ) in the combustion process. Based on the same working principle, mixing can also be studied using streams of different gaseous species. The downside of this method is that when more than two streams are present, species sampling becomes more difficult and time consuming.

## 11.5 John Zink COOL *flow* Physical Modeling Case Study

### 11.5.1 Introduction

The prototype was a field erected boiler with two natural gas firing burners. The burners shared a common windbox. The purpose of the study was to ensure that each burner receives the same amount of combustion air with even peripheral velocity distributions through the engineering of a baffle system based on John Zink's COOL *flow* physical modeling study.

Figures 11.6 and 11.7 show the burner being installed in the prototype and the scale physical model of the air supply duct and burner/windbox system, respectively. The objective of this scale model study was to develop a set of windbox baffles designed to provide an even combustion air mass flow distribution between the two burners, uniform peripheral flow entering each burner, and the elimination of tangential velocities within each burner. The major constraint in achieving these objectives was the air distribution arrangement and the internal dimensions of the windbox. Considering that air in the combustion process accounts for approximately 94% of the mass flow, numerous observations on boiler combustion



FIGURE 11.6 Cutaway view of the burner to be installed on the prototype.

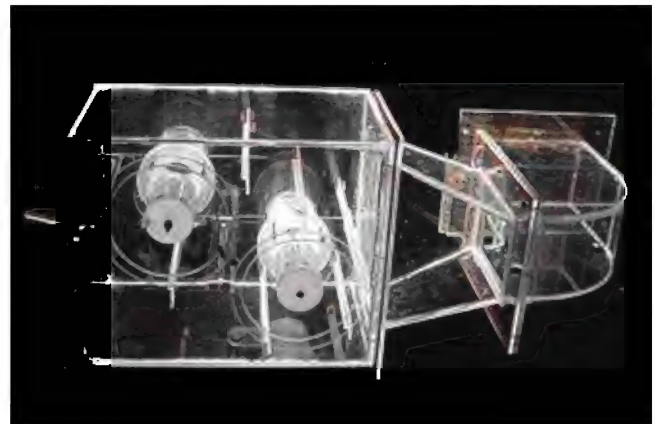


FIGURE 11.7 Scale physical model of the combustion air system.

systems have shown that the correct air distribution and peripheral entry condition is a key factor in the achievement of high performance (low  $\text{NO}_x$ , low excess  $\text{O}_2$ , and low  $\text{CO}$ ). The purpose of each objective relates to a specific burner performance parameter is described next.

Mass flow deviations are minimized to enable lower postcombustion  $\text{O}_2$ ,  $\text{CO}$ , and  $\text{NO}_x$ . The lowest postcombustion  $\text{O}_2$  concentration possible is constrained by the burner most starved for air. This starved burner will generate a high  $\text{CO}$  concentration and consequently the total  $\text{O}_2$  must be raised to minimize the formation of  $\text{CO}$  in that burner. By equalizing the air flow to each burner and assuring that the fuel flow is equal, the  $\text{O}_2$  can be lowered until the  $\text{CO}$  starts to increase equally for all burners. Lower  $\text{O}_2$  has additional benefits of lower  $\text{NO}_x$  formation (see Chapter 15) and higher thermal efficiency (see Chapter 12).

The equalization of the peripheral air velocity at the burner inlet will result in equal mass flow of air around and through the periphery of the swirler. The result of this



equal air mass flow distribution through the swirler will be a fully developed and balanced air vortex at the center of the outlet of the swirler.<sup>5</sup> Flame stability and turndown of the burner depend on the condition of this vortex. Unequal air distribution results in an asymmetrical vortex leading to a flame that is more sensitive to pressure variations, limited in turndown ratio, sensitive to FGR on flame instability at lower loads, difficult in light-off by the igniter, and sensitive to flame scanning operation.

The creation of swirling air is a fundamental requirement for many burners. Louvered burners are designed to create a controlled swirl by rotating the entire air mass. Unfortunately, if the air has tangential velocities entering the burner, these velocities may act counter to the design of the burner, either working against the designed swirl of the burner (opposite swirl direction), or providing excessive swirl (same swirl direction). Uncontrolled swirl may create a problem at high turndown rates. At low loads (e.g., 10%), excess O<sub>2</sub> is typically 11%–13%. By having the entire mass swirling improperly, the fuel may be diluted to the point where flame stability becomes marginal.

### 11.5.2 Boiler Technical Data—(Basis for the Model)

Boiler Type	Field Erected
No. of burners:	2
Maximum combustion air flow: (based on natural gas with 10% excess air)	134,366 kg/h
Nominal combustion air temperature:	40°C (104°F)
Model scale:	1/8
Model air temperature:	32°C (90°F)
Model airflow:	1,937 kg/h

### 11.5.3 Modeling Criteria

The following criteria were applied to ensure optimum performance of the burners:

- Mass flow differences for each burner shall be within  $\pm 2\%$  of mean, in the model.
- Peripheral air distribution velocity differences shall be less than  $\pm 10\%$  of the mean.
- Swirls shall be eliminated if possible or kept to a practical minimum.

### 11.5.4 Scale Model Description

As shown in Figure 11.7, the model was built using acrylic sheets at a 1/8th scale. This included the combustion air ducting from the force draft fan outlet through the windbox and the burners. Cold flow modeling was performed using air at ambient temperature as the working fluid for the combustion air. Quantitative

air flow measurements were taken using a Pitot tube. Observation of the flow field was performed using the analog helium bubble flow visualization technique.

### 11.5.5 Instrumentation

Extensive quantitative data were obtained by air flow modeling. A miniature calibrated Pitot tube, combined with an electronic manometer was used to measure the velocity profile in the duct of the model. However, to measure the peripheral distribution of velocities around the inlet of burners, a custom-made miniature Pitot tube was used. Since this Pitot tube was not calibrated, absolute values were not recorded. These readings were only used to compare velocities from one point to another and no units are given for the results. Since the geometry of the model burner is well known, the total flow through each burner can be determined by integrating the velocity profile over the measurement area. A straight bladed spinner was used to determine the swirl at the exit of burner.

### 11.5.6 Modeling Procedure

The model was initially run at maximum continuous rating for a baseline condition. The velocity profiles were set to the design conditions at the model entrance. The mass flow readings, peripheral distribution, and swirl were then recorded. Baffle plates were then installed strategically within the model and the mass flow, peripheral distribution, and swirl were then remeasured.

### 11.5.7 Physical Modeling Results

#### 11.5.7.1 Mass Flow Distribution

Table 11.1 shows the mass flow data recorded during the baseline and after modification testing. Table 11.1 shows a significant disparity of mass flow rates between the two burners. Burner No.1 was severely starved for air with a 57.6% mass deficit. This can potentially lead to a number of operating issues including, for example, combustion stability, high concentration of unburned hydrocarbon

**TABLE 11.1**

Mass Flow Measurements

**Mass Flow Measurements**

<i>Baseline</i>	
Burner #	% of average
1	42.4%
2	157.6%
<i>After installing baffle solutions</i>	
Burner #	% of average
1	100.3%
2	99.7%

and CO in the exhaust flue gases, and elongated flame that may cause hot spots on heat transfer tubes. On the other hand, burner No. 2 had a high percentage of excess air. The availability of abundant oxygen in a high temperature combustion zone with the presence of a large amount of nitrogen can lead to high NO<sub>x</sub> emissions.

The mass flow rates with the implementation of a baffle system are also shown in Table 11.1. The variations of mass flow between the two burners were corrected to within  $\pm 0.3$ .

#### 11.5.7.2 Primary Air Velocity Distribution

Pitot tube measurements of the axial velocities exiting the burner are shown in Figures 11.8 through 11.11.

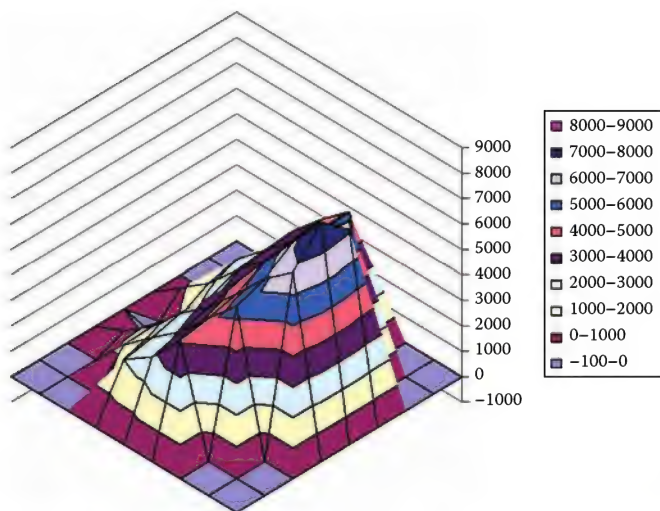


FIGURE 11.8  
Burner no. 1 exit air velocity—Baseline.

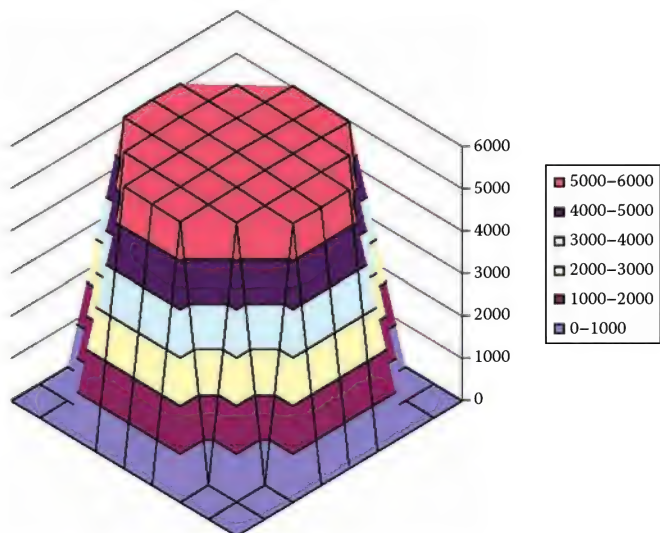


FIGURE 11.9  
Burner no. 1 exit air velocity—After modifications.

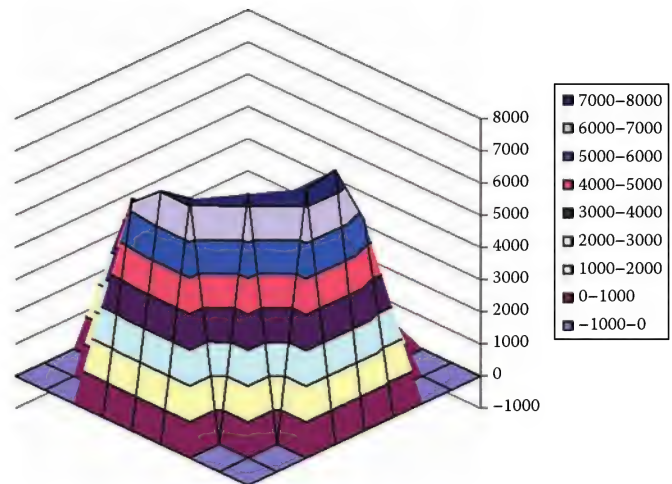


FIGURE 11.10  
Burner no. 2 exit air velocity—Baseline.

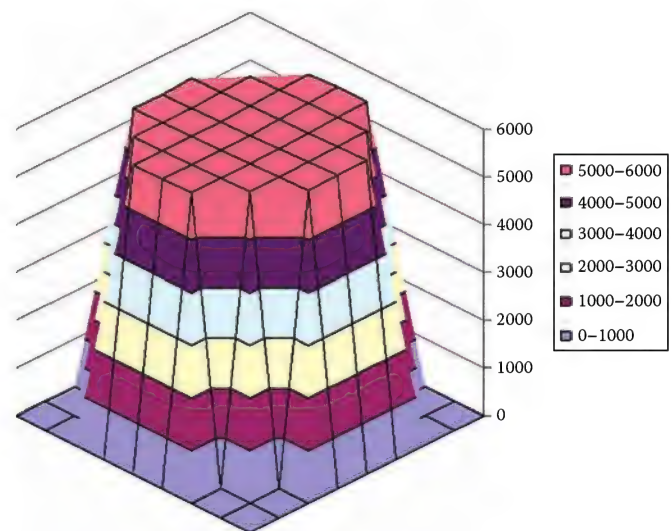


FIGURE 11.11  
Burner no. 2 exit air velocity—After modifications.

The numbers corresponding to the measurements are directly from an uncalibrated Pitot tube and do not represent the true local velocity magnitude. However, they do represent the relative velocity profiles across the burner exits.

Figures 11.8 and 11.10 show that the axial velocities exiting both burners were severely skewed toward one side of the burner exit. Such air flow distribution will cause parts of the burner to starve for air while other parts to operate with high excess air. The results will be similar to the mass flow maldistribution discussed earlier, but on a more localized scale for each individual burner. Such uneven peripheral air distribution should be corrected to allow the burners to function properly.



Figures 11.9 and 11.11 show the burner exit axial velocities with the baffle solution implemented. More uniform velocity profiles similar to that of a plug flow can be seen.

### 11.5.7.3 Burner Exit Peripheral Air Velocity Distribution

Measurements of relative axial velocity distributions along the peripheries of the burners and swirl numbers are shown in Figures 11.12 and 11.13. Peripheral velocity distributions (the red lines) at burner exits vary from +21.1% from the mean velocity to -19.8%. With the baffle solution implemented, the range of axial peripheral velocity deviation from the mean velocity is reduced to a range of +2.7% to -3.9%. The baffle solution also eliminated the swirl in both burners.

### 11.5.8 Summary of Case Study

This case study demonstrated the importance of air supply system designs in achieving optimal operations of the burners, and hence the boiler. Physical modeling is a powerful and effective technique for understanding the fluid flow and for developing solutions to the flow-related issues. Based on the Buckingham theorem and the self-similar nature of turbulent flows, the solutions developed in the scale model can be directly translated to prototype design and operation. Even in today's business world where computer simulations are widely used (see Chapter 13), physical modeling continues to demonstrate its value and power in improving the energy efficiency, environment performance, and product quality of a variety of industrial processes.

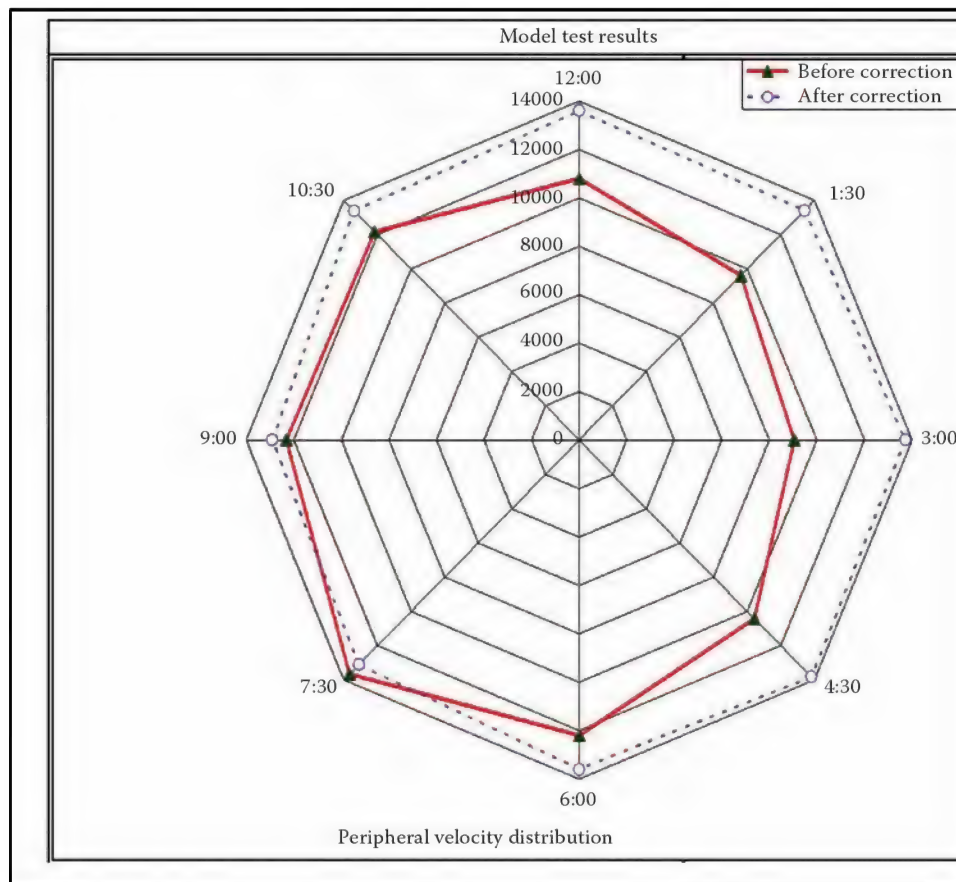


FIGURE 11.12 Burner no. 1 peripheral velocity distribution.



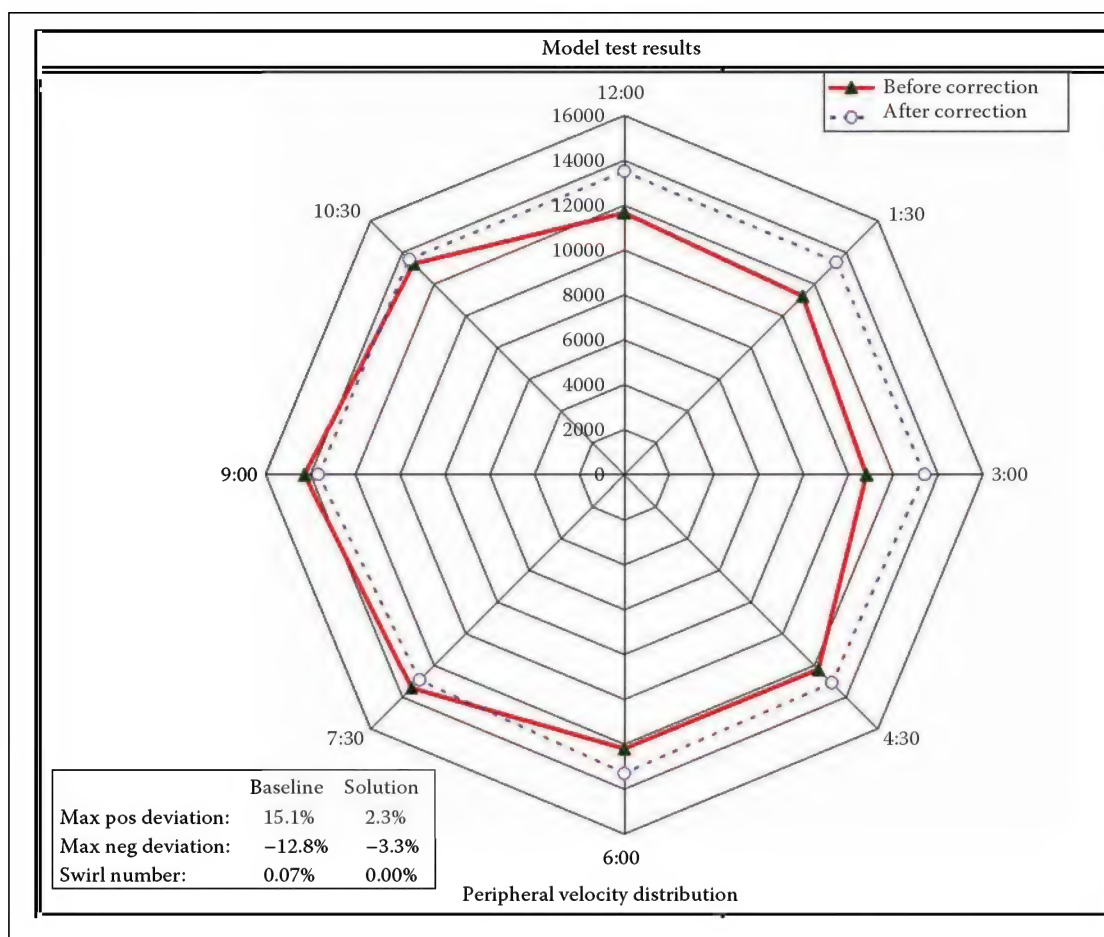


FIGURE 11.13

Burner no. 2 peripheral velocity distribution.

## References

1. Jian, C. Q., Physical Modeling in Combustion Systems, Chapter 10 in *Industrial Combustion Testing*, C. E. Baukal, (Ed.), Boca Raton, FL: CRC Press, 2011.
2. Schlichting, H., *Boundary Layer Theory*, New York: McGraw-Hill, 1979.
3. Panton, R. L., *Incompressible Flow*, New York: John Wiley & Sons, 1984.
4. Hinze, J. O., *Turbulence*, New York: McGraw-Hill, 1959.
5. Batchelor, G. K., *An Introduction to Fluid Dynamics*, Cambridge, U.K.: Cambridge University Press, 1983.

This page intentionally left blank

# 12

## Thermal Efficiency\*

Charles E. Baukal, Jr. and Wes Bussman

### CONTENTS

12.1	Introduction .....	339
12.2	Problems with Leaks .....	342
12.2.1	Reduced Thermal Efficiency .....	342
12.2.2	Increased NOx Emissions.....	343
12.2.3	Poor Burner Performance .....	343
12.2.4	After-Burning .....	345
12.2.5	Increased Metal Oxidation and Stress.....	345
12.2.6	Other Problems .....	345
12.3	Leak Sources/Causes.....	345
12.3.1	Leaky Combustors.....	345
12.3.2	Improperly Sealed Openings .....	345
12.3.3	Burners Out of Service .....	346
12.3.4	Improper Operation .....	347
12.4	Leak Size and Location .....	347
12.5	Finding Leaks .....	348
12.5.1	Dark Regions .....	348
12.5.2	Smoke Testing.....	349
12.5.3	IR Camera .....	349
12.5.4	Peeling Paint .....	349
12.6	Mitigating Leaks .....	349
12.6.1	Control Furnace Pressure .....	349
12.6.2	Fix Leaks .....	350
12.6.3	Operate as Many Burners as Possible .....	350
12.7	Conclusion .....	351
12.8	Recommendation .....	351
	References.....	351

### 12.1 Introduction

Combustion has been the foundation of worldwide industrial development for the past 200 years.<sup>1</sup> Industry relies heavily on the combustion process as shown in Table 12.1. The major uses for combustion in industry are shown in Table 12.2. Hewitt et al.<sup>2</sup> have listed some of the common heating applications used in industry, as shown in Table 12.3. As can be seen in Figure 12.1, the worldwide demand for energy continues to increase. Most of the energy

(84%) is produced by the combustion of fossil fuels like petroleum, natural gas, and coal (see Figure 12.2). According to the U.S. Department of Energy, the demand in the industrial sector is projected to increase by 0.8% per year to the year 2020.<sup>3</sup> Figure 12.3 shows that the industrial sector is one of the largest U.S. energy consumers. Figure 12.4 shows the projected energy source and end use for the United States in 2010. This again highlights the importance of industrial combustion.

There are many factors that impact the thermal efficiency of an industrial combustion process. Some of

\* The material in this chapter is adapted from Baukal, C.E. and Bussman, W.R., Air infiltration effects on industrial combustion efficiency, in *Fuel Efficiency*, (ed.) J.K. Bernard, Nova Science Publishers, Hauppauge, New York, pp. 101–134, 2011.



TABLE 12.1

## Importance of Combustion to Industry

Industry	% Total Energy From (At the Point of Use)		
	Steam	Heat	Combustion
Petroleum refining	29.6	62.6	92.2
Forest products	84.4	6.0	90.4
Steel	22.6	67.0	89.6
Chemicals	49.9	32.7	82.6
Glass	4.8	75.2	80.0
Metal casting	2.4	67.2	69.6
Aluminum	1.3	17.6	18.9

Source: U.S. Department of Energy (DOE), *Industrial Combustion Vision: A Vision by and for the Industrial Combustion Community*, U.S. DOE, Washington, DC, 1998.

TABLE 12.2

## Major Process Heating Operations

<i>Metal melting</i>	<i>Drying</i>
Steel making	Surface film drying
Iron and steel melting	Rubber, plastic, wood, glass products drying
Non-ferrous melting	Coal drying
<i>Metal heating</i>	Food processing
Steel soaking, reheat, ladle preheating	Animal food processing
Forging	<i>Calcining</i>
Non-ferrous heating	Cement, lime, soda ash
<i>Metal heat treating</i>	Alumina, gypsum
Annealing	<i>Clay firing</i>
Stress relief	Structural products
Tempering	Refractories
Solution heat treating	Agglomeration
Aging	Iron, lead, zinc
Precipitation hardening	<i>Smelting</i>
<i>Curing and forming</i>	Iron, copper, lead
Glass annealing, tempering, forming	<i>Non-metallic materials melting</i>
Plastics fabrication	Glass
Gypsum production	<i>Other heating</i>
<i>Fluid heating</i>	Ore roasting
Oil and natural gas production	Textile manufacturing
Chemical/petroleum feedstock preheating	Food production
Distillation, visbreaking, hydrotreating, hydrocracking, delayed coking	<i>Aluminum anode baking</i>
<i>Bonding</i>	
Sintering, brazing	

Source: U.S. Department of Energy (DOE), *Industrial Combustion Vision: A Vision by and for the Industrial Combustion Community*, U.S. DOE, Washington, DC, 1998.

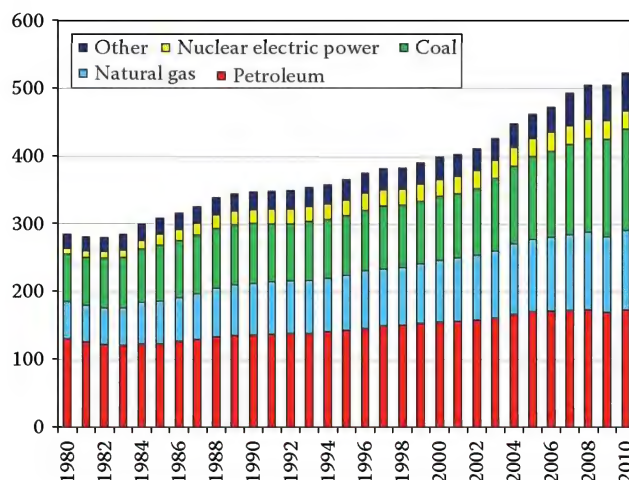


FIGURE 12.1

Historical (1980-2010) world energy consumption. (From Energy Information Administration.)

TABLE 12.3

## Examples of Processes in the Process Industries Requiring Industrial Combustion

Process Industry	Examples of Processes Using Heat
Steel making	Smelting of ores, melting, annealing
Chemicals	Chemical reactions, pyrolysis, drying
Non-metallic minerals (bricks, glass, cement and other refractories)	Firing, kilning, drying, calcining, melting, forming
Metal manufacture (iron and steel, and non-ferrous metals)	Blast furnaces and cupolas, soaking and heat treatment, melting, sintering, annealing
Paper and printing	Drying

Source: Adapted from U.S. Department of Energy, *Energy Information Administration, Annual Energy Outlook 2008*, Report DOE/EIA-0384 (2008), Washington, DC, 2009.

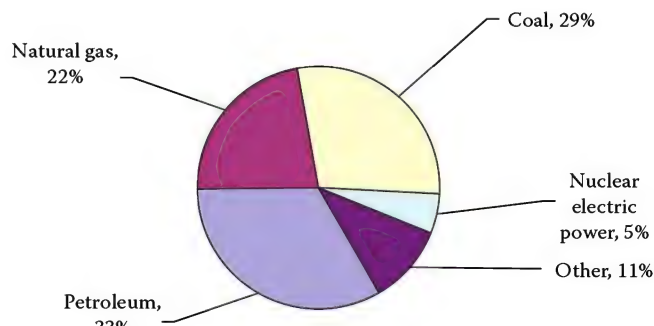


FIGURE 12.2

2010 World energy consumption. (From Energy Information Administration.)

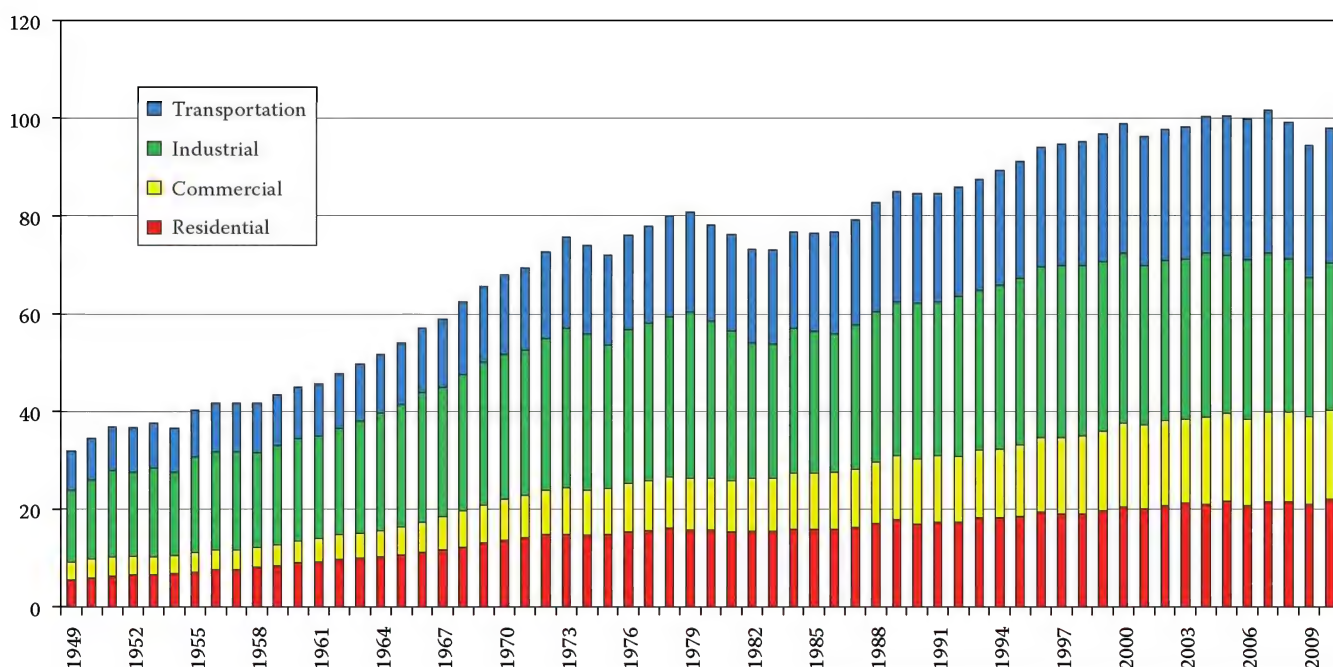


FIGURE 12.3

U.S. energy consumption by industry sector. (From Energy Information Administration.)

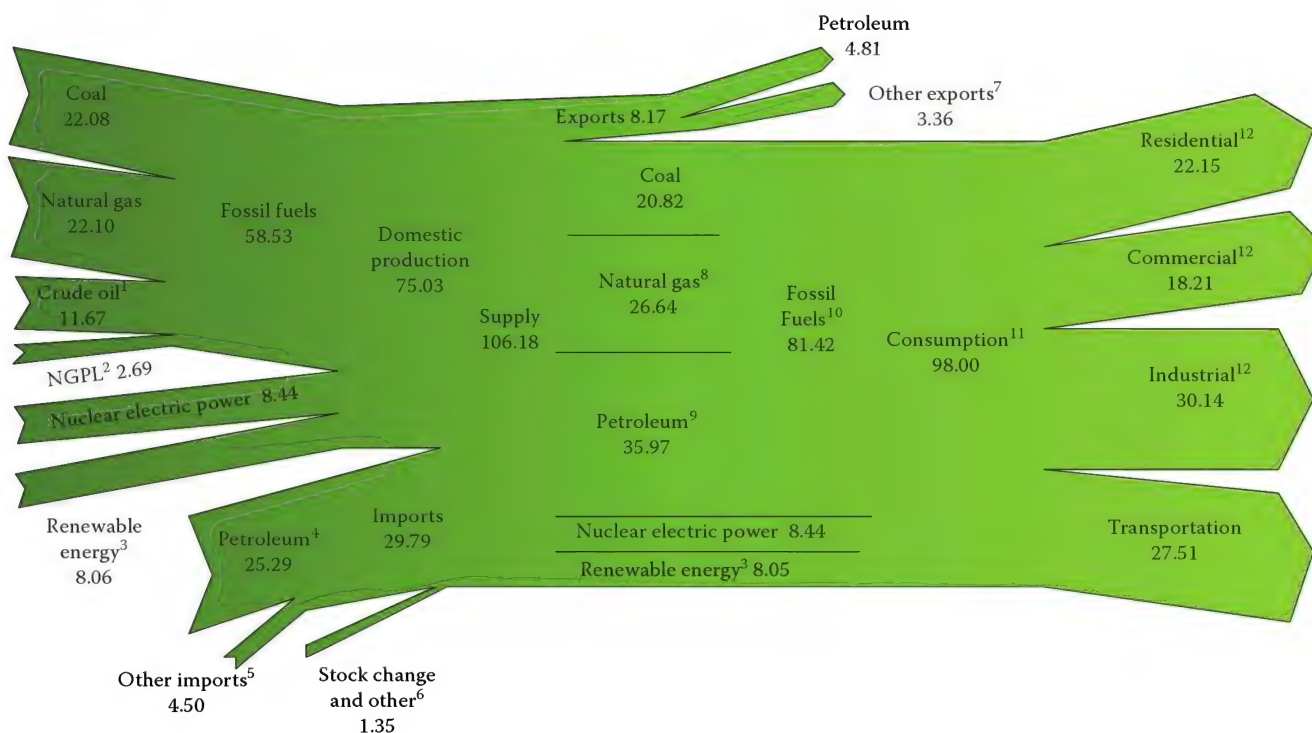


FIGURE 12.4

2010 Energy flow by source and end use in the United States. (From Energy Information Administration.)

these include too little or too much excess combustion air (see Chapter 4), inadequate insulation (see Volume 2), high exhaust gas temperatures (see Chapter 4), and excessive air infiltration (this chapter).<sup>4</sup> Even a relatively small reduction in fuel efficiency from air

infiltration correlates to a tremendous amount of energy because of the high consumption rates. Conversely, even a slight improvement in fuel efficiency by reducing air infiltration can save a large amount of energy,<sup>5,6</sup> which indirectly reduces pollution emissions as less

fuel is combusted. Annex G in American Petroleum Institute Standard 560 provides some guidelines for measuring the efficiency in fired process heaters.<sup>7</sup>

## 12.2 Problems with Leaks

Many industrial combustors are notoriously leaky for a variety of reasons, which are discussed in the next section. There are many potential problems caused by these leaks. Some of the major problems are discussed in this section.

### 12.2.1 Reduced Thermal Efficiency

Ideally, a combustor should be supplied with just the right amount of air to completely burn all of the fuel, which is referred to as the stoichiometric or theoretical amount of air (see Chapter 4). However, in actual practice, industrial combustors operate with an excess amount of combustion air due to imperfect mixing of the air and fuel and to accommodate swings in variables like fuel composition and ambient conditions. It is common for heaters and furnaces to operate with about 10%–15% excess air, which corresponds to about 2%–3% excess  $O_2$ .

A Sankey diagram schematically shows the energy flow in and out of a system. Figure 12.5 shows a Sankey diagram for a generic furnace. The major energy flow into the furnace is the chemical energy stored in the fuel. There are numerous energy flows out of the furnace. The available heat is defined as the gross heating value of the fuel minus the energy carried out by the flue gas (“Moist” + “Dry” “Flue Gas Losses”).

Increasing the amount of excess air in a combustion process decreases heater efficiency because some of the energy released during combustion is wasted due

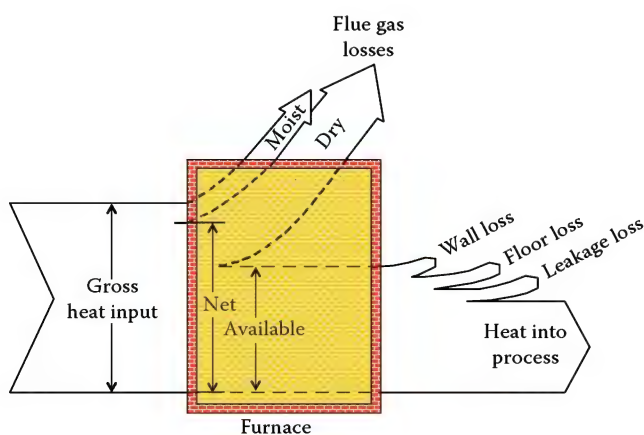


**FIGURE 12.5**  
Sankey diagram for the energy flows into and out of a furnace.

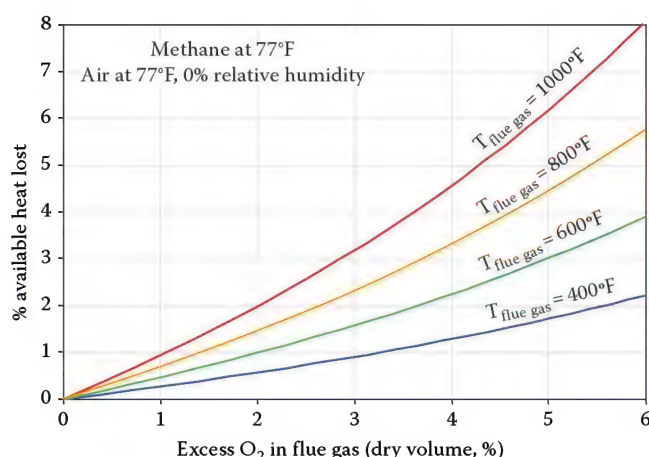


**FIGURE 12.6**  
Available heat lost due to increased excess  $O_2$  as a function of the flue gas exit temperature for methane as the fuel.

to heating the excess air from ambient temperature to the stack gas exit temperature.<sup>8,9</sup> Storm<sup>10</sup> argues that one of the best ways to improve the efficiency of large coal-fired boilers is to minimize the amount of “stealth” air in-leakage. Figure 12.6 shows how much available heat is lost as the amount of excess air (usually determined by measuring the excess  $O_2$  in the flue gas) increases. The graph also shows that more available heat is lost as the flue gas temperature increases. In general, most plants try to keep the flue gas temperature below about 400°F (200°C) if possible to maximize thermal efficiency. They do not want to go below the dew point of the exhaust gases for fear of causing condensation that could corrode the equipment. Figure 12.7 is a similar plot, but for a fixed flue gas temperature 400°F (200°C) and multiple fuels. Again, it can be seen that increasing excess air reduces thermal efficiency. Therefore, excessive air infiltration can significantly reduce thermal efficiency.<sup>11</sup>

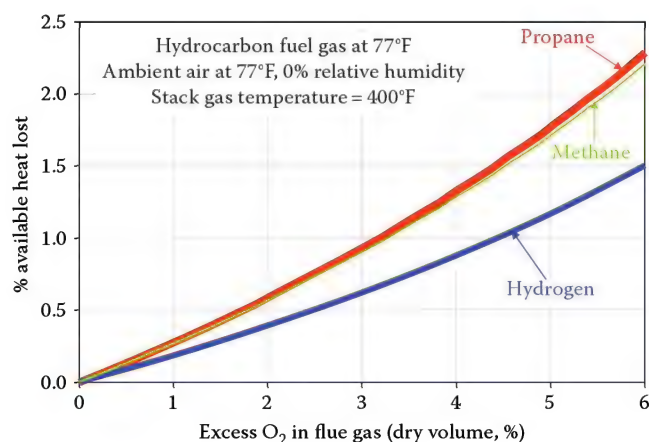


**FIGURE 12.7**  
Available heat lost due to increased excess  $O_2$  as a function of the fuel for a fixed flue gas exit temperature (400°F).



Changes in ambient air conditions can indirectly affect furnace efficiency, since these conditions affect both the combustion air flowing through the burners and the air leaking into the combustor.<sup>12</sup> For example, as the ambient air temperature decreases, more air flows (on a mass basis) for a given pressure drop. Therefore, for a fixed furnace negative pressure and ambient pressure, more air will leak into a combustor when the air is colder. The combination of increased air flow and lower air temperatures associated with colder ambient temperatures means that the thermal efficiency is reduced compared to leaks with warmer ambient temperatures.

### 12.2.2 Increased NO<sub>x</sub> Emissions

High air infiltration into a combustor can adversely affect pollution emissions for two reasons. The first is that the reduced thermal efficiency described earlier requires more fuel to be combusted for a given production rate.<sup>13</sup> Burning more fuel produces more emissions. The second reason is that operating with too much excess O<sub>2</sub> can increase NO<sub>x</sub> emissions (see Chapter 14).<sup>14</sup> Figure 12.8 shows some experimental data that demonstrate how NO<sub>x</sub> increases with excess O<sub>2</sub>. When there is not enough O<sub>2</sub> available to fully combust the fuel, NO<sub>x</sub> formation is not as significant. However, when there is excess O<sub>2</sub> available after the fuel has been combusted, the combination of high flame temperature and excess O<sub>2</sub> causes NO<sub>x</sub> emissions to increase.

Ambient conditions can indirectly impact pollution emissions by increasing excess O<sub>2</sub> if proper adjustments to the combustor are not made.<sup>15</sup> For example, Figure 12.9 shows how the ambient air temperature and humidity can dramatically impact CO emissions. If a heater is tuned to operate at 2% excess O<sub>2</sub> with an ambient air

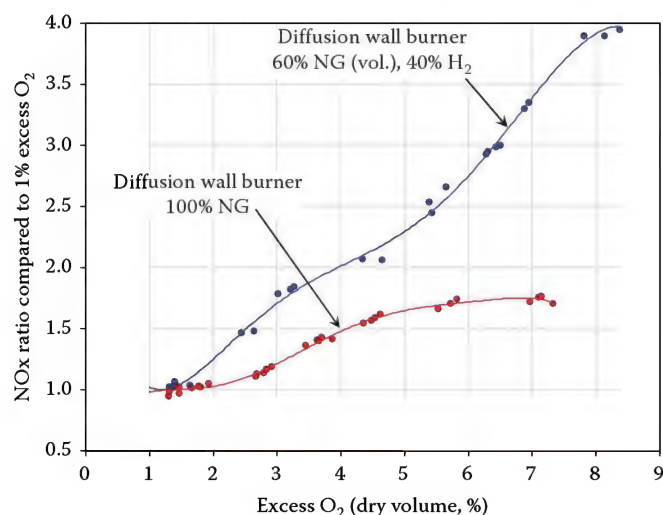


**FIGURE 12.8**  
Ratio of NO<sub>x</sub> formed at a given excess O<sub>2</sub> level compared to the amount of NO<sub>x</sub> formed at 1% excess O<sub>2</sub>.

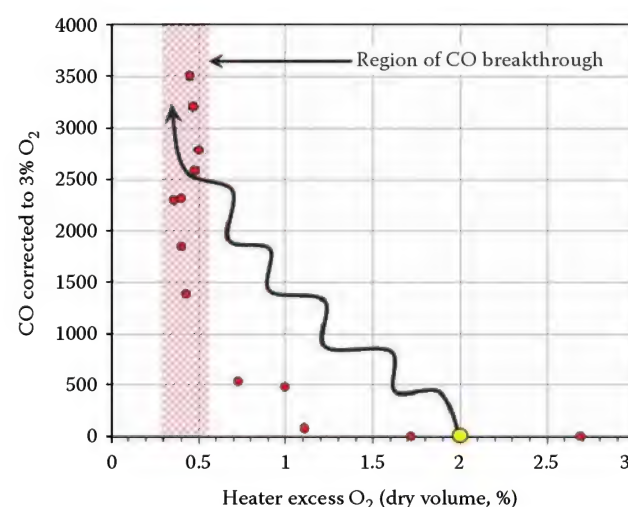
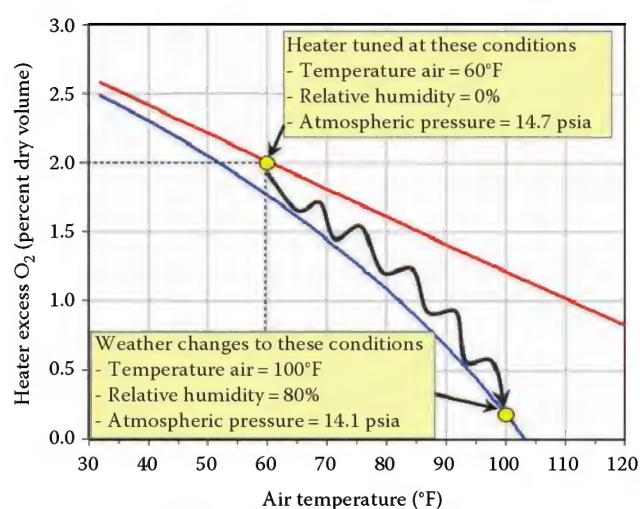


**FIGURE 12.9**

Example demonstrating how variations in ambient temperature and humidity can result in dramatic changes in CO emissions. (From Bussman, W. and Baukal, C.E., *Energy*, 34, 1624, 2009. Courtesy of Elsevier.)

temperature of 60°F (16°C) and humidity of 0%, when the ambient air temperature and humidity increase to 100°F (38°C) and 80%, respectively, the CO increases from zero to thousands of parts per million (ppm). This assumes no adjustments are made to the heater. NO<sub>x</sub> emissions are also impacted by changes in the ambient air temperature and humidity. Atmospheric pressure, wind, and rain also can impact emissions for combustors located outside, such as process heaters.

### 12.2.3 Poor Burner Performance

Process burners will be used here as an example to show how air infiltration can adversely affect burner performance. The best place to measure the excess O<sub>2</sub> in a process heater (see Figure 12.10) is at the top (roof) of the radiant section (sometimes referred to as the arch or

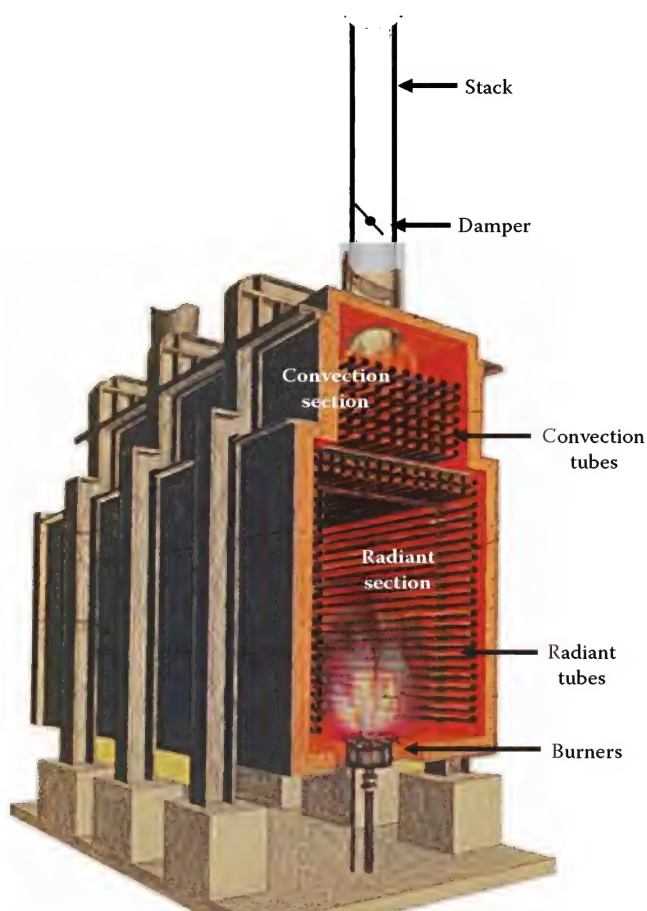


**FIGURE 12.10**  
Cabin-style process heater.

bridgewall)<sup>16</sup> for two important reasons. The first is that this is generally far enough downstream of the burners that the combustion process has gone to completion so the excess  $O_2$  should not be changing at that point. The second reason is that there is usually very high air leakage in the downstream convection section due to the multiplicity of tube penetrations into the heater, which are often not properly sealed. Measuring downstream of the convection section could falsely indicate there is plenty of  $O_2$  for combustion, when that might not be the case in the radiant section where combustion should be taking place.

One of the problems with large amounts of air infiltration into the radiant section is that the excess  $O_2$  measured at the arch might be within acceptable limits, even though a large portion of the air might not be going through the burners. Therefore, it is possible to measure plenty of  $O_2$  at the arch and yet have very poor flame quality at the burners because not enough of the air is flowing through the burners to properly complete combustion.<sup>17</sup> Process burners are designed assuming that all of the air needed for combustion will enter through the burner air inlet. Figure 12.11 shows an example in an actual process heater of what happens when there is not enough air flowing through the burners for complete combustion. The figure shows long flames with yellow tails, signifying that the flames were lacking  $O_2$  for complete combustion. After the burner air registers were opened slightly to increase the combustion air flow rate, the flames shortened to their design length, with no traces of yellow.

Excessive air infiltration into the radiant section can indirectly cause poor burner performance because not

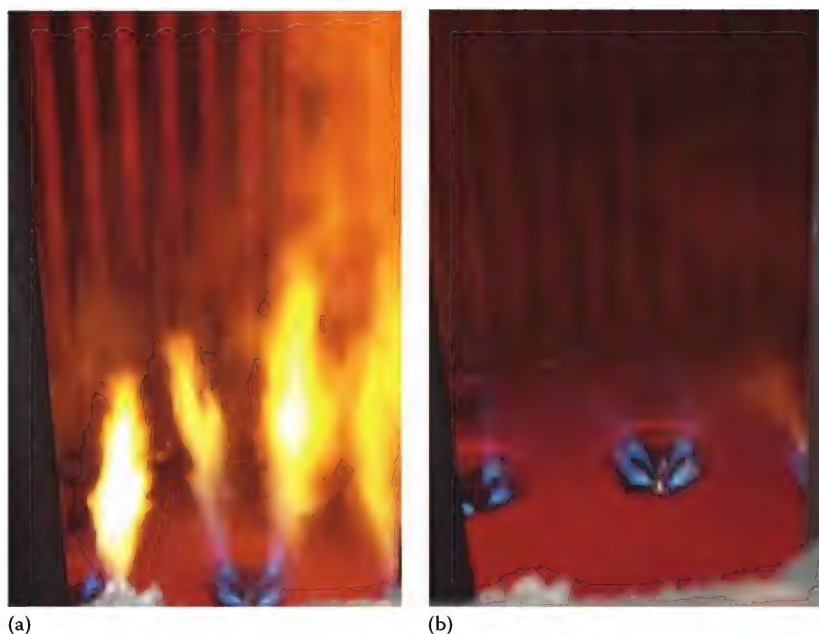


**FIGURE 12.11**  
Process burners in a cabin heater: (a) <0.5% excess  $O_2$  and (b) 1.5% excess  $O_2$ .



enough of the air is flowing through the burner as designed. This results in longer flames, which could cause flame impingement on the process tubes in the convection section. Longer flames could also adversely affect the heat flux profile in the heater. See Volume 2 for a more detailed discussion of these problems and recommended solutions. All of these problems adversely affect fuel efficiency indirectly because more fuel needs to be combusted for a given unit of production.

### 12.2.4 After-Burning

When there is significant air infiltration in the downstream section of a combustion system (e.g., the convection section of a process heater or the posttreatment control system in a boiler) and the measured excess  $O_2$  level is within the target range, there may not be enough combustion air flowing through the burners as designed. In addition to poor burner performance, this can also lead to incomplete combustion in the primary section of the combustor due to inadequate mixing and residence time, even if the measured excess  $O_2$  at the exhaust is within the target limits. Products of incomplete combustion (e.g., CO and unburned hydrocarbons) may then exit the primary section of the combustor and enter the downstream section. If air leakage into the downstream section is significant, the hot products of incomplete combustion normally burn rapidly in the presence of the additional  $O_2$ , which is typically referred to as after-burning. This additional heat in the downstream section may damage equipment, which is not designed for continuous exposure to flames caused by after-burning. This indirectly reduces fuel efficiency because of improper heat distribution and because the combustion system may need to be shut down more frequently for repairs, which leads to unproductive operation.

### 12.2.5 Increased Metal Oxidation and Stress

Reed<sup>18</sup> noted that process tubes in a heater can be damaged by excessive air leakage. The damage is believed to be caused by accelerated oxidation and thermal stresses of the tubes in the vicinity of the air leaks. The atmosphere in an operating heater consists mostly of hot inert gases such as nitrogen, carbon dioxide, and water vapor. The incoming cold tramp air provides oxygen for oxidation that contacts heated tubes causing increased metal oxidation. The cold tramp air contacting the hot process tubes also increases the thermal stress on the tubes. Excessive air infiltration into any combustor could also cause metal in the furnace to be more rapidly oxidized and thermally stressed. Again, this indirectly reduces fuel efficiency because of the increased time required for repairs.

### 12.2.6 Other Problems

Excessive air leakage into a boiler can contribute to poor furnace performance, slagging, fouling, and excessive levels of carbon-in-ash content.<sup>19</sup> All of these reduce fuel efficiency because of unproductive operations and poor heat transfer performance.

---

## 12.3 Leak Sources/Causes

There are many potential sources and causes of leaks in industrial combustors. They have been grouped into several categories that are described next.

### 12.3.1 Leaky Combustors

Industrial combustors may be leaky due to poor design or inadequate maintenance. Many combustors have been in service for many years. Some combustors such as process heaters are located outside and are therefore subject to the weather, which further accelerates deterioration. Combustors are typically very large with many welds and bolted connections that could fail leading to leaks. Some of these combustors are also subject to thermal cycling due to repeated shutdowns and start-ups, for example, batch processes and routine maintenance. Those combustors located outside are also subject to the changes in ambient temperatures due to normal weather fluctuations. The expansion and contraction of the combustors leads to cracks in the refractory lining and in the metal shell. These cracks are normally small enough that they are not easily seen and may go unnoticed and unrepaired. Cumulatively, numerous small leaks can lead to a large amount of air infiltration. Those cracks provide a path for tramp ambient air to leak into the combustors.

### 12.3.2 Improperly Sealed Openings

Industrial combustors are typically designed to have a number of openings used for a variety of purposes. Access doors are used for entering the combustor for inspection and maintenance. Nozzles may be used for injecting snuffing steam to put out fires in the combustor and to purge the combustor prior to start-up. Some combustors, such as process heaters, have tube penetrations that allow the tubes carrying the process fluid to enter and exit the heater. Sight ports permit visual inspection of the heater during operation. Explosion doors are used to relieve over-pressures in a combustor. Smaller penetrations are used to insert instruments into the combustor to measure, for example, tube skin temperatures, flue gas temperatures, excess  $O_2$ , and combustor draft.





**FIGURE 12.12**  
Air leak around a tube penetration in the convection section.



**FIGURE 12.13**  
Open sight port in the floor of a process heater.

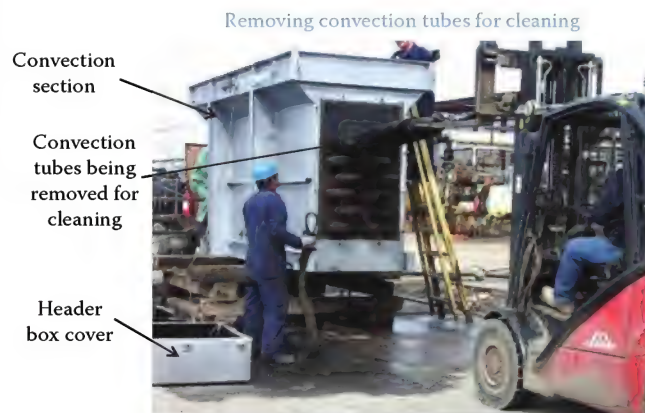
These combustor penetrations may be improperly sealed. Figure 12.12 shows a photo of a tube penetration through the convection section of a process heater. An attempt was made to seal the opening with blanket refractory. Notice that much of the blanket is now gone, most likely due to the effects of weather. Figure 12.13 shows an example of an open sight port located at the bottom of an operating process heater. It is sometimes convenient for the operators to keep sight ports open for easy viewing, but that allows a large amount of tramp air to enter the heater.

Figure 12.14 shows a poorly sealed sight port on the side of a process heater. The sight port door consists only of a piece of uninsulated metal without any gasket material to minimize air infiltration. Improperly sealed openings can lead to a large ingress of tramp air.

The header box used to cover the tube penetrations in a process heater is an example of an opening that is difficult to seal (see Figure 12.15). These header boxes are designed to minimize air leakage through the penetrations and typically have an access door for



**FIGURE 12.14**  
Poorly sealed sight port on the side of a process heater.



**FIGURE 12.15**  
Example of a convection section removed so that tubes can be cleaned.

inspection and clean out. While these doors normally have some type of gasket to help keep them sealed, the seal may be degraded after the doors have been opened and closed several times.<sup>15</sup> Reed<sup>15</sup> noted that in one case, after sealing the header box leaks, the burner air registers had to be opened to supply the required combustion air.

### 12.3.3 Burners Out of Service

In a combustor with multiple burners, there may be certain conditions that require one or more of the burners to be taken out of service. One example is when some burner components need to be serviced, such as when

the fuel injectors in process burners are plugged and need to be cleaned.<sup>20</sup> Another example is when very little heat is needed, such as when a combustor is being warmed up slowly after a refractory repair. It may not be possible to turn all of the burners down to a low enough firing rate, which means that some of the burners may need to be turned off to reduce the firing duty to a low enough level. Simply turning off the fuel to a natural draft burner, without closing off the combustion air inlets, means there will be large openings in the heater at locations with high negative pressures; both of which cause high air infiltration.

### 12.3.4 Improper Operation

Improperly operating an industrial combustion process could increase air infiltration. For example, process heaters used in the chemical and petrochemical industry are designed to operate with the combustion chamber, usually referred to as the radiant section, at a slightly negative pressure (draft). However, if a process heater is operated at a significantly higher negative pressure (referred to as “high draft”) than designed, then air leakage may increase dramatically. This high draft condition typically occurs when the stack damper is wide open and the burner air registers/dampers are nearly closed.<sup>21</sup> High draft increases the amount of air drawn into the heater through cracks and other openings.

## 12.4 Leak Size and Location

It is obvious that the size of an opening is important for how much tramp air leaks into a combustor. Figure 12.16 shows the amount of air leakage

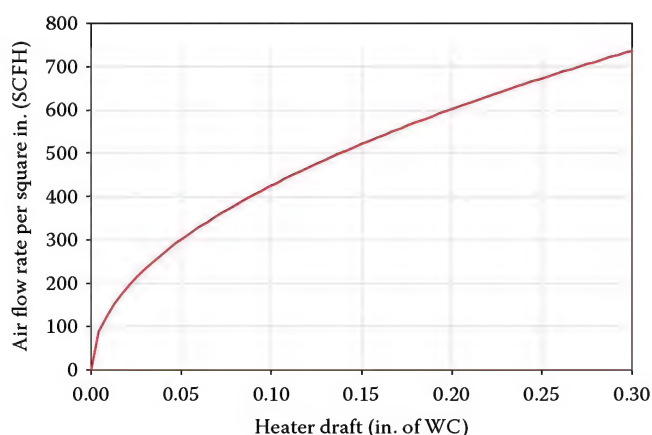


**FIGURE 12.16**  
Air infiltration as a function of heater draft.

(standard cubic feet per hour or SCFH) per unit opening area (square inches) as a function of the heater draft (inches of water column).

For example, assume that the burner damper for a single out-of-service burner in a process heater has been left open. A common process burner throat diameter is 16 in. (41 cm), which equates to a 201 in<sup>2</sup> (1300 cm<sup>2</sup>) opening. Assume the heater draft at the floor is 0.30 in. of water column (WC) (7.5 kPa). From the graph in Figure 12.16 for a draft of 0.30 in. WC (7.5 kPa), the leak rate would be about 740 SCFH/in<sup>2</sup> (3.25 SCMH/cm<sup>2</sup>). Therefore, the leak rate would be (740 SCFH/in<sup>2</sup>) (201 in<sup>2</sup>) = 149,000 SCFH (4,200 SCMH). For a heater firing  $100 \times 10^6$  Btu/h (29 MW), the combustion air flow with 15% excess air (3% excess O<sub>2</sub>) would be approximately  $1.20 \times 10^6$  ft<sup>3</sup>/h ( $34 \times 10^3$  m<sup>3</sup>/h) assuming the fuel is methane (CH<sub>4</sub>). The calculated leak rate equates to approximately 14% of the stoichiometric air flow. This means that if the target excess O<sub>2</sub> was 3%, which is a typical level, then nearly all of the excess air would be coming from the out-of-service burner. It would also mean that the operating burners would have only about 0.8% excess combustion air. That would likely produce long lazy flames with high levels of CO emissions due to incomplete combustion and possibly unstable flames due to lack of O<sub>2</sub> to combust the fuel flowing through the burners.

In addition to the leak size, the leak location may also be important in determining the amount of air infiltration. As shown in Figure 12.16, the air leakage rate increases with the draft level. Figure 12.17 shows the draft profile in a typical natural draft process heater. The highest draft (most negative) is at the floor, which is used to pull in the air for combustion through the natural draft burners, since no fans or blowers are used. The lowest draft (least negative pressure) in the radiant section is at the top of the radiant section (arch). This means that leaks in the floor of the heater (e.g., see Figure 12.13) will allow more tramp air infiltration than leaks through the wall near the arch, for a given size leak opening, because of the difference in draft levels at the two locations.

Another aspect regarding the location of leaks is associated with gas flow patterns inside the combustor. For example, the general flow in a vertically-fired process heater (e.g., Figure 12.10), near the floor-mounted burners, is upward due to both the outlet gas velocities from the burners which are pointing upward, and from the buoyancy of the hot combustion products. Tramp air leaking into a heater near the burners would most likely be carried upward. The coldest part of the radiant section is typically near the process tubes that carry the hydrocarbon fluids being heated by the heater. The gas flow near the tubes is typically downward because those gases are cooler than, for example, the combustion



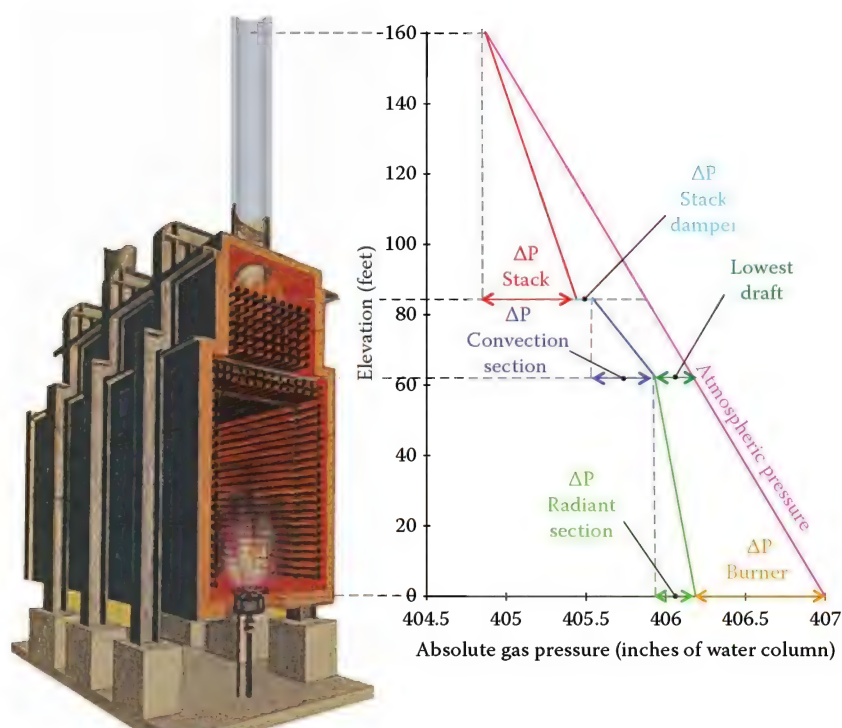


FIGURE 12.17

Typical draft profile in a process heater ( $\Delta P$  = pressure drop).

products coming from the burners. If there is a leak near the process tubes, the tramp air entering the heater may flow downward because it too is much cooler than the combustion products flowing upward near the center of the heater. The actual gas flow patterns in a combustion process can be complicated, so ambient air leaking into a heater may flow in a variety of directions, depending on the leak location.

tubes or centers of the burners) include the outline of an access door at the center near the floor, a sight port to the left of the bottom burner, and two snuffing steam inlets to the right of the access door. The dark regions around these openings indicate that some ambient air is leaking through them and cooling the opening.

## 12.5 Finding Leaks

There are a variety of ways to find locations where tramp air enters into an industrial combustor. Some of the more common methods are discussed in this section.

### 12.5.1 Dark Regions

A relatively simple method of finding air leaks is to look inside an operating combustor and find any dark regions, other than the load. These dark regions normally indicate cooler regions where air may be leaking in. Figure 12.18 shows a photo of an endwall in an operating process heater. The process tubes are located on the left side of the photo. Three burners are firing on the endwall. Several dark regions (not including the process

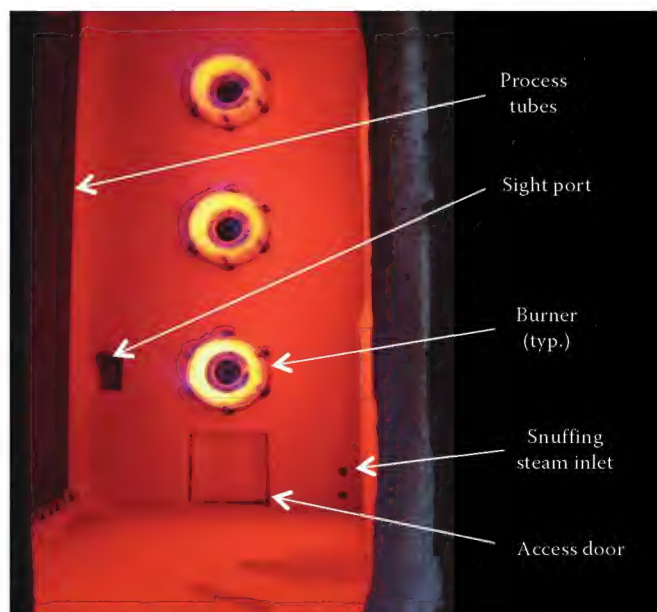


FIGURE 12.18

End wall photo of an operating process heater.



### 12.5.2 Smoke Testing

Another method that is used to find tramp air leaks is with smoke. Two techniques are most commonly used. The first technique uses a handheld smoke generator. For combustors operating at a negative pressure, such as process heaters, smoke is introduced outside of and near the walls of an operating combustor, particularly near joints and penetrations. If a noticeable amount of smoke is drawn into the combustor, it indicates that there is a significant leak in that location. The leak may be repaired at that time (e.g., with a high temperature silicone sealant), or it may be marked for future repair (e.g., welding cracks in the metal shell).

The second method to find leaks using smoke requires a smoke bomb, or some other method for generating large quantities of smoke. The smoke is introduced into the inlet of a fan or blower that is attached to the combustor (see Figure 12.19). It is important to note that this must be done when the combustor is not firing. During the test, the stack damper and burner dampers (air registers) are fully closed. All other openings such as sight ports and access doors are also closed. An external air blower is connected to the combustor to pressurize it. When smoke is introduced into the fan inlet, it enters into the combustor and will exit the combustor at locations where there are openings. The location of these leaks can then be marked and repaired after the test is completed.

### 12.5.3 IR Camera

Another method that can be used to find air leaks in a heater is with an infrared (IR) camera. Figure 12.20 shows a thermal image of the side of a process heater. The colors indicate temperature where the darker the color, the higher the temperature. Notice that the side of the heater is essentially dark, except in the vicinity

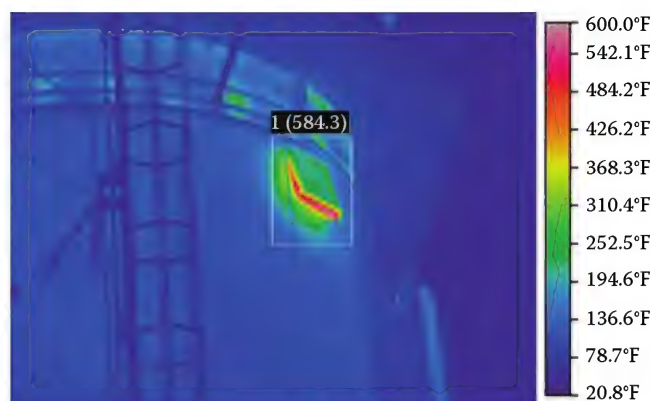


FIGURE 12.20

Thermal image showing a partially open explosion door.

of an explosion door, which is designed to relieve significant overpressures in the heater. In this case, the explosion door was not properly sealed and appeared to be partially open, which allows a significant amount of heat to escape from the heater. Since the pressure inside the heater at this location in the radiant section should be negative, tramp air is likely entering the heater around that explosion door. An IR camera can be used to photograph the outside of a combustor to look for hot spots where significant amounts of heat are radiating out, and where significant amounts of tramp air may be leaking in.

### 12.5.4 Peeling Paint

Another visual method that can sometimes be used to indirectly find tramp air leaks is to inspect the paint on the skin of a combustor. If the paint is discolored or burned off in certain areas, it could indicate there are significant openings in the combustor at those locations that are allowing heat to escape and tramp air to enter.

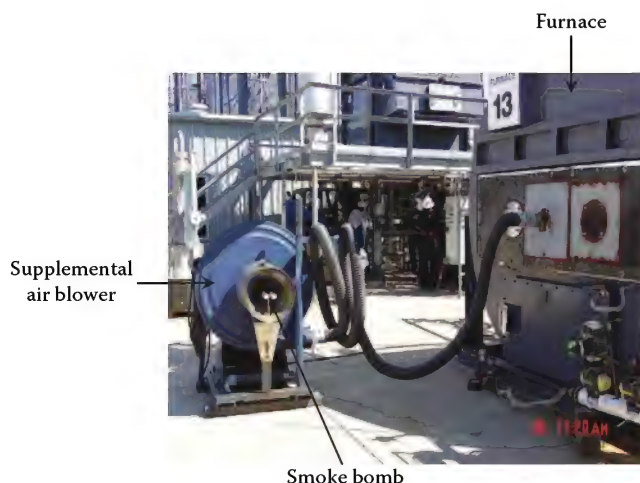


FIGURE 12.19

Smoke bomb test to find leaks in a heater.

## 12.6 Mitigating Leaks

### 12.6.1 Control Furnace Pressure

One important and easy method for minimizing air infiltration into a combustor is to control the pressure inside the furnace, preferably automatically.<sup>22</sup> For example, in a process heater this means properly controlling the draft levels inside the heater. If the draft is excessively high (much more negative than designed), then more air will be pulled into the heater than if it is at the target level (typically about  $-0.1$  in. WC or  $-25$  Pa at the arch). One reason why a heater might be operated with a high draft is to increase the combustion air flow through the

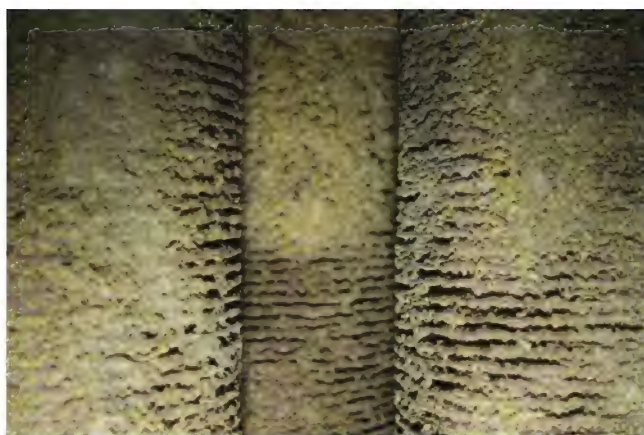


**FIGURE 12.21**  
Plugged convection section tubes.

burners if they are being operated beyond their maximum design firing rate to increase the throughput in the heater. Another reason might be that the convection section is partially plugged (see Figure 12.21), necessitating more draft to allow enough flow through the convection section due to the increased pressure drop. While the draft at the exit of the plugged convection section may be close to the design condition, the draft before the convection section (e.g., in the radiant section) may be much higher than design, causing higher tramp air infiltration. Therefore, convection sections should be regularly inspected and cleaned (see Figure 12.15) to minimize the pressure drop. Combustors should be operated at their design pressure.

Changes in the ambient air conditions can impact the air infiltration into an industrial combustor. For example, for a fixed set of furnace operating conditions, more air will infiltrate into a combustor when the air is colder and less humid.<sup>9</sup>

### 12.6.2 Fix Leaks

Another obvious way to mitigate tramp air infiltration is to fix the leaks in the heater. This can be a time-consuming and tedious process because of the sheer size of most industrial combustors. It also needs to be an ongoing process as new cracks will often develop after old cracks have been sealed. At a minimum, cracks should be sealed during each major maintenance shutdown. As previously discussed, it is particularly important to seal the leaks in combustor locations where the pressures are negative. However, as pointed out by McNeill and Peppers<sup>23</sup>, air “leaks are hard to find and permanently fix. Stop one leak, and more will inevitably appear.” This illustrates the importance of constant vigilance to find and seal air leaks in industrial combustors, which should be an ongoing activity and not a once-and-done event.



**FIGURE 12.22**  
Sight port refractory plug seal. (Courtesy of Thorpe Corp., Houston, TX.)

It is also important to properly seal other combustor openings such as sight ports (see Figure 12.14) and explosion doors (see Figure 12.20). Figure 12.22 shows an example of a specially designed refractory plug seal used to minimize heat escaping through the sight port and minimize air infiltration through the sight port. A refractory gasket around the opening, between the sight port door and the heater, further improves the seal. Figure 12.23 shows a specially designed sight port that uses a quartz window so the inside of the heater can be seen without opening the port. An interior shutter is spring loaded, so it shields the quartz from the heat, but can be easily retracted by pushing a lever, without ever opening the sight port. That sight port design also minimizes air leaks by providing a tight seal around the quartz window. This window design is also safer as personnel are not exposed to hot gases when they look through this sight port.

Another example of sealing leaks is demonstrated in Figure 12.24, which shows high temperature seals designed to minimize air infiltration around process tube penetrations through the walls of a process heater.<sup>24</sup> Because of thermal expansion, these seals need to be flexible so they can move as the tubes expand and contract. Properly sealing combustor penetrations helps mitigate air infiltration.

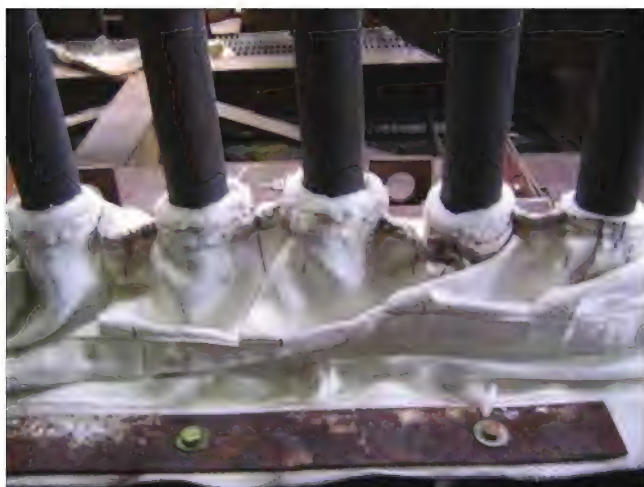
### 12.6.3 Operate as Many Burners as Possible

An indirect method of minimizing air infiltration is to operate as many burners as possible, that is, do not take burners out of service unless it is necessary. As demonstrated in Section 12.4, air leakage through an out-of-service burner can be large if the burner damper (air register) has not been closed. Even when the burner damper is closed, there is still some air



**FIGURE 12.23**

Sight port designed to reduce air leaks and protect operators against hot furnace flue gases, high radiant heat, and positive pressure surges in the heater.

**FIGURE 12.24**

Engineered tube seals. (Courtesy of Thorpe Corp., Houston, TX.)

leakage through the burner because the damper is not designed to be air tight. Since natural draft burners are typically located where the heater negative pressure is high, any openings in out-of-service burners can lead to high air infiltration.

## 12.7 Conclusion

Air infiltration into industrial combustors can reduce thermal efficiency, increase pollution emissions such as NO<sub>x</sub>, degrade burner performance, and cause after-burning in downstream sections. There are many possible sources for air leaks including leaky combustion chambers, improperly sealed openings, and out-of-service burners. Both the size and the location of the leaks are important because both directly impact how much tramp air is drawn into the combustor. There are many ways to find the leaks including visual inspection inside the combustor looking for dark regions, using smoke outside an operating combustor to see where it is drawn in, using smoke inside a combustor which is not operating to see where it comes out, thermal images of the outside of the combustor to see where heat may be leaking out and air possibly leaking in, and checking the paint on the combustor shell to see if there are places where the paint has been discolored or burned off.

## 12.8 Recommendation

Because of their significant impact on heater performance, air leaks need to be mitigated, particularly those that are large and in locations where the combustor pressure is very negative. An important recommendation is to operate the combustor at the design draft level, because excessively high negative pressures increase tramp air infiltration. Cracks in the shell of combustors need to be repaired on a regular basis. Penetrations need to be sealed. Tube seals and specially designed sight ports are examples of devices specifically made to minimize air leaks. Another important recommendation to ensure plant operators, engineers, and maintenance personnel are properly trained (see Chapter 17) so that they fully understand the importance of air infiltration and that plant personnel are vigilant in fixing leaks in their industrial combustors.

## References

1. U.S. Department of Energy (DOE). *Industrial Combustion Vision: A Vision by and for the Industrial Combustion Community*, U.S. Department of Energy: Washington, DC, 1998.
2. Hewitt, G.F., Shires, G.L., and Bott, T.R., *Process Heat Transfer*, Boca Raton, FL: CRC Press LLC, 1994.



3. U.S. Department of Energy, *Energy Information Administration*. Annual Energy Outlook 2008, Report DOE/EIA-0384(2008), Washington, DC, released June 26, 2009.
4. Trinks, W., Mawhinney, M.H., Shannon, R.A., Reed, R.J., and Garvey, J.R., *Industrial Furnaces*, 6th edn., New York: John Wiley & Sons, 2004.
5. Petrick, M. and Pellegrino, J. *The Potential for Reducing Energy Utilization in the Refining Industry*, Argonne National Laboratory Report ANL/ESD/TM-158, U.S. Department of Energy: Washington, DC, 1999.
6. Lawrence Berkeley National Laboratory and Resource Dynamics Corporation, *Improving Process Heating System Performance: A Sourcebook for Industry*, 2nd edn., U.S. Department of Energy and Industrial Heating Equipment Association: Washington, DC, 2007.
7. ANSI/API Standard 560, *Fired Heaters for General Refinery Service*, 4th edn., American Petroleum Institute: Washington, DC, August 2007.
8. Chen, Q.L., Yin, Q.H., Wang, S.P., and Hua, B., Energy-use analysis and improvement for delayed coking units, *Energy*, 2004, 29, 2225–2237.
9. Reed, R.J., *The North American Combustion Handbook, Vol. I: Combustion, Fuels, Stoichiometry, Heat Transfer, Fluid Flow*, 3rd edn., North American Mfg. Co.: Cleveland, OH, 1986.
10. Storm, R.F., How stealth combustion losses lower plant efficiency, *Power*, 2005, 149(2), 62–74.
11. Mullinger, P. and Jenkins, B., *Industrial and Process Furnaces*, Elsevier: Oxford, U.K., 2008.
12. Bussman, W. and Baukal, C.E., Ambient condition effects on process heater efficiency, *Energy*, 2009, 34, 1624–1635.
13. Baukal, C., Waibel, D., and Webster, T., Plant-wide NO<sub>x</sub> reduction strategies, *Proceedings of the Industrial Energy Technology Conference*, New Orleans, LA, May 9–12, 2006.
14. Baukal, C.E., *Industrial Combustion Pollution and Control*, Marcel Dekker: New York, 2004.
15. Bussman, W. and Baukal, C.E., Ambient condition effects on process heater emissions, *Proceedings of the International Mechanical Engineering Congress & Exhibition*, Paper IMECE2008–68284, Boston, MA, November 2008.
16. Baukal, C.E. (ed.), *The John Zink Combustion Handbook*, CRC Press: Boca Raton, FL, 2001.
17. Baukal, C.E. (ed.), *Industrial Burners Handbook*, CRC Press: Boca Raton, FL, 2004.
18. Reed, R.D., *Furnace Operations*, 3rd edn., Gulf Publishing: Houston, TX, 1981.
19. Storm, R.F., Storm, S.K., and Hall, S.G., Managing air to improve combustion efficiency, *Power*, 2007, 151(10), 64–70.
20. Baukal, C., Johnson, B., Vaughn, K., and Pappe, M., Burner fuel tips, *Process Heating*, 2010, 17(2), 11–13.
21. Rajan, G.G., *Optimizing Energy Efficiencies in Industry*, McGraw-Hill: New York, 2003.
22. IHEA, *Combustion Technology Manual*, 5th edn., Industrial Heating Equipment Association: Arlington, VA, 1994.
23. McNeill, H.F. and Peppers, D., Sealing boiler cracks once and for all, *Power*, 2005, 149(5), 29–34.
24. West, K. and Hodel, A.E., Refractory/ceramic fiber insulation boosts ethylene heater efficiency, *Chemical Processing*, 1995, 58(8), 50–52.

# 13

## CFD-Based Combustion Modeling

Michael A. Lorra and Shirley X. Chen

### CONTENTS

13.1	Introduction .....	353
13.2	Computational Fluid Dynamics Model Background .....	355
13.2.1	Transport Equations .....	355
13.2.2	Turbulence Models .....	356
13.2.3	Algebraic Models .....	356
13.2.4	One- and Two-Equation Models .....	356
13.2.4.1	$k$ - $\epsilon$ Turbulence Model .....	357
13.2.4.2	$k$ - $\epsilon$ Turbulence Model Boundary Conditions .....	359
13.2.5	Other Turbulence Modeling Approaches .....	361
13.3	Computational Fluid Dynamics-Based Combustion Submodels .....	361
13.3.1	Regimes of Turbulent Combustion .....	361
13.3.2	Reaction Kinetics .....	363
13.3.3	Eddy Breakup Model .....	364
13.3.4	Eddy Dissipation Combustion Model .....	364
13.3.5	Eddy Dissipation Concept .....	365
13.3.6	Mixture Fraction Approach for Equilibrium or Finite Rate Chemistry .....	365
13.3.7	Pollutant Chemistry Models .....	367
13.4	Radiation Models .....	367
13.4.1	P-1 Radiation Model .....	368
13.4.2	Discrete Ordinates Radiation Model .....	368
13.4.3	Monte Carlo Method .....	370
13.4.4	Gas-Radiation Properties .....	370
13.4.5	Weighted Sum of Gray Gases Model .....	370
13.4.6	Effect of Soot on Thermal Radiation .....	370
13.5	Solution Methodology .....	371
13.5.1	Problem Setup: Preprocessing .....	371
13.5.2	Solution Convergence .....	373
13.5.3	Analysis of Results: Postprocessing .....	374
13.6	Summary .....	376
	Nomenclature .....	378
	References .....	378

### 13.1 Introduction

Computational fluid dynamics (CFD) has become a widely accepted tool to help in the design and operation of equipment in various industries. It evolved from a tool to simulate isothermal flow distribution in simpler

geometries, as, for example, flow distribution in combustion equipment, see also Figure 13.1, to a generic tool that is theoretically capable of simulating complex flow phenomena with respect to geometry and physics.

Simulation of reactive flows with complex reaction mechanisms, convective and radiative heat transfer, phase changes of liquid material, and volatilization

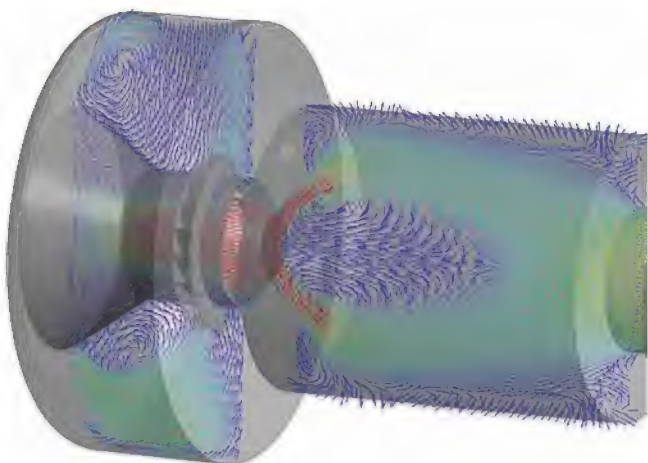


**FIGURE 13.1**  
Investigation of an isothermal flow field.

of coal particles are now capabilities of commercially available CFD packages. However, even today there are still some caveats that limit the use of a CFD model for a certain application or problem at hand:

- Limited theoretical understanding of the physics involved in reactive flow systems:  
This includes uncertainty in fundamental chemical reaction kinetics for complex fuels (higher hydrocarbons), the understanding and mathematical description of the chaotic nature of turbulent mixing, the more complex heterogeneous chemistry related to liquids or solids (e.g., soot formation, catalysis, evaporation of multicomponent droplets, etc.
- Uncertainty of thermodynamic properties:  
One problem of using CFD models for complex combustion systems such as incinerators stems from the lack of thermodynamic data of species involved in the combustion process. The datasets available and accepted worldwide include a variety of hydrocarbon species ranging from C1 to C10, including all intermediate radicals. As soon as the process involves more “exotic” species, as, for example, various sulfur compounds, thermodynamic data becomes unavailable or various sources might offer differing data.
- The large disparity in both spatial and temporal time scales in typical reacting flow systems:  
To capture the flow characteristics responsible for momentum transfer one needs to resolve the flow to the smallest characteristic size (i.e., Kolmogorov scale), typically in the order of magnitude of micrometers for most laboratory flows. This poses a major problem for the model of full scale combustion chambers in a way that

is efficient enough to be achievable for computations on a reasonable number of computers in a reasonable amount of time.

- Uncertainty of boundary conditions:  
For a range of applications, the exact boundary conditions are unknown and can only be estimated or given as a “temporal snapshot.” One example here would be a CFD model of a ground flare exposed to ambient conditions with varying conditions for wind speed and wind direction. Data can be obtained for median values as recorded by discrete measuring stations like weather stations in airports, but the local conditions, also affected by the surrounding terrain, remain unknown. This prompts the need for an extended domain to capture topographical data in order to obtain a solution that is more representative for the impact of any given wind condition to the object of interest. An example is shown in Figures 13.2 and 13.3, showing the

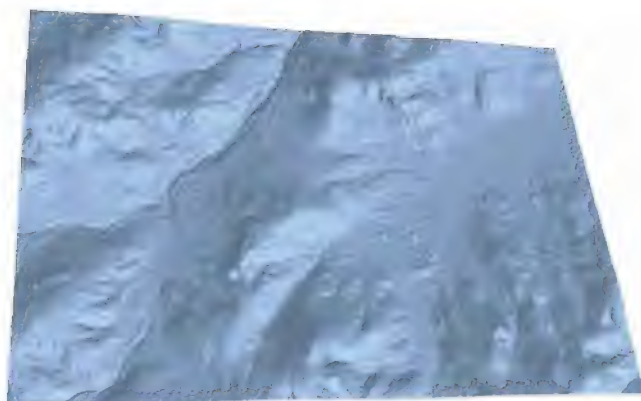


**FIGURE 13.2**  
Original topographic data.

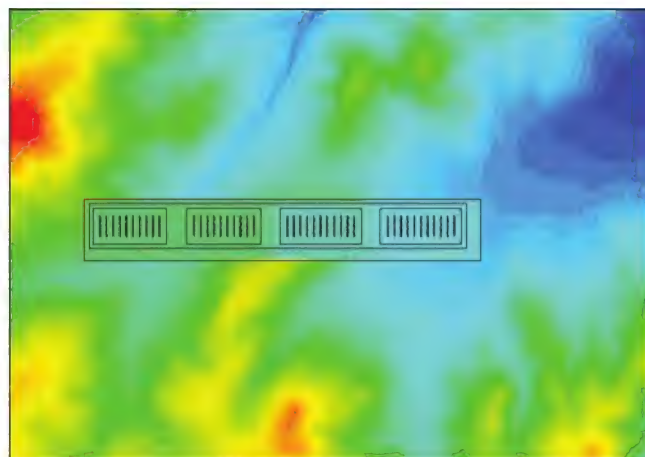


**FIGURE 13.3**  
Representation of topographical data in a CFD model (blue showing lower elevation, red showing higher elevation).



original topographical data and the representation in a CFD model, respectively. The blue color in Figure 13.2 depicts lower ground elevation; the red indicates higher ground elevation.

A CFD code or a specific submodel for this code has a three-fold basis:

1. The development of a CFD code or specific submodel requires the understanding of the physical phenomena involved in any fluid dynamic process.
2. The “real world” physics of the flow phenomena must be translated into mathematical relationships. The developer of a CFD model (or submodel) would have to find the functional or parametric relationship between cause and effect.
3. Due to the complexity of nonlinear mathematics, the governing equations describing the flow phenomenon must be solved using numerical algorithms to make those compatible for a computer.

Error in any one translates into erroneous predictions, and failing to understand the limitations of each can lead to incorrect conclusions and potentially catastrophic results. For optimal use, an engineer utilizing CFD code must understand the physics, the mathematics, and the numerical approach to determine if a simulation produces sound results. In addition, knowledge about the application that has to be modeled is crucial to determine if the results are correct within its context. When used appropriately, CFD can help reduce development cycle time, potentially improves efficiency of a process, or can extend the lifetime of the equipment.

Figures 13.4 and 13.5 are an example of the use of CFD for a new burner development. In a project like this, results



**FIGURE 13.4**  
Close-up view of a burner in a test furnace.

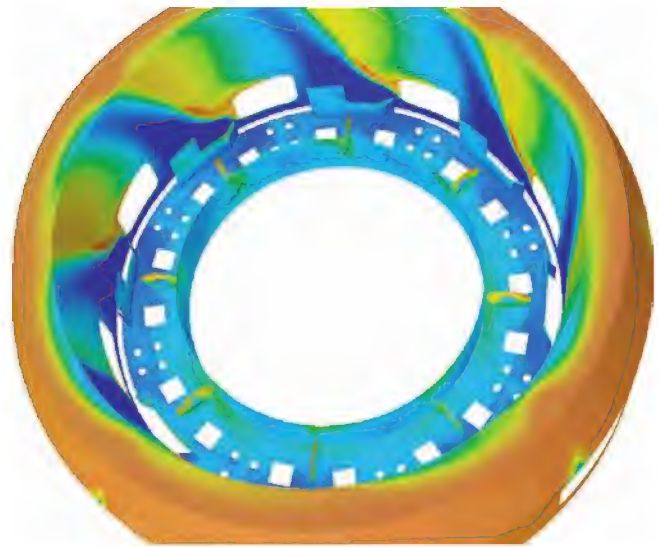


**FIGURE 13.5**  
Representation of a process burner, colored by temperature (blue showing low temperatures, red high temperatures).

from the real world, established through measurements in a test furnace and the results from a CFD model can complement each other leading to shorter development times.

## 13.2 Computational Fluid Dynamics Model Background

All CFD codes have evolved from similar backgrounds being based on the semi-implicit pressure linked equations (SIMPLE) algorithm, which solves a set of nonlinear coupled partial differential equations (PDEs) describing the conservation of mass, momentum, and energy, described later. To illustrate the mathematical basis from which CFD codes are derived, a brief review of the general make up of a CFD code is given in the following section.

### 13.2.1 Transport Equations

Non-reactive turbulent fluid flow is modeled using the steady-form of the Navier–Stokes equations by assuming a continuous flow field described locally by the general conservation of mass and momentum:<sup>1</sup>

$$\frac{D\rho}{Dt} = -\rho(\nabla \cdot \underline{v}) \quad (13.1)$$

$$\rho \frac{D\underline{v}}{Dt} = -\nabla p - \nabla \cdot \underline{\tau} + \rho \underline{g} \quad (13.2)$$

where  $D/Dt$  is the total (or substantial) derivative.

These equations may be simplified by assuming steady-state flow of a Newtonian fluid. If the fluid is

assumed to be noncompressible, the dilatation ( $\nabla \cdot \vec{v}$ ) can also be used to further simplify the equations. A non-compressible assumption is applicable to low Mach number flows (i.e., Mach No.  $< 0.3$ ) and for incompressible fluids. Given these simplifying assumptions, the general conservation or transport equations for mass and momentum for steady flow can be written in Cartesian tensor notation as

$$\frac{\partial(\rho u_j)}{\partial x_j} = 0 \quad (13.3)$$

$$\frac{\partial(\rho u_i u_j)}{\partial x_j} = -\frac{\partial P}{\partial x_i} + \frac{\partial \tau_{ij}}{\partial x_j} + \rho f_i \quad (13.4)$$

$$\tau_{ij} = \mu \left( \frac{\partial u_i}{\partial x_j} + \frac{\partial u_j}{\partial x_i} \right) + \left( \frac{2}{3} \mu - \mu_B \right) \frac{\partial u_k}{\partial x_k} \delta_{ij} \quad (13.5)$$

Similarly, a transport equation can be written for any conserved scalar,  $\Phi$ s:

$$\frac{\partial(\rho \Phi u_j)}{\partial x_j} = \frac{\partial}{\partial x_j} \left( \Gamma_\Phi \frac{\partial \Phi}{\partial x_j} \right) + S_\Phi \quad (13.6)$$

These equations are valid for all flow regimes from laminar to turbulent. However, for all practical purposes, these equations cannot be solved directly for turbulent flows. Hence the need for a statistical approach to model turbulent flow regimes. The approach is rather simplistic; a simple decomposition into mean values and fluctuations with a zero mean value:

$$\Phi = \bar{\Phi} + \phi'' \quad (13.7)$$

where  $\bar{\Phi} = \overline{\rho \Phi} / \bar{\rho}$  and  $\overline{\rho \phi''} = 0$ , but  $\bar{\phi''} \neq 0$ .

Applying this decomposition to all variables except density and pressure, the conservation equations (Equations 13.3 through 13.6) are transformed into the mass-averaged or Favre-averaged transport equations:

$$\frac{\partial(\bar{\rho} \tilde{u}_j)}{\partial x_j} = 0 \quad (13.8)$$

$$\frac{\partial(\bar{\rho} \tilde{u}_i \tilde{u}_j)}{\partial x_j} = -\frac{\partial \bar{P}}{\partial x_i} + \frac{\partial}{\partial x_j} \left( \bar{\tau}_{ij} - \overline{\rho u_i'' u_j''} \right) + \bar{\rho} f_i \quad (13.9)$$

$$\frac{\partial(\bar{\rho} \tilde{\Phi} u_j)}{\partial x_j} = \frac{\partial}{\partial x_j} \left( \bar{\Gamma}_\Phi \frac{\partial \tilde{\Phi}}{\partial x_j} - \overline{\rho \phi'' u_j''} \right) + \bar{S}_\Phi \quad (13.10)$$

These represent the turbulent transport equation set for non-reacting flow. However, as a result of the

averaging procedure, several additional variables called Favre-stresses ( $\overline{\rho u_i'' u_j''}$ ) and Favre-fluxes ( $\overline{\rho \phi'' u_j''}$ ) have been introduced. These stresses and fluxes represent the mean-momentum transport and the mean-scalar transport by turbulent diffusion. Additional equations are required to solve for these new turbulent transport variables.

### 13.2.2 Turbulence Models

There are generally four types of turbulence models commonly used in engineering practice:

1. Algebraic models
2. One-equation models
3. Two-equation models
4. Second-order closure models

Wilcox<sup>2</sup> and Rodi<sup>3</sup> provide good reviews of various methods of turbulence modeling. Most of the models, which fall into one of the first three categories, have an underlying commonality, which is the Boussinesq approximation. The Boussinesq approximation assumes that the Reynolds-stress tensor is proportional to the mean strain-rate tensor, for every location in a turbulent flow. The constant of proportionality between the Reynolds-stress tensor and the mean strain-rate tensor is the eddy viscosity ( $\mu_T$ ).

### 13.2.3 Algebraic Models

Many algebraic models calculate an eddy viscosity from the Prandtl mixing-length hypothesis, given by

$$\mu_T = \rho \left( l_m^2 \right) \left| \frac{\partial U}{\partial y} \right| \quad (13.11)$$

where

$l_m$  is the mixing length  
 $U$  is the mean velocity

Algebraic models are not very general, because the mixing length depends on the flow scenario (i.e., jet, boundary layer, pipe flow, etc.). Therefore, an expression for the mixing length must be obtained for each type of flow when using an algebraic model.

### 13.2.4 One- and Two-Equation Models

One- and two-equation models attempt to overcome the difficulties with the Prandtl mixing-length hypothesis by solving transport equations for quantities that are related to the type of flow. In the aforementioned

algebraic model, there is a direct link between the fluctuating velocity scale and the mean velocity gradients, as shown by Equation 13.11. In one- and two-equation models, the link between the fluctuating velocity scale and the mean velocity gradients is found by solving one or more transport equations. Wilcox<sup>2</sup> describes two, more recent, one-equation turbulence models, which appear to show promise. The Baldwin–Barth<sup>4</sup> model employs a transport equation for the turbulent Reynolds number and the Spalart–Allmaras<sup>5</sup> model employs a transport equation for the eddy viscosity.

Prandtl chose the turbulent kinetic energy as the basis for a turbulent velocity scale

$$k = \frac{1}{2} \overline{u'_i u'_i} = \frac{1}{2} (\overline{u'^2} + \overline{v'^2} + \overline{w'^2}) \quad (13.12)$$

The eddy viscosity can be computed using the Kolmogorov–Prandtl expression:

$$\mu_T = C_1 \rho \sqrt{k} l \quad (13.13)$$

where

$k$  is the turbulent kinetic energy

$l$  is the turbulence length scale

$C_1$  is the constant of proportionality

Wilcox<sup>2</sup> provides a derivation of the Reynolds-stress equation, obtained by taking moments of the Navier–Stokes equation. The Reynolds-stress equation is a tensor equation, and by taking the trace of it, a transport equation is obtained for turbulence kinetic energy. This transport equation for the turbulence kinetic energy forms the basis for a number of one- and two-equation turbulence models. The turbulence kinetic energy transport equation has various terms, which have been given physical interpretations. Included in the terms is a dissipation term ( $\epsilon$ ), which represents the rate at which turbulence kinetic energy is converted to thermal internal energy. From the turbulence kinetic energy equation,  $\epsilon$  is the product of the viscosity and the square of the fluctuating vorticity. Therefore, based on dimensional arguments, the dissipation ( $\epsilon$ ) should be related to the turbulence kinetic energy and length scale:

$$\epsilon = \frac{C_2 k^{3/2}}{l} \quad (13.14)$$

where  $C_2$  is the constant of proportionality.

#### 13.2.4.1 $k$ - $\epsilon$ Turbulence Model

A turbulent flow is a flow with a wide range of temporal and length scales. Figure 13.6 is an example of a typical

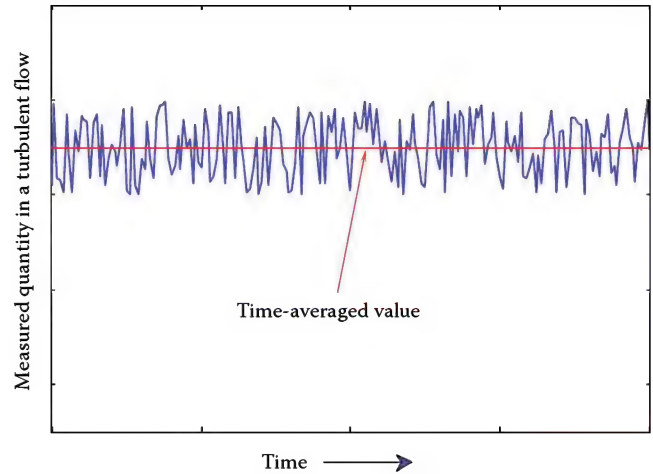


FIGURE 13.6

Point measurement of a scalar in a turbulent flow.

point measurement (e.g., pressure or velocity) within a turbulent flow.

Within a turbulent flow, the quantities of interest—such as pressure and velocity—fluctuate in an apparently random fashion. Analysis shows that these quantities are not truly random.<sup>6</sup> Information revealed by spectral analysis of point measurements indicates that there are ranges of temporal and length scales which contain significant energy (the large or integral scales) and smaller scales where this turbulent energy is dissipated by viscous processes. The energy cascade is the mechanism by which energy is moved from the large scales to the small scales. For more information on the physics of turbulent flows, the reader should refer to Ref. [6].

Prediction of turbulent flow from the Reynolds-averaged (time-averaged) or Favre-averaged conservation equations requires closure approximations. This is because the time-averaged conservation equations contain terms that are not known. In the case of the momentum equations, the time averaging of the convection terms leads to the Reynolds stresses:  $\rho \overline{u'^2}$ ,  $\rho \overline{v'^2}$ ,  $\rho \overline{w'^2}$ ,  $\rho \overline{u'v'}$ ,  $\rho \overline{u'w'}$ ,  $\rho \overline{v'w'}$ .

Closure approximations are required to solve the Reynolds averaged conservation equations.

The workhorse turbulence model used in furnace simulations is the standard  $k$ - $\epsilon$  model.<sup>16</sup> The popularity of this model can be ascribed to its relative simplicity (e.g., compared to a Reynolds stress model) and its good performance in a variety of engineering flows. Its weaknesses include its performance in unconfined flows, in rotating and swirling flows, and in flows with large strains, such as curved boundary layers. The Reynolds stress model (RSM) addresses some of these performance issues. RSM is much more computationally demanding because it involves seven extra PDEs rather than the two of the  $k$ - $\epsilon$  model. However, in a typical combustion calculation, the number of PDEs solved



is typically quite large, so adding five more may be easily justified if the quality of the prediction improves.

A number of variants of the classical  $k$ - $\epsilon$  model exist. The classical  $k$ - $\epsilon$  model uses a single eddy viscosity in all directions. The nonlinear  $k$ - $\epsilon$  model by Speziale<sup>7</sup> addresses this assumption, which is known to be poor even in relatively simple flows. Another development in  $k$ - $\epsilon$  modeling is the renormalization group (RNG)  $k$ - $\epsilon$  model of Yakhot et al.<sup>8</sup> Its performance in complex flows has been promising, so much so that several of the commercial CFD code vendors have implemented the RNG  $k$ - $\epsilon$  model. The realizable  $k$ - $\epsilon$ <sup>9</sup> represents yet another variant recently introduced. The advantages and limitations of these turbulence models are discussed in more detail in Ref. [10].

Perhaps the most commonly used turbulence model for practical flow problems is the  $k$ - $\epsilon$  model. The earliest developments related to the  $k$ - $\epsilon$  model were by Chou,<sup>11</sup> Davidov,<sup>12</sup> and Harlow and Nakayama.<sup>13</sup> The most well-known paper on the  $k$ - $\epsilon$  model is that of Jones and Launder,<sup>14</sup> which according to Wilcox<sup>2</sup> has almost reached the status of the Boussinesq and Reynolds papers within the turbulence modeling community. The  $k$ - $\epsilon$  model is based on the turbulence kinetic energy transport equation discussed earlier, and a second transport equation for the dissipation rate. The equation for the dissipation rate ( $\epsilon$ ) is derived by taking a moment of the Navier–Stokes equation using the fluctuating vorticity.

Although several turbulence models have been proposed,<sup>15</sup> the  $k$ - $\epsilon$  turbulence model, originally proposed by Harlow and Nakayama,<sup>13</sup> remains the most widely used model to describe practical flow systems.<sup>7</sup> The  $k$ - $\epsilon$  turbulence model employs a modified version of the Boussinesq hypothesis

$$-\overline{u_i''u_j''} = -\nu_t \left( \frac{\partial \tilde{u}_i}{\partial x_j} + \frac{\partial \tilde{u}_j}{\partial x_i} \right) - \frac{2}{3} (\nu_t \nabla \cdot \vec{v} + k) \delta_{ij} \quad (13.15)$$

where  $\nu_t$  is known as the eddy diffusivity or turbulent viscosity. This approach allows the molecular viscosity to be replaced with the eddy (or turbulent) diffusivity, which allows the instantaneous transport equations (Equations 13.3 through 13.6) to be modeled using the mean-value equations (Equations 13.8 through 13.10). A disadvantage to this approach is the need to assume isotropic eddy diffusivity. However, given this assumption and the specific velocity- and length-scales ( $u'$ ,  $l'$ ):

$$\begin{aligned} u' &\approx \sqrt{k} \\ l' &\approx C_\mu \frac{k^{3/2}}{\epsilon} \end{aligned} \quad (13.16)$$

where the turbulent kinetic energy  $k$  can be defined as

$$k = \frac{1}{2} \overline{u_i u_i} = \frac{1}{2} (\overline{u_1 u_1} + \overline{u_2 u_2} + \overline{u_3 u_3}) \quad (13.17)$$

Given these definitions, additional transport equations for the turbulent kinetic energy  $k$  and the dissipation rate of turbulent kinetic energy,  $\epsilon$  can be written, respectively:

$$\begin{aligned} \frac{\partial k}{\partial t} + \vec{v} \cdot \nabla k &= \frac{1}{\rho} \nabla \cdot \left( \frac{\nu_t}{\sigma_k} \nabla k \right) + G - \epsilon \\ G &= \frac{\nu_t}{\sigma_k} \left[ 2 \nabla^2 \vec{v} + \sum_{i=1, i \neq j}^3 \sum_{j=1}^3 \left( \frac{\partial u_i}{\partial x_j} + \frac{\partial u_j}{\partial x_i} \right) \right] \end{aligned} \quad (13.18)$$

$$\frac{\partial \epsilon}{\partial t} + \vec{u} \cdot \nabla \epsilon = \frac{1}{\rho} \nabla \cdot \left( \frac{\nu_t}{\sigma_\epsilon} \nabla \epsilon \right) + f_1 c_1 G \left( \frac{\epsilon}{k} \right) - f_2 c_2 \left( \frac{\epsilon^2}{k} \right) \quad (13.19)$$

with the eddy viscosity defined as

$$\nu_t = \frac{f_\mu C_\mu k^2}{\epsilon} \quad (13.20)$$

Several key “empirical” constants are required by the  $k$ - $\epsilon$  turbulence model. An accepted set of constants is shown in Table 13.1.

These values are those originally proposed by Launder and Spalding,<sup>16</sup> but differ slightly from those reported by other researchers.<sup>15,17,18</sup> This may be because these constants are based on simple two-dimensional (2D) flows and adjustment may be required to simulate more complex flows. Regardless, this fact and the other simplifying assumptions suggest that the flow results be closely scrutinized when applying any CFD code using this turbulence model to simulate complex flow systems. The application of the  $k$ - $\epsilon$  turbulence model requires boundary conditions for both  $k$  and  $\epsilon$ .

Boundary layer theory could be used to derive the equations for flow near the wall, but to reduce computer storage and run times the  $k$ - $\epsilon$  turbulence model uses wall functions instead. The Van Driest hypothesis on turbulent flow near walls is used to derive wall functions consistent with the logarithmic law of the wall.<sup>16</sup> These functions relate the dependent variables near the

TABLE 13.1

Universal “Empirical” Constants Used in the Standard  $k$ - $\epsilon$  Turbulence Model

Constant	$C_\mu$	$C_1$	$C_2$	$\sigma_k$	$\sigma_\epsilon$	$\kappa$
Value	0.09	1.44	1.92	1.0	1.3	0.4187

TABLE 13.2

Cartesian Differential Equation Set

$\frac{\partial(\bar{\rho}\tilde{u}\phi)}{\partial x} + \frac{\partial(\bar{\rho}\tilde{v}\phi)}{\partial y} + \frac{\partial(\bar{\rho}\tilde{w}\phi)}{\partial z} - \frac{\partial}{\partial x}\left(\Gamma_\phi \frac{\partial(\phi)}{\partial x}\right) - \frac{\partial}{\partial y}\left(\Gamma_\phi \frac{\partial(\phi)}{\partial y}\right) - \frac{\partial}{\partial z}\left(\Gamma_\phi \frac{\partial(\phi)}{\partial z}\right) = S_\phi$			
Equation	$\phi$	$\Gamma_\phi$	$S_\phi$
Continuity	1	0	0
X-momentum	$\tilde{u}$	$\mu_e$	$-\frac{\partial p}{\partial x} + \frac{\partial}{\partial x}\left(\mu_e \frac{\partial \tilde{u}}{\partial x}\right) + \frac{\partial}{\partial y}\left(\mu_e \frac{\partial \tilde{v}}{\partial x}\right) + \frac{\partial}{\partial z}\left(\mu_e \frac{\partial \tilde{w}}{\partial x}\right) + \bar{\rho}g_x - \frac{2}{3}\bar{\rho}\tilde{k}$
Y-momentum	$\tilde{v}$	$\mu_e$	$-\frac{\partial p}{\partial y} + \frac{\partial}{\partial x}\left(\mu_e \frac{\partial \tilde{u}}{\partial y}\right) + \frac{\partial}{\partial y}\left(\mu_e \frac{\partial \tilde{v}}{\partial y}\right) + \frac{\partial}{\partial z}\left(\mu_e \frac{\partial \tilde{w}}{\partial y}\right) + \bar{\rho}g_y - \frac{2}{3}\bar{\rho}\tilde{k}$
Z-momentum	$\tilde{w}$	$\mu_e$	$-\frac{\partial p}{\partial z} + \frac{\partial}{\partial x}\left(\mu_e \frac{\partial \tilde{u}}{\partial z}\right) + \frac{\partial}{\partial y}\left(\mu_e \frac{\partial \tilde{v}}{\partial z}\right) + \frac{\partial}{\partial z}\left(\mu_e \frac{\partial \tilde{w}}{\partial z}\right) + \bar{\rho}g_z - \frac{2}{3}\bar{\rho}\tilde{k}$
Mixture fraction	Z	$\frac{\mu_e}{\sigma_f}$	0
Mixture fraction variance	$\tilde{g}$	$\frac{\mu_e}{\sigma_g}$	$-\frac{C_{g1}\mu_e}{\sigma_g} + \left[\left(\frac{\partial \tilde{f}}{\partial x}\right)^2 + \left(\frac{\partial \tilde{f}}{\partial y}\right)^2 + \left(\frac{\partial \tilde{f}}{\partial z}\right)^2\right] - C_{g2}\bar{\rho}\tilde{g}\frac{\tilde{\epsilon}}{\tilde{k}}$
Turbulent energy	$\tilde{k}$	$\frac{\mu_e}{\sigma_k}$	$G - \bar{\rho}\tilde{\epsilon}$
Dissipation rate	$\tilde{\epsilon}$	$\frac{\mu_e}{\sigma_\epsilon}$	$\left(\frac{\tilde{\epsilon}}{\tilde{k}}\right)(c_1G - c_2\bar{\rho}\tilde{\epsilon})$

where

$$G = \mu_e \left\{ 2 \left[ \left( \frac{\partial \tilde{u}}{\partial x} \right)^2 + \left( \frac{\partial \tilde{v}}{\partial y} \right)^2 + \left( \frac{\partial \tilde{w}}{\partial z} \right)^2 \right] + \left( \frac{\partial \tilde{u}}{\partial y} + \frac{\partial \tilde{v}}{\partial x} \right)^2 + \left( \frac{\partial \tilde{u}}{\partial z} + \frac{\partial \tilde{w}}{\partial x} \right)^2 + \left( \frac{\partial \tilde{v}}{\partial z} + \frac{\partial \tilde{w}}{\partial y} \right)^2 \right\}$$

wall to those in the bulk flow field. Given the turbulence model with the necessary boundary conditions, the full equation set may be written (Tables 13.2 and 13.3).

As shown, each equation is conveniently cast into a general convection–diffusion form with the off terms collected on the right-hand side (RHS), the specific terms depend on the coordinate system selected. Examining the  $\Theta$ -momentum equation (Table 13.3) helps illustrate the meaning of each term:

$$\begin{aligned} & r \frac{\partial(\bar{\rho}\tilde{u}\tilde{w})}{\partial x} + \frac{\partial(r\bar{\rho}\tilde{v}\tilde{w})}{\partial r} + \frac{\partial(\bar{\rho}\tilde{w}\tilde{w})}{\partial \theta} - r \frac{\partial}{\partial x} \left( \mu_e \frac{\partial \tilde{w}}{\partial x} \right) \\ & - \frac{\partial}{\partial r} \left( r \mu_e \frac{\partial \tilde{w}}{\partial r} \right) - \frac{\partial}{\partial \theta} \left( \frac{\mu_e}{r} \frac{\partial \tilde{w}}{\partial \theta} \right) = - \frac{\partial p}{\partial \theta} + r \frac{\partial}{\partial x} \left( \frac{\mu_e}{r} \frac{\partial \tilde{u}}{\partial \theta} \right) \\ & + \frac{\partial}{\partial r} \left( \mu_e \frac{\partial \tilde{v}}{\partial \theta} - \mu_e \tilde{w} \right) + \frac{\partial}{\partial \theta} \left[ \left( \frac{\mu_e}{r} \right) \left( \frac{\partial \tilde{w}}{\partial \theta} + 2r \frac{\partial \tilde{v}}{\partial r} \right) \right] \\ & + \mu_e \left( \frac{\partial \tilde{w}}{\partial r} + \frac{1}{r} \frac{\partial \tilde{v}}{\partial \theta} - \frac{\tilde{w}}{r} \right) - \bar{\rho}\tilde{v}\tilde{w} + r\bar{\rho}g_\theta \end{aligned} \quad (13.21)$$

The first three terms of Equation 13.21 represent the net rate of momentum addition to a volume element by convection from the three direction components.

The fourth, fifth, and sixth terms represent the corresponding diffusion terms. When the turbulence model solves for the individual Reynolds stresses, the diffusion terms do not only strictly represent molecular diffusion, but also include momentum contributions due to the turbulent motion of the fluid. The first term on the RHS of Equation 13.21 represents the pressure force on the volume element. All other terms on the RHS of the equation represent either a source or sink term for momentum (e.g., gravity force, centripetal forces, etc.)

#### 13.2.4.2 $k$ - $\epsilon$ Turbulence Model Boundary Conditions

Establishing boundary conditions for the  $k$ - $\epsilon$  turbulence model results from an order of magnitude analysis of the boundary layer momentum equation in the log layer. The log layer is an overlap region between the viscous sublayer and the defect layer, where the law of the wall applies. An order of magnitude analysis of the boundary layer momentum equation suggests that convection, pressure gradient, and molecular diffusion terms can be neglected. Applying these simplifications to the transport equations for  $k$  and  $\epsilon$  (13.18 and 13.19) results in relations for  $k$  and  $\epsilon$  at the boundaries, which are referred to as wall functions. The standard wall functions are given by the following two equations.

TABLE 13.3

Cylindrical Differential Equation Set

$$r \frac{\partial(\bar{\rho}\tilde{u}\phi)}{\partial x} + \frac{\partial(r\bar{\rho}\tilde{v}\phi)}{\partial r} + \frac{\partial(r\bar{\rho}\tilde{w}\phi)}{\partial \theta} - r \frac{\partial}{\partial x} \left( \Gamma_\phi \frac{\partial(\phi)}{\partial x} \right) - \frac{\partial}{\partial r} \left( r\Gamma_\phi \frac{\partial(\phi)}{\partial r} \right) - \frac{\partial}{\partial \theta} \left( \frac{\Gamma_\phi}{r} \frac{\partial(\phi)}{\partial \theta} \right) = S_\phi$$

Equation	$\phi$	$\Gamma_\phi$	$S_\phi$
Continuity	1	0	0
$r$ -momentum	$\tilde{u}$	$\mu_e$	$-r \frac{\partial p}{\partial x} + r \frac{\partial}{\partial x} \left( \mu_e \frac{\partial \tilde{u}}{\partial x} \right) + \frac{\partial}{\partial r} \left( r\mu_e \frac{\partial \tilde{v}}{\partial x} \right) + \frac{\partial}{\partial \theta} \left( \mu_e \frac{\partial \tilde{w}}{\partial x} \right) + r\bar{\rho}g_x - \frac{2}{3}r\bar{\rho}\tilde{k}$
$\theta$ -momentum	$\tilde{v}$	$\mu_e$	$-r \frac{\partial p}{\partial r} + r \frac{\partial}{\partial x} \left( \mu_e \frac{\partial \tilde{u}}{\partial r} \right) + \frac{\partial}{\partial r} \left( r\mu_e \frac{\partial \tilde{v}}{\partial r} \right) + \frac{\partial}{\partial \theta} \left( \mu_e \frac{\partial \tilde{w}}{\partial r} - \frac{\tilde{w}}{r} \right) - \frac{2\mu_e}{r} \frac{\partial \tilde{w}}{\partial \theta} - \frac{2\tilde{v}\mu_e}{r} + \bar{\rho}\tilde{w}^2 + r\bar{\rho}g_r - \frac{2}{3}\bar{\rho}\tilde{k}$
$z$ -momentum	$\tilde{w}$	$\mu_e$	$-\frac{\partial p}{\partial \theta} + r \frac{\partial}{\partial x} \left( \frac{\mu_e}{r} \frac{\partial \tilde{u}}{\partial \theta} \right) + \frac{\partial}{\partial r} \left( \mu_e \frac{\partial \tilde{v}}{\partial \theta} - \mu_e \tilde{w} \right) - \bar{\rho}\tilde{v}\tilde{w} + \frac{\partial}{\partial \theta} \left[ \left( \frac{\mu_e}{r} \right) \left( \frac{\partial \tilde{w}}{\partial \theta} - 2\tilde{v} \right) \right] + \mu_e \left( \frac{\partial \tilde{w}}{\partial r} + \frac{1}{r} \frac{\partial \tilde{w}}{\partial \theta} - \frac{\tilde{w}}{r} \right) + r\bar{\rho}g_\theta - \frac{2}{3}r\bar{\rho}\tilde{k}$
Mixture fraction	$\tilde{f}$	$\frac{\mu_e}{\sigma_f}$	0
Mixture fraction variance	$\tilde{g}$		$-\frac{C_{g1}\mu_e r}{\sigma_g} + \left[ \left( \frac{\partial \tilde{f}}{\partial x} \right)^2 + \left( \frac{\partial \tilde{f}}{\partial r} \right)^2 + \left( \frac{1}{r} \frac{\partial \tilde{f}}{\partial \theta} \right)^2 \right] - C_{g2}r\bar{\rho}\tilde{g} \frac{\tilde{g}}{\tilde{k}}$
Turbulent energy	$\tilde{k}$	$\frac{\mu_e}{\sigma_k}$	$r(G - \bar{\rho}\tilde{\epsilon})$
Dissipation rate	$\tilde{\epsilon}$	$\frac{\mu_e}{\sigma_\epsilon}$	$\left( r \frac{\tilde{\epsilon}}{\tilde{k}} \right) (c_1 G - c_2 \bar{\rho}\tilde{\epsilon})$

where

$$G = \mu_e \left\{ 2 \left[ \left( \frac{\partial \tilde{u}}{\partial x} \right)^2 + \left( \frac{\partial \tilde{v}}{\partial r} \right)^2 + \left( \frac{1}{r} \frac{\partial \tilde{v}}{\partial \theta} + \frac{\tilde{v}}{r} \right)^2 \right] + \left( \frac{\partial \tilde{u}}{\partial r} + \frac{\partial \tilde{v}}{\partial x} \right)^2 + \left( \frac{1}{r} \frac{\partial \tilde{u}}{\partial \theta} + \frac{\partial \tilde{w}}{\partial x} \right)^2 + \left( \frac{1}{r} \frac{\partial \tilde{v}}{\partial \theta} + \frac{\partial \tilde{w}}{\partial r} - \frac{\tilde{w}}{r^2} \right)^2 \right\}$$

Standard wall functions for  $k$ :

$$k = \frac{u_\tau^2}{\sqrt{C_\mu}} \quad (13.22)$$

Standard wall functions for  $\epsilon$ :

$$\epsilon = \frac{k^{3/2} C_\mu^{3/4}}{\kappa y} : \quad (13.23)$$

where

 $u_\tau$  is the friction velocity,  $u_\tau = \sqrt{\tau_w/\rho}$  $\tau_w$  is the wall shear stress $\kappa$  is the Kármán constant ( $\kappa \approx 0.4$ ) $y$  is the distance measured normal from the wall

The wall functions (13.22 and 13.23) are applied to the node adjacent to the wall, which should lie within the log layer region. The law of the wall equation (13.24) is used to find the friction velocity ( $u_\tau$ ) at the node adjacent to the wall, and then the wall functions are used to specify  $k$  and  $\epsilon$ .

$$U = u_\tau \left[ \frac{1}{\kappa} \ln \left( \frac{u_\tau y}{\nu} \right) + B_1 \right] \quad (13.24)$$

where

 $U$  is the mean velocity $\nu$  is the kinematic viscosity $B_1$  is a constant

If the surface is smooth, Equation 13.24 should be used; however, if the surface is not smooth, an equivalent equation to 13.24 is given by Equation 13.25 and was developed by Nikuradse. Equations 13.24 and 13.25 are given in most engineering fluid mechanics texts, such as Roberson and Crowe.<sup>19</sup>

$$U = u_\tau \left[ \frac{1}{\kappa} \ln \left( \frac{y}{k_s} \right) + B_2 \right] \quad (13.25)$$

where

 $k_s$  is the surface roughness height $B_2$  is a constant



Wilcox<sup>2</sup> notes that numerical solutions are sensitive to the location of the node adjacent to the surface and recommends using near-wall grids. Another potential problem with using wall functions is that theoretically they do not apply for flows that separate from the wall. Finally, Wilcox points out that the standard  $k$ - $\epsilon$  model with standard wall functions does not perform well for boundary layers with adverse pressure gradients. Kim and Choudhury<sup>20</sup> have proposed modifications to the standard  $k$ - $\epsilon$  wall functions to account for adverse pressure gradient.

### 13.2.5 Other Turbulence Modeling Approaches

The vorticity that characterizes turbulent flow has a large range of length and time scales that can exist in relatively close proximity to one another. When Reynolds-averaged Navier–Stokes (RANS) equations are utilized to simulate turbulent flow, all of the turbulent fluctuations are modeled using algebraic approximations rather than directly calculated which results in a significant reduction in computational requirements. Various other approaches exist that are used to compute the turbulent relationships that exist in flowing systems. Three of the more popular methodologies are known as direct numerical simulation (DNS), large-eddy simulation (LES)<sup>21</sup> and detached eddy simulation (DES). DNS can be categorically neglected for this class of problems because the computational demands are far in excess of current computational resources as an applicable tool for furnace simulations.<sup>22,23</sup> DNS looks at solving the Navier–Stokes equations over the complete range of time and length scales present in a particular system. Perhaps the greatest issue with DNS is that the computational domain must be big enough to accommodate the largest length scales present, with a grid small enough to allow for resolution of the smallest scales where kinetic energy dissipation occurs. This criterion insures that the number of grid points required to solve a problem of practical size will be quite large as compared to more conventional RANS type calculations. By way of example, the number of grid points required in each direction of a 3D calculation is proportional to  $Re^{3/4}$ , the Reynolds number based upon the magnitude of the velocity fluctuations and the integral scale. Hence, for  $Re = 10^6$  (which is not unusual for flows in typical engineering systems), the resulting grid requirement for a 3D simulation would be on the order of  $10^{13}$ . While the results of such calculations would contain very useful information, the current limits of available computer hardware make routine use of this approach to solve practical engineering problems prohibitive. In addition to the large grid requirements, the time scale required for this approach is constrained to very small time steps to capture the fluctuations at the very small end

of the range, which further increases the computational load. Currently, DNS is used to solve small, low-Reynolds number flow circumstances based upon simple geometries.

LES is positioned between DNS and the RANS approaches. This approach separates the range of length scales (eddies) into two groups. The first consists of relatively large eddies that can be numerically simulated and represent the majority of the turbulent energy. These are generally constrained more by boundary conditions and domain geometries. The second group is comprised of small eddies, which are more influenced by molecular viscous forces. The second group tends to be more isotropic and, therefore, it is easier to justify the use of numerical approximations to model them. Hence, the simulation rationale focuses upon the direct resolution of the large eddies and filtering out eddies smaller than some lower limit or smaller than the local grid resolution and allowing them to be modeled. A significant issue related to the utilization of the LES approach is the “communication” that must occur between the simulation of the two groups as large eddies degrade to smaller ones. The impact this has on grid requirements is that much coarser grids than are required by DNS can be used, although the grid requirements for LES are still much greater than for the Reynolds-/Favre-averaged approaches. The recent improvements in computer hardware performance have allowed this approach to be considered for engineering analysis.

---

## 13.3 Computational Fluid Dynamics–Based Combustion Submodels

This section discusses the modeling of combustion chemistry in petrochemical applications. The focus of this section is on methods for modeling the interaction of turbulence with combustion chemistry. This is an area of intense current research, and some of this research is briefly discussed as it pertains to current CFD calculations as well as near-future CFD calculations. There are several relatively new turbulence/chemistry interaction models (such as CMC and joint-probability density function [PDF] transport models) which are not currently available for use in any of the commercial CFD packages. We can hope that this situation will change soon and these models will be available for more widespread use.

### 13.3.1 Regimes of Turbulent Combustion

Damköhler numbers are ratios of a fluid dynamical time scale to a chemical time scale.<sup>24</sup> In a turbulent flow, there

are a variety of time scales, such as the integral scale (a convective scale) and the Kolmogorov scale (a viscous scale). There are also a variety of chemical time scales because of the many chemical reactions that accompany the combustion of even a simple molecule such as  $\text{CH}_4$ . Frequently, combustion problems are described as being in the high Damköhler or flamelet regime. The term flamelet is used because of the notion that within a turbulent non-premixed flame, the actual combustion reactions take place within small layers termed flamelets. These flamelets are so small that they are not affected by the turbulent motions within the fluid, instead molecular diffusion effects dominate and the structure of the reaction zone is that of a laminar flame (albeit a strained laminar flame). Following Bray,<sup>22</sup> the Damköhler number is defined as

$$\text{Da} = \frac{t_T}{t_\kappa} = \frac{ku_L^0}{\epsilon l_L^0} \quad (13.26)$$

where

The subscript  $L$  and superscript 0 refer to an unstretched laminar flame

The subscript  $T$  refers to the scale of the turbulence

In cases where non-premixed combustion is studied, it is common to use the velocity and length scales (the laminar premixed flame speed and thickness) as representative of the relevant chemical scales. The Karlovitz number is

$$\text{Ka} = \frac{t_L^0}{t_\kappa} = \frac{t_L}{\sqrt{\nu/\epsilon}} \quad (13.27)$$

where the subscript  $\kappa$  refers to the Kolmogorov time scale.

When the laminar flame time is less than the Kolmogorov scale (i.e.,  $\text{Ka} < 1$ ), the flame is considered to be a laminar flame stretched by a turbulent flow. Combustion in this regime is referred to as flamelet combustion. When the Damköhler number is less than one, the time scale of larger turbulent eddies has become smaller than the chemical time scale. In these conditions, the combustion process is described as a well-stirred reaction zone. For intermediate values of  $\text{Da}$  and  $\text{Ka}$ , combustion is said to occur in distributed reaction zones. This term indicates that the turbulent flow can affect the structure of the reaction zone, in contrast to the flamelet regime, but the turbulent mixing is not so fast that the reaction can be considered to occur under well-stirred conditions.

Using the relationships for the Damköhler number as described earlier, two physical limits have been

identified.<sup>25</sup> The first, referred to as the “frozen” limit, occurs when

$$\text{Da} \rightarrow 0 \quad (13.28)$$

In this case, the reaction time ( $t_r$ ) is much larger than the flow time ( $t_T$ ), and kinetic effects are negligible compared to mixing effects.

Conversely, the second limit, referred to as the “fast chemistry” limit, occurs when

$$\text{Da} \rightarrow \infty \quad (13.29)$$

In this case, the reaction time is very short (fast reactions) relative to the mixing time. Many diffusion flames in environments that shift the chemical equilibrium to the product side are approximated well by the latter limit. For high temperature combustion chemistry, it can be assumed that the homogeneous reaction kinetics are sufficiently fast so that gas mixing is controlling factor for the conversion of reactants to the products. This is commonly referred to as the “mixed-is-burnt” assumption.

Given the large disparity between short reaction time scales and long mixing time scales, chemical activity may be confined to an infinitesimally thin layer commonly referred to as a “flamelet” or “flamesheet”.<sup>26</sup> This assumption allows flame chemistry to be approximated using local thermodynamic equilibrium without significant error. This assumption is not valid for reactions that are considered slow as, for example, the formation of thermal  $\text{NO}_x$ . In these cases, the reaction time scale and the mixing time scale are of similar magnitude:

$$\text{Da} \approx O(1) \quad (13.30)$$

In order to get a satisfactory solution, the finite-rate chemistry must be coupled with the turbulent fluid mechanics calculations. Because turbulent effects must be included in the kinetic scheme, global mechanisms are generally used to avoid solving individual transport equations for each species in a detailed kinetics mechanism.

In general, a differentiation has to be made for types of flames as there are

- Premixed
- Partially premixed
- Non-premixed or diffusion flames

Depending on the Reynolds, Damköhler, and Karlovitz numbers, a further separation has to be made in laminar, turbulent, wrinkled, corrugated flames, and homogeneous reaction zones.<sup>27</sup> Since almost every flow regime

in a technical combustion application is highly turbulent, the laminar flame modeling will not be included in this discussion. Further information on laminar reaction systems can be found in Kee et al.,<sup>28,29</sup> Glarborg et al.,<sup>30</sup> and Rogg.<sup>31–33</sup>

The type of turbulent flame to be modeled determines the combustion submodel to be used.

For the premixed flames, the models available are

- Progress variable,  $C$
- Transport equation for the flame front,  $G$
- Eddy break up (EBU), Eddy dissipation combustion model (EDX), and the eddy dissipation concept (EDC)

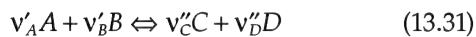
For non-premixed combustion, the models available are

- Presumed PDF with equilibrium chemistry (adiabatic and nonadiabatic)
- Presumed PDF with finite rate chemistry (flamelet model)
- EBU, EDX, and EDC

Turbulent premixed flames have proven to be much more difficult to model than their non-premixed counterparts.<sup>34</sup> In a turbulent, mixing-limited non-premixed flame, the flame structure is governed by turbulent mixing, a reasonably well-understood phenomena. The ideal turbulent premixed flame consists of a flame sheet propagating at some flame speed with respect to the fluid around it, which is itself undergoing turbulent motions. The consequence of superposing flame propagation and turbulent fluid motions is that premixed flame modeling is much more challenging than non-premixed flames.<sup>23</sup> For this reason, most commercial CFD codes only include limited support for premixed flame modeling.

### 13.3.2 Reaction Kinetics

The general form for a reaction with educts  $A$  and  $B$  and the products  $C$  and  $D$  can be written as



where  $v_i$  is the stoichiometric coefficient.

The reaction rate can formally be written as the product of the reaction rate coefficient and all participating species.

$$r_i = \left( \frac{dc_i}{dt} \right) = k c_1^{a_1} c_2^{a_2} c_3^{a_3} \cdots c_N^{a_N} \quad (13.32)$$

with the reaction coefficient  $k$ , the reaction order  $a_i$ , and the species  $c_i$ , where the concentration of each species  $i$  is defined as

$$c_i = \frac{\rho_i Y_i}{M} \quad (13.33)$$

with  $M$  as the mean molar mass of the mixture. The rate coefficient  $k$  can be written in general form as

$$k = A T^m e^{\left( -\frac{E_A}{RT} \right)}, \quad (13.34)$$

with  $R$  as the gas constant (8.3143 kJ/mol K). The parameters here are the pre-exponential Arrhenius factor  $A$ , the temperature exponent  $m$ , and the activation energy  $E_A$ .

The final formulation for a concentration change of species  $i$ , over all elementary reactions  $k$  can be formulated as

$$\frac{\partial c_i}{\partial t} = \sum_{k=1}^M (v''_{i,k} - v'_{i,k}) (A T^m)_k \exp\left(-\frac{E_k}{RT}\right) \prod_{j=1}^N \left( \frac{\rho Y_j}{W_j} \right)^{v'_{j,k}} \quad (13.35)$$

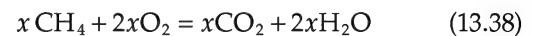
or written as reaction rate:

$$\frac{\partial c_i}{\partial t} W_i = \dot{Y}_i = W_i \sum_{k=1}^K v_{i,k} r_k \quad (13.36)$$

Finally, the additional source term for the equation for energy conservation. The total released energy can be written as the sum of the product of reaction enthalpy  $H$  and the concentration change of species  $i$ .

$$q_r = \sum_{k=1}^K q_k = \sum_{k=1}^K \left( \frac{\Delta H_k}{v_{i,k}} \right) \left( \frac{dc_i}{dt} \right)_k = - \sum_{i=1}^N h_i \omega_i \quad (13.37)$$

These equations are generally valid for all reaction mechanisms, either for a model with a detailed reaction mechanism including hundreds of reactions or a simplified global reaction as, for example, the conversion of methane:



The difficulty at hand for the formulation of a global reaction mechanism lies in the fact that the Arrhenius parameters as described earlier become unavailable for a global reaction, since a global reaction tries to describe a process that includes a large number of elementary reactions and intermediate species.



However, there are well-documented sources<sup>35</sup> for the formulation of Arrhenius parameters of global reactions for the combustion of hydrocarbon fuels.

The implementation of a reaction mechanism into a CFD model requires the formulation of a transport equation of the mass fraction of any species involved in the combustion model setup.

The equation governing the species transport is

$$\frac{\partial}{\partial t} \rho Y_i + \nabla \cdot (\rho \vec{u} Y_i) = \nabla \cdot (\rho D_i \nabla Y_i) + \dot{Y}_i \quad (13.39)$$

with  $\dot{Y}_i$  the source term of the species  $i$ . The determination of that source term can be done according to aforementioned equations, or due to the complexity and number of involved species using approaches, which reduce the computational effort.

### 13.3.3 Eddy Breakup Model

The eddy break up (EBU) model was developed by Spalding<sup>36</sup> for the calculation of turbulent, premixed flame with irreversible one-step reaction. The assumption was that the rate of reaction is totally controlled by dissipation of eddies either containing unburned fuel or burned hot gases. The reaction rate of the unburned mixture  $\dot{Y}_{Fv}$  as to be used in Equation 13.37 is determined by the decay rate of these eddies.

$$\dot{Y}_{F,eddy} = C(1 - \tau) \rho \left| \frac{du}{dy} \right| \quad (13.40)$$

following the mixing length hypothesis.

In order to estimate the actual rate of fuel consumption, we have to take into account the kinetically controlled reaction rate as defined by

$$\dot{Y}_{F,kin} = A Y_F Y_{O_2} \exp\left(\frac{-E_A}{RT}\right) \quad (13.41)$$

where

$A$  is the pre-exponential factor

$E_A$  is the activation energy

$R$  is the gas constant

The actual rate of fuel consumption can be determined by

$$\dot{Y}_{F,actual} = \frac{1}{\frac{1}{\tau \dot{Y}_{kin}} + \frac{1}{\dot{Y}_{eddy}}} \quad (13.42)$$

The major drawback of this approach is the assumption of homogeneous distribution and perfect mixing of fuel

and oxidant. The formulation would only be valid for a turbulent, premixed flame with homogeneous distribution of fuel/air and flue gas pockets.

### 13.3.4 Eddy Dissipation Combustion Model

A development of the EBU model is the eddy dissipation combustion (EDX) model formulated by Magnussen and Hjertager.<sup>37</sup> He takes into account the unmixedness of fuel and oxidizer and postulates that the rate of combustion will be determined by the turbulent intermixing of fuel and oxygen eddies on a molecular scale, or in other words by dissipation of these eddies. The reaction rate can be written down in general form as

$$\dot{Y}_i = C \bar{Y}_i \frac{\epsilon}{k} \quad (13.43)$$

where

$C$  is a constant depending on the structure of the flame

$\bar{Y}_i$  is the time-averaged concentration

This approach acknowledges the distribution and unmixedness of fuel oxidizer and hot products, and is therefore valid also for the calculation of non-premixed flames. The actual reaction rate is determined by the minimum of these criteria:

The reaction rate is determined by the following:

1. The concentration of fuel

$$\dot{Y}_F = A \bar{Y}_F \frac{\epsilon}{k} \quad (13.44)$$

where

$A = 4.0$

$\bar{Y}_F$  is the time-averaged fuel concentration

2. The reaction rate is determined by the concentration of oxygen

$$\dot{Y}_{O_2} = A \frac{\bar{Y}_{O_2}}{r_{O_2}} \frac{\epsilon}{k} \quad (13.45)$$

with  $Y_{O_2}$  the local mean oxygen concentration and  $r_{O_2}$  the stoichiometric oxygen requirement.

3. The reaction rate is limited by the presence of hot products

$$\dot{Y}_{Pr} = AB \frac{\bar{Y}_{Pr}}{1 + r_{O_2}} \frac{\epsilon}{k} \quad (13.46)$$

with  $A = 4.0$ ,  $B = 0.5$ ,  $\bar{Y}_{Pr}$  the local mean product concentration, and  $r_{O_2}$  the stoichiometric oxygen requirement.

### 13.3.5 Eddy Dissipation Concept

The disadvantage of the EDX approach is the fact that still global reactions have to be used. An extension of these models is the EDC.<sup>38</sup> This model is still based on the eddy dissipation along the turbulent energy cascade, but differentiates between areas of chemical reaction—the so-called fine structure region and their surrounding non-reactive regions. These fine structures are situated at the end of the turbulent energy cascade. There, length scale is that of eddies in Kolmogorov scale, where the species are mixed on a molecular level and react as the energy level meets their respective activation energy. The chemistry inside of these fine structures can be treated as perfectly stirred reactor.

This model takes into account that the dissipation is not homogeneously distributed in the computational domain, but takes place mainly in strained areas, the separating area from the reacting and non-reacting volumes. Magnussen proposes the following definition for the mass fraction contained in these fine structures:

$$\gamma = \left( \frac{u^*}{u'} \right)^3 \quad (13.47)$$

where

$u^*$  is the characteristic velocity of the fine structure  
 $u'$  is the turbulent velocity

Any mass transfer from surrounding non-reacting fluid into these fine structures follows the expression

$$\dot{m} = 2 \frac{u^*}{L^*} \gamma^* \quad (13.48)$$

where the characteristic velocity  $u^*$  and the characteristic length  $L^*$  can be expressed with

$$u^* = 1.74 (\nu \epsilon)^{1/4} \quad (13.49)$$

and

$$L^* = 1.43 \frac{\nu^{3/4}}{\epsilon^{1/4}} \quad (13.50)$$

where

$\nu$  is the kinematic viscosity  
 $\epsilon$  is the rate of dissipation of turbulent energy

Assuming isotropic turbulence, the mass fraction of the fine structure and the mass transfer between the fine structure and the surrounding can be written as

$$\gamma^* = 9.7 \left( \frac{\nu \epsilon}{k^2} \right)^{3/4} \quad (13.51)$$

and for the mass transfer

$$\dot{m} = 23.6 \left( \frac{\nu \epsilon}{k^2} \right)^{1/4} \frac{\epsilon}{k} \quad (13.52)$$

If we assume that the reactions inside of the fine structures are infinitely fast, the mass transfer between the surrounding fluid and the fine structure itself limits the reaction rate. Therefore, the rate of reaction can be written depending on the mass transfer

$$\dot{Y}_F = 23.6 \left( \frac{\nu \epsilon}{k^2} \right)^{1/4} \frac{\epsilon}{k} \bar{Y}_{\min} \quad (13.53)$$

where  $\bar{Y}_{\min}$  is the smallest concentration of  $Y_F$  or  $Y_{O_2}$ , limiting the reaction rate. It cannot be assumed that all fine structures are on the same temperature level, so the concentration of hot products has to be taken into account. A correction factor

$$\chi = \frac{\bar{Y}_{Pr} / (1 + r_{O_2})}{\bar{Y}_{Pr} / (1 + r_{O_2}) + Y_F} \quad (13.54)$$

is introduced and the final expression for the reaction rate is

$$\dot{Y}_F = 23.6 \left( \frac{\nu \epsilon}{k^2} \right)^{1/4} \frac{\epsilon}{k} \chi \bar{Y}_{\min} \quad (13.55)$$

The main advantage of this approach is the possibility to include elementary reactions to describe the kinetics within the fine structures. Since any given set of reactions has only to be solved within these small regions, the computational time can be reduced significantly.

### 13.3.6 Mixture Fraction Approach for Equilibrium or Finite Rate Chemistry

Another modeling approach is the PDF-approach with finite rate or equilibrium chemistry. The mixture fraction concept plays a central role in reducing a turbulent nonpremixed flame to a mixing problem. The mixture fraction is a conserved scalar, meaning that it is convected and diffused by fluid motions and gradients, but it is neither created nor destroyed. The mixture fraction,  $Z$  represents the mass fraction of fluid at a particular location that originated with the fuel stream. The pure fuel stream then will have  $Z = 1$ , while the oxidant stream will have  $Z = 0$ .

In a turbulent flow, the mixture fraction  $Z$  fluctuates at a given point with time. A PDF for these fluctuations can be defined so that the probability of  $Z$  lying between some value  $x$  and  $x + dx$  is  $P(x)dx$ .

This approach is often applied to turbulent flames using a presumed PDF for the mixture fraction. The schematics for an adiabatic calculation are shown in Refs. [39,40].

The mixture fraction  $Z$  is defined as an element mass fraction of matter originating from the fuel stream. It is a so-called conserved scalar, because elements are conserved during combustion and it is not influencing directly the underlying fluid mechanics. The element mass fraction of an element  $i$  in an  $N$ -species mixture, is

$$Z_i = \sum_{j=1}^N a_{ji} Y_j \frac{M_i^{atom}}{M_j}, \quad (13.56)$$

where

$a_{ij}$  is the number of atoms  $i$  in species  $j$

$M_j$  is the molecular weight of species  $j$

$M_i^{atom}$  is the atomic mass of atom  $i$

The mixture fraction  $Z$  is defined as linear combination of  $Z_i$ , where it is 0 in the oxidizer stream and 1 in the fuel. In a two-feed system with a fuel stream mass flow  $\dot{m}_1$  and an oxidizer stream mass flow  $\dot{m}_2$ , the mixture fraction represents the mass fraction of the fuel stream locally in the unburned mixture

$$Z = \frac{\dot{m}_1}{\dot{m}_1 + \dot{m}_2} = \frac{Z_F}{Y_{F,1}} = 1 - \frac{Z_O}{Y_{O_2,2}} \quad (13.57)$$

where

$Y_{F,1}$  is the mass fraction of fuel in the fuel stream

$Y_{O_2,2}$  is the mass fraction of oxygen in the oxidizer stream

$Z_F$  and  $Z_O$  are the fuel element mass fraction coming from the fuel and respectively coming from the oxidizer stream. The fuel element mass fraction  $Z_F$  is equivalent to the sum of fuel atoms. In the case of hydrocarbon combustion, it is equal to

$$Z_F = Z_C + Z_H \quad (13.58)$$

The mixture fraction in the presence of combustion can be written as

$$Z = \frac{\nu Y_F - Y_{O_2} + Y_{O_2,2}}{\nu Y_{F,1} - Y_{O_2,2}} \quad (13.59)$$

For the case of a stoichiometric mixture with  $\nu Y_F = Y_{O_2}$ , the stoichiometric mixture fraction  $Z_{st}$  can be calculated via

$$Z_{st} = \frac{Y_{O_2,2}}{\nu Y_{F,1} - Y_{O_2,2}} = \left[ 1 + \frac{\nu Y_{F,1}}{Y_{O_2,2}} \right]^{-1} \quad (13.60)$$

In order to include this approach into a CFD model, two additional equations have to be solved. The first one is the conservation equation for the mixture fraction  $Z$

and the second one is the conservation equation for the mixture fraction variance  $Z''$ .

The transport equation for the mixture fraction  $Z$  as it is represented in a flow simulation

$$\begin{aligned} & \frac{\partial(\rho u Z)}{\partial x} + \frac{\partial(\rho v Z)}{\partial y} + \frac{\partial(\rho w Z)}{\partial z} \\ & = \left( D_f + \frac{\mu_t}{Sc_f} \right) \left( \frac{\partial^2 Z}{\partial x^2} + \frac{\partial^2 Z}{\partial y^2} + \frac{\partial^2 Z}{\partial z^2} \right) = 0 \end{aligned} \quad (13.61)$$

and the transport equation for the mixture fraction variance  $Z''$

$$\begin{aligned} & \frac{\partial(\rho u g)}{\partial x} + \frac{\partial(\rho v g)}{\partial y} + \frac{\partial(\rho w g)}{\partial z} - \left( D_g + \frac{\mu_t}{Sc_g} \right) \left( \frac{\partial^2 g}{\partial x^2} + \frac{\partial^2 g}{\partial y^2} + \frac{\partial^2 g}{\partial z^2} \right) \\ & = 2 \frac{\mu_t}{Sc_g} \left( \frac{\partial Z}{\partial x} + \frac{\partial Z}{\partial y} + \frac{\partial Z}{\partial z} \right)^2 - 2\rho \frac{\epsilon}{k} g \end{aligned} \quad (13.62)$$

The PDF integration is commonly done by a presumed PDF, using the  $\beta$ -PDF. Other PDF shapes such as a clipped Gaussian function and a double delta function are discussed in Ref. [18]. The equilibrium chemistry assumption is poor in flames that are lifted or flames near extinction.

The  $\beta$ -function is defined as

$$\text{Beta}(\alpha, \chi) = \frac{\Gamma(\alpha)\Gamma(\chi)}{\Gamma(\alpha + \chi)}, \quad (13.63)$$

where

$$\alpha = Z \left( \frac{Z(1-Z)}{Z''^2} - 1 \right) \quad (13.64)$$

and

$$\beta = (1-Z) \left( \frac{Z(1-Z)}{Z''^2} - 1 \right) \quad (13.65)$$

with

$$\Gamma(\varphi) = \int_0^\infty t^{\varphi-1} e^{-t} dt \quad (13.66)$$

The shape of the  $\beta$ -function is shown in Figure 13.7.

This graph shows the distribution for some values of mixture fraction and several values for the mixture fraction variance  $Z''$ .



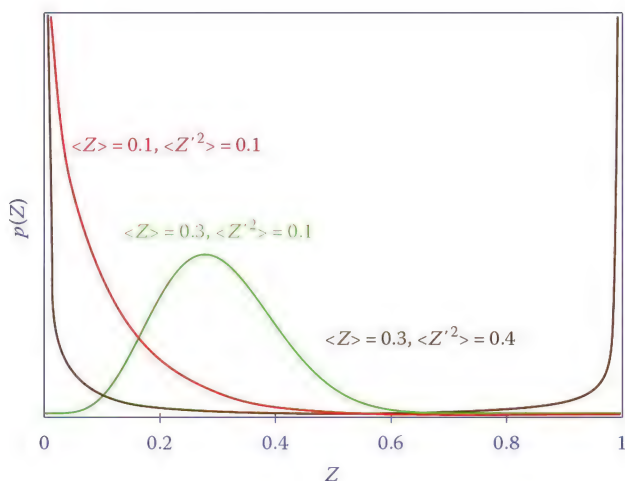


**FIGURE 13.7**  
Plot of the  $\beta$ -function for several values of  $Z$  and  $Z''$ .

The mass fraction of any species and the temperature distribution after integration over  $\beta$ -function can be determined with

$$\tilde{Y}(Z, Z'') = \int Y(Z) P(Z, Z'') dz \quad (13.67)$$

and

$$\tilde{T}(Z, Z'') = \int T(Z) P(Z, Z'') dz \quad (13.68)$$

A graph of the calculated temperatures of a methane–air flame for different variances  $Z''$  can be found elsewhere.<sup>41</sup>

An alternative to the equilibrium chemistry discussion in the previous paragraph is the laminar flamelet model. In this model, the relationship between the state of the mixture and the mixture fraction  $f$  is determined by a laminar diffusion flame calculation. Peters<sup>42</sup> introduced this idea, which assumes that the reaction length scale,  $L_R$ , is much smaller than the Kolmogorov length scale,  $L_K$ . Bilger<sup>43</sup> has criticized the classical flamelet method, claiming that for most nonpremixed flames of interest, the flamelet criterion,  $L_R < L_K$ , is violated. Bish and Dahm<sup>44</sup> discuss the concept further and attempt to eliminate what they view as a key limitation of the method: its assumption that the reaction layers are bounded by pure fuel on one side and pure oxidizer on the other. Their strained dissipation and reaction layer (SDRL) model is based on the one-dimensionality of the reaction layer, but does not assume the reaction layer to be thin relative to the dissipative scales.

The classical flamelet model's assumption that the reaction zones are bounded by pure fuel on one side and pure oxidizer on the other is severe in light of the  $\text{NO}_x$  control strategies used in practical combustion systems.  $\text{NO}_x$  control is predicated on entraining cooled combustion products into the reaction zone, and the proportion

of these gases entrained varies along the length of the flame. The effect of this flue gas entrainment is to reduce flame temperatures and dilute the reactants. Both of these effects are effective at reducing  $\text{NO}_x$  formation.

Research of models of non-premixed combustion continues at a fervent pace. Pope's<sup>34</sup> joint PDF methods appear promising because they have the ability to treat finite rate kinetics and eliminate the closure problems. Bilger's<sup>45</sup> conditional moment closure (CMC) method also is a promising model for nonpremixed combustion modeling. Both of these models are applicable to premixed combustion as well.<sup>22</sup> These models are still subjects of active research and academic debate. It does not appear that these models have been implemented in any of the commercial CFD packages at this time.

### 13.3.7 Pollutant Chemistry Models

Pollutant emissions are among the most important drivers for the development of an improved burner design or furnace layout. The permitted emission levels of  $\text{NO}_x$  and  $\text{SO}_x$  from petrochemical plants and refineries continue to decrease. To respond to this challenge, burner manufacturers strive to develop burners that produce lower and lower emissions. In addition, furnace manufacturers and other vendors develop post-combustion technologies such as SCR (selective catalytic reduction) and SNCR (selective non-catalytic reduction) to reduce  $\text{NO}_x$  in the stack (see Chapter 15 and Volume 3). Sulfur scrubbers are used to reduce  $\text{SO}_x$  levels in stack gases.

Two different models for the turbulence/chemistry interaction are proposed by Pope (see, e.g., Pope<sup>34</sup>) and Bilger.<sup>45</sup> The PDF model described in this paper is not the assumed-PDF discussed at length earlier. This method solves for the transport and production of the scalar joint PDF and is extremely computationally expensive since a Monte Carlo solution algorithm must be used. There is a particularly interesting comment in the introduction of that article that says, "a realistic target for agreement between experiment and prediction might be  $\pm 20\%$  and  $\pm 30\%$ ." The flame studied in this paper is a simple diluted hydrogen jet flame. If the most sophisticated turbulence/chemistry models currently under research applied to a very simple flame in a very simple geometry can only be expected to yield an accuracy of  $\pm 30\%$ , then how accurately can  $\text{NO}_x$  emissions be predicted?

## 13.4 Radiation Models

Radiative transport from a non-gray gas (the products of combustion) to the furnace walls and tubes (with the process fluid flowing inside) whose emissivity is temperature

dependent is the primary mode of heat transfer. The interaction between these physical processes is of considerable importance. The turbulence/chemistry interaction has been well studied for many years, particularly for non-premixed systems. More recently, the interaction between turbulence and radiative emission from a non-gray gas with properties has been studied.<sup>46</sup>

Typical petrochemical furnaces consist of a radiant section and a convection section. These regions are so named because of the dominant mode of heat transfer. In the radiant section, refractory surface temperatures can be higher than 2200°F (1200°C). Radiant heat is incident on the process tubes both from the high temperature surfaces and directly from the flame. Accurate modeling of the heat delivered to the process fluid requires an accurate prediction of the radiant intensity inside the furnace. In addition, accurate prediction of radiation from the flame is necessary to accurately predict emissions. For example, Barlow<sup>47</sup> notes that the different radiation models can affect NO<sub>x</sub> predictions as much as the different turbulence/chemistry interaction models evaluated in the paper.

Thermal radiation transport presents a difficult problem because of the number of independent variables. The radiation transport equation (RTE) describes radiation transport in an absorbing, emitting, and scattering media. The equation is<sup>48</sup>

$$\frac{\partial I_{\lambda}}{\partial s} = \kappa_{\lambda} I_{b\lambda} - \beta_{\lambda} I_{\lambda} + \frac{\sigma_{s\lambda}}{4\pi} \int_{4\pi} I_{\eta}(\vec{s}_i) \Phi(\vec{s}_i, \vec{s}) d\Omega_i \quad (13.69)$$

Radiant intensity is a function of location, (three coordinates in a 3D problem) direction, (two angular independent variables), and wavelength (one independent variable varying from 0 to infinity). This means that the problem of radiative transport is a 6D problem. A common approach is to remove the wavelength dependence by making gray media approximations (see Chapter 7).

There are many solution methods in solving the general RTE equation. Here, we provide a brief introduction to the major methods and especially those having close relationships with CFD simulations in petrochemical furnaces.

#### 13.4.1 P-1 Radiation Model

The P-1 radiation model is basically the general P-N approximation<sup>61</sup> when N is set to one, which is the lowest-order form of P-N formulation. Although there are higher-order applications like P-3<sup>60</sup> in relatively simple geometries, P-1 is the most popular method since it reduces the RTE equation to a relatively simple PDE by expressing radiative intensity with generalized Fourier series and spherical harmonics.<sup>64</sup>

The P-1 model may take into account scattering effects and could produce reasonable results with optically

thick media. Fortunately, most combustion applications are in this optically thick range. However, the P-1 method may have significant inaccuracy in optically thin media and at the same time with strongly anisotropic characteristics, especially when surface emission is much stronger than media emission.

For example, it was pointed out by Sazhin et al.,<sup>57</sup> that the P-1 model overestimates the radiative heat fluxes from localized heat sources in optically thin media. On the other hand, they also concluded that P-1 model is capable of accounting for the radiative exchange between gas and particles. The results of coal combustion simulation in an industrial furnace using the P-1 model are shown to be in reasonable agreement with the experimental observations.

#### 13.4.2 Discrete Ordinates Radiation Model

The discrete ordinates method, also called S<sub>N</sub>-method was first proposed and developed by Chandrasekhar<sup>49,50</sup> as an analytic approach in his research on atmospheric radiative transfer. The method was then extensively investigated and applied to neutron transport field by Lathrop et al.<sup>51</sup> With the fast development of petroleum and power generation industries, accurate calculation of radiative heat transfer in emitting, absorbing, and scattering media became more and more important. This led to early studies and applications of the discrete ordinates method in radiative heat transfer problems during the 1970s to 1980s, mainly by the works of Fiveland and coworkers<sup>52–56</sup> as well as Truelove and coworkers.<sup>57,58</sup>

The discrete ordinates method transforms the RTE equation into a set of simultaneous PDEs; Modest provided detailed evolution of the theory and extensive discussions in his book. To simplify the problem, consider a gray medium where all equations are valid with spectral dependent cases as well. Equation 13.67 then takes the following form:

$$\frac{dI(r, \vec{s})}{ds} = k(r)I_b(r) - \beta(r)I(r, \vec{s}) + \frac{\sigma(r)}{4\pi} \int_{4\pi} I(r, \vec{s}') \Phi(r, \vec{s}', \vec{s}) d\Omega' \quad (13.70)$$

In the previous equation, the radiative intensity  $I$  is a function of  $r$  and direction vector  $\vec{s}$ , here  $r$  represents the position including three space coordinates ( $x$ ,  $y$ , and  $z$ ) and  $\vec{s}$  is the unit vector of the intensity direction including two direction coordinates ( $\theta$ ,  $\phi$ ) in  $4\pi$  solid angle. Here,  $\beta$  is the extinction coefficient;  $\sigma$  is the scattering albedo of the medium; and  $\Phi$  is the scattering phase function.

Using the discrete ordinates method, Equation 13.68 will be solved along a number of specified directions  $\vec{s}_i$  ( $i = 1, 2, 3, \dots, n$ ) and the whole  $4\pi$  solid angle integral term will be replaced by numerical quadrature.

This results in the following equations instead of Equation 13.68:

$$\frac{dI(r, \vec{s}_i)}{ds_i} = k(r)I_b(r) - \beta(r)I(r, \vec{s}_i) + \frac{\sigma(r)}{4\pi} \sum_{j=1}^n w_j I(r, \vec{s}_j) \Phi(r, \vec{s}_i, \vec{s}_j), \quad i = 1, 2, 3, \dots, n \quad (13.71)$$

where,  $w_j$  in the previous equation is the quadrature weight. The direction  $\vec{s}_i$  in  $4\pi$  solid angles could be expressed as

$$\begin{aligned} \vec{s}_i &= \cos(\vec{s}_i, \vec{x}) \cdot \vec{x} + \cos(\vec{s}_i, \vec{y}) \cdot \vec{y} + \cos(\vec{s}_i, \vec{z}) \cdot \vec{z} \\ &= \xi_i \cdot \vec{x} + \eta_i \cdot \vec{y} + \mu_i \cdot \vec{z} \end{aligned} \quad (13.72)$$

Here,  $\vec{x}$ ,  $\vec{y}$ , and  $\vec{z}$  are principal unit vectors. Once the intensities in specified ordinate directions in  $4\pi$  solid angle are obtained, the radiative heat flux and incident radiation could be calculated by their definition formulas as follows:

$$\vec{q}(r) = \int_{4\pi} I(r, \vec{s}) \vec{s} d\Omega \equiv \sum_{i=1}^n w_i I_i(r) \vec{s}_i \quad (13.73)$$

$$G(r) = \int_{4\pi} I(r, \vec{s}) d\Omega \equiv \sum_{i=1}^n w_i I_i(r) \quad (13.74)$$

Please note that the heat flux is a vector with magnitude and direction. In Cartesian coordinates, the three components are expressed as

$$\begin{aligned} q_x(x, y, z) &= \int_{4\pi} I(x, y, z, \vec{s}) \cdot \cos(\vec{s}, \vec{x}) \cdot d\Omega \\ &\equiv \sum_{i=1}^n w_i I_i(x, y, z) \cdot \cos(\vec{s}_i, \vec{x}) \end{aligned} \quad (13.75)$$

$$\begin{aligned} q_y(x, y, z) &= \int_{4\pi} I(x, y, z, \vec{s}) \cdot \cos(\vec{s}, \vec{y}) \cdot d\Omega \\ &\equiv \sum_{i=1}^n w_i I_i(x, y, z) \cdot \cos(\vec{s}_i, \vec{y}) \end{aligned} \quad (13.76)$$

$$\begin{aligned} q_z(x, y, z) &= \int_{4\pi} I(x, y, z, \vec{s}) \cdot \cos(\vec{s}, \vec{z}) \cdot d\Omega \\ &\equiv \sum_{i=1}^n w_i I_i(x, y, z) \cdot \cos(\vec{s}_i, \vec{z}) \end{aligned} \quad (13.77)$$

Usually the more directions that are chosen or the higher the order of discrete ordinates, the more accurate the results will be, but at a much higher cost of computational resources and slower convergence speed. Several different sets of directions and weights based

**TABLE 13.4**

Discrete Ordinates for the  $S_N$  Approximation ( $N = 2, 4$ , and  $6$ )

Order of Approximation	Ordinates		Weights	
	$\xi$	$\eta$	$\mu$	$w$
$S_2$ (symmetric)	0.5773503	0.5773503	0.5773503	1.5707963
$S_2$ (nonsymmetrical)	0.5000000	0.7071068	0.5000000	1.5707963
$S_4$	0.2958759	0.2958759	0.9082483	0.5235987
	0.2958759	0.9082483	0.2958759	0.5235987
	0.9082483	0.2958759	0.2958759	0.5235987
	0.1838670	0.1838670	0.9656013	0.1609517
$S_6$	0.1838670	0.6950514	0.6950514	0.3626469
	0.1838670	0.9656013	0.1838670	0.1609517
	0.6950514	0.1838670	0.6950514	0.3626469
	0.6950514	0.6950514	0.1838670	0.3626469
	0.9656013	0.1838670	0.1838670	0.1609517
	0.9656013	0.1838670	0.1838670	0.1609517

Source: Modest, M.F., *Radiative Heat Transfer*, McGraw-Hill, New York, 1993.

on different principles can be found in the literature.<sup>59,60</sup> Generally, there are three criteria of the 0th, first, and second moments to satisfy. Table 13.4 showing  $S_2$ ,  $S_4$ , and  $S_6$  approximations is reproduced from Modest.<sup>61</sup>

The beauty of the discrete ordinates method is that it can be carried out to any higher order and accuracy. But as a consequence of the spatial discretization technique, similar to the “numerical diffusion” in CFD calculations, the discrete ordinates method may cause “false scattering” leading to physically unrealistic solutions. Also, as the consequence of angular discretization approach, discrete ordinates can have the so-called “ray effect.” Between two ordinate directions, there may be some control volumes that do not receive any energy from distant emission sources. Both false scattering and the ray effect may lead to physically impossible results. By refining the control volume mesh and increasing discrete ordinate directions (higher order), both numerical errors can be reduced.

So far, a brief introduction to the standard form of discrete ordinates method has been presented. This standard form is hard to implement into fluid dynamics flow and heat transfer computations. One of the several reasons is that it is difficult to apply to irregular geometries, because it is hard to find a set of directions and weights to calculate heat fluxes at irregular wall boundaries without errors. In order to overcome those difficulties, it is logical for people to use the finite volume method, or a modified discrete ordinates method in radiation calculation for reacting flow simulations. The finite volume method is easier to implement into the control volume CFD scheme and combined heat transfer problems.

The finite volume method actually calculates the solid angle integral term by exact integration through a fully finite volume approach in direction. By doing so, the energy is conservative. The directional domain of  $4\pi$  is divided into  $n$  solid angles. Assuming radiative intensity in



the finite solid angle is a constant or defined by simple formulas. Numerical errors can be incurred due to solid angle overhang; however, this can be improved by pixilation.

### 13.4.3 Monte Carlo Method

Monte Carlo is a statistical method, which is described as solving a mathematic problem through a statistical sampling technique. When dealing with radiative heat transfer, the Monte Carlo method means solving thermal radiation problems by tracing the history of bundles of photons (or rays) from their points of emission to their points of absorption. Depending on how a ray is traced, the Monte Carlo ray tracing method has two popular algorithms: forward Monte Carlo ray tracing (FMCRT) and reverse (or backward) Monte Carlo ray tracing (RMCRT). Both FMCRT and RMCRT trace a ray in the same way, but in FMCRT, the tracing is on how much energy is lost along the path of the ray; while in RMCRT, the tracing is on how much intensity contributes to the point of interest from the reversed paths.<sup>62</sup>

One of the advantages of the Monte Carlo method is that it can solve even the most complicated problem with relative ease. As the complexity of the problem increases, the solution effort increases much less rapidly than with conventional techniques. The Monte Carlo method may be the only method that can satisfactorily deal with the effects of irregular radiative properties (non-ideal directional and/or non-gray behavior.) The disadvantage of the Monte Carlo method is the unavoidable statistical error it may have. The Monte Carlo method can also be computationally intensive depending on the size of samples and accuracy requirement. Many researchers are trying to improve the efficiency of Monte Carlo programs.<sup>58,63</sup>

The Monte Carlo method takes a much different approach from other methods. In the Monte Carlo method, individual photons of radiant energy are emitted, reflected, and absorbed by both solid surfaces and participating media using ray tracing algorithms. This method provides a very elegant approach to treating non-gray radiation as well as the directional dependence of radiation. Its use is limited by its computational cost if high accuracy is required.

Siegel and Howell<sup>64</sup> and Modest<sup>61</sup> provide extensive discussion of the solution methods for radiation in participating media. These texts discuss the accuracy, computational effort, and limitations of the various models. The reader should consult these books for more discussion on these solution methods.

### 13.4.4 Gas-Radiation Properties

Molecular gas radiation is an important mode of heat transfer in gas-fired furnaces. Radiative emission from nonluminous hydrocarbon flames is mostly due to the

H<sub>2</sub>O and CO<sub>2</sub> species present in the products of combustion. Radiation from these gases is fairly well understood, but a rigorous treatment of this radiation requires significant computational resources. For instance, Mazumder and Modest<sup>46</sup> considered 10 radiative bands in modeling emission from a hydrocarbon flame. This means that they solved the RTE for 10 different intensities. In a large-scale furnace calculation, such a model would be extremely computationally demanding.

Quantum mechanics postulates that molecular gases emit and absorb gases only at distinct wavenumbers, called spectral lines. However, in reality these distinct lines are broadened by several mechanisms including collision broadening, natural line broadening, and Doppler broadening. These individual lines are characterized by a line strength and a line width. These lines are caused by quantum transitions in the vibrational or rotational state of a molecule. Frequently, vibrational and rotational transitions occur simultaneously, leading to a tightly clustered array of lines around a given vibrational transition. This subject is beyond the scope of the present chapter. The intent is to illustrate the complexity of modeling a radiating gas.

### 13.4.5 Weighted Sum of Gray Gases Model

The weighted sum of gray gases model<sup>64</sup> provides formulas for computing the emissivity of a gas volume as a function of its temperature and partial pressures of CO<sub>2</sub> and H<sub>2</sub>O. The model assumes the gas is a mixture of radiating gases that is transparent between the absorption bands. The weighted sum of gray gases model is probably the most widely used method to calculate radiation within combustion gases. The computational cost of radiation transport can be very high compared to the flow solver portion of a simulation because of the large number of independent variables in the RTE. In practice, it is usually reasonable to lag the calculation of the RTE for a number of flow solver iterations, with the actual number dependent on the solver in use and stability requirements.

### 13.4.6 Effect of Soot on Thermal Radiation

The presence of soot in a flame can significantly increase the flame emissivity. Predicting soot formation within a flame is very difficult because soot is formed in fuel-rich regions of a flame when the temperature is high. Models such as Khan and Greeves<sup>65</sup> and Tesner et al.<sup>66</sup> allow the prediction of soot concentrations, but these models are very empirical and cannot be expected to provide accurate quantitative results.

Soot within a flame is caused by the combustion of hydrocarbons under fuel-rich conditions. Soot is visually observed as a yellow-red brightness in the flame. C<sub>2</sub> hydrocarbons and higher have more tendency to soot, while methane does not normally produce a sooty

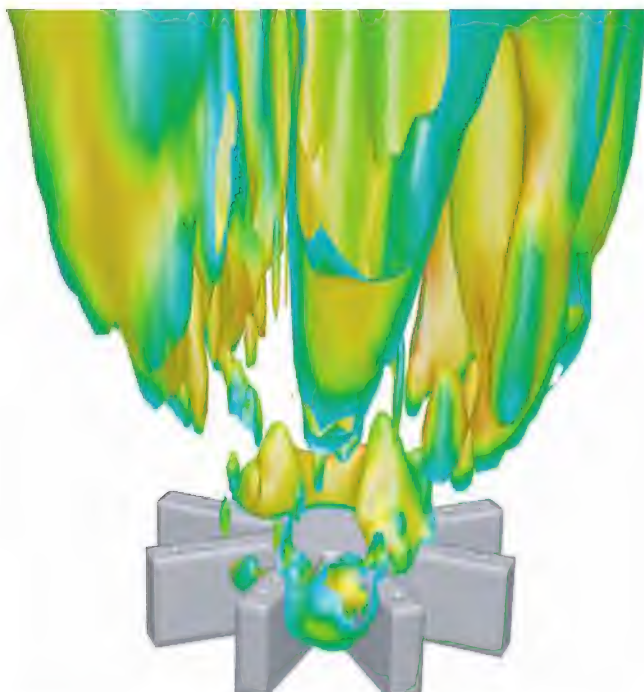


**FIGURE 13.8**  
Representation of a luminous flame utilizing a soot model.

flame. Soot has a strong impact on flame radiation. Emission from soot in flames is frequently much larger than the gas radiation emitted by the flame.<sup>48</sup> In some applications, (oil firing, in particular) soot emissions from the flame are regulated by environmental agencies. In flaring applications, smokeless (smoke results from unoxidized soot particles leaving the flame) operation is frequently guaranteed by the flare vendor for some range of conditions. In petrochemical applications, the gases flared are a wide range of hydrocarbons, typically ranging in molecular weight from 16 to 40. These gases have components such as ethylene and acetylene, which are known precursors to soot formation. However, the calculated soot concentration from those models could be used for the qualitative representation of a luminous flame, either in a combustion furnace, or as shown in Figure 13.8 for a flare burner under ambient conditions.

Current CFD codes (limited by physical model availability) cannot predict smoking from these large, buoyant flare fires, but current LES work in this area appears promising.

## 13.5 Solution Methodology

There are many schemes used to discretize the PDEs of fluid flows onto different types of meshes. Since the primary focus of this chapter is applied CFD where mesh types by necessity include tetrahedral cells, the

two important discretization schemes are the finite volume method and the finite element method. The finite volume method is clearly the method of choice in the industry today for large-scale computations of turbulent flows. The dominant software products commercially available for these problems almost exclusively use the finite volume method. There are occasions when other methods, such as the finite difference method, are used.

### 13.5.1 Problem Setup: Preprocessing

The pre-processing phase of a problem includes all the steps from the initial problem definition through the beginning of computations. In typical problems, this includes geometry creation, mesh generation, model selection, fluid property specification, and enabling and setting up the appropriate submodels.

At this stage, the scope of the geometry to be studied should be considered. In many cases, it is difficult to determine where to place the outside boundaries of a CFD model. Flow conditions must be known at all the inlets. Therefore, for instance, putting a flow inlet just downstream of an elbow would probably be a poor choice because it would be difficult to know the velocity and pressure profiles at such a location. This issue is particularly important if heat transfer has to be considered. Thermal boundary conditions are typically difficult to specify, requiring considerable physical insight into a problem.

It is also important to consider the capabilities of the software and computer hardware to be used when specifying a problem. For instance, if the software's only turbulence model is the standard  $k$ - $\epsilon$  model, then studying a high swirling isothermal flow (where standard  $k$ - $\epsilon$  is known to perform poorly) may generate erroneous results. On the other hand, if one is aware of this limitation and recognizes that the turbulence model will not accurately predict the axial and tangential momentum of the swirl, a conscious decision can be made to neglect the portions of the solution that are expected to be poor and only use the results that are expected to be meaningful.

The capability of a CFD package to treat complex geometries is an important consideration for industrial applications, see also Figures 13.9 and 13.10 as examples.

The geometries encountered in low emissions burners frequently employ complicated shapes and jet angles. The purpose of these geometries is to precisely control when and where the fuel is oxidized. These combustion control strategies are critical to the performance of the equipment. CFD models must be able to accurately capture the effect of these complex geometries in order to be useful.

Figure 13.11 shows a rendered view of a CFD model of a burner tip with a local mesh refinement. As one can see, the drill port sizes are resolved without the use of tetrahedral cells, which would increase the computational



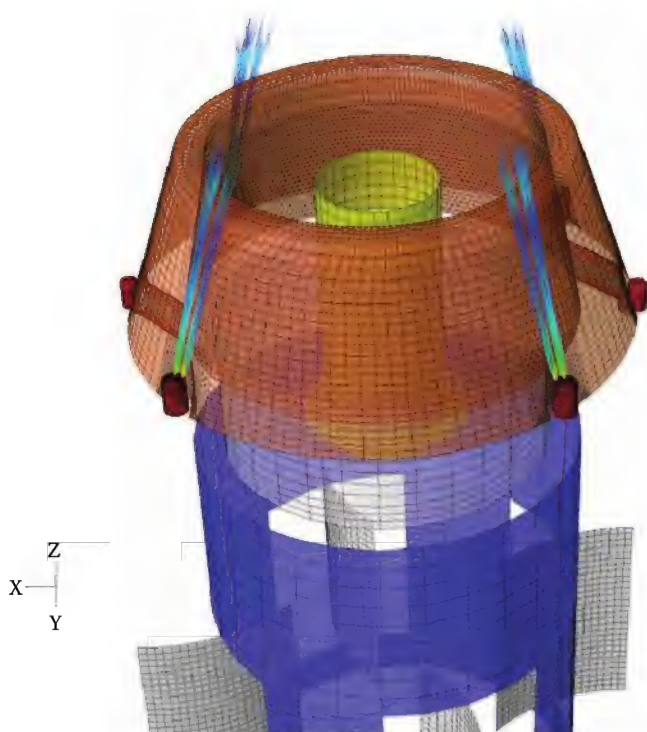


**FIGURE 13.9**  
Discretized geometry of a typical process burner.

effort disproportionately. However, such detail is necessary to treat complex geometries to accurately model the performance of the modeled burner.

A simplified burner model may be used to reduce the overall complexity of the CFD model. Here, experience has shown that a model must resolve each fuel jet to

capture the governing physics that result in flame shape and spread inside a furnace. In all cases, experience is required to understand what level of detail is required for a specific burner/furnace system. In some cases, one may avoid analyzing the full system geometry. On the other hand, one should include as much of the domain as is practically reasonable given available computer resources.

Recent developments of software vendors of CFD software now allow the discretization of those details with very high accuracy, without the downside of creating huge numbers of cells and therefore increase accuracy of the results without increasing computational time.

Generating a computational mesh for this type of geometries is a well-known bottleneck in a CFD analysis. Improvements in mesh generation technology greatly benefit industrial CFD users as they allow more and more of the actual geometry to be included in the CFD model. In addition, mesh generation improvements frequently simplify the process of modifying an existing geometry. To obtain a solution, the mathematical expressions describing physical phenomena must be reduced to simplified but analogous discrete algebraic equations that require solution at discrete points representing specific subvolumes of the overall computational domain.<sup>67</sup> This replacement of “continuum” equations with those utilizing discrete numbers is referred to as discretization. Hence, the simulation becomes possible with the associated computational load related to the number of discrete points where values of conserved scalars are calculated in the general domain. These discrete points are referred to as grid points and the collection of grid points represents a computational mesh. Once the calculation within

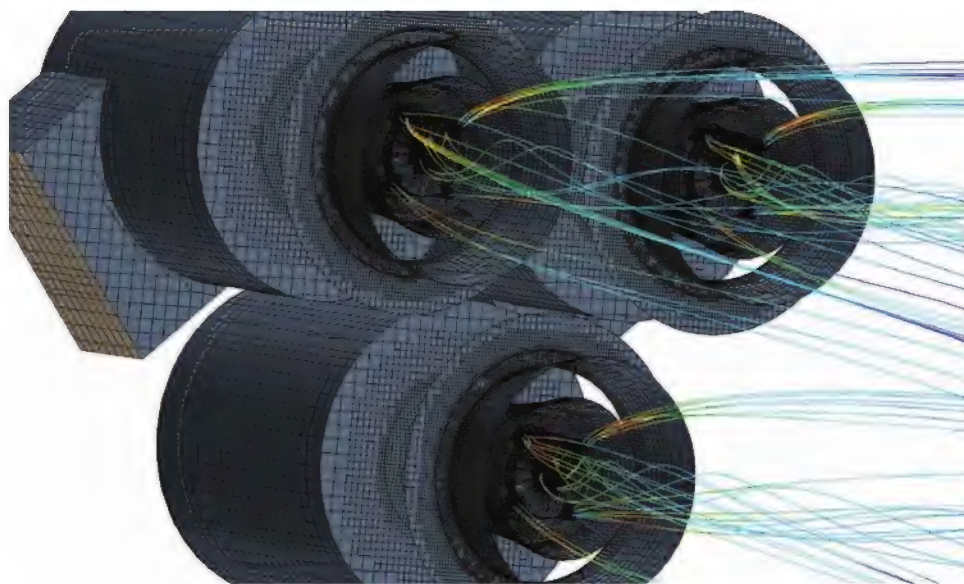


**FIGURE 13.10**  
Discretized geometry of a typical boiler burner.



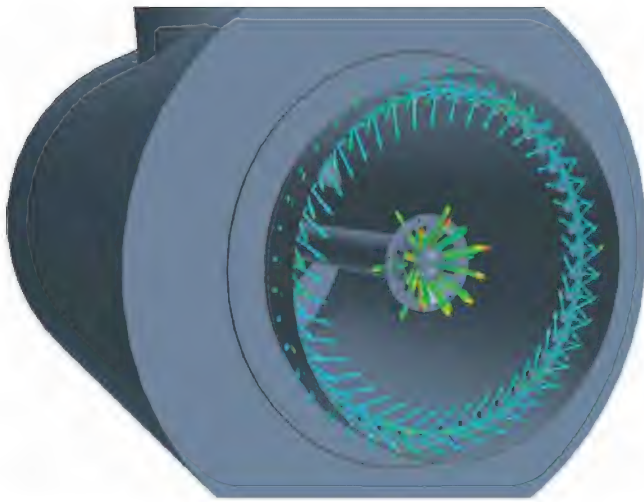


FIGURE 13.11

Close-up view of primary and secondary tips. The view shows fuel jets (indicated by the vectors in the image) issuing from those tips.

the domain is broken down into these discrete points, the closed form of the mathematical expressions can be expressed as a series of algebraic equations. This allows for numerical solution of the various flow-field variables at each of the grid points. For definition, if the PDE form of the conservation relationships is used, the resulting methodology is known as a finite difference scheme. If the integral form of the equations is used, the resulting technique is known as the finite volume method.

The arrangement of the discrete points mentioned earlier is referred to as the computational mesh or grid and provides a segmented approximation of the system geometry to be analyzed or simulated by a CFD model. The density or number of grid points in any one portion of the computational domain should be sufficient to resolve the important geometric features, as well as capture the significant physics (e.g., boundary layer, shear layer, recirculation zone, reaction layer, etc.). The density of grid points typically varies from one region of the domain to another to help resolve these features. In practice, many times it is not feasible or even necessary to resolve the computational domain in this way, since some details might be of less importance for the sought solution. If, for example, the engineer is only interested in the general flow field and temperature distribution in a larger combustion chamber, the resolution of the boundary layer on the walls of that combustion chamber might become less important. This also means that whoever generates a model has to define the scope and purpose of this CFD model. For an aeronautical engineer developing a new design of an airplane wing, it is more important to take care of resolving the exact flow including the behavior in the boundary layer across that wing. Similarly, a combustion engineer must resolve the exact flow at a wall of a large furnace. This might change, however, if the purpose of the model

is the calculation of heat transfer to the tubes in a radiant section of a furnace. Then the boundary layer becomes important again to obtain a more accurate result for the convective heat transfer to those tubes. With today's computational capabilities, a CFD model is still a compromise between the real-world physics and the results of the CFD model. With increasing computational capacities, that gap becomes decreasingly smaller.

Generally, it is acknowledged that greater grid densities (i.e., larger number of elements describing the domain), produce more accurate simulation results.

### 13.5.2 Solution Convergence

After generating the mesh and setting up the problem for solution, the calculations begin. Typically, the momentum equations are solved for each velocity component, the turbulence equations are solved for the respective turbulence variables, and the continuity equation is left for the pressure field. A key issue in CFD is solving for the pressure gradient source terms, found in the momentum equations, since the pressure fields for enclosed flows are usually unknown. CFD codes use traditionally the SIMPLE algorithm for solving the equations of motion and continuity in a decoupled fashion, by transforming the continuity equation into a pressure correction equation. The codes use a tri-diagonal algorithm to solve the PDEs for each variable along a line on each plane of the computational space. The variables are solved in succession, starting with a velocity component and ending with one of the turbulence variables. Since the PDEs are solved in a decoupled fashion, only 4–5 “microiterations” are required per variable. A complete cycle through the equation set, termed a macroiteration, resolves the nonlinear coupling between equations to a prespecified convergence criterion. Overall convergence typically requires between 2,000 and 10,000 macroiterations. CFD codes iterate on each equation individually, the equation coupling necessitates simultaneous convergence of the entire equation set. Various methods have been used to measure convergence, compare convergence rates of each equation, and determine when the required level of convergence is obtained. Typically, the error used to track convergence represents the residual for each FDE as shown:

$$R_{\phi}^0 = A_E \phi_E + A_W \phi_W + A_N \phi_N + A_S \phi_S + A_T \phi_T + A_B \phi_B + S_U - A_P \phi_P \quad (13.78)$$

where

$A_P \phi_P$  represents the computational node and the other  $A_i \phi_i$ 's represent the neighboring nodes

$S_U$  represents the source term (RHS of equations shown earlier)

$R_{\phi}$  represents the residual or relative error in the equation

In other words, a balance around each computational cell is made. As the solution converges, the residual is getting smaller and convergence achieved if  $R_\phi$  falls below a (to be defined) threshold. Comparison of errors from each of the seven equations is difficult because of the relative magnitude of the coefficients ( $A_i$ 's) for each equation. Normalization is also difficult due to the range of variable and source term magnitudes within each equation. Without comparison of the convergence of each equation, it is impossible to determine when "overall" convergence is achieved or which equation is slowing the convergence process. This phase of the CFD analysis does not usually require a lot of effort unless severe convergence problems are encountered. Normally, all that is required of the analyst is to observe the progress of the CFD code toward convergence and perhaps adjust under-relaxation factors and adapt the grid. It is always the stated goal to obtain a solution that is grid independent, but in practice, it usually is too time consuming to refine the mesh such that the obtained solution can be proven grid independent.

### 13.5.3 Analysis of Results: Postprocessing

A typical CFD simulation provides on the order of  $10^8$ – $10^{10}$  discrete numerical outputs. For example, a

simulation with 5,000,000 nodes and 11 variables per node (pressure, density, three velocity components,  $k$ ,  $\epsilon$ , temperature, mixture fraction, variance of mixture fraction, and irradiation) would generate 55,000,000 numbers. If the various chemical species are considered as well as the detailed results of a discrete ordinates model, the number of variables per node could easily exceed 50, leading to 250,000,000 numerical results. The generation of 2D plots (for instance, temperature vs. position along the burner centerline), contour plots, velocity vector plots, streamline plots, and combinations and animations of these outputs are necessary for the analyst to understand the results of a simulation. The production of these different sorts of outputs becomes very important in communicating the results of a simulation. This is especially true when the intended audience is not composed of CFD specialists. Current post-processing packages have the ability to add lighting to a model, which makes the images more realistic to the viewer.

Figure 13.12 shows an example of using the rendering capabilities of a CFD package to generate an image with photorealistic qualities. Images such as Figure 13.12 can take anywhere from several seconds to several minutes for current generation scientific workstations to render depending on the number of lights applied, the number of surfaces in the scene, and the complexity of

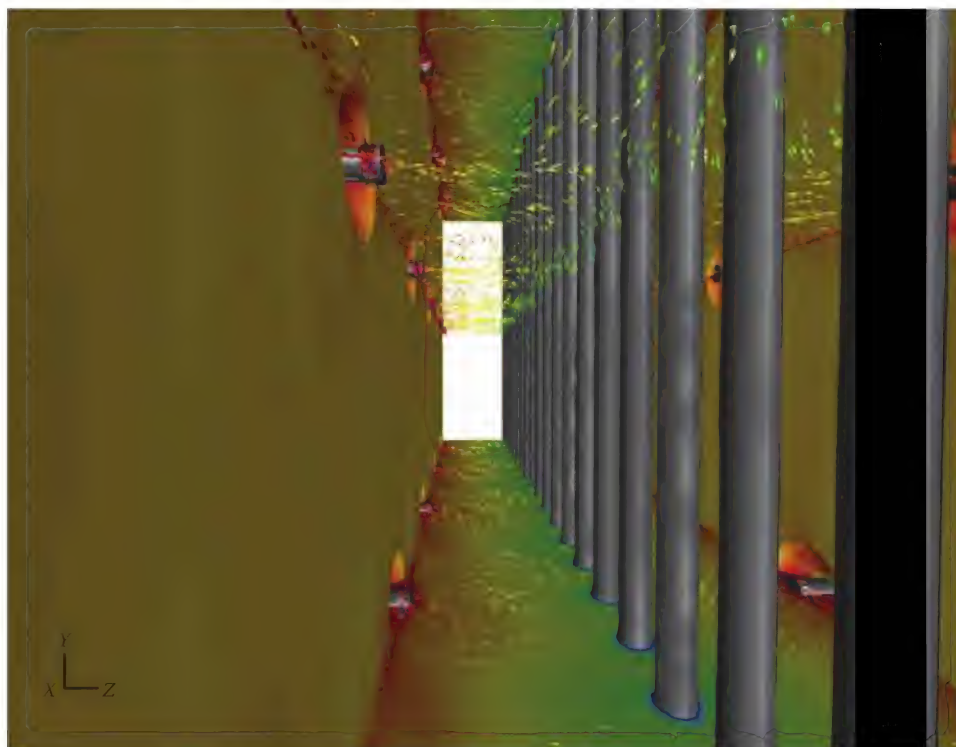
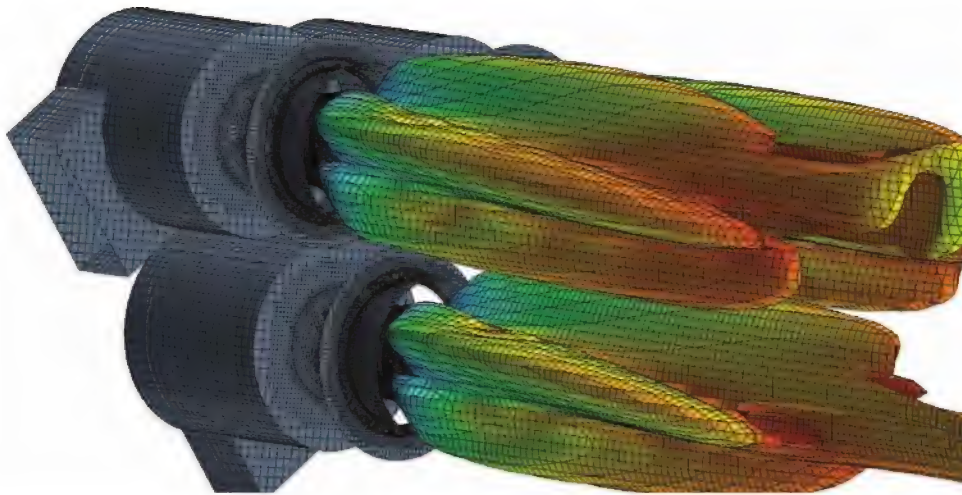


FIGURE 13.12

Rendered view inside an ethylene cracker showing flow patterns near the premixed radiant wall burners. (Courtesy of John Zink Co., Tulsa, OK)





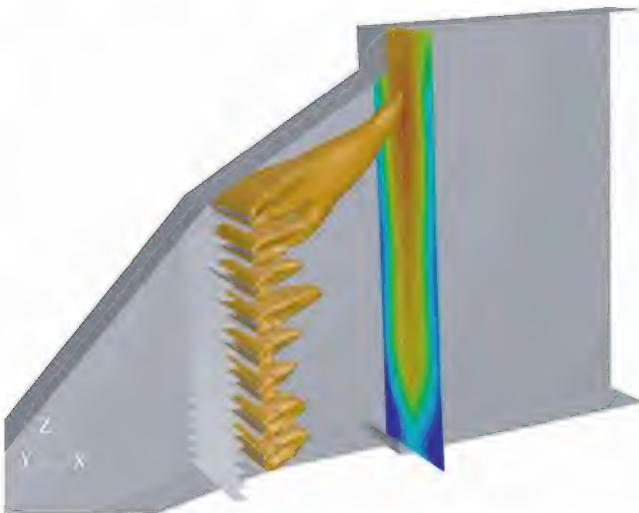
**FIGURE 13.13**  
Illustration of a flame envelope defined as an isocontour of 2500 ppm CO.

these surfaces. High-performance virtual reality environments must be able to regenerate these scenes many times per second.

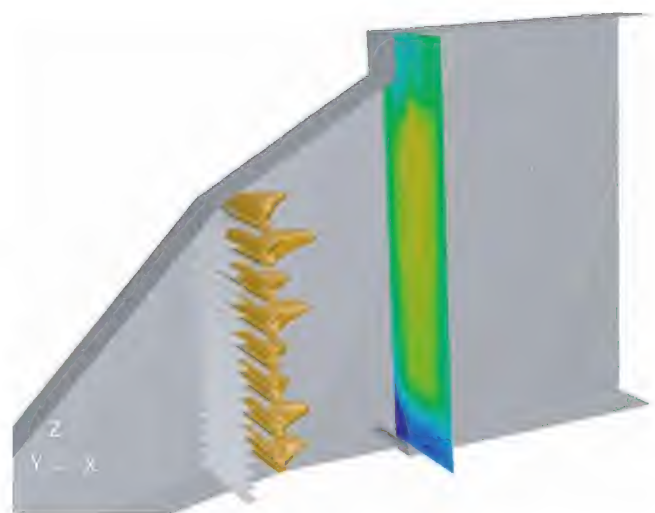
In addition to still images, animations can be effectively used to illustrate CFD results. Animated velocity vectors and streamlines illustrate the path of fluid flow in internal and external flow problems very well. Sweeping planes showing either velocity vectors or filled contour maps of a scalar result can quickly present information about an entire 3D simulation. Some output requires knowledge about the process, or the underlying physics, like, for example, the picture shown in Figure 13.13.

Figure 13.13 is a representation of a flame shape. Flame shapes are not a direct output (quantitative solution) of a CFD model, but must be derived from other

calculated quantities such as the concentration of CO in this example. Pictures like these require the CFD engineer to understand the underlying physics of a CFD model and its interpretation. Relationships like these can also be used for the improved understanding of mixing mechanisms. Figures 13.14 and 13.15 show an isocontour similar to the one in Figure 13.13. However, the value of CO is biased here toward much smaller values to illustrate the mixing of the oxidizer, here coming from a gas turbine, with fuel released from the duct burners. A proper interpretation of these pictures leads to the conclusion that the mixing of oxidizer with fuel for the two top-most burners is insufficient leading to a larger combustion product envelope. A CFD model helped investigating this issue and offer a solution, as shown in Figure 13.15.



**FIGURE 13.14**  
Illustration of combustion products indicating poor mixing between fuel and oxidizer.



**FIGURE 13.15**  
Smaller combustion product envelopes indicate improved mixing between oxidizer and fuel.



Generating effective presentations like these, including still images and animations, is a time-consuming task, since the CFD engineer has to understand the problem and find a way to convey the results to the “customer” in a way that is descriptive and easy to understand. Creating a suitable image to make a specific argument frequently requires the analyst to look at and reject a large number of candidate images. It also requires significant expertise from the CFD analyst. It is certainly true that CFD results can be misinterpreted or misapplied to lead to an incorrect conclusion. In addition, in an industrial setting, the audience will frequently not have the expertise required to assess the quality of a simulation.

### 13.6 Summary

CFD modeling of industrial furnaces is a valuable tool, which can be used profitably. CFD modeling can help identify the cause of problems and it can be used to test solutions. In addition, CFD modeling can be a valuable design tool for combustion equipment in the petrochemical industry. It is also clear that CFD has not achieved the status of stress analysis in terms of ease of use. In many cases, engineers without advanced understanding of the physics do stress analysis of mechanical designs and obtain

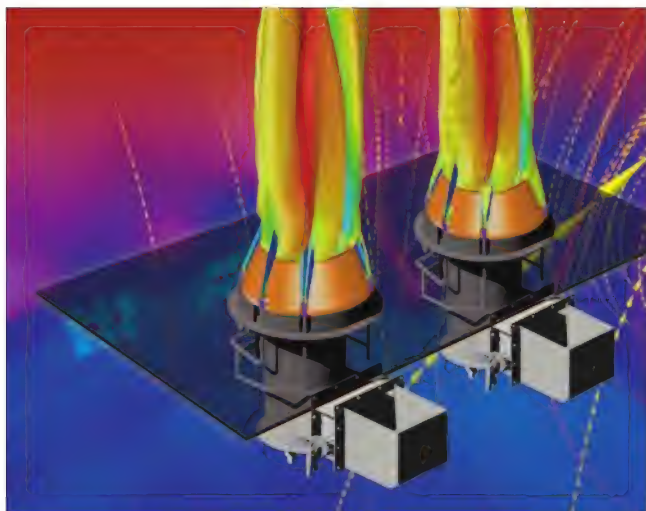


FIGURE 13.16  
CFD model of two burners.

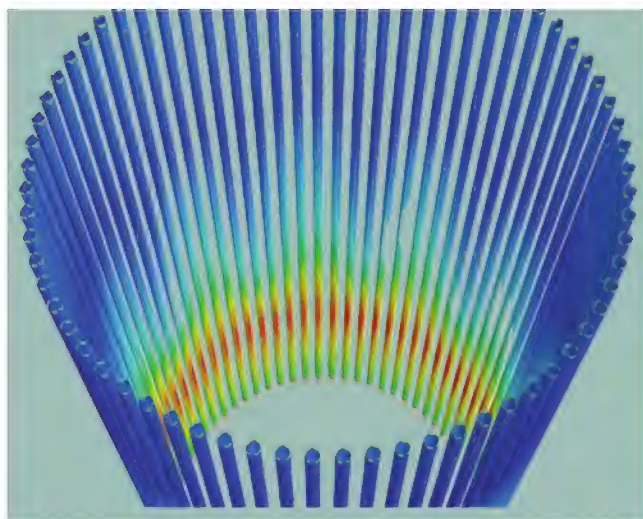


FIGURE 13.17  
CFD simulation optimizes burner performance leading to uniform heat flux on process tubes.

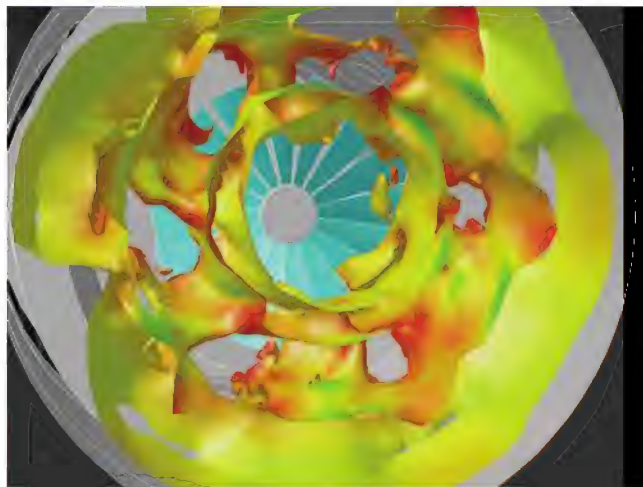
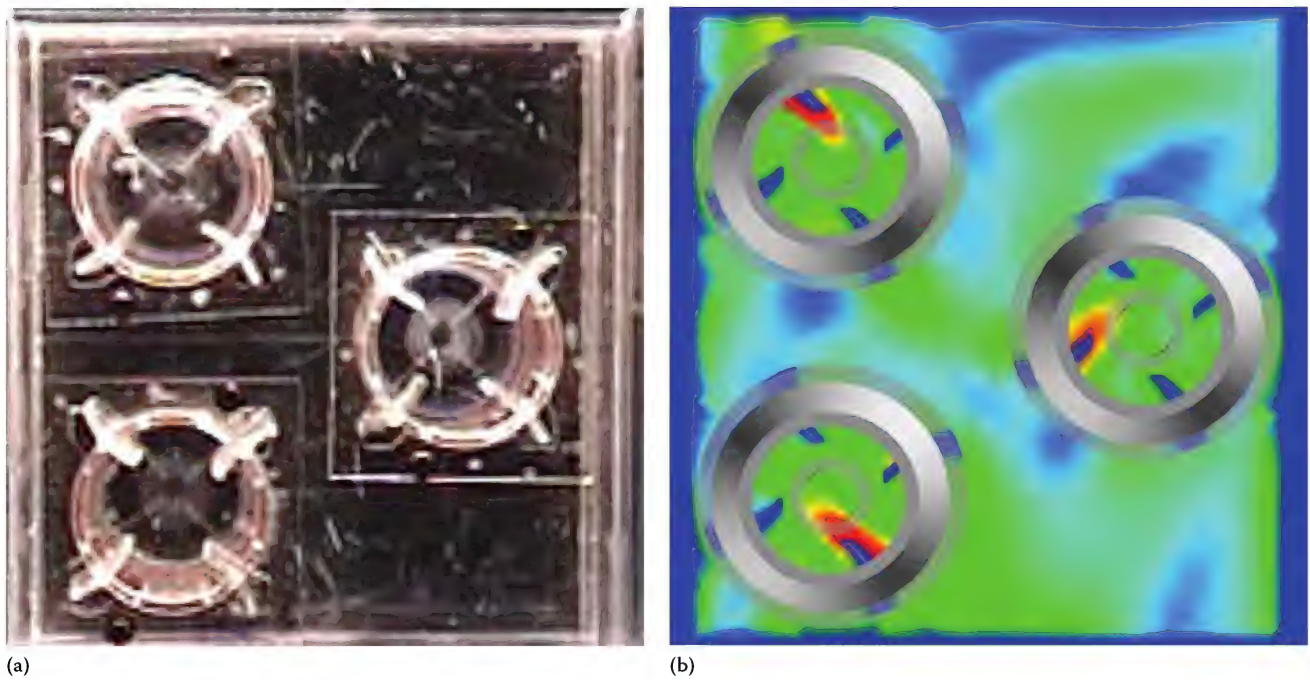
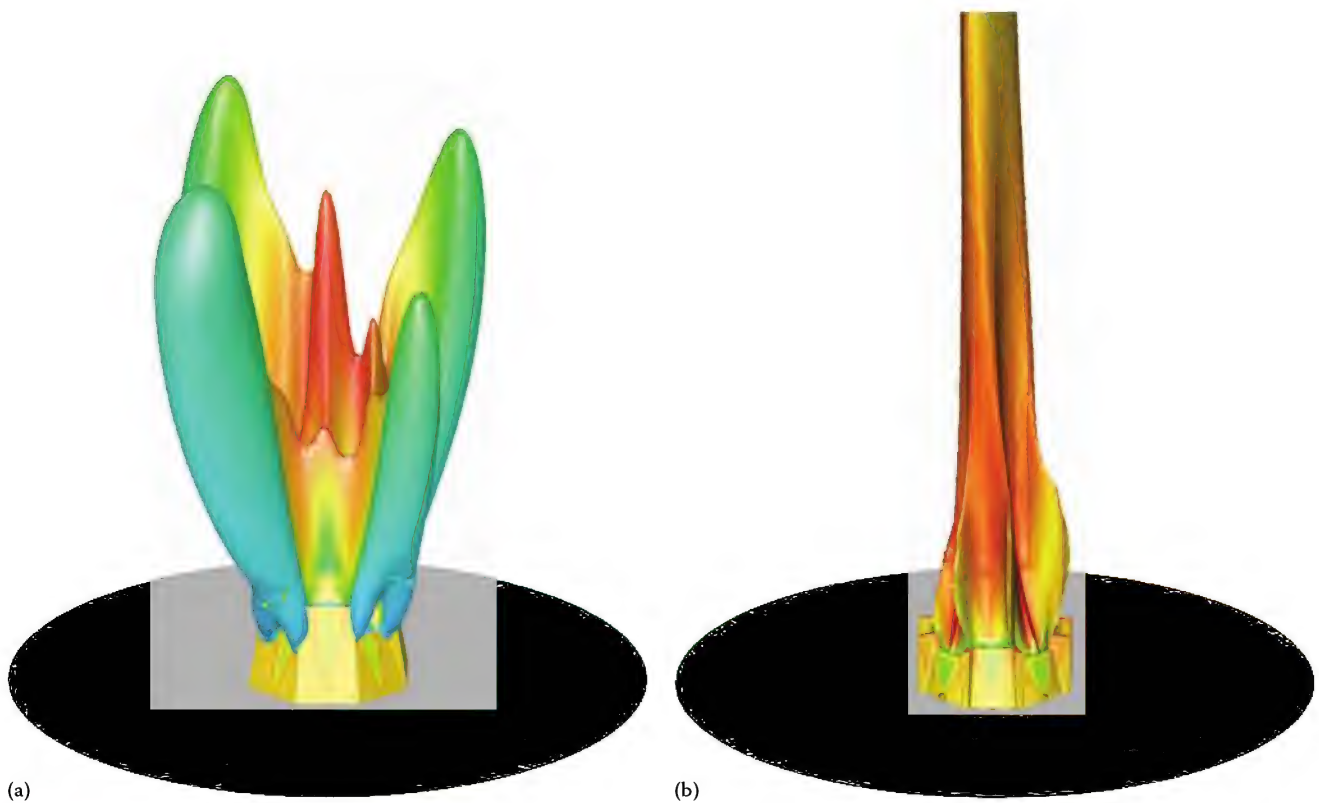


FIGURE 13.18  
Improved flame pattern maximizes burner performance.

reasonable results. With CFD analysis, especially the study of combustion systems, this is not the case. Understanding and interpreting the results of a CFD model requires a thorough understanding of the underlying physics. In a typical furnace model, the science involved is multi-disciplinary, involving heat transfer, fluid flow, and combustion kinetics.<sup>68</sup> For additional examples of CFD output, see Figures 13.16 through 13.20.

**FIGURE 13.19**

Combining John Zink's (a) physical and (b) CFD simulation capabilities allows them to provide comprehensive solutions for their customers.

**FIGURE 13.20**

(a) Before—testing reveals a wide flame with an unacceptable appearance. CFD calculations indicate flame spreading out above the burner tile. (b) After—Design modifications were developed using CFD simulation. Results show a more desirable flame profile within the burner tile geometry.



## Nomenclature

$A$	difference coefficient composed of convection/diffusion terms
$Da$	Damköhler number: ratio of reaction time to flow time
$f$	general body force in momentum equation
$g$ (kg m/s <sup>2</sup> )	gravity
$I$ (W/m <sup>2</sup> sr)	radiation intensity
$k$ (m <sup>2</sup> /s <sup>2</sup> )	turbulent kinetic energy
$K_s$	scattering coefficient
$K_a$	adsorption coefficient
$l_F$ (m)	reaction zone thickness used to define Damköhler number
$l_t$ (m)	turbulent length scale used to define Damköhler number
$p$ (N/m <sup>2</sup> )	pressure
$r$ (m)	cylindrical coordinate position variable
$R$	residual or relative equation error
$S_\phi$	source term in conservation equations for general property
$S_L$ (m/s)	laminar flame speed
$t_{flow}$ (s)	characteristic time for flow to adjust to imposed shear
$t_{rxn}$ (s)	characteristic time for chemical species to react with each other
$u$ (m/s)	axial gas velocity
$v$ (m/s)	radial gas velocity
$v'$	turbulence intensity used to define Damköhler number
$w$ (m/s)	tangential gas velocity
$x$ (m)	Cartesian coordinate position variable
$y$ (m)	Cartesian coordinate position variable
$z$ (m)	Cartesian coordinate position variable
$\delta_{ij}$	Kronecker delta
$\varepsilon$ (m <sup>2</sup> /s <sup>2</sup> )	kinetic energy dissipation rate
$\mu$ (kg/m s)	viscosity
$\mu_b$ (kg/m s)	bulk viscosity
$\mu_e$ (kg/m s)	eddy viscosity
$\nu$ (m <sup>2</sup> /s)	eddy diffusivity used in $k$ - $\varepsilon$ turbulence model
$\rho$ (kg/m <sup>3</sup> )	density
$\tau$ (kg/m s <sup>2</sup> )	viscous stress tensor
$\Gamma_\phi$	general transport coefficient for transport property $\phi$
$\Phi$	conserved scalar
$\Phi$	general transport property
$\Omega$	represents a solid angle in RTE
$\Psi$	dimensionless position variable, difference equation truncation
$\Psi$	truncation error from difference equation

## Overlines

$\bar{\quad}$	time averaged value
$\sim$	Favre or mass weighted averaged value
$\rightarrow$	vector quantity

## Superscripts

$'$	fluctuating portion of instantaneous value
$o$	initial value
$p$	center point in difference scheme

## Subscripts

$i, j, k$	indices representing coordinate directions in 3-space
$\Phi$	general transport property
$E, W, N, S, T, B$	East, West, North, South, Top, Bottom—relative directions in grid

## References

1. Bird, R.B., Stewart, W.E., and Lightfoot, E.N., *Transport Phenomena*, John Wiley & Sons, New York, 1960.
2. Wilcox, D.C., *Turbulence Modeling for CFD*, DCW Industries, Inc., La Canada, CA, 1993.
3. Rodi, W., *Turbulence Models and Their Application in Hydraulics—A State of the Art Review*, 3rd edn., Association for Hydraulic Research, Delft, the Netherlands, 1993.
4. Baldwin, B.S. and Barth, T.J., A one-equation turbulence transport model for high Reynolds number wall-bounded flows, NASA TM-102847, 1990.
5. Spalart, P.R. and Allmaras, S.R., A one-equation turbulence model for aerodynamic flows, AIAA Paper 92-439, Reno, NV, 1992.
6. Libby, P.A., *Introduction to Turbulence*, Taylor & Francis, New York, 1996.
7. Speziale, C.G., On non-linear  $k$ - $l$  and  $k$ - $\varepsilon$  models of turbulence, *Journal of Fluid Mechanics*, 178, 459–478, 1987.
8. Yakhot, V. et al., Development of turbulence models for shear flows by a double expansion technique, *Physics of Fluids A*, 4(7), 1510–1520, 1992.
9. Shih, T.-H., Liou, W.W., Shabbir, A., and Zhu, J., A new  $k$ - $\varepsilon$  Eddy-viscosity model for high Reynolds number turbulent flows—Model development and validation, *Computers Fluids*, 24(3), 227–238, 1995.
10. Versteeg, H.K. and Malalasekera, W., *An Introduction to Computational Fluid Dynamics. The Finite Volume Method*, Addison Wesley Longman Limited, Essex, England, 1995.
11. Chou, P.Y., On the velocity correlations and the solution of the equations of turbulent fluctuation, *Quarterly of Applied Mathematics*, 3, 38–54, 1945.
12. Davidov, B.I., On the statistical dynamics of an incompressible fluid, *Doklady Akademii Nauk SSSR*, 136, 47–50, 1961.



13. Harlow, F.H. and Nakayama, P.I., Transport of turbulence energy decay rate, Los Alamos National Laboratory, University of California, Los Alamos, NM, Report LA-3854, 1968.
14. Jones, W.P. and Launder, B.E., The prediction of laminarization with a two-equation model of turbulence, *International Journal of Heat and Mass Transfer*, 15, 301–314, 1972.
15. Nallasamy, M., A critical evaluation of various turbulence models as applied to internal fluid flows, NASA TP-2474, Marshall Space Flight Center, Huntsville, AL, May, 1985.
16. Launder, B.E. and Spalding, D.B., *Mathematical Models of Turbulence*, Academic Press, London, U.K., 1972.
17. Lilleheie, N.I., Ertesvag, I., Bjorge, T., Byggstoyl, S., and Magnussen, B.F., Modeling and chemical reactions: Review of turbulence and combustion models, NEI-DK-286, DE90 760249, SINTEF/The Norwegian Institute of Technology, Division of Thermodynamics, Norway, July 11, 1989.
18. Jones, W.P. and Whitelaw, J.H., Calculation methods for reacting turbulent flows: A review, *Combustion and Flame*, 48, 1–26, 1982.
19. Roberson, J.A. and Crowe, C.T., *Engineering Fluid Mechanics*, Houghton Mifflin, Boston, MA, 1975.
20. Kim, S.E. and Choudhury, D., A near wall treatment using wall functions sensitized to pressure gradient, ASME FED Vol. 217, Separated and Complex Flows, ASME, 1995.
21. Oran, E.S. and Boris, J.P., *Numerical Simulation of Reactive Flow*, 2nd edn., Cambridge University Press, Cambridge, U.K., 2001.
22. Bray, K.N.C., The challenge of turbulent combustion, *Proceedings of the 26th Symposium (International) on Combustion*, Vol. 1, pp. 1–26, The Combustion Institute, Pittsburgh, PA, 1996.
23. Warnatz, J., Mass, U., and Dibble, R.W., *Combustion: Physical and Chemical Fundamentals, Modeling and Simulation, Experiments, Pollutant Formation*, Springer-Verlag, Berlin, Germany, 1995.
24. Williams, F.A., *Combustion Theory*, Addison-Wesley, New York, 1985.
25. Law, C.K., Dynamics of stretched flames, chemical and physical processes in combustion, *Fall Technical Meeting*, The Eastern States Section, Clearwater Beach, FL, pp. C1–C11, 1984.
26. Peters, N., Length scales in laminar and turbulent flames, *Prog. Astro. Aero.*, 35, 155–183, 1991.
27. Borghi, R., Turbulent combustion modelling, *Progress in Energy Combustion Science*, 14, 245–292, 1988.
28. Kee, R.J. et al., Chemkin II: A FORTRAN chemical kinetics package for the analysis of gas-phase chemical kinetics, Sandia Report SAND 89-8009B-UC706, 1989, Reprinted 1992.
29. Kee, R.J. et al., SENKIN: A FORTRAN program for predicting homogeneous gas phase chemical kinetics with sensitivity analysis, Sandia-Report SAND 87-8248UC401, Reprinted 1991.
30. Glarborg, P. et al., PSR: A FORTRAN program for modelling well-stirred reactors, Sandia-Report SAND 86-8209UC4, Reprinted 1992.
31. Rogg, B., RUN-1DL: The Cambridge universal laminar flamelet computer code, in *Reduced Kinetic Mechanisms for Application in Combustion Systems*, Appendix C, N. Peters and B. Rogg (Eds.), Springer-Verlag, Berlin-Heidelberg, Germany, 1993.
32. Rogg, B., *RUN-1DL: The Universal Laminar Flame and Flamelet Computer Code*, User Manual, 1994.
33. Rogg, B., Numerical modelling and computation of reactive stagnation-point-flows, in *Computers and Experiments in Fluid Flow*, pp. 75–85, G.M. Carlomagno and C.A. Brebbia (Eds.), Springer-Verlag, Berlin, Germany, 1989.
34. Pope, S.B., Computations of turbulent combustion: Progress and challenges, *Proceedings of the 23rd Symposium (International) on Combustion*, The Combustion Institute, Pittsburgh, PA, 1990.
35. Westbrook, C.K. and Dryer, F.L., Chemical kinetic modeling of hydrocarbon combustion, *Progress in Energy Combustion Science*, 10, 1–57, 1984.
36. Spalding, D.B., Mixing and chemical reaction in steady confined turbulent flames, *Proceedings of the 13th Symposium (International) on Combustion*, The Combustion Institute, Pittsburgh, PA, pp. 649–657, 1971.
37. Magnussen, B.F. and Hjertager, B.H., On mathematical modeling of turbulent combustion with special emphasis on soot formation and combustion, *Proceedings of the 16th Symposium (International) on Combustion*, The Combustion Institute, Pittsburgh, PA, pp. 719–727, 1977.
38. Magnussen, B.F., Hjertager, B.H., Olsen, J.G., and Bhaduri, D., Effects of turbulent structure and local concentrations on soot formation and combustion in  $C_2H_2$  diffusion flames, *Proceedings of the 17th Symposium (International) on Combustion*, The Combustion Institute, Pittsburgh, PA, pp. 1383–1393, 1978.
39. Lorra, M., Investigation of  $NO_x$  reduction in turbulent exhaust gas flows with reburning methods using experimental and mathematical modeling regarding detailed reaction mechanisms using the laminar flamelet theory, PhD Thesis, Ruhr-Universitaet Bochum, Bochum, Germany, 1999 (in German).
40. Lorra, M. and Kremer, H., Mathematical modelling and experimental evaluation of  $NO_x$  reduction at glass melting furnaces with reburning, *Proceedings of the Fifth International Conference of Combustion Technologies for a Clean Environment*, Lisbon, Portugal, 1999.
41. Lorra, M., Schnepfer, C., and Stephen, S., Investigation of a duct burner design using CFD capabilities in conjunction with full-scale experiments, *Proceedings of the Sixth European Conference on Industrial Furnaces and Boilers*, Estoril, Portugal, 2002.
42. Peters, N., Laminar flamelet models in non-premixed turbulent combustion, *Progress in Energy and Combustion Science*, 10, 319–339, 1984.
43. Bilger, R.W., The structure of turbulent nonpremixed flames, *Proceedings of the 22nd Symposium (International) on Combustion*, The Combustion Institute, Pittsburgh, PA, 1988.
44. Bish, E.S. and Dahm, W.J.A., Strained dissipation and reaction layer analyses of nonequilibrium chemistry in turbulent reaction flows, *Combustion and Flame*, 100(3), 457–464, 1995.

45. Bilger, R.W., Conditional moment closure for turbulent reacting flow, *Physics of Fluids A*, 5, 436–444, 1993.
46. Mazumder, S. and Modest, M.F., Turbulence-radiation interactions in nonreactive flow of combustion gases, *Journal of Heat Transfer*, 121(3), 726–729, 1998.
47. Barlow, R.S., Nitric oxide formation in dilute hydrogen jet flames: Isolation of the effects of radiation and turbulence-chemistry submodels, *Combustion and Flame*, 117, 4–31, 1999.
48. Modest, M.F., *Radiative Heat Transfer*, McGraw-Hill, New York, 1993.
49. Chandrasekhar, S., *Radiative Transfer*, Oxford University Press, Oxford, U.K., 1950.
50. Chandrasekhar, S., *Radiative Transfer*, Dover Publications, New York, 1960.
51. Lathrop, K.D., Use of discrete-ordinate methods for solution of photon transport problems, *Nuclear Science and Engineering*, 24, 381–388, 1966.
52. Fiveland, W.A., A discrete ordinates method for predicting radiative heat transfer in axisymmetric enclosure, ASME Paper No. 82-HT-20, 1982.
53. Fiveland, W.A., Three-dimensional radiative heat-transfer solutions by the discrete-ordinates method, *Journal of Thermophysics and Heat Transfer*, 2(4), 309–316, 1988.
54. Fiveland, W.A. and Jamaluddin, A.S., Three-dimensional spectral radiative heat transfer solutions by the discrete ordinates method. *Journal of Thermophysics and Heat Transfer*, 5(3), 335–339, 1991.
55. Fiveland, W.A. and Jessee, J.P., Mathematical modeling of pulverized coal combustion in axisymmetric geometries, *Proceedings of the ASME/EPRI Joint Power Generation Conference*, Phoenix, AZ, 1994.
56. Fiveland, W.A. and Jessee, J.P., Comparison of discrete ordinates formulations for radiative heat transfer in multidimensional geometries, *Journal of Thermophysics and Heat Transfer*, 9(1), 47–54, 1995.
57. Sazhin, S.S., Sazhina, E.M., Faltsi-Saravelou, O., and Wild, P., The P-1 model for thermal radiation transfer: Advantages and limitations, *Fuel*, 75(3), 289–294, 1996.
58. Mazumder, S. and Kersch, A., A fast Monte-Carlo scheme for thermal radiation in semiconductor processing applications, *Numerical Heat Transfer, Part B*, 37, 185–199, 2000.
59. Thurgood, C.P., Pollard, A., and Becker, H.A. The  $T_N$  quadrature set for the discrete ordinates method, *ASME Journal of Heat Transfer*, 117(4), 1068–1070, 1995.
60. Bayazitoglu, Y. and Higenyi, J., The higher-order differential equations of radiative transfer: P3 approximation, *AIAA Journal*, 17, 424–431, 1979.
61. Modest, M.F., *Radiative Heat Transfer*, Academic Press, An imprint of Elsevier Science, San Diego, CA, 2003.
62. Sun, X. and Smith, P.J., A parametric case study in radiative heat transfer using the Reverse Monte-Carlo Ray-tracing with full-spectrum k-distribution method, *Journal of Heat Transfer*, 132(2), 024501, 2009.
63. Zeeb, C.N., Performance and accuracy enhancements of radiative heat transfer modeling via Monte Carlo, PhD Dissertation, Colorado State University, Fort Collins, CO, October 2002.
64. Siegel, R. and Howell, J.R., *Thermal Radiation Heat Transfer*, Hemisphere, Washington, DC, 1992.
65. Khan, I.M. and Greeves, G., A method for calculating the formation and combustion of soot in diesel engines, in *Heat Transfer in Flames*, Chapter 25, N.H. Afgan and J.M. Beer (Eds.), Scripta, Washington, DC, 1974.
66. Tesner, P.A., Snegiriova, T.D., and Knorre, V.G., Kinetics of dispersed carbon formation, *Combustion and Flame*, 17, 253–260, 1971.
67. Anderson, J.D., Jr., *Computational Fluid Dynamics—The Basics with Applications*, p. 125, McGraw-Hill, New York, 1995.
68. Baukal, C.E., Gerstein, V.Y., and Li, X., *Computational Fluid Dynamics in Industrial Combustion*, CRC Press, Boca Raton, FL, 2001.

# 14

## *Pollutant Emissions\**

Charles E. Baukal, Jr., I.-Ping Chung, Steve Londerville, James G. Seebold, and Richard T. Waibel

### CONTENTS

14.1	Introduction .....	382
14.1.1	Emissions in the Hydrocarbon and Petrochemical Industries .....	384
14.1.2	Conversions .....	384
14.2	Combustibles .....	387
14.2.1	CO and Unburned Fuel.....	387
14.2.2	Volatile Organic Compounds.....	388
14.3	Particulates .....	391
14.3.1	Combustion-Generated Particulates.....	391
14.3.2	Parameters Controlling Combustion-Generated Particulates .....	391
14.3.3	Measuring Methods .....	391
14.3.3.1	Bacharach Method .....	392
14.3.3.2	Opacity Method .....	392
14.3.3.3	Method 5 or ISO-9096.....	392
14.4	Carbon Dioxide .....	397
14.4.1	CO <sub>2</sub> Generation.....	398
14.4.2	CO <sub>2</sub> Capture.....	398
14.4.3	CO <sub>2</sub> Transport.....	398
14.4.4	CO <sub>2</sub> Storage .....	398
14.4.5	CO <sub>2</sub> Usage .....	399
14.5	SO <sub>x</sub> .....	399
14.6	Hazardous Air Pollutants.....	399
14.6.1	Experimental Setup .....	399
14.6.1.1	Experimental Facility .....	399
14.6.1.2	Full-Scale Burner Tests .....	401
14.6.2	Experimental Results .....	401
14.6.2.1	No Systematic Variation.....	401
14.6.2.2	High Velocity Jet Mixing Produces Low PICs .....	403
14.6.2.3	Turn-Down vs. Mixing Rate.....	405
14.6.2.4	BERL-Field Connection .....	405
14.6.2.5	Refinery Fuel Gas, Natural Gas Equivalency.....	406
14.6.2.6	No Effect of Burner Type .....	406
14.6.2.7	Detection Limits.....	407
14.6.2.8	Results of the Final Full-Scale Trials .....	407
14.6.2.9	Summary .....	411
14.6.3	Process Heater, Petroleum Refinery Emissions Factors .....	412
14.7	Dioxins and Furans .....	413
	References.....	414

\* This includes pollution emissions other than nitrogen oxides (NO<sub>x</sub>) which are covered in Chapter 15.



14.1 Introduction

The purpose of this chapter is to alert the interested reader about the potential effects on pollutant emissions of the combustion processes in the petrochemical and hydrocarbon industries. There continues to be increasing interest in reducing pollutant emissions of all types from all combustion processes. One prognosticator predicts this will continue well into the future.<sup>1</sup> These pollutants have deleterious effects on both the environment and on the health of humans and animals.

Efforts are underway from a broad cross section of organizations to improve existing techniques and to develop new techniques for minimizing pollution. Table 14.1 shows the air quality standards for ambient air concentrations of six criteria pollutants identified by the U.S. Environmental Protection Agency. Figure 14.1 shows that 127 million people in the United States are living in counties where the ambient air quality does not meet at least one health-based standard, where the primary pollutants are ozone and particulate matter.<sup>2</sup>

Figure 14.2 shows that since the Clean Air Act Amendment was passed in the United States in 1970,

TABLE 14.1  
U.S. National Ambient Air Quality Standards (NAAQS) as of October 2011

Pollutant	Primary/Secondary	Averaging Time	Level	Form
Carbon monoxide	Primary	8 h	9 ppm	Not to be exceeded more than once per year
		1 h	35 ppm	
Lead	Primary and secondary	Rolling 3 month average	0.15 µg/m <sup>3</sup>	Not to be exceeded
Nitrogen dioxide	Primary	1 h	100 ppb	98th percentile, averaged over 3 years
	Primary and secondary	Annual	53 ppb	Annual mean
Ozone	Primary and secondary	8 h	0.075 ppm	Annual fourth-highest daily maximum 8-h concentration, averaged over 3 years
Particle pollution	PM <sub>2.5</sub>	Annual	15 µg/m <sup>3</sup>	Annual mean, averaged over 3 years
		24 h	35 µg/m <sup>3</sup>	98th percentile, averaged over 3 years
	PM <sub>10</sub>	24 h	150 µg/m <sup>3</sup>	Not to be exceeded more than once per year on average over 3 years
Sulfur dioxide	Primary	1 h	75 ppb	99th percentile of 1 h daily maximum concentrations, averaged over 3 years
	Secondary	3 h	0.5 ppm	Not to be exceeded more than once per year

Source: U.S. Environmental Protection Agency, Our nation’s air: Status and trends through 2008, Report EPA-454/R-09-002, Washington, DC, February 2010.

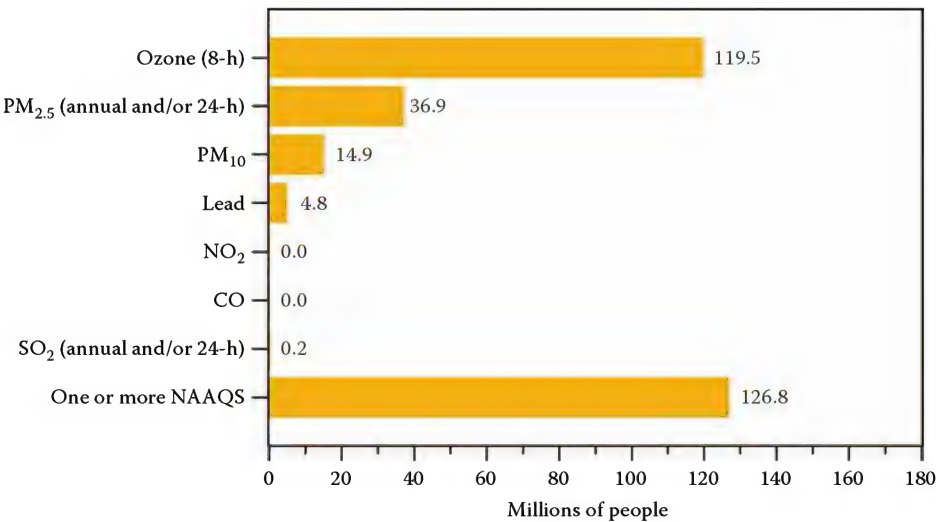


FIGURE 14.1  
Number of people (in millions) living in counties with air quality concentrations above the level of the primary (health-based) National Ambient Air Quality Standards (NAAQS) in 2008. (From U.S. Environmental Protection Agency, *Our Nation’s Air: Status and Trends through 2008*, Report EPA-454/R-09-002, Washington, DC, February 2010.)

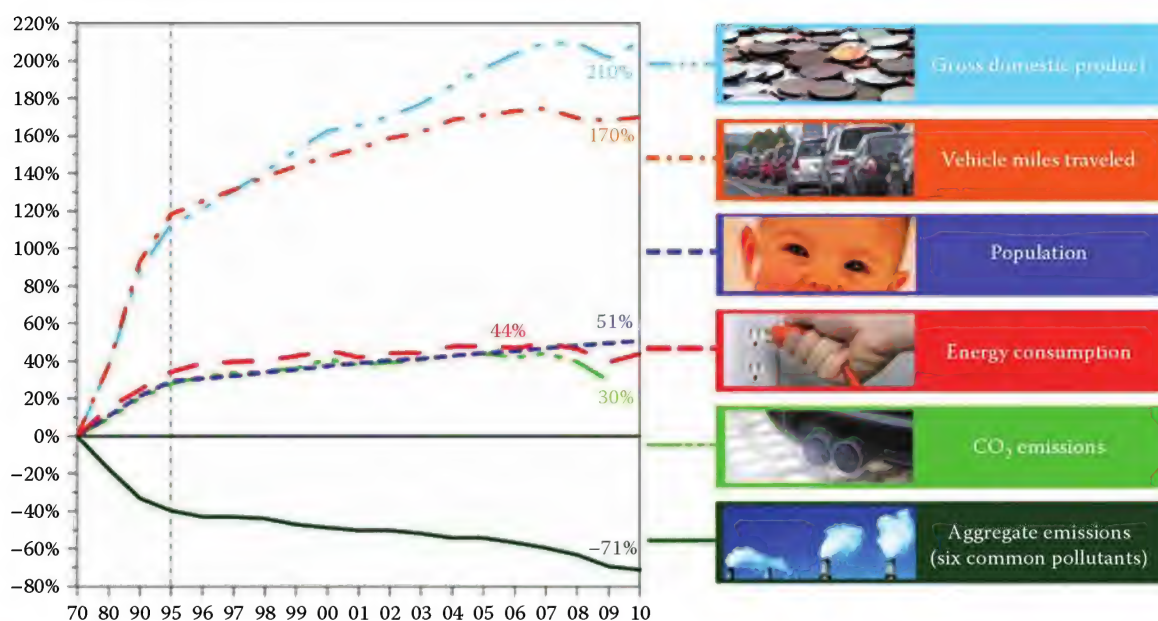


FIGURE 14.2

Comparison of growth measures (gross domestic product, vehicle miles traveled, population, and energy consumption) and emissions (CO<sub>2</sub> and aggregate emissions) from 1970 to 2010 in the United States. (From U.S. Environmental Protection Agency, *Our Nation's Air: Status and Trends through 2008*, Report EPA-454/R-09-002, Washington, DC, February 2010.)

there has been significant growth in many categories that drive energy consumption such as gross domestic product, vehicle miles traveled, and population. Energy consumption directly influences many air pollutants—the more fuel consumed, the more emissions generated. However, due to increased emphasis on reducing pollution, aggregate emissions have actually dropped significantly despite the growth in energy consumption. Much of this decline is due to advancements in technologies such as burners and engines, where less

pollution is generated compared to previous generations of equipment.

Figure 14.3 shows the distribution of air pollution emissions by pollutant type and by source category. The category of interest here is “Industrial and Other Processes” that includes hydrocarbon and petrochemical facilities. While there are other pollutants potentially produced in those industries, this chapter is only concerned with the air pollutants resulting from the combustion processes. For typical gaseous fuels, the

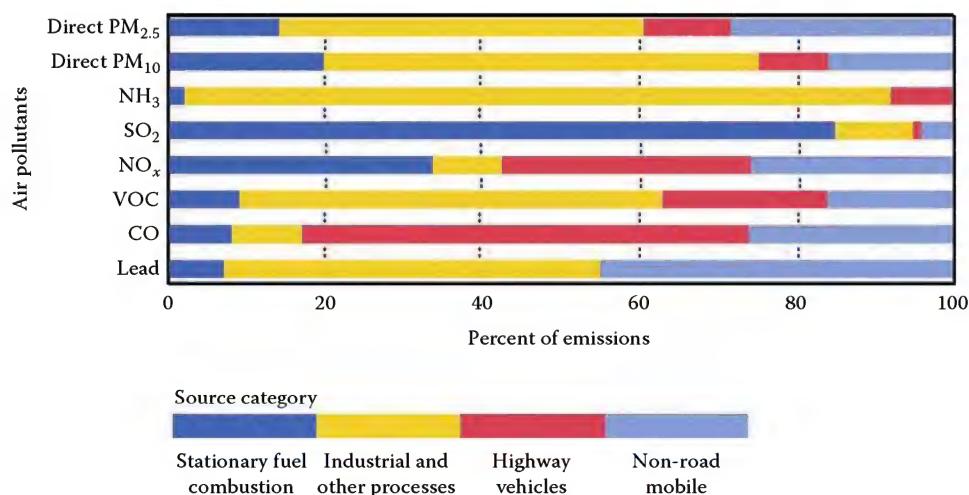


FIGURE 14.3

Distribution of air pollution emissions by pollutant type and source category. (From U.S. Environmental Protection Agency, *Our Nation's Air: Status and Trends through 2008*, Report EPA-454/R-09-002, Washington, DC, February 2010.)

TABLE 14.2

Combustion Emission Factors (lb/10<sup>6</sup> Btu) by Fuel Type

Fuel Type	SO <sub>x</sub>	NO <sub>x</sub>	CO	Particulates	VOCs
Distillate fuel	0.160	0.140	0.0361	0.010	0.002
Residual fuel	1.700	0.370	0.0334	0.080	0.009
Other oils	1.700	0.370	0.0334	0.080	0.009
Natural gas	0.000	0.140	0.0351	0.003	0.006
Refinery gas	0.000	0.140	0.0340	0.003	0.006
Liquefied petroleum gas	0.000	0.208	0.0351	0.007	0.006
Propane	0.000	0.208	0.0351	0.003	0.006
Steam coal	2.500	0.950	0.3044	0.720	0.005
Petroleum coke	2.500	0.950	0.3044	0.720	0.005
Electricity	1.450	0.550	0.1760	0.400	0.004

Source: U.S. Department of Energy Office of Industrial Technology, Petroleum—Industry of the future: Energy and environmental profile of the U.S. Petroleum Refining Industry, U.S. DOE, Washington, DC, December 1998.

two major pollutants are nitrogen dioxide and carbon monoxide (CO). Figure 14.1 shows that these are not currently ambient air concerns compared to the other four criteria pollutants (ozone, particulate matter, lead, and sulfur dioxide). There are numerous factors that affect the pollutant emissions generated from the combustion of fuels. The U.S. Dept. of Energy has classified emission factors by fuel type for petroleum refining, as shown in Table 14.2.<sup>3</sup> An EPA report identified the following heater design parameters that affect NO<sub>x</sub> emissions from process heaters: fuel type, burner type, combustion air preheat, firebox temperature, and draft type.<sup>4</sup> The important factors that influence pollution are considered here.

#### 14.1.1 Emissions in the Hydrocarbon and Petrochemical Industries

The Western States Petroleum Association (WSPA) and the American Petroleum Institute (API) worked with the California Air Resources Board (CARB) to develop air toxic emission factors for the petroleum industry.<sup>5</sup> Source data were provided in 18 groups. Some of those groups of relevance here include both refinery-gas fired and fuel oil-fired boilers and heaters fired on natural gas, refinery gas, oil, and a combination of natural gas and refinery oil. The U.S. Environmental Protection Agency has compiled an extensive list of emission factors for a wide range of industrial processes.<sup>6</sup> Chapter 1 of AP-42 concerns external combustion sources and focuses on the fuel type. Sections 14.3 through 14.5 of AP-42 concern fuel oil combustion, natural gas combustion, and liquefied petroleum gas combustion, respectively. Chapter 5 of AP-42 concerns the petroleum industry, where the reader is referred to Sections 14.3 and 14.4

for boilers and process heaters using fuel oil and natural gas, respectively. Chapter 6 of AP-42 concerns the organic chemical process industry. Reis<sup>7</sup> has written a general book on environmental issues in petroleum engineering, including drilling and production operations. Baukal<sup>8</sup> has written a general purpose book on pollution emissions and control in a wide range of industries including the hydrocarbon and petrochemical industries.<sup>8</sup> API Recommended Practice 556 gives some guidelines for instrumentation used to make pollutant emission measurements in gas-fired heaters.<sup>9</sup>

#### 14.1.2 Conversions

It is often necessary to convert pollutant measurements (e.g., NO<sub>x</sub> and CO) into a standard basis for both regulatory and comparison purposes. The concentration of each pollutant is measured at the stack in dry parts per million by volume (ppmvd). One conversion that is often necessary is from the measured O<sub>2</sub> level in the exhaust gases to a standard basis O<sub>2</sub> level. The method for converting measurements to a standard basis is given by<sup>10</sup>

$$\text{ppm}_{\text{corr}} = \text{ppm}_{\text{meas}} \left( \frac{20.9 - \text{O}_{2\text{ref}}}{20.9 - \text{O}_{2\text{meas}}} \right) \quad (14.1)$$

where

ppm<sub>meas</sub> is the measured pollutant concentration in flue gases (ppmvd)

ppm<sub>corr</sub> is the pollutant concentration corrected to a reference O<sub>2</sub> basis (ppmvd)

O<sub>2meas</sub> is the measured O<sub>2</sub> concentration in flue gases (vol. %, dry basis)

O<sub>2ref</sub> is the reference O<sub>2</sub> basis (vol. %, dry basis)

#### Example 14.1

Given: Measured CO = 20 ppmvd, measured O<sub>2</sub> = 2% on a dry basis.

Find CO at 3% O<sub>2</sub> on a dry basis.

Solution: ppm<sub>meas</sub> = 20, O<sub>2meas</sub> = 2, O<sub>2ref</sub> = 3

$$\text{ppm}_{\text{corr}} = (20) \left( \frac{20.9 - 3}{20.9 - 2} \right) = 18.9 \text{ ppmvd}$$

This example shows that CO values will be lower when the basis O<sub>2</sub> is higher than the measured O<sub>2</sub> because higher O<sub>2</sub> levels mean more air dilution and therefore lower CO concentrations. The reverse is true when the basis O<sub>2</sub> is lower than the measured O<sub>2</sub> level.

Another correction that may be required is to convert the measured pollutants from a measured furnace



temperature to a different reference temperature. This may be required when a burner is tested at one furnace temperature and needs to be modified to find out the equivalent at the another furnace temperature. The correction for temperature is

$$\text{ppm}_{\text{corr}} = \text{ppm}_{\text{meas}} \left( \frac{T_{\text{ref}} - T_{\text{basis}}}{T_{\text{meas}} - T_{\text{basis}}} \right) \quad (14.2)$$

where

$\text{ppm}_{\text{meas}}$  is the measured pollutant concentration in flue gases (ppmvd)

$\text{ppm}_{\text{corr}}$  is the pollutant concentration corrected to a reference temp. basis (ppmvd)

$T_{\text{ref}}$  is the reference furnace temperature (°F)

$T_{\text{meas}}$  is the measured furnace temperature (°F)

$T_{\text{basis}}$  is the basis furnace temperature (°F)

#### Example 14.2

Given: Measured  $\text{NO}_x = 20$  ppmvd, measured furnace temp. =  $1800^\circ\text{F}$ .

Find  $\text{NO}_x$  at a reference temperature of  $2000^\circ\text{F}$ .

Solution:  $\text{ppm}_{\text{meas}} = 20$ ,  $T_{\text{meas}} = 1800^\circ\text{F}$ , assume  $T_{\text{ref}} = 400^\circ\text{F}$

$$\text{ppm}_{\text{corr}} = (20) \left( \frac{2000 - 400}{1800 - 400} \right) = 22.9 \text{ ppmvd}$$

There are two things to notice in the previous example. The first is that the basis temperature was chosen as  $400^\circ\text{F}$  ( $200^\circ\text{C}$ ), which is an empirically determined value that applies to many burners commonly used in the hydrocarbon and petrochemical industries. However, this equation should be used with care for more unique burner designs and when there is a very large difference between the measured and the reference furnace temperatures. The second thing to notice is that the  $\text{NO}_x$  increases when the reference temperature is higher than the measured temperature and vice versa. As will be shown later in Chapter 15,  $\text{NO}_x$  generally increases with the furnace temperature.

These two corrections can also be combined into a single correction when both the measured  $\text{O}_2$  level and furnace temperature are different from the reference  $\text{O}_2$  level and furnace temperature:

$$\text{ppm}_{\text{corr}} = \text{ppm}_{\text{meas}} \left( \frac{20.9 - \text{O}_{2\text{ref}}}{20.9 - \text{O}_{2\text{meas}}} \right) \left( \frac{T_{\text{ref}} - T_{\text{basis}}}{T_{\text{meas}} - T_{\text{basis}}} \right) \quad (14.3)$$

where the variables are defined earlier.

#### Example 14.3

Given: Measured  $\text{NO}_x = 20$  ppmvd, measured  $\text{O}_2 = 2\%$  on a dry basis, measured furnace temp. =  $1800^\circ\text{F}$ .

Find  $\text{NO}_x$  at  $3\% \text{O}_2$  on a dry basis at a reference temperature of  $2000^\circ\text{F}$ .

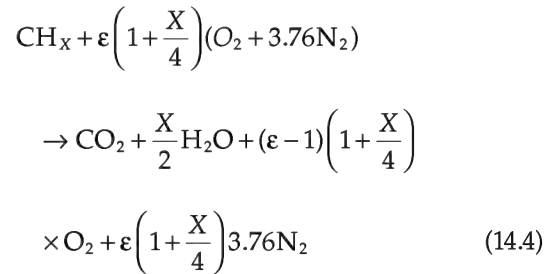
Solution:  $\text{ppm}_{\text{meas}} = 20$ ,  $\text{O}_{2\text{meas}} = 2$ ,  $\text{O}_{2\text{ref}} = 3$ ,  $T_{\text{meas}} = 1800^\circ\text{F}$ , assume  $T_{\text{ref}} = 400^\circ\text{F}$

$$\text{ppm}_{\text{corr}} = (20) \left( \frac{20.9 - 3}{20.9 - 2} \right) \left( \frac{2000 - 400}{1800 - 400} \right) = 21.6$$

In this case, the increase in  $\text{NO}_x$  due to the temperature correction is greater than the reduction in  $\text{NO}_x$  due to the higher  $\text{O}_2$  reference.

Some very common simple conversion calculations for gaseous emissions that are frequently used are introduced next. Common examples of gaseous emissions are  $\text{NO}_2$ ,  $\text{CO}$ , and  $\text{SO}_2$ . As ppmvd varies with the amount of  $\text{O}_2$  in the stack, it is sometimes necessary to establish a reference percentage of  $\text{O}_2$  such as 100 ppm  $\text{NO}_x$  at  $3\% \text{O}_2$ .

In order to establish the percentage of excess air, the dry  $\text{O}_2$  needs to be known vs. excess air. This can be computed from the general HC reaction as follows:



From the products of the general form of hydrocarbons reactions given earlier, we now have

$$\text{O}_2\%_{\text{dry}} = \frac{(\epsilon - 1) \left( 1 + \frac{x}{4} \right) 100}{1 + (\epsilon - 1) \left( 1 + \frac{x}{4} \right) + \epsilon \left( 1 + \frac{x}{4} \right) 3.76} \quad (14.5)$$

where

$$\left( \frac{H}{C} \right)_{\text{mole}} = "X" \quad (14.6)$$

Substituting  $\epsilon = \frac{\% \text{Excess Air}}{100} + 1$  and simplifying a unique relationship between measured oxygen and excess air is

obtained. A general relation for EA and O<sub>2</sub> dry for any HC fuel is given by:

$$\text{O}_2\% \text{dry} = \frac{1}{\left( \frac{1}{1 + \frac{X}{4}} + 3.76 \right) \frac{1}{\text{EA}} + .0476} \quad (14.7)$$

Back solving for the EA, the EA as a function of O<sub>2</sub> dry is given by:

$$\text{EA}\% = \frac{\left( \frac{1}{1 + \frac{X}{4}} + 3.76 \right)}{\left[ \frac{1}{\text{O}_2\% \text{dry}} - .0476 \right]} \quad (14.8)$$

It is often necessary to calculate mass emission rate per Btu produced  $\left( \frac{\text{lb}}{10^6 \text{ Btu}} \right)$  from parts per million (ppmvd). Using the general chemical equation for fuel oxidation given earlier, the following can be computed

$$\begin{aligned} & \left( \frac{n \text{ ppmvd}}{10^6} \right) \frac{\text{lb}_{\text{mole Chem}}}{\text{lb}_{\text{mole FG}}} \times \frac{\text{lb}_{\text{mole}} \left( \frac{\text{FG}}{F} \right)}{\text{lb}_{\text{mole}}} \times \frac{\text{lb}_{\text{mole Fuel}}}{\text{MW}_F \text{ lb Fuel}} \\ & \times \frac{\text{MW}_{\text{chem}} \text{ lb}_m}{\text{lb}_{\text{mole Chem}}} \times \frac{\text{lb}_m \text{ Fuel}}{\text{HHV}} \times \frac{10^6 \text{ Btu}}{\text{million}} = \frac{n \text{ lb}_m}{10^6 \text{ Btu}} \end{aligned}$$

where  $n$  ppmvd is the ppmvd of chemical  $n$

$$\left( \frac{\text{FG}}{F} \right)_{\text{dry, vol}} = 1 + (\epsilon - 1) \left( 1 + \frac{X}{4} \right) + \epsilon \left( 1 + \frac{X}{4} \right) \quad (14.9)$$

Substituting  $\epsilon = \frac{\% \text{Excess Air}}{100} + 1$  and simplifying,

$$\begin{aligned} & \frac{n \text{ ppmvd MW}_n}{\text{HHV}(12 + X)} \left[ \left( 1 + \left( 1 + \frac{X}{4} \right) \right) \left( \frac{4.76 \text{ EA}}{100} + 3.76 \right) \right] \\ & = \frac{\text{lb}_m n}{10^6 \text{ Btu}} \quad (14.10) \end{aligned}$$

The preceding equation is a general relationship between a product species in dry PPM by volume and  $\left( \frac{\text{lb}}{10^6 \text{ Btu}} \right)$  for any chemical compound, with a fuel HHV = Btu/lb<sub>m</sub> and EA = % excess air and the molecular weight of chemical  $n$ . It is applicable for all HC fuels, both gas and liquids that are mostly composed of HCs.

It is also common to use units of  $\frac{\text{g}}{\text{NM}^3}$ . The conversion is as follows:

$$\begin{aligned} & \left( \frac{\text{lb}_m n}{10^6 \text{ Btu}} \right) \left( \frac{453.6 \text{ g}}{\text{lb}_m} \right) \left( \frac{\text{HHV Btu}}{\text{lb}_m} \right) \left( \frac{\text{lb}_m \text{ Fuel}}{\text{lb}_m \text{ FG}} \right) \left( \frac{\text{lb}_m \text{ FG}}{\text{NM}^3} \right) \\ & = \frac{\text{g } n}{\text{NM}^3} \end{aligned}$$

#### Example 14.4

Given: Fuel = CH<sub>4</sub>, HHV = 23,875 Btu/lb<sub>m</sub>

Required: NO<sub>2</sub> emission = 0.1 lb<sub>m</sub>/10<sup>6</sup> Btu

Find PPM at 20% EA on a dry basis

Solution: MW<sub>NO<sub>2</sub></sub> = 46, X = 4, EA = 20%

$$\begin{aligned} & \frac{x \text{ ppm}(46)}{23,875 \times (12 + 4)} \left[ 1 + \left( 1 + \frac{4}{4} \right) \left( \frac{4.76 \times 20}{100} + 3.76 \right) \right] \\ & = 0.1 \frac{\text{lb}_m}{10^6 \text{ Btu}} \end{aligned}$$

$$x = 79.66 \text{ ppm}$$

It is important to note here that the mass emission rates for NO<sub>x</sub> are always expressed as NO<sub>2</sub> and the ppmvd measured in the stack can be all NO<sub>x</sub> in ppm since the compounds only contain one atom of nitrogen.

#### Example 14.5

Given: Fuel = CH<sub>4</sub>, HHV = 23,875 Btu/lb<sub>m</sub>

Required: CO emission = 0.2 lb<sub>m</sub>/10<sup>6</sup> Btu

Find ppm at 20% EA on a dry basis

Solution: MW CO = 28, X = 4, EA = 20%

$$\begin{aligned} & \frac{x \text{ PPM}(28)}{23,875(12 + 4)} \left[ 1 + \left( 1 + \frac{4}{4} \right) \left( \frac{4.76 \times 20}{100} + 3.76 \right) \right] \\ & = 0.2 \frac{\text{lb}_m}{10^6 \text{ Btu}} \end{aligned}$$

$$x = 261.8 \text{ ppm}$$

The earlier-given two examples show the PPM values necessary to achieve certain mass flow rates for NO<sub>2</sub> and CO. It is often necessary to measure the emission and back calculate the mass emission rate as shown in Example 14.3.

#### Example 14.6

Given: Fuel = CH<sub>4</sub>, HHV = 23,875 Btu/lb<sub>m</sub>

$x = 140 \text{ ppm NO}_x$  at 4% O<sub>2</sub> dry

Find EA% and lb<sub>m</sub>/10<sup>6</sup> Btu

Solution: MW<sub>NO<sub>2</sub></sub> = 46, X = 4, O<sub>2</sub>% dry = 4%

$$EA\% = \frac{\left( \frac{1}{1 + \frac{4}{4}} + 3.76 \right)}{\left[ \frac{1}{4} - .0476 \right]} = 21\%$$

$$\frac{140 \text{ PPM}(46)}{23,875(12 + 4)} \left[ \left( 1 + \left( 1 + \frac{4}{4} \right) \right) \left( \frac{4.76 \times 21}{100} + 3.76 \right) \right]$$

$$= 0.177 \frac{\text{lb}_m}{10^6 \text{ Btu}}$$

In liquids, solids, and sometimes gaseous fuels, elemental nitrogen compounds exist that convert partially to  $\text{NO}_x$ . The following example shows a general method to compute this contribution. It is important to note that these computed  $\text{NO}_x$  emissions are in addition to thermal and prompt  $\text{NO}_x$  and are a function of fuel bound nitrogen only.

#### Example 14.7

Given: Firing #6 oil, FBN = 0.3%, Excess air = 25%, and API gravity = 20

Find Fuel  $\text{NO}_2$  contribution given 40% conversion in  $\frac{\text{lb}_m}{10^6 \text{ Btu}}$  and ppmvd

Solution: HHV = 18,740 Btu/lb<sub>m</sub>, For API gravity = 20; %C = 88.01, and %H = 10.99

$$\left( \frac{\text{H}}{\text{C}} \right)_{\text{mole}} = \frac{10.99 \text{ lb}_m \text{H}}{88.10 \text{ lb}_m \text{C}} \times \frac{12 \text{ lb}_m \text{C}}{\text{mole C}} \times \frac{\text{mole H}}{1 \text{ lb}_m \text{H}} = 1.50$$

$$\left( \frac{0.3 \text{ lb}_m \text{N}}{100 \text{ lb}_m \text{Fuel}} \right) \left( \frac{1 \text{ lb}_{\text{mole}} \text{N}}{14 \text{ lb}_m \text{N}} \right) \left( \frac{1 \text{ lb}_{\text{mole}} \text{NO}_2}{1 \text{ mole N}} \right) \left( \frac{46 \text{ lb}_m \text{NO}_2}{\text{lb}_{\text{mole}} \text{NO}_2} \right)$$

$$\times \left( \frac{1 \text{ lb}_m \text{Fuel}}{18,470 \text{ Btu}} \right) \left( \frac{10^6 \text{ Btu}}{\text{million Btu}} \right) = 0.53 \frac{\text{lb}_m \text{NO}_2}{10^6 \text{ Btu}} (40\%)$$

$$= 0.21 \frac{\text{lb}_m}{10^6 \text{ Btu}}$$

$$\frac{x \text{ PPM}(46)}{18,740(12 + 1.5)} \left[ 1 + (1.375) \left( \frac{4.76(25)}{100} + 3.76 \right) \right]$$

$$= 0.21 \frac{\text{lb}_m}{10^6 \text{ Btu}}$$

$$x = 147 \text{ ppm}$$

It should be noted that the conversion of elemental fuel bound nitrogen compounds to  $\text{NO}_x$  varies widely from about 4% to 100% and generally are a function of fuel type and concentration. Low concentrations in gaseous fuels are near 100%. High concentrations in solid and liquid fuels range from 20% to 80%. Staging techniques can reduce this conversion in solid and liquid fuels up to 80% lower conversion.

## 14.2 Combustibles

This section has been broken into two types of combustibles. The first involves the incomplete combustion of the fuel which usually produces CO and, in some limited cases, not all of the hydrocarbon fuel is consumed and passes through the combustor unreacted. The second type of combustible is volatile organic compounds (VOCs), which are generally only important in a limited number of processes, typically involving contaminated or otherwise hazardous waste streams.

### 14.2.1 CO and Unburned Fuel

CO is generally produced in trace quantities in many combustion processes as a product of incomplete combustion. CO is a flammable gas, which is nonirritating, colorless, odorless, tasteless, and normally noncorrosive. It is highly toxic and acts as a chemical asphyxiant by combining with hemoglobin in the blood that normally transports oxygen inside the body. The affinity of CO for hemoglobin is approximately 300 times more than the affinity of oxygen for hemoglobin.<sup>11</sup> CO preferentially combines with hemoglobin to the exclusion of oxygen so that the body becomes starved for oxygen, which can eventually lead to asphyxiation. Therefore, CO is a regulated pollutant with specific emissions guidelines depending on the application and the geographical location.

CO is generally produced by the incomplete combustion of a carbon-containing fuel. Normally, a combustion system is operated slightly fuel lean (excess  $\text{O}_2$ ) to ensure complete combustion and to minimize CO emissions. Figure 14.4 shows the calculated CO as a function of the equivalence ratio (ratio of 1 is stoichiometric, >1 is fuel rich, and <1 is fuel lean). Because these are adiabatic calculations with very high flame temperatures, the dissociation in the flame produces high quantities of CO even under fuel lean conditions. This is graphically shown in Figure 14.5 where much more CO is produced at higher gas temperatures, all other variables remaining the same.

Figures 14.6 and 14.7 show the effects on CO production of air and fuel preheating, respectively. In both cases, the higher flame temperatures produced by preheating cause more CO formation as the preheat temperature increases. Figure 14.8 shows the effect of fuel composition for  $\text{H}_2/\text{CH}_4$  blends. As expected, higher concentrations of  $\text{H}_2$  produce less CO and for pure  $\text{H}_2$ , no CO is generated. Similarly, Figure 14.9 shows the effect of fuel composition for  $\text{CH}_4/\text{N}_2$  blends. Higher concentrations of  $\text{N}_2$  both reduce the flame temperature and the concentration of carbon available to make CO, which both reduce CO generation.



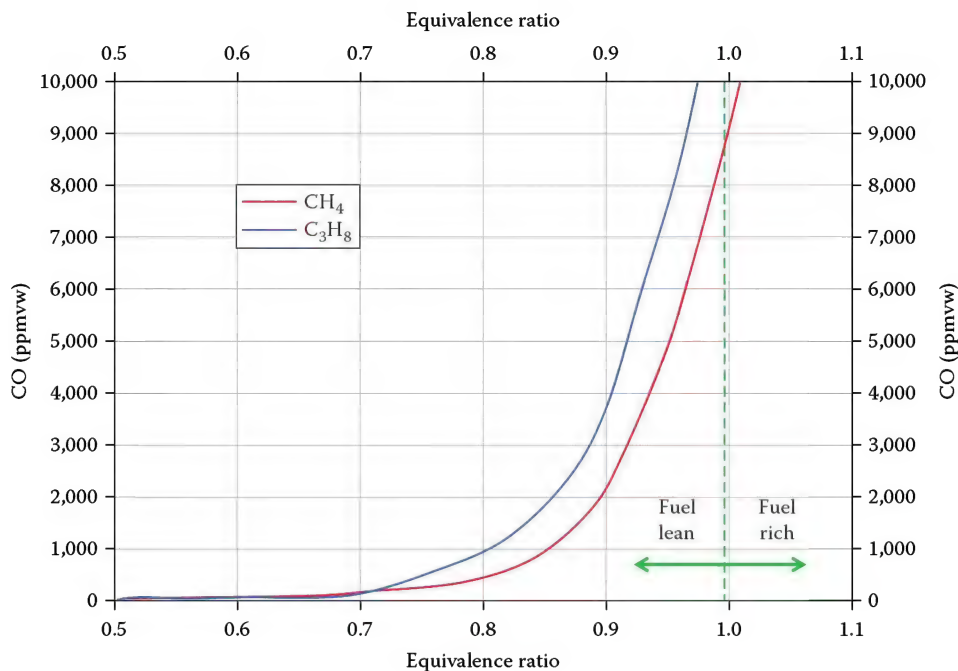


**FIGURE 14.4**  
Adiabatic equilibrium CO as a function of equivalence ratio for air/fuel flames.

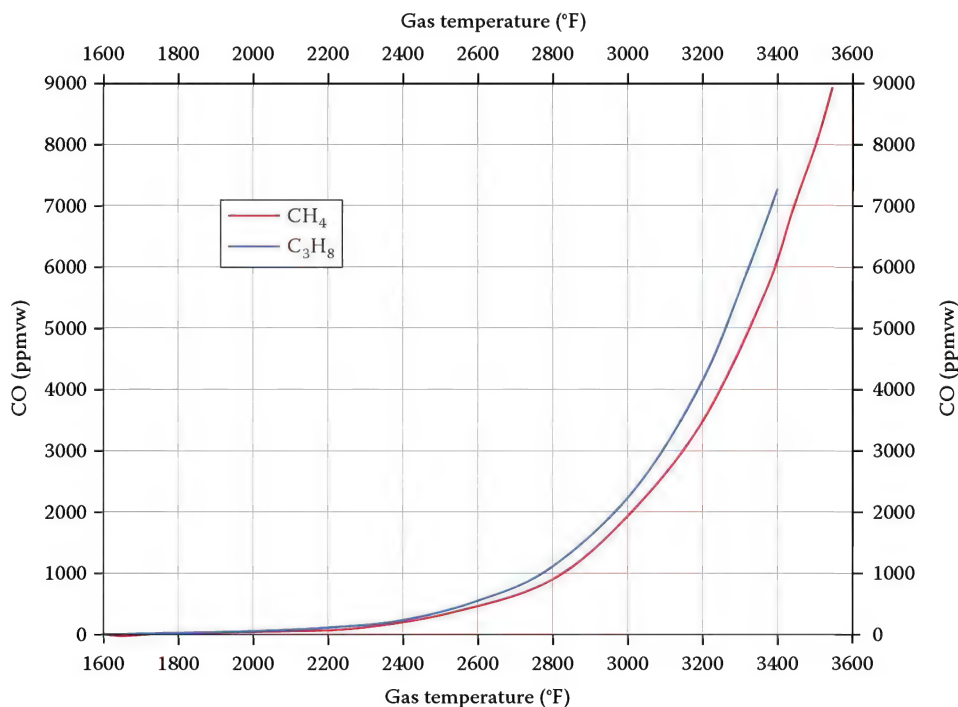


**FIGURE 14.5**  
Adiabatic equilibrium CO as a function of gas temperature for stoichiometric air/fuel flames.

### 14.2.2 Volatile Organic Compounds

VOCs are generally low molecular weight aliphatic and aromatic hydrocarbons like alcohols, ketones, esters, and aldehydes.<sup>12</sup> Typical VOCs include benzene, acetone, acetaldehyde, chloroform, toluene, methanol, and

formaldehyde. These compounds are considered to be regulated pollutants because they can cause photochemical smog and depletion of the ozone layer if they are released into the atmosphere. They are not normally produced in the combustion process, but they may be

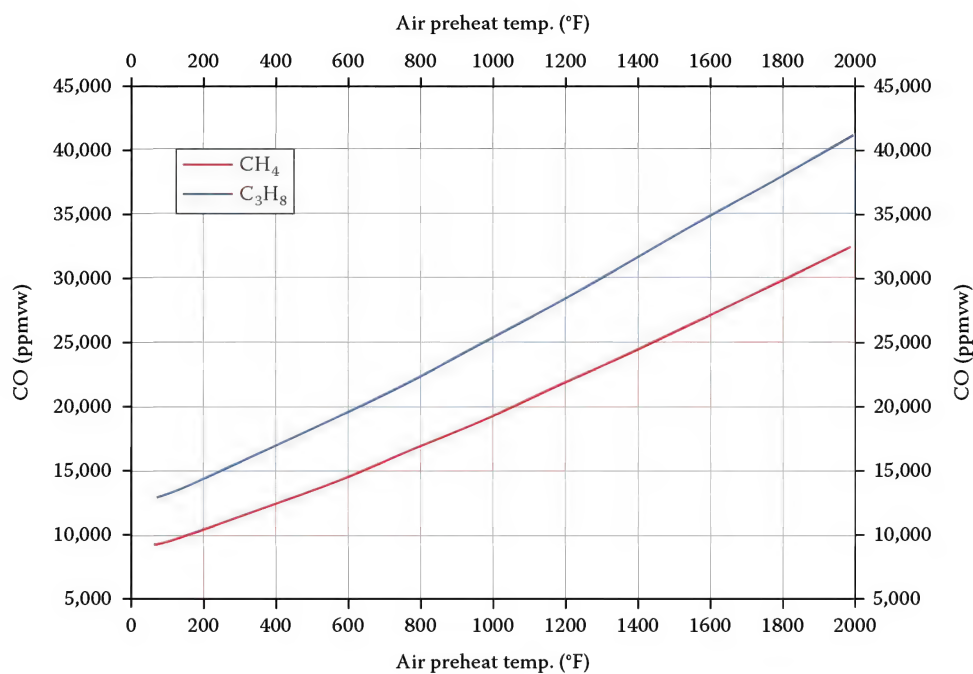


FIGURE 14.6

Adiabatic equilibrium CO as a function of air preheat temperature for stoichiometric air/fuel flames.

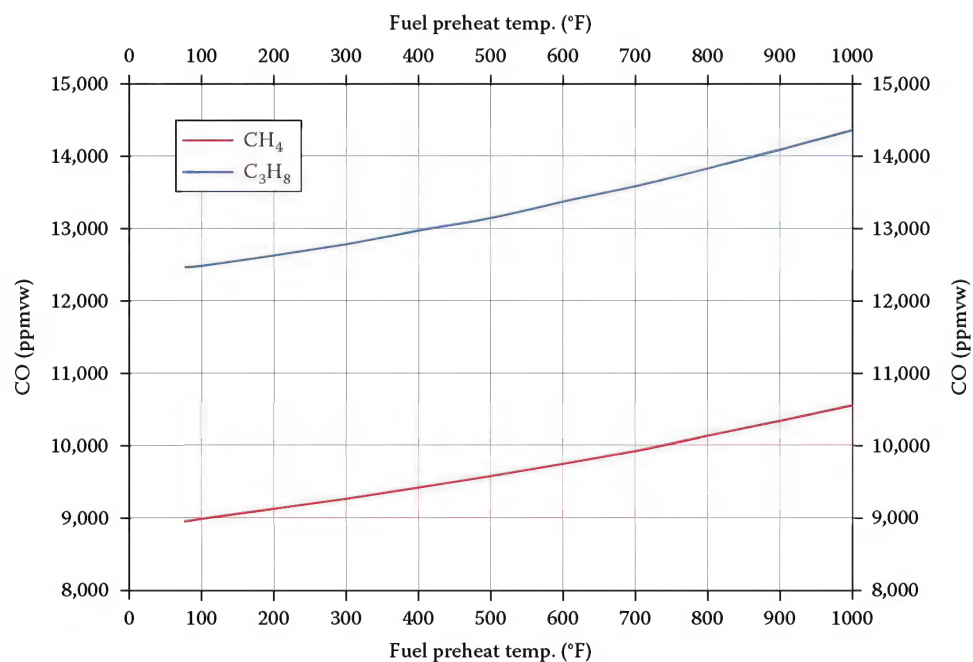
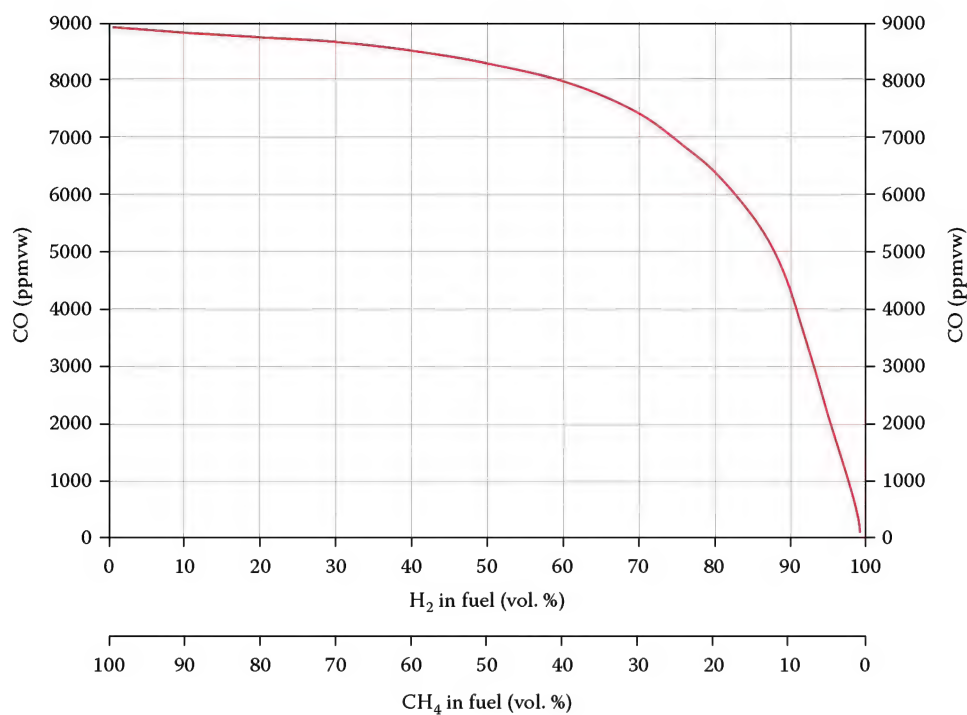


FIGURE 14.7

Adiabatic equilibrium CO as a function of fuel preheat temperature for a stoichiometric air/CH<sub>4</sub> flame.

contained in the material that is being heated, such as in the case of a contaminated hazardous waste in a waste incinerator (see Thermal Oxidizers in Volume 3). In that case, the objective of the heating process is usually to volatilize the VOCs out of the waste and combust them before they can be emitted into the atmosphere.

There are two strategies for removing VOCs from the waste gases of a combustion process.<sup>12</sup> One is to separate and recover them using techniques like carbon adsorption or condensation. The other method involves oxidizing the VOCs to CO<sub>2</sub> and H<sub>2</sub>O. This process includes techniques like thermal oxidation (see Vol. 3 on Thermal



**FIGURE 14.8**  
Adiabatic equilibrium CO as a function of fuel composition (CH<sub>4</sub>/H<sub>2</sub>) for a stoichiometric air/fuel flame.

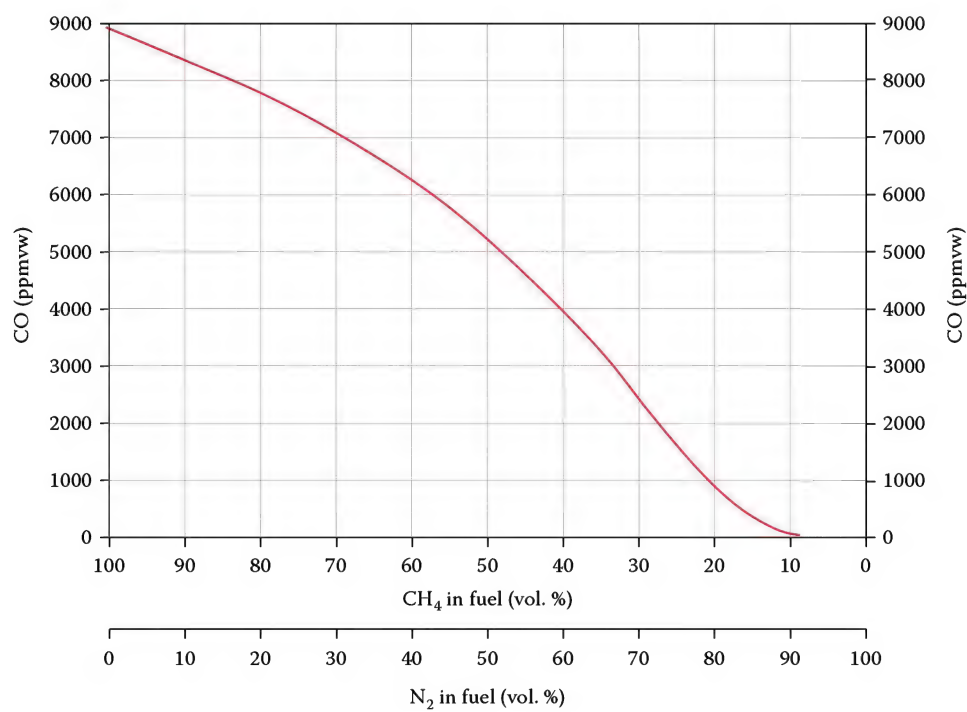


**FIGURE 14.9**  
Adiabatic equilibrium CO as a function of fuel composition (CH<sub>4</sub>/N<sub>2</sub>) for a stoichiometric air/fuel flame.



Oxidation), catalytic oxidation, and biooxidation. One common way to ensure complete destruction of VOCs in waste incinerators is to add an afterburner or secondary combustion chamber, which may or may not have a catalyst, after the main or primary combustion chamber.<sup>13</sup>

---

### 14.3 Particulates

The impact of particulate emissions on human health has been studied extensively. Some examples are listed in the references.<sup>14–18</sup> This section concentrates on particulate generation and measuring methods in industries for particulate pollutant emissions.

Usually, gas firing and light oil firing do not generate particulate emissions that impact the environment. Heavy oils like No. 6 cause concern on particulate emissions. Heavy oil flames tend to generate particulates due to high carbon contents and the difficulty in fully oxidizing droplets prior to exiting the stack.

#### 14.3.1 Combustion-Generated Particulates

Combustion-generated particles are called soot. Under certain conditions, even gaseous fuels may produce soot. Fuels that have a higher carbon-to-hydrogen mass ratio tend to produce more soot than fuels with a lower ratio. For example, propane ( $C_3H_8$ ), which has a C:H mass ratio of about 4.5 is more likely to produce soot than methane ( $CH_4$ ), which has a C:H mass ratio of about 3.0. For clean burning fuels like natural gas, it is more difficult to produce sooty flames compared to other fuels, such as oil and coal, which have little hydrogen and a high concentration of carbon.

Soot can be produced by operating in a very fuel rich mode or by the incomplete combustion of the fuel due to poor mixing. Flames containing more soot are more luminous and tend to radiate heat more efficiently than flames containing less soot, which tend to be transparent (see Chapter 7). Soot particles generally consist of high molecular weight polycyclic hydrocarbons. Ideally, soot is expected to be generated at the beginning of the flame and to be destroyed before exiting the flame. In this way, no particulates would be emitted to the environment. However, in reality, soot particles are sometimes quenched or “frozen,” making them difficult to incinerate; they are then emitted with the exhaust products. The quenching could be caused by contact with cold gases or possibly by impingement on a cool surface, such as a boiler tube.

Soot particles can cling to the exhaust ductwork, clogging the ductwork, and other pollution treatment

equipment in the system. This creates equipment maintenance problems. In addition, most industrial heating processes have a regulated limit for particulate emission.

#### 14.3.2 Parameters Controlling Combustion-Generated Particulates

Particulate emissions depend on many variables. Some of them are controlled by the burner or oil gun design. In addition to the oil gun or burner designs, oil gun operation conditions must be considered. Atomization quality is the main driving force affecting particulate generation—the better the atomization, the fewer the particulate emissions. This is discussed in detail in Volume 1, Chapter 10: Oil Atomization and Volume 3, Chapter 2: Oil Burners.

The other parameters that are not related to the oil gun or the burner are (1) oil quality and (2) furnace environment. Heavy oil usually contains some solid particles. Any particulates that are originally contained in the oil will leave the furnace with the exhaust products. The chemical composition of the particulates may be changed, but the overall mass is approximately constant. The original particulate loading can be quite significant. This should be noted when considering the particulate emissions.

As previously discussed, the furnace environment also influences particulate emissions. The two most important parameters are the furnace temperature and the residence time. Particulates will be generated when the soot particle is quenched. Therefore, the hotter the furnace is, the lower the particulate emissions are. The residence time is the time that a particle spends in the furnace. The longer the residence time, the more chance the soot particles would be burnt out; consequently, the less the particulate emissions will be. Therefore, particulate emissions might be different for two different furnaces even though the oil guns or oil burners are the same with similar operation conditions.

#### 14.3.3 Measuring Methods

Many methods are used in industry for particulate measurements, for example, Bacharach method,<sup>19</sup> Opacity method,<sup>20</sup> Method 5,<sup>21</sup> and ISO-9096.<sup>22</sup> The Bacharach and Opacity methods are qualitative. The Method 5 and ISO-9096 method are quantitative. Method 5 is recommended by the U.S. EPA and usually used for industrial compliance. In European countries, ISO-9096 is well accepted. The procedure and instrument required for Method 5 are very similar to those in ISO-9096. ISO-9096 is a concise version of the U.S. EPA Method 5.



FIGURE 14.10

Bacharach smoke tester included a hand pump, filter papers, and spot scale sheet.

#### 14.3.3.1 Bacharach Method

The Bacharach method is specified in U.S. Standard ASTM D1256-56 and in German Standard DIN51-402. The Bacharach smoke tester is a hand pump to suck the exhaust gases from the stack as shown in Figure 14.10. Filter paper is installed inside the suction tube, which is connected to the hand pump. After 10 full strokes of the hand pump, the filter paper is filled with particulates. Then, the filter paper is removed and compared with the Bacharach smoke spot scale, which consists of 10 spots from 0 to 9. Scale 0 is the lightest color with the least particulate emissions and scale 9 is the darkest color with the worst particulate emissions.

To achieve accurate sampling, it is suggested to hold each stroke for several seconds at the end of stroke. Also, pull the stroke as steadily as possible so that each stroke is about 3–4 s. Every 10th sample, the sampling tube should be cleaned and the pump should be purged with several quick strokes by pumping air without the filter paper.

#### 14.3.3.2 Opacity Method

In the simplest definition, opacity can be defined as the amount of light blocked by a medium, measured as a percentage from 0 to 100. An opacity of zero means that no light is blocked and all passes through the medium. An opacity of 100 means that 100% of the light is blocked. A more rigorous definition often used in opacity meters is<sup>23</sup>

$$\text{Opacity} = 1 - e^{(-Db)} \quad (14.11)$$

where

$D$  is the duct size, length of light beam

$b$  is the light extinction coefficient of the medium proportional to the volumetric portion of the particles in the flow

The earliest attempt to measure opacity was developed by Maximilian Ringelmann in Paris. In the late 1800s, Ringelmann developed the Ringelmann smoke charts that were introduced in the United States in 1904 and adopted as a standard in 1910. Six charts were created ranging from all white to all black corresponding to charts 0–5.<sup>24</sup> Comparing stack opacity to these charts was used for many years as the standard measure of opacity.

The EPA has adopted Method 9<sup>25</sup> as a standard to determine opacity, “Visual determination of the Opacity of Emissions from Stationary Sources.” This method uses trained and certified observers to determine opacity by visual observation; not significantly different than that of Ringelmann charts of 100 years ago.

Today, it is common for local air quality districts to use both EPA Method 9 and/or opacity measuring instruments. These instruments must be certified to standard specification.<sup>26</sup> Opacity in stack plumes is caused by the presence of particles in the plume that scatter light. These particles are generally generated from solid and liquid fuels and are a combination of ash, carbon loss, and sulfur-related compounds. The formation of these particles is covered in other chapters under oil burners (see Volume 3, Chapter 2), atomization (see Chapter 10), and solid fuels (see Chapter 5).

For the same mass particulate emission rates, the opacity can change significantly according to the size of the particles. Generally, smaller particle size distributions will result in high light scatter and higher opacity. For instance, 1  $\mu\text{m}$  particles produce 8 times greater opacity than 10  $\mu\text{m}$  particles. However, this is not continuous and peaks at about 0.8  $\mu\text{m}$ . Below 0.8  $\mu\text{m}$ , this trend reverses and further reduction in particles below 0.8  $\mu\text{m}$  results in lower opacity. In actual systems, most particulates are greater than 1  $\mu\text{m}$ .<sup>27</sup>

#### 14.3.3.3 Method 5 or ISO-9096

Method 5 is a quantity measurement and requires a special instrument, that is, a particulate sampling train as illustrated in Figure 14.11. When performing Method 5, Methods 1, 2, 3, and 4 will be automatically included: Method 1—Sample and Velocity Traverses for Stationary Sources; Method 2—Determination of Stack Gas Velocity and Volumetric Flow Rate (Type S Pitot Tube); Method 3—Gas Analysis for Carbon Dioxide, Oxygen, Excess air, and Dry Molecular Weight; Method 4—Determination of Moisture Content in Stack Gas; and Method 5—Determination of Particulate Emissions from Stationary Sources.

In the sampling train, the flue gas is sucked into the sampling probe by a motor-driven suction pump.



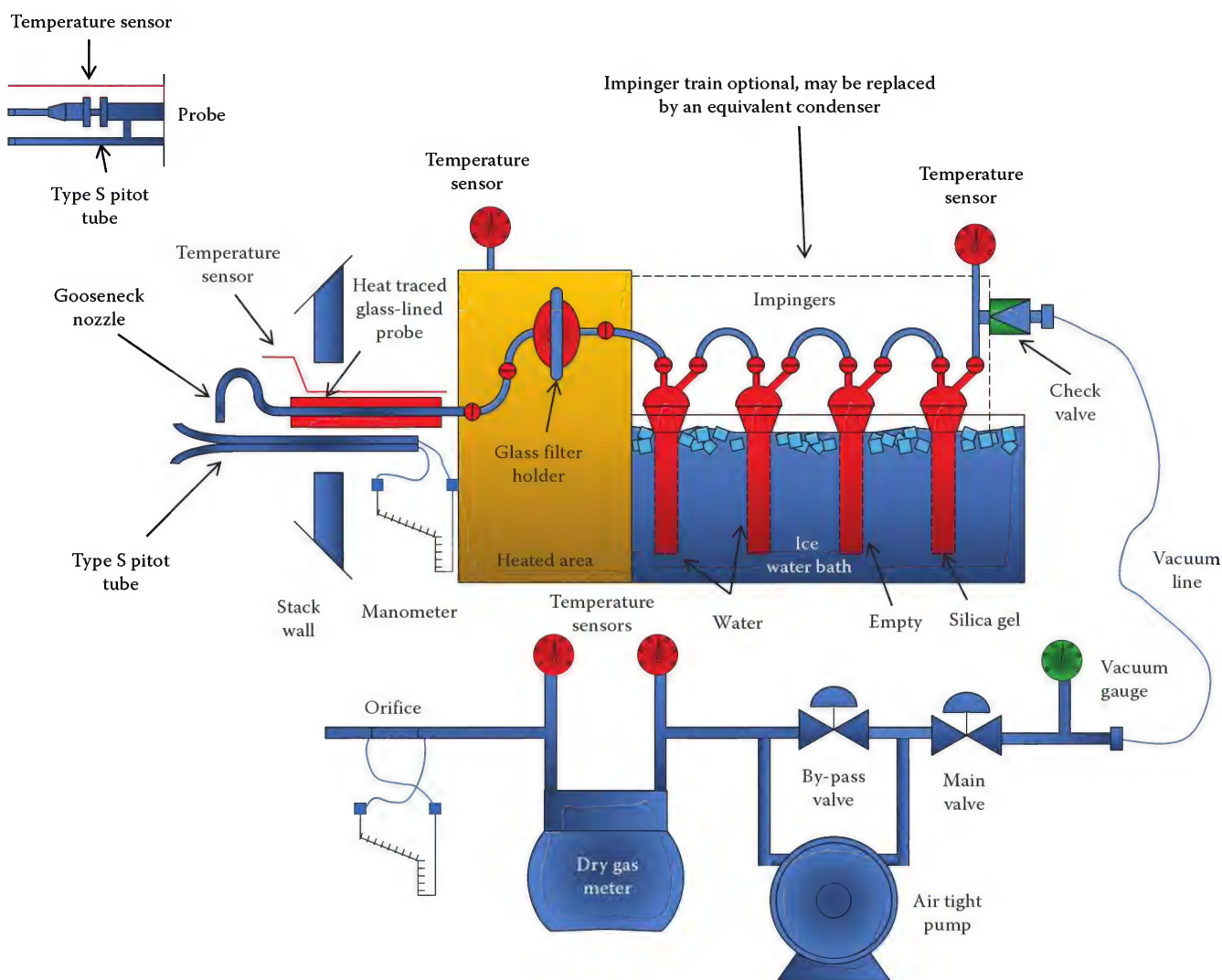


**FIGURE 14.11**  
Particulate sampling train.

The flue gas passes through filter paper, an impinger train, control valves, and a dry gas meter. The particulates are collected in the filter paper and some of them may deposit on the sampling line, which requires collection also. The moisture is collected in the impingers.

The reason that Method 5 procedures are so complicated is due to the requirement for isokinetic sampling. An isokinetic condition is where the velocity entering the sampling probe is the same as the velocity of the combustion gas in the stack. Isokinetic sampling is the only way to get true particulate concentration from particulate-suspended fluid flow.<sup>28-32</sup> When performing isokinetic sampling, a sample is taken without distorting the streamlines. If the sample rate is too low or too high with respect to the environmental gas velocity, errors will result in the particulate concentration measurements.

A simple schematic, as illustrated in Figure 14.12, demonstrates the deviation of sampling concentrations at different isokinetic variations. Isokinetic variation is the ratio of sampling nozzle suction velocity to the environmental gas velocity. At 100% isokinetic variation, as shown in Figure 14.12a, the nozzle sampling velocity is the same as the environmental gas velocity. A true particulate concentration is obtained. If isokinetic variation is less than 100% as indicated in Figure 14.12b, the nozzle sampling velocity is lower than the environmental gas velocity resulting in sampling streamlines represented by the dashed lines. Small particles follow the streamlines and escape from the nozzle. The large particles go straight into the nozzle. Therefore, the nozzle collects more large particles and less small particles than the environmental stream. The measured particulate concentration,



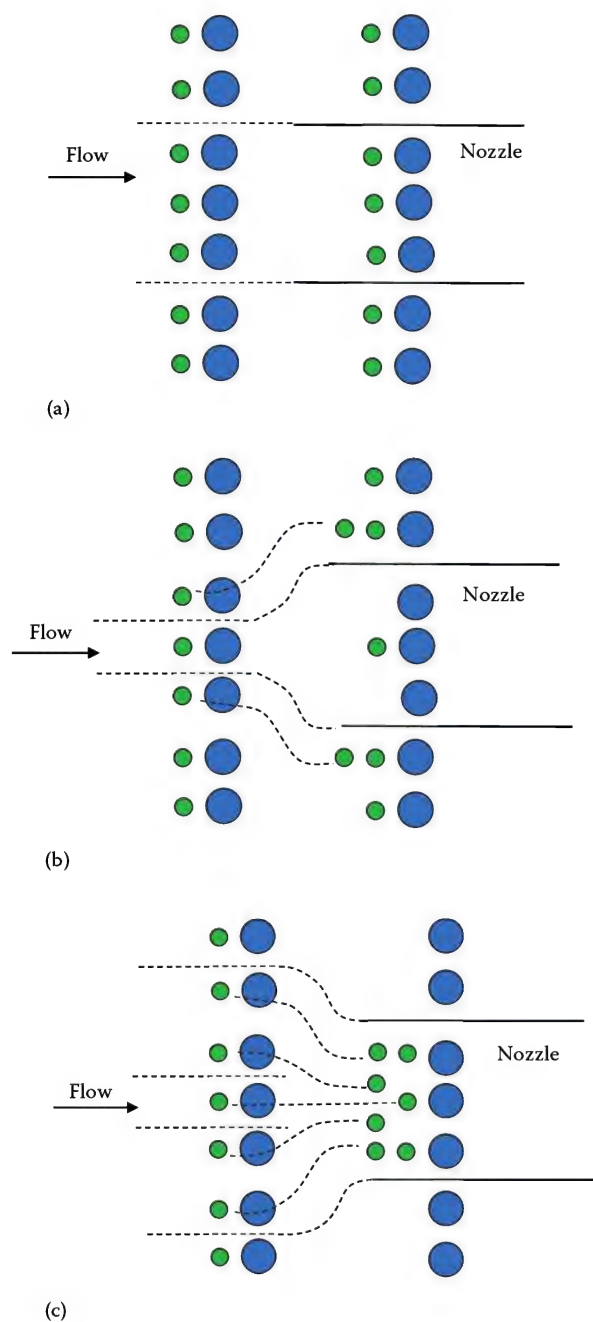


FIGURE 14.12

Sampling at different isokinetic variations. (a) 100 % isokinetic sampling, (b) less than 100 % isokinetic sampling, and (c) more than 100 % isokinetic sampling

therefore, is higher than the true value. For isokinetic variation larger than 100%, as shown in Figure 14.12c, the situation becomes reversed. The nozzle collects more small particles and less large particles than the environmental gas. The particulate concentration is thus lower than the true value.

To achieve isokinetic sampling, the stack gas velocity needs to be determined first. To measure stack velocity accurately, a complicated instrument as indicated in Figure 14.11 is required. Before performing any measurements, those instruments have to be carefully calibrated. This involves tedious preparation and calibration procedures. The whole procedure for Method 5 includes three major parts: (1) preparation, (2) on-site measurements, and (3) particulate recovery.

#### 14.3.3.3.1 Preparation

Preparation includes: (1) determination of sampling points, (2) instrument calibration, and (3) filter paper preparation.

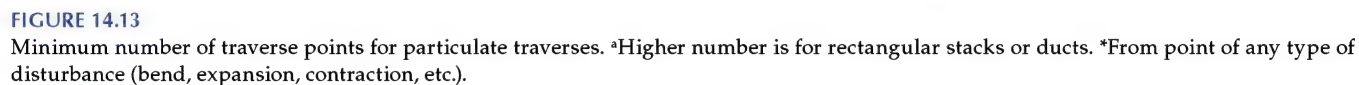
When combustion gas exits out of the stack, the velocity distribution inside the stack is not uniform and its bulk velocity varies with the heat loads in the furnace. In order to obtain a representative particulate concentration of the exhaust gas, the sampling probe must be moved to various points across the stack. Method 1 provides a guideline for selecting the representative measuring points across the stack.

Every stack has its own structure and the location of the sampling opening is different for different furnaces. Method 1 suggests that the number of traverse points in the stack should follow the guideline as shown in Figure 14.13. As for the location of traverse points, it is determined by Table 14.3. When any of the traverse points fall within one inch of the stack walls, relocate them away from the stack walls to: (1) a distance of 1 in. (2.5 cm) or (2) a distance equal to the nozzle inside diameter, whichever is larger.

At each sampling point, the isokinetic condition must be maintained. Method 2 describes the techniques for determining the stack gas velocity and volumetric flow rate. The measurements in Method 2 are necessary for the determination of the nozzle diameter and the suction rate of an isokinetic sample probe.

Methods 3 and 4 describe how to measure the molecular weight and the moisture content of the stack gas, which are required for determining the pressure drop in a pitot tube. The pitot tube (see Volume 2, Chapter 7) is an instrument used to measure the gas velocity based on Bernoulli's principle. Bernoulli's principle states that the static pressure in a fluid decreases as the velocity of the fluid increases (see Chapter 9). Bernoulli's equation can be found in any fluid dynamics textbook.<sup>33</sup>

Due to the particulate contents in the stack gas, a special pitot tube, a Type S as shown in Figure 14.14, is usually used. The Type S pitot tube has several advantages over the standard type pitot tube. It has large sensing openings that minimize the chance of plugging in heavy particulate concentrations, and provides a higher  $\Delta p$  reading than a



### Location of Traverse Points in Circular Stacks

[illegible]

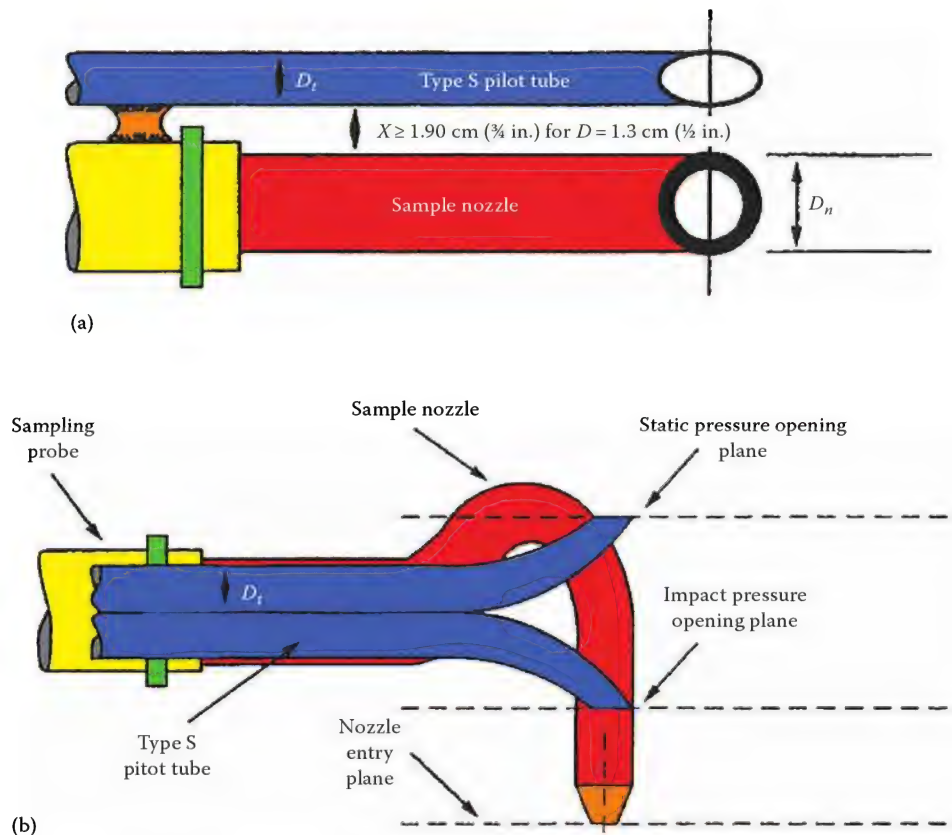


FIGURE 14.14

Type S pitot tube. (a) Bottom view, showing minimum pitot tube-nozzle separation. (b) Side view, to prevent pitot tube from interfering with gas flow streamlines approaching the nozzle. The impact pressure opening plane of the pitot tube shall be even with or above the nozzle entry plane.

standard pitot tube, which is beneficial in measuring low gas velocities.

The Type S pitot tube is not a designated standard and therefore it should be calibrated against a standard pitot tube, whose calibration factor is known. This is the first calibration procedure that is required. During calibration, the  $C_p$  value is obtained as indicated in Equation 14.12. The equation is used to calculate the flue gas velocity from pitot tube pressure drop reading ( $\Delta p$ ).

$$V_s = K_p C_p \sqrt{\frac{T_s \Delta p}{P_s M_s}} \quad (14.12)$$

where

- $V_s$  is the flue gas velocity (ft/s)
- $K_p$  is the unit factor =  $85.49 \text{ ft/s } ((\text{lb/lb mol}) (\text{in. Hg}) / (^\circ\text{R})(\text{in. H}_2\text{O}))^{1/2}$
- $C_p$  is the pitot tube coefficient
- $T_s$  is the stack gas temperature ( $^\circ\text{R}$ )
- $\Delta p$  is the velocity head of the stack gas (in. H<sub>2</sub>O)
- $P_s$  is the absolute stack gas pressure (in. Hg)

$M_s$  is the stack gas molecular weight (lb/lb mol)

The other calibration involved is the orifice meter. To measure the suction pump volumetric flow rate,  $Q_m$ , an orifice meter is installed to indicate the flow rate based on the following equation:

$$Q_m = K_m \sqrt{\frac{T_m \Delta H}{P_m M_m}} \quad (14.13)$$

where

- $K_m$  is the orifice meter calibration factor
- $T_m$  is the gas temperature
- $\Delta H$  is the pressure differential across orifice (in. H<sub>2</sub>O)
- $M_m$  is the molecular weight of gas passing through meter (lb/lb mol)

The  $K_m$  value is unknown and obtained by calibrating through different suction volume flow rates,  $Q_m$ .

After the instruments have been calibrated, the filter paper should be prepared. The filter paper should be desiccated for at least 24 h or be dried in an oven for 2–3 h. The dried filter paper needs to be weighed to a precision of the nearest 0.1 mg.



#### 14.3.3.3.2 On-Site Measurements

The furnace should maintain a steady heat load. Before sampling particulates, the stack gas velocity and volume flow rate have to be measured so that an isokinetic condition can be set. Before measuring, the sampling line needs to be leak-checked by blowing through one leg opening of the Type S pitot tube until 7.6 cm (3 in.) water column pressure shows on the manometer. Then, the opening is closed off. The pressure has to be stable at least for 15 s.

Based on the number of traverse points that were obtained from the aforementioned preparation procedure, the pitot tube is moved across all the traverse points and the  $\Delta p$  readings on the manometer are recorded. The stack gas velocity is calculated based on Equation 14.12 and the stack gas volume flow rate is corrected to the standard condition, which is 68°F (20°C) and 29.92 in. Hg (0.03989 bar).

Since the suction pump in the sampling train has a limited range of volumetric variation, a correct probe nozzle diameter has to be selected to attain isokinetic velocity. The probe nozzle diameter,  $D_n$ , can be estimated as follows:

$$D_n = \sqrt{\frac{0.0358 Q_m P_m}{T_m C_p (1 - B_{ws})}} \sqrt{\frac{T_s M_s}{P_s \Delta p_{ave}}} \quad (14.14)$$

where

$D_n$  is the nozzle diameter (in.)

$Q_m$  is the volumetric flow rate of suction pump (cfm)

$P_m$  is the absolute meter pressure (in. Hg)

$T_m$  is the dry gas meter temperature (°R)

$B_{ws}$  is the moisture content of the stack gas

$M_s$  is the gas molecular weight

$P_s$  is the gas pressure

$\Delta p_{ave}$  is the average velocity head of the stack gas across the stack (in. H<sub>2</sub>O)

After the nozzle size is determined, the meter pump rate read by  $\Delta H$  is varied with the pitot tube reading of  $\Delta p$ . There is a linear relationship between these two readings:

$$\Delta H = K \Delta p \quad (14.15)$$

The factor,  $K$ , is expressed as follows:

$$K = 846.72 D_n^4 \Delta H @ C_p^2 (1 - B_{ws})^2 \frac{M_m}{M_s} \frac{T_m}{T_s} \frac{P_s}{P_m} \quad (14.16)$$

where

$$\Delta H @ = \frac{0.9244}{K_m^2} \quad (14.17)$$

The value of  $K_m$  is established from Equation 14.13 when calibrating the orifice meter.

The sampling instrument usually has several different nozzle sizes. The nozzle that is closest to the estimation from Equation 14.14 is chosen. The pre-weighted filter paper is then installed into the filter holder. Approximately,

100 mL (6.1 in.<sup>3</sup>) of water is filled into the first two impingers and 200–300 g (0.44–0.66 lb) silica gel is put into the fourth impinger. The third impinger is left empty. The water impingers and silica gel impinger are all weighted.

The instrument needs to be checked for leakage and proper function. The ice is then placed into the condenser box of the sampling train. The probe and filter have to be maintained at operating temperature, that is, 248 ± 25°F (120 ± 14°C).

The probing time for each traverse point has to be at least 2.5 min. If the number of traverse points is low, the probing time at each traverse point should be longer. The total sample volume should be at least 30 dscf (0.85 dscm), where d represents dry gas, or total sampling time should be at least 60 min.

#### 14.3.3.3.3 Particulate Recovery

The procedure of recovering particulates is important. The particulates should be recovered not only from the filter paper, but also from the filter holder and fittings. All the particulates and filter paper are put in a container to be oven-dried and weighed.

Other particulates that are on the probe nozzle, lines, and fittings are washed with acetone. The washed acetone is collected in the other container. The container is then evaporated to dryness at ambient temperature and pressure, and desiccated for 24 h before weighing.

The silicone gel and water impingers are weighed before and after sampling. The weight difference is used for calculating stack gas moisture content. The dry gas volume flow rate is required when evaluating the isokinetic variation.

As described earlier, if the experiment is 100% isokinetic variation, the measurement is the true particulate concentration. If isokinetic variation is less than 100%, the measurement is larger than the true isokinetic value. If isokinetic variation is larger than 100%, the measurement is less than the true isokinetic value. Usually, when the isokinetic variation is within ±20%, the particulate measurements deviation is around 10%. If isokinetic variation is off too much, the measurement is not accurate.

Performing Method 5 measurements requires correct instrument calibrations, rigorous leakage checking, and accurate calculations. It is not an easy task. It is highly recommended to have trained professionals to perform the test for accurate results.

## 14.4 Carbon Dioxide

Carbon dioxide (CO<sub>2</sub>) is a colorless, odorless, inert gas that does not support life since it can displace oxygen and act as an asphyxiant. It is found naturally in the atmosphere at concentrations averaging 0.03% or 300 ppmv. Concentrations of 3%–6% can cause

headaches, dyspnea, and perspiration. Concentrations of 6%–10% can cause headaches, tremors, visual disturbance, and unconsciousness. Concentrations above 10% can cause unconsciousness eventually leading to death.

Some studies indicate that CO<sub>2</sub> is a greenhouse gas that contributes to global warming. A greenhouse gas is a gas in the atmosphere that absorbs and emits radiation within the thermal infrared range. This process is the fundamental cause of the greenhouse effect.

#### 14.4.1 CO<sub>2</sub> Generation

There are a number of different anthropogenic sources of CO<sub>2</sub> emissions. Predominately, the emissions are from the combustion of fossil fuels. CO<sub>2</sub> is produced when a fuel containing carbon is combusted. The International Energy Agency (IEA)<sup>34</sup> has estimated the CO<sub>2</sub> emissions from various sources worldwide in the year 2000. They reported that emissions of CO<sub>2</sub> from fossil fuels globally totaled about 23.5 GtCO<sub>2</sub> per year. Of this, close to 60% were attributed to large stationary emissions sources, such as power generation, cement production, refineries, iron, and steel industry, petrochemical industry, and oil and gas processing. Therefore, reduction of CO<sub>2</sub> emissions is mainly targeted at those stationary sources.

#### 14.4.2 CO<sub>2</sub> Capture

Many schemes have been suggested for reduction of CO<sub>2</sub> emissions including energy efficiency improvement, fuel switching, nuclear power, solar power, wind power, renewable sources of energy, and CO<sub>2</sub> capture and storage (CCS). In this section, only CCS is discussed since this technology is mainly applied to large industrial stationary CO<sub>2</sub> production sources.

Broadly, there are three types of technologies for CCS: postcombustion, precombustion, and oxy/fuel combustion.

In post-combustion capture, CO<sub>2</sub> is removed after the combustion of a carbon-containing fuel. Instead of being discharged directly into the atmosphere, the flue gas is passed through equipment that separates most of the CO<sub>2</sub>. The separation is achieved by passing the flue gas in close contact with a liquid absorbent or solid sorbent that is capable of capturing CO<sub>2</sub>. Other schemes such as separation with membranes or by cryogenic distillation are also used. These technologies are well developed, adapted mainly from the acid gas removal process. The acid gas removal process is to remove hydrogen sulfide (H<sub>2</sub>S), CO<sub>2</sub>, or similar contaminants in raw natural gas or other gas mixtures in natural gas industries.

For pre-combustion technology, the fossil fuel is partially oxidized to generate syngas (CO and H<sub>2</sub>). The syngas is then reacted with steam in a catalytic reactor to convert CO into CO<sub>2</sub> and generate more H<sub>2</sub>. After that, the CO<sub>2</sub> is separated, usually by a physical or chemical absorption process, resulting in a hydrogen-rich fuel. Compared to

post-combustion technology, the resulting CO<sub>2</sub> in this technology can be captured in a relatively pure stream.

The other way to obtain pure CO<sub>2</sub> stream is oxy/fuel combustion.<sup>35</sup> The fuel is burned with pure oxygen instead of air, resulting in a flue gas that is mainly CO<sub>2</sub> and H<sub>2</sub>O. If fuel is combusted using pure oxygen, the flame temperature will be extremely high. The CO<sub>2</sub> and/or H<sub>2</sub>O-rich flue gas can be recirculated back to the combustion chamber to lower the flame temperature. The advantage of oxy/fuel combustion is little NO<sub>x</sub> emissions if there is any due to no nitrogen in the combustion process (assuming little if any N<sub>2</sub> in the fuel and air leakage into the combustor). The detailed discussion on CO<sub>2</sub> capture technologies can be found in reference [34].

#### 14.4.3 CO<sub>2</sub> Transport

After CO<sub>2</sub> is collected, it needs to be transported to a storage area. Two methods are currently in use for transport of CO<sub>2</sub>: pipeline and motorized transport (ship, road, and rail tankers). Pipelines are more common. CO<sub>2</sub> is typically compressed to above 8 MPa (1160 psig) at ambient temperature to avoid two-phase flow. In the United States, over 30 MtCO<sub>2</sub> per year are sent through more than 2500 km (1600 mi) of pipeline to the sites in Texas for enhanced oil recovery (EOR). For acid gas applications, the CO<sub>2</sub> waste stream could be reinjected back to the gas wells. Deep injection of liquid wastes, and acid gas disposal (mixtures of CO<sub>2</sub> and H<sub>2</sub>S) have been conducted in Canada and the United States since 1990.

In some locations, transport of CO<sub>2</sub> by ship may be more economically attractive, particularly when CO<sub>2</sub> has to be moved over a long distance or overseas. According to one source,<sup>36</sup> marine transportation is more cost-effective than pipelines for distances greater than 1000 km (620 mi) and amounts smaller than a few million tons per annum. Currently, CO<sub>2</sub> transported by ship takes place on a small scale mainly because of limited demand. CO<sub>2</sub> transported by ship is held at a pressure of 0.7 MPa (101 psig). Road and rail tankers also are technically feasible options. These systems transport CO<sub>2</sub> at temperatures of –20°C (–4°F) and pressures of 2 MPa (290 psig). However, they are uneconomical compared to pipelines and ships, except on a very small scale.

#### 14.4.4 CO<sub>2</sub> Storage

Most large-scale CO<sub>2</sub> storage is underground. Four options exist for geological storage: (1) use of depleted oil and gas reservoirs; (2) use in enhanced coal bed methane (ECBM) recovery; (3) injection in deep saline formations; and (4) use in EOR. In each case, CO<sub>2</sub> is injected in dense form.

Geological storage of CO<sub>2</sub> is ongoing in three industrial-scale projects: the Sleipner project in the North Sea, the Weyburn project in Canada, and the In Salah project

in Algeria. As for EOR, it is mostly in Texas, United States, where EOR commenced in the early 1970s. Much of the  $\text{CO}_2$  injected for EOR is produced with the oil, from which it is separated and then reinjected.

#### 14.4.5 $\text{CO}_2$ Usage

Except for large quantities of  $\text{CO}_2$  used for EOR, a large portion of  $\text{CO}_2$  recovered is used to make chemicals. Industrial usage for  $\text{CO}_2$  includes chemical production—for example, urea, refrigerants, inert agents in food packaging, carbonation of beverages, industrial gas welding systems, fire extinguishers, water treatment, calcium carbonate precipitation (paper industry), and many other small-scale applications. Currently, the total industrial use is approximately 120  $\text{MtCO}_2$  per year worldwide, excluding use for EOR. This amount is small compared to the emissions from major sources generated by human activities, that is, 13,500  $\text{MtCO}_2$  per year.<sup>36</sup> Therefore, global  $\text{CO}_2$  reduction, such as alternative energy usage, is necessary.

#### 14.5 $\text{SO}_x$

Sulfur oxides, usually referred to as  $\text{SO}_x$ , include  $\text{SO}$ ,  $\text{S}_2\text{O}$ ,  $\text{S}_n\text{O}$ ,  $\text{SO}_2$ ,  $\text{SO}_3$ , and  $\text{SO}_4$  of which  $\text{SO}_2$  and  $\text{SO}_3$  are of particular importance in combustion processes.<sup>37</sup> Sulfur dioxide ( $\text{SO}_2$ ) tends to be preferred at higher temperatures while  $\text{SO}_3$  is more preferred at lower temperatures.<sup>38</sup> Since most combustion processes are at high temperatures,  $\text{SO}_2$  is the more predominant form of  $\text{SO}_x$  emitted from systems containing sulfur. For combustion at low excess air levels, more  $\text{SO}_2$  is produced and less  $\text{SO}_3$  is produced.<sup>39</sup>

$\text{SO}_2$  is a colorless gas with a pungent odor that is used in a variety of chemical processes. It can be very corrosive in the presence of water. It is considered a pollutant because of the choking effect it can cause on the human respiratory system. It is also damaging to green plants, which are more sensitive to  $\text{SO}_2$  than people and animals. When  $\text{SO}_2$  is released into the atmosphere, it can produce acid rain by combining with water to produce sulfuric acid ( $\text{H}_2\text{SO}_4$ ). Sulfuric acid is very corrosive and can cause considerable damage to the environment.

It is often assumed that any sulfur in a combustor will be converted to  $\text{SO}_2$  that will then be carried out with the exhaust gases.<sup>40</sup> The sulfur may come from the fuel or from the raw materials used in the production process. Fuels like heavy oil and coal generally contain significant amounts of sulfur while gaseous fuels like natural gas tend to contain little if any sulfur. The two strategies for minimizing or eliminating  $\text{SO}_x$  are (1) removing the sulfur from the incoming fuel or raw materials and (2) removing the  $\text{SO}_x$  from the exhaust stream using a variety of dry and wet scrubbing techniques.<sup>41</sup> One dry

scrubbing technique is limestone injection. After use, the combined limestone and sulfur can be used in gypsum board. New membrane separation technologies are another reduction technique being developed.

#### 14.6 Hazardous Air Pollutants

In the United States, the 1990 Amendments to the Clean Air Act promulgated new regulations by the U.S. Environmental Protection Agency on emissions of hazardous air pollutants (HAPs) from process heaters and industrial boilers used in the petroleum, petrochemical, and chemical sectors.<sup>42</sup> Unfortunately, the science upon which to base those regulations was extremely limited and the paucity of field data then extant was severely flawed. To address those deficiencies, a 4-year \$7-million fundamental study on the origin and fate of trace emissions from gaseous hydrocarbon external combustion was initiated by a government–university–industry collaboration.<sup>43</sup> This collaboration produced fundamental knowledge and phenomenological understanding in two important areas, one basic and one applied:

- A flame is an extraordinarily effective reactor. From a basic standpoint, the program elucidated why and how the hot, rich diffusive zones are prolific manufacturers of a myriad of reaction intermediates from the light, partially oxygenated species through the heavy Polycyclic aromatic hydrocarbon (PAHs).
- Emissions of products of incomplete combustion (PICs) from typical petroleum industry burners are extremely low. From the applied standpoint, the program elucidated why and how the highly reactive diffusive jets of typical petroleum industry burners are extremely effective in destroying the myriad of reaction intermediates that are manufactured in the hot, rich zones.

This section discusses that study on HAPs in the refinery, chemical, and petrochemical industries. Some relevant references on HAPs are given in Refs. [44–69].

##### 14.6.1 Experimental Setup

###### 14.6.1.1 Experimental Facility

The experimental facility in which full-scale petroleum industry burners were tested is illustrated in Figure 14.15. The Burner Engineering Research Laboratory (BERL) located at the Combustion Research Facility, Sandia National Laboratories (Livermore, California)



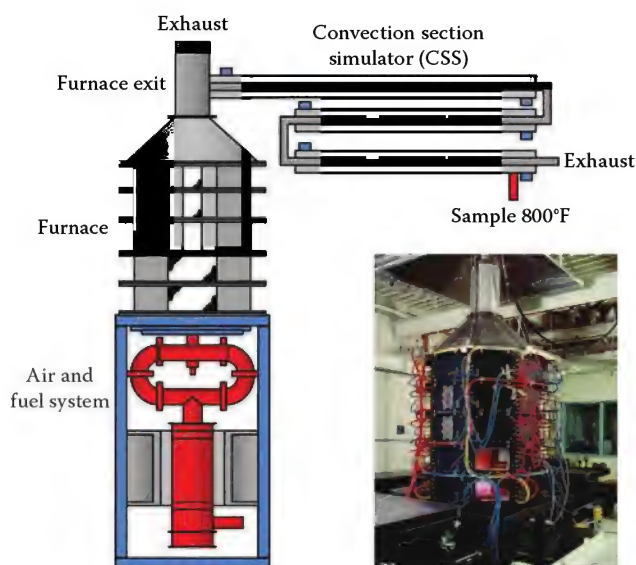


FIGURE 14.15  
BERL experimental facility. (Courtesy of Sandia.)

provided controlled, stable, and well characterized operating conditions for full-scale burners. The BERL also featured laser diagnostic and air emissions testing capabilities that allowed complete characterization of industrial burner flames and emissions.

The experimental rig accommodated up to a 900 kW ( $3 \times 10^6$  Btu/h) full-scale burner. It consisted of two distinct sections: the furnace section and the convection section simulator (CSS) that is illustrated in Figure 14.16. The walls of the furnace section were water-cooled for radiative extraction of heat from the combustion gases. From the furnace section, the combustion gases flowed to the quartz-lined CSS, which was designed to duplicate the exit temperature profile seen in full-scale process heaters.

While BERL was optimized for the study of flame structure, petroleum refinery process heaters are optimized for efficiency and economy. Because of this, a petroleum refinery process heater employs a convection section for additional heat extraction before rejecting the combustion gases to atmosphere, a feature that was originally not needed in BERL. Since previous kinetics studies indicated that a significant amount of reaction chemistry may occur in the convection section, a fact that was verified in this study, a CSS was added to BERL. Instead of an actual

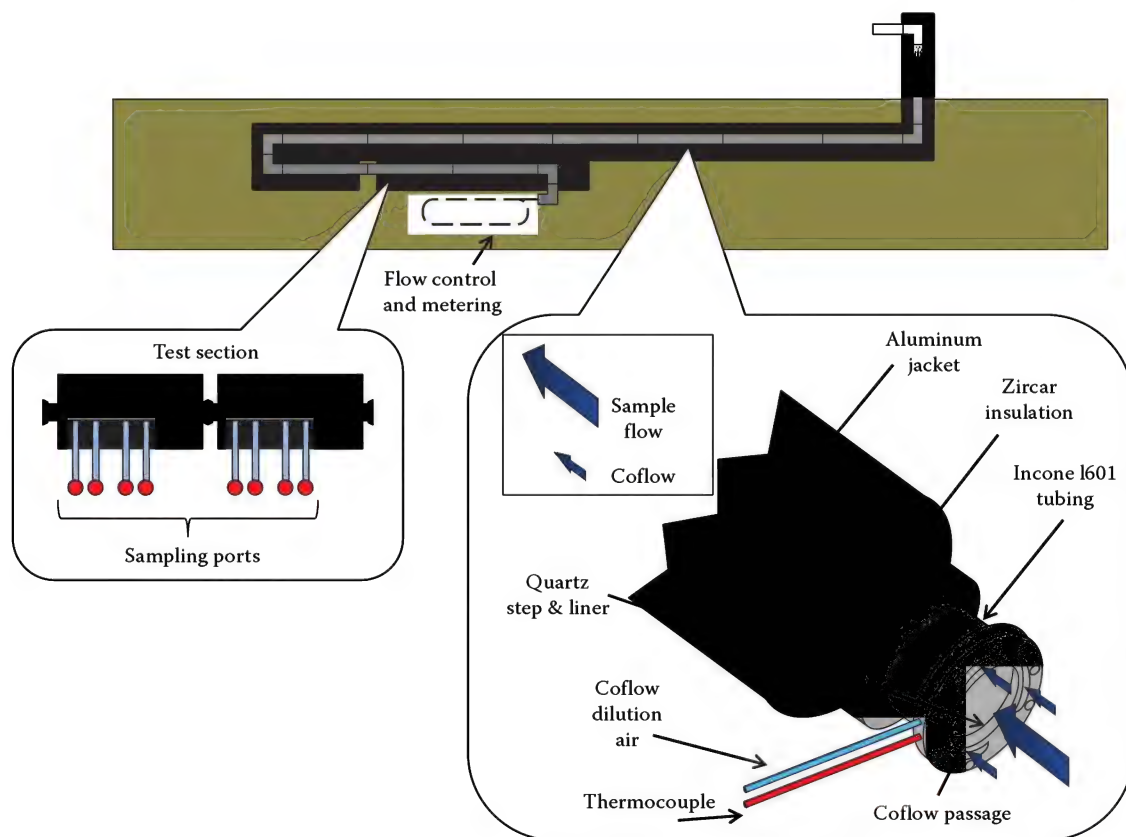


FIGURE 14.16  
CSS. (Adapted from Seebold, J.G. and Waibel, R.T., Products of incomplete combustion (PIC) from petroleum, petrochemical & chemical sector process heaters and industrial boilers, 10th International Congress on Combustion By-Products and Their Health Effects, Ischia, Italy, June 17–20, 2007.)

convection section, the project team decided to construct a CSS. The CSS closely matched the temperature-time profiles of petroleum refinery process heaters over a range of mean cooling rates. Mixing was accomplished by adding a series of steps and miters to the walls of the CSS that created turbulence in the gas flow. Catalytic effects between the gas stream and the CSS were prevented by lining all parts of the CSS exposed to the gas stream with quartz. The CSS is illustrated in Figure 14.16. Sample locations were chosen to ensure that the sample obtained represented the flue gas exhaust stream and desired sample conditions. Flue gas slipstreams were pulled from BERL both before and after the CSS. This combined approach enabled the flexibility to study independently the effects of both flame characteristic variability and exhaust temperature/residence time variability on PICs formation and destruction.

#### 14.6.1.2 Full-Scale Burner Tests

A conventional diffusion flame burner (CDFB) is illustrated in Figure 14.17. This CDFB has all of the fuel injection tips in the combustion air stream inside the burner tile. The near stoichiometric, turbulent diffusion mixing of the fuel and air results in high flame temperatures and high  $\text{NO}_x$  levels.

A low  $\text{NO}_x$  diffusion flame burner (LDFB) is illustrated in Figure 14.18. This LDFB has both primary and staged fuel injection tips located in the furnace on the periphery of the burner tile. Both the primary fuel and staged fuel entrain furnace gases prior to mixing with

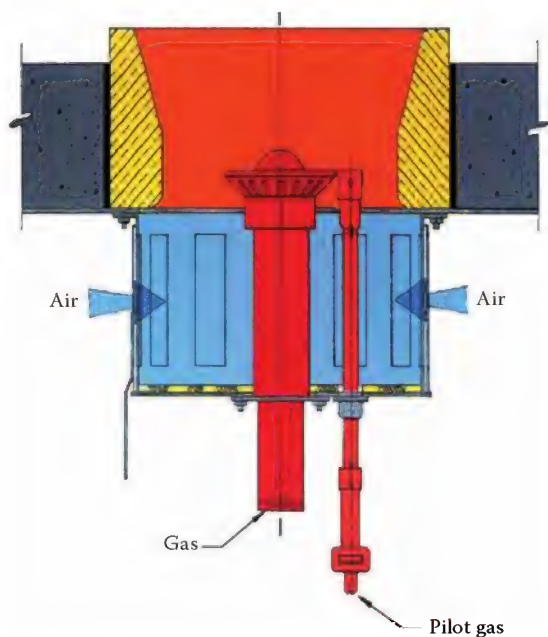


FIGURE 14.17  
CDFB

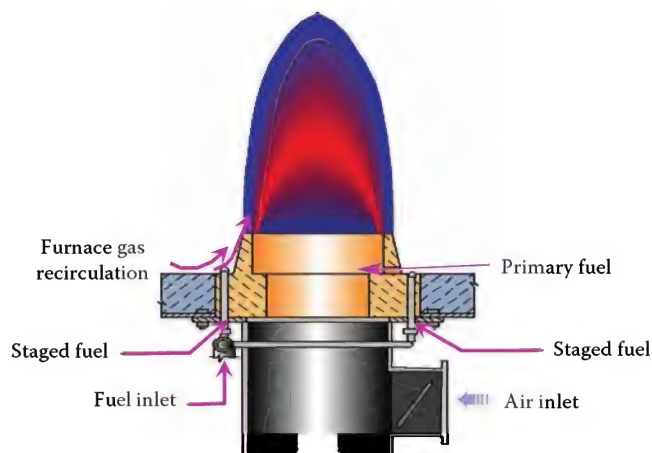


FIGURE 14.18  
Low  $\text{NO}_x$  diffusion flame burner (LDFB).

air. The inert furnace gases dilute the fuel stream minimizing prompt  $\text{NO}_x$  and reduce peak flame temperatures minimizing thermal  $\text{NO}_x$ .

#### 14.6.2 Experimental Results

##### 14.6.2.1 No Systematic Variation

In this program, it was found that the nature of the gaseous hydrocarbon fuel mixture did not make much difference, neither in the total PIC emissions nor in the individual species levels. This observation includes natural gas, which is itself another hydrocarbon mixture; that is, there is no reason to distinguish "refinery fuel gas" from "natural gas." Almost stochastic in nature, the individual species levels seemed to be dependent less upon physics and chemistry and more upon the vagaries of the sophisticated sampling methods and precise analytical techniques that are required to detect them in the minute concentrations in which they appear in the combustion products.

In Figures 14.19 through 14.22, these facts are illustrated by the mass emission of total hydrocarbons. Except for an operationally unrealistic super-aerated (450% stoichiometric air) case, there was no significant effect of heating value, combustion zone stoichiometry, propylene or ethylene spikes, or hydrogen content.

The heating value variation was achieved at the constant base case 16% hydrogen content by increasing the proportion of propane in the hydrogen/natural gas/propane mixture. The field-operational typical  $\pm 15\%$  theoretical air variation around the base case 125% was extended substoichiometrically in the combustion zone to 50% or one-half of the air theoretically required for complete combustion with overfire air added to simulate a leaky furnace while still maintaining the base case 125% theoretical air in the stack; additionally, in other tests to be discussed later, the combustion air was

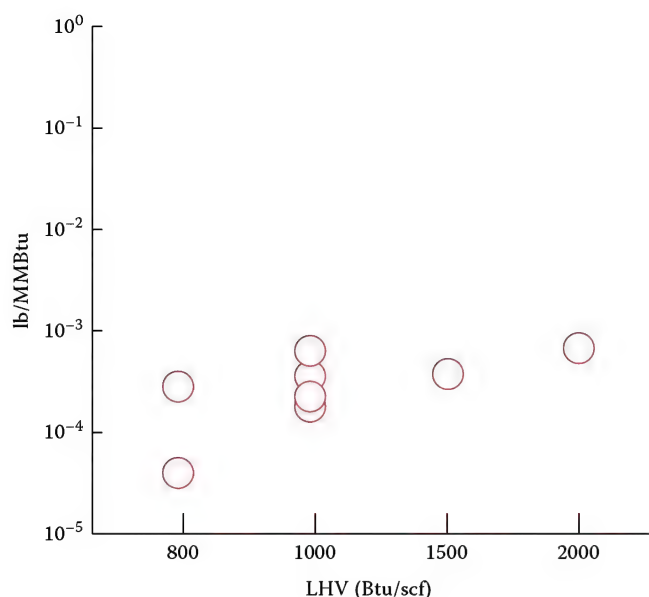


FIGURE 14.19

CDFB total hydrocarbon emissions versus heating value of HC fuel mixture. (Adapted from Seebold, J.G. and Waibel, R.T., Products of incomplete combustion (PIC) from petroleum, petrochemical & chemical sector process heaters and industrial boilers, *10th International Congress on Combustion By-Products and Their Health Effects*, Ischia, Italy, June 17–20, 2007.)

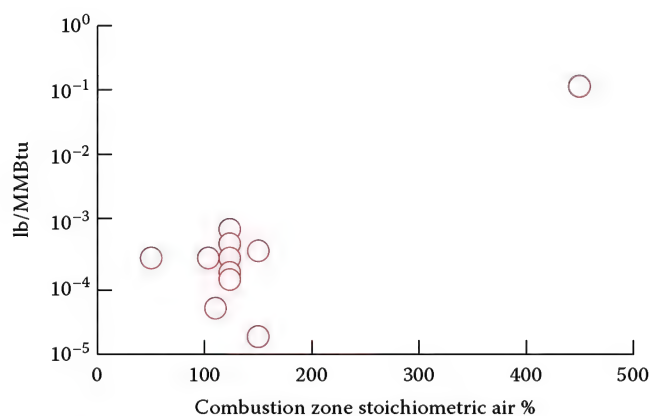


FIGURE 14.20

CDFB total hydrocarbon emissions versus combustion zone stoichiometry. (Adapted from Seebold, J.G. and Waibel, R.T., Products of incomplete combustion (PIC) from petroleum, petrochemical & chemical sector process heaters and industrial boilers, *10th International Congress on Combustion By-Products and Their Health Effects*, Ischia, Italy, June 17–20, 2007.)

limited to less than 50% of theoretical right through and out the stack. The theoretical air variation was extended superstoichiometrically in the combustion zone to 450% or four-and-half times the air theoretically required for complete combustion simply by increasing the air delivery to the burner.

The absence of systematic variability in the trace emissions of PICs in hydrocarbon gaseous external

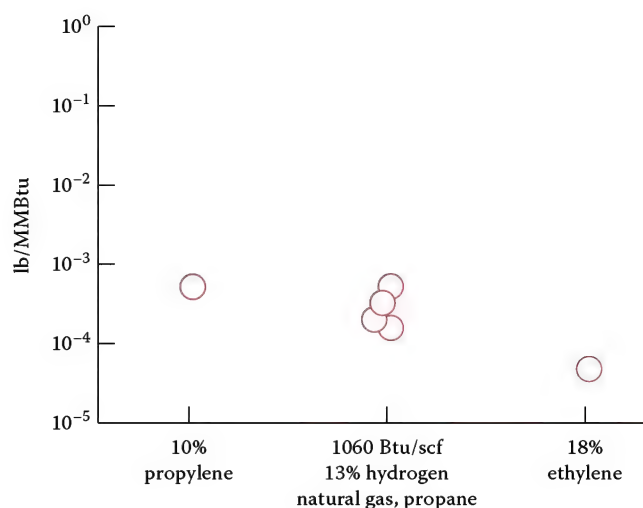


FIGURE 14.21

CDFB total hydrocarbon emissions versus propylene and ethylene spikes. (Adapted from Seebold, J.G. and Waibel, R.T., Products of incomplete combustion (PIC) from petroleum, petrochemical & chemical sector process heaters and industrial boilers, *10th International Congress on Combustion By-Products and Their Health Effects*, Ischia, Italy, June 17–20, 2007.)

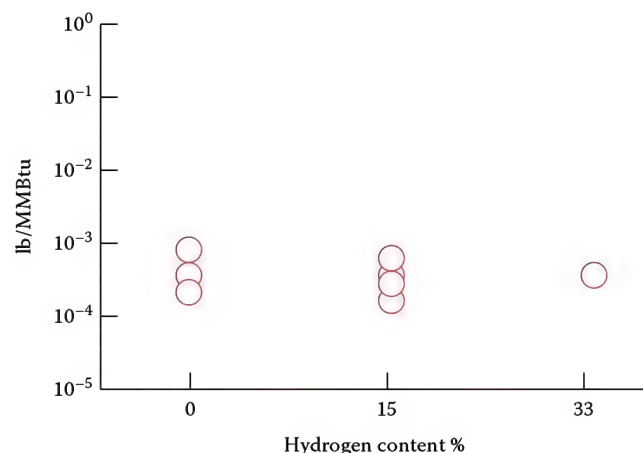


FIGURE 14.22

CDFB total hydrocarbon emissions versus hydrogen content of HC fuel mixture. (Adapted from Seebold, J.G. and Waibel, R.T., Products of incomplete combustion (PIC) from petroleum, petrochemical & chemical sector process heaters and industrial boilers, *10th International Congress on Combustion By-Products and Their Health Effects*, Ischia, Italy, June 17–20, 2007.)

combustion is illustrated in Figures 14.23 and 14.24. The reproducibility of the reference regulatory base cases ("A1" was a 1050 Btu/scf mixture of 16% hydrogen, natural gas, and propane while "A4" was 1050 Btu/scf natural gas) remained good throughout all of the CDFB trials in test sequences A, B, and C. While test sequence A spanned a broad range of fuel compositions and operating conditions around the normal operation base cases A1 and A4, there was



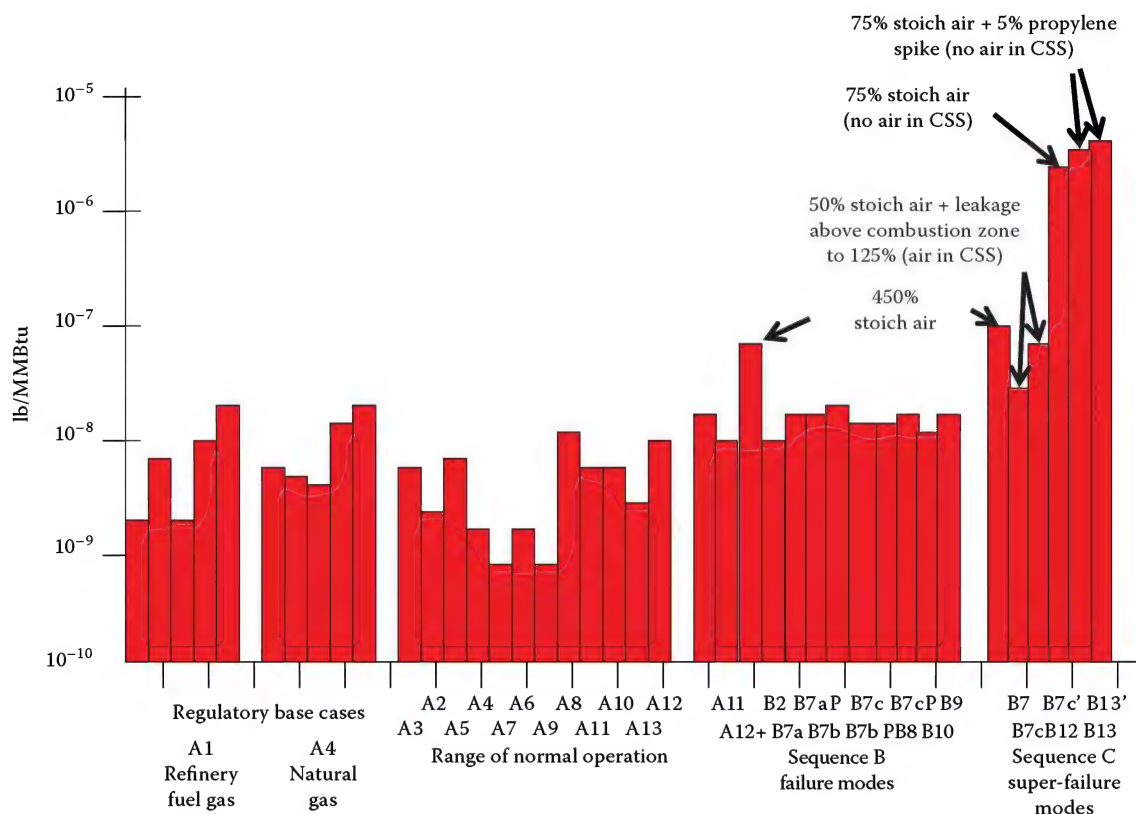


FIGURE 14.23

CDFB total PAH at stack outlet. (Adapted from Seebold, J.G. and Waibel, R.T., Products of incomplete combustion (PIC) from petroleum, petrochemical & chemical sector process heaters and industrial boilers, *10th International Congress on Combustion By-Products and Their Health Effects*, Ischia, Italy, June 17–20, 2007.)

no systematic variation in emissions; all emissions remained exceedingly low and the small differences were well within the typical bounds of experimental variability.

PAH emissions as high as those reported in some field tests could not be reproduced even in the sequence B “failure mode” tests. In the sequence C “super-failure mode” trials, stack emissions up to  $2 \times 10^{-6}$  lb-PAH/MMBtu (e.g., B13’ in Figures 14.23 and 14.24) were measured, as high as any in the “real-world” field data base. These high emissions are often attributed, but without much definition and no detailed understanding, to the so-called “gross mixing failures.”

As illustrated in Figures 14.23 and 14.24, to generate high stack emissions from gaseous hydrocarbon mixtures in external combustion, severe fuel–air mixing failures were required, egregious hypothetical extreme combustion conditions that would hardly be tolerated nor permitted to persist in any well-run plant.

To sustain these conclusions, it was important to confirm that the CSS did not sequester PAHs nor otherwise produce misleading results. The suitability of the

CSS was confirmed by direct calibration runs, injecting known PAH concentrations in an inert, but otherwise identical-condition flow, and confirming by direct measurement that what went in did, in fact, come out. Furthermore, it may be observed that in the actual test runs in which there was virtually no air in the CSS, the inlet PAHs came through virtually unreacted (e.g., B12, B12’, and B13’ in Figure 14.24), just as they should have done, while in the presence of excess air, which is the usual case in the field, and just as the program’s kinetic modeling led to the expectation, the high CSS-inlet (furnace-outlet) PAH concentrations were consumed (e.g., B7C and B7C’ in Figure 14.24) before the flue gas emerged into the atmosphere.

#### 14.6.2.2 High Velocity Jet Mixing Produces Low PICs

The strong mixing potential of sonic jets is well known. In the case of choked jets exhausted to atmosphere, for instance, it is common for an initially toxic composition rapidly to automix down to harmless concentrations. In the case of the multiple, small reacting jets of the CDFB, surrounded as they are (under normal

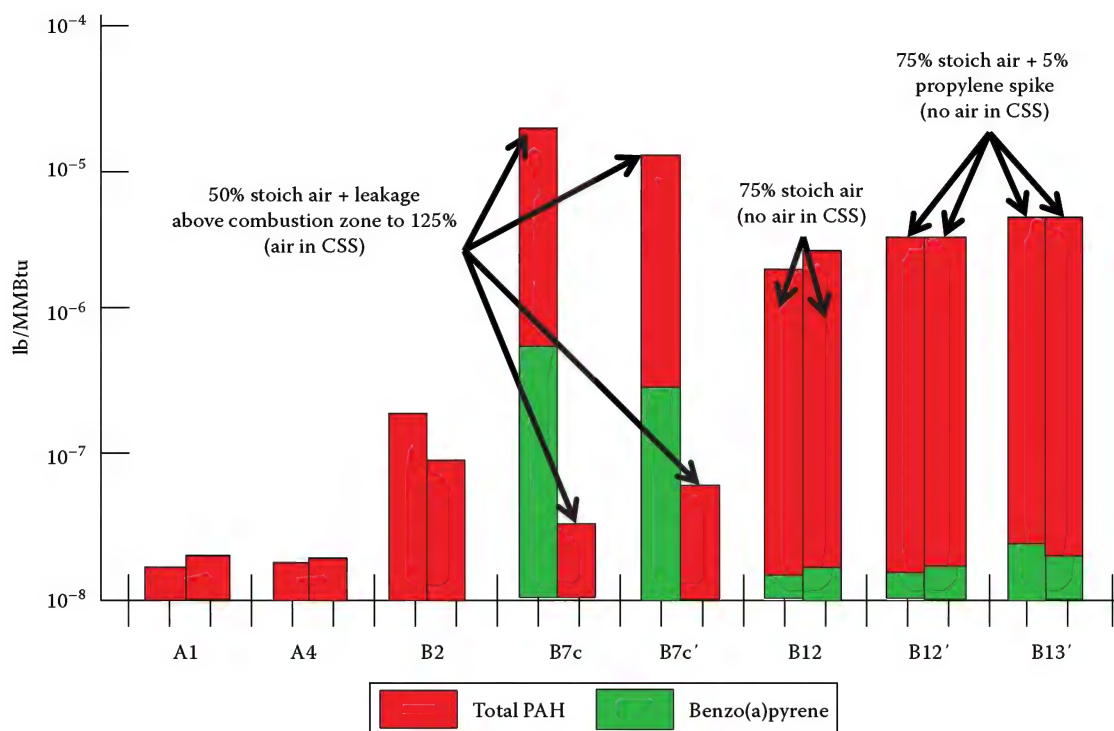


FIGURE 14.24

CDFB total PAH and benzo(a)pyrene at furnace outlet compared to stack outlet. (Adapted from Seebold, J.G. and Waibel, R.T., Products of incomplete combustion (PIC) from petroleum, petrochemical & chemical sector process heaters and industrial boilers, 10th International Congress on Combustion By-Products and Their Health Effects, Ischia, Italy, June 17–20, 2007.)

conditions) with an excess supply of oxidant (air), similar behavior would be expected.

Early in the program, it was hypothesized that the hot, rich combustion regions that are necessarily present in a diffusion flame ought to be prolific generators of individual hydrocarbon species in all possible elemental molecular combinations. The early stirred-reactor, plug-flow computations carried out by Lawrence Livermore National Laboratory supported the hypothesis, while later the laboratory flame measurements carried out at the UCLA Chemical Engineering Laboratory, as well as the research furnace experiments carried out at the BERL, confirmed it. The Lawrence Livermore calculations also suggested that, in the presence of excess air, the individual hydrocarbon species that are necessarily profusely generated in the rich zone would subsequently quickly be consumed to near-extinction, a prediction that was seen borne out time and time again in the full-scale burner trials carried out at the BERL.

Most significant, particularly in light of the results of the last-completed "Sequence E" super-failure mode trials, are the results of Sandia's application of a two-stage Lagrangian jet model to a typical CDFB jet. Based upon the observed flame structure of the conventional burner, the jet model was applied twice: first to the individual jet flames that emerge from the burner

tips inside the quarl and again for the merged jet exiting the quarl; thereafter, when mixing is completed, a plug-flow reactor model was utilized to represent the remaining flow to the furnace exit. To give confidence in the results, it may be observed that the model predicted a final CO level of 2 ppm, consistent with the measured level below the detection limit of 5 ppm, and a final NO<sub>x</sub> concentration of 106 ppm, compared with the measured value of 118 ppm. As shown in Figure 14.25, the jet model predicted that individual hydrocarbon species should be produced to significant levels within the in-quarl flames, but should be consumed well within the substoichiometric regime, both just as was shown.

In Figure 14.25, "theoretical air (%)" may also to be interpreted as "x" or length along the axis of the jet. Initially, where the reactions are just beginning, there is nothing but the original fuel reactants and oxidant in abundance. As the reactants and oxidant begin to mix, the reacting part of the "reacting jet" begins, too, and the reaction products start to appear. Then, as more and more air is mixed into the jet, with theoretical air% increasing, but still well within the substoichiometric regime, the reaction products peak and then are rapidly consumed even before the mixture reaches stoichiometric.

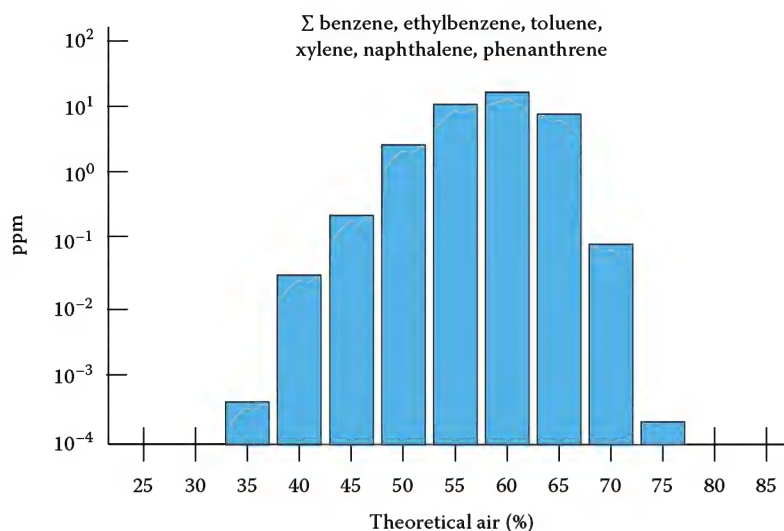


FIGURE 14.25

Lagrangian jet model predictions. (Adapted from Seebold, J.G. and Waibel, R.T., Products of incomplete combustion (PIC) from petroleum, petrochemical & chemical sector process heaters and industrial boilers, *10th International Congress on Combustion By-Products and Their Health Effects*, Ischia, Italy, June 17–20, 2007.)

The prediction confirmed that PIC species, manufactured in abundance in the hot, rich, diffusive regime, are subsequently consumed in the high-mixing-potential jet well before it reaches even stoichiometric conditions. This is extremely significant with regard to its implication upon the robustness of practical combustion systems in the field. Moreover, it is perhaps remarkable to note that, in the “sequence E” super-failure mode full-scale trials carried out at the BERL, it was not until severely substoichiometric conditions (stoichiometric ratio <0.80) were achieved in the combustion zone and maintained right through and out the stack to the atmosphere, and just as predicted by the Lagrangian jet model, that high levels of PICs emerged.

This helps explain why the CDFB, composed as it is of burner tips out of which there emerge high-mixing-potential jets surrounded by an abundant supply of oxidant, simply has to be a low PICs burner. Perhaps, only when this high mixing potential might be compromised, as, for example, in the case of extreme turn down and its attendant low velocity mixing or, especially, in the presence of liquid droplets that may not even vaporize prior to escaping the intended gaseous “mixing zone,” might higher levels of PICs be expected to escape to the atmosphere.

#### 14.6.2.3 Turn-Down vs. Mixing Rate

In Figure 14.26 are shown some results of experimentation with a real-time total PAH meter carried out at several burner firing rates in the BERL. The expected sharp drop-off with increasing theoretical air can be seen, but well within the substoichiometric regime, is evidently

confirmed and that the drop-off “knee” was sharply defined by this pioneering research effort. Moreover, it can be seen that the knee shifts toward higher theoretical air as the jet mixing potential declines at reduced burner firing rates (reduced gas pressure reduces the momentum flux of the fuel jets), just as would be expected and perhaps signaling the breakdown of the burner’s individual reacting jets. Perhaps, it is not surprising, therefore, that similar trends have been reported (*viz.*, higher PICs under turndown conditions) in some field tests.

#### 14.6.2.4 BERL-Field Connection

Shown superimposed on the charts in Figures 14.27 and 14.28 is the range of measurements by one company on five process heaters of markedly different configuration firing refinery fuel gas, one with air-staged low NO<sub>x</sub> burners, two with fuel-staged ultralow NO<sub>x</sub> burners, one with raw gas burners and one with premix burners. Like the proprietary field measurements made by some CRADA-signatory companies, the 1993–1994 source testing results that were commissioned by the non-CRADA-signatory company were obtained following the general recognition of the poor quality of the *ca.*1989–1990 WSPA Pooled Source Testing campaign. The light hydrocarbons for which PERF 92-19 sampled in support of the chemical kinetic modeling aspects of the program were not reported in the WSPA tests and probably not sought, there being no reason to do so, but all of the compounds of regulatory importance were; *viz.*, “aldehydes” (formaldehyde, acetaldehyde); “VOC” (benzene, toluene, ethylbenzene, xylenes); and “POM”



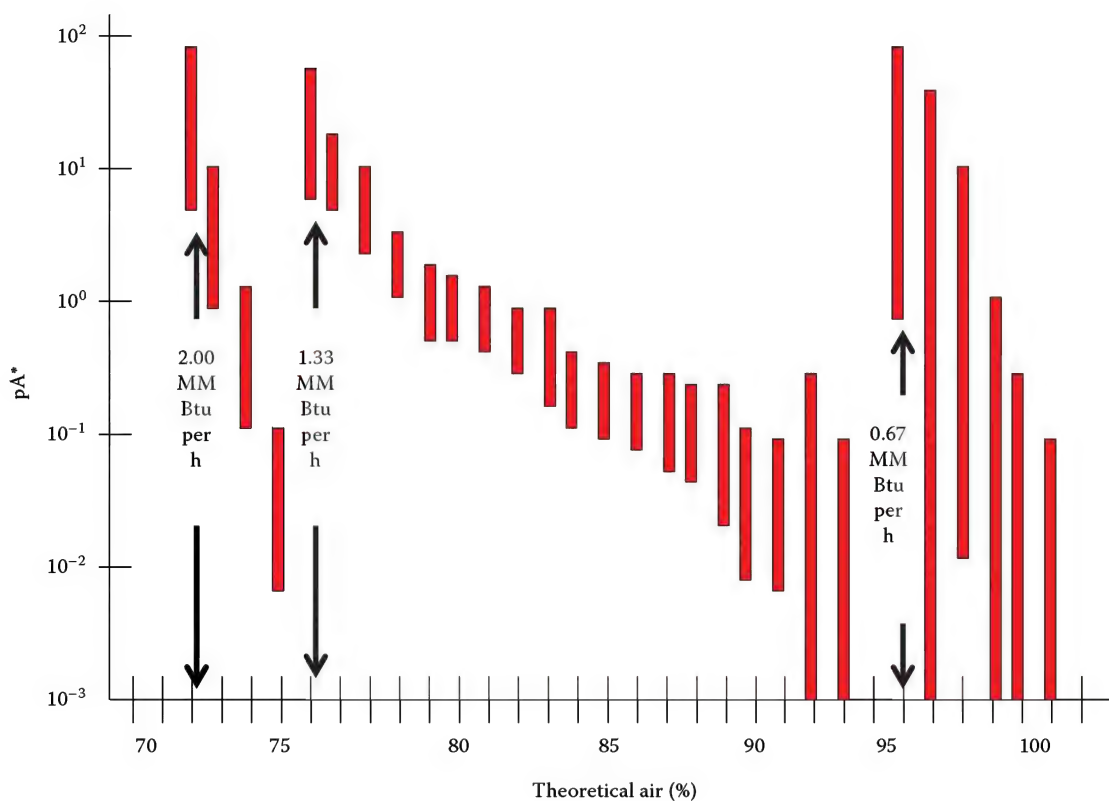


FIGURE 14.26

CDFB photoionization current (pA) versus theoretical air (%). (Adapted from Seebold, J.G. and Waibel, R.T., Products of incomplete combustion (PIC) from petroleum, petrochemical & chemical sector process heaters and industrial boilers, *10th International Congress on Combustion By-Products and Their Health Effects*, Ischia, Italy, June 17–20, 2007.)

(naphthalene through dibenz(a,h)anthracene) and, in contrast to earlier industry testing, this very high quality field campaign was conducted with suitably low detection limits.

The comparison shown in Figures 14.27 and 14.28 illustrates what has been suggested elsewhere; viz., that the high mixing potential reacting jets make petroleum industry burners firing gaseous hydrocarbon fuels highly effective low PICs burners; that detailed differences among burners, process heater designs, and gaseous hydrocarbon fuel compositions are unimportant; and that the connection between the full-scale BERL trials and high quality field measurements is strong indeed. Field measurement campaigns with adequately low limits of detection in which “nondetects” do not play any substantial role in determining the reported emissions produce, for gaseous hydrocarbon external combustion, substantially the same results as were obtained at full scale by this program in the BERL.

In connection with the droplet hypothesis and the production of higher than expected POM emissions, and also of interest in relation to the “BERL-field connection” is an account of the determination of emissions levels of HAPs from the combustion of a #2 oil, a #5 oil, a low sulfur #6 oil, and a high sulfur #6 oil in

a full-scale firetube industrial boiler.<sup>70</sup> The emissions of aldehydes and VOCs for the various oils compared favorably with those obtained during the full-scale gaseous combustion burner trials carried out under the PERF 92-19 CRADA at the BERL, but the POM emissions were higher by about an order of magnitude.

#### 14.6.2.5 Refinery Fuel Gas, Natural Gas Equivalency

Elsewhere it has been shown, for a broad range of combustion conditions, the total hydrocarbon emissions resulting from the external combustion of natural gas and a variety of refinery fuel gas mixtures in which it is easily seen that there is no reason to distinguish refinery fuel gas from natural gas, the latter being itself just another mixture of hydrocarbon gases. Figures 14.29 and 14.30 illustrate the same equivalency on but a speciated basis, there being only small, statistically insignificant differences in the individual species’ emissions.

#### 14.6.2.6 No Effect of Burner Type

The exhaustive exploration of the combustion parameter space with the CDFB demonstrated the robustness

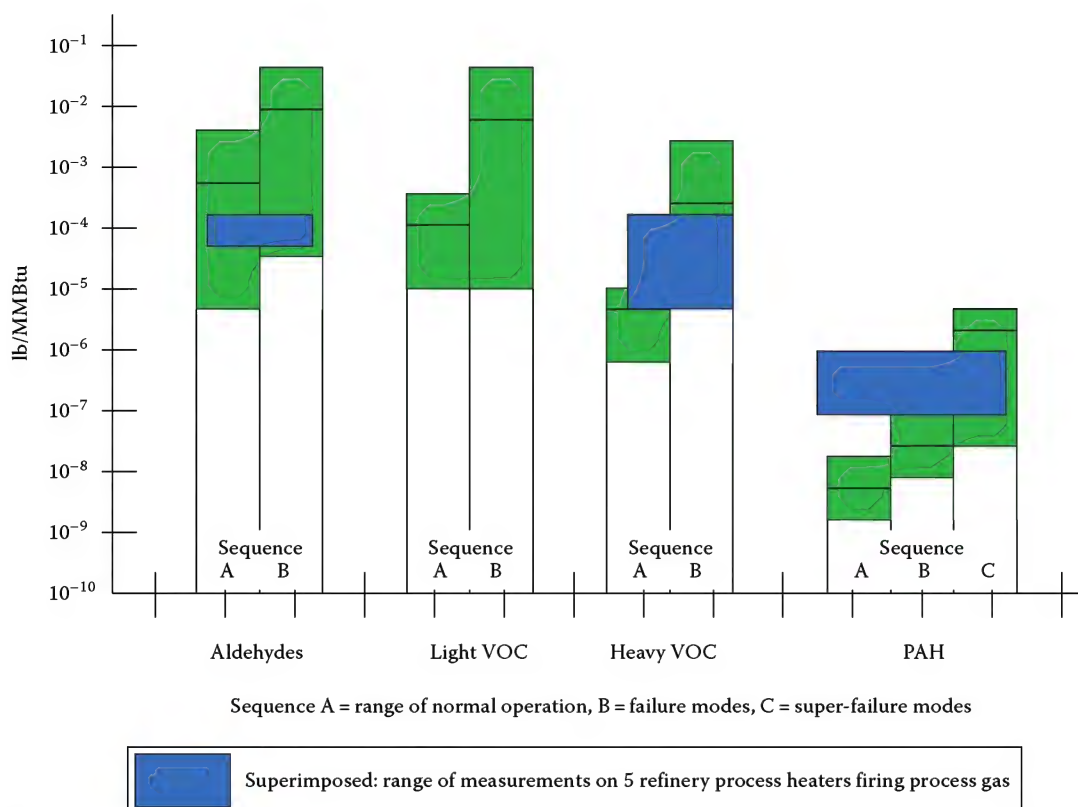


FIGURE 14.27

Range and average of emissions at the stack outlet for the CDFB. (Adapted from Seebold, J.G. and Waibel, R.T., Products of incomplete combustion (PIC) from petroleum, petrochemical & chemical sector process heaters and industrial boilers, *10th International Congress on Combustion By-Products and Their Health Effects*, Ischia, Italy, June 17–20, 2007.)

of hydrocarbon gaseous external combustion in producing ultralow PIC emissions. This was even when subjected to extreme mixing failures imposed by, for example, a partially blocked quarl, plugged or reversed burner tips, or even air starvation with overfire leakage air. This suggested the ultralow  $\text{NO}_x$  LDFB would prove also to be an ultralow PICs burner. Indeed, because of the more intense mixing in the LDFB as compared with the CDFB owing to internal self-recirculation, it was predicted that the trace PIC emissions might become a little “tracer,” as it were, and they did. The lack of any important impact on trace PIC emissions of greatly altered mixing owing to changing the burner type is illustrated in Figure 14.30 for the normal operation regulatory base cases. In the hypothetical extreme failure-mode tests, a similar lack of significant impact on PIC emissions was seen.

#### 14.6.2.7 Detection Limits

“Nondetects” recorded at high limits of detection are worse than useless. Thus, at the inception of this program, in part due to the well-known inadequacies of what few field testing programs had been carried

out, it was concluded that QA/QC was of the utmost importance and, in particular, that detection limits much lower than those that had been achieved in the field tests would be needed to gain useful data. In this regard, it is worth noting that the emission concentrations in Figure 14.30 are expressed in parts per *quadrillion* and that to reliably detect the exceedingly low levels of polycyclic organic matter (“POM”) that were produced under typical operating conditions, detection limits *less than 100 parts per quadrillion* were required to be achieved. This program’s thoroughly documented and highly accurate finding of no effect of burner type, conventional vs. low  $\text{NO}_x$ , nevertheless seems to be corroborated by the field database as illustrated in Figure 14.31.

#### 14.6.2.8 Results of the Final Full-Scale Trials

In the final sequence of full-scale trials, through egregious excursions into the super- and substoichiometric combustion regimes, some systematic behavior (vs. stoichiometric ratio) was finally shown. Perhaps, a PAH surrogate (benzene) was found. This answered a question left over from previous trials about the ultra-superstoichiometric hydrocarbon PICs whether they

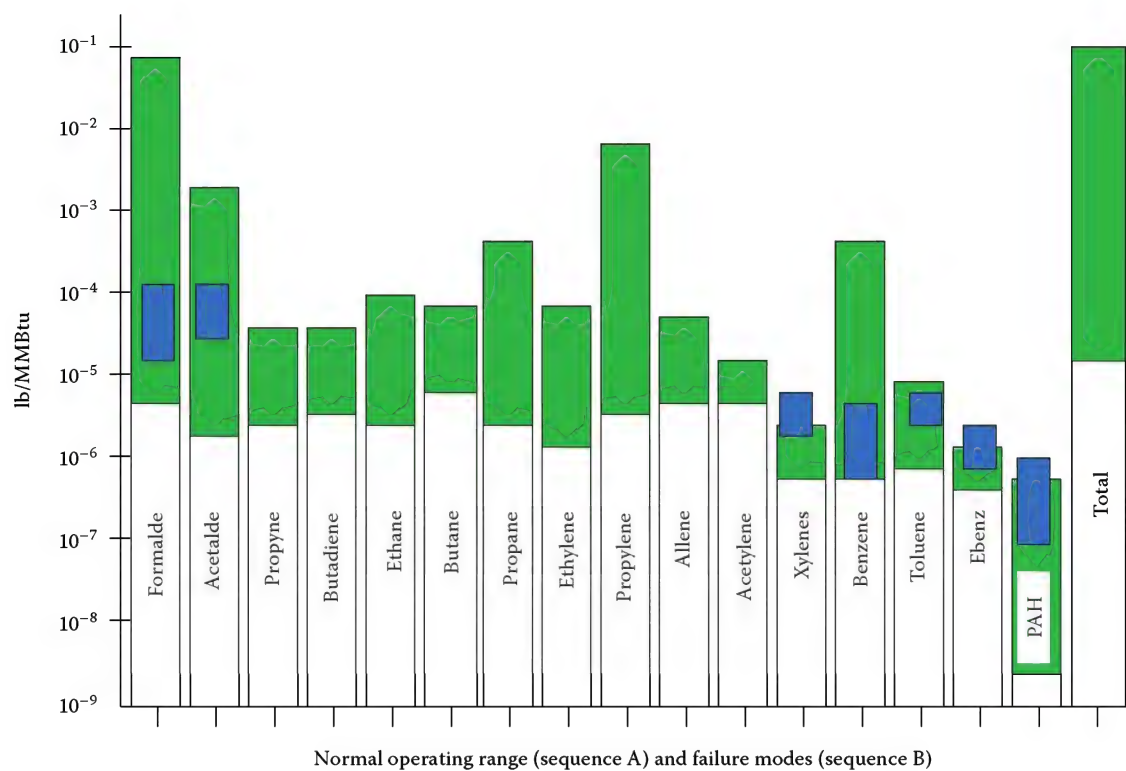


**FIGURE 14.28** Range of measurements of HAPs at the stack outlet for the CDFB. (Adapted from Seebold, J.G. and Waibel, R.T., Products of incomplete combustion (PIC) from petroleum, petrochemical & chemical sector process heaters and industrial boilers, 10th International Congress on Combustion By-Products and Their Health Effects, Ischia, Italy, June 17–20, 2007.)

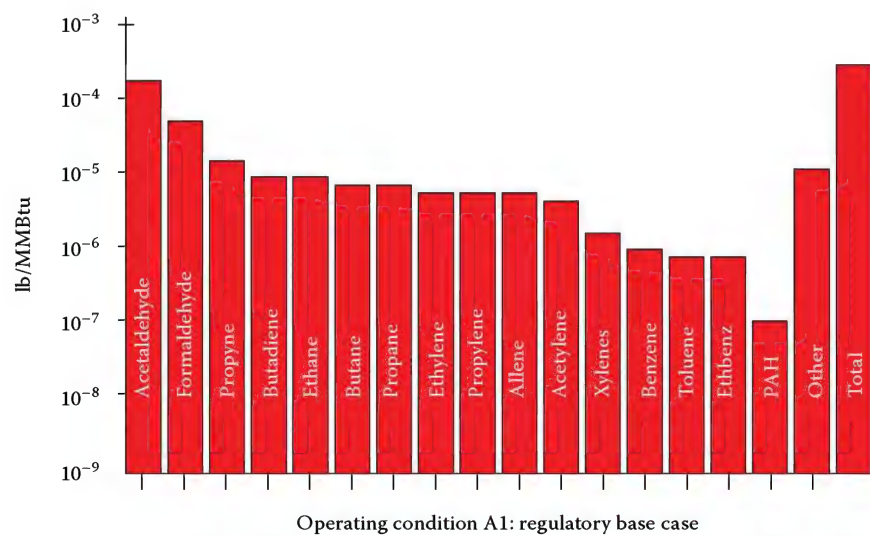


**FIGURE 14.29** Emissions for refinery fuel gas (16% H<sub>2</sub>, propane, natural gas) for the CDFB. (Adapted from Seebold, J.G. and Waibel, R.T., Products of incomplete combustion (PIC) from petroleum, petrochemical & chemical sector process heaters and industrial boilers, 10th International Congress on Combustion By-Products and Their Health Effects, Ischia, Italy, June 17–20, 2007.)



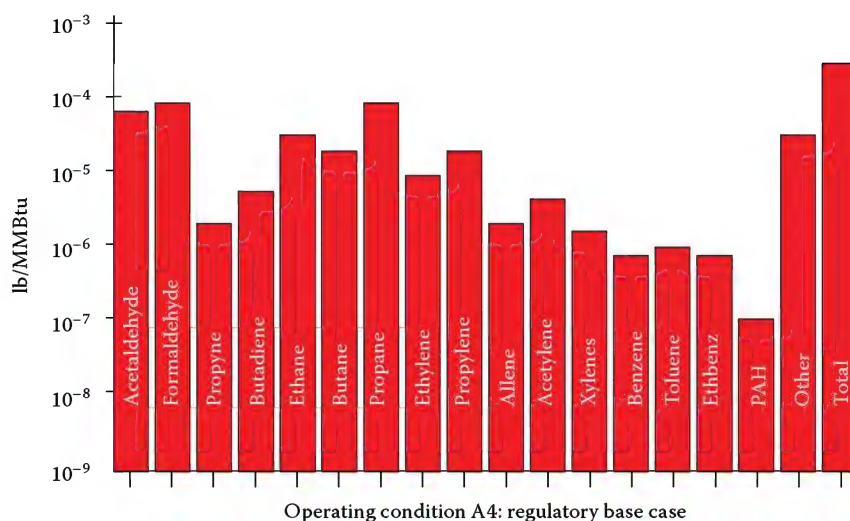


FIGURE 14.30

Range of emissions for natural gas and refinery fuel gas for the CDFB and the ultralow NO<sub>x</sub> diffusion burner. (Adapted from Seebold, J.G. and Waibel, R.T., Products of incomplete combustion (PIC) from petroleum, petrochemical & chemical sector process heaters and industrial boilers, 10th International Congress on Combustion By-Products and Their Health Effects, Ischia, Italy, June 17–20, 2007.)

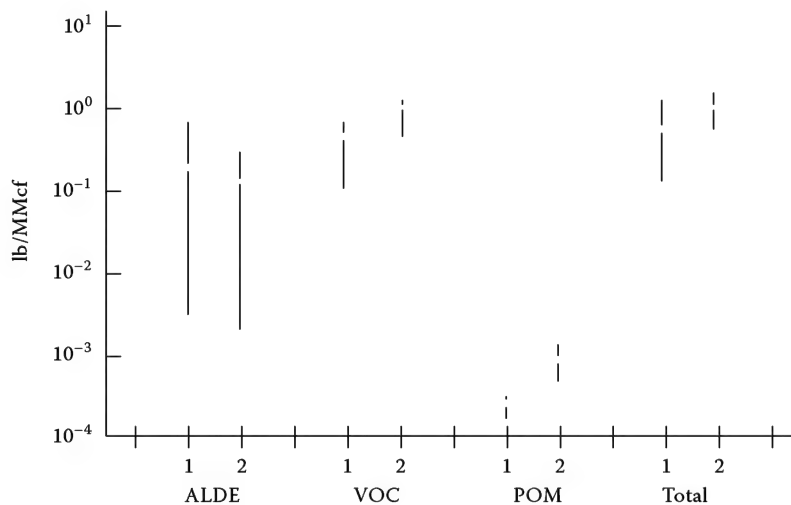


FIGURE 14.31

Emission factor comparison for low NO<sub>x</sub> burner and conventional burner. (Adapted from Seebold, J.G. and Waibel, R.T., Products of incomplete combustion (PIC) from petroleum, petrochemical & chemical sector process heaters and industrial boilers, 10th International Congress on Combustion By-Products and Their Health Effects, Ischia, Italy, June 17–20, 2007.)

were reaction products (yes) or simply unreacted fuel fragments (no). It was also “discovered” (yet again) that CO and HC are poor surrogates, at least in the case of hydrocarbon gaseous external combustion.

As shown in Figure 14.32, at severely substoichiometric conditions maintained right through and out the stack to the atmosphere, total PAH emissions 4 rings and greater as great as 98 parts per million (ppm) at the furnace exit (“in” = inlet to the CSS) and 2.5 ppm at the stack exit (“out”) were observed, with corresponding benzo(a)pyrene emissions of 130 parts per billion (ppb) and 40 ppb. Note that

the emission levels are expressed in parts per *trillion* and that detection limits in some cases *below 100 parts per quadrillion* were required to be achieved. In the quest for a surrogate for PAH emissions, as may be seen in Figure 14.33, it appears that benzene (shown blue), at least in the severely substoichiometric regime, has some promise. Figures 14.34 and 14.35 simply serve to illustrate the fact that neither carbon monoxide (“CO”) nor total hydrocarbon (“HC”) have any promise whatsoever as PAH surrogates.

Similar to the deeply substoichiometric trials, prior highly aerated tests emphasized the trace polycyclic

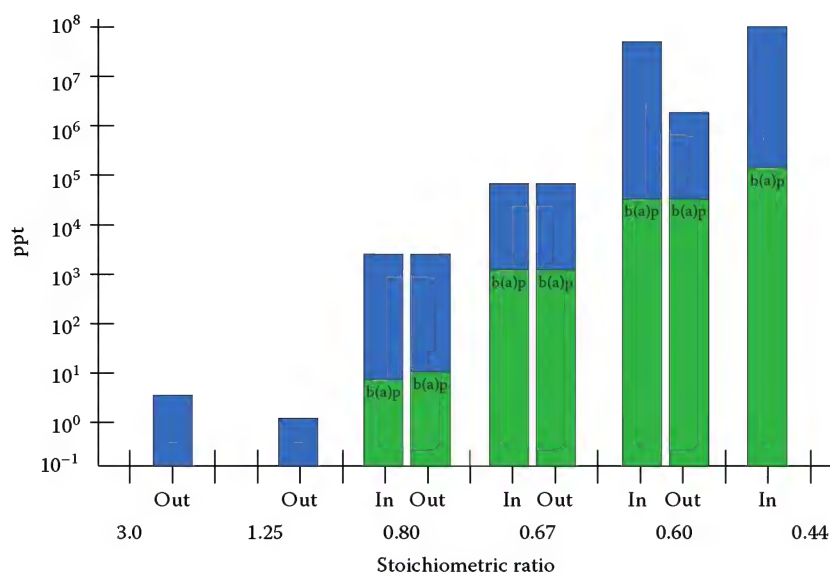


FIGURE 14.32

Total PAH emissions 4 rings and greater versus stoichiometric ratio. (Adapted from Seebold, J.G. and Waibel, R.T., Products of incomplete combustion (PIC) from petroleum, petrochemical & chemical sector process heaters and industrial boilers, 10th International Congress on Combustion By-Products and Their Health Effects, Ischia, Italy, June 17–20, 2007.)

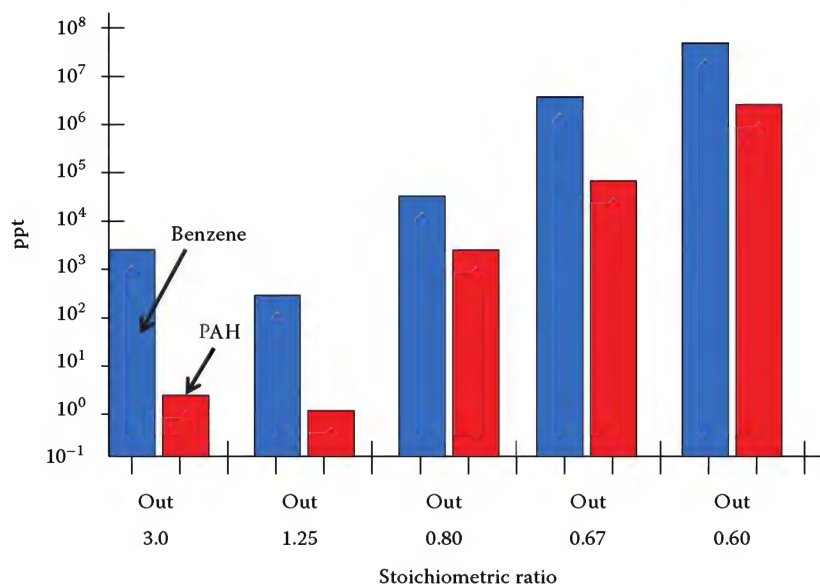


FIGURE 14.33

Benzene and PAH emissions versus stoichiometric ratio for the CDFB. (Adapted from Seebold, J.G. and Waibel, R.T., Products of incomplete combustion (PIC) from petroleum, petrochemical & chemical sector process heaters and industrial boilers, 10th International Congress on Combustion By-Products and Their Health Effects, Ischia, Italy, June 17–20, 2007.)

organic hydrocarbon emissions but, nevertheless, showed high total hydrocarbon emissions, as well. In sequence E, the reason for rerunning the superstoichiometric case (stoichiometric ratio [SR] = 3.0) and, as always, the regulatory base case (SR = 1.25) for comparison, was to add stack exit aldehyde and heavy volatile organic compound measurements in order to determine whether or not those high total hydrocarbons were reaction products or merely

unburned fuel fragments. In Figure 14.36, the hydrocarbon emissions (shown in yellow) are largely accounted for by reaction products, mainly aldehydes.

Finally, Figure 14.37 illustrates again (with the exception of the heavy VOCs that include benzene, ethyl benzene, xylenes, and toluene) that systematic behavior (vs. SR) can be forced by excursions into the severely super- and substoichiometric regimes.

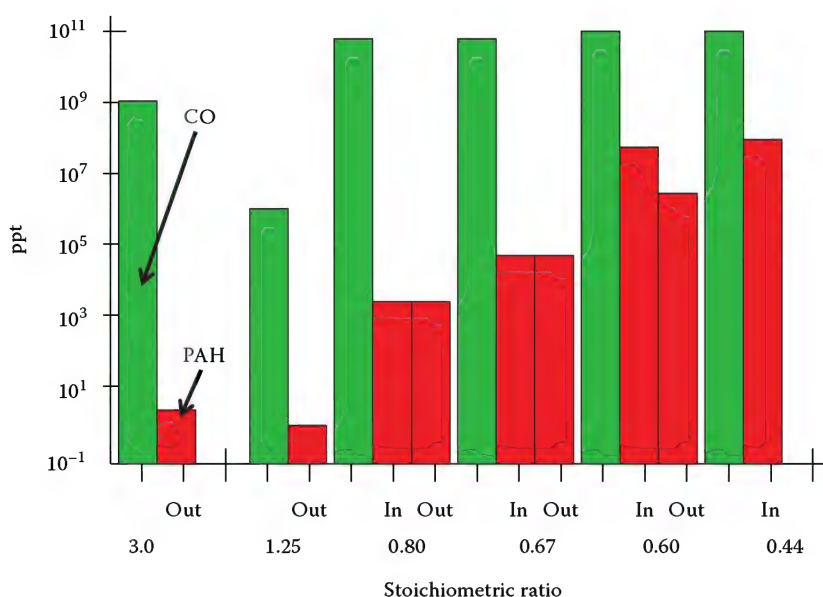


FIGURE 14.34

CO and PAH emissions versus stoichiometric ratio for the CDFB. (Adapted from Seebold, J.G. and Waibel, R.T., Products of incomplete combustion (PIC) from petroleum, petrochemical & chemical sector process heaters and industrial boilers, *10th International Congress on Combustion By-Products and Their Health Effects*, Ischia, Italy, June 17–20, 2007.)

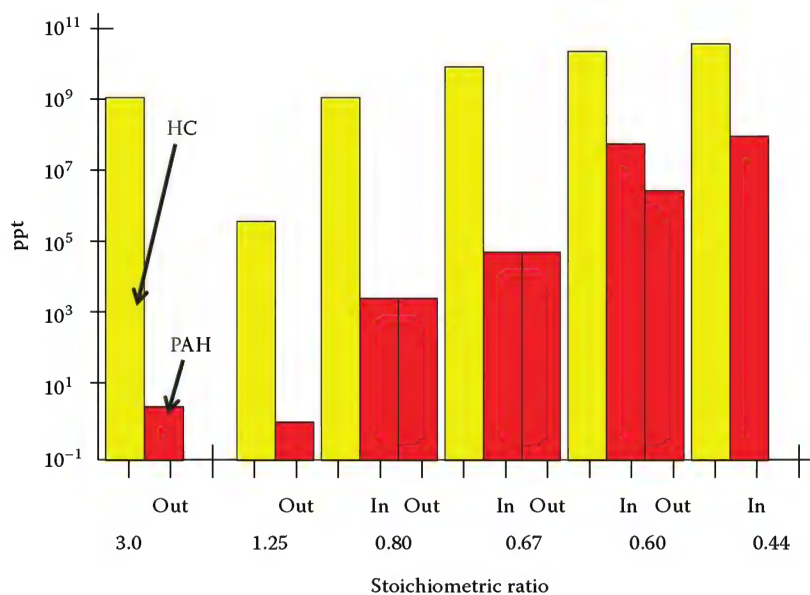


FIGURE 14.35

HC and PAH emissions versus stoichiometric ratio for the CDFB. (Adapted from Seebold, J.G. and Waibel, R.T., Products of incomplete combustion (PIC) from petroleum, petrochemical & chemical sector process heaters and industrial boilers, *10th International Congress on Combustion By-Products and Their Health Effects*, Ischia, Italy, June 17–20, 2007.)

#### 14.6.2.9 Summary

Jet-mixed hydrocarbon gaseous diffusion flames, such as those produced by the burners that are typically used in petroleum industry process heaters and industrial boilers, produce exceedingly low PIC emissions. The nature of the hydrocarbon gaseous fuel mixture makes

little difference, neither in the total emissions nor in the individual species concentrations; that there is no reason to distinguish between process gas and natural gas, the latter being itself merely just another mixture of hydrocarbon gases; that the individual hydrocarbon species levels as measured depend mainly upon the vagaries



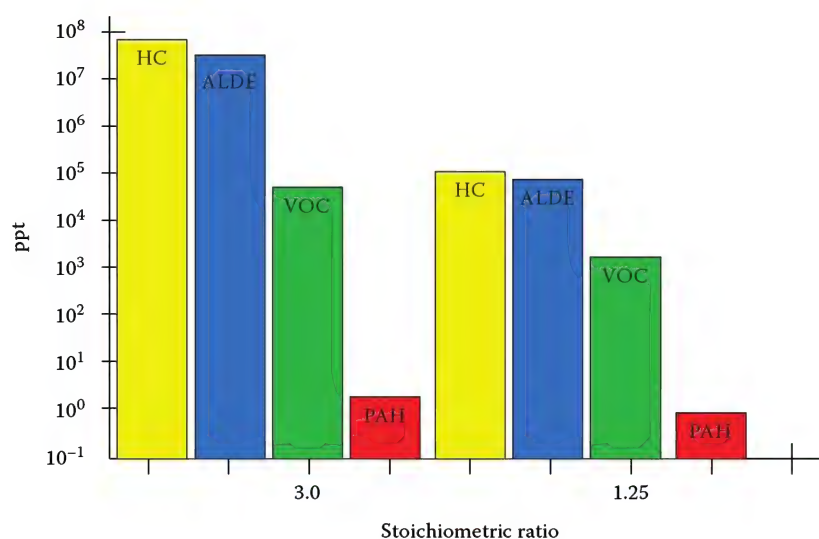


FIGURE 14.36

HC, aldehyde, VOC, and PAH emissions versus stoichiometric ratio for the CDFB. (Adapted from Seebold, J.G. and Waibel, R.T., Products of incomplete combustion (PIC) from petroleum, petrochemical & chemical sector process heaters and industrial boilers, *10th International Congress on Combustion By-Products and Their Health Effects*, Ischia, Italy, June 17–20, 2007.)

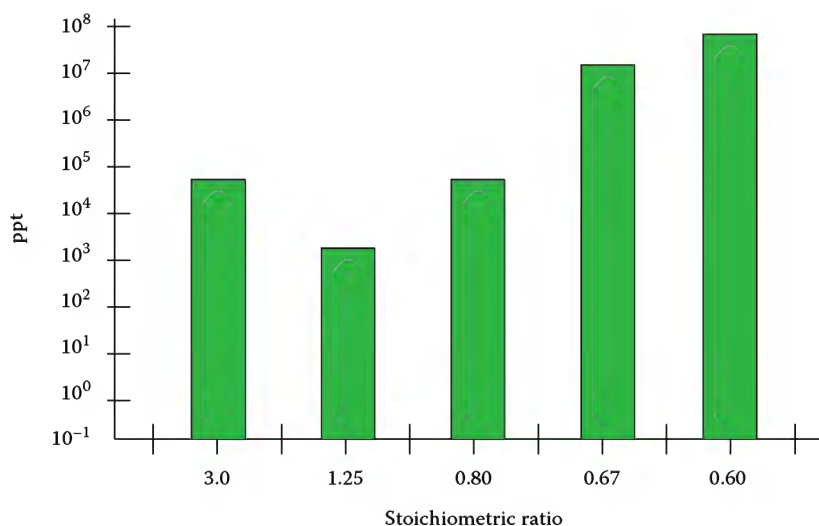


FIGURE 14.37

Total heavy VOC emissions versus stoichiometric ratio for the CDFB. (Adapted from Seebold, J.G. and Waibel, R.T., Products of incomplete combustion (PIC) from petroleum, petrochemical & chemical sector process heaters and industrial boilers, *10th International Congress on Combustion By-Products and Their Health Effects*, Ischia, Italy, June 17–20, 2007.)

of the sophisticated sampling methods and precise analytical techniques that are required to detect them all in the minute concentrations in which they appear in the combustion products; that, despite their markedly different mixing patterns, both the CDFB and today's ultralow  $\text{NO}_x$  burner are ultralow PIC burners; that all of this is true for an exceedingly broad range of hydrocarbon gaseous combustion conditions; and that high quality field measurement campaigns produce results that are the same as those obtained in this program in the

BERL. In short, the jet-mixed hydrocarbon gaseous combustion process is extremely robust, producing ultralow PIC emissions even when subjected to extreme mixing failures.

#### 14.6.3 Process Heater, Petroleum Refinery Emissions Factors

As indicated in Figures 14.27 and 14.28, competent field measurement campaigns (i.e., those carried out

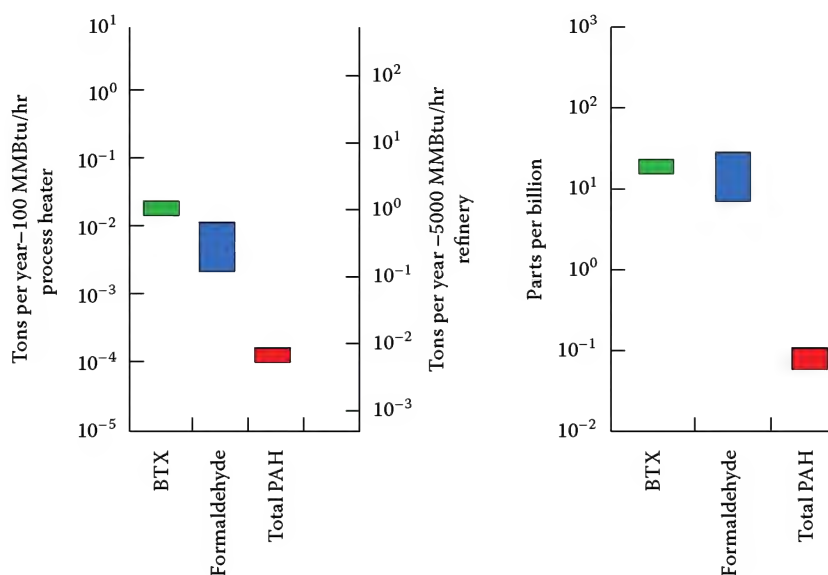


FIGURE 14.38

Typical process heater, petroleum refinery emissions factors. (Adapted from Seebold, J.G. and Waibel, R.T., *Products of incomplete combustion (PIC) from petroleum, petrochemical & chemical sector process heaters and industrial boilers*, 10th International Congress on Combustion By-Products and Their Health Effects, Ischia, Italy, June 17–20, 2007.)

with adequately low limits of detection in which “non-detects” do not play any substantial role in determining the reported “emissions”) produce, for jet-mixed gaseous hydrocarbon external combustion, substantially the same results as were obtained at full scale by this program in the BERL. Following completion of the PERF 92-19 CRADA Project, a more extensive comparison with a broad range of field data was carried out that confirmed that the landmark PERF data and actual field data from the “WSPA-CATEF” database compared well.<sup>42</sup> While the test methods used in the PERF 92-19 CRADA program were far more sensitive than those used in most field tests, the agreement between the PERF and field results nevertheless demonstrates the excellent representativeness of the PERF data for jet-mixed gaseous hydrocarbon external combustion.

Given the excellent agreement of all data sources, in the subsequent analysis referred to earlier, it seemed reasonable to combine all data to develop robust emission factors applicable to all gas-fired industrial boilers and process heaters which, in turn, enabled reliable characterization of PIC emissions from a typical gas-fired process heater and a typical petroleum refinery.<sup>71</sup> The result is shown in Figure 14.38. Calculated organic PIC mass emissions in tons per year are shown for a hypothetical process heater or industrial boiler with a fuel heat input value of 100 MMBtu/h (29 MW), which is in the same order of magnitude as those commonly found in petroleum industry facilities such as refineries and natural gas processing plants. The total heat input to gas-fired

combustion equipment in a typical oil refinery is on the order of 5000 MMBtu/h (1500 MW). Organic PIC mass emissions from a refinery of this size, estimated in the same way, are also shown in Figure 14.38. The equivalent gas concentrations are also shown to emphasize that these mass emission rates correspond to exceedingly low concentrations measured in parts per billion.

## 14.7 Dioxins and Furans

This class of pollutants includes the carbon–hydrogen–oxygen–halogen compounds and has received considerable attention from both the general public and from regulatory agencies because of the potential health hazards associated with them. Dioxins generally refer to polychlorinated dibenzo-p-dioxin (PCDD) compounds while furans generally refer to polychlorinated dibenzofuran (PCDF) compounds. Some of the potential health risks include toxicity because of the poisoning effect on cell tissues, carcinogenicity because cancerous growth may be stimulated, mutagenicity because of possible mutations in cell structure or function, and teratogenicity because of the potential changes to fetal tissue.<sup>13</sup> The over 200 dioxin/furan compounds are regulated in certain industries, particularly in waste incineration, and also in certain geographical locations for a wide range of applications, especially in Europe.

In the vast majority of cases, dioxin/furan emissions result from some contaminant in the load materials

being heated in the combustor. A quick scan of most of the textbooks on combustion shows that these emissions are essentially ignored because they are not generally produced in the flame, except in certain limited cases. This is primarily because there are not usually any halogens in either the fuel or the oxidizer to produce dioxins or furans. An exception is the case when waste materials are burned as a fuel by direct injection into a flame. One example is the destruction of waste solvents that may be injected into an incinerator through the burner.

## References

1. J.A. Stanislaw, Petroleum industry faces tectonic shifts changing global energy map, *Oil Gas J.*, 97(50), 8–14, 1999.
2. U.S. Environmental Protection Agency, *Our Nation's air: Status and Trends through 2008*, Report EPA-454/R-09-002, Washington, DC, February 2010.
3. U.S. Department of Energy Office of Industrial Technology, Petroleum—Industry of the future: Energy and environmental profile of the U.S. Petroleum Refining Industry, U.S. DOE, Washington, DC, December 1998.
4. S.A. Shareef, C.L. Anderson, and L.E. Keller, *Fired Heaters: Nitrogen Oxides Emissions and Controls*, U.S. Environmental Protection Agency, Research Triangle Park, NC, EPA Contract No. 68-02-4286, June 1988.
5. D. Hansell and G. England, *Air Toxic Emission Factors for Combustion Sources Using Petroleum Based Fuels*, Vol. 3, Energy and Environmental Research Corp., Irvine, CA, 1998 (available at [www.api.org/step/piep.htm](http://www.api.org/step/piep.htm)).
6. U.S. EPA, *AP-42: Compilation of Air Pollutant Emission Factors*, 5th edn., U.S. Environmental Protection Agency, Washington, DC, January 1995.
7. J.C. Reis, *Environmental Control in Petroleum Engineering*, Gulf Publishing, Houston, TX, 1996.
8. C.E. Baukal, *Industrial Combustion Pollution and Control*, Marcel Dekker, New York, 2004.
9. American Petroleum Institute Recommended Practice 556, *Instrumentation, Control, and Protective Systems for Gas Fired Heaters*, 2nd edn., API, Washington, DC, April 2011.
10. American National Standards Institute/American Society of Mechanical Engineers, Performance Test Code PTC 19.10, Part 10: Flue and exhaust gas analyses, American Society of Mechanical Engineers, New York, 1981.
11. K. Ahlberg (ed.), *AGA Gas Handbook*, AGA AB, Lidingö, Sweden, 1985.
12. S. Setia, VOC emissions—Hazards and techniques for their control, *Chem. Eng. World*, XXXI (9), 43–47, 1996.
13. W.R. Niessen, *Combustion and Incineration Processes*, 2nd edn., Marcel Dekker Inc., New York, 1995.
14. M. Lippmann and R. Albert, The effect of particle size on the regional deposition of inhaled aerosols in human respiratory tract, *Am. Ind. Hyg. Assoc. J.*, 30, 257–275, 1969.
15. J. Heyder, L. Armbruster, J. Gebhart et al., Total deposition of aerosol particles in human respiratory tract for nose and mouth breathing, *J. Aerosol Sci.*, 6, 311–320, 1975.
16. L. Armbruster and H. Breuer, Investigation into defining inhalable dust, *Ann. Occup. Hyg.*, 26, 21–32, 1982.
17. S.C. Soderholm, *Particle Size-Selective Sampling in the Work Place. Report of ACGIH Technical Committee on Air Sampling Procedures*, pp. 27–32. American Conference of Governmental Industrial Hygienists, Cincinnati, OH, 1985.
18. I.P. Chung, R.F. Phalen, and D. Dunn-Rankin, Predicted aerosol aspiration efficiency for infants, children, and adults, *Appl. Occup. Environ. Hyg.*, 8(7), 1993.
19. U.S. Department of Commerce, Bacharach Test Method—Installation Standards of the National Oil Fuel Institute, New York, ASTM Designation D2156—65, 1965, also in *German Standard DIN 51402*.
20. Environmental Protection Agency Method 9—Determination of Stack Plume Opacity, 40 CFR (Code of Federal Regulation) Chapter 1 Part 60 Appendixes A—Standards of Performance for New Stationary Sources Test Methods, 1907, revised as July 1995.
21. Environmental Protection Agency Method 5—Determination of Particulate Emissions from Stationary Sources, 40 CFR (Code of Federal Regulation) Chapter 1 Part 60 Appendixes A—Standards of Performance for New Stationary Sources Test Methods, 1970, revised as July 1995.
22. ISO 9096, International Standard ISO 9096: *Stationary Source Emissions—Determination and mass flow rate of particulate material in gas-carrying ducts*, International Organization for Standardization, 2003, American National Standards Institute, Washington, DC.
23. H.C. Van de Hulst, *Light Scattering by Small Particles*, Dover Publications, New York, 1981.
24. Circular 8333, *Ringelmann Smoke Chart Bureau of Mines*, Revision of IC 7718, Washington, DC, May 1967.
25. 40 CFR Chapter 1, Part 60, Appendix A, Method 9, Visual Determination of the Opacity of Emissions from Stationary Sources, July 1, 2000, published by the Office of the Federal Register National Archives and Records Administration, Washington, DC.
26. CFR 40 Chapter I, Part 60.1, Appendix B, Performance Specifications 1, Specifications and Test Procedures for Opacity Continuous Emission Monitoring Systems in Stationary Sources, July 1, 2000, published by the Office of the Federal Register National Archives and Records Administration, Washington, DC.
27. S. Hersh, S.E. Kerho, D. Giovanni, and D. Mormile, ASME 87-JPGC-FACT-15, Reductions in carbonaceous particulate matter emissions from oil fired utility boilers through improvements in atomizer performance, presented at ASME/IEEE Power Generation Conference, Miami Beach, Florida, October 4–8, 1987, American Society of Mechanical Engineers, New York, NY.
28. C.N. Davies and M. Subari, Aspiration above wind velocity of aerosols with thin-walled nozzles facing and at right angles to the wind direction, *J. Aerosol Sci.*, 13, 59–71, 1982.
29. I.P. Chung and D. Dunn-Rankin, Numerical simulation of two-dimensional cylindrical blunt sampling in viscous flow, *J. Aerosol Sci.*, 23, 217–232, 1992.



30. I.P. Chung and D. Dunn-Rankin, The effect of bluntness and orientation on two-dimensional samplers in calm air, *Aerosol Sci. Technol.*, 19, 371–380, 1993.
31. I.P. Chung, T. Trinh, and D. Dunn-Rankin, Experimental investigation of a two-dimensional cylindrical sampler, *J. Aerosol Sci.*, 25(5), 935–955, 1994.
32. I.P. Chung and D. Dunn-Rankin, Experimental investigation of air flow around blunt aerosol samplers, *J. Aerosol Sci.*, 28(2), 289–305, 1997.
33. F.M. White, *Fluid Mechanics*, McGraw-Hill Book Co., New York, p.159, 1979.
34. IEA, CO<sub>2</sub> emissions from fuel combustion, 1971–2001, OECD/IEA, Paris, 2003.
35. C.E. Baukal, *Oxygen-Enhanced Combustion*, CRC Press, Boca Raton, FL, 1998.
36. B. Metz, O. Davidson, H. de Coninck, M. Loos, and L. Meyer, *Carbon Dioxide Capture and Storage*, Prepared by Working Group III of the Intergovernmental Panel on Climate Change, Cambridge University Press, Cambridge, U.K., 2005.
37. E.D. Weil, Sulfur compounds, in *Kirk-Othmer Encyclopedia of Chemical Technology*, 3rd edn., Vol. 22, John Wiley & Sons, New York, 1983.
38. C.T. Bowman, Chemistry of gaseous pollutant formation and destruction, in *Fossil Fuel Combustion*, ed., W. Bartok and A.F. Sarofim, John Wiley & Sons, New York, 1991.
39. American Petroleum Institute, Burners for fired heaters in general refinery services, API Recommended Practice 535, 2nd edn., Washington, DC, January 2006.
40. C.R. Bruner, *Handbook of Incineration Systems*, McGraw-Hill, New York, 1991.
41. S.R. Turns, *An Introduction to Combustion*, McGraw-Hill, New York, 1996.
42. G.C. England, T.P. McGrath, L. Gilmer, J.G. Seebold, M. Lev-On, and T. Hunt, Hazardous air pollutant emissions from gas-fired combustion sources: Emissions and the effects of design and fuel type, *Chemosphere*, 42(5–7), 745–764, 2001.
43. J.G. Seebold and R.T. Waibel, Products of incomplete combustion (PIC) from petroleum, petrochemical & chemical sector process heaters and industrial boilers, *10th International Congress on Combustion By-Products and Their Health Effects*, Ischia, Italy, June 17–20, 2007.
44. CARB, *Stationary Source Test Methods, Volume III: Methods for Determining Emissions of Toxic Air contaminants from Stationary Sources*, Monitoring and Laboratory Division, California Air Resources Board, El Monte, CA, 1991.
45. J.F. Collins, J.P. Brown, S.V. Dawson, and M.A. Marty, Risk assessment for benzo[a]pyrene, *Regul. Toxicol. Pharm.*, 13, 170–184, 1991.
46. G.F. Simes, *Preparation Aids for the Development of Category II Quality Assurance Project Plans*, U.S. Environmental Protection Agency, EPA/600/8-91/004, Cincinnati, OH, 1991.
47. D.W. Hansell, G.C. England, N. Soelberg, W.R. Seeker, M. Lev-On, and S. Folwarkow, *Development of Air Toxics Emissions Factors for Petroleum Industry Combustion Devices, Air and Waste Management Association 85th Annual Meeting and Exhibition* (Publication No. 92-98.02), Kansas City, MO, 1992.
48. EPRI, *Electric Utility Trace Substances Synthesis Report*, Electric Power Research Institute, Palo Alto, CA, TR-104614, 1994.
49. W.J. Pitz, C.K. Westbrook, A.E. Lutz, R.J. Kee, S.M. Senkan, and J.G. Seebold, Numerical modeling capabilities for the simulation of toxic by-products formation in combustion processes, *Combust. Sci. Technol.*, 101, 383–396, 1994.
50. M.J. Castaldi, A. Vincitore, and S.M. Senkan, Micro-structures of hydrocarbon flames: Methane, *Combust. Sci. Technol.*, 107, 1–19, 1995.
51. S.S. Chao and A. Attari, Characterization and measurement of natural gas trace constituents, Final Report, Contract No. 5089-253-1832, Gas Research Institute, Chicago, IL, 1995.
52. C.F. Edwards and P.J. Goix, Effect of fuel composition and excess air on VOC emissions and flame structure of a small-scale industrial burner, *Fourth International Congress on Toxic Combustion By-Products*, Berkeley, CA, 1995.
53. M.J. Castaldi and S.M. Senkan, Micro-structures of hydrocarbon flames: Ethane, *Combust. Sci. Tech.*, 116, 167, 1996.
54. M.J. Castaldi and S.M. Senkan, PAH formation in premixed flame of ethane, *Combust. Sci. Tech.*, 116–117, 167–181, 1996.
55. C.F. Edwards and P.J. Goix, Effect of fuel gas composition and excess air on VOC emissions from a small-scale, industrial style burner, *Combust. Sci. Tech.*, 116–117(1–6), 375, 1996.
56. D.W. Hansell, Development of toxic emission factors from source test data collected under the air toxics hot spots program, Final Report, California Air Resources Board, Sacramento, CA, 1996.
57. D.W. Hansell, Updated air toxics emission factors for petroleum industry combustion equipment, Final Report, Western States Petroleum Association and American Petroleum Institute, Sacramento, CA, 1996.
58. N.M. Marinov, W.J. Pitz, C.K. Westbrook, M.J. Castaldi, and S.M. Senkan, Modeling of aromatic and polycyclic aromatic hydrocarbon formation in premixed methane and ethane flames, *Combust. Sci. Tech.*, 116–117, 211–287, 1996.
59. C. Rossi-Lane, D. Stein, and R. Himes, *Gas-Fired Boiler and Turbine Air Toxics Summary Report*, Gas Research Institute, Chicago, IL, GRI-95/0200, 1996.
60. S.M. Senkan and M.J. Castaldi, Formation of polycyclic aromatic hydrocarbons (PAH) in hydrocarbon combustion: Comparative new results from premixed flames, *Combust. Flame*, 107, 141–150, 1996.
61. C.M. Gittins, M.J. Castaldi, S.M. Senkan et al., Real-time quantitative analysis of combustion-generated polycyclic aromatic hydrocarbons by resonance-enhanced multiphoton ionization time-of-flight mass spectrometry, *Anal. Chem.*, 69(3), 286–293, 1997.
62. D.W. Hansell, *Analysis of HAP Emission Factors from Petroleum Industry Combustion Devices*, Energy and Environmental Research Corporation, Irvine, CA, 1997.
63. J.W. Huang, I. Onal, and S.M. Senkan, Formation of trace byproducts in the premixed flames of CH<sub>3</sub>Cl/C<sub>2</sub>H<sub>4</sub>, *Environ. Sci. Technol.*, 31(5), 1372–1381, 1997.

64. T.M. McGrath, G.C. England, and D. Jones, The origin and fate of toxic combustion byproducts in refinery heaters: research to enable efficient compliance with the clean air act, air toxics measurements, Final Report, Energy and Environmental Research Corporation, Irvine, CA, 1997.
65. M.J. Castaldi and S. Senkan, Real-time, ultrasensitive monitoring of air toxics by laser photoionization time-of-flight mass spectrometry, *J. Air Waste Mgmt.*, 48(1), 77–81, 1998.
66. A.M. Vincitore and S. Senkan, Polycyclic aromatic hydrocarbon formation in opposed flow diffusion flames of ethane, *Combust. Flame*, 114(1–2), 259–266, 1998.
67. N.M. Marinov, W.J. Pitz, C.K. Westbrook, A.K. Lutz, A.M. Vincitore, and S.M. Senkan, Chemical kinetic modeling of a methane opposed flow diffusion flame and comparison to experiments, *27th Symposium (International) on Combustion*, The Combustion Institute, Pittsburgh, PA, pp. 605–613, 1998.
68. N.M. Marinov, W.J. Pitz, C.K. Westbrook, A.M. Vincitore, M.J. Castaldi, and S. Senkan, Aromatic and polyaromatic hydrocarbon formation in a laminar premixed *n*-butane flame, *Combust. Flame*, 114(1–2), 192–213, 1998.
69. N.M. Marinov, W.J. Pitz, and C.K. Westbrook, *The Formation of Aromatics and PAHs in Flames, Plenary Lecture at the Joint Meeting of the British, German and French Sections of the Combustion Institute*, Nancy, France, 18–21, 1999.
70. C.A. Miller and J.V. Ryan, Characterization of air toxics from an oil-fired firetube boiler, *J. AWMA*, 46, 742–748, 1996.
71. U.S. EPA, AP-42: Compilation of air pollutant emission factors, Draft section 1.4—Natural Gas Combustion. U.S. Environmental Protection Agency, Washington, DC, 1997.

# 15

## *NO<sub>x</sub> Emissions*

Charles E. Baukal, Jr. and Wes Bussman

### CONTENTS

15.1	Introduction .....	418
15.2	Theory .....	420
15.2.1	Formation Mechanisms .....	420
15.2.1.1	Thermal NO <sub>x</sub> .....	420
15.2.1.2	Prompt NO <sub>x</sub> .....	421
15.2.1.3	Fuel NO <sub>x</sub> .....	421
15.2.2	Important Factors Affecting NO <sub>x</sub> .....	421
15.2.2.1	Air–Fuel Ratio (Stoichiometry) .....	422
15.2.2.2	Gas Temperature .....	423
15.2.2.3	Air and Fuel Preheat Temperature .....	423
15.2.2.4	Fuel Composition .....	424
15.2.2.5	Air–Fuel Mixing .....	426
15.3	Regulations .....	427
15.3.1	Units .....	428
15.3.2	Conversions .....	428
15.3.3	Hydrocarbon and Petrochemical Industry Regulations .....	430
15.4	Measurement Techniques .....	430
15.5	Abatement Strategies .....	431
15.5.1	Pretreatment .....	432
15.5.1.1	Fuel Switching .....	432
15.5.1.2	Additives .....	432
15.5.1.3	Fuel Pretreatment .....	432
15.5.1.4	Oxidizer Switching .....	433
15.5.2	Combustion Modification .....	433
15.5.2.1	Air Preheat Reduction .....	433
15.5.2.2	Low Excess Air .....	433
15.5.2.3	Staging .....	434
15.5.2.4	Gas Recirculation .....	435
15.5.2.5	Ultralean Premix .....	436
15.5.2.6	Water Injection .....	438
15.5.2.7	Reburning .....	438
15.5.2.8	Burner Out-of-Service (BOOS) .....	438
15.5.2.9	Burner Spacing .....	439
15.5.2.10	Pulsed Combustion .....	439
15.5.2.11	Flameless Combustion .....	439
15.5.2.12	Low NO <sub>x</sub> Burners .....	440
15.5.3	Process Modification .....	442
15.5.3.1	Reduced Production .....	443
15.5.3.2	Electrical Heating .....	443
15.5.3.3	Improved Thermal Efficiency .....	443
15.5.3.4	Product Switching .....	443



15.5.4	Post-Treatment .....	444
15.5.4.1	Selective Catalytic Reduction .....	444
15.5.4.2	Selective Non-Catalytic Reduction .....	446
15.5.4.3	Catalytic Reduction .....	448
15.5.4.4	Other .....	449
15.5.5	Implementing Strategies .....	449
15.5.5.1	General Implementation .....	449
15.5.5.2	More Specific Implementation .....	450
15.6	Pilot-Scale Test Results .....	450
15.6.1	Conventional Burner .....	451
15.6.1.1	Fuel Composition Effects .....	451
15.6.1.2	Fuel Gas Tip Design .....	454
15.6.1.3	Summary .....	455
15.6.2	Furnace Temperature Effects on NOx .....	459
15.6.2.1	Introduction .....	459
15.6.2.2	Furnace Temperature Measurement .....	460
15.6.2.3	Test Results .....	461
15.6.2.4	Conclusions .....	461
15.6.3	Ghost NOx .....	463
15.6.3.1	Introduction .....	463
15.6.3.2	Test Description .....	466
15.6.3.3	Results .....	467
15.6.4	Down-Fired Burner .....	469
	References .....	474

## 15.1 Introduction

NO<sub>x</sub> refers to oxides of nitrogen.<sup>1-23</sup> These generally include nitrogen monoxide, also known as nitric oxide (NO), and nitrogen dioxide (NO<sub>2</sub>). They may also include nitrous oxide (N<sub>2</sub>O), also known as laughing gas, as well as other less common combinations of nitrogen and oxygen such as nitrogen tetroxide (N<sub>2</sub>O<sub>4</sub>).

In most high temperature heating applications, the majority of the NO<sub>x</sub> exiting the exhaust stack is in the form of nitric oxide (NO).<sup>4</sup> NO is a colorless gas that rapidly combines with O<sub>2</sub> in the atmosphere to form NO<sub>2</sub> (Figure 15.1). NO is poisonous to humans and can cause irritation of the eyes and throat, tightness of the chest, nausea, headache, and gradual loss of strength. Prolonged exposure to NO can cause violent coughing, difficulty in breathing, cyanosis, and could be fatal. *Science* magazine named nitric oxide as its 1992 Molecule of the Year.<sup>5</sup> The reason is that NO is absolutely essential in human physiology. A growing body of research indicates its importance in many things such as aiding digestion, regulating blood pressure, and acting as a messenger in the nervous system. It is also a promising drug in the treatment of persistent pulmonary hypertension which is a life threatening lung condition affecting about 4000 babies each year.

In most high temperature combustion processes, NO<sub>2</sub> is a significant fraction of the total NO<sub>x</sub> exiting the stack, although it is generally not as much as NO. NO<sub>2</sub> is a reddish-brown gas that has a suffocating odor. It is highly toxic and hazardous because of its ability to cause delayed chemical pneumonitis and pulmonary edema. NO<sub>2</sub> vapors are a strong irritant to the pulmonary tract. Inhalation may also cause irritation of the eyes and throat, tightness of the chest, headache, nausea, and gradual loss of strength. Severe symptoms may be delayed and include cyanosis, increased difficulty in breathing, irregular

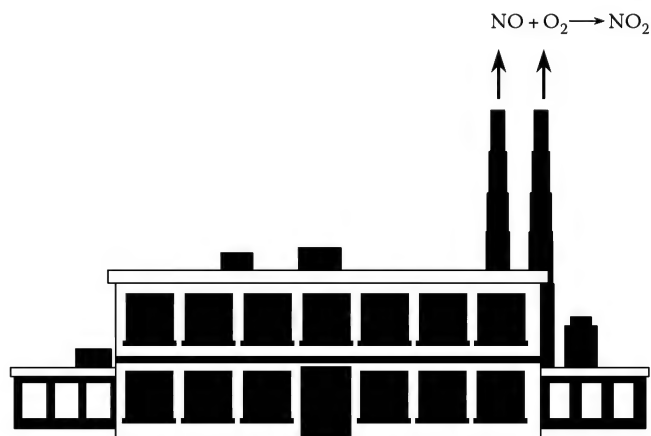


FIGURE 15.1

Schematic of NO exiting a stack and combining with O<sub>2</sub> to form NO<sub>2</sub>.

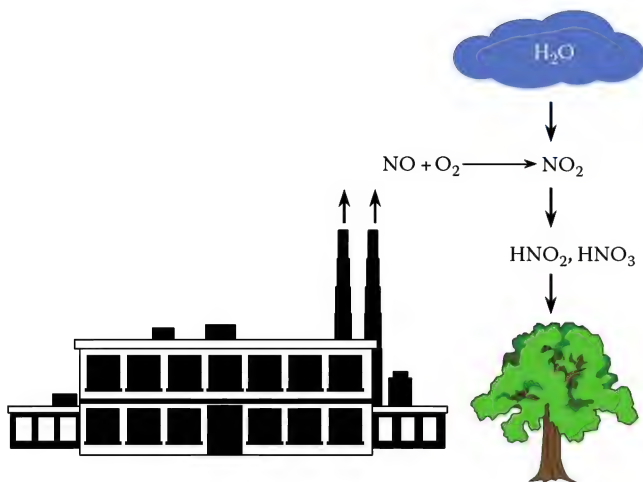


FIGURE 15.2  
Schematic of acid rain.

respiration, fatigue, and possible death due to pulmonary edema. Chronic or repeated exposure to  $\text{NO}_2$  could cause a permanent decrease in pulmonary function. Intermittent low-level  $\text{NO}_2$  exposure may also induce kidney, liver, spleen, red blood cell, and immune system alterations.<sup>6</sup>

In addition, to the poisoning effect that  $\text{NO}_x$  has on humans, there are also other problems associated with these chemicals. In the lower atmosphere,  $\text{NO}$  reacts with oxygen to form ozone ( $\text{O}_3$ ), as well as  $\text{NO}_2$ . Ozone is also a health hazard, which can cause respiratory problems in humans.  $\text{NO}_2$  is extremely reactive and is a strong oxidizing agent. It reacts violently on contact with alcohols, hydrocarbons, organic materials, and fuels.  $\text{NO}_2$  decomposes on contact with water to produce nitrous acid ( $\text{HNO}_2$ ) and nitric acid ( $\text{HNO}_3$ ) which are highly corrosive (see Figure 15.2). When  $\text{NO}_2$  forms in the atmosphere and comes in contact with moisture, acid rain is produced. Acid rain is destructive to many things it contacts, including plants, trees, and man-made structures like buildings, bridges, and statues (see Figure 15.3<sup>7,8</sup>). Another problem with  $\text{NO}_2$  is its

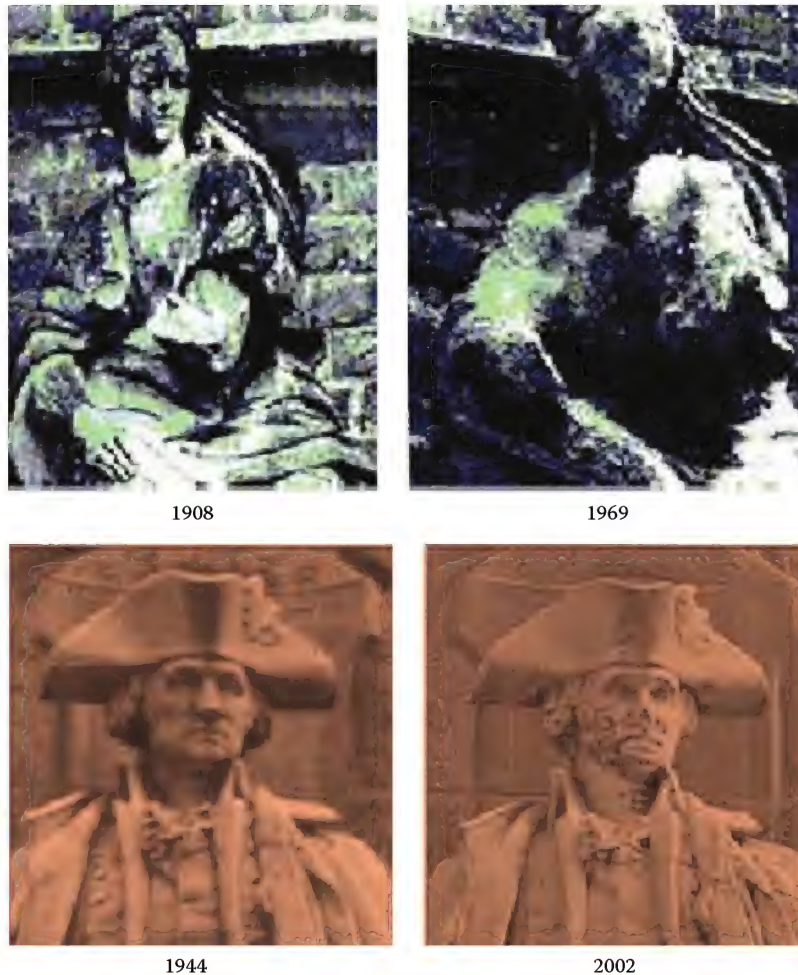
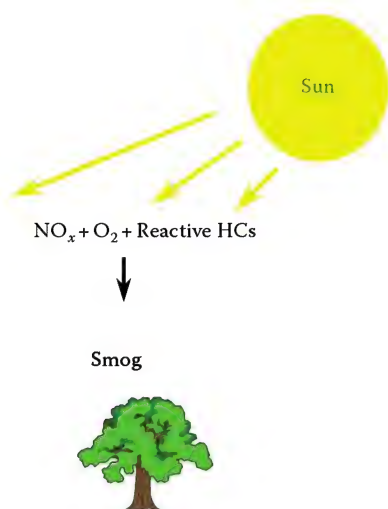


FIGURE 15.3  
Acid rain deterioration examples.



**FIGURE 15.4**  
Schematic of smog formation.

contribution to smog. When sunlight contacts a mixture of  $\text{NO}_2$  and unburned hydrocarbons in the atmosphere, photochemical smog is produced (see Figure 15.4).

Many combustion processes operate at elevated temperatures and high excess air levels. The combustion products may have long residence times in the combustion chamber. These conditions produce high thermal efficiencies and product throughput rates. Unfortunately, these conditions also favor the formation of  $\text{NO}_x$ . Only about 5% of typical  $\text{NO}_x$  sources in an industrial region of the United States come from industrial sources, compared to 44% from highway and

off-road vehicles<sup>9</sup> as seen in Figure 14.3. Figure 15.5 shows that  $\text{NO}_x$  emissions for petroleum refineries are comparable to other industries.<sup>10</sup>

## 15.2 Theory

### 15.2.1 Formation Mechanisms

There are three generally accepted mechanisms for  $\text{NO}_x$  production: thermal, prompt, and fuel. These are each discussed briefly in this section.

#### 15.2.1.1 Thermal $\text{NO}_x$

Thermal  $\text{NO}_x$  is formed by the high temperature reaction of nitrogen with oxygen, by the well-known Zeldovich mechanism.<sup>11</sup> It is given by the simplified reaction:



The reaction of the so-called extended Zeldovich mechanism is



Thermal  $\text{NO}_x$  increases exponentially with temperature (Figure 15.8). Above about 2000°F (1100°C), it is generally the predominant mechanism in combustion processes,

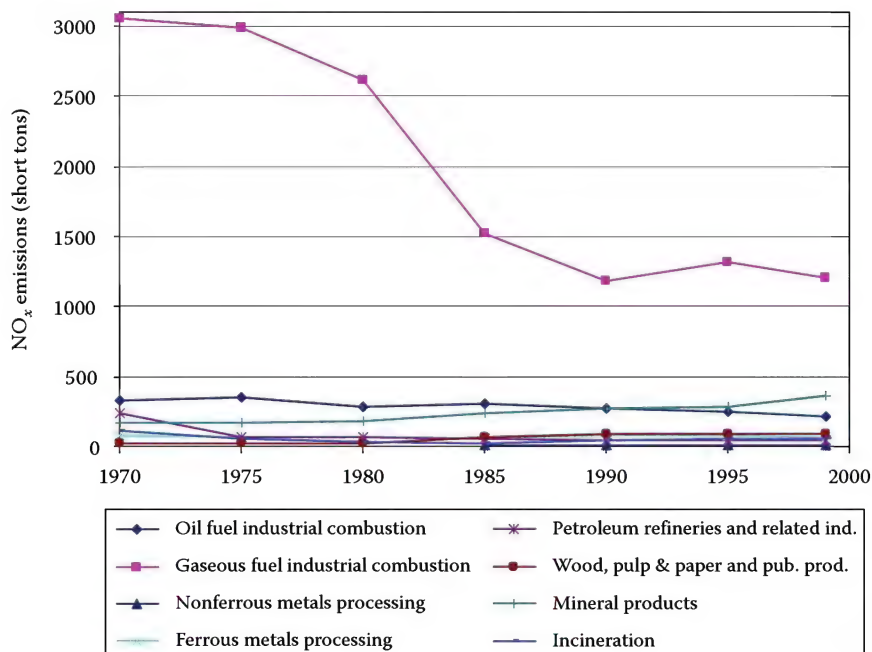


**FIGURE 15.5**  
 $\text{NO}_x$  emissions in the United States between 1970 and 1999 based on the process. (From Elkins, J. et al., National air quality and emissions trends report, 1999, U.S. Environmental Protection Agency, Washington, DC, Report EPA 454/R-01-004, 2001.)



making it important in most high temperature heating applications. This means that this mechanism becomes even more important when the combustion air is pre-heated or enriched with oxygen,<sup>44</sup> both of which increase the flame temperature.

Results from laboratory experiments provided the information necessary to develop an empirical relationship for high temperature (i.e., thermal) NO formation. This empirical relationship reveals several important parameters that affect NO formation:<sup>12</sup>

$$[\text{NO}] = K_1 t e^{K_2/T} [\text{N}_2][\text{O}_2]^{1/2} \quad (15.5)$$

where

$[\text{NO}]$  is the volume concentration of NO (ppm)

$K_1$  is  $5.2 \times 10^{17}$

$K_2$  is  $-72,300$

$t$  is the residence time (s), valid for 0–5 s

$T$  is the temperature (K), valid for range 1800°C–2000°C

$[\text{N}_2]$  is the volume concentration of  $\text{N}_2$

$[\text{O}_2]$  is the volume concentration of  $\text{O}_2$

### Example 15.1

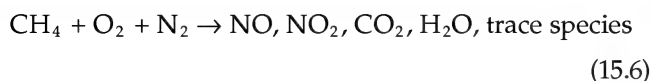
If  $t = 2$  s,  $T = 1975^\circ\text{C}$ ,  $[\text{N}_2] = 0.7$  (70%  $\text{N}_2$  by volume), and  $[\text{O}_2] = 0.30$  (30%  $\text{O}_2$  by volume), then find  $[\text{NO}]$

$$[\text{NO}] = 5.2 \times 10^{17} (2\text{s}) e^{-72300/2248 \text{ K}} [0.70][0.30]^{1/2} = 4295 \text{ ppm}$$

This empirical equation is only valid over a fairly narrow range of conditions, but it shows the impact of various parameters. NO is linearly dependent on residence time, but only up to 5 s; thereafter, NO is approximately constant. NO is exponentially dependent on temperature, linearly dependent on  $\text{N}_2$  concentration, and dependent on the square root of  $\text{O}_2$  concentration. In most industrial combustion processes, the concentration of  $\text{N}_2$  is generally large and approximately fixed, while the concentration of  $\text{O}_2$  is relatively small and somewhat variable. In general, increasing the residence time, the temperature, the  $\text{N}_2$  concentration, and/or the  $\text{O}_2$  concentration in the high temperature zone all increase NO<sub>x</sub>. Of these variables, the only one that cannot usually be influenced significantly is the  $\text{N}_2$  concentration. The NO<sub>x</sub> reduction techniques utilizing combustion modification (see Section 15.5.2) are based on reducing the peak flame temperature, the residence time in the flame zone, and the excess  $\text{O}_2$  concentration.

#### 15.2.1.2 Prompt NO<sub>x</sub>

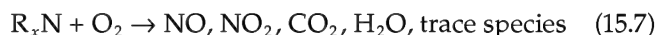
Prompt NO<sub>x</sub> is formed by the relatively fast (“prompt”) reaction between nitrogen, oxygen, and hydrocarbon radicals.<sup>13</sup> It is given by the following overall reaction:



In reality, this very complicated process consists of hundreds of reactions. The hydrocarbon radicals are intermediate species formed during the combustion process. Prompt NO<sub>x</sub> is generally an important mechanism in lower temperature combustion processes.

#### 15.2.1.3 Fuel NO<sub>x</sub>

Fuel NO<sub>x</sub> is formed by the oxidation of nitrogen contained in the fuel<sup>14</sup> and is given by the following overall reaction:



An example of “fuel” ( $\text{R}_x\text{N}$ ) is ammonia ( $\text{NH}_3$ ) where nitrogen is chemically bound to hydrogen atoms. In reality, there are many intermediate reactions for this formation mechanism as indicated in Figure 15.6. Fuel NO<sub>x</sub> is not a concern for high-quality gaseous fuels like natural gas (NG) or propane, which normally have no organically bound nitrogen. Although, sometimes NG may contain some nitrogen in the form of  $\text{N}_2$  that contribute to NO<sub>x</sub> formation, this, however, would not be an example of fuel NO<sub>x</sub> because the nitrogen is not organically bound.

Sometimes fuel NO<sub>x</sub> may be important when oil (e.g., residual fuel oil), coal, or waste fuels are used which may contain significant amounts of organically bound nitrogen. Table 15.1 shows that heavy oil (residual fuel) produces much more NO<sub>x</sub> per unit energy (lb/MMBtu) than light oil (distillate fuel), generally because heavy oils contain more organically bound nitrogen than lighter oils.<sup>15</sup> The challenge with fuel NO<sub>x</sub> is that it is dependent not only on both the operating conditions and amount of nitrogen in the fuel, but also on the composition and specific characteristics of the fuel.<sup>16</sup> This makes it challenging to estimate emissions without making measurements.

Table 15.2 shows typical thermal and fuel NO<sub>x</sub> emissions for process heaters.<sup>17</sup> The amount of fuel-bound nitrogen converted to NO<sub>x</sub> ranges from 15% to 100%.<sup>17</sup> The higher the conversion efficiency, the lower the nitrogen content in the fuel.

#### 15.2.2 Important Factors Affecting NO<sub>x</sub>

There are many factors that impact NO<sub>x</sub> formation. These include the oxidizer and fuel compositions and temperatures, the ratio of the fuel to the oxidizer, the burner and heater designs, the furnace and flue gas temperatures, and the operational parameters of the combustion system (e.g., furnace air infiltration). Some of these factors are considered next.

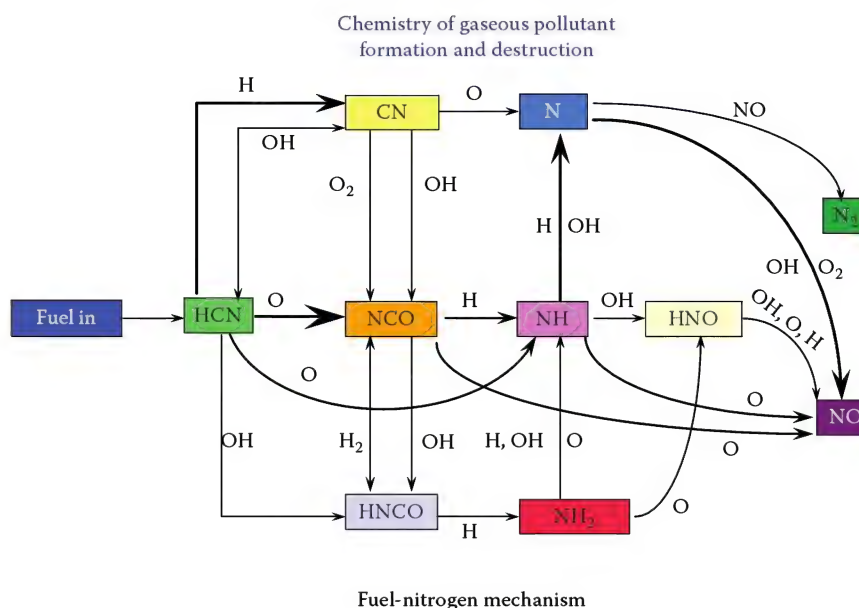


**FIGURE 15.6**  
Schematic of fuel NO<sub>x</sub> formation pathways.

**TABLE 15.1**

NO<sub>x</sub> Emission Factors by Fuel Type

Fuel Type	Emission Factor (lb/MMBtu)
Distillate fuel	0.140
Residual fuel	0.370
Other oils	0.370
Natural gas	0.140
Refinery gas	0.140
LPG	0.208
Coal	0.950
Petroleum coke	0.950
Electricity	0.550

Source: Pellegrino, J. et al., Energy and environmental profile of the U.S. petroleum refining industry, report prepared by Energetics, Inc. for the U.S. Department of Energy, November 2007.

**TABLE 15.2**

Uncontrolled NO<sub>x</sub> Emission Factors for Typical Process Heaters

Model Heater Type	Uncontrolled Emission Factor, lb/10 <sup>6</sup> Btu		
	Thermal NO <sub>x</sub>	Fuel NO <sub>x</sub>	Total NO <sub>x</sub> <sup>a</sup>
ND, natural gas-fired <sup>b</sup>	0.098	N/A	0.098
MD, natural gas-fired <sup>b</sup>	0.197	N/A	0.197
ND, distillate oil-fired	0.140	0.060	0.200
ND, residual oil-fired	0.140	0.280	0.420
MD, distillate oil-fired	0.260	0.060	0.320
ND, residual oil-fired	0.260	0.280	0.540
ND, pyrolysis, natural gas-fired	0.104	N/A	0.104
ND, pyrolysis, high-hydrogen fuel gas-fired <sup>c</sup>	0.140 <sup>d</sup>	N/A	0.140

Source: Sanderford, E.B., Alternative control techniques document – NO<sub>x</sub> emissions from process heaters, U.S. Environmental Protection Agency report EPA-453/R-93-015, February, 1993.

Note: N/A = Not applicable; ND = Natural draft; MD = Mechanical draft; Table 2-1 on p. 2-3 of Sanderford, EPA document, 1993.

<sup>a</sup> Total NO<sub>x</sub> = Thermal NO<sub>x</sub> + Fuel NO<sub>x</sub>.

<sup>b</sup> Heaters firing refinery fuel gas with up to 50 mole percent hydrogen can have up to 20% higher NO<sub>x</sub> emissions than similar heaters firing NG.

<sup>c</sup> High-hydrogen fuel gas is fuel gas with 50 mole percent or greater hydrogen content.

<sup>d</sup> Calculated assuming approximately 50 mole percent hydrogen.

### 15.2.2.1 Air–Fuel Ratio (Stoichiometry)

Figure 15.7 shows the predicted (theoretical) NO (in parts per million by volume on a wet basis or ppmvw) as a function of the air-to-fuel ratio (stoichiometry) for an air/CH<sub>4</sub> flame under adiabatic equilibrium conditions. Notice that the NO concentration increases at fuel-lean conditions (equivalence ratio <1) and decreases at fuel-rich conditions (equivalence ratio >1). Figure 4.6 shows a plot of the adiabatic equilibrium flame temperature for an air/CH<sub>4</sub> flame as a function of the flame equivalence ratio. Notice that the flame temperature for the air/CH<sub>4</sub> flame is very dependent on the stoichiometry. This figure helps explain why, for example, NO<sub>x</sub>

is reduced dramatically under fuel-rich conditions. One reason is because of the dramatic reduction in the flame temperature. Another reason is related to the chemistry. In a reducing atmosphere, CO is formed preferentially to NO; this is exploited in some of the NO<sub>x</sub> reduction techniques. An example of this technique is methane reburn (see Section 15.5.2.7).<sup>18</sup> The exhaust gases from the combustion process flow through a zone that is at reducing conditions. NO<sub>x</sub> is reduced back to N<sub>2</sub>. Any CO that may have formed in the reduction zone and any other unburned fuels are then combusted downstream of the reduction zone. However, they are combusted at temperatures well below those found in the main combustion process; these lower temperatures are not favorable to NO<sub>x</sub> formation.

Another thing to notice in Figure 15.7 is that NO<sub>x</sub> also decreases under very fuel-lean (oxidizing or excess O<sub>2</sub>) conditions. This is because of the reduced flame temperature caused by all the diluent excess air (see Figure 4.6). One technology that takes advantage of this principle is called ultralean premix (see Section 15.5.2.5). With this technology, part of the fuel burns under very fuel-lean conditions with the balance of the fuel being added somewhere else in the system (e.g., downstream of the ultralean zone). Overall, the system operates at slightly fuel-lean conditions (low excess O<sub>2</sub> levels).

### 15.2.2.2 Gas Temperature

Figure 15.8 shows the predicted NO<sub>x</sub> as a function of gas temperature for stoichiometric air/fuel flames under adiabatic equilibrium conditions. This plot shows

the importance of the gas temperature on thermal NO<sub>x</sub> formation. Notice that the NO<sub>x</sub> rises rapidly at temperatures above about 2000°F (1100°C) for all three fuel cases shown. This demonstrates the exponential increase in thermal NO<sub>x</sub> as a function of temperature. Many combustion modification strategies used for reducing NO<sub>x</sub> emissions involve lowering the flame temperature because it has such a large impact on NO<sub>x</sub>. For example, one strategy is to inject water (usually in the form of steam) into the flame in order to reduce NO<sub>x</sub> by cooling the flame to a lower temperature where NO<sub>x</sub> formation is less favorable (see Section 15.5.2.6). However, water injection reduces the thermal efficiency of the heater because it is an added heat load.

### 15.2.2.3 Air and Fuel Preheat Temperature

Figure 15.9 shows how NO<sub>x</sub> increases with combustion air preheat temperature. Air preheating is commonly used to help increase the overall thermal efficiency of the heating process by recovering energy from the flue gases and transferring it to the incoming combustion air. However, it can dramatically increase NO<sub>x</sub> emissions because of the strong temperature dependence of NO formation. Figure 4.7 shows the adiabatic flame temperature increases approximately linearly with air preheating. The increase in NO emissions mimics the increase in flame temperature.

Figure 15.10 shows how NO<sub>x</sub> increases with the fuel preheat temperature. Fuel preheating is another method used to improve the overall thermal efficiency of a heating process. Figure 4.8 shows how the adiabatic flame temperature increases due to fuel preheating. The

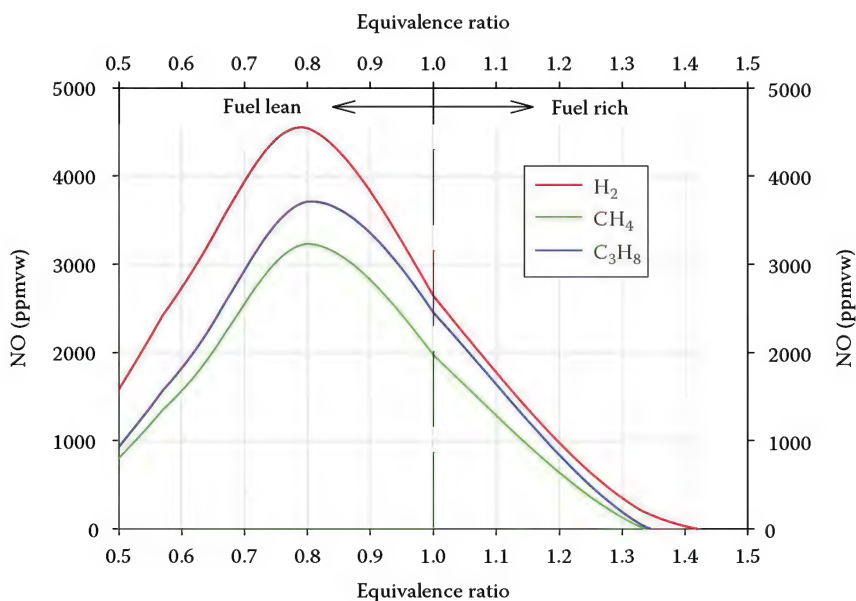


**FIGURE 15.7**  
Adiabatic equilibrium NO as a function of equivalence ratio for air/fuel flames.



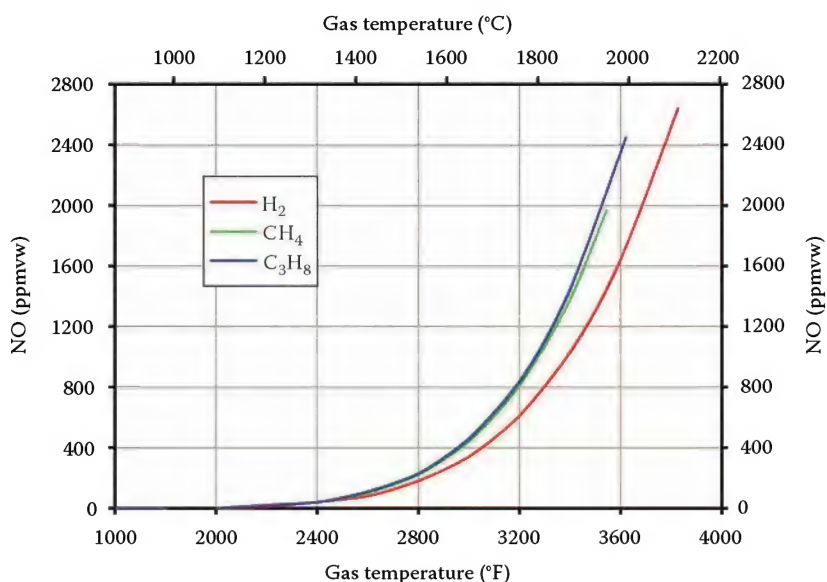


FIGURE 15.8

Adiabatic equilibrium NO as a function of gas temperature for stoichiometric air/fuel flames.

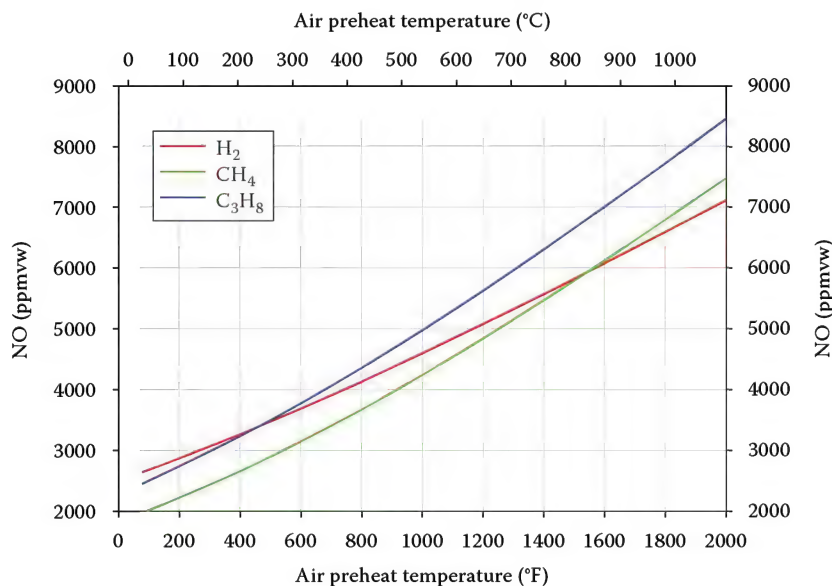


FIGURE 15.9

Adiabatic equilibrium NO as a function of air preheat temperature for stoichiometric air/fuel flames.

increase in NO<sub>x</sub> emissions follows the same pattern as the increase in flame temperature. Fuel preheating is usually less important for NO<sub>x</sub> formation as compared to air preheating for a given preheat temperature because the mass flow rate of air is typically much greater than the mass flow rate of fuel.

#### 15.2.2.4 Fuel Composition

Figure 15.11 shows how the fuel composition affects NO for a blend of CH<sub>4</sub> and H<sub>2</sub>. First, it is important to note that NO increases as the H<sub>2</sub> content in the blend increases. This is similar to the effect on the adiabatic

flame temperature as shown in Figure 4.9. The second observation is that the effect is not linear between pure CH<sub>4</sub> and pure H<sub>2</sub>. That is, NO<sub>x</sub> increases more rapidly as the H<sub>2</sub> content increases. The third observation is that there is a significant difference between the two extremes as the NO<sub>x</sub> ranges from a little less than 2000 ppmvw to a little more than 2600 ppmvw.

Figure 15.12 shows how the fuel composition affects NO for a blend of CH<sub>4</sub> and N<sub>2</sub>. NO (ppmvw) drops off rapidly as the N<sub>2</sub> concentration in the fuel blend increases. At 100% N<sub>2</sub>, the “fuel” produces no NO (nor does it produce any heat!). The additional quantity of

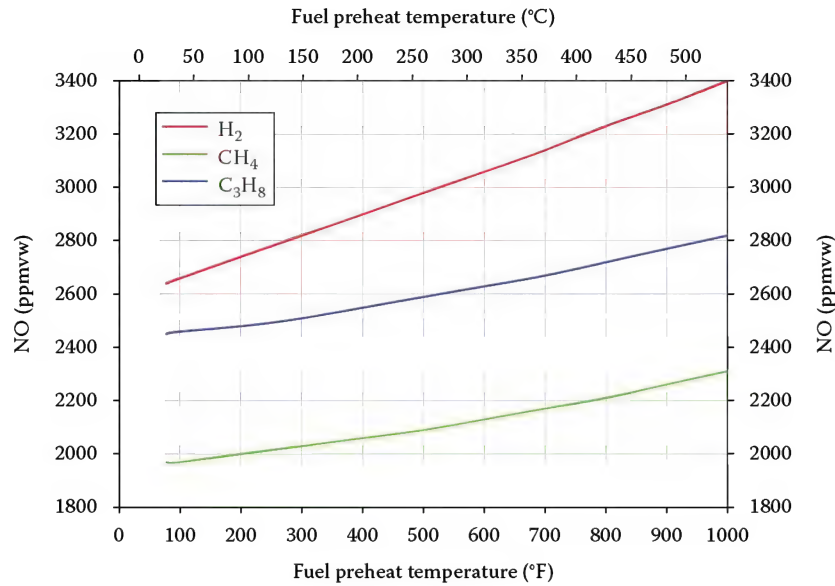


FIGURE 15.10

Adiabatic equilibrium NO as a function of fuel preheat temperature for a stoichiometric air/CH<sub>4</sub> flame.

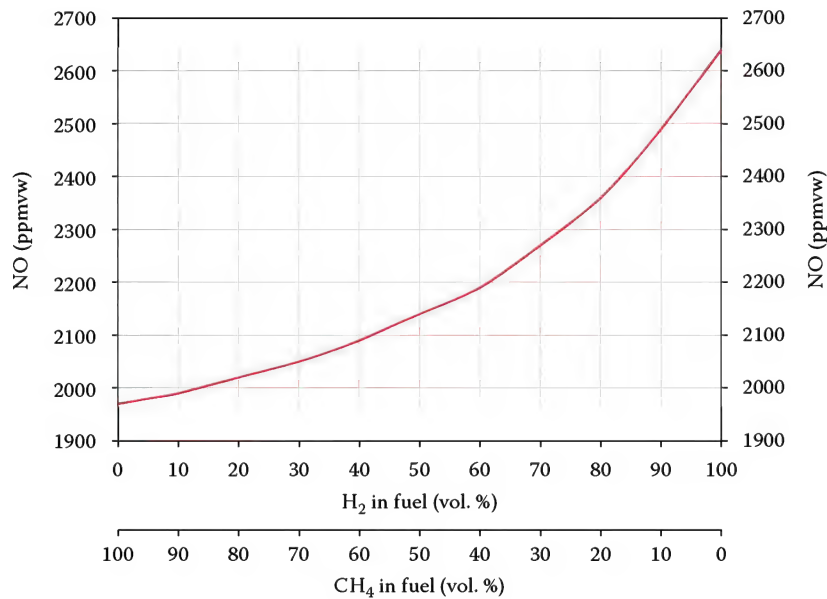


FIGURE 15.11

Adiabatic equilibrium NO as a function of fuel composition (CH<sub>4</sub>/H<sub>2</sub>) for a stoichiometric air/fuel flame.

N<sub>2</sub> in the fuel does not increase NO<sub>x</sub> because of the increased availability of N<sub>2</sub> to make NO<sub>x</sub> since there is already plenty of N<sub>2</sub> available from the combustion air.

Another aspect of NO<sub>x</sub> determined by fuel composition is the organically bound nitrogen content in liquid fuels. The higher the nitrogen content, the more the NO<sub>x</sub> generated, although it is not a linear correlation. Figure 15.13 shows that the experimentally determined conversion ratio  $r_N$  of fuel-bound nitrogen to NO<sub>2</sub> in a variety of compounds decreases with fuel-nitrogen content with  $r_N$  defined as

$$r_N = \frac{E_{\text{NO}_2}}{\xi_N} \frac{M_N}{M_{\text{NO}_2}} H_u \quad (15.8)$$

where

$E_{\text{NO}_2}$  is the NO<sub>2</sub> emissions value in mg of NO<sub>2</sub>/kWh

$\xi_N$  is the fuel-bound nitrogen content

$M_N$  and  $M_{\text{NO}_2}$  are the molar masses of nitrogen and nitrogen dioxide

$H_u$  is the net calorific value of the sample<sup>19</sup>

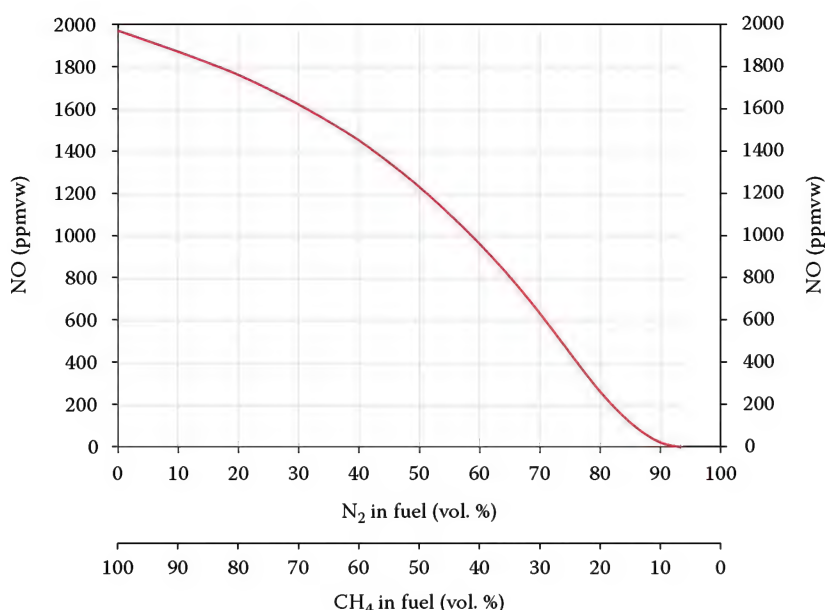


FIGURE 15.12

Adiabatic equilibrium NO as a function of fuel composition ( $\text{CH}_4/\text{N}_2$ ) for a stoichiometric air/fuel flame.

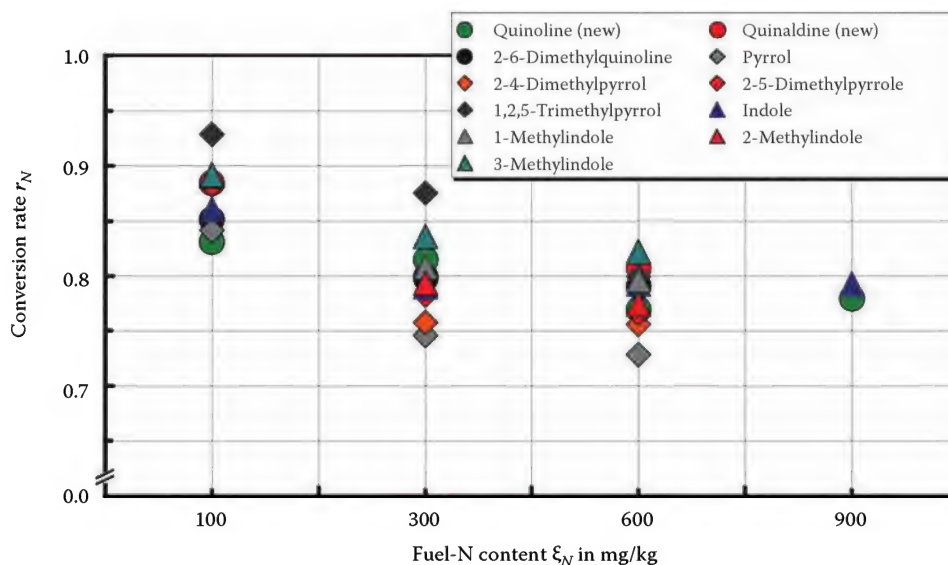


FIGURE 15.13

Conversion ratio of fuel-bound nitrogen to  $\text{NO}_2$  of various nitrogen-containing fuels as a function of fuel-nitrogen content. (From Medeiros, A. et al., *Clean Air*, 8(4), 359, 2007.)

Figure 15.14 shows some experimental data gathered from John Zink burners firing oils with different levels of fuel-bound nitrogen. The data again show that the conversion efficiency declines as the amount of fuel-bound nitrogen increases, although the actual shape of the curve is dependent on the burner design.

#### 15.2.2.5 Air–Fuel Mixing

The mixing of the air and fuel, which is related to the burner design, directly impacts  $\text{NO}_x$  emissions.<sup>20</sup>

Figure 15.15 shows a diagram of the relative effects of both the air/fuel mixture ratio and the general type of burner design (premix vs. diffusion). Note that the actual shapes of these curves depend on several factors, particularly the actual burner design; therefore, the curves are only meant to be representative, which is why no specific  $\text{NO}_x$  levels are given.

The  $\text{NO}_x$  for premix flames has the same general shape as that predicted by adiabatic equilibrium calculations as shown in Figure 15.7. However, the magnitude of  $\text{NO}_x$  from actual premixed flames is generally



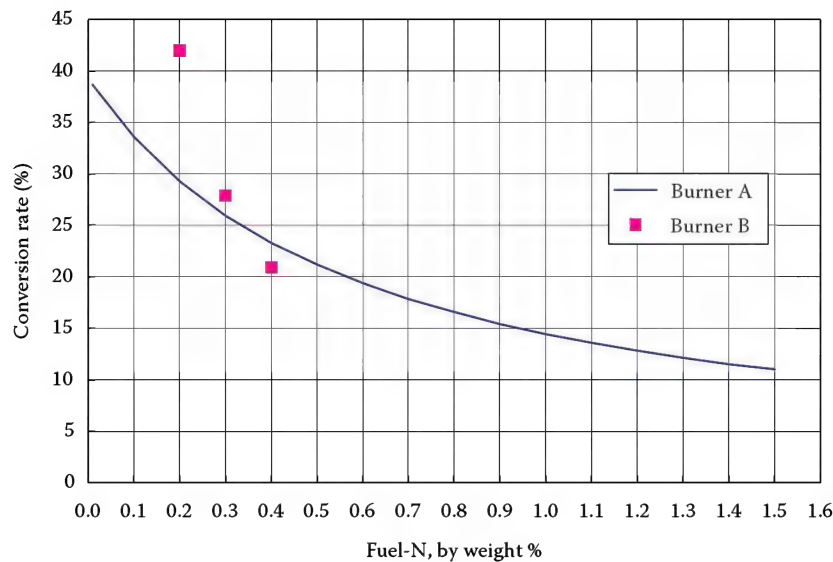


**FIGURE 15.14**  
Conversion rate of fuel-bound nitrogen to NO<sub>x</sub> for two different oil-fired burners.

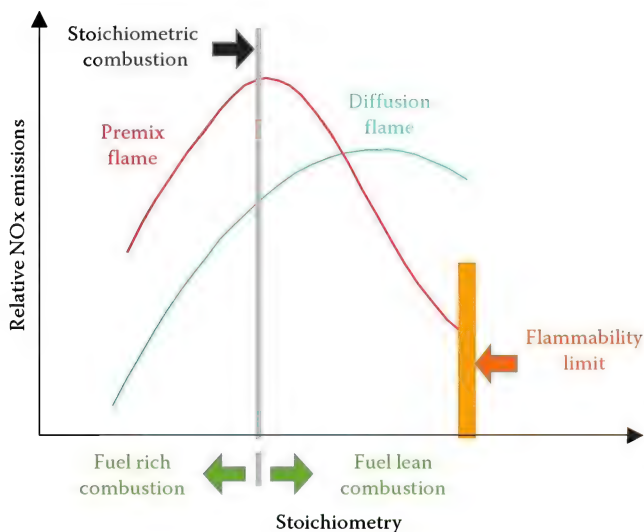


**FIGURE 15.15**  
Relative NO<sub>x</sub> versus air/fuel ratio for premix and diffusion flames.

much less than predicted by adiabatic calculations because actual flames radiate heat and therefore are at lower temperatures as compared to adiabatic conditions. Notice that the peak NO<sub>x</sub> occurs approximately at the air/fuel ratio where most industrial combustion systems are operated.

Assuming all other variables are the same, diffusion flames produce less NO<sub>x</sub> than premixed flames because of the delayed mixing. In a diffusion flame, the fuel and air mix over some distance after exiting the burner, which depends on the specific design. Heat is being continually released as the fuel and air continue to mix; therefore, diffusion flames typically do not reach the same peak temperatures as premix

flames do. As shown in Figure 15.8, NO<sub>x</sub> is very temperature dependent, so the lower peak temperatures for diffusion flames generate less NO<sub>x</sub> compared to premix flames.

The shape of the curve for the diffusion flame is also different than for the premix flame because of the delayed mixing. The peak NO<sub>x</sub> is shifted to a more fuel-lean mixture for diffusion flames. While overall the flame is more fuel lean, the actual air/fuel mixture ratio varies considerably depending on location. Higher overall levels of excess air result in zones in the flame that are closer to stoichiometric conditions while the air and fuel are still mixing. Then, there are other zones in the flame that still have high excess air levels where the fuel still has not completely mixed with the air. Those zones serve to absorb heat from the more stoichiometric zones, which reduces the peak flame temperatures, which also reduces NO<sub>x</sub> compared to premixed flames. At high enough excess air levels, NO<sub>x</sub> levels decline as well for diffusion flames because of the flame quenching.

### 15.3 Regulations

Due to the many health and environmentally related problems caused by NO<sub>2</sub>, it is considered to be one of the six criteria pollutants identified by the U.S. Environmental Protection Agency (EPA). As such, it is strictly regulated to ensure that ambient air concentrations do not exceed the National Ambient Air Quality Standards (NAAQS). Figure 14.1 shows that of the six criteria

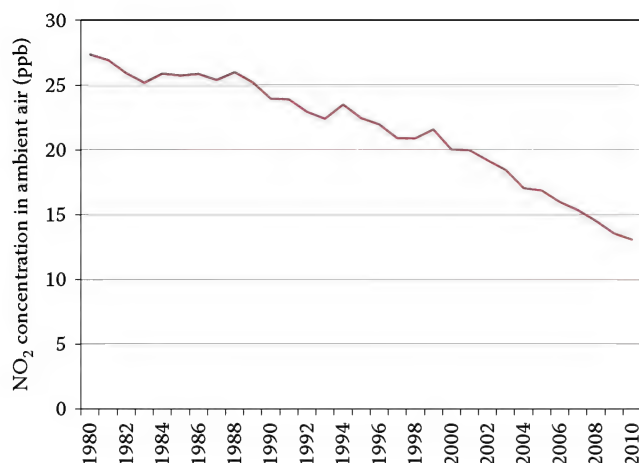


FIGURE 15.16

National NO<sub>2</sub> ambient air quality trends. (From U.S. Environmental Protection Agency, Nitrogen Dioxide, <http://www.epa.gov/airtrends/nitrogen.html>, accessed September 14, 2012.)

pollutants, NO<sub>2</sub> is not as much a concern at the present time compared to ozone and particulate matter. Figure 15.16 shows that average ambient air concentrations of NO<sub>2</sub> (in ppb = parts per billion) are well below the current U.S. national standard. Regulations are effectively controlling NO<sub>2</sub> emissions at this time.

Regulations for NO<sub>x</sub> vary by country and region. Countries such as the United States, Japan, and Germany have among the strictest regulations in the world. Perhaps the most stringent standards in the world are those enforced by the South Coast Air Quality Management District (SCAQMD) that governs the greater Los Angeles area.

### 15.3.1 Units

Baukal and Eleazer<sup>21</sup> have discussed potential sources of confusion in the existing NO<sub>x</sub> regulations which include the wide variety of units that have been used, reporting on either a dry or wet sample basis, measuring NO, but reporting NO<sub>2</sub>, and reporting on a volume vs. a mass basis.

Historically, governing bodies have sprung up regionally to regulate particular sources. The governing bodies have generally adopted units related to a traditional industry metric; this has led to a wide variety of NO<sub>x</sub> units. For example, internal combustion engines are generally regulated on a gram per brake horsepower (g/bhp) basis—a mass-based unit normalized by the output power of the engine. Gas turbines, on the other hand, are generally regulated on a part per million (ppm) basis. Because this unit is volume based, it must be referenced to a standard condition. Gas turbines usually operate near 15% excess oxygen, and traditionally NO<sub>x</sub> measurement requires removal of water before analysis. Therefore, gas turbines often use a ppm measurement referenced on a dry volume basis (ppmvd) to 15% oxygen.

On the other hand, one typically operates industrial boilers and process heaters nearer to 3% excess oxygen. Therefore, NO<sub>x</sub> emissions from those units are generally referenced as ppmvd corrected to 3% oxygen. However, these processes may also be regulated on a mass basis normalized by the heat release of the burner; for example, pounds per million Btu (lb/MMBtu). Large electrical utilities operate their boilers under very tight oxygen limits. Therefore, some U.S. agencies regulate utility boilers on a pound per megawatt basis (lb/MW). A further complication is whether to normalize the unit by gross output power (Gross MW; based on the HHV) or to subtract parasitic power losses (Net MW). Some regulatory agencies use SI units such as grams per normal cubic meter (g/Nm<sup>3</sup>).

### 15.3.2 Conversions

It is often necessary to convert pollutant measurements (e.g., NO<sub>x</sub> and CO) into a standard basis for both regulatory and comparison purposes. One conversion that is often necessary is from the measured O<sub>2</sub> level in the exhaust gases to a standard basis O<sub>2</sub> level. The method for converting measurements to a standard basis is given by<sup>22</sup>

$$\text{ppm}_{\text{corr}} = \text{ppm}_{\text{meas}} \left( \frac{20.9 - \text{O}_{2\text{ref}}}{20.9 - \text{O}_{2\text{meas}}} \right) \quad (15.9)$$

where

ppm<sub>meas</sub> is the measured pollutant concentration in flue gases (ppmvd)

ppm<sub>corr</sub> is the pollutant concentration corrected to a reference O<sub>2</sub> basis (ppmvd)

O<sub>2meas</sub> is the measured O<sub>2</sub> concentration in flue gases (vol. %, dry basis)

O<sub>2ref</sub> is the reference O<sub>2</sub> basis (vol. %, dry basis)

#### Example 15.2

Given: Measured NO<sub>x</sub> = 20 ppmvd, measured O<sub>2</sub> = 2% on a dry basis.

Find NO<sub>x</sub> at 3% O<sub>2</sub> on a dry basis.

Solution: ppm<sub>meas</sub> = 20, O<sub>2meas</sub> = 2, O<sub>2ref</sub> = 3

$$\text{ppm}_{\text{corr}} = (20) \left( \frac{20.9 - 3}{20.9 - 2} \right) = 18.9 \text{ ppmvd}$$

This example shows that NO<sub>x</sub> values will be lower when the basis O<sub>2</sub> is higher than the measured O<sub>2</sub> because higher O<sub>2</sub> levels mean more air dilution and therefore lower NO<sub>x</sub> concentrations. The reverse is true when the basis O<sub>2</sub> is lower than the measured O<sub>2</sub> level. Note that some regulations do not allow correcting emissions to a lower value.

Another correction that may be required is to convert the measured pollutants from a measured furnace

temperature to a different reference temperature. This may be required when a burner is tested at one furnace temperature and needs to be adjusted to determine the equivalent at another furnace temperature. The correction for temperature is

$$\text{ppm}_{\text{corr}} = \text{ppm}_{\text{meas}} \left( \frac{T_{\text{ref}} - T_{\text{basis}}}{T_{\text{meas}} - T_{\text{basis}}} \right) \quad (15.10)$$

where

$\text{ppm}_{\text{meas}}$  is the measured pollutant concentration in flue gases (ppmvd)

$\text{ppm}_{\text{corr}}$  is the pollutant concentration corrected to a reference temperature basis (ppmvd)

$T_{\text{ref}}$  is the reference furnace temperature (°F)

$T_{\text{meas}}$  is the measured furnace temperature (°F)

$T_{\text{basis}}$  is the basis furnace temperature (°F)

#### Example 15.3

Given: Measured NOx = 20 ppmvd, measured furnace temperature = 1800°F.

Find NOx at a reference temperature of 2000°F.

Solution:  $\text{ppm}_{\text{meas}} = 20$ ,  $T_{\text{meas}} = 1800^\circ\text{F}$ , assume  $T_{\text{basis}} = 400^\circ\text{F}$

$$\text{ppm}_{\text{corr}} = (20) \left( \frac{2000 - 400}{1800 - 400} \right) = 22.9 \text{ ppmvd}$$

There are two things to notice in the aforementioned example. The first is that the basis temperature was chosen as 400°F, which is an empirically determined value that applies to many burners commonly used in the hydrocarbon and petrochemical industries. This correction is only valid for a moderate difference between the measured and corrected temperatures of no more than 200°F (110°C) or is degree symbol. However, this equation should be used with care for other burner designs and when there is a very large difference between the measured and the reference furnace temperatures. The second observation is that the NOx increases when the reference temperature is higher than the measured temperature and vice versa. As will be shown later, NOx generally increases with the furnace temperature.

These two corrections can also be combined into a single correction when both the measured O<sub>2</sub> level and furnace temperature are different from the reference O<sub>2</sub> level and furnace temperature:

$$\text{ppm}_{\text{corr}} = \text{ppm}_{\text{meas}} \left( \frac{20.9 - \text{O}_{2\text{ref}}}{20.9 - \text{O}_{2\text{meas}}} \right) \left( \frac{T_{\text{ref}} - T_{\text{basis}}}{T_{\text{meas}} - T_{\text{basis}}} \right) \quad (15.11)$$

where the variables have been previously defined.

#### Example 15.4

Given: Measured NOx = 20 ppmvd, measured O<sub>2</sub> = 2% on a dry basis, measured furnace temp. = 1800°F.

Find NOx at 3% O<sub>2</sub> on a dry basis at a reference temperature of 2000°F.

Solution:  $\text{ppm}_{\text{meas}} = 20$ ,  $\text{O}_{2\text{meas}} = 2$ ,  $\text{O}_{2\text{ref}} = 3$ ,  $T_{\text{meas}} = 1800^\circ\text{F}$ , assume  $T_{\text{basis}} = 400^\circ\text{F}$

$$\text{ppm}_{\text{corr}} = (20) \left( \frac{20.9 - 3}{20.9 - 2} \right) \left( \frac{2000 - 400}{1800 - 400} \right) = 21.6 \text{ ppmvd}$$

In this case, the increase in NOx due to the temperature correction is greater than the reduction in NOx due to the higher O<sub>2</sub> reference.

It is important to be able to convert field measurements to specific units in order to determine whether the emissions from a specific burner or heater are below the permitted limits. In most cases, NOx is measured on a ppmvd basis. The following examples will show how to convert these units to a specific basis.

#### Example 15.5

Given: Fuel = methane with a gross or higher heating value of 1012 Btu/ft<sup>3</sup>, NO = 20 ppmvd, measured O<sub>2</sub> = 2% on a dry basis.

Find NOx as NO<sub>2</sub> in lb/10<sup>6</sup> Btu (gross).

Solution: First calculate dry flue gas products.

Global chemical reaction:  $\text{CH}_4 + x(\text{O}_2 + 3.76\text{N}_2) = \text{CO}_2 + 2\text{H}_2\text{O} + y\text{O}_2 + 3.76x\text{N}_2$

where  $\text{O}_2 + 3.76\text{N}_2$  is the composition of air (79% N<sub>2</sub>, 21% O<sub>2</sub>, by volume)

1. Given 2% O<sub>2</sub> in dry flue gases:

$$\frac{y}{1 + y + 3.76x} = 0.02$$

2. O atom balance:

$$2x = 2 + 2 + 2y = 4 + 2y \quad \text{or,} \quad x = 2 + y$$

Solving (1) and (2) simultaneously,

$$\begin{aligned} \text{CH}_4 + 2.188(\text{O}_2 + 3.76\text{N}_2) \\ = \text{CO}_2 + 2\text{H}_2\text{O} + 0.188\text{O}_2 + 8.23\text{N}_2 \end{aligned}$$

This shows the moles of products for each mole of CH<sub>4</sub>. Note that the NO in the flue products has been ignored because it is only in trace amounts. Assume that all NO is converted to NO<sub>2</sub> in the atmosphere.

$$\begin{aligned} 1 \times 10^6 \text{ Btu (gross)} / (1012 \text{ Btu/ft}^3 \text{ CH}_4) \\ = 988 \text{ ft}^3 \text{ of CH}_4 \end{aligned}$$



$$(988 \text{ ft}^3 \text{ of CH}_4)(1 + 0.188 + 8.23)$$

$$= 9305 \text{ ft}^3 \text{ of dry combustion}$$

products at STP per  $10^6$  Btu

Given 20 ppmvd  $\text{NO}_2$

$$= (20 \text{ ft}^3 \text{ NO}_2 / 10^6 \text{ ft}^3 \text{ dry products})$$

$$(9305 \text{ ft}^3 \text{ dry products} / 10^6 \text{ Btu})$$

$$= 0.186 \text{ ft}^3 \text{ NO}_2 / 10^6 \text{ Btu}$$

$$\text{Density of NO}_2 = 0.111 \text{ lb/ft}^3$$

Mass of  $\text{NO}_2$  in exhaust products

$$= (0.186 \text{ ft}^3 \text{ NO}_2 / 10^6 \text{ Btu})(0.111 \text{ lb NO}_2 / \text{ft}^3 \text{ NO}_2)$$

$$= 0.021 \text{ lb NO}_2 / 10^6 \text{ Btu (HHV)}$$

### 15.3.3 Hydrocarbon and Petrochemical Industry Regulations

The U.S. EPA regulates emissions in the hydrocarbon and chemical processing industries (HPI and CPI, respectively; see Chapter 2). At the state level, additional agencies are free to adopt more stringent regulations. Examples are the California Air Resources Board (CARB)<sup>23</sup> and the Texas Natural Resource Conservation Commission (TNRCC).<sup>24</sup>

Some states have even more local agencies such as California's SCAQMD<sup>25</sup> regulating the greater Los Angeles area, or the Bay Area Air Quality Management District (BAAQMD)<sup>26</sup> regulating the greater San Francisco area. The general trend is toward more stringent regulation. The large number of governing bodies shows the general public support for stricter pollution control at all levels of government.

## 15.4 Measurement Techniques

Accurate measurements of pollutants, such as NO and CO, from industrial sources are increasingly important in view of strict air-quality regulations. Based on such measurements, companies may have to pay significant fines, reduce production, install expensive flue-gas treatment systems, buy NO<sub>x</sub> credits in certain non-attainment areas, or change the production process to a less polluting technology. If compliance is achieved, however, the company may continue its processes without interruption and, if their emissions are below permitted limits, sell their NO<sub>x</sub> credits.

Numerous studies have been done and recommendations made on the best ways to sample hot gases from high temperature furnaces (see Chapter 14 and reference<sup>27</sup> for more details). For example, EPA Method 7E<sup>28</sup> applies to gas samples extracted from an exhaust stack that are analyzed with a chemiluminescent analyzer. A typical sampling system is shown in Figure 15.17. The major components are a heated sampling probe, heated filter, heated sample line, moisture removal system, pump, flow control valve, and then the analyzer. The EPA method states that the sample probe may be made of glass, stainless steel, or other equivalent materials. The probe should be heated to prevent water in the combustion products from condensing inside the probe. Mandel<sup>29</sup> notes that the equipment cost for the gas analysis system is relatively small compared to the maintenance and repair costs.

The effects of probe materials, such as metal and quartz, as well as the probe cooling requirements, have been investigated for sampling gases in combustion systems.<sup>30</sup> Several studies have found that both metal and quartz probe materials can significantly affect NO measurements in air/fuel combustion systems, especially under fuel-rich conditions with high CO concentrations.<sup>31,32</sup> However, the NO readings were not affected under fuel-lean conditions.

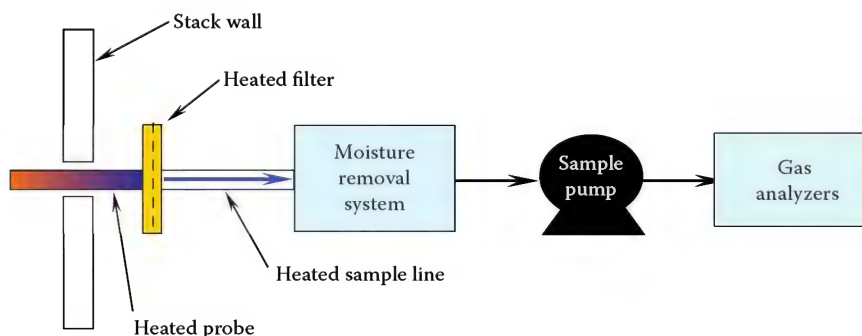


FIGURE 15.17

Sampling system schematic as recommended by the U.S. EPA.

## 15.5 Abatement Strategies

Before air quality regulations, flue gases from combustion processes were vented directly to the atmosphere. As air quality laws tightened and the public's awareness increased, industry began looking for new strategies to curb NOx emissions. The four general strategies for reducing NOx emissions are discussed next (see schematic in Figure 15.18).<sup>33</sup> Table 15.3 shows a summary of NOx control techniques developed for the U.S. EPA.<sup>34</sup> Table 15.4 shows typical NOx reduction efficiencies as functions of the burner draft type (natural or forced), fuel (distillate or residual oil), and reduction

technique.<sup>17</sup> The NOx emissions from gas-fired process heating equipment are highly variable (see Table 15.5).<sup>74</sup> Therefore, the technique(s) chosen to reduce NOx emissions are very site and equipment dependent. This section is not intended to be exhaustive, but is representative and includes many of the commonly used techniques for minimizing NOx emissions.

The U.S. EPA<sup>35</sup> published a compendium of NOx control technologies including those specifically for process heaters. Reese et al.<sup>36</sup> prepared a useful review of common NOx control technologies. Muzio and Quartucy<sup>37</sup> presented an interesting history of NOx control and have an extensive reference list. Tomita<sup>38</sup> has edited a compendium of NOx suppression techniques

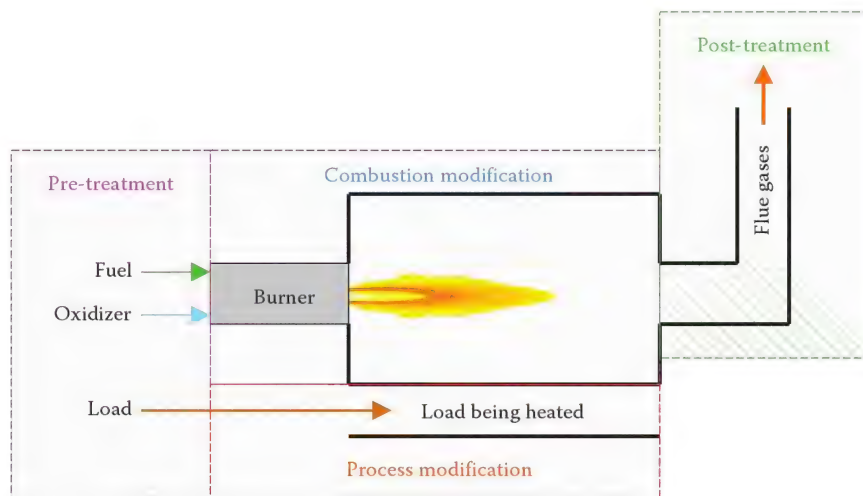


**FIGURE 15.18**  
Schematic of four general strategies for reducing NOx emissions.

**TABLE 15.3**

Summary of NOx Control Techniques

Technique	Principle of Operation	Status of Development	Limitations	Applications	
				Near-Term	Long-Term
Combustion modification	Suppress thermal NOx through reduced flame temperature, reduced O <sub>2</sub> level; suppress fuel NOx through delaying fuel/air mixing or reduced O <sub>2</sub> level in primary flame	Operational for point sources; pilot-scale and full-scale studies on combined modifications, operational problems, and advanced design concepts for area sources	Degree of control limited by operational problems	Retrofit utility, industrial boilers, gas turbines, improved designs, new utility boilers	Optimized design area, point sources
Flue gas–noncombustion tail gas treatment	Additional absorption of NOx to HNO <sub>3</sub> ; conversion of NOx to NH <sub>4</sub> NO <sub>3</sub> ; reduction of NOx to N <sub>2</sub> by catalytic treatment	Operational for existing and new nitric acid plants meeting NSPS; pilot scale feasibility studies for conventional combustion systems	New wet processes developing experience in applications; old catalytic processes have high costs, interference by fuel sulfur of metallic compounds	Noncombustion sources (nitric acid plants)	Possible supplement to combustion modifications; simultaneous SOx/NOx removal

Source: U.S. Environmental Protection Agency, Nitrogen oxide control for stationary combustion sources, U.S. EPA report EPA/625/5-86/020, 1986; U.S. EPA., Control techniques for nitrogen oxides emissions from stationary sources, EPA Report 450/1-78-001, U.S. Environmental Protection Agency, Washington, DC, 1978.

TABLE 15.4

Reduction Efficiencies for NO<sub>x</sub> Control Techniques

Draft and Fuel Type	Control Technique	Total Effective NO <sub>x</sub> Reduction Percent
ND, distillate	(ND) LNB	40
	(MD) LNB	43
	(ND) ULNB	76
	(MD) ULNB	74
	SNCR <sup>a</sup>	60
	(MD) SCR	75
	(MD) LNB + FGR	43
	(ND) LNB + SNCR	76
	(MD) LNB + SNCR	77
	(MD) LNB + SCR	86
ND, residual	(ND) LNB	27
	(MD) LNB	33
	(ND) ULNB	77
	(MD) ULNB	73
	SNCR	60
	(MD) SCR	75
	(MD) LNB + FGR	28
	(ND) LNB + SNCR	71
	(MD) LNB + SNCR	73
	(MD) LNB + SCR	83
MD, distillate	(MD) LNB	45
	(MD) ULNB	74
	(MD) SNCR	60
	(MD) SCR	75
	(MD) LNB + FGR	48
	(MD) LNB + SNCR	78
	(MD) LNB + SCR	92
MD, residual	(MD) LNB	37
	(MD) ULNB	73
	(MD) SNCR	60
	(MD) SCR	75
	(MD) LNB + FGR	34
	(MD) LNB + SNCR	75
	(MD) LNB + SCR	91

Source: Sanderford, E.B., Alternative control techniques document – NO<sub>x</sub> emissions from process heaters, U.S. Environmental Protection Agency report EPA-453/R-93-015, February, 1993.

Note: MD = mechanical draft; ND = natural draft; LNB = low NO<sub>x</sub> burner; ULNB = ultralow NO<sub>x</sub> burner; SNCR = selective non-catalytic reduction; SCR = selective catalytic reduction; FGR = flue gas recirculation.

<sup>a</sup> Reduction efficiencies for ND or MD SNCR are equal.

that is a useful reference. Adouane<sup>39</sup> has written a book on the subject of fuel-bound NO<sub>x</sub> from low calorific fuels. The U.S. EPA also has a site dedicated to nitrogen dioxide.<sup>40</sup>

### 15.5.1 Pretreatment

The first NO<sub>x</sub> reduction strategy is pretreatment, which is a preventative technique to minimize NO<sub>x</sub> generation.

TABLE 15.5

NO<sub>x</sub> Control Technologies in Process Heaters

Control Technology	Controlled Emissions	Percent Reduction
Low-NO <sub>x</sub> burners	0.1–0.3 lb/MMBtu	25–65
Staged air lances	Not available	35–51
Fiber burner	10–20 ppm	
Ammonia injection	Not available	43–70
Urea injection + low NO <sub>x</sub> burner	Not available	55–70
SCR	20–40 ppm	65–90
SCR + Low NO <sub>x</sub> burner	25–40 ppm	70–90

Source: Bluestein, J., NO<sub>x</sub> Controls for gas-fired industrial boilers and combustion equipment: A survey of current practices, Gas Research Institute, Chicago, IL, report GRI-92/0374, 1992.

Note: Uncontrolled emissions are in the range of 0.1–0.53 lb/MMBtu.

In pretreatment, the incoming feed materials (fuel, oxidizer, and/or the material being heated) are treated in such a way as to reduce NO<sub>x</sub>. Some of these treatments include fuel switching, using additives, fuel treatment, and oxidizer switching.

#### 15.5.1.1 Fuel Switching

Fuel switching is simply replacing a more polluting fuel with a less polluting fuel. For example, fuel oils generally contain some organically bound nitrogen that produces fuel NO<sub>x</sub>. NG does not normally contain any organically bound nitrogen and usually has low quantities of molecular nitrogen (N<sub>2</sub>). Partial or complete substitution of NG for fuel oil can significantly reduce NO<sub>x</sub> emissions by reducing fuel NO<sub>x</sub>. Figure 15.11 shows that CH<sub>4</sub> produces less NO<sub>x</sub> than H<sub>2</sub> because of the difference in flame temperatures. Fuels composed entirely of hydrogen can produce twice as much NO<sub>x</sub> as fuels with no hydrogen.<sup>41</sup> Fuel switching may or may not be an option depending on the availability of fuels and on the economics of switching to a different fuel.

#### 15.5.1.2 Additives

Another type of pretreatment involves adding a chemical to the incoming feed materials (raw materials, fuel, or oxidizer) to reduce emissions by changing the chemistry of the combustion process. One example would be injecting ammonia into the combustion air stream as a type of in situ de-NO<sub>x</sub> process (see Section 15.5.4.2). Several factors must be considered to determine the viability of this option. These include economics, the effects on the process, and the ease of blending chemicals into the process.

#### 15.5.1.3 Fuel Pretreatment

A third type of pretreatment involves treating the incoming fuel prior to its use in the combustion



process. An example would be removing fuel-bound nitrogen from fuel oil or removing molecular nitrogen ( $N_2$ ) from NG. The latter is generally not very effective because of the  $N_2$  in the combustion air. This technique is normally an expensive process depending on how much treatment must be done and how the fuel is treated. For example, it is generally more difficult to remove nitrogen from fuel oil than from NG. In Europe, some NG supplies have as much as 15%  $N_2$  by volume. If only a few percent  $N_2$  needs to be removed from that type of NG, this can be done relatively easily and inexpensively with adsorption or membrane separation techniques.

MacKenzie et al.<sup>42</sup> discuss the four common techniques for separating nitrogen from producer gas, particularly for improving the quality of fuel gases removed from naturally occurring NG reserves. These techniques include single high pressure column process, double column (high and low pressure) process, three column (high, intermediate, and low pressure) process, and two column (high and low pressure) process. Simulations were done to show the differences in power requirements among the four techniques as a function of the inlet nitrogen concentration.

#### 15.5.1.4 Oxidizer Switching

The fourth type of pretreatment is oxidizer switching, where a different oxidizer is used. Air is the most commonly used oxidizer. It can be shown that a substantial NOx reduction can be achieved by using pure oxygen, instead of air, for combustion.<sup>43</sup> For example, in the extreme case of combusting a fuel like  $CH_4$  with pure  $O_2$ , instead of air that contains 79%  $N_2$  by volume, it is possible to completely eliminate NOx as no  $N_2$  is present to produce NOx. For example, if  $H_2$  is combusted with pure  $O_2$ , the global reaction can be represented by



By drastically reducing the  $N_2$  content in the system, NOx is usually reduced. However, there are significant challenges to using high purity oxygen, instead of air, for combustion.<sup>44</sup> This technique has not been used widely in the hydrocarbon and petrochemical industries, but could become more popular in the future as the cost of oxygen continues to decline as less expensive methods for separating oxygen from air are developed.

### 15.5.2 Combustion Modification

The second general strategy for reducing NOx is known as combustion modification. Combustion modification

reduces NOx formation by changing the combustion process. Combustion modification methods are usually less capital intensive than most post-treatment methods. In many cases, there is a limit to how much NOx reduction can be achieved using these methods.

There are numerous methods that have been used to modify the combustion process for low NOx. A popular method is low NOx burner design where specially designed burners generate less NOx than previous burner technologies. Low NOx burners may incorporate a number of techniques for minimizing NOx including flue gas recirculation, staging, pulse combustion, and advanced mixing. Many of the more common combustion modification techniques are discussed next.

#### 15.5.2.1 Air Preheat Reduction

One combustion modification technique is reducing the combustion air preheat temperature. As shown in Figure 15.9, reducing the level of air preheat can significantly reduce NOx emissions. Reducing air preheat significantly reduces NOx for processes that use heat recuperation. However, air preheat reduction also reduces the overall system efficiency as shown in Figure 4.11. The loss of efficiency can be somewhat mitigated if the heater is equipped with a convection section. This is an easy strategy to implement and may be cost effective if the lost efficiency is more than offset by the cost of alternative NOx reduction techniques.

It is possible to achieve low NOx using high levels of air preheat using a specially designed combustion system that utilizes advanced mixing combined with intense internal flue gas recirculation and strict  $O_2$  control in the flame zone.<sup>45,46</sup> This technology reduces energy consumption because of a heat recovery system used to preheat the combustion air which is built into the high temperature air combustion (HiTAC) burner. Reducing energy consumption also indirectly reduces all pollution emissions because less fuel is consumed which means less pollution is produced.

#### 15.5.2.2 Low Excess Air

As shown in Figure 15.7, excess air causes NOx emissions to increase at excess air levels near stoichiometric conditions (0% excess air). Notice, however, that at higher excess air levels, NOx actually decreases. There are two primary reasons for this increase in NOx near low levels of excess air and then subsequent decrease at higher levels. The first concerns chemistry and the priority of reacting with available oxygen. Hydrogen is the most reactive element and reacts first with oxygen to form  $H_2O$ . Next, carbon reacts with oxygen. If there is enough

oxygen available and sufficient temperature and mixing, then the carbon and oxygen react to form  $\text{CO}_2$ . The least reactive element in the H–C–N mixture to react with any remaining oxygen is nitrogen. If there is not enough oxygen (fuel-rich or substoichiometric conditions) available to fully react with carbon, then significant amounts of CO are typically produced and very little NOx is generated. Some excess oxygen is required to react with the nitrogen to form NOx. The second reason for the increase in NOx near low levels of excess air (near stoichiometric conditions) is that the flame temperature (see Figure 4.6) is high under those conditions. The combination of available oxygen and high temperatures leads to high NOx. Most combustion systems are designed to operate near stoichiometric conditions, with low levels of excess air to maximize thermal efficiency (see Chapter 12). It is also desirable to operate with low levels of excess air to minimize NOx emissions as well. The lower limit on target excess air levels is usually CO generation where CO can spike up dramatically (sometimes called “CO breakthrough”) if there is insufficient  $\text{O}_2$ , mixing, and temperature (see Chapter 14). Since both NOx and CO typically need to be minimized, a system designed to minimize both will often be operated at the lowest possible excess  $\text{O}_2$  level without producing high levels of CO.

Excess air generally comes from two sources: the combustion air supplied to the burner and air infiltration into the heater. Excess air produced by either source is detrimental to NOx emissions. Excess air increases NOx formation by providing additional  $\text{N}_2$  and  $\text{O}_2$  that can combine in a high temperature reaction zone to form NO. In many cases, NOx can be reduced by simply reducing the excess air through the burners.

Air infiltration (see Chapter 12), sometimes referred to as “tramp air,” into a combustion system affects the excess air in the combustor and can affect NOx emissions. The quantity and location of the leakage are important. Small leaks far from the burners are not nearly as detrimental in terms of NOx emissions as large leaks near the flames. By reducing air infiltration (leakage) into the furnace, NOx can be reduced because excess  $\text{O}_2$  generally increases NOx at levels common in industrial combustion systems.<sup>47,48</sup>

Reducing excess air is also beneficial in helping increase thermal efficiency. Any unnecessary air absorbs heat that is carried out of the stack with the exhaust products.<sup>49</sup> However, there is a practical limit to the minimum target excess  $\text{O}_2$ . Since the mixing of the fuel and air in a diffusion flame burner is not perfect, some excess air is necessary to ensure both complete combustion of the fuel and minimization of CO emissions. The limit on reducing the excess air is CO emissions. If the excess  $\text{O}_2$  is reduced too much, then CO emissions will increase. CO is not only a pollutant, but it is also an

indication that the fuel is not being fully combusted, resulting in lower system efficiencies.

There are some special techniques that control the  $\text{O}_2$  in the flame to minimize NOx; one example is pulsed combustion (see Section 15.5.2.10). Pulsed combustion has been shown to reduce NOx because alternating very fuel rich and very fuel-lean combustion zones minimize NOx formation. The overall stoichiometry of the oxidizer and fuel is maintained by controlling the pulsations. Pulsed combustion has not been used in many industrial combustion processes at this time. This is due to some operational problems, especially the high frequency cycling of the switching valves that causes them to wear out more quickly.

### 15.5.2.3 Staging

Staged combustion is an effective technique for lowering NOx. Staging means that some of the fuel or oxidizer or both is added downstream of the main combustion zone. The fuel, oxidizer, or both may be staged into the flame. For example, there may be primary and secondary fuel inlets where a portion of the fuel is injected into the main flame zone and the balance of the fuel is injected downstream of that main flame zone. In fuel staging, some of the fuel is directed into the primary combustion zone while the balance is directed into secondary and even tertiary zones in some cases (see Figures 1.48 and 1.49). This makes the primary zone fuel lean, which is less conducive to NOx formation when compared to stoichiometric conditions. The excess  $\text{O}_2$  from the primary zone is then used to combust the fuel added in the secondary and sometimes even tertiary zones. While the overall stoichiometry may be the same as in a conventional burner, the peak flame temperature is much lower in the staged fuel case because the combustion process is staged over some distance while heat is simultaneously being released from the flame. The lower peak temperatures in the staged fuel flame help to reduce the NOx emissions. Then, fuel staging is effective for two reasons: (1) the peak flame temperatures are reduced which reduces NOx and (2) the fuel-rich chemistry in the primary flame zone also reduces NOx. Waibel et al.<sup>50</sup> have shown that fuel staging is one of the most cost effective methods for reducing NOx in process heaters. Figure 15.19 shows an example of a staged fuel burner.

In air staging, some of the combustion air is directed into the primary combustion zone while the balance is directed into secondary and even tertiary zones in some cases (see Figures 1.46 and 1.47). This makes the primary zone fuel rich, which is less conducive to NOx formation when compared to stoichiometric conditions. The unburned combustibles from the primary zone are then combusted in secondary and tertiary zones.

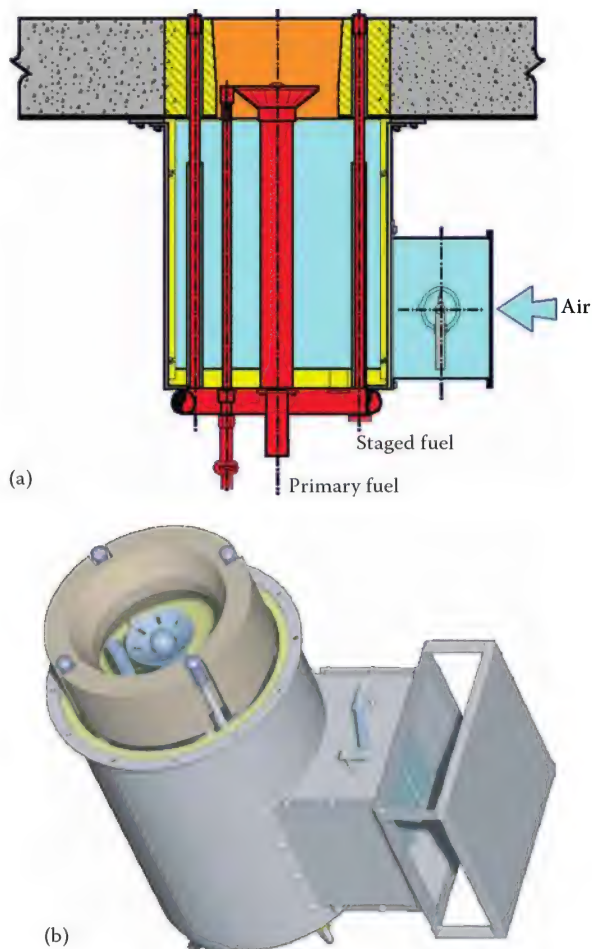


**FIGURE 15.19**  
Example of a staged fuel burner: (a) 2D cutaway drawing and (b) 3D drawing.

While the overall stoichiometry may be the same as in a conventional burner, the peak flame temperatures are much lower in the staged air case because the combustion process is staged over some distance while heat is simultaneously being released from the flame. The lower temperatures in the staged air flame help to reduce the NO<sub>x</sub> emissions. Figure 15.20 is an example of a staged air burner commonly used in down-fired hydrogen reformer furnaces.

#### 15.5.2.4 Gas Recirculation

Gas recirculation is a process that causes the products of combustion to be recirculated back into the flame. It may seem at first to be counterproductive to recirculate hot flue gases back into the flame since NO<sub>x</sub> increases with temperature. However, although the combustion products are hot, they are considerably cooler than the flame itself. The cooler furnace or flue gases act as a diluent, reducing the flame temperature, which in turn reduces NO<sub>x</sub> (see Figure 15.8). Advanced mixing techniques use carefully designed burner aerodynamics to control the mixing of the fuel and the oxidizer. The goals of this technique are to avoid hot spots and make the flame temperature uniform, to increase the heat release from the flame, which lowers the flame temperature, and to control the chemistry in the flame zone to minimize NO<sub>x</sub> formation.

There are two common ways to recirculate combustion exhaust products through a flame—furnace gas recirculation (FuGR) and flue gas recirculation (FGR). In FGR, exhaust gases are recirculated from the exhaust stack or flue back through the burner (Figure 1.39). This requires some type of fan or fuel eductor system to circulate the gases external to the furnace and back through the burner. The burner must be designed to handle both the added flow and elevated temperature of the recirculated

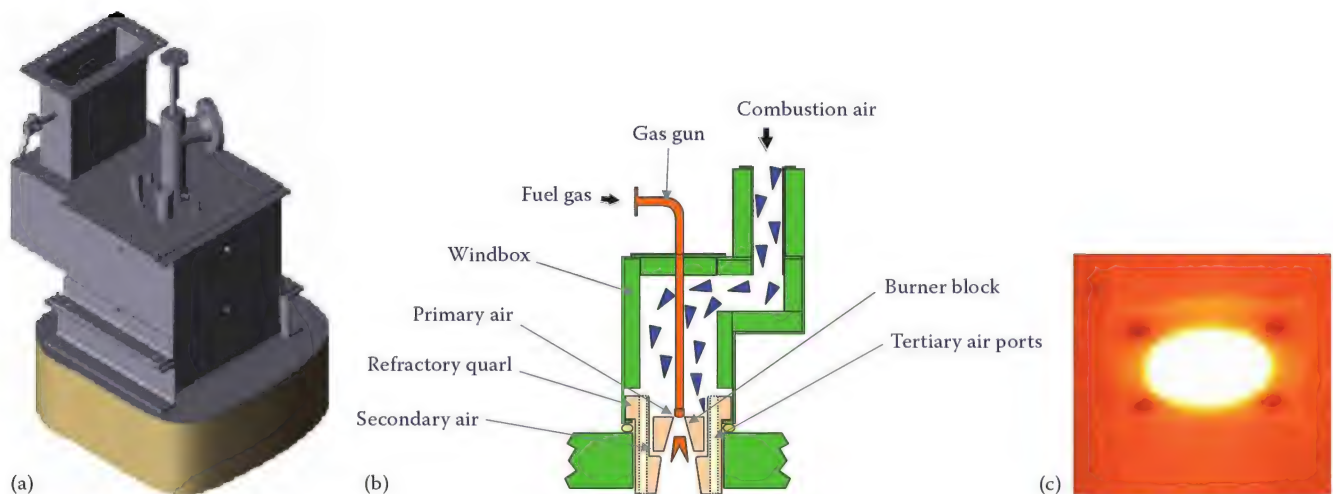


**FIGURE 15.20**  
Example of a staged air burner (Hamworthy DFR burner): (a) drawing, (b) schematic, and (c) photo of a burner in operation.



gases that are often partially or fully blended with the combustion air. Garg<sup>51</sup> estimates NO<sub>x</sub> reductions of up to 50% using FIGR.

In FuGR, the combustion products are recirculated inside the furnace back toward the burner and are inspirated into the flame to moderate its temperature (see Figure 15.21). Figure 15.22 is an example of a burner that uses FuGR to reduce NO<sub>x</sub> emissions. The Halo™ burner uses a specially shaped Coanda surface on the top of the tile to control the air–fuel mixing and to enhance furnace gas entrainment into the flame.<sup>52</sup> The unique design allows for more furnace gas entrainment compared to other burner designs, which cannot entrain as much furnace gas because of stability issues where the flame can become so diluted that the mixture is no longer flammable (see Chapters 3 and 4). The difference with the Halo burner design is that the furnace gases are not as uniformly mixed with the air and fuel so there is a region that is still flammable, despite higher levels of furnace gas entrainment.

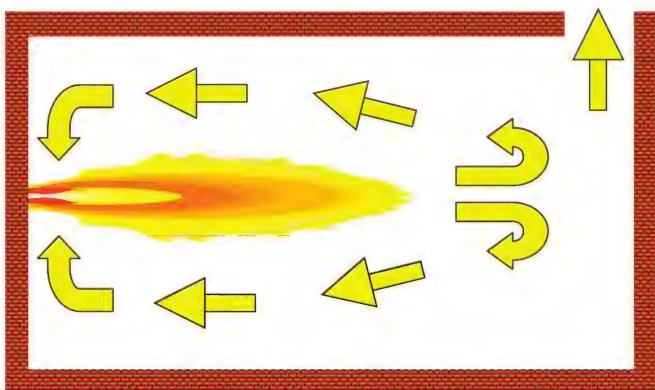


FIGURE 15.21  
Schematic of FuGR.

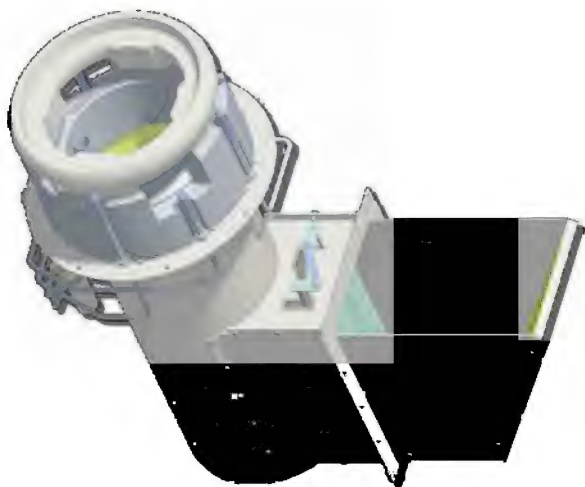


FIGURE 15.22  
Example of a burner incorporating FuGR (John Zink Halo™ burner).

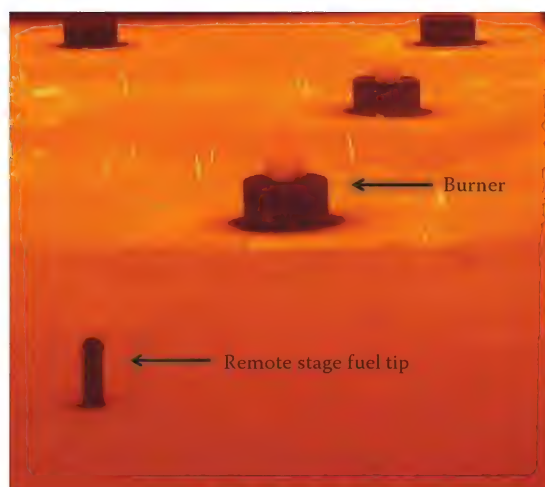


FIGURE 15.23  
Remote stage fuel tip.

Another method utilizing the FuGR technique is called remote stage fuel injection.<sup>53</sup> A remote staged furnace burner configuration includes placement of secondary fuel gas nozzles remote from the burners (see Figure 15.23). This configuration brings about an increased mixing of secondary fuel with furnace flue gases as illustrated in Figure 15.24. As a result, the temperature of the burning fuel gas is lowered reducing NO<sub>x</sub> emission and providing flameless combustion as shown in Figure 15.25.

There are some important advantages of FuGR as compared to FIGR. When using the FIGR technique, an additional hot fan may be needed to extract flue gases from the stack and deliver it to the burners. In some cases, if the flue gas temperatures are low enough, it may be possible to use the combustion air fan to pull both combustion air and flue gases and send them to the burners. This is commonly done in boiler burner applications where the flue gas temperature is generally fairly low. However, even if an additional fan is not needed, additional power is required to move the flue gases from the exhaust stack to the burners. Another potential disadvantage of using FIGR is that additional ductwork may need to be insulated. Finally, the physical size of the burner usually needs to be larger to accommodate the added flow of the recirculated flue gases. The burner components may also need to be modified to handle the higher flue gas temperatures.

#### 15.5.2.5 Ultralean Premix

A relatively new development in industrial burner technology for reducing NO<sub>x</sub> is called lean premix.<sup>54</sup> Lean premix involves running the primary part of the flame with as much air as possible and as little fuel as possible—that is, to make the air–fuel mixture as fuel lean as possible. This is not conducive to NO<sub>x</sub> emissions as

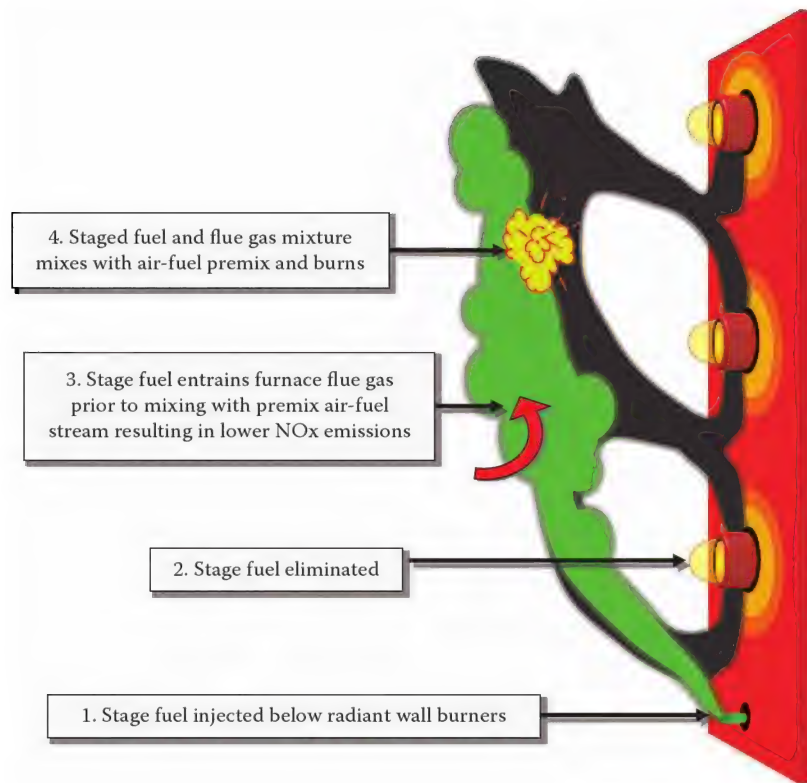


FIGURE 15.24

Illustration showing how the remote stage method provides lower NO<sub>x</sub> emissions.



(a)



(b)

FIGURE 15.25

Radiant wall burners firing (a) without remote staging, NO<sub>x</sub> = 24 ppmvd and (b) with remote staging, NO<sub>x</sub> = 16 ppmvd.

previously shown in Figure 15.7. The main challenge with operating the primary zone near the lean flammability limit is to maintain flame stability. Ren et al.<sup>55</sup> discuss the use of lean premix combined with methane reforming as an option to either preheating the fuel or adding expensive components like hydrogen or carbon monoxide to the fuel to increase stability. Both of those techniques add cost and complexity to the combustion system. As previously shown, the addition of hydrogen also increases flame temperatures and usually NO<sub>x</sub> emissions.

Lean premix technology utilizes the principle that air-fuel mixtures with significantly higher than stoichiometric levels of air (referred to as fuel lean) produce less NO<sub>x</sub> as shown in Figure 15.7. The primary reason this technique lowers the NO<sub>x</sub> emissions is because it lowers the flame temperatures as shown in Figure 4.6; as discussed earlier, lower flame temperatures can dramatically reduce NO<sub>x</sub>. This principle may seem to contradict the discussion in Section 15.5.2.2 where low or excess air levels are recommended to reduce NO<sub>x</sub>. Notice how NO<sub>x</sub> emissions peak in Figure 15.7 at slightly fuel-lean conditions and then steadily decline as the air-fuel mixture becomes leaner. The reason for this peak is the combination of available oxygen and high flame temperatures as previously discussed in Section 15.2.2. Although there is even more available oxygen at very lean conditions, the flame temperature is much lower

which produces less NO<sub>x</sub>. The air–fuel ratio for ultra-lean premix is typically limited to the lower flammability limit of the mixture. If the mixture is too lean, the flame can become unstable or even go out because there is not enough fuel to sustain combustion.

#### 15.5.2.6 Water Injection

Many of the combustion modification methods attempt to reduce the temperature of the flame to lower NO<sub>x</sub> emissions. In some cases, this may result in a reduction in combustion efficiency.<sup>56</sup> Another NO<sub>x</sub> reduction technique is to inject water into the flame. However, the water absorbs heat from the flame and carries some of that energy out with the exhaust gases, preventing the transfer of much of that energy to the load, so the efficiency is usually reduced.

Another form of water injection is to inject steam. There are several advantages to using steam as compared to liquid water. One advantage is that steam is much hotter than liquid water and includes the latent heat of vaporization needed to change the liquid water to a vapor. When liquid water is injected into a combustion process, it can put a large heat load on the process because liquid water can absorb a large amount of energy before vaporizing due to its high latent heat of vaporization. Steam puts a much smaller load on the process because it absorbs less energy than liquid water; therefore, it does not reduce the thermal efficiency as much as liquid water. Another reason for using steam instead of liquid water is that steam is already in vapor form and mixes readily with the combustion gases. Liquid water must be injected through nozzles to form a fine mist to disperse it uniformly into the combustion gases. Therefore, it is often easier to blend steam into the combustion products compared to liquid water. The advantage of water injection is that the water flow rate can be easily adjusted to get variable levels of NO<sub>x</sub> reduction. Fine-tuning is not generally as easy with some of the other NO<sub>x</sub> reduction methods.

#### 15.5.2.7 Reburning

Reburning is a technique similar to fuel staging, but uses a slightly different strategy. An example is methane reburn. The methane reburn technique injects some methane in the exhaust gas, usually well after the primary combustion zone, where the gases are at a lower temperature. As previously shown in Figure 15.7, fuel-rich conditions are not favorable to NO<sub>x</sub>. As the exhaust gases from the combustion process flow through this fuel rich reducing zone, NO<sub>x</sub> is reduced back to N<sub>2</sub> and O<sub>2</sub>. Any CO and other unburned fuels in the exhaust gases are then combusted downstream of the reburn zone at temperatures well below those found in the main

combustion process. These lower temperature reactions are less favorable to NO<sub>x</sub> formation so the net effect is that NO<sub>x</sub> is reduced. This is a type of nitrogen reformer.<sup>57</sup>

There are some challenges with this technique. One is to get proper injection of the reburning gas into the exhaust products. Another challenge is that the reburn zone must be capable of sustaining combustion. It is important that the gas be injected in a lower temperature region of the process in order to minimize NO<sub>x</sub> formation. For example, the gas may need to be injected in a previously uninsulated portion of ductwork that may have to be replaced with higher temperature materials and insulated. A third challenge is trying to take advantage of some of the energy produced during the reburning. In some cases, a heat recovery system may need to be added in order to increase the overall thermal system efficiency.

Dagaut et al.<sup>57</sup> have shown that the reburning fuel has some effect on NO<sub>x</sub> reduction. For the fuels considered, the ranking from lowest to highest NO<sub>x</sub> reduction was as follows: methane, NG, ethane, ethylene, and acetylene. Zamansky et al.<sup>58</sup> showed experimentally that adding nitrogen agents like ammonia, urea, and sodium salts into the flue gases with a delay time of 0.1–0.5 s after injection of the reburning fuel can enhance the reburning process. At that point in the process, the oxygen content in the flue gases has been depleted to the point that the injection of nitrogen agents does not promote NO generation. The enhanced NO reduction can be explained by the presence of additional active radicals that promote the reduction.

Miller et al.<sup>59</sup> experimentally demonstrated that fuel-lean reburning can reduce NO<sub>x</sub> emissions in exhaust gas streams. The application of reburning in field applications has often been restricted to overall fuel-rich or reducing conditions in the reburning zone. This research shows it is technically possible to utilize reburning for NO<sub>x</sub> reduction of up to 50% in fuel-lean (up to 6% O<sub>2</sub> in the flue gases) environments. Watts et al.<sup>60</sup> have written a brief review of the use of reburn technology to reduce NO<sub>x</sub> emissions in coal-fired boilers. Braun-Unkhoff et al.<sup>61</sup> compared experimental data on reburning technology applied on a large scale with numerical predictions. There is a good correlation between the measurements and predictions. Wendt<sup>62</sup> has shown that non-ideal mixing can enhance the effectiveness of reburning for diffusion flames.

#### 15.5.2.8 Burner Out-of-Service (BOOS)

This is a technique primarily used in boilers where the fuel is turned off to the upper burners, while maintaining the airflow.<sup>63</sup> The fuel removed from the upper burners is then redirected to the lower burners, while maintaining the same airflow to the lower burners. Therefore, the overall fuel and airflow to the boiler remains the same,



but is redistributed; this makes the lower burners fuel rich, which is less conducive to NO<sub>x</sub> formation due to the lower flame temperatures and fuel-rich chemistry. The upper burners, running on air only, provide the rest of the air needed to fully combust the fuel. Rather than air staging in individual burners, the BOOS technique stages air over the entire boiler. This technique is relatively inexpensive to implement. Ensuring proper heat distribution is important to prevent overheating the tubes or derating the firing capacity.

#### 15.5.2.9 Burner Spacing

The interaction between burners, especially low NO<sub>x</sub> burners, can increase NO<sub>x</sub> emissions. These burners are designed to have carefully controlled mixing, for example, fuel staging, to minimize the peak temperatures in the flame, which reduces NO. However, if the burners are spaced too closely together, the designed mixing is disturbed, which normally increases NO<sub>x</sub> emissions. This is a relatively new problem because of the advent of low NO<sub>x</sub> burners that produce less intense flames (softer flame) than many older-style burners. The reduced intensity makes the flames more susceptible to the gas flow patterns in a combustor; including the gas flow from adjacent burners.

There are two common options to mitigate the problem of flame interaction between burners: modify the burner design to accommodate the tight spacing or modify the spacing to accommodate the low NO<sub>x</sub> burners. Except in new furnace construction or in a major furnace rebuild, modifying the burner spacing is usually not the preferred option because of the high cost of modifying the furnace. However, modifying the burner design is also not necessarily an easy proposition either. If the flames are shortened, for example, by intensifying the mixing between the fuel and the combustion air, this normally increases NO<sub>x</sub> emissions. In some cases, it may be possible to modify the burners only where they come in close contact with adjacent burners. For example, one technique would be to reduce or eliminate fuel staging in the region between adjacent burners. If the burner has fuel nozzles around the perimeter, those closest to adjacent burners can be eliminated or have smaller outlet ports to reduce the fuel flow.

#### 15.5.2.10 Pulsed Combustion

Pulsed combustion is another technique that can be used to reduce NO<sub>x</sub> emissions (e.g., Ref. [64]), although it can also increase NO<sub>x</sub> under certain conditions (e.g., Ref. [65]). Pulsed combustion currently has only been used in a limited number of industrial combustion applications. Martins et al.<sup>66</sup> experimentally studied NO<sub>x</sub> emissions from a Rijke-type pulse combustor. While the system efficiency increased with pulse combustion compared

to non-pulse combustion, NO<sub>x</sub> emissions also increased. Kegasa<sup>67</sup> experimentally showed that forced oscillating combustion can reduce NO<sub>x</sub> emissions under certain circumstances of a particular oscillation frequency, phase difference between the fuel and the air, and duty ratio. Barham et al.<sup>68</sup> studied the effect of the flapper valve thickness on the operation of a pulsed combustor including pollutant emissions. The experimental results indicated that increasing the air/fuel ratio decreased NO<sub>x</sub> emissions and did not have a significant impact on the system thermal efficiency. CO emissions were minimized at a specific air/fuel ratio.

#### 15.5.2.11 Flameless Combustion

The so-called flameless combustion is where the flame is not visible to the naked human eye. There are several possible causes for an invisible flame. One is that the combustor is so hot that the radiation from the hot walls may overwhelm the viewer's eyes so that the flame cannot be seen. Using certain lenses, such as a cobalt lens, can usually reduce the background radiation enough so the flame can then be seen. Another example of when a flame may be invisible is when the fuel, for example hydrogen, burns very clearly. In a hydrogen production plant, operators sometimes walk around with straw brooms in front of them so that if there is a hydrogen fire they cannot see, the broom acts as a flame detector and will catch fire before the operator accidentally walks into the flame. It is important to use straw brooms because plastic brooms may put off an odor or toxic fumes, which can substantially increase the overall pollutant emissions in a plant. Small hydrogen flames can be particularly difficult to see outdoors on a bright sunny day. Hydrogen burns very clearly because there is no soot in the flame due to the complete absence of any carbon.

The flameless combustion of interest here does not refer to the two previous examples, but rather to a flame generated by a specially designed burner. It is not the lack of a visible flame itself that produces low NO<sub>x</sub>, but rather the carefully controlled mixing that produces a very uniform temperature flame. Flames from these burners are invisible to the naked eye even when the furnace is not very hot or when the fuel does not normally burn clearly with a conventional burner. Figure 15.26 shows an example of a flameless combustion system where the fuel is injected at one location and the oxidizer is injected at another location at some distance away from the fuel. The fuel and air mix and burn over a very large volume which tends to make much more homogeneous temperature distributions as compared to conventional burners; this can dramatically reduce the hot spots that promote NO<sub>x</sub> generation. The more uniform temperatures usually lead to invisible flames and low NO<sub>x</sub> emissions. However, combustion systems usually cannot be operated in the

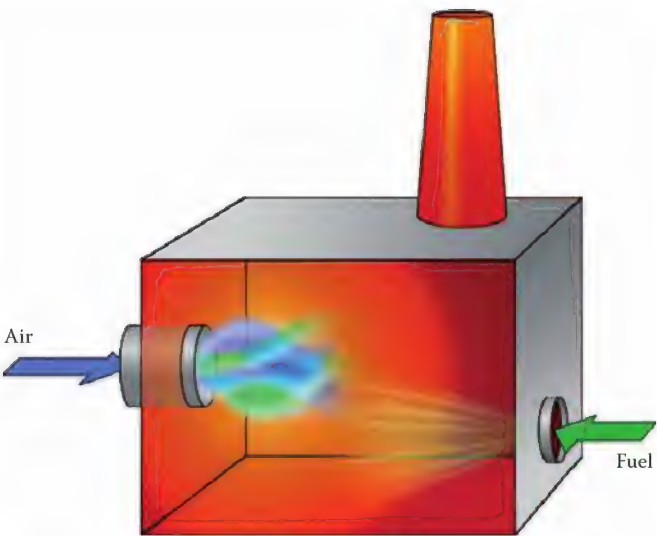


FIGURE 15.26  
Flameless combustion system.

flameless mode until the combustor is above the autoignition temperature of the air/fuel mixture; otherwise, the flames could become unstable increasing the potential for an incident. Conventional burners are often used to heat the flameless system above the autoignition temperature; once above the autoignition temperature, the system is switched into flameless mode.

One of the challenges of this technology is detecting the “flame.” Conventional flame detectors such as flame rods or flame scanners often have trouble getting a strong enough signal when the system is in the flameless mode. Thermocouples can be used, but they do not react as quickly as flame rods and flame scanners. Because of the significant safety concerns of this technology, it has not been a popular technique to the present time, but may become more important in the future when some of the operational issues are sufficiently resolved.

There are variations of flameless combustion. Figure 15.27 shows an example of a burner that has the



FIGURE 15.27  
TANGENT™ technology low NOx thermal oxidizer burner.

capability of producing invisible flames and very low NOx in thermal oxidizers. In this design, the fuel and air both flow through a common burner, which can be operated in multiple modes: conventional burner or a flameless burner. The advantage is that the same burner can be used to heat the combustor before switching to flameless mode. This technology has been demonstrated to produce NOx levels close to zero and is a very promising option for the future.

15.5.2.12 Low NOx Burners

Garg<sup>69</sup> discussed the use of low NOx burners to achieve emission reductions compared to standard gas burners. Table 15.6 shows typical NOx reductions using various low NOx burner techniques. An EPA study found that ultralow NOx burners were the most cost-effective means to reduce NOx.<sup>17</sup>

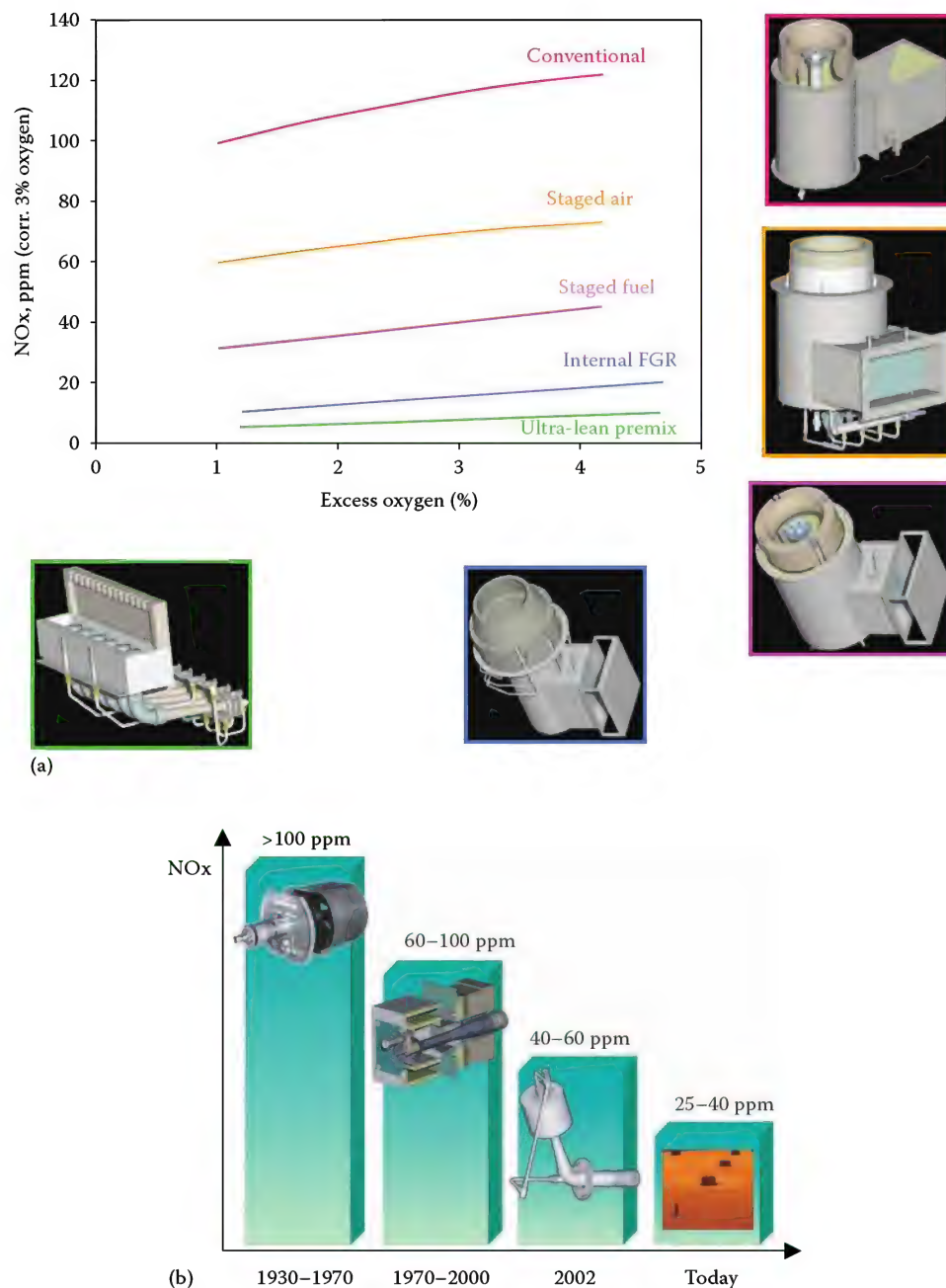
Low NOx burners incorporate some of the techniques discussed in this section such as air and fuel staging, FuGR, and ultralean premix. “Low NOx” is a relative term because there is no agreed-upon definition of exactly what “low” means, such as a specific value of NOx emissions. A low NOx burner for one manufacturer might be an ultralow NOx burner for another.

Figure 15.28a shows a graph of the history of low NOx burner development for round flame process burners since the passage of the Clean Air Act Amendment in the United States in 1970. Going from top to bottom, the curves are for increasingly more modern technologies with the oldest at the top and most modern at the bottom. The graph shows two things: NOx emissions have significantly decreased with each new generation of technology and NOx emissions increase with excess air level for the range given (see Section 15.5.2.2). Today’s lowest NOx burners can be in the single digits for NOx depending on the operating conditions such as fuel composition and combustor temperature. Figure 15.28b shows a similar graph, but for radiant wall burners. Radiant wall burners are commonly used in cracking furnaces. These furnaces

TABLE 15.6  
NOx Reductions for Different Low-NOx Burner Types

Burner Type	Typical NOx Reductions (%)
Staged-air burner	25–35
Staged-fuel burner	40–50
Low-excess-air burner	20–25
Burner with external flue gas recirculation (FGR)	50–60
Burner with internal flue gas recirculation	40–50
Air or fuel-gas staging with internal FGR	55–75
Air or fuel-gas staging with external FGR	60–80

Source: Garg, A., Specify better low-NOx burners for furnaces, *Chem. Eng. Prog.*, 90(1), 46, 1994.

**FIGURE 15.28**

History of low NO<sub>x</sub> burner development for (a) round flame burners and (b) radiant wall burners, firing on gaseous fuels.

are generally hotter than process heaters, which means the NO<sub>x</sub> levels are typically higher due to the higher temperatures compared to round flame burners; all other things being the same. These graphs are only representative. One could expect that new technologies will add additional and even lower curves in the future since the downward trend of lower NO<sub>x</sub> is evident.

An example of a low NO<sub>x</sub> burner is the COOLstar™ burner (Figure 15.29).<sup>70</sup> This design solves some of the previous issues associated with low NO<sub>x</sub> burners. It is

easier to retrofit in existing heaters because of its compact size, which reduces some of the burner-to-burner interaction issues with previous designs. It produces shorter flames and has a higher turndown ratio as compared to many other low NO<sub>x</sub> burners. One of the unique aspects of this patented burner<sup>71</sup> is the folded flame pattern that produces a shorter flame length compared to other low NO<sub>x</sub> burners. This is produced primarily by the combination of the burner tile shape and the fuel injection pattern. A variety of NO<sub>x</sub> reduction



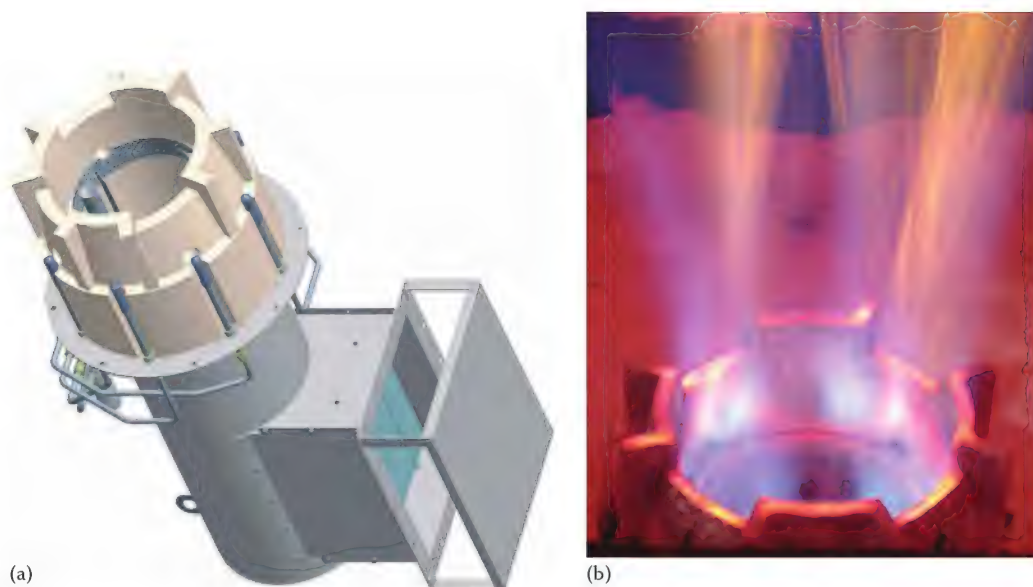


**FIGURE 15.29**  
COOLstar burner: (a) drawing and (b) photograph.

techniques have been used in the burner design including fuel gas staging, internal flue gas recirculation, and advanced mixing concepts. The burner was developed through a combination of computational fluid dynamics (CFD) modeling<sup>72</sup> (see Chapter 13) and experimentation. Figure 15.30 shows how CFD was used to identify problems with the initial design and to show the improved design. Subsequent field testing validated the design.

### 15.5.3 Process Modification

There are a number of techniques that may be employed to change the existing process in such a way as to reduce NO<sub>x</sub> emissions. These methods are often more extreme and expensive and are usually not used except under somewhat unique circumstances. These methods must be analyzed on a case-by-case basis to verify if they are viable.

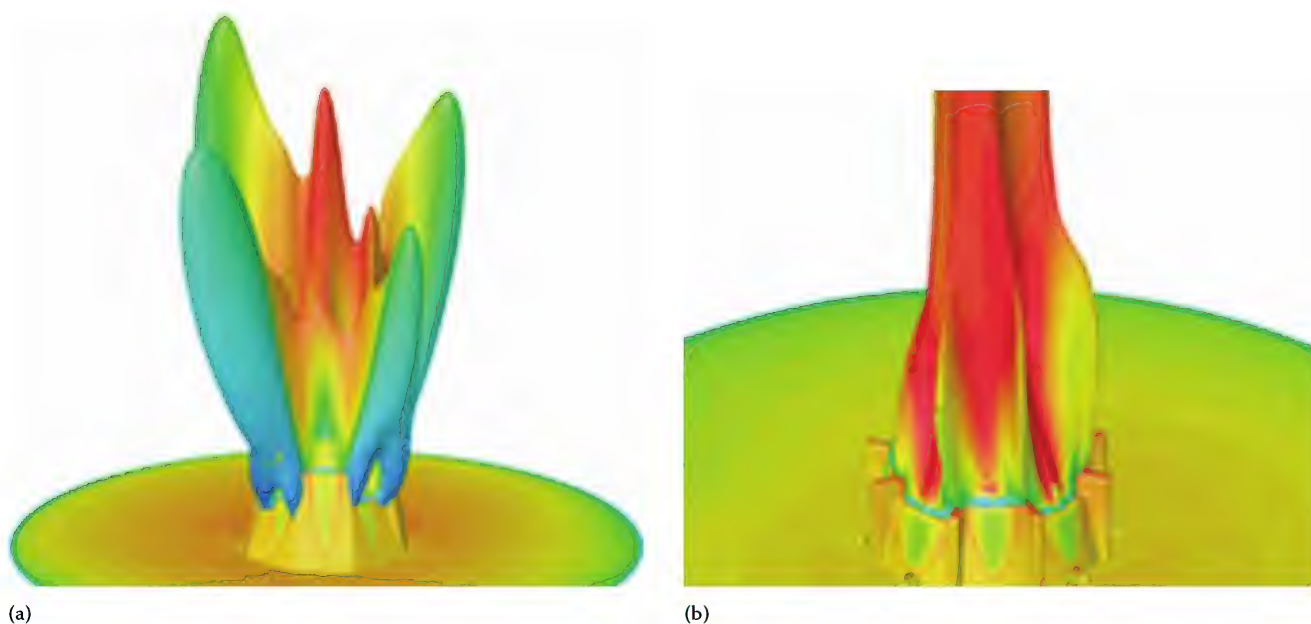


**FIGURE 15.30**  
Computational fluid dynamic modeling of the COOLstar burner: (a) initial design and (b) revised design. (From Chung, I.-P. et al., *Hydrocarbon Engineering*, 10(8), 77, 2005.)

### 15.5.3.1 Reduced Production

If the total mass of NO<sub>x</sub> emitted from a plant is too high, an alternative is to reduce the firing rate, which means a corresponding reduction in production. The reduction in NO<sub>x</sub> is proportional to the reduction in firing rate; that is, the less fuel burned, the less NO<sub>x</sub> formed. Obviously, this is generally not a preferred alternative because reduced production means reduced revenue. However, depending on the costs to reduce NO<sub>x</sub>, this could be the most economical alternative.

In boilers, reducing the firing rate reduces the overall temperature inside the boiler, which reduces the thermal NO<sub>x</sub> formation.<sup>73</sup> This technique is known as *derating* and is not desirable if the boiler is capacity limited, but in certain situations it may be a viable alternative.

### 15.5.3.2 Electrical Heating

One process modification that is sometimes used to minimize or eliminate NO<sub>x</sub> emissions is to replace some or all of the fossil-fuel-fired energy with electrical energy. The electrical energy produces no NO<sub>x</sub> emissions at the point of use and moves the emissions to the power plant. In general, the resulting NO<sub>x</sub> emissions at the power plant are often lower than at an industrial site because of the strict limits imposed on the power plant and the various methods employed to minimize NO<sub>x</sub> which are often more cost effective on a unit mass basis because of the economies of scale.

There are a number of potential problems with this method. The first is that the economics are usually very unfavorable when replacing fossil fuels with electrical energy. In most hydrocarbon and petrochemical processes, the fuel used in the heaters is a by-product that is available at little or no cost. Electrical energy is often much more expensive than even purchased fossil fuels like NG or oil. Besides the higher operating costs, there would be substantial capital costs involved in converting some or all of the existing fossil energy heating to electricity. In addition to the removal of the existing burners, there would be a cost for the new electrical heaters and often large costs of installing electrical substations that may be required for all of the additional power. In many locations, large additional sources of electricity are not readily available, so a new source of electricity may need to be built at the plant, such as a cogeneration facility. However, although the electrical costs may be reduced in that scenario because the transmission losses are much lower, the NO<sub>x</sub> emissions are now at a different location at the plant site and little may then be gained in

reducing overall NO<sub>x</sub> emissions for the plant. It is possible, in the future, that government regulators may consider the net NO<sub>x</sub> generated during the production of a product and could include the NO<sub>x</sub> formed in the generation of electricity. This would make replacement of fossil energy with electricity less attractive as most of the power generated in the United States is by fossil-fuel-fired power plants.

### 15.5.3.3 Improved Thermal Efficiency

By making a heating process more efficient, less fuel needs to be burned for a given unit of production (see Chapter 12). Since the firing rate is directly proportional to the NO<sub>x</sub> emissions, less fuel used equals less NO<sub>x</sub> produced. There are many ways to improve the efficiency of a process. A few representative examples will be given. One way is to repair the refractory to reduce air infiltration leaks on an existing heater.<sup>49</sup> This is often relatively inexpensive and saves fuel while reducing NO<sub>x</sub>. Another way is to add heat recovery to the heating process that does not have it currently. The heat recovery could be in several forms. One method is to preheat the incoming combustion air. As discussed in Section 15.5.2.1, this can increase NO<sub>x</sub> emissions due to the higher flame temperatures if it is not done properly. Another method is to add a convection section onto a heater that does not presently have one; this has other operational benefits as well and is often a good choice. A more drastic method of increasing the thermal efficiency of a heating process is to replace an old heater with a new, more modern design. This may make sense if the existing heater is very old, is high maintenance, and is not easily repairable or upgradeable. In that scenario, the payback may be fast enough to justify replacing the old leaky heater.

### 15.5.3.4 Product Switching

Another radical process modification that can reduce NO<sub>x</sub> is to switch the product being made to one that requires less energy to produce. In a process heater, this would involve replacing the existing process fluid with one that requires less energy to heat. For example, heavier crude oils require more energy to process than lighter, purer crudes so less energy would be needed to process purer crudes. Less energy consumption means less NO<sub>x</sub> generated. However, this is usually not an option and is only considered under extreme circumstances. In the earlier-given example, purer or "sweeter" crudes are much more expensive raw materials than less pure or more "sour" crudes. Therefore, the savings in energy and the NO<sub>x</sub> reduction may be more than offset by the higher raw material costs.

### 15.5.4 Post-Treatment

The fourth strategy for minimizing NO<sub>x</sub> is known as post-treatment. Post-treatment removes NO<sub>x</sub> from the exhaust gases after the NO<sub>x</sub> has already been formed in the combustion chamber. SO<sub>x</sub> emissions are typically removed by reaction with a reagent like lime (CaO) to form particles that can be scrubbed out of the exhaust gas stream. However, there is no comparable inexpensive reagent and scrubbing system for NO<sub>x</sub>. Another problem is that the reaction of NO<sub>2</sub> with water to form nitric acid is much slower than the comparable reactions for SO<sub>x</sub>. The reaction is too slow to go to completion under normal conditions in the short time NO<sub>x</sub> is in the treatment equipment. Therefore, a variety of other techniques are used to remove NO<sub>x</sub> from exhaust gas streams. The general strategy is to use a reducing agent, such as CO, CH<sub>4</sub>, other hydrocarbons, or ammonia, to remove the oxygen from the NO and convert it into N<sub>2</sub> and O<sub>2</sub>. Often some type of catalyst is required for the reactions.

Two of the most common methods of post-treatment are selective catalytic reduction (SCR) and selective non-catalytic reduction (SNCR).<sup>74</sup> Wet techniques for post-treatment include oxidation–absorption, oxidation–absorption–reduction, absorption–oxidation, and absorption–reduction. Dry techniques for post-treatment, besides SCR and SNCR, include activated carbon beds, electron beam radiation, and reaction with hydrocarbons. One of the advantages of post-treatment methods is that multiple exhaust streams can be treated simultaneously, thus achieving economies of scale. Most of the post-treatment methods are relatively simple to retrofit to existing processes.

Many of these techniques are fairly sophisticated and are not trivial to operate and maintain in industrial furnace environments. For example, the catalytic reduction techniques require a catalyst that may become plugged or poisoned fairly quickly by dirty flue gases. Post-treatment methods are often capital intensive. They usually require stopping production if there is a malfunction of the treatment equipment. In addition, post-treatment does not normally benefit the combustion process in any way. For example, it does not increase production or energy efficiency, so it is strictly an additional cost. Some trade organizations like the American Petroleum Institute have issued recommended practices for post-combustion NO<sub>x</sub> control for fired equipment.<sup>75</sup>

#### 15.5.4.1 Selective Catalytic Reduction

SCR (see Volume 3, Chapter 8) involves injecting an NO<sub>x</sub>-reducing chemical into an exhaust stream in the presence of a catalyst within a specific temperature window. This

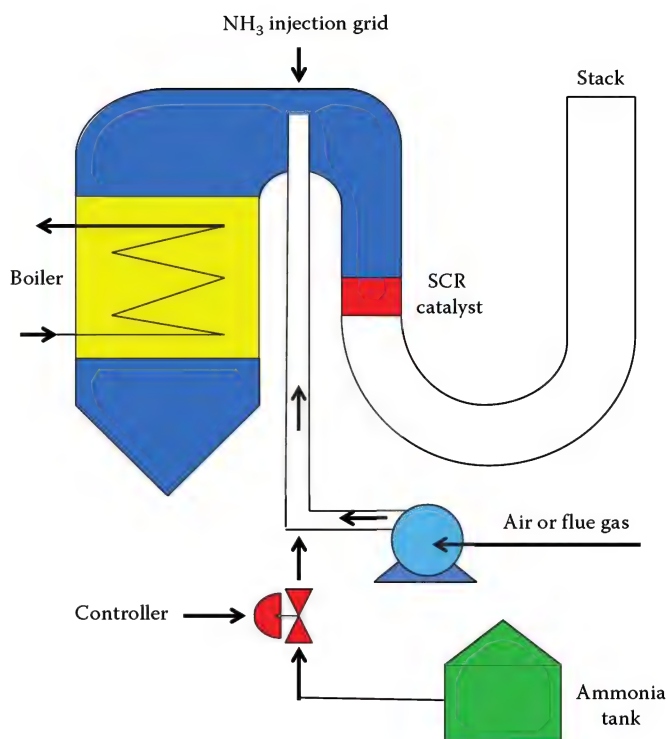


FIGURE 15.31

Schematic of the selective catalytic reduction process. (Adapted from Chuang, K.T. and Sanger, A.R., 5.20 Gaseous emission control: Physical and chemical separation, in *Environmental Engineers' Handbook*, 2nd edn., Eds. D.H.F. Liu, B.G. Lipták, Lewis Publishers, Boca Raton, FL, 1997.)

process, applied to a boiler, is shown in Figure 15.31.<sup>76</sup> The chemical is typically ammonia and the temperature window is approximately 500°F–1100°F (230°C–600°C). Figure 15.32 shows how the gas temperature affects the NO<sub>x</sub> removal efficiency for an SCR process. The NO<sub>x</sub>

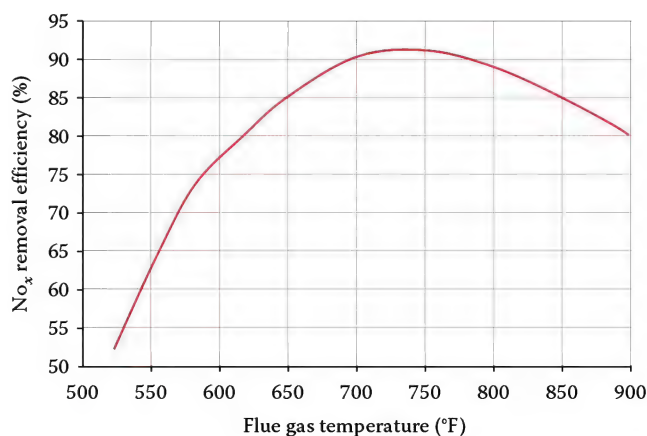
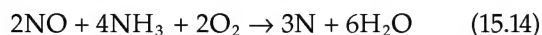
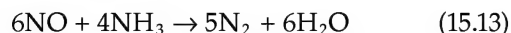


FIGURE 15.32

NO<sub>x</sub> removal efficiency versus temperature for SCR. (Adapted from Mussatti, D.C. et al., Section 4.2: NO<sub>x</sub> post-combustion, Selective catalytic reduction, Chapter 2 in *Air Pollution Control Cost Manual*, 6th edn., Ed. D.C. Mussatti, Report EPA/452/B-02-001, U.S. Environmental Protection Agency, Washington, DC, January 2002.)



and NH<sub>3</sub> react on the catalyst surface to form N<sub>2</sub> and H<sub>2</sub>O. The major reactions are



The ammonia may be in the form of anhydrous ammonia, which is nearly 100% pure ammonia or mixed with water, where the ammonia concentration is typically in the range of 20%–30%. SCR using ammonia as the reductant or reagent typically uses one of three types of catalysts: noble metal, base metal, and zeolites.<sup>77</sup> A common catalyst configuration used in SCR processes is shown in Figure 15.33.<sup>78</sup> The noble metals are normally wash coated onto an inert ceramic or metal monolith. These are used to treat particle-free, low sulfur exhausts. Base metal catalysts are either wash coated or extruded into honeycombs and are only used in particle-free exhausts. Zeolites may be wash coated or extruded into honeycombs and can function at higher temperatures (650°F–940°F or 343°C–504°C). The most commonly used commercial SCR catalyst is vanadia supported on a high surface area anatase titania. Heck and Farrauto<sup>79</sup> recommend the following catalysts depending upon the temperature range:

- Low temperature (175°C–250°C or 350°F–480°F): platinum
- Medium temperature (300°C–450°C or 570°F–840°F): vanadium
- High temperature (350°C–600°C or 660°F–1100°F): zeolite

An overall schematic of SCR is shown in Figure 15.34. The U.S. EPA has prepared a helpful manual for estimating the cost of air pollution control using various techniques, which includes a chapter on SCR for NO<sub>x</sub> control.<sup>80</sup>

There are a number of potential problems and challenges with SCR techniques. The catalyst introduces a pressure drop into the system, which often increases the power requirements for the gas handling equipment. The catalyst may become plugged or fouled in dirty exhaust streams, which is especially a challenge when firing liquid fuels like residual oil. The catalyst may also become poisoned or deactivated under certain conditions.<sup>81</sup> The ammonia must be properly injected into the flue gases to achieve proper mixing, must be injected at the right location to be in the proper temperature window, and must be injected in the proper amount to obtain adequate NO<sub>x</sub> reduction without allowing an excessive amount of ammonia to slip through unreacted. Using poor quality ammonia, usually caused by inadequate quality of the water mixed with the ammonia, can lead to mineral deposit buildup on handling and vaporization equipment.<sup>82</sup> The presence of certain chemicals in certain concentrations can significantly affect the performance of an SCR.<sup>83</sup> SCR systems are not very tolerant of constantly changing conditions as a stable window of operation is required for optimum efficiency. Another problem is handling the spent catalyst. Figure 15.35 shows how the activity of the catalyst declines over time. Regeneration is often the most attractive option, but may be more expensive than buying new catalyst. Disposal of the spent catalyst may be expensive as it may be classified as a hazardous waste, especially if the catalyst contains vanadium as is commonly the case. An EPA study found that SCR was the most expensive means to reduce NO<sub>x</sub>.<sup>17</sup> SCR systems are capital intensive, have high operating costs, and require significant amounts of space in the plant that is often difficult to find.

Research continues on finding new combinations of chemicals, catalysts, and catalyst supports for economically reducing NO<sub>x</sub>. For example, research is looking at NO<sub>x</sub> reduction methods using ammonia with both supported

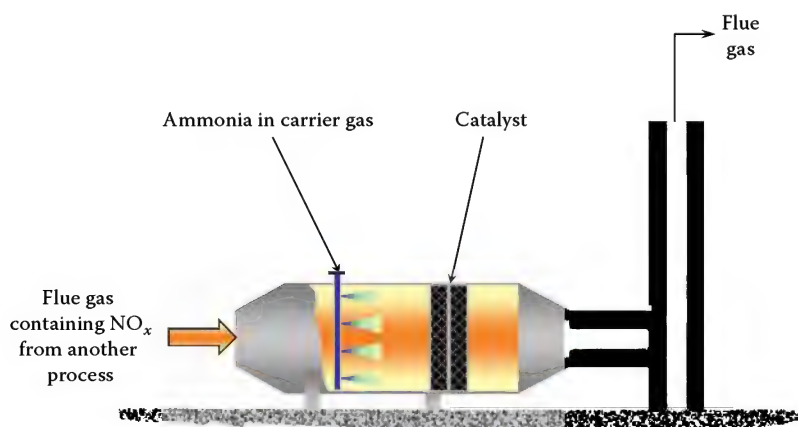


FIGURE 15.33

Common catalyst configuration used in SCR systems. (From Melton, P. and Graham, K., Thermal oxidizers, Chapter 21 in *The John Zink-Hamworthy Combustion Handbook*, CRC Press, Boca Raton, FL, 2001.)

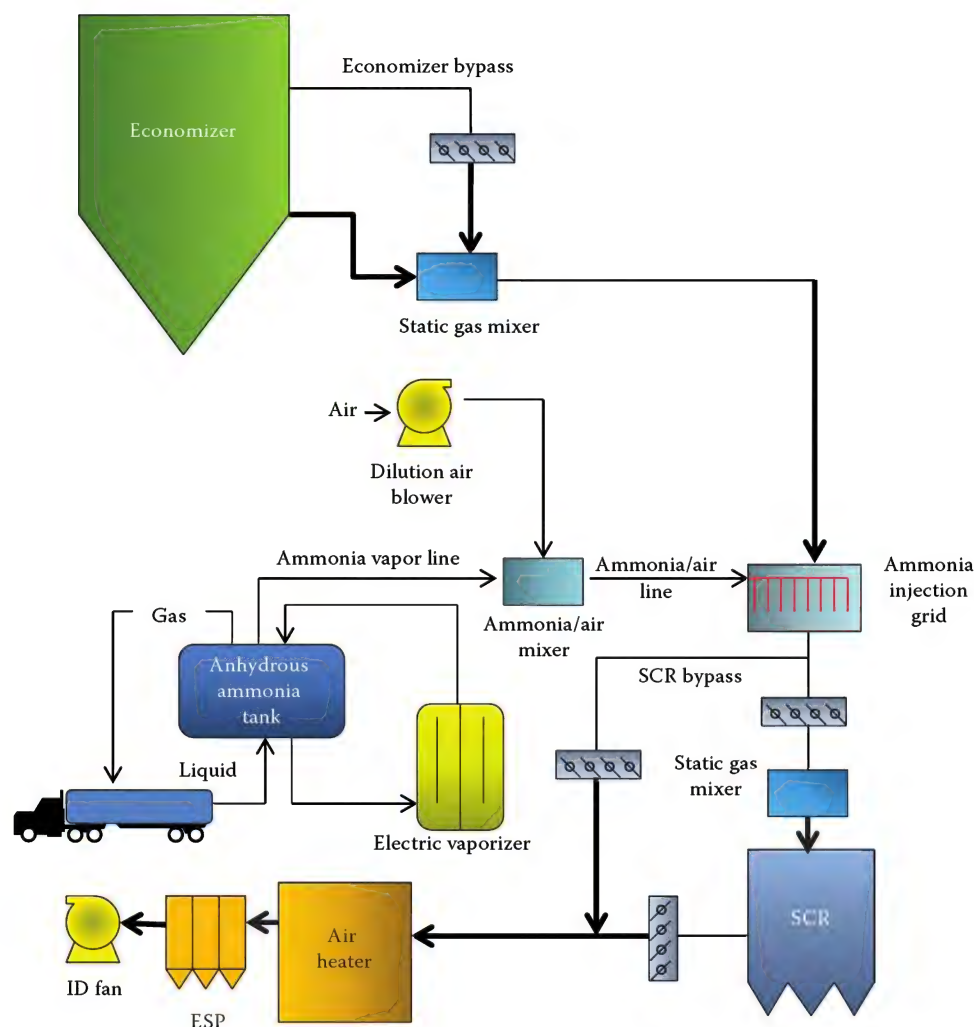


FIGURE 15.34

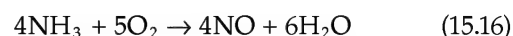
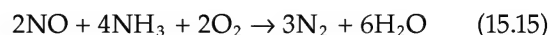
SCR process flow diagram. (Adapted from Mussatti, D.C. et al., Section 4.2: NO<sub>x</sub> post-combustion, Selective catalytic reduction, Chapter 2 in *Air Pollution Control Cost Manual*, 6th edn., Ed. D.C. Mussatti, Report EPA/452/B-02-001, U.S. Environmental Protection Agency, Washington, DC, January 2002.)

and unsupported vanadia catalysts.<sup>84</sup> Ozkan et al.<sup>85</sup> have edited a book that includes a wide range of research in the general area of SCR. Aerogels of titania, silica, and vanadia are being investigated for use in SCR processes.<sup>86</sup>

Laplante and Lindenhoff<sup>87</sup> discuss the use of SCRs in refineries to meet the increasingly more stringent NO<sub>x</sub> regulations. Reductions of up to 95% are possible. According to the authors, this may be the only currently available technology to achieve single digit NO<sub>x</sub> performance. The NO<sub>x</sub> catalyst is made of fiber-reinforced titanium oxide carrier that is impregnated with vanadium oxide and tungsten oxide on the catalyst surface. The catalyst is assembled into modules for ease of handling and installation.

from a combustion process within a specific temperature window. No catalyst is involved in the process, which is one advantage over SCR. The most commonly used chemicals are ammonia and urea. Other chemicals like hydrogen, hydrogen peroxide, and methanol may be added to improve the performance and lower the minimum threshold temperature.

The Exxon thermal DeNO<sub>x</sub><sup>TM</sup> process<sup>88,89</sup> is one common SNCR technique using ammonia that is employed in a wide variety of industrial applications. The following reactions show how NO<sub>x</sub> is reduced to N<sub>2</sub> using this technique:



#### 15.5.4.2 Selective Non-Catalytic Reduction

SNCR (Figure 15.36) involves injecting NO<sub>x</sub>-reducing chemicals, such as ammonia, into the exhaust products

The optimum temperature window, without the addition of other chemicals to increase the temperature

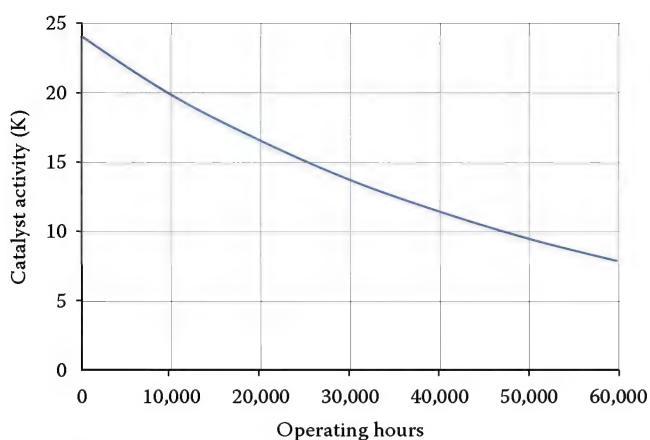
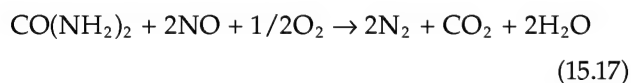


FIGURE 15.35

Typical catalyst deactivation for an SCR as a function of operating time. (Adapted from Adapted from Mussatti, D.C. et al., Section 4.2: NO<sub>x</sub> post-combustion, Selective catalytic reduction, Chapter 2 in *Air Pollution Control Cost Manual*, 6th edn., Ed. D.C. Mussatti, Report EPA/452/B-02-001, U.S. Environmental Protection Agency, Washington, DC, January 2002.)

window, is 1600°F–2200°F (870°C–1200°C). The effect of temperature on NO<sub>x</sub> reduction performance is shown in Figure 15.37.<sup>90</sup>

The Nalco Fuel Tech NO<sub>x</sub>OUT<sup>®</sup> process, originally patented by the Electric Power Research Institute (EPRI),<sup>91</sup> is a common SNCR technique employing urea:



The optimum temperature window, without the addition of other chemicals to increase the temperature window, is 1600°F–2000°F (870°C–1100°C). At higher temperatures, the reagent (e.g., ammonia or urea) can

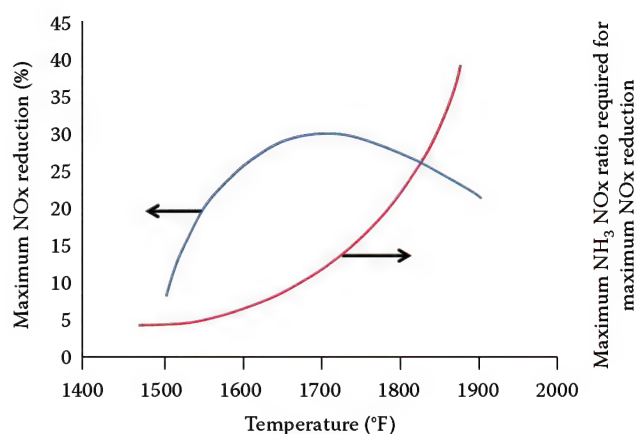


FIGURE 15.37

SNCR temperature window. (Adapted from Schnelle, K.B. and Brown, C.A., *Air Pollution Control Technology Handbook*, CRC Press, Boca Raton, FL, 2002.)

actually oxidize and make NO, which is both counter-productive and wastes reagent. Rota et al.<sup>92</sup> experimentally and numerically studied the NO<sub>x</sub>OUT process in the temperature range from 950 to 1450 K (1250°F–2150°F) using a laboratory reactor. The experiments showed that the process is very effective in a narrow temperature window of 1250–1300 K (1800°F–1900°F). The nitrogen in the reducing agent and the O<sub>2</sub> concentration in the gas being treated are also important parameters in the removal process. For the conditions studied, the CO/NO ratio did not significantly affect the removal efficiency.

Besides the temperature operating window, residence time is another important factor for optimum performance. Sufficient reaction time can effectively broaden the operating window.<sup>93</sup> Figure 15.38 shows how increasing the residence time from 100 to 500 ms (milliseconds) greatly expands the operating window and improves

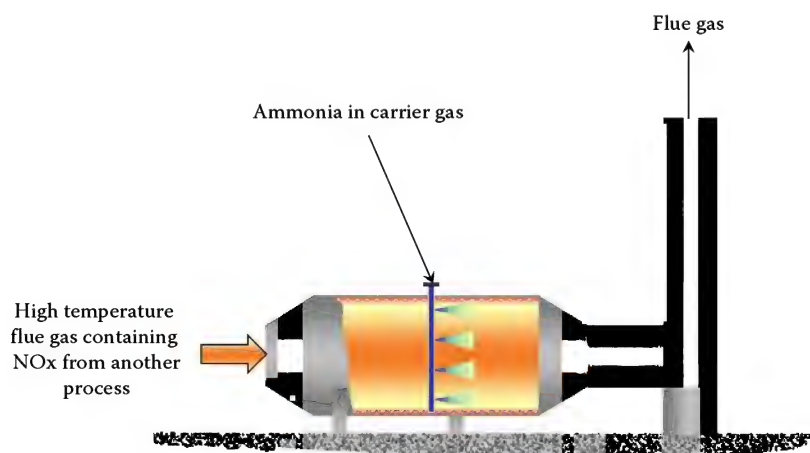


FIGURE 15.36

Selective non-catalytic reduction system. (From Melton, P. and Graham, K., Thermal oxidizers, Chapter 21 in *The John Zink Combustion Handbook*, CRC Press, Boca Raton, FL, 2001.)



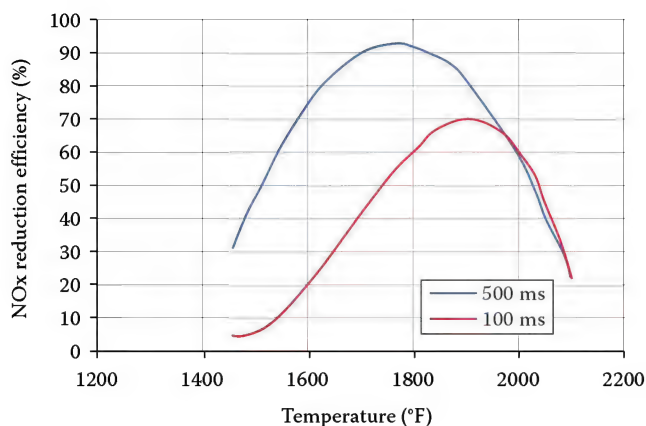


FIGURE 15.38

Effect of residence time on SNCR NO<sub>x</sub> reduction efficiency. (Adapted from Mussatti, D.C., et al., Section 4.2: NO<sub>x</sub> post-combustion, Selective noncatalytic reduction, Chapter 1 in *Air Pollution Control Cost Manual*, 6th edn., Ed. D.C. Mussatti, Report EPA/452/B-02-001, U.S. Environmental Protection Agency, Washington, DC, January 2002.)

the NO<sub>x</sub> reduction efficiency.<sup>94</sup> Mixing is also an important factor for maximizing NO<sub>x</sub> removal efficiencies.<sup>95</sup>

There are many potential problems with SNCR. The first is the initial capital and ongoing operating costs, which are usually significantly more than non-post-treatment techniques like low NO<sub>x</sub> burners. Although the use of SNCR decreases NO<sub>x</sub>, it may increase other undesirable emissions such as CO, N<sub>2</sub>O, and NH<sub>3</sub> (which can occur if the injected chemicals slip through the exhaust without reacting, referred to as ammonia slip).<sup>17</sup> However, as shown in Figure 15.39, the NO<sub>x</sub> removal efficiency increases as the ammonia slip increases so that acceptable limits must be determined either by design or regulatory

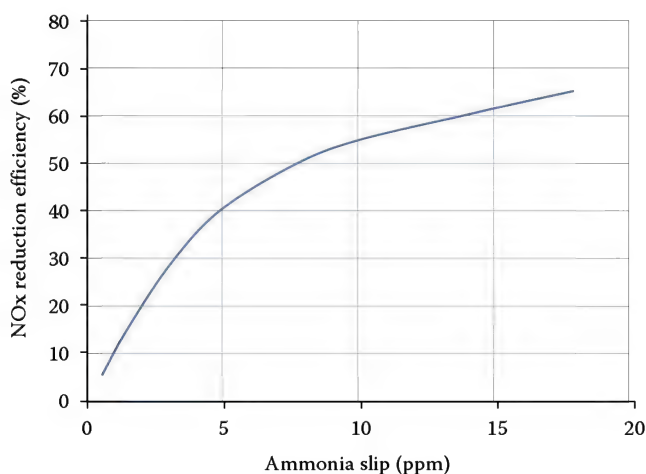


FIGURE 15.39

Effect of ammonia slip on SNCR NO<sub>x</sub> reduction efficiency. (Adapted from Mussatti, D.C., et al., Section 4.2: NO<sub>x</sub> post-combustion, Selective noncatalytic reduction, Chapter 1 in *Air Pollution Control Cost Manual*, 6th edn., Ed. D.C. Mussatti, Report EPA/452/B-02-001, U.S. Environmental Protection Agency, Washington, DC, January 2002.)

constraints. There are also safety concerns with transporting and storing ammonia (NH<sub>3</sub>) used in SNCR because of the health hazards of ammonia in the event of a spill or leak. Other major challenges of this technology include:

- Finding the proper location in the process to inject the chemicals (the chemicals must be injected where the flue gases are within a relatively narrow temperature window for optimum efficiency).
- Injecting the proper amount of chemicals (too much will cause some chemicals to slip through unreacted and too little will not get sufficient NO<sub>x</sub> reductions).
- Obtaining the proper mixing of the chemicals with the flue gas products (there must be both adequate mixing and residence time for the reactions to go to completion).

Both physical modeling and computer modeling are often used to determine the optimal place, amount, and method of injection.

Under ideal laboratory conditions, SCNRs can be shown to achieve significant NO<sub>x</sub> reductions. However, in practical applications the reductions are usually much less due to the nonuniformity of the temperature profile in the combustor, difficulties with completely mixing the nitrogen agent (ammonia, urea, cyanuric acid, etc.) into the exhaust stream, limited residence times, and ammonia slip. These can reduce the effectiveness by up to 50%. Zamansky et al.<sup>96</sup> experimentally and computationally demonstrated that it is possible to alleviate these practical problems with the injection of inexpensive and non-toxic inorganic salts such as sodium carbonate with the nitrogen agent. The results showed that the inorganic salts could significantly broaden the effective temperature window, which can be a significant obstacle in industrial processes due to the nonhomogeneity of the gas temperatures. The U.S. EPA has prepared a helpful manual for estimating the cost of air pollution control using various techniques, which includes a chapter on SNCR for NO<sub>x</sub> control.<sup>94</sup>

#### 15.5.4.3 Catalytic Reduction

Another post-treatment method of reducing NO<sub>x</sub> is referred to as catalytic cleaning.<sup>97</sup> In this process, NO formed during combustion is converted into N<sub>2</sub> in the presence of a catalyst according to the basic reaction:

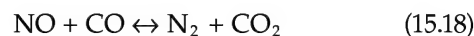


Figure 15.40 shows a schematic of a typical catalytic reduction system.

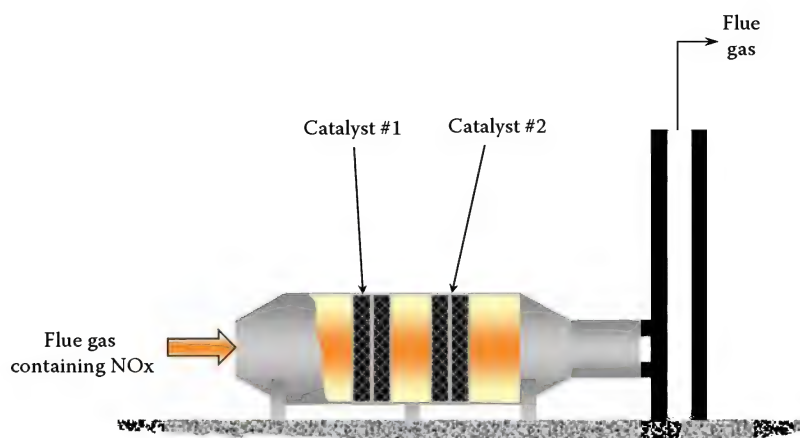


FIGURE 15.40

Catalytic cleaning NO<sub>x</sub> reduction system. (From Baukal, C.E., *Industrial Combustion Pollution and Control*, Marcel Dekker, New York, 2004.)

In the application of this technology to recuperative radiant tube burners, the catalyst is placed in the recuperator section of the burner in a position where the gases will be in the proper temperature range in order to optimize the catalytic reactions. A second catalyst is located further downstream in the burner to oxidize the CO. The flue gas temperatures and excess air ratios in the vicinity of the catalysts affect the efficiency of the reduction processes. NO<sub>x</sub> reductions of up to 87% are projected for this newly developed process. The advantage of this technique compared to SCR and SNCR is that no reagent is needed. However, further work is required to make catalytic cleaning effective in industrial combustion applications.

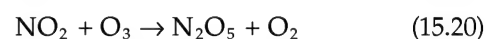
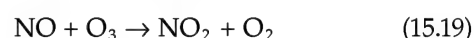
#### 15.5.4.4 Other

There are many other post-treatment NO<sub>x</sub> control technologies. Several examples are given in this section. Thomas and Vanderschuren<sup>98</sup> describe the use of hydrogen peroxide (H<sub>2</sub>O<sub>2</sub>) to reduce NO<sub>x</sub> emissions in a wet absorption process. Their work shows that there is an optimum concentration of H<sub>2</sub>O<sub>2</sub> beyond which there is no increase in NO<sub>x</sub> removal efficiency. A packed tower scrubber can be used to remove NO<sub>x</sub> from gases using a wet absorption process.

A technique currently under development is termed non-thermal plasma.<sup>99</sup> A pulsed corona discharge generates short high frequency pulses that increase radical production in an exhaust stream. These radicals then make it easier to transform the toxic pollutants into benign compounds. A key to the use of these plasmas is that they have little effect on the bulk carrier gas and preferentially react with the trace constituents. A catalyst is used to convert the radical species produced by the plasma into benign species. In one form of this technology, NO and NO<sub>2</sub> are oxidized to N<sub>2</sub>O<sub>5</sub>, the removal of which is described in the following.

Another new development is a device called a fungal vapor-phase bioreactor that is designed to remove NO and VOCs from waste gas streams.<sup>100</sup> This technology, generally referred to as biofiltration, shows a resistance to adverse operating conditions and is able to maintain high removal efficiencies over an extended period of time; a problem with some other post-treatment technologies. Removal efficiencies exceeding 90% for both NO<sub>x</sub> and VOCs have been demonstrated on a bench-scale apparatus.

A relatively new technique referred to as low-temperature oxidation with absorption converts NO and NO<sub>2</sub> into another form of NO<sub>x</sub> (N<sub>2</sub>O<sub>5</sub>) that is very soluble and is easily removed with a wet scrubber:<sup>90</sup>



In this technique, the oxidizer is ozone, which can be generated using either air or pure oxygen. The process takes place at about 300°F (150°C) which makes it impractical for many industrial combustion processes unless the flue gases are cooled prior to reaching the ozone. At temperatures above about 500°F (260°C), ozone decomposes very rapidly. The process can have NO<sub>x</sub> removal efficiencies as high as 99%. Other reactions with CO and SO<sub>2</sub> are slow compared to the NO<sub>x</sub> reactions and do not compete for the ozone.

### 15.5.5 Implementing Strategies

#### 15.5.5.1 General Implementation

Before determining an appropriate NO<sub>x</sub> reduction strategy, the baseline data from the various emission sources in the plant must be collected. This should be compared



to the target emission requirement to determine how much total reduction is needed. As discussed earlier, there are many potential choices for reducing NOx emissions. The specific strategy chosen will depend on many factors that vary by plant. This section describes some general strategies that will apply in many cases, although the specific order of priority may vary somewhat, depending on the situation.

The first task that should be accomplished in most cases is to tune up each combustion system, if this has not been done recently. To do this, the flue gases from each exhaust stack must be analyzed for composition (CO, NOx, and O<sub>2</sub>) and temperature. The CO and NOx measurements indicate the pollutant emissions. The CO, O<sub>2</sub>, and temperature can be used to determine the thermal efficiency. Too much CO or too much O<sub>2</sub> usually indicate reduced thermal efficiency. The system should ideally be operated at a fairly low O<sub>2</sub> level, without excessive CO emissions. However, low O<sub>2</sub> by itself does not necessarily mean a properly operating system. O<sub>2</sub> coming from leaks in the furnace, instead of through the burner, often indicates poor combustion control. Furnace leaks should be sealed to minimize tramp air infiltration (see Chapter 12). Fuel injectors should be inspected to make sure they are clean and not excessively eroded, since dirty or eroded fuel tips can reduce burner performance (see Volume 2). Tuning up the combustion system is often the most cost-effective strategy because it improves thermal efficiency while reducing emissions per unit of production.

If more NOx reduction is required, the next step is to investigate upgrading or replacing old high NOx burners with new low NOx burners. This can often be accomplished while a furnace is still in operation, with minimal impact on production. As previously discussed, low NOx burners are usually the most cost-effective equipment upgrade for reducing NOx (see Section 15.5.2.12). This may only need to be performed on the most polluting heaters, depending on how much NOx reduction is needed. Other types of combustion modifications may also be employed depending on how much NOx reduction is required.

If further NOx reduction is needed, post-treatment methods are often then considered. In many cases, it is more cost effective to treat multiple flue gas streams in a single post-treatment system such as an SCR. This will depend on the proximity of the exhaust stacks and the availability of space to locate a post-treatment system, which can often be fairly large. Unfortunately, most of these systems can only be installed during a turnaround, so this would usually have to be scheduled well in advance of a required reduction in emissions.

Except under special circumstances, pretreatment and process modification techniques are often the last option to be considered. They are generally more

radical in nature and more expensive. In many cases, process modifications are not a viable option.

#### 15.5.5.2 More Specific Implementation

Several hypothetical examples are provided next to illustrate various NOx reduction implementation plans and the factors that should be considered when developing these plans. The first example assumes that relatively minor NOx reductions are needed to meet new regulations that will become effective in the next 2 years. All of the heaters, furnaces, and boilers have already been inspected and tuned up recently, and most are already equipped with low NOx burners. A turnaround is planned in the next 18 months and there is available space to install post-treatment equipment in one part of the plant. In this scenario, the best alternative may be to install post-treatment equipment in that part of the plant to treat several flue gas streams from heaters in close proximity to each other.

The next example assumes that moderate NOx reductions are needed in a plant installing a new cogeneration facility. A significant amount of steam will become available as a result of this new cogeneration plant. This might suggest using steam injection into some of the heaters, furnaces, and boilers to reduce NOx emissions. Since all of the combustors at this plant are equipped with some type of heat recuperation (e.g., convection sections), there should not be any significant reduction in thermal efficiency caused by the steam injection. Large-scale steam injection is often not an option at many plants because there is not sufficient excess steam available.

The last example assumes the permitted NOx emissions will need to be significantly reduced over the next 5 years. In year 1, tramp air leakage and excess O<sub>2</sub> are reduced in all of the heaters, furnaces, and boilers in the plant to improve thermal efficiency and reduce emissions. Existing burners are inspected and serviced as required to ensure peak performance. In years 2–3, existing high NOx burners are replaced with ultralow NOx burners on several selected heaters. In years 4 and 5, SCR systems are added to some of the heaters that are clustered in close proximity to each other. This staging of the implementation allows the plant to schedule the modifications around the production needs, spread the cost over time, and determine the effectiveness of initial upgrades before implementing more costly upgrades later.

---

### 15.6 Pilot-Scale Test Results

This section gives some example test results for full scale burner testing in pilot-scale test burners. These were single burner tests and are given to show some representative test data.



## 15.6.1 Conventional Burner

### 15.6.1.1 Fuel Composition Effects

The composition of the fuel supplied to a combustion system has a significant impact on the NO<sub>x</sub> emissions (e.g., see Figure 15.11). In the petrochemical and chemical process industries, there is a very wide range of fuel blends used for process heating (see Chapter 3). These fuels are often by-products from a refining process. They typically contain hydrocarbons ranging from C<sub>1</sub> to C<sub>4</sub>, hydrogen, and inert gases like N<sub>2</sub> and CO<sub>2</sub>. In a given plant or refinery, burners used in process heaters may need to be capable of firing on multiple fuels that are present at different times (e.g., start-up, normal operation, upset conditions, etc.). In many cases, the NO<sub>x</sub> emissions from the heaters may not exceed a given value regardless of what fuel composition is being fired. Therefore, it is critical that the effects of the fuel composition on NO<sub>x</sub> emissions be understood and quantified to ensure that permitted values are not exceeded.

This section shows the results of an extensive series of tests to study the effects of fuel composition on NO<sub>x</sub> emissions from an industrial-scale burner.<sup>101</sup> The data provide additional insight into effects on NO<sub>x</sub> over the entire range of fuel compositions consisting of various fractions of three primary components: H<sub>2</sub>, C<sub>3</sub>H<sub>8</sub>, and CH<sub>4</sub>. Figures 15.41 through 15.43 show how NO<sub>x</sub> theoretically varies for 2-component fuel mixtures of CH<sub>4</sub>–C<sub>3</sub>H<sub>8</sub>, CH<sub>4</sub>–H<sub>2</sub> and C<sub>3</sub>H<sub>8</sub>–H<sub>2</sub>, respectively. These figures show the predicted adiabatic equilibrium NO concentrations for flames with 15% excess air. Figure 15.44 shows a ternary diagram of the calculated adiabatic flame temperatures (Figure 15.44a) over the range of 3-component fuel blends tested and another ternary diagram showing the predicted adiabatic equilibrium NO (Figure 15.44b) for 3-component fuel blends containing CH<sub>4</sub>, C<sub>3</sub>H<sub>8</sub>, and H<sub>2</sub> combusted with 15% excess air.

Testing was conducted using a conventional-type (i.e., not low NO<sub>x</sub>) burner (see Figure 15.45) with a

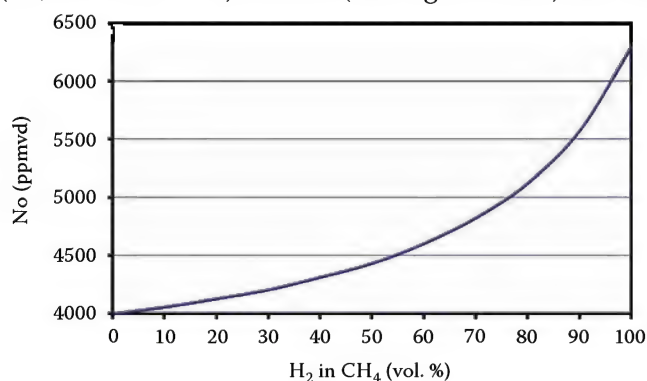


FIGURE 15.41

Adiabatic equilibrium NO as a function of the fuel blend composition for H<sub>2</sub>/CH<sub>4</sub> blends combusted with 15% excess air where both the fuel and the air are at ambient temperature and pressure.

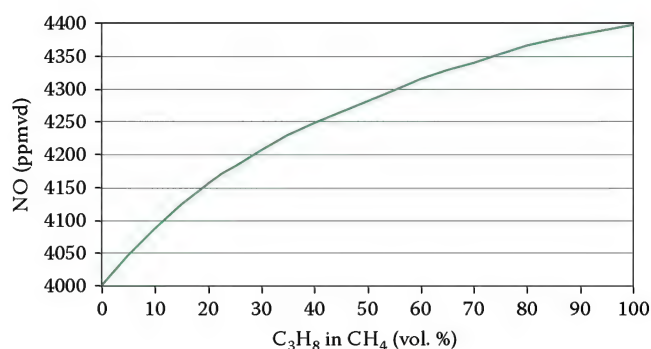


FIGURE 15.42

Adiabatic equilibrium NO as a function of the fuel blend composition for C<sub>3</sub>H<sub>8</sub>/CH<sub>4</sub> blends combusted with 15% excess air where both the fuel and the air are at ambient temperature and pressure.

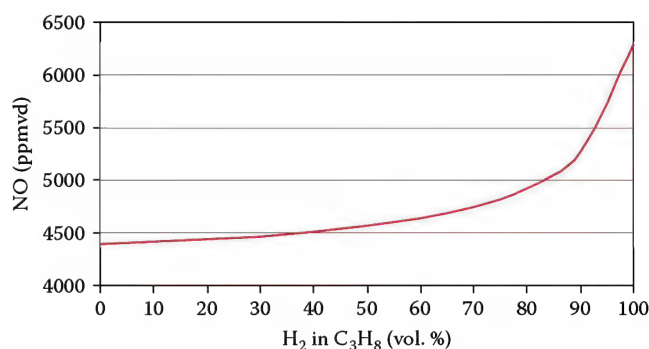


FIGURE 15.43

Adiabatic equilibrium NO as a function of the fuel blend composition for H<sub>2</sub>/C<sub>3</sub>H<sub>8</sub> blends combusted with 15% excess air where both the fuel and the air are at ambient temperature and pressure.

single fuel gas tip and flame holder (see Figure 15.46). The burner was fired vertically upward in a rectangular furnace (see Figure 15.47). The test furnace was a rectangular heater 8 ft (2.4 m) wide, 12 ft (3.7 m) long, and 15 ft (4.6 m) tall. The furnace was cooled by a water jacket on all four walls. The interior of the water-cooled walls was covered with varying layers of refractory lining to achieve the desired furnace temperature. The burner was tested at a nominal heat release rate of  $7.5 \times 10^6$  Btu/h (2.2 MW).

A velocity thermocouple (also known as a suction thermocouple or suction pyrometer—(see Vol. 2, Chapter 7) was used to measure the furnace and stack gas temperatures. The furnace draft was measured with an automatic, temperature-compensated, pressure transducer as well as an inclined manometer connected to a pressure tap in the furnace floor. Fuel flow rates were measured using calibrated orifice meters, fully corrected for temperature and pressure. Emission levels were measured using state-of-the-art continuous emissions monitors (CEMs) to measure emissions species concentrations of NO<sub>x</sub>, CO, and O<sub>2</sub>.

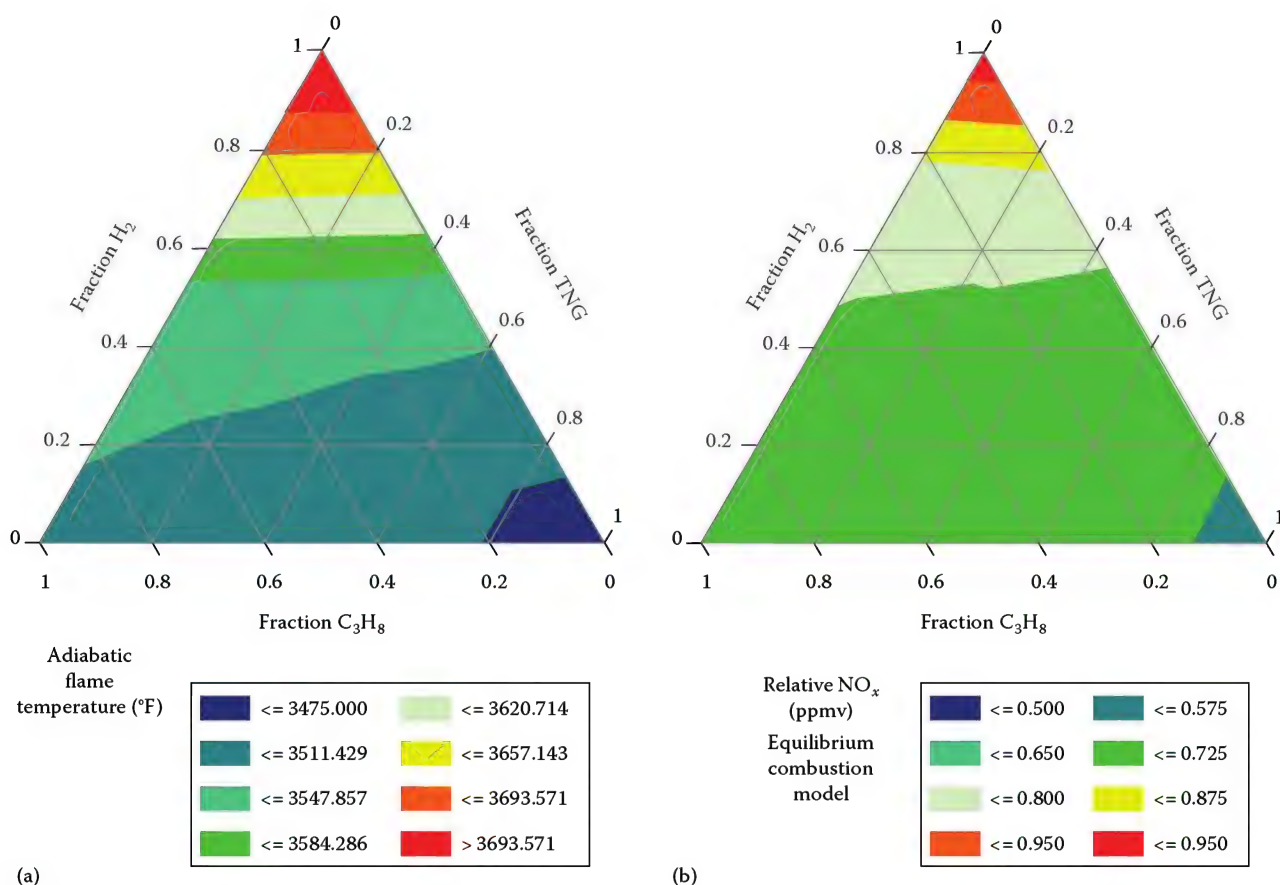


FIGURE 15.44

Ternary plot of adiabatic equilibrium (a) temperature and (b) relative NO (fraction of the maximum value) as a function of the fuel blend composition for H<sub>2</sub>/CH<sub>4</sub>/C<sub>3</sub>H<sub>8</sub> blends combusted with 15% excess air where both the fuel and the air are at ambient temperature and pressure.

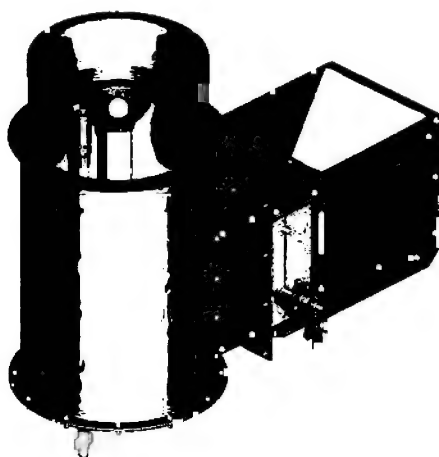


FIGURE 15.45

Raw gas (VYD) burner.

The experimental matrix consisted of firing the burner at a constant heat release ( $7.5 \times 10^6$  Btu/h or 2.2 MW) and excess air level (15%) with 15 different fuel blends comprised of varying amounts of H<sub>2</sub>, C<sub>3</sub>H<sub>8</sub>, and Tulsa NG (TNG). The nominal composition by volume of TNG is 93.4% CH<sub>4</sub>, 2.7% C<sub>2</sub>H<sub>6</sub>, 0.60% C<sub>3</sub>H<sub>8</sub>, 0.20%

C<sub>4</sub>H<sub>10</sub>, 0.70% CO<sub>2</sub>, and 2.4% N<sub>2</sub>. For testing and analysis purposes, TNG was treated as a single fuel component for convenience. TNG, which is comprised of approximately 93% CH<sub>4</sub>, is a more economical choice than pure CH<sub>4</sub> for experimental work and the analysis is simplified by treating it as a single component. All 15 fuel

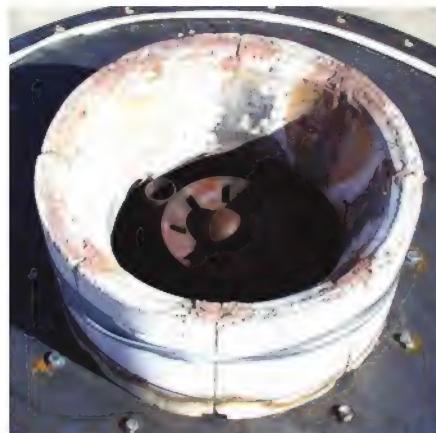
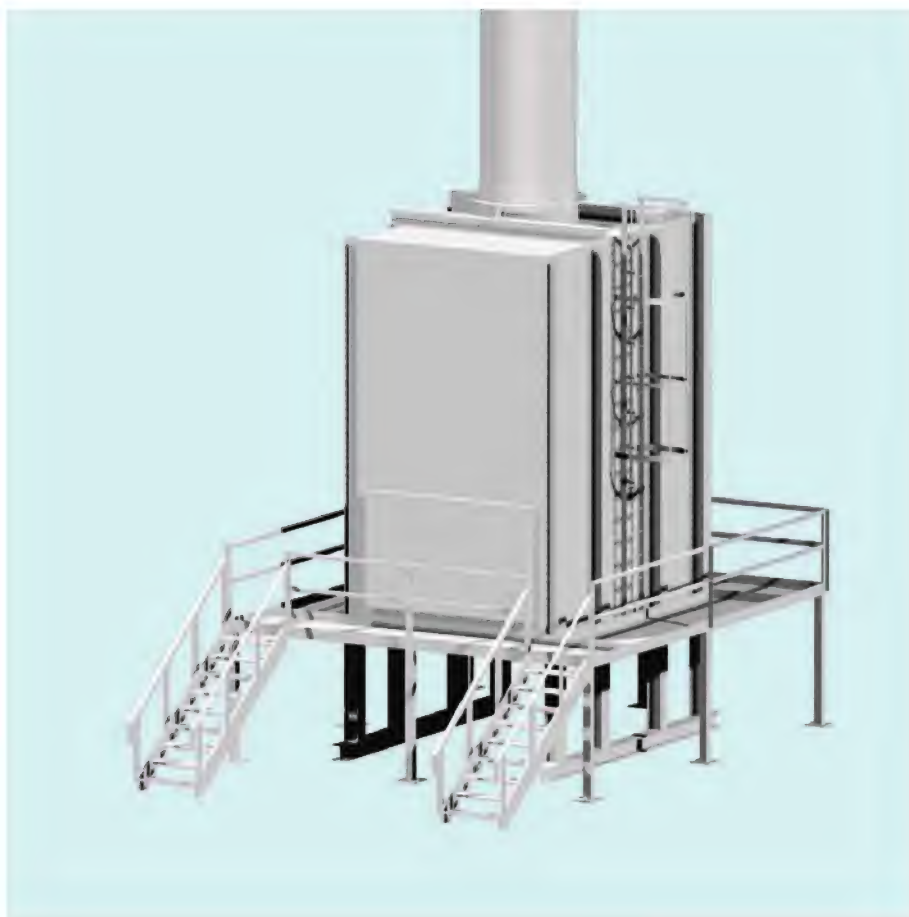


FIGURE 15.46

VYD burner closeup.



**FIGURE 15.47**  
Test furnace.

compositions were tested on each of six different fuel gas tips, which differed in port diameter sizes, to enable the acquisition of additional information regarding effects resulting from differing fuel pressures.

Figure 15.48 shows the variation in relative measured NO<sub>x</sub> emissions resulting from different concentrations (volume basis) of H<sub>2</sub> in a fuel blend composed with a balance of TNG for each of the six different fuel gas tips tested. The plot, which illustrates NO<sub>x</sub> levels on a concentration basis, shows the correlation between increased H<sub>2</sub> content and higher NO<sub>x</sub> emission levels. The slope of the profile is exponentially increasing, qualitatively similar to that predicted by the plotted theoretical calculations shown previously in Figure 15.41. The effect of H<sub>2</sub> is significant, with the sharpest increase in NO<sub>x</sub> levels taking place as concentration levels of H<sub>2</sub> in the fuel mixture rise from 75% to 100%.

The variation in relative measured NO<sub>x</sub> emissions resulting from different concentrations (volume basis) of C<sub>3</sub>H<sub>8</sub> in a fuel blend composed with a balance of TNG is shown in Figure 15.49. The slope of the increase in NO<sub>x</sub> levels corresponding to increased concentrations of C<sub>3</sub>H<sub>8</sub> is shown to be relatively constant or slightly

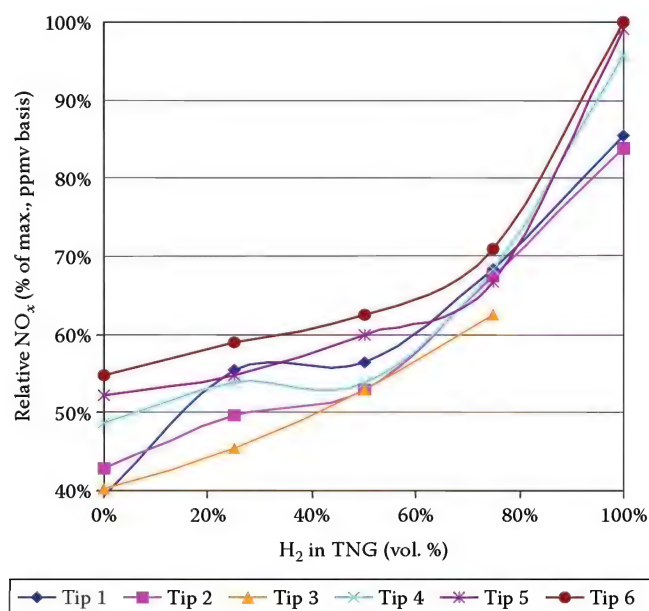


**FIGURE 15.48**  
Measured NO<sub>x</sub> (percent of the maximum ppmv value) as a function of the fuel blend composition for H<sub>2</sub>/TNG blends combusted with 15% excess air where both the fuel and the air were at ambient temperature and pressure.



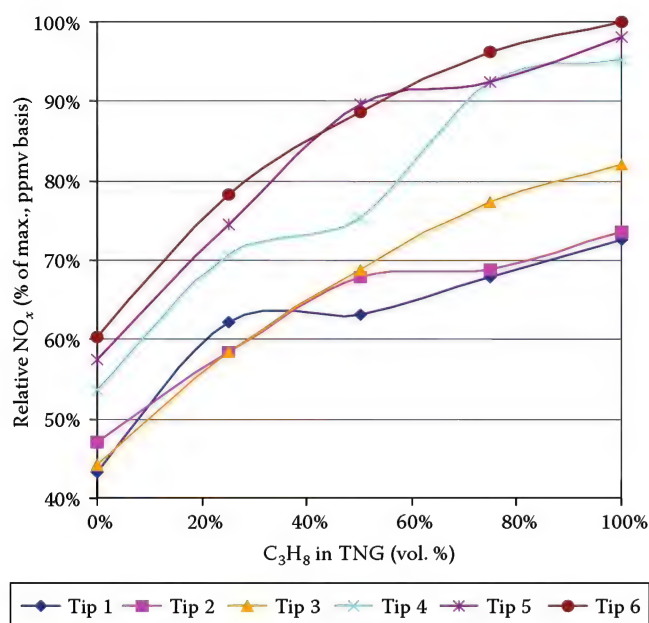


FIGURE 15.49

Measured NO<sub>x</sub> (percent of the maximum ppmv value) as a function of the fuel blend composition for C<sub>3</sub>H<sub>8</sub>/TNG blends combusted with 15% excess air where both the fuel and the air were at ambient temperature and pressure.

declining over the gradient in C<sub>3</sub>H<sub>8</sub> concentration, in contrast with the exponentially increasing profile of the H<sub>2</sub>-TNG plot in Figure 15.48. The profile showing the effect of C<sub>3</sub>H<sub>8</sub> content is also seen to be similar to the corresponding calculated trends shown previously in Figure 15.42.

Figure 15.50 shows the final two-component fuel blend results being examined, which describe the variation in relative measured NO<sub>x</sub> emissions resulting from different concentrations (volume basis) of H<sub>2</sub> in a fuel blend composed with a balance of C<sub>3</sub>H<sub>8</sub>. The upper plot, which shows measured relative NO<sub>x</sub> on a volume concentration basis, illustrates that for a given tip geometry and port size the measured NO<sub>x</sub> concentrations actually decrease slightly with increasing H<sub>2</sub> content up to 75% H<sub>2</sub> content, then sharply increase with H<sub>2</sub> concentration.

Due to the decrease in total dry products of combustion from the burning of H<sub>2</sub> expressing NO<sub>x</sub> in terms of concentration (ppmv) does not fully represent the actual mass rate of NO<sub>x</sub> emissions produced. The lower plot, which shows the variation in measured NO<sub>x</sub> levels on a mass per unit heat release basis, illustrates that the overall emissions of NO<sub>x</sub> on a mass basis decrease with increasing fuel hydrogen content and continue to decrease or remain relatively flat even in the high-hydrogen content region which produced a sharp increase in NO<sub>x</sub> levels on a volume concentration basis.

### 15.6.1.2 Fuel Gas Tip Design

Three-component interaction results were also examined by considering results from several of the tested fuel gas tip designs. Figures 15.51 through 15.53 show contoured ternary plots of variation in relative measured NO<sub>x</sub> levels corresponding to different fractions of H<sub>2</sub>, C<sub>3</sub>H<sub>8</sub>, and TNG in the fuel blend. Plots for three tip designs are shown. The tips differ only in fuel port area size, which results in different fuel pressures for a given heat release on each tip. The results are shown for tips in order of increasing port area size, or in other words, decreasing fuel pressure levels for the design heat release. Two plots are shown for each of three tips, with one illustrating NO<sub>x</sub> levels on a volume concentration basis and the other illustrating NO<sub>x</sub> levels on a mass per unit heat release basis. Higher fuel pressures produce higher fuel gas jet velocities and lower pressures produce lower jet velocities. The fuel jet velocity affects the mixing of the air and fuel, which impacts NO<sub>x</sub> emissions.

For each given tip, the highest NO<sub>x</sub> emissions on a concentration basis occurred in the high-hydrogen content region, while the highest NO<sub>x</sub> emissions on a mass per unit heat release basis occur in the high-propane region. The contoured gradients illustrate the interaction of the three fuel components and how each of the components affects NO<sub>x</sub> emission in different regions of the fuel mixture, such as the steep NO<sub>x</sub> concentration gradients in the high-hydrogen content regions. The effect of C<sub>3</sub>H<sub>8</sub> content can be seen to dominate the NO<sub>x</sub> level gradients on a mass per unit heat release basis with a relatively constant slope. It is also interesting to note that NO<sub>x</sub> levels overall appear to increase as fuel gas tips change from having less open fuel port area (higher fuel pressures for a given heat release) to having greater open fuel port area (lower fuel pressure for a given heat release).

Figure 15.54 shows ternary plots of fuel composition effects on NO<sub>x</sub> at a nominal constant fuel pressure of 21 psig (145 kPag). This analysis, made possible by testing a range of fuel gas tips, enables the examination of fuel composition effects on NO<sub>x</sub> emissions relatively independently from fuel pressure variations. A qualitative comparison of the plot on the left with the theoretical plots previously shown in Figure 15.44 reveals that, on a volume concentration basis, the change in NO<sub>x</sub> level as a function of fuel composition, for a relatively constant pressure and constant heat release, varies similarly to the trends predicted by the adiabatic flame temperature variation and predicted relative NO<sub>x</sub> concentrations from the equilibrium combustion model over the same regions. This result is expected due to the well-established correlation of the dependence of thermal NO<sub>x</sub> formation on flame

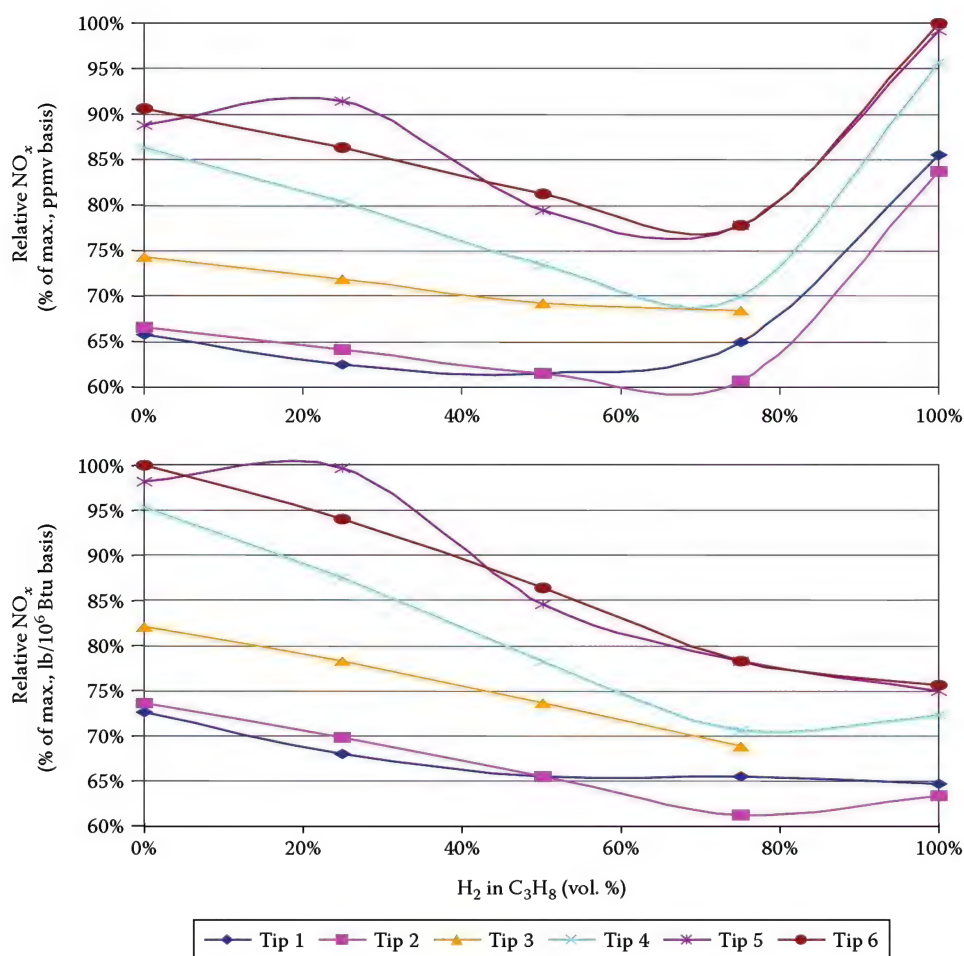


FIGURE 15.50

Measured NO<sub>x</sub> (percent of the maximum value in both ppmv and lb/MMBtu) as a function of the fuel blend composition for H<sub>2</sub>/C<sub>3</sub>H<sub>8</sub> blends combusted with 15% excess air where both the fuel and the air were at ambient temperature and pressure.

temperature. The mass basis plot in Figure 15.54b, shows that variation in NO<sub>x</sub> levels with fuel composition, from a constant fuel pressure perspective, are less severe than seen in the analysis of a single fuel gas tip with fixed port sizes, for which fuel pressures may vary greatly to maintain a given heat release with fuel composition variation.

From both the two-component and three-component analyses it is evident that fuel pressure has a significant effect on NO<sub>x</sub> emission levels. Figure 15.55 shows a plot of relative NO<sub>x</sub> levels vs. fuel pressure for each of the 15 different fuels tested. This plot shows a consistent decrease in NO<sub>x</sub> levels correlated with an increase in fuel pressure. This phenomenon is explained by the burner configuration, which allows significant amounts of inert flue gas to be entrained into the flame zone (see Section 15.5.2.4) with increasing fuel jet momentum, thus decreasing thermal NO<sub>x</sub> formation.

### 15.6.1.3 Summary

Figure 15.56 shows an overall view of the data collected from all six tips with each of the 15 different fuel compositions (90 data points in total) from both an NO<sub>x</sub> volume concentration basis and mass per unit heat release viewpoint. The plots use fuel pressure and adiabatic flame temperatures as the primary axes to illustrate some overall trends. The plot of relative NO<sub>x</sub> concentration levels shows the minimum NO<sub>x</sub> levels occur in the region with the lowest adiabatic flame temperature and highest fuel pressures. Inversely the highest NO<sub>x</sub> concentration levels are found in the region of high adiabatic flame temperatures and low fuel pressures, when high concentrations of hydrogen are present. The mass per unit heat release NO<sub>x</sub> levels are also at a minimum in the same region as the concentration-based profiles; however, the maximum NO<sub>x</sub> levels, when measured on a mass basis, are not

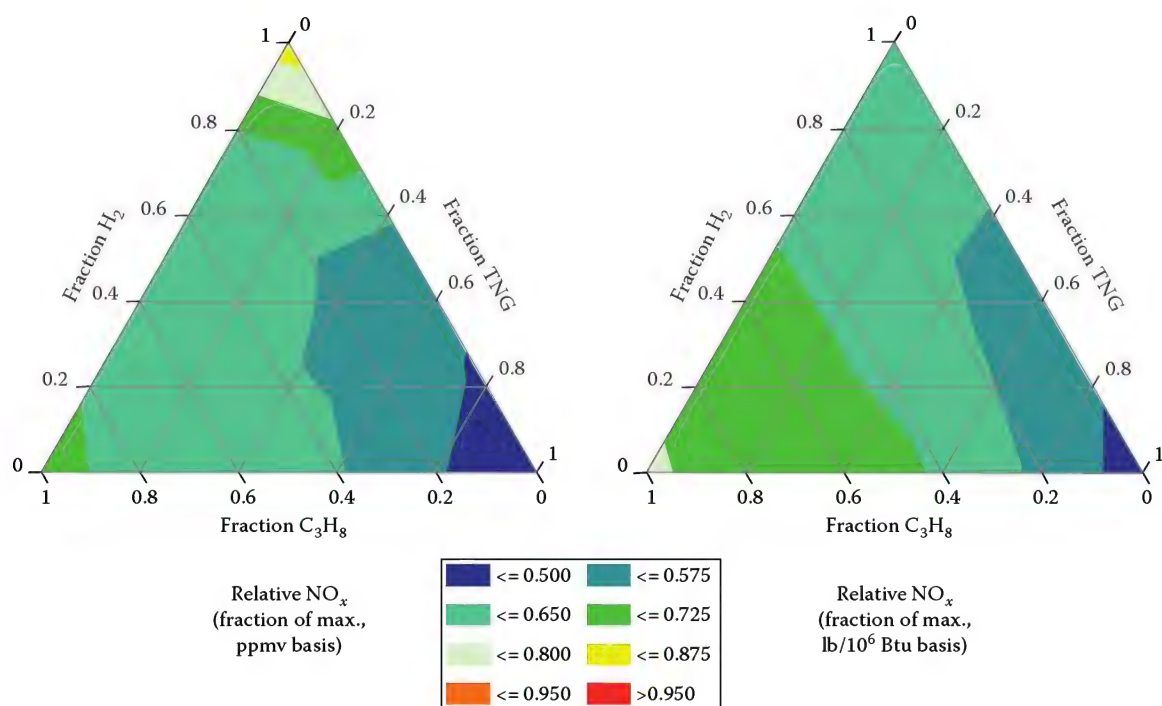


FIGURE 15.51

Measured NO<sub>x</sub> (fraction of the maximum value in both ppmv and lb/MMBtu) as a function of the fuel blend composition for TNG/H<sub>2</sub>/C<sub>3</sub>H<sub>8</sub> blends combusted with 15% excess air where both the fuel and the air were at ambient temperature and pressure for gas tip #2.

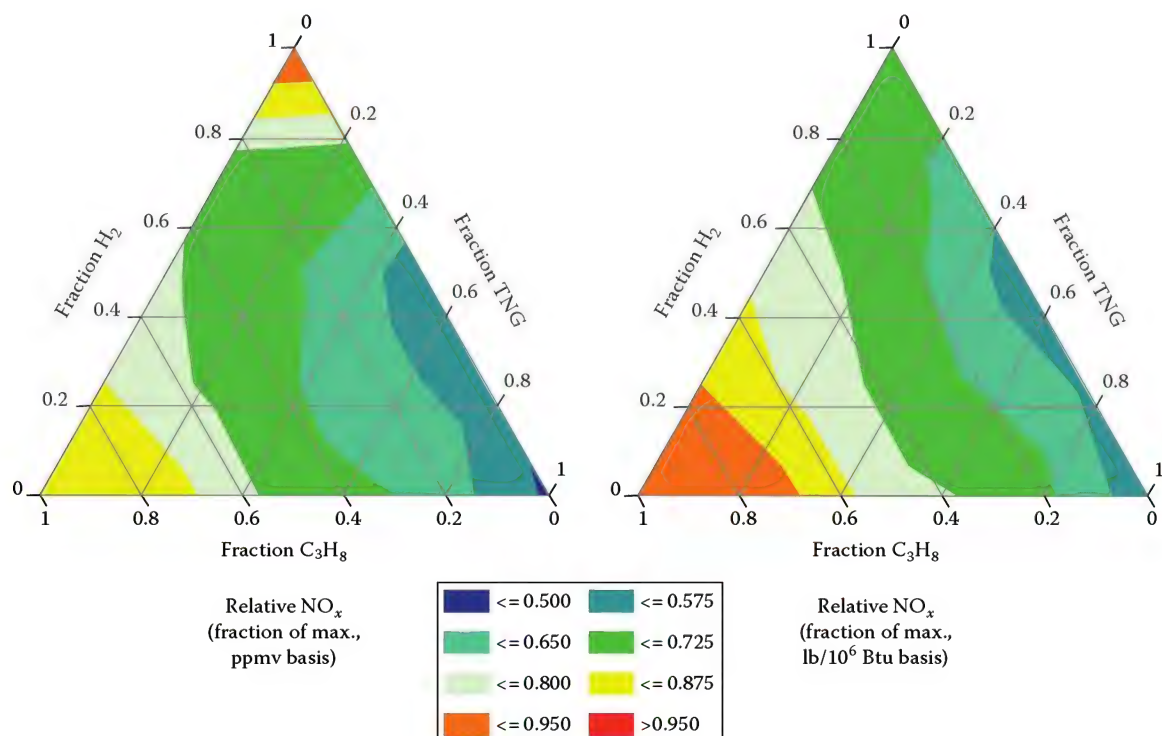


FIGURE 15.52

Measured NO<sub>x</sub> (fraction of the maximum value in both ppmv and lb/MMBtu) as a function of the fuel blend composition for TNG/H<sub>2</sub>/C<sub>3</sub>H<sub>8</sub> blends combusted with 15% excess air where both the fuel and the air were at ambient temperature and pressure for gas tip #4.



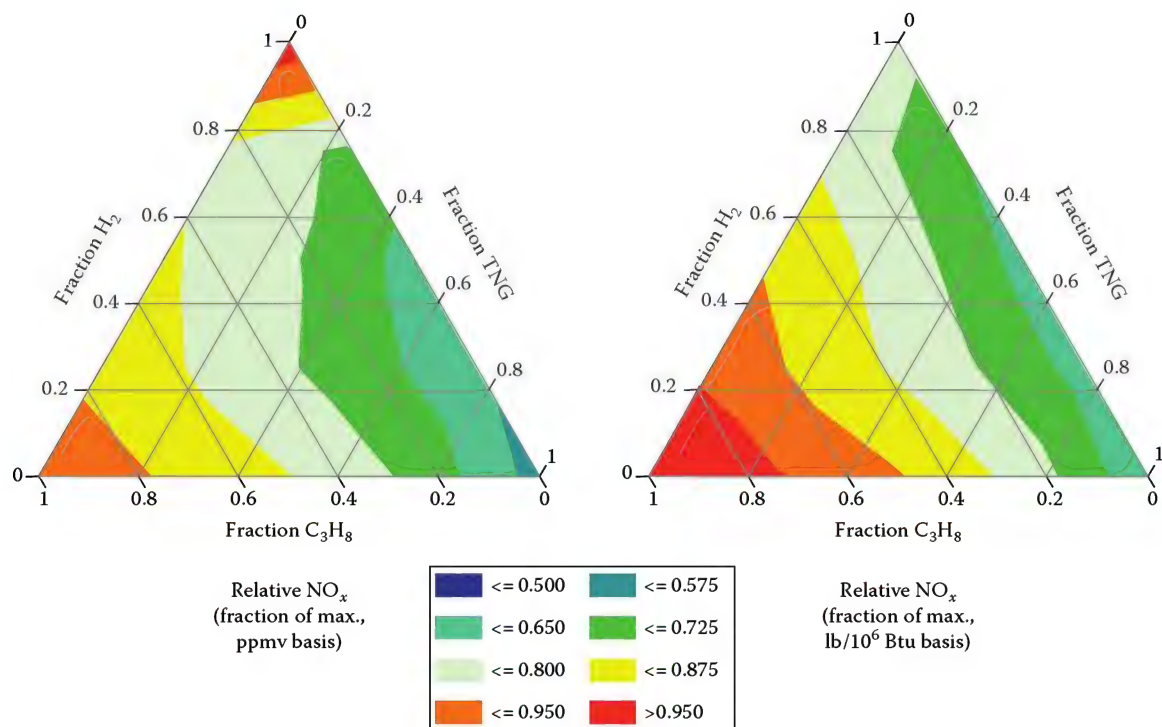


FIGURE 15.53

Measured NO<sub>x</sub> (fraction of the maximum value in both ppmv and lb/MMBtu as a function of the fuel blend composition for TNG/H<sub>2</sub>/C<sub>3</sub>H<sub>8</sub> blends combusted with 15% excess air where both the fuel and the air were at ambient temperature and pressure for gas tip #6.

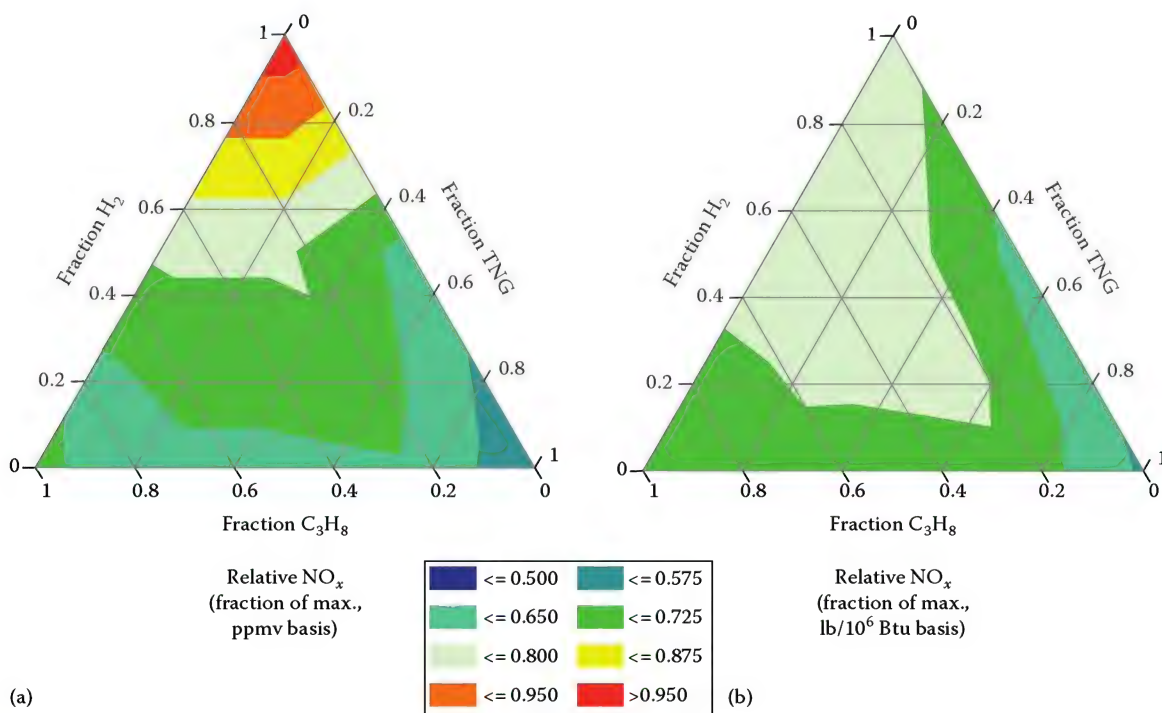


FIGURE 15.54

Measured NO<sub>x</sub> (fraction of the maximum value) in (a) ppmv and (b) lb/MMBtu as a function of the fuel blend composition for TNG/H<sub>2</sub>/C<sub>3</sub>H<sub>8</sub> blends combusted with 15% excess air where both the fuel and the air were at ambient temperature and pressure for a constant fuel gas pressure of 21 psig.

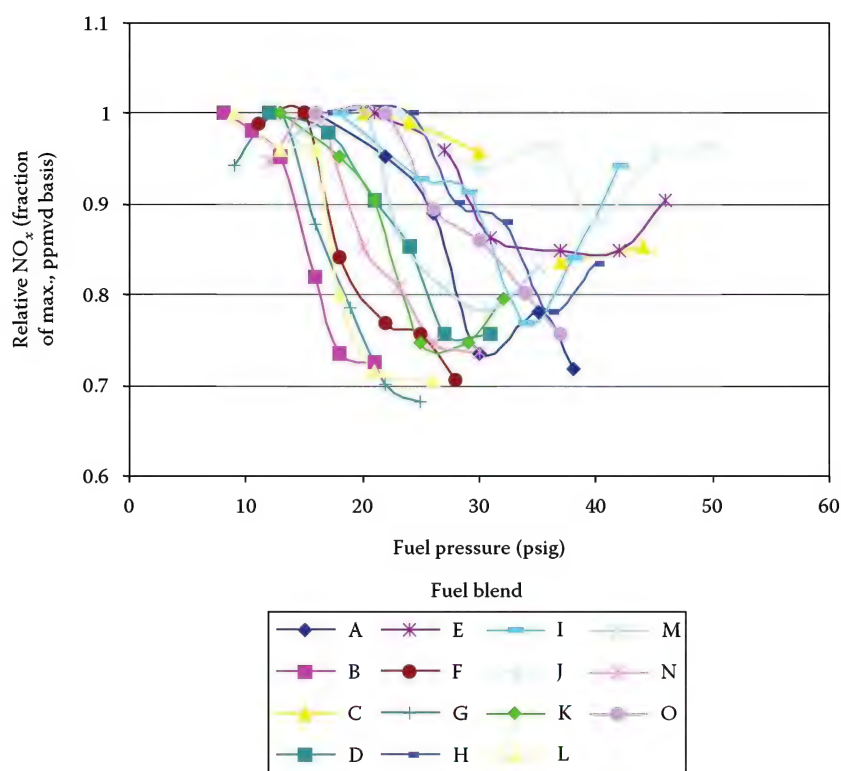


FIGURE 15.55

Measured NO<sub>x</sub> (fraction of the maximum value in ppmvd) as a function of the fuel pressure for all 15 different TNG/H<sub>2</sub>/C<sub>3</sub>H<sub>8</sub> blends (A through O) combusted with 15% excess air where both the fuel and the air were at ambient temperature and pressure.

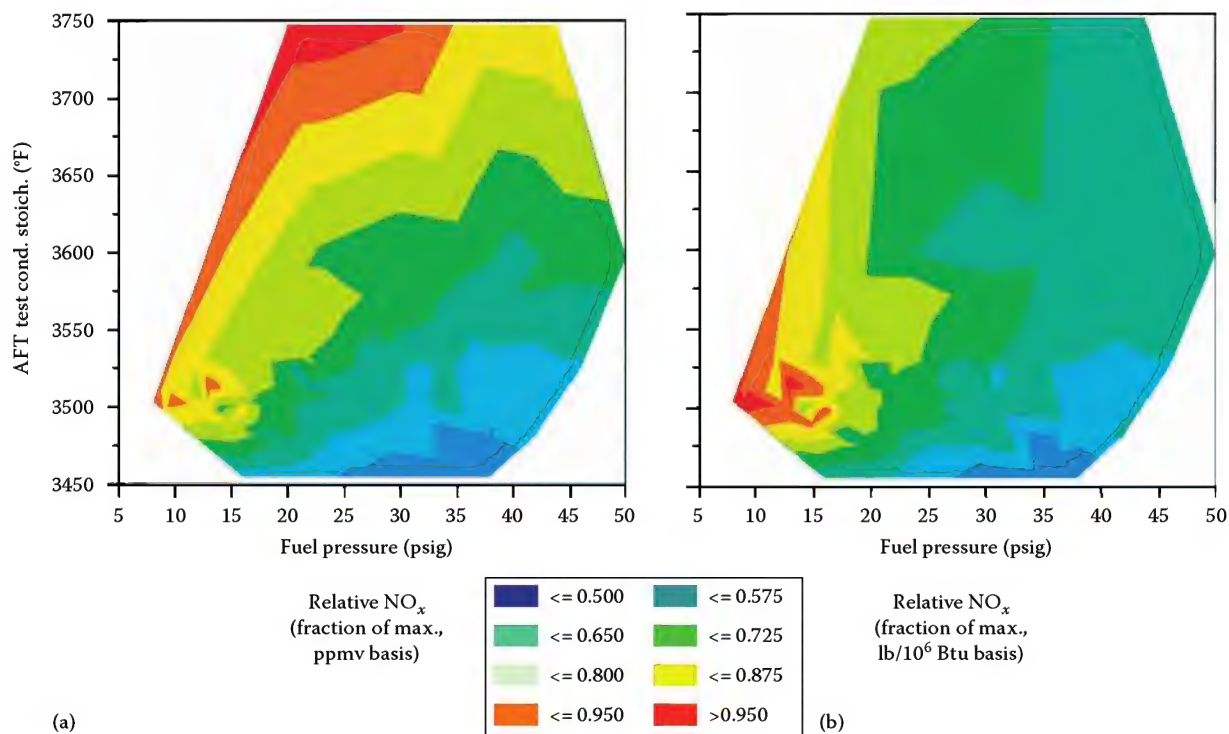


FIGURE 15.56

Measured NO<sub>x</sub> (fraction of the maximum value) in (a) ppmv and (b) lb/MMBtu as a function of the fuel blend composition, fuel gas pressure and calculated adiabatic flame temperature for TNG/H<sub>2</sub>/C<sub>3</sub>H<sub>8</sub> blends combusted with 15% excess air where both the fuel and the air were at ambient temperature and pressure.

found in the same region, but occur in areas of lowest fuel pressures with a mildly elevated adiabatic flame temperature, which correspond to high C<sub>3</sub>H<sub>8</sub> concentration regions. These overall trends concur with the previously discussed results and agree with the correlations shown by the three-component and two-component interaction analyses.

Adiabatic flame temperature and fuel pressure are both identified as significant fundamental parameters affecting NO<sub>x</sub> emission levels when considering the effect of fuel composition on NO<sub>x</sub> levels. For a conventional burner, with NO<sub>x</sub> on a concentration basis, the adiabatic flame temperature is dominant, with fuel pressure remaining significant in affecting NO<sub>x</sub> emission levels. The highest NO<sub>x</sub> levels on a volume concentration basis occurred at the highest hydrogen content fuel compositions at lower fuel pressures. On a mass per heat release basis however, the highest relative NO<sub>x</sub> levels were achieved for fuel compositions containing large fractions of C<sub>3</sub>H<sub>8</sub>. This appears to result from some combined characteristics of a high-propane mixture including: very low fuel pressure for a given heat release in comparison with the other fuels; somewhat higher adiabatic flame temperature than CH<sub>4</sub>; and a substantially larger amount of total dry products of combustion produced for a given heat release when compared with H<sub>2</sub>. In summary, the results of this work provide both quantitative and qualitative information to improve emission performance prediction and design of burners with application to a wide variation of fuel compositions.

## 15.6.2 Furnace Temperature Effects on NO<sub>x</sub><sup>102,103</sup>

### 15.6.2.1 Introduction

It has been well documented that NO<sub>x</sub> emissions increase with firebox temperature, assuming other variables are held constant. For example, suppose a burner is operating with a given fuel composition at a constant heat release, excess air level, and furnace temperature. If the furnace temperature were to increase due to a reduction in the heat transfer to the process tubes, NO<sub>x</sub> emissions would typically increase. In most gas firing applications, the NO<sub>x</sub> increase is due primarily to the increase in the reaction rate of oxygen and nitrogen at elevated temperatures. This NO<sub>x</sub> formation mechanism is called thermal NO<sub>x</sub>, which rises rapidly at gas temperatures above about 2000°F (1100°C) as demonstrated in the graph in Figure 15.8.

The American Petroleum Institute Recommended Practice 535 (API 535)<sup>104</sup> provides a published curve that demonstrates how the NO<sub>x</sub> emitted from a burner, firing at a given operating condition, is estimated to increase with furnace temperature (Figure 15.57).

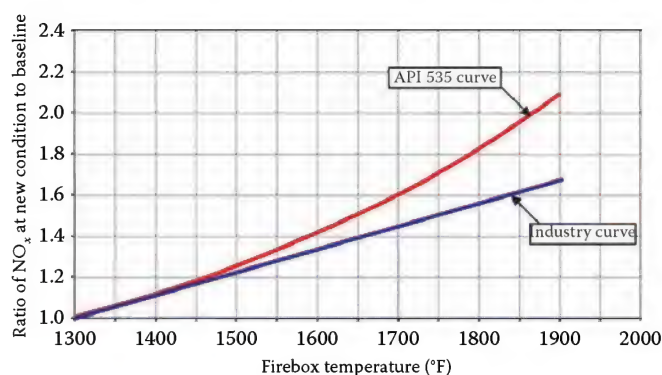


FIGURE 15.57

Effects of firebox temperature on NO<sub>x</sub>. (From Bussman, W. et al., The effect of firebox temperature on NO<sub>x</sub> emissions, *Proceeding of 2004 Air and Waste Management Conference*, Paper# 04-A-664-AWMA, Indianapolis, IN, June 2004.)

To approximate the variation in NO<sub>x</sub> emissions with firebox temperature, the known NO<sub>x</sub> is multiplied by the ratio of the values at each firebox temperature.

### Example 15.6

Assume a burner is generating 20 ppm NO<sub>x</sub> by volume on a dry basis (ppmvd) at a firebox temperature of 1600°F. What would happen to the NO<sub>x</sub> if the firebox temperature were to increase to 1800°F under identical burner firing conditions? Using the API 535 curve as shown in Figure 15.57, the increase in NO<sub>x</sub> can be estimated as follows:

$$\begin{aligned} \text{NO}_{x_{1800^{\circ}\text{F}}} &= \text{NO}_{x_{1600^{\circ}\text{F}}} \\ &\times \frac{\text{Ratio of NO}_x \text{ at new condition to baseline at } 1800^{\circ}\text{F}}{\text{Ratio of NO}_x \text{ at new condition to baseline at } 1600^{\circ}\text{F}} \\ \text{NO}_{x_{1800^{\circ}\text{F}}} &= 20 \times \frac{1.8}{1.4} = 25.7 \text{ ppm} \end{aligned}$$

This shows that the NO<sub>x</sub> is predicted to increase by nearly 30% with only a 200°F increase in furnace temperature.

The API 535 guidelines mention that the choice of burner can affect the variation in NO<sub>x</sub> emissions with firebox temperature. Although API 535 provides no reference to what style of burners were used to generate the curve or at what firing conditions, it has been used extensively in the burner industry to estimate the NO<sub>x</sub> emissions.

It was recognized that NO<sub>x</sub> emissions did not always follow the API 535 curve, so a new curve (see Figure 15.57) was developed by the industry to help improve NO<sub>x</sub> estimates. This curve provided information needed to reasonably estimate NO<sub>x</sub> emissions at various firebox temperatures for the so-called standard NO<sub>x</sub> burners. It predicts less of an increase in NO<sub>x</sub> with temperature than API 535. Notice that the two curves are similar up to about 1450°F, after which the difference becomes more significant.



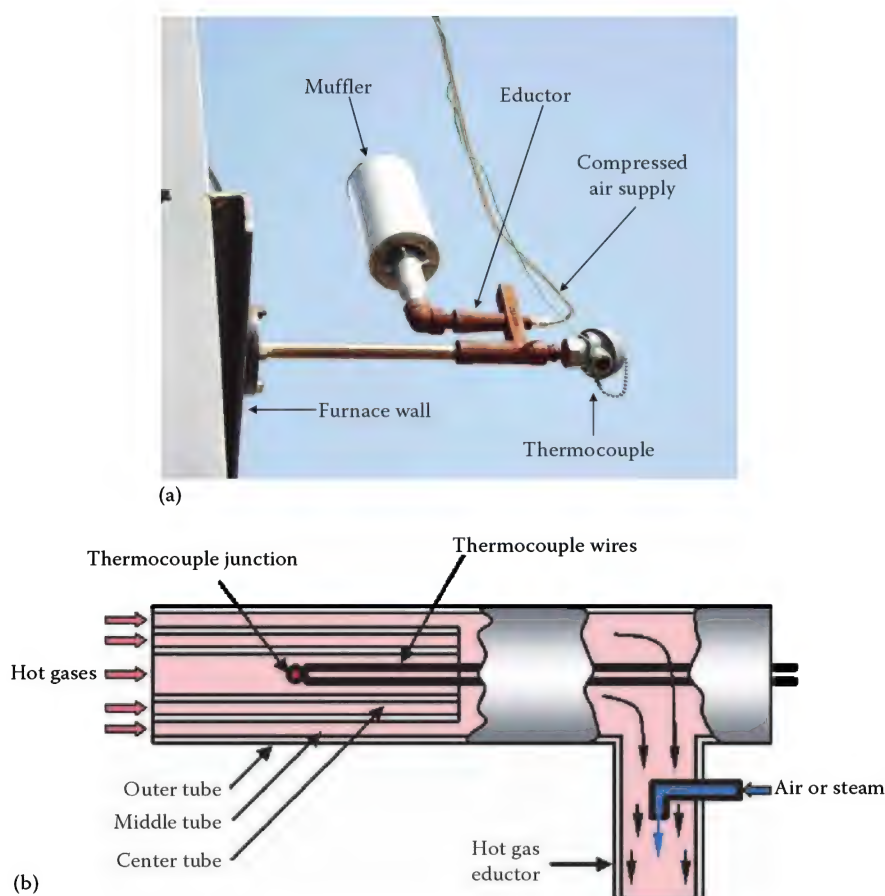


**FIGURE 15.58**

Velocity thermocouple (suction pyrometer): (a) photo and (b) schematic. (From Bussman, W. et al., The effect of firebox temperature on NO<sub>x</sub> emissions, *Proceeding of 2004 Air and Waste Management Conference*, Paper# 04-A-664-AWMA, Indianapolis, IN, June 2004.)

Some burner designs began to change considerably in the early 1990s, after the California regulations significantly reduced NO<sub>x</sub> requirements. Some of these new designs began to use a strategy that diluted the fuel with flue gas and air prior to combustion.<sup>105</sup> Today, due to tightened NO<sub>x</sub> regulations in many parts of the world, burner designs have further changed by using even more aggressive fuel dilution strategies. Test data gathered at The John Zink Research and Development Test Center demonstrated that these low NO<sub>x</sub> burner designs did not trend with either the API 535 curve or with the industry-developed curve. This discrepancy led to an effort to better understand the differences in NO<sub>x</sub> trends as a function of firebox temperature.<sup>102</sup>

Two styles of burners were tested for the effect of firebox temperature on NO<sub>x</sub>: (1) diffusion (sometimes called raw gas) burners and (2) partially premixed burners. Multiple burner configurations for each style, designed to simulate burners that generate varying degrees of NO<sub>x</sub>, were tested under different operating conditions.

#### 15.6.2.2 Furnace Temperature Measurement

During the testing, furnace temperatures were measured using suction pyrometers. The suction pyrometer uses an eductor system to aspirate furnace gases across a thermocouple that is recessed inside of a radiation shield as illustrated in Figure 15.58. This configuration maximizes the convection heat transfer to the thermocouple while minimizing radiation exchange between the thermocouple and its surroundings. Unshielded thermocouples can give temperatures up to 200°F (93°C) lower than a velocity thermocouple, because of radiation effects. Without proper correction, using unshielded thermocouples can lead to significant errors in accurately predicting NO<sub>x</sub> emissions. There have been instances where customers claimed that new low NO<sub>x</sub> burners did not meet NO<sub>x</sub> emissions guarantees. Upon further investigation, it was determined that the actual firebox temperature was significantly higher than specified by the customer. The higher temperatures naturally increase NO<sub>x</sub> emissions (see Figure 15.8). Therefore, it is critical that furnace temperatures are properly measured to predict expected NO<sub>x</sub> emission levels.

### 15.6.2.3 Test Results

Various types of diffusion and partially premixed burners producing a range of NO<sub>x</sub> emissions were tested. The fuel for all tests was 100% TNG which consisted of >90% methane. The furnace temperature was controlled using multiple insertable water-cooled lances where the insertion depth controlled the cooling surface area. The excess O<sub>2</sub> level in the exhaust products was varied from 2% to 4%. A forced-draft air preheater was used to control the temperature of the combustion air feeding the diffusion burners. The temperature of the pre-heated air was varied from ambient to 500°F (260°C).

Figure 15.59 shows the effect of firebox temperature on the NO<sub>x</sub> ratio for three different types of diffusion-style burners producing various levels of NO<sub>x</sub>. Here, standard, low, and ultralow NO<sub>x</sub> refers to NO<sub>x</sub> emissions of approximately 100, 30, and 10 ppmvd, respectively, at a firebox temperature of 1950°F (1070°C). All data were collected firing the burners at an excess O<sub>2</sub> level of 3%. The vertical axis is plotted as a ratio of NO<sub>x</sub> at the new condition to the baseline condition at 1300°F (700°C), similar to the API 535 curve discussed earlier. The baseline NO<sub>x</sub> value was determined by fitting an exponential curve through the data and extrapolating the NO<sub>x</sub> value at a firebox temperature of 1300°F (700°C). An exponential fit was used because thermal NO<sub>x</sub> is exponentially dependent on temperature (Figure 15.8). Notice that NO<sub>x</sub> depends on the type of burner. The data indicate that the more NO<sub>x</sub> the burner generates, the less sensitive it is to the NO<sub>x</sub> ratio at various firebox temperatures.

Figure 15.60 shows the effect of firebox temperature on the NO<sub>x</sub> ratio at O<sub>2</sub> levels of 2% and 4%, for the three

types of diffusion burners tested. The burners were tested at a heat release of  $3.5 \times 10^6$  Btu/h (1 MW). In all cases, the data indicate the furnace O<sub>2</sub> has an effect on the NO<sub>x</sub> ratio. The low and high NO<sub>x</sub> burners had similar trends where the NO<sub>x</sub> ratio was more sensitive at an O<sub>2</sub> level of 2% than at 4%. However, the ultralow NO<sub>x</sub> burner was more sensitive at 4% O<sub>2</sub>.

Figure 15.61 shows the effects of firebox temperature on NO<sub>x</sub> at various air pre-heat temperatures for the three diffusion burners tested. For the pre-heat temperatures tested, the data show that combustion air temperature did not substantially influence the response of the NO<sub>x</sub> ratio, regardless of whether the burner was a high, low, or ultralow NO<sub>x</sub> design. This suggests that air preheat may not substantially influence the mixing rate of the air, fuel, and furnace flue gases. If the mixing rate of the gases were substantially altered, there might be more variation in the NO<sub>x</sub> levels.

Two similar low NO<sub>x</sub> partially premixed burners were tested. Again, the NO<sub>x</sub> trends were somewhat different as shown in Figure 15.62, even for fairly similar style burners. Both increased faster than the API 535 curve. Figure 15.63 shows that diffusion and partially premixed burners with similar NO<sub>x</sub> levels produce similar increases in NO<sub>x</sub> as a function of firebox temperature.

### 15.6.2.4 Conclusions

There are several important conclusions regarding the effects of furnace temperature on NO<sub>x</sub>. The furnace temperature must be accurately measured to ensure that

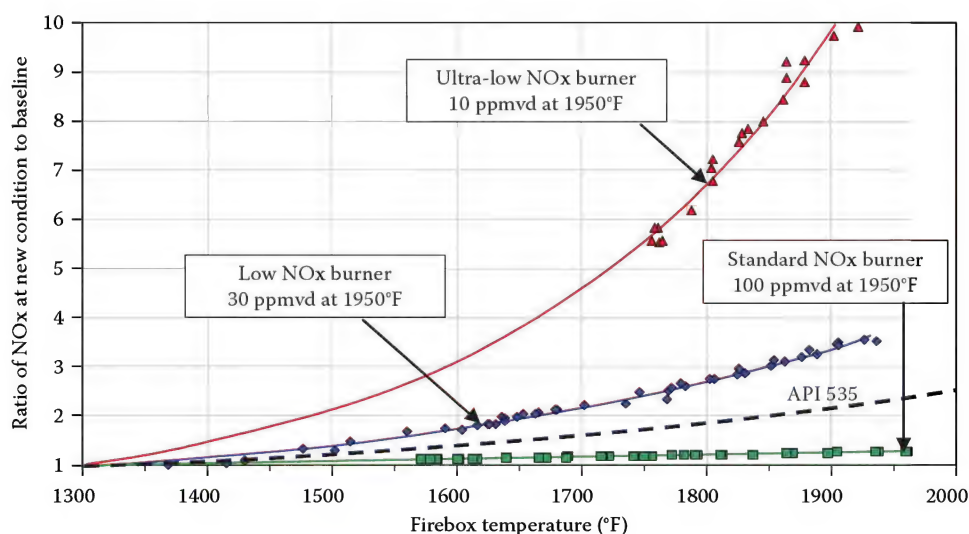


FIGURE 15.59

Effect of firebox temperature on NO<sub>x</sub> for various types of diffusion burners firing NG at 3% excess O<sub>2</sub>. (From Bussman, W. et al., The effect of firebox temperature on NO<sub>x</sub> emissions, *Proceeding of 2004 Air and Waste Management Conference*, Paper# 04-A-664-AWMA, Indianapolis, IN, June 2004.)

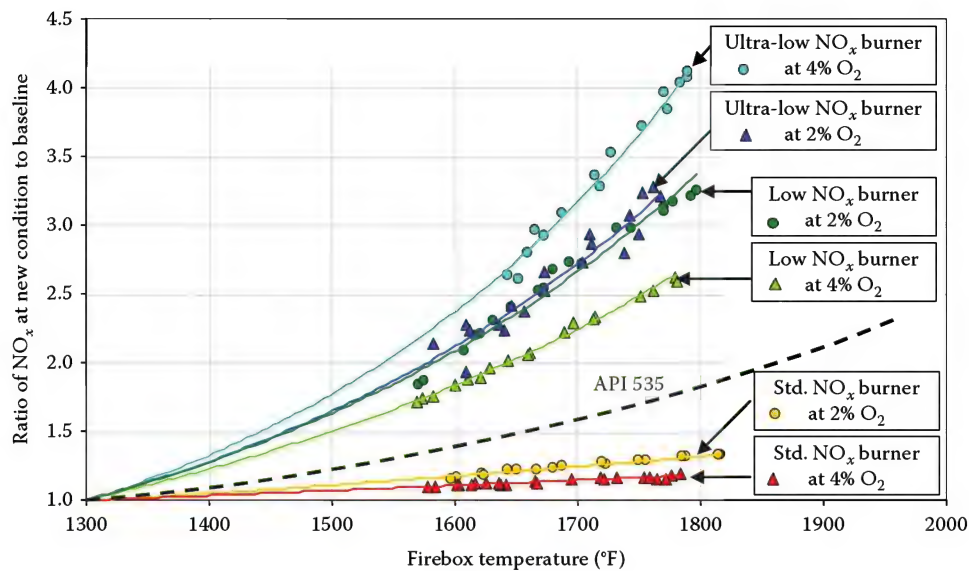


FIGURE 15.60

Effect of firebox temperature on NO<sub>x</sub> for various types of diffusion burners firing NG at various excess O<sub>2</sub> levels. (From Bussman, W. et al., The effect of firebox temperature on NO<sub>x</sub> emissions, *Proceeding of 2004 Air and Waste Management Conference*, Paper# 04-A-664-AWMA, Indianapolis, IN, June 2004.)

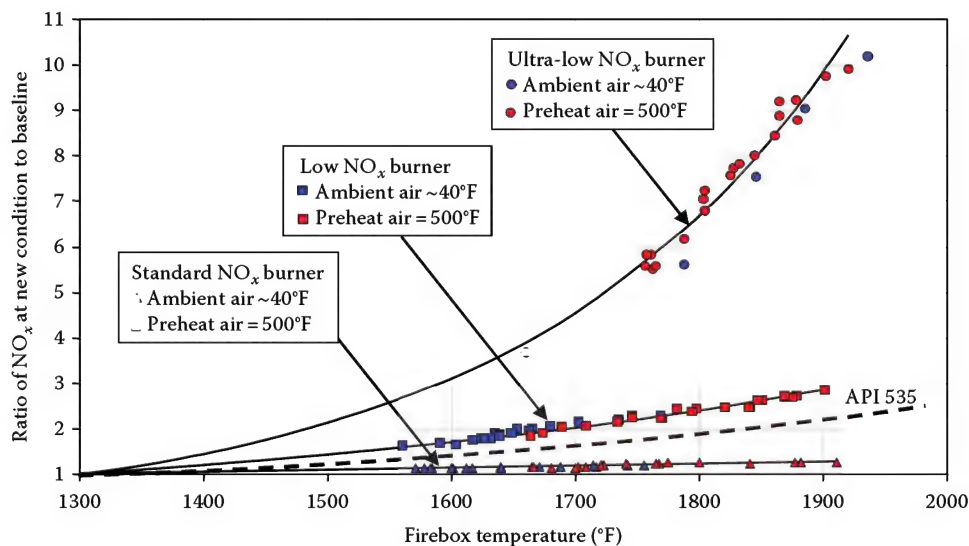


FIGURE 15.61

Effect of firebox temperature on NO<sub>x</sub> for various types of diffusion burners firing NG at 3% excess O<sub>2</sub> and various air preheat temperatures. (From Bussman, W. et al., The effect of firebox temperature on NO<sub>x</sub> emissions, *Proceeding of 2004 Air and Waste Management Conference*, Paper# 04-A-664-AWMA, Indianapolis, IN, June 2004.)

NO<sub>x</sub> predictions are not underestimated. Test data indicate that the more NO<sub>x</sub> the burner generated, the less sensitive it was to the NO<sub>x</sub> ratio at various firebox temperatures. The furnace O<sub>2</sub> had a significant effect on the NO<sub>x</sub> ratio, while combustion air temperature did not substantially influence the NO<sub>x</sub> ratio, regardless of whether the burner was a standard, low, or ultralow NO<sub>x</sub> design.

More importantly, the API 535 and industry correction curves could produce substantial errors in estimating NO<sub>x</sub> at firebox temperatures significantly different from

the known baseline. These two methods do not include the effects of burner design, excess O<sub>2</sub> level, or air preheat temperature. Other parameters such as fuel composition may also be important as shown in Figure 15.11. A general rule-of-thumb is that these corrections should only be used if the temperature difference between the baseline and the new operating condition is less than about 150°F (66°C). At higher differences, actual NO<sub>x</sub> data should be used where possible for more accurate predictions.



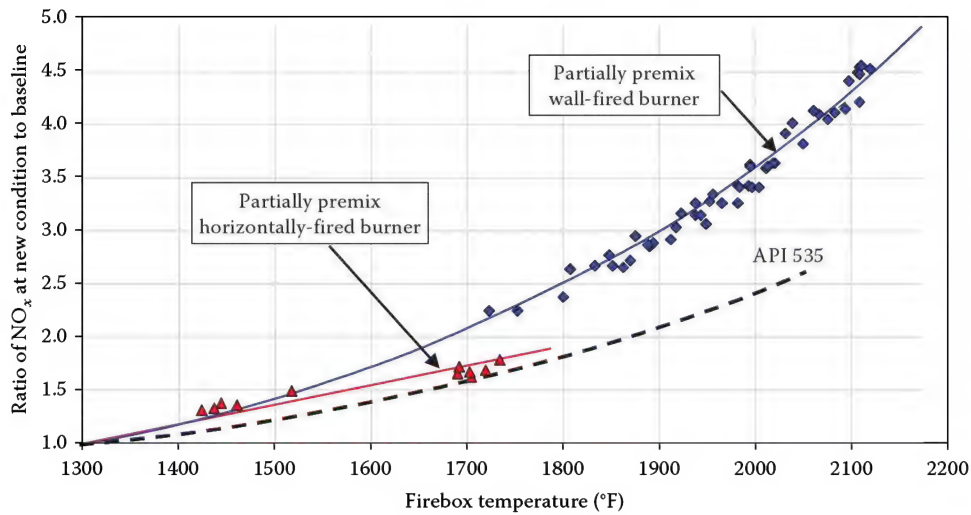


**FIGURE 15.62**

Effect of firebox temperature on NO<sub>x</sub> for various types of partially premixed burners firing NG at 3% excess O<sub>2</sub>. (From Bussman, W. et al., The effect of firebox temperature on NO<sub>x</sub> emissions, *Proceeding of 2004 Air and Waste Management Conference*, Paper# 04-A-664-AWMA, Indianapolis, IN, June 2004.)

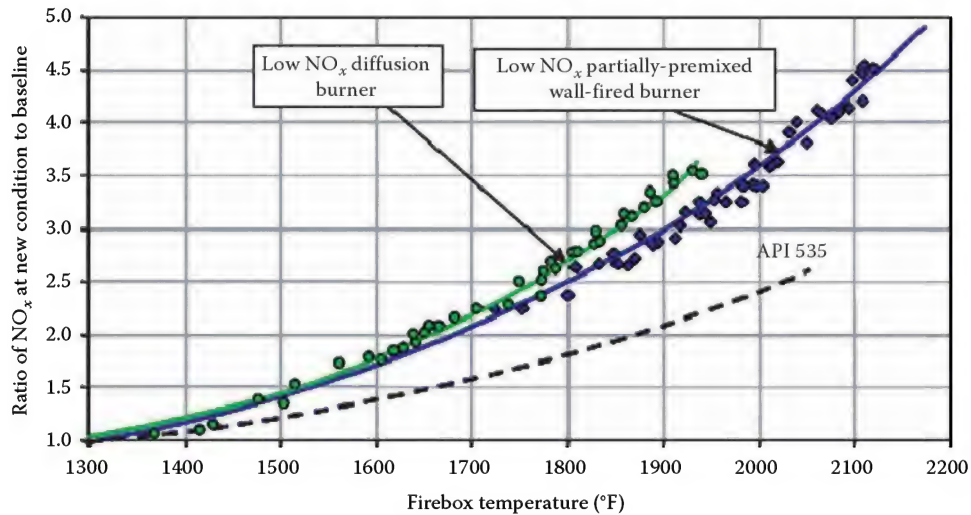


**FIGURE 15.63**

Effect of firebox temperature on NO<sub>x</sub> for diffusion and partially premixed low NO<sub>x</sub> burners firing on NG at 3% excess O<sub>2</sub>. (From Bussman, W. et al., The effect of firebox temperature on NO<sub>x</sub> emissions, *Proceeding of 2004 Air and Waste Management Conference*, Paper# 04-A-664-AWMA, Indianapolis, IN, June 2004.)

### 15.6.3 Ghost NO<sub>x</sub><sup>106</sup>

#### 15.6.3.1 Introduction

This section considers some experiments designed to study the potential error associated with the overall NO<sub>x</sub> (NO + NO<sub>2</sub>) emissions from process heaters. Field data suggest that the nitrogen oxide (NO<sub>x</sub> = NO + NO<sub>2</sub>) readings can be significantly different depending on the sample location within the furnace. For example, field data show that the NO<sub>x</sub> emissions in the furnace stack can be as much as 50% higher than for a sample

extracted before the convection section. This anomaly is referred to here as “ghost NO<sub>x</sub>.”

There are many possible hypotheses for why the “ghost NO<sub>x</sub>” anomaly might occur.

1. NO<sub>x</sub> meter does not measure NO<sub>2</sub>, only NO.
2. NO<sub>2</sub> readily dissolves in water during sampling.
3. NO<sub>2</sub> catalytically decomposes in the convection section.
4. Thermal NO<sub>x</sub> formation increases due to longer residence time.

5. NO<sub>x</sub> emissions are not uniformly distributed in the radiant section.
6. NO<sub>2</sub> to NO reduction converter in analyzer is not efficient.
7. NO<sub>x</sub> formation chemistry produces additional NO<sub>x</sub> in the convection section.

One or a combination of these could be a culprit in the NO<sub>x</sub> anomaly. Each of these hypotheses is briefly discussed next.

#### 15.6.3.1.1 NO<sub>x</sub> Meter Only Reads NO, Not NO<sub>2</sub>

Some NO<sub>x</sub> meters used in the field are not capable of reading NO<sub>2</sub>, but only the NO emissions. With these types of meters, NO<sub>2</sub> is calculated. For example, some portable meters do not directly measure NO<sub>2</sub>. Usually, the NO reading is multiplied by a correction factor with a value of about 1.05 to give an estimate of the total NO<sub>x</sub> (NO + NO<sub>2</sub>) emissions. This correction factor assumes that the NO<sub>2</sub> accounts for 5% of the total NO<sub>x</sub> emissions. Note that newer portable meters can measure both NO and NO<sub>2</sub>.

A typical burner, with NO<sub>x</sub> emissions of 30–50 ppm on a dry volume basis (ppmdv), will usually have about a 5%–10% NO<sub>2</sub> contribution to the total NO<sub>x</sub> based on previous test data. However, with new ultralow NO<sub>x</sub> burners, the NO<sub>2</sub> contribution may be significantly higher. "Some manufacturers and researchers have asserted that newer turbines with single-digit NO<sub>x</sub> concentrations may emit 50%–90% of the total NO<sub>x</sub> as NO<sub>2</sub>."<sup>107</sup>

#### 15.6.3.1.2 NO<sub>2</sub> Readily Dissolves in Water

Measuring NO<sub>2</sub> is the primary problem when determining the total NO<sub>x</sub> concentrations. NO<sub>2</sub> is highly soluble in water. If water is present in the flue gas sample line, the NO<sub>2</sub> will readily dissolve in it, yielding a low NO<sub>x</sub> reading. So, if a long sample line, that is not heat traced or insulated, is used to collect data in the radiant section and a short, heat traced sample line is used in the stack, it is possible that water could condense in the radiant section sample line and absorb more NO<sub>2</sub>. A critical step in proper sample conditioning is to prevent contact of gaseous NO<sub>2</sub> with condensed water;<sup>107</sup> this could result in a lower NO<sub>x</sub> reading in the radiant section than in the stack.

#### 15.6.3.1.3 Catalytic Decomposition of NO<sub>2</sub> through the Convection Section

Data in the literature show that NO<sub>2</sub> can dissociate into NO, N<sub>2</sub>, and O<sub>2</sub> if it comes in contact with a metal oxide at a high temperature.<sup>108–110</sup> The amount of dissociation depends largely on the type of metal oxide, and the temperature and composition of the surrounding gas. Data show that NO<sub>2</sub> cannot decompose to form NO if the metal does not have an oxide layer formed.<sup>108</sup>

**TABLE 15.7**

Data for NO<sub>2</sub> Decomposition over Metal Oxides at 773 K (842°F)

Catalyst	% NO <sub>2</sub> Conversion to NO
CO <sub>3</sub> O <sub>4</sub>	88.6
CuO	89.7
MnO <sub>2</sub>	87.0
V <sub>2</sub> O <sub>5</sub>	11.9
NiO	89.1
Fe <sub>2</sub> O <sub>3</sub>	80.6
SnO <sub>2</sub>	21.2
ZnO	7.3
Cr <sub>2</sub> O <sub>3</sub>	31.5
CeO <sub>2</sub>	88.3
TiO <sub>2</sub>	29.8
SiO <sub>2</sub>	1.6
ZrO <sub>2</sub>	37.8
Al <sub>2</sub> O <sub>3</sub>	36.1
MgO	17.8
La <sub>2</sub> O <sub>3</sub>	33.9
Nd <sub>2</sub> O <sub>3</sub>	89.9
CaO	19.9

Source: Reprinted from Shimokawabe, M. et al., *Applied Catalysis A: General*, 85, 129, 1992. With permission from Elsevier.

Certain metal oxides can exhibit high activity for decomposition of NO<sub>2</sub> to NO, while others show very little. Table 15.7 shows data for NO<sub>2</sub> decomposition over some common metal oxides at a temperature of 723 K (842°F).<sup>108</sup>

The literature suggests that many metal oxides approach a conversion equilibrium value with respect to reaction at a temperature of about 450°C (840°F). That temperature is usually in the range of the gas temperature and process tube skin temperatures in the convection section of a conventional process furnace. Therefore, it is possible that as the furnace flue gases flow through the convection section, the NO<sub>2</sub> reacts with the metal oxides on the process tubes to form NO, N<sub>2</sub>, and O<sub>2</sub>. If this reaction occurred in the convection section of a furnace, it would likely result in a higher NO concentration in the stack than in the radiant section.

Usually the first several rows of tubes ("shock tubes") in the convection section of a furnace are high alloy steel. At locations higher in the convection section, where the flue gas temperature is cooler and the tubes are not exposed to the direct radiation from the firebox, the tube material may be carbon steel. The composition of metal oxide formed on the tube depends on the material as illustrated in Figure 15.64.<sup>111</sup> This is a schematic showing the effect of chromium in Fe–Cr alloys on oxide scale structure based on isothermal oxidation



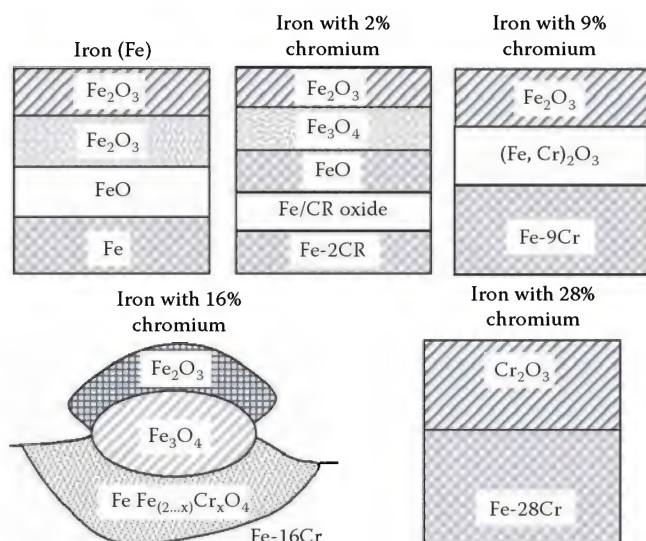


FIGURE 15.64

Schematic showing the effect of chromium in Fe-Cr allows an oxide scale structure based on isothermal oxidation studies at 1000°C (1800°F). (From Bussman, W. et al., Ghost NO<sub>x</sub>, Control #28, Air & Waste Management Association's 98th Annual Conference and Exhibition, Minneapolis, MN, June 21–24, 2005.)

studies at 1000°C (1800°F). Notice that for pure iron (Fe) and alloys with less than 16% chromium (Cr), the outer layer of metal oxide formed is Fe<sub>2</sub>O<sub>3</sub>. From Table 15.7, Fe<sub>2</sub>O<sub>3</sub> is very efficient at converting NO<sub>2</sub> to NO (80.6% at a temperature of 450°C or 840°F). Notice that the alloy with 28% chromium (310 stainless steel is 24%–26% Cr) produces an oxide scale composed of Cr<sub>2</sub>O<sub>3</sub>. In Table 15.7, Cr<sub>2</sub>O<sub>3</sub> is not as efficient at converting NO<sub>2</sub> to NO (31.5% at a temperature of 450°C or 840°F). Therefore, this suggests that higher alloy tubes with high chromium content may not produce as much “ghost NO<sub>x</sub>” as tubes with less chromium.

#### 15.6.3.1.4 NO<sub>x</sub> Formation due to Increased Residence Time

Thermal NO<sub>x</sub> is produced by the reaction of atmospheric oxygen and nitrogen at elevated temperatures, and is considered to be the dominant mechanism in industrial gas-fired combustion. The amount of thermal NO<sub>x</sub> formed depends largely on the temperature of the gas and the residence time. The higher the temperature and the longer the residence time, the more NO<sub>x</sub> is formed. This hypothesis suggests that a NO<sub>x</sub> reading in the radiant section could be lower than in the stack because additional NO<sub>x</sub> is generated due to the longer residence time as the gas flows through the convection section to the stack.

This hypothesis probably does not account for the “ghost NO<sub>x</sub>” anomaly, however, because very high temperatures are required to produce a substantial amount of thermal NO<sub>x</sub>. The flue gas temperature just below the convection section might be as high as 2200°F

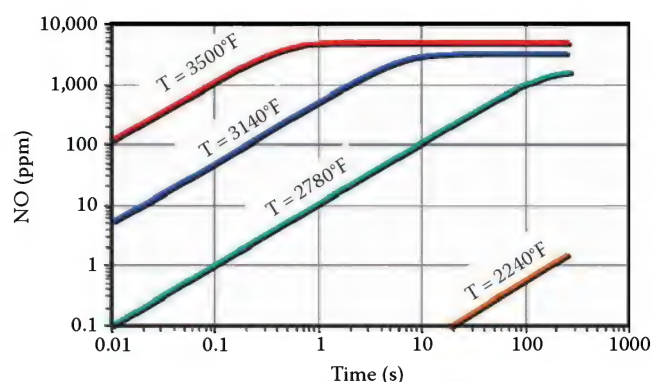


FIGURE 15.65

A plot showing predicted NO concentration as a function of time for various exhaust gas temperatures. (From Bussman, W. et al., Ghost NO<sub>x</sub>, Control #28, Air & Waste Management Association's 98th Annual Conference and Exhibition, Minneapolis, MN, June 21–24, 2005.)

(1200°C) in some instances, but quickly cools as the flue gas flows through the convection section. These relatively cool gas temperatures probably do not account for the substantial increase in NO<sub>x</sub> emissions observed from the radiant section to the stack as demonstrated in Figure 15.65. The plot in Figure 15.65 shows predicted NO concentration as a function of time for various exhaust gas temperatures. These calculations are based on an approximate solution of the Zeldovich mechanism with 3% O<sub>2</sub> in the exhaust.<sup>112</sup> The results demonstrate that at a flue gas temperature of 2240°F (1230°C), which is a typical flue gas temperature entering into the convection section of an ethylene cracking furnace, approximately 200 s of residence time is required to increase the NO concentration by 1 ppm. There is not enough additional residence time to account for the observed increase in NO<sub>x</sub>.

#### 15.6.3.1.5 Distribution of NO<sub>x</sub> Emissions in the Furnace

Experimental results from a refinery furnace and testing in a pilot-scale test furnace clearly demonstrate that high gradients in NO<sub>x</sub> concentration, just before the convection section, exist (data will be shown later). For example, over a span of only 20 in. (51 cm) in the large-scale pilot test furnace, the NO<sub>x</sub> concentration varied from 50 to 58 ppmvd. The NO<sub>x</sub> concentration in the stack was approximately 56 ppmvd. These data clearly demonstrate that one must be careful in using readings within the radiant section as the total emissions from the furnace. This also demonstrates that the gradient in NO<sub>x</sub> concentration could also be a culprit for the “ghost NO<sub>x</sub>” anomaly. Care must be taken where measurements are made. Traverses across the flow area are recommended in case the concentration of NO<sub>x</sub> is not uniform.

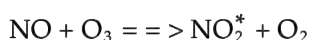
Another potential cause for the difference in NO<sub>x</sub> readings before and after the convection section could



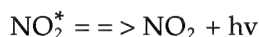
be the formation of a high temperature plume in the center of the furnace. This phenomenon has been known to occur in furnaces with larger cross sections. A higher temperature plume of gas develops in the center of the furnace, with cooler gases close to the walls. This plume can penetrate into the convection section, leading to continued thermal NO<sub>x</sub> formation.

#### 15.6.3.1.6 NO<sub>2</sub> to NO Reduction Converter Efficiency

Nitric oxide reacts with ozone to produce chemiluminescence. When a sample gas containing NO and ozone gas are mixed in a container (reactor), the following reaction occurs:



where NO<sub>2</sub><sup>\*</sup> is an NO<sub>2</sub> molecule in an excited state. When the NO<sub>2</sub> molecules in the excited state return to the ground state, the excitation energy is emitted as light:



Since the degree of luminescence is directly proportional the amount of NO molecules, the concentration of NO in the sample gas can be determined by measuring the intensity of light emitted. To measure NO<sub>x</sub> (NO + NO<sub>2</sub>), the NO<sub>2</sub> is reduced into NO by a reduction converter. The total NO<sub>x</sub> can then be detected as the original exhaust concentration of NO plus the NO concentration resulting from NO<sub>2</sub> to NO conversion. These converters are usually high-temperature devices that contain a reducing surface, typically molybdenum or carbon.<sup>113</sup> The reduction converter used in the laboratory tests reported here was stainless steel coated with molybdenum. Notice in Table 15.7 that molybdenum oxide scale (MnO<sub>2</sub>) is very efficient at converting NO<sub>2</sub> to NO (87% at a temperature of 450°C or 840°F).

Typically, a new reduction converter can convert about 90%–95% of the NO<sub>2</sub> to NO. However, after a period of use, the converter's efficiency deteriorates substantially. This has been demonstrated in previous tests using the same laboratory analyzer. Therefore, two analyzers might not provide identical NO<sub>x</sub> readings if the reduction converter efficiency is not the same for each analyzer, even though each was calibrated on the same NO span gas.

#### 15.6.3.1.7 NO<sub>x</sub> Formation Chemistry

Other NO<sub>x</sub> formation mechanisms within the convection section are also possible. For example, the formation of the N<sub>2</sub>O intermediate is important in lower temperature fuel-lean combustion applications like lean

premix.<sup>114</sup> The NNH route is another potential intermediate route that should be investigated.<sup>115</sup>

The role of prompt NO<sub>x</sub> formation may have been important in the convection section. It is possible that HCN or NH<sub>3</sub> were present and then converted to NO in the convection section. This effect can be enhanced if there is O<sub>2</sub> stratification in the furnace. All of these potential chemistry effects were beyond the scope of this investigation.

#### 15.6.3.2 Test Description

The laboratory tests were performed in a pilot scale test furnace. Figure 15.66 is a schematic showing the laboratory test arrangement. The setup allowed for a sample probe to be inserted at three locations just before the convection section or at three locations in the middle of the convection section as shown in Figure 15.66. The probe depth could also be adjusted to various depths within the convection section. The flue gas sample was pulled through a heat-traced Teflon tube to a remotely located chemiluminescent NO<sub>x</sub> analyzer. Flue gas samples were also collected from a sample port located approximately 10' (3 m) below the top of the furnace and stack exit plane. Those samples were also pulled through a heat-traced Teflon tube to the same NO<sub>x</sub> analyzer.

Tests were performed using state-of-the-art CEMs to measure emissions species concentrations of NO<sub>x</sub>, CO, and O<sub>2</sub>. Stack samples were continuously extracted at high flow rates to minimize response time. A continuous sample was fed to a condenser/conditioner, which cooled the sample to 1°C dew point. Once the moisture was removed, the dry sample flowed to the CEM for species analysis.

The reduction converter efficiency was determined using NO<sub>2</sub> span gas with 16.5 ppm. With this span gas, the analyzer read a value of 14.6 ppm, for a conversion efficiency of 88%. This compared very favorably with the 87% conversion efficiency reported in Table 15.7 for MnO<sub>2</sub>.

Field tests were also performed in a full-scale ethylene cracking furnace comprised of multiple floor and wall burners operating at a total heat release of approximately 235 × 10<sup>6</sup> Btu/h (68.9 MW). The setup allowed for a sample probe to be inserted at various locations through sight ports within the furnace radiant section and crossover section located just before the convection section. The probe length was approximately 10' (3 m) long and could be adjusted to various depths within the furnace. The flue gas sample was pulled through a heat-traced Teflon tube to a remotely located CEM.

Tests were performed using state-of-the-art CEMs. Stack samples were continuously extracted at high flow rates to measure emissions species concentrations of NO<sub>x</sub>, CO, and O<sub>2</sub>. A continuous sample was fed to a condenser/conditioner, which cools the sample to 1°C dew point. Once the moisture was removed, the dry sample

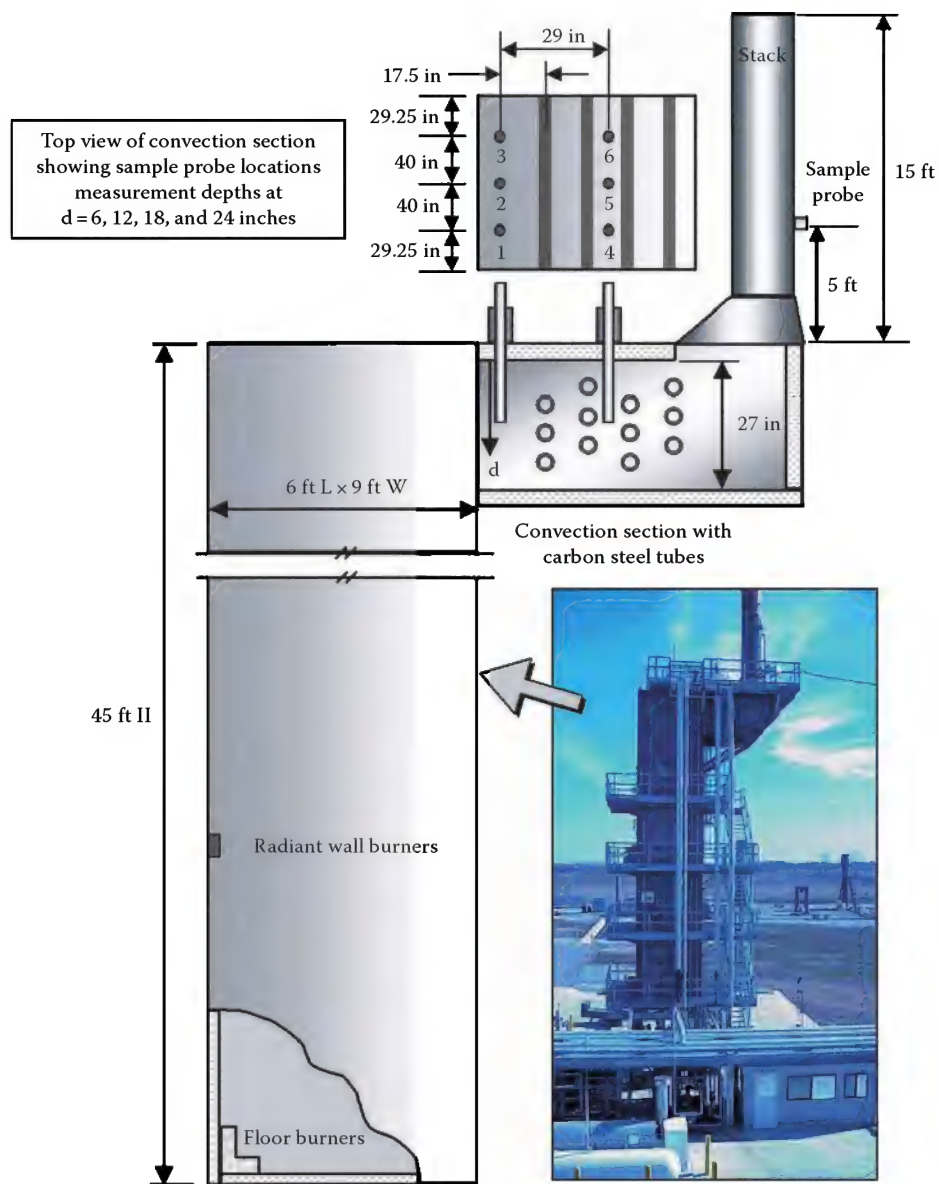


FIGURE 15.66

Schematic showing test furnace and sample probe locations. (From Bussman, W. et al., Ghost NO<sub>x</sub>, Control #28, *Air & Waste Management Association's 98th Annual Conference and Exhibition*, Minneapolis, MN, June 21–24, 2005.)

flowed to the CEM for species analysis. The reduction converter efficiency of 96% was determined using NO<sub>2</sub> span gas.

### 15.6.3.3 Results

The laboratory tests are considered first. Figure 15.67a and b are plots of the NO at locations before and in the middle of the convection section at various depths. These data were collected at a total furnace heat release of  $14.7 \times 10^6$  Btu/h (4.3 MW) burning 100% TNG (>90% CH<sub>4</sub>) at 3% O<sub>2</sub> in the dry exhaust products. The

data clearly show that the NO<sub>x</sub> concentration varied by a maximum of 15% over a distance of 18 in. (46 cm) through the convection section, demonstrating that the NO<sub>x</sub> was highly stratified within the convection section.

The stratification of NO<sub>x</sub> might have been due to recirculating flow patterns inside the furnace. It is speculated that the flow pattern of furnace flue gases might look similar to that as illustrated in Figure 15.68. As the hot combustion products turn 90° into the convection section, they create a recirculation zone in the upper corner of the furnace. Also, in Figure 15.68 is a streak photograph showing small particles flowing through two 90° elbows.<sup>116</sup> Notice in this photograph

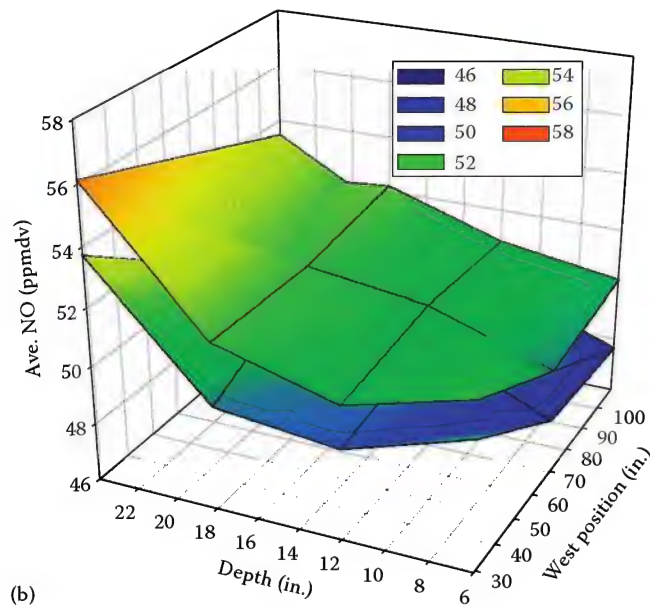
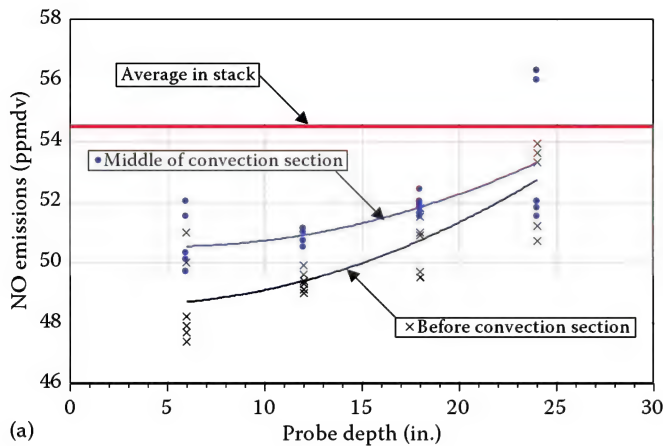


FIGURE 15.67

(a) NO emissions at locations before and in the middle of the convection section at various depths and (b) top surface is in middle of convection section, bottom surface before convection section. (From Bussman, W. et al., Ghost NO<sub>x</sub>, Control #28, Air & Waste Management Association's 98th Annual Conference and Exhibition, Minneapolis, MN, June 21–24, 2005.)

that there is a small recirculation zone in the upper corner of the first 90° elbow. This recirculation zone, containing relatively cool gas, might extend into the convection section of the furnace and create the NO<sub>x</sub> stratification observed.

Also, notice in Figure 15.68 that the NO appears to be slightly lower at a location before the convection section than at a location in the middle of the convection section for all depths tested. This suggests that the carbon steel convection tubes might be acting as a catalyst and converting the NO<sub>2</sub> to NO, one of the possible culprits for the "ghost NO<sub>x</sub>" anomaly.

Figure 15.69a and b are plots of NO<sub>x</sub> (NO + NO<sub>2</sub>) at locations before and in the middle of the convection

section at various depths. The data clearly show that NO<sub>x</sub> varied by a maximum of 11% over a distance of 18 in. (46 cm). Notice that the NO<sub>x</sub> appeared to be lower at a location before the convection section than at a location in the middle of the convection section, for all depths tested. It is unclear why this occurred because the total NO<sub>x</sub> (NO + NO<sub>2</sub>) should be conserved between these two locations. Perhaps the recirculation pattern in the upper corner of the firebox created this anomaly. At a probe depth of 24 in. (61 cm), the average NO<sub>x</sub> in the stack appears to be in the center of the data scatter for NO<sub>x</sub> collected at various locations in the convection section.

The convection tube skin temperature in the test furnace might not have been high enough to provide substantial conversion of NO<sub>2</sub> to NO. In the first few rows

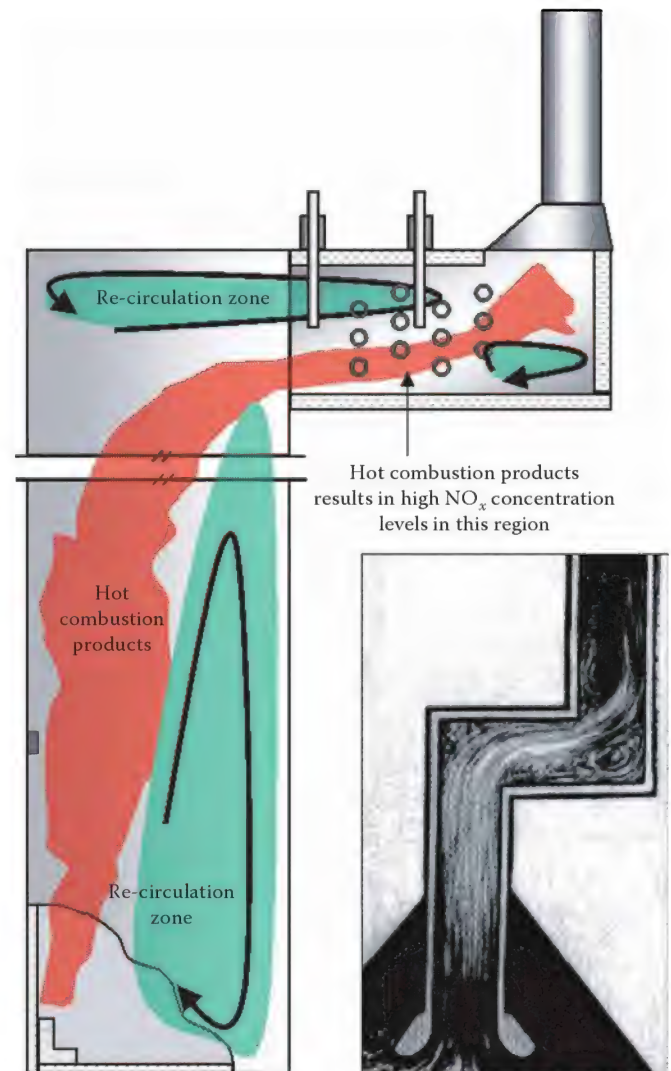
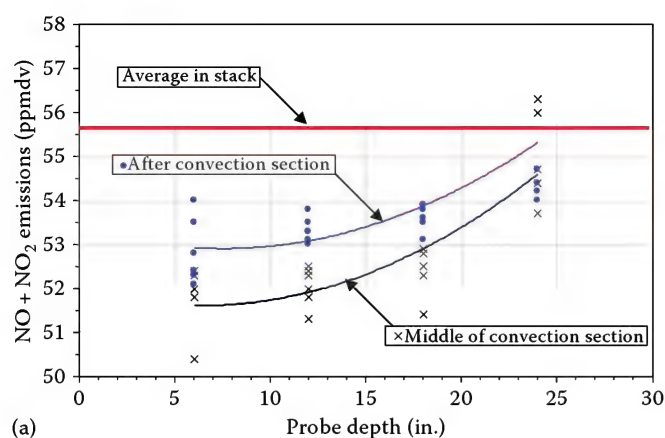


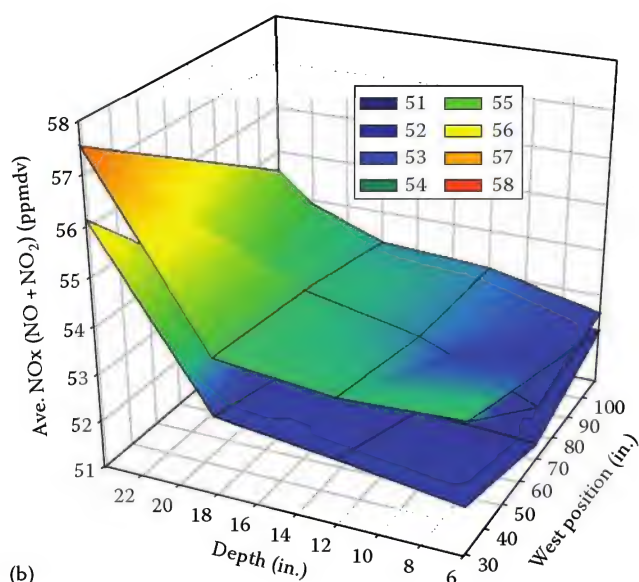
FIGURE 15.68

Illustration showing theorized flow pattern within test furnace. Also shown is a streak photograph of particles flowing through two 90° turns. (From Bussman, W. et al., Ghost NO<sub>x</sub>, Control #28, Air & Waste Management Association's 98th Annual Conference and Exhibition, Minneapolis, MN, June 21–24, 2005.)





(a)



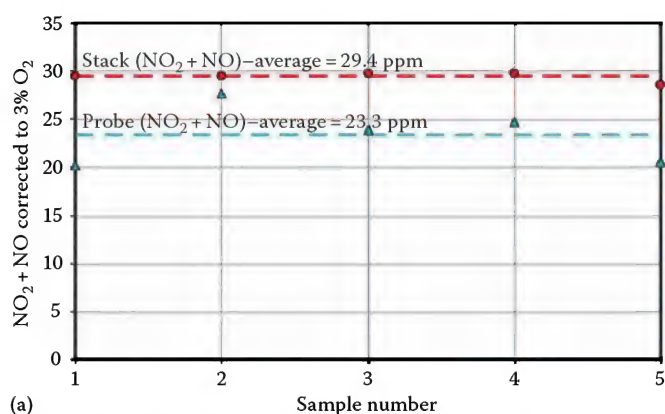
(b)

**FIGURE 15.69**

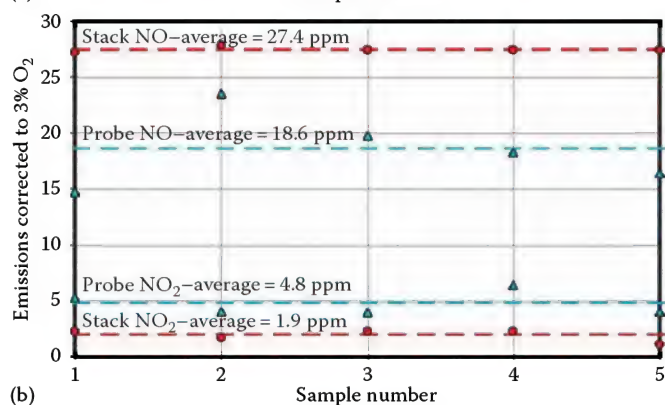
(a) NO<sub>x</sub> (NO + NO<sub>2</sub>) at locations before and in the middle of the convection section at various depths and (b) top surface is in middle of convection section, bottom surface before convection section. (From Bussman, W. et al., *Ghost NO<sub>x</sub>, Control #28, Air & Waste Management Association's 98th Annual Conference and Exhibition*, Minneapolis, MN, June 21–24, 2005.)

of the convection section of a typical ethylene cracking furnace, the tube skin temperature can reach values above 1800°F (980°C).

Next, the field test results were considered. Figure 15.70a is a plot of the NO<sub>x</sub> (NO + NO<sub>2</sub>), corrected to 3% O<sub>2</sub>, at various locations in the upper 10 ft (3 m) of the radiant section. These data were collected at a total furnace heat release of  $235 \times 10^6$  Btu/h (68.9 MW) burning a typical refinery fuel at approximately 5.7% O<sub>2</sub> in the stack. The data show that the overall average NO<sub>x</sub> value was 26% lower in the upper zone of the radiant section than at the stack exit. The data also show that variations in probe readings within the radiant section varied significantly (approximately 40%), but were fairly constant at the stack exit.



(a)



(b)

**FIGURE 15.70**

(a) NO<sub>x</sub> (NO + NO<sub>2</sub>) at various locations in the upper 10' (3 m) of the radiant section of the field test furnace and (b) NO and NO<sub>2</sub> at various locations in the upper 10' (3.0 m) of the radiant section of the field test furnace. (From Bussman, W. et al., *Ghost NO<sub>x</sub>, Control #28, Air & Waste Management Association's 98th Annual Conference and Exhibition*, Minneapolis, MN, June 21–24, 2005.)

Figure 15.70b is a plot of the NO and NO<sub>2</sub> at various locations in the upper 10 ft (3 m) of the radiant section; the data correspond to the plotted values in Figure 15.70a. The data show that the overall average NO<sub>2</sub> value was 152% lower in the stack than in the upper zone of the radiant section. However, the NO was 147% higher in the stack than in the upper zone of the radiant section. This trend appears to suggest NO<sub>2</sub> was converted to NO as the flue gas passed through the convection section.

#### 15.6.4 Down-Fired Burner<sup>117</sup>

Hydrogen has become more prominent in the recent past because of the potential it holds to improve the environmental performance of fuels as well as its use as an energy source.<sup>118</sup> Steam methane reforming (SMR) has become the technology of choice for producing hydrogen because it is relatively simple, and cost-effective.<sup>119,120</sup>

Typical SMR furnaces are designed with several rows of burners that fire vertically down from the ceiling

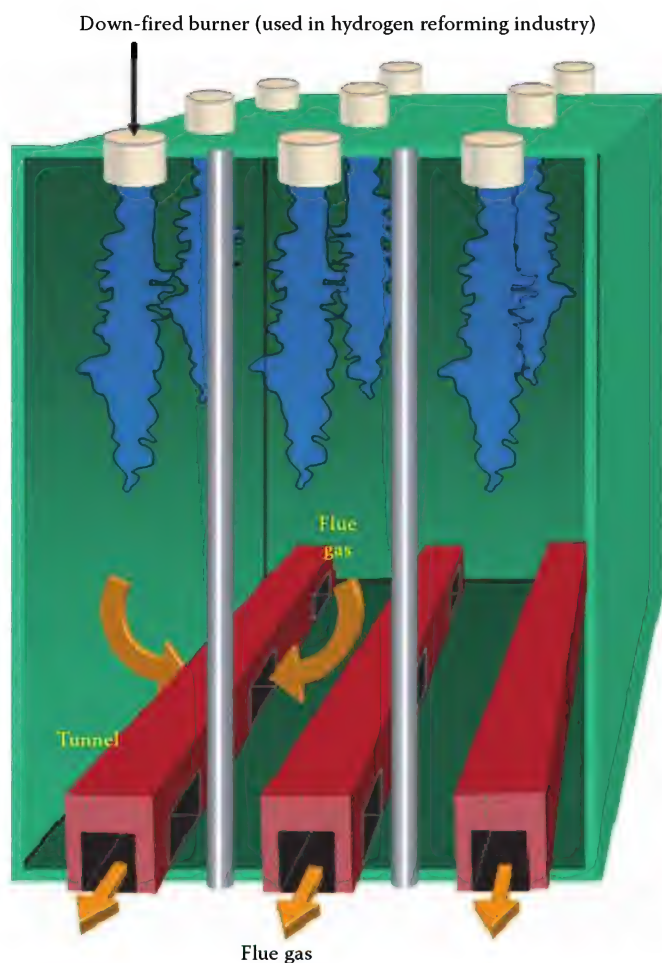


FIGURE 15.71

Schematic showing the layout of a typical reforming furnace. (From Bussman, W. et al., Low NO<sub>x</sub> down-fired burners for reforming furnaces, *Air & Waste Management Association's 101st Annual Conference and Exhibition*, Paper #219, Portland, OR, June 2008.)

of the furnace<sup>121</sup> as illustrated in Figure 15.71. These burners, referred to as down-fired burners, are located between multiple rows of catalyst-filled process tubes. Burners are fired from the ceiling because the catalyst-filled tubes demand the maximum heat density near the incoming feed at the top of the furnace to start the reforming reaction inside the tubes.

Burners located in the outer rows are commonly designed to fire at a lower heat release than the burners located in the inner rows; typically the outer row of burners fire about 65% of the heat release of the inner burners and are referred to here as the 65% capacity burners. The outer rows of burners fire at a lower heat release because there is only one row of tubes to absorb the heat from the flames, whereas the center row, referred to as the 100% capacity burners, has two rows of tubes absorbing heat (Figure 15.71).

Down-fired burners are often dual-fuel burners firing both a makeup fuel and a waste gas. The makeup

fuel is usually NG or refinery fuel gas; although, other fuels are used such as naphtha, No. 2 fuel oil, diesel oil, or a propane/butane gas fuel (see Chapter 3). Typically, start-up of the furnace is accomplished by firing the makeup gas that is generally supplied at a pressure ranging from 25 to 35 psig. The waste gas consists of a pressure swing adsorption (PSA) off-gas usually referred to as tail gas. This fuel gas is a low-pressure (2–3 psig), low heating value fuel produced as a by-product of a PSA process, a key purification component in the steam reforming hydrogen production process. A typical PSA composition is 17% CH<sub>4</sub>, <1% H<sub>2</sub>O, 28% H<sub>2</sub>, 44% CO<sub>2</sub>, 10% CO, and <1% N<sub>2</sub>. The makeup fuel and PSA gas can be blended together before the burner, but are usually supplied to the burner in separate manifolds (Figure 15.73).

The most significant variables influencing NO<sub>x</sub> emissions from a down-fired burner include (1) furnace temperature, (2) combustion air temperature, (3) burner turndown, (4) percent excess air, (5) percent PSA gas duty, and (6) composition of PSA gas. Figure 15.74 shows the effects of furnace temperature on NO<sub>x</sub> emissions for a conventional, low NO<sub>x</sub>, and ultralow NO<sub>x</sub> down-fired burner. Notice that the ultralow NO<sub>x</sub> and low NO<sub>x</sub> burners are more sensitive to furnace temperature than the conventional type burner design.

The MK-II burner (Figure 15.73) was fired in a pilot-scale test furnace (Figure 15.72). Figure 15.75 shows the effects of combustion air temperature on NO<sub>x</sub> emissions at several burner turndown conditions firing the ultralow NO<sub>x</sub> burner. The NO<sub>x</sub> emissions were corrected to 1900°F (1000°C) and 3% O<sub>2</sub> with units of pounds per million Btu on a dry volume basis (lb<sub>m</sub>/10<sup>6</sup> Btu, dry vol.). The data were generated with the burner firing 55% of the total heat release on PSA gas with the balance as NG makeup fuel. Over the range of firing capacities tested, the furnace temperature varied from approximately 1750°F to 2050°F (954°C–1120°C). For all test cases, the furnace O<sub>2</sub> concentration was approximately 3% on a dry volume basis.

Figure 15.75 clearly shows that NO<sub>x</sub> increased as the combustion air temperature increased. The data show that NO<sub>x</sub> approximately doubled as the combustion air temperature increased from ambient temperature to 800°F (430°C) ° is degree symbol. This trend is largely attributed to the increase in flame temperature, resulting in the increased rate of thermal NO<sub>x</sub>.

The data in Figure 15.75 also show that NO<sub>x</sub> decreases as burner heat release increases. For example, for a combustion air temperature of 600°F (300°C), NO<sub>x</sub> decreases from 0.045 to 0.03 lb<sub>m</sub>/10<sup>6</sup> Btu as the heat release increases from 6 to 9 million Btu/h (2 to 3 MW). One explanation for this trend is that as the fuel pressure decreases, it loses its efficiency at entraining furnace flue gas; this





**FIGURE 15.72**

Test furnace and MK-II™ burner. (From Bussman, W. et al., Low NO<sub>x</sub> down-fired burners for reforming furnaces, *Air & Waste Management Association's 101st Annual Conference and Exhibition*, Paper #219, Portland, OR, June 2008.)

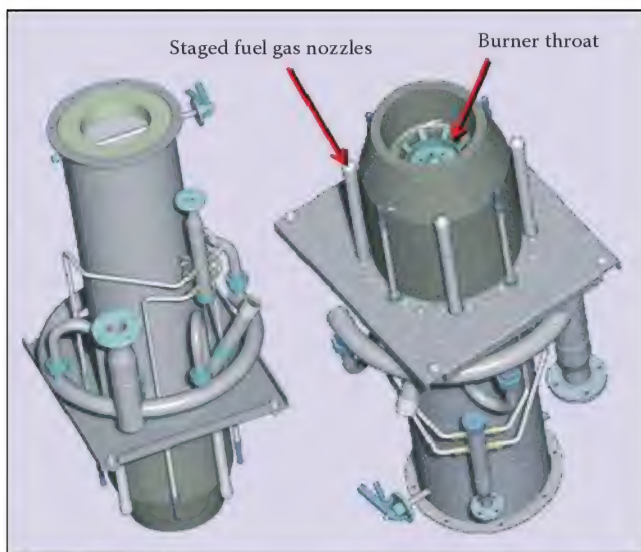


**FIGURE 15.73**

Schematic of the MK-II™ burner. (From Bussman, W. et al., Low NO<sub>x</sub> down-fired burners for reforming furnaces, *Air & Waste Management Association's 101st Annual Conference and Exhibition*, Paper #219, Portland, OR, June 2008.)

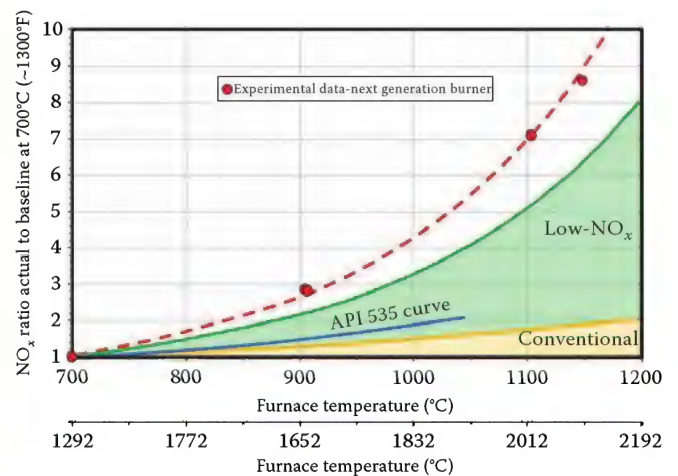


**FIGURE 15.74**

Effects of furnace temperature on NO<sub>x</sub> emissions. (From Bussman, W. et al., Low NO<sub>x</sub> down-fired burners for reforming furnaces, *Air & Waste Management Association's 101st Annual Conference and Exhibition*, Paper #219, Portland, OR, June 2008.)



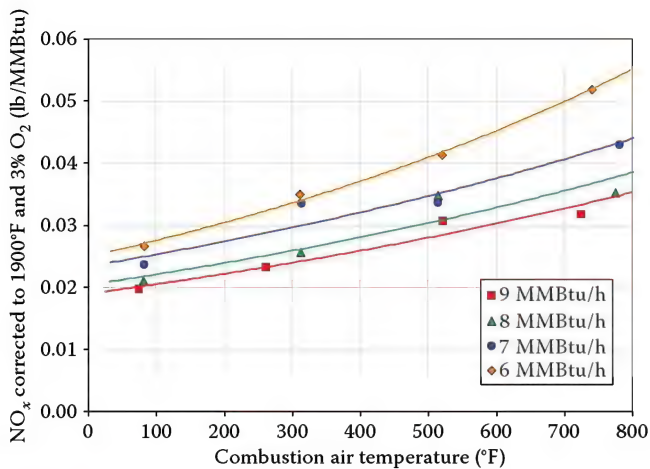


**FIGURE 15.75**

Effects of combustion air temperature on NOx emissions at various turn-down conditions. (From Bussman, W. et al., Low NOx down-fired burners for reforming furnaces, *Air & Waste Management Association's 101st Annual Conference and Exhibition*, Paper #219, Portland, OR, June 2008.)

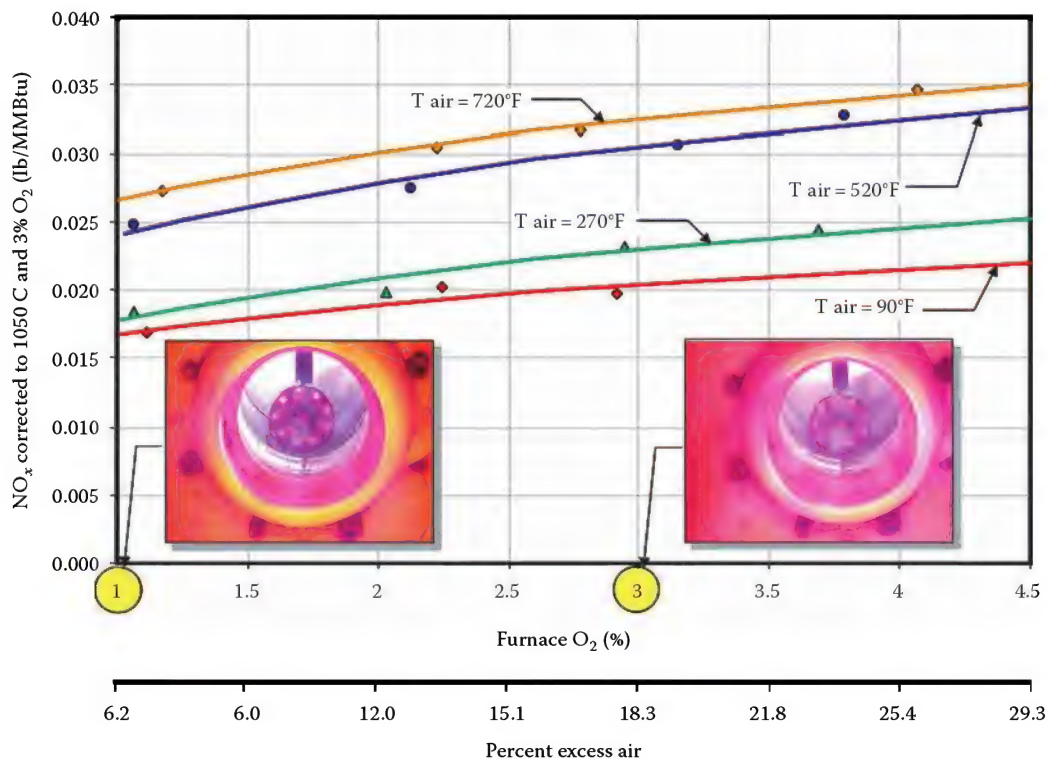
causes the flame temperature to increase, resulting in higher NOx.

Figure 15.76 shows the effects of percent excess air on NOx for various combustion air temperatures. The data show that as the percent excess air (or furnace O<sub>2</sub> concentration) increases, NOx increases. Also included in Figure 15.76 are photographs of the burner firing at an

O<sub>2</sub> concentration of 1% (6.2% excess air) and 3% (18.3% excess air). These photographs show that at an O<sub>2</sub> concentration of 3% the flame is more visible compared to the burner operating at 1% O<sub>2</sub>. These photographs demonstrate that increasing the O<sub>2</sub> concentration alters the flame appearance by causing more intense combustion in the near-burner region. When this occurs, flue gas entrainment and mixing with the fuel prior to combustion is reduced, leading to increased NOx emissions.

Figure 15.77 shows photographs of an ultralow NOx, low NOx, and conventional style burner technology firing inside a test furnace. Notice the bright yellow, intense flame produced by the conventional burner. This appearance indicates the flame temperature was much hotter than the light-blue flames produced by the low-NOx burners. The light-blue flames produced by the low-NOx burners indicate that the fuel was entraining substantial amounts of flue gas prior to combustion, resulting in flames that were much cooler than the flame produced by the conventional burner.

The data in Figure 15.78 show that as the proportion of PSA gas increased, NOx decreased. This trend occurred because the PSA gas consisted of a substantial amount of CO<sub>2</sub> gas. CO<sub>2</sub> is an inert gas that acts as a ballast to absorb heat during combustion. By absorbing heat, the flame temperature is reduced, resulting in lower NOx emissions as demonstrated in Figure 15.80. The three photographs



**FIGURE 15.76**

Effects of furnace O<sub>2</sub> concentration (excess air) on NOx emissions at various combustion air temperatures. (From Bussman, W. et al., Low NOx down-fired burners for reforming furnaces, *Air & Waste Management Association's 101st Annual Conference and Exhibition*, Paper #219, Portland, OR, June 2008.)

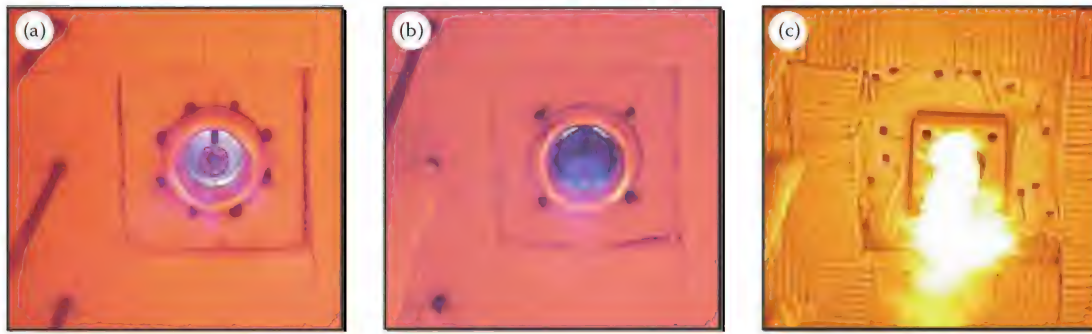


FIGURE 15.77

Photographs of (a) MK-II™, (b) low-NO<sub>x</sub>, and (c) conventional burner technologies. (From Bussman, W. et al., Low NO<sub>x</sub> down-fired burners for reforming furnaces, *Air & Waste Management Association's 101st Annual Conference and Exhibition*, Paper #219, Portland, OR, June 2008.)

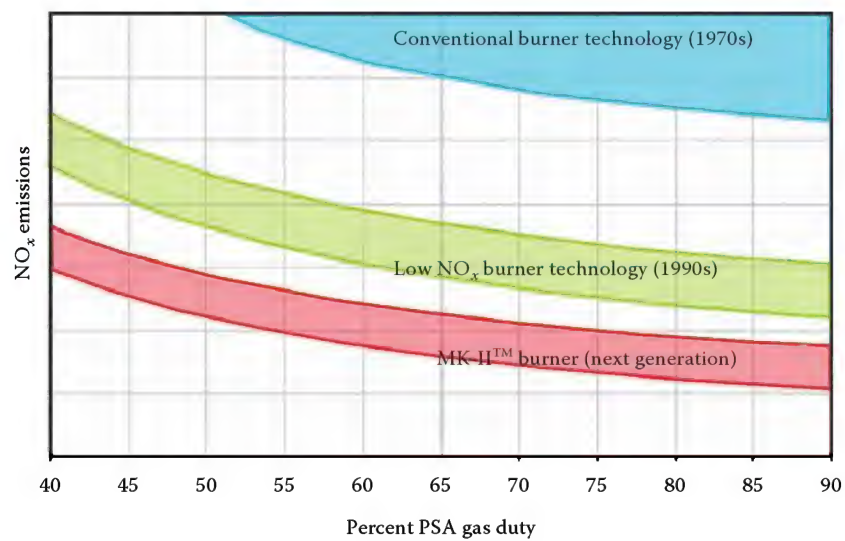


FIGURE 15.78

Comparison of NO<sub>x</sub> emissions for the conventional, low-NO<sub>x</sub> and MK-II™ burner technologies. (From Bussman, W. et al., Low NO<sub>x</sub> down-fired burners for reforming furnaces, *Air & Waste Management Association's 101st Annual Conference and Exhibition*, Paper #219, Portland, OR, June 2008.)

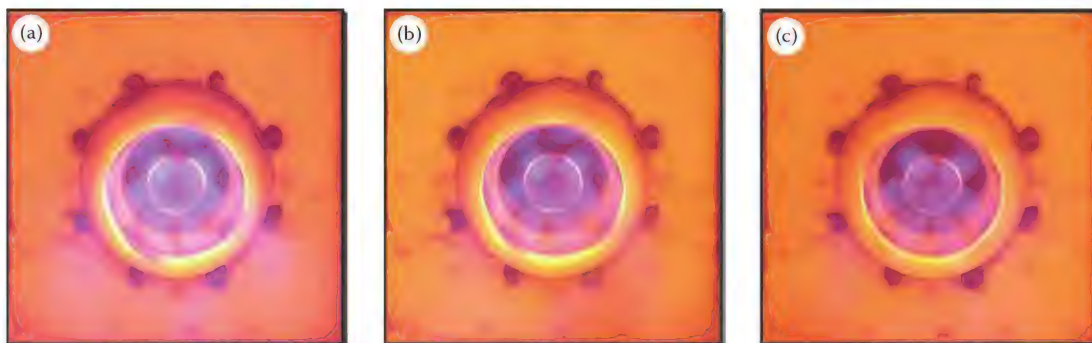
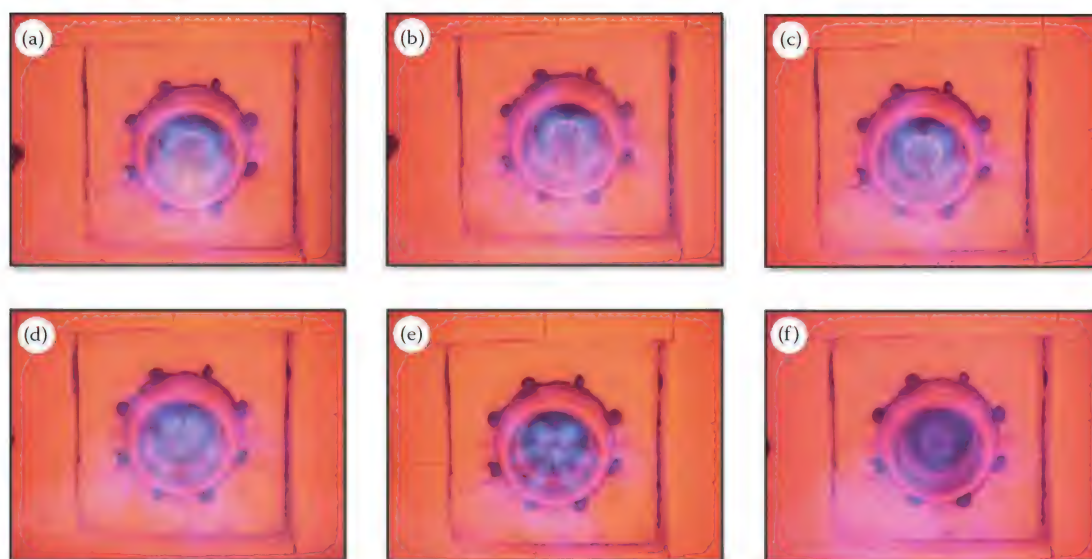


FIGURE 15.79

Effects of percent PSA gas duty on flame appearance firing the MK-II™ burner. The percent PSA gas duty is (a) 65%, (b) 75%, and (c) 88%. (From Bussman, W. et al., Low NO<sub>x</sub> down-fired burners for reforming furnaces, *Air & Waste Management Association's 101st Annual Conference and Exhibition*, Paper #219, Portland, OR, June 2008.)





**FIGURE 15.80**

Effects of PSA gas composition on flame appearance firing the MK-II™ burner at a constant heat release. The percent CO<sub>2</sub> in each photograph is (a) 10%, (b) 20%, (c) 30%, (d) 40%, (e) 50%, and (f) 60%. (From Bussman, W. et al., Low NO<sub>x</sub> down-fired burners for reforming furnaces, *Air & Waste Management Association's 101st Annual Conference and Exhibition*, Paper #219, Portland, OR, June 2008.)

in Figure 15.79 show the low NO<sub>x</sub> burner firing with 65%, 75%, and 88% of the duty with PSA gas. Notice that the flame became more translucent as the PSA proportion increased. A translucent flame suggests a cooler flame temperature as compared to a light-blue flame.

The PSA gas composition can have a significant impact on NO<sub>x</sub>. Figure 15.80 shows an ultralow NO<sub>x</sub> burner firing with various amounts of CO<sub>2</sub> in the PSA gas firing at a constant heat release. Notice as the CO<sub>2</sub> concentration increased, the flame appearance became more translucent; again, this flame appearance is associated with lower NO<sub>x</sub> emissions.

## References

1. C.E. Baukal, *Industrial Combustion Pollution and Control*, Marcel Dekker, New York, 2004.
2. C.E. Baukal, Everything you need to know about NO<sub>x</sub>, *Metal Finishing*, 103, 11, 18–24, 2005.
3. C.E. Baukal, NO<sub>x</sub> 101: A primer on controlling this highly regulated pollutant, *Process Heating*, 15, 2, 34–37, 2008.
4. U.S. Environmental Protection Agency, Nitrogen oxide control for stationary combustion sources, U.S. EPA report EPA/625/5-86/020, 1986.
5. E. Culotta and D.E. Khoshland, NO news is good news, *Science*, 258, 5050, 1862–1865, 1992.
6. M. Sandell, Putting NO<sub>x</sub> in a box, *Pollution Engineering*, 30, 3, 56–58, 1998.
7. New York Conservationists for Kids, New York Department of Environmental Conservation, <http://www.dec.ny.gov/education/77189.html>, accessed September 14, 2012.
8. Environmental Degradation of Marble, European Chemistry Thematic Network, [www.whatischemistry.unina.it/en/martmarmo.html](http://www.whatischemistry.unina.it/en/martmarmo.html) accessed July 27, 2012.
9. M. Moreton and S. Beal, Controlling NO<sub>x</sub> emissions, *Pollution Engineering International*, Winter, pp. 14–16, 1998.
10. J. Elkins, N. Frank, J. Hemby, D. Mintz, J. Szykman, A. Rush, T. Fitz-Simons, T. Rao, R. Thompson, E. Wildermann, and G. Lear, National air quality and emissions trends report, 1999. U.S. Environmental Protection Agency, Washington, DC, Report EPA 454/R-01-004, 2001.
11. Y.B. Zeldovich, The oxidation of nitrogen in combustion and explosions, *Acta Physicochimica* (USSR), 21, 557–628, 1946.
12. D.J. MacKinnon, Nitric oxide formation at high temperatures, *Journal of the Air Pollution Control Association*, 24, 3, 237–239, 1974.
13. C.P. Fenimore, Formation of nitric oxide in premixed hydrocarbon flames, *Proceedings of the Combustion Institute*, 13, 373–380, 1971.
14. T. Yamamoto, T. Kuwahara, K. Nakaso, and T. Yamamoto, Kinetic study of fuel NO formation from pyrrole type nitrogen, *Fuel*, 93, 213–220, 2012.
15. J. Pellegrino, S. Brueske, T. Carole, and H. Andres, Energy and environmental profile of the U.S. petroleum refining industry, report prepared by Energetics, Inc. for the U.S. Department of Energy, November 2007.
16. I. Vermeulen, C. Block, and C. Vandecasteele, Estimation of fuel-nitrogen oxide emissions from the element composition of the solid or waste fuel, *Fuel*, 94, 75–80, 2012.
17. E.B. Sanderford, Alternative control techniques document – NO<sub>x</sub> emissions from process heaters, U.S. Environmental Protection Agency report EPA-453/R-93-015, February, 1993.
18. U.S. Environmental Protection Agency, Alternative control techniques – NO<sub>x</sub> emissions from utility boilers, U.S. EPA report EPA-453/R-94-023, 1994.



19. A. Medeiros, R. Edenhofer, K. Lucka, and H. Köhne, Steady-state determination of fuel-bond (sic) nitrogen in diesel and industrial gas oil, *Clean Air*, 8, 4, 359–371, 2007.
20. J. Singer (ed.), *Combustion Fossil Power*, 4th edn., Combustion Engineering, Inc., Windsor, CT, 1991.
21. C.E. Baukal and P.B. Eleazer, Quantifying NO<sub>x</sub> for industrial combustion processes, *Journal of the Air & Waste Management Association*, 48, 1, 52–58, 1998.
22. American National Standards Institute/American Society of Mechanical Engineers, Performance Test Code PTC 19.10, Part 10: *Flue and Exhaust Gas Analyses*, American Society of Mechanical Engineers, New York, 1981.
23. California Air Resources Board, <http://www.arb.ca.gov/homepage.htm> (accessed December 16, 2011).
24. Texas Commission on Environmental Quality, <http://www.tceq.state.tx.us/> (accessed on December 16, 2011).
25. South Coast Air Quality Management District, <http://aqmd.gov/> (accessed December 16, 2011).
26. Bay Area Air Quality Management District, <http://www.baaqmd.gov/> (accessed on December 16, 2011).
27. C.E. Baukal, Pollution emissions, Chapter 7 in *Industrial Combustion Testing*, Ed. C.E. Baukal, CRC Press, Boca Raton, FL, 2010.
28. U.S. Government, Code of Federal Regulations 40, Part 60, Revised July 1, 1994, Washington, DC.
29. S.B. Mandel, What is the total cost for emissions monitoring? *Hydrocarbon Processing*, 76, 1, 99–102, 1997.
30. M.C. Drake, Kinetics of nitric oxide formation in laminar and turbulent methane combustion, Gas Research Institute, Chicago, IL, Report No. GRI-85/0271, 1985.
31. M.F. Zabielski, L.G. Dodge, M.B. Colket, and D.J. Seery, The optical and probe measurement of NO: A comparative study, *Eighteenth Symposium (International) on Combustion*, The Combustion Institute, Pittsburgh, PA, 1991, 1981.
32. A. Berger and G. Rotzoll, Kinetics of NO reduction by CO on quartz glass surfaces, *Fuel*, 74, 452, 1995.
33. C. Baukal, D. Waibel, and T. Webster, Plant-wide NO<sub>x</sub> reduction strategies, presented at the *Industrial Energy Technology Conference*, New Orleans, LA, May 9–12, 2006.
34. U.S. EPA. Control techniques for nitrogen oxides emissions from stationary sources, EPA Report 450/1-78-001, U.S. Environmental Protection Agency, Washington, DC, 1978.
35. L.M. Campbell, D.K. Stone, and G.S. Shareef, Sourcebook: NO<sub>x</sub> control technology data, U.S. Environmental Protection Agency Report EPA-600/2-91-029, Research Triangle Park, NC, July 1991.
36. J.L. Reese, R. Batten, G.L. Molianen, C.E. Baukal, R. Borkowicz, and D.O. Czerniak, State of the art of NO<sub>x</sub> emission control technologies, ASME Paper 94-JPGC-EC-15, 1994.
37. L.J. Muzio and G.C. Quartucy, Implementing NO<sub>x</sub> control: Research to application, *Progress in Energy and Combustion Science*, 23, 3, 233–266, 1997.
38. A. Tomita, *Emissions Reduction: NO<sub>x</sub>/SO<sub>x</sub> Suppression*, Elsevier Science, New York, 2001.
39. B. Adouane, *Towards a Clean Combustion of LCV Gas: NO<sub>x</sub> from Fuel-Bound Nitrogen*, VDM Verlag Dr. Müller, Saarbrücken, Germany, 2009.
40. Nitrogen Dioxide, U.S. Environmental Protection Agency <http://www.epa.gov/airquality/nitrogenoxides/>
41. H.M. Goma, L.G. Hackemesser, and D.T. Cindric, NO<sub>x</sub>/CO emissions and control in ethylene plants, *Environmental Progress*, 10, 4, 267–272, 1991.
42. D. MacKenzie, I. Cheta, and D. Burns. Removing nitrogen. *Hydrocarbon Engineering*, 7, 11, 57–63, 2002.
43. C.E. Baukal and A.I. Dalton, Nitrogen oxide measurements in oxygen enriched air-NG combustion systems, *Proceedings of Second Fossil Fuel Combustion Symposium*, ASME PD-Vol. 30, New Orleans, LA, January 15, pp. 75–79, 1990.
44. C.E. Baukal (Ed.), *Oxygen-Enhanced Combustion*, CRC Press, Boca Raton, FL, 1998.
45. H. Tsuji, A.K. Gupta, T. Hasegawa, M. Katsuki, K. Kishimoto, and M. Morita, *High Temperature Air Combustion: From Energy Conservation to Pollution Reduction*, CRC Press, Boca Raton, FL, 2003.
46. W. Yang and W. Blasiak, High temperature air combustion for steam reformers, *Hydrocarbon Processing*, 84, 9, 115–122, 2005.
47. W. Bussman and C. Baukal, Ambient conditions impact CO and NO<sub>x</sub> emissions: Part I, *Petroleum Technology Quarterly*, 14, 3, 93–99, 2009.
48. W. Bussman and C. Baukal, Ambient conditions impact CO and NO<sub>x</sub> emissions: Part II, *Petroleum Technology Quarterly*, 14, 4, 37–41, 2009.
49. C. Baukal and W. Bussman, Air infiltration effects on industrial combustion efficiency, Chapter 4 in *Fuel Efficiency*, Ed. J.K. Bernard, Nova Science Publishers, Inc., Hauppauge, NY, pp. 101–134, 2011.
50. R. Waibel, D. Nickeson, L. Radak, and W. Boyd, Fuel staging for NO<sub>x</sub> control, in *Industrial Combustion Technologies*, Ed. M.A. Lukasiewicz, American Society of Metals, Warren, PA, pp. 345–350, 1986.
51. A. Garg, Trimming NO<sub>x</sub>, *Chemical Engineering*, 99, 11, 122–124, 1992.
52. R. Poe, A. Patel, C. Baukal, and D. Wright, Advanced combustion system for cracking furnaces, *Petroleum Technology Quarterly*, 12, 3, 113–117, 2007.
53. W. Bussman, R. Waibel, C. Baukal, R. Ruiz, and I. Chung, Remote staged furnace burner configurations and methods, U.S. Patent, US 7,153,129 B2, December 26, 2006.
54. J.G. Seebold, R.T. Waibel, and T.L. Webster, Control refinery NO<sub>x</sub> emissions cost-effectively, *Hydrocarbon Processing*, 80, 11, 55–59, 2001.
55. J.-Y. Ren, F.-N. Egolfopoulos, and T.T. Tsotsis, NO<sub>x</sub> emission control of lean methane-air combustion with addition of methane reforming products, *Combustion Science Technology*, 174, 181–205, 2002.
56. H.L. Shelton, Find the right low-NO<sub>x</sub> solution, *Environmental Engineering World*, November–December, 2, 6, 24–27, 1996.
57. P. Dagaut, J. Luche, F. Lecomte, and M. Cathonnet, The kinetics of C<sub>1</sub> to C<sub>4</sub> hydrocarbons-NO reactions in relation with reburning, *Proceedings of 5th European Conference on Industrial Furnaces and Boilers*, Lisbon, Portugal, Vol. 2, pp. 499–509, 2000.
58. V.M. Zamansky, L. Ho, P.M. Maly, and W.R. Seeker, Reburning promoted by nitrogen- and Sodium-Containing Compounds, *Twenty-Sixth Symposium (International) on Combustion*, The Combustion Institute, Pittsburgh, PA, pp. 2075–2082, 1996.

59. C.A. Miller, A.D. Touati, J. Becker, and J.O.L. Wendt, NO<sub>x</sub> Abatement by fuel-lean reburning: Laboratory combustor and pilot-scale package boiler results, *Twenty-Seventh Symposium (International) on Combustion*, The Combustion Institute, Pittsburgh, PA, pp. 3189–3195, 1998.
60. J.U. Watts, A. Mann, J. Harvilla, and D. Engelhardt, NO<sub>x</sub> control by utilization of reburn technologies in the United States, *Fifth International Conference on Technologies and Combustion for a Clean Environment*, The Combustion Institute – Portuguese Section, Lisbon, Portugal, Vol. 2, pp. 1017–1021, 1999.
61. M. Braun-Unkhoff, P. Frank, S. Koger, and W. Leuckel, Evaluation of NO<sub>x</sub> reburning models under large scale conditions, *Fifth International Conference on Technologies and Combustion for a Clean Environment*, The Combustion Institute – Portuguese Section, Lisbon, Portugal, Vol. 2, pp. 1023–1032, 1999.
62. J.O.L. Wendt, Pollutant Formation in Furnaces: NO<sub>x</sub> and Fine Particulates, *Proceedings of 5th European Conference on Industrial Furnaces and Boilers*, Lisbon, Portugal, Vol. 1, pp. 129–156, 2000.
63. J. Colannino, Low-cost techniques reduce boiler NO<sub>x</sub>, *Chemical Engineering*, 100, 2, 100–106, 1993.
64. M. Fregeau and J.C. Hermanson, CO/NO<sub>x</sub> emissions of strongly pulsed jet diffusion flames, *Combustion Science and Technology*, 181, 3, 536–554, 2009.
65. C.A. Martins, J.A. Carvalho, Jr., C.A.G. Veras, M.A. Ferreira, and P.T. Lacava, Experimental measurements of the NO<sub>x</sub> and CO concentrations operating in oscillatory and non-oscillatory burning conditions, *Fuel*, 85, 1, 84–93, 2006.
66. C.A. Martins, J.A. Carvalho, M.A. Ferreira, and C.A.G. Veras, An experimental investigation of NO<sub>x</sub> formation in a Rijke type pulse combustor, *Fifth International Conference on Technologies and Combustion for a Clean Environment*, The Combustion Institute – Portuguese Section, Lisbon, Portugal, Vol. 1, pp. 489–494, 1999.
67. A. Kegasa, NO<sub>x</sub> reduction effect of forced oscillating combustion, *Fifth International Conference on Technologies and Combustion for a Clean Environment*, The Combustion Institute – Portuguese Section, Lisbon, Portugal, Vol. 1, pp. 495–500, 1999.
68. P. Barham, K.J.A. Hargreaves, H. Ipakchi, and W.C. Maskell, Emission characteristics and influence of flap-per valve thickness upon operation of a premixed pulsed combustor, *Fifth International Conference on Technologies and Combustion for a Clean Environment*, The Combustion Institute – Portuguese Section, Lisbon, Portugal, Vol. 1, pp. 481–488, 1999.
69. A. Garg, Specify better low-NO<sub>x</sub> burners for furnaces, *Chemical Engineering Progress*, 90, 1, 46–49, 1994.
70. I.-P. Chung, D. Meinen, R. Poe, J. Lewallen, C. Baukal, and C. Schnepfer, Solving the low NO<sub>x</sub> dilemma, *Hydrocarbon Engineering*, 10, 8, 77–80, 2005.
71. I.-P. Chung, J. Chambers, C. Schnepfer, R. Poe, J. Jayakaran, R. Waibel, M. Claxton, M. Zimola, and D. Foote, Compact low NO<sub>x</sub> gas burner apparatus and methods, U.S. Patent 6,695,609, issued February 24, 2004.
72. C. Baukal, V. Gershtein, and X. Li (Eds.), *Computational Fluid Dynamics in Industrial Combustion*, CRC Press, Boca Raton, FL, 2001.
73. J. Colannino, NO<sub>x</sub> reduction for stationary sources, *AIPE Facilities*, January/February, 63–66, 1996.
74. J. Bluestein, NO<sub>x</sub> Controls for gas-fired industrial boilers and combustion equipment: A survey of current practices, Gas Research Institute, Chicago, IL, report GRI-92/0374, 1992.
75. API Recommended Practice 536, Post-combustion NO<sub>x</sub> control for fired equipment in general refinery services, 1st edn., American Petroleum Institute, Washington, DC, March 1998.
76. K.T. Chuang and A.R. Sanger, 5.20 Gaseous emission control: Physical and chemical separation, in *Environmental Engineers' Handbook*, 2nd edn., Eds. D.H.F. Liu, B.G. Lipták, Lewis Publishers, Boca Raton, FL, 1997.
77. C.J. Pereira and M.D. Amiridis, NO<sub>x</sub> control from stationary sources, in *Reduction of Nitrogen Oxide Emissions*, Eds. U.S. Ozkan, S.K. Agarwal, G. Marcelin, American Chemical Society, Washington, DC, 1995.
78. P. Melton and K. Graham, Thermal oxidizers, Chapter 21 in *The John Zink-Hamworthy Combustion Handbook*, CRC Press, Boca Raton, FL, 2001.
79. R.M. Heck and R.J. Farrauto, *Catalytic Air Pollution Control: Commercial Technology*, Van Nostrand Reinhold, New York, 1995.
80. D.C. Mussatti, R. Srivastava, P.M. Hemmer, and R. Strait, Section 4.2: NO<sub>x</sub> post-combustion, Selective catalytic reduction, Chapter 2 in *Air Pollution Control Cost Manual*, 6th edn., Ed. D.C. Mussatti, Report EPA/452/B-02-001, U.S. Environmental Protection Agency, Washington, DC, January 2002.
81. E. Hums and G.W. Spitznagel, Deactivation behavior of selective catalytic reduction of DeNO<sub>x</sub> catalysts, in *Reduction of Nitrogen Oxide Emissions*, Eds. U.S. Ozkan, S.K. Agarwal, G. Marcelin, American Chemical Society, Washington, DC, 1995.
82. D. Divinia, Fine-tune SCR operations, *Hydrocarbon Processing*, 84, 1, 81–82, 2005.
83. B.W.-L. Jang, J.J. Spivey, M.C. Kung, B. Yang, and H.H. Kung, Low-temperature selective catalytic reduction of NO by hydrocarbons in the presence of O<sub>2</sub> and H<sub>2</sub>O. In *Reduction of Nitrogen Oxide Emissions*, Eds. U.S. Ozkan, S.K. Agarwal, G. Marcelin. American Chemical Society, Washington, DC, 1995.
84. U.S. Ozkan, Y. Cai, and M.W. Kumthekar, Selective catalytic reduction of nitric oxide with ammonia over supported and unsupported vanadia catalysts. In *Catalytic Control of Air Pollution*, Eds. R.G. Silver, J.E. Sawyer, J.C. Summers. American Chemical Society, Washington, DC, 1992.
85. U.S. Ozkan, S.K. Agarwal, and G. Marcelin (Eds.), *Reduction of Nitrogen Oxide Emissions*, American Chemical Society, Washington, DC, 1995.
86. M.D. Amiridis, B.K. Na, and E.I. Ko, Selective catalytic reduction of NO by NH<sub>3</sub> over aerogels of titania, silica, and vanadia. In *Reduction of Nitrogen Oxide Emissions*, Eds. U.S. Ozkan, S.K. Agarwal, G. Marcelin. American Chemical Society, Washington, DC, 1995.

87. M.P. Laplante and P. Lindenhoff, How low can you go?—Catalytic NO<sub>x</sub> reduction in refineries, *World Refining*, 13, 2, 46–51, 2002.
88. R.K. Lyon, Method for the reduction of the concentration of NO in combustion effluents using ammonia, U.S. Patent 3,900,554, issued August 19, 1975.
89. R.K. Lyon, The NH<sub>3</sub>-NO-O<sub>2</sub> reaction, *International Journal of Chemical Kinetics*, 8, 2, 315–318, 1976.
90. K.B. Schnelle and C.A. Brown, *Air Pollution Control Technology Handbook*, CRC Press, Boca Raton, FL, 2002.
91. J.K. Arand, L.J. Muzio, and J.G. Sotter, Urea reduction of NO<sub>x</sub> in combustion effluents, U.S. Patent 4,208,386, issued June 17, 1980.
92. R. Rota, D. Antos, E.F. Zanoelo, and M. Morbidelli, Experimental and modeling analysis of the NO<sub>x</sub>OUT process, *Chemical Engineering Science*, 57, 27–38, 2002.
93. M.L. Lin, J.R. Comparato, and W.H. Sun, Applications of urea-based selective noncatalytic reduction in hydrocarbon processing industry. In *Reduction of Nitrogen Oxide Emissions*, Eds. U.S. Ozkan, S.K. Agarwal, G. Marcelin. American Chemical Society, Washington, DC, 1995.
94. D.C. Mussatti, R. Srivastava, P.M. Hemmer, and R. Strait, Section 4.2: NO<sub>x</sub> post-combustion, Selective noncatalytic reduction, Chapter 1 in *Air Pollution Control Cost Manual*, 6th edn., Ed. D.C. Mussatti, Report EPA/452/B-02-001, U.S. Environmental Protection Agency, Washington, DC, January 2002.
95. R. Rota, E.F. Zanoela, M. Morbidelli, and S. Carra, Effect of mixing on selective non-catalytic nitric oxide reduction, *Fifth International Conference on Technologies and Combustion for a Clean Environment*, The Combustion Institute – Portuguese Section, Lisbon, Portugal, Vol. 1, pp. 119–128, 1999.
96. V.M. Zamansky, P.M. Maly, L. Ho, V.V. Lissianski, D. Rusli, and W.C. Gardiner, Promotion of selective non-catalytic reduction of NO by sodium carbonate, *Twenty-Seventh Symposium (International) on Combustion*, The Combustion Institute, Pittsburgh, PA, pp. 1443–1449, 1998.
97. M. Naslund and N. Lindskog, Catalytic cleaning in radiant tube burners reduces NO<sub>x</sub> emissions, *Industrial Heating*, LXVIII, 8, 41–46, 2001.
98. D. Thomas and J. Vanderschuren, The use of hydrogen peroxide for the NO<sub>x</sub> reduction in wet processes, in *Chemical Industry and Environment II*, Vol. 2, Eds. N. Piccinini, R. Delorenzo, Politecnico di Torino, Torino, Italy, 1996.
99. I. Orlandini and U. Riedel, Modelling of NO and HC removal by non-thermal plasmas, *Combustion Theory and Modelling*, 5, 447–462, 2001.
100. J.R. Woertz, K.A. Kinney, and P.J. Szaniszló, A fungal vapor-phase bioreactor for the removal of nitric oxide from waste gas streams, *Journal of the Air & Waste Management Association*, 51, 895–902, 2001.
101. R.R. Hayes, C.E. Baukal, and D. Wright, Fuel composition effects on NO<sub>x</sub>, presented at the 2000 American Flame Research Committee International Symposium, Newport Beach, CA, September 2000.
102. W. Bussman, C. Baukal, and J. Colannino, The effect of firebox temperature on NO<sub>x</sub> emissions, *Proceeding of 2004 Air and Waste Management Conference*, Paper# 04-A-664-AWMA, Indianapolis, IN, June 2004.
103. W. Bussman and C. Baukal, Changing temperatures, *Hydrocarbon Engineering*, 12, 9, 127–131, 2007.
104. American Petroleum Institute, *Burners for Fired Heaters in General Refinery Services*, API Recommended Practice 535, 2nd edn., American Petroleum Institute, Washington, DC, January 2006.
105. C. Baukal (Ed.), *Industrial Burners Handbook*, CRC Press, Boca Raton, FL, 2004.
106. W. Bussman, C. Baukal, and D. Waibel, Ghost NO<sub>x</sub>, Control #28, *Air & Waste Management Association's 98th Annual Conference and Exhibition*, Minneapolis, MN, June 21–24, 2005.
107. D. Fitz, Quantification of uncertainties in continuous measurement systems for low-NO<sub>x</sub> emissions from stationary sources, California Energy Commission, Sacramento, CA, October 2001.
108. M. Shimokawabe, A. Ohi, and N. Takezawa, Catalytic decomposition of nitrogen dioxide over various metal oxides, *Applied Catalysis A: General*, 85, 129–133, 1992.
109. A. Vijn, Sabatier-balandin interpretation of the catalytic decomposition of nitrous oxide on metal-oxide semiconductors, *Journal of Catalysis*, 31, 51–54, 1973.
110. L. Wikstrom and K. Nobe, Catalytic dissociation of nitrogen dioxide, *I&EC Process Design and Development*, 4, 2, 191, 1965.
111. G. Lai, *High-Temperature Corrosion of Engineering Alloys*, ASM International, Materials Park, OH, 1990.
112. D. Chang, Equilibrium and Kinetics: NO<sub>x</sub>, ATM/ECI 149 Lecture F'03.
113. Vaught Engineering Inc., Low NO<sub>x</sub> measurement: Gas turbine plants – final report on review of current measuring and monitoring practices, ASME International Report, CRTD Vol. 52, 1999.
114. S.M. Correa, A Review of NO<sub>x</sub> formation under gas-turbine combustion conditions, *Combustion Science and Technology*, 87, 329–362, 1992.
115. A.N. Hayhurst and E.M. Hutchinson, Evidence for a new way of producing NO via NNH in fuel-rich flames at atmospheric pressure, *Combustion and Flame*, 114, 274–279, 1998.
116. I.E. Idelchik, *Handbook of Hydraulic Resistance*, Hemisphere Publishing Corporation, New York, 1986.
117. W. Bussman, J. Lewallen, and C. Baukal, Low NO<sub>x</sub> down-fired burners for reforming furnaces, *Air & Waste Management Association's 101st Annual Conference and Exhibition*, Paper #219, Portland, OR, June 2008.
118. I. Dybkjaer, What are the options for hydrogen plant revamps?, *Hydrocarbon Processing*, 84, 2, 63–67, 2005.
119. V.K. Khanna, Hydrogen generation – a brief review, *Hydrocarbon Processing*, 80, 7, 86A–86D, 2001.
120. K. Ruthardt, K.R. Radtke, and J. Larsen, Hydrogen trends, *Hydrocarbon Engineering*, 10, 11, 41–46, 2005.
121. H. Gunardson, *Industrial Gases in Petrochemical Processing*, Marcel Dekker, New York, 1998.



This page intentionally left blank

# 16

## Noise

Wes Bussman, Jay Karan, Carl-Christian Hantschk, and Edwin Schorer

### CONTENTS

16.1	Fundamentals of Sound .....	480
16.1.1	Introduction .....	480
16.1.2	Basics of Sound .....	481
16.1.2.1	Sound Pressure Level and Frequency .....	481
16.1.2.2	Decibel .....	483
16.1.2.3	Sound Power Level .....	484
16.1.2.4	Threshold of Hearing .....	484
16.1.2.5	Threshold of Pain .....	485
16.1.2.6	Correction Scales .....	485
16.1.3	Measurements .....	486
16.1.3.1	Overall Sound Level and How to Add dB Values .....	488
16.1.3.2	Atmospheric Attenuation .....	489
16.2	Industrial Noise Pollution .....	490
16.2.1	OSHA Requirements .....	492
16.2.2	International Requirements .....	492
16.2.3	Noise Sources and Environment Interaction .....	492
16.3	Mechanisms of Industrial Combustion Equipment Noise .....	493
16.3.1	Combustion Roar and Combustion Instability Noise .....	493
16.3.1.1	Flare Combustion Roar .....	493
16.3.1.2	Flare Combustion Instability Noise .....	497
16.3.1.3	Burner Combustion Noise .....	498
16.3.1.4	Burner Combustion Instability Noise .....	499
16.3.2	Fan Noise .....	499
16.3.3	Gas Jet Noise .....	499
16.3.3.1	Gas Jet Mixing Noise .....	499
16.3.3.2	Shock-Associated Noise .....	500
16.3.4	Valve and Piping Noise .....	501
16.4	Noise Abatement Techniques .....	502
16.4.1	Flare Noise Abatement Techniques .....	502
16.4.2	Burner Noise Abatement Techniques .....	504
16.4.3	Valve and Piping Noise Abatement Techniques .....	505
16.4.4	Fan Noise Abatement Techniques .....	507
16.5	Analysis of Combustion Equipment Noise .....	507
16.5.1	Multiple Burner Interaction .....	507
16.5.2	High-Pressure Flare .....	508
16.5.3	Atmospheric Attenuation Example .....	509
	Glossary .....	509
	References .....	511
	Bibliography .....	511

## 16.1 Fundamentals of Sound

### 16.1.1 Introduction

Silence is golden

—Anonymous

Noise is referred to as unwanted sound; it is a common by-product of our mechanized civilization and is an insidious danger in industrial environments. Noise pollution is usually a local problem and so is not viewed on the same scale of importance as the more high-profile industrial emissions like  $\text{NO}_x$ , CO, and particulates (see Chapters 14 and 15). Nonetheless, it is an environmental pollutant of significant impact.

Serious concern is merited when a pollutant can result in either environmental damage or human discomfort. Considering the impact on people, noise is most often a source of annoyance, but it can also have more detrimental effects, such as causing physical injury. Noise-related injuries range from short-term discomfort to permanent hearing loss. According to recent statistics, more than 20 million Americans are exposed to hazardous sound levels on a regular basis. There are approximately 28 million

Americans who have some degree of hearing loss: about one-third of these—more than 9 million—have been affected, at least in part, by exposure to excessive noise.

The sense of hearing is a fragile and vital function of the human body. It resembles the sense of vision, more so than the other senses, because permanent and complete damage can occur quite easily in an industrial environment. So noise pollution has been recognized as a safety concern for a long time and has been appropriately regulated.

Although personnel safety may be the most important concern, noise pollution has several other significant side effects. Sometimes combustion performance must be balanced with noise performance and in some extreme cases, the performance of the equipment must be compromised somewhat to achieve the noise performance required. To those in relatively remote or unpopulated areas, it may seem unthinkable that equipment performance could be compromised for the sake of noise control. However, given the age and economic drivers of the petroleum refining and chemical industries, it is now common to find plants located in densely populated areas (see Figure 16.1). Industry located in close proximity to residential areas or busy commercial facilities can create levels of noise that the people in the neighborhood find objectionable, resulting in regulations aimed



**FIGURE 16.1**  
Community located close to an industrial plant. (Photograph from Dreamstime.)



at controlling noise emissions. Within the industrial site itself, the immediate issue with noise is employee safety. In addition to the concern with physical safety, it has been found that reduction in noise levels contributes to improved employee work performance and morale.

Equipment is also affected by noise. In most cases, these effects lie in the area of vibration control and are beyond the scope of this chapter. Suffice it to say that noise and mechanical vibration usually occur together. High levels of mechanical vibration are accompanied by high levels of noise and vice versa. Vibration leads to mechanical fatigue, which reduces equipment life. The effects of fatigue are frequently accepted as normal wear and tear if the equipment life cycle spans a reasonable duration. In extreme cases, the effects of vibration may be more rapidly manifested, such as in the case of premature cracking and spalling of hard refractory linings in furnaces.

This chapter is written as a practical guide, as well as a reference, for engineers involved in the design, operation, or maintenance of combustion equipment (see Volume 2)—be it burners, furnaces, flares, or thermal oxidizers (see Volume 3). In addition, because this chapter provides a comprehensive coverage of the fundamentals of sound, the creative engineer will also be able to extend his or her knowledge to analyze other noise-producing industrial equipment.

### 16.1.2 Basics of Sound

What is sound? An interesting question one may have been asked before is “If a tree falls in the forest and nobody is around to hear it, does it still make a sound?” (see Figure 16.2). Webster’s dictionary defines sound as “That which is heard.” So, according to this definition, the tree will not make a sound as it falls. Obviously, an engineer will find this definition inadequate for technical purposes. The definition provided by the *Handbook of Noise Measurement* is more accurate: “Sound is the vibration of particles in a gas, liquid or solid.”<sup>1</sup>

Sound is propagated through any medium in waves that take the form of pressure peaks (compressions) and troughs (rarefactions) as illustrated in Figure 16.3. The pressure wave travels through the medium at the speed of sound in that medium. The auditory system in humans and most animals senses the impingement of these pressure waves on a tissue membrane and converts them to electrical impulses that are then sent to the brain where they are interpreted as the information we receive from the sound.

Figure 16.4 shows a cross-section of the human ear. Sound is collected and funneled into the ear canal by the outer ear. At the end of the ear canal, the sound impinges on the ear drum. The bones of the middle ear convey the ear drum’s vibration to the inner ear. The inner ear consists of a fluid-filled membrane called the



**FIGURE 16.2**  
Tree falling in the forest. (Courtesy of Dreamstime.)

cochlea, that has tiny hair cells on the inside. The hair cells sense the vibration conveyed to the cochlea and convert the vibrations into nerve pulses which are then conveyed to the brain through the auditory nerve.

In reality, most naturally occurring sounds are composites of different pressure levels at various frequencies. On the other hand, a pure tone is a sound at only one frequency. Any pure tone can be uniquely identified by two of its properties, namely, pressure level and frequency. A tuning fork is an example of a pure tone generator. Naturally occurring pure tone generators are rare. Even musical instruments create notes that have significant pressure levels at two or three multiples, or harmonics, of the fundamental frequency of the note.

#### 16.1.2.1 Sound Pressure Level and Frequency

Pressure level defines the loudness of the sound, while frequency defines the pitch or tone of the sound. Pressure level is the amplitude of the compression, or rarefaction, of the pressure wave. The common unit of pressure level is decibel, abbreviated to “dB.” Frequency is the number of pressure waves that pass by an arbitrary point of reference, in a given unit of time. As such, the measure of sound frequency can be cycles per second (cps), and as with electricity, the commonly used unit is Hertz (Hz); 1 Hz = 1 cps.

Another important quantity in the description of sound waves is the speed of sound which is typically

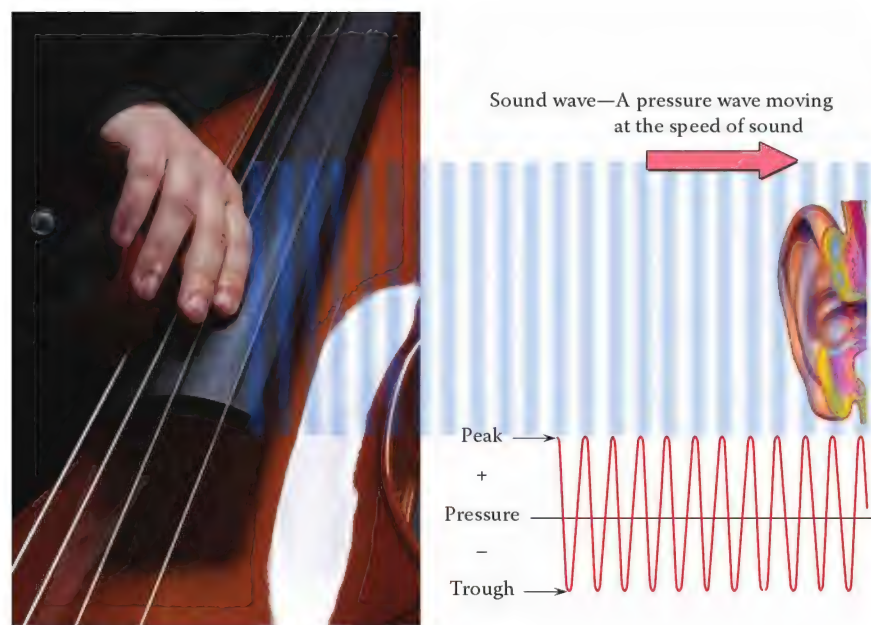


**FIGURE 16.3**  
Pressure peaks and troughs. (Photograph of base from Dreamstime.)

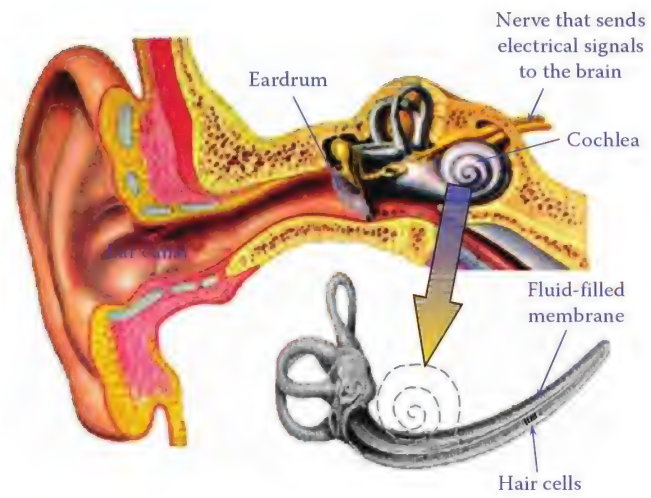


**FIGURE 16.4**  
Cross-section of the human ear.

designated by the letter  $c$ . The speed of sound describes the velocity at which a sound wave propagates through the ambient air or other fluids (e.g., water). In other words, the speed of sound describes the distance a sound wave propagates per unit of time. The length of a sound wave is another important quantity in the description of sound. The wavelength,  $\lambda$ , describes the distance between one wave crest and the next, i.e., between one point of maximum compression in the sound wave to the next. The frequency  $f$ , speed of sound  $c$ , and wavelength  $\lambda$  are related as follows:

$$c = \lambda f \tag{16.1}$$

The speed at which a sound wave propagates depends mainly on the type of fluid and the temperature of the fluid. Table 16.1 gives some examples for the speed of sound in different media and at different temperatures. The typical range of human hearing extends from 20 Hz to 20 kHz. Young children can hear frequencies slightly higher than 20 kHz but this ability diminishes with age. This trend of reduced high-frequency sensitivity continues with advancing age. Loss of hearing in humans in the later stages of life typically

**TABLE 16.1**  
Speed of Sound in Different Media  
and at Different Temperatures

Fluid	Temperature (°C)	Speed of Sound, $c$ (m/s)
Air, dry	-40	307
	20	320
	0	332
	20	344
	40	356
Hydrogen	20	1316
Methane	20	448
Ethylene	20	331
Water	0	1403
	40	1529
	80	1555
	100	1543
Steel	20	5180
Soft rubber	20	54



**TABLE 16.2**

The 10 Octave Bands

Full Octave Band Standards	
Octave Band (Hz)	Center Frequency (Hz)
22–44	31.5
44–88	63
88–177	125
177–355	250
355–710	500
710–1420	1,000
1,420–2,840	2,000
2,840–5,680	4,000
5,680–11,360	8,000
11,360–22,720	16,000

manifests itself as diminished sensitivity to frequencies from 10 to 20 kHz. Mechanically, this is due to the deterioration of the fine hair cells in the basilar membrane.

It is important to note that the ear is not equally sensitive over the entire range from 20 Hz to 20 kHz. This is vital to understanding how noise affects us and how noise control is implemented. The human ear is much less sensitive to sound at the extremes of low and high frequencies and we will discuss this in more detail later in the chapter.

The wide range of frequencies in our hearing range may be conveniently handled by breaking it up into octave bands. Each octave band represents a doubling in frequency. Table 16.2 shows the 10 octave bands that

cover the hearing range and the center frequencies that can be used to represent each octave band. Each octave band extends over seven fundamental musical notes.

### 16.1.2.2 Decibel

The unit of sound level, the decibel, is difficult to visualize and warrants some explanation. While it is possible to quantify sound in units of either power or pressure, neither unit is convenient to use because in practice one has to deal with sounds that extend over a very large range of power or pressure values. For example, the sound power of a whisper is  $10^{-9}$  W, while the sound power of a jet plane is  $10^3$  W. The range of these two sound sources spans  $10^{12}$  W. The decibel, a dimensionless unit, was invented in order to represent these large ranges conveniently.

In the 1960s, Bell Laboratories coined the term “decibel.” The “deci” stands for the base 10 log scale on which the decibel is based and the “bel” was meant to represent Bell Labs. See Figure 16.5 for how decibel relates to watts.

In Figure 16.5, the  $y$ -axis corresponds to the sound power in watts, and follows a base-10 scale. The  $x$ -axis corresponds to the sound power level in dB (PWL). The line provides the relationship between the sound power and the PWL; for example, a PWL of 120 dB is equal to a sound power of 1 W. As an illustration of the  $\log_{10}$  relationship, note that 110 dB is equal to one-tenth of a watt 0.1 (0.1 W) and 100 dB is equal to a hundredth of a watt (0.01 W).

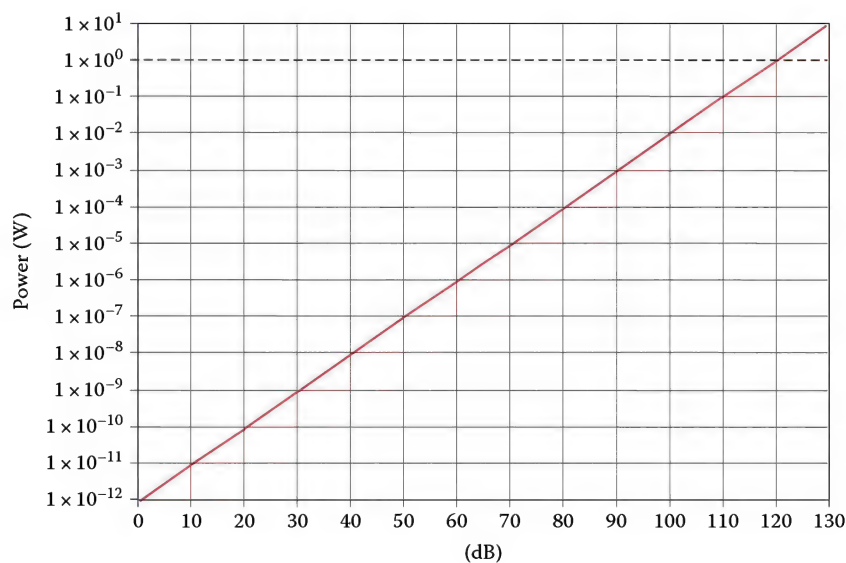


**FIGURE 16.5**  
Relationship of decibels to watts.



The following are useful equations that may be used to calculate sound pressure and power levels, in dB, from the equivalent pressure and power units.

$$L_p \text{ (dB)} = 20 \log_{10} \left( \frac{P}{2 \times 10^{-5}} \right) \quad (16.2)$$

$$L_w \text{ (dB)} = 10 \log_{10} \left( \frac{W}{1 \times 10^{-12}} \right) \quad (16.3)$$

where

$L_p$  is the sound pressure level (dB)  
 $L_w$  is the sound power level (dB)  
 $P$  is the sound pressure (N/m<sup>2</sup>)  
 $W$  is the sound power (W)

### 16.1.2.3 Sound Power Level

There is a subtle but important difference between the terms PWL, and sound pressure level (SPL). PWL is used to indicate the total energy emitting ability of a sound source. In other words, sound power is a characteristic of the sound source itself. SPL, on the other hand, is used to indicate the intensity of sound received at any point of interest, from one or more sources. The illustration in Figure 16.6 shows the formula to calculate the SPL to be expected at a distance  $r$  from a spherically radiating source of power level  $L_w$ :

$$L_p = L_w - 10 \log_{10}(4\pi r^2) + 10.5 \quad (16.4)$$

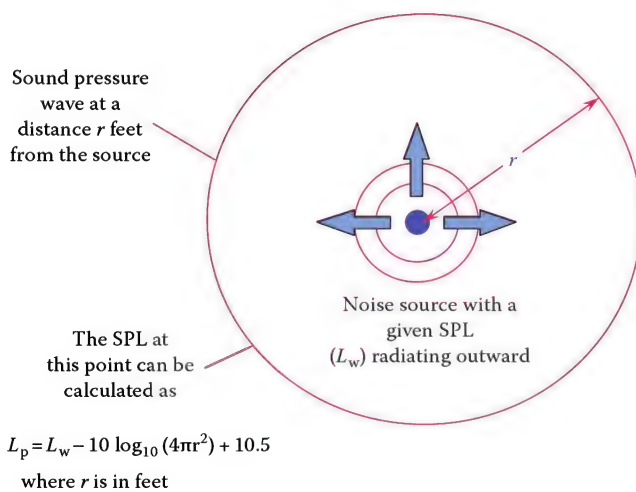


**FIGURE 16.6**  
Calculating SPL at a distance  $r$ .

where

$L_p$  is the sound pressure level (dB)  
 $L_w$  is the sound power level (dB)  
 $r$  is the distance from source (ft)

Equation 16.4 is only valid exactly if the following conditions are fulfilled:

- Noise radiation from the source is uniform and equal in every direction.
- The source is small compared to the distance  $r$ .
- There is no relevant noise contribution from other sources at the point of interest.
- There is no relevant influence on the noise at the point of interest from sound reflecting surfaces nearby.

If the aforementioned conditions are sufficiently fulfilled, then Equation 16.4 cannot only be used to calculate the SPL expected at a certain distance  $r$  from the source (knowing the PWL  $L_w$ ), but it can also be used to back-calculate the PWL of a source from a measurement of the SPL at a known distance  $r$  from the source. The latter procedure is a technique that is standardized in DIN EN ISO 3744.<sup>2</sup>

If the aforementioned conditions, however, are not fulfilled, then the SPL predicted at a certain distance from a sound source could differ significantly from the level actually measured, or the PWL of a source back-calculated from a measurement of the SPL can differ significantly from the real PWL of the source. In this context, it is important to keep in mind that the PWL is an intrinsic property of the source which is independent from the environment while the SPL not only depends on the distance to the source, but is also influenced by other sound sources, the environment (reflecting surfaces, etc.), and the sound propagation conditions (temperature, atmospheric pressure, wind, barriers, etc.).

### 16.1.2.4 Threshold of Hearing

Figure 16.7 reveals a map of the threshold of hearing in humans. The  $y$ -axis represents the SPL in dB and the  $x$ -axis represents frequency. Any SPL that falls below the curve at any given frequency will be inaudible to humans. For example, a SPL of 30 dB at 63 Hz will be inaudible; whereas, a SPL of 70 dB at the same 63 Hz frequency will be audible. Humans are most sensitive to sounds in the so-called "mid-frequencies" from 1 kHz to about 5 kHz. This is generally the range of frequencies of the human voice and many other important common sounds. Additionally, at a constant level,

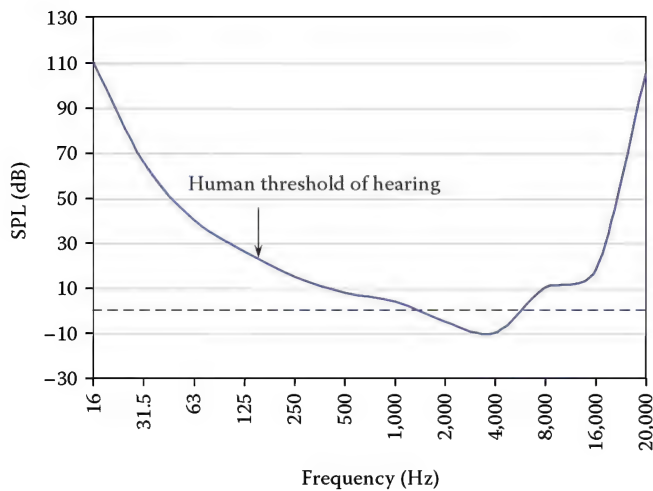


**FIGURE 16.7**  
Threshold of hearing in humans.

sound with a low or very high frequency will not have the same loudness sensation as that in the medium frequency range. For example, a 100 Hz tone at a SPL of 50 dB is perceived as the same loudness as a 1000 Hz tone at SPL of 40 dB.<sup>3</sup>

#### 16.1.2.5 Threshold of Pain

Figure 16.8 shows the threshold of pain superimposed on the threshold of hearing. Fortunately, the curve representing the threshold of pain is relatively flat. In general, a SPL of over 120 dB at any frequency will cause pain. An important observation that can be derived from the two curves is that if a sound is audible at very low or very high frequencies, persons subject to this sound are very close to experiencing pain.

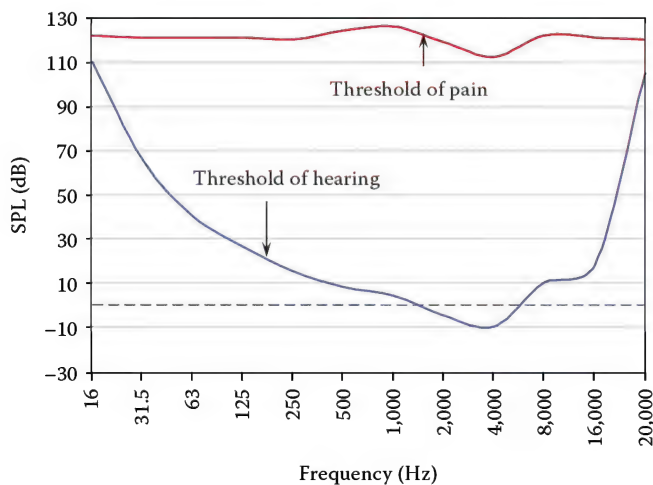


**FIGURE 16.8**  
Threshold of hearing and threshold of pain in humans.

#### 16.1.2.6 Correction Scales

Sound meters are capable of measuring with equal sensitivity over the entire audible range. However, because humans do not hear with equal sensitivity at all frequencies, the sound meter's measurement needs to be modified to quantify what really affects humans. This can be done using a correction curve. The most common correction is the A-scale correction curve which resembles an idealized inverse of the threshold of hearing curve (refer to Figure 16.9). An A-weighted sound level correlates reasonably well with hearing-damage risk in industry and with subjective annoyance for a wide category of industrial and community noises. After applying the A-scale correction, the unit of SPL becomes the dBA scale. Figure 16.10 shows a typical burner noise curve as measured by a noise meter (flat scale) and the result after applying A-scale correction.

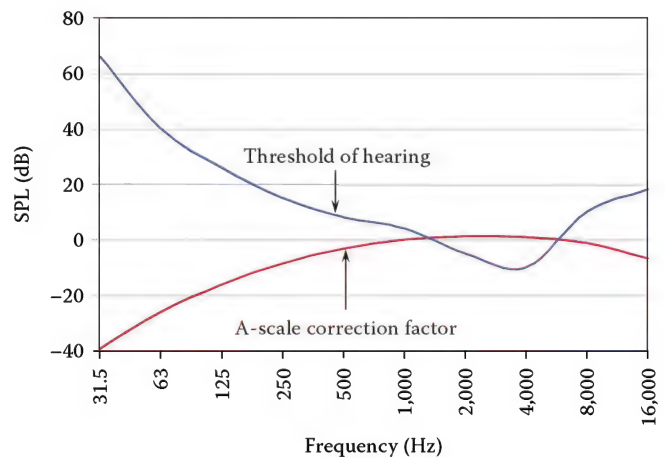


**FIGURE 16.9**  
A-weighted scale for human hearing threshold.

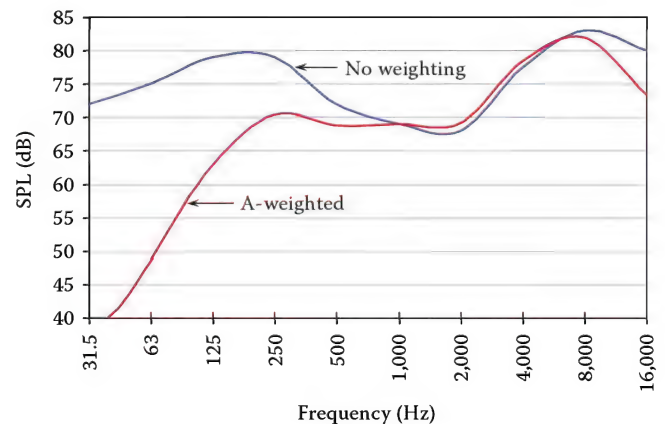


**FIGURE 16.10**  
A-weighted burner noise curve.

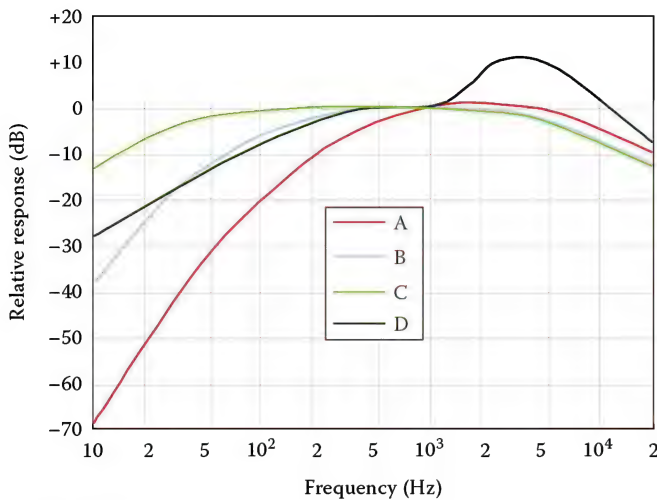


**FIGURE 16.11**  
Weighting curves A, B, C, and D.

The other, less used correction scales are named, as might be expected, B, C, and D. Referring to Figure 16.11, one can see that the C-scale is essentially flat over the range of interest and the B-scale lies somewhere between the A- and C-scales. Given an understanding of the influence of low-frequency sounds, one finds that the B- and C-scales do not apply adequate correction in the lower frequencies. Finally, the D-scale is different from the others in that it has a pronounced correction in the range of 2–5 kHz. The D-scale was devised for the aircraft industry and is rarely used otherwise.

### 16.1.3 Measurements

A simple schematic of a noise meter is shown in Figure 16.12. The microphone is designed with a transducer that transforms pressure variations in air to a corresponding electrical signal. Since the electrical signal generated by the microphone is relatively small in magnitude, a preamplifier is needed to boost the

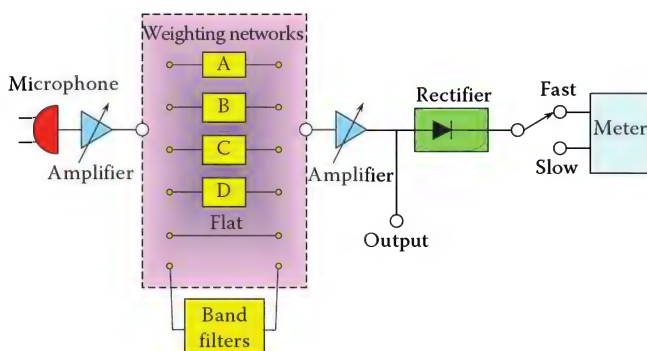


**FIGURE 16.12**  
Block diagram of a sound level meter.

signal before it can be analyzed, measured, or displayed. Special weighting networks are used to shape the signal spectrum and apply the various correction scales discussed earlier. The weighted signal then passes through a second output amplifier into a meter. The meter and associated electronic circuits detect the approximate root-mean-square (rms) value of the signal and display it in units of dB.

Noise meters range from the simplest—microphone and needle gauge—to sophisticated digital signal processing (DSP) equipped analyzers. The more sophisticated analyzers are equipped with fast Fourier transform (FFT) capabilities that aid in accurate narrow band analysis. In general, spectrum analyzers allow the user to map the SPL at different frequencies, or in other words, generate a curve of the sound over different frequencies. However, there is a significant difference between instruments that make one measurement per octave band and those that slice the octave band up into several intervals and make a measurement at each interval. Typically, instruments are capable of carrying out

1. Octave band measurements
2. One-third octave band measurements
3. Narrow-band measurements

Table 16.3 shows the usual octave and one-third octave bands. As the name suggests, a one-third octave band instrument makes three measurements in each octave as opposed to the single measurement of the octave band instrument. A narrow-band instrument, on the other hand, uses DSP to implement FFT analysis, and in the current state of the art, FFT analysis allows the analyzed frequency range to be sliced up into a large number of smaller intervals, limited in number only by the measured time interval's length and the available computer power.

Figure 16.13 provides a comparison of the same sound spectrum as analyzed using three different frequency band intervals: octave band, one-third octave band, and narrow band. This comparison shows that the additional resolution provided by narrower band methods can be of vital importance. In this example the level at 1 kHz, as recorded by the octave band instrument, is 90 dB; on the one-third octave instrument, it is 85 dB, and on the narrow-band instrument it is 70 dB. The lower resolution measurements produce higher values due to the spill-over influence of the nearby peak at 1.8 kHz. In addition, in implementing noise control for this source, it is very valuable to know that it is the narrow peak at 1.8 kHz that is driving the maximum noise. This knowledge helps to zero-in on the source.



TABLE 16.3

Octave and One-Third Octave Bands

Band	Octave			One-Third Octave		
	Lower Band Limit	Center	Upper Band Limit	Lower Band Limit	Center	Upper Band Limit
12	11	16	22	14.1	16	17.8
13				17.8	20	22.4
14				22.4	25	28.2
15	22	31.5	44	28.2	31.5	35.5
16				35.5	40	44.7
17				44.7	50	56.2
18	44	63	88	56.2	63	70.8
19				70.8	80	89.1
20				89.1	100	112
21	88	125	177	112	125	141
22				141	160	178
23				178	200	224
24	177	250	355	224	250	282
25				282	315	355
26				355	400	447
27	355	500	710	447	500	562
28				562	630	708
29				708	800	891
30	710	1,000	1,420	891	1,000	1,122
31				1,122	1,250	1,413
32				1,413	1,600	1,778
33	1,420	2,000	2,840	1,778	2,000	2,239
34				2,239	2,500	2,818
35				2,818	3,150	3,548
36	2,840	4,000	5,680	3,548	4,000	4,467
37				4,467	5,000	5,623
38				5,623	6,300	7,079
39	5,680	8,000	11,360	7,079	8,000	8,913
40				8,913	10,000	11,220
41				11,220	12,500	14,130
42	11,360	16,000	22,720	14,130	16,000	17,780
43				17,780	20,000	22,390

**Note:** The advantages of making broad band analyses of sound using octave or one-third octave band filter sets are that less time is needed to obtain data and the instrumentation required to measure the data is less expensive. The main disadvantage is the loss of detailed information about the sound which is available from narrow-band (FFT) analyzers.

However, as with many things, there is a cost associated with high performance. For most applications, a one-third octave analysis is usually adequate. The advantages of making broad band analyses using octave or one-third octave band filter sets are that less time is needed to obtain data and the instrumentation required to measure the data is less expensive.

When making sound measurements, several factors regarding the nature of the source should be considered. For example, whether the source is a true point

source in space (sound radiating spherically), whether the source is located close to a flat surface (sound radiating hemispherically), or between two flat surfaces (sound radiating a quarter of a sphere), will make a difference in how the measurement needs to be performed. However, a detailed discussion of measurement issues is beyond the scope of this chapter and the reader may use some of the more comprehensive works in the list of references at the end of this chapter. The American Petroleum Institute has issued a recommended practice for measuring noise from fired process heaters.<sup>4</sup>

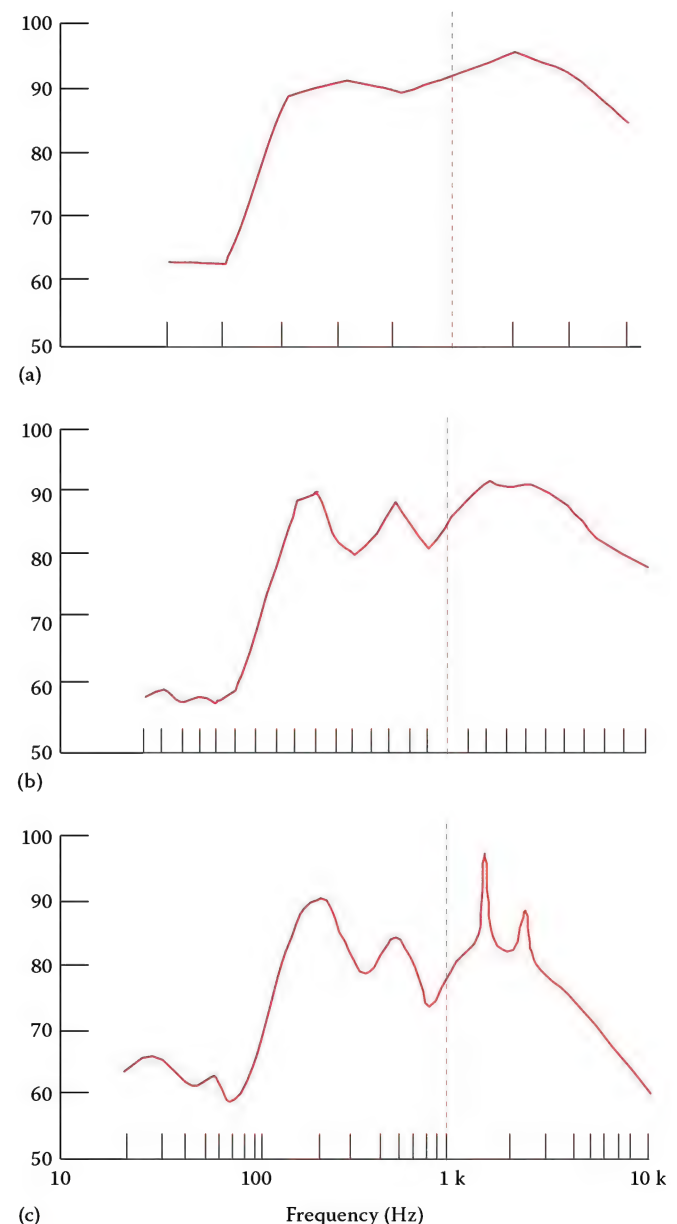


FIGURE 16.13

Same sound spectrum on three different intervals. (a) Octave band spectrum, (b) one-third octave band spectrum, and (c) narrow-band spectrum.

16.1.3.1 Overall Sound Level and How to Add dB Values

As mentioned earlier, most sounds are composites of several different levels at different frequencies. This is especially true of industrial noise. A typical burner noise curve is shown in Figure 16.14. As can be seen, there are significantly higher levels in two frequency zones, both of which will contribute to the apparent intensity experienced by a person working in the vicinity of the burner. It is difficult to describe this sound without using either a diagram like the one shown or a table listing various SPLs occurring in the different octave bands. The “overall sound level,” a single number, has been devised to represent such composite sound curves conveniently. If a single number is to be used to represent the whole curve, then it is not practical to use the average of the various levels in the octave bands, since this number would be less than the levels at the peaks and the peaks have the most influence on the listener. Therefore, one must not confuse the average with the overall sound level.

The overall sound level is calculated by adding the individual levels in the various octave bands. In columns 1 and 2 of Table 16.4, the burner sound curve has been split up into its component levels in each octave band. In column 3, the A-weighted correction has similarly been split up and listed. Column 4 gives the A-corrected values for the sound curve by simply subtracting column 3 from column 2. Now, the values in column 4 must be combined to obtain the A-weighted overall sound level.

Since the decibel is based on a log<sub>10</sub> scale, simple addition cannot be used. For example, if two values of equal

TABLE 16.4

A-Weighting of the Burner Sound Curve from Figure 16.14

Frequency (Hz)	SPL (dB)	A-Scale CF (dB)	SPL (dBA)
31.5	72	-39	33
63	75	-26	49
125	79	-16	63
250	79	-9	70
500	72	-3	69
1,000	69	0	69
2,000	68	1	69
4,000	78	1	79
8,000	83	-1	82
16,000	80	-7	73

magnitude are added, say 100 dB and 100 dB, the result is 103 dB. The formula used to add SPLs is as follows:

$$L_{total} (dB) = 10 \log_{10} \left( \sum_{i=1}^n 10^{0.1L_i} \right) \\ = 10 \log_{10} \left( 10^{0.1L_1} + 10^{0.1L_2} + 10^{0.1L_3} + \dots \right) \quad (16.5)$$

where

- $L_{total}$  is the total SPL level (dB)
- $L_i$  is each individual level (dB)
- $n$  is the number of SPLs to be added

To demonstrate how to use this equation, consider the following example:

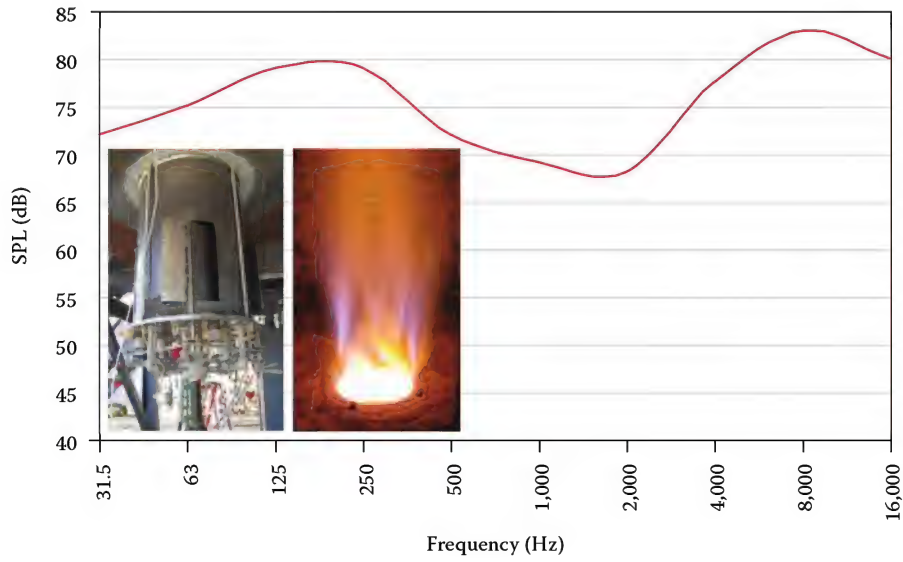


FIGURE 16.14  
Typical burner noise curve.

**Example 16.1**

Add the following SPLs together: 88, 92, and 86 dB

$$L_{\text{total}}(\text{dB}) = 10 \log_{10}(10^{0.1 \times 88} + 10^{0.1 \times 92} + 10^{0.1 \times 86}) = 94.17 \text{ dB}$$

Some simple rules of thumb can be used to perform quick estimates. They are as follows:

1. When adding dB values that are of equal magnitude or that differ by 1, the sum is 3 dB added to the greater number.
2. When the two values are different by 2–3 dB, then the sum is 2 dB added to the greater number.
3. When adding two values that differ by 4–9 dB, then the sum is 1 dB added to the greater number.
4. For values that differ by 8 dB or more, the sum is just the larger number.
5. Always start with the smallest number in the list and add it to the next larger number.

To better understand why these rules work, refer to the chart in Figure 16.5. From the chart it can be seen that 1 W is equal to 120 dB.

$$1 \text{ W} = 120 \text{ dB}$$

$$1 \text{ W} = 120 \text{ dB}$$

$$2 \text{ W} = 123 \text{ dB}$$

On the chart, 2 W registers 123 dB on the line. Similarly, the reason that numbers 10 dB or more in difference are neglected is because

$$1.0 \text{ W} = 120 \text{ dB}$$

$$0.1 \text{ W} = 110 \text{ dB}$$

$$1.1 \text{ W} = 120 \text{ dB}$$

Since the 110 dB contributes only a 0.1 W, it is neglected in the approximation. The example becomes more vivid when adding two numbers that differ by 20 dB or more.

$$1.00 \text{ W} = 120 \text{ dB}$$

$$0.01 \text{ W} = 100 \text{ dB}$$

$$1.01 \text{ W} = 120 \text{ dB}$$

Rule number 5 is especially necessary when adding a list that contains several numbers that are almost equal in value and one or more that are 10 dB greater, such as in a list that contains six values of 90 dB and one value of 100 dB. If we begin to add from the 100 dB value we will arrive at a wrong result. It should be noted that the rules

**TABLE 16.5**

Addition Rules

What is the overall dBA level?			
Frequency Hz	SPL dB	A-scale CF dB	SPL dBA
31.5	72	-39	33
63	75	-26	49
125	79	-16	63
250	79	-9	70
500	72	-3	69
1,000	69	0	69
2,000	68	1	69
4,000	78	1	79
8,000	83	-1	82
16,000	80	-7	73

Overall sound level = 85 dBA

Caution: Overall SPL does not = average SPL

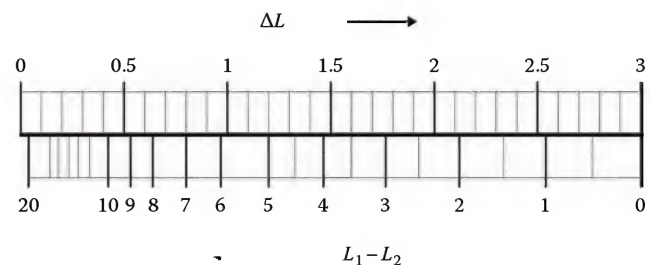
provided are approximations. For exact calculations, the formulas should be used.

Table 16.5 shows the effect of applying the addition rules to the values generated by breaking up the burner noise curve. At the end of the addition list, 1 dB has been added to compensate for any errors due to approximation.

As an alternative to using the aforementioned rules of thumb for level addition, the nomogram in Figure 16.15 can be used to determine the sum of the two levels  $L_1$  and  $L_2$ : For a certain difference between the two levels  $L_1$  and  $L_2$  in the lower scale of the nomogram, the corresponding level increase  $\Delta L$  to be added to the higher one of the two levels can be found in the upper part of the nomogram. For example, add the following pressure levels: 90 dB + 90 dB. The difference between these two values is zero. Locating zero on the lower scale of the nomogram, one finds a value of 3 directly above it; therefore, 90 dB + 90 dB = 93 dB.

**16.1.3.2 Atmospheric Attenuation**

When a sound wave travels through still air, it is absorbed or attenuated by the atmosphere. Over a



**FIGURE 16.15**  
Nomogram for noise level addition.



couple of hundred feet, the atmosphere does not significantly attenuate the sound; however, over a few thousand feet, the sound level can be substantially reduced. The amount of sound that is attenuated in still air largely depends on the atmospheric temperature and relative humidity. Figure 16.16 depicts the atmospheric attenuation for aircraft-to-ground propagation in SPL per 1000 ft (300 m) distance for center frequencies of 500, 1000, 2000, 4000, and 8000 Hz. Notice that the atmospheric attenuation is larger at higher frequencies than at lower frequencies. For example, suppose that we are 1000 ft (300 m) away from a noise source and that the atmospheric temperature and relative humidity is 80°F (27°C) and 10%, respectively. The plots in Figure 16.16 show that the atmospheric attenuation for 500 Hz is approximately 2 dB whereas for 8000 Hz the attenuation is 55 dB.

Atmospheric attenuation, outdoors, can also be affected by turbulence, fog, rain, and snow. Typically, the more turbulence present in the air, the more the attenuation. There appears to be conflicting evidence as to whether or not fog attenuates sound. It is recommended that no excess attenuation be assigned to fog or light precipitation.

## 16.2 Industrial Noise Pollution

Thus far, sound has been discussed. So what is noise? An all-encompassing definition would be that noise is any undesirable sound. By saying this, the concept is introduced that what is considered to be noise is somewhat subjective, and depends on several temporal and circumstantial factors.

For example, it is not unusual for a person to encounter SPLs of 100–110 dB at a sporting event, in a stadium full of cheering fans, and yet not be perturbed by it. On the contrary, the barely 45 dB sound of a dripping faucet may cause considerable annoyance in the quiet of the night. Table 16.6 gives some examples of noise levels.

Industrial noise pollution is a major concern for society as a whole. In a recent survey, the effects of exposure to noise in refinery workers were studied extensively. A cross-section of workers in different divisions/units was chosen. It was found that noise levels averaged 87–88 dBA in the aromatic and paraffin facilities and 89 dBA in alkylation facilities. In comparison, workers in the warehouse, health clinics, laboratories, and offices were, generally, found to be exposed to much lower levels.

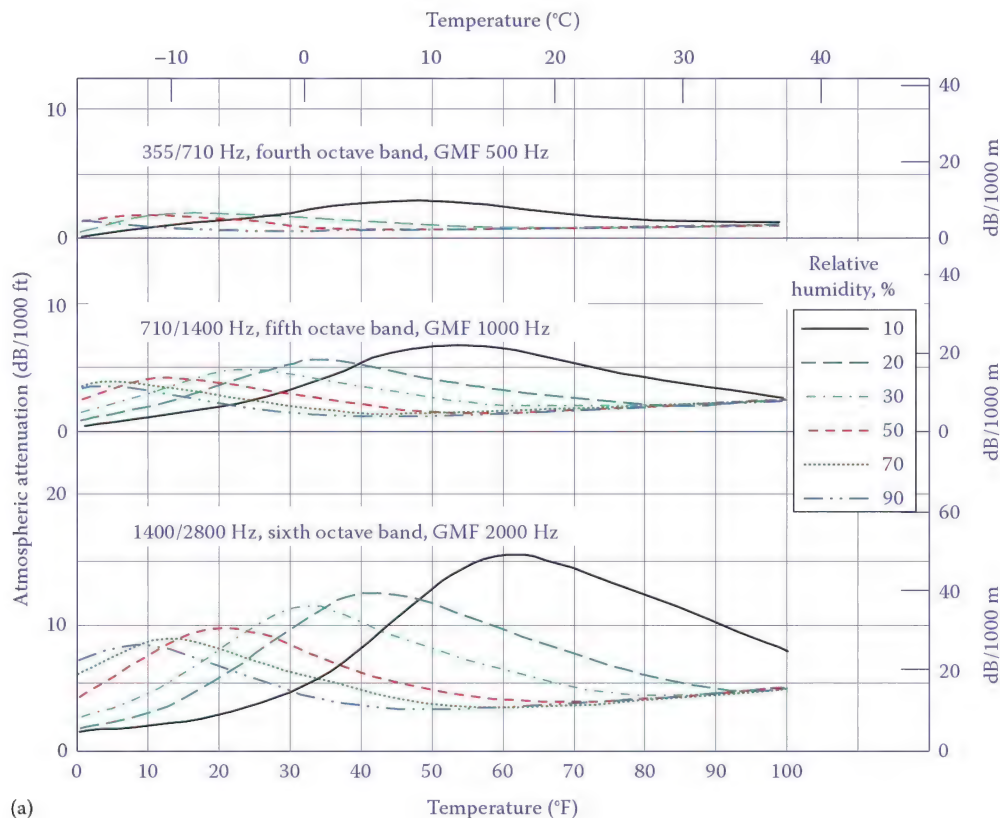


**FIGURE 16.16**

Atmospheric attenuation for (a) fourth, fifth, and sixth octave bands. (Adapted from Beranek, L.L., *Noise and Vibration Control*, McGraw Hill Book Co., New York, 1971.)

(continued)

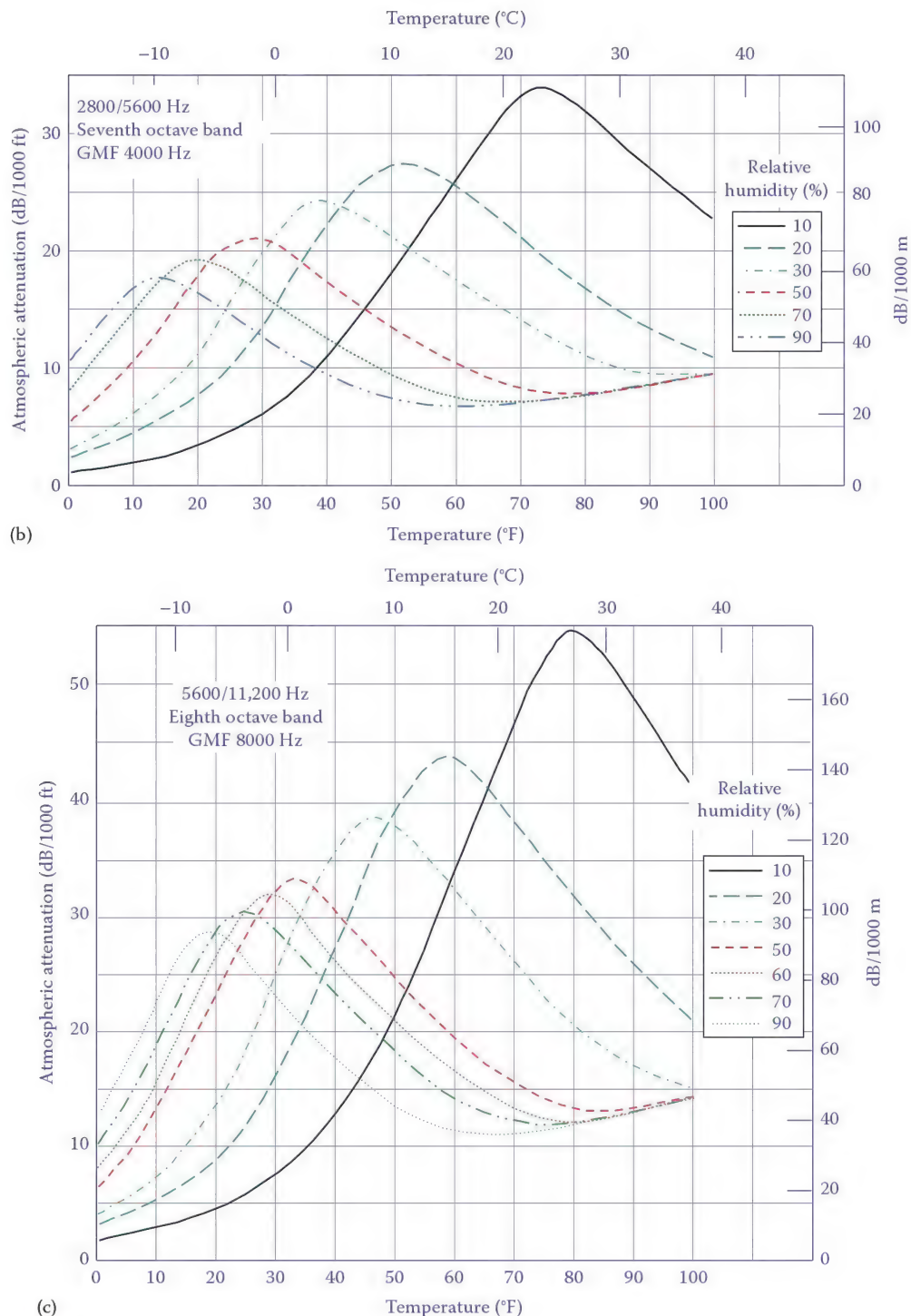


FIGURE 16.16 (continued)

Atmospheric attenuation for (b) seventh octave band and (c) eighth octave band. (Adapted from Beranek, L.L., *Noise and Vibration Control*, McGraw Hill Book Co., New York, 1971.)

Noise can damage hearing, and can cause physical or mental stress (increased pulse rate, high blood pressure, nervousness, sleep disorders, lack of concentration, and irritability). Irreparable damage can be caused by single transient sound events with peak levels exceeding 140 dBA (e.g., shots or explosions). Long-duration

exposure to noise exceeding 85 dBA can lead to short-term reversible hearing impairment and long-term exposure to levels higher than 85 dBA can cause permanent hearing loss.

The following is a mathematical model based on empirical data (ISO 1999) used to calculate the maximum

TABLE 16.6

Sound Levels of Various Sources

Threshold of hearing	0 dBA
Rustle of leaves	10 dBA
Normal conversation (at 1 M)	30 dBA
Min level in Chicago at night	40 dBA
City street, very busy traffic	70 dBA
Noisiest spot at Niagara Falls	85 dBA
Threshold of pain	120 dBA
Jet engine (at 50 M)	130 dBA
Rocket (at 50 M)	200 dBA

permissible continuous noise level at the work place that will not lead to permanent hearing loss:

$$L_{A,m}(\text{dBA}) < 85 + 10 \log_{10} \left( \frac{24}{T_n} \right) \quad (16.6)$$

where  $T_n$  is the daily noise exposure time (h).

Wearing ear protection devices at continuous noise levels greater than 85 dBA can prevent or reduce the danger of permanent hearing damage. There are two levels of protection commonly used by industrial workers to reduce noise levels: earplugs and ear muffs as shown in Figure 16.17. Earplugs can lower the noise level by 5–45 dB, depending on the type of plug, sound frequency, and how well the user inserts them into the ear. Ear muffs are designed to cover the entire ear and typically reduce noise levels by 5–50 dB depending on the type of ear muff and the frequency of the sound.

### 16.2.1 OSHA Requirements

Title 29 CFR, section 1910.95 of the U.S. Occupational Safety and Health Act (OSHA) pertains to the protection of workers from potentially hazardous noise. Table 16.7 shows OSHA permissible noise exposure levels.



FIGURE 16.17  
Typical earplugs and muffs.

TABLE 16.7

OSHA Permissible Noise Exposure

Duration per Day (h)	SPL (dBA) (Slow Response)
8.0	90
6.0	92
4.0	95
3.0	97
2.0	100
1.5	102
1.0	105
0.5	110
0.25 or less	115

Note: Exposure to impulsive or impact noise should not exceed 140 dBA.

OSHA requires that the employer must provide protection against the effects of noise exposure when the sound levels exceed those shown in Table 16.7. When the daily noise exposure consists of two or more periods of noise exposure at different levels, their combined effect should be considered rather than the individual effects of each. According to OSHA the exposure factor (EF) is defined as<sup>5</sup>

$$EF = \frac{C_1}{T_1} + \frac{C_2}{T_2} + \frac{C_3}{T_3} + \dots + \frac{C_n}{T_n} \quad (16.7)$$

where

$C_n$  is the total time of exposure at a specific noise level  
 $T_n$  is the total time of exposure permitted at that level and shown in Table 16.7

If the EF exceeds 1.0, the employee's exposure is above OSHA limits. If OSHA identifies such a situation, a citation may be issued and a grace period defined in which the employer must correct the violation or face penalties as high as \$10,000 per day.

### 16.2.2 International Requirements

Regulations aimed at protecting individuals from industrial noise pollution have been enforced in almost all industrialized countries. The noise caused in industries and the work place is generally taken as a serious issue.

Most countries have adopted 85 dBA as the limit for the permissible noise. At any work place with sound levels exceeding 85 dBA, ear protection devices must be worn and workers exposed to this level should have their hearing level checked periodically.

### 16.2.3 Noise Sources and Environment Interaction

The predominant individual sources of noise in chemical and petrochemical plants are burners (process



furnaces, steam boilers, and flares), fans, compressors, blowers, pumps, electric motors, steam turbines, gears, valves, exhausts to open air, conveyors, and silos, airborne splash noise from cooling towers, coal mills, and loading and unloading of raw and finished materials.

Although noise pollution caused by industrial sectors is minor compared to that caused by road and rail traffic, industrial noise receives more attention due to public representation. ISO 1996 provides information on how to measure and assess environmental noise, which can be used to help determine regulations for noise protection in residential neighborhoods located near industrial areas.

National or local authorities must enforce noise limits that should not be exceeded in the neighborhood. The magnitude of limiting values, additional charges for tonality and impulsive noise, and the legalities change not only from country to country, but sometimes within different states and regions in the same country. In general, nighttime noise limits are 10–15 dB lower than that for the daytime.

### 16.3 Mechanisms of Industrial Combustion Equipment Noise

There are four major mechanisms of noise production in combustion equipment. They can be categorized as either predominantly high-frequency or low-frequency sources. They are as follows:

1. Low-frequency noise sources
  - a. Combustion roar and instability
  - b. Fan noise
2. High-frequency noise sources
  - a. Gas jet noise
  - b. Piping and valve noise

#### 16.3.1 Combustion Roar and Combustion Instability Noise

To better understand combustion roar, the mixing process taking place between the fuel and the oxidant on a very minute scale is considered. It is known that a well-blended mixture of fuel and air will burn very rapidly if the mixture is within the flammability limits for that fuel. On the other hand, a raw fuel stream that depends on turbulence and momentum to mix in the ambient

air and achieve flammable mixture, tends to create a slower combustion process. In either case, when regions in the mixing process form a flammable mixture and encounter a source of ignition, combustion takes place. The closer an air-fuel mixture is to stoichiometry prior to encountering an ignition source, the more rapid the combustion.

When combustion occurs near stoichiometric conditions, more of the energy released is converted into noise. For example, Figure 16.18 shows a test flare operating at the same flow rate of fuel, but with different degrees of mixing. The photograph on the left shows a flame with a high degree of mixing between the fuel and ambient air; notice this produces a short, crisp flame that burns smokelessly. The photograph on the right, however, shows the same flare operating at the same fuel flow rate, but with poor mixing between the fuel and ambient air. For this condition, notice that the flame is not as crisp (softer) and is significantly larger. Although the fuel flow rate is the same for each of these cases, the combustion noise generated is significantly different. The well-mixed flame (photograph on the left) is about 5 dB higher in noise emissions than the poorly mixed flame (photograph on the right).

The noise emitted from each small region of rapidly combusting mixture adds up to create what is called combustion roar. Therefore, combustion roar is largely a function of how rapidly the fuel is being burned. In addition, in the context of combustion equipment like burners and flares, usually the larger the fuel flow rate, the more the turbulence in the combustion process. Since turbulence directly influences the mixing rate, high turbulence processes also produce more combustion roar. Thus, it is more accurate to state that the level of combustion roar generated by a combustion process is a function of the amount of fuel burned and how rapidly one arranges to burn it.

##### 16.3.1.1 Flare Combustion Roar

It has been recognized for a long time that the noise emitted from a normal operating flare has two mechanisms at work; namely, combustion roar and gas jet noise. Combustion roar typically resides in the lower frequency region of the audible frequency spectrum, while gas jet noise occurs in the higher frequencies, as illustrated in Figure 16.19.

As previously mentioned, the amount of combustion roar emitted from a flare, generally, depends on how fast the waste gas stream mixes with the ambient air. A waste gas stream that exits a flare tip with a low velocity and



FIGURE 16.18

Test flare at John Zink test site in Tulsa, OK. Combustion of identical fuel flow rates with different degrees of mixing. Total noise emissions of the flame in the photograph on the left are about 5 dB higher than that of the flare flame in the photograph on the right.

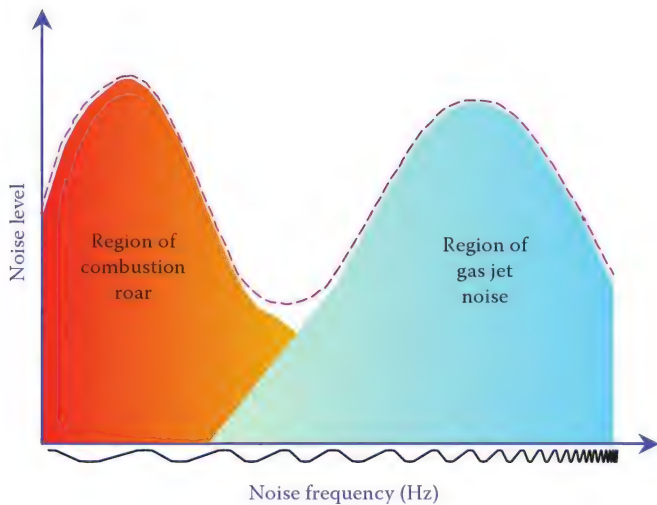


FIGURE 16.19

Typical noise signature emitted from a flare.

low levels of turbulence will mix slowly with the ambient air and burn relatively quietly. These types of flames are called buoyancy-dominated flames. Conversely a waste gas stream that exits a flare tip with a high velocity and high levels of turbulence will burn much faster and create substantially more combustion noise for the same heat release rate. These high velocity flames are referred

to as momentum-dominated flames. Increasing the rate at which the waste gas burns, results in “bigger explosions” of the air-fuel mixture. These “bigger explosions” create larger disturbances in the atmosphere resulting in higher levels of combustion roar.

Combustion roar emitted from a flare flame is not highly directional and is considered to be a monopole source. That is, it is analogous to a spherical balloon whose surface is expanding and shrinking at various frequencies and emitting uniform spherical waves.

High levels of turbulence in a flare flame are usually desirable because it helps reduce radiation and increase the smokeless capacity of the flare. Unfortunately, high levels of turbulence increase combustion roar. Unlike the solution for flare radiation reduction, it is not practical to increase the height of a flare stack or boom to reduce combustion noise because even doubling the flare stack height would reduce the SPL at the flare base by only about 6 dB (see Equation 16.4). In addition, combustion roar is a low-frequency sound that can travel a great distance without being substantially attenuated by the atmosphere. The noise signature of low-frequency combustion roar typically consists of a broadband spectrum with a single peak.

Flare flames emit combustion noise over a broad spectrum of frequencies. The maximum (peak) noise level typically occurs at a frequency of about 63 Hz.



**TABLE 16.8**

Calculation of the Typical Combustion Noise Spectrum of a Stable Burning Flare from the Overall Sound Pressure Level (OASPL)

Frequency (Hz)	Resultant Noise Spectrum (dB)
31.5	OASPL-5
63	OASPL-4
125	OASPL-9
250	OASPL-15
500	OASPL-20
1000	OASPL-21
2000	OASPL-24
4000	OASPL-28
8000	OASPL-34

If one knows the OASPL emitted from a flare, the combustion noise spectrum can be estimated by subtracting the values shown in Table 16.8<sup>6</sup> from the OASPL. Notice that at frequencies above about 500 Hz, the noise contribution from flare combustion becomes relatively insignificant.

A typical method for estimating the sound power level in dB (PWL) emitted from a flare flame is to relate the energy released from the combustion of the waste gas stream (chemical energy) to the noise energy liberated by the combustion. The ratio of noise energy to chemical energy released from the combustion is called the thermoacoustic efficiency (TAE). For a stable burning flare, the TAE typically varies between  $1 \times 10^{-9}$  and  $3 \times 10^{-6}$ . The value of the TAE largely depends on the turbulent mixing of the waste gas with ambient air; the faster the mixing, the higher the TAE.

A flare flame that is highly turbulent, such as the high-pressure flare in Figure 16.20, can have a TAE on the order of  $1 \times 10^{-6}$ . However, flames with low levels of turbulence, such as low-pressure flares or a butane lighters (Figure 16.21) for example, can have a TAE on the order of  $1 \times 10^{-9}$ . For every order of magnitude that the TAE changes, the SPL will change by 10 dB. For example, the difference in SPL for a TAE of  $1 \times 10^{-6}$  and  $1 \times 10^{-9}$  is 30 dB.

Figure 16.22 is a photograph of an engineer collecting noise levels from a flare using a noise meter. Data collection is important because it allows for the TAE of flares to be determined; this information can then be used to model the level of combustion roar emitted from a flare. To demonstrate how the TAE is determined from experimental data consider the following example:

**FIGURE 16.20**

Photograph of a high-pressure and low-pressure flare burning the same fuel.

**FIGURE 16.21**

Shadow photograph of a burning butane lighter.





FIGURE 16.22  
Engineer measuring flare noise.

### Example 16.2

**Given:** A flare burning a waste gas stream with a heat release of  $5000 \times 10^6$  Btu/h (1465 MW). Noise measurements show that the SPL 400 ft (120 m) from the flame is 100 dB. Estimate the TAE of the flare flame.

**Solution:** The sound power emitted from the flame,  $W$ , can be determined as follows (see also Equations 16.3 and 16.4):

$W$ (watts)

$$= 1 \times 10^{-12} \left[ \text{antilog}_{10} \left( \frac{L_p + 10 \log_{10}(4\pi r^2) - 10.5}{10} \right) \right] \quad (16.8)$$

where

$L_p$  is the SPL in dB (100 dB for the example)

$r$  is the distance from the flame in feet (400 ft for the example)

Substituting these values into Equation 16.8 gives  $W = 1792$  W. The TAE is then calculated to be

$$\begin{aligned} \text{TAE} &= \frac{\text{Acoustical power}}{\text{Thermal power}} \\ &= \frac{1792 \text{ W}}{1465 \times 10^6 \text{ W}} = 1.2 \times 10^{-6} \end{aligned}$$

Since the TAE is on the order of magnitude of  $1 \times 10^{-6}$ , one would expect that the flame would be highly turbulent and momentum-dominated.

Figure 16.23 shows data obtained from field measurements of the PWL emitted from a number of industrial flares operating at different loads.<sup>7</sup> This data includes combustion roar as well as the noise

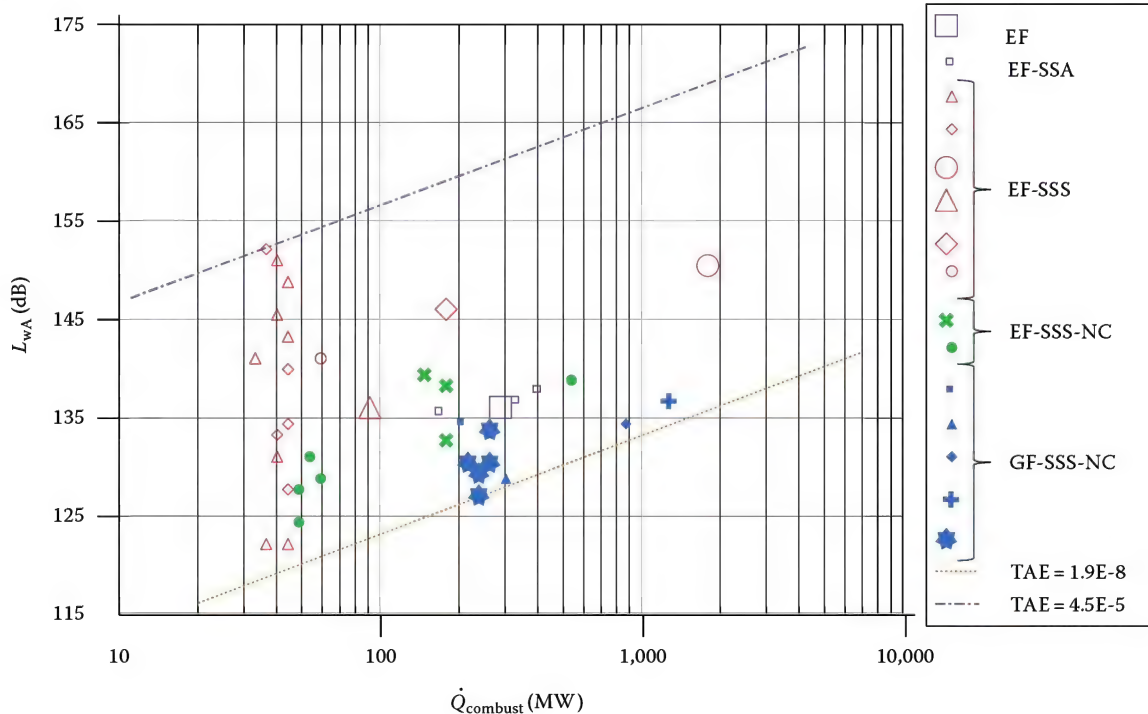


FIGURE 16.23

PWL  $L_w$  calculated from measured noise data, plotted versus heat release rate,  $\dot{Q}_{\text{combust}}$ , for different types of industrial flares under various operating conditions. EF, elevated (single-point) flare; GF, (enclosed) ground flare; SSA, smoke suppression by air; SSS, smoke suppression by steam; NC, equipped with advanced noise control.

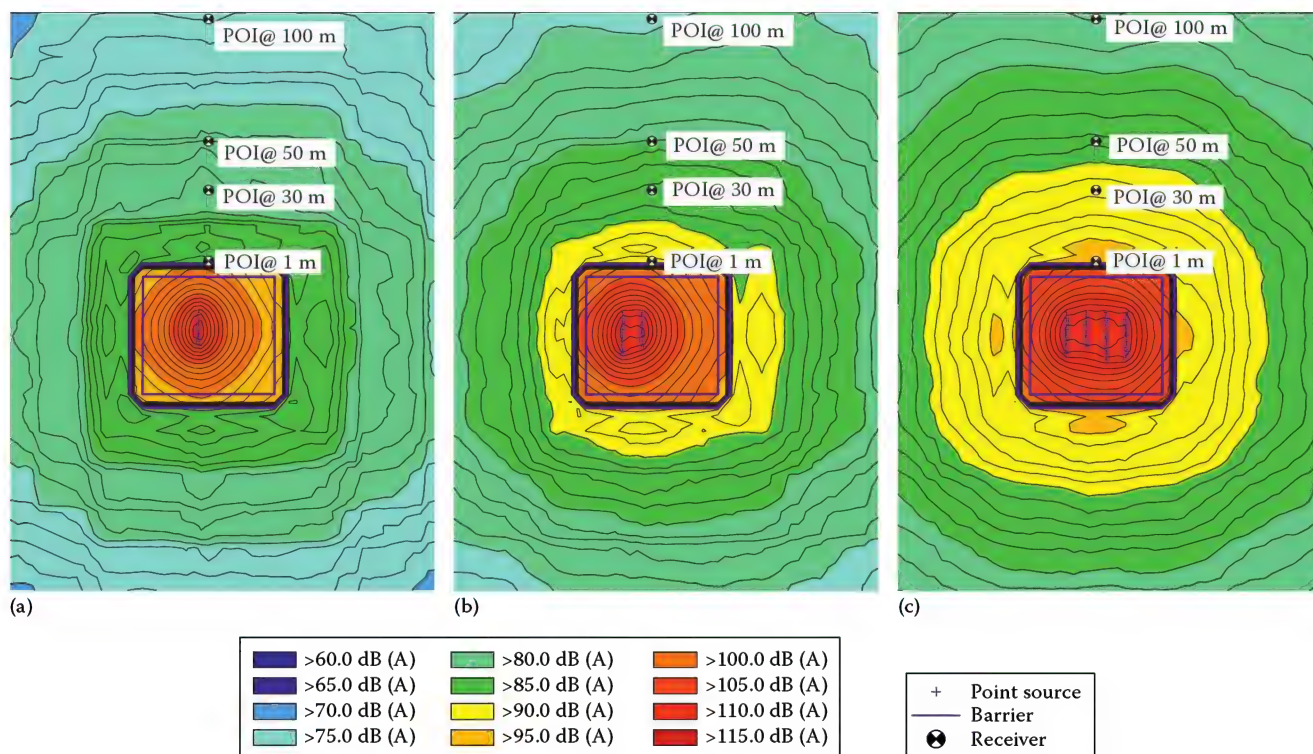


FIGURE 16.24

Predicted sound pressure field contour plots for a multipoint LRGO flare system. (a) First stage in operation; (b) stages 1 and 2 in operation; (c) all stages in operation.

emitted from valves, injectors, smoke suppression devices, etc. during data collection. The two lines in the figure represent constant TAE corresponding to the maximum and minimum values of the data set; the minimum TAE is  $1.9 \times 10^{-8}$  and maximum TAE is  $4.5 \times 10^{-5}$ . A central problem with using this approach for determining the TAE lies in applying it to a whole flare system instead of the combustion process alone. Doing so means that TAE becomes a “lumped parameter” incorporating all effects that have an impact on the acoustical behavior of the flare, i.e., noise emissions from valves, injectors, smoke suppression devices, etc. as well as any noise control measures installed. Alternative approaches to evaluating TAE can be found in the literature.<sup>8</sup>

Another problem with using the TAE concept to predict combustion noise is that it does not take the frequency characteristics of the noise emissions into account. Frequency characteristics are very important for the design of adequate noise control measures and will also determine the human perception of the noise emissions since the ear’s sensitivity for noise is frequency-dependent (see Section 16.1).

Additional challenges arise for spatially extended flare systems that can no longer be treated as point sources. Prediction of the noise emissions of a grade-mounted multipoint flare system requires the correct modeling

not only of the individual burners and their combustion and jet noise emissions, but also of the arrangement of the burners in the flare pit and the effect of the radiation fence surrounding the burner array. Figure 16.24 shows the calculated sound pressure field contour plots for a multipoint, so-called linear relief gas oxidizer (LRGO) flare system at different operating conditions.

In summary, it can be concluded that the TAE concept applied to flare systems will usually only allow a very rough estimate of the actual noise emissions and the associated effect of these emissions on persons in the neighborhood of the flare. In some cases, the results can be dramatically different than the actual situation. A key issue in developing reliable noise prediction tools for flares that are more generally applicable in a broad range of operating conditions lies in a proper treatment of the individual sources that contribute to the overall noise emissions of a flare system.

### 16.3.1.2 Flare Combustion Instability Noise

If a flame lifts too far above a flare tip, it can become unstable. An unstable flame will periodically lift and then reattach to the flare tip and create a low-frequency rumbling noise. Typically, this rumbling noise occurs in the frequency range of 5–10 Hz and is usually called combustion instability. Being as low in frequency as it is, combustion



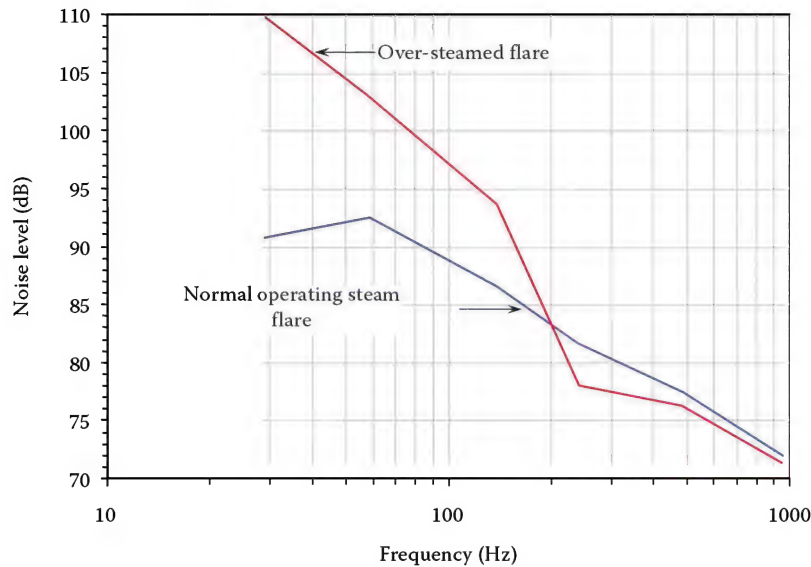


FIGURE 16.25

SPL emitted from a steam-assisted flare operating at normal conditions and at over-steamed conditions (combustion instability).

instability noise is usually inaudible, but can travel over several miles without being substantially attenuated by the atmospheric air. When there are reports of shaking the walls and windows of buildings in the vicinity of a flare, it is usually due to combustion instability.

If too much steam or air is added in the base of a flare tip, the waste gas stream can be over-aerated causing the flame to periodically lift and reattach at the tip. This periodic lifting and reattachment of the flame from the flare tip is the mechanism responsible for creating the low-frequency rumbling noise. Combustion instability noise can usually be reduced by lowering the steam flow rate to a steam-assisted flare or by lowering the blower air flow rate to an air-assisted flare. Figure 16.25 graphically depicts a typical steam-assisted flare operating under both normal conditions as well as over-steamed conditions.<sup>9</sup> Note that the combustion noise frequency shifts substantially to a lower region and the level dramatically increases when the flare is over-steamed.

### 16.3.1.3 Burner Combustion Noise

Like flares, burner combustion noise is an unwanted sound associated with combustion roar and combustion instability. In many situations, the combustion noise can be the dominant source of noise emitted from a burner. Combustion roar and combustion instability are quite complex by nature. The literature contains a variety of combustion noise and combustion instability prediction techniques for burners operating in a furnace. Most of these prediction techniques are based on experimental studies that attempt to correlate the acoustic power radiated by the burner/furnace geometry, laminar burning

velocity of the air-fuel mixture, and various turbulence parameters such as the turbulent length scale and intensity. This section does not attempt to discuss these prediction techniques in detail, but gives a broad and general discussion of combustion roar and combustion instability noise using some of the results from these studies.

Figure 16.14 is a plot showing a typical noise spectrum emitted from a burner operating under normal conditions in a furnace. Notice that the noise spectrum has two peak frequencies associated with it; the high-frequency noise contribution is from the fuel gas jets while the low-frequency contribution is from the combustion roar. As with combustion roar emitted from flares, burner combustion roar is associated with a smooth broad band spectrum having relatively low conversion efficiency from chemical energy to noise (TAE): in the range of  $1 \times 10^{-9}$  to  $1 \times 10^{-6}$ . However, the combustion noise spectrum associated with a burner and a flare is not similar. The reason is that a flame burning in the open atmosphere will behave differently compared to a flame that is burning in an enclosed chamber such as a furnace.

The combustion roar associated with flares typically peaks at a frequency of approximately 63 Hz while the combustion roar associated with burners can vary in the 200–500 Hz range. Burner noise can have a spectrum shape and amplitude that can vary with many factors. These factors include the (1) internal shape of the furnace, (2) design of the burner muffler, plenum, and tile, (3) acoustic properties of the furnace lining, (4) transmission of the noise into the fuel and air supply system, and (5) transmissive and reflective characteristics of the furnace walls and stack.



#### 16.3.1.4 Burner Combustion Instability Noise

Combustion instability within a furnace is characterized by a high amplitude low-frequency noise often resembling the puffing sound of a steam locomotive. This type of noise can create significant pressure fluctuations within a furnace that can cause damage to the structure and radiate high noise levels to the surroundings.

Figure 16.26 is a plot showing the SPL for a gas burner operating under normal conditions and with instability. It is obvious that the SPL increases substantially when the operation is accompanied by instability. Combustion instability noise has a high efficiency of conversion of chemical energy to noise (TAE). Typically the TAE from burner combustion instability is in the range of  $1 \times 10^{-4}$ .<sup>10</sup>

The oscillations caused by combustion instability are naturally damped by pressure drop losses through the burner and furnace, and therefore cannot be sustained unless energy is provided. These steady oscillations are sustained by energy extracted from the rapid expansion of the air-fuel mixture upon reaction. Over the years, furnace operators have used several techniques in an attempt to eliminate combustion instability. Some of these techniques include modifying the (1) furnace stack height, (2) internal volume of the furnace, (3) acoustical properties of the furnace lining, (4) pressure drop through the burner by varying the damper position, (5) fuel port diameter, (6) location of the pilot, and (7) flame stabilization techniques.

#### 16.3.2 Fan Noise

The noise emitted from industrial fans typically consists of two noise components: broadband and discrete tones. Vortex shedding of the moving blades and the interaction

of the turbulence with the solid constructed parts of the fan create the broadband noise. This broadband noise is of the dipole type, meaning that the noise is directional. On the other hand, the discrete tones are created by the periodic interactions of the rotating blades and nearby upstream and downstream surfaces. Discrete tonal noise is usually the loudest at the frequency at which a blade passes a given point. The tonal frequency is easily calculated by multiplying the number of blades times the impeller rotation speed in revolutions per second.

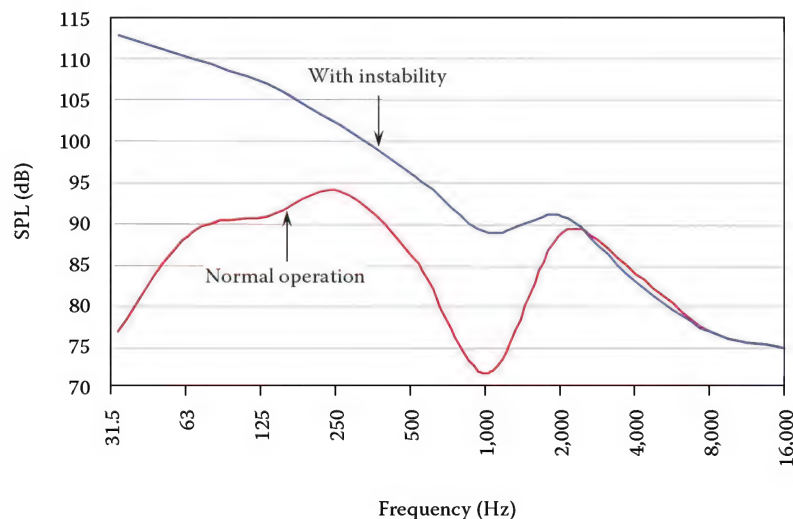
The broadband and discrete tonal noise emitted from fans can radiate from both the suction and pressure side of a fan and through the fan casing. The noise can radiate downstream through the ducting and discharge into the environment at an outlet. Fan and duct systems should include provisions to control this noise if residential areas are located nearby. Installation of mufflers and silencers on the suction and the discharge sides of the fan, as well as wrapping of the casing and the ducts are common methods for reducing fan noise.

#### 16.3.3 Gas Jet Noise

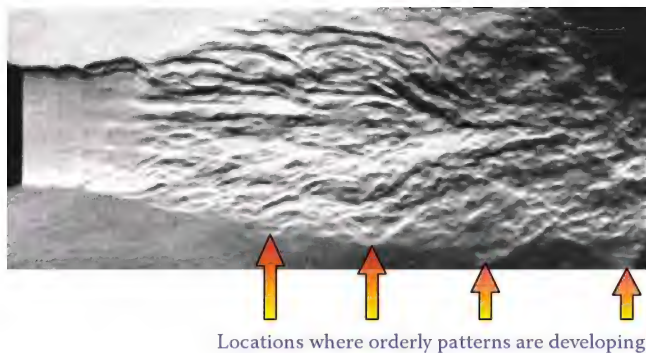
Gas jet noise is very common in the combustion industry and in many instances it can be the dominant noise source within a combustion system. The noise created when a high-speed gas jet exits into an ambient gas usually consists of two principal components: gas jet mixing noise and shock-associated noise.<sup>11</sup>

##### 16.3.3.1 Gas Jet Mixing Noise

Studies have shown that a high-speed gas jet exiting a nozzle will develop a large-scale orderly pattern as



**FIGURE 16.26**  
Burner SPL normal and with instability.

**FIGURE 16.27**

Development of orderly wave patterns within a high-speed gas jet.

shown in Figure 16.27. This orderly structure is known as the “global instability” or “preferred mode” of the jet. The presence of both the small-scale turbulent eddies within the jet and the large-scale structure is responsible for the gas jet mixing noise.

The source of gas jet mixing noise begins near the nozzle exit and extends several nozzle diameters downstream. Near the nozzle exit, the scale of the turbulent eddies is small and predominantly responsible for the high-frequency component of the jet mixing noise. The lower frequencies are generated further downstream of the nozzle exit where the large-scale orderly pattern of the gas jet exists.

Gas jet mixing noise consists of a broadband frequency spectrum. The frequency at which the spectrum peaks depends on several factors including the (1) diameter of the nozzle, (2) Mach number of the gas jet, and (3) temperature ratio of the fully expanded jet to the ambient gas. In the flare and burner industry, gas jet mixing noise typically peaks somewhere between 2,000 and 16,000 Hz.

The overall SPL created by gas jet mixing depends on several variables including the (1) distance from the gas jet, (2) angle of the observer relative to the gas jet centerline, (3) Mach number, (4) fully expanded gas jet area, and (4) density ratio of the fully expanded jet to the ambient gas.

The maximum overall SPL of gas jet mixing noise occurs at an angle between approximately  $15^{\circ}$ – $30^{\circ}$  relative to the centerline of the gas jet as illustrated in Figure 16.28.<sup>11</sup>

As one moves in either direction from this angle, the noise level typically drops off significantly. For example, the overall SPL created by gas jet mixing can be reduced as much as 25 dB when one moves from an angle of maximum noise level ( $15^{\circ}$ – $30^{\circ}$ ) to an angle directly behind the nozzle ( $180^{\circ}$ ).

### 16.3.3.2 Shock-Associated Noise

When a flare or burner operates above a certain fuel pressure, a marked change occurs in the structure of

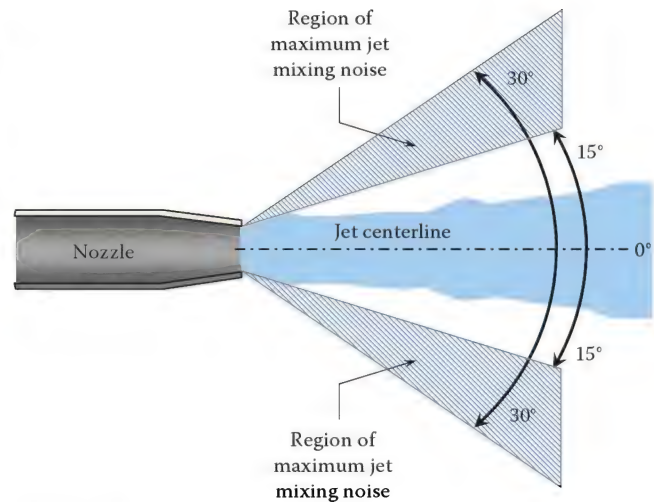
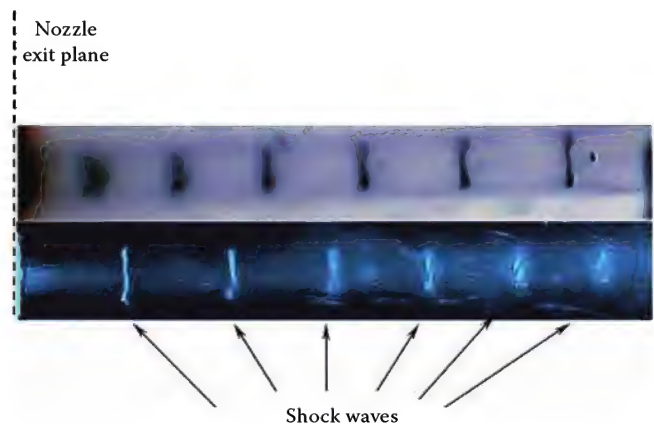
**FIGURE 16.28**

Illustration showing the region of maximum jet mixing noise.

the gas jet. Above a certain pressure called the critical pressure, the gas jet develops a structure of shock waves downstream of the nozzle as shown in Figure 16.29. The critical pressure of a gas jet typically occurs at a pressure of 12–15 psig (0.8–1 barg), depending on the gas composition and temperature. These shock cells consist of compression and expansion waves that repeatedly compress and expand the gas as it moves downstream. Using Schlieren photography, several investigators have seen as many as seven shock cells downstream of a nozzle. These shock cells are responsible for creating two additional components of gas jet noise: screech tones and broadband shock-associated noise.

Screech tones are distinct narrow-band frequency sounds that can be described as a “whistle” or “screech.” The literature reports that these tones are emitted from the fourth and fifth shock cells downstream of the nozzle exit as shown in Figure 16.30.<sup>12</sup>

**FIGURE 16.29**

Photograph showing shock waves downstream of an air jet.

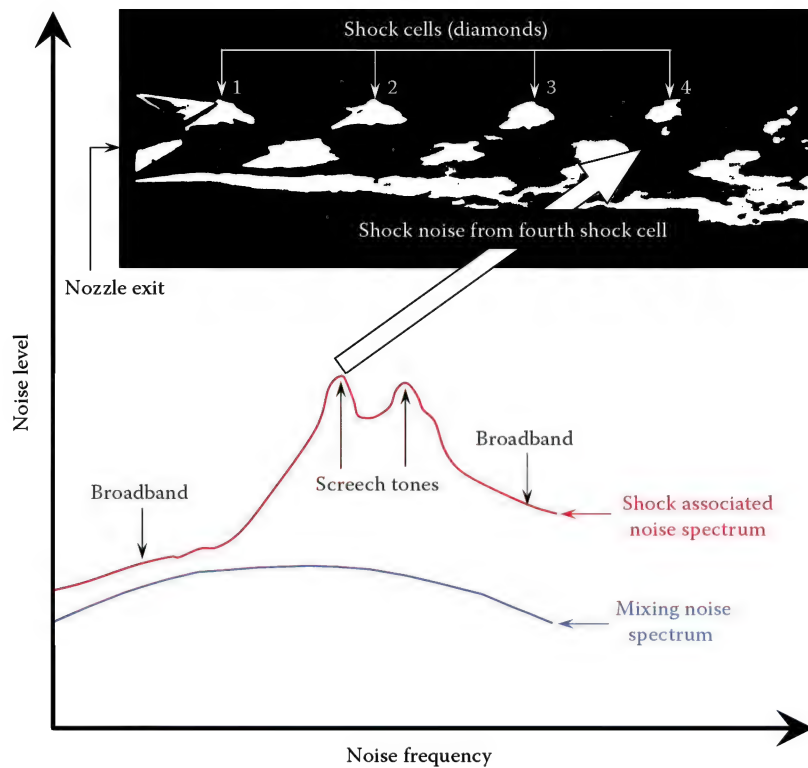


**FIGURE 16.30**  
Screech tone emissions.

The sound waves from these shock cells propagate upstream, where they interact with the shear layer at the nozzle exit. This interaction then creates oscillating instability waves within the gas jet. When these instability waves propagate downstream they interfere with the fourth and fifth shock cells causing them to emit the screech tones. Screech tone noise is not highly directional (monopole noise source), unlike gas jet mixing noise.

Broadband shock-associated noise occurs when the turbulent eddies within the gas jet pass through shock waves. The shock waves appear to suddenly distort the turbulent eddies which creates a noise that can range over several octave bands. The broadband, shock-associated peak frequency noise typically occurs at a higher frequency than the screech tone peak frequency.

#### 16.3.4 Valve and Piping Noise

When a gas flowing steadily in a pipe encounters a valve, a change in the flow pattern and pressure will occur that can create turbulence and shock waves downstream of the valve. Typically, when valves are partially closed, creating a reduction in flow area, the small flow passage behaves much like an orifice and produces jet noise. As discussed earlier, turbulence and shock waves create mixing noise and shock-associated noise. This noise can

radiate downstream through the pipe and exhaust into the environment at an outlet and/or radiate through the pipe wall not only into the space near the valve itself, as illustrated in Figure 16.31, but also at relatively large distances from the valve.

Usually, butterfly valves and ball valves are noisier than globe valves. Butterfly valves and ball valves

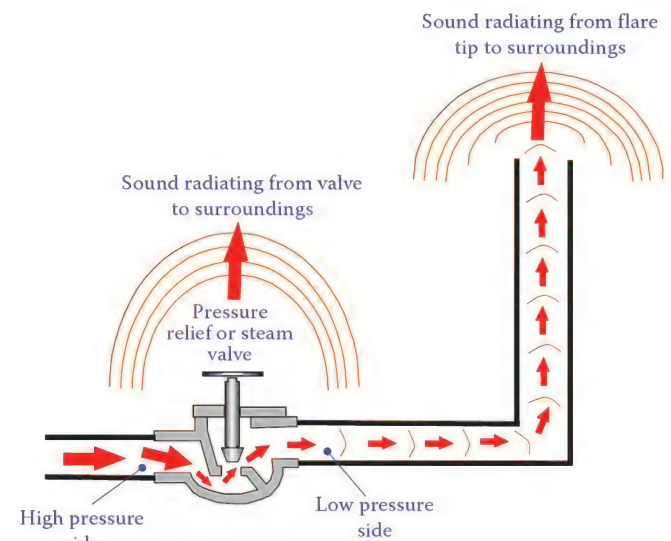


**FIGURE 16.31**  
Noise radiating from a valve.



typically have a smaller vena contracta than a globe valve operating at the same pressure drop which results in higher levels of mixing and shock-associated noise. As a general guideline when the pressure ratio across a valve is less than approximately 3, the mixing noise and shock-associated noise are within about the same order of magnitude. However, for pressure ratios greater than 3, shock noise usually dominates mixing noise.<sup>13</sup> There are several methods used for reducing the noise emitted from a valve. These include sound-absorptive wrapping of the pipes and the valve casings and the installation of silencers between the valve and the connected pipes. In addition, special low-noise valve designs with multiple pressure drop stages exist that generate less noise than standard designs.

## 16.4 Noise Abatement Techniques

There are three places noise can be reduced: at the source, in the path between the source and personnel, and on the personnel.<sup>14</sup> The ideal place to stop noise is at the source. There are several techniques used in the flare and burner industry to reduce the noise at the source, but these techniques have limitations. Ear protection can reduce noise relative to the personnel using it; unfortunately, a plant operator cannot ask a surrounding community or workers within a nearby office building to wear ear protection when the noise levels become a problem. The most common method for reducing noise is in the path between the source and personnel, using silencers, plenums, and mufflers. The purpose of this section is to discuss the most common and effective noise abatement techniques utilized in the flare and burner industry.

### 16.4.1 Flare Noise Abatement Techniques

The following individual sound sources can contribute to the overall noise emissions of flares:

1. Combustion process
2. Gas jet and flow noise of the released gases
3. Smoke suppression equipment
  - a. Jet and flow noise by steam and air injection
  - b. Combustion air fans
4. Pilot burners
5. Valves (gas and steam side) and connected piping

As previously discussed the two principal sources of noise emitted from industrial flares are combustion roar and gas jet noise. Inhibiting the rate at which the air and fuel streams mix can reduce the level of combustion roar; however, this noise abatement technique generally tends to reduce the smokeless performance and increase thermal radiation (see Chapter 8) and flame length. Reducing the mixing rate of the air and fuel stream in order to lower combustion roar levels usually does not justify the accompanying sacrifices in the performance of a flare.

In such cases, enclosed flares may provide one solution. Enclosed flares are designed to completely hide a flare flame in order to reduce noise and thermal radiation levels. The design of these flare systems typically consists of an insulated enclosure with a wall around the air inlets, as shown in the photograph in Figure 16.32. These types of flares can substantially reduce noise emissions as compared to open elevated flares.

There are several abatement techniques commonly used to reduce the gas jet noise emitted from flares. Such techniques include mufflers, water injection, and modifications to the nozzle geometry. Mufflers are most commonly used on steam-assisted flares to abate the high-pressure steam jet noise as shown in Figure 16.33.

In most flare systems, steam is supplied to nozzles at a pressure of 100–150 psig (7–10 barg). These high-pressure steam jets produce high-frequency mixing and shock-associated noise. A number of flare muffler styles have been used in the industry with varying degrees of noise abatement performance. Many of these mufflers are designed with a fiber material several inches thick placed on the inside. Mufflers usually do a good job of absorbing the high-frequency steam jet noise, as demonstrated by the data in Figure 16.34. This plot shows the noise spectrum emitted from a steam-assisted flare operating with and without a muffler on the lower steam jets. The data

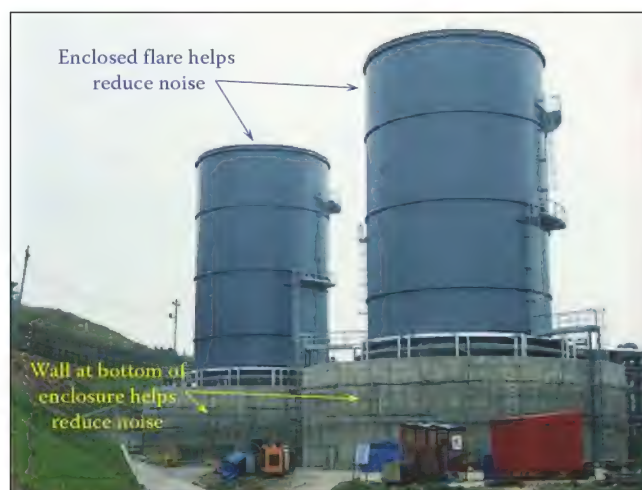


**FIGURE 16.32**  
Photograph of two enclosed flares.

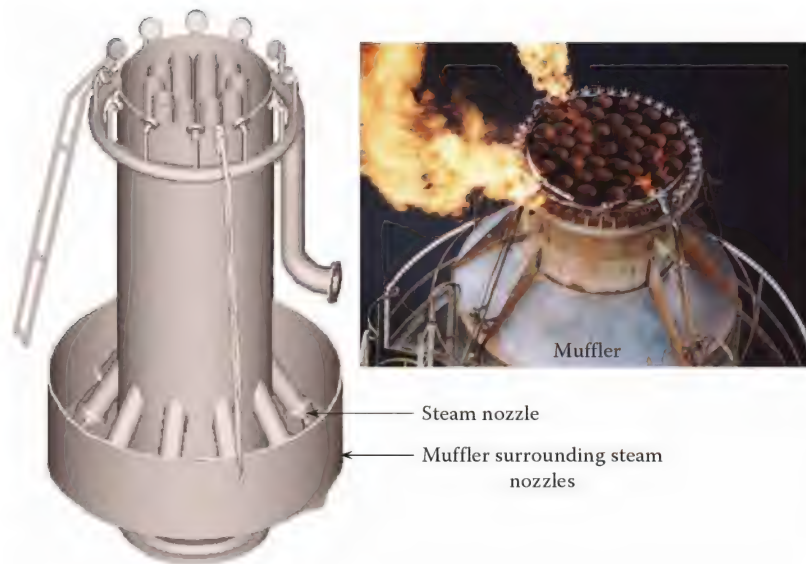


**FIGURE 16.33**  
A steam-assisted flare with a muffler.

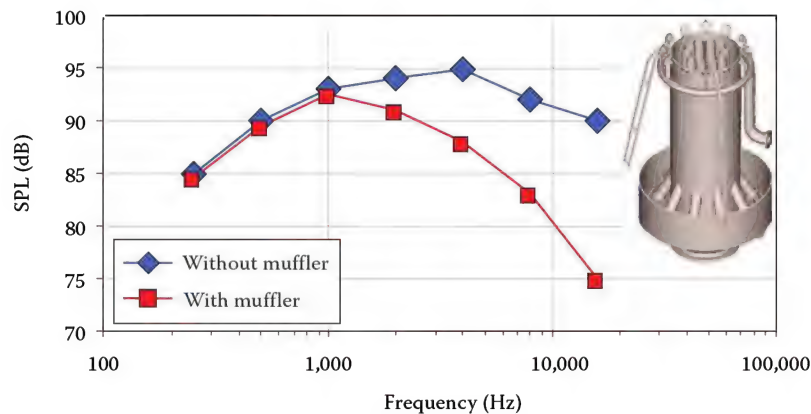


**FIGURE 16.34**  
Steam jet noise emitted with and without muffler.

clearly show that mufflers are more efficient at absorbing the higher noise frequencies than the lower ones.

Instead of using a muffler, noise from steam injector nozzles in steam-assisted flares can also be decreased by reducing the amount of steam required to ensure smokeless combustion. This method of (indirect) noise control does not call for any mufflers or other sound absorbing devices: its working principle is that less noise is generated because of the lower steam pressure and flow rate. Figure 16.35 shows the PWL spectra of the noise emitted from two types of steam-assisted flares. The data are for the two flares burning the same type and flow rate of fuel with the steam flow adjusted as to just obtain smokeless combustion. To do so, the more efficient XP flare tip uses less steam and, therefore, emits less noise.

In high-pressure flaring applications, gas jet noise can be the major source of noise. In 2000, the John Zink Company developed a unique method for reducing gas jet noise from

high-pressure flares by injecting water into the waste gas stream near the flare nozzle exit (see Figure 16.36).<sup>15</sup> The water injection method appears to substantially reduce the shock-associated noise as shown in Figure 16.37. This plot depicts the noise spectrum emitted from a John Zink high-pressure flare operating with and without water injection. Schlieren photography shows that water injection does not eliminate the downstream shock cell structure, but does appear to alter its appearance. This suggests that water injection suppresses the feedback mechanism responsible for growth of the gas jet instability that leads to screech tones.

Gas jet noise reduction using water injection is more pronounced when flaring high-molecular-weight gases as compared to low-molecular-weight gases at the same operating pressure. Test data show that high-molecular-weight gases are more dominated by screech tone noise than low-molecular-weight gases operating at the same



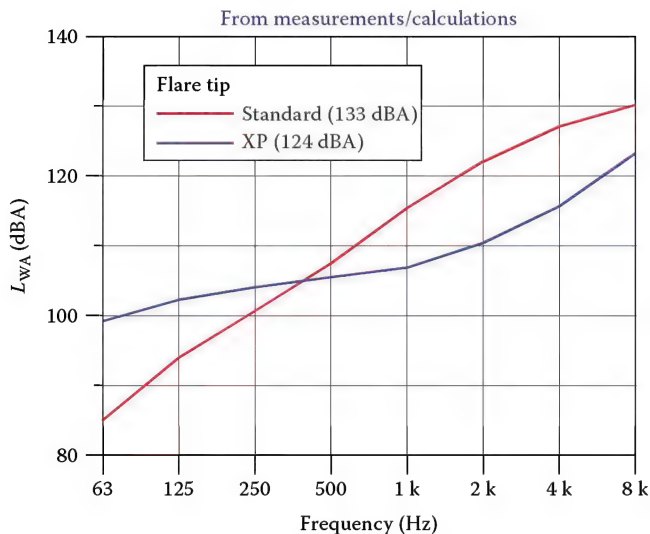


FIGURE 16.35

Example for noise abatement in steam-assisted flares by reducing the amount of steam required to ensure smokeless combustion. A-weighted PWL for a standard flare tip (overall PWL 133 dBA) and a modern John Zink Company XP flare tip (124 dBA). Values measured (XP) and calculated based on measurements (standard tip).

pressure, which explains why gas jet noise reduction, using water injection, is more pronounced when flaring high-molecular-weight gases.

It is very common in the flare industry to design a flare using several small-diameter nozzles in order to reduce

the A-weighted gas jet noise level. Gas jet noise emitted from high-pressure flares usually peaks at a frequency between approximately 2,000 and 16,000 Hz. The peak frequency is a function of several variables, but is most affected by the diameter of the nozzle. For example, a 1-in. (25 mm) diameter gas jet nozzle will peak at a frequency between 2000 and 4000 Hz, whereas a 1/4-in. (6.4 mm) diameter gas jet nozzle will peak between 8,000 and 16,000 Hz. To the human ear, a group of several smaller-diameter gas jet nozzles will appear quieter than a single larger nozzle operating at the same pressure and mass flow rate; the primary reason being that the group of smaller nozzles will peak at a higher frequency, where the human ear is less sensitive. Designing a flare with many small-diameter nozzles is not always practical or economical to build. Some large-capacity flare designs would require several thousand nozzles to substantially reduce the gas jet noise.

#### 16.4.2 Burner Noise Abatement Techniques

Typical sound sources contributing to the overall noise emissions of burners used in industrial heaters and furnaces are as follows:

- Combustion process
- Gas jet noise of the fuel gas at the burner
- Pilot burners
- Combustion air fan
- Steam or air injection for fuel atomization
- Control valves and connected pipes

The most important of the aforementioned sound sources, typically, are the (1) combustion roar from the combustion process itself, which resides in the frequency range of approximately 100–1000 Hz, and the (2) gas jet noise, which typically ranges between 4,000 and 16,000 Hz. The mid-to-high-frequency noise is the most annoying and damaging to the ear. Several techniques have been used to suppress the noise emitted within the mid-to-high frequencies. Four common techniques used to reduce noise in industrial burners are the following:

1. Sound absorption in the burner plenum
2. Mufflers at air inlets of natural draft burners
3. Acoustically optimized furnace wall construction
4. Acoustical treatment of the air ducts in forced draft burners

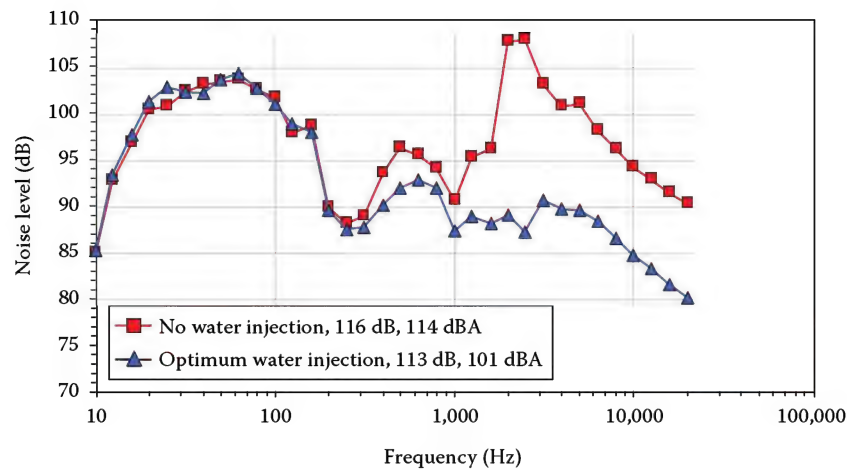
Figure 16.38 shows a plot of the SPL as a function of the frequency for a burner operating with and without a muffler. Clearly, without the muffler, the noise level is higher especially in the higher frequency region.



FIGURE 16.36

Water injected into a high-pressure flare.





**FIGURE 16.37**  
Noise spectrum from a high-pressure flare with and without water injection.

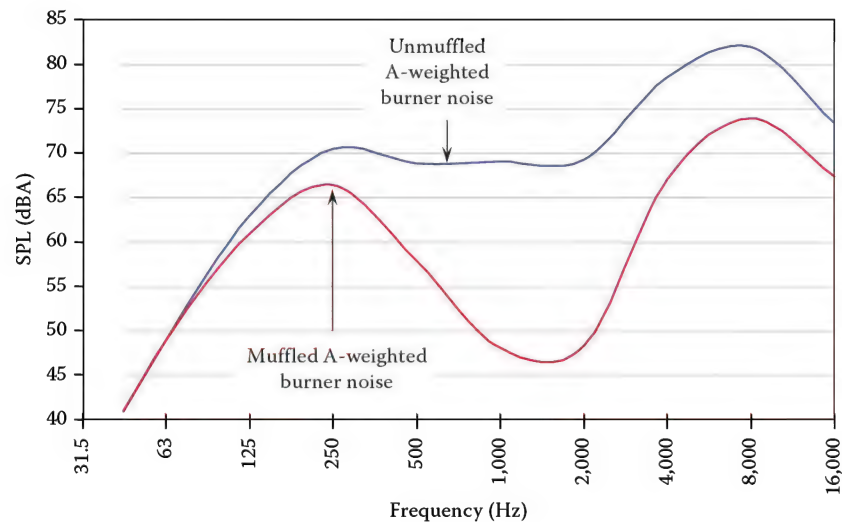


**FIGURE 16.38**  
Sound pressure versus frequency for a burner operating with and without a muffler.

The performance of burner mufflers can be optimized through their size, but also through design. For example, Figure 16.39 shows a muffler located at the air intake of a natural draft burner in two different designs. Although these two mufflers are similar in size, the muffler shown on the left side will provide better performance than the muffler shown on the right side. By designing the muffler with a 90° turn, the sound wave is required to impact the muffler wall and change directions several times before exiting the muffler. Each time the sound wave impacts the wall and changes direction, energy is lost resulting in lower noise emissions.

When space is limited around a furnace, designing each burner with a muffler can be a problem. In some cases

common plenum chambers for groups of burners can be used as shown in Figure 16.40. Properly designed plenum chambers can provide a reduction in burner noise emissions in addition to the reduction achieved by the mufflers.

#### 16.4.3 Valve and Piping Noise Abatement Techniques

Valve and piping noise abatements include sound-absorptive wrapping of the pipes and valve casings, installation of silencers between the valves and the connecting pipes, and the use of low-noise valve designs with multiple pressure stages. Acoustical pipe lagging is similar to thermal pipe insulation. However, whereas acoustical pipe lagging also provides excellent

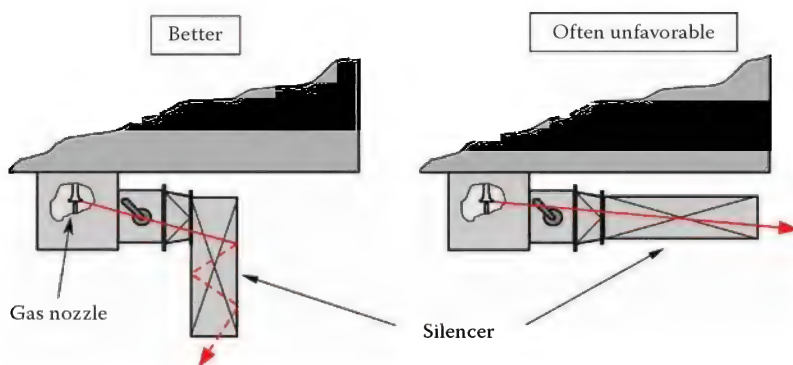
**FIGURE 16.39**

Illustration showing two different muffler designs. Although the mufflers are similar in size, the design on the left side provides better noise reduction performance than the design on the right side.

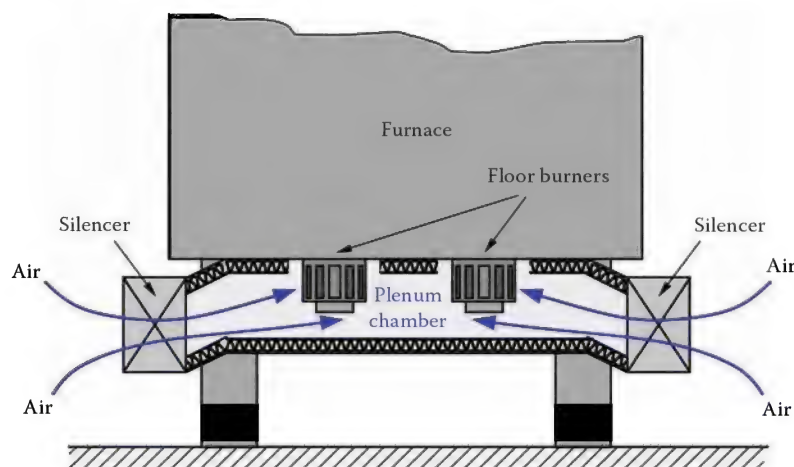
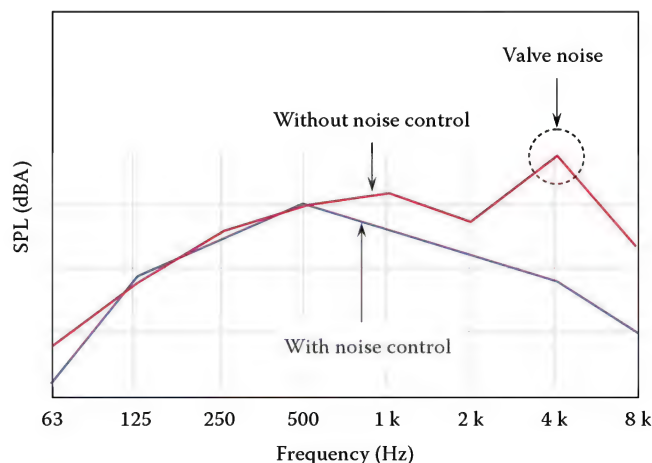
**FIGURE 16.40**

Illustration showing a common plenum chamber for floor burners in a furnace.

thermal insulation, many thermal insulations provide only poor noise control. Rigid insulations for cold service (such as foam glass installed on smaller-diameter pipes) can actually aggravate the noise situation by conducting the noise to the outer surface. Although acoustical energy radiated per unit area of insulated and jacketed pipe is less than for the same noninsulated pipe, the surface area of an insulated and jacketed pipe is greater. The product of these two factors can cause larger-diameter jacketed pipes to radiate more noise than bare pipes.<sup>16</sup>

Piping requiring acoustical treatment in a typical petrochemical plant is often in cold service. These lagging systems have to be both thermal and acoustical insulators. For that reason, fibrous insulation followed by an outer leaded aluminum jacket is commonly used. Sometimes, very noisy pipes need a layer of impregnated vinyl sandwiched between layers of fibrous insulation, called a septum system.<sup>16</sup>

Figure 16.41 shows an example of noise emitted from a steam control valve located at the base of an elevated, steam-assisted flare. In the original configuration, a

**FIGURE 16.41**

Noise emissions from a steam control valve. "Without noise control" refers to an uninsulated pipe equipped with a butterfly valve. "With noise control" refers to insulated pipe equipped with a low-noise valve.

standard butterfly valve is used and neither the valve nor the connecting steam piping is insulated. During these tests the waste gas flow rate was very low; therefore the flare noise emissions were not significant. The data show that the noise emissions are dominated by the valve noise with a peak frequency of 4000 Hz. After installing a low-noise valve and acoustically insulating the steam pipes, the noise emissions at frequencies of 1000 Hz and above are significantly reduced. Noise emissions at 500 Hz and below remain unchanged because these are dominated by the combustion noise coming from the flare tip.

#### 16.4.4 Fan Noise Abatement Techniques

Fan noise can usually be addressed similar to valve and piping noise:

1. Silencers can be installed at the suction and pressure sides of the fan particularly for fans communicating with the atmosphere on either the suction or the pressure side and thereby cut down on noise coming out of these portals.
2. Acoustically enclose the fan casing to address noise radiated from or transmitted through the casing surface.
3. Acoustically isolate the ductwork leading to and from a fan.

At the design stage, one may consider the use of low-noise motors and the use of impellers with more blades and reduced tip speed, etc.

### 16.5 Analysis of Combustion Equipment Noise

#### 16.5.1 Multiple Burner Interaction

A burner manufacturer will typically guarantee a burner noise level at a location 3 ft (1 m) directly in front of the muffler. When several burners are installed in a furnace, however, the noise level 3 ft (1 m) from the burner may be higher than for a single burner due to the noise contribution from surrounding burners. The purpose of this section is to give an example that illustrates the noise level increase due to noise emitted from surrounding burners.

##### Example 16.3

**Given:** Assume a furnace with a simple burner configuration, as illustrated in Figure 16.42, with burner B operating alone, and the noise level is 85 dB at location 2.

**Find:** How is the noise level determined at location 2 when all burners are operating?

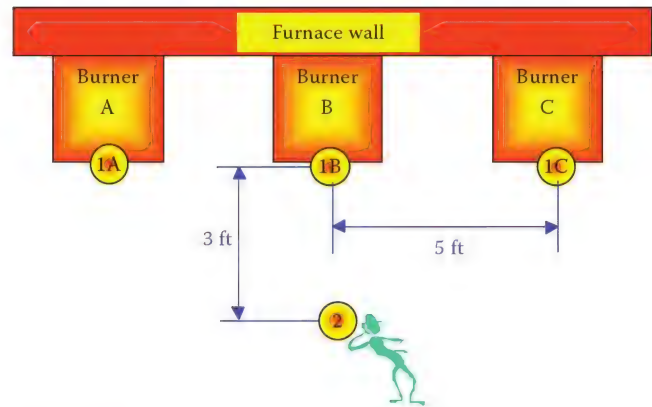


FIGURE 16.42

Illustration used for burner noise example.

**Solution:** First, find the PWL,  $L_w$ , emitted from each burner, assuming that the noise is emitted at the muffler exit at points 1A, 1B, and 1C. Assume that the noise spreads over a uniform sphere from each of these points. The PWL can be calculated as follows (see Equation 16.4):

$$L_w = L_p - 10 \log_{10} \left( \frac{1}{4\pi r^2} \right) - 10.5 \quad (16.10)$$

where

$L_p$  is the SPL

$r$  is the distance from the source (ft)

The noise level 3 ft (1 m) from burner B (location 2) is 85 dB when it is operating alone. From Equation 16.10,  $L_{wB} = 95.03$  dB. Assuming that all burners are operating at the same conditions, the PWL must be 95.0 dB for each one. The SPL contribution,  $L_p$ , can now be calculated at location 2 when burner A is operating alone by solving Equation 16.10 for  $L_p$ :

$$L_p = L_w + 10 \log_{10} \left( \frac{1}{4\pi r^2} \right) + 10.5 \quad (16.11)$$

For this case  $L_{wA} = 95.03$  and  $r = (5^2 + 3^2)^{0.5} = 5.83$  ft. Substituting these values into Equation 16.11 gives  $L_{pA} = 79.2$  dB. This is the SPL contribution emitted from burner A measured at location 2. Since the distance from burner C to location 2 is the same, we know that the SPL contribution from burner C at location 2,  $L_{pC}$ , is also 79.2 dB. The total SPL at location 2 can be determined by adding the SPL contribution from each burner (79.2 dB + 79.2 dB + 85 dB).

$$L_{p\text{total}} = 10 \log_{10} (10^{0.1L_{pA}} + 10^{0.1L_{pB}} + 10^{0.1L_{pC}}) = 86.8 \text{ dB}$$

For this example, the noise level will be approximately 1.6 dB higher when all the burners are operating than if burner B is operating alone.



### 16.5.2 High-Pressure Flare

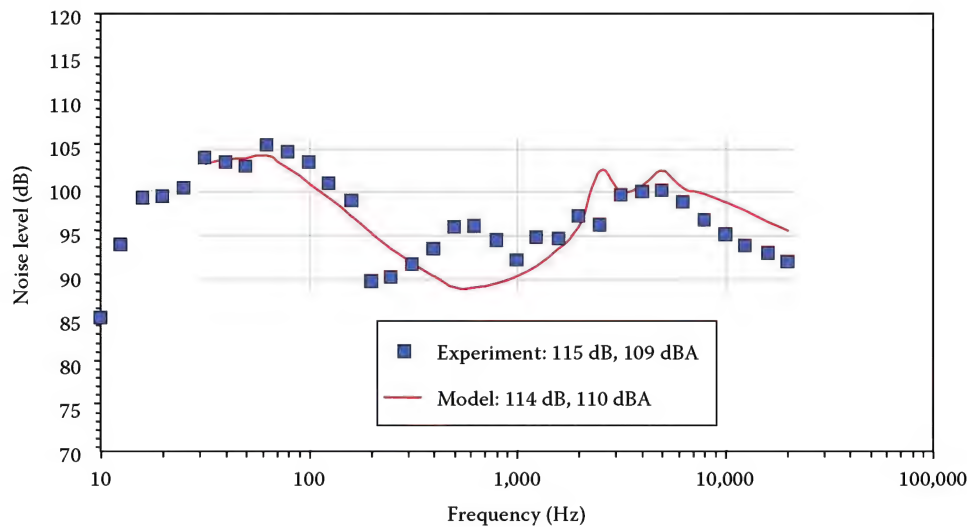
Figure 16.43 is a plot showing the SPL spectrum of a high-pressure flaring event burning natural gas in a 3.5 in. (8.9 cm) diameter flare tip. The symbols and the lines represent the noise spectrum gathered using a real-time sound-level meter and mathematical modeling results, respectively. The SPL spectrum consists of two major peaks; a low-frequency peak that corresponds to the combustion roar and a high-frequency peak that corresponds to the gas jet noise. The intermediate peak is a result of piping and valve noise. Notice that the combustion roar peaks at a frequency of approximately 63 Hz, which is typical for a stable burning open flare.

Figure 16.44 is a plot showing the noise contributions separately based on the mathematical model.

Notice that the gas jet mixing noise is a broadband frequency spectrum, while the screech noise occurs over a fairly narrow bandwidth.

The screech noise would not exist if the flare were operated below the critical gas pressure. Below the critical gas pressure, shock waves, which cause screech noise, do not form. The summation of the combustion roar, gas jet mixing noise, and screech noise provides the total SPL prediction emitted from the flare.

The OASPL determined experimentally and calculated using the mathematical model is summarized in Table 16.9. Notice that in this particular example the OASPL, on a dBA scale, is dominated by the gas jet noise. If this 3.5 in. (8.9 cm) diameter flare were designed with several smaller-diameter ports, having the same total exit area, then the gas jet noise would



**FIGURE 16.43**  
SPL spectrum for high-pressure flaring.

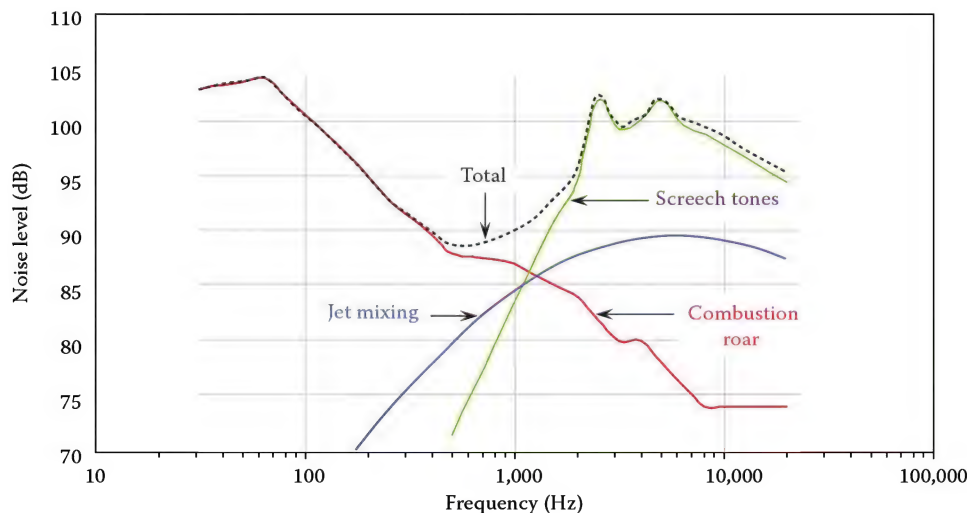


**FIGURE 16.44**  
Noise contributions separately based on the mathematical model.

TABLE 16.9

OASPL Determined Experimentally and Using the Mathematical Model

	Jet Mixing Noise	Screech Noise	Combustion Roar	Total
<i>Model</i>				
dB	105.7	105.1	113.0	114.3
dBA	105.2	105.3	97.4	108.6
<i>Experiment</i>				
dB	—	—	—	113.7
dBA	—	—	—	109.2

shift to higher frequencies. If the diameter of these ports were small enough to substantially shift the frequency of the gas jet noise, then the combustion noise would dominate on the dBA scale.

### 16.5.3 Atmospheric Attenuation Example

Figure 16.45 shows an example of the SPL received from a flare calculated at various distances and for different atmospheric attenuation. Notice at a distance of 1500 ft (460 m) from the flare, the noise level peaks at about 80 dBA, while at 3000 ft (910 m) the peak reduces to about 74 dBA if atmospheric attenuation is not taken into account. When the atmospheric attenuation is taken into account, depending on the ambient temperature and humidity level considered (see Section 16.1.3.2), there is further reduction in noise levels. It is important to note that the contribution in each case is significant. Given the particular atmospheric conditions in this example, the attenuation has created a significant difference. The 10 dB attenuation (from 74 to 64 dBA) amounts to the sound

intensity reduction equal to one-tenth of its intensity at 3000 ft (910 m) without atmospheric attenuation. Hence, it should be noted that measurements at large distances may vary significantly on different days for the same equipment, if the atmospheric conditions are significantly different.

The effect of wind is even stronger and the SPL at 1000 m (3300 ft) distance from a noise source may differ by more than 20 dB for downwind conditions as compared to upwind conditions.

## Glossary

**Absorption:** Conversion of sound energy into another form of energy, usually heat, when passing through an acoustical medium.

**Absorption coefficient:** Ratio of sound absorbing effectiveness, at a specific frequency, of a unit area of acoustical absorbent to a unit area of perfectly absorptive material.

**Acoustics:** Science of the production, control, transmission, reception, and effects of sound and of the phenomenon of hearing.

**Ambient noise:** All-pervasive noise associated with a given environment.

**Anechoic room:** Room whose boundaries effectively absorb all incident sound over the frequency range of interest, thereby creating essentially free field conditions.

**Audibility threshold:** Sound pressure level, for a specified frequency, at which humans with normal hearing begin to respond.

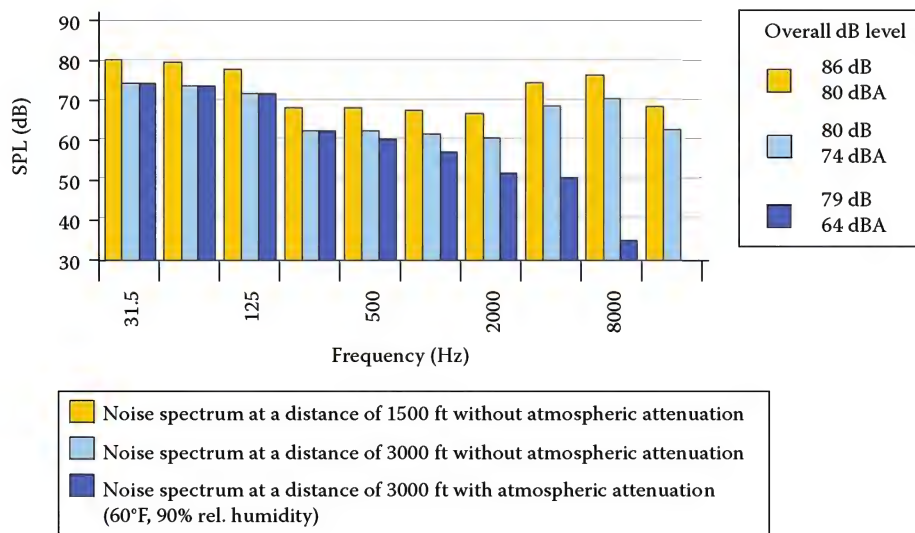


FIGURE 16.45

Effect of distance on flare noise.

**Background noise:** Ambient noise level above which signals must be presented or noise sources measured.

**Decibel scale:** Linear numbering scale used to define a logarithmic amplitude scale, thereby compressing a wide range of amplitude values to a small set of numbers.

**Diffraction:** Scattering of radiation at an object smaller than one wavelength and the subsequent interference of the scattered wavefronts.

**Diffuse field:** Sound field in which the SPL is the same everywhere, and the flow of energy is equally probable in all directions.

**Diffuse sound:** Sound that is completely random in phase; sound that appears to have no single source.

**Directivity factor:** Ratio of the mean-square pressure (or intensity) on the axis of a transducer at a certain distance to the mean-square pressure (or intensity) that a spherical source radiating the same power would produce at that point.

**Far field:** Distribution of acoustic energy at a much greater distance from a source than the linear dimensions of the source itself. See also diffraction.

**Free field:** An environment in which there are no reflective surfaces within the frequency region of interest.

**Hearing loss:** An increase in the threshold of audibility due to disease, injury, age, or exposure to intense noise.

**Hertz (Hz):** Unit of frequency measurement, representing cycles per second.

**Infrasound:** Sound at frequencies below the audible range, that is, below about 16 Hz.

**Isolation:** Resistance to the transmission of sound by materials and structures.

**Loudness:** Subjective impression of the intensity of a sound.

**Masking:** Process by which the threshold of audibility of one sound is raised by the presence of another (masking) sound.

**Near field:** That part of a sound field, usually within about two wavelengths of a noise source, where there is no simple relationship between sound level and distance.

**Noise emission level:** dBA level measured at a specified distance and direction from a noise source, in an open environment, above a specified type of surface; generally follows the recommendation of a national or industry standard.

**Noise reduction coefficient (NRC):** Arithmetic average of the sound absorption coefficients of a material at 250, 500, 1000, and 2000 Hz.

**Phon:** Loudness level of a sound, numerically equal to the SPL of a 1 kHz free progressive wave, which is judged by reliable listeners to be as loud as the unknown sound.

**Pink noise:** Broadband noise whose energy content is inversely proportional to frequency (−3 dB per octave or −10 dB per decade).

**Power spectrum level:** Level of the power in a band 1 Hz wide referred to a given reference power.

**Reverberation:** Persistence of sound in an enclosure after a sound source has been stopped. Reverberation time is the time (in seconds) required for sound pressure at a specific frequency to decay 60 dB after a sound source is stopped.

**Root-mean-square (RMS):** The square root of the arithmetic average of a set of squared instantaneous values.

**Sabine:** Measure of sound absorption of a surface. One metric sabine is equivalent to 1 m<sup>2</sup> of perfectly absorptive surface.

**Sound:** Energy transmitted by pressure waves in air or other materials which is the objective cause of the sensation of hearing. Commonly called noise if it is unwanted.

**Sound intensity:** Rate of sound energy transmission per unit area in a specified direction.

**Sound level:** Level of sound measured with a sound level meter and one of its weighting networks. When A-weighting is used, the sound level is given in dBA.

**Sound level meter:** An electronic instrument for measuring the RMS of sound in accordance with an accepted national or international standard.

**Sound power:** Total sound energy radiated by a source per unit time.

**Sound power level:** Fundamental measure of sound power, defined as

$$L_w = 10 \log \frac{P}{P_0} \text{ dB}$$

where

$P$  is the RMS value of sound power (Watts)

$P_0$  is  $1 \times 10^{-12}$  (Watts)

**Sound pressure:** Dynamic variation in atmospheric pressure. The pressure at a point in space minus the static pressure at that point.

**Sound pressure level:** Fundamental measure of sound pressure defined as

$$L_p = 20 \log \frac{P}{P_0} \text{ dB}$$

where

$P$  is the RMS value (unless otherwise stated) of sound pressure (Pascal)

$P_0$  is  $2 \times 10^{-5}$  (Pascal)



**Sound transmission loss:** Ratio of the sound energy emitted by an acoustical material or structure to the energy incident upon the opposite side.

**Standing wave:** A periodic wave having a fixed distribution in space that is the result of interference of progressive waves of the same frequency and kind. Characterized by the existence of maximum and minimum amplitudes that are fixed in space.

**Thermoacoustic efficiency:** A value used to characterize the amount of combustion noise emitted from a flame. Defined as the ratio of the acoustical power emitted from the flame to the total heat release rate of the flame.

**Ultrasound:** Sound at frequencies above the audible range, that is, above about 20 kHz.

**Wavelength:** Distance measured perpendicular to the wavefront in the direction of propagation between two successive points in the wave, which are separated by one period. Equal to the ratio of the speed of sound in the medium to the fundamental frequency.

**Weighting network:** An electronic filter in a sound level meter that approximates, under defined conditions, the frequency response of the human ear. The A-weighting network is most commonly used.

**White noise:** Broadband noise having constant energy per unit of frequency.

## References

1. A.P.G. Peterson, *Handbook of Noise Measurement*, 9th edn., GenRad, Westford, MA, 1980.
2. ISO 3744, Acoustics—Determination of sound power levels and sound energy levels of noise sources using sound pressure—Engineering methods for an essentially free field over a reflecting plane, 2010.
3. W. Daiminger, K.R. Fritz, E. Schorer, and B. Stüber, *Ullmann's Encyclopedia of Industrial Chemistry*, Vol. B7, VCH, Weinheim, Germany, 1995, pp. 384–401.
4. API, *Recommended Practice 531M: Measurement of Noise from Fired Process Heaters*, Reaffirmed Edition, American Petroleum Institute, Washington, DC, August 1995.
5. A. Thumann, and R.K. Miller, *Secrets of Noise Control*, Fairmont Press, Atlanta, GA, 1974.
6. O.C. Leite, Predict flare noise and spectrum, *Hydrocarb. Process.*, 68, 55, 1988.
7. Müller-BBM, GmbH: Noise emissions of different flare systems—field measurements taken in various refineries and petrochemical plants. Proprietary data, 1990–2004.
8. Verein Deutscher Ingenieure, VDI 3732, Standard noise levels of technical sound sources—Flares, VDI guideline, 1999.
9. W. Bussman and J. White, Steam-assisted flare testing, John Zink Co. Internal Report, September 1996.
10. A.A. Putnam, *Combustion Noise in the Handheld Industry*, Battelle Columbus Laboratories, Columbus, OH.
11. L.L. Beranek and I.L. Ve'r, *Noise and Vibration Control Engineering*, John Wiley & Sons, Inc., New York, 1992.
12. H. Shen and C.K.W. Tam, Numerical simulation of the generation of axisymmetric mode jet screech tones, *AIAA J.*, 36(10), 1801, October 1998.
13. L.L. Beranek, *Noise and Vibration Control*, McGraw Hill Book Co., New York, 1971.
14. Allied Witan Co., *Noise Facts and Control*, Company brochure, North Royalton, OH, 1976.
15. W.R. Bussman and D. Knott, Unique concept for noise and radiation reduction in high-pressure flaring, *OTC Conference*, Houston, TX, 2000.
16. L.D. Frank and D.R., Dembicki, Lower plant noise with lagging, *Hydrocarb. Process.*, 71(8), 83–85, 1992.

## Bibliography

- Energy Conservation Resources Board, Noise Control, Directive 038, dated February 16, 2007, <http://www.ercb.ca/docs/documents/directives/Directive038.pdf>, accessed 1 August 2012.
- Brief, R.S. and R.G. Confer, Interpreting noise dosimeter results based on different noise standards, *Am. Ind. Hyg J.*, 36(9), 677–682, 1975.
- Crow, S.C. and F.H. Champagne, Orderly structure in jet turbulence, *J. Fluid Mech.*, 48(3), 547–591, 1971.
- Diserens, A.H. Personal noise dosimetry in refinery and chemical plants, *J. Occup. Med.*, 16(4), 255–257, 1974.
- Gharabegian, A. and J.E. Peat, Saudi petrochemical plant noise control, *J. Environ. Eng.*, 112(6), 1026–1040, 1986.
- HFP Acoustical Consultants, Effect of flow parameters on flare stack generator noise, *Proceedings of Spring Environmental Noise Conference: Innovations in Noise Control for the Energy Industry*, Banff, AB, Canada, April 19–22, 1998.
- IEC 61672-1, Electroacoustics—Sound level meters—Part 1: Specifications, 2002.
- ISO 1683, Acoustics—Preferred reference values for acoustical and vibratory levels, 2008.
- ISO 532, Acoustics—Method for calculating loudness level, 1975.
- ISO 1996-1, Acoustics—Description, measurement and assessment of environmental noise - Part 1: Basic quantities and assessment procedures, 2003.
- ISO 3744, Acoustics—Determination of sound power levels and sound energy levels of noise sources using sound pressure—Engineering methods for an essentially free field over a reflecting plane, 2010.
- ISO 8297, Acoustics—Determination of sound power levels of multisource industrial plants for evaluation of sound pressure levels in the environment—Engineering method, 1994.

- ISO 9614-1, Acoustics—Determination of sound power levels of noise sources using sound intensity—Part 1: Measurement at discrete points, 1993.
- ISO 9613-1, Acoustics—Attenuation of sound during propagation outdoors—Part 1: Calculation of the absorption of sound by the atmosphere, 1993.
- ISO 9613-2, Acoustics—Attenuation of sound during propagation outdoors—Part 2: General method of calculation, 1996.
- Lang, W.W. Ed., A commentary on noise dosimetry and standards, *Proceedings of the Noise Congress-75*, Gaithersburg, MD, September 15–17, 1975.
- Maling, Jr., J.C. Ed., Start-up silencers for a petrochemical complex, *Proceedings of the International Conference on Noise Control Engineering*, Honolulu, HI, December 3–5, 1984.
- Powell, A. On the noise emanating from a two dimensional jet above the critical pressure, *The Aeronautical Quarterly*, 4, 103, 1953.
- Reed, R. *Furnace Operations*, Gulf Publishing, Houston, TX, 1981.
- Ribner, H.S. Perspectives on jet noise, *AIAA J.*, 19(12), 1513, 1981.
- Roberts, J.P., Gas Combustion Noise, PhD thesis, London University, London, U.K., 1971.
- Seebold, G. and A.S. Hersh, Control flare steam noise, *Hydrocarb. Process.*, 51, 140, 1971.
- Selle, G.K. Steam-assisted flare eliminates environmental concerns of smoke and noise, *Hydrocarb. Process.*, 73(12), 77–78, 1994.
- Shivashankara, B.N., W.C. Strahle, and J.C. Henkley, Combustion noise radiation by open turbulent flames, Paper 73-1025, *AIAA Aero-Acoustics Conference*, Seattle, WA, 1973.
- Straitz, J.F. Improved flare design, *Hydrocarb. Process.*, 73(10), 61–66, 1994.
- Thomas, A. and G.T. Williams, Flame Noise: sound emission from spark-ignited bubbles of combustion gas, *Proc. Roy. Soc., A*, 294, 449, 1966.
- Zwicker, E. and H. Fastl, *Psychoacoustics—Facts and Models*, Springer Verlag, Berlin, Germany, 1990.

# 17

## *Combustion Training*

Charles E. Baukal, Jr. and Myra N. Crawford-Fanning

### CONTENTS

17.1	Introduction.....	514
17.2	Participants.....	514
17.2.1	Students.....	515
17.2.1.1	Engineers.....	515
17.2.1.2	Operators.....	515
17.2.1.3	Others .....	515
17.2.2	Instructors.....	516
17.2.2.1	Employer .....	516
17.2.2.2	Supplier.....	516
17.2.2.3	University.....	517
17.2.3	Training Coordinators.....	517
17.3	Learning Styles.....	517
17.4	Subject Matter Categories.....	519
17.4.1	Fundamentals.....	519
17.4.2	Operations.....	520
17.5	Training Providers.....	520
17.5.1	Internal Providers .....	521
17.5.1.1	Forms of Internal Providers.....	521
17.5.1.2	Advantages of Internal Providers.....	522
17.5.1.3	Disadvantages of Internal Providers.....	523
17.5.2	External Providers .....	524
17.5.2.1	Forms of External Providers.....	525
17.5.2.2	Advantages of External Providers.....	525
17.5.2.3	Disadvantages of External Providers.....	526
17.5.3	Hybrid Providers .....	526
17.5.3.1	Forms of Hybrid Training.....	527
17.5.3.2	Advantages of Hybrid Training.....	527
17.5.3.3	Disadvantages of Hybrid Training.....	528
17.6	Training Locations.....	528
17.6.1	Institution.....	528
17.6.2	On-Site .....	528
17.6.3	Hub.....	529
17.6.4	Online.....	529
17.7	Training Organizations.....	530
17.7.1	ASTD.....	530
17.7.2	PTECH Organizations .....	531
17.8	Other Considerations .....	532
17.8.1	Instructor Training .....	532
17.8.1.1	Preparation.....	532
17.8.1.2	Presentation Skills.....	532
17.8.1.3	Behind the Scenes .....	533
17.8.1.4	Tools .....	534



17.8.1.5	Apparel.....	535
17.8.1.6	Checklist.....	535
17.8.1.7	Introduction and Closing.....	536
17.8.2	Accreditation .....	537
17.9	Case Studies.....	538
17.9.1	British Petroleum .....	538
17.9.1.1	Importance of Training .....	538
17.9.1.2	Training Partnership .....	538
17.9.1.3	Customized Operator Training.....	539
17.9.1.4	Results.....	541
17.9.1.5	Conclusions.....	542
17.9.2	Shintech.....	542
17.9.2.1	Course Design .....	543
17.9.2.2	Training .....	544
17.9.2.3	Results.....	544
17.9.2.4	Conclusions.....	546
17.10	Recommendations .....	546
	References.....	547

## 17.1 Introduction

Improper installation, operation, or maintenance of industrial combustion equipment could result in serious incidents, which is why training is recommended by organizations like the National Fire Protection Association (NFPA).<sup>1</sup> This training is recommended for those involved with fired equipment and usually includes operators and engineers.

The Institute of Continuing Professional Development (ICPD, 2010) defines continuing professional development as “the systematic maintenance and improvement of knowledge, skills and competence, and the enhancement of learning, undertaken by an individual throughout his or her working life.” Padfield and Schaufelberger (p. 8)<sup>2</sup> defined continuing education as including “all those processes that contribute to the advancement of an individual’s knowledge, skill, understanding, competence, and general professional and personal development.” Continuing education, continuing professional development, and professional development are all related terms that generally concern learning outside the normal workplace.<sup>3</sup>

A related term is *training*, which can be defined as “a planned effort by a company to facilitate employees’ learning of job-related competencies” where the competencies include “knowledge, skills, or behaviors that are critical for successful job performance” (p. 3).<sup>4</sup> Jacobs and Park<sup>5</sup> believe that workforce learning is the most inclusive term for the many ways that employees learn in organizations.

There are many types of continuing education, including both informal and formal training. Informal

training is generally unplanned and initiated by the individual, although it could include sanctioned learning, such as mentoring, coaching, and special assignments. For example, reading journals and magazines and attending conferences help keep employees current with changes in technology. Formal training may be defined as “planned learning activities that are intended to help individuals acquire specific areas of knowledge, awareness, and skills” and “mostly involves institutionally sponsored and endorsed programs, which would include almost all training and development (T&D) programs that organizations offer” (p. 140).<sup>5</sup> For example, on-the-job training is typically done by pairing a less experienced employee with a more experienced one who is the instructor. Employees may also take formal classes with instructors that may be for credit and possibly even leading to an advanced degree.

**Note:** This chapter contains many illustrations from and references to the John Zink Company and the John Zink Institute (JZI) as these are the organizations with which the authors are both associated and most familiar.

## 17.2 Participants

There are a number of participants who may be involved in combustion training. The most important are the students themselves who are typically engineers or operators. The instructors or trainers are responsible for delivering the course content. They may come from a variety of organizations such as the employee’s company, universities, or suppliers. Another type of

participant considered in this section is the training coordinator. These coordinators are responsible for making the arrangements for the students' organization. These three types of participants are briefly discussed in the following sections.

### 17.2.1 Students

The students are the most important participants in any training program. If they do not learn the material covered in a course, then the training has been a failure, despite the best efforts of the instructors and the training coordinators. At most plants, the two most important constituencies for training are engineers and operators. While they may work for the same organization, they generally have significantly different needs, which is why they have been separated here. Sometimes it may be preferred to have separate classes specifically designed to meet the needs of these two types of students. There may also be some other types of students such as college students, college professors, equipment suppliers, government regulators, and any others involved in industrial combustion equipment.

#### 17.2.1.1 Engineers

Engineers generally have a college degree in some field of engineering (e.g., mechanical, chemical, electrical, civil, or petroleum), although there are some "engineers" who do not have a degree in engineering. Engineers with degrees in engineering have taken many math and science classes and generally have a strong background in the fundamentals related to those subjects. Those with degrees in mechanical and chemical engineering will also have taken courses in subjects such as fluid flow, heat transfer, and chemistry (covered elsewhere in this book), which are important topics when discussing industrial combustion.

However, unless an engineer has an advanced degree related to combustion, they generally will have had few, if any, classes in combustion. Even if they have taken a college course in combustion, it is not likely to have covered industrial combustion as discussed in this book. Therefore, engineers normally need training in the specific types of combustion equipment used by their organization. Depending on how long it has been since an engineer has taken relevant courses (e.g., heat transfer) and how frequently they have used a particular subject in their job, they may or may not need a refresher in some of the basics. Even if they have not used a subject for some time, they will have different training needs compared to, say, an operator, for example, who likely has never had any formal training in that subject.

Another important consideration for training engineers is their responsibility within a given organization which usually varies significantly compared to

operators. Engineers are generally more concerned about overall performance such as thermal efficiency and pollution emissions, compared to operators who are generally more interested in other things, such as reliability and operability. Both engineers and operators will be interested in subjects such as safety because of its importance for preventing personnel from getting injured and because both types of participants will likely have had little, if any, formal training in combustion safety.

In general, training for engineers may be more theoretical compared to training for operators which may be more practical. This is sometimes a difficult balance to achieve when both types of participants are in the same class. One way to handle this is with prerequisite online training where students can go at whatever pace they need so that they can begin their classes with a minimum expected level of prerequisite knowledge.

#### 17.2.1.2 Operators

Operators are responsible for the safe and reliable use of the equipment. They generally have different training needs compared to engineers. For example, operators need to ensure there are no unplanned equipment problems that could cause a heater to be shutdown unexpectedly. That means operators need to be very knowledgeable about detecting problems and fixing them before they lead to much larger problems. Operators monitor the equipment on a daily basis, where engineers may see the same equipment on a much less frequent basis. Operators need to be knowledgeable about preventative maintenance. They may do some of this maintenance or they may communicate with a maintenance group to handle these issues. Whether they actually do the maintenance or not, they need to be knowledgeable about what needs to be done and when, to make sure the equipment is available for continued operation.

Operators usually have little, if any, formal training in subjects such as heat transfer, fluid flow, and chemistry. If these subjects will be covered in a training course on industrial combustion equipment, it should be assumed this is the first time these students will have taken those topics and that it will not be refresher training. In general, operators will be less interested in theory and more interested in the practical implementation of what they are being taught.

#### 17.2.1.3 Others

There are a number of other potential types of students that may take a course in industrial combustion. One type is college students, especially those studying and doing research in the area of combustion. Baukal et al.<sup>6,7</sup> describe industrial combustion training for university students, delivered by a combustion equipment supplier.<sup>6,7</sup> Part

of this training included the students visiting the supplier to see combustion equipment in actual operation. College professors involved in combustion research may take industrial combustion training to better understand how equipment is used in industry to more precisely tailor their research to the needs in industry.

Another potential type of student includes suppliers who work with industrial equipment, but do not actually use that equipment. For example, these suppliers might supply fans, blowers, flame arrestors, refractory materials, flame detectors, ignition systems, control valves, pollution detection equipment, and other related equipment. Suppliers may be taking a combustion course to learn more about how their products are being used so they can be further improved.

Government regulators may take an industrial combustion training course to better understand how the equipment is being used so proper regulations can be written and implemented. It is certainly more difficult to write good regulations without a proper understanding of the context. Administrative assistants, company buyers, and other office personnel may attend training so that they may better understand phone calls from customers explaining their type of equipment, understand conversations during departmental meetings, and better meet the needs of the customer.

## 17.2.2 Instructors

The instructors are responsible for delivering the course content to the students. They may come from a variety of sources and often have a variety of backgrounds. Two key requirements for the instructors are that they should be very knowledgeable of the subject matter and they should be skilled presenters. Some of the typical sources of instructors are discussed in the following sections.

### 17.2.2.1 Employer

Employers may provide instructors to train their fellow employees. This could be in a variety of formats. In on-the-job training, a more experienced employee mentors a less experienced employee in specific policies and procedures. This usually takes place over an extended period of time. The trainee or apprentice usually “passes the course” when the experienced employee is satisfied that the trainee has acquired the necessary knowledge and skills to do the job. The curriculum is usually very fluid and varies depending on the preferences of the mentor. The length of the training may also vary considerably depending on the mentor and apprentice, as well as on the context. For example, if the unit where the mentor and apprentice work is particularly busy, the training may take more time because the mentor may have less available time for training.

Another type of trainer for an employer is someone dedicated either full-time or part-time to training. These trainers may have a training background or they may have been subject matter experts (SMEs) with many years of experience who are now teaching. This type of trainer often teaches in a traditional classroom to multiple students. The courses may range in length from less than a day to many months depending on the scope of training required. For example, a refresher course will typically be fairly short, while training of new employees will take much longer depending on the position. Some companies train new employees as part of a cohort where a group goes through training at the same time. There may be multiple trainers in that scenario, but usually one person oversees the entire program who is sometimes referred to as the training coordinator. This position is discussed in more detail in Section 17.2.3.

### 17.2.2.2 Supplier

In the past, it was fairly common for organizations to have resident experts in a wide range of technologies. For example, most refineries had experts in process heaters, pumps, valves, reactors, and other common equipment in the plant. To save money, many of the specialists in the plant were replaced by a smaller group of generalists who had less specific knowledge about any given equipment, but more knowledge broadly of the equipment in the plant. To complement the generalists, larger organizations often had specialists as a corporate function who would visit plants to help as needed. Today, many plants do not have the same level of expertise on-site that they have had in the past so they often rely on the equipment suppliers for help including training. Since the suppliers designed and built the equipment, they have specialized knowledge that is often needed by end users. The suppliers then may be available to train employees in the plant. These external trainers are sometimes referred to as external providers (see Section 17.5.2). However, the suppliers may not have intimate knowledge of the process where the equipment is used, so sometimes suppliers may partner with the plant to jointly deliver training which is sometimes referred to as a hybrid provider (see Section 17.5.3).

The potential problem with suppliers providing training is that the information may be slanted toward their equipment. If the plant only uses equipment from a single supplier, this may not be a problem; but if the plant uses equipment from multiple suppliers, using one supplier to provide training is potentially problematic as the single supplier may not be able or willing to speak about competitors' equipment. If the training is somewhat generic, this may not be an issue, but if detailed and specific knowledge and skills are needed, using a single supplier to train may not be the optimal solution.



There are many potential benefits to using a supplier to provide training. They are probably more knowledgeable about their equipment than anyone at the end user's site. They typically know about issues industry-wide and are not limited to issues only at a given site or for a given company. They often have training materials specifically developed for their equipment, and they usually have experienced trainers who update and deliver the content on a regular basis.

### 17.2.2.3 University

Companies may partner with universities to teach certain types of content. University instructors are another type of external provider (see Section 17.5.2). Typically this type of instructor will focus more on the theory side of the process or equipment. However, in some cases, training provided by a university professor can be very targeted when that professor has an established relationship with the organization, possibly through joint research programs. Many engineering professors do consulting in addition to their normal university duties. They are generally very experienced presenters, although their audience is normally college students who are usually much younger than personnel working in industry. It is important that the professor training the plant employees is also a skilled trainer of adults.<sup>8-10</sup> According to the theory of andragogy, adults should be taught differently than children and even young adults attending college right after high school.<sup>11</sup>

### 17.2.3 Training Coordinators

Many organizations have one or more persons dedicated to the administration of the training program. At plant sites, these persons are often called training coordinators. Besides the administration of the training program, these people also typically do some training. They organize the training to ensure employees receive the proper training which is usually determined in conjunction with supervisors and plant management. Training coordinators make sure adequate facilities are available to conduct the training and work with management to schedule the training. For example, during a turnaround, it may be advantageous to train some who are not directly involved with the turnaround, but it would not be wise to schedule training for others who are intimately involved in the turnaround.

Plant coordinators try to keep up-to-date on the latest information and technology regarding training. They may also train other trainers in presentation skills. They work with plant management to determine when new types of training may be needed. For example, after an incident, it may be recommended that certain types of job positions receive certain types of training to avoid

future incidents. Another example is when new equipment is installed in the plant and personnel need to be trained on installation, operation, troubleshooting, and maintaining that equipment. Plant training coordinators serve as the hub for all functions related to training in the plant. Plant training coordinators may also be a mediator between the training supplier and their purchasing department as they prepare to submit a required purchase order and service agreement to assure that training has been approved and payment will be made.

---

## 17.3 Learning Styles

There is an important aspect of training that is often forgotten: *Make Learning and Training Fun*. It may have taken years for some to actually believe that training can be fun, but it has since become an expectation and has been proven to be effective, if the activities are completed with a purpose. Not all learners see through the same mental lens. There are many paths into the learner's mind. If a trainer only utilizes one path of learning, the results are going to be less successful. A variety of delivery techniques benefits all types of learners because it keeps learning interesting and engaging. There is a golden rule that trainers know very well: People retain 10% of what they read, 20% of what they hear, 30% of what they see, 50% of what they hear and see, 70% of what they say, and 90% of what they say and do.<sup>12</sup>

*"One must learn by doing the thing, for though you think you know it—you have no certainty until you try." Sophocles, 5th c. B.C.*

Several techniques may be used to strengthen retention and understanding. A trainer cannot expect the participants to walk out of the classroom and apply the knowledge without allowing time for practice. There are three types of learners in the room: *prisoners* (they made me come, I know it all ... I could be teaching this class...), *vacationers* (Whew! 8 hours away from that phone, I'm in the AC, which beach do I hit first, in a nice hotel, no kids, mind is somewhere else) and *learners/explorers* (call them the sponges. WOW! They may come in as LEs but the goal is to keep them there).

After much study and researching, trainers learn that there are other thoughts and opinions regarding adult learning. Malcolm Knowles, known as the father of adult learning theory, shares in his book *The Adult Learner: A Neglected Species*, published in 1973, six assumptions to adult learning. Some think that the Knowles assumptions overlap themselves, so much so that Ann Herrmann-Nehdi developed the *Neurolinguistic Programming* (NLP) theory, which narrows it down to three types of learning

styles, making it easier for trainers to understand.<sup>13</sup> These include visual, auditory, and kinesthetic learning styles. To summarize each, visual learners prefer pictures, graphs, and illustrations. “Show me,” is their motto. Auditory learners pay close attention to every word, voice, and sound present in the classroom. “Tell me,” is their motto. Kinesthetic learners are “hands-on” learners. They enjoy class activities. Their motto is “Let me do it.” Identifying which participant prefers which particular learning style may be difficult at first, but experienced instructors generally can do so before the first lunch break. It is important to silently identify the learning styles and types of learners early and make every attempt to engage them, praise them, challenge them, and eventually have them all leave as satisfied participants.

Dave Meier, founder of The Center for Accelerated Learning in 1980, takes this concept to another level.<sup>14</sup> Accelerated learning (AL) has only one goal: to get results. There is a difference between AL and fun-games, gimmicky, “creative” approaches that do not really bring results or have a purpose. They are used more to take up time or even waste time. The theory behind AL is to blend both fun and serious lecture in a way that enhances learning and produces positive outcomes using the following principles:

1. Total learner involvement enhances learning.
2. Learning is not the passive storage of information, but the active creation of knowledge.
3. Collaboration among learners greatly enhances learning.
4. Activity-centered learning events are often superior to presentation-centered ones.

5. Activity-centered learning events can be designed in a fraction of the time it takes to design presentation-centered ones.

Examples of activities that may be incorporated into a training session include the following:

- Quiz cards—serve as a review of the previous discussions (see Figure 17.1)
- Molecule modules—class activity to share connection between various chemicals (see Figure 17.2.)

It is important to continue to research the Internet, attend conferences/workshops, and take part in events to learn of new activities that may be used in training sessions to enhance learning. Many participants did not sign up for the course to hear a lecture the entire session. Sivasailam “Thiagi” Thiagarajan reminds trainers that lecturers ignore the fact that real learning requires active participation, not passive listening; lecturers tend to focus on what they want to tell the audience rather than on what members of the audience want to know; and lecturers do not receive useful feedback.<sup>15</sup> Thiagi suggests that the facilitator or instructor continues to observe the reaction of the participants throughout the program and periodically switch between the passive and active facilitator/instructor role.

In summary, Craig Strachan, a keynote and seminar speaker, has prepared what he calls, *The A–Z of Public Speaking*.<sup>16</sup> Perhaps it could be used as a checklist before entering the classroom.

- Have a great *attitude* on and off the stage
- *Body language* and gestures enhance the message



FIGURE 17.1

Quiz cards example. (From Powell, D., *Training Treasures—The Visual Idea Book for Creative Trainers and Presenters*, special edition, Pfeiffer, San Francisco, CA, 2007.)



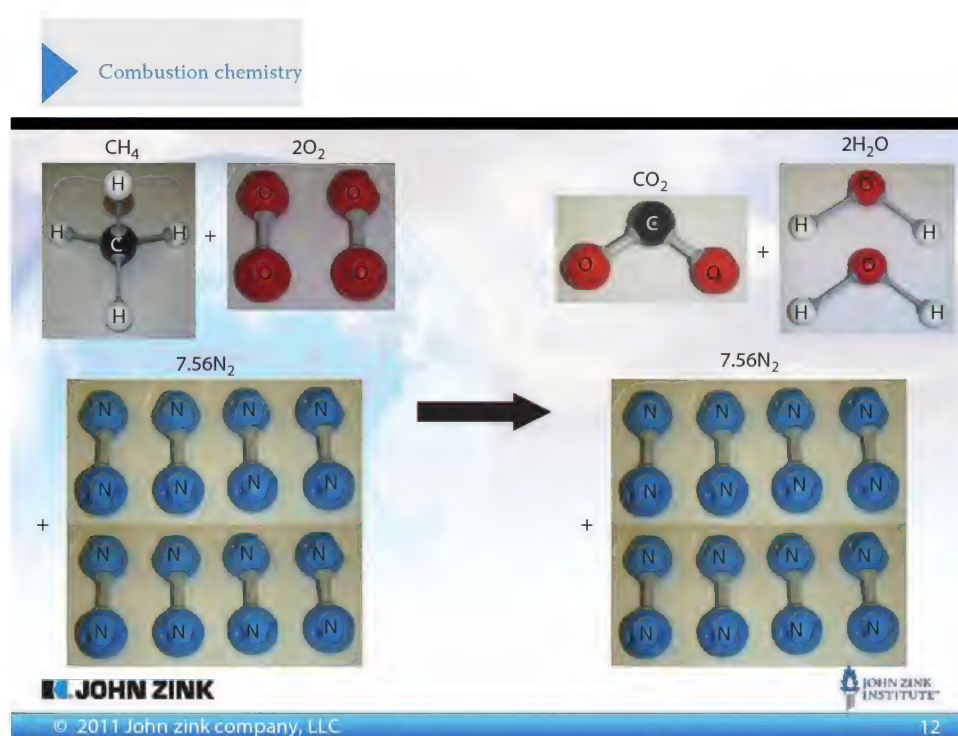


FIGURE 17.2  
Molecule modules example.

- Make *connections* with the audience
- *Delivery* and content are key
- Speak with *energy* and *enthusiasm*
- *Facts* tell, stories sell
- *Get* to the point
- Use *humor* to make connections
- *Inspire* the audience
- Use original *Jokes*
- *Know* the audience
- Record and *listen* to one's speeches
- What is the *message*?
- *Notice* how the audience is responding to the speech
- Speak at every *opportunity* (stage time!)
- Is *PowerPoint* enhancing or detracting from the speech?
- *Q* cards can be useful—especially for a long presentation
- *Rehearse* the presentation
- *Simple* messages are easy to understand
- Stick to the *time* allotted
- Does the audience *understand* the message?
- Use *visual*, auditory, and kinesthetic phrases—address all the senses

- *When in doubt*, leave it out
- Use real-life examples
- *You* are not the star
- Zzzzz—do not put the audience to sleep<sup>17</sup>

## 17.4 Subject Matter Categories

There are many ways that subject matter could be categorized. It could be based on the type of process or equipment. It could be based on the unit in the plant. It could be by job or task function. Here, subject matter has been broadly categorized as fundamentals and operations, which encompasses some of the other methods. For example, operations would cover specific equipment in the plant such as valves, compressors, piping, and reactor vessels. It would also cover specific job functions such as outside operators who are responsible for the operation of specific equipment. Often the most powerful training includes aspects of both fundamentals and operations. Both of these categories are briefly discussed in the following sections.

### 17.4.1 Fundamentals

“Fundamentals” refers to the basic theory behind a process or piece of equipment. One philosophy for training is that personnel should be taught what they need



to do, but not necessarily why they are doing it. While that philosophy may be more efficient in terms of the amount of time required for training, it unnecessarily narrows the amount of knowledge a student has about the process or equipment. If an issue arises that has not been covered in the training, the student may not be properly equipped to think through how to handle that issue as they have not been given an adequate foundation that includes the theory behind the process or equipment. This does not mean everyone needs to know how to design every process in the plant from scratch, which would not be possible nor is it necessary. It does mean that those involved should at least have a working understanding of some of the basics.

An example can illustrate this philosophy. Most plant operators know the weather can have a significant impact on equipment performance, but they may not understand why or be able to predict what will happen based on weather forecasts. One of the pollution emissions from a process heater, nitric oxide or NO, usually decreases when the air humidity increases (see Chapter 15).<sup>18,19</sup> This is simply because the added water in the air reduces the flame temperature, which reduces NO. By learning one of the fundamental principles of NO formation—anything that increases temperature normally increases NO, assuming all other variables are held constant—plant operators would also be able to understand what happens when the air temperature increases or decreases, which happens frequently during the normal atmospheric temperature fluctuations due to the changes in weather from day to day and season to season. If the plant is operating close to their allowable pollution limits, relatively simple adjustments can be made to compensate for things like the weather which are beyond the control of the plant. This can help the plant avoid costly penalties for going over their permitted limits. Some basic understanding of the fundamentals can help operators make better decisions as it is virtually impossible to cover all possible scenarios in a training course.

#### 17.4.2 Operations

Training focused on operations may include topics such as installation, operations, troubleshooting, and maintenance (see Volume 2). This general type of subject matter covers the practical aspects of equipment and processes. This nuts-and-bolts training often has a hands-on component. Where training on the fundamentals is usually more knowledge-based, training on operations is usually more skills-based. Operations-type training may include examples of the right way to do things and the wrong way to do things, including the consequences of doing things the wrong way.

One of the challenges with operations-type training is that it may be difficult to practice skills on operating

equipment. It is rarely possible to simulate abnormal, even emergency, situations in an operating plant, because of the potential safety and financial ramifications. In those conditions, other techniques may need to be employed during the training so employees are adequately prepared to handle nonroutine conditions. Simulators are routinely used to demonstrate the proper procedures for handling a wide range of conditions without adversely affecting plant production.<sup>20</sup> Actual equipment not installed in the plant, scale models, cut-aways, photographs, drawings, and videos are other methods that may be used to train personnel in plant operations.

---

### 17.5 Training Providers

Small- and medium-sized organizations often need to partner with other organizations to provide training for their employees.<sup>21</sup> Even the largest organizations are not able to provide all of the continuing education needed by their employees.<sup>22</sup> There are several reasons for this. Many organizations no longer have as many experts in-house as in the past, due to *right-sizing*. Employees at the organization may not be SMEs or trained instructors. There may also not be enough employees needing certain types of specialized training to justify internally developing and delivering the necessary courses. The volume of training may be too much for the available staff within an organization.<sup>21</sup> For these reasons, organizations rely on outside providers to deliver the training they cannot provide themselves. This is often referred to as *outsourcing*. Outsourcing in the context of T&D can be defined as

Entering into a long-term relationship with an external resource so as to leverage the capabilities and capacity of that resource. Outsourcing is done to better respond to demands for learning solutions that are technology-based, manage training's costs, decrease cycle time, accelerate development and delivery, and avoid investment in developing the training function (p. 2).<sup>24</sup>

According to a January 2011 survey by the Human Capital Media Advisory Group, over half of all organizations outsource at least some of their training.<sup>22</sup>

The challenge is how to deliver training when and where it is needed, at a reasonable cost. Continuing education must be relevant and should be designed to solve industrial problems.<sup>25</sup> Continuing professional education (CPE) must be related to professional practice to help professionals make decisions about situations they encounter.<sup>26</sup> This means that training providers should deliver training that employees can use in their

jobs. This is consistent with Knowles' theory of adult learning referred to as *andragogy* where one of his key assumptions is that learning should be relevant to the learner.<sup>44</sup> Training courses should be developed and delivered according to recommended adult learning principles such as using the prior experiences of the learner and making the content usable for the learner.

The individual employee, employers, academia, professional societies, government, and other education providers (e.g., suppliers) all have a role in continuing education.<sup>27,28</sup> Ultimately, individual employees are responsible for their own continuing education.<sup>29</sup> Employers are responsible for providing the time and financial support to continually educate their employees. Employers also offer many specialized courses relevant to their own operations, especially on-the-job training. Academia both provides continuing education and helps to develop a mindset in undergraduate students for life-long learning. Professional societies and trade organizations help set guidelines and standards for, encourage, and deliver continuing education. Governments set regulations for licensing engineers and develop policies that can encourage continuing education. Other (usually for-profit) education providers offer a wide range of continuing education courses for the ongoing training of workers. Suppliers and customers can provide specific training on their technologies and processes.

Employer-sponsored continuing education dwarfs that offered by any other type of provider and possibly more than all other providers combined.<sup>30</sup> While much has been written, for example, on continuing education offered by universities, relatively little has been written about employer-sponsored continuing education.

Continuing education is provided by many different sources, including traditional nonprofit institutions (e.g., universities, and professional/trade organizations), corporate universities, and commercial content providers.<sup>31</sup> Note that here the distinction between the types of providers is made based on who delivers the training, not where the training is held. For example, some refer to *employer-sponsored* continuing education as any courses organized by the employer including in-house seminars, workshops, and courses regardless of who actually delivers the training (e.g., Ref. [27]). Here, the employer delivering training content is referred to as an *internal* provider. Providers outside the organization delivering training for the employer are referred to as *external* providers. The combination of the employer and an outside provider partnering together to deliver training is referred to as a *hybrid* provider.

Continuing education courses include all types of technical (e.g., equipment, processes, computing software), management (e.g., leadership, employment law, enhancing team performance), and soft skills (e.g., communication, listening, presentation skills) courses.

Technical training can be defined as "the process to obtain or transfer knowledge, skills, and abilities needed to carry out a specific activity or task, related to a specific scientific, mechanical, or specialized discipline, function, or profession."<sup>32</sup> Management and soft skills courses may be broadly categorized as human resources training. Course formats include face-to-face (F2F), online, and a combination of both.

The experiences of the JZI will be used to illustrate some of the different types of continuing education providers discussed here. JZI is part of the John Zink Company, LLC (JZC) which manufactures industrial combustion equipment. The primary purpose of JZI is to help clients safely use that equipment while maximizing thermal efficiency and uptime and minimizing pollutant emissions. JZI provides continuing education courses primarily for engineers and operators in the hydrocarbon and petrochemical industries. These courses range from one to three days in length and are offered at its training facilities (Tulsa, Oklahoma, USA and Dudelange, Luxembourg), at customer facilities (referred to as on-site), and at central locations, such as university campuses or hotels located near multiple plants (referred to as a hub).

### 17.5.1 Internal Providers

The amount of continuing education offered at the workplace surpasses that of all other providers combined.<sup>29</sup> Cervero does not identify who provides the training, only where it is delivered.<sup>29</sup> Some organizations have set up sophisticated training programs, sometimes referred to as *corporate universities*, to provide ongoing training for their employees.<sup>33,34</sup> Some examples include the University of Toyota, Motorola University, and Schwab University.<sup>35</sup> IBM estimated its internal education program was equivalent to a 40,000 student university with a 6,000 member staff and faculty.<sup>36</sup>

#### 17.5.1.1 Forms of Internal Providers

Training delivered by the employer comes in a variety of forms. The least formal and probably the most common is on-the-job training, sometimes referred to as job shadowing or apprenticeship, where a more experienced employee trains a less experienced employee. For example, a new engineer on a chemical production unit may be paired up with an experienced engineer who trains the new engineer on the processes and procedures in that unit.

Another type of internal training is where SMEs train their fellow employees in their area of expertise. Craig and Evers<sup>37</sup> refer to these SMEs as *employee educators* and note that using employee SMEs to teach their colleagues "reflects a common belief of many corporate managers that those who actually performed the job are those best

qualified to teach it.” For example, some refineries have an expert who is very knowledgeable in all aspects of process heaters. That person can help train new employees on the basics as well as help experienced operators and engineers to optimally run their heaters, including recommending what can be done to improve the operations. This type of training may be formally conducted in the classroom, informally in the plant, or a combination of both. As an example, JZI sponsors Lunch-and-Learn internal courses where JZC’s SMEs teach their colleagues on a particular area of technology. These are voluntary courses held over lunch which are generally well attended.

Another type of on-the-job training is referred to as *shared practice* where employees learn from each other during the course of working together.<sup>38</sup> Finnish development engineers from two high-technology companies were observed working together over the course of a 5–6 week period. This ethnographic study showed that the practice of design engineering is a highly social process. In this type of workplace learning, engineers learn from each other, often while working on projects together. This type of continuing education differs from the first two described earlier because it does not involve formal mentoring between more experienced and less experienced employees, nor does it necessarily involve an SME. Working together on projects requires collaboration, problem-solving, and the ability to handle conflict, often leading to a sense of community, which are important skills that can be learned through shared practice.

Internal trainers for an organization sometimes purchase course materials that they can either deliver essentially as is or that they can modify according to the needs of their organization. Internal trainers may also develop their own materials, particularly on topics that are very specific to their plant. For example, trainers may develop materials for a particular unit in the plant which might include process and instrumentation diagrams, equipment specifications, operating manuals, and other documentation such as past safety incidents.

#### 17.5.1.2 Advantages of Internal Providers

There are many advantages of training provided by the employer, which Gräfen<sup>39</sup> argues is the most effective. The training is very focused and targeted to the specific needs of the organization, which is in a unique position to know its own knowledge and skill deficiencies as well as those of its individual employees. Training can be provided on the specific equipment in the plant, rather than on generic equipment. For example, employees working with process heaters only need to know how to operate and maintain the process heaters in their own plant, not the endless varieties that exist in the industry. Training materials may include drawings and manuals of the actual equipment in the plant. This

makes the training more targeted and time efficient, as well as easier to engage the students since they are learning about the exact equipment they operate.

Internal instructors usually know the organization, its products and services, and the customers it serves. They often also know the students who are fellow employees. This helps the instructors tailor the materials and teaching methods to the needs of both the organization and the students. It is often possible to have multiple SMEs in the organization teach their areas of expertise in a single course. For example, JZI sometimes uses a dozen instructors to teach a 2 day course held in Tulsa where the SMEs are located. Each instructor may only teach for an hour or two on their particular area of expertise, but the students often get the most qualified instructor in the organization for that topic. This may not be practical for a course held at a significant distance away from the organization.

The format and duration of the training can be easily adjusted as appropriate. For example, in plants that run 24 hours a day, seven days a week, there are multiple shifts that may need to receive training. Internal instructors can easily adjust their schedules to provide training to cover the shifts in a timely manner. This may mean teaching certain days and times one week and different days and times another week. While this is possible with external providers, it will likely be much more expensive and more challenging to schedule. Another related factor is that internal courses may be more cost-effectively delivered to very small groups of students. For example, if a new employee is hired just after a particular class has been given or if some employees missed a training class for some reason (e.g., vacation), internal instructors can relatively easily give the course to those few employees at the convenience of both the students and instructors. The cost of bringing in an external provider, especially if there are significant travel and living expenses involved, can be very high per student when training a small number of employees.

Students and instructors can discuss topics with less concern about legal and competitive issues when they all work for the same organization. One of the problems with training classes consisting of students from competing organizations is that detailed and proprietary information cannot be shared which provides a competitive advantage. There is also the concern of possible antitrust violations if certain types of information, such as product pricing, are shared. Even if all of the students are from the same organization but the instructor is not, sharing proprietary information can be a problem, unless some type of confidentiality agreement has been executed. When students and instructors are from the same organization, they can share important and specific details that can enhance the learning experience and maximize the benefit to the organization.



### 17.5.1.3 Disadvantages of Internal Providers

There are some potential disadvantages of internal providers. The first is that training for the typical employer is not their primary mission, which is usually to earn a profit. This means that training may not receive the support and resources necessary to provide consistent quality continuing education for the employees.<sup>40</sup>

Another disadvantage is that training is often limited to the knowledge within the given organization. This means that students may not always get the advantage of learning industry best practices. This has been the experience of JZI. Many on-site classes have proven to be learning experiences for the plants that are often not aware of certain best practices in the industry. For example, start-up procedures for burners and heaters vary somewhat depending on the plant and the specific equipment. Some procedures are more effective than others. Since heater accidents typically occur during start-up, using the best available procedures can significantly enhance safety, while failure to use proper procedures could lead to accidents. External providers are more likely to know the industry best practices if they work with many different organizations across that industry.

While an advantage of this type of provider is the capability to train on the specific equipment the student will be using, a potential disadvantage is that this equipment may not be available for the full range of training exercises. If the equipment has a large impact on production, students may only be able to make limited adjustments to avoid adversely affecting production. This means the student may receive little, if any, training on the actual equipment on those conditions that rarely occur, such as emergency situations, start-up, and shutdown. Some type of simulator may be needed to train for those special operating conditions that occur infrequently.

Another potential disadvantage is that internal instructors may be too familiar with the students who are also colleagues, which could lead them to be too easy or too hard on certain individuals. For example, an instructor may not challenge a student who is a superior for fear of possible job repercussions, while an instructor might be overly harsh on a colleague with a reputation for not taking their work seriously enough or on one they do not like. External instructors may be less biased toward the students than internal instructors.

Another potential problem with classes taught by internal instructors and consisting only of internal students is that some students may be hesitant to ask questions for fear of how they might appear to their colleagues. While instructors may state the adage that there is no such thing as a stupid question, it may be difficult to convince students while they are in the presence of their colleagues, especially supervisors. This can be handled by giving students other alternatives for asking questions such as

writing them down anonymously or discussing issues with instructors privately during breaks or outside of class.

The U.S. Occupational Safety and Health Administration (OSHA) standard 1910.120 Appendix E recommends that instructors should have “documented experience in their area of instruction.”<sup>41</sup> Depending on the size and sophistication of the internal training organization, instructors may be asked to teach subjects for which they may not be truly qualified in order to save time and money. Conversely, instructors may not know or be willing to admit they are not qualified to teach certain topics. A different type of problem related to the quality of the instructors concerns their teaching ability. If the internal instructors are SMEs, they may be experts in their subject area, but they may not be trained on how to teach adults.<sup>42–44</sup>

For courses that are taught infrequently, it is more likely that the quality of internally delivered courses will not be as good as it is for external organizations teaching the same courses on a more frequent basis. For example, JZI teaches various types of process burner courses many times per year. One specific example is an on-site process burner class taught at a large oil refinery in Texas City, Texas (see Section 17.9.1).<sup>45</sup> JZI continuously updates the course materials with new photos and videos as they become available. A typical plant may only teach a course like that a few times a year (if that often). Because of other priorities, that course is not likely to receive as much attention from internal instructors compared to other courses they teach more frequently.

Unless required by some external organization such as governments or customers, very few internally developed and delivered continuing education courses are accredited. There are many possible reasons for this. The first is that the added expense is not usually justified unless accreditation is required by law or by customers such as in their requests for proposals for services or equipment. This is particularly the case for internal courses that are offered infrequently or involve relatively few employees. Another important reason is that most engineering organizations do not have the personnel, policies, and procedures in place to become accredited and then to maintain that accreditation. Initial accreditation is often a lengthy and costly process. Maintaining accreditation is similarly rigorous and requires discipline on the part of the organization. Since training is not the primary function of most organizations, accreditation is not usually a priority, especially in an era of *right-sizing* when most employees are already stretched to the limit and have little time for nonessential activities. For most engineering organizations, accreditation of their own formal continuing education courses is not viewed as a competitive advantage. Lack of accreditation suggests that internally developed and delivered courses may not have adequate quality assurance.

### 17.5.2 External Providers

There are many potential reasons why an organization might use external providers to deliver training. Some of these reasons include gaining flexibility to better control the workload during fluctuating business cycles, outsourcing training for subjects outside core competencies, increasing options for managing the training budget, and using specific expertise to support new strategies or projects.<sup>23</sup> Smaller organizations often need to use external providers because they do not have the staff to deliver all their training requirements.<sup>46</sup>

There are many types of external providers that deliver continuing education courses. These are broadly categorized here as universities, professional and trade organizations, commercial training organizations, government, suppliers, and customers. Each of these is briefly discussed next including some examples of each.

Universities are a major provider of continuing education, typically with more emphasis on theory.<sup>25</sup> One university source for continuing education courses is the National Technological University (NTU), now part of Walden University, which is a consortium of over 50 engineering-degree granting institutions.<sup>47</sup> NTU provides both Masters level engineering courses for degrees and nearly 500 continuing professional education noncredit courses. The noncredit courses are generally 3–5 hours in length and are available in a wide range of formats to accommodate working professionals.

Stanford University developed one of the largest instructional television networks in the world and partnered with industry to offer a wide range of distance continuing education courses.<sup>48</sup>

Industry sometimes partners with universities to provide continuing education where the universities deliver the training. One example of this partnership is the JZI Visiting Scholars program. JZI invites well-known combustion engineering professors to lecture at JZC on topics related to their particular area of research expertise. This helps educate JZC's engineers on the latest developments in the field and strengthens the company's ties with academia. Noncredit continuing education courses can be developed by universities in conjunction with industry to meet employee development needs.<sup>49</sup> Examples of courses include Programmable Logic Controllers and Industrial Motor Control. These courses are not normally taught in engineering degree programs because they are too technology specific, but they are needed by engineers using those technologies in their jobs. Industry sometimes provides input on what should be included in these courses and may even supply supplemental materials such as photos, videos, models, or actual equipment, but the courses are delivered by the universities.

Universities delivering online courses are sometimes characterized as virtual universities, which can

be defined as "an electronic representation of the features of a real university."<sup>50</sup> While both employee and employer agree that continuing education is important, the real challenge is time for the employee who is busy with work and family responsibilities and often finds it difficult to regularly attend classes held on a specific day and time each week.<sup>51</sup> This is an important reason why distance education has expanded rapidly for delivering continuing education.<sup>52</sup> These virtual universities help meet the demand for continuing education any time and any place.

Professional societies are an important source of CPE courses. Engineering societies are generally organized around a specific branch of engineering such as the Institute for Electrical and Electronics Engineers which offers both classroom and online courses related to electrical engineering.<sup>53</sup> Professional societies are probably better suited to provide continuing education where the focus is longer term, compared to company-developed training programs that tend to be short-term focused.<sup>54</sup> Professional societies have some advantages over university and industry training programs such as the flexibility to use the best instructors anywhere a course is needed.<sup>55</sup>

Another type of professional organization of particular interest here is the societies dedicated to engineering education. The international umbrella organization is the International Federation of Engineering Education Societies.<sup>56</sup> Several of the member societies are used as examples here. An objective of the ASEE is to bring together industry, education, and government to further engineering education.<sup>57</sup> One of the stated objectives of both the European Society for Engineering Education and the International Association for Continuing Engineering Education is to develop and strengthen cooperation between education and industry.<sup>58,59</sup> These engineering education societies both encourage and provide continuing education and training for engineers.

Another category of external continuing education providers is nonprofit industry trade organizations, which have been largely ignored in most discussions of continuing education providers. In contrast to professional societies, trade organizations focus on specific industries or technologies, rather than on a particular branch of engineering. One example is the European Powder Metallurgy Association (EPMA) which offers distance education courses on CD-ROM on powder metallurgy.<sup>60</sup> Another example is the American Petroleum Institute which formed the API University that offers a wide range of classroom courses related to the petroleum industry, including courses on API standards.<sup>61</sup> EPMA and API focus on specific industries. The Instrument Society of America is an example of a trade organization focused on a particular area of technology, and offers a range of classes related to controls and instrumentation.<sup>62</sup>

As an example of partnering with trade associations, JZI has provided training arranged by local industry

groups for engineers in the hydrocarbon and petrochemical industries in a variety of cities. These courses are designed for the specific group of engineers in a particular region. For example, in the Gulf Coast region of the United States, pollution emissions are of specific interest due to stringent government regulations, so JZI has delivered training on reducing pollution to chemical engineers working in the plants in that region.

There are many for-profit educational organizations, including independent consultants, specializing in delivering continuing education. The Center for Professional Advancement offers over 350 accredited technical training courses, both F2F and online, in 18 applied industrial technologies all over the world.<sup>63</sup> PDHengineer.com offers online continuing education courses for professional engineers to maintain their licenses.<sup>64</sup> The Educational Program Innovations Center (EPIC) is a Canadian organization that provides non-degree F2F and distance continuing education courses.<sup>65</sup> The role of these organizations is primarily to provide topical short courses.<sup>66</sup>

Some government agencies offer continuing education. For example, the U.S. Environmental Protection Agency has established the Air Pollution Training Institute and offers a wide range of training courses, both classroom and online, related to air pollution.<sup>67</sup> The U.S. Occupational Safety and Health Administration established the OSHA Training Institute which sponsors a wide range of training courses, such as industrial hygiene, hazardous materials, and ergonomics.<sup>68</sup>

Many suppliers offer continuing education related to their products and services, sometimes for a fee and sometimes at little or no cost. Delivering technical training not only to its own employees, but also to its customers and partners, may be a strategic objective for an organization.<sup>31</sup> Suppliers and manufacturers often have other motives related to continuing education besides making money from training.<sup>69</sup> These may include the marketing exposure for their products, gaining new customers, increasing user satisfaction, improving safety related to the use of their products, and getting candid feedback related to their products. JZI is an example of a supplier offering continuing education to help JZC customers better use its products. JZI provides dozens of courses on technologies related to combustion equipment such as process burners, boiler burners, flares, and vapor combustors. These are generally short (one to three days long), intense, and concentrated on a particular area of technology.

Another type of external provider is customers. No substantial discussion of this type of provider was found in the literature. This can be a potentially very powerful type of provider as customers could provide information that may not be readily available within the supplier's organization. For example, in the authors' organization, customers often have complicated refineries and chemical plants and there is relatively lesser knowledge on particular

aspects of those processes within the organization. While training on these processes is available from consultants, it would be particularly beneficial to receive that training from the customer's perspective, especially regarding any problem areas related to the products supplied by the organization. The more knowledgeable the supplier is regarding the customer's needs, the better for both the supplier and the customer. There are some potential challenges with this type of provider as the information may be biased toward a particular customer's operations, there could be some intellectual property concerns, and there would have to be some significant benefits to the customer to dedicate resources to training suppliers.

#### **17.5.2.1 Forms of External Providers**

External providers deliver a wide range of courses in a variety of formats in many locations. Formats include F2F, distance, and a combination of both. Locations include at the provider's site, at the client's site, or at other locations such as hotels and university campuses. JZI offers both F2F and online courses<sup>70</sup> that are delivered at its training facility in Tulsa, at client locations all over the world, at hotels in hub cities, and at universities.

#### **17.5.2.2 Advantages of External Providers**

There are many potential advantages of using external providers. The most important is getting trainers who are experts in a specific subject area. A particular advantage of professional societies is access to a wider variety of experienced experts compared to other providers.<sup>28</sup> As a supplier continuing education provider, JZI is part of JZC which has been designing and building industrial combustion equipment for over 80 years. JZC is a world-renowned expert on the equipment it makes. Using its vast experience in training classes gives the students the benefit of that experience and expertise, including industry best practices related to that equipment.

A related advantage of external providers is the custom training resources they may have. For example, JZC has a world-class test facility (see Figure 1.56) that can be used for demonstrations for the classes held in Tulsa.<sup>71</sup> JZI has developed a furnace simulator used strictly for training purposes, where students can virtually experience a variety of conditions and practice making adjustments without the fear of jeopardizing production in an operating plant.<sup>19</sup> JZC also has a virtual reality conference room used to view computational fluid dynamic simulation results in 3-D, which is used to demonstrate principles taught in class.<sup>72</sup>

Accreditation of continuing engineering courses has been recognized internationally as a problem.<sup>73</sup> The European Union and the United States are partnering in a transatlantic program called Development of



Accreditation in Engineering Training and Education (DAETE) to address this issue.<sup>74</sup> While some external providers have accredited courses, this is much less common for internal providers, as previously discussed. Accreditation is likely to become more important in the future, particularly regarding licensing of engineers, to ensure that continuing education meets some minimum quality standards. For example, JZI is designated as an authorized provider by the International Association for Continuing Education and Training (IACET).<sup>75</sup> This means JZI's program meets the stringent requirements developed by IACET, and is therefore authorized to offer Continuing Education Units (CEUs) to students meeting certain requirements when taking a course. These requirements vary by the accrediting organization, but often include attending at least a certain amount of the course, passing a test at the end of the course, and completing a course evaluation. JZI also has some specific courses accredited by the API under its Training Provider Certification Program (TPCP).<sup>76</sup> Accredited training providers normally undergo periodic audits to maintain their accreditation to ensure the accreditor's standards are being met. For example, one IACET standard requires that instructors disclose any commercial interests in products and services discussed during their presentation.<sup>77</sup> One reason why suppliers sometimes provide training is to help sell their products and services. This is generally strongly discouraged if not forbidden by accrediting agencies, which may be a reason for an organization to use accredited external providers to avoid training that is overtly commercialized.

A potential important advantage of an external provider for an employer is cost savings. It is usually not cost-effective for employers to match the educational capabilities of organizations dedicated specifically to training on topics outside the areas of expertise for the employer. When selecting an external provider, the employer often has multiple options which means the cost may be lower due to competition between providers.

### 17.5.2.3 Disadvantages of External Providers

One of the key disadvantages of external providers is the added out-of-organization costs. While there are certain costs for internal courses, those expenses may be viewed differently as the costs for internally developed and delivered courses do not leave the organization. Company trainers and training facilities are generally part of the operating budget, while costs for externally provided training usually receive much more scrutiny and may be more difficult to justify, especially during times of tight budgets.

Another potential disadvantage of an external provider is that the course content may be somewhat generic, particularly if the students are from multiple organizations with varying technologies. This means

there may be considerable wasted time for students who do not use the technology being covered at various points in the course. It also usually means that even when the technology being covered is used by the student, it may not be discussed in very great depth because of time constraints when multiple versions of a technology are being covered. For example, at JZI's process burner courses held in Tulsa, many different types of burners are covered but none in great depth due to time constraints. If all students are from the same organization, the external provider can usually tailor the course to specifically cover the technology used by that organization. For example, JZI offers start-up training at the client's site on the particular equipment being used. This type of training would be difficult for internal trainers unfamiliar with that equipment to develop and deliver.

A further potential disadvantage may be possible conflicts of interest.<sup>78</sup> This could occur where a supplier offering training may unduly influence students to purchase their equipment which could have negative safety and environmental ramifications. For example, a supplier making equipment that generates more pollution than other suppliers' equipment could minimize the importance of pollution in a training class, while overemphasizing the importance of other features where its equipment is superior.

### 17.5.3 Hybrid Providers

An alternative continuing education provider is a combination of internal and external providers. Two or more organizations can create an alliance to develop and deliver some type of training. This form of arrangement has been described as co-sourcing, share-sourcing, strategic sourcing, and in-between sourcing.<sup>79</sup> Note that the collaboration between providers considered here is more narrowly defined than by others. For example, there is increasing collaboration between providers, particularly between employers and universities, to deliver CPE.<sup>29</sup> However, that collaboration primarily concerns employers hiring universities to deliver courses tailored to their needs, where those courses are taught entirely by the university. Beder<sup>80</sup> described four forms of collaboration in CPE: co-sponsorship, referral, coordination/control, and donor relationships. These refer more to the administration of, and payment for, courses, rather than to the delivery. Kost<sup>81</sup> suggested joint instruction as a potential form of collaboration between industry and academic institutions, although he did not elaborate or give any examples. Here, collaboration between providers specifically includes *co-teaching*, where all providers teach a portion of the course. It is important to note that relatively little is known about cooperative relationships in continuing education.<sup>82</sup> Most of the literature concerning cooperative relationships in continuing education involves primarily higher education (e.g., Ref. [83])

and continuing medical education (e.g., Ref. [84]), where organizations are working together, but not usually co-teaching. It is argued here that even less is known about cooperative relationships in continuing education where providers jointly teach a given course. Some examples of such relationships are given later in this section.

While a contractual arrangement is certainly one type of relationship, the more powerful form is where there is a mutual alliance between the organizations where all benefit in some way. The objective is to produce more effective training through synergy than could be provided by the individual organizations. Collaborative relationships among organizations may take several forms, which are discussed as follows.

#### 17.5.3.1 Forms of Hybrid Training

One type of hybrid training is where multiple organizations partner together to develop and deliver courses. One example is EuroPACE which is a European non-profit consortium of universities and educational organizations that develop online courses, including those for continuing education, through networked e-learning projects between members.<sup>85</sup>

Another form of hybrid training is where competitors work together to offer noncompetitive training of benefit to the industry. This is sometimes called *coopetition*, where competitors cooperate on noncompetitive areas such as training.<sup>31</sup> For example, teaching safety and environmental best practices is generally good for the entire industry. While the most common form of this would be papers presented at a technical conference, it could also be in the form of seminars designed to train inexperienced employees or possibly even those outside the industry such as university students or government regulators. Fink et al.<sup>86</sup> described a European consortium of 17 telecom companies in six countries and six universities that joined together to provide continuing professional development training for engineers on noncompetitive topics in multiple languages. JZI sponsored an international flare symposium where equipment designers, industrial end users, academia, and government, all participated to share information and recommend future research programs. State-of-the-art technologies, best practices, and industry problems were discussed which would have been difficult for any one organization to do.

JZI partnered with a heater manufacturer to jointly deliver a 2 day training course on process heaters and burners at Texas A&M University, Kingsville Texas, sponsored by an organization of petrochemical plants in the Corpus Christi, Texas area. This format provided students (mostly engineers from plants in the area) with instructors from top suppliers of particular technologies, in facilities designed for training, and located conveniently for plants in a given region.

Another JZI experience concerned partnering with a particular customer to deliver a series of training classes to different sets of operators in a particular plant. The training materials from both organizations were merged together to give students the combination of the specific equipment, procedures, and processes of the plant, along with industry best practices. Instructors from both organizations delivered the content.

#### 17.5.3.2 Advantages of Hybrid Training

Internal SMEs teamed with external SMEs have the potential to deliver customized training that combines the strengths of both. The internal SMEs are experts in their organization's processes and procedures. They can effectively train fellow employees on how things are done in their own organization, but do not necessarily have knowledge of industry best practices or of potential problems that could occur, but which have not occurred in their own organization. External SMEs may know industry best practices, but may not know the details of a particular organization's operations and experiences. JZI partnered with a refinery to jointly deliver a process heater training course. This was a powerful combination because the students learned about specific issues in their plant as well as those in the industry. One of the more important topics in that course was safety. Because of the large quantities of fuel used in a process heater, incidents can be very dangerous. The refinery SME used pictures of incidents that occurred in its plants, while JZI showed pictures of incidents that occurred in other companies' plants in the industry. The incidents in the students' organization were powerful because they demonstrated what had already happened in that organization. The incidents outside the organization were powerful because they demonstrated what could happen if proper procedures were not followed. Also, detailed analyses of the internal incidents were discussed, which is not usually possible with external incidents because those analyses are rarely shared outside the organization.

Another potential benefit of a hybrid course is a better blend of theory and practice in the case when industry partners with academia. Industry is very familiar with the application of the technologies used in their facilities, but may not be as familiar with the theory or with the most recent developments in an area of technology. Academia is usually less familiar with actual practice but is well versed in the theory and recent advancements in a field, particularly if the university instructors are actively involved in research in that field. For example, JZI has partnered with a world-renowned combustion engineering professor to teach a course on combustion dynamics along with a JZC SME. The professor provides the theory and current research on the subject, while the JZC SME provides the practical industrial examples.

### 17.5.3.3 Disadvantages of Hybrid Training

Hybrid training courses may take more preparation time than those taught by a single organization, whether internal or external. More coordination is required to determine which organizations will cover what topics. Training materials need to be meshed together to eliminate duplication, ensure coherence, and handle any areas where there are conflicts. For example, in a course jointly taught by JZI with a refinery, there were some policies and procedures that differed related to start-up between the organization and industry common practices. In that case, the refinery's procedures took precedence because they were even more rigorous than the generally accepted industry best practices.

Another potential disadvantage of hybrid training is that the training methods and styles of the multiple collaborating organizations may be significantly different which could reduce the learning effectiveness as students may need to continuously adapt to the various styles used. The course materials may be different. For example, one organization may use one type of template for its slides while another is likely to use a different template. If these are not harmonized, the course may appear to lack cohesiveness. A related problem is the potential discontinuity of having multiple instructors from different organizations teaching at different times during the course. For some students who enjoy the variety, this may be an advantage. For others who prefer more continuity, this could be distracting. The course should be designed to minimize the distractions of multiple instructors and teaching styles.

Other potential problems are the legal issues that could arise with multiple organizations, particularly when competitors are collaborating. For example, one organization may have a different legal disclaimer than another organization. These may need to be harmonized which is not always an easy task. Another legal issue that could be a concern is ownership of the combined training materials. After a joint course has been completed, can one organization use another organization's materials in future courses that may not include the other organization? This, of course, can be resolved prior to the start of the course, but added time may be needed to handle these issues.

operators from around the world who are looking to optimize their plant or maximize their career.

The North American Process Technology Alliance (NAPTA) provides a plethora of industry and educational institutions who offer technical programs for all ages. Some include Baker Hughes, ConocoPhillips, ONEOK, Sinclair Oil, Fractionation Research Institute (FRI), JZC, Murray State College, Northeastern State University, Northern Oklahoma College, Tulsa Community College, Tulsa Technology Center, Pioneer Technology Center, and Oklahoma Department of Career and Technology Education. A complete listing is available by contacting NAPTA ([www.naptaonline.org](http://www.naptaonline.org)).

Many of these organizations offer scholarships, certification, and accreditation. The JZI is one of the few to offer accreditation and certification provided by IACET, API, and the Accrediting Council for Continuing Education and Training (ACCET).

### 17.6.2 On-Site

Field service personnel have the responsibility to visit various refineries around the world and often they discover the need for training. JZI became aware of the need and began offering on-site training courses: basically, taking the classroom to the refinery. "Stay there. JZI will bring the classroom to the workplace."

There are some advantages of teaching a class at the plant location. When a company has chosen to offer on-site training, they are able to have the majority of their operators and engineers in the facility training room at one time, all discussing issues that pertain particularly to their own equipment. Customization is another advantage to on-site training. A survey may be distributed to the plant in advance, asking for specific information regarding their training session. This survey basically asks for the desired outcome of the training session, what problems currently exist at their location, how many participants, how many shifts, and how many days are allowed to cover the training session. A basic agenda may be given, but the on-site coordinator and the instructor may see the need for additional topics to cover. Subject to economic conditions, many facilities have limited resources. Therefore, allowing two or three of their operators to be away from the refinery at the same time can be critical to their daily operation. Conducting an on-site training allows several operators and engineers to attend the same 1 day course together, receiving the same information regarding fundamentals, troubleshooting, and maintenance of combustion. They are able to discuss current issues and perhaps resolve them as a group. If there is a need for various night shift workers to attend a training session, arrangements can be made to offer the training to them during their shift hours. Another advantage is the ability to

---

## 17.6 Training Locations

### 17.6.1 Institution

There are many institutions, colleges, and universities that offer combustion, process technology, and instructional training courses. The JZI, JZC's educational organization, offers combustion training to engineers and



take the classroom to the field. It is recommended that this be done in small groups to allow all the participants the ability to hear the instructor. At this time, problem areas can be emphasized visually to all attendees and then a discussion can take place on location or back in the classroom. This can be noted as a “hands-on” experience for the participants.

Oftentimes, it is difficult for a company to send their operators and engineers to a 2-day or 3-day course offered offsite. The reason may be limited resources, budget constraints, or conflicts in the company schedule. Funding several operators and engineers to attend training offsite can be costly. They must consider airfare, lodging, and meals. The non-productive days for traveling can also cost the company, especially if it means traveling on a Saturday or Sunday. For hourly employees, the company would be responsible for paying overtime to the employee, if applicable.

There are also some potential disadvantages for on-site courses. When a company decides to conduct on-site training rather than sending their employees offsite, generally only two or three SMEs are assigned to conduct the training. Although the outcomes are generally positive, they do not have the advantage of hearing other SMEs in the field of combustion. When operators or engineers attend offsite courses, several instructors may be available to share their expertise and answer questions. Many times the space available for on-site training is limited. On-site training space can range from a small trailer located on the plant premises to a break room in the middle of several offices. Not all plants are equipped with an actual training room that has a projector, large projector screen, adequate table, and writing space or chairs designed for long periods of sitting. The noise level surrounding the available training space may also be high and distracting. All of these may become a disadvantage for the participants as well as the instructors and can create a negative learning experience.

When on-site training sessions are held at the customer's facility, there is a possibility that participants may get called away to assist coworkers or to take a phone call. Oftentimes, participants do not see the urgency to return to the classroom after a short break or lunch break. This causes a disruption in the classroom as they return to their seats, after the session has started.

As noted in the previous section, oftentimes the attendees include supervisors of one or two groups of those present. This may cause participants to hesitate to answer questions honestly and speak of current issues that they are experiencing because they know it may be of a different opinion than that of their supervisor, who is also present in the classroom. Whereas, when they attend an offsite course, they generally attend without their supervisor and are more open during discussions about issues at their facility.

Overall, on-site training at a customer's facility may not have all the advantages of attending offsite training courses, but it is definitely a benefit to the company. Providing a learning opportunity for operators and engineers to learn proper operating skills, expand their safety knowledge of their equipment, and learn how to troubleshoot issues they have on a daily basis is crucial. It can be a win-win for all parties involved.

### 17.6.3 Hub

In addition to offering on-site courses, companies may select to offer a hub training session in a particular city or state. “Hub” refers to a centralized location, similar to how airlines use hub cities to efficiently move people and packages from one location to another. In this case, the instructors and students are all brought to a convenient location, typically in a city where multiple plants are located.

Some companies may identify only a small group of employees who are in need of training or a refresher course, but not enough to justify the expenses to have on-site training at their facility or send their employees to an offsite course. Field service personnel are then challenged to find other refineries in a particular area that also have small groups of employees needing training. If other regionalized interest is found, a centralized location is identified and an announcement and notification is sent to all refineries within a certain geographic radius that a provider will offer a course on a particular date.

There are some specific advantages of hub classes. Companies are able to send their employees to a location within driving distance which lowers travel and lodging expenses. This training is typically a short (e.g., 1 day) course, so employees are not usually away from the plant for very long. Hub training also allows great networking to take place. Generally, the participants are all in the same line of work so they have the opportunity to share non-competitive operating experiences and discuss ideas and solutions.

### 17.6.4 Online

Since the late 1990s, online training, sometimes referred to as e-learning (electronic learning), computer-based training (CBT) or web-based training (WBT) has made its way into the learning environment. All of these forms are growing in popularity and are available from many companies. JZC currently uses web-based safety training to supplement in-house training. Modules are available on nearly a hundred different topics. Some operations personnel view a new safety topic on a weekly basis. Each module has an instructional section that includes text, graphics, audio, and sometimes video, followed by a quiz to demonstrate that the key

concepts have been grasped. Training records for each employee are automatically updated after the quiz has been successfully completed. Another version of this form of training is where a live class is conducted over the Internet including e-mail interaction between participants in a type of on-line chat room. A related type is where the class lectures can be viewed either through a television or through the Internet with e-mail used to ask the instructor questions. This method, though not live, is ongoing over the course of the semester. More and more universities are offering some form of web-based training.

Another form of CBT could be a specially designed home study course using a workbook and CD-ROMs where the student could go over the materials at their own pace. Some limit is normally placed on how long they have to complete the course. Tests are mailed to the training organization to be graded and then returned to the student with comments. Instructors can be called or e-mailed if the student has any questions.

JZI has gone a step further and offers an online course entitled, "Process Burner Theory."<sup>70</sup> This is an online course designed to provide basic fundamentals of combustion, fluid flow, and heat transfer as they pertain to burners used in process heaters and furnaces. The course consists of 16 modules, each of which takes approximately 15 min to complete *via* the Internet. There is a quiz given after each module to check for understanding and achievement. This is a great tool for those operators who really need a foundation in the combustion field, but are not able to travel to attend a JZI Tulsa training course. They are able to "get an education right from their desktop."<sup>87</sup>

## 17.7 Training Organizations

### 17.7.1 ASTD

Most careers provide a professional organization that offers support and resources; the training profession is no exception. The American Society for Training and Development (ASTD) is the world's largest membership association for training professionals.<sup>88</sup> ASTD takes pride in offering support, content, and resources to workplace learning and performance. With over 70,000 members and associates from all over the world, there are thousands of organizations, government and academia, consulting firms, and product and service suppliers who meet regularly to offer support to trainers in their city or surrounding area.

ASTD began in 1942 during a training committee meeting of the API held in New Orleans, Louisiana.

In 1964, the association changed its name to the American Society for Training & Development. In 2000, the organization chose to refer to itself just by the letters ASTD to recognize that the profession looks far beyond training in its quest to create a better working environment for all involved. ASTD offers various resources for learning and development to all members. Members are able to view up-to-date ideas, trends, and best practices by subscribing to the T&D magazine or reviewing resources available on the ASTD online library.

State and national ASTD conferences are offered annually in various cities. Over 125 local chapters in the United States and over 20 international partners from around the world attend these conferences. Attendees have the opportunity to walk away with numerous training ideas and training materials. The networking opportunity that is available at these conferences is priceless. Smaller regional conferences like Learning Transfer, LearnNow, and "Telling Ain't Training" are also offered for those who desire specific and detailed training.

As the use of technology has grown in many learning environments, the ASTD TechKnowledge® Conference and Exposition has become a popular event. Also, it facilitates the connection of other ASTD members through social media platforms.

Many trainers and employees are looking for training certification. ASTD offers the Certified Professional in Learning and Performance (CPLP) credential for individuals in the workplace learning and development field. There are also over 40 certified programs and workshops aligned with the Areas of Expertise in ASTD's Competency Model in theory, practice, and application (see Figure 17.3).

The ASTD Competency Model was created in partnership among ASTD, Development Dimension International (DDI), and Rothwell & Associates (R&A). This model provides a strategic plan for training professionals. The model serves as a guideline for trainers as they prepare their training sessions or may be used as a guideline for monthly ASTD chapter speakers. This allows the members to reflect on how they may apply the presenter's material once they return to their work environment.

As a trainer, it is beneficial to become involved in a local ASTD chapter or ASTD nationals. Members have access to a bank of presenters, speakers, and consultants to share with their human resource department when the need arises for the training of employees. Networking with other trainers allows the opportunity to share ideas and best practices which makes provision for growth and enhancement to one's training career.

**ASTD Mission:** Empower professionals to develop knowledge and skills successfully.

**ASTD Vision:** Create a world that works better.

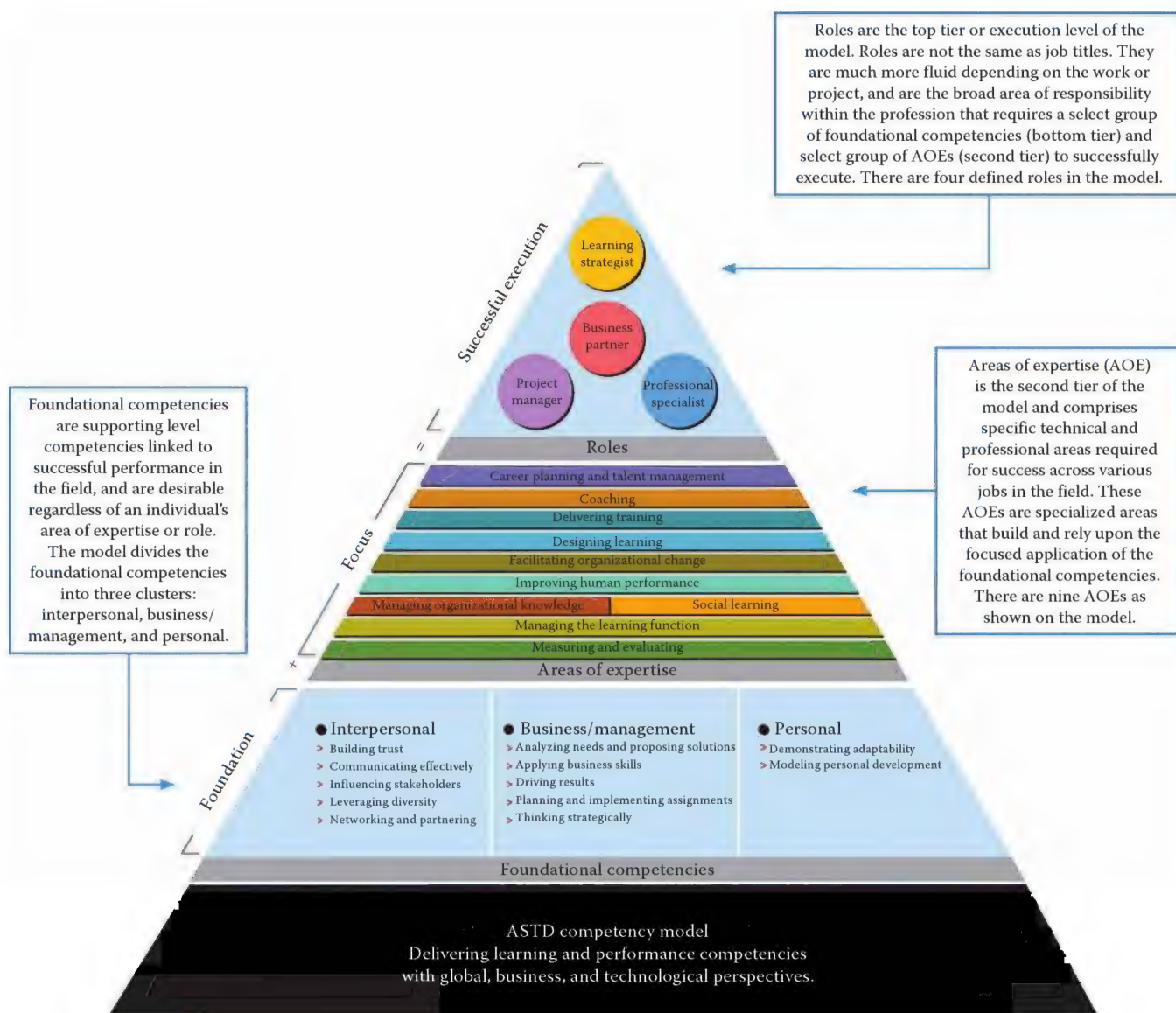


FIGURE 17.3

ASTD competency model. (With permission of the American Society for Training and Development (ASTD), Competency Model, <http://www.astd.org/Communities-of-Practice/Career-Development/Competency-Model>, accessed 14 September 2012. © 2011. All rights reserved.)

### 17.7.2 PTECH Organizations

A recent API study analyzed all the factors that affect a plant's efficiency. According to the study, human error had the greatest impact on asset utilization. An American Chemical Society study concluded that when plants hire qualified, trained workers, companies documented an average savings of \$16,000 for every new hire made. It is also possible for companies to see an increase in plant asset utilization from one to four percent. The question then becomes, "Where should a company search for qualified plant workers?"

The Process Technology (PTECH) program provides classroom instruction and practical experience to prepare students for employment in a variety of

process-related jobs.<sup>89</sup> The material prepares individuals to monitor, operate, and maintain equipment used in the processing of raw material into marketable chemical/petrochemical products. This includes instruction in materials handling, extraction, distillation, evaporation, drying, absorption, heat transfer, and reaction processes. It also includes chemical and fire safety, codes and standards, and general plant day-to-day operations. Students involved in PTECH programs participate in a curriculum that emphasizes safe and efficient work practices, basic occupational skills and employability skills. The content is organized into competency-based courses of instruction which evaluate specific occupational competencies. Each student is



required to successfully complete the competency exam before receiving credit for participating in the program. The PTECH program generally requires a 2 year educational commitment and much of that time is hands-on experience in a lab similar to one at an actual processing plant.

Refineries have discovered that hiring PTECH graduates may decrease employee selection costs up to 80% or even 90%, reduce 2 year new employee turnover up to 50%, drop job-training costs up to 40%, and result in up to 37% fewer safety-related incidents. Process Technology positions are not only available in oil refineries, power plants, or chemical plants, but they exist in pulp and paper manufacturing, water treatment plants, power generation plants, food and beverage processing, and pharmaceutical plants.

After gaining employment, PTECH graduates soon learn to approach each workday with curiosity and flexibility. Graduates may begin the day by performing basic duties, but due to customer demands, weather changes, unexpected equipment malfunctions, and new technology, the day may end with unexpected adventure. PTECH employees often work rotating shifts, some only working 12 hour shifts/14 days per month. These hours are a huge attraction to those looking for a career choice. The pay and benefits are often compared to college graduates who have attended college for 4 years or more. There is a famous story of a PTECH graduate who brags to his neighbor who is an engineer for NASA of his six-figure salary. The graduate spoke of several bonuses of \$4000 or more received within one year. In the meantime, the neighbor only recalls a one-time bonus of \$100. The story ends with the neighbor informing his wife of a career change to process technology.<sup>90</sup>

After successfully completing the curriculum, a State Certificate of Achievement or an Associate of Science Degree, PTECH graduates soon discover the advantage of entering a workforce where there are more PTECH positions than there are qualified employees. Today, not many college graduates have that experience.

The average age of a process technology operator today is 50, which means as many as half of all process operators will be eligible for retirement within the next 5–10 years. This will likely create a situation in the refinery workforce of not having enough trained workers available to replace the retirees. Therefore, there are organizations and corporations who support PTECH graduates and work with employers to help meet the demand.

The NAPTA, formerly known as the Gulf Coast Process Technology Alliance (GCPTA) is an organization that provides educational support to those who are seeking a process technology career. NAPTA interacts closely with several colleges that have endorsed the process technology curriculum. These endorsed colleges have an active advisory committee, have completed a

comprehensive program audit, and have been approved for endorsement. Both are closely involved and supportive of developing standards for PTECH programs to assure that qualified graduates are prepared for today's process technology workforce.

---

## 17.8 Other Considerations

### 17.8.1 Instructor Training

#### 17.8.1.1 Preparation

Perhaps one remembers their first speech and their teachers encouraged them to stand up tall, hands to the side, look into the audience, and speak up. Honestly, they were on to something that speakers could use many years later. Not only are these simple tips that training organizations often use, but there are others that are highly recommended.

A well-known mentor and trainer, Bob Pike is famous for reminding speakers that preparation is essential to achieving an outstanding training outcome.<sup>91</sup> To do that, he recommends the six “P”s of an effective presentation: “Proper Preparation and Practice Prevents Poor Performance.” A part of that preparation is enhancing a person's presentation skills.

According to a 1977 survey mentioned in *The Book of Lists* by David Wallechinsky, Irving Wallace and Amy Wallace,<sup>92</sup> speaking in front of others is the one thing people fear the most—even more than death!<sup>93</sup> Even the most educated and technologically savvy person can become a bundle of nerves when asked to speak in front of others; including the president of a company! Researchers who study human behavior have indicated that, when one considers the key components of communication, there is little difference between talking to one or two people or an entire room of course participants. One's tone of voice, body language, and passion about the subject may apply to both, but in order to become a great presenter, one must master being direct, interesting, and informative.

A favorite presentation method is what can be called the “NEWS AT TEN METHOD.” Tell the audience what you are going to tell them. Tell them! Tell them what you have told them.<sup>94</sup>

#### 17.8.1.2 Presentation Skills

Great presenters have two qualities: appropriate skills and confidence to use those skills well.<sup>95</sup> These skills should include good eye contact, great posture, and appropriate facial expressions and hand gestures (non-verbal aspects). Most exhibit timely pauses and silences and speak with clarity. Good presenters engage the

audience by encouraging participation, inviting questions throughout, and answering questions well. They are careful in the appropriate use of clichés, diction, slang or vulgarities, gender references, acronyms, and jargon. It is imperative that a good speaker knows their audience!

Utilizing listening skills is another very important tool for a presenter. This may sound strange and one may ask, "How can one listen and talk at the same time?" Here are questions to ask oneself while speaking:

- Is your audience on board with you?
- Are they following you?
- Are you speaking over their heads or do you need to take it up a notch?
- Did they fail to laugh at what you thought was really funny?
- Is your energy level equal to theirs or is it too high or too low?
- Are you racing ahead of them, speaking too fast?

It has been said many times, "know your audience." This includes being "tuned in" to the audience throughout the presentation. This is achieved by "listening" to the audience for both their verbal and nonverbal queues.

As one reflects back on the best speakers that they have ever heard, one common element most likely experienced was their *passion* for their topic. Although, a presenter may have passion for their subject, the other key presentation elements are not guaranteed to fall into place. In the training industry, a SME is often called upon to present a particular topic. Yes, they will most likely have a passion for their topic because it is in their field of expertise, but that does not guarantee that they have taken the time to hone their presentation skills. Therefore, it is important to remember that not all SMEs are good presenters. Although the presenter is an expert in their field and very knowledgeable of the topic, the material may not be received well by the participants simply because it was not presented well. The presenter's tone, body language, and mood often affect the audience more than the actual presentation. Trainers step up to the podium with different presentation styles. It is important to identify one's style and enhance it. Several presenters may be given the same topic, same agenda and outline, yet each will most likely deliver the content in a different manner. This is great because there are various levels of learners. Audiences may range from high-level executives or supervisors or engineers to new operators or employees who have not heard a majority of the content being presented. Whatever a person's style may be, they must remember the key elements of a great presenter. These elements improve the likelihood of the information being received, understood, and placed in practice.

### 17.8.1.3 Behind the Scenes

Training needs to be assessed to determine how to design and develop the training course. Once this step has been taken, it is time to check in on one's presentation skills. Although it may seem easy and simple to follow, practice is highly recommended. As the saying goes, "it's easier said than done." So, prepare instructors with tools to succeed by using Pike's suggestion notes in the beginning of this section. Pike believes that 80% of being a good trainer and getting people involved depends upon adequate preparation. Participants rarely know what went on behind the scenes, but they will notice if the presenter did not take time to prepare. It is recommended to make every effort to be ready for the first participant who enters the class; first impressions are very important.

Establishing an environment conducive to learning is a critical aspect of starting a training session with positive momentum. Facilitators may spend hours the day before (and sometimes late hours) arranging the tables and chairs, arranging the manuals and student packets for participants to gather as they enter, assuring that all have a writing utensil, notepad, or even a highlighter to note "ah ha!" information received. Preparing name tags and/or name tents are useful tools not only for the participants to network, but it also allows the instructor to identify the student by name and not, "you in the green shirt." Some instructors utilize hands-on materials, such as product equipment, puzzles, handouts, etc. It is important to have those items available and ready for use. Although most of these tasks are the responsibility of the facilitator, it is helpful to the instructor to know in advance that these things are available to the participants in case they want to reference them during their presentation.

The room arrangement may have a significant impact on a presentation. The speaker should review the learning objectives. Consider if the learning objectives require participants to construct a product, work in groups to achieve an outcome, or play a game designed for learning? If so, is the classroom arranged in such a way that allows movement without confusion? Arranging the room in advance to meet the course objectives is fundamental to preparation and gives comfort to the presenter. The presentation will flow with ease as the presenter advances from one concept or activity to the next. Therefore, preparing the classroom just minutes before start time is *not* recommended.

Many trainers and facilitators take the following tasks for granted and fail to check room temperature, lighting, outside noises, visibility of all visual aids from every angle of the classroom, projector and screens, restrooms, emergency exits, room capacity (fire code), adequate learning space for each participant (9 ft<sup>2</sup>/person table space), microphones, a full easel pad, markers, extra pens/paper/manuals, backup instructor in case the assigned

instructor becomes sick or unavailable. Perhaps there are several others to add to this list. Prepare, prepare, prepare!

#### 17.8.1.4 Tools

Today, many trainers have become very comfortable using a PowerPoint presentation; however, one must not allow PowerPoint to become a crutch while presenting. PowerPoint is a very effective tool to use. It provides various visual aids for better understanding, especially for those who are visual learners. But, when it is overused, the electronic slides can lose their effectiveness. Using too many graphics and various backgrounds within one presentation may cause confusion. Conversely, displaying only text on slide after slide can be boring and show a lack of preparation/creativity on the part of the presenter. A rule to remember: prepare a cheat sheet of the presentation. One never knows when the projector or PC might decide to malfunction.

Many companies recommend that all company sponsored presentations use one basic template (see Figure 17.4). This template should be very minimal, and not overpower the information noted on each slide. From a legal perspective, each slide should also include course title and copyright information; it may be helpful if a page from the hardcopy version is separated from the entire presentation.

Visuals should support the training and not distract from it. They are most effective when<sup>96</sup>

- They are relevant to the subject.
- They are visible and understandable.
- Page orientation is consistent, using either landscape or portrait.
- Words are large enough to read.

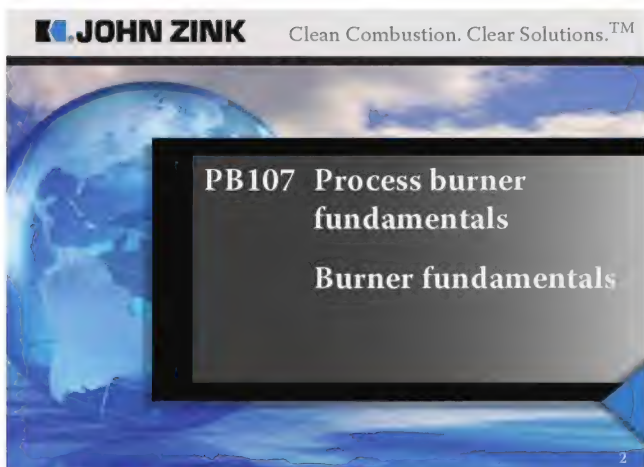


FIGURE 17.4  
Example of a PowerPoint template slide.

- They are oriented to the listener: “Here are four ideas you will...”.
- Color is used appropriately.
- The typeface varies in boldness and size (although not too much).
- The print is in both upper and lower typeface.
- The typeface enhances the readability (usually a sans serif font).
- Bullets delineate each point.
- They enhance the speaker’s performance rather than replace it.
- The visual becomes an extension of the speaker.
- They are tied together with a common element, for example, a sketch or graphic.
- They are customized for the group.

Compare the following two sentences:<sup>97</sup>

USING ALL CAPS INCREASES READING DIFFICULTY AND ELIMINATES USING ALL CAPS WITH SINGLE WORDS FOR EMPHASIS.

Using upper- and lower-case INCREASES readability and allows the use of ALL CAPS for emphasis.

Most trainers can relate to the 6 × 6 rule when preparing their presentations. This simply refers to the number of lines down and words across the visual (slide). Other tips to remember are as follows:

- When presenting a list, design it so the text can be revealed one line at a time.
- To further emphasize the line item, change the color of the newest item or have the previous items fade subtly. (*Try not to overdo this action.*)
- Headings should be about 44 pt and body 32 pt, but no less than 24 pt.
- Select one primary transition throughout the content for each module (too many types of transitions are distracting).
- Limit colors to two per slide plus black.
- Fade to black to signal a new module or to pause for discussion or an activity. (*This can be achieved by selecting “ctrl” and letter “b” on the keyboard.*)
- Use a subtle background.
- Ensure that there is enough contrast between typeface and background; light on dark is preferred.
- Use clip art sparingly and do not try to be cute. (*Important to obtain permission to use the clip art.*)



- When using animation, select one type and use throughout a module or content section.
- Keep sound effects brief, and make sure they add impact. (*Remember to check the volume level and speakers in advance.*)

Remember when instructors only had overhead transparencies and/or a flip chart? They were not all that bad. They can also be used as great tools today. It is still important that they are prepared in the same manner as a PowerPoint presentation. It is highly recommended and timesaving to prepare flip chart pages in advance. Perhaps make a few notes on pages and then use a sticky note on the side as a reminder as to when to share that information. Perhaps the instructor is not the greatest artist and may need to trace an object or picture from a professional. That is highly acceptable. Just remember to do that in advance. Plan, plan, plan ahead!

Today there are post-it note flip charts. What a neat invention! These are great for trainers to utilize because they enable a presenter to remove a paper (point) from the easel and place it on a visible wall for participants to reference at a later time. Perhaps one may want to encourage participants to add comments to a large sheet on the wall by attaching a smaller post-it note from their student packet if they have another comment relating to that discussion. Wow! A class activity opportunity!

Do not forget about handouts. Handouts reinforce the key points that a presenter is trying to make and serve as a reference once participants return back to their workplace. They may also provide additional information that was not added to the final presentation; need to know *vs.* nice to know discussion. Be careful of the timing of distributing handouts. If the handouts are distributed too early (before the point of the discussion), the participants may become distracted and not pay attention to the current discussion. For example: During instructor workshops, presenters often wait until the very end of the workshop to distribute handouts. They serve as a summary, not a crutch or sign of laziness and excuse to say, "It's in the handout."

Remember that handouts are a reflection of the speaker and their company. They are takeaways so it is important that they look professional, are easy to read, and are of good printing quality. An acronym to remember is **CRISP**: Colorful, Readable, Interactive, Simple, Pictures, if possible (graphics, diagrams, etc.).<sup>98</sup>

### 17.8.1.5 Apparel

Many work environments allow employees to dress business casual and some even allow casual attire; perhaps jeans on Fridays. It is recommended that the trainer maintain a professional look. Obviously, if the

presenter is outside with the operators offering training on specific equipment, the requirement will be different. The presenter can still make sure their hard hat is clean, boots are presentable, and protective clothing or coveralls are clean. In the classroom where several instructors are presenting, the decision may be made to wear identical shirts during training sessions. Not only will this better the chances of a professional look worn by all presenting, but it also allows participants to easily identify the instructors when they have a question or concern.

Sometimes trainers may become nervous or find themselves in an uncomfortable situation and reach for items to jiggle or toss. Because of this, it is recommended that trainers remove all coins or small items from their pant pockets before stepping up to the podium. This avoids the opportunity for participants to hear the jingle tune as they play with the coins in their pockets. In an effort to appear fashionable, women may desire to wear bulky and noisy jewelry. This fashion statement is not recommended. This may sound minimal, but any movement or the chance of jewelry getting caught on equipment could cause maximum distraction. Today, high heels are a fashion must for women. Great! Just be mindful if there are plans to interact with participants and how quickly the presenter will need to do so; in this case lower heels may work better. A good technique is to take the attention off the speaker early and involve the participants in a class activity or discussion.

### 17.8.1.6 Checklist

Ready, set, speak! Langevin Learning has provided a sample checklist that can be used to evaluate trainers.<sup>99</sup> Perhaps this checklist better summarizes attributes instructors may review as they strive to become good presenters.

Presentation skills:

- Clarity
- AV usage
- Avoidance of speech filters
- Expertise in subject
- Confidence

Organization:

- Appropriate amount of material
- Objective clearly stated
- Pace
- Time management
- Handling of materials

## Lesson structure:

- Introduction
- Feedback to learners
- Transition from phase to phase
- Reviews/summaries

## Climate/rapport:

- Enthusiasm
- Has fun
- Friendly/warm
- Casual/relaxed
- Use of learners' names
- Paid attention to all learners

## Response to learners:

- Responds to signs of difficulty
- Flexibility
- Noticed learner reactions
- Listened

## Questioning:

- Questions are clear
- Handling of incorrect answers
- Answered questions well

## Involvement:

- Encourages participation
- Invites questions
- Held attention
- Participation was spread

## Nonverbals:

- Voice
- Enunciation
- Eye contact
- Posture
- Facial expression
- Gestures
- Pauses and silences
- Nervousness controlled

## Results:

- Objectives met
- Learners receptive

This checklist may appear long and fearful, but it is possible to achieve 98% of the tasks after an instructor's second or third round at the podium. It is important to relax and enjoy presenting to the class. Giving a presentation is not about being perfect as much as personable.<sup>100</sup>

**17.8.1.7 Introduction and Closing**

Start the course by introducing the speaker and offering a story or icebreaker. The Internet is a great source of icebreakers. There are many available to use and tweak to the preferred training style and/or topic; tie it in and get them interested. Often icebreakers or stories come to a person in the middle of the night. Write them down! Darren LaCroix, 2011 World Champion Speaker, encouraged participants at a North Eastern Oklahoma ASTD retreat to keep a story library. Darren explained how he maintains an electronic folder full of events that he has turned into stories or icebreakers.<sup>101</sup> This way, a story is just a click away and he is always prepared when called upon to deliver.

Darren also shared *The Triangle of WOW*. Each side of the triangle represented a goal that every presenter should try to achieve when communicating. They are **Material**: words that are chosen, **Delivery**: manner in which the topic is communicated and **Setting**: atmosphere in which the subject is communicated.

Icebreakers can be used to arrange the participants in groups to enhance networking with others outside their peers. For example: The Bob Pike Group provides a simple and quick icebreaker entitled, "Line up by Experience." Basically, the instructor will ask participants to stand and move toward a designated wall. The instructor will ask participants to line up according to years of experience, perhaps as an operator or engineer in the petrochemical industry. This activity can be customized to the audience. Perhaps, line up participants by years of teaching experience. The instructor will need to designate which portion of the line is the lower end *vs.* the higher end of experience. It is recommended that participants are encouraged to line up quickly and try to do so with minimal discussion.

Once participants have formed a straight line, the instructor will then ask the participants to count off by numbering themselves according to the number of tables available in the room. (e.g., If there are five tables, then number themselves one through five.) After this is complete, identify which table is #1, #2, etc. Then ask that all those who are #1, please gather their belongings and move to table #1, and proceed until #5 participants are reached.

The outcome of this icebreaker forces the participants to sit with others outside their comfort zone and provides different skill levels at each table. The more advanced operators or engineers are able to mentor the

less experienced ones throughout the training session, during break conversations, lunch, or class activities. This creates a great start to their learning experience. It also gives participants another clue that they are not attending a “normal” training session. Perhaps, they may enjoy themselves along with learning a new skill or technique.<sup>102</sup>

It is important for presenters to share their credentials and experience in the field. Be brief! Be careful to not bore them with reciting the entire resume! A key point to remember: the quickest way to connect with the audience is to share personal failures and flaws. Sharing success after success tends to lead the participants to think, “Sure, he can do it, but I doubt that I can. He’s perfect!” Begin by identifying with the audience in both personal success and failures. Give the impression that the entire room is open to share knowledge and, hopefully, gain a few tools and tips that will enhance their daily activities. Although one may be the SME, remain open to hearing experiences and ideas from others in the room.

If introductions have not taken place, this is a good time to have participants introduce themselves. To save time and lower the nervousness of the participants, prepare a slide of questions that will remind them of what information to provide (see Figure 17.5). Once this is done, inform them of why they are present; WIIFM (What’s in it for me). Share the topic objectives and inform them that, in addition to learning, they are encouraged to enjoy the class and have fun.

It is just as important to close the presentation or training session properly as it was to start it properly. Often the closing moments are used to wrap up all discussions, gather takeaway items, handouts and materials and move the focus to returning to their workplace, hotel or catching their flight home. Participants are generally eager to leave and are not 100% tuned into any

discussions. This should not dissuade the instructor from asking if all the learning objectives and expectations have been met.

One closing activity may be for participants to verbalize to a table partner one or two action items that they will take away from their training session and implement immediately or in the near future at their workplace. Allow enough time for participants to share their experience and exchange contact information with those they have met during their stay.

Closing with another story is recommended. This calms the participants as they quiet down to hear the end of the story. Especially if the training session was started with a great story! For closing activities and stories visit [www.ebbweb.com](http://www.ebbweb.com).

It is also important to allow participants to offer feedback, positive as well as negative in some type of writing format. Comments provided by participants are an advantage to the instructors and facilitators providing the training. They allow feedback, suggestions, and room for improvement areas that will enhance the next training session. JZI offers feedback time after each presentation or topic is presented while it is fresh on the learner’s mind. Allowing them to not enter their name or personal information encourages honesty and completed evaluations.

If possible, encourage a company representative to stand by the exit doors and offer thanks to each participant, encouragement to continue to strive for excellence, and wish them well. Thank them for coming and ask that they tell others about their experience and refer them to the next training session. This provides one last positive experience for them upon leaving.

### 17.8.2 Accreditation

Accreditation refers to an independent third party giving approval to some aspect of a training program. There are numerous accrediting organizations as well as different types of accreditation. These will be briefly discussed in this section. Accreditation should be considered by an organization hiring an outside party to do training. Accreditation is a measure of quality that shows the training organization meets the rigorous standards set by the accrediting body. For example, most accrediting bodies require that instructors disclose any conflicts of interest. This may be particularly important when hiring a supplier to do training as the course could be a glorified sales presentation if the supplier is not required to meet any accreditation requirements.

Some accrediting organizations, such as the API under their TPCP,<sup>75</sup> accredit individual courses. Some accrediting organizations, such as the IACET,<sup>74</sup> accredit entire programs. There are also some accreditors that

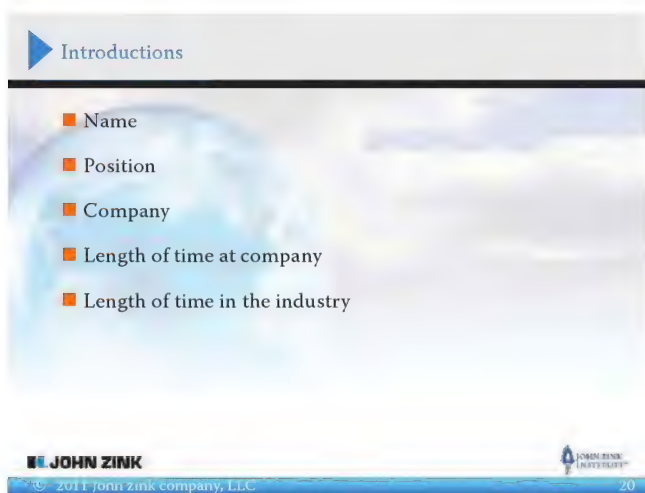


FIGURE 17.5  
Example of an introduction slide.



accredit a group of courses leading to a certificate, such as the ANSI.<sup>76</sup> Note that some accrediting bodies, such as the ACCET are officially recognized by government agencies such as the U.S. Department of Education.<sup>103</sup>

## 17.9 Case Studies

### 17.9.1 British Petroleum<sup>45</sup>

The British Petroleum (BP) Texas City refinery (see Figure 17.6) is one of the largest and most complex in the world. Located on a 1,200-acre site, it has a crude oil capacity of 460,000 barrels/day and nearly 2,000 direct employees. This section describes a partnership between BP and the JZC to deliver classroom training on fired heater operations to process operators.

Operator training can and should be done in a variety of ways. Some types of refresher training may best be done online. Training on a specific unit is usually best conducted on the job where an experienced operator trains a less-experienced operator. Training on upset conditions that would be difficult, if not impossible, to simulate with the actual operating equipment is usually best conducted using a process simulator. Training on general theory and best practices is often preferred in the classroom where students and instructors can interact and discuss principles that can be applied to their processes. The last type is of interest here.



FIGURE 17.6

BP, Texas City, Texas refinery. (From Valencia et al., *Hydrocarbon Process.*, 87(11), 55, 2008.)

#### 17.9.1.1 Importance of Training

There are many reasons why operator training is important. One survey found that the three top objectives for operating plants are to improve safety, increase process knowledge, and improve plant profit.<sup>104</sup> The most important objective is safety, to ensure that operators can properly respond to abnormal situations.<sup>105</sup> This includes handling situations they may never have actually encountered before, but which could happen, similar to airline pilots who train for many possible situations that rarely, if ever, occur. This means the operators must have a deep enough understanding of the process to enable them to safely handle abnormal situations and identify potential hazards.

Sustaining and improving the performance of process plant operators is a key element of operational excellence.<sup>106</sup> This is accomplished in a variety of ways including, for example, proper procedures, documentation, audits, mentoring/coaching, automation and controls, maintenance, and training (both off and on the job). There are many elements of operational excellence, including safety, efficiency, productivity, and environmental compliance. It is therefore critical that operators are adequately trained to meet the demands of operational excellence.

Plant operators must be able to quickly and accurately troubleshoot and diagnose process upsets and equipment problems.<sup>107</sup> Failure to do so can lead to lost production, off-spec product, equipment damage, and possibly even catastrophic events. Related to troubleshooting is process optimization, which means maximizing production while minimizing costs and meeting environmental regulations. This means that operators should be trained both to handle problems and to look for ways to improve processes even when nothing appears to be wrong. Proper training can sensitize operators about warning signals and what adjustments are needed in the circumstances encountered.

#### 17.9.1.2 Training Partnership

BP's unit-specific operations training department partnered with the JZC to develop a general 1 day training course for fired heater operations. This course was one component of a more comprehensive operator training program that BP put together which also included a classroom-lead process fired heater simulator and unit-specific fired heater training conducted by the BP unit training coordinators. The JZI, the training organization for JZC, delivers training courses all over the world, including at plant sites. While there is a standardized curriculum for a typical 1 day course, most on-site classes are customized to the equipment in the plant. BP's unit-specific operations training department

developed their desired course outline, learning objectives, and outcomes including a student learning assessment. A pilot course was developed by JZC and delivered to a cross functional group of BP personnel, including training general personnel, engineers, and operations supervisors. The materials were fine-tuned to meet BP's requirements before rolling it out to the Texas City Site operations organization.

One of the benefits for a plant partnering with an experienced training organization is the accumulation of industry-wide best practices. JZC personnel have worked in virtually every refinery in the world. They have seen a wide range of both problems and best practices. This experience is invaluable for training because it exposes a particular plant to potential issues that even their experienced operators may rarely, if ever, have encountered.

Most JZI courses are accredited by the IACET, which means that CEUs are given to students who can demonstrate that they have met the course requirements, which includes successfully passing a post-course examination. One of the requirements of accreditation requires student privacy where test results can be given to others only with written permission from the student. BP decided to forego CEUs for this training because they wanted to see all test results. BP also chose to make the course requirements more stringent than those required by the IACET accreditation.

### 17.9.1.3 Customized Operator Training

The objectives for the course were to improve overall understanding, define common fired heater terminology, follow proper and safe operating procedures, increase heater thermal efficiency, reduce pollutant emissions, and provide tools for troubleshooting problems. The agenda shown in Table 17.1 was developed for the course to meet those objectives. The primary thrusts of the training were safety, reducing pollution emissions, maximizing thermal efficiency, and providing troubleshooting tools. These were addressed throughout the course. For example, while section three specifically addressed combustion safety, it was designed to provide the foundation for other discussions on safety

in later sections. Detailed theory and equations were kept to a minimum because the course was designed for operators, so the information had to be practical and easily applied to daily operations.

Sixteen classes were conducted in 2007, with an average class size of 13, to ensure good interaction between students and instructors. Each student received a color copy of the PowerPoint slides used during the training. Figure 17.7 shows an example of a typical slide which has a picture of actual equipment and a drawing showing more details of free-standing diffusion (raw gas) burners. One copy of the *John Zink Combustion Handbook*<sup>108</sup> was provided to each class for use as a reference. That book is used as a text in other JZI classes, and although it includes practical information, it is designed primarily for engineers rather than operators. Each student also received a laminated flowchart, designed for use in the plant, for setting the oxygen and draft levels for natural draft and balanced draft heaters.

The students were introduced to each course by a BP Manufacturing Department Leader, followed by the unit-specific operations training Project Manager. They helped provide context, expectations, and motivation for the class. The students then took a closed-book pretest consisting of 15 questions requiring fill-in-the-blank answers. No multiple choice or true or false questions were used where students might have been able to correctly guess the answers even though they may not have actually known the answers a priori.

The classes were designed to be highly interactive, emphasizing the Socratic teaching style where the instructor asks the students several questions and instructs based upon the responses. For example, Figure 17.8a shows three burners firing horizontally in a process heater (not at BP). The students were asked to determine what might have been wrong with the burners. Then they were shown a picture of the back of the burners (Figure 17.8b) which shows that the air registers were closed on the two burners with bright yellow flames. Throughout the course, many photos, animations, and short video clips were shown of process heaters that had problems. The students were asked to determine the problems and recommend solutions. This format exposed them to many potential problems they may never have encountered, but which they might encounter or which they could avoid in the future by taking the proper actions. For example, video clips of burners flashing back were shown during the class. These clips were taken at the JZC Test Facility under highly controlled conditions. Those clips exposed students to the sights and sounds of flashbacks in case they ever encounter them in their own heaters.

**TABLE 17.1**

Course Outline

Section	Title	Length (h)
1	Introduction	1
2	Combustion fundamentals	1
3	Combustion safety	1
4	Process heater fundamentals	1
5	Burner fundamentals	2
6	Heater operations	2



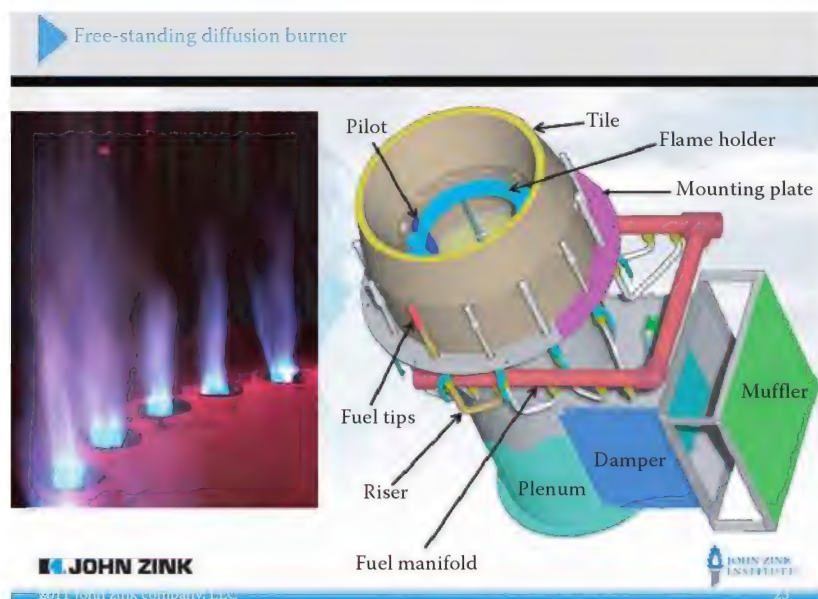


**FIGURE 17.7**  
Free-standing diffusion burner slide. (From Valencia et al., *Hydrocarbon Process.*, 87(11), 55, 2008.)



(a)



(b)

**FIGURE 17.8**  
(a) Irregular flame patterns in an operating process heater and (b) closed air registers on the two improperly adjusted burners. (From Valencia et al., *Hydrocarbon Process.*, 87(11), 55, 2008.)

The course was designed to show operators both good and poor heater operations. Many examples were shown of a variety of problems found in actual operating heaters in many plants. Figure 17.9a shows an example of improperly adjusted burners in a process heater (not at BP). Both the furnace draft and excess  $O_2$  were well out of the desired specifications. The flames were irregular and were not producing the desired heat flux pattern on the floor. Figure 17.9b shows the same burners in the same heater, after they were properly adjusted. These adjustments can be easily made by operators once they have

been properly trained. Figure 17.10 shows a schematic of flame rollover in a cabin heater. Burners are firing up along the wall, but the flames are rolling over into the process tubes, which is very undesirable and can cause a premature shutdown. Possible causes and solutions were discussed for this and other related problems. Students received practice troubleshooting in the classroom using the tools they learned. They also were able to discuss the problems with their colleagues and the instructors.

An important element of the class is that it was designed to be fun. While there is no doubt that a lot



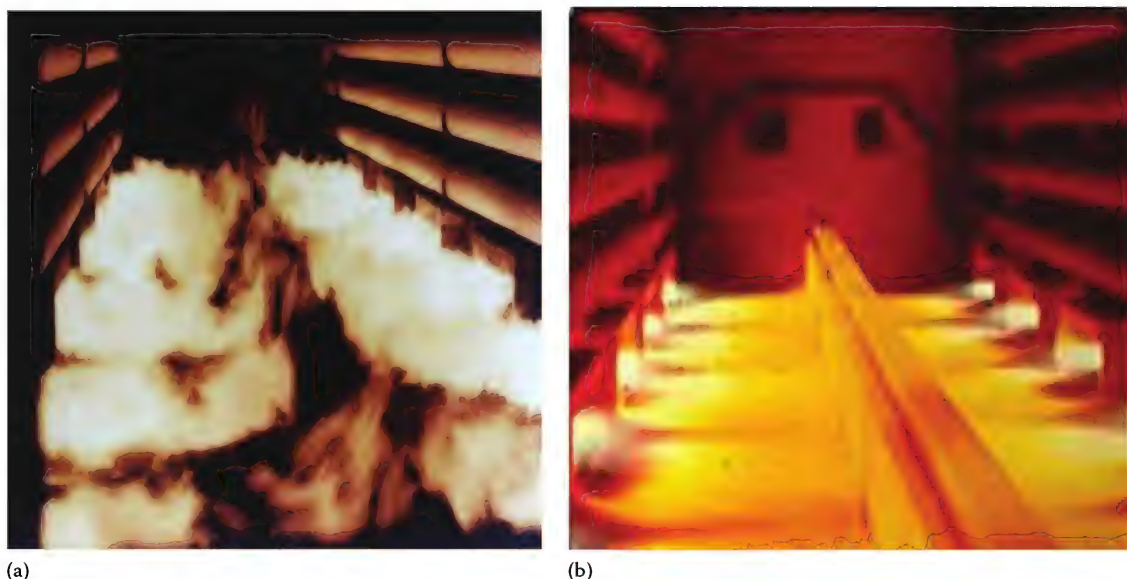


FIGURE 17.9

Burners firing across the floor in a process heater (a) before adjustment and (b) after adjustment. (From Valencia et al., *Hydrocarbon Process.*, 87(11), 55, 2008.)

of new material was covered over the course of the day, humor and games were used to help engage the students. For example, as a review of the posttest, students were divided into two teams that competed in a game of Jeopardy (see Figure 17.11). The winning team members received a nice prize, so the competition was often fierce.

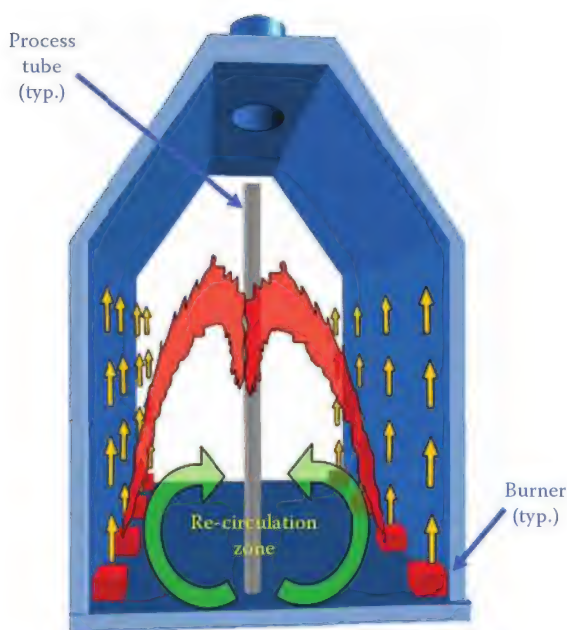


FIGURE 17.10

Schematic of flame rollover in a cabin heater. (From Valencia et al., *Hydrocarbon Process.*, 87(11), 55, 2008.)



FIGURE 17.11

Main computer screen for Jeopardy game used to review for final test. (From Valencia et al., *Hydrocarbon Process.*, 87(11), 55, 2008.)

### 17.9.1.4 Results

The students taking this course ranged in experience from as little as a few months to more than thirty years. Very experienced operators still benefited from the training because they gained a deeper understanding of the reasons for various procedures. For example, a burner that is pulsing or huffing is unsafe and needs to be corrected immediately. The operator may know to reduce the fuel flow to the burner, but may not know why or what could happen if the wrong action is taken.

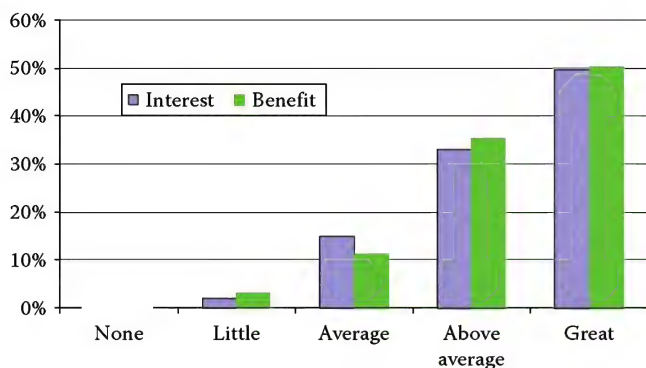


FIGURE 17.12

Overall ratings by students on their interest in and the benefit of each course section. (From Valencia et al., *Hydrocarbon Process.*, 87(11), 55, 2008.)

Knowing the why behind the procedures helps the operations personnel to better handle abnormal operations they may never have encountered.

The posttest questions were identical to the pretest questions, so a direct comparison could be made between what students knew before and after taking the course. After 16 classes and over 200 students, there was a sizeable improvement between pretest and posttest scores as a result of the course. The average pretest score was 33% and the average posttest score was 94%. Students were given anonymous course evaluations and asked to rate their interest in and the benefit of each topic using a Likert scale ranging from 1 to 5 where 1 = none and 5 = great. The overall average rating for all topics was 4.3. One student wrote, "Learning was made fun and interesting." Another wrote, "I know more about heaters than when I came to class!" Figure 17.12 shows a summary of the overall student evaluations for the course. The blue bars show interest in the content and the green bars show how much the students benefited from the class. The vast majority of students found the course interesting and beneficial. The course materials were continuously revised based on student feedback. For example, students in the earlier classes felt there was too much material, so duplicate and superfluous information was deleted in later classes.

#### 17.9.1.5 Conclusions

Operator training is critical for the safe, environmentally sound, and efficient operation of a plant. Partnerships between plants and external training organizations can effectively help meet some operator training requirements. Specific objectives should be developed so the materials and learning experiences can be designed to meet those objectives. Certain types of training are

better done in the classroom with a limited number of students to promote interaction and engagement. Some type of assessment tool, such as a posttest, should be used to quantify learning and ensure that key concepts have been grasped. Ideally the training should be fun to fully engage the students, particularly operators who may not be as comfortable in the classroom as, for example, degreed engineers. Some type of course evaluation is important so adjustments can be made as appropriate to continuously improve the content and instruction methods.

#### 17.9.2 Shintech<sup>109</sup>

Shintech began construction of its new Plaquemine Louisiana manufacturing facility (see Figure 17.13) in October 2005. The facility is located on a 1725 acre site, and it manufactures chlorine, caustic soda, and vinyl chloride monomer (VCM). Historically, Shintech has manufactured only polyvinyl chloride (PVC). This new plant is Shintech's first integrated complex. The new manufacturing facility employs state-of-the-art environmental technologies and is subject to the most stringent environmental controls in the country.

JZC manufactures thermal oxidation systems (see Volume 3, Chapter 7) used to destroy unwanted wastes.<sup>107</sup> Thermal oxidizers (TOs) are commonly used to treat volatile organic compounds (VOCs) and carbon monoxide



FIGURE 17.13

Shintech plant in Plaquemine, Louisiana. (From Gilder et al., *Hydrocarbon Process.*, 89(11), 55, 2010.)





**FIGURE 17.14**  
Photo of part of the thermal oxidation system during installation.  
(From Gilder et al., *Hydrocarbon Process.*, 89(11), 55, 2010.)

(CO) emissions because of their very high destruction and removal efficiencies.<sup>110</sup> Thermal oxidation can be defined as, “the process of oxidizing combustible materials by raising their temperature above the autoignition point in the presence of oxygen and maintaining it at high temperature for sufficient time to complete combustion to carbon dioxide and water.”<sup>111</sup> Training at customer plant sites is typically from one to three days long and is customized to the equipment in the specific plant. JZI works with the plant to determine a suitable course agenda.

Shintech partnered with JZI to offer a customized TO training to 37 of its plant operators for the start-up of its new facility. A photo of part of the thermal oxidation system is shown in Figure 17.14. The course was offered with optional CEU credits that were available to any students meeting the following criteria: take (not pass) a pretest, attend at least 80% of the course contact time, pass (at least 80%) a posttest, and complete an anonymous course evaluation. JZI is authorized to offer CEUs through its accreditation by the IACET.

### 17.9.2.1 Course Design

The course was designed to give operators at the new facility a good idea of both the *what* and the *why* of operating the equipment. All too often, operators are trained, sometimes hurriedly and haphazardly, by existing experienced operators. The new operators may learn *what* to do, but not the *why* behind the *what*. It is also fairly common for long-time operators not to understand some of the basics because these basics were never taught to them. The *why* is important because it helps operators better understand the cause and effects that can impact safety, thermal efficiency (and, therefore, operating costs), productivity, and pollutant emissions. For example, Figure 17.15 shows a slide describing the potential problem of “blow-off” if a burner is over-fired. Moving from left to right shows what happens as the air/fuel mixture velocity is increased. When the

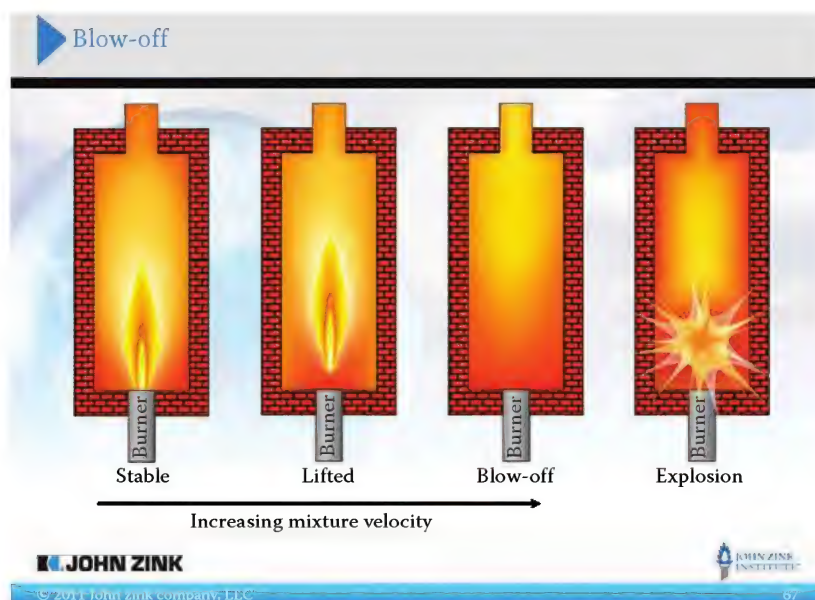


**FIGURE 17.15**  
Series of furnaces showing the progression towards blow-off of a burner flame. (From Gilder et al., *Hydrocarbon Process.*, 89(11), 55, 2010.)



last furnace on the far right appears in the slide animation, the sound effect of an explosion is heard to help reinforce the point of the danger of going beyond the design firing limit for the burner. The *why* also better prepares operators to react to new situations that may not have been covered in formal training sessions. The course content included basics that apply to any equipment of this type, along with very detailed and specific information on the equipment in this particular plant.

The course had the following sections:

1. Combustion and thermal oxidizer basics
2. Safety overview and warnings
3. Overall equipment familiarization
4. Detailed walkthrough of equipment
5. Detailed blower, boiler, absorber, scrubber, and demister detail
6. Detailed walkthrough of P&IDs
7. Drawings review
8. Pre-start-up and refractory cure out
9. Normal start-up and shutdown
10. Logic demonstration and DCS screens
11. Normal maintenance
12. Troubleshooting
13. Drawings

Each student received a three-ring binder containing the color PowerPoint slides. Adequate room was provided for them to make notes in the manual as desired. Some of the students received their manuals prior to the start of the class and came prepared with questions to ask. Statistics for all types of training show that retention of the material diminishes fairly quickly after the training has been completed. The student manual can be quickly and easily referenced as often as needed to refresh previously studied information. Although operators do not generally receive their own copy of the operation and maintenance manual, the student manual contains much of the same information including many of the written operating procedures.

### 17.9.2.2 Training

The training was conducted over three consecutive days, followed by a 4th day about 6 weeks later on a couple of specific pieces of equipment. Although most of the time was spent in the classroom, there were many short sessions spent outside at the equipment going over the specifics after reviewing the basics in the classroom. The plant had not been commissioned yet, so the equipment was installed, but not operational. While this did not allow the operators to do live training, it did permit

operators from all shifts to attend classes together during normal working hours. This produced a great deal of interaction and feedback between participants and with the instructors. Another important aspect of the training was that supervisors were present during most of the sessions, which sent a strong message about the importance of the class.

The format of the training was designed to be very interactive. While colorful PowerPoint slides (e.g., see Figure 17.16) were used to guide the discussion, operators were encouraged to ask questions and make comments at any time. This was encouraged in part through subject-oriented fun games, such as poker and bingo. Every time a participant asked or answered a question, they were given a random card from a poker deck. For the poker game, the student with the best poker hand at the end of the day received a nice prize. For the bingo game, cards were drawn from a deck until someone had enough matching cards to win. The more cards a student had, the more chances of winning, so this encouraged continuous and frequent participation. Other token gifts were also given out during the training as deemed appropriate by the instructors (e.g., to a student asking a particularly good question).

Short video clips and brief plant visits were used to break up the lecture periods and to help keep students engaged in the materials. Videos are particularly powerful when demonstrating potential problems, such as flashback from a burner, that may not have been previously experienced at a particular plant, but which could happen under certain circumstances. This is analogous to airline pilots who train in simulators to react to situations they hope they never encounter, but for which they are prepared to handle just in case.

The actual equipment drawings for this plant were used during the training to help familiarize the operators with the equipment and with the operating procedures. To make it even more realistic, photos were taken of individual components that would display on the drawings when clicked. For example, clicking on the symbol of a valve would show a picture of the actual valve in the plant (see Figure 17.17). This helped personalize the training and made it easier for the operators to connect the drawings to the actual equipment.

### 17.9.2.3 Results

Identical fifteen-question pretests and posttests were given to the students to measure learning. The pretest assessed students' knowledge prior to taking the class. The average pretest and posttest scores were 52% and 99%, respectively. The difference between the scores is an indicator of what was learned in the training.

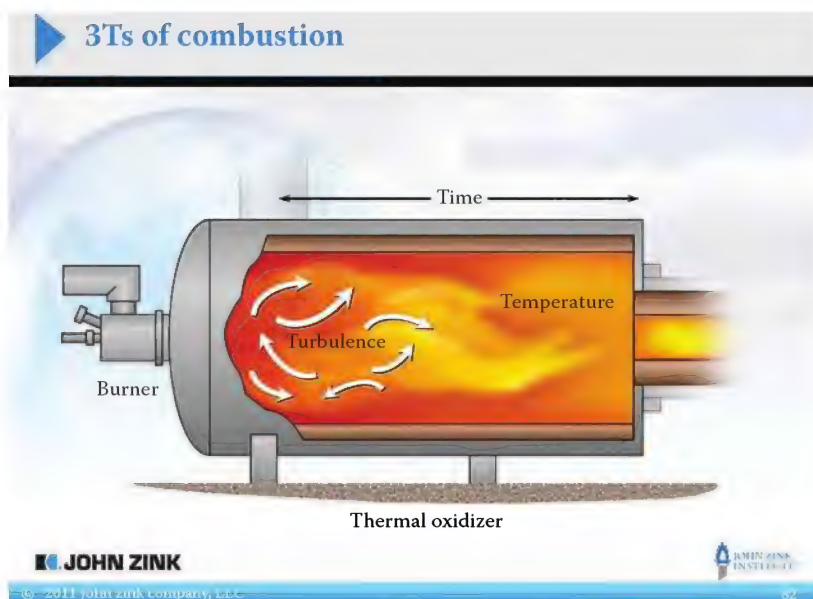


FIGURE 17.16

Slide showing the 3Ts of combustion: time, temperature, and turbulence. (From Gilder et al., *Hydrocarbon Process.*, 89(11), 55, 2010.)

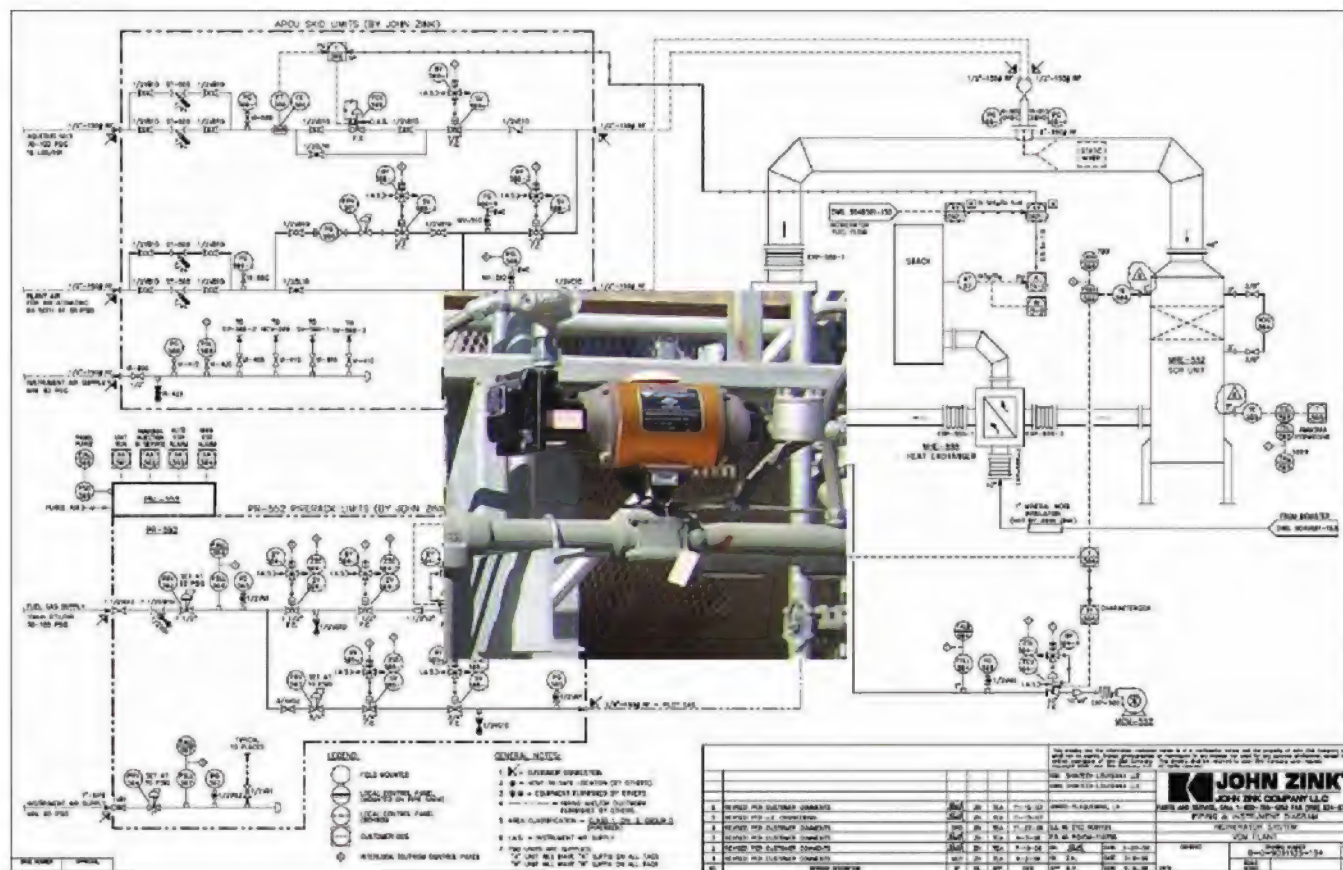


FIGURE 17.17

Animated P&ID with a picture of an actual control valve. (From Gilder et al., *Hydrocarbon Process.*, 89(11), 55, 2010.)

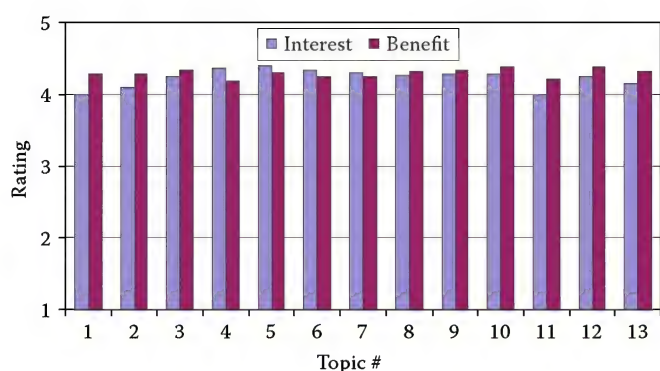


FIGURE 17.18

Student ratings of interest and benefit of each course topic. (From Gilder et al., *Hydrocarbon Process.*, 89(11), 55, 2010.)

Students were also given a questionnaire at the end of the course to assess their level of satisfaction with the course. Students did not put their name on the forms, although their name was checked off a list to show they completed the evaluation, which is one of the requirements for receiving credits for the course. A five-point Likert scale was used, where 1 = none, 2 = little, 3 = average, 4 = above average, and 5 = great. Students rated each section of the course according to their interest in the topic and its benefit to them. There was also a space to write in any comments they may have had on the topic. Figure 17.18 shows the averaged results by interest and benefit for each topic. The results show that, on average, students found all topics to be of “above-average” interest and benefit.

Another part of the questionnaire asked students for written comments on the instructors and material. Some of the instructor comments included “Very Knowledgeable,” “Excellent,” and “Very Thorough.” Some students felt more time should have been spent on start-up, shutdown, and troubleshooting and less time on the drawings. Content and coverage is always the challenge with a group of students having a wide range of backgrounds and experiences. Note that all students met the necessary requirements and received CEUs for the class.

#### 17.9.2.4 Conclusions

Properly training plant operators is critical to ensure equipment is operating safely, while maximizing efficiency and productivity and minimizing pollution emissions. Operators need to understand some basic information about the equipment, as well as the details on their specific installation. Although not always possible, it is particularly beneficial to have all operators together in the same class to enhance discussion and mutual learning. Training should be customized to the needs of the plant and incorporate techniques such as

fun games to promote interaction among the participants and instructors. Ideally, there should be a “hands-on” portion of the training where instructors use the actual equipment during demonstrations. Pretesting and post-testing are effective tools to show that operators have learned the key points in the training.

### 17.10 Recommendations

There is growing concern about the effectiveness of CPE, most of which focuses on abstract knowledge rather than on practical application.<sup>24</sup> To improve program effectiveness, the best solution for an organization depends on a number of factors but is often a combination of providers. Organizations need to select the best way of sourcing their training needs,<sup>112</sup> which means selecting the best provider for the specific type of continuing education. Internal providers are often best suited for an organization’s core competencies where there are available SMEs who have specialized and proprietary knowledge that may only be available inside the organization and because the organization may not want to share this information which gives them a competitive advantage. This is particularly important for processes and products that are not protected by patents, but are instead trade secrets where the organization must closely protect the information to maintain that competitive advantage. Training that is strategic to the organization should preferably be developed and delivered by internal providers.<sup>46</sup> The more complicated the topic, the more likely it will need to be taught by internal technical experts.<sup>32</sup>

For some types of training, external providers may be best suited to deliver certain courses. This might be for technologies or skills where the expertise lies outside the organization and where this knowledge does not by itself give the organization a competitive advantage. It might also be necessary when the training resources lie outside the organization, such as specialized hardware or software. For example, the operation and maintenance of a pump in a chemical plant is usually not considered to be knowledge that offers a competitive advantage. For this type of noncompetitive training, the plant may decide that it is best delivered by an external provider such as a supplier. In the past, it was much more common for plants to have specialists who knew a great deal about particular aspects of the operation, such as particular processes or types of equipment. However, the trend toward leaner operations has eliminated many of these specialists, so plants rely much more on suppliers and consultants



for that specialized knowledge. Another example where an external training provider would be the best choice is when an organization purchases a new piece of equipment that it has not previously used, and for which there are no experienced users in the organization. Specialized training may even be included as part of the purchase.<sup>32</sup> JZI often trains clients at the plant site when the clients purchase technology that is new to the plant. These are often short, half-day sessions covering safety, operation, maintenance, and trouble-shooting of the equipment.

For certain types of training, a combination of providers may be the best solution. One example might be when competitors collaborate to train on noncompetitive topics such as safety, health, and the environment. It is in the best interests of an industry to keep people safe and healthy and not to harm the environment. Incidents that injure plant personnel and damage the environment often bring bad publicity to all organizations in an industry, even those that were not involved in the incidents. Another reason why a hybrid provider might be the best choice is when the specific knowledge of a given organization is combined with industry best practices. An SME in the organization provides the former, while an SME in the industry provides the latter. The internal SME can teach what has happened in their organization, while the external SME can teach what has happened in other organizations in the industry.

One example of using multiple types of continuing education providers is BP (Texas City, Texas), which used a combination of solutions for a four-day heater operations training course.<sup>45</sup> BP hired a supplier to teach a 1 day class using a customized computer simulator to train on specific operating units in the plant. They hired JZI to teach a 1 day class on process burners and heaters. BP used experienced operators to conduct 2 day hands-on training sessions on the actual equipment in the plant. This arrangement of multiple providers received high marks from plant personnel, because the best providers were used to teach each portion of the course.

It is unrealistic to expect that all continuing education required by an organization can be provided using only internal resources. "Due to increasing focus on cost control and complex learning technologies in educating adults in the workforce, companies realize that in-house development and management alone are insufficient."<sup>113</sup> External continuing education providers should be used as appropriate, particularly when the expertise on a certain subject is outside the organization. In some cases, the best option may be a hybrid combination of instructors from both internal and external sources. The primary goal for the organization should be to select qualified instructors, whether they are inside or outside the organization, for the given continuing education subject.

## References

1. NFPA 86 (2011), *Standard for Ovens and Furnaces*, 2011 edition, National Fire Protection Association, Quincy, MA.
2. Padfield, C. and Schaufelberger, W. (1998), Lifelong learning in engineering education: A call to action (Brussels: Soci  t   Europ  enne pour la Formation des Ing  nieurs).
3. Dirkx, J. M. (2011), Work-related learning in the United States: Past practices, paradigm shifts, and policies of partnership. In Malloch, M., Cairns, L., Evans, K., and O'Connor, B. N. (eds.), *The Sage Handbook of Workplace Learning*, Sage, London, U.K.
4. Noe, R. A. (2005), *Employee Training and Development*, 3rd edn., McGraw-Hill, New York.
5. Jacobs, R. L. and Park, Y. (2009), A proposed framework of workplace learning: Implications for theory development and research in human resource development, *Human Resource Development* 8(2), 133–150.
6. Baukal, C., Colannino, J., Bussman, W., and Price, G. (2010), Industry instructors for a specialized elective course, *Paper AC2010–67, Proceedings of the American Society for Engineering Education Annual Conference and Exhibition*, Louisville, KY, June 20–23, 2010.
7. Baukal, C., Price, G., Matsson, J., Bussman, W., and Olson, S. (2011), Industry adjuncts: Lessons learned, *Paper AC2011–2248, Proceedings of the American Society for Engineering Education Annual Conference and Exhibition*, Vancouver, British Columbia, Canada, June 26–29, 2011.
8. Darkenwald, G. G. and Merriam, S. B. (1982), *Adult Education: Foundations of Practice*, Harper & Row, New York.
9. Praeger, R. R., Ponticell, J. A., and Gordon, E. E. (1998), *Enhancing Learning in Training and Adult Education*, Praeger, Westport, CT.
10. Merriam, S. B., Caffarella, R. S., and Baumgartner, L. M. (2007), *Learning in Adulthood: A Comprehensive Guide*, Jossey-Bass, San Francisco, CA.
11. Knowles, M. S., Holton, E. G., and Swanson, R. A. (2005), *The Adult Learner*, Elsevier, Boston, MA.
12. Communication for the Safety Professional, Robert Kornikau and Frank McElroy, National Safety Council: Chicago (1975), p. 370.
13. Elaine Biech, *Training for Dummies*, Wiley Publishing, Inc., Hoboken, NJ, 2005, pp. 28–32.
14. Dave Meier (2000), *The Accelerated Learning Handbook*, McGraw Hill Companies, Inc. New York.
15. The Thiagi Group, Improving Performance Playfully, [www.thiagi.com](http://www.thiagi.com), accessed 20 July 2012.
16. Craigstrachan.com—Keep Talking, The A-Z of public speaking, <http://www.craigstrachan.com/blog/2008/09/the-a-z-of-public-speaking.html>, September 3, 2008, accessed 30 July 2012.
17. EdgeNet, Exclusive Community for Members of World Champions' EDGE, <http://www.worldchampionsedenet.com>; <http://www.craigstrachan.com>, accessed 30 July 2012.

18. Baukal, C. and Bussman, W. (2009), Ambient condition impact CO and NO<sub>x</sub> emissions: Part I, *Pet. Technol. Q.* 14(3), 93–99.
19. Baukal, C. and Bussman, W. (2009), Ambient condition impact CO and NO<sub>x</sub> emissions: Part II, *Pet. Technol. Q.* 14(4), 37–41.
20. Baukal, C. and Bussman, W. (2009), Simulator for teaching process heater operating principles, Paper presented at the 2009 American Society of Engineering Education conference, June 14–17, 2009, Austin, TX.
21. Forrester, K., Payne, J., and Ward, K. (1995), *Workplace learning: perspectives on education, training and work*, Avebury Aldershot, U.K.
22. Cole, H. P., Moss, J., Gohs, F. X., Lacefield, W. E., Barfield, B. J., and Blythe, D. K. (1984), *Measuring Learning in Continuing Education for Engineers and Scientists*, Oryx Press, Phoenix, AZ.
23. Anderson, C. (2011), Outsource training to transfer knowledge, *Chief Learning Officer* 10(5), 52–55.
24. Hale, J. (2006), *Outsourcing Training and Development: Factors for Success*, Pfeiffer, San Francisco, CA.
25. Weimar, B. (1992), Assumptions about university-industry relationship in continuing professional education: A re-assessment, *Eur. J. Educ.* 27(4), 379–396.
26. Cervero, R. M. (1992), Professional practice, learning, and continuing education: An integrated perspective, *Int. J. Lifelong Educ.* 11(2), 91–101.
27. National Research Council (1985), *Engineering Education and Practice in the United States: Continuing Education of Engineers*, National Academy Press, Washington, DC.
28. Heinke, G. W. (1991), Continuing professional education for engineers in Canada: Whose responsibility is it, and how do we get it going? *Int. J. Cont. Eng. Educ. Lifelong Learn.* 1(4), 319–333.
29. Houle, C. O. (1980), *Continuing Learning in the Professions*, Jossey-Bass, San Francisco, CA.
30. Cervero, R. M. (2001), Continuing professional education in transition, 1981–2000, *Int. J. Lifelong Educ.* 20(1/2), 16–30.
31. Bourne, J., Harris, D., and Mayadas, F. (2005), Online engineering education: Learning anywhere, anytime, *J. Async. Learn. Net.* 9(1), 15–41.
32. Combs, Wendy, L. and Davis, Bettina M. (2010), *Demystifying Technical Training: Partnership, Strategy, and Execution*, Pfeiffer, San Francisco, CA.
33. Meister, J. C. (2001), The brave new world of corporate education, *Chron. High. Educ.* 47(22), B10–B11.
34. Lui-Abel, A. (2011), Identifying and classifying corporate universities in the United States. In Malloch, M., Cairns, L., Evans, K., and O'Connor B. N. (eds.), *The Sage Handbook of Workplace Learning*, Sage, London, U.K.
35. Allen, M. (2002), *The Corporate University Handbook: Designing, Managing, and Growing a Successful Program*, AMACOM, New York.
36. Balm, G. J. (1990), Continuing engineering education at IBM, *Int. J. Cont. Eng. Educ. Lifelong Learn.* 1(1), 98–103.
37. Craig, R. L. and Evers, C. J. (1981), Employers as educators: The 'shadow education system'. In Gold G. ed., *Business and Higher Education: Toward New Alliances*, Jossey-Bass, San Francisco, CA, pp. 29–46.
38. Collin, K. (2008), Development engineers' work and learning as shared practice, *Int. J. Lifelong Educ.* 27(4), 379–397.
39. Gräfen, H. (1991), Continuing education: An investment for the future, *Int. J. Cont. Eng. Educ. Lifelong Learn.* 1(2), 121–128.
40. Cervero, R. M. (1988), *Effective Continuing Education for Professionals*, Jossey-Bass, San Francisco, CA.
41. OSHA (2010), *Training Curriculum Guideline—(Non-mandatory)*, U.S. Occupational Safety and Health Administration, Washington, DC, [http://www.osha.gov/pls/oshaweb/owa-disp.show\\_document?p\\_table=STANDARDS&p\\_id=9770](http://www.osha.gov/pls/oshaweb/owa-disp.show_document?p_table=STANDARDS&p_id=9770)
42. Cross, K. P. (1981), *Adults as Learners: Increasing Participation and Facilitating Learning*, Jossey-Bass, San Francisco, CA.
43. Merriam, S. B. and Caffarella, R. S. (1999), *Learning in Adulthood: A Comprehensive Guide*, 2nd edn., Jossey-Bass, San Francisco, CA.
44. Knowles, M. S., Holton, E. F., and Swanson, R. A. (2005), *The Adult Learner*, 6th edn., Elsevier, Burlington, MA.
45. Valencia, R., Link, D., Baukal, C., and McGuire, J. (2008), Consider classroom training for plant operators, *Hydrocarbon Process.* 87(11), 55–59.
46. Blanchard, P. N. and Thacker, J. W. (2004), *Effective Training: Systems, Strategies, and Practices*, 2nd edn., Pearson, Upper Saddle River, NJ.
47. Baldwin, L. V. and Johnson, G. R. (2001), NTU: The working professional's university, *Int. J. Eng. Educ.* 17(2), 108–118.
48. Dipaolo, A. (1995), The Stanford instructional television network: A partnership with industry, *Euro. J. Eng. Educ.* 20(2), 243–246.
49. Anwar, S. and Curley, W. G. (2000), Partnering with industry to provide continuing and distance education programs in engineering and technology: A case study, Paper presented at the 2000 American Society of Engineering Education Annual Conference & Exhibition: Engineering Education Beyond the Millennium, June 18–21, 2000, St. Louis, Missouri, MO.
50. Bodendorf, F. and Swain, P. H. (2001), Virtual universities in engineering education, *Int. J. Eng. Educ.* 17(2), 102–107.
51. Fink, F. K. (2001), Integration of engineering education and productive engineering, *8th World Conference on Continuing Engineering Education*, May 12–16, 2001, Toronto, Ontario, Canada.
52. Baukal, C. (2010), Continuing engineering education through distance learning, *Euro. J. Eng. Educ.* 35(2), 225–233.
53. Institute for Electrical and Electronics Engineers (2010), <http://www.ieee.org/index.html>, accessed 30 July 2012.
54. Van Horn, J. H. (1977), Industry/professional society interaction, *Eng. Educ.* 64(4), 285–287.
55. Abramson, H. I. (1977), How one professional society provides continuing education, *Eng. Educ.* 64(4), 287–289.
56. International Federation of Engineering Education Societies (2010), <http://www.ifees.net/>, accessed 30 July 2012.
57. American Society for Engineering Education (2010), <http://www.asee.org/>, accessed 30 July 2012.

58. European Society for Engineering Education (2010), <http://www.sefi.be/>, accessed 30 July 2012.
59. International Association for Continuing Engineering Education (2010), <http://www.iacee.org/>, accessed 30 July 2012.
60. European Commission (2002), *Distance Learning; Leonardo da Vinci Series: Good Practices*, Commission of the European Communities, Brussels, Belgium.
61. American Petroleum Institute (2010), API University, <http://www.api.org/apiu/>, accessed 30 July 2012.
62. Instrument Society of America (2010), <http://www.isa.org/>, accessed 30 July 2012.
63. Center for Professional Advancement (2010), <http://www.cfpa.com/>, accessed 30 July 2012.
64. PDHengineer.com (2010), <http://www.pdhengineer.com/>, accessed 30 July 2012.
65. EPIC (2010), <http://www.epic-edu.com/>, accessed 30 July 2012.
66. Anderson, R. M. (1977), An educator views the limitations of professional societies, *Eng. Educ.* 67(4), 289–291.
67. U.S. Environmental Protection Agency (2010), Air Pollution Training Institute, <http://www.epa.gov/apti/>, accessed 30 July 2012.
68. U.S. Occupational and Safety & Health Administration (2010) OSHA Training Institute, <http://www.osha.gov/dte/oti/index.html>, accessed 30 July 2012.
69. Suleiman, A. (1983), Private enterprise: The independent provider? In M. R. Stern, M. R. (ed), *Power and Conflict in Continuing Professional Education*, Wadsworth, Belmont, CA, pp. 136–144.
70. Baukal, C. (2008), Web-based supplemental training in continuing engineering education courses, Paper presented at the World Conference on Continuing Engineering Education, May 20–23, 2008, Atlanta, GA.
71. Hong, J., Baukal, C., Schwartz, R., and Fleifil, M. (2006), Industrial-scale flare testing, *Chem. Eng. Prog.* 102(5), 35–39.
72. Jian, C. Q., Lorra, M. A., McCorkle, D. and Bryden, K. M. (2006), Applications of virtual engineering in combustion equipment development and engineering, Paper presented at the 2006 ASME International Mechanical Engineering Congress and Exposition. Paper No. IMECE2006-14362, November 5–10, 2006, Chicago, IL.
73. Jones, M. (2010), 7.2.6 Continuing engineering education and professional development. In UNESCO, *Engineering: Issues, Challenges and Opportunities for Development*, United Nations Educational, Scientific and Cultural Organization Paris, France (<http://unesdoc.unesco.org/images/0018/001897/189753e.pdf>), 329–332.
74. DAETE (2011), Development of accreditation in engineering training and education, <http://daete.up.pt/>, accessed 30 July 2012.
75. International Association for Continuing Education and Training (2010), <http://www.iacet.org/>
76. American Petroleum Institute (2010b), API Training Provider Certification Program, <http://www.api.org/Certification-Programs/Training-Provider-TPCP.aspx>, accessed 30 July 2012.
77. ANSI/IACET 1-2007 (2007), *Standards for Continuing Education and Training*, American National Standards Institute, Washington, DC.
78. Dutta, D. (2010), *Lifelong Learning Imperative in Engineering: Summary of a Workshop*, The National Academies Press, Washington, DC, <http://www.nap.edu/catalog/12866.html>
79. Salopek, J. J. (1998), Outsourcing, insourcing, and in-between sourcing, *Training and Development* 52(7), 51–56.
80. Beder, H. (1987), Collaboration as a competitive strategy. In Baden, C. (ed.), *Competitive Strategies for Continuing Education*, Jossey-Bass, San Francisco, CA, pp. 85–95.
81. Kost, R. J. (1980), Competition and innovation in continuing education. In H. J. Alford (ed.), *Power and Conflict in Continuing Education: Survival and Prosperity for All?* Wadsworth, Belmont, CA, pp. 38–51.
82. Hohmann, L. (1980), Professional continuing education. In Alford H. J. (ed.), *Power and Conflict in Continuing Education: Survival and Prosperity for All?* Wadsworth, Belmont, CA, pp. 83–94.
83. Boyd, D. J. (1994), Enhancing continuing education through partnerships: The importance of cooperation and collaboration. *Proceedings of the Annual Meeting of the Association for Continuing Higher Education*, Toronto, Ontario, Canada, October 22–24, 1994. [www.eric.ed.gov/PDFS/ED381644.pdf](http://www.eric.ed.gov/PDFS/ED381644.pdf)
84. Shershneva, M. B., Mullikin, E. A., Loose, A-S, and Olson, C. A. (2008), Learning to collaborate: A case study of performance improvement CME, *J. Cont. Educ. Health Prof.* 28(3), 140–147.
85. EuroPACE (2010), <http://www.europace.org/>, accessed 30 July 2012.
86. Fink, F. K., Tongeren, S. V., Simak, B., Nemeth, B., Nemeth, G., Mazet, L., and Ramos, F. (1999), Continuing professional development programs in university-industry co-operations, *Paper presented at the 29th ASEE/IEEE Frontiers in Education Conference*, Vol. 1, pp. 117b-15–117b-20, November 10–13, 1999, San Juan, Puerto Rico.
87. John Zink Institute (2012), *Process Technology Training Guide, 2011–2012*. [www.johnzink.com/training-classes/](http://www.johnzink.com/training-classes/), accessed 30 July 2012.
88. American Society for Training and Development, [www.astd.org](http://www.astd.org), accessed September 14, 2012.
89. North American Process Technology Alliance, [www.naptaonline.org](http://www.naptaonline.org), accessed September 14, 2012.
90. Alvin Community College Process Technology: An Education that Pays (video) [www.alvincollege.edu/process-technology/default.htm](http://www.alvincollege.edu/process-technology/default.htm), accessed 30 July 2012.
91. Pike, Robert W. (1989, 1994, 2003), CSP/CPAE-speakers hall of fame, *Creative Training Techniques Handbook, Third Edition Tips, Tactics, and How-To's for Delivering Effective Training*, HRD Press, Inc, Amherst, MA.
92. David Wallechinsky, Irving Wallace and Amy Wallace, *The Book of Lists*, Cassell, London, 1977.
93. Joyful Public Speaking (from fear to joy) [www.joyful-publicspeaking.blogspot.com/2009](http://www.joyful-publicspeaking.blogspot.com/2009).
94. Paula Thomas, Premier Presentations Services, <http://www.premier-presentation.co.uk/TIPS.htm>, accessed 30 July 2012.
95. Datta Groover, founder of Higher Speech would like to add another important skill; LISTENING.



96. Elaine Biech (2005), *Training for Dummies*, Wiley Publishing, Inc., Hoboken, NJ.
97. Robert, W. Pike, (2003), *Creative Training Techniques Handbook*, 3rd edn., HRD Press, Amherst, MA, pp. 88–89.
98. *Approved Trainer of Registered Technician— Tips for Trainers Michigan State University*
99. Langevin Learning Services, <http://www.langevin.com>, accessed 30 July 2012.
100. Private communication with Patricia Fripp, CSP, CPA, 2012.
101. Darren Lacroix, Speech at ASTD retreat, *The Humor Institute, Inc.*, 2007 [www.DarrenLacroix.com](http://www.DarrenLacroix.com), accessed 30 July 2012.
102. Rich Meiss & Doug McCallum, *S.C.O.R.E Super Closers Openers Review Energizers for Enhanced Training Results*, The Bob Pike Group, 2007.
103. U.S. Dept. of Education, Accreditation in the United States, [http://www2.ed.gov/admins/finaid/accred/accreditation\\_pg6.html](http://www2.ed.gov/admins/finaid/accred/accreditation_pg6.html) (accessed on January 24, 2012).
104. Hill, D. (2005), Operator training practices revealed, *Hydrocarbon Process*. 84(6), 17.
105. Wilkins, M. (2006), Benchmarking consortium includes operator training, *Hydrocarbon Process*. 85(11), 15–16, 2006.
106. Pankoff, J. A. (2005), Improve and sustain process plant operator performance, *Hydrocarbon Process*. 84(7), 97–99.
107. Smith, K. (2002), Refine your approach to process troubleshooting and optimization, *Hydrocarbon Process*. 81(6), 63–66.
108. Baukal, C. (ed.) (2001), *The John Zink Combustion Handbook*, CRC Press, Boca Raton, FL.
109. Gilder, T., Campbell, D., Robertson, T., and Baukal, C. (2010), Customize operator training for your thermal oxidizers, *Hydrocarbon Process*. 89(11), 55–59.
110. Schnelle, K. B. and Brown, C. A. (2002), Thermal oxidation for VOC control, Chapter 13. In *Air Pollution and Control Technology Handbook*, CRC Press, Boca Raton, FL.
111. Moretti, E. C. (2002), Reduce VOC and HAP emissions, *Chem. Eng. Prog.* 98(6), 30–40.
112. Derosé, G. J. (1999), *Outsourcing Training and Education*, American Society for Training & Development, Alexandria, VA.
113. Malloch, M., Cairns, L., Evans, K., and O'Connor, B. N. (eds.) (2011), *The Sage Handbook of Workplace Learning*, Sage, London, U.K.

## Appendix A: Units and Conversions

TABLE A.1

### Prefixes

Multiplier	Prefix	Symbol
$10^{18}$	Exa	E
$10^{15}$	Peta	P
$10^{12}$	Tera	T
$10^9$	Giga	G
$10^6$	Mega	M
$10^3$	Kilo	k
$10^2$	Hecto	h
10	Deca	da
$10^{-1}$	Deci	d
$10^{-2}$	Centi	c
$10^{-3}$	Milli	m
$10^{-6}$	Micro	$\mu$
$10^{-9}$	Nano	n
$10^{-12}$	Pico	p
$10^{-15}$	Femto	f
$10^{-18}$	Atto	a

Source: Annamalai, K. and Puri, I.K.,  
Combustion Science and Engineering,  
Table A.1A, CRC Press, Boca Raton,  
FL, p. 981, 2007.

TABLE A.2

### Basic Units, Conversions, and Molecular Properties

#### Area

1 acre = 4046.9 m<sup>2</sup>  
 $1 \text{ m}^2 = 10^{-6} \text{ km}^2 = 10^4 \text{ cm}^2 = 10^6 \text{ mm}^2$   
 $1 \text{ m}^2 = 10.764 \text{ ft}^2 = 1550 \text{ in.}^2$   
 $1 \text{ ft}^2 = 144 \text{ in.}^2 = 0.0929 \text{ m}^2$   
 1 hectare = 10,000 m<sup>2</sup> = 2.5 acres = 108,000 ft<sup>2</sup>

#### Density

$1 \text{ g/cm}^3 = 1 \text{ kg/L} = 1000 \text{ kg/m}^3 = 62.43 \text{ lb}_m/\text{ft}^3 = 0.03613 \text{ lb}_m/\text{in.}^3$   
 $1 \text{ kg/m}^3 = 0.06243 \text{ lb}_m/\text{ft}^3$ ,  $1 \text{ lb}_m/\text{ft}^3 = 16.018 \text{ kg/m}^3$   
 Specific gravity = density/reference density  
 For liquids, reference density of water at 15.74°C (60°F) = 999 kg/m<sup>3</sup>,  
 62.4 lb/ft<sup>3</sup>  
 For gases, reference density of air at 15.74°C (60°F) = 1.206 kg/m<sup>3</sup>

#### Energy

1 eV  $\approx 1.602 \times 10^{-19}$  J.  
 1 mBtu = 1 kBtu = 1000 Btu, 1 mmBtu = 1000 kBtu =  $10^6$  Btu  
 1 TBtu =  $10^9$  Btu or 1 GBtu  
 1 quad =  $10^{15}$  Btu or  $1.05 \times 10^{15}$  kJ or  $2.93 \times 10^{11}$  kWh = 172.4 million  
 barrels of crude oil  
 $1 \text{ kWh} = 0.0036 \text{ GJ} = 3.6 \text{ MJ} = 3412 \text{ Btu}$ , 1 hp h = 0.00268 GJ =  
 2.68 MJ = Btu  
 $1 \text{ Btu} = 778.14 \text{ ft lb}_f = 1.0551 \text{ kJ}$ ,  $1 \text{ kJ} = 0.94782 \text{ Btu} = 25,037 \text{ lb}_m \text{ ft/s}^2$   
 1 cal = 4.1868 J, 1 (food) cal = 1000 cal or 1 kcal

TABLE A.2 (continued)

### Basic Units, Conversions, and Molecular Properties

$1 \text{ kJ/kg} = 0.43 \text{ Btu/lb}$ ,  $1 \text{ Btu/lb} = 2.326 \text{ kJ/kg}$ ,  $1 \text{ kg/GJ} = 1 \text{ g/MJ} =$   
 $2.326 \text{ lb}_m/\text{mmBtu}$   
 $1 \text{ Btu/SCF} = 37 \text{ kJ/m}^3$ ,  $1 \text{ m}^3/\text{GJ} = 37.3 \text{ ft}^3/\text{mmBtu}$ ,  $1 \text{ lb}_m/\text{mmBtu} =$   
 $0.430 \text{ kg/GJ} = 0.430 \text{ g/MJ}$   
 1 Therm =  $10^5 \text{ Btu} = 1.055 \times 10^5 \text{ kJ}$   
 $1 \text{ hp} = 0.7064 \text{ Btu/s} = 0.7457 \text{ kW} = 745.7 \text{ W} = 550 \text{ lb}_f \text{ ft/s} =$   
 $42.41 \text{ Btu/min}$   
 1 boiler HP = 33,475 Btu/h,  $1 \text{ Btu/h} = 1.0551 \text{ kJ/h}$   
 1 barrel (42 gallons) of crude oil = 5,800,000 Btu = 6120 MJ  
 1 gallon of gasoline = 124,000 Btu = 131 MJ  
 1 gallon of heating oil = 139,000 Btu = 146.7 MJ  
 1 gallon of diesel fuel = 139,000 Btu = 146.7 MJ  
 1 barrel of residual fuel oil = 6,287,000 Btu = 6633 MJ  
 1 cubic foot of natural gas = 1,026 Btu = 1.082 MJ  
 1 gallon of propane = 91,000 Btu = 96 MJ  
 1 short ton of coal = 20,681,000 Btu = 21,821 MJ

#### Force

$1 \text{ lb}_f = 4.4482 \text{ N} = 32.174 \text{ lb}_m \cdot \text{ft/s}^2$  or  $g_c = 32.174 \text{ lb}_m \text{ ft/s}^2 \text{ lb}_f$

#### Ideal Gas Law

$PV = RT$ ;  $PV = mRT$ ;  $PV = n\bar{R}T$ ,  $P\bar{v} = \bar{R}T$ ,  
 $\bar{R} = 8.314 \text{ kPa m}^3/\text{kmol K} = 0.08314 \text{ bar m}^3/\text{kmol K}$   
 $= 1.986 \text{ Btu/lb mol } ^\circ\text{R} = 1545 \text{ ft lb}_f/\text{lb mol } ^\circ\text{R}$   
 $= 0.7299 \text{ atm ft}^3/\text{lb mol } ^\circ\text{R}$

#### Length/Velocity

1 in. = 0.0254 m  
 1 ft = 12 in. = 0.3048 m  
 1 mile = 5280 ft = 1609.3 m  
 1 statute mile = 0.87 nmi = 1.609 km  
 1 nautical mile = 1.15 smi = 1.85 km  
 $1 \text{ mi/h} = 1.46667 \text{ ft/s} = 0.447 \text{ m/s} = 1.609 \text{ km/h}$   
 $1 \text{ m/s} = 3.2808 \text{ ft/s} = 2.237 \text{ mi/h} = 1.96 \text{ kt} = 1.15 \text{ smi/h} = 3.63 \text{ km/h}$   
 Speed of light in vacuum,  $c = 2.998 \times 10^8 \text{ m/s}$   
 Sound speed =  $\sqrt{\gamma RT}$

#### Mass

1 teragram (Tg) = 1 million metric tonnes  
 Mass of an electron = 0.5 MeV (1 MeV =  $10^6$  eV; for mass,  
 use  $E = mc^2$ ) =  $9.109 \times 10^{-31} \text{ kg}$   
 Mass of proton = 940 MeV =  $1.67 \times 10^{-27} \text{ kg}$ , Mass of neutron =  
 $1.675 \times 10^{-27} \text{ kg}$   
 $1 \text{ lb}_m = 0.45359 \text{ kg} = 7000 \text{ grains}$   
 1 short ton = 2000 lb = 907.2 kg  
 1 long ton = 2240 lb or 1016.1 kg  
 1 metric ton = 1000 kg  
 1 ounce = 28.3495 g  
 $1 \text{ kg} = 2.2046 \text{ lb}$

(continued)

TABLE A.2 (continued)

## Basic Units, Conversions, and Molecular Properties

**Molecular Properties**1 Angstrom =  $1.0 \times 10^{-10}$  m $N_{\text{Avog}} = 6.023 \times 10^{26}$  molecules/kmol for a molecular substance

(e.g., oxygen)

 $= 6.023 \times 10^{26}$  atoms/atom mole for an atomic substance (e.g., He)Boltzmann constant,  $k_B = 1.38 \times 10^{-26}$  kJ/molecule KPlanck's constant,  $h_P = 6.626 \times 10^{-37}$  kJ s/moleculeStefan-Boltzmann constant,  $\sigma = 5.66961 \times 10^{-11}$  kW/m<sup>2</sup>K<sup>4</sup>Charge of an electron =  $1.602 \times 10^{-19}$  coulombs, orbit radius (nm) =  $0.0529n^2$ ,  $n$ : orbit numberEnergy level of an orbit (eV) =  $13.56/n^2$ **Numbers** $\ln x = 2.303 \log_{10} x$  $\log_{10} x = 0.4343 \ln x$  $e = 2.718$  $\pi = 3.142$ 

1 deg = 0.0175 radians

**Pressure**1 bar =  $10^5$  Pa, 1 mm Hg = 133.3 Pa

1 in Hg = 3.387 kPa = 0.491 psi

1 in water (4°C) = 0.03613 psi

1 atm =  $14.696 \text{ lb}_f/\text{in}^2 = 1.0133 \text{ bar} = 10.3323 \text{ mm of H}_2\text{O (4°C)} = 760 \text{ mm of Hg (0°C)}$ 1 psi =  $1 \text{ lb}_f/\text{in}^2 = 144 \text{ lb}_f/\text{ft}^2 = 6.894 \text{ kPa} = 6894 \text{ Pa} = 27.653$ 

in water (4°C)

**Specific Heat**

1 Btu/lb °F = 4.1868 kJ/kg °C

1 kJ/kg °C = 0.23885 Btu/lb °F

**Temperature** $T(^{\circ}\text{C}) = (T(^{\circ}\text{F}) - 32) * (5/9)$  $T(^{\circ}\text{F}) = T(^{\circ}\text{C}) * 1.8 + 32$  $T(\text{K}) = T(^{\circ}\text{C}) + 273.15$  $T(^{\circ}\text{R}) = T(^{\circ}\text{F}) + 459.67$  $1^{\circ}\text{R} = 0.556 \text{ K}$ ,  $1 \text{ K} = 1.8^{\circ}\text{R}$ 

To convert electron volts into the corresponding temperature in Kelvin, multiply by 11,604.

**Volume**1 m<sup>3</sup> = 1000 L1 fluid ounce =  $29.5735 \text{ cm}^3 = 0.0295735 \text{ L}$ 1 m<sup>3</sup>/kg = 1000 L/kg =  $16.02 \text{ ft}^3/\text{lb}$ , 1 m<sup>3</sup>/GJ =  $37.26 \text{ ft}^3/\text{mmBtu}$ 1 ft<sup>3</sup>/lb<sub>m</sub> =  $0.062428 \text{ m}^3/\text{kg}$ 

1 U.S. gallon = 128 fluid ounce = 3.786 L

1 barrel = 42 U.S. gallons = 35 imperial gallons =  $158.98 \text{ L} = 5.615 \text{ ft}^3 = 231 \text{ in}^3 = 0.1337 \text{ ft}^3$ 

TABLE A.2 (continued)

## Basic Units, Conversions, and Molecular Properties

Volume of 1 kmol (SI) and 1 lb mol (English) of an ideal gas at STP conditions as defined below:

Scientific or SATP	U.S. Standard (1976) or ISA	Chemists' Standard or CSA	NTP (Gas Industry)
25°C (77°F), 101.3 kPa (14.7 psi, 29.92 in. of Hg)	15°C (60°F), 101.33 kPa (1 atm, 14.696 psi, 29.92 in. of Hg)	0°C (32°F), 101.33 kPa (1 atm, 14.7 psi, 29.92 in. of Hg)	20°C (65°F), 101.33 kPa (1 atm)
24.5 m <sup>3</sup> /kmol (392 ft <sup>3</sup> /lb mol)	23.7 m <sup>3</sup> /kmol (375.6 ft <sup>3</sup> /lb mol)	22.4 m <sup>3</sup> /kmol (359.2 ft <sup>3</sup> /lb mol)	23.89 m <sup>3</sup> /kmol (382.7 ft <sup>3</sup> /lb mol)

SATP, standard ambient temperature and pressure; ISA, International Standard Atmosphere; NTP, normal temperature and pressure.

## Air Composition

Species	Mole %	Mass %	Molecular Weight
Ar	0.934	1.288287	39.948
CO <sub>2</sub>	0.0314	0.047715	44.01
N <sub>2</sub>	78.084	75.51721	28.01
O <sub>2</sub>	20.9476	23.14489	32
Ne	0.001818	0.001267	20.18
He	0.000524	7.24E-05	4.0026
Krypton	0.000114	0.00033	83.8
Xe	8.70E-06	3.94E-05	131.3
H <sub>2</sub>	0.00005	3.48E-06	2.016
CH <sub>4</sub>	0.0002	0.000111	16.043
N <sub>2</sub> O	0.00005	7.6E-05	44.013
SO <sub>2</sub> , NO <sub>2</sub> , CO, I <sub>2</sub>	0.000235	—	—

Source: Annamalai, K. and Puri, I.K., *Combustion Science and Engineering*, Table A.1A, CRC Press, Boca Raton, FL, p. 981, 2007.

Note: Molecular weight (mass) of air = 28.96 kg/kmol.



TABLE A.3

Atomic Weights for Common Elements

Name	Symbol	Atomic Number	Atomic Weight
Aluminum	Al	13	26.98
Antimony	Sb	51	121.76
Argon	Ar	18	39.95
Arsenic	As	33	74.92
Barium	Ba	56	137.32
Beryllium	Be	4	9.01
Bismuth	Bi	83	208.98
Boron	B	5	10.811
Bromine	Br	35	79.90
Cadmium	Cd	48	112.41
Calcium	Ca	20	40.08
Carbon	C	6	12.01
Cesium	Cs	55	132.91
Chlorine	Cl	17	35.45
Chromium	Cr	24	52.00
Cobalt	Co	27	58.93
Copper	Cu	29	63.55
Fluorine	F	9	19.00
Germanium	Ge	32	72.61
Gold	Au	79	196.97
Helium	He	2	4.00
Hydrogen	H	1	1.01
Indium	In	49	114.82
Iodine	I	53	126.90
Iridium	Ir	77	192.22
Iron	Fe	26	55.85
Krypton	Kr	36	83.80
Lead	Pb	82	207.20
Lithium	Li	3	6.94
Magnesium	Mg	12	24.31
Manganese	Mn	25	54.94
Mercury	Hg	80	200.59
Molybdenum	Mo	42	95.94
Neon	Ne	10	20.18
Nickel	Ni	28	58.69
Nitrogen	N	7	14.01
Oxygen	O	8	16.00
Palladium	Pd	46	106.42
Phosphorus	P	15	30.97
Platinum	Pt	78	195.08
Plutonium	Pu	94	244.00
Potassium	K	19	39.10
Radium	Ra	88	226.00
Radon	Rn	86	222.00
Rhodium	Rh	45	102.91
Selenium	Se	34	78.96
Silicon	Si	14	28.09

TABLE A.3 (continued)

Atomic Weights for Common Elements

Name	Symbol	Atomic Number	Atomic Weight
Silver	Ag	47	107.87
Sodium	Na	11	22.99
Strontium	Sr	38	87.62
Sulfur	S	16	32.07
Tantalum	Ta	73	180.95
Thallium	Tl	81	204.38
Tin	Sn	50	118.71
Titanium	Ti	22	47.87
Tungsten	W	74	183.84
Uranium	U	92	238.03
Vanadium	V	23	50.94
Xenon	Xe	54	131.29
Zinc	Zn	30	65.39
Zirconium	Zr	40	92.22

Source: Annamalai, K. and Puri, I.K., *Combustion Science and Engineering*, Table A.1B, CRC Press, Boca Raton, FL, p. 985, 2007.

This page intentionally left blank

## Appendix B: Physical Properties of Materials

TABLE B.1

Physical Properties of Pipe

Nominal Pipe Size, OD (in.)	Schedule Number			Wall Thickness (in.)	ID (in.)	Inside Area (in. <sup>2</sup> )	Metal Area (in. <sup>2</sup> )	Sq. Ft. Outside Surface (per ft)	Sq. Ft. Inside Surface (per ft)	Weight per ft (lb)	Weight of Water per ft (lb)	Moment of Inertia (in. <sup>4</sup> )	Section Modulus (in. <sup>3</sup> )	Radius Gyration (in.)
	a	b	c											
1/8 0.405	—	—	10S	0.049	0.307	0.0740	0.0548	0.106	0.0804	0.186	0.0321	0.00088	0.00437	0.1271
	40	Std	40S	0.068	0.269	0.0568	0.0720	0.106	0.0705	0.245	0.0246	0.00106	0.00525	0.1215
	80	XS	80S	0.095	0.215	0.0364	0.0925	0.106	0.0563	0.315	0.0157	0.00122	0.00600	0.1146
1/4 0.540	—	—	10S	0.065	0.410	0.1320	0.0970	0.141	0.1073	0.330	0.0572	0.00279	0.01032	0.1694
	40	Std	40S	0.088	0.364	0.1041	0.1250	0.141	0.0955	0.425	0.0451	0.00331	0.01230	0.1628
	80	XS	80S	0.119	0.302	0.0716	0.1574	0.141	0.0794	0.535	0.0310	0.00378	0.01395	0.1547
3/8 0.675	—	—	10S	0.065	0.545	0.2333	0.1246	0.177	0.1427	0.423	0.1011	0.00586	0.01737	0.2169
	40	Std	40S	0.091	0.493	0.1910	0.1670	0.177	0.1295	0.568	0.0827	0.00730	0.02160	0.2090
	80	XS	80S	0.126	0.423	0.1405	0.2173	0.177	0.1106	0.739	0.0609	0.00862	0.02554	0.1991
1/2 0.840	—	—	10S	0.083	0.674	0.3570	0.1974	0.220	0.1765	0.671	0.1547	0.01431	0.0341	0.2692
	40	Std	40S	0.109	0.622	0.3040	0.2503	0.220	0.1628	0.851	0.1316	0.01710	0.0407	0.2613
	80	XS	80S	0.147	0.546	0.2340	0.3200	0.220	0.1433	1.088	0.1013	0.02010	0.0478	0.2505
3/4 1.050	160	—	—	0.187	0.466	0.1706	0.3830	0.220	0.1220	1.304	0.0740	0.02213	0.0527	0.2402
	—	XXS	—	0.294	0.252	0.0499	0.5040	0.220	0.0660	1.714	0.0216	0.02425	0.0577	0.2192
	—	—	5S	0.065	0.920	0.6650	0.2011	0.275	0.2409	0.684	0.2882	0.02451	0.0467	0.349
1 1.315	—	—	10S	0.083	0.884	0.6140	0.2521	0.275	0.2314	0.857	0.2661	0.02970	0.0566	0.343
	40	Std	40S	0.113	0.824	0.5330	0.3330	0.275	0.2157	1.131	0.2301	0.0370	0.0706	0.334
	80	XS	80S	0.154	0.742	0.4320	0.4350	0.275	0.1943	1.474	0.1875	0.0448	0.0853	0.321
1 1/4 1.660	160	—	—	0.218	0.614	0.2961	0.5700	0.275	0.1607	1.937	0.1284	0.0527	0.1004	0.304
	—	XXS	—	0.308	0.434	0.1479	0.7180	0.275	0.1137	2.441	0.0641	0.0579	0.1104	0.284
	—	—	5S	0.065	1.185	1.1030	0.2553	0.344	0.3100	0.868	0.478	0.0500	0.0760	0.443
1 1/2 1.900	—	—	10S	0.109	1.097	0.9450	0.4130	0.344	0.2872	1.404	0.409	0.0757	0.1151	0.428
	40	Std	40S	0.133	1.049	0.8640	0.4940	0.344	0.2746	1.679	0.374	0.0874	0.1329	0.421
	80	XS	80S	0.179	0.957	0.7190	0.6390	0.344	0.2520	2.172	0.311	0.1056	0.1606	0.407
2 2.375	160	—	—	0.250	0.815	0.5220	0.8360	0.344	0.2134	2.844	0.2261	0.1252	0.1903	0.387
	—	XXS	—	0.358	0.599	0.2818	1.0760	0.344	0.1570	3.659	0.1221	0.1405	0.2137	0.361
	—	—	5S	0.065	1.530	1.839	0.326	0.434	0.401	1.107	0.797	0.1038	0.1250	0.564
2 1/2 2.875	—	—	10S	0.109	1.442	1.633	0.531	0.434	0.378	1.805	0.707	0.1605	0.1934	0.550
	40	Std	40S	0.140	1.380	1.496	0.669	0.434	0.361	2.273	0.648	0.1948	0.2346	0.540
	80	XS	80S	0.191	1.278	1.283	0.881	0.434	0.335	2.997	0.555	0.2418	0.2913	0.524
3 3.500	160	—	—	0.250	1.160	1.057	1.107	0.434	0.304	3.765	0.458	0.2839	0.342	0.506
	—	XXS	—	0.382	0.896	0.631	1.534	0.434	0.2346	5.214	0.2732	0.341	0.411	0.472
	—	—	5S	0.065	1.770	2.461	0.375	0.497	0.463	1.274	1.067	0.1580	0.1663	0.649
3 1/2 4.000	—	—	10S	0.109	1.682	2.222	0.613	0.497	0.440	2.085	0.962	0.2469	0.2599	0.634
	40	Std	40S	0.145	1.610	2.036	0.799	0.497	0.421	2.718	0.882	0.310	0.326	0.623
	80	XS	80S	0.200	1.500	1.767	1.068	0.497	0.393	3.631	0.765	0.391	0.412	0.605
4 4.500	160	—	—	0.281	1.338	1.406	1.429	0.497	0.350	4.859	0.608	0.483	0.508	0.581
	—	XXS	—	0.400	1.100	0.950	1.885	0.497	0.288	6.408	0.412	0.568	0.598	0.549
	—	—	5S	0.065	2.245	3.960	0.472	0.622	0.588	1.604	1.716	0.315	0.2652	0.817
4 1/2 5.000	—	—	10S	0.109	2.157	3.650	0.776	0.622	0.565	2.638	1.582	0.499	0.420	0.802
	40	Std	40S	0.154	2.067	3.360	1.075	0.622	0.541	3.653	1.455	0.666	0.561	0.787
	80	XS	80S	0.218	1.939	2.953	1.477	0.622	0.508	5.022	1.280	0.868	0.731	0.766
5 5.563	160	—	—	0.343	1.689	2.240	2.190	0.622	0.442	7.444	0.971	1.163	0.979	0.729
	—	XXS	—	0.436	1.503	1.774	2.656	0.622	0.393	9.029	0.769	1.312	1.104	0.703
	—	—	5S	0.083	2.709	5.76	0.728	0.753	0.709	2.475	2.499	0.710	0.494	0.988
	—	—	10S	0.120	2.635	5.45	1.039	0.753	0.690	3.531	2.361	0.988	0.687	0.975

(continued)



TABLE B.1 (continued)

## Physical Properties of Pipe

Nominal Pipe Size, OD (in.)	Schedule Number			Wall Thickness (in.)	ID (in.)	Inside Area (in. <sup>2</sup> )	Metal Area (in. <sup>2</sup> )	Sq. Ft. Outside Surface (per ft)	Sq. Ft. Inside Surface (per ft)	Weight per ft (lb)	Weight of Water per ft (lb)	Moment of Inertia (in. <sup>4</sup> )	Section Modulus (in. <sup>3</sup> )	Radius Gyration (in.)
	a	b	c											
2 1/2	40	Std	40S	0.203	2.469	4.79	1.704	0.753	0.646	5.793	2.076	1.530	1.064	0.947
2.875	80	XS	80S	0.276	2.323	4.24	2.254	0.753	0.608	7.661	1.837	0.193	1.339	0.924
	160	—	—	0.375	2.125	3.55	2.945	0.753	0.556	10.01	1.535	2.353	1.637	0.894
	—	XXS	—	0.552	1.771	2.46	4.030	0.753	0.464	13.70	1.067	2.872	1.998	0.844
	—	—	5S	0.083	3.334	8.73	0.891	0.916	0.873	3.03	3.78	1.301	0.744	1.208
	—	—	10S	0.120	3.260	8.35	1.274	0.916	0.853	4.33	3.61	1.822	1.041	1.196
3	40	Std	40S	0.216	3.068	7.39	2.228	0.916	0.803	7.58	3.20	3.02	1.724	1.164
3.500	80	XS	80S	0.300	2.900	6.61	3.020	0.916	0.759	10.25	2.864	3.90	2.226	1.136
	160	—	—	0.437	2.626	5.42	4.210	0.916	0.687	14.32	2.348	5.03	2.876	1.094
	—	XXS	—	0.600	2.300	4.15	5.470	0.916	0.602	18.58	1.801	5.99	3.43	1.047
	—	—	5S	0.083	3.834	11.55	1.021	1.047	1.004	3.47	5.01	1.960	0.980	1.385
	—	—	10S	0.120	3.760	11.10	1.463	1.047	0.984	4.97	4.81	2.756	1.378	1.372
3 1/2	40	Std	40S	0.226	3.548	9.89	2.68	1.047	0.929	9.11	4.28	4.79	2.394	1.337
4.000	80	XS	80S	0.318	3.364	8.89	3.68	1.047	0.881	12.51	3.85	6.28	3.14	1.307
	—	—	5S	0.083	4.334	14.75	1.152	1.178	1.135	3.92	6.40	2.811	1.249	1.562
	—	—	10S	0.120	4.260	14.25	1.651	1.178	1.115	5.61	6.17	3.96	1.762	1.549
	40	Std	40S	0.237	4.026	12.73	3.17	1.178	1.054	10.79	5.51	7.23	3.21	1.510
	80	XS	80S	0.337	3.826	11.50	4.41	1.178	1.002	14.98	4.98	9.61	4.27	1.477
4.500	120	—	—	0.437	3.626	10.33	5.58	1.178	0.949	18.96	4.48	11.65	5.18	1.445
	160	—	—	0.531	3.438	9.28	6.62	1.178	0.900	22.51	4.02	13.27	5.90	1.416
	—	XXS	—	0.674	3.152	7.80	8.10	1.178	0.825	27.54	3.38	15.29	6.79	1.374
	—	—	5S	0.109	5.345	22.44	1.868	1.456	1.399	6.35	9.73	6.95	2.498	1.929
	—	—	10S	0.134	5.295	22.02	2.285	1.456	1.386	7.77	9.53	8.43	3.03	1.920
5	40	Std	40S	0.258	5.047	20.01	4.30	1.456	1.321	14.62	8.66	15.17	5.45	1.878
5.563	80	XS	80S	0.375	4.813	18.19	6.11	1.456	1.260	20.78	7.89	20.68	7.43	1.839
	120	—	—	0.500	4.563	16.35	7.95	1.456	1.195	27.04	7.09	25.74	9.25	1.799
	160	—	—	0.625	4.313	14.61	9.70	1.456	1.129	32.96	6.33	30	10.8	1.760
	—	XXS	—	0.750	4.063	12.97	11.34	1.456	1.064	38.55	5.62	33.6	12.1	1.722
	—	—	5S	0.109	6.407	32.20	2.231	1.734	1.677	5.37	13.98	11.85	3.58	2.304
6	—	—	10S	0.134	6.357	31.70	2.733	1.734	1.664	9.29	13.74	14.4	4.35	2.295
	40	Std	40S	0.280	6.065	28.89	5.58	1.734	1.588	18.97	12.51	28.14	8.5	2.245
	80	XS	80S	0.432	5.761	26.07	8.40	1.734	1.508	28.57	11.29	40.5	12.23	2.195
	120	—	—	0.562	5.501	23.77	10.70	1.734	1.440	36.39	10.30	49.6	14.98	2.153
	160	—	—	0.718	5.189	21.15	13.33	1.734	1.358	45.30	9.16	59	17.81	2.104
6.625	—	XXS	—	0.864	4.897	18.83	15.64	1.734	1.282	53.16	8.17	66.3	20.03	2.060
	—	—	5S	0.109	8.407	55.5	2.916	2.258	2.201	9.91	24.07	26.45	6.13	3.01
	—	—	10S	0.148	8.329	54.5	3.94	2.258	2.180	13.40	23.59	35.4	8.21	3.00
	20	—	—	0.250	8.125	51.8	6.58	2.258	2.127	22.36	22.48	57.7	13.39	2.962
	30	—	—	0.277	8.071	51.2	7.26	2.258	2.113	24.70	22.18	63.4	14.69	2.953
8	40	Std	40S	0.322	7.981	50.0	8.40	2.258	2.089	28.55	21.69	72.5	16.81	2.938
	60	—	—	0.406	7.813	47.9	10.48	2.258	2.045	35.64	20.79	88.8	20.58	2.909
	80	XS	80S	0.500	7.625	45.7	12.76	2.258	1.996	43.39	19.80	105.7	24.52	2.878
	100	—	—	0.593	7.439	43.5	14.96	2.258	1.948	50.87	18.84	121.4	28.14	2.847
	120	—	—	0.718	7.189	40.6	17.84	2.258	1.882	60.63	17.60	140.6	32.6	2.807
8.625	140	—	—	0.812	7.001	38.5	19.93	2.258	1.833	67.76	16.69	153.8	35.7	2.777
	—	XXS	—	0.875	6.875	37.1	21.30	2.258	1.800	72.42	16.09	162	37.6	2.757
	160	—	—	0.906	6.813	36.5	21.97	2.258	1.784	74.69	15.80	165.9	38.5	2.748
	—	—	5S	0.134	10.482	86.3	4.52	2.815	2.744	15.15	37.4	63.7	11.85	3.75
	—	—	10S	0.165	10.420	85.3	5.49	2.815	2.728	18.70	36.9	76.9	14.3	3.74
	20	—	—	0.250	10.250	82.5	8.26	2.815	2.683	28.04	35.8	113.7	21.16	3.71
	—	—	—	0.279	10.192	81.6	9.18	2.815	2.668	31.20	35.3	125.9	23.42	3.70
	30	—	—	0.307	10.136	80.7	10.07	2.815	2.654	34.24	35.0	137.5	25.57	3.69

TABLE B.1 (continued)

## Physical Properties of Pipe

Nominal Pipe Size, OD (in.)	Schedule Number			Wall Thickness (in.)	ID (in.)	Inside Area (in. <sup>2</sup> )	Metal Area (in. <sup>2</sup> )	Sq. Ft. Outside Surface (per ft)	Sq. Ft. Inside Surface (per ft)	Weight per ft (lb)	Weight of Water per ft (lb)	Moment of Inertia (in. <sup>4</sup> )	Section Modulus (in. <sup>3</sup> )	Radius Gyration (in.)
	a	b	c											
10 10.750	40	Std	40S	0.365	10.020	78.9	11.91	2.815	2.623	40.48	34.1	160.8	29.9	3.67
	60	XS	80S	0.500	9.750	74.7	16.10	2.815	2.553	54.74	32.3	212	39.4	3.63
	80	—	—	0.593	9.564	71.8	18.92	2.815	2.504	64.33	31.1	244.9	45.6	3.60
	100	—	—	0.718	9.314	68.1	22.63	2.815	2.438	76.93	29.5	286.2	53.2	3.56
	120	—	—	0.843	9.064	64.5	26.24	2.815	2.373	89.20	28.0	324	60.3	3.52
	140	—	—	1.000	8.750	60.1	30.6	2.815	2.291	104.13	26.1	368	68.4	3.47
	160	—	—	1.125	8.500	56.7	34.0	2.815	2.225	115.65	24.6	399	74.3	3.43
	—	—	5S	0.165	12.420	121.2	6.52	3.34	3.25	19.56	52.5	129.2	20.27	4.45
	—	—	10S	0.180	12.390	120.6	7.11	3.34	3.24	24.20	52.2	140.5	22.03	4.44
	20	—	—	0.250	12.250	117.9	9.84	3.34	3.21	33.38	51.1	191.9	30.1	4.42
12 12.750	30	—	—	0.330	12.090	114.8	12.88	3.34	3.17	43.77	49.7	248.5	39.0	4.39
	—	Std	40S	0.375	12.000	113.1	14.58	3.34	3.14	49.56	49.0	279.3	43.8	4.38
	40	—	—	0.406	11.938	111.9	15.74	3.34	3.13	53.53	48.5	300	47.1	4.37
	—	XS	80S	0.500	11.750	108.4	19.24	3.34	3.08	65.42	47.0	362	56.7	4.33
	60	—	—	0.562	11.626	106.2	21.52	3.34	3.04	73.16	46.0	401	62.8	4.31
	80	—	—	0.687	11.376	101.6	26.04	3.34	2.978	88.51	44.0	475	74.5	4.27
	100	—	—	0.843	11.064	96.1	31.5	3.34	2.897	107.20	41.6	562	88.1	4.22
	120	—	—	1.000	10.750	90.8	36.9	3.34	2.814	125.49	39.3	642	100.7	4.17
	140	—	—	1.125	10.500	86.6	41.1	3.34	2.749	139.68	37.5	701	109.9	4.13
	160	—	—	1.312	10.126	80.5	47.1	3.34	2.651	160.27	34.9	781	122.6	4.07
14 14.000	10	—	—	0.250	13.500	143.1	10.80	3.67	3.53	36.71	62.1	255.4	36.5	4.86
	20	—	—	0.312	13.376	140.5	13.42	3.67	3.5	45.68	60.9	314	44.9	4.84
	30	Std	—	0.375	13.250	137.9	16.05	3.67	3.47	54.57	59.7	373	53.3	4.82
	40	—	—	0.437	13.126	135.3	18.62	3.67	3.44	63.37	58.7	429	61.2	4.80
	—	XS	—	0.500	13.000	132.7	21.21	3.67	3.4	72.09	57.5	484	69.1	4.78
	—	—	—	0.562	12.876	130.2	23.73	3.67	3.37	80.66	56.5	537	76.7	4.76
	60	—	—	0.593	12.814	129.0	24.98	3.67	3.35	84.91	55.9	562	80.3	4.74
	—	—	—	0.625	12.750	127.7	26.26	3.67	3.34	89.28	55.3	589	84.1	4.73
	—	—	—	0.687	12.626	125.2	28.73	3.67	3.31	97.68	54.3	638	91.2	4.71
	80	—	—	0.750	12.500	122.7	31.2	3.67	3.27	106.13	53.2	687	98.2	4.69
16 16.000	—	—	—	0.875	12.250	117.9	36.1	3.67	3.21	122.66	51.1	781	111.5	4.65
	100	—	—	0.937	12.126	115.5	38.5	3.67	3.17	130.73	50.0	825	117.8	4.63
	120	—	—	1.093	11.814	109.6	44.3	3.67	3.09	150.67	47.5	930	132.8	4.58
	140	—	—	1.250	11.500	103.9	50.1	3.67	3.01	170.22	45.0	1127	146.8	4.53
	160	—	—	1.406	11.188	98.3	55.6	3.67	2.929	189.12	42.6	1017	159.6	4.48
	10	—	—	0.250	15.500	188.7	12.37	4.19	4.06	42.05	81.8	384	48	5.57
	20	—	—	0.312	15.376	185.7	15.38	4.19	4.03	52.36	80.5	473	59.2	5.55
	30	Std	—	0.375	15.250	182.6	18.41	4.19	3.99	62.58	79.1	562	70.3	5.53
	—	—	—	0.437	15.126	179.7	21.37	4.19	3.96	72.64	77.9	648	80.9	5.50
	40	XS	—	0.500	15.000	176.7	24.35	4.19	3.93	82.77	76.5	732	91.5	5.48
16 16.000	—	—	—	0.562	14.876	173.8	27.26	4.19	3.89	92.66	75.4	813	106.6	5.46
	—	—	—	0.625	14.750	170.9	30.2	4.19	3.86	102.63	74.1	894	112.2	5.44
	60	—	—	0.656	14.688	169.4	31.6	4.19	3.85	107.50	73.4	933	116.6	5.43
	—	—	—	0.687	14.626	168.0	33.0	4.19	3.83	112.36	72.7	971	121.4	5.42
	—	—	—	0.750	14.500	165.1	35.9	4.19	3.8	122.15	71.5	1047	130.9	5.40
	80	—	—	0.842	14.314	160.9	40.1	4.19	3.75	136.46	69.7	1157	144.6	5.37
	—	—	—	0.875	14.250	159.5	41.6	4.19	3.73	141.35	69.1	1193	154.1	5.36
	100	—	—	1.031	13.938	152.6	48.5	4.19	3.65	164.83	66.1	1365	170.6	5.30
	120	—	—	1.218	13.564	144.5	56.6	4.19	3.55	192.29	62.6	1556	194.5	5.24
	140	—	—	1.437	13.126	135.3	65.7	4.19	3.44	223.50	58.6	1760	220.0	5.17

(continued)

TABLE B.1 (continued)

## Physical Properties of Pipe

Nominal Pipe Size, OD (in.)	Schedule Number			Wall Thickness (in.)	ID (in.)	Inside Area (in. <sup>2</sup> )	Metal Area (in. <sup>2</sup> )	Sq. Ft. Outside Surface (per ft)	Sq. Ft. Inside Surface (per ft)	Weight per ft (lb)	Weight of Water per ft (lb)	Moment of Inertia (in. <sup>4</sup> )	Section Modulus (in. <sup>3</sup> )	Radius Gyration (in.)
	a	b	c											
18 18.000	160	—	—	1.593	12.814	129.0	72.1	4.19	3.35	245.11	55.9	1894	236.7	5.12
	10	—	—	0.250	17.500	240.5	13.94	4.71	4.58	47.39	104.3	549	61.0	6.28
	20	—	—	0.312	17.376	237.1	17.34	4.71	4.55	59.03	102.8	678	75.5	6.25
	—	Std	—	0.375	17.250	233.7	20.76	4.71	4.52	70.59	101.2	807	89.6	6.23
	30	—	—	0.437	17.126	230.4	24.11	4.71	4.48	82.06	99.9	931	103.4	6.21
	—	XS	—	0.500	17.000	227.0	27.49	4.71	4.45	93.45	98.4	1053	117.0	6.19
	40	—	—	0.562	16.876	223.7	30.8	4.71	4.42	104.75	97.0	1172	130.2	6.17
	—	—	—	0.625	16.750	220.5	34.1	4.71	4.39	115.98	95.5	1289	143.3	6.15
	—	—	—	0.687	16.626	217.1	37.4	4.71	4.35	127.03	94.1	1403	156.3	6.13
	60	—	—	0.750	16.500	213.8	40.6	4.71	4.32	138.17	92.7	1515	168.3	6.10
	—	—	—	0.875	16.250	207.4	47.1	4.71	4.25	160.04	89.9	1731	192.8	6.06
	80	—	—	0.937	16.126	204.2	50.2	4.71	4.22	170.75	88.5	1834	203.8	6.04
	100	—	—	1.156	15.688	193.3	61.2	4.71	4.11	207.96	83.7	2180	242.2	5.97
	120	—	—	1.375	15.250	182.6	71.8	4.71	3.99	244.14	79.2	2499	277.6	5.90
	140	—	—	1.562	14.876	173.8	80.7	4.71	3.89	274.23	75.3	2750	306	5.84
20 20.000	160	—	—	1.781	14.438	163.7	90.7	4.71	3.78	308.51	71.0	3020	336	5.77
	10	—	—	0.250	19.500	298.6	15.51	5.24	5.11	52.73	129.5	757	75.7	6.98
	—	—	—	0.312	19.376	294.9	19.30	5.24	5.07	65.40	128.1	935	93.5	6.96
	20	Std	—	0.375	19.250	291.0	23.12	5.24	5.04	78.60	126.0	1114	111.4	6.94
	—	—	—	0.437	19.126	287.3	26.86	5.24	5.01	91.31	124.6	1286	128.6	6.92
	30	XS	—	0.500	19.000	283.5	30.6	5.24	4.97	104.13	122.8	1457	145.7	6.90
	—	—	—	0.562	18.876	279.8	34.3	5.24	4.94	116.67	121.3	1624	162.4	6.88
	40	—	—	0.593	18.814	278.0	36.2	5.24	4.93	122.91	120.4	1704	170.4	6.86
	—	—	—	0.625	18.750	276.1	38.0	5.24	4.91	129.33	119.7	1787	178.7	6.85
	—	—	—	0.687	18.626	272.5	41.7	5.24	4.88	141.71	118.1	1946	194.6	6.83
	—	—	—	0.750	18.500	268.8	45.4	5.24	4.84	154.20	116.5	2105	210.5	6.81
	60	—	—	0.812	18.376	265.2	48.9	5.24	4.81	166.40	115.0	2257	225.7	6.79
	—	—	—	0.875	18.250	261.6	52.6	5.24	4.78	178.73	113.4	2409	240.9	6.77
	80	—	—	1.031	17.938	252.7	61.4	5.24	4.70	208.87	109.4	2772	277.2	6.72
	100	—	—	1.281	17.438	238.8	75.3	5.24	4.57	256.10	103.4	3320	332	6.63
24 24.000	120	—	—	1.500	17.000	227.0	87.2	5.24	4.45	296.37	98.3	3760	376	6.56
	140	—	—	1.750	16.500	213.8	100.3	5.24	4.32	341.10	92.6	4220	422	6.48
	160	—	—	1.968	16.064	202.7	111.5	5.24	4.21	379.01	87.9	4590	459	6.41
	10	—	—	0.250	23.500	434	18.65	6.28	6.15	63.41	188.0	1316	109.6	8.40
	—	—	—	0.312	23.376	430	23.20	6.28	6.12	78.93	186.1	1629	135.8	8.38
	20	Std	—	0.375	23.250	425	27.83	6.28	6.09	94.62	183.8	1943	161.9	8.35
	—	—	—	0.437	23.126	420	32.4	6.28	6.05	109.97	182.1	2246	187.4	8.33
	—	XS	—	0.500	23.000	415	36.9	6.28	6.02	125.49	180.1	2550	212.5	8.31
	30	—	—	0.562	22.876	411	41.4	6.28	5.99	140.80	178.1	2840	237.0	8.29
	—	—	—	0.625	22.750	406	45.9	6.28	5.96	156.03	176.2	3140	261.4	8.27
	40	—	—	0.687	22.626	402	50.3	6.28	5.92	171.17	174.3	3420	285.2	8.25
	—	—	—	0.750	22.500	398	54.8	6.28	5.89	186.24	172.4	3710	309	8.22
	60	—	—	0.968	22.064	382	70.0	6.28	5.78	238.11	165.8	4650	388	8.15
	80	—	—	1.218	21.564	365	87.2	6.28	5.65	296.36	158.3	5670	473	8.07
	100	—	—	1.531	20.938	344	108.1	6.28	5.48	367.40	149.3	6850	571	7.96
	120	—	—	1.812	20.376	326	126.3	6.28	5.33	429.39	141.4	7830	652	7.87
	140	—	—	2.062	19.876	310	142.1	6.28	5.20	483.13	134.5	8630	719	7.79



TABLE B.1 (continued)

## Physical Properties of Pipe

Nominal Pipe Size, OD (in.)	Schedule Number			Wall Thickness (in.)	ID (in.)	Inside Area (in. <sup>2</sup> )	Metal Area (in. <sup>2</sup> )	Sq. Ft. Outside Surface (per ft)	Sq. Ft. Inside Surface (per ft)	Weight per ft (lb)	Weight of Water per ft (lb)	Moment of Inertia (in. <sup>4</sup> )	Section Modulus (in. <sup>3</sup> )	Radius Gyration (in.)
	a	b	c											
	160	—	—	2.343	19.314	293	159.4	6.28	5.06	541.94	127.0	9460	788	7.70
	10	—	—	0.312	29.376	678	29.1	7.85	7.69	98.93	293.8	3210	214	10.50
30	20	—	—	0.500	29.000	661	46.3	7.85	7.59	157.53	286.3	5040	336	10.43
30.000	30	—	—	0.625	28.750	649	57.6	7.85	7.53	196.08	281.5	6220	415	10.39

Source: Table A.2, *JZ Handbook*, 1st edn., p. 704.

<sup>a</sup> ASA B36.10 Steel-pipe schedule numbers.

<sup>b</sup> ASA B36.10 Steel-pipe nominal wall-thickness designations.

<sup>c</sup> ASA B36.19 Stainless-steel-pipe schedule numbers.

TABLE B.2

Commercial Copper Tubing<sup>a</sup>

Size, OD		Wall Thickness			Flow Area		Surface Area			
in.	mm	in.	mm	gage	in. <sup>2</sup>	mm <sup>2</sup>	Metal Area (in. <sup>2</sup> )	Inside (ft <sup>2</sup> /ft)	Outside (ft <sup>2</sup> /ft)	Weight (lb/ft)
1/8	3.2	0.030	0.76	A	0.003	1.9	0.012	0.017	0.033	0.035
3/16	4.76	0.030	0.76	A	0.013	8.4	0.017	0.034	0.049	0.058
1/4	6.4	0.030	0.76	A	0.028	18.1	0.021	0.050	0.066	0.080
1/4	6.4	0.049	1.24	18	0.018	11.6	0.031	0.038	0.066	0.120
5/16	7.94	0.032	0.81	21A	0.048	31.0	0.028	0.065	0.082	0.109
3/8	9.53	0.032	0.81	21A	0.076	49.0	0.033	0.081	0.098	0.134
3/8	9.53	0.049	1.24	18	0.060	38.7	0.050	0.072	0.098	0.195
1/2	12.7	0.032	0.81	21A	0.149	96.1	0.047	0.114	0.131	0.182
1/2	12.7	0.035	0.89	20L	0.145	93.6	0.051	0.113	0.131	0.198
1/2	12.7	0.049	1.24	18K	0.127	81.9	0.069	0.105	0.131	0.269
1/2	12.7	0.065	1.65	16	0.108	69.7	0.089	0.97	0.131	0.344
5/8	15.9	0.035	0.89	20A	0.242	156	0.065	0.145	0.164	0.251
5/8	15.9	0.040	1.02	L	0.233	150	0.074	0.143	0.164	0.285
5/8	15.9	0.049	1.24	18K	0.215	139	0.089	0.138	0.164	0.344
3/4	19.1	0.035	0.89	20A	0.363	234	0.079	0.178	0.196	0.305
3/4	19.1	0.042	1.07	L	0.348	224	0.103	0.174	0.196	0.362
3/4	19.1	0.049	1.24	18K	0.334	215	0.108	0.171	0.196	0.418
3/4	19.1	0.065	1.65	16	0.302	195	0.140	0.162	0.196	0.542
3/4	19.1	0.083	2.11	14	0.268	173	0.174	0.151	0.196	0.674
7/8	22.2	0.045	1.14	L	0.484	312	0.117	0.206	0.229	0.455
7/8	22.2	0.065	1.65	16K	0.436	281	0.165	0.195	0.229	0.641
7/8	22.2	0.083	2.11	14	0.395	255	0.206	0.186	0.229	0.800
1	25.4	0.065	1.65	16	0.594	383	0.181	0.228	0.262	0.740
1	25.4	0.083	2.11	14	0.546	352	0.239	0.218	0.262	0.927
1 1/8	28.6	0.050	1.27	L	0.825	532	0.176	0.268	0.294	0.655
1 1/8	28.6	0.065	1.65	16K	0.778	502	0.216	0.261	0.294	0.839
1 1/4	31.8	0.065	1.65	16	0.985	636	0.242	0.293	0.327	0.938
1 1/4	31.8	0.083	2.11	14	0.923	596	0.304	0.284	0.327	1.18
1 3/8	34.9	0.055	1.40	L	1.257	811	0.228	0.331	0.360	0.884
1 3/8	34.9	0.065	1.65	16K	1.217	785	0.267	0.326	0.360	1.04
1 1/2	38.1	0.065	1.65	16	1.474	951	0.294	0.359	0.393	1.14
1 1/2	38.7	0.083	2.11	14	1.398	902	0.370	0.349	0.393	1.43
1 5/8	41.3	0.060	1.52	L	1.779	1148	0.295	0.394	0.425	1.14
1 5/8	41.3	0.072	1.83	K	1.722	1111	0.351	0.388	0.425	1.36
2	50.8	0.083	2.11	14	2.642	1705	0.500	0.480	0.628	1.94
2	50.8	0.109	2.76	12	2.494	1609	0.620	0.466	0.628	2.51
2 1/8	54.0	0.070	1.78	L	3.095	1997	0.449	0.520	0.556	1.75
2 1/8	54.0	0.083	2.11	14K	3.016	1946	0.529	0.513	0.556	2.06
2 5/8	66.7	0.080	2.03	L	4.77	3078	0.645	0.645	0.687	2.48
2 5/8	66.7	0.095	2.41	13K	4.66	3007	0.760	0.637	0.687	2.93
3 1/8	79.4	0.090	2.29	L	6.81	4394	0.950	0.771	0.818	3.33
3 1/8	79.4	0.109	2.77	12K	6.64	4284	1.034	0.761	0.818	4.00

TABLE B.2 (continued)

Commercial Copper Tubing<sup>a</sup>

Size, OD		Wall Thickness			Flow Area		Surface Area			
in.	mm	in.	mm	gage	in. <sup>2</sup>	mm <sup>2</sup>	Metal Area (in. <sup>2</sup> )	Inside (ft <sup>2</sup> /ft)	Outside (ft <sup>2</sup> /ft)	Weight (lb/ft)
3 5/8	92.1	0.100	2.54	L	9.21	5942	1.154	0.897	0.949	4.29
3 5/8	92.1	0.120	3.05	11K	9.00	5807	1.341	0.886	0.949	5.12
4 1/8	104.8	0.110	2.79	L	11.92	7691	1.387	1.022	1.080	5.38
4 1/8	104.8	0.134	3.40	10K	11.61	7491	1.682	1.009	1.080	6.51

Source: *The CRC Handbook of Mechanical Engineering*, CRC Press, Boca Raton, FL, 1998; Table A.3, *JZ Handbook*, 1st edn. p. 709.

Note: The table above gives dimensional data and weights of copper tubing used for automotive, plumbing, refrigeration, and heat exchanger services. For additional data see the standards handbooks of the Copper Development Association, Inc., the ASTM standards, and the "SAE Handbook."

Dimensions in this table are actual specified measurements, subject to accepted tolerances. Trade size designations are usually by actual OD, except for water and drainage tube (plumbing), which measures 1/8 in. larger OD. A 1 1/2 in. plumbing tube, for example, measures 5/8 in. OD, and a 2 in. plumbing tube measures 2 1/8 in. OD.

**Key to Gage Sizes**

Standard-gage wall thicknesses are listed by numerical designation (14–21), BWG or Stubs gage. These gage sizes are standard for tubular heat exchangers. The letter A designates SAE tubing sizes for automotive service. Letter designations *K* and *L* are the common sizes for plumbing services, soft or hard temper.

**Other Materials**

These same dimensional sizes are also common for much of the commercial tubing available in aluminum, mild steel, brass, bronze, and other alloys. Tube weights in this table are based on copper at 0.323 lb/in<sup>3</sup>. For other materials the weights should be multiplied by the following approximate factors:

Aluminum	0.30
Monel	0.96
Mild steel	0.87
Stainless steel	0.89
Brass	0.95

<sup>a</sup> Compiled and computed.



This page intentionally left blank

## Appendix C: Properties of Gases and Liquids

**TABLE C.1**

Properties of Gases at Atmospheric Pressure (101.3 kPa = 14.7 psia): Air (Gas Constant = 286.8 J/(kg K) = 53.3 ft lbf/lbm °R;  $\gamma = c_p/c_v = 1.4$ )

Temp, $T$		Density, $\rho$		Specific Heat, $c_p$		Kinematic Viscosity, $\nu$		Thermal Conductivity, $k$		Thermal Diffusivity, $\alpha$		Prandtl Number, $Pr$
K	°R	kg/m <sup>3</sup>	lbm/ft <sup>3</sup>	J/kg · K	BTU/lbm · °R	m <sup>2</sup> /s	ft <sup>2</sup> /s	W/m · K	BTU/h · ft · °R	m <sup>2</sup> /s	ft <sup>2</sup> /h	
100	180	3.601	0.225	1026.6	0.245	1.923 × 10 <sup>-6</sup>	2.070 × 10 <sup>-5</sup>	0.009246	0.005342	0.02501 × 10 <sup>-6</sup>	0.0869	0.770
150	270	2.368	0.148	1009.9	0.241	4.343	4.674	0.013735	0.007936	0.05745	0.223	0.753
200	360	1.768	0.110	1006.1	0.240	7.490	8.062	0.01809	0.01045	0.10165	0.394	0.739
250	450	1.413	0.0882	1005.3	0.240	9.49	10.2	0.02227	0.02287	0.13161	0.510	0.722
300	540	1.177	0.0735	1005.7	0.240	15.68	16.88	0.02624	0.01516	0.22160	0.859	0.708
350	630	0.998	0.0623	1009.0	0.241	20.76	22.35	0.03003	0.01735	0.2983	1.156	0.697
400	720	0.883	0.0551	1014.0	0.242	25.90	27.88	0.03365	0.01944	0.3760	1.457	0.689
450	810	0.783	0.489	1020.7	0.244	28.86	31.06	0.037.7	0.02142	0.4222	1.636	0.683
500	900	0.705	0.0440	1029.5	0.245	37.90	40.80	0.04038	0.02333	0.5564	2.356	0.680
550	990	0.642	0.0401	1039.2	0.248	44.34	47.73	0.04360	0.02519	0.6532	2.531	0.680
600	1000	0.589	0.0367	1055.1	0.252	51.34	55.26	0.04659	0.02682	0.7512	2.911	0.680
650	1170	0.543	0.0339	1063.5	0.254	58.51	62.98	0.00953	0.02862	0.8578	3.324	0.682
700	1260	0.503	0.0314	1075.2	0.257	66.25	7131	0.05230	0.030023	0.9672	3.748	0.684
750	1350	0.471	0.0594	1085.6	0.259	73.91	79.56	0.05509	0.03183	1.0774	4.175	0.686
800	1440	0.441	0.0275	1097.8	0.262	8229	88.58	0.05779	0.03339	1.1951	4.631	0.689
850	1530	0.415	0.0259	1109.5	0.265	90.75	97.68	0.06028	0.03483	1.3097	5.075	0.692
900	1620	0.393	0.0245	1121.2	0.268	99.3	107	0.06279	0.03628	1.4278	5.530	0.696
950	1710	0.372	0.0232	1132.1	0.270	108.2	116.5	0.06525	0.03770	1.5510	6.010	0.699
1000	1800	0.352	0.0220	1141.7	0.273	117.8	126.8	0.06752	0.03901	1.6779	6502	0.702
1100	1980	0.320	0.0120	1160	0.277	138.6	149.2	0.0732	0.0423	1.969	7.630	0.704
1200	2160	0.295	0.0184	1179	0.282	159.1	171.3	0.0782	0.0423	1.969	7.630	0.707
1300	2340	0.271	0.0189	1197	0.286	182.1	196.0	0.0837	0.0434	2.583	10.01	0.705
1400	2520	0.252	0.0157	1214	0.290	205.5	221.2	0.0891	0.0515	2.920	11.32	0.705
1500	2700	0.236	0.0147	1230	0.294	229.1	246.6	0.0946	0.0547	3.262	1264	0.705
1600	2880	0.221	0.0138	1248	0.298	254.5	273.9	0.100	0.0578	3.609	13.98	0.705
1700	3060	0.208	0.0130	1267	0.303	280.5	301.9	0.105	0.0607	3.977	15.41	0.705
1800	3240	0.197	0.0123	1287	0.307	308.1	331.6	0.111	0.0641	4.379	16.97	0.704
1900	3420	0.186	0.0115	1309	0.383	338.5	364.4	0.117	0.0676	4.811	18.64	0.704
2000	3600	0.176	0.0110	1338	0.320	369.0	397.2	0.124	0.0716	5.260	20.38	0.702
2100	3780	0.168	0.0105	1372	0.328	399.6	430.1	0.131	0.0757	5.715	22.15	0.700
2200	3960	0.160	0.0100	1419	0.339	432.6	465.6	0.139	0.0803	6120	2372	0.707
2300	4140	0.154	0.00955	1482	0.354	464.0	499.4	0.149	0.0861	6.540	25.34	0.710
2400	4320	0.146	0.00905	1574	0376	504.0	542.5	0.161	0.0930	7.020	27.20	0.718
2500	4500	0.139	0.00868	1688	0.403	543.5	585.0	0.175	0.101	7.441	28.83	0.730

Source: Janna, W.S., *Engineering Heat Transfer*, 2nd edn., Table D.1, CRC Press, Boca Raton, FL, p. 654, 2000.

TABLE C.2

Properties of Gases at Atmospheric Pressure (101.3 kPa = 14.7 psia): Nitrogen (Gas Constant = 296.8 J/(kg K) = 55.16 ft lbf/lbm °R;  $\gamma = c_p/c_v = 1.40$ )

Temp, $T$		Density, $\rho$		Specific Heat, $c_p$		Kinematic Viscosity, $\nu$		Thermal Conductivity, $k$		Thermal Diffusivity, $\alpha$		Prandtl Number, $P_r$
K	°R	kg/m <sup>3</sup>	lbm/ft <sup>3</sup>	J/kg · K	BTU/lbm · °R	m <sup>2</sup> /s	ft <sup>2</sup> /s	W/m · K	BTU/h · ft · °R	m <sup>2</sup> /s	ft <sup>2</sup> /h	
100	180	3.4808	0.2173	1072.2	0.2561	$1.971 \times 10^{-6}$	$2.122 \times 10^{-5}$	0.009450	0.005460	$0.025319 \times 10^{-4}$	0.09811	0.786
200	360	1.7108	0.1068	1042.9	0.2491	7.568	8.146	0.01824	0.01054	0.10224	0.3962	0.747
300	540	1.1421	0.0713	1040.8	0.2486	15.63	16.82	0.02620	0.01514	0.22044	0.8542	0.713
400	720	0.8538	0.0533	1045.9	0.2498	25.74	27.71	0.03335	0.01927	0.3734	1.447	0.691
500	900	0.6824	0.0426	1055.5	0.2521	37.66	40.54	0.03984	0.02302	0.5530	2.143	0.684
600	1080	0.5687	0.0355	1075.6	0.2569	51.19	55.10	0.04580	0.02646	0.7486	2.901	0.686
700	1260	0.4934	0.0308	1096.9	0.2620	65.13	70.10	0.05123	0.02960	0.9466	3.668	0.691
800	1440	0.4277	0.0267	1122.5	0.2681	81.46	87.68	0.05609	0.03241	1.1685	4.528	0.700
900	1620	0.3796	0.0237	1146.4	0.2738	91.06	98.02	0.06070	0.03507	1.3946	5.404	0.711
1000	1800	0.3412	0.0213	1167.7	0.2789	117.2	126.2	0.06475	0.03741	1.6250	6.297	0.724
1100	1980	0.3108	0.0194	1185.7	0.2382	136.0	146.4	0.06850	0.03958	1.8591	7.204	0.736
1200	2160	0.2851	0.0178	1203.7	0.2875	156.1	168.0	0.07184	0.04151	2.0932	8.111	0.748

Source: Janna, W.S., *Engineering Heat Transfer*, 2nd edn., Table D.5, CRC Press, Boca Raton, FL, p. 657, 2000.

TABLE C.3

Properties of Gases at Atmospheric Pressure (101.3 kPa = 14.7 psia): Oxygen (Gas Constant = 260 J/(kg K) = 48.3 ft lbf/lbm °R;  $\gamma = c_p/c_v = 1.40$ )

Temp, $T$		Density, $\rho$		Specific Heat, $c_p$		Kinematic Viscosity, $\nu$		Thermal Conductivity, $k$		Thermal Diffusivity, $\alpha$		Prandtl Number, $P_r$
K	°R	kg/m <sup>3</sup>	lbm/ft <sup>3</sup>	J/kg · K	BTU/lbm · °R	m <sup>2</sup> /s	ft <sup>2</sup> /s	W/m · K	BTU/h · ft · °R	m <sup>2</sup> /s	ft <sup>2</sup> /h	
100	180	3.9118	0.2492	947.9	0.2264	$1.946 \times 10^{-6}$	$2.095 \times 10^{-5}$	0.00903	0.00522	$0.023876 \times 10^{-4}$	0.09252	0.815
150	270	2.6190	0.1635	917.8	0.2192	4.387	4.722	0.01367	0.00790	0.05688	0.2204	0.773
200	360	1.9559	0.1221	913.1	0.2181	7.593	8.173	0.01824	0.01054	0.10214	0.3958	0.745
250	450	1.5618	0.0975	915.7	0.2187	11.45	12.32	0.02259	0.01305	0.15794	0.6120	0.725
300	540	1.3007	0.0812	920.3	0.2198	15.86	17.07	0.02676	0.01546	0.22353	0.8662	0.709
350	630	1.1133	0.0695	929.1	0.2219	20.80	22.39	0.03070	0.01774	0.2968	1.150	0.702
400	720	0.9755	0.0609	942.0	0.2250	26.18	28.18	0.03461	0.02000	0.3768	1.460	0.695
450	810	0.8682	0.0542	956.7	0.2285	31.99	34.43	0.03828	0.02212	0.4609	1.786	0.694
500	900	0.7801	0.0487	972.2	0.2322	38.37	41.27	0.04173	0.02411	0.5502	2.132	0.697
550	990	0.7096	0.0443	988.1	0.2360	45.05	48.49	0.04517	0.02610	0.6441	2.496	0.700
600	1080	0.6508	0.0406	1004.4	0.2399	52.15	56.13	0.04882	0.02792	0.7399	2.867	0.704

Source: Janna, W.S., *Engineering Heat Transfer*, 2nd edn. Table D.6, CRC Press, Boca Raton, FL, p. 658, 2000.



TABLE C.4

Properties of Gases at Atmospheric Pressure (101.3 kPa = 14.7 psia): Carbon Dioxide (Gas Constant = 188.9 J/(kg K) = 35.11 ft lbf/lbm °R;  $\gamma = c_p/c_v = 1.30$ )

Temp, $T$		Density, $\rho$		Specific Heat, $c_p$		Kinematic Viscosity, $\nu$		Thermal Conductivity, $k$		Thermal Diffusivity, $\alpha$		Prandtl Number, $Pr$
K	°R	kg/m <sup>3</sup>	lbm/ft <sup>3</sup>	J/kg · K	BTU/lbm · °R	m <sup>2</sup> /s	ft <sup>2</sup> /s	W/m · K	BTU/h · ft · °R	m <sup>2</sup> /s	ft <sup>2</sup> /h	
220	396	2.4733	0.1544	783	0.187	$4.490 \times 10^{-6}$	$4.833 \times 10^{-5}$	0.010805	0.006243	$0.05920 \times 10^{-4}$	0.2294	0.818
250	450	2.1657	0.1352	804	0.192	5.813	6.257	0.012884	0.007444	0.07401	0.2868	0.793
300	540	1.7973	0.1122	871	0.208	8.321	8.957	0.016572	0.009575	0.10588	0.4103	0.770
350	630	1.5362	0.0959	900	0.215	11.19	12.05	0.02047	0.01183	0.14808	0.5738	0.755
400	720	1.3424	0.0838	942	0.225	14.39	15.49	0.02461	0.01422	0.19463	0.7542	0.738
450	810	1.1918	0.0744	980	0.234	17.90	19.27	0.02897	0.01674	0.24813	0.9615	0.721
500	900	1.0732	0.0670	1013	0.242	21.67	23.33	0.03352	0.01937	0.3084	1.195	0.702
550	990	0.9739	0.0608	1047	0.250	25.74	27.71	0.03821	0.02208	0.3750	1.453	0.685
600	1080	0.8938	0.0558	1076	0.257	30.02	32.31	0.04313	0.02491	0.4483	1.737	0.668

Source: Janna, W.S., *Engineering Heat Transfer*, 2nd edn., Table D.2, CRC Press, Boca Raton, FL, p. 655, 2000.

TABLE C.5

Properties of Gases at Atmospheric Pressure (101.3 kPa = 14.7 psia): Water Vapor or Steam (Gas Constant = 461.5 J/(kg K) = 85.78 ft lbf/lbm °R;  $\gamma = c_p/c_v = 1.33$ )

Temp, $T$		Density, $\rho$		Specific Heat, $c_p$		Kinematic Viscosity, $\nu$		Thermal Conductivity, $k$		Thermal Diffusivity, $\alpha$		Prandtl Number, $Pr$
K	°R	kg/m <sup>3</sup>	lbm/ft <sup>3</sup>	J/kg · K	BTU/lbm · °R	m <sup>2</sup> /s	ft <sup>2</sup> /s	W/m · K	BTU/h · ft · °R	m <sup>2</sup> /s	ft <sup>2</sup> /h	
380	684	0.5863	0.0366	2060	0.492	$2.16 \times 10^{-6}$	$2.33 \times 10^{-5}$	0.0246	0.0142	$0.2036 \times 10^{-4}$	0.789	1.060
400	720	0.5542	0.0346	2014	0.481	2.42	2.61	0.0261	0.0151	0.2338	0.906	1.040
450	810	0.4902	0.0306	1980	0.473	3.11	3.35	0.0299	0.0173	0.307	1.19	1.010
500	900	0.4005	0.0275	1985	0.474	3.86	4.16	0.0339	0.0196	0.387	1.50	0.996
550	990	0.4005	0.0250	1997	0.477	4.70	5.06	0.0379	0.0219	0.475	1.84	0.991
600	1080	0.3652	0.0228	2026	0.484	5.66	6.09	0.0422	0.0244	0.573	2.22	0.986
650	1170	0.3380	0.0211	2056	0.491	6.64	7.15	0.0464	0.0268	0.666	2.58	0.995
700	1260	0.3140	0.0196	2085	0.498	7.75	8.31	0.0505	0.0292	0.772	2.99	1.000
750	1350	0.2931	0.0183	2119	0.506	8.88	9.56	0.0549	0.0317	0.883	3.42	0.005
800	1440	0.2739	0.0171	2152	0.514	10.20	10.98	0.0592	0.0342	1.001	3.88	1.010
850	1530	0.2579	0.0161	2186	0.522	11.52	12.40	0.0637	0.0368	1.130	4.38	1.019

Source: Janna, W.S., *Engineering Heat Transfer*, 2nd edn., Table D.7, CRC Press, Boca Raton, FL, p. 659, 2000.

TABLE C.6

Thermodynamic Properties of Steam: Temperature Table (SI Units)

$T_{\text{sat}}$ (°C)	$P_{\text{sat}}$ (kPa)	Specific Volume (m <sup>3</sup> /kg)			Internal Energy (kJ/kg)			Enthalpy (kJ/kg)			Entropy (kJ/kg K)		
		$\nu_f$	$\nu_{fg}$	$\nu_g$	$u_f$	$u_{fg}$	$u_g$	$h_f$	$h_{fg}$	$h_g$	$s_f$	$s_{fg}$	$s_g$
0	0.61	0.001000	206.13	206.13	0.00	2,373.9	2,373.9	0.0	2,500.0	2,500.0	-0.0012	9.1590	9.1578
5	0.87	0.001000	147.20	147.20	21.04	2,361.1	2,382.1	21.0	2,489.6	2,510.6	0.0757	8.9510	9.0267
10	1.23	0.001000	106.36	106.36	42.02	2,347.8	2,389.8	42.0	2,478.4	2,520.4	0.1509	8.7511	8.9020
15	1.71	0.001001	78.036	78.037	62.95	2,333.7	2,396.7	63.0	2,466.8	2,529.7	0.2244	8.5582	8.7827
20	2.34	0.001002	57.801	57.802	83.86	2,319.9	2,403.7	83.9	2,455.0	2,538.9	0.2965	8.3718	8.6684
25	3.17	0.001003	43.446	43.447	104.75	2,305.5	2,410.3	104.8	2,443.1	2,547.9	0.3672	8.1919	8.5591
30	4.24	0.001004	32.907	32.908	125.63	2,291.6	2,417.2	125.6	2,431.2	2,556.8	0.4367	8.0180	8.4546
35	5.62	0.001006	25.250	25.251	146.50	2,277.3	2,423.8	146.5	2,419.2	2,565.7	0.5049	7.8496	8.3545
40	7.37	0.001008	19.536	19.537	167.37	2,263.2	2,430.6	167.4	2,407.3	2,574.6	0.5720	7.6864	8.2584
45	9.58	0.001010	15.262	15.263	188.24	2,249.1	2,437.3	188.3	2,395.3	2,583.5	0.6381	7.5281	8.1662
50	12.33	0.001012	12.046	12.047	209.12	2,234.7	2,443.8	209.1	2,383.2	2,592.3	0.7031	7.3745	8.0776
55	15.74	0.001014	9.5771	9.5781	230.01	2,220.4	2,450.4	230.0	2,371.1	2,601.1	0.7672	7.2253	7.9925
60	19.92	0.001017	7.6776	7.6786	250.91	2,206.0	2,456.9	250.9	2,358.9	2,609.8	0.8303	7.0804	7.9107
65	25.00	0.001020	6.1996	6.2006	271.83	2,191.6	2,463.4	271.9	2,346.6	2,618.4	0.8926	6.9394	7.8320
70	31.15	0.001023	5.0452	5.0462	292.76	2,177.0	2,469.7	292.8	2,334.2	2,626.9	0.9540	6.8023	7.7563
75	38.54	0.001026	4.1328	4.1338	313.70	2,162.3	2,476.0	313.7	2,321.6	2,635.4	1.0146	6.6687	7.6834
80	47.35	0.001029	3.4074	3.4085	334.67	2,147.6	2,482.3	334.7	2,309.8	2,643.7	1.0744	6.5387	7.6131
85	57.80	0.001032	2.8276	2.8286	355.65	2,132.8	2,488.4	355.7	2,296.2	2,651.9	1.1335	6.4118	7.5453
90	70.10	0.001036	2.3604	2.3614	376.66	2,117.8	2,494.5	376.7	2,283.3	2,660.0	1.1917	6.2881	7.4798
95	84.52	0.001039	1.9806	1.9817	397.69	2,102.8	2,500.5	397.8	2,270.2	2,668.0	1.2493	6.1673	7.4166
100	101.32	0.001043	1.6689	1.6699	418.75	2,087.9	2,506.6	418.9	2,257.0	2,675.8	1.3062	6.0492	7.3554
105	120.80	0.001047	1.4142	1.4152	439.83	2,072.8	2,512.6	440.0	2,243.6	2,683.6	1.3624	5.9338	7.2962
110	143.27	0.001051	1.2063	1.2074	460.95	2,057.2	2,518.2	461.1	2,230.0	2,691.1	1.4179	5.8209	7.2388
115	169.07	0.001056	1.0350	1.0361	482.10	2,041.3	2,523.4	482.3	2,216.3	2,698.6	1.4728	5.7105	7.1833
120	198.55	0.001060	0.89100	0.8921	503.28	2,025.4	2,528.7	503.5	2,202.3	2,705.8	1.5271	5.6023	7.1293
125	232.11	0.001065	0.76938	0.7704	524.51	2,009.6	2,534.1	524.8	2,188.2	2,712.9	1.5807	5.4962	7.0770
130	270.15	0.001070	0.66702	0.6681	545.78	1,993.6	2,539.4	546.1	2,173.8	2,719.9	1.6338	5.3922	7.0261
135	313.09	0.001075	0.58074	0.5818	567.09	1,977.3	2,544.4	567.4	2,159.2	2,726.6	1.6864	5.2902	6.9766
140	361.39	0.001080	0.50739	0.5085	588.46	1,960.9	2,549.3	588.8	2,144.3	2,733.1	1.7384	5.1900	6.9284
145	415.53	0.001085	0.44462	0.4457	609.88	1,944.3	2,554.2	610.3	2,129.1	2,739.4	1.7899	5.0916	6.8815
150	475.99	0.001091	0.39100	0.3921	631.35	1,927.5	2,558.8	631.9	2,113.6	2,745.5	1.8409	4.9948	6.8358
155	543.30	0.001096	0.34514	0.3462	652.89	1,910.3	2,563.2	653.5	2,097.8	2,751.3	1.8915	4.8996	6.7911
160	618.00	0.001102	0.30566	0.3068	674.50	1,892.8	2,567.3	675.2	2,081.7	2,756.9	1.9416	4.8059	6.7475
165	700.68	0.001108	0.27131	0.2724	696.18	1,875.1	2,571.3	697.0	2,065.2	2,762.2	1.9912	4.7135	6.7048
170	791.86	0.001114	0.24141	0.2425	717.93	1,857.2	2,575.2	718.8	2,048.4	2,767.2	2.0405	4.6224	6.6630
175	892.20	0.001121	0.21538	0.2165	739.77	1,839.0	2,578.8	740.8	2,031.2	2,772.0	2.0894	4.5325	6.6220
180	1,002.3	0.001127	0.19266	0.1938	761.69	1,820.5	2,582.1	762.8	2,013.6	2,776.4	2.1380	4.4437	6.5817
185	1,122.9	0.001134	0.17272	0.1739	783.70	1,803.6	2,585.3	785.0	1,995.5	2,780.5	2.1862	4.3559	6.5421
190	1,254.5	0.001141	0.15513	0.1563	805.80	1,782.4	2,588.3	807.2	1,977.1	2,784.3	2.2341	4.2691	6.5032
195	1,398.0	0.001148	0.13964	0.1408	828.01	1,762.9	2,590.9	829.6	1,958.1	2,787.8	2.2817	4.1834	6.4651
200	1,553.9	0.001156	0.12597	0.1271	850.32	1,743.0	2,593.3	852.1	1,938.8	2,790.9	2.3290	4.0986	6.4276
205	1,723.1	0.001164	0.11386	0.1150	872.74	1,722.7	2,595.4	874.7	1,918.9	2,793.6	2.3761	4.0147	6.3908
210	1,906.3	0.001172	0.10307	0.1042	895.28	1,702.0	2,597.3	897.5	1,898.5	2,796.0	2.4230	3.9314	6.3544
215	2,104.3	0.001180	0.09345	0.0946	917.94	1,681.0	2,598.9	920.4	1,877.6	2,798.0	2.4696	3.8485	6.3181
220	2,317.8	0.001189	0.08486	0.0860	940.73	1,659.5	2,600.2	943.5	1,856.2	2,799.7	2.5161	3.7661	6.2821
225	2,547.8	0.001198	0.07716	0.0784	963.66	1,637.6	2,601.3	966.7	1,834.2	2,800.9	2.5623	3.6841	6.2464
230	2,795.0	0.001208	0.07022	0.0714	986.73	1,615.4	2,602.2	990.1	1,811.7	2,801.8	2.6084	3.6025	6.2109
235	3,060.3	0.001218	0.06400	0.0652	1,010.0	1,592.7	2,602.7	1,033.7	1,788.6	2,802.3	2.6544	3.5213	6.1757
240	3,344.7	0.001228	0.05851	0.0597	1,033.6	1,569.1	2,602.5	1,037.5	1,764.8	2,802.3	2.7002	3.4404	6.1406
245	3,649.0	0.001239	0.05353	0.0548	1,056.9	1,545.2	2,602.1	1,061.4	1,740.5	2,801.9	2.7460	3.3597	6.1057

TABLE C.6 (continued)

Thermodynamic Properties of Steam: Temperature Table (SI Units)

$T_{\text{sat}}$ (°C)	$P_{\text{sat}}$ (kPa)	Specific Volume (m <sup>3</sup> /kg)			Internal Energy (kJ/kg)			Enthalpy (kJ/kg)			Entropy (kJ/kg K)		
		$\nu_f$	$\nu_{fg}$	$\nu_g$	$u_f$	$u_{fg}$	$u_g$	$h_f$	$h_{fg}$	$h_g$	$s_f$	$s_{fg}$	$s_g$
250	3,974.2	0.001250	0.04893	0.0502	1,080.7	1,521.0	2,601.7	1,085.6	1,715.5	2,801.2	2.7917	3.2792	6.0708
255	4,321.3	0.001262	0.04471	0.0460	1,104.6	1,496.7	2,601.3	1,110.1	1,689.9	2,800.0	2.8373	3.1986	6.0359
260	4,691.2	0.001275	0.04086	0.0421	1,128.8	1,471.9	2,600.7	1,134.8	1,663.5	2,798.3	2.8829	3.1180	6.0009
265	5,085.0	0.001288	0.03738	0.0387	1,153.2	1,446.4	2,599.6	1,159.8	1,636.5	2,796.3	2.9286	3.0372	5.9657
270	5,503.8	0.001302	0.03424	0.0355	1,177.9	1,420.3	2,598.1	1,185.1	1,608.7	2,793.7	2.9743	2.9560	5.9303
275	5,948.6	0.001317	0.03139	0.0327	1,202.8	1,393.4	2,596.3	1,210.7	1,580.1	2,790.8	3.0200	2.8745	5.8945
280	6,420.5	0.001333	0.02878	0.0301	1,228.1	1,366.0	2,594.0	1,236.6	1,550.8	2,787.4	3.0660	2.7924	5.8584
285	6,920.8	0.001349	0.02639	0.0277	1,253.7	1,337.9	2,591.6	1,263.0	1,520.6	2,783.6	3.1121	2.7097	5.8218
290	7,450.6	0.001366	0.02418	0.0255	1,279.6	1,297.7	2,577.3	1,289.8	1,477.9	2,767.7	3.1585	2.6262	5.7847
295	8,011.1	0.001385	0.02214	0.0235	1,306.0	1,265.5	2,571.5	1,317.1	1,442.8	2,759.9	3.2052	2.5417	5.7469
300	8,603.7	0.001404	0.02025	0.0217	1,332.8	1,232.0	2,564.8	1,344.9	1,406.2	2,751.1	3.2523	2.4560	5.7083
305	9,214.4	0.001425	0.01850	0.0199	1,360.2	1,197.5	2,557.6	1,373.3	1,367.9	2,741.2	3.3000	2.3688	5.6687
310	9,869.4	0.001447	0.01688	0.0183	1,388.0	1,161.1	2,549.2	1,402.3	1,327.8	2,730.1	3.3483	2.2797	5.6279
315	10,561.	0.001470	0.01538	0.0169	1,416.5	1,123.0	2,539.6	1,432.1	1,285.5	2,717.6	3.3973	2.1884	5.5858
320	11,289.	0.001499	0.01398	0.0155	1,445.7	1,083.0	2,528.7	1,462.6	1,240.9	2,703.5	3.4473	2.0947	5.5420
325	12,056.	0.001528	0.01267	0.0142	1,475.5	1,040.9	2,516.4	1,494.0	1,193.6	2,687.3	3.4984	1.9979	5.4962
330	12,862.	0.001561	0.01143	0.0130	1,506.2	996.3	2,502.5	1,526.3	1,143.3	2,669.6	3.5507	1.8973	5.4480
335	13,712.	0.001598	0.01026	0.0119	1,537.8	949.0	2,486.8	1,559.7	1,089.6	2,649.3	3.6045	1.7922	5.3967
340	14,605.	0.001639	0.00914	0.0108	1,570.4	898.7	2,469.0	1,594.3	1,032.2	2,626.5	3.6601	1.6820	5.3420
345	15,545.	0.001686	0.00808	0.0098	1,606.3	842.1	2,448.4	1,632.5	967.7	2,600.2	3.7176	1.5658	5.2834
350	16,535.	0.001741	0.00706	0.0088	1,643.0	780.5	2,423.5	1,671.8	897.2	2,569.0	3.7775	1.4416	5.2191
355	17,577.	0.001808	0.00605	0.0079	1,682.1	710.9	2,393.0	1,713.9	817.3	2,531.2	3.8400	1.3054	5.1454
360	18,675.	0.001896	0.00504	0.0069	1,726.2	629.5	2,355.7	1,761.6	723.7	2,485.3	3.9056	1.1531	5.0587
365	19,833.	0.002016	0.00400	0.0060	1,777.9	531.0	2,308.9	1,817.8	610.3	2,428.1	3.9746	0.9822	4.9569
370	21,054.	0.002225	0.00274	0.0050	1,843.3	394.1	2,237.3	1,890.1	451.9	2,342.0	4.0476	0.7555	4.8030
374.4	22,090.	0.00315	0.00000	0.00315	2,029.6	0.0	2,029.6	2,099.3	0.0	2,099.3	4.4298	0.0	4.4298

Source: Properties obtained from software, STEAMCALC, John Wiley & Sons, New York, 1983; *Introduction to Thermal and Fluid Engineering*, CRC Table A.3, p. 901.



TABLE C.7

Thermodynamic Properties of Steam: Pressure Table (SI Units)

$P_{\text{sat}}$ (kPa)	$T_{\text{sat}}$ (°C)	Specific Volume (m³/kg)			Internal Energy (kJ/kg)			Enthalpy (kJ/kg)			Entropy (kJ/kg K)		
		$v_f$	$v_{fg}$	$v_g$	$u_f$	$u_{fg}$	$u_g$	$h_f$	$h_{fg}$	$h_g$	$s_f$	$s_{fg}$	$s_g$
1.00	7.0	0.001000	129.08	129.08	29.40	2,356.1	2,385.5	29.4	2,485.2	2,514.6	0.1058	8.8704	8.9763
1.50	13.0	0.001001	88.067	88.068	54.68	2,339.3	2,394.0	54.7	2,471.4	2,526.3	0.1956	8.6337	8.8292
2.00	17.5	0.001001	67.073	67.074	73.41	2,326.8	2,400.2	73.4	2,460.9	2,534.3	0.2607	8.4642	8.7249
2.50	21.1	0.001002	54.290	54.291	88.41	2,316.7	2,405.1	88.4	2,452.4	2,540.8	0.3120	8.3322	8.6442
3.00	24.1	0.001003	45.751	45.752	100.96	2,308.0	2,409.0	101.0	2,445.3	2,546.2	0.3545	8.2240	8.5786
3.50	26.7	0.001003	39.483	39.484	111.81	2,300.9	2,412.7	111.8	2,439.1	2,550.9	0.3908	8.1324	8.5233
4.00	29.0	0.001004	34.779	34.780	121.37	2,294.5	2,415.9	121.4	2,433.6	2,555.0	0.4226	8.0529	8.4756
4.50	31.0	0.001005	31.128	31.129	129.95	2,288.6	2,418.6	130.0	2,428.7	2,558.7	0.4509	7.9827	8.4336
5.00	32.9	0.001005	28.194	28.195	137.73	2,283.3	2,421.0	137.7	2,424.3	2,562.0	0.4764	7.9197	8.3961
5.50	34.6	0.001006	25.773	25.774	144.86	2,278.4	2,423.3	144.9	2,420.2	2,565.0	0.4996	7.8626	8.3622
6.00	36.2	0.001006	23.742	23.743	151.45	2,274.0	2,425.4	151.5	2,416.4	2,567.9	0.5209	7.8104	8.3313
6.50	37.7	0.001007	22.013	22.014	157.58	2,269.8	2,427.4	157.6	2,412.9	2,570.5	0.5407	7.7623	8.3030
7.00	39.0	0.001007	20.522	20.523	163.31	2,266.0	2,429.3	163.3	2,409.6	2,572.9	0.5590	7.7177	8.2768
7.50	40.3	0.001008	19.225	19.226	168.70	2,262.3	2,431.0	168.7	2,406.5	2,575.2	0.5763	7.6762	8.2524
8.00	41.5	0.001008	18.086	18.087	173.79	2,258.9	2,432.7	173.8	2,403.6	2,577.4	0.5924	7.6372	8.2296
8.50	42.7	0.001009	17.080	17.081	178.61	2,255.6	2,434.2	178.6	2,400.8	2,579.4	0.6077	7.6006	8.2083
9.00	43.8	0.001009	16.185	16.186	183.19	2,252.5	2,435.7	183.2	2,398.2	2,581.4	0.6222	7.5660	8.1881
9.50	44.8	0.001010	15.383	15.384	187.56	2,249.5	2,437.1	187.6	2,395.7	2,583.2	0.6359	7.5332	8.1691
10.00	45.8	0.001010	14.660	14.661	191.74	2,246.7	2,438.4	191.7	2,393.3	2,585.0	0.6490	7.5021	8.1511
15.00	54.0	0.001014	10.020	10.021	225.83	2,223.2	2,449.0	225.8	2,373.5	2,599.4	0.7544	7.2548	8.0092
20.00	60.1	0.001017	7.6483	7.6493	251.28	2,205.7	2,457.0	251.3	2,358.7	2,610.0	0.8314	7.0779	7.9093
25.00	65.0	0.001020	6.2015	6.2025	271.80	2,191.6	2,463.3	271.8	2,346.6	2,618.4	0.8925	6.9396	7.8321
30.00	69.1	0.001022	5.2277	5.2287	289.09	2,379.5	2,468.6	289.1	2,336.3	2,625.5	0.9433	6.8260	7.7693
35.00	72.7	0.001024	4.5249	4.5259	304.11	2,169.0	2,473.1	304.1	2,327.4	2,631.5	0.9869	6.7295	7.7164
40.00	75.9	0.001026	3.9918	3.9929	317.42	2,159.7	2,477.1	317.5	2,319.4	2,636.8	1.0253	6.6455	7.6707
45.00	78.7	0.001028	3.5744	3.5755	329.40	2,151.3	2,480.7	329.4	2,312.2	2,641.6	1.0595	6.5710	7.6305
50.00	81.3	0.001030	3.2389	3.2398	340.31	2,143.6	2,483.9	340.4	2,305.5	2,645.9	1.0904	6.5042	7.5946
60.00	86.0	0.001033	2.7305	2.7316	359.66	2,129.9	2,489.6	359.7	2,293.7	2,653.5	1.1446	6.3880	7.5326
70.00	90.0	0.001036	2.3638	2.3648	376.49	2,117.9	2,494.4	376.6	2,283.4	2,659.9	1.1913	6.2891	7.4804
80.00	93.5	0.001038	2.0859	2.0869	391.43	2,107.2	2,498.7	391.5	2,274.1	2,665.6	1.2323	6.2029	7.4352
90.00	96.7	0.001041	1.8667	1.8678	404.90	2,097.7	2,502.6	405.0	2,265.7	2,670.7	1.2689	6.1265	7.3954
100.00	99.6	0.001043	1.6898	1.6908	417.20	2,089.0	2,506.2	417.3	2,258.0	2,675.3	1.3020	6.0578	7.3598
101.32	100.0	0.001043	1.66895	1.6700	418.74	2,087.9	2,506.6	418.8	2,257.0	2,675.8	1.3062	6.0493	7.3554
125.00	106.0	0.001048	1.36965	1.3707	444.01	2,069.7	2,513.7	444.1	2,240.9	2,685.1	1.3734	5.9113	7.2847
150.00	111.4	0.001053	1.15612	1.1572	466.74	2,052.9	2,519.6	466.9	2,226.3	2,693.2	1.4330	5.7904	7.2234
175.00	116.1	0.001057	1.00248	1.0035	486.58	2,037.9	2,524.5	486.8	2,213.4	2,700.1	1.4844	5.6873	7.1717
200.00	120.2	0.001060	0.88498	0.8860	504.25	2,024.7	2,529.0	504.5	2,201.7	2,706.2	1.5295	5.5974	7.1269

225.00	124.0	0.001064	0.79229	0.7934	520.22	2,012.8	2,533.0	520.5	2,191.1	2,711.5	1.5700	5.5175	7.0874
250.00	127.4	0.001067	0.71751	0.7186	534.82	2,001.9	2,536.7	535.1	2,181.2	2,716.3	1.6066	5.4455	7.0521
275.00	130.6	0.001070	0.65602	0.6571	548.30	1,991.7	2,540.0	548.6	2,172.1	2,720.7	1.6401	5.3800	7.0201
300.00	133.5	0.001073	0.60457	0.6056	560.83	1,982.1	2,542.9	561.2	2,163.5	2,724.6	1.6710	5.3199	6.9910
325.00	136.3	0.001076	0.56082	0.5619	572.57	1,973.1	2,545.7	572.9	2,155.4	2,728.3	1.6998	5.2643	6.9641
350.00	138.9	0.001079	0.52305	0.5241	583.60	1,964.6	2,548.2	584.0	2,147.7	2,731.6	1.7266	5.2126	6.9392
375.00	141.3	0.001081	0.49007	0.4911	594.03	1,956.6	2,550.6	594.4	2,140.3	2,734.8	1.7519	5.1642	6.9161
400.00	143.6	0.001084	0.46105	0.4621	603.93	1,948.9	2,552.8	604.4	2,133.3	2,737.7	1.7757	5.1187	6.8944
425.00	145.8	0.001086	0.43534	0.4364	613.36	1,941.6	2,554.9	613.8	2,126.6	2,740.4	1.7982	5.0758	6.8740
450.00	147.9	0.001088	0.41242	0.4135	622.35	1,934.5	2,556.9	622.8	2,120.1	2,743.0	1.8196	5.0352	6.8548
475.00	149.9	0.001091	0.39188	0.3930	630.97	1,927.7	2,558.7	631.5	2,113.9	2,745.4	1.8400	4.9966	6.8366
500.00	151.8	0.001093	0.37336	0.3745	639.24	1,921.2	2,560.4	639.8	2,107.9	2,747.6	1.8595	4.9598	6.8193
550.00	155.5	0.001097	0.34129	0.3424	654.86	1,908.7	2,563.5	655.5	2,096.4	2,751.8	1.8960	4.8910	6.7871
600.00	158.8	0.001101	0.31443	0.3155	669.42	1,896.9	2,566.3	670.1	2,085.5	2,755.6	1.9298	4.8278	6.7576
650.00	162.0	0.001104	0.29151	0.2926	683.06	1,885.8	2,568.8	683.8	2,075.2	2,759.0	1.9613	4.7692	6.7305
700.00	164.9	0.001108	0.27168	0.2728	695.93	1,875.3	2,571.2	696.7	2,065.4	2,762.1	1.9907	4.7146	6.7053
750.00	167.7	0.001111	0.25439	0.2555	708.11	1,865.3	2,573.4	708.9	2,056.0	2,765.0	2.0183	4.6634	6.6817
800.00	170.4	0.001115	0.23919	0.2403	719.68	1,855.7	2,575.4	720.6	2,047.0	2,767.6	2.0445	4.6152	6.6597
850.00	172.9	0.001118	0.22572	0.2268	730.71	1,846.5	2,577.2	731.7	2,038.4	2,770.0	2.0692	4.5696	6.6388
900.00	175.3	0.001121	0.21372	0.2148	741.27	1,837.7	2,578.9	742.3	2,030.0	2,772.3	2.0928	4.5264	6.6192
950.00	177.7	0.001124	0.20295	0.2041	751.39	1,829.1	2,580.5	752.5	2,021.9	2,774.3	2.1152	4.4853	6.6005
1,000	179.9	0.001127	0.19322	0.1943	761.11	1,820.8	2,581.9	762.2	2,014.0	2,776.3	2.1367	4.4460	6.5827
1,100	184.1	0.001133	0.17631	0.1774	779.52	1,805.1	2,584.6	780.8	1,999.0	2,779.8	2.1771	4.3725	6.5495
1,200	187.9	0.001138	0.16209	0.1632	796.71	1,790.2	2,586.9	798.1	1,984.7	2,782.8	2.2145	4.3047	6.5191
1,300	191.6	0.001143	0.14998	0.1511	812.87	1,776.1	2,589.0	814.4	1,971.1	2,785.4	2.2493	4.2417	6.4910
1,400	195.0	0.001148	0.13956	0.1407	828.13	1,762.7	2,590.8	829.7	1,958.0	2,787.8	2.2820	4.1829	6.4649
1,500	198.3	0.001153	0.13050	0.1317	842.61	1,749.8	2,592.4	844.3	1,945.5	2,789.8	2.3127	4.1277	6.4405
1,600	201.4	0.001158	0.12254	0.1237	856.39	1,737.3	2,593.7	858.2	1,933.4	2,791.7	2.3418	4.0757	6.4176
1,700	204.3	0.001163	0.11549	0.1167	869.56	1,725.4	2,595.0	871.5	1,921.7	2,793.3	2.3695	4.0265	6.3960
1,800	207.1	0.001167	0.10918	0.1104	882.18	1,713.9	2,596.1	884.3	1,910.4	2,794.7	2.3958	3.9797	6.3755
1,900	209.8	0.001172	0.10351	0.1047	894.30	1,702.7	2,597.0	896.5	1,899.4	2,795.9	2.4210	3.9350	6.3559
2,000	212.4	0.001176	0.09839	0.0996	905.97	1,691.9	2,597.9	908.3	1,888.7	2,797.0	2.4450	3.8922	6.3372
2,250	218.4	0.001186	0.08751	0.0887	933.41	1,666.2	2,599.6	936.1	1,863.1	2,799.2	2.5012	3.7925	6.2936
2,500	223.9	0.001196	0.07873	0.0799	958.75	1,642.1	2,600.9	961.7	1,839.0	2,800.7	2.5525	3.7015	6.2540
2,750	229.1	0.001206	0.07147	0.0727	982.37	1,619.4	2,601.8	985.7	1,816.0	2,801.7	2.5997	3.6178	6.2176
3,000	233.8	0.001215	0.06538	0.0666	1,004.5	1,597.9	2,602.4	1,008.2	1,794.0	2,802.2	2.6437	3.5402	6.1839
3,250	238.3	0.001225	0.06028	0.0615	1,025.4	1,577.0	2,602.5	1,029.4	1,772.9	2,802.3	2.6848	3.4676	6.1524
3,500	242.5	0.001234	0.05594	0.0572	1,045.3	1,556.8	2,602.1	1,049.6	1,752.6	2,802.2	2.7234	3.3995	6.1229
3,750	246.5	0.001242	0.05208	0.0533	1,064.2	1,537.6	2,601.8	1,068.8	1,732.9	2,801.7	2.7600	3.3350	6.0950
4,000	250.3	0.001251	0.04864	0.0499	1,082.2	1,519.3	2,601.5	1,087.2	1,713.9	2,801.1	2.7947	3.2739	6.0686
5,000	263.9	0.001285	0.03811	0.0394	1,147.9	1,451.9	2,599.8	1,154.3	1,642.4	2,796.7	2.9186	3.0548	5.9734

(continued)

**TABLE C.7 (continued)**

Thermodynamic Properties of Steam: Pressure Table (SI Units)

$P_{\text{sat}}$ (kPa)	$T_{\text{sat}}$ (°C)	Specific Volume (m <sup>3</sup> /kg)			Internal Energy (kJ/kg)			Enthalpy (kJ/kg)			Entropy (kJ/kg K)		
		$v_f$	$v_{fg}$	$v_g$	$u_f$	$u_{fg}$	$u_g$	$h_f$	$h_{fg}$	$h_g$	$s_f$	$s_{fg}$	$s_g$
6,000	275.5	0.001319	0.03109	0.0324	1,205.6	1,390.4	2,596.0	1,213.5	1,576.9	2,790.5	3.0251	2.8655	5.8906
7,000	285.8	0.001352	0.02603	0.0274	1,257.8	1,333.5	2,591.3	1,267.2	1,515.7	2,782.9	3.1194	2.6965	5.8159
8,000	295.0	0.001385	0.02214	0.0235	1,305.9	1,265.8	2,571.7	1,317.0	1,442.9	2,759.9	3.2050	2.5421	5.7471
9,000	303.3	0.001418	0.01907	0.0205	1,351.0	1,209.3	2,560.3	1,363.7	1,380.9	2,744.7	3.2840	2.3981	5.6821
10,000	311.0	0.001452	0.01658	0.0180	1,393.7	1,153.8	2,547.5	1,408.2	1,319.5	2,727.7	3.3580	2.2616	5.6196
11,000	318.1	0.001489	0.01450	0.0160	1,434.6	1,098.6	2,533.1	1,451.0	1,258.0	2,709.0	3.4283	2.1305	5.5588
12,000	324.7	0.001527	0.01273	0.0143	1,474.0	1,043.3	2,517.3	1,492.4	1,196.0	2,688.4	3.4958	2.0028	5.4986
13,000	331.0	0.001568	0.01119	0.0128	1,512.4	987.6	2,499.9	1,532.8	1,133.1	2,665.8	3.5611	1.8771	5.4382
14,000	336.9	0.001612	0.00984	0.0114	1,549.8	931.1	2,480.9	1,572.4	1,068.8	2,641.2	3.6249	1.7520	5.3769
15,000	342.4	0.001661	0.00862	0.0103	1,586.6	873.4	2,460.0	1,611.5	1,002.8	2,614.3	3.6877	1.6265	5.3142
16,000	347.7	0.001715	0.00752	0.0092	1,626.1	810.1	2,436.2	1,653.6	930.4	2,584.0	3.7498	1.4996	5.2494
17,000	352.3	0.001769	0.00660	0.0084	1,660.2	750.3	2,410.5	1,690.3	862.5	2,552.8	3.8054	1.3819	5.1872
18,000	357.0	0.001839	0.00566	0.0075	1,698.6	680.8	2,379.4	1,731.7	782.6	2,514.3	3.8652	1.2481	5.1134
19,000	361.4	0.001926	0.00475	0.0067	1,740.1	603.6	2,343.6	1,776.7	693.9	2,470.5	3.9249	1.1063	5.0312
20,000	365.7	0.002037	0.00384	0.0059	1,785.8	515.1	2,300.9	1,826.6	591.9	2,418.5	3.9846	0.9568	4.9414
21,000	369.8	0.002208	0.00281	0.0050	1,839.7	401.7	2,241.4	1,886.0	460.8	2,346.8	4.0443	0.7681	4.8124
22,000	373.7	0.002623	0.00114	0.0038	1,944.6	174.0	2,118.6	2,002.3	199.0	2,201.3	4.1042	0.4563	4.5605
22,090	374.4	0.00315	0.00000	0.00315	2,029.6	0.0	2,029.6	2,099.3	0.0	2,099.3	4.4298	0.0	4.4298

Source: Properties obtained from software, *STEAMCALC*, John Wiley & Sons, New York, 1983; *Introduction to Thermal and Fluid Engineering*, CRC Table A.4, p. 904.



TABLE C.8

Thermodynamic Properties of Steam: Superheated Vapor Table (SI Units)

$P$ (kPa)	$T$ (°C)	$v$ (m <sup>3</sup> /kg)	$u$ (kJ/kg)	$h$ (kJ/kg)	$s$ (kJ/kg K)
10 ( $T_{\text{sat}} = 45.8^\circ\text{C}$ )					
	100	17.196	2516.2	2688.1	8.4498
	150	19.513	2588.2	2783.3	8.6893
	200	21.826	2661.2	2879.5	8.9040
	250	24.136	2735.5	2976.8	9.0996
	300	26.446	2811.2	3075.6	9.2799
	350	28.754	2888.3	3175.9	9.4476
	400	31.063	2967.1	3277.7	9.6048
	450	33.371	3047.4	3381.1	9.7530
	500	35.679	3129.4	3486.2	9.8935
	550	37.987	3213.1	3593.0	10.027
	600	40.295	3298.5	3701.5	10.155
	650	42.603	3385.7	3811.7	10.278
	700	44.911	3474.5	3923.7	10.396
	750	47.219	3565.2	4037.4	10.510
	800	49.526	3657.6	4152.9	10.620
	850	51.834	3751.8	4270.2	10.727
50 ( $T_{\text{sat}} = 81.3^\circ\text{C}$ )					
	100	3.4182	2512.0	2682.9	7.6959
	150	3.8894	2586.0	2780.5	7.9413
	200	4.3561	2659.8	2877.6	8.1583
	250	4.8206	2734.5	2975.6	8.3551
	300	5.2840	2810.5	3074.7	8.5360
	350	5.7468	2887.8	3175.1	8.7040
	400	6.2092	2966.6	3277.1	8.8614
	450	6.6715	3047.1	3380.6	9.0098
	500	7.1336	3129.1	3485.8	9.1504
	550	7.5956	3212.9	3592.6	9.2843
	600	8.0575	3298.3	3701.2	9.4123
	650	8.5193	3385.5	3811.4	9.5351
	700	8.9811	3474.4	3923.4	9.6532
	750	9.4428	3565.0	4037.2	9.7672
	800	9.9045	3657.5	4152.7	9.8775
	850	10.366	3751.7	4270.0	9.9843
100 ( $T_{\text{sat}} = 99.6^\circ\text{C}$ )					
	100	1.6956	2506.4	2676.0	7.3610
	150	1.9363	2583.1	2776.8	7.6146
	200	2.1724	2658.1	2875.3	7.8347
	250	2.4062	2733.3	2974.0	8.0329
	300	2.6388	2809.6	3073.5	8.2146
	350	2.8708	2887.1	3174.2	8.3831
	400	3.1025	2966.1	3276.4	8.5407
	450	3.3340	3046.6	3380.0	8.6893
	500	3.5654	3128.8	3485.3	8.8300
	550	3.7966	3212.5	3592.2	8.9640
	600	4.0277	3298.0	3700.8	9.0921
	650	4.2588	3385.2	3811.1	9.2149
	700	4.4898	3474.1	3923.1	9.3331
	750	4.7208	3564.8	4036.9	9.4471
	800	4.9518	3657.3	4152.4	9.5574
	850	5.1827	3751.5	4269.8	9.6643

TABLE C.8 (continued)

Thermodynamic Properties of Steam: Superheated Vapor Table (SI Units)

$P$ (kPa)	$T$ (°C)	$v$ (m <sup>3</sup> /kg)	$u$ (kJ/kg)	$h$ (kJ/kg)	$s$ (kJ/kg K)
101.32 ( $T_{\text{sat}} = 100.0^\circ\text{C}$ )					
	150	1.9109	2583.1	2776.7	7.6084
	200	2.1439	2658.0	2875.3	7.8286
	250	2.3747	2733.3	2973.9	8.0268
	300	2.6043	2809.6	3073.4	8.2085
	350	2.8334	2887.1	3174.2	8.3770
	400	3.0621	2966.1	3276.3	8.5347
	450	3.2905	3046.6	3380.0	8.6832
	500	3.5189	3128.7	3485.3	8.8240
	550	3.7471	3212.5	3592.2	8.9580
	600	3.9752	3298.0	3700.8	9.0860
	650	4.2033	3385.2	3811.1	9.2089
	700	4.4313	3474.1	3923.1	9.3271
	750	4.6593	3564.8	4036.9	9.4411
	800	4.8872	3657.3	4152.4	9.5513
	850	5.1152	3751.5	4269.8	9.6582
200 ( $T_{\text{sat}} = 120.2^\circ\text{C}$ )					
	150	0.9596	2577.2	2769.1	7.2804
	200	1.0804	2654.5	2870.6	7.5072
	250	1.1989	2730.9	2970.7	7.7084
	300	1.3162	2807.8	3071.1	7.8916
	350	1.4329	2885.8	3172.4	8.0610
	400	1.5492	2965.0	3274.9	8.2192
	450	1.6653	3045.7	3378.8	8.3682
	500	1.7813	3128.0	3484.3	8.5092
	550	1.8971	3211.9	3591.3	8.6434
	600	2.0129	3297.4	3700.0	8.7716
	650	2.1286	3384.7	3810.4	8.8945
	700	2.2442	3473.7	3922.5	9.0128
	750	2.3598	3564.4	4036.4	9.1268
	800	2.4754	3656.9	4152.0	9.2372
	850	2.5909	3751.1	4269.3	9.3441
300 ( $T_{\text{sat}} = 133.5^\circ\text{C}$ )					
	150	0.6338	2570.8	2760.9	7.0779
	200	0.7164	2650.8	2865.7	7.3122
	250	0.7965	2728.5	2967.4	7.5165
	300	0.8753	2806.1	3068.7	7.7014
	350	0.9535	2884.4	3170.5	7.8717
	400	1.0314	2963.9	3273.4	8.0305
	450	1.1091	3044.8	3377.6	8.1798
	500	1.1866	3127.2	3483.2	8.3211
	550	1.2639	3211.2	3590.4	8.4554
	600	1.3413	3296.9	3699.2	8.5838
	650	1.4185	3384.2	3809.7	8.7068
	700	1.4957	3473.2	3921.9	8.8252
	750	1.5728	3564.0	4035.8	8.9393
	800	1.6499	3656.5	4151.5	9.0497
	850	1.7270	3750.8	4268.9	9.1566

(continued)

TABLE C.8 (continued)

Thermodynamic Properties of Steam: Superheated Vapor Table (SI Units)

$P$ (kPa)	$T$ (°C)	$v$ (m <sup>3</sup> /kg)	$u$ (kJ/kg)	$h$ (kJ/kg)	$s$ (kJ/kg K)
400 ( $T_{\text{sat}} = 143.6^\circ\text{C}$ )					
	150	0.4707	2563.9	2752.2	6.9287
	200	0.5343	2647.0	2860.7	7.1712
	250	0.5952	2726.0	2964.1	7.3789
	300	0.6549	2804.3	3066.2	7.5655
	350	0.7139	2883.1	3168.6	7.7367
	400	0.7725	2962.9	3271.9	7.8961
	450	0.8309	3044.0	3376.3	8.0458
	500	0.8892	3126.5	3482.2	8.1873
	550	0.9474	3210.6	3589.5	8.3219
	600	1.0054	3296.3	3698.5	8.4504
	650	1.0635	3383.7	3809.0	8.5735
	700	1.1214	3472.7	3921.3	8.6919
	750	1.1793	3563.5	4035.3	8.8062
	800	1.2372	3656.1	4151.0	8.9166
	850	1.2951	3750.4	4268.4	9.0236
600 ( $T_{\text{sat}} = 158.8^\circ\text{C}$ )					
	200	0.3521	2639.0	2850.2	6.9669
	250	0.3939	2720.8	2957.2	7.1819
	300	0.4344	2800.6	3061.3	7.3719
	350	0.4742	2880.3	3164.8	7.5451
	400	0.5136	2960.7	3268.9	7.7057
	450	0.5528	3042.2	3373.8	7.8562
	500	0.5919	3125.0	3480.1	7.9982
	550	0.6308	3209.3	3587.7	8.1332
	600	0.6696	3295.1	3696.9	8.2619
	650	0.7084	3382.6	3807.7	8.3853
	700	0.7471	3471.8	3920.1	8.5039
	750	0.7858	3562.7	4034.2	8.6182
	800	0.8245	3655.3	4150.0	8.7287
	850	0.8631	3749.7	4267.6	8.8358
800 ( $T_{\text{sat}} = 170.4^\circ\text{C}$ )					
	200	0.2608	2630.4	2839.1	6.8156
	250	0.2932	2715.5	2950.1	7.0388
	300	0.3241	2796.9	3056.2	7.2326
	350	0.3544	2877.5	3161.0	7.4079
	400	0.3842	2958.5	3265.8	7.5697
	450	0.4137	3040.4	3371.4	7.7209
	500	0.4432	3123.5	3478.0	7.8635
	550	0.4725	3208.0	3586.0	7.9988
	600	0.5017	3294.0	3695.4	8.1278
	650	0.5309	3381.6	3806.3	8.2514
	700	0.5600	3470.9	3918.9	8.3702
	750	0.5891	3561.9	4033.1	8.4846
	800	0.6181	3654.6	4149.1	8.5953
	850	0.6471	3749.0	4266.7	8.7024

TABLE C.8 (continued)

Thermodynamic Properties of Steam: Superheated Vapor Table (SI Units)

$P$ (kPa)	$T$ (°C)	$v$ (m <sup>3</sup> /kg)	$u$ (kJ/kg)	$h$ (kJ/kg)	$s$ (kJ/kg K)
1000 ( $T_{\text{sat}} = 179.9^\circ\text{C}$ )					
	200	0.2059	2621.4	2827.3	6.6930
	250	0.2328	2710.0	2942.8	6.9251
	300	0.2580	2793.1	3051.1	7.1229
	350	0.2824	2874.7	3157.1	7.3003
	400	0.3065	2956.3	3262.7	7.4633
	450	0.3303	3038.5	3368.8	7.6154
	500	0.3540	3121.9	3475.9	7.7585
	550	0.3775	3206.6	3584.2	7.8942
	600	0.4010	3292.8	3693.8	8.0235
	650	0.4244	3380.6	3805.0	8.1473
	700	0.4477	3470.0	3917.7	8.2662
	750	0.4710	3561.0	4032.0	8.3808
	800	0.4943	3653.8	4148.1	8.4916
	850	0.5175	3748.3	4265.8	8.5988
1500 ( $T_{\text{sat}} = 198.3^\circ\text{C}$ )					
	250	0.15199	2695.4	2923.4	6.7093
	300	0.16971	2783.3	3037.8	6.9183
	350	0.18654	2867.4	3147.2	7.1014
	400	0.20292	2950.6	3255.0	7.2677
	450	0.21906	3034.0	3362.5	7.4219
	500	0.23503	3118.1	3470.6	7.5664
	550	0.25089	3203.3	3579.7	7.7030
	600	0.26666	3289.9	3689.9	7.8331
	650	0.28237	3378.0	3801.5	7.9574
	700	0.29803	3467.6	3914.7	8.0767
	750	0.31364	3558.9	4029.4	8.1917
	800	0.32921	3651.8	4145.7	8.3027
	850	0.34475	3746.5	4263.6	8.4101
2000 ( $T_{\text{sat}} = 212.4^\circ\text{C}$ )					
	250	0.11145	2679.5	2902.4	6.5451
	300	0.12550	2772.9	3023.9	6.7671
	350	0.13856	2860.0	3137.1	6.9565
	400	0.15113	2944.8	3247.1	7.1263
	450	0.16343	3029.3	3356.1	7.2826
	500	0.17556	3114.2	3465.3	7.4286
	550	0.18757	3200.0	3575.1	7.5662
	600	0.19950	3287.0	3686.0	7.6970
	650	0.21137	3375.4	3798.1	7.8218
	700	0.22318	3465.3	3911.6	7.9416
	750	0.23494	3556.8	4026.7	8.0569
	800	0.24667	3649.9	4143.2	8.1681
	850	0.25836	3744.7	4261.5	8.2758

TABLE C.8 (continued)

Thermodynamic Properties of Steam: Superheated Vapor Table (SI Units)

$P$ (kPa)	$T$ (°C)	$v$ (m <sup>3</sup> /kg)	$u$ (kJ/kg)	$h$ (kJ/kg)	$s$ (kJ/kg K)
2500 ( $T_{\text{sat}} = 223.9^{\circ}\text{C}$ )					
	250	0.08699	2662.2	2879.7	6.4076
	300	0.09893	2762.0	3009.3	6.6446
	350	0.10975	2852.2	3126.6	6.8409
	400	0.12004	2938.9	3239.1	7.0145
	450	0.13005	3024.6	3349.7	7.1730
	500	0.13987	3110.3	3459.9	7.3205
	550	0.14958	3196.6	3570.6	7.4592
	600	0.15921	3284.1	3682.1	7.5906
	650	0.16876	3372.8	3794.7	7.7161
	700	0.17827	3462.9	3908.6	7.8362
	750	0.18772	3554.6	4024.0	7.9518
	800	0.19714	3648.0	4140.8	8.0633
	850	0.20653	3742.9	4259.3	8.1712
3000 ( $T_{\text{sat}} = 233.8^{\circ}\text{C}$ )					
	250	0.07055	2643.2	2854.9	6.2855
	300	0.08116	2750.6	2994.1	6.5399
	350	0.09053	2844.3	3115.9	6.7437
	400	0.09931	2932.9	3230.9	6.9213
	450	0.10779	3019.8	3343.1	7.0822
	500	0.11608	3106.3	3454.5	7.2312
	550	0.12426	3193.2	3566.0	7.3709
	600	0.13234	3281.1	3678.1	7.5031
	650	0.14036	3370.2	3791.3	7.6291
	700	0.14832	3460.6	3905.6	7.7497
	750	0.15624	3552.5	4021.2	7.8656
	800	0.16412	3646.0	4138.4	7.9774
	850	0.17197	3741.1	4257.1	8.0855
4000 ( $T_{\text{sat}} = 250.3^{\circ}\text{C}$ )					
	300	0.058835	2725.8	2961.2	6.3622
	350	0.066448	2827.6	3093.4	6.5835
	400	0.073377	2920.6	3214.1	6.7699
	450	0.079959	3010.0	3329.8	6.9358
	500	0.086343	3098.2	3443.6	7.0879
	550	0.092599	3186.4	3556.8	7.2298
	600	0.098764	3275.2	3670.2	7.3636
	650	0.10486	3364.9	3784.3	7.4907
	700	0.11090	3455.9	3899.5	7.6121
	750	0.11690	3548.2	4015.8	7.7287
	800	0.12285	3642.1	4133.5	7.8411
	850	0.12878	3737.6	4252.7	7.9496

TABLE C.8 (continued)

Thermodynamic Properties of Steam: Superheated Vapor Table (SI Units)

$P$ (kPa)	$T$ (°C)	$v$ (m <sup>3</sup> /kg)	$u$ (kJ/kg)	$h$ (kJ/kg)	$s$ (kJ/kg K)
5000 ( $T_{\text{sat}} = 263.9^{\circ}\text{C}$ )					
	300	0.045302	2698.2	2924.7	6.2085
	350	0.051943	2809.9	3069.6	6.4512
	400	0.057792	2907.7	3196.6	6.6474
	450	0.063252	3000.0	3316.2	6.8188
	500	0.068495	3090.0	3432.5	6.9743
	550	0.073603	3179.5	3547.5	7.1184
	600	0.078617	3269.2	3662.3	7.2538
	650	0.083560	3359.6	3777.4	7.3820
	700	0.088447	3451.1	3893.4	7.5044
	750	0.093289	3543.9	4010.4	7.6216
	800	0.098094	3638.2	4128.7	7.7345
	850	0.102867	3734.0	4248.3	7.8435
6000 ( $T_{\text{sat}} = 275.6^{\circ}\text{C}$ )					
	300	0.036146	2667.1	2884.0	6.0669
	350	0.042223	2790.9	3044.2	6.3354
	400	0.047380	2894.3	3178.6	6.5429
	450	0.052104	2989.7	3302.3	6.7202
	500	0.056592	3081.7	3421.3	6.8793
	550	0.060937	3172.5	3538.1	7.0258
	600	0.065185	3263.1	3654.2	7.1627
	650	0.069360	3354.3	3770.4	7.2922
	700	0.073479	3446.4	3887.2	7.4154
	750	0.077552	3539.6	4004.9	7.5333
	800	0.081588	3634.3	4123.8	7.6467
	850	0.085592	3730.4	4243.9	7.7562
7000 ( $T_{\text{sat}} = 285.8^{\circ}\text{C}$ )					
	300	0.029459	2631.9	2838.1	5.9299
	350	0.035234	2770.6	3017.2	6.2301
	400	0.039922	2880.4	3159.8	6.4504
	450	0.044132	2979.1	3288.1	6.6343
	500	0.048087	3073.2	3409.8	6.7971
	550	0.051890	3165.4	3528.6	6.9460
	600	0.055591	3257.0	3646.1	7.0846
	650	0.059218	3348.9	3763.4	7.2153
	700	0.062788	3441.6	3881.1	7.3394
	750	0.066312	3535.3	3999.5	7.4580
	800	0.069798	3630.3	4118.9	7.5720
	850	0.073253	3726.7	4239.5	7.6818

Source: *Introduction to Thermal and Fluid Engineering*, CRC Table A.5, p. 907.



TABLE C.9  
Combustion Data for Hydrocarbons (Metric and English Units)

Hydrocarbon	Formula	Higher Heating Value (Vapor)		Theor. Air/ Fuel Ratio (by mass)	Max Flame Speed		Adiabatic Flame Temp (in Air)		Ignition Temp (in Air)		Flash Point		Flammability Limits (in Air) (% by volume)	
		kJ/kg	Btu/lbm		m/s	ft/s	°C	°F	°C	°F	°C	°F	°C	°F
Paraffins or alkanes														
Methane	CH <sub>4</sub>	55,533	23,875	17.195	0.34	1.1	1,918	3,484	705	1,301	Gas	Gas	5.0	15.0
Ethane	C <sub>2</sub> H <sub>6</sub>	51,923	22,323	15.899	0.40	1.3	1,949	3,540	520–630	968–1,166	Gas	Gas	3.0	12.5
Propane	C <sub>3</sub> H <sub>8</sub>	50,402	21,669	15.246	0.40	1.3	1,967	3,573	466	871	Gas	Gas	2.1	10.1
Isobutane	C <sub>4</sub> H <sub>10</sub>	49,593	21,321	14.984	0.37	1.2	1,973	3,583	405	761	–60	–76	1.86	8.41
Isobutane	C <sub>4</sub> H <sub>10</sub>	49,476	21,271	14.984	0.37	1.2	1,973	3,583	462	864	–83	–117	1.80	8.44
Isopentane	C <sub>5</sub> H <sub>12</sub>	49,067	21,095	15.323	0.40	1.3	2,232	4,050	309	588	< –40	< –40	1.40	7.80
Isopentane	C <sub>5</sub> H <sub>12</sub>	48,955	21,047	15.323	0.37	1.2	2,235	4,055	420	788	< –51	< –60	1.32	9.16
Neopentane	C <sub>5</sub> H <sub>12</sub>	48,795	20,978	15.323	0.34	1.1	2,238	4,060	450	842	Gas	Gas	1.38	7.22
Neohexane	C <sub>6</sub> H <sub>14</sub>	48,767	20,966	15.238	0.40	1.3	2,221	4,030	248	478	–22	–7	1.25	7.00
Neohexane	C <sub>6</sub> H <sub>14</sub>	48,686	20,931	15.238	0.37	1.2	2,235	4,055	425	797	–48	–54	1.19	7.58
Isopentane	C <sub>7</sub> H <sub>16</sub>	48,506	20,854	15.141	0.40	1.3	2,196	3,985	223	433	–4	25	1.00	6.00
Isopentane	C <sub>7</sub> H <sub>16</sub>	48,437	20,824	15.141	0.37	1.2	2,224	4,035	454	849	—	—	1.08	6.69
Isopentane	C <sub>8</sub> H <sub>18</sub>	48,371	20,796	15.093	—	—	—	—	220	428	13	56	0.95	3.20
Isopentane	C <sub>8</sub> H <sub>18</sub>	48,311	20,770	15.093	0.34	1.1	—	—	447	837	–12	10	0.76	5.94
Olefins or alkenes														
Ethylene	C <sub>2</sub> H <sub>4</sub>	50,325	21,636	14.807	0.67	2.2	2,343	4,250	490	914	Gas	Gas	2.75	28.6
Propylene	C <sub>3</sub> H <sub>6</sub>	48,958	21,048	14.807	0.43	1.4	2,254	4,090	458	856	gas	gas	2.00	11.1
Butylene	C <sub>4</sub> H <sub>8</sub>	48,506	20,854	14.807	0.43	1.4	2,221	4,030	443	829	Gas	Gas	1.98	9.65
Isobutylene	C <sub>4</sub> H <sub>8</sub>	48,234	20,737	14.807	0.37	1.2	—	—	465	869	Gas	Gas	1.80	9.00
Isopentene	C <sub>5</sub> H <sub>10</sub>	48,195	20,720	14.807	0.43	1.4	2,296	4,165	298	569	—	—	1.65	7.70
Aromatics														
Benzene	C <sub>6</sub> H <sub>6</sub>	42,296	18,184	13.297	0.40	1.3	2,266	4,110	562	1,044	–11	12	1.35	6.65
Toluene	C <sub>7</sub> H <sub>8</sub>	43,033	18,501	13.503	0.37	1.2	2,232	4,050	536	997	4	40	1.27	6.75
p-Xylene	C <sub>8</sub> H <sub>10</sub>	43,410	18,663	13.663	—	—	2,210	4,010	464	867	17	63	1.00	6.00
Other hydrocarbons														
Acetylene	C <sub>2</sub> H <sub>2</sub>	50,014	21,502	13.297	1.40	4.6	2,632	4,770	406–440	763–824	Gas	Gas	2.50	81.0
Naphthalene	C <sub>10</sub> H <sub>8</sub>	40,247	17,303	12.932	—	—	2,260	4,100	515	959	79	174	0.90	5.9

Source: Created from Multiple Sources.

TABLE C.10

Chemical, Physical, and Thermal Properties of Gases: Gases and Vapors, Including Fuels and Refrigerants, English and Metric Units

Common Name(s)	Acetylene (Ethyne)	Butadiene	<i>n</i> -Butane	Isobutane (2-Methyl Propane)
Chemical Formula	C <sub>2</sub> H <sub>2</sub>	C <sub>4</sub> H <sub>6</sub>	C <sub>4</sub> H <sub>10</sub>	C <sub>4</sub> H <sub>10</sub>
Refrigerant Number	—	—	600	600a
Chemical and physical properties				
Molecular weight	26.04	54.09	58.12	58.12
Specific gravity, air = 1	0.90	1.87	2.07	2.07
Specific volume, ft <sup>3</sup> /lb	14.9	7.1	6.5	6.5
Specific volume, m <sup>3</sup> /kg	0.93	0.44	0.405	0.418
Density of liquid (at atm bp), lb/ft <sup>3</sup>	43.0		37.5	37.2
Density of liquid (at atm bp), kg/m <sup>3</sup>	693.		604.	599.
Vapor pressure at 25°C, psia			35.4	50.4
Vapor pressure at 25°C, MN/m <sup>2</sup>			0.024 4	0.347
Viscosity (abs), lbm/ft·s	6.72 × 10 <sup>-6</sup>		4.8 × 10 <sup>-6</sup>	
Viscosity (abs), centipoises <sup>a</sup>	0.01		0.007	
Sound velocity in gas, m/s	343	226	216	216
Thermal and thermo dynamic properties				
Specific heat, <i>c<sub>p</sub></i> , Btu/lb·°F or cal/g·°C	0.40	0.341	0.39	0.39
Specific heat, <i>c<sub>p</sub></i> , J/kg·K	1 674.	1 427.	1 675.	1 630.
Specific heat ratio, <i>c<sub>p</sub></i> / <i>c<sub>v</sub></i>	1.25	1.12	1.096	1.10
Gas constant <i>R</i> , ft lb/lb·°R	59.3	28.55	26.56	26.56
Gas constant <i>R</i> , J/kg·°C	319	154.	143.	143.
Thermal conductivity, Btu/h·ft·°F	0.014		0.01	0.01
Thermal conductivity, W/m °C	0.024		0.017	0.017
Boiling point (sat 14.7 psia), °F	-103	24.1	31.2	10.8
Boiling point (sat 760 mm), °C	-75	-4.5	-0.4	-11.8
Latent heat of evap. (at bp), Btu/lb	264		165.6	157.5
Latent heat of evap. (at bp), J/kg	614 000		386 000	366 000
Freezing (melting) point, °F (1 atm)	-116	-164.	-217.	-229
Freezing (melting) point, °C (1 atm)	-82.2	-109.	-138	-145
Latent heat of fusion, Btu/lb	23.		19.2	
Latent heat of fusion, J/kg	53 500		44 700	
Critical temperature, °F	97.1		306	273.
Critical temperature, °C	36.2	171.	152.	134.
Critical pressure, psia	907.	652.	550.	537.
Critical pressure, MN/m <sup>2</sup>	6.25		3.8	3.7
Critical volume, ft <sup>3</sup> /lb			0.070	
Critical volume, m <sup>3</sup> /kg			0.004 3	
Flammable (yes or no)	Yes	Yes	Yes	Yes
Heat of combustion, Btu/ft <sup>3</sup>	1 450	2 950	3 300	3 300
Heat of combustion, Btu/lb	21 600	20 900	21 400	21 400
Heat of combustion, kJ/kg	50 200	48 600	49 700	49 700

(continued)

TABLE C.10 (continued)

Chemical, Physical, and Thermal Properties of Gases: Gases and Vapors, Including Fuels and Refrigerants, English and Metric Units

Common Name(s)	1-Butene (Butylene)	<i>cis</i> -2-Butene	<i>trans</i> -2-Butene	Isobutene
Chemical Formula	C <sub>4</sub> H <sub>8</sub>	C <sub>4</sub> H <sub>8</sub>	C <sub>4</sub> H <sub>8</sub>	C <sub>4</sub> H <sub>8</sub>
Refrigerant Number	—	—	—	—
Chemical and physical properties				
Molecular weight	56.108	56.108	56.108	56.108
Specific gravity, air = 1	1.94	1.94	1.94	1.94
Specific volume, ft <sup>3</sup> /lb	6.7	6.7	6.7	6.7
Specific volume, m <sup>3</sup> /kg	0.42	0.42	0.42	0.42
Density of liquid (at atm bp), lb/ft <sup>3</sup>				
Density of liquid (at atm bp), kg/m <sup>3</sup>				
Vapor pressure at 25°C, psia				
Vapor pressure at 25°C, MN/m <sup>2</sup>				
Viscosity (abs), lbm/ft·s				
Viscosity (abs), centipoises <sup>a</sup>				
Sound velocity in gas, m/s	222	223.	221.	221.
Thermal and thermodynamic properties				
Specific heat, <i>c<sub>p</sub></i> , Btu/lb·°F or cal/g·°C	0.36	0.327	0.365	0.37
Specific heat, <i>c<sub>p</sub></i> , J/kg K	1 505.	1 368.	1 527.	1 548.
Specific heat ratio, <i>c<sub>p</sub></i> / <i>c<sub>v</sub></i>	1.112	1.121	1.107	1.10
Gas constant <i>R</i> , ft lb/lb·°F	27.52			
Gas constant <i>R</i> , J/kg·°C	148.			
Thermal conductivity, Btu/h ft °F				
Thermal conductivity, W/m °C				
Boiling point (sat 14.7 psia), °F	20.6	38.6	33.6	19.2
Boiling point (sat 760 mm), °C	−6.3	3.7	0.9	−7.1
Latent heat of evap. (at bp), Btu/lb	167.9	178.9	174.4	169.
Latent heat of evap. (at bp), J/kg	391 000	416 000.	406 000.	393 000.
Freezing (melting) point, °F (1 atm)	−301.6	−218.	−158.	
Freezing (melting) point, °C (1 atm)	−185.3	−138.9	−105.5	
Latent heat of fusion, Btu/lb	16.4	31.2	41.6	25.3
Latent heat of fusion, J/kg	38 100	72 600.	96 800.	58 800.
Critical temperature, °F	291.			
Critical temperature, °C	144.	160.	155.	
Critical pressure, psia	621.	595.	610.	
Critical pressure, MN/m <sup>2</sup>	4.28	4.10	4.20	
Critical volume, ft <sup>3</sup> /lb	0.068			
Critical volume, m <sup>3</sup> /kg	0.004 2			
Flammable (yes or no)	Yes	Yes	Yes	Yes
Heat of combustion, Btu/ft <sup>3</sup>	3 150	3 150.	3 150.	3 150.
Heat of combustion, Btu/lb	21 000	21 000.	21 000.	21 000.
Heat of combustion, kJ/kg	48 800	48 800.	48 800.	48 800.



TABLE C.10 (continued)

Chemical, Physical, and Thermal Properties of Gases: Gases and Vapors, Including Fuels and Refrigerants, English and Metric Units

Common Name(s)	Carbon Dioxide	Carbon Monoxide	Ethane	Ethylene (Ethene)
Chemical Formula	CO <sub>2</sub>	CO	C <sub>2</sub> H <sub>6</sub>	C <sub>2</sub> H <sub>4</sub>
Refrigerant Number	744	—	170	1150
Chemical and physical properties				
Molecular weight	44.01	28.011	30.070	28.054
Specific gravity, air = 1	1.52	0.967	1.04	0.969
Specific volume, ft <sup>3</sup> /lb	8.8	14.0	13.025	13.9
Specific volume, m <sup>3</sup> /kg	0.55	0.874	0.815	0.87
Density of liquid (at atm bp), lb/ft <sup>3</sup>	—	—	28.	35.5
Density of liquid (at atm bp), kg/m <sup>3</sup>	—	—	449.	569.
Vapor pressure at 25°C, psia	931.	—	—	—
Vapor pressure at 25°C, MN/m <sup>2</sup>	6.42	—	—	—
Viscosity (abs), lbm/ft s	9.4 × 10 <sup>-6</sup>	12.1 × 10 <sup>-6</sup>	64. × 10 <sup>-6</sup>	6.72 × 10 <sup>-6</sup>
Viscosity (abs), centipoises <sup>a</sup>	0.014	0.018	0.095	0.010
Sound velocity in gas, m/s	270.	352.	316.	331.
Thermal and thermodynamic properties				
Specific heat, c <sub>p</sub> , Btu/lb °F or cal/g °C	0.205	0.25	0.41	0.37
Specific heat, c <sub>p</sub> , J/kg K	876.	1 046.	1 715.	1 548.
Specific heat ratio, c <sub>p</sub> /c <sub>v</sub>	1.30	1.40	1.20	1.24
Gas constant R, ft lb/lb·°F	35.1	55.2	51.4	55.1
Gas constant R, J/kg·°C	189.	297.	276.	296.
Thermal conductivity, Btu/h ft °F	0.01	0.014	0.010	0.010
Thermal conductivity, W/m °C	0.017	0.024	0.017	0.017
Boiling point (sat 14.7 psia), °F	-109.4 <sup>b</sup>	-312.7	-127.	-155.
Boiling point (sat 760 mm), °C	-78.5	-191.5	-88.3	-103.8
Latent heat of evap. (at bp), Btu/lb	246.	92.8	210.	208.
Latent heat of evap. (at bp), J/kg	572 000.	216 000.	488 000.	484 000.
Freezing (melting) point, °F (1 atm)	—	-337.	-278.	-272.
Freezing (melting) point, °C (1 atm)	—	-205.	-172.2	-169.
Latent heat of fusion, Btu/lb	—	12.8	41.	51.5
Latent heat of fusion, J/kg	—	—	95 300.	120 000.
Critical temperature, °F	88.	-220.	90.1	49.
Critical temperature, °C	31.	-140.	32.2	9.5
Critical pressure, psia	1 072.	507.	709.	741.
Critical pressure, MN/m <sup>2</sup>	7.4	3.49	4.89	5.11
Critical volume, ft <sup>3</sup> /lb	—	0.053	0.076	0.073
Critical volume, m <sup>3</sup> /kg	—	0.003 3	0.004 7	0.004 6
Flammable (yes or no)	No	Yes	Yes	Yes
Heat of combustion, Btu/ft <sup>3</sup>	—	310.	—	1 480.
Heat of combustion, Btu/lb	—	4 340.	22 300.	20 600.
Heat of combustion, kJ/kg	—	10 100.	51 800.	47 800.

(continued)

TABLE C.10 (continued)

Chemical, Physical, and Thermal Properties of Gases: Gases and Vapors, Including Fuels and Refrigerants, English and Metric Units

Common Name(s)	Hydrogen	Methane	Nitric Oxide	Nitrogen
Chemical Formula	H <sub>2</sub>	CH <sub>4</sub>	NO	N <sub>2</sub>
Refrigerant Number	702	50	—	728
Chemical and physical properties				
Molecular weight	2.016	16.044	30.006	28.013 4
Specific gravity, air = 1	0.070	0.554	1.04	0.967
Specific volume, ft <sup>3</sup> /lb	194.	24.2	13.05	13.98
Specific volume, m <sup>3</sup> /kg	12.1	1.51	0.814	0.872
Density of liquid (at atm bp), lb/ft <sup>3</sup>	4.43	26.3		50.46
Density of liquid (at atm bp), kg/m <sup>3</sup>	71.0	421.		808.4
Vapor pressure at 25°C, psia				
Vapor pressure at 25°C, MN/m <sup>2</sup>				
Viscosity (abs), lbm/ft-s	6.05 × 10 <sup>-6</sup>	7.39 × 10 <sup>-6</sup>	12.8 × 10 <sup>-6</sup>	12.1 × 10 <sup>-6</sup>
Viscosity (abs), centipoises <sup>a</sup>	0.009	0.011	0.019	0.018
Sound velocity in gas, m/s	1 315.	446.	341.	353.
Thermal and thermo dynamic properties				
Specific heat, <i>c<sub>p</sub></i> , Btu/lb·°F or cal/g·°C	3.42	0.54	0.235	0.249
Specific heat, <i>c<sub>p</sub></i> , J/kg·K	14 310.	2 260.	983.	1 040.
Specific heat ratio, <i>c<sub>p</sub></i> / <i>c<sub>v</sub></i>	1.405	1.31	1.40	1.40
Gas constant <i>R</i> , ft lb/lb·°F	767.	96.	51.5	55.2
Gas constant <i>R</i> , J/kg·°C	4 126.	518.	277.	297.
Thermal conductivity, Btu/h-ft·°F	0.105	0.02	0.015	0.015
Thermal conductivity, W/m·°C	0.018 2	0.035	0.026	0.026
Boiling point (sat 14.7 psia), °F	-423.	-259.	-240.	-320.4
Boiling point (sat 760 mm), °C	20.4 K	-434.2	-151.5	-195.8
Latent heat of evap. (at bp), Btu/lb	192.	219.2		85.5
Latent heat of evap. (at bp), J/kg	447 000.	510 000.		199 000.
Freezing (melting) point, °F (1 atm)	-434.6	-296.6	-258.	-346.
Freezing (melting) point, °C (1 atm)	-259.1	-182.6	-161.	-210.
Latent heat of fusion, Btu/lb	25.0	14.	32.9	11.1
Latent heat of fusion, J/kg	58 000.	32 600.	76 500.	25 800.
Critical temperature, °F	-399.8	-116.	-136.	-232.6
Critical temperature, °C	-240.0	-82.3	-93.3	-147.
Critical pressure, psia	189.	673.	945.	493.
Critical pressure, MN/m <sup>2</sup>	1.30	4.64	6.52	3.40
Critical volume, ft <sup>3</sup> /lb	0.53	0.099	0.033 2	0.051
Critical volume, m <sup>3</sup> /kg	0.033	0.006 2	0.002 07	0.003 18
Flammable (yes or no)	Yes	Yes	No	No
Heat of combustion, Btu/ft <sup>3</sup>	320.	985.	—	—
Heat of combustion, Btu/lb	62 050.	2 2900.	—	—
Heat of combustion, kJ/kg	144 000.		—	—

(continued)

TABLE C.10 (continued)

Chemical, Physical, and Thermal Properties of Gases: Gases and Vapors, Including Fuels and Refrigerants, English and Metric Units

Common Name(s)	Nitrous Oxide	Oxygen	Propane	Propylene (Propene)
Chemical Formula	N <sub>2</sub> O	O <sub>2</sub>		C <sub>3</sub> H <sub>6</sub>
Refrigerant Number	744A	732	290	1270
Chemical and physical properties				
Molecular weight	44.012	31.998 8	44.097	42.08
Specific gravity, air = 1	1.52	1.105	1.52	1.45
Specific volume, ft <sup>3</sup> /lb	8.90	12.24	8.84	9.3
Specific volume, m <sup>3</sup> /kg	0.555	0.764	0.552	0.58
Density of liquid (at atm bp), lb/ft <sup>3</sup>	76.6	71.27	36.2	37.5
Density of liquid (at atm bp), kg/m <sup>3</sup>	1 227.	1 142.	580.	601.
Vapor pressure at 25°C, psia			135.7	166.4
Vapor pressure at 25°C, MN/m <sup>2</sup>			0.936	1.147
Viscosity (abs), lbm/ft s	10.1 × 10 <sup>-6</sup>	13.4 × 10 <sup>-6</sup>	53.8 × 10 <sup>-6</sup>	57.1 × 10 <sup>-6</sup>
Viscosity (abs), centipoises <sup>a</sup>	0.015	0.020	0.080	0.085
Sound velocity in gas, m/s	268.	329.	253.	261.
Thermal and thermodynamic properties				
Specific heat, $c_p$ , Btu/lb·°F				
or cal/g·°C	0.21	0.220	0.39	0.36
Specific heat, $c_p$ , J/kg·K	879.	920.	1 630.	1 506.
Specific heat ratio, $c_p/c_v$	1.31	1.40	1.2	1.16
Gas constant $R$ , ft lb/lb·°F	35.1	48.3	35.0	36.7
Gas constant $R$ , J/kg·°C	189.	260.	188.	197.
Thermal conductivity, Btu/h·ft·°F	0.010	0.015	0.010	0.010
Thermal conductivity, W/m °C	0.017	0.026	0.017	0.017
Boiling point (sat 14.7 psia), °F	-127.3	-297.3	-44.	-54.
Boiling point (sat 760 mm), °C	-88.5	-182.97	-42.2	-48.3
Latent heat of evap. (at bp), Btu/lb	161.8	91.7	184.	188.2
Latent heat of evap. (at bp), J/kg	376 000.	213 000.	428 000.	438 000.
Freezing (melting) point, °F (1 atm)	-131.5	-361.1	-309.8	-301.
Freezing (melting) point, °C (1 atm)	-90.8	-218.4	-189.9	-185.
Latent heat of fusion, Btu/lb	63.9	5.9	19.1	
Latent heat of fusion, J/kg	149 000.	13 700.	44 400.	
Critical temperature, °F	97.7	-181.5	205.	197.
Critical temperature, °C	36.5	-118.6	96.	91.7
Critical pressure, psia	1 052.	726.	618.	668.
Critical pressure, MN/m <sup>2</sup>	7.25	5.01	4.26	4.61
Critical volume, ft <sup>3</sup> /lb	0.036	0.040	0.073	0.069
Critical volume, m <sup>3</sup> /kg	0.002 2	0.002 5	0.004 5	0.004 3
Flammable (yes or no)	No	No	Yes	Yes
Heat of combustion, Btu/ft <sup>3</sup>	—	—	2 450.	2 310.
Heat of combustion, Btu/lb	—	—	21 660.	21 500.
Heat of combustion, kJ/kg	—	—	50 340.	50 000.

Source: *The CRC Press Handbook of Thermal Engineering*, CRC Press, Boca Raton, FL, 2000; *JZ Handbook*, 1st edn., Table B.4, p. 719.

Note: The properties of pure gases are given at 25°C (77°F, 298 K) and atmospheric pressure (except as stated).

<sup>a</sup> For N·s/m<sup>2</sup> divide by 1000.



TABLE C.11

Burning Velocities of Various Fuels

	$\phi = 0.7$	$\phi = 0.8$	$\phi = 0.9$	$\phi = 1.0$	$\phi = 1.1$	$\phi = 1.2$	$\phi = 1.3$	$\phi = 1.4$	$S_{\max}$	$\phi$ at $S_{\max}$
Saturated hydrocarbons										
Ethane	30.6	36.0	40.6	44.5	47.3	47.3	44.4	37.4	47.6	1.14
Propane			42.3	45.6	46.2	42.4	34.3		46.4	1.06
<i>n</i> -Butane		38.0	42.6	44.8	44.2	41.2	34.4	25.0	44.9	1.03
Methane		30.0	38.3	43.4	44.7	39.8	31.2		44.8	1.08
<i>n</i> -Pentane		35.0	40.5	42.7	42.7	39.3	33.9		43.0	1.05
<i>n</i> -Heptane		37.0	39.8	42.2	42.0	35.5	29.4		42.8	1.05
2,2,4-Trimethylpentane		37.5	40.2	41.0	37.2	31.0	23.5		41.0	0.98
2,2,3-Trimethylpentane		37.8	39.5	40.1	39.5	36.2			40.1	1.00
2,2-Dimethylbutane		33.5	38.3	39.9	37.0	33.5			40.0	0.98
Isopentane		33.0	37.6	39.8	38.4	33.4	24.8		39.9	1.01
2,2-Dimethylpropane			31.0	34.8	36.0	35.2	33.5	31.2	36.0	1.10
Unsaturated hydrocarbons										
Acetylene		107	130	144	151	154	154	152	155	1.25
Ethylene	37.0	50.0	60.0	68.0	73.0	72.0	66.5	60.0	73.5	1.13
Propyne		62.0	66.6	70.2	72.2	71.2	61.0		72.5	1.14
1,3-Butadiene			42.6	49.6	55.0	57.0	56.9	55.4	57.2	1.23
<i>n</i> -1-Heptyne		46.8	50.7	52.3	50.9	47.4	41.6		52.3	1.00
Propylene			48.4	51.2	49.9	46.4	40.8		51.2	1.00
<i>n</i> -2-Pentene		35.1	42.6	47.8	46.9	42.6	34.9		48.0	1.03
2,2,4-Trimethyl-3-pentene		34.6	41.3	42.2	37.4	33.0			42.5	0.98
Substituted alkyls										
Methanol		34.5	42.0	48.0	50.2	47.5	44.4	42.2	50.4	1.08
Isopropyl alcohol		34.4	39.2	41.3	40.6	38.2	36.0	34.2	41.4	1.04
Triethylamine		32.5	36.7	38.5	38.7	36.2	28.6		38.8	1.06
<i>n</i> -Butyl chloride	24.0	30.7	33.8	34.5	32.5	26.9	20.0		34.5	1.00
Allyl chloride	30.6	33.0	33.7	32.4	29.6				33.8	0.89
Isopropyl mercaptan		30.0	33.5	33.0	26.6				33.8	0.44
Ethylamine		28.7	31.4	32.4	31.8	29.4	25.3		32.4	1.00
Isopropylamine		27.0	29.5	30.6	29.8	27.7			30.6	1.01
<i>n</i> -Propyl chloride		24.7	28.3	27.5	24.1				28.5	0.93
Isopropyl chloride		24.8	27.0	27.4	25.3				27.6	0.97
<i>n</i> -Propyl bromide	No ignition									
Silanes										
Tetramethylsilane	39.5	49.5	57.3	58.2	57.7	54.5	47.5		58.2	1.01
Trimethylethoxysilane	34.7	41.0	47.4	50.3	46.5	41.0	35.0		50.3	1.00
Aldehydes										
Acrolein	47.0	58.0	66.6	65.9	56.5				67.2	0.95
Propionaldehyde		37.5	44.3	49.0	49.5	46.0	41.6	37.2	50.0	1.06
Acetaldehyde		26.6	35.0	41.4	41.4	36.0	30.0		42.2	1.05
Ketones										
Acetone		40.4	44.2	42.6	38.2				44.4	0.93
Methyl ethyl ketone		36.0	42.0	43.3	41.5	37.7	33.2		43.4	0.99
Esters										
Vinyl acetate	29.0	36.6	39.8	41.4	42.1	41.6	35.2		42.2	1.13
Ethyl acetate		30.7	35.2	37.0	35.6	30.0			37.0	1.00
Ethers										
Dimethyl ether		44.8	47.6	48.4	47.5	45.4	42.6		48.6	0.99
Diethyl ether	30.6	37.0	43.4	48.0	47.6	40.4	32.0		48.2	1.05
Dimethoxymethane	32.5	38.2	43.2	46.6	48.0	46.6	43.3		48.0	1.10
Diisopropyl ether		30.7	35.5	38.3	38.6	36.0	31.2		38.9	1.06

TABLE C.11 (continued)

## Burning Velocities of Various Fuels

	$\phi = 0.7$	$\phi = 0.8$	$\phi = 0.9$	$\phi = 1.0$	$\phi = 1.1$	$\phi = 1.2$	$\phi = 1.3$	$\phi = 1.4$	$S_{\max}$	$\phi$ at $S_{\max}$
Thio ethers										
Dimethyl sulfide		29.9	31.9	33.0	30.1	24.8			33.0	1.00
Peroxides										
Di- <i>t</i> -butyl peroxide		41.0	46.8	50.0	49.6	46.5	42.0	35.5	50.4	1.04
Aromatic compounds										
Furan	48.0	55.0	60.0	62.5	62.4	60.0			62.9	1.05
Benzene		39.4	45.6	47.6	44.8	40.2	35.6		47.6	1.00
Thiophane	33.8	37.4	40.6	43.0	42.2	37.2	24.6		43.2	1.03
Cyclic compounds										
Ethylene oxide	57.2	70.7	83.0	88.8	89.5	87.2	81.0	73.0	89.5	1.07
Butadiene monoxide		36.6	47.4	57.8	64.0	66.9	66.8	64.5	67.1	1.24
Propylene oxide	41.6	53.3	62.6	66.5	66.4	62.5	53.8		67.0	1.05
Dihydropyran	39.0	45.7	51.0	54.5	55.6	52.6	44.3	32.0	55.7	1.08
Cyclopropane		40.6	49.0	54.2	55.6	53.5	44.0		55.6	1.10
Tetrahydropyran	44.8	51.0	53.6	51.5	42.3				53.7	0.93
Cyclic compounds										
Tetrahydrofuran			43.2	48.0	50.8	51.6	49.2	44.0	51.6	1.19
Cyclopentadiene	36.0	41.8	45.7	47.2	45.5	40.6	32.0		47.2	1.00
Ethylenimine		37.6	43.4	46.0	45.8	43.4	38.9		46.4	1.04
Cyclopentane	31.0	38.4	43.2	45.3	44.6	41.0	34.0		45.4	1.03
Cyclohexane			41.3	43.5	43.9	38.0			44.0	1.08
Inorganic compounds										
Hydrogen	102	120	145	170	204	245	213	290	325	1.80
Carbon disulfide	50.6	58.0	59.4	58.8	57.0	55.0	52.8	51.6	59.4	0.91
Carbon monoxide					28.5	32.0	34.8	38.0	52.0	2.05
Hydrogen sulfide	34.8	39.2	40.9	39.1	32.3				40.9	0.90
Propylene oxide	74.0	86.2	93.0	96.6	97.8	94.0	84.0	71.5	97.9	1.09
Hydrazine	87.3	90.5	93.2	94.3	93.0	90.7	87.4	83.7	94.4	0.98
Furfural	62.0	73.0	83.3	87.0	87.0	84.0	77.0	65.5	87.3	1.05
Ethyl nitrate	70.2	77.3	84.0	86.4	83.0	72.3			86.4	1.00
Butadiene monoxide	51.4	57.0	64.5	73.0	79.3	81.0	80.4	76.7	81.1	1.23
Carbon disulfide	64.0	72.5	76.8	78.4	75.5	71.0	66.0	62.2	78.4	1.00
<i>n</i> -Butyl ether		67.0	72.6	70.3	65.0				72.7	0.91
Methanol	50.0	58.5	66.9	71.2	72.0	66.4	58.0	48.8	72.2	1.08
Diethyl cellosolve	49.5	56.0	63.0	69.0	69.7	65.2			70.4	1.05
Cyclohexene										
Monoxide	54.5	59.0	63.5	67.7	70.0	64.0			70.0	1.10
Epichlorohydrin	53.0	59.5	65.0	68.6	70.0	66.0	58.2		70.0	1.10
<i>n</i> -Pentane		50.0	55.0	61.0	62.0	57.0	49.3	42.4	62.9	1.05
<i>n</i> -Propyl alcohol	49.0	56.6	62.0	64.6	63.0	50.0	37.4		64.8	1.03
<i>n</i> -Heptane	41.5	50.0	58.5	63.8	59.5	53.8	46.2	38.8	63.8	1.00
Ethyl nitrite	54.0	58.8	62.6	63.5	59.0	49.5	42.0	36.7	63.5	1.00
Pinene	48.5	58.3	62.5	62.1	56.6	50.0			63.0	0.95
Nitroethane	51.5	57.8	61.4	57.2	46.0	28.0			61.4	0.92
Isooctane		50.2	56.8	57.8	53.3	50.5			58.2	0.98
Pyrrole		52.0	55.6	56.6	56.1	52.8	48.0	43.1	56.7	1.00
Aniline		41.5	45.4	46.6	42.9	37.7	32.0		46.8	0.98
Dimethyl formamide		40.0	43.6	45.8	45.5	40.7	36.7		46.1	1.04

Source: The compilation of laminar flame speed data given in tables is from Gibbs and Calcote, *J. Chem. Eng. Data*, 4, 2226, 1959; *Combustion Science and Engineering*, CRC Table A.39D, p. 1057.

Note:  $T = 25^\circ\text{C}$  (air–fuel temperature);  $P = 1\text{ atm}$  (0.31 mol %  $\text{H}_2\text{O}$  in air); burning velocity  $S$  as a function of equivalence ratio  $\phi$  in cm/s. The data are for premixed fuel–air mixtures at  $100^\circ\text{C}$  and 1 atm pressure; 0.31 mol %  $\text{H}_2\text{O}$  in air; burning velocity  $S$  as a function of  $\phi$  in cm/s.

This page intentionally left blank



## Appendix D: Properties of Solids

TABLE D.1

Thermal Properties of Selected Metallic Elements at 293 K (20°C) or 528°R (65°F)

Element	Specific Gravity	Specific Heat, $c_p$		Thermal Conductivity, $k$		Diffusivity, $\alpha$		Melting Temperature	
		J/(kg K)	BTU/(lbm °R)	W/(m K)	BTU/(h ft °R)	m <sup>2</sup> /s × 10 <sup>6</sup>	ft <sup>2</sup> /s × 10 <sup>3</sup>	K	°R
Aluminum	2.702	896	0.214	236	136	97.5	1.05	933	1680
Beryllium	1.850	1750	0.418	205	118	63.3	0.681	1550	2790
Chromium	7.160	440	0.105	91.4	52.8	29.0	0.312	2118	3812
Copper	8.933	383	0.0915	399	231	116.6	1.26	1356	2441
Gold	19.300	129	0.0308	316	183	126.9	1.37	1336	2405
Iron	7.870	452	0.108	31.1	18.0	22.8	0.245	1810	3258
Lead	11.340	129	0.0308	35.3	20.4	24.1	0.259	601	1082
Magnesium	1.740	1017	0.243	156	90.1	88.2	0.949	923	1661
Manganese	7.290	486	0.116	7.78	4.50	2.2	0.0236	1517	2731
Molybdenum	10.240	251	0.0600	138	79.7	53.7	0.578	2883	5189
Nickel	8.900	446	0.107	91	52.6	22.9	0.246	1726	3107
Platinum	21.450	133	0.0318	71.4	41.2	25.0	0.269	2042	3676
Potassium	0.860	741	0.177	103	59.6	161.6	1.74	337	607
Silicon	2.330	703	0.168	153	88.4	93.4	1.01	1685	3033
Silver	10.500	234	0.0559	427	247	173.8	1.87	1234	2221
Tin	5.750	227	0.0542	67.0	38.7	51.3	0.552	505	909
Titanium	4.500	611	0.146	22.0	12.7	8.0	0.0861	1953	3515
Tungsten	19.300	134	0.0320	179	103	69.2	0.745	3653	6575
Uranium	19.070	113	0.0270	27.4	15.8	12.7	0.137	1407	2533
Vanadium	6.100	502	0.120	31.4	18.1	10.3	0.111	2192	3946
Zinc	7.140	385	0.0920	121	69.9	44.0	0.474	693	1247

Source: Data from several sources; Janna, W.S., *Engineering Heat Transfer*, 2nd edn., Table B.1, CRC Press, Boca Raton, FL, p. 643, 2000.

Notes: Density =  $\rho$  = specific gravity × 62.4 lbm/ft<sup>3</sup> = specific gravity × 1000 kg/m<sup>3</sup>.

Diffusivity =  $\alpha$ ; for aluminum,  $\alpha$  m<sup>2</sup>/s × 10<sup>6</sup> = 97.5; so  $\alpha$  = 97.5 × 10<sup>-6</sup> m<sup>2</sup>/s.

Also,  $\alpha$  =  $k/\rho c_p$ .

Thermal Properties of Selected Alloys											
Alloy Name	Composition	Specific Gravity	Specific Heat, <i>c</i> <sub>p</sub>		Thermal Conductivity, <i>k</i>		Diffusivity, <i>α</i>		Coeff. of Linear Expansion		Approximate Melting Point
			J/(kg K)	BTU/(lbm °R)	W/(m K)	BTU/(h ft °R)	m²/s × 10 <sup>5</sup>	ft²/s × 10 <sup>4</sup>	μ m/m K	μ in./in. °F	°C
Aluminum alloy 3003, H14	ASTM B221	2.73			155.7	90			23.2	12.9	649
Aluminum alloy 2017, T6	ASTM B221	2.8			164.4	95			22.9	12.7	641
Aluminum alloy 380	ASTM SC84B	2.7			96.9	56			20.9	11.6	566
Copper alloy 70	95 Al, 5 Cu	2.787	833	0.199	164	94.7	6.676	7.187			
	87 Al, 13 Si	2.659	871	0.208	164	94.7	7.099	7.642			
	ASTM B152, B124, B133, B1, B2, B3	8.91			389.3	225			16.7	9.3	1082
	ASTM B30, No. 4A	8.7			72.7	42			18.0	10.0	996
	ASTM B36, B134, B135	8.47			119.4	69			18.9	10.5	932
Aluminum bronze 5	ASTM B169, Alloy A; ASTM B124, B150	7.8			70.9	41			16.6	9.2	1038
Copper alloy 25	ASTM B194	8.25			12.1	7			16.7	9.3	927
	95 Cu, 5 Al	8.666	410	0.0979	83	47.9	2.330	2.508			
	75 Cu, 25 Sn	8.666	343	0.0819	26	15.0	0.859	0.925			
	85 Cu, 9 Sn, 6 Zn	8.714	385	0.0920	61	35.2	1.804	1.942			
	70 Cu, 30 Zn	8.522	385	0.0920	111	64.1	3.412	3.673			
Aluminum-silver alloy	62 Cu, 15 Ni, 22 Zn	8.618	394	0.0941	24.9	14.4	0.733	0.789			
Aluminum-nickel alloy	60 Cu, 40 Ni	8.922	410	0.0979	22.7	13.1	0.612	0.659			
Nickel alloy 30%	30%	8.95			29.4	17			15.3	8.5	1227
Nickel alloy 55-45	55-45 (Constantan)	8.9			22.5	13			14.6	8.1	1260
Cast iron		7.86			72.7	42			12.2	6.8	1538
	ASTM A48-48, Class 25	7.2			45.0	26			12.1	6.7	1177
Cast iron	ASTM A47	7.32							11.9	6.6	1232
Cast iron	ASTM A339, A395	7.2			32.9	19			13.5	7.5	1149
Cast iron	type 2	7.3			39.8	23			17.3	9.6	1232
Cast iron	4 C	7.272	420	0.100	52	30.0	1.702	1.832			
	0.5 CH	7.849	460	0.110	59	34.1	1.626	1.750			

Table 1. Mechanical properties of various materials (continued)											
Material		Tensile strength (MPa)		Yield strength (MPa)		Elongation at break (%)		Modulus of elasticity (GPa)		Density (g/cm³)	
Carbon steel	AISI-SAE 1020	7.86			51.9	30				12.1	6.7
	1 C	7.801	473	0.113	43	24.8	1.172	1.262			
	1.5 C	7.753	486	0.113	36	20.8	0.970	1.040			
Steel	1 Cr	7.865	460	0.110	61	35.2	1.665	1.792			
	5 Cr	7.833	460	0.110	40	23.1	1.110	1.195			
	10 Cr	7.785	460	0.110	31	17.9	0.867	0.933			
Nickel steel	15 Cr, 10 Ni	7.865	460	0.110	19	11.0	0.526	0.577			
	20 Cr, 15 Ni	7.833	460	0.110	15.1	8.72	0.415	0.447			
Steel	10 Ni	7.945	460	0.110	26	15.0	0.720	0.775			
	20 Ni	7.993	460	0.110	19	11.0	0.526	0.566			
	40 Ni	8.169	460	0.110	10	5.78	0.279	0.300			
Inconel	60 Ni	8.378	460	0.110	19	11.0	0.493	0.531			
	80 Ni, 15 C	8.522	460	0.110	17	9.82	0.444	0.478			
Inconel	40 Ni, 15 C	8.073	460	0.110	11.6	6.70	0.305	0.328			
	1 Mn	7.865	460	0.110	50	28.9	1.388	1.494			
Inconel	5 Mn	7.849	460	0.110	22	12.7	0.637	0.686			
	1 Si	7.769	460	0.110	42	24.3	1.164	1.164			
Inconel	5 Si	7.417	460	0.110	19	11.0	0.555	0.597			
	Type 304	8.02	461	0.110	14.4	8.32	0.387	0.417	17.3	9.6	1427
Inconel	Type 347	7.97	461	0.110	14.3	8.26	0.387	0.417			
	1 W	7.913	448	0.107	66	31.1	1.858	2.000			
Inconel	5 W	8.073	435	0.104	54	31.2	1.525	1.642			
Lead		11.35			34.6	20			29.5	16.4	327
Aluminum lead (hard)		10.9			29.4	17			27.2	15.1	290
Aluminum alloy	AZ31B	1.77			77.9	45			26.1	14.5	627
	ASTM B160, B161, B162	8.89			60.6	35			11.9	6.6	1441
Aluminum alloy (over 18% alloy weight)	ASTM B122, No. 2	8.8			32.9	19			16.2	9.0	1110
Commercial titanium		5			17.3	10			8.8	4.9	1816
	ASTM B69	7.14			107.3	62			32.4	18.0	418
Inconel, commercial		6.5			17.3	10			5.2	2.9	1843
Aluminum alloy (HD)	ASTM A297-63T	7.6			2.6	1.5			16.6	9.2	1482
	C	3.94			8.7	5			11.3	6.3	1288
	X, annealed	8.25			15.6	9			12.1	6.7	1399
	alloy 25 (L605)	9.15			9.5	5.5			13.7	7.6	1371
		8.47			19.0	11			13.3	7.4	1349
50-50		8.89			45.0	26			23.6	13.1	216

Sourced from multiple sources.



TABLE D.3

Thermal Properties of Selected Building Materials and Insulations at 293 K (20°C) or 528°R (65°F)

Material	Specific Gravity	Specific Heat, $c_p$		Thermal Conductivity, $k$		Diffusivity, $\alpha$	
		J/(kg K)	BTU/(lbm °R)	W/(m K)	BTU/(h ft °R)	m <sup>2</sup> /s × 10 <sup>5</sup>	ft <sup>2</sup> /s × 10 <sup>6</sup>
Asbestos	0.383	816	0.195	0.113	0.0653	0.036	3.88
Asphalt	2.120			0.698	0.403		
Bakelite	1.270			0.233	0.135		
Brick							
Carborundum (50%SiC)	2.200			5.82	3.36		
Common	1.800	840	0.201	0.38–0.52	0.22–0.30	0.028–0.034	3.0–3.66
Magnesite (50%MgO)	2.000			2.68	1.55		
Masonry	1.700	837	0.200	0.658	0.38	0.046	5.0
Silica (95%SiO <sub>2</sub> )	1.900			1.07	0.618		
Cardboard				0.14–0.35	0.08–0.2		
Cement (hard)				1.047	0.605		
Clay (48.7%moist)	1.545	880	0.210	1.26	0.728	0.101	10.9
Coal (anthracite)	1.370	1260	0.301	0.238	0.137	0.013–0.015	1.4–1.6
Concrete(dry)	0.500	837	0.200	0.128	0.074	0.049	5.3
Cork board	0.150	1880	0.449	0.042	0.0243	0.015–0.044	1.6–4.7
Cork (expanded)	0.120			0.036	0.0208		
Earth (diatomaceous)	0.466	879	0.210	0.126	0.072	0.031	3.3
Earth (clay with 28% moist)	1.500			1.51	0.872		
Earth (sandy with 8% moist)	1.500			1.05	0.607		
Glass fiber	0.220			0.035	0.02		
Glass (window pane)	2.800	800	0.191	0.81	0.47	0.034	3.66
Glass (wool)	0.200	670	0.160	0.040	0.023	0.028	3.0
Granite	2.750			3.0	1.73		
Ice at 0°C	0.913	1830	0.437	2.22	1.28	0.124	13.3
Kapok	0.025			0.035	0.02		
Linoleum	0.535			0.081	0.047		
Mica	2.900			0.523	0.302		
Pine bark	0.342			0.080	0.046		
Plaster	1.800			0.814	0.47		

Source: Janna, W.S., *Engineering Heat Transfer*, 2nd edn., Table B.3, CRC Press, Boca Raton, FL, p. 645, 2000.Notes: Density =  $\rho$  = specific gravity × 62.4 lbm/ft<sup>3</sup> = specific gravity × 1000 kg/m<sup>3</sup>.Diffusivity =  $\alpha$ ; for asbestos,  $\alpha \times 10^3 = 0.036$  m<sup>2</sup>/s; so  $\alpha = 0.036 \times 10^{-3}$  m<sup>2</sup>/s also,  $\alpha = k/\rho c_p$ .

This page intentionally left blank



**The John Zink Hamworthy Combustion Handbook,  
Second Edition: Volume 1 – Fundamentals**

Edited by Charles E. Baukal, Jr.,  
John Zink Company, LLC, Tulsa, Oklahoma, USA

Despite the length of time it has been around, its importance, and vast amounts of research, combustion is still far from being completely understood. Issues regarding the environment, cost, and fuel consumption add further complexity, particularly in the process and power generation industries. Dedicated to advancing the art and science of industrial combustion, **The John Zink Hamworthy Combustion Handbook, Second Edition: Volume 1 – Fundamentals** gives you a strong understanding of the basic concepts and theory.

Under the leadership of Charles E. Baukal, Jr., top combustion engineers and technologists from John Zink Hamworthy Combustion examine the interdisciplinary fundamentals – including chemistry, fluid flow, and heat transfer – as they apply to industrial combustion.

**What's New in This Edition**

- Expanded to three volumes, with **Volume 1** focusing on fundamentals
- Extensive updates and revisions throughout
- Updated information on HPI/CPI industries, including alternative fuels, advanced refining techniques, emissions standards, and new technologies
- Expanded coverage of the physical and chemical principles of combustion
- New practices in coal combustion, such as gasification
- The latest developments in cold-flow modeling, CFD-based modeling, and mathematical modeling
- Greater coverage of pollution emissions and NO<sub>x</sub> reduction techniques
- New material on combustion diagnostics, testing, and training
- More property data useful for the design and operation of combustion equipment
- Coverage of technologies such as metallurgy, refractories, blowers, and vapor control equipment

The first of three volumes in the expanded second edition of the bestselling *The John Zink Combustion Handbook*, this comprehensive volume – featuring color illustrations throughout – helps you broaden your understanding of industrial combustion to better meet the challenges of this field.



**CRC Press**

Taylor & Francis Group  
an informa business

[www.taylorandfrancisgroup.com](http://www.taylorandfrancisgroup.com)

6000 Broken Sound Parkway, NW  
Suite 300, Boca Raton, FL 33487  
711 Third Avenue  
New York, NY 10017  
2 Park Square, Milton Park  
Abingdon, Oxon OX14 4RN, UK

K11814

ISBN: 978-1-4398-3962-1



9 0000



9 781439 839621

[www.crcpress.com](http://www.crcpress.com)